

# Natural **BIODYNAMICS**



Vladimir G Ivancevic • Tijana T Ivancevic





This page intentionally left blank

# Natural **BIODYNAMICS**



**Vladimir G. Ivancevic**

Defence Science & Technology Organisation, Australia

**Tijana T. Ivancevic**

University of Adelaide, Australia



NEW JERSEY • LONDON • SINGAPORE • BEIJING • SHANGHAI • HONG KONG • TAIPEI • CHENNAI

*Published by*

World Scientific Publishing Co. Pte. Ltd.

5 Toh Tuck Link, Singapore 596224

USA office: 27 Warren Street, Suite 401-402, Hackensack, NJ 07601

UK office: 57 Shelton Street, Covent Garden, London WC2H 9HE

**British Library Cataloguing-in-Publication Data**

A catalogue record for this book is available from the British Library.

**NATURAL BIODYNAMICS**

Copyright © 2005 by World Scientific Publishing Co. Pte. Ltd.

*All rights reserved. This book, or parts thereof, may not be reproduced in any form or by any means, electronic or mechanical, including photocopying, recording or any information storage and retrieval system now known or to be invented, without written permission from the Publisher.*

For photocopying of material in this volume, please pay a copying fee through the Copyright Clearance Center, Inc., 222 Rosewood Drive, Danvers, MA 01923, USA. In this case permission to photocopy is not required from the publisher.

ISBN 981-256-534-5

*Dedicated to*  
*Nitya, Atma and Kali*

This page intentionally left blank

# Preface

This book is a result of two and a half decades of authors' struggles with *human-like biodynamics* (*biodynamics*, for short), a highly complex and synergetic subject, which needs rigorous mathematical analysis to become *totally predictive*, but apparently defies it. This work has been realized in the form of the world-leading human-motion simulator called *Human Biodynamics Engine* (developed in the Land Operations Division, Defence Science & Technology Organisation, Australia).

To get an idea of biodynamics complexity at the purely mechanical level, consider for a moment a human spine. Even if we ignore the highly irregular multi-vertebral geometry, a popular 'spinal column' is not columnar at all; it is a chain of 26 flexibly-coupled rigid bodies, including 25 movable spinal joints, each with three rotations (restricted to about 6–7 angular degrees in average) as well as three translations (each restricted to about 5 millimeters), which gives a total number of 150 constraint degrees of freedom (DOF). To perform a predictive analysis of the mechanism of a very common 'back pain' syndrome, in which there is no evidence at all for any tissue damage (measured by X-ray, CT, PET or functional MRI scans), and yet the patient suffers from spastic pain and drastically reduced motion capability — we need to take into account *all* 150 DOF. Dynamically speaking, we have a chain of 25 constrained Euclidean  $SE(3)$  groups acting in all movable spinal joints, and we need to develop a rigorous kinematics and dynamics, as well as a hierarchical control model for this chain — to be able to accurately predict/control all possible motions (between any initial and final body configurations) and prevent spinal injuries, and thus efficiently cope with the back pain syndrome.

Spine is just one of many examples in which current biomechanics (or biomedical engineering) tries to *predict* and *control* the behavior of highly

complex physiological systems using trivial models, like a very popular 1 DOF *inverted pendulum model* for the whole human body that has more than 300 DOF driven by more than 600 muscles, or similarly popular ‘Hybrid III’ crash-test dummy, that has one cylinder for the spine and one for the neck.<sup>1</sup> Toy models might be good for educational purposes, to *explain* natural phenomena, but they *cannot* really *predict* or *control* anything that is considerably more complex. To be able to accurately predict/control a complex natural phenomenon, a tentative model’s complexity necessarily approaches the complexity of the original, at least from the dynamical & control perspective. The core question in modelling natural phenomena is: “How would *Nature* solve this complex engineering problem?” Our suggested answer is: “Surely not by *over-simplification* (so-common today, considering a spine to be a ‘column’, or even a ‘stick’), but rather by consistent, continuous and smooth inner logic, which makes ‘all the components fit together nicely’ – that we call *natural biodynamics*.” The aim of this book is to offer a plausible mathematical answer to such questions and show that rigorous engineering analysis and prediction of holistic biodynamic problems *is* possible. What we really want is to understand the *manifoldness* of natural biodynamics. In this attempt, we start with pure mechanics, but we inevitably have to go beyond and above the realm of mechanics, into the higher realm of modern *brain-like control*.

Today we see a fashion of engineers mimicking the ways of Nature: – e.g., measuring motion and impact accelerations in various athletes, pilots and crash-test dummies, using three-axial accelerometers, which actually

---

<sup>1</sup> *Human Biodynamics Engine* (HBE) is a generalized Hamiltonian system with 264 DOF, including 132 rotational DOF (considered active) and 132 translational DOF (considered passive). Passive joint dynamics models visco-elastic properties of intervertebral discs, joint tendons and muscle ligaments as a nonlinear spring-damper system. Active joint dynamics is driven by 264 *nonlinear muscular actuators*, each with its own excitation-contraction dynamics (following traditional biomechanical models) and two-level neural-like control. The lower control level resembles *spinal-reflex positive and negative force feedbacks* (stretch and Golgi reflexes). The higher control level resembles cerebellum’s postural stabilization and velocity control (modelled as a high-dimensional Lie-derivative controller). The HBE includes over 2000 body parameters, all derived from individual user data, using standard biomechanical tables. It models stabilizing and reaching body movements at a spot, walking and running with any speed and a generic crash simulator. The HBE incorporates a new theory of soft neuro-musculo-skeletal injuries, much more sensitive than the traditional Principal Loading Hypothesis (of tension, compression, bending and shear) for spinal and other neuro-musculo-skeletal injuries. It is based on the concept of the local Jolts and Torque-Jolts, which are the time derivatives of the total forces and torques localized in each joint at a particular time instant.

resemble bio-accelerometers embedded in human semicircular canals (fluid-filled loops that form part of the labyrinth inside the inner ear); – e.g., control on Lie  $SO(3)$ -group actually mimics the action of six extraocular muscles of the human eye, etc.

Now, what is ‘Natural Biodynamics’? In essence, it is mathematical unity in biodynamics diversity as well as natural diversity in mathematical unity. In other words, it is discovering *biodynamic laws* in ‘real world’ and utilizing these laws to understand, predict and control/prevent other natural phenomena (like various injuries). To explain this, let us start with the second word, ‘*Biodynamics*’, the main subject of this book. We define biodynamics as a union of *nonlinear dynamics* and *biological complexity*. Its research area is the intersection between mathematical physiology and humanoid robotics. In other words, biodynamics can be defined as *human-like neuro-mechanics*, with two distinct organizational levels:

- Lower-mechanical level; and
- Higher-neural level.

The mechanical level is clearly more structured and rigorous, with the fully developed mathematical machinery. Here, we follow the slogan of Ralph Abraham [Abraham and Shaw (1992)]: “...*dynamics is geometry of behavior*...” and therefore, this part is dominated by differential geometric and topological variations to the central theme of our *covariant force law*:

**force 1-form-field = mass distribution  $\times$  acceleration vector-field**

On the other hand, the neural level is one of the most complex phenomena in our world and its scientific methodology is yet in its early development phase. Therefore, the mechanical part of the text is written in a ‘strong mathematical’ form, while the neural part is written in an inevitably ‘weak physiological’ form. However, even in this weak neural part, we try to follow the path-showing words of Paul Dirac [Dirac (1930)]: “...The main object of physical science is not the provision of pictures, but is the formulation of laws governing phenomena and the application of these laws to the discovery of new phenomena...” The same fundamental scientific idea, in the words of Roger Penrose [Penrose (1997)], reads: “...These will not be ‘botanical’ sections, telling you in detail what is here and what is there in our Universe, but rather I want to concentrate upon understanding the actual laws which govern the way the world behaves.” Neural part of biodynamics is supposed to give a brain-like reflection of the mechanical covariant force law. It is



the sensory-motor [lat. *sensus* = sense; *motor* = mover] coordination and control.

Now, the main attribute, '*Natural*', which is supposed to 'explain' the subject of the book, is clearly associated with Nature. How? Both biophysically and mathematically. More precisely, the keyword natural in this book represents a combination of the following two ideas:

- *Global* mathematical idea of natural transformations (i.e., functorial, or categorical maps) – which represents *unity in diversity* (i.e., mathematical unity in natural diversity); and
- *Local* biophysical idea of Haken's synergetics, i.e., self-organized learning dynamics, which implies the order emerging from chaos by cooperation of subsystems – which represents *diversity in unity* (i.e., natural diversity in mathematical unity).

The combination of these two ideas, which we believe enables us to understand the manifoldness of natural biodynamics, is the concept of *biodynamic manifold*.

Theory of categories and functors is a synthetic metalanguage of modern mathematics, visually depicted using commutative diagrams. The core of the higher biodynamics is the global sensory-motor coordination/control, which in categorical language defines the *neuro-muscular adjunction*

$$\text{Coordination} := \text{Sensory Path} \dashv \text{Motor Path}$$

between the two functorial neural pathways

$$(\text{Sensory}, \text{Motor}) : \text{Brain} \rightleftarrows \text{Body}.$$

It is an open system, generalized from the simple system's stimulus-response map (i.e., input-output, or cause-effect relation). Its other physiological meanings are: reaction, association, and integration.

On the other hand, the adaptive synergetics describes the local learning process according to the basic formula:

$$\text{New Value} = \text{Old Value} + \text{Innovation},$$

including all basic synergetic forms: 'unsupervised' self-organization, emergence of dynamic patterns, coherent nonlinear oscillations, nonequilibrium phase transitions, as well as symmetry braking instabilities.

In our opinion, these two ideas together form unique and natural scientific machinery for understanding, prediction and control of both human and artificial systems of the highest complexity.

If we manage to bring a new light into this subject, we will find the solution (at least in principle) for the three main biodynamics applications:

- (i) Understanding the true mechanics of injuries and pathology of the human motion, which is a paradigm of general human behavior;
- (ii) Biomechanical modelling for computer-assisted surgical planning; and
- (iii) Design of a super-robot, to help disabled people.

Therefore, the purpose of this book is to investigate the subject of 'biodynamics' using the method of 'natural' mathematics and biophysics. A reader may say: it's all right about the subject (and its possible applications), but why using this 'overkill' methodology. The answer that we propose is this: It is true that the human mind prefers linear and simplistic solutions, but we cannot attempt to solve an immensely complex problem using a simplistic method. As Madam A. Ehresmann says, "Any representation of a complex system by the traditional models based on ordinary and partial differential equations can be valid only locally and temporarily." On the other hand, a trivial method (compared to the complexity of the problem) can give only a trivial solution. As we are dealing with the problem of the highest possible complexity, we need the scientific method that matches that complexity (which is unfortunately not common in science today). In our opinion, we have borrowed the strongest machinery from both mathematics and (bio)physical sciences. We call this machinery *natural*.

The book contains seven chapters and appendix. The first two chapters have introductory character: the official introduction is given in the first chapter, where the problem of human-like biodynamics is stated 'in plain English,' including the most important historical remarks; the second chapter introduces the 'natural' language of biodynamics. The next three chapters develop the lower biodynamics, in terms of natural geometry, mechanics and topology. Here the keyword 'natural' predominantly means 'functorial', as this part is simpler in nature and naturally more rigorous. The last two chapters are devoted to the higher biodynamics, from modern nonlinear control and brain-like point of view. Here the keyword 'natural' predominantly means 'synergetic', as this part is much more complex and consequently much more fuzzy. The appendix is of a textbook nature, giving brief introduction into the background knowledge necessary for comprehensive understanding of the main text.

Biodynamics operates on four different biophysical levels of organization (using a top-down classification):

- (1) Level of a whole neuro-musculo-skeletal system;
- (2) Level of a single muscle and/or a single neural network;

- (3) Cellular level of a single muscle-fibre and/or a single neuron;
- (4) Molecular muscular and neural level.

Here, the first three macroscopic levels are governed by classical biodynamics, while the fourth (molecular) level is governed by quantum biodynamics.

Although the book includes several medical sections, its goal is not to cure certain surgical phenomena (like traumas and injuries), but rather to understand, predict and control/prevent their occurrence, especially recurrence.

The target audience for this book includes applied mathematicians, physicists, robotics and general engineering scientists, as well as various postgraduate (and last year undergraduate) students with stronger mathematical background and general interest in biodynamics as well as complex, human-like synergetic systems. Although wrapped in categorical formalism, (usually 'reserved for pure mathematics'), the mathematics developed in the text is intentionally informal to be accessible for the wider audience. Therefore, although presenting a chapter on differential-geometric methods and a chapter on topological methods, this book is not a textbook in differential geometry or (algebraic) topology. It just uses the strongest tools that contemporary mathematics offers to deal with our 'natural biodynamics reality', driven by the *immortal spirit of David Hilbert*:

"We must know! We shall know!"

V. Ivancevic

Defence Science & Technology Organisation, Australia

e-mail: [Vladimir.Ivancevic@dsto.defence.gov.au](mailto:Vladimir.Ivancevic@dsto.defence.gov.au)

T. Ivancevic

School of Mathematics,

The University of Adelaide, Australia

e-mail: [Tijana.Ivancevic@adelaide.edu.au](mailto:Tijana.Ivancevic@adelaide.edu.au)

Adelaide,

August 2005

# Acknowledgments

Our warmest appreciation must go to Professor J.C. Misra, a true pioneer in human biodynamics.

The authors also wish to thank Land Operations Division, Defence Science & Technology Organisation, Australia, for the support in developing the *Human Biodynamics Engine* (HBE) and all HBE-related text in this monograph.

Finally, we express our gratitude to the World Scientific Publishing Company, and especially to Ms. Zhang Ji and Mr. Rhaimie Wahap.

This page intentionally left blank

# Glossary of Frequently Used Symbols

## General

- ‘iff’ means ‘if and only if’;
- ‘r.h.s’ means ‘right hand side’; ‘l.h.s’ means ‘left hand side’;
- *Einstein’s summation convention over repeated indices* (not necessarily one up and one down) *is assumed in the whole text*, unless explicitly stated otherwise.

## Sets

- $\mathbb{N}$  – natural numbers;  
 $\mathbb{Z}$  – integers;  
 $\mathbb{R}$  – real numbers;  
 $\mathbb{C}$  – complex numbers;  
 $\mathbb{H}$  – quaternions;  
 $\mathbb{K}$  – number field of real numbers, complex numbers, or quaternions.

## Maps

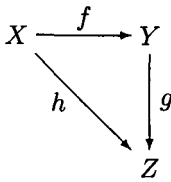
$f : A \rightarrow B$  – a function, (or map) between sets  $A \equiv \text{Dom } f$  and  $B \equiv \text{Cod } f$ ;

$\text{Ker } f = f^{-1}(e_B)$  – a kernel of  $f$ ;

$\text{Im } f = f(A)$  – an image of  $f$ ;

$\text{Coker } f = \text{Cod } f / \text{Im } f$  – a cokernel of  $f$ ;

$\text{Coim } f = \text{Dom } f / \text{Ker } f$  – a coimage of  $f$ ;



— a commutative diagram, requiring  $h = g \circ f$ .

## Derivatives

$C^k(A, B)$  – set of  $k$ –times differentiable functions between sets  $A$  to  $B$ ;

$C^\infty(A, B)$  – set of *smooth* functions between sets  $A$  to  $B$ ;

$C^0(A, B)$  – set of *continuous* functions between sets  $A$  to  $B$ ;

$f'(x) = \frac{df(x)}{dx}$  – derivative of  $f$  with respect to  $x$ ;

$\dot{x}$  – total time derivative of  $x$ ;

$\partial_t \equiv \frac{\partial}{\partial t}$  – partial time derivative;

$\partial_{x^i} \equiv \partial_i \equiv \frac{\partial}{\partial x^i}$  – partial coordinate derivative;

$\dot{f} = \partial_t f + \partial_{x^i} f \dot{x}^i$  – total time derivative of the scalar field  $f = f(t, x^i)$ ;

$u_t \equiv \partial_t u$ ,  $u_x \equiv \partial_x u$ ,  $u_{xx} \equiv \partial_{x^2} u$  – only in partial differential equations;

$L_{x^i} \equiv \partial_{x^i} L$ ,  $L_{\dot{x}^i} \equiv \partial_{\dot{x}^i} L$  – coordinate and velocity partial derivatives of the Lagrangian function;

$d$  – exterior derivative;

$d^n$  – coboundary operator;

$\partial_n$  – boundary operator;

$\nabla = \nabla(g)$  – Levi-Civita affine connection on a smooth manifold  $M$  with Riemannian metric tensor  $g = g_{ij}$ ;

$\Gamma_{jk}^i$  – Christoffel symbols of the connection  $\nabla$ ;

$\nabla_X T$  – covariant derivative of the tensor-field  $T$  with respect to the vector-field  $X$ , defined by means of  $\Gamma_{jk}^i$ ;

$T_{;x^i}$  – covariant derivative of the tensor-field  $T$  with respect to the coordinate basis  $\{x^i\}$ ;

$\ddot{T} \equiv \frac{DT}{dt}$  – absolute (intrinsic, or Bianchi) derivative of the tensor-field  $T$  upon the parameter  $t$ ; e.g., acceleration vector is the *absolute time derivative* of the velocity vector,  $a^i = \dot{v}^i \equiv \frac{Dv^i}{dt}$ ; note that in general,  $a^i \neq \dot{v}^i$  – this is crucial for *proper definition of Newtonian force* (see Appendix);

$\mathcal{L}_X T$  – Lie derivative of the tensor-field  $T$  in direction of the vector-field  $X$ ;

$[X, Y]$  – Lie bracket (commutator) of two vector-fields  $X$  and  $Y$ ;

$\{F, G\}$  – Poisson bracket of two functions  $F$  and  $G$ ;

$\{F, G\}$  – Lie-Poisson bracket of two functions  $F$  and  $G$ .

## Manifolds and Fibre Bundles

$M$  – manifold, usually the biodynamic configuration manifold;

$TM$  – tangent bundle of the manifold  $M$ ;

$\pi_M : TM \rightarrow M$  – natural projection;

$T^*M$  – cotangent bundle of the manifold  $M$ ;

$(E, \pi, M)$  – a vector bundle with total space  $E$ , base  $M$  and projection  $\pi$ ;

$(E, p, M, F)$  – a fibre bundle with total space  $E$ , base  $M$ , projection  $p$  and standard fibre  $F$ ;

$J^k(M, N)$  – bundle of  $k$ -jets of smooth functions between manifolds  $M, N$ .

## Groups

$G$  – usually a general Lie group;

$GL(n)$  – general linear group with real coefficients in dimension  $n$ ;

$SO(n)$  – group of rotations in dimension  $n$ ;

$T^n$  – toral (Abelian) group in dimension  $n$ ;

$Sp(n)$  – symplectic group in dimension  $n$ ;

$T(n)$  – group of translations in dimension  $n$ ;

$SE(n)$  – Euclidean group in dimension  $n$ ;

$H_n(M) = \text{Ker } \partial_n / \text{Im } \partial_{n-1}$  –  $n$ th homology group of the manifold  $M$ ;

$H^n(M) = \text{Ker } d^n / \text{Im } d^{n-1}$  –  $n$ th cohomology group of the manifold  $M$ .

## Other Spaces and Operators

$C^k(M)$  – space of  $k$ -differentiable functions on the manifold  $M$ ;

$\Omega^k(M)$  – space of  $k$ -forms on the manifold  $M$ ;

$\mathfrak{g}$  – Lie algebra of a Lie group  $G$ , i.e., the tangent space of  $G$  at its identity element;

$Ad(g)$  – adjoint endomorphism; recall that *adjoint representation* of a Lie group  $G$  is the linearized version of the action of  $G$  on itself by conjugation, i.e., for each  $g \in G$ , the inner automorphism  $x \mapsto gxg^{-1}$  gives a linear transformation  $Ad(g) : \mathfrak{g} \rightarrow \mathfrak{g}$ , from the Lie algebra  $\mathfrak{g}$  of  $G$  to itself;

$nD$  space (group, system) means  $n$ -dimensional space (group, system), for  $n \in \mathbb{N}$ ;

$\lrcorner$  – interior product, or contraction, of a vector-field and a one-form;

$\oint$  – Feynman path integral symbol, denoting integration over continuous spectrum of smooth paths and summation over discrete spectrum of



Markov chains; e.g.,  $\oint \mathcal{D}[x] e^{iS[x]}$  denotes the path integral (i.e., sum-over-histories) over all possible paths  $x^i = x^i(t)$  defined by the Hamilton action,  $S[x] = \frac{1}{2} \int_{t_0}^{t_1} g_{ij} \dot{x}^i \dot{x}^j dt$ , while  $\oint \mathcal{D}[\Phi] e^{iS[\Phi]}$  denotes the path integral over all possible fields  $\Phi^i = \Phi^i(x)$  defined by some field action  $S[\Phi]$ .

## Categories

$\mathcal{S}$  – all sets as objects and all functions between them as morphisms;

$\mathcal{V}$  – all vector spaces as objects and all linear maps between them as morphisms;

$\mathcal{G}$  – all groups as objects, all homomorphisms between them as morphisms;

$\mathcal{A}$  – Abelian groups as objects, homomorphisms between them as morphisms;

$\mathcal{AL}$  – all algebras (over a given number field  $\mathbb{K}$ ) as objects, all their homomorphisms between them as morphisms;

$\mathcal{T}$  – all topological spaces as objects, all continuous functions between them as morphisms;

$\mathcal{TG}$  – all topological groups as objects, their continuous homomorphisms as morphisms;

$\mathcal{M}$  – all smooth manifolds as objects, all smooth maps between them as morphisms;

$\mathcal{M}_n$  –  $n$ D manifolds as objects, their local diffeomorphisms as morphisms;

$\mathcal{LG}$  – all Lie groups as objects, all smooth homomorphisms between them as morphisms;

$\mathcal{LAL}$  – all Lie algebras (over a given field  $\mathbb{K}$ ) as objects, all smooth homomorphisms between them as morphisms;

$\mathcal{TB}$  – all tangent bundles as objects, all smooth tangent maps between them as morphisms;

$\mathcal{T}^*\mathcal{B}$  – all cotangent bundles as objects, all smooth cotangent maps between them as morphisms;

**Symplec** – all symplectic manifolds (i.e., physical phase-spaces), all symplectic maps (i.e., canonical transformations) between them as morphisms;

**Hilbert** – all Hilbert spaces and all unitary operators as morphisms.

# Contents

<i>Preface</i>	vii
<i>Glossary of Frequently Used Symbols</i>	xv
1. Introduction	1
1.1 The Problem of Natural Biodynamics . . . . .	1
1.2 A Brief History of Biodynamics . . . . .	3
1.3 Mechanical Basis of Biodynamics . . . . .	8
1.3.1 Natural Galilei Group . . . . .	9
1.3.2 Newtonian Equations of Motion . . . . .	10
1.3.3 Calculus of Variations . . . . .	11
1.3.4 Lagrangian Equations of Motion . . . . .	12
1.3.5 Hamiltonian Equations of Motion . . . . .	13
1.3.6 Lagrangian Flows on Biodynamic Manifolds . . . . .	14
1.4 Conservative versus Dissipative Hamiltonian Dynamics . . . . .	15
1.4.1 Dissipative Systems . . . . .	16
1.4.2 Thermodynamic Equilibrium . . . . .	18
1.4.3 Nonlinearity . . . . .	19
1.4.4 The Second Law of Thermodynamics . . . . .	19
1.4.5 Geometry of Phase Space . . . . .	21
1.5 Neural Basis of Biodynamics . . . . .	23
2. Natural Language of Biodynamics	25
2.1 Categorical Metalanguage . . . . .	25
2.1.1 Preliminaries from Calculus, Algebra and Topology . . . . .	25
2.1.1.1 Notes From Calculus . . . . .	26

2.1.1.2	Notes from Set Theory . . . . .	28
2.1.1.3	Notes from General Topology . . . . .	28
2.1.1.4	Commutative Diagrams . . . . .	32
2.1.1.5	Groups and Related Algebraic Structures . .	35
2.1.2	Categories . . . . .	39
2.1.3	Functors . . . . .	43
2.1.4	Natural Transformations . . . . .	45
2.1.5	Limits and Colimits . . . . .	47
2.1.6	The Adjunction . . . . .	47
2.1.7	$n$ -Categories . . . . .	49
2.1.7.1	Generalization to 'Big' $n$ -Categories . . . .	49
2.1.7.2	Topological Structure of $n$ -Categories . . .	54
2.1.8	Algebra in Abelian Categories . . . . .	57
2.1.9	Fundamental Biodynamic Adjunction . . . . .	59
2.2	The Basics of Dynamics . . . . .	60
2.2.1	Ordinary Differential Equations . . . . .	60
2.2.2	Linear Autonomous Dynamics . . . . .	63
2.2.2.1	The Flow of a Linear ODE . . . . .	63
2.2.2.2	Canonical Linear Flows in $\mathbb{R}^2$ . . . . .	65
2.2.2.3	Topological Equivalence . . . . .	67
2.3	Chaos and Synergetics in Biodynamics . . . . .	68
2.3.1	Prototype of Chaotic and Synergetic Systems . . . .	73
2.3.2	Chaotic Systems and Biomorphs . . . . .	75
2.3.2.1	Simulation Examples: Chaotic Systems . . .	75
2.3.2.2	Simulation Examples: Biomorphic Systems .	81
2.3.3	Controlling Chaos within the Chaos Theory . . . . .	82
2.3.3.1	Exploiting Critical Sensitivity . . . . .	82
2.3.3.2	Lyapunov exponents and KY-dimension . .	85
2.3.3.3	Kolmogorov-Sinai entropy . . . . .	87
2.3.3.4	Chaos Control by Ott, Grebogi and Yorke .	89
2.3.3.5	Floquet Stability Analysis and OGY Control	92
2.3.3.6	Jerk Functions of Simple Chaotic Flows . .	97
2.3.4	The Basic Hamiltonian Model of Biodynamics . . . .	101
2.3.5	The Basics of Haken's Synergetics . . . . .	102
2.3.5.1	Phase Transitions . . . . .	104
2.3.5.2	Mezoscopic Derivation of Order Parameters	106
2.3.6	Macro-Synergetic Control of Biodynamics . . . . .	109

3.1	Motivation for Geometry in Biodynamics . . . . .	114
3.2	Biodynamic Manifold $M$ . . . . .	117
3.2.1	Definition of the Manifold $M$ . . . . .	118
3.2.2	Smooth Maps Between Manifolds . . . . .	120
3.3	Biodynamic Bundles . . . . .	121
3.3.1	The Tangent Bundle of the Manifold $M$ . . . . .	121
3.3.2	The Cotangent Bundle of the Manifold $M$ . . . . .	123
3.4	Sections of Biodynamic Bundles . . . . .	124
3.4.1	Biodynamic Evolution and Flow . . . . .	125
3.4.2	Vector-Fields and Their Flows . . . . .	126
3.4.2.1	Vector-Fields on $M$ . . . . .	126
3.4.2.2	Integral Curves as Biodynamic Trajectories . . . . .	127
3.4.2.3	Biodynamic Flows on $M$ . . . . .	131
3.4.2.4	Categories of ODEs . . . . .	132
3.4.3	Differential Forms on $M$ . . . . .	133
3.4.3.1	1-Forms on $M$ . . . . .	134
3.4.3.2	$k$ -Forms on $M$ . . . . .	135
3.4.3.3	Exterior Differential Systems . . . . .	137
3.4.3.4	Exterior Derivative on $M$ . . . . .	138
3.4.3.5	De Rham Complex and Homotopy Operators . . . . .	140
3.4.3.6	Stokes Theorem and De Rham Cohomology . . . . .	142
3.4.3.7	Euler-Poincaré Characteristics of $M$ . . . . .	143
3.4.3.8	Duality of Chains and Forms on $M$ . . . . .	144
3.4.3.9	Other Exterior Operators on $M$ . . . . .	146
3.4.4	Geometry of Nonlinear Dynamics . . . . .	148
3.5	Lie Categories in Biodynamics . . . . .	152
3.5.1	Lie Derivative in Biodynamics . . . . .	152
3.5.1.1	Lie Derivative on Functions . . . . .	152
3.5.1.2	Lie Derivative of Vector Fields . . . . .	155
3.5.1.3	Derivative of the Evolution Operator . . . . .	157
3.5.1.4	Lie Derivative of Differential Forms . . . . .	158
3.5.1.5	Lie Derivative of Various Tensor Fields . . . . .	159
3.5.1.6	Lie Algebras . . . . .	161
3.5.2	Lie Groups in Biodynamics . . . . .	162
3.5.2.1	Lie Groups and Their Lie Algebras . . . . .	162
3.5.2.2	Actions of Lie Groups on $M$ . . . . .	167
3.5.2.3	Basic Biodynamic Groups . . . . .	169
3.5.2.4	Groups of Joint Rotations . . . . .	171
3.5.2.5	Special Euclidean Groups of Joint Motions . . . . .	175

3.5.3	Group Structure of the Biodynamic Manifold $M$ . .	180
3.5.3.1	Purely Rotational Biodynamic Manifold . .	180
3.5.3.2	Reduction of the Rotational Manifold . . . .	182
3.5.3.3	The Complete Biodynamic Manifold . . . .	184
3.5.3.4	Realistic Human Spine Manifold . . . . .	184
3.5.4	Lie Symmetries in Biodynamics . . . . .	185
3.5.4.1	Lie Symmetry Groups . . . . .	185
3.5.4.2	Prolongations . . . . .	188
3.5.4.3	Special Biodynamic Equations . . . . .	194
3.6	Riemannian Geometry in Biodynamics . . . . .	195
3.6.1	Local Riemannian Geometry on $M$ . . . . .	196
3.6.1.1	Riemannian Metric on $M$ . . . . .	197
3.6.1.2	Geodesics on $M$ . . . . .	201
3.6.1.3	Riemannian Curvature on $M$ . . . . .	202
3.6.2	Global Riemannian Geometry on $M$ . . . . .	205
3.6.2.1	The Second Variation Formula . . . . .	205
3.6.2.2	Gauss–Bonnet Formula . . . . .	208
3.6.2.3	Ricci Flow on $M$ . . . . .	209
3.6.2.4	Structure Equations on $M$ . . . . .	212
3.6.2.5	Basics of Morse Theory . . . . .	213
3.6.2.6	Basics of (Co)Bordism Theory . . . . .	215
3.7	Symplectic Geometry in Biodynamics . . . . .	217
3.7.1	Symplectic Algebra . . . . .	217
3.7.2	Symplectic Geometry on $M$ . . . . .	218
3.8	Impulse Biodynamics and Synthetic Geometry . . . . .	220
3.8.1	Delta Spikes . . . . .	220
3.8.2	Kick Dynamics . . . . .	222
3.8.2.1	Deterministic Delayed Kicks . . . . .	222
3.8.2.2	Random Kicks and Langevin Equation . . .	223
3.8.3	Distributions and Synthetic Differential Geometry . .	226
3.8.3.1	Distributions . . . . .	227
3.8.3.2	Synthetic Calculus in Euclidean Spaces . . .	229
3.8.3.3	Spheres and Balls as Distributions . . . . .	231
3.8.3.4	Stokes Theorem for Unit Sphere . . . . .	233
3.8.3.5	Time Derivatives of Expanding Spheres . . .	234
3.8.3.6	The Wave Equation . . . . .	235
3.9	A Quick Look at Modern Geometrodynamics . . . . .	237
3.9.1	Einstein Equations . . . . .	237
3.9.2	$n$ –Categories in Physics . . . . .	237

3.9.3	Quantum Geometry Framework . . . . .	240
3.10	3D Modelling and Animation in Biodynamics . . . . .	242
3.10.1	Essentials of Human Animation . . . . .	242
3.10.1.1	Motion Capture-Based Human Animation . . . . .	243
3.10.1.2	Virtual Muscular Dynamics in 3D-Graphics . . . . .	244
3.10.2	Curves and Surfaces in Geometric Modelling . . . . .	245
3.10.2.1	Power Basis Form of a Curve . . . . .	246
3.10.2.2	Bezier Curves . . . . .	247
3.10.2.3	Rational Bezier Curves . . . . .	249
3.10.3	B-Spline Basis Functions . . . . .	249
3.10.3.1	DeBoor-Cox Recursive Definition . . . . .	250
3.10.3.2	Derivatives of B-Spline Basis Functions . . . . .	250
3.10.4	B-Spline Curves and Surfaces in Geometric Modelling . . . . .	251
3.10.4.1	Definition of B-Spline Curves . . . . .	251
3.10.4.2	Properties of B-Spline Curves . . . . .	251
3.10.4.3	Derivatives of a B-Spline Curve . . . . .	252
3.10.4.4	Definition of B-Spline Surfaces . . . . .	253
3.10.4.5	Properties of B-Spline Surfaces . . . . .	253
3.10.4.6	Derivatives of a B-Spline Surface . . . . .	254
3.10.5	NURBS Curves and Surfaces . . . . .	255
3.10.5.1	Definition of NURBS Curves . . . . .	255
3.10.5.2	Properties of NURBS Curves . . . . .	255
3.10.5.3	Definition of NURBS Surfaces . . . . .	256
3.10.5.4	Properties of NURBS Surfaces . . . . .	257
3.11	Kinematics of Biomechanical Chains . . . . .	257
3.11.1	3D Transformation Matrix . . . . .	257
3.11.2	A Multilink Kinematic Chain . . . . .	258
3.11.3	CNS Representation of the Body Posture . . . . .	259
3.11.4	Transformation Matrix Used in Computer Graphics . . . . .	260
4.	Natural Mechanics of Biodynamics . . . . .	261
4.1	Lagrangian Formalism in Biodynamics . . . . .	261
4.2	Hamiltonian Formalism in Biodynamics . . . . .	265
4.2.1	Nonlinear Dynamics in Hamiltonian Form . . . . .	267
4.2.1.1	Real 1-DOF Hamiltonian Dynamics . . . . .	267
4.2.1.2	Complex One-DOF Hamiltonian Dynamics . . . . .	276
4.2.1.3	Library of Basic Hamiltonian Systems . . . . .	279
4.2.1.4	n-DOF Hamiltonian Dynamics . . . . .	286
4.2.2	Hamiltonian Geometry in Biodynamics . . . . .	289

4.2.3	Hamilton–Poisson Geometry in Biodynamics . . . . .	292
4.2.3.1	Hamilton–Poisson Biodynamic Systems . . . . .	294
4.2.4	Completely Integrable Hamiltonian Systems . . . . .	298
4.2.4.1	Liouville Theorem . . . . .	298
4.2.4.2	Action–Angle Variables . . . . .	299
4.2.5	Ergodicity . . . . .	301
4.2.5.1	Ergodicity in Hamiltonian Systems . . . . .	301
4.2.5.2	Dynamical Systems and Hyperbolicity . . . . .	302
4.2.5.3	Ergodic Theory and Nontrivial Recurrence . . . . .	305
4.2.5.4	Nonuniformly Hyperbolic Trajectories . . . . .	306
4.2.5.5	Systems with Nonzero Lyapunov Exponents . . . . .	307
4.3	Quantum Formalism in Nano–Biodynamics . . . . .	310
4.3.1	Quantum Mechanics in Biological Matter . . . . .	310
4.3.2	Dirac’s Canonical Quantization . . . . .	311
4.3.2.1	Quantum States and Operators . . . . .	312
4.3.2.2	Quantum Pictures . . . . .	318
4.3.2.3	Spectrum of a Quantum Operator . . . . .	320
4.3.2.4	General Representation Model . . . . .	324
4.3.2.5	Direct Product Space . . . . .	325
4.3.2.6	State–Space for $n$ Quantum Particles . . . . .	326
4.3.2.7	Quantum Measurement and Penrose Paradox . . . . .	328
4.3.3	The Problem of Quantum Measurement and Entropy . . . . .	330
4.3.3.1	The Classical Apparatus . . . . .	331
4.3.3.2	Quantum Object . . . . .	331
4.3.3.3	Adiabatic Measurement Lagrangians . . . . .	333
4.3.3.4	The Stern–Gerlach Experiment . . . . .	334
4.3.3.5	Work and Heat . . . . .	335
4.3.3.6	Statistical Thermodynamics . . . . .	336
4.3.3.7	Friction in a Macroscopic Apparatus . . . . .	338
4.3.3.8	Low Velocity Projective Measurements . . . . .	340
4.3.3.9	Information and Entropy . . . . .	341
4.3.4	Von Neumann’s Density Matrix Quantization . . . . .	342
4.3.4.1	Dissipative Quantum Formalism . . . . .	344
4.3.5	Geometric Quantization . . . . .	345
4.3.5.1	Motivation . . . . .	345
4.3.5.2	Geometric Prequantization . . . . .	347
4.4	Variational Formalism in Biodynamics . . . . .	351
4.4.1	Biodynamic Action Functional . . . . .	351
4.4.2	Lagrangian Action . . . . .	352

4.4.3	Hamiltonian Action . . . . .	353
4.4.4	Noether Theorem . . . . .	354
4.4.5	Hamiltonian–Action Formulation of Biodynamics . .	356
4.4.6	Feynman Quantum Action . . . . .	359
4.5	Nonholonomic Biodynamics . . . . .	364
4.5.1	Lagrangian Approach . . . . .	364
4.5.2	Hamiltonian Approach . . . . .	366
4.5.3	Biodynamic Example: Bicycle Dynamics . . . . .	368
4.6	Stochastic Formalism in Biodynamics . . . . .	370
4.6.1	Markov Stochastic Processes . . . . .	372
4.6.2	Statistical Mechanics of Oscillator Chains . . . . .	374
4.7	Muscular Excitation–Contraction Dynamics . . . . .	376
4.7.1	Human Musculo–Skeletal System . . . . .	376
4.7.1.1	Human Skeleton . . . . .	376
4.7.1.2	Human Joints . . . . .	378
4.7.1.3	Human Muscular System . . . . .	379
4.7.1.4	Human Energy Flow . . . . .	381
4.7.1.5	Equivalent Muscular Actuator . . . . .	385
4.7.2	Molecular Muscular Dynamics . . . . .	385
4.7.3	Mezoscopic Muscular Dynamics . . . . .	386
4.7.3.1	Myocybernetics . . . . .	392
4.7.4	Macroscopic Muscular Dynamics . . . . .	392
4.7.4.1	Soft Tissue Dynamics of Relaxed Muscles . .	392
4.7.4.2	Classical Hill’s Model . . . . .	395
4.7.4.3	Biodynamics of Load–Lifting . . . . .	396
4.8	Lie Functors in Biodynamics . . . . .	403
4.8.1	Lie–Lagrangian Biodynamic Functor . . . . .	403
4.8.1.1	Joint Kinematics . . . . .	403
4.8.1.2	Exterior Lagrangian Dynamics . . . . .	405
4.8.2	Lie–Hamiltonian Biodynamic Functor . . . . .	410
4.8.2.1	The Abstract Functor Machine . . . . .	412
4.8.2.2	Muscle–Driven Hamiltonian Biodynamics . .	413
4.8.3	Stochastic–Lie–Hamiltonian Biodynamic Functor . .	414
4.8.4	Fuzzy–Stochastic–Lie–Hamiltonian Functor . . . . .	416
4.9	Mechanics of Spinal Injuries . . . . .	419
4.9.1	Spinal Dislocations, Disclinations and Fractures . . .	420
4.9.2	Measuring the Risk of Local Intervertebral Injuries .	420
4.9.2.1	Biodynamic Jerk Functions . . . . .	424
4.9.3	Measuring the Risk of Vertebral Fractures . . . . .	426



4.9.3.1	Research on Bone Injuries . . . . .	426
5.	Natural Topology of Biodynamics . . . . .	427
5.1	Category of (Co)Chain Complexes in Biodynamics . . . . .	427
5.1.1	(Co)Homologies in Abelian Categories Related to $M$ . . . . .	428
5.1.2	Reduction and Euler–Poincaré Characteristic . . . . .	430
5.2	Natural Duality in Biodynamics . . . . .	431
5.2.1	Geometric Duality Theorem for $M$ . . . . .	431
5.2.1.1	Lie–Functorial Proof . . . . .	432
5.2.1.2	Geometric Proof . . . . .	433
5.2.2	Topological Duality Theorem for $M$ . . . . .	437
5.2.2.1	Cohomological Proof . . . . .	437
5.2.2.2	Homological Proof . . . . .	439
5.2.3	Lagrangian Versus Hamiltonian Duality . . . . .	439
5.2.4	Globally Dual Structure of Rotational Biodynamics . . . . .	440
5.3	Topological Phase Transitions and Hamiltonian Chaos . . . . .	441
5.3.1	Phase Transitions in Hamiltonian Systems . . . . .	441
5.3.2	Geometry of the Largest Lyapunov Exponent . . . . .	444
5.3.3	Euler Characteristics of Hamiltonian Systems . . . . .	447
5.4	The Covariant Force Functor . . . . .	452
6.	Natural Control and Self–Organization in Biodynamics . . . . .	453
6.1	The Basics of Classical Control and Stability . . . . .	455
6.1.1	Introduction to Feedback Control . . . . .	455
6.1.2	Linear Stationary Systems and Operators . . . . .	460
6.1.2.1	Basics of Kalman State–Space Theory . . . . .	460
6.1.2.2	Regulator Problem . . . . .	461
6.1.2.3	End Point Control Problem . . . . .	462
6.1.2.4	Servomechanism Problem . . . . .	463
6.1.2.5	Repetitive Mode Problem . . . . .	463
6.1.2.6	Feedback Changes the Operator . . . . .	464
6.1.3	Stability and Boundedness . . . . .	465
6.1.4	Lyapunov’s Stability Method . . . . .	468
6.1.5	Graphical Techniques for Nonlinear Systems . . . . .	469
6.1.5.1	Describing Function Analysis . . . . .	470
6.2	The Basis of Modern Geometric Control . . . . .	472
6.2.1	Feedback Linearization . . . . .	472
6.2.1.1	Exact Feedback Linearization . . . . .	472

6.2.1.2	Relative Degree . . . . .	476
6.2.1.3	Approximative Feedback Linearization . . .	478
6.2.2	Controllability . . . . .	481
6.2.2.1	Linear Controllability . . . . .	481
6.2.2.2	Nonlinear Controllability . . . . .	482
6.2.2.3	Controllability Condition . . . . .	484
6.2.2.4	Distributions . . . . .	485
6.2.2.5	Foliations . . . . .	486
6.3	Modern Control Techniques for Mechanical Systems . . . .	487
6.3.1	Abstract Control System . . . . .	487
6.3.2	Controllability of a Linear Control System . . . . .	488
6.3.3	Affine Control System and Local Controllability . . .	489
6.3.4	Hamiltonian Control and Maximum Principle . . . .	490
6.3.4.1	Hamiltonian Control Systems . . . . .	490
6.3.4.2	Pontryagin's Maximum Principle . . . . .	493
6.3.4.3	Affine Control Systems . . . . .	494
6.4	Locomotion Systems and Human Gait . . . . .	496
6.4.1	Control of Locomotion Systems . . . . .	496
6.4.1.1	Stratified Kinematic Controllability . . . . .	497
6.4.1.2	The Distributions Approach . . . . .	499
6.4.1.3	The Exterior Differential Systems Approach . . . .	499
6.4.1.4	On the Existence and Uniqueness of Solutions . . .	501
6.4.1.5	Trajectory Generation Problem . . . . .	502
6.4.2	Gait Biodynamics . . . . .	504
6.5	Biodynamic Control Policy, Learning and Self-Organization . . .	508
6.5.1	Control Policy Learning by Robots . . . . .	508
6.5.1.1	Direct Learning of the Control Policy . . . . .	509
6.5.1.2	Indirect Learning of the Control Policy . . . . .	510
6.5.1.3	Learning of Motor Control Components . . . . .	512
6.5.2	Pathways to Self-Organization in Biodynamics . . . .	512
6.5.3	Neuro-Muscular Excitation-Contraction Dynamics . . .	514
6.5.3.1	Motor Units . . . . .	514
6.5.3.2	Darwinian Oscillatory Neural Net . . . . .	514
6.5.3.3	Recurrent Neuro-Muscular Model . . . . .	517
6.5.3.4	Autogenetic Reflex Motor-Servo . . . . .	519
6.5.3.5	Biodynamics Control . . . . .	520
6.5.4	Lie-Adaptive Biodynamic Control . . . . .	524
6.6	Essentials of Biodynamic Measurement: Kalman Filtering and Inertial Navigation . . . . .	526

6.6.0.1	Kalman Filter Basics . . . . .	526
6.6.0.2	Inertial Navigation . . . . .	532
6.6.0.3	Adaptive Estimation in Biomechanics . . . . .	536
6.7	Humanoid Robotics . . . . .	537
6.7.1	Honda Humanoid Series . . . . .	537
6.7.2	Cerebellar Robotics . . . . .	538
7.	Natural Brain Dynamics and Sensory–Motor Integration . . . . .	541
7.1	Introduction to Brain . . . . .	542
7.2	Human Nervous System . . . . .	549
7.2.1	Building Blocks of the Nervous System . . . . .	550
7.2.1.1	Neuronal Circuits . . . . .	552
7.2.1.2	Basic Brain Partitions and Their Functions . . . . .	556
7.2.1.3	Nerves . . . . .	558
7.2.1.4	Action potential . . . . .	559
7.2.1.5	Synapses . . . . .	561
7.2.2	Reflex Action: the Basis of CNS Activity . . . . .	566
7.2.3	The Spinal Cord Pathways . . . . .	568
7.2.3.1	Spinal Lower Motor Neurons . . . . .	569
7.2.3.2	Central Pattern Generators in the Spinal Cord . . . . .	575
7.2.3.3	Influence of Higher Centers . . . . .	576
7.2.4	First Look at the Brain . . . . .	578
7.2.5	Motor Pathways . . . . .	581
7.2.5.1	Primary Motor Cortex . . . . .	581
7.2.5.2	Motor Association/Premotor Cortical Areas . . . . .	584
7.2.6	Subcortical Motor ‘Side Loops’ . . . . .	587
7.2.6.1	The Cerebellum . . . . .	588
7.2.6.2	The Basal Ganglia . . . . .	594
7.2.6.3	Cerebellar Movement Control . . . . .	596
7.2.7	Human Senses and their Pathways . . . . .	600
7.2.8	The Human–Like Vision . . . . .	603
7.2.8.1	Extraocular $SO(3)$ –Muscles . . . . .	604
7.2.8.2	Retina . . . . .	606
7.2.8.3	Cornea . . . . .	607
7.2.8.4	Iris . . . . .	608
7.2.8.5	Pursuit Eye Control and Motion Perception . . . . .	610
7.2.8.6	Optical Flow . . . . .	613
7.2.9	The Visual Pathway . . . . .	615
7.2.9.1	Light Reflex and 3D Vision . . . . .	619

7.2.10	Differential Geometry of the Striate Cortex . . . . .	620
7.2.11	Auditory and Vestibular Pathways . . . . .	622
7.2.11.1	The Inner Ear . . . . .	622
7.2.11.2	Auditory Transduction . . . . .	623
7.2.11.3	Central Auditory Pathways . . . . .	624
7.2.11.4	The Vestibular System . . . . .	626
7.2.11.5	The Semicircular Canals . . . . .	626
7.2.11.6	The Vestibulo–Ocular Reflex . . . . .	627
7.2.11.7	The Utricle and Saccule . . . . .	628
7.2.11.8	Mechanics of the Semicircular Canals . . . . .	629
7.2.11.9	Endolymph Flow in the Semicircular Canals . . . . .	630
7.2.12	Somatosensory Pathways . . . . .	632
7.2.12.1	The Discriminative Touch System . . . . .	633
7.2.12.2	The Pain and Temperature System . . . . .	634
7.2.12.3	The Proprioceptive System . . . . .	635
7.3	The Sensory–Motor Adjunction . . . . .	638
7.3.1	Summary on Sensory–Motor Pathways . . . . .	638
7.3.2	Sensory–Motor Control . . . . .	642
7.3.2.1	Multisensory Integration for Motor Planning . . . . .	645
7.3.2.2	The Sensory–Motor Adjunction . . . . .	649
7.3.3	The Central Biomechanical Adjunction . . . . .	649
7.3.3.1	Postural Control Experiments . . . . .	652
7.3.3.2	Learning Arm Movement Control . . . . .	655
7.3.4	Mechanism of Brain Injuries . . . . .	658
7.3.4.1	Basic Dynamics of Brain Injuries . . . . .	658
7.3.4.2	Research on Head and Brain Injuries . . . . .	661
7.4	Brain Dynamics . . . . .	661
7.4.1	Microscopic Neurodynamics of Microtubules . . . . .	662
7.4.1.1	Biochemistry of Microtubules . . . . .	662
7.4.1.2	Kink Soliton Model of MT–Dynamics . . . . .	664
7.4.2	Mezoscopic Neurodynamics of Action Potentials . . . . .	667
7.4.2.1	Hodgkin–Huxley Model . . . . .	667
7.4.2.2	FitzHugh–Nagumo Model . . . . .	671
7.5	Biological Neural Nets . . . . .	672
7.5.1	Phase Dynamics of Oscillatory Neural Nets . . . . .	672
7.5.1.1	Kuramoto Synchronization Model . . . . .	675
7.5.1.2	Lyapunov Chaotic Synchronization . . . . .	676
7.5.2	Complex Networks Dynamics . . . . .	678
7.5.2.1	Continuum Limit of the Kuramoto Network . . . . .	679

7.5.2.2	Path-Integral Approach to Complex Nets . . .	679
7.5.3	Complex Adaptive Systems . . . . .	681
7.5.4	Noise Delayed Bifurcation in Coupled Neurons . . .	684
7.5.4.1	The Theta-Neuron . . . . .	684
7.5.4.2	Coupled Theta-Neurons . . . . .	685
7.5.5	Classification of 'Spiking' Neuron Models . . . . .	688
7.5.6	Weakly Connected and Canonical Neural Nets . . . .	692
7.5.7	Quantum Brain Model . . . . .	694
7.5.8	Open Liouville Neurodynamics and Self-Similarity .	698
7.5.8.1	Hamiltonian Framework . . . . .	700
7.5.8.2	Conservative Classical System . . . . .	700
7.5.8.3	Conservative Quantum System . . . . .	700
7.5.8.4	Open Classical System . . . . .	701
7.5.8.5	Continuous Neural Network Dynamics . . .	702
7.5.8.6	Open Quantum System . . . . .	703
7.5.8.7	Non-Critical Stringy MT-Dynamics . . . .	704
7.5.8.8	Equivalence of Neurodynamic Forms . . . .	704
7.6	Artificial Neural Nets in Biodynamics . . . . .	705
7.6.1	Biological Versus Artificial Neural Nets . . . . .	705
7.6.2	Common Discrete ANNs . . . . .	707
7.6.2.1	Multilayer Perceptrons . . . . .	707
7.6.2.2	Summary of Supervised Learning Methods .	719
7.6.2.3	Other Standard ANNs . . . . .	720
7.6.2.4	Fully Recurrent ANNs . . . . .	727
7.6.2.5	Dynamical Games and Recurrent ANNs . .	728
7.6.2.6	Complex-Valued ANNs . . . . .	731
7.6.3	Common Continuous ANNs . . . . .	732
7.6.3.1	Neurons as Functions . . . . .	733
7.6.3.2	Basic Activation and Learning Dynamics . .	735
7.6.3.3	Standard Models of Continuous Nets . . . .	736
7.7	Distinguished ANN Models . . . . .	741
7.7.1	Generalized Kohonen's SOM . . . . .	741
7.7.1.1	The Winner Relaxing Kohonen Algorithm .	742
7.7.1.2	The Magnification Factor . . . . .	743
7.7.1.3	Magnification Exponent . . . . .	744
7.7.2	Dynamics of Hopfield's Associative Recurrent Nets .	745
7.7.2.1	Ising-Spin Neurons . . . . .	745
7.7.2.2	Graded-Response Neurons . . . . .	746
7.7.2.3	Hopfield's Overlaps . . . . .	747

7.7.2.4	Overlap Dynamics . . . . .	749
7.7.2.5	Hebbian Learning Dynamics . . . . .	750
7.7.3	A Self-Organizing Bidirectional Competitive Net . . . . .	753
7.8	Fuzzy Logic in Biodynamics . . . . .	755
7.8.1	The Concept of Fuzziness . . . . .	755
7.8.1.1	‘Fuzzy Thinking’ . . . . .	755
7.8.1.2	Fuzzy Sets . . . . .	756
7.8.1.3	Fuzziness of the Real World . . . . .	757
7.8.1.4	Fuzzy Entropy . . . . .	758
7.8.2	Fuzzy Inference Engine . . . . .	761
7.8.3	Fuzzy Logic Control . . . . .	764
7.8.3.1	Fuzzy Control of Biodynamic Jerks . . . . .	768
7.8.3.2	Characteristics of Fuzzy Control . . . . .	769
7.8.3.3	Evolving Connectionist Systems . . . . .	770
7.8.4	High-Resolution FAM Agents . . . . .	771
7.8.4.1	Generic Nonlinear MIMO Systems . . . . .	772
7.8.4.2	Alternative MIMO Systems . . . . .	775
7.8.4.3	Biodynamics Example: Tennis Game . . . . .	777
7.9	Natural System in a Category . . . . .	783
7.9.1	Categorical Patterns and Hierarchical Links . . . . .	783
7.9.2	A General Natural System . . . . .	786
7.9.3	The Category of Neurons . . . . .	787
7.9.4	Memory Evolutionary System . . . . .	787
7.9.5	Neural System in a Category . . . . .	789
7.10	Brain-Mind Functorial Machines . . . . .	792
7.10.1	Neurodynamic 2-Functor . . . . .	792
7.10.2	Solitary ‘Thought Nets’ and the Emerging Mind . . . . .	795
7.10.2.1	Synergetic ‘Thought Solitons’ . . . . .	795
7.11	Body-Mind Adjunction and Natural Psychodynamics . . . . .	800
7.11.1	Natural Psychodynamics in the Life Space Foam . . . . .	801
7.11.1.1	Six Faces of the Life Space Foam . . . . .	806
7.11.1.2	General Formalism . . . . .	806
7.11.1.3	Motion and Decision Making in $LSF_{paths}$ . . . . .	810
7.11.1.4	Force-Fields and Memory in $LSF_{fields}$ . . . . .	814
7.11.1.5	Geometries, Topologies and Noise in $LSF_{geom}$ . . . . .	816
7.12	Brain-Like Control in a Nutshell . . . . .	818
7.12.1	Functor Control Machine . . . . .	820
7.12.2	Spinal Control Level . . . . .	822
7.12.3	Cerebellar Control Level . . . . .	827

7.12.4	Cortical Control Level . . . . .	830
7.12.5	A Note on Muscular Training . . . . .	833
7.12.6	Errors in Motion Control: Locomotor Injuries . . . . .	836

Appendix A		837
A.1	Basic Formulas from Tensor Analysis . . . . .	837
A.1.1	General Functional Transformation . . . . .	837
A.1.1.1	Transformation of Coordinates . . . . .	838
A.1.1.2	Scalar Invariants . . . . .	839
A.1.1.3	Vectors and Covectors . . . . .	839
A.1.1.4	Second-Order Tensors . . . . .	840
A.1.1.5	Higher-Order Tensors . . . . .	842
A.1.1.6	Tensor Symmetry . . . . .	842
A.1.2	Euclidean Tensors . . . . .	844
A.1.2.1	Basis Vectors and the Metric Tensor in $\mathbb{R}^n$ . . . . .	844
A.1.2.2	Tensor Products in $\mathbb{R}^n$ . . . . .	845
A.1.3	Tensor Derivatives on Riemannian Manifolds . . . . .	846
A.1.3.1	Christoffel's Symbols . . . . .	846
A.1.3.2	Geodesics . . . . .	847
A.1.3.3	The Covariant Derivative . . . . .	847
A.1.3.4	Vector Differential Operators . . . . .	848
A.1.3.5	The Absolute Derivative . . . . .	849
A.1.4	The Covariant Force Law in Biodynamics . . . . .	853
A.1.5	The Essence of Natural Hamiltonian Biodynamics . . . . .	855
A.1.6	Neuro-Hamiltonian Control in Biodynamics . . . . .	856
A.2	Frequently Used Neurophysiological Terms . . . . .	857
A.3	Modern 3D Neuroimaging . . . . .	880
A.3.1	Nuclear Magnetic Resonance in 2D Medical Imaging . . . . .	880
A.3.2	3D Magnetic Resonance Imaging of Human Brain . . . . .	881
A.3.3	Diffusion MRI in 3D Volume . . . . .	882
A.3.4	Imaging Diffusion with MRI . . . . .	883
A.3.5	3D Diffusion Tensor . . . . .	884
A.3.6	Brain Connectivity Studies . . . . .	887
A.3.7	Brain Waves and Independent Component Analysis . . . . .	888
A.4	Complex Functions, Manifolds and Hilbert Spaces . . . . .	889
A.4.1	Complex Numbers and Vectors . . . . .	889
A.4.1.1	Quaternions and Rotations . . . . .	890
A.4.2	Complex Functions . . . . .	894
A.4.3	Complex Manifolds . . . . .	898

A.4.4 Hilbert Space . . . . .	902
A.5 Classical Lie Theory . . . . .	904
A.5.1 Basic Tables of Lie Groups and Their Lie Algebras . . . . .	904
A.5.2 Representations of Lie groups . . . . .	907
A.5.3 Root Systems and Dynkin Diagrams . . . . .	908
A.5.3.1 Definitions . . . . .	908
A.5.3.2 Classification . . . . .	909
A.5.3.3 Dynkin Diagrams . . . . .	910
A.5.3.4 Root Systems and Lie Theory . . . . .	913
A.5.4 Simple and Semisimple Lie Groups and Algebras . . . . .	913
A.6 Phase Transitions, Partition Function and Noise . . . . .	915
A.6.1 Equilibrium Phase Transitions . . . . .	915
A.6.1.1 Classification of Phase Transitions . . . . .	916
A.6.1.2 Basic Properties of Phase Transitions . . . . .	918
A.6.2 Landau's Theory of Phase Transitions . . . . .	921
A.6.3 Partition Function . . . . .	922
A.6.3.1 Classical Partition Function . . . . .	923
A.6.3.2 Quantum Partition Function . . . . .	924
A.6.3.3 Vibrations of Coupled Oscillators . . . . .	925
A.6.4 Noise-Induced Nonequilibrium Phase Transitions . . . . .	930
A.6.4.1 General Zero-Dimensional System . . . . .	931
A.6.4.2 General $d$ -Dimensional System . . . . .	934
A.7 <i>Mathematica</i> <sup>TM</sup> Derivation of Main Biodynamic Functions . . . . .	938
A.7.1 Load-Lifting Biodynamics . . . . .	938
A.7.2 Brain-Like Control Functions . . . . .	939
A.7.2.1 Spinal FC-level . . . . .	939
A.7.2.2 Cerebellar FC-level . . . . .	941
A.7.2.3 Cortical FC-level . . . . .	942
A.7.3 Anatomical Description of Human Movements . . . . .	944
A.7.3.1 Movements in Synovial Joints . . . . .	944
A.7.3.2 Examples of Sport Movements . . . . .	945
<i>Bibliography</i> . . . . .	947
<i>Index</i> . . . . .	979



This page intentionally left blank

## Chapter 1

# Introduction

In this introductory part, we first define the problem of human-like biodynamics, with main historical remarks and brief description of both lower, mechanical and higher, neural parts of biodynamics. Secondly, we introduce the global-functorial and local-synergetic language of biodynamics, as our main tools for understanding mathematical unity in biodynamic diversity and natural diversity in mathematical unity, respectively.

In the first chapter, we first state the problem of natural biodynamics, then we give a brief history of classical biodynamics. After that, we give a brief of lower, mechanical biodynamics, including the so-called dissipative structures. We conclude with a brief of higher, neural biodynamics.

### 1.1 The Problem of Natural Biodynamics

In this section we state the problem of natural biodynamics. We shall use the phrase **human-like biodynamics** (or just **biodynamics**, for short) to cover both *biomechanically-realistic human biodynamics* and *biologically similar humanoid (machine) biodynamics*. This biodynamics is extremely complex, multi-dimensional, highly nonlinear and hierarchical. About 640 muscles are available to man for complete motion of his skeleton of over 200 bones. The *control* of a system with so many degrees of freedom (DOF, for short) would at first seem beyond analytical treatment [Vukobratovic (1975)]. The task is made even more difficult by the fact that, apart from the basic feedback mechanisms, the brain control mechanism is still largely unknown<sup>1</sup>.

---

<sup>1</sup>To illustrate the complexity of the problem, we need to say that the most powerful contemporary artificial neural networks, which are high-speed parallel super-computers, with many hidden layers of 'neurons' and lots of 'synaptic' weights,

If we deliberately neglect the control mechanism, and also, instead of real skeletal muscles consider idealized ones, the so-called ‘equivalent muscular actuators’, we still have the major problem: *nonlinear dynamics with several hundreds of nonlinearly coupled variables is inevitably chaotic*. And yet, we all know that the motion of an ordinary healthy human being is not chaotic at all. The problem can be stated at a purely mechanical level, and it is clearly much harder than the classical unsolved  $n$ -body problem. So, how can we deal with it? To tackle this problem, we obviously need much stronger techniques than the standard ones used either in the *restricted 3-body problem* (see [Meyer and Hall (1992)]) or in the low-dimensional *chaos control* as proposed by Ott–Grebogi–Yorke (see [Ott *et al.* (1990)]). Do we really need some totally new mathematics to deal with ‘our reality’, as proposed by R. Penrose [Penrose (1989)]? Though aware of the complexity of the problem of human-like biodynamics, we still try to deal with it using the most powerful techniques of contemporary mathematics and physics. Here comes our ‘natural’ machinery, embracing from the unique point of view the above mentioned and other fundamental techniques of mechanics, differential geometry and algebraic topology, as well as nonlinear control and brain theory.

This book is about mathematical modelling of complex real-world phenomena (see Figure 1.1), using a combination of algebraic, numerical and graphical techniques [Stuart (1999)]. The primary focus in this book is on conceptual understanding of the manifoldness of natural biodynamics, both in its conceptual unity (using the categorical metalanguage) and its realistic diversity (using the self-organizing synergetics).

To be able to predict dynamics of human motion we need first to understand it as it really is, in its ‘realistic order of complexity’. This problem is hard, but the bonus that we get from it is a contribution to understanding the general dynamics of human behavior, of which the dynamics of human movement is a special, prototype case, governed by our *covariant force law* (see subsection A.1.4 in Appendix),

$$F_i = mg_{ij}a^j, \quad \text{that ‘in plain English’ reads :}$$

**force 1-form–field = mass distribution  $\times$  acceleration vector–field**

still belong to the taxonomy of ‘Rana Computatrix’, [Arbib (1998)] i.e., ‘computational frog’. Even microtubules, protein polymers constructing the cytoskeleton of biological neurons have the crucial *learning* ability [Hameroff and Penrose (1996); Dustin (1984)]. On the other hand, the number of possible inter-neuronal connections in the human brain is roughly estimated as ‘1 followed by ten million kilometers of zeros’ [Anochin (1980)].

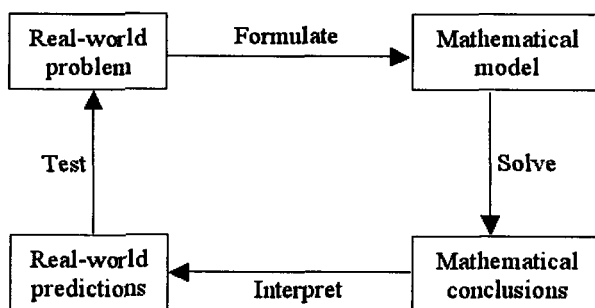


Fig. 1.1 General process of mathematical modelling.

## 1.2 A Brief History of Biodynamics

In this section we give a brief review of classical biodynamics. Many attempts have been made in the biomechanics and robotics literature to create a general model/theory of human-like motion. The earliest systematic study of human and animal (loco)motion principles appears to be due to Muybridge, who in 1877 invented a type of motion-picture camera which was used to obtain the first photographic record of the successive phases of a number of quadruped gaits [Muybridge (1957)].

An overall hierarchical-control philosophy of the biodynamics of human locomotion was proposed in 1940s by N.A. Bernstein [Bernstein (1947); Bernstein (1967); Bernstein (1935)], the father of former Soviet school of biomechanics. He applied the Pavlov–Anochin physiological theory of *conditional reflexes* and *functional systems* [Anochin (1980)] to the analysis of human motion and formulated its basic building blocks in terms of (linear) ordinary differential equations<sup>2</sup>.

Only sequences of foot lifting and placing were considered by Muybridge, leading to the ‘finite-state’ theory of animal locomotion and bioengineering control systems proposed by Tomovic and McGhee in 1966 [Tomovic and

<sup>2</sup>Much of human biodynamics is explained in Bernstein’s words: ‘As in orchestra, each instrument plays its individual score, so in the act of human walking each joint reproduces its own curve of movements and each center of gravity performs its sequence of accelerations, each muscle produces its melody of efforts, full with regularly changing but stable details. And in like manner, the whole of this ensemble acts in unison with a single and complete rhythm, fusing the whole enormous complexity into clear and harmonic simplicity. The consolidator and manager of this complex entity, the conductor and at the same time the composer of the analyzed score, is of course the central nervous system’ [Bernstein (1935)].

McGhee (1966)]. This finite-state theory eventually led to a kinematic theory of quadruped stability, proposed by McGhee and Frank in 1968 [McGhee and Frank (1968)]. They first discovered that the total number of theoretically possible connected quadruped gaits was 5040. They realized further that any study of locomotion stability must include some spatial properties of gaits as well as their temporal properties, and proposed the first kinematic model of quadruped locomotion, consisting of a rigid body and four noninertial legs.

Real dynamic analysis of human (loco)motion was first proposed by Chow and Jacobson in 1970 *via* optimal programming [Chow and Jacobson (1970)]. They tried, using a criterion of minimum power, to achieve driving torques in the hip and knee and the appropriate 'optimal' trajectories of corresponding joints. To solve this optimization problem they made various mechanical and mathematical simplifications. They employed a seven-segment model of the human body, restricted to the sagittal-plane gait in the two basic configurations. This was the first attempt to solve the inverse dynamic problem by the use of Lagrange's equations.

Bernstein's followers, Moreinis and Gritzenko, developed and investigated the mathematical and physical model of the human locomotor system in 1974 in order to learn about the dynamic characteristics both of a healthy man and of one using prosthesis [Moreinis and Grycenko (1974)]. They formulated model with nine DOF by the use of Lagrange's equations and solved the inverse dynamic problem: the joint kinematics are given experimentally and the objective is to find the forcing functions (joint torques and reaction forces) causing the desired locomotor task.

Vukobratovic, the father of the former Yugoslav school of robotics, with his PhD students, finally solved the inverse problem of anthropomorphic locomotion. In a series of papers and Springer books published between 1973 and 1980 [Vukobratovic *et al.* (1982–1989)], they developed computer methods for automatic-setting mathematical models of anthropomorphic mechanisms. This was based on D'Alembert's and kinetostatic principles and Newton–Euler, Lagrange and Gibbs–Appell equations. The programs were written in Fortran and later translated to C-language, adapted to all computers existing at that period. Vukobratovic also formulated the so-called 'half-inverse' method of gait synthesis, in which the dynamics of the motion of the legs is inversely solved, and simultaneously the compensatory dynamics of the upper body (with two DOF) solved directly. Sophisticated methods were also developed for hierarchical adaptive control design in-

cluding open and closed kinematic chains plus actuators in the form of DC drives, stability and sensitivity analysis.

After Bernstein, a small number of authors, both in robotics and in the biomechanics literature, have considered the forward dynamic problem: given the forcing functions (joint torques and reaction forces), the objective is to determine the resulting joint kinematics in various simple tasks of human motion. The formulation of highly nonlinear systems of differential equations of motion was a difficult task, especially with complicated kinematic chains with ten or more DOF. The solution of these equations for fixed or variable initial and/or boundary conditions was more difficult and the problem of control more difficult again. The best-known forward dynamical models in the biomechanical literature are those presented by Huston and Passerello [Huston and Passerello (1971)], Aleshinsky and Zatsiorsky [Aleshinsky and Zatsiorsky (1978)] and Hemami and Wyman [Hemami and Wyman (1979)], all of which include muscular input torques in the form of Hill's model [Hill (1938)] of muscular contraction.

Much of this research is summarized in the mid and late 1970s in the work of H. Hatze, the founder of Austrian biomechanics school. Hatze attempted to develop:

- General 'myocybernetic' control model of skeletal muscle [Hatze (1977a); Hatze (1978); Hatze (1980)], and
- Complete set of control equations for the human musculo-skeletal system [Hatze (1977b); Hatze (1981)].

His muscle-control model involves excitation dynamics of neuro-muscular inputs (motor units) and contraction dynamics based on Huxley's sliding-filament theory of muscle contraction [Huxley and Niedergerke (1954); Huxley (1957)]. Based on his muscle-control model, Hatze developed his 'hominoid dynamics' by the use of Lagrange's equations of the second and the first kind. He described the motion of the 17 major (interacting) segments of the human body, subjected to a variety of external and internal forces and torques, including the internal torques produced by the 46 major muscle groups of the body. His model had 42 DOF for three-dimensional (3D, for short) motion and 21 DOF for planar motion. The model was simulated on CDC Cyber 174 computer and successfully predicted the take-off phase of the long jump.

In describing and predicting human motion dynamics, Hatze's hominoid model was much more powerful than all other published models in both the robotic and the biomechanical literature, before him and even a decade af-

ter him. In one sense, he solved the problem of the dynamics of human motion. However, his muscular and humanoid models were both very complicated and included a large number of nonlinear differential equations. For example, in the sagittal-plane simulation of the take-off phase of the long-jump, he used a humanoid state-space vector of dimension 42 and a muscular state-space vector of dimension 230. His papers have rarely been cited in the literature and subsequent authors, both in robotics and in biomechanics, have made fresh attempts on the problems Hatze has already solved in a more general way.

After Hatze's work, the most important research in the dynamics of anthropomorphic motion has moved into the realm of artificial intelligence. Much of this work has been done in the USA, mainly at MIT, and most of the rest in Japan. Before 1990 it was based on Lisp in the USA and Prolog computing in Japan. Since 1990 the majority of human motion dynamics research has been based on artificial neural networks and fuzzy logic. In both periods, authors tried to avoid formulating and solving large systems of differential equations. Satisfactory results have been achieved in the analysis and design of performing some specific motion tasks, but without substantial underlying mathematics, physics and physiology.

On the other hand, *humanoid robots* are human-like, anthropomorphic mechanisms with complex, muscle driven, biodynamics with many activated DOF and hierarchical brain-like control. In other words, humanoid biodynamics is supposed to closely resemble biodynamics of human motion (see [Ivancevic and Snoswell (2001); Ivancevic (2002); Ivancevic (2004); Ivancevic and Pearce (2001b); Ivancevic (2005); Ivancevic (1991); Ivancevic and Pearce (2001a)] for technical details on biomechanically-realistic human/humanoid biodynamics).

Since the early papers of Vukobratovic (see [Vukobratovic (1970); Vukobratovic *et al.* (1970); Vukobratovic and Stepanenko (1972); Vukobratovic and Stepanenko (1973); Vukobratovic (1975); Vukobratovic *et al.* (1982–1989); Vukobratovic *et al.* (1990)]), the vast body of research has been done in relation to kinematics, dynamics and control of anthropomorphic robots (see [Igarashi and Nogai (1992); Hurmuzlu (1993); Shih *et al.* (1993); Shih and Klein (1993); Lieh (1994); Channon *et al.* (1996); Seward *et al.* (1996); Has (1998); Sardain *et al.* (1999)]). Some of the biped models had the ability of passive dynamic walking [McGeer (1990)] and others had powered walking ability [Pratt and Pratt (1998)]. The previous decade was dominated by various solutions to the kinematic problems of redundancy and singularities [Yoshikawa (1984);

Seraji (1989)]. The last decade of the twentieth century has been characterized mostly by extensive use of intelligent, adaptive, neuro-fuzzy-genetic control (see [Chiel *et al.* (1992); Dorigo and Schnepf (1993); Hat (1996); Pribe *et al.* (1997); Schaal and Atkeson (1998); Schaal (1999)]), and 3D-graphics animation [Ko and Badler (1996)].

In this book, we attempt to deal with the general biodynamics problem, in its full mechanical and physiological complexity, following *geometric spirit* of Riemann, Poincaré and the Hilbert 6th problem. For this cause we propose a spectrum of mathematical, physical, biological and engineering tools, wrapped in the 'natural', i.e., functorial and synergetic machinery (see [MacLane (1971); Haken (1993)]). Within this framework we will explore geometric mechanics of Arnold–Abraham–Marsden–Mihor type (see [Arnold (1989); Abraham and Marsden (1978); Abraham *et al.* (1988); Marsden and Ratiu (1999); Michor (2001)]), topology of Morse–Hodge–Eilenberg–Steenrod type (see [Steenrod (1951); Dieudonne (1988); Switzer (1975); Dodson and Parker (1997)]), Isidori–Shastri type nonlinear control theory (see [Isidori (1989)]), and Zadeh–Hopfield–Grossberg–Kosko–Arbib brain theory (see [Kosko (1992); Haykin (1994); Arbib (1998)]). These theories, filled with our own research (see [Ivancevic and Snoswell (2001); Ivancevic (2002); Ivancevic (2004); Ivancevic and Pearce (2001b); Ivancevic (2005); Ivancevic (1991); Ivancevic and Pearce (2001a)] are the building blocks in our comprehension of the human-like biodynamics.

A practically-reasoning (or, simple-minded) reader might ask himself whether all this machinery is really necessary. Now, instead of our own reply, we rather cite here an extract from the *Nobel Lecture of Richard Feynman*: "The fact that electrodynamics can be written in so many ways – the differential equations of Maxwell, various minimum principles with fields, minimum principles without fields, all different kinds of ways, was something I knew, but I have never understood. It always seems odd to me that the fundamental laws of physics, when discovered, can appear in so many different forms that are not apparently identical at first, but, with a little mathematical fiddling you can show the relationship. An example of that is the Schrödinger equation and the Heisenberg formulation of quantum mechanics. I do not know why this is – it remains *mystery*, but it was something I learned from experience. There is always another way to say the same thing that does not look at all like the way you said it before. I do not know what the reason for this is. I think it is somehow a representation



of the simplicity of *Nature*. A thing like the inverse square law is just right to be represented by the solution of Poisson's equation, which, therefore, is a very different way to say the same thing that does not look at all like the way you said it before. I do not know what it means, that *Nature* chooses these curious forms, but maybe that is a way of defining *simplicity*. Perhaps a thing is simple if you can describe it fully in several different ways without immediately knowing that you are describing the same thing."

On the other hand, *David Hilbert* (1862–1943) said in 1900: "The conviction of the solvability of every mathematical problem is a powerful incentive to the worker. We hear within us the perpetual call: There is the problem. Seek its solution. You can find it by pure reason, for in mathematics there is no *ignorabimus*." ... And, he continued in 1930: "We ought not to believe those who today, adopting a philosophical air and a tone of superiority, prophesy the decline of culture and are content with the 'unknowable' in a self-satisfied way. For us there is no unknowable, and in my opinion there is also none whatsoever for the natural sciences. In place of the foolish 'unknowable', let our watchword on the contrary be: We must know! We shall know!"

### 1.3 Mechanical Basis of Biodynamics

In this section we briefly describe lower, mechanical part of biodynamics. The foundations of the part of mechanics that deals with the motion of point-particles were laid by Isaac Newton in 1687, in his celebrated book *Philosophiae Naturalis Principia Mathematica*. This classic work does not consist of a carefully thought-out system of axioms in the modern sense, but rather of a number of statements of various significance and generality, depending on the state of knowledge at the time. We shall take his *second law* as our starting point: 'Force equals mass times acceleration' (although Newton himself stated this law as 'Force equals the rate of change of momentum', see Hamiltonian formalism, below). Letting  $x_i(t)$  to be Cartesian coordinates, in  $N$ -dimensional ( $ND$ ) Euclidean space  $\mathbb{R}^N$ , of the  $i$ th particle as a function of time, this means

$$m_i \ddot{x}_i(t) = F_i(x_i), \quad (i = 1, \dots, N; \text{ no summation}), \quad (1.1)$$

where 'overdot'  $\dot{x} = dx/dt$  denotes the time derivative of  $x$  (as will *always* be the case in this book),  $F_i$  denotes the force on the  $i$ th particle. In nature, so far as we know, there are just four fundamental forces: the strong, weak,

electromagnetic, and gravitational forces. The first two fundamental forces operate at the subatomic level, outside the realm of classical mechanics, so in this chapter we shall only discuss gravitation and electromagnetism.

The exact expressions for the forces in (1.1) are rather complicated in their full generality, but, surprisingly, they both simplify greatly in the Newtonian limit where the velocities of the particles are much less than the speed of light. They are the gradients of the Newtonian and Coulombic potentials (see [Thirring (1979)])

$$F_i(x_i) = \sum_{j \neq i} \frac{x_j - x_i}{|x_j - x_i|^3} (km_i m_j - e_i e_j),$$

where  $k$  is the gravitational constant and  $e_i$  is the charge of the  $i$ th particle.

Newtonian mechanics researches the motion of systems of material points in the 3D Euclidean space  $E^3$ . In  $E^3$  acts a 6D group (consisting of three rotations and three translations) of space motions. Essential terms and theorems of Newtonian mechanics are invariant with respect to this group, as well as with respect to the extended Galilei group of space-time transformations.

Newton's potential mechanical system is given with the masses of its 'material points' and potential energy. The system motions preserving the potential energy correspond to the conservation laws.

Newton's equations enable us to analyze up to the end a series of important mechanical problems, for example, the problem of motion in a central field.

### 1.3.1 *Natural Galilei Group*

The *Galilei group* is the group of transformations in space and time that connect those Cartesian systems that are termed 'inertial frames' in Newtonian mechanics. The most general relationship between two such frames is the following. The origin of the time scale in the inertial frame  $S'$  may be shifted compared with that in  $S$ ; the orientation of the Cartesian axes in  $S'$  may be different from that in  $S$ ; the origin  $O$  of the Cartesian frame in  $S'$  may be moving relative to the origin  $O$  in  $S$  at a uniform velocity. The transition from  $S$  to  $S'$  involves ten parameters; thus the Galilei group is a ten parameter group (see also (3.5.2.3) below). The basic assumption inherent in Galilei-Newtonian relativity is that there is an absolute time scale, so that the only way in which the time variables used by two different 'inertial observers' could possibly differ is that the zero of time for one of

them may be shifted relative to the zero of time for the other.

Galilei space-time structure involves the following three elements:

- (1) *World*, as a 4D affine space  $A^4$ . The points of  $A^4$  are called *world points* or *events*. The parallel transitions of the world  $A^4$  form a linear (i.e., Euclidean) space  $\mathbb{R}^4$ .
- (2) *Time*, as a linear map  $t : \mathbb{R}^4 \rightarrow \mathbb{R}$  of the linear space of the world parallel transitions onto the real 'time axes'. Time interval from the event  $a \in A^4$  to  $b \in A^4$  is called the number  $t(b-a)$ ; if  $t(b-a) = 0$  then the events  $a$  and  $b$  are called synchronous. The set of all mutually synchronous events consists a 3D affine space  $A^3$ , being a subspace of the world  $A^4$ . The kernel of the mapping  $t$  consists of the parallel transitions of  $A^4$  translating arbitrary (and every) event to the synchronous one; it is a linear 3D subspace  $\mathbb{R}^3$  of the space  $\mathbb{R}^4$ .
- (3) *Distance (metric)* between the synchronous events,

$$\rho(a, b) = \| a - b \|, \quad \text{for all } a, b \in A^3,$$

given by the scalar product in  $\mathbb{R}^3$ . The distance transforms arbitrary space of synchronous events into the well known 3D Euclidean space  $E^3$ .

The space  $A^4$ , with the Galilei space-time structure on it, is called Galilei space. Galilei group is the group of all possible transformations of the Galilei space, preserving its structure. The elements of the Galilei group are called Galilei transformations. Therefore, Galilei transformations are affine transformations of the world  $A^4$  preserving the time intervals and distances between the synchronous events.

The direct product  $\mathbb{R} \times \mathbb{R}^3$ , of the time axes with the 3D linear space  $\mathbb{R}^3$  with a fixed Euclidean structure, has a natural Galilei structure. It is called Galilei coordinate system.

### 1.3.2 Newtonian Equations of Motion

Recall that Newtonian *causality-determination principle* states: *initial state of a mechanical system* (a totality of positions and velocities of the system points in an arbitrary time point) *uniquely determines all its motion*. In other words, if we know all initial conditions and forces acting on the system at initial moment, we can predict its future behavior.

Let real  $N$ -dimensional ( $ND$ , for short) linear space  $\mathbb{R}^N$ , ( $N = 3n$ ), denote the Euclidean configuration space for a mechanical system of  $n$

points. A family of maps  $x_i : \mathbb{R} \rightarrow \mathbb{R}^N$ , ( $i = 1, \dots, N$ ) of the real time axis  $\mathbb{R}$  into the configuration space  $\mathbb{R}^N$  is usually called *motion in the Galilei coordinate system*  $\mathbb{R} \times \mathbb{R}^3$ .

According to the Newton's determination-causality principle, all motions of a system are uniquely determined by its initial position ( $x_i(t_0) \in \mathbb{R}^N$ ) and initial velocities ( $\dot{x}_i(t_0) \in \mathbb{R}^N$ ).

Particularly, initial position and velocities determine acceleration. Therefore, the smooth function (i.e., the function belonging to the class  $C^\infty$ )  $F : \mathbb{R}^N \times \mathbb{R}^N \times \mathbb{R} \rightarrow \mathbb{R}^N$  exists, satisfying the Newtonian equation of motion (1.1), which can be rewritten as

$$\ddot{x}_i = F(x_i, \dot{x}_i, m_i, t), \quad (i = 1, \dots, n).$$

It follows, from the standard theorem on the existence and uniqueness of the solution of a system of ordinary differential equations with smooth r.h.s in Hausdorff spaces (such as the real Euclidean space  $\mathbb{R}^N$ ), that the function  $F = F(x_i, \dot{x}_i, m_i, t)$  and initial conditions  $x(t_0)$  and  $\dot{x}(t_0)$  uniquely determine the system motion.

The form of the function  $F$  of any concrete mechanical system is obtained by experiment. From the mathematical point of view, the form of  $F$  for any system constitutes the definition of the system.

Particularly, the motion of a *potential system* (i.e.,  $n$  point-particles with masses  $m_i$  in the potential field with potential energy  $U = U(x_i)$ ) is given by the set of equations

$$m_i \ddot{x}_i = -\partial_{x_i} U, \quad (\partial_{x_i} \equiv \frac{\partial}{\partial x_i}; i = 1, \dots, n; \text{ no summation}).$$

The total mechanical energy (i.e., the sum of kinetic and potential energies) of a potential system is conserved, i.e.,

$$E = \frac{1}{2} m_i \dot{x}_i^2 + U(x_i) = \text{const.}$$

### 1.3.3 Calculus of Variations

Recall that *calculus of variations* seeks to find the path, curve, surface, etc., for which a given function has a *stationary value*, which, in physical problems, is usually a minimum or maximum (see e.g., [Forsyth (1960)]). Mathematically, this involves finding stationary values of integrals of the

form

$$S[x] = \int_a^b f(y, \dot{y}, x) dx.$$

Integral  $S[x]$  has an extremum *iff* the *Euler-Lagrange differential equation* is satisfied, i.e., *iff*

$$\frac{\partial f}{\partial y} - \frac{d}{dx} \left( \frac{\partial f}{\partial \dot{y}} \right) = 0.$$

The fundamental lemma of calculus of variations states that, if

$$S[x] = \int_a^b M(x) h(x) dx = 0$$

for all  $h(x)$  with continuous second partial derivatives, then

$$M(x) = 0 \quad \text{on } (a, b).$$

The calculus of variations is the basis of Lagrangian dynamics, as well as global Riemannian geometry (see chapters 3 and 4).

#### 1.3.4 Lagrangian Equations of Motion

Let  $x$  be a vector of an  $N$ D Euclidean coordinate space  $\mathbb{R}^N$ ,  $\gamma = \{t, x : x = x(t), t_0 \leq t \leq t_1\}$  – be a curve of  $(N + 1)$ D Galilei coordinate system  $\mathbb{R} \times \mathbb{R}^3$ , and  $L : \mathbb{R}^N \times \mathbb{R}^N \times \mathbb{R} \rightarrow \mathbb{R}^N$  – be a function of  $2N + 1$  arguments. Now holds the theorem: necessary and sufficient condition for the curve to be the extremal of the functional

$$S(\gamma) = \int_{t_0}^{t_1} L(x, \dot{x}, t) dt$$

on the space of curves  $x(t)$ , connecting the two points  $(t_0, x_0)$ ,  $(t_1, x_1)$ , is that along this path the Euler-Lagrange's equations

$$\frac{d}{dt} \frac{\partial L}{\partial \dot{x}} - \frac{\partial L}{\partial x} = 0$$

are satisfied. Therefore, the motion  $x(t)$  in the Galilei coordinate system  $\mathbb{R} \times \mathbb{R}^3$  is defined by the extremal path of the functional  $\int L dt$ . It implies that in an arbitrary coordinate system the Euler-Lagrange's equations of motion (written in this coordinate system) are valid. So we can choose the most suitable coordinates  $(q^1, \dots, q^N)$  in the *configuration space* of the system with  $n$  material points ( $N = 3n - k$ ,

where  $k$  denotes the number of *holonomic*, i.e., time-independent constraints). This configuration space, spanned by the generalized coordinates  $q^i$ , ( $i = 1, \dots, N$ ), is technically called the system's *configuration manifold*, and represents the central geometrical object in biodynamics. Now we have the usual mechanical interpretation:  $q^i$  and  $\dot{q}^i$  are respectively generalized coordinates and velocities, the difference  $T - U$  between kinetic and potential energy of the system is called Lagrange's function or Lagrangian  $L(q^i, \dot{q}^i, t)$ , partials  $\partial L / \partial \dot{q}^i = p_i$  are called generalized momenta, partials  $\partial L / \partial q^i = Q_i$  are called generalized forces, integral  $\int L(q, \dot{q}, t) dt$  is called the Hamilton's action, and Lagrange's equations of motion are the extremals of the Hamilton's action (see [Goldstein (1980); Arnold (1989); Abraham and Marsden (1978); Abraham *et al.* (1988); Marsden and Ratiu (1999)])

$$\frac{d}{dt} \frac{\partial L}{\partial \dot{q}^i} - \frac{\partial L}{\partial q^i} = 0. \quad (1.2)$$

Lagrange's equations of motion form the system of  $N$  differential equations of the second order, and its solution depends on  $2N$  arbitrary constants, given by the boundary conditions  $q^i(t_0) = q_0$ , and  $q^i(t_1) = q_1$ .

### 1.3.5 Hamiltonian Equations of Motion

Consider an  $N\dot{D}$  system of Lagrange's equations  $\dot{p}_i = \partial L / \partial q^i$  (with  $p_i = \partial L / \partial \dot{q}^i$ ), as given by Lagrangian  $L: \mathbb{R}^N \times \mathbb{R}^N \times \mathbb{R} \rightarrow \mathbb{R}^N$ . This system is equivalent to the system of  $2N$  equations of the first order – the Hamiltonian equations (see [Goldstein (1980); Arnold (1989); Abraham and Marsden (1978); Abraham *et al.* (1988); Marsden and Ratiu (1999); Puta (1993)])

$$\dot{p}_i = -\frac{\partial H}{\partial q^i}, \quad \dot{q}^i = \frac{\partial H}{\partial p_i}, \quad (1.3)$$

where  $H(p_i, q^i, t) = p_i \dot{q}^i - L$  is the *Legendre transformation* of the Lagrange's function (here and in the following text, summation convention upon repeated indices is used). It is called the Hamilton's function or Hamiltonian, and represents the total mechanical energy  $T + U$  of the system considered.

For the simplest example of a 1D motion,

$$\begin{aligned}\ddot{q} &= -\frac{\partial U}{\partial q}, & p &= \dot{q}, \\ T &= \frac{1}{2} \dot{q}^2, & U &= U(Q), \\ H &= \frac{p^2}{2} + U(q),\end{aligned}$$

and Hamilton's equations (1.3) read

$$\dot{q} = p, \quad \dot{p} = -\frac{\partial H}{\partial q}.$$

### 1.3.6 Lagrangian Flows on Biodynamic Manifolds

Let  $\Gamma$  be a smooth  $k$ D surface in a  $3n$ D configuration space of  $n$  material point-particles  $m_1, \dots, m_n$ , given by their  $n$  radius vectors  $\mathbf{r}^1, \dots, \mathbf{r}^n$ . Let  $\mathbf{q} = (q^1, \dots, q^k)$  are coordinates on  $\Gamma : \mathbf{r}^i = \mathbf{r}^i(\mathbf{q})$  (here  $i = 1, \dots, 3n - k$ ). Dynamical system described by Lagrangian equations (1.2), rewritten here in vector form

$$\frac{d}{dt} \frac{\partial L}{\partial \dot{\mathbf{q}}} = \frac{\partial L}{\partial \mathbf{q}}, \quad \text{with} \quad L = \frac{1}{2} m_i \dot{\mathbf{r}}^i + U(\mathbf{q}),$$

is called the system of  $n$  point-particles connected by  $3n - k$  ideal *holonomic constraints*. The surface  $\Gamma$  is called the configuration space of the system with constraints, and it appears to be a smooth (i.e., differentiable) manifold.

The intuitive picture of a smooth surface becomes analytic with the concept of a manifold. On the small scale, i.e., locally, a manifold looks like a Euclidean space, so that infinitesimal operations like differentiation may be defined on it. In general, a manifold is a smooth  $ND$  hyper-surface, that might be embedded into a  $\mathbb{R}^{N+1}$ . In case of a human-like biodynamic manifold, it has an additional Lie group structure, consisting of constrained *special Euclidean groups of rigid body motions*, as depicted in Figure 1.2 (see chapter 3 for details).

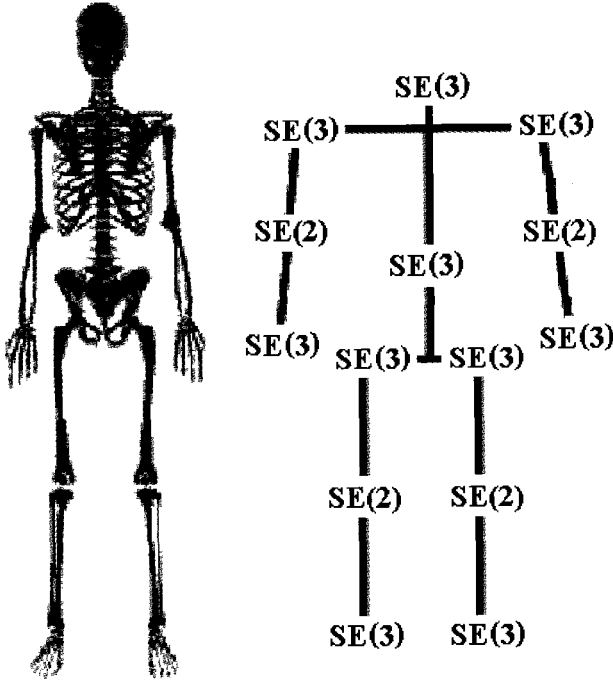


Fig. 1.2 A whole-body biodynamic manifold, with reduced spinal movability.

#### 1.4 Conservative versus Dissipative Hamiltonian Dynamics

Recall that *conservative-reversible systems* are in classical dynamics described by Hamilton's equations (1.3), also written as

$$\dot{q}^i = \partial_{p_i} H, \quad \dot{p}_i = \partial_{q^i} H, \quad (i = 1, \dots, n), \quad (1.4)$$

with a *constant Hamiltonian energy function*

$$H = H(q, p) = E_{kin}(p) + E_{pot}(q) = E = \text{const.} \quad (1.5)$$

Conservative dynamics visualizes the time evolution of a system in a *phase space*  $P$ , in which the coordinates are  $q^i$  and  $p_i$ . The instantaneous state of the system is the *representative point*  $(q, p)$  in  $P$ . As time varies, the representative point  $(q, p)$  describes the *phase trajectory*. A particular case



of a phase trajectory is the *position of equilibrium*, in which both  $\dot{q}^i = 0$  and  $\dot{p}_i = 0$  (see [Ivancevic (1991); Ivancevic (2004)]).

#### 1.4.1 Dissipative Systems

In addition to *conservative-reversible* systems, we must consider systems that give rise to *irreversible processes* and *dissipative structures* of *Nobel Laureate Ilya Prigogine* (see [Nicolis and Prigogine (1977); Ivancevic (1991)]).

A typical example is a chemical reaction in which a molecule of species *A* (say the hydroxyl radical OH) can combine with a molecule of species *B* say molecular hydrogen H<sub>2</sub>) to produce one molecule of species *C* and one molecule of species *D* (respectively H<sub>2</sub>O and atomic hydrogen H in our example). This process is symbolized



in which  $k$  is the rate constant, generally a function of temperature and pressure. On the l.h.s of (1.6), the *reactants* *A* and *B* combine and disappear in the course of time, whereas on the r.h.s the *products* *C* and *D* are formed and appear as the reaction advances. The rate at which particles of species *A* are consumed is proportional to the frequency of encounters of molecules of *A* and *B* – which, if the system is dilute, is merely proportional to the product of their concentrations,  $c$ ,

$$\dot{c}_A = -k c_A c_B. \quad (1.7)$$

Clearly, if we reverse time,  $t' = -t$ , and denote by  $c'_A$ ,  $c'_B$  the values of the concentrations as functions of  $t'$ , (1.7) becomes

$$\dot{c}_A = k c_A c_B,$$

and describes a process in which  $c_A$  would be produced instead of being consumed. This is certainly not equivalent to the phenomenon described by (1.7).

Further examples are *heat conduction*, given by *Fourier equation*

$$\partial_t T = \kappa \nabla^2 T, \quad \kappa > 0, \quad \left( \partial_t \equiv \frac{\partial}{\partial t} \right), \quad (1.8)$$

and *diffusion*, described by *Fick equation*

$$\partial_t T = D \nabla^2 c, \quad D > 0. \quad (1.9)$$

Here  $T$  is the temperature,  $c$  is the concentration of a certain substance dissolved in the fluid,  $\kappa$  is the heat diffusivity coefficient and  $D$  is the mass diffusivity. Both experiments and these two equations show that when a slight temperature variation (respectively, inhomogeneity) is imposed in an isothermal (respectively, uniform) fluid, it will *spread out* and eventually disappear.

Again, if we reverse time, we get the completely different laws

$$\partial_t T = -\kappa \nabla^2 T, \quad \partial_t c = -D \nabla^2 c,$$

describing a situation in which an initial temperature or concentration disturbance would be amplified rather than damped.

Both the *concentration* and the *temperature* variables are examples of so-called *even variables*, whose sign does not change upon time reversal. In contrast, the *momentum of a particle* and the *convection velocity of a fluid* are *odd variables*, since they are ultimately expressed as time derivatives of position-like variables and change their sign with time reversal.

This leads us to the following general property of the evolution equation of a dissipative system. Let  $\{X_i\}$  denote a complete set of macroscopic variables of such a system. *Dissipative evolution laws* have the form

$$\partial_t X_i = F_i(\{X_j\}, \lambda), \quad (1.10)$$

where  $\lambda$  denote *control parameters*, and  $F_i$  are functions of  $\{X_i\}$  and  $\lambda$ .

The basic feature of (1.10) is that, whatever the form of the functions  $F_i$ , in the absence of constraints they must reproduce the steady state of equilibrium

$$F_i(\{X_{j,eq}\}, \lambda_{eq}) = 0. \quad (1.11)$$

More generally, for a nonequilibrium steady state,

$$F_i(\{X_{j,s}\}, \lambda_s) = 0. \quad (1.12)$$

These relations impose certain restrictions. For instance, the evolution laws must ensure that positive values are attained for temperature or chemical concentrations that come up as solutions, or that detailed balance is attained. This is an important point, for it shows that the analysis of physical systems cannot be reduced to a mathematical game. In many respects physical systems may be regarded as highly atypical, specific, or nongeneric from the mathematical point of view. In these steady state relations, the

*nonlinearity*, relating the control parameters  $\lambda$  to the steady state values  $X_{j,s}$ , begins to play the prominent role.

### 1.4.2 Thermodynamic Equilibrium

In mechanics, (static) equilibrium is a particular 'state of rest' in which both the velocities and the accelerations of all the material points of a system are equal to zero. By definition the net balance of forces acting on each point is zero at each moment. If this balance is disturbed, equilibrium will be broken. This is what happens when a piece of metal fractures under the effect of load (see [Nicolis and Prigogine (1977); Ivancevic (1991)]).

Now, the notion of *thermodynamic equilibrium* is sharply different (see Appendix). Contrary to mechanical equilibrium, the molecules constituting the system are subject to forces that are not balanced and move continuously in all possible directions unless the temperature becomes very low. 'Equilibrium' refers here to some collective properties  $\{X_i\}$  characterizing the system as a whole, such as temperature, pressure, or the concentration of a chemical constituent.

Consider a system  $\{X_i\}$  embedded in a certain environment  $\{X_{ie}\}$ . Dynamic role of the sets of properties  $\{X_i\}$  and  $\{X_{ie}\}$  resides primarily in their exchanges between the system and the environment. For instance, if the system is contained in a vessel whose walls are perfectly rigid, permeable to heat but impermeable to matter, one of these quantities will be identical to the temperature,  $T$  and will control the exchange of energy in the form of heat between the system and its environment.

We say that the system is in thermodynamic equilibrium if it is completely identified with its environment, that is, if the properties  $X_i$  and  $X_{ie}$  have identical values. In the previous example, thermodynamic equilibrium between the system and its surroundings is tantamount to  $T = T_e$  at all times and at all points in space. But because the walls of the vessel are impermeable to matter, system and environment can remain highly differentiated in their chemical composition,  $c$ . If the walls become permeable to certain chemical substances  $i$ , thermodynamic equilibrium will prevail when the system and the environment become indistinguishable as far as those chemicals are concerned. In simple cases this means that the corresponding composition variables will satisfy the equality  $c_i = c_{ie}$ , but more generally equilibrium will be characterized by the equality for a quantity known as the chemical potential,  $\mu_i = \mu_{ie}$ . Similarly, if the walls of the vessel are not rigid, the system can exchange mechanical energy with its

environment. Equilibrium will then also imply the equality of pressures,  $p = p_e$ .

According to the above definitions, equilibrium is automatically a stationary state,  $\partial X_i / \partial t = 0$ : the properties  $X_i$  do not vary with time. As they are identical in the properties  $X_i$ , the system and the environment have nothing to exchange. We express this by saying that there are no net *fluxes* across the system,

$$J_i^{eq} = 0. \quad (1.13)$$

### 1.4.3 Nonlinearity

Here is a simple example. Let  $X$  be the unique state variable,  $k$  a parameter, and let  $\lambda$  represent the applied constraint. We can easily imagine a mechanism such as  $A \rightleftharpoons X \rightleftharpoons D$  in which  $X$  evolves according to

$$\dot{X} = \lambda - kX,$$

yielding a stationary state value given by  $\lambda - kX_s = 0$ , or  $X_s = \lambda/k$ . In the linear law linking the steady state value  $X_s$  to the control parameter  $\lambda$  the behavior is bound to be qualitatively similar to that in equilibrium, even in the presence of strongly correlated nonequilibrium constraints. In the nonlinear law linking the steady state value  $X_s$  to the control parameter  $\lambda$  there is an unlimited number of possible forms describing nonlinear dependencies. For the certain values of  $\lambda$  the system can present several distinct solutions.

Nonlinearity combined with *nonequilibrium constraints* allows for multiple solutions and hence for the diversification of the behaviors presented by a system (see [Nicolis and Prigogine (1977); Ivancevic (1991)]).

### 1.4.4 The Second Law of Thermodynamics

According to this law there exists a function of the state variables (usually chosen to be the *entropy*,  $S$ ) of the system that varies monotonically during the approach to the unique final state of thermodynamic equilibrium:

$$\dot{S} \geq 0 \quad (\text{for any isolated system}). \quad (1.14)$$

It is usually interpreted as a *tendency to increased disorder*, i.e., an irreversible trend to maximum disorder.

The above interpretation of entropy and a second law is fairly obvious for systems of *weakly interacting particles*, to which the arguments developed by Boltzmann referred.

For strongly interacting systems the above interpretation does not apply in a straightforward manner since, we know that for such systems there exists the possibility of evolving to more ordered states through the mechanism of chapter *phase transitions* (see Appendix, as well as *synergetics* in chapter 2 and *topological phase transitions* in chapter 5).

Let us now turn to nonisolated systems, which exchange energy or matter with the environment. The entropy variation will now be the sum of two terms. One, entropy flux,  $d_e S$ , is due to these exchanges; the other, entropy production,  $d_i S$ , is due to the phenomena going on within the system. Thus the entropy variation is

$$\dot{S} = \frac{d_i S}{dt} + \frac{d_e S}{dt}. \quad (1.15)$$

For an isolated system  $d_e S = 0$ , and (1.15) together with (1.14) reduces to  $dS = d_i S \geq 0$ , the usual statement of the second law. But even if the system is nonisolated,  $d_i S$  will describe those (irreversible) processes that would still go on even in the absence of the flux term  $d_e S$ . We thus require the following extended form of the second law:

$$\dot{S} \geq 0 \quad (\text{nonisolated system}). \quad (1.16)$$

As long as  $d_i S$  is strictly positive, irreversible processes will go on continuously within the system. Thus,  $d_i S > 0$  is equivalent to the condition of dissipativity as time irreversibility. If, on the other hand,  $d_i S$  reduces to zero, the process will be reversible and will merely join neighboring states of equilibrium through a slow variation of the flux term  $d_e S$ .

Among the most common irreversible processes contributing to  $d_i S$  are chemical reactions, heat conduction, diffusion, viscous dissipation, and relaxation phenomena in electrically or magnetically polarized systems. For each of these phenomena two factors can be defined: an appropriate internal *flux*,  $J_i$ , denoting essentially its rate, and a driving *force*,  $X_i$ , related to the maintenance of the nonequilibrium constraint. A most remarkable feature is that  $d_i S$  becomes a *bilinear form* of  $J_i$  and  $X_i$ . The following table summarizes the fluxes and forces associated with some commonly observed irreversible phenomena (see [Nicolis and Prigogine (1977); Ivancevic (1991)])

Phenomenon	Flux	Force	Rank
Heat conduction	Heat flux, $\mathbf{J}_{th}$	$grad(1/T)$	Vector
Diffusion	Mass flux, $\mathbf{J}_d$	$-[grad(\mu/T) - \mathbf{F}]$	Vector
Viscous flow	Pressure tensor, $\mathbf{P}$	$(1/T) grad \mathbf{v}$	Tensor
Chemical reaction	Rate of reaction, $\omega$	Affinity of reaction	Scalar

In general, the fluxes  $J_k$  are very complicated functions of the forces  $X_i$ . A particularly simple situation arises when their relation is linear, then we have the celebrated *Onsager relations* (named after *Nobel Laureate Lars Onsager*),

$$J_i = L_{ik}X_k, \quad (1.17)$$

in which  $L_{ik}$  denote the set of *phenomenological coefficients*. This is what happens near equilibrium where they are also symmetric,  $L_{ik} = L_{ki}$ . Note, however, that certain states far from equilibrium can still be characterized by a linear dependence of the form of (1.17) that occurs either accidentally or because of the presence of special types of regulatory processes.

#### 1.4.5 Geometry of Phase Space

Now, we reduce (1.10) to the *temporal* systems, in which there is no space dependence in the operator  $F_i$ , so that  $\partial \rightarrow d$ , and we have

$$\dot{X}_i = F_i(\{X_j\}, \lambda), \quad i = 1, \dots, n. \quad (1.18)$$

Moreover, we restrict ourselves to autonomous systems, for which  $F_i$  does not depend explicitly on time, a consequence being that the trajectories in phase space are invariant. Note that in a Hamiltonian system  $n$  must be even and  $F_i$  must reduce to the characteristic structure imposed by (1.4).

A first kind of phase space trajectory compatible with (1.18) is given by

$$\dot{X}_i = 0. \quad (1.19)$$

It includes as particular cases the states of mechanical equilibrium encountered in conservative systems and the steady states encountered in dissipative systems. In phase space such trajectories are quite degenerate, since they are given by the solutions of the  $n$  algebraic equations for  $n$  unknowns,  $F_i = 0$ . They are represented by *fixed points*.

If (1.19) is not satisfied, the representative point will not be fixed but will move along a phase space trajectory defining a curve. The line element

along this trajectory for a displacement corresponding to  $(dX_1, \dots, dX_n)$  along the individual axes is given by Euclidean metrics

$$ds^2 = \sum_i dX_i^2 = \sum_i F_i^2 dt. \quad (1.20)$$

Thus, the projections of the tangent of the curve along the axes are given by

$$\frac{dX_\alpha}{ds} = \frac{F_\alpha}{\sqrt{\sum_i F_i^2}}, \quad (1.21)$$

and are well defined everywhere. The points belonging to such curves are called *regular points*. In contrast, the tangent on the fixed points is *ill-defined* because of the simultaneous vanishing of all  $F_i$ 's. Therefore, the fixed points could be also referred to as the singular points of the flow generated by (1.18). The set of fixed points and phase space trajectories constitutes the *phase portrait* of a dynamical system.

One property that plays a decisive role in the structure of the phase portrait relates to the *existence-uniqueness theorem* of the solutions of ordinary differential equations. This important result of A. Cauchy asserts that *under quite mild conditions on the functions  $F_i$ , the solution corresponding to an initial condition not on a fixed point exists and is unique for all times in a certain interval  $(0, \tau)$ , whose upper bound  $\tau$  depends on the specific structure of the functions  $F_i$* . In the phase space representation, the theorem automatically rules out the intersection of two trajectories in any regular point (see [Nicolis and Prigogine (1977); Ivancevic (1991)]).

A second structure of great importance is the *existence and structure of invariant sets of the flow*. By this we mean objects embedded in the phase space that are bounded and are mapped onto themselves during the evolution generated by (1.18). An obvious example of an invariant set is the ensemble of fixed points. Another is a closed curve in phase space representing a periodic motion.

The *impossibility of self-intersection of the trajectories* and the *existence of invariant sets* of a certain form (fixed points, limit circles,...) determine, to a large extent, the structure of the phase portrait in 2D phase spaces, and through it the type of behavior that may arise. *In three or more dimensions*, however, the constraints imposed by these properties are much less severe, since the trajectories have many more possibilities to avoid each other by 'gliding' within the 'gaps' left between invariant sets, thus implying the

*possibility for chaos.*

In principle, the solution of (1.18) constitutes a *well-posed problem*, in the sense that *a complete specification of the state  $(X_1, \dots, X_n)$  at any one time allows prediction of the state at all other times.* But in many cases such a complete specification may be operationally meaningless. For example, in a Hamiltonian system composed of particles whose number is of the order of Avogadro's number, or in a chaotic regime, it is no longer meaningful to argue in terms of individual trajectories. New modes of approach are needed, and one of the most important is a description of the system in terms of *probability concepts*. For this purpose we consider not the rather special case of a single system, but instead focus attention on the *Gibbs ensemble* of a very large number of identical systems, which are in general in different states, but all subject to exactly the same constraints. They can therefore be regarded as emanating from an initial ensemble of systems whose representative phase points were contained in a certain phase space volume  $V_0$  (see [Nicolis and Prigogine (1977); Ivancevic (1991)]).

## 1.5 Neural Basis of Biodynamics

In this section we briefly describe higher, neural part of biodynamics. Higher biodynamics is the science of *sensory-motor coordination*, which is performed by the *nervous system*. The general function of the nervous system is to orchestrate the integration and communication of other body systems. These processes are accomplished by *nerve impulses* and are facilitated by *neurons* throughout the body. In greatly simplified terms, a typical biological neuron has (see Figure 1.3):

- (1) A branching dendritic tree that collects signals from many other neurons in a limited area;
- (2) A cell body that integrates collected signals and generates a response signal (as well as manages metabolic functions); and
- (3) A long branching axon that distributes the response through contacts with dendritic trees of many other neurons.

The response of each neuron is a relatively simple nonlinear function of its inputs and is largely determined by the strengths of the connections from its inputs. In spite of the relative simplicity of the individual units, systems containing many neurons can generate complex and interesting behaviors.



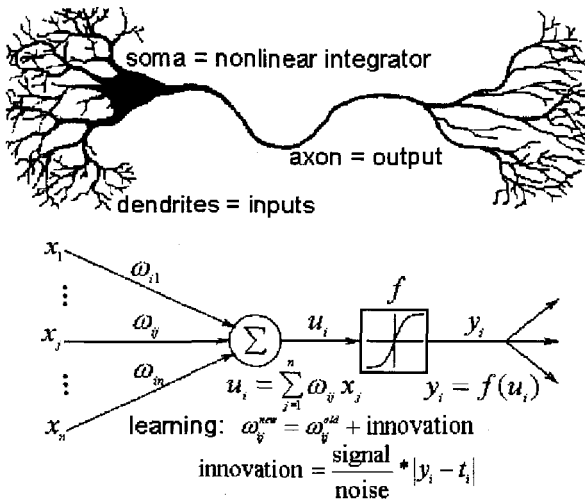


Fig. 1.3 Biological neuron (up) and activation dynamics of an artificial neurons (down); here,  $x_j$  are inputs,  $y_i$  are outputs,  $w_{ij}$  are synaptic weights to be adjusted/adapted by the learning process,  $t_i$  are targets, and  $f$  is a nonlinear, most often sigmoidal (e.g., tanh) function.

On the other hand, the so-called *artificial neural networks* (ANNs, for short) are *parallel, distributed computational systems* [Rumelhart and McClelland (1987)], with ability of *biological-like learning* [Sejnowski *et al.* (1988)]. The learning, whose structure is based on that of the animal *nervous system* [Hebb (1949)], generally performs according to the basic formula: *New Value* = *Old Value* + *Innovation*, where *Innovation* is possibly dependent either on informational *signal/noise* ratio, or on psychological *award/punishment* ratio. In engineering terminology, ANNs are distributed, adaptive, generally nonlinear learning machines built from many different *processing elements* (PEs), resembling animal *neurons* (see Figure 1.3), each possibly having a (small amount of) local *memory*. The PEs are connected by either unidirectional, or bidirectional, *communication channels*, resembling *synaptic-like interconnections*, which carry numerical data, or signals. The PEs operate only on their local data and on the inputs  $x$  they receive via the connections. The interconnectivity defines the ANN *topology*. The signals flowing on the connections are scaled by adjustable parameters called *synaptic weights*  $w$ . The PEs sum all these contributions and produce an output that is a nonlinear (static) function of the sum.

## Chapter 2

# Natural Language of Biodynamics

The purpose of this chapter is to introduce the natural language of biodynamics to be used in the later chapters. Its *functorial* part introduces the unity-in-diversity metalanguage of both classical ('small') categories and modern ('big')  $n$ -categories, as well as associated algebraic and topological preliminaries. Its *synergetic* part introduces the diversity-in-unity language of dynamics, chaos theory and Haken's synergetics.

### 2.1 Categorical Metalanguage

In this section we introduce our global, categorical metalanguage, as a main tool to see *unity in diversity*, mathematical unity in natural biodynamics diversity. In modern mathematical sciences whenever one defines a new class of mathematical objects, one proceeds almost in the next breath to say what kinds of maps between objects will be considered [Switzer (1975)]. A general framework for dealing with situations where we have some *objects* and *maps between objects*, like sets and functions, vector spaces and linear operators, points in a space and paths between points, etc. – provides the modern metalanguage of categories. Categories are mathematical universes. For this reason, in this book we extensively use this language, mainly following its founder, S. MacLane [MacLane (1971)].

#### 2.1.1 Preliminaries from Calculus, Algebra and Topology

Before defining categories, functors and natural transformations, we give the necessary preliminaries from calculus, algebra and point-set topology.

### 2.1.1.1 Notes From Calculus

**Functions.** Recall that a *function*  $f$  is a *rule* that assigns to each element  $x$  in a set  $A$  exactly one element, called  $f(x)$ , in a set  $B$ . A function could be thought of as a *machine*  $[[f]]$  with  $x$ -input (the *domain* of  $f$  is the set of all possible inputs) and  $f(x)$ -output (the *range* of  $f$  is the set of all possible outputs) [Stuart (1999)]

$$x \rightarrow [[f]] \rightarrow f(x).$$

There are four possible ways to represent a function: (i) verbally (by a description in words); (ii) numerically (by a table of values); (iii) visually (by a graph); and (iv) algebraically (by an explicit formula). The most common method for visualizing a function is its graph. If  $f$  is a function with domain  $A$ , then its *graph* is the set of ordered input-output pairs

$$\{(x, f(x)) : x \in A\}.$$

**Algebra of Functions.** Let  $f$  and  $g$  be functions with domains  $A$  and  $B$ . Then the functions  $f + g$ ,  $f - g$ ,  $fg$ , and  $f/g$  are defined as follows [Stuart (1999)]

$$\begin{aligned} (f + g)(x) &= f(x) + g(x) & \text{domain} &= A \cap B, \\ (f - g)(x) &= f(x) - g(x) & \text{domain} &= A \cap B, \\ (fg)(x) &= f(x)g(x) & \text{domain} &= A \cap B, \\ \left(\frac{f}{g}\right)(x) &= \frac{f(x)}{g(x)} & \text{domain} &= \{x \in A \cap B : g(x) \neq 0\}. \end{aligned}$$

**Compositions of Functions.** Given two functions  $f$  and  $g$ , their *composition*  $f \circ g$  is defined by

$$(f \circ g)(x) = f(g(x)).$$

The  $(f \circ g)$ -machine is composed of the  $g$ -machine (first) and then the  $f$ -machine [Stuart (1999)],

$$x \rightarrow [[g]] \rightarrow g(x) \rightarrow [[f]] \rightarrow f(g(x)).$$

For example, suppose that  $y = f(u) = \sqrt{u}$  and  $u = g(x) = x^2 + 1$ . Since  $y$  is a function of  $u$  and  $u$  is a function of  $x$ , it follows that  $y$  is ultimately a function of  $x$ . We compute this by substitution

$$y = f(u) = f \circ g = f(g(x)) = f(x^2 + 1) = \sqrt{x^2 + 1}.$$

**The Chain Rule.** If  $f$  and  $g$  are both differentiable and  $h = f \circ g$  is the composite function defined by  $h(x) = f(g(x))$ , then  $h$  is differentiable and  $h'$  is given by the product [Stuart (1999)]

$$h'(x) = f'(g(x)) g'(x).$$

In Leibniz notation, if  $y = f(u)$  and  $u = g(x)$  are both differentiable functions, then

$$y' = \frac{dy}{dx} = \frac{dy}{du} \frac{du}{dx}.$$

The reason for the name *chain rule* becomes clear if we add another link to the chain. Suppose that we have one more differentiable function  $x = h(t)$ . Then, to compute the derivative of  $y$  with respect to  $t$ , we use the chain rule twice,

$$\dot{y} = \frac{dy}{dt} = \frac{dy}{du} \frac{du}{dx} \frac{dx}{dt}.$$

**Integration and Change of Variables.** Based on the chain rule, under the certain hypotheses (such as a one-to-one  $C^0$  map  $T$  with a nonzero *Jacobian determinant*  $\left| \frac{\partial(x, \dots)}{\partial(u, \dots)} \right|$  that maps a region  $S$  onto a region  $R$ , see [Stuart (1999)]) we have the following substitution formulas:

1. for a single integral,

$$\int_R f(x) dx = \int_S f(x(u)) \left| \frac{\partial x}{\partial u} \right| du,$$

2. for a double integral,

$$\iint_R f(x, y) dA = \iint_S f(x(u, v), y(u, v)) \left| \frac{\partial(x, y)}{\partial(u, v)} \right| dudv,$$

3. for a triple integral,

$$\iiint_R f(x, y, z) dV = \iiint_S f(x(u, v, w), y(u, v, w), z(u, v, w)) \left| \frac{\partial(x, y, z)}{\partial(u, v, w)} \right| dudvdw,$$

4. similarly for  $n$ -tuple integrals. (For the basics of complex-variable theory, see Appendix).

### 2.1.1.2 Notes from Set Theory

Given a function  $f : A \rightarrow B$ , the set  $A$  is called the *domain* of  $f$ , and denoted  $\text{Dom } f$ . The set  $B$  is called the *codomain* of  $f$ , and denoted  $\text{Cod } f$ . The codomain is not to be confused with the *range* of  $f(A)$ , which is in general only a subset of  $B$ .

A function  $f : X \rightarrow Y$  is called *injective* or *one-to-one* or an *injection* if for every  $y$  in the codomain  $Y$  there is at most one  $x$  in the domain  $X$  with  $f(x) = y$ . Put another way, given  $x$  and  $x'$  in  $X$ , if  $f(x) = f(x')$ , then it follows that  $x = x'$ . A function  $f : X \rightarrow Y$  is called *surjective* or *onto* or a *surjection* if for every  $y$  in the codomain  $\text{Cod } f$  there is at least one  $x$  in the domain  $X$  with  $f(x) = y$ . Put another way, the *range*  $f(X)$  is equal to the codomain  $Y$ . A function is *bijective* iff it is both injective and surjective. Injective functions are called the *monomorphisms*, and surjective functions are called the *epimorphisms* in the *category of sets* (see below).

A *relation* is any subset of a *Cartesian product* (see below). By definition, an *equivalence relation*  $\alpha$  on a set  $X$  is a relation which is *reflexive*, *symmetrical* and *transitive*, i.e., relation that satisfies the following three conditions:

- (1) *Reflexivity*: each element  $x \in X$  is equivalent to itself, i.e.,  $x\alpha x$ ,
- (2) *Symmetry*: for any two elements  $x, x' \in X$ ,  $x\alpha x'$  implies  $x'\alpha x$ , and
- (3) *Transitivity*:  $a \leq b$  and  $b \leq c$  implies  $a \leq c$ .

Similarly, a relation  $\leq$  defines a *partial order* on a set  $S$  if it has the following properties:

- (1) *Reflexivity*:  $a \leq a$  for all  $a \in S$ ,
- (2) *Antisymmetry*:  $a \leq b$  and  $b \leq a$  implies  $a = b$ , and
- (3) *Transitivity*:  $a \leq b$  and  $b \leq c$  implies  $a \leq c$ .

A *partially ordered set* (or *poset*) is a set taken together with a partial order on it. Formally, a partially ordered set is defined as an ordered pair  $P = (X, \leq)$ , where  $X$  is called the *ground set* of  $P$  and  $\leq$  is the partial order of  $P$ .

### 2.1.1.3 Notes from General Topology

*Topology* is a kind of *abstraction* of Euclidean geometry, and also a natural framework for the study of *continuity*. Euclidean geometry is abstracted by regarding triangles, circles, and squares as being the same basic object.

Continuity enters because in saying this one has in mind a *continuous deformation* of a triangle into a square or a circle, or any arbitrary shape. On the other hand, a disk with a hole in the center is topologically different from a circle or a square because one cannot create or destroy holes by continuous deformations. Thus using topological methods one does not expect to be able to identify a geometric figure as being a triangle or a square. However, one does expect to be able to detect the presence of gross features such as holes or the fact that the figure is made up of two disjoint pieces etc. In this way topology produces theorems that are usually qualitative in nature – they may assert, for example, the existence or non-existence of an object. They will not in general, provide the means for its construction [Nash and Sen (1983)].

Let  $X$  be any set and  $Y = \{X_\alpha\}$  denote a collection, finite or infinite of subsets of  $X$ . Then  $X$  and  $Y$  form a *topological space* provided the  $X_\alpha$  and  $Y$  satisfy:

- (1) Any finite or infinite subcollection  $\{Z_\alpha\} \subset X_\alpha$  has the property that  $\cup Z_\alpha \in Y$ , and
- (2) Any *finite subcollection*  $\{Z_{\alpha_1}, \dots, Z_{\alpha_n}\} \subset X_\alpha$  has the property that  $\cap Z_{\alpha_i} \in Y$ .

The set  $X$  is then called a topological space and the  $X_\alpha$  are called *open sets*. The choice of  $Y$  satisfying (2) is said to give a topology to  $X$ .

Now, given two topological spaces  $X$  and  $Y$ , a *function* (or, a *map*)  $f: X \rightarrow Y$  is *continuous* if the inverse image of an open set in  $Y$  is an open set in  $X$ .

The main general idea in topology is to study spaces which can be continuously deformed into one another, namely the idea of *homeomorphism*. If we have two topological spaces  $X$  and  $Y$ , then a map  $f: X \rightarrow Y$  is called a homeomorphism iff

- (1)  $f$  is continuous, and
- (2) There exists an inverse of  $f$ , denoted  $f^{-1}$ , which is also continuous.

Definition (2) implies that if  $f$  is a homeomorphism then so is  $f^{-1}$ . Homeomorphism is the main topological example of *reflexive, symmetrical and transitive relation*, i.e., *equivalence relation*. Homeomorphism divides all topological spaces up into *equivalence classes*. In other words, a pair of topological spaces,  $X$  and  $Y$ , belong to the same equivalence class if they are homeomorphic.

The second example of topological equivalence relation is *homotopy*. While homeomorphism generates equivalence classes whose members are topological spaces, homotopy generates equivalence classes whose members are continuous maps (or,  $C^0$ -maps). Consider two continuous maps  $f, g : X \rightarrow Y$  between topological spaces  $X$  and  $Y$ . Then the map  $f$  is said to be *homotopic* to the map  $g$  if  $f$  can be continuously deformed into  $g$  (see below for the precise definition of homotopy). Homotopy is an equivalence relation which divides the space of continuous maps between two topological spaces into equivalence classes [Nash and Sen (1983)].

Another important notions in topology are *covering*, *compactness* and *connectedness*. Given a family of sets  $\{X_\alpha\} = X$  say, then  $X$  is a *cover* of another set  $Y$  if  $\cup X_\alpha$  contains  $Y$ . If all the  $X_\alpha$  happen to be open sets the cover is called an *open cover*. Now consider the set  $Y$  and all its possible open coverings. The set  $Y$  is *compact* if for every open covering  $\{X_\alpha\}$  with  $\cup X_\alpha \supset Y$  there always exists a finite subcovering  $\{X_1, \dots, X_n\}$  of  $Y$  with  $X_1 \cup \dots \cup X_n \supset Y$ .<sup>1</sup> Again, we define a set  $Z$  to be *connected* if it cannot be written as  $Z = Z_1 \cup Z_2$ , where  $Z_1$  and  $Z_2$  are both open and  $Z_1 \cap Z_2$  is an empty set.

Let  $A_1, A_2, \dots, A_n$  be closed subspaces of a topological space  $X$  such that  $X = \cup_{i=1}^n A_i$ . Suppose  $f_i : A_i \rightarrow Y$  is a function,  $1 \leq i \leq n$ , iff

$$f_i|_{A_i \cap A_j} = f_j|_{A_i \cap A_j}, 1 \leq i, j \leq n. \quad (2.1)$$

In this case  $f$  is continuous iff each  $f_i$  is. Using this procedure we can define a  $C^0$ -function  $f : X \rightarrow Y$  by cutting up the space  $X$  into closed subsets  $A_i$  and defining  $f$  on each  $A_i$  separately in such a way that  $f|_{A_i}$  is obviously continuous; we then have only to check that the different definitions agree on the *overlaps*  $A_i \cap A_j$ .

The *universal property of the Cartesian product*: let  $p_X : X \times Y \rightarrow X$ , and  $p_Y : X \times Y \rightarrow Y$  be the *projections* onto the first and second factors, respectively. Given any pair of functions  $f : Z \rightarrow X$  and  $g : Z \rightarrow Y$  there is a unique function  $h : Z \rightarrow X \times Y$  such that  $p_X \circ h = f$ , and  $p_Y \circ h = g$ . Function  $h$  is continuous iff both  $f$  and  $g$  are. This property characterizes

<sup>1</sup>The notion of compactness is fundamental for biodynamic control. Namely, the basic (kinematic) unit of the biodynamic manifold is the special Euclidean group  $SE(3)$ . This group is non-compact, which means that it does not admit a natural metric generated by the segment's kinetic energy, and therefore there is not a natural control. However, its two subgroups, the group of rotations  $SE(3)$  and the group of translations  $\mathbb{R}^3$  are both compact, admitting the natural quadratic metric forms given by the kinetic energy. This implies the existence of (muscular-like) optimal controls in the sense of geodesics (see chapter 3).

$X/\alpha$  up to homeomorphism. In particular, to check that a given function  $h : Z \rightarrow X$  is continuous it will suffice to check that  $p_X \circ h$  and  $p_Y \circ h$  are continuous.

The *universal property of the quotient*: let  $\alpha$  be an equivalence relation on a topological space  $X$ , let  $X/\alpha$  denote the space of equivalence classes and  $p_\alpha : X \rightarrow X/\alpha$  the natural projection. Given a function  $f : X \rightarrow Y$ , there is a function  $f' : X/\alpha \rightarrow Y$  with  $f' \circ p_\alpha = f$  iff  $x\alpha x'$  implies  $f(x) = f(x')$ , for all  $x \in X$ . In this case  $f'$  is continuous iff  $f$  is. This property characterizes  $X/\alpha$  up to homeomorphism.

Now we return to the fundamental notion of homotopy. Let  $I$  be a compact unit interval  $I = [0, 1]$ . A *homotopy* from  $X$  to  $Y$  is a continuous function  $F : X \times I \rightarrow Y$ . For each  $t \in I$  one has  $F_t : X \rightarrow Y$  defined by  $F_t(x) = F(x, t)$  for all  $x \in X$ . The functions  $F_t$  are called the 'stages' of the homotopy. If  $f, g : X \rightarrow Y$  are two continuous maps, we say  $f$  is homotopic to  $g$ , and write  $f \simeq g$ , if there is a homotopy  $F : X \times I \rightarrow Y$  such that  $F_0 = f$  and  $F_1 = g$ . In other words,  $f$  can be continuously deformed into  $g$  through the stages  $F_t$ . If  $A \subset X$  is a subspace, then  $F$  is a homotopy relative to  $A$  if  $F(a, t) = F(a, 0)$ , for all  $a \in A, t \in I$ .

The homotopy relation  $\simeq$  is an equivalence relation. To prove that we have  $f \simeq f$  is obvious; take  $F(x, t) = f(x)$ , for all  $x \in X, t \in I$ . If  $f \simeq g$  and  $F$  is a homotopy from  $f$  to  $g$ , then  $G : X \times I \rightarrow Y$  defined by  $G(x, t) = F(x, 1 - t)$ , is a homotopy from  $g$  to  $f$ , i.e.,  $g \simeq f$ . If  $f \simeq g$  with homotopy  $F$  and  $g \simeq h$  with homotopy  $G$ , then  $f \simeq h$  with homotopy  $H$  defined by

$$H(x, t) = \begin{cases} F(x, t), & 0 \leq t \leq 1/2 \\ G(x, 2t - 1), & 1/2 \leq t \leq 1. \end{cases}$$

To show that  $H$  is continuous we use the relation (2.1).

In this way, the set of all  $C^0$ -functions  $f : X \rightarrow Y$  between two topological spaces  $X$  and  $Y$ , called the *function space* and denoted by  $Y^X$ , is partitioned into equivalence classes under the relation  $\simeq$ . The equivalence classes are called *homotopy classes*, the homotopy class of  $f$  is denoted by  $[f]$ , and the set of all homotopy classes is denoted by  $[X; Y]$ .

If  $\alpha$  is an equivalence relation on a topological space  $X$  and  $F : X \times I \rightarrow Y$  is a homotopy such that each stage  $F_t$  factors through  $X/\alpha$ , i.e.,  $x\alpha x'$  implies  $F_t(x) = F_t(x')$ , then  $F$  induces a homotopy  $F' : (X/\alpha) \times I \rightarrow Y$  such that  $F' \circ (p_\alpha \times 1) = F$ .

Homotopy theory has a range of applications of its own, outside topology and geometry, as for example in proving Cauchy theorem in complex



variable theory (see Appendix), or in solving nonlinear equations of artificial neural networks (see subsection (7.6.2.1) below).

A *pointed set*  $(S, s_0)$  is a set  $S$  together with a distinguished point  $s_0 \in S$ . Similarly, a *pointed topological space*  $(X, x_0)$  is a space  $X$  together with a distinguished point  $x_0 \in X$ . When we are concerned with pointed spaces  $(X, x_0), (Y, y_0)$ , etc., we always require that all functions  $f : X \rightarrow Y$  shall preserve base points, i.e.,  $f(x_0) = y_0$ , and that all homotopies  $F : X \times I \rightarrow Y$  be relative to the base point, i.e.,  $F(x_0, t) = y_0$ , for all  $t \in I$ . We denote the homotopy classes of base point-preserving functions by  $[X, x_0; Y, y_0]$  (where homotopies are relative to  $x_0$ ).  $[X, x_0; Y, y_0]$  is a pointed set with base point  $f_0$ , the constant function:  $f_0(x) = y_0$ , for all  $x \in X$ .

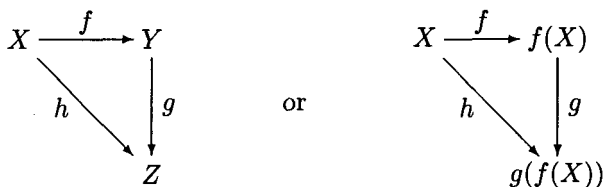
A *path*  $\gamma(t)$  from  $x_0$  to  $x_1$  in a topological space  $X$  is a continuous map  $\gamma : I \rightarrow X$  with  $\gamma(0) = x_0$  and  $\gamma(1) = x_1$ . Thus  $X^I$  is the space of all paths in  $X$  with the compact-open topology. We introduce a relation  $\sim$  on  $X$  by saying  $x_0 \sim x_1$  iff there is a path  $\gamma : I \rightarrow X$  from  $x_0$  to  $x_1$ .  $\sim$  is clearly an equivalence relation, and the set of equivalence classes is denoted by  $\pi_0(X)$ . The elements of  $\pi_0(X)$  are called the *path components*, or *0-components* of  $X$ . If  $\pi_0(X)$  contains just one element, then  $X$  is called *path connected*, or *0-connected*. A *closed path*, or *loop* in  $X$  at the point  $x_0$  is a path  $\gamma(t)$  for which  $\gamma(0) = \gamma(1) = x_0$ . The *inverse loop*  $\gamma^{-1}(t)$  based at  $x_0 \in X$  is defined by  $\gamma^{-1}(t) = \gamma(1 - t)$ , for  $0 \leq t \leq 1$ . The *homotopy of loops* is the particular case of the above defined homotopy of continuous maps.

If  $(X, x_0)$  is a pointed space, then we may regard  $\pi_0(X)$  as a pointed set with the 0-component of  $x_0$  as a base point. We use the notation  $\pi_0(X, x_0)$  to denote  $\pi_0(X, x_0)$  thought of as a pointed set. If  $f : X \rightarrow Y$  is a map then  $f$  sends 0-components of  $X$  into 0-components of  $Y$  and hence defines a function  $\pi_0(f) : \pi_0(X) \rightarrow \pi_0(Y)$ . Similarly, a base point-preserving map  $f : (X, x_0) \rightarrow (Y, y_0)$  induces a map of pointed sets  $\pi_0(f) : \pi_0(X, x_0) \rightarrow \pi_0(Y, y_0)$ . In this way defined  $\pi_0$  represents a 'functor' from the 'category' of topological (point) spaces to the underlying category of (point) sets (see the next section).

#### 2.1.1.4 Commutative Diagrams

S. MacLane says that the category theory was born with an observation that many properties of mathematical systems can be unified and simplified by a presentation with *commutative diagrams of arrows* [MacLane (1971)]. Each arrow  $f : X \rightarrow Y$  represents a function (i.e., a map, transformation,

operator); that is, a source (domain) set  $X$ , a target (codomain) set  $Y$ , and a rule  $x \mapsto f(x)$  which assigns to each element  $x \in X$  an element  $f(x) \in Y$ . A typical diagram of sets and functions is



This diagram is *commutative* iff  $h = g \circ f$ , where  $g \circ f$  is the usual composite function  $g \circ f : X \rightarrow Z$ , defined by  $x \mapsto g(f(x))$ .

Similar commutative diagrams apply in other mathematical, physical and computing contexts; e.g., in the ‘category’ of all topological spaces, the letters  $X, Y$ , and  $Z$  represent topological spaces while  $f, g$ , and  $h$  stand for continuous maps. Again, in the category of all groups,  $X, Y$ , and  $Z$  stand for groups,  $f, g$ , and  $h$  for homomorphisms.

Less formally, composing maps is like following directed paths from one object to another (e.g., from set to set). In general, a diagram is commutative iff any two paths along arrows that start at the same point and finish at the same point yield the same ‘homomorphism’ via compositions along successive arrows. Commutativity of the whole diagram follows from commutativity of its triangular components (depicting a ‘commutative flow’, see Figure 2.1). Study of commutative diagrams is popularly called ‘diagram chasing’, and provides a powerful tool for mathematical thought.

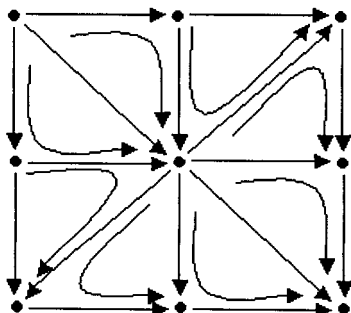
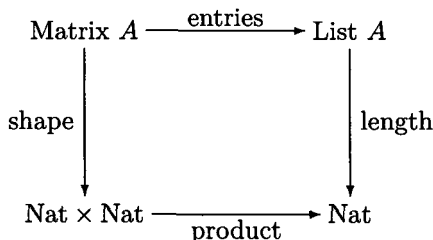


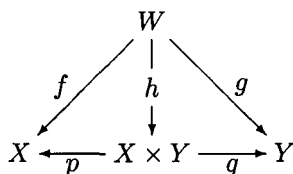
Fig. 2.1 A *commutative flow* (denoted by curved arrows) on a *triangulated digraph*. Commutativity of the whole diagram follows from commutativity of its triangular components.

As an example from linear algebra, consider an elementary diagrammatic description of matrices, using the following *pull-back diagram* [Barry (1993)]:



asserts that a matrix is determined by its shape, given by a pair of natural numbers representing the number of rows and columns, and its data, given by the matrix entries listed in some specified order.

Many properties of mathematical constructions may be represented by *universal properties* of diagrams [MacLane (1971)]. Consider the *Cartesian product*  $X \times Y$  of two sets, consisting as usual of all ordered pairs  $\langle x, y \rangle$  of elements  $x \in X$  and  $y \in Y$ . The projections  $\langle x, y \rangle \mapsto x$ ,  $\langle x, y \rangle \mapsto y$  of the product on its 'axes'  $X$  and  $Y$  are functions  $p : X \times Y \rightarrow X$ ,  $q : X \times Y \rightarrow Y$ . Any function  $h : W \rightarrow X \times Y$  from a third set  $W$  is uniquely determined by its composites  $p \circ h$  and  $q \circ h$ . Conversely, given  $W$  and two functions  $f$  and  $g$  as in the diagram below, there is a unique function  $h$  which makes the following diagram commute:



This property describes the Cartesian product  $X \times Y$  uniquely; the same diagram, read in the category of topological spaces or of groups, describes uniquely the Cartesian product of spaces or of the direct product of groups.

The construction 'Cartesian product' is technically called a 'functor' because it applies suitably both to the sets and to the functions between them; two functions  $k : X \rightarrow X'$  and  $l : Y \rightarrow Y'$  have a function  $k \times l$  as their Cartesian product:

$$k \times l : X \times Y \rightarrow X' \times Y', \quad \langle x, y \rangle \mapsto \langle kx, ly \rangle.$$

### 2.1.1.5 Groups and Related Algebraic Structures

As already stated, the basic functional unit of lower biodynamics is the special Euclidean group  $SE(3)$  of rigid body motions. In general, a *group* is a pointed set  $(G, e)$  with a *multiplication*  $\mu : G \times G \rightarrow G$  and an *inverse*  $\nu : G \rightarrow G$  such that the following diagrams commute [Switzer (1975)]:

$$\begin{array}{c}
 \begin{array}{ccccc}
 G & \xrightarrow{(e, 1)} & G \times G & \xrightarrow{(1, e)} & G \\
 & \searrow 1 & \downarrow \mu & \nearrow 1 & \\
 & & G & & 
 \end{array} \\
 (1) \\
 (e \text{ is a two-sided identity}) \\
 \\
 \begin{array}{ccc}
 G \times G \times G & \xrightarrow{\mu \times 1} & G \times G \\
 \downarrow 1 \times \mu & & \downarrow \mu \\
 G \times G & \xrightarrow{\mu} & G
 \end{array} \\
 (2) \\
 (\text{associativity}) \\
 \\
 \begin{array}{ccccc}
 G & \xrightarrow{(\nu, 1)} & G \times G & \xrightarrow{(1, \nu)} & G \\
 & \searrow e & \downarrow \mu & \nearrow e & \\
 & & G & & 
 \end{array} \\
 (3) \\
 (\text{inverse}).
 \end{array}$$

Here  $e : G \rightarrow G$  is the constant map  $e(g) = e$  for all  $g \in G$ .  $(e, 1)$  means the map such that  $(e, 1)(g) = (e, g)$ , etc. A group  $G$  is called *commutative* or *Abelian group* if in addition the following diagram commutes

$$\begin{array}{ccc}
 G \times G & \xrightarrow{T} & G \times G \\
 & \searrow \mu & \nearrow \mu \\
 & & G
 \end{array}$$

where  $T : G \times G \rightarrow G \times G$  is the switch map  $T(g_1, g_2) = (g_2, g_1)$ , for all  $(g_1, g_2) \in G \times G$ .

A group  $G$  *acts* (on the left) on a set  $A$  if there is a function  $\alpha : G \times A \rightarrow$

A such that the following diagrams commute [Switzer (1975)]:

$$\begin{array}{ccc}
 A & \xrightarrow{(e, 1)} & G \times A \\
 & \searrow 1 & \downarrow \alpha \\
 & & A
 \end{array}
 \quad (1)$$

$(e, 1)(x) = (e, x) \quad \text{for all } x \in A$

$$\begin{array}{ccccc}
 G \times G \times A & \xrightarrow{1 \times \alpha} & G \times A \\
 \mu \times 1 \downarrow & & \downarrow \alpha \\
 G \times A & \xrightarrow{\alpha} & A
 \end{array}
 \quad (2)$$

The *orbits* of the action are the sets  $Gx = \{gx : g \in G\}$  for all  $x \in A$ .

Given two groups  $(G, *)$  and  $(H, \cdot)$ , a *group homomorphism* from  $(G, *)$  to  $(H, \cdot)$  is a function  $h : G \rightarrow H$  such that for all  $x$  and  $y$  in  $G$  it holds that

$$h(x * y) = h(x) \cdot h(y).$$

From this property, one can deduce that  $h$  maps the identity element  $e_G$  of  $G$  to the identity element  $e_H$  of  $H$ , and it also maps inverses to inverses in the sense that  $h(x^{-1}) = h(x)^{-1}$ . Hence one can say that  $h$  is *compatible* with the *group structure*.

The *kernel*  $\text{Ker } h$  of a group homomorphism  $h : G \rightarrow H$  consists of all those elements of  $G$  which are sent by  $h$  to the identity element  $e_H$  of  $H$ ,

$$\text{Ker } h = \{x \in G : h(x) = e_H\}.$$

The *image*  $\text{Im } h$  of a group homomorphism  $h : G \rightarrow H$  consists of all elements of  $H$  which are sent by  $h$  to  $H$ , i.e.,

$$\text{Im } h = \{h(x) : x \in G\}.$$

The kernel is a *normal subgroup* of  $G$  and the image is a *subgroup* of  $H$ . The homomorphism  $h$  is *injective* (and called a *group monomorphism*) iff  $\text{Ker } h = e_G$ , i.e., iff the kernel of  $h$  consists of the identity element of  $G$  only.

Similarly, a *ring* is a set  $S$  together with two binary operators  $+$  and  $*$  (commonly interpreted as addition and multiplication, respectively) satisfying the following conditions:

- (1) Additive associativity: For all  $a, b, c \in S$ ,  $(a + b) + c = a + (b + c)$ ,
- (2) Additive commutativity: For all  $a, b \in S$ ,  $a + b = b + a$ ,
- (3) Additive identity: There exists an element  $0 \in S$  such that for all  $a \in S$ ,  
 $0 + a = a + 0 = a$ ,
- (4) Additive inverse: For every  $a \in S$  there exists  $-a \in S$  such that  $a + (-a) = (-a) + a = 0$ ,
- (5) Multiplicative associativity: For all  $a, b, c \in S$ ,  $(a * b) * c = a * (b * c)$ ,
- (6) Left and right distributivity: For all  $a, b, c \in S$ ,  $a * (b + c) = (a * b) + (a * c)$   
 and  $(b + c) * a = (b * a) + (c * a)$ .

A ring (the term introduced by *D. Hilbert*) is therefore an Abelian group under addition and a semigroup under multiplication. A ring that is commutative under multiplication, has a unit element, and has no divisors of zero is called an *integral domain*. A ring which is also a commutative multiplication group is called a *field*. The simplest rings are the integers  $\mathbb{Z}$ , polynomials  $\mathbb{R}[x]$  and  $\mathbb{R}[x, y]$  in one and two variables, and square  $n \times n$  real matrices.

An *ideal* is a subset  $\mathcal{I}$  of elements in a ring  $R$  which forms an additive group and has the property that, whenever  $x$  belongs to  $R$  and  $y$  belongs to  $\mathcal{I}$ , then  $xy$  and  $yx$  belong to  $\mathcal{I}$ . For example, the set of even integers is an ideal in the ring of integers  $\mathbb{Z}$ . Given an ideal  $\mathcal{I}$ , it is possible to define a factor ring  $R/\mathcal{I}$ .

A ring is called *left* (respectively, *right*) *Noetherian* if it does not contain an infinite ascending chain of left (respectively, right) ideals. In this case, the ring in question is said to satisfy the ascending chain condition on left (respectively, right) ideals. A *ring* is said to be *Noetherian* if it is both left and right Noetherian. If a ring  $R$  is Noetherian, then the following are equivalent: (i)  $R$  satisfies the ascending chain condition on ideals, (ii) every ideal of  $R$  is finitely generated, and (iii) every set of ideals contains a maximal element.

A *module* is a mathematical object in which things can be added together commutatively by multiplying coefficients and in which most of the rules of manipulating vectors hold. A module is abstractly very similar to a vector space, although in modules, coefficients are taken in rings which are much more general algebraic objects than the fields used in vector spaces.

A module taking its coefficients in a ring  $R$  is called a module over  $R$  or  $R$ -module. Modules are the basic tool of homological algebra.

Examples of modules include the set of integers  $\mathbb{Z}$ , the cubic lattice in  $d$  dimensions  $\mathbb{Z}^d$ , and the group ring of a group.  $\mathbb{Z}$  is a module over itself. It is closed under addition and subtraction. Numbers of the form  $n\alpha$  for  $n \in \mathbb{Z}$  and  $\alpha$  a fixed integer form a submodule since, for  $(n, m) \in \mathbb{Z}$ ,  $n\alpha \pm m\alpha = (n \pm m)\alpha$  and  $(n \pm m)$  is still in  $\mathbb{Z}$ . Also, given two integers  $a$  and  $b$ , the smallest module containing  $a$  and  $b$  is the module for their greatest common divisor,  $\alpha = GCD(a, b)$ .

A module  $M$  is a *Noetherian module* if it obeys the ascending chain condition with respect to inclusion, i.e., if every set of increasing sequences of submodules eventually becomes constant. If a module  $M$  is Noetherian, then the following are equivalent: (i)  $M$  satisfies the ascending chain condition on submodules, (ii) every submodule of  $M$  is finitely generated, and (iii) every set of submodules of  $M$  contains a maximal element.

Let  $I$  be a partially ordered set. A *direct system* of  $R$ -modules over  $I$  is an ordered pair  $\{M_i, \varphi_j^i\}$  consisting of an indexed family of modules  $\{M_i : i \in I\}$  together with a family of homomorphisms  $\{\varphi_j^i : M_i \rightarrow M_j\}$  for  $i \leq j$ , such that  $\varphi_i^i = 1_{M_i}$  for all  $i$  and such that the following diagram commutes whenever  $i \leq j \leq k$

$$\begin{array}{ccc} M_i & \xrightarrow{\varphi_k^i} & M_k \\ & \searrow \varphi_k^j & \nearrow \varphi_j^i \\ & M_j & \end{array}$$

Similarly, an *inverse system* of  $R$ -modules over  $I$  is an ordered pair  $\{M_i, \psi_i^j\}$  consisting of an indexed family of modules  $\{M_i : i \in I\}$  together with a family of homomorphisms  $\{\psi_i^j : M_j \rightarrow M_i\}$  for  $i \leq j$ , such that  $\psi_i^i = 1_{M_i}$  for all  $i$  and such that the following diagram commutes whenever  $i \leq j \leq k$

$$\begin{array}{ccc} M_k & \xrightarrow{\psi_i^k} & M_i \\ & \searrow \psi_j^k & \nearrow \psi_i^j \\ & M_j & \end{array}$$

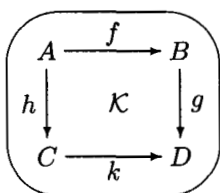
## 2.1.2 Categories

A category is a generic mathematical structure consisting of a collection of *objects* (sets with possibly additional structure), with a corresponding collection of *arrows*, or *morphisms*, between objects (agreeing with this additional structure). A category  $\mathcal{K}$  is defined as a pair  $(\text{Ob}(\mathcal{K}), \text{Mor}(\mathcal{K}))$  of generic objects  $A, B, \dots$  in  $\text{Ob}(\mathcal{K})$  and generic arrows  $f : A \rightarrow B$ ,  $g : B \rightarrow C, \dots$  in  $\text{Mor}(\mathcal{K})$  between objects, with *associative composition*:

$$A \xrightarrow{f} B \xrightarrow{g} C = A \xrightarrow{f \circ g} C,$$

and *identity* (loop) arrow. (Note that in topological literature,  $\text{Hom}(\mathcal{K})$  or  $\text{hom}(\mathcal{K})$  is used instead of  $\text{Mor}(\mathcal{K})$ ; see [Switzer (1975)]).

A category  $\mathcal{K}$  is usually depicted as a *commutative diagram* (i.e., a diagram with a common *initial object*  $A$  and *final object*  $D$ ):



To make this more precise, we say that a *category*  $\mathcal{K}$  is defined if we have:

- (1) A *class of objects*  $\{A, B, C, \dots\}$  of  $\mathcal{K}$ , denoted by  $\text{Ob}(\mathcal{K})$ ;
- (2) A *set of morphisms*, or *arrows*  $\text{Mor}_{\mathcal{K}}(A, B)$ , with elements  $f : A \rightarrow B$ , defined for any *ordered pair*  $(A, B) \in \mathcal{K}$ , such that for two different pairs  $(A, B) \neq (C, D)$  in  $\mathcal{K}$ , we have  $\text{Mor}_{\mathcal{K}}(A, B) \cap \text{Mor}_{\mathcal{K}}(C, D) = \emptyset$ ;
- (3) For any *triplet*  $(A, B, C) \in \mathcal{K}$  with  $f : A \rightarrow B$  and  $g : B \rightarrow C$ , there is a *composition* of morphisms

$$\text{Mor}_{\mathcal{K}}(B, C) \times \text{Mor}_{\mathcal{K}}(A, B) \ni (g, f) \rightarrow g \circ f \in \text{Mor}_{\mathcal{K}}(A, C),$$

written schematically as

$$\frac{f : A \rightarrow B, \quad g : B \rightarrow C}{g \circ f : A \rightarrow C}.$$

If we have a morphism  $f \in \text{Mor}_{\mathcal{K}}(A, B)$ , (otherwise written  $f : A \rightarrow B$ , or  $A \xrightarrow{f} B$ ), then  $A = \text{dom}(f)$  is a *domain* of  $f$ , and  $B = \text{cod}(f)$  is a *codomain* of  $f$  (of which *range* of  $f$  is a subset) and denoted  $B = \text{ran}(f)$ .



To make  $\mathcal{K}$  a category, it must also fulfill the following two properties:

- (1) *Associativity of morphisms*: for all  $f \in \text{Mor}_{\mathcal{K}}(A, B)$ ,  $g \in \text{Mor}_{\mathcal{K}}(B, C)$ , and  $h \in \text{Mor}_{\mathcal{K}}(C, D)$ , we have  $h \circ (g \circ f) = (h \circ g) \circ f$ ; in other words, the following diagram is commutative

$$\begin{array}{ccc}
 A & \xrightarrow{h \circ (g \circ f) = (h \circ g) \circ f} & D \\
 f \downarrow & & \uparrow h \\
 B & \xrightarrow{g} & C
 \end{array}$$

- (2) *Existence of identity morphism*: for every object  $A \in \text{Ob}(\mathcal{K})$  exists a unique identity morphism  $1_A \in \text{Mor}_{\mathcal{K}}(A, A)$ ; for any two morphisms  $f \in \text{Mor}_{\mathcal{K}}(A, B)$ , and  $g \in \text{Mor}_{\mathcal{K}}(B, C)$ , compositions with identity morphism  $1_B \in \text{Mor}_{\mathcal{K}}(B, B)$  give  $1_B \circ f = f$  and  $g \circ 1_B = g$ , i.e., the following diagram is commutative:

$$\begin{array}{ccccc}
 A & \xrightarrow{f} & B & \xrightarrow{g} & C \\
 & \searrow f & \downarrow 1_B & \nearrow g & \\
 & & B & & 
 \end{array}$$

The set of all morphisms of the category  $\mathcal{K}$  is denoted

$$\text{Mor}(\mathcal{K}) = \bigcup_{A, B \in \text{Ob}(\mathcal{K})} \text{Mor}_{\mathcal{K}}(A, B).$$

If for two morphisms  $f \in \text{Mor}_{\mathcal{K}}(A, B)$  and  $g \in \text{Mor}_{\mathcal{K}}(B, A)$  the equality  $g \circ f = 1_A$  is valid, then the morphism  $g$  is said to be *left inverse* (or *retraction*), of  $f$ , and  $f$  *right inverse* (or *section*) of  $g$ . A morphism which is both right and left inverse of  $f$  is said to be *two-sided inverse* of  $f$ .

A morphism  $m : A \rightarrow B$  is called *monomorphism* in  $\mathcal{K}$  (i.e., *one-to-one*, or *injection* map), if for any two parallel morphisms  $f_1, f_2 : C \rightarrow A$  in  $\mathcal{K}$  the equality  $m \circ f_1 = m \circ f_2$  implies  $f_1 = f_2$ ; in other words,  $m$  is monomorphism if it is *left cancellable*. Any morphism with a left inverse is monomorphism.

A morphism  $e : A \rightarrow B$  is called *epimorphism* in  $\mathcal{K}$  (i.e., *onto*, or *surjection* map), if for any two morphisms  $g_1, g_2 : B \rightarrow C$  in  $\mathcal{K}$  the equality  $g_1 \circ e = g_2 \circ e$  implies  $g_1 = g_2$ ; in other words,  $e$  is epimorphism if it is *right cancellable*. Any morphism with a right inverse is epimorphism.

A morphism  $f : A \rightarrow B$  is called *isomorphism* in  $\mathcal{K}$  (denoted as  $f : A \cong B$ ) if there exists a morphism  $f^{-1} : B \rightarrow A$  which is a two-sided inverse of  $f$  in  $\mathcal{K}$ . The relation of isomorphism is reflexive, symmetric, and transitive, i.e., equivalence relation.

For example, an isomorphism in the category of sets is called a set-isomorphism, or a *bijection*, in the category of topological spaces is called a topological isomorphism, or a *homeomorphism*, in the category of differentiable manifolds is called a differentiable isomorphism, or a *diffeomorphism*.

A morphism  $f \in \text{Mor}_{\mathcal{K}}(A, B)$  is *regular* if there exists a morphism  $g : B \rightarrow A$  in  $\mathcal{K}$  such that  $f \circ g \circ f = f$ . Any morphism with either a left or a right inverse is regular.

An object  $T$  is a *terminal object* in  $\mathcal{K}$  if to each object  $A \in \text{Ob}(\mathcal{K})$  there is exactly one arrow  $A \rightarrow T$ . An object  $S$  is an *initial object* in  $\mathcal{K}$  if to each object  $A \in \text{Ob}(\mathcal{K})$  there is exactly one arrow  $S \rightarrow A$ . A *null object*  $Z \in \text{Ob}(\mathcal{K})$  is an object which is both initial and terminal; it is unique up to isomorphism. For any two objects  $A, B \in \text{Ob}(\mathcal{K})$  there is a unique morphism  $A \rightarrow Z \rightarrow B$  (the composite through  $Z$ ), called the *zero morphism* from  $A$  to  $B$ .

A notion of subcategory is analogous to the notion of subset. A subcategory  $\mathcal{L}$  of a category  $\mathcal{K}$  is said to be a *complete subcategory* iff for any objects  $A, B \in \mathcal{L}$ , every morphism  $A \rightarrow B$  of  $\mathcal{L}$  is in  $\mathcal{K}$ .

The standard categories that we will use in this book are:

- $\mathcal{S}$  – all sets as objects and all functions between them as morphisms;
- $\mathcal{PS}$  – all pointed sets as objects and all functions between them preserving base point as morphisms;
- $\mathcal{V}$  – all vector spaces as objects and all linear maps between them as morphisms;
- $\mathcal{B}$  – Banach spaces over  $\mathbb{R}$  as objects and bounded linear maps between them as morphisms;
- $\mathcal{G}$  – all groups as objects, all homomorphisms between them as morphisms;
- $\mathcal{A}$  – Abelian groups as objects, homomorphisms between them as morphisms;
- $\mathcal{AL}$  – all algebras (over a given field  $\mathbb{K}$ ) as objects, all their homomorphisms between them as morphisms;
- $\mathcal{T}$  – all topological spaces as objects, all continuous functions between them as morphisms;
- $\mathcal{PT}$  – pointed topological spaces as objects, continuous functions be-

tween them preserving base point as morphisms;

- $\mathcal{TG}$  – all topological groups as objects, their continuous homomorphisms as morphisms;
- $\mathcal{M}$  – all smooth manifolds as objects, all smooth maps between them as morphisms;
- $\mathcal{M}_n$  –  $n$ D manifolds as objects, their local diffeomorphisms as morphisms;
- $\mathcal{LG}$  – all Lie groups as objects, all smooth homomorphisms between them as morphisms;
- $\mathcal{LAL}$  – all Lie algebras (over a given field  $\mathbb{K}$ ) as objects, all smooth homomorphisms between them as morphisms;
- $\mathcal{TB}$  – all tangent bundles as objects, all smooth tangent maps between them as morphisms;
- $\mathcal{T}^*\mathcal{B}$  – all cotangent bundles as objects, all smooth cotangent maps between them as morphisms.

A *groupoid* is a category in which every morphism is invertible. A typical groupoid is the *fundamental groupoid*  $\Pi_1(X)$  of a topological space  $X$ . An object of  $\Pi_1(X)$  is a point  $x \in X$ , and a morphism  $x \rightarrow x'$  of  $\Pi_1(X)$  is a homotopy class of paths  $f$  from  $x$  to  $x'$ . The *composition* of paths  $g : x' \rightarrow x''$  and  $f : x \rightarrow x'$  is the path  $h$  which is ‘ $f$  followed by  $g$ ’. Composition applies also to homotopy classes, and makes  $\Pi_1(X)$  a category and a groupoid (the inverse of any path is the same path traced in the opposite direction).

A *group* is a groupoid with one object, i.e., a *category with one object* in which *all morphisms are isomorphisms*. Therefore, if we try to generalize the concept of a group, keeping associativity as an essential property, we get the notion of a category.

A category is *discrete* if every morphism is an identity. A *monoid* is a category with one object. A *group* is a category with one object in which every morphism has a two-sided inverse under composition.

*Homological algebra* was the progenitor of category theory (see e.g., [Dieudonne (1988)]). Generalizing L. Euler’s formula  $f + v = e + 2$  for the faces, vertices and edges of a convex polyhedron, E. Betti defined *numerical invariants of spaces* by formal addition and subtraction of faces of various dimensions; H. Poincaré formalized these and introduced homology. E. Noether stressed the fact that these calculations go on in Abelian groups, and that the operation  $\partial_n$  taking a face of dimension  $n$  to the alternating sum of faces of dimension  $n-1$  which form its boundary is a homomorphism,

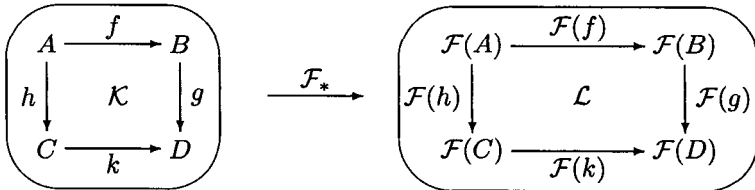
and it also satisfies  $\partial_n \cdot \partial_{n+1} = 0$ . There are many ways of approximating a given space by polyhedra, but the quotient  $H_n = \text{Ker } \partial_n / \text{Im } \partial_{n+1}$  is an invariant, the *homology group*. Since Noether, the groups have been the object of study instead of their dimensions, which are the *Betti numbers* (see chapter 5 for details).

### 2.1.3 Functors

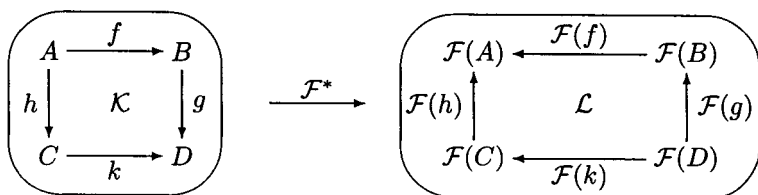
In algebraic topology, one attempts to assign to every topological space  $X$  some algebraic object  $\mathcal{F}(X)$  in such a way that to every  $C^0$ -function  $f : X \rightarrow Y$  there is assigned a homomorphism  $\mathcal{F}(f) : \mathcal{F}(X) \rightarrow \mathcal{F}(Y)$  (see [Switzer (1975); Dodson and Parker (1997)]). One advantage of this procedure is, e.g., that if one is trying to prove the non-existence of a  $C^0$ -function  $f : X \rightarrow Y$  with certain properties, one may find it relatively easy to prove the non-existence of the corresponding algebraic function  $\mathcal{F}(f)$  and hence deduce that  $f$  could not exist. In other words,  $\mathcal{F}$  is to be a ‘homomorphism’ from one category (e.g.,  $\mathcal{T}$ ) to another (e.g.,  $\mathcal{G}$  or  $\mathcal{A}$ ). Formalization of this notion is a *functor*.

A functor is a generic *picture* projecting one category into another. Let  $\mathcal{K} = (\text{Ob}(\mathcal{K}), \text{Mor}(\mathcal{K}))$  be a *source* (or domain) *category* and  $\mathcal{L} = (\text{Ob}(\mathcal{L}), \text{Mor}(\mathcal{L}))$  be a *target* (or codomain) *category*. A functor  $\mathcal{F} = (\mathcal{F}_O, \mathcal{F}_M)$  is defined as a pair of maps,  $\mathcal{F}_O : \text{Ob}(\mathcal{K}) \rightarrow \text{Ob}(\mathcal{L})$  and  $\mathcal{F}_M : \text{Mor}(\mathcal{K}) \rightarrow \text{Mor}(\mathcal{L})$ , preserving categorical symmetry (i.e., commutativity of all diagrams) of  $\mathcal{K}$  in  $\mathcal{L}$ .

More precisely, a *covariant functor*, or simply a *functor*,  $\mathcal{F}_* : \mathcal{K} \rightarrow \mathcal{L}$  is a *picture* in the target category  $\mathcal{L}$  of (all objects and morphisms of) the source category  $\mathcal{K}$ :



Similarly, a *contravariant functor*, or a *cofunctor*,  $\mathcal{F}^* : \mathcal{K} \rightarrow \mathcal{L}$  is a *dual picture* with reversed arrows:



In other words, a *functor*  $\mathcal{F} : \mathcal{K} \rightarrow \mathcal{L}$  from a *source* category  $\mathcal{K}$  to a *target* category  $\mathcal{L}$ , is a pair  $\mathcal{F} = (\mathcal{F}_O, \mathcal{F}_M)$  of maps  $\mathcal{F}_O : \text{Ob}(\mathcal{K}) \rightarrow \text{Ob}(\mathcal{L})$ ,  $\mathcal{F}_M : \text{Mor}(\mathcal{K}) \rightarrow \text{Mor}(\mathcal{L})$ , such that

- (1) If  $f \in \text{Mor}_{\mathcal{K}}(A, B)$  then  $\mathcal{F}_M(f) \in \text{Mor}_{\mathcal{L}}(\mathcal{F}_O(A), \mathcal{F}_O(B))$  in case of the *covariant* functor  $\mathcal{F}_*$ , and  $\mathcal{F}_M(f) \in \text{Mor}_{\mathcal{L}}(\mathcal{F}_O(B), \mathcal{F}_O(A))$  in case of the *contravariant* functor  $\mathcal{F}^*$ ;
- (2) For all  $A \in \text{Ob}(\mathcal{K}) : \mathcal{F}_M(1_A) = 1_{\mathcal{F}_O(A)}$ ;
- (3) For all  $f, g \in \text{Mor}(\mathcal{K})$ : if  $\text{cod}(f) = \text{dom}(g)$ , then  
 $\mathcal{F}_M(g \circ f) = \mathcal{F}_M(g) \circ \mathcal{F}_M(f)$  in case of the *covariant* functor  $\mathcal{F}_*$ , and  
 $\mathcal{F}_M(g \circ f) = \mathcal{F}_M(f) \circ \mathcal{F}_M(g)$  in case of the *contravariant* functor  $\mathcal{F}^*$ .

Category theory originated in algebraic topology, which tried to assign algebraic invariants to topological structures. The golden rule of such *invariants* is that they should be *functors*. For example, the *fundamental group*  $\pi_1$  is a functor. Algebraic topology constructs a group called the *fundamental group*  $\pi_1(X)$  from any topological space  $X$ , which keeps track of how many holes the space  $X$  has. But also, any map between topological spaces determines a homomorphism  $\phi : \pi_1(X) \rightarrow \pi_1(Y)$  of the fundamental groups. So the fundamental group is really a functor  $\pi_1 : \mathcal{T} \rightarrow \mathcal{G}$ . This allows us to completely transpose any situation involving *spaces* and *continuous maps* between them to a parallel situation involving *groups* and *homomorphisms* between them, and thus reduce some topology problems to algebra problems.

Also, singular homology in a given dimension  $n$  assigns to each topological space  $X$  an Abelian group  $H_n(X)$ , its *nth homology group* of  $X$ , and also to each continuous map  $f : X \rightarrow Y$  of spaces a corresponding homomorphism  $H_n(f) : H_n(X) \rightarrow H_n(Y)$  of groups, and this in such a way that  $H_n(X)$  becomes a functor  $H_n : \mathcal{T} \rightarrow \mathcal{A}$ .

The leading idea in the *use of functors in topology* is that  $H_n$  or  $\pi_n$  gives an algebraic picture or image not just of the topological spaces  $X, Y$  but also of all the continuous maps  $f : X \rightarrow Y$  between them.

Similarly, there is a functor  $\Pi_1 : \mathcal{T} \rightarrow \mathcal{G}$ , called the ‘fundamental groupoid functor’, which plays a very basic role in algebraic topology. Here’s how we get from any space  $X$  its ‘fundamental groupoid’  $\Pi_1(X)$ . To say what the groupoid  $\Pi_1(X)$  is, we need to say what its objects and morphisms are. The objects in  $\Pi_1(X)$  are just the *points* of  $X$  and the morphisms are just certain equivalence classes of *paths* in  $X$ . More precisely, a morphism  $f : x \rightarrow y$  in  $\Pi_1(X)$  is just an equivalence class of continuous paths from  $x$  to  $y$ , where two paths from  $x$  to  $y$  are decreed equivalent if one can be continuously deformed to the other while not moving the endpoints. (If this equivalence relation holds we say the two paths are ‘homotopic’, and we call the equivalence classes ‘homotopy classes of paths’ (see [MacLane (1971); Switzer (1975)]).

For each category  $\mathcal{K}$ , the *identity functor*  $I_{\mathcal{K}}$  takes every  $\mathcal{K}$ -object and every  $\mathcal{K}$ -morphism to itself.

Given a category  $\mathcal{K}$  and its subcategory  $\mathcal{L}$ , we have an *inclusion functor*  $\text{In} : \mathcal{K} \rightarrow \mathcal{K}$ .

Given a category  $\mathcal{K}$ , a *diagonal functor*  $\Delta : \mathcal{K} \rightarrow \mathcal{K}$  takes each object  $A \in \mathcal{K}$  to the object  $(A, A)$  in the product category  $\mathcal{K} \times \mathcal{K}$ .

Given a category  $\mathcal{K}$  and a category of sets  $\mathcal{S}$ , each object  $A \in \mathcal{K}$  determines a *covariant Hom-functor*  $\mathcal{K}[A, \_] : \mathcal{K} \rightarrow \mathcal{S}$ , a *contravariant Hom-functor*  $\mathcal{K}[\_, A] : \mathcal{K} \rightarrow \mathcal{S}$ , and a *Hom-bifunctor*  $\mathcal{K}[\_, \_] : \mathcal{K}^{\text{op}} \times \mathcal{K} \rightarrow \mathcal{S}$ .

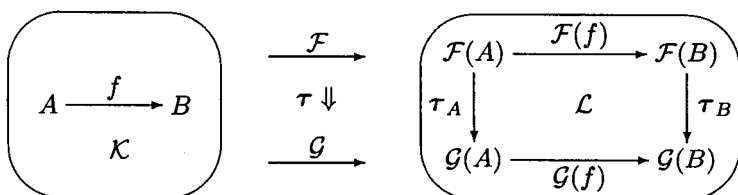
A functor  $\mathcal{F} : \mathcal{K} \rightarrow \mathcal{L}$  is a *faithful functor* if for all  $A, B \in \text{Ob}(\mathcal{K})$  and for all  $f, g \in \text{Mor}_{\mathcal{K}}(A, B)$ ,  $\mathcal{F}(f) = \mathcal{F}(g)$  implies  $f = g$ ; it is a *full functor* if for every  $h \in \text{Mor}_{\mathcal{L}}(\mathcal{F}(A), \mathcal{F}(B))$ , there is  $g \in \text{Mor}_{\mathcal{K}}(A, B)$  such that  $h = \mathcal{F}(g)$ ; it is a *full embedding* if it is both full and faithful.

A *representation of a group* is a functor  $\mathcal{F} : \mathcal{G} \rightarrow \mathcal{V}$ .

Similarly, we can define a *representation of a category* to be a functor  $\mathcal{F} : \mathcal{K} \rightarrow \mathcal{V}$  from the 2-category  $\mathcal{K}$  (a ‘big’ category including all ordinary, or ‘small’ categories, see subsection (2.1.7.1) below) to the category of vector spaces  $\mathcal{V}$ . In this way, a category is a generalization of a group and group representations are a special case of category representations.

#### 2.1.4 Natural Transformations

A *natural transformation* (i.e., a *functor morphism*)  $\tau : \mathcal{F} \rightarrow \mathcal{G}$  is a map between two functors of the same variance,  $(\mathcal{F}, \mathcal{G}) : \mathcal{K} \rightrightarrows \mathcal{L}$ , preserving categorical symmetry:



More precisely, all functors of the same variance from a source category  $\mathcal{K}$  to a target category  $\mathcal{L}$  form themselves objects of the *functor category*  $\mathcal{L}^{\mathcal{K}}$ . Morphisms of  $\mathcal{L}^{\mathcal{K}}$ , called *natural transformations*, are defined as follows.

Let  $\mathcal{F} : \mathcal{K} \rightarrow \mathcal{L}$  and  $\mathcal{G} : \mathcal{K} \rightarrow \mathcal{L}$  be two functors of the same variance from a category  $\mathcal{K}$  to a category  $\mathcal{L}$ . Natural transformation  $\mathcal{F} \xrightarrow{\tau} \mathcal{G}$  is a family of morphisms such that for all  $f \in \text{Mor}_{\mathcal{K}}(A, B)$  in the source category  $\mathcal{K}$ , we have  $\mathcal{G}(f) \circ \tau_A = \tau_B \circ \mathcal{F}(f)$  in the target category  $\mathcal{L}$ . Then we say that the *component*  $\tau_A : \mathcal{F}(A) \rightarrow \mathcal{G}(A)$  is *natural in A*.

If we think of a functor  $\mathcal{F}$  as giving a *picture* in the target category  $\mathcal{L}$  of (all the objects and morphisms of) the source category  $\mathcal{K}$ , then a natural transformation  $\tau$  represents a set of morphisms mapping the picture  $\mathcal{F}$  to another picture  $\mathcal{G}$ , preserving the commutativity of all diagrams.

An invertible natural transformation, such that all components  $\tau_A$  are isomorphisms) is called a *natural equivalence* (or, *natural isomorphism*). In this case, the inverses  $(\tau_A)^{-1}$  in  $\mathcal{L}$  are the components of a natural isomorphism  $(\tau)^{-1} : \mathcal{G} \xrightarrow{*} \mathcal{F}$ . Natural equivalences are among the most important *metamathematical constructions* in algebraic topology (see [Switzer (1975)]).

For example, let  $\mathcal{B}$  be the category of Banach spaces over  $\mathbb{R}$  and bounded linear maps. Define  $D : \mathcal{B} \rightarrow \mathcal{B}$  by taking  $D(X) = X^* =$  Banach space of bounded linear functionals on a space  $X$  and  $D(f) = f^*$  for  $f : X \rightarrow Y$  a bounded linear map. Then  $D$  is a cofunctor.  $D^2 = D \circ D$  is also a functor. We also have the identity functor  $1 : \mathcal{B} \rightarrow \mathcal{B}$ . Define  $T : 1 \rightarrow D \circ D$  as follows: for every  $X \in \mathcal{B}$  let  $T(X) : X \rightarrow D^2X = X^{**}$  be the *natural inclusion* – that is, for  $x \in X$  we have  $[T(X)(x)](f) = f(x)$  for every  $f \in X^*$ .  $T$  is a natural transformation. On the subcategory of finite-dimensional Banach spaces  $T$  is even a natural equivalence. The largest subcategory of  $\mathcal{B}$  on which  $T$  is a natural equivalence is called the category of reflexive Banach spaces [Switzer (1975)].

As S. Eilenberg and S. MacLane first observed, ‘category’ has been defined in order to define ‘functor’ and ‘functor’ has been defined in order to define ‘natural transformation’ [MacLane (1971)].

### 2.1.5 Limits and Colimits

In abstract algebra constructions are often defined by an abstract property which requires the existence of unique morphisms under certain conditions. These properties are called *universal properties*. The *limit* of a functor generalizes the notions of inverse limit and product used in various parts of mathematics. The dual notion, *colimit*, generalizes direct limits and direct sums. Limits and colimits are defined via universal properties and provide many examples of *adjoint functors*.

A *limit* of a covariant functor  $\mathcal{F} : \mathcal{J} \rightarrow \mathcal{C}$  is an object  $L$  of  $\mathcal{C}$ , together with morphisms  $\phi_X : L \rightarrow \mathcal{F}(X)$  for every object  $X$  of  $\mathcal{J}$ , such that for every morphism  $f : X \rightarrow Y$  in  $\mathcal{J}$ , we have  $\mathcal{F}(f)\phi_X = \phi_Y$ , and such that the following *universal property* is satisfied: for any object  $N$  of  $\mathcal{C}$  and any set of morphisms  $\psi_X : N \rightarrow \mathcal{F}(X)$  such that for every morphism  $f : X \rightarrow Y$  in  $\mathcal{J}$ , we have  $\mathcal{F}(f)\psi_X = \psi_Y$ , there exists precisely one morphism  $u : N \rightarrow L$  such that  $\phi_X u = \psi_X$  for all  $X$ . If  $\mathcal{F}$  has a limit (which it need not), then the limit is defined up to a unique isomorphism, and is denoted by  $\lim \mathcal{F}$ .

Analogously, a *colimit* of the functor  $\mathcal{F} : \mathcal{J} \rightarrow \mathcal{C}$  is an object  $L$  of  $\mathcal{C}$ , together with morphisms  $\phi_X : \mathcal{F}(X) \rightarrow L$  for every object  $X$  of  $\mathcal{J}$ , such that for every morphism  $f : X \rightarrow Y$  in  $\mathcal{J}$ , we have  $\phi_Y \mathcal{F}(X) = \phi_X$ , and such that the following universal property is satisfied: for any object  $N$  of  $\mathcal{C}$  and any set of morphisms  $\psi_X : \mathcal{F}(X) \rightarrow N$  such that for every morphism  $f : X \rightarrow Y$  in  $\mathcal{J}$ , we have  $\psi_Y \mathcal{F}(X) = \psi_X$ , there exists precisely one morphism  $u : L \rightarrow N$  such that  $u\phi_X = \psi_X$  for all  $X$ . The colimit of  $\mathcal{F}$ , unique up to unique isomorphism if it exists, is denoted by  $\text{colim } \mathcal{F}$ .

Limits and colimits are related as follows: A functor  $\mathcal{F} : \mathcal{J} \rightarrow \mathcal{C}$  has a colimit iff for every object  $N$  of  $\mathcal{C}$ , the functor  $X \mapsto \text{Mor}_{\mathcal{C}}(\mathcal{F}(X), N)$  (which is a covariant functor on the dual category  $\mathcal{J}^{op}$ ) has a limit. If that is the case, then  $\text{Mor}_{\mathcal{C}}(\text{colim } \mathcal{F}, N) = \lim \text{Mor}_{\mathcal{C}}(\mathcal{F}(-), N)$  for every object  $N$  of  $\mathcal{C}$ .

### 2.1.6 The Adjunction

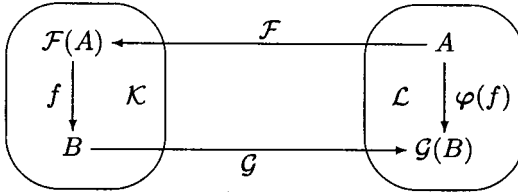
The most important functorial operation is adjunction; as S. MacLane once said, “Adjoint functors arise everywhere” [MacLane (1971)].

The *adjunction*  $\varphi : \mathcal{F} \dashv \mathcal{G}$  between two functors  $(\mathcal{F}, \mathcal{G}) : \mathcal{K} \rightleftarrows \mathcal{L}$  of *opposite variance* [Kan (1958)], represents a *weak functorial inverse*



$$\frac{f : \mathcal{F}(A) \rightarrow B}{\varphi(f) : A \rightarrow \mathcal{G}(B)}$$

forming a *natural equivalence*  $\varphi : \text{Mor}_{\mathcal{K}}(\mathcal{F}(A), B) \xrightarrow{\varphi} \text{Mor}_{\mathcal{L}}(A, \mathcal{G}(B))$ . The adjunction isomorphism is given by a *bijective correspondence* (a one-to-one and onto map on objects)  $\varphi : \text{Mor}(\mathcal{K}) \ni f \rightarrow \varphi(f) \in \text{Mor}(\mathcal{L})$  of isomorphisms in the two categories,  $\mathcal{K}$  (with a representative object  $A$ ), and  $\mathcal{L}$  (with a representative object  $B$ ). It can be depicted as a (non-commutative) diagram



In this case  $\mathcal{F}$  is called *left adjoint*, while  $\mathcal{G}$  is called *right adjoint*.

In other words, an *adjunction*  $\mathcal{F} \dashv \mathcal{G}$  between two functors  $(\mathcal{F}, \mathcal{G})$  of opposite variance, from a source category  $\mathcal{K}$  to a target category  $\mathcal{L}$ , is denoted by  $(\mathcal{F}, \mathcal{G}, \eta, \varepsilon) : \mathcal{K} \rightleftarrows \mathcal{L}$ . Here,  $\mathcal{F} : \mathcal{L} \rightarrow \mathcal{K}$  is the *left (upper) adjoint functor*,  $\mathcal{G} : \mathcal{K} \rightarrow \mathcal{L}$  is the *right (lower) adjoint functor*,  $\eta : 1_{\mathcal{L}} \rightarrow \mathcal{G} \circ \mathcal{F}$  is the *unit natural transformation* (or, *front adjunction*), and  $\varepsilon : \mathcal{F} \circ \mathcal{G} \rightarrow 1_{\mathcal{K}}$  is the *counit natural transformation* (or, *back adjunction*).

For example,  $\mathcal{K} = \mathcal{S}$  is the category of sets and  $\mathcal{L} = \mathcal{G}$  is the category of groups. Then  $\mathcal{F}$  turns any set into the *free group* on that set, while the ‘forgetful’ functor  $\mathcal{F}^*$  turns any group into the *underlying set* of that group. Similarly, all sorts of other ‘free’ and ‘underlying’ constructions are also left and right adjoints, respectively.

Right adjoints preserve categorical *limits*, and left adjoints preserve *colimits*.

The category  $\mathcal{C}$  is called a *cocomplete category* if every functor  $\mathcal{F} : \mathcal{J} \rightarrow \mathcal{C}$  has a colimit. The following categories are cocomplete:  $\mathcal{S}, \mathcal{G}, \mathcal{A}, \mathcal{T}$ , and  $\mathcal{PT}$ .

The importance of adjoint functors lies in the fact that every functor which has a left adjoint (and therefore is a right adjoint) is continuous. In the category  $\mathcal{A}$  of Abelian groups, this e.g., shows that the kernel of a product of homomorphisms is naturally identified with the product of the kernels. Also, limit functors themselves are continuous. A covariant functor

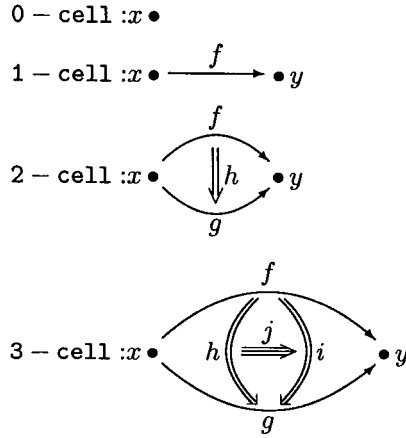
$\mathcal{F} : \mathcal{J} \rightarrow \mathcal{C}$  is *cocontinuous* if it transforms colimits into colimits. Every functor which has a right adjoint (and is a left adjoint) is cocontinuous.

The *analogy* between *adjoint functors* and *adjoint linear operators* relies upon a deeper analogy: just as in quantum theory the inner product  $\langle \phi, \psi \rangle$  represents the *amplitude* to pass from  $\phi$  to  $\psi$ , in category theory  $\text{Mor}(A, B)$  represents the *set of ways* to go from  $A$  to  $B$ . These are to Hilbert spaces as categories are to sets. The analogues of adjoint linear operators between Hilbert spaces are certain adjoint functors between 2-Hilbert spaces [Baez (1997); Baez and Dolan (1998)]. Similarly, the *adjoint representation* of a Lie group  $G$  is the linearized version of the action of  $G$  on itself by conjugation, i.e., for each  $g \in G$ , the inner automorphism  $x \mapsto gxg^{-1}$  gives a linear transformation  $\text{Ad}(g) : \mathfrak{g} \rightarrow \mathfrak{g}$ , from the Lie algebra  $\mathfrak{g}$  of  $G$  to itself.

### 2.1.7 *n*-Categories

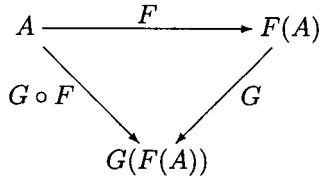
#### 2.1.7.1 Generalization to ‘Big’ *n*-Categories

If we think of a point in geometric space (either natural, or abstract) as an *object* (or, a 0-cell), and a path between two points as an *arrow* (or, a 1-morphism, or a 1-cell), we could think of a ‘path of paths’ as a 2-arrow (or, a 2-morphism, or a 2-cell), and a ‘path of paths of paths’ (or, a 3-morphism, or a 3-cell), etc. Here a ‘path of paths’ is just a continuous 1-parameter family of paths from between source and target points, which we can think of as tracing out a 2D surface, etc. In this way we get a ‘skeleton’ of an *n*-category, where a 1-category operates with 0-cells (objects) and 1-cells (arrows, causally connecting *source* objects with *target* ones), a 2-category operates with all the cells up to 2-cells [Bénabou (1967)], a 3-category operates with all the cells up to 3-cells, etc. This skeleton clearly demonstrates the *hierarchical self-similarity* of *n*-categories:

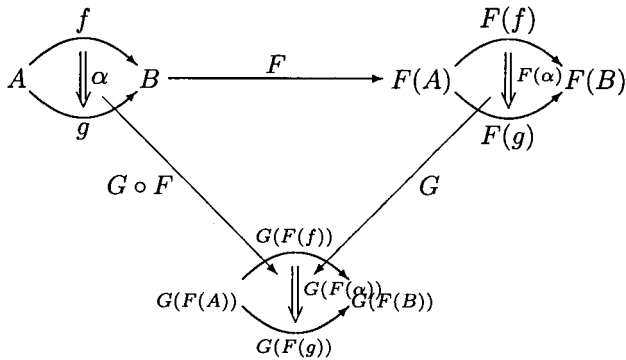


where triple arrow goes in the third direction, perpendicular to both single and double arrows. Categorical composition is defined by pasting arrows.

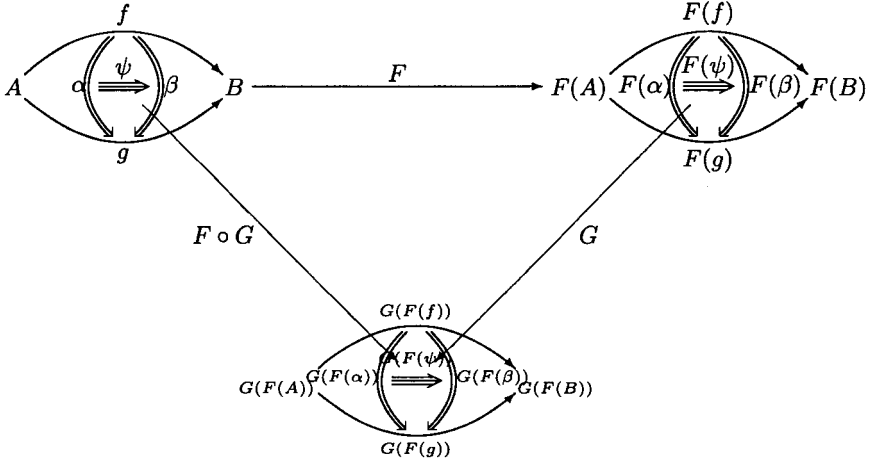
In this way defined, a 1-category can be depicted as a commutative triangle:



a 2-category is a commutative triangle:



a 3-category is a commutative triangle:



etc., up to  $n$ -categories.

Many deep-sounding results in mathematical sciences are obtained by the process of *categorification*<sup>2</sup> of the high school mathematics [Crane and Frenkel (1994); Baez and Dolan (1998)].

An  $n$ -category is a generic mathematical structure consisting of a collection of objects, a collection of arrows between objects, a collection of 2-arrows between arrows [Bénabou (1967)], a collection of 3-arrows between 2-arrows, and so on up to  $n$  [Baez (1997); Baez and Dolan (1998); Leinster (2002); Leinster (2003); Leinster (2004)].

More precisely, an  $n$ -category (for  $n \geq 0$ ) consists of:

- 0-cells, or objects,  $A, B, \dots$
- 1-cells, or arrows,  $A \xrightarrow{f} B$ , with a composition

$$A \xrightarrow{f} B \xrightarrow{g} C = A \xrightarrow{g \circ f} C$$

- 2-cells, 'arrows between arrows',  $A \begin{array}{c} \xrightarrow{f} \\ \Downarrow \alpha \\ \xrightarrow{g} \end{array} B$ , with vertical compo-

<sup>2</sup>Categorification means replacing sets with categories, functions with functors, and equations between functions by natural equivalences between functors. Iterating this process requires a theory of  $n$ -categories.

sitions (denoted by  $\circ$ ) and horizontal compositions (denoted by  $*$ ), respectively given by

$$\begin{array}{c} f \\ \curvearrowright \\ A \xrightarrow{g} B \\ \curvearrowleft \\ h \end{array} \Downarrow \alpha \quad = \quad \begin{array}{c} f \\ \curvearrowright \\ A \xrightarrow{h} B \\ \curvearrowleft \end{array} \Downarrow \beta \circ \alpha$$

and

$$\begin{array}{c} f \\ \curvearrowright \\ A \xrightarrow{g} A' \\ \curvearrowleft \end{array} \Downarrow \alpha \quad \begin{array}{c} f' \\ \curvearrowright \\ A' \xrightarrow{g'} A'' \\ \curvearrowleft \end{array} \Downarrow \alpha' \quad = \quad \begin{array}{c} f' \circ f \\ \curvearrowright \\ A \xrightarrow{g' \circ g} A'' \\ \curvearrowleft \end{array} \Downarrow \alpha' * \alpha$$

- 3-cells, 'arrows between arrows

$$\begin{array}{c} f \\ \curvearrowright \\ A \xrightarrow{\alpha} B \\ \curvearrowleft \\ g \end{array} \quad \begin{array}{c} \Gamma \\ \hline \end{array} \quad \begin{array}{c} \beta \\ \curvearrowleft \\ B \end{array}$$

between arrows',  $A \xrightarrow{\alpha} B$  (where the  $\Gamma$ -arrow goes in

a direction perpendicular to  $f$  and  $\alpha$ ), with various kinds of vertical, horizontal and mixed compositions,

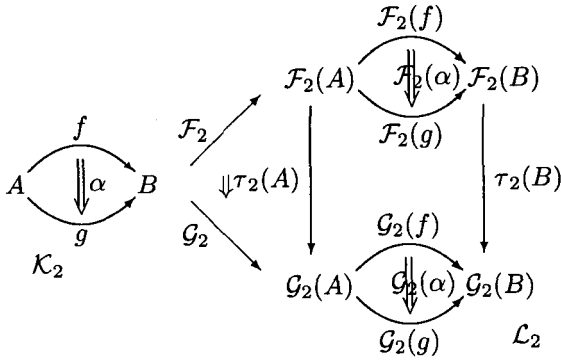
- etc., up to  $n$ -cells.

Calculus of  $n$ -categories has been developed as follows. First, there is  $\mathcal{K}_2$ , the 2-category of all ordinary (or small) categories.  $\mathcal{K}_2$  has categories  $\mathcal{K}, \mathcal{L}, \dots$  as objects, functors  $\mathcal{F}, \mathcal{G} : \mathcal{K} \Rightarrow \mathcal{L}$  as arrows, and natural transformations, like  $\tau : \mathcal{F} \rightarrow \mathcal{G}$  as 2-arrows.

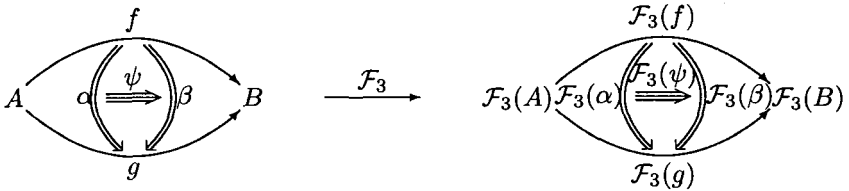
In a similar way, the arrows in a 3-category  $\mathcal{K}_3$  are 2-functors  $\mathcal{F}_2, \mathcal{G}_2, \dots$  sending objects in  $\mathcal{K}_2$  to objects in  $\mathcal{K}_2$ , arrows to arrows, and 2-arrows to 2-arrows, strictly preserving all the structure of  $\mathcal{K}_2$

$$\begin{array}{c} f \\ \curvearrowright \\ A \xrightarrow{g} B \\ \curvearrowleft \end{array} \Downarrow \alpha \quad \xrightarrow{\mathcal{F}_2} \quad \begin{array}{c} \mathcal{F}_2(f) \\ \curvearrowright \\ \mathcal{F}_2(A) \xrightarrow{\mathcal{F}_2(g)} \mathcal{F}_2(B) \\ \curvearrowleft \end{array} \Downarrow \mathcal{F}_2(\alpha)$$

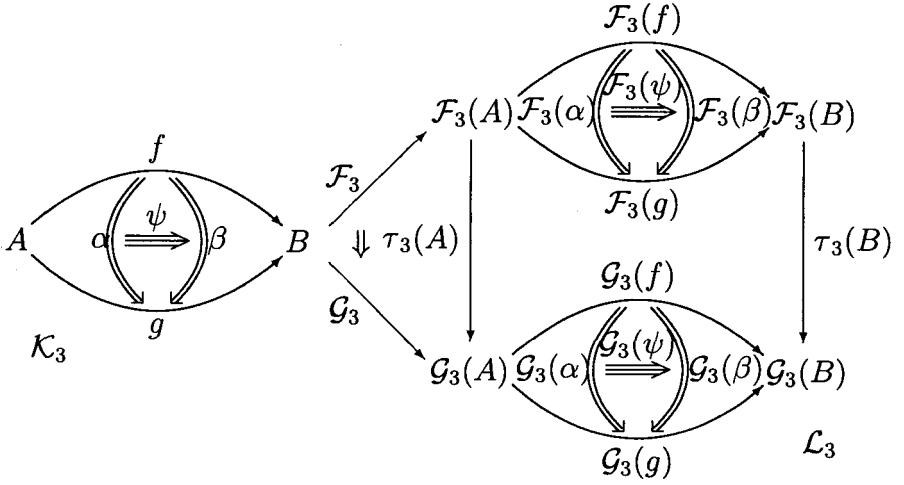
The 2-arrows in  $\mathcal{K}_3$  are 2-natural transformations, like  $\tau_2 : \mathcal{F}_2 \xRightarrow{2} \mathcal{G}_2$  between 2-functors  $\mathcal{F}_2, \mathcal{G}_2 : \mathcal{K}_2 \rightarrow \mathcal{L}_2$  that sends each object in  $\mathcal{K}_2$  to an arrow in  $\mathcal{L}_2$  and each arrow in  $\mathcal{K}_2$  to a 2-arrow in  $\mathcal{L}_2$ , and satisfies natural transformation-like conditions. We can visualize  $\tau_2$  as a prism going from one functorial picture of  $\mathcal{K}_2$  in  $\mathcal{L}_2$  to another, built using commutative squares:



Similarly, the arrows in a 4-category  $\mathcal{K}_4$  are 3-functors  $\mathcal{F}_3, \mathcal{G}_3, \dots$  sending objects in  $\mathcal{K}_3$  to objects in  $\mathcal{L}_3$ , arrows to arrows, and 2-arrows to 2-arrows, strictly preserving all the structure of  $\mathcal{K}_3$



The 2-arrows in  $\mathcal{K}_4$  are 3-natural transformations, like  $\tau_3 : \mathcal{F} \xRightarrow{3} \mathcal{G}$  between 3-functors  $\mathcal{F}_3, \mathcal{G}_3 : \mathcal{K}_3 \rightarrow \mathcal{L}_3$  that sends each object in  $\mathcal{K}_3$  to a arrow in  $\mathcal{L}_3$  and each arrow in  $\mathcal{K}_3$  to a 2-arrow in  $\mathcal{L}_3$ , and satisfies natural transformation-like conditions. We can visualize  $\tau_3$  as a prism going from one picture of  $\mathcal{K}_3$  in  $\mathcal{L}_3$  to another, built using commutative squares:



### 2.1.7.2 Topological Structure of $n$ -Categories

We already emphasized the topological nature of ordinary category theory. This fact is even more obvious in the general case of  $n$ -categories (see [Leinster (2002); Leinster (2003); Leinster (2004)]).

**Homotopy Theory.** Any topological manifold  $M$  gives rise to an  $n$ -category  $\Pi_n(M)$  (its *fundamental  $n$ -groupoid*), in which 0-cells are *points* in  $M$ ; 1-cells are *paths* in  $M$  (i.e., parameterized continuous maps  $f : [0, 1] \rightarrow M$ ); 2-cells are *homotopies* (denoted by  $\simeq$ ) of *paths* relative to endpoints (i.e., parameterized continuous maps  $h : [0, 1] \times [0, 1] \rightarrow M$ ); 3-cells are *homotopies of homotopies* of paths in  $M$  (i.e., parameterized continuous maps  $j : [0, 1] \times [0, 1] \times [0, 1] \rightarrow M$ ); categorical *composition* is defined by *pasting* paths and homotopies. In this way the following ‘homotopy skeleton’ emerges:

$$\begin{aligned}
 0\text{-cell} &: x \bullet & x &\in M; \\
 1\text{-cell} &: x \bullet \xrightarrow{f} \bullet y & f &: x \simeq y \in M, \\
 & f : [0, 1] \rightarrow M, f : x \mapsto y, y = f(x), f(0) = x, f(1) = y; \\
 & \text{e.g., linear path: } f(t) = (1 - t)x + ty;
 \end{aligned}$$

$$2\text{-cell} : x \bullet \begin{array}{c} \xrightarrow{f} \\ \Downarrow h \\ \xrightarrow{g} \end{array} \bullet y \quad h : f \simeq g \in M,$$

$$h : [0, 1] \times [0, 1] \rightarrow M, \quad h : f \mapsto g, \quad g = h(f(x)),$$

$$h(x, 0) = f(x), \quad h(x, 1) = g(x), \quad h(0, t) = x, \quad h(1, t) = y$$

$$\text{e.g., linear homotopy: } h(x, t) = (1 - t)f(x) + tg(x);$$

$$3\text{-cell} : x \bullet \begin{array}{c} \xrightarrow{f} \\ \begin{array}{c} \curvearrowright \\ h \end{array} \begin{array}{c} \xrightarrow{j} \\ \Downarrow \\ \xrightarrow{i} \end{array} \begin{array}{c} \curvearrowleft \\ g \end{array} \\ \xrightarrow{g} \end{array} \bullet y \quad j : h \simeq i \in M,$$

$$j : [0, 1] \times [0, 1] \times [0, 1] \rightarrow M, \quad j : h \mapsto i, \quad i = j(h(f(x)))$$

$$j(x, t, 0) = h(f(x)), \quad j(x, t, 1) = i(f(x)),$$

$$j(x, 0, s) = f(x), \quad j(x, 1, s) = g(x),$$

$$j(0, t, s) = x, \quad j(1, t, s) = y$$

$$\text{e.g., linear composite homotopy: } j(x, t, s) = (1 - t)h(f(x)) + ti(f(x)).$$

If  $M$  is a *smooth* manifold, then all included paths and homotopies need to be *smooth*. Recall that a *groupoid* is a category in which every morphism is invertible; its special case with only one object is a *group*.

**Category  $TT$ .** Topological  $n$ -category  $TT$  has:

- 0-cells: topological spaces  $X$
- 1-cells: continuous maps  $X \xrightarrow{f} Y$

- 2-cells: homotopies  $h$  between  $f$  and  $g : X \begin{array}{c} \xrightarrow{f} \\ \Downarrow h \\ \xrightarrow{g} \end{array} Y$

i.e., continuous maps  $h : X \times [0, 1] \rightarrow Y$ , such that  $\forall x \in X, h(x, 0) = f(x)$  and  $h(x, 1) = g(x)$



- 3-cells: homotopies between homotopies :  $X \begin{array}{c} \xrightarrow{f} \\ \text{homotopy} \\ \xrightarrow{g} \end{array} Y$   
i.e., continuous maps  $j : X \times [0, 1] \times [0, 1] \rightarrow Y$ .

**Category  $\mathcal{CK}$ .** Consider an  $n$ -category  $\mathcal{CK}$ , which has:

- 0-cells: chain complexes  $A$  (of Abelian groups, say)
- 1-cells: chain maps  $A \xrightarrow{f} B$
- 2-cells: chain homotopies  $A \begin{array}{c} \xrightarrow{f} \\ \text{homotopy} \\ \xrightarrow{g} \end{array} B$ ,  
i.e., maps  $\alpha : A \rightarrow B$  of degree 1
- 3-cells  $A \begin{array}{c} \xrightarrow{f} \\ \text{homotopy} \\ \xrightarrow{g} \end{array} B$ : homotopies between homotopies,  
i.e., maps  $\Gamma : A \rightarrow B$  of degree 2 such that  $d\Gamma - \Gamma d = \beta - \alpha$ .

There ought to be some kind of map  $\mathcal{CC} : \mathcal{TT} \Rightarrow \mathcal{CK}$  (see [Leinster (2002); Leinster (2003); Leinster (2004)]).

**Categorification.** Categorification is the process of finding category-theoretic analogs of set-theoretic concepts by replacing sets with categories, functions with functors, and equations between functions by natural isomorphisms between functors, which in turn should satisfy certain equations of their own, called ‘coherence laws’. Iterating this process requires a theory of  $n$ -categories.

Categorification uses the following analogy between set theory and category theory [Crane and Frenkel (1994); Baez and Dolan (1998)]:

Set Theory	Category Theory
elements	objects
equations between elements	isomorphisms between objects
sets	categories
functions	functors
equations between functions	natural isomorphisms between functors

Just as sets have elements, categories have objects. Just as there are functions between sets, there are functors between categories. Now, the proper analog of an equation between elements is not an equation between objects, but an isomorphism. Similarly, the analog of an equation between functions is a natural isomorphism between functors.

### 2.1.8 Algebra in Abelian Categories

An *Abelian category* is a certain kind of category in which morphisms and objects can be added and in which kernels and cokernels exist and have the usual properties. The motivating prototype example of an Abelian category is the category of Abelian groups  $\mathcal{A}$ . Abelian categories are the framework for homological algebra (see [Dieudonne (1988)]).

Given a homomorphism  $f : A \rightarrow B$  between two objects  $A \equiv \text{Dom } f$  and  $B \equiv \text{Cod } f$  in an Abelian category  $\mathcal{A}$ , then its *kernel*, *image*, *cokernel* and *coimage* in  $\mathcal{A}$  are defined respectively as:

$$\begin{aligned} \text{Ker } f &= f^{-1}(e_B), & \text{Coker } f &= \text{Cod } f / \text{Im } f, \\ \text{Im } f &= f(A), & \text{Coim } f &= \text{Dom } f / \text{Ker } f, \end{aligned}$$

where  $e_B$  is a unit of  $B$  [Dodson and Parker (1997)].

In an Abelian category  $\mathcal{A}$  a *composable* pair of arrows,

$$\bullet \xrightarrow{f} B \xrightarrow{g} \bullet$$

is *exact* at  $B$  iff  $\text{Im } f \equiv \text{Ker } g$  (equivalence as subobjects of  $B$ ) – or, equivalently, if  $\text{Coker } f \equiv \text{Coim } g$  [MacLane (1971)].

For each arrow  $f$  in an Abelian category  $\mathcal{A}$  the *triangular identities* read

$$\text{Ker}(\text{Coker}(\text{Ker } f)) = \text{Ker } f, \quad \text{Coker}(\text{Ker}(\text{Coker } f)) = \text{Coker } f.$$

The diagram (with 0 the null object)

$$0 \longrightarrow A \xrightarrow{f} B \xrightarrow{g} C \longrightarrow 0 \quad (2.2)$$

is a *short exact sequence* when it is exact at  $A$ , at  $B$ , and at  $C$ .

Since  $0 \rightarrow a$  is the zero arrow, exactness at  $A$  means just that  $f$  is *monic* (i.e., one-to-one, or injective map); dually, exactness at  $C$  means that  $g$  is *epic* (i.e., onto, or surjective map). Therefore, (2.2) is equivalent to

$$f = \text{Ker } g, \quad g = \text{Coker } f.$$

Similarly, the statement that  $h = \text{Coker } f$  becomes the statement that the sequence

$$A \xrightarrow{f} B \xrightarrow{g} C \longrightarrow 0$$

is exact at  $B$  and at  $C$ . Classically, such a sequence was called a short right exact sequence. Similarly,  $k = \text{Ker } f$  is expressed by a short left exact sequence

$$0 \longrightarrow A \xrightarrow{f} B \xrightarrow{g} C.$$

If  $\mathcal{A}$  and  $\mathcal{A}'$  are Abelian categories, an *additive functor*  $\mathcal{F} : \mathcal{A} \rightarrow \mathcal{A}'$  is a functor from  $\mathcal{A}$  to  $\mathcal{A}'$  with

$$\mathcal{F}(f + f') = \mathcal{F}f + \mathcal{F}f',$$

for any parallel pair of arrows  $f, f' : b \rightarrow c$  in  $\mathcal{A}$ . It follows that  $\mathcal{F}0 = 0$ .

A functor  $\mathcal{F} : \mathcal{A} \rightarrow \mathcal{A}'$  between Abelian categories  $\mathcal{A}$  and  $\mathcal{A}'$  is, by definition, *exact* when it preserves all finite limits and all finite colimits. In particular, an exact functor preserves kernels and cokernels, which means that

$$\text{Ker}(\mathcal{F}f) = \mathcal{F}(\text{Ker } f) \quad \text{and} \quad \text{Coker}(\mathcal{F}f) = \mathcal{F}(\text{Coker } f);$$

then  $\mathcal{F}$  also preserves images, coimages, and carries exact sequences to exact sequences. By construction of limits from products and equalizers and dual constructions,  $\mathcal{F} : \mathcal{A} \rightarrow \mathcal{A}'$  is exact iff it is additive and preserves kernels and cokernels.

A functor  $\mathcal{F}$  is *left exact* when it preserves all finite limits. In other words,  $\mathcal{F}$  is left exact iff it is additive and  $\text{Ker}(\mathcal{F}f) = \mathcal{F}(\text{Ker } f)$  for all  $f$ :

the last condition is equivalent to the requirement that  $\mathcal{F}$  preserves short left exact sequences.

Similarly, a functor  $\mathcal{F}$  is *right exact* when it preserves all finite colimits. In other words,  $\mathcal{F}$  is right exact iff it is additive and  $\text{Coker}(\mathcal{F}f) = \mathcal{F}(\text{Coker } f)$  for all  $f$ : the last condition is equivalent to the requirement that  $\mathcal{F}$  preserves short right exact sequences.

In an Abelian category  $\mathcal{A}$ , a *chain complex* is a sequence

$$\dots \longrightarrow c_{n+1} \xrightarrow{\partial_{n+1}} c_n \xrightarrow{\partial_n} c_{n-1} \longrightarrow \dots$$

of composable arrows, with  $\partial_n \partial_{n+1} = 0$  for all  $n$ . The sequence need not be exact at  $c_n$ ; the deviation from exactness is measured by the  *$n$ th homology object*

$$H_n c = \text{Ker}(\partial_n : c_n \longrightarrow c_{n-1}) / \text{Im}(\partial_{n+1} : c_{n+1} \longrightarrow c_n).$$

Similarly, a *cochain complex* in an Abelian category  $\mathcal{A}$  is a sequence

$$\dots \longrightarrow w_{n+1} \xrightarrow{d_{n+1}} w_n \xrightarrow{d_n} w_{n-1} \longrightarrow \dots$$

of composable arrows, with  $d_n d_{n+1} = 0$  for all  $n$ . The sequence need not be exact at  $w_n$ ; the deviation from exactness is measured by the  *$n$ th cohomology object*

$$H^n w = \text{Ker}(d_{n+1} : w_n \longrightarrow w_{n+1}) / \text{Im}(d_n : w_{n-1} \longrightarrow w_n).$$

A *cycle* is a chain  $C$  such that  $\partial C = 0$ . A *boundary* is a chain  $C$  such that  $C = \partial B$ , for any other chain  $B$ .

A *cocycle* (a *closed form*) is a cochain  $\omega$  such that  $d\omega = 0$ . A *coboundary* (an *exact form*) is a cochain  $\omega$  such that  $\omega = d\theta$ , for any other cochain  $\theta$ .

See chapter 5 about the further development of topology in biodynamics.

### 2.1.9 Fundamental Biodynamic Adjunction

We shall end this section on the categorical metalanguage by formulating the *fundamental biodynamic adjunction* (as adapted from R. Penrose (see [Penrose (1989); Penrose (1994); Penrose (1997)])), in the form :

## PLATONIC WORLD OF MATHEMATICAL TRUTHS

$$\mathcal{F}^U \uparrow \quad \dashv \quad \downarrow \mathcal{F}_D$$

## NATURAL WORLD OF BIODYNAMICS

Here the upward functor, *realization*,  $\mathcal{F}^U$  represents emerging mathematical structures from the natural world of biodynamics, while the downward functor, *manifestation*,  $\mathcal{F}_D$  represents emerging biodynamic functions from the Platonic world of mathematics. The essential biodynamic adjunction is the philosophy of the present book. It offers a mathematical solution to the fundamental question: How would Nature solve this engineering problem? This adjunction represents the mathematical unity in biodynamics diversity as well as the natural diversity in mathematical unity.

This abstract biodynamic adjunction will get its concrete physiological manifestation in the form of coordination-adjunction, *sensory*  $\dashv$  *motor* : *brain*  $\rightleftharpoons$  *body*, which is the main theme of the last chapter on brain-like biodynamic control.

## 2.2 The Basics of Dynamics

In this section we give a simple, linear description of basic dynamics, to be generalized later (with the help of geometric manifold theory) into modern nonlinear dynamics of our *covariant force law*,  $F_i = m g_{ij} a^j$ .

### 2.2.1 Ordinary Differential Equations

In this section we consider *systems of ordinary differential equations* (ODEs) of the form

$$\dot{x} = f(x), \tag{2.3}$$

where  $x = (x_1, \dots, x_n) \in \mathbb{R}^n$  and  $f : \mathbb{R}^n \rightarrow \mathbb{R}^n$ . Since the r.h.s of (7.8.4.3) does not depend on  $t$  explicitly, the ODE is called *autonomous ODE*. If  $f$

is a linear function, i.e.,

$$f(x) = Ax,$$

where  $A$  is an  $n \times n$  matrix of real numbers, the ODE is *linear*. In general  $f$  is *nonlinear*. The vector  $x \in \mathbb{R}^n$  is called the *state vector* of the system, and  $\mathbb{R}^n$  is called the *state-space*.

The function  $f$  can be interpreted as a *vector-field* on the state-space  $\mathbb{R}^n$ , since it associates with each  $x \in \mathbb{R}^n$  an element  $f(x)$  on  $\mathbb{R}^n$ , which can be interpreted as a vector

$$f(x) = (f_1(x), \dots, f_n(x))$$

situated at  $x$ .

A *solution* of the ODE (7.8.4.3) is a function  $\psi : \mathbb{R}^n \rightarrow \mathbb{R}^n$  which satisfies

$$\dot{\psi}(t) = f(\psi(t)) \quad (2.4)$$

for all  $t \in R$  (the domain of  $\psi$  may be a finite interval  $(\alpha, \beta)$ ).

The image of the solution function  $\psi$  in  $\mathbb{R}^n$  is called an *orbit* of the ODE. Equation (7.8.4.3) implies that the vector-field  $f$  at  $x$  is tangent to the orbit through  $x$ . The state of the physical system that is being analyzed is represented by a point  $x \in \mathbb{R}^n$ . The evaluation of the system in time is described by the motion of this point along an orbit of the ODE in  $\mathbb{R}^n$ , with  $t$  as time. In this interpretation, the ODE implies that the *vector-field*  $f$  is the *velocity* of the moving point in the state-space (this should not be confused with the physical velocity of a physical particle).

One cannot hope to find exact solutions of a nonlinear ODE (7.8.4.3) for  $n \geq 2$  (except in very special cases). One thus has to use either qualitative methods, perturbative methods, or numerical methods, in order to deduce the behavior of the physical system. The aim of *qualitative analysis* is to understand the qualitative behavior of typical solutions of the ODE, e.g., the *long-term behavior* as  $t \rightarrow \infty$  of typical solutions. One is also interested in questions of *stability* and the possible existence of *bifurcations*.

The starting point in the qualitative analysis of an autonomous ODE (7.8.4.3) in  $\mathbb{R}^n$  is to locate the zeros of the vector-field, i.e., to find all  $a \in \mathbb{R}^n$  such that

$$f(a) = 0.$$

If  $f(a) = 0$ , then  $\psi(t) = a$ , for all  $t \in \mathbb{R}$ , and it is a solution of the ODE, since  $\dot{\psi}(t) = f(\psi(t))$  is satisfied trivially for all  $t \in \mathbb{R}$ . A constant solution  $\psi(t) = a$  describes an *equilibrium state* of the physical system, and hence the point  $a \in \mathbb{R}^n$  is called an *equilibrium point* of the ODE. More precisely, given an ODE  $\dot{x} = f(x)$  in  $\mathbb{R}^n$ , any point  $a \in \mathbb{R}^n$  which satisfies  $f(a) = 0$ , is an equilibrium point of the ODE.

We are interested in the stability of equilibrium states. In order to address this question it is necessary to study the behavior of the orbits of the ODE close to the equilibrium points. The idea is to consider the linear approximation of the vector-field  $f: \mathbb{R}^n \rightarrow \mathbb{R}^n$  at an equilibrium point. We thus assume that the function  $f$  is of class  $C^1(\mathbb{R}^n)$  (i.e., that the partial derivatives of  $f$  exist and are  $C^0$ -functions on  $\mathbb{R}^n$ .)

The *derivative matrix* (or, *Jacobian matrix*) of  $f: \mathbb{R}^n \rightarrow \mathbb{R}^n$  is the  $n \times n$  matrix  $Df(x)$  defined by

$$Df(x) = \left( \frac{\partial f_i}{\partial x_j} \right), \quad (i, j = 1, \dots, n),$$

where the  $f_i$  are the component functions of  $f$ .

The *linear approximation* of  $f$  is written in terms of the derivative matrix,

$$f(x) = f(a) + Df(a)(x - a) + R_1(x, a), \quad (2.5)$$

where  $Df(a)(x - a)$  denotes the  $n \times n$  derivative matrix evaluated at  $a$ , acting on the vector  $(x - a)$ , and  $R_1(x, a)$  is the *error term*. An important result from advanced calculus is that if  $f$  is of class  $C^0$ , then the magnitude of the error  $\|R_1(x, a)\|$  tends to zero faster than the magnitude of the displacement  $\|x - a\|$ . Here  $\|\cdot\|$  denotes the Euclidean norm on  $\mathbb{R}^n$  (i.e.,  $\|x\| = \sqrt{x_1^2 + \dots + x_n^2}$ ). This means that in general,  $R_1(x, a)$  will be small compared to  $Df(a)(x - a)$ , for  $x$  sufficiently close to  $a$ .

If  $a \in \mathbb{R}^n$  is an equilibrium point of the ODE  $\dot{x} = f(x)$ , we can use (2.5) to write the ODE in the form

$$\text{NL:} \quad \dot{x} = Df(a)(x - a) + R_1(x, a),$$

assuming that  $f$  is of class  $C^0$ . We let  $y = x - a$ , and with the nonlinear ODE (NL) above, we associate the following linear ODE (L),

$$\text{L:} \quad \dot{y} = Df(a)y,$$

which is called the *linearization* of the NL at the equilibrium point  $a \in \mathbb{R}^n$ . The question is when do solutions of L approximate the solutions of the NL

near  $x = a$ ? In general the approximation is valid, but in special situations, the approximation can fail.

## 2.2.2 Linear Autonomous Dynamics

### 2.2.2.1 The Flow of a Linear ODE

Fundamental theorem for linear autonomous ODEs states that if  $A$  is an  $n \times n$  real matrix then the initial value problem

$$\dot{x} = Ax, \quad x(0) = a \in \mathbb{R}^n \quad (2.6)$$

has the unique solution

$$x(t) = e^{tA}a, \quad \text{for all } t \in \mathbb{R}. \quad (2.7)$$

(Here  $a$  is the state at time  $t = 0$  and  $e^{tA}$  is the state at time  $t$ ). To prove the existence, let  $x(t) = e^{tA}a$  then

$$\begin{aligned} \frac{dx}{dt} &= \frac{d(e^{tA}a)}{dt} = Ae^{tA}a = Ax, \\ x(0) &= e^0a = Ia = a, \end{aligned}$$

shows that  $x(t)$  satisfies the initial value problem (2.6) (here  $I$  denotes the  $n \times n$  identity matrix).

To prove the uniqueness, let  $x(t)$  be any solution of (2.6). It follows that

$$\frac{d}{dt} [e^{-tA}x(t)] = 0.$$

Thus  $e^{-tA}x(t) = C$ , a constant. The initial condition implies that  $C = a$  and hence  $x(t) = e^{tA}a$ .

The unique solution of the ODE (2.6) is given by (2.7) for all  $t$ . Thus, for each  $t \in \mathbb{R}$ , the matrix  $e^{tA}$  maps

$$a \mapsto e^{tA}a.$$

The set  $\{e^{tA}\}_{t \in \mathbb{R}}$  is a 1-parameter family of linear maps of  $\mathbb{R}^n$  into  $\mathbb{R}^n$ , and is called the *linear flow* of the ODE (for comparison with the general flow notion, see section (3.4.2.3) below).

We write

$$g^t = e^{tA}$$



– to denote the flow. The flow describes the evolution in time of the physical system for all possible initial states. As the physical system evolves in time, one can think of the state vector  $x$  as a moving point in state space, its motion being determined by the flow  $g^t = e^{tA}$ . The linear flow satisfies two important properties, which also hold for nonlinear flows.

The linear flow  $g^t = e^{tA}$  satisfies:

$$\begin{aligned} \text{F1 : } \quad & g^0 = I, \quad \text{identity map,} \quad \text{and} \\ \text{F2 : } \quad & g^{t_1+t_2} = g^{t_1} \circ g^{t_2}, \quad \text{composition.} \end{aligned}$$

Note that properties F1 and F2 imply that the flow  $\{g^t\}_{t \in \mathbb{R}}$  forms a *group* under composition of maps.

The flow  $g^t$  of the ODE (2.6) partitions the state-space  $\mathbb{R}^n$  into subsets called *orbits*, defined by

$$\gamma(a) = \{g^t a : t \in \mathbb{R}\}.$$

The set  $\gamma(a)$  is called the orbit of the ODE through  $a$ . It is the image in  $\mathbb{R}^n$  of the solution curve  $x(t) = e^{tA}a$ . It follows that for  $a, b \in \mathbb{R}^n$ , either  $\gamma(a) = \gamma(b)$  or  $\gamma(a) \cap \gamma(b) = \emptyset$ , since otherwise the uniqueness of solutions would be violated.

For example, consider

$$\dot{x} = Ax, \quad \text{for all } x \in \mathbb{R}^2;$$

with

$$A = \begin{pmatrix} 0 & 1 \\ -1 & 0 \end{pmatrix},$$

the linear flow is

$$e^{tA} = \begin{pmatrix} \cos t & \sin t \\ -\sin t & \cos t \end{pmatrix}.$$

The *action of the flow* on  $\mathbb{R}^2$ ,  $a \mapsto e^{tA}a$  corresponds to a *clockwise rotation about the origin*. Thus if  $a \neq 0$ , the orbit  $\gamma(a)$  is a circle centered at the origin passing through  $a$ . The origin is a *fixed point* of the flow, since  $e^{tA}0 = 0$ , for all  $t \in \mathbb{R}$ . The orbit  $\gamma(0) = \{0\}$  is called a *point orbit*. All other orbits are called *periodic orbits* since  $e^{2\pi A}a = a$ , i.e., the flow maps onto itself after a time  $t = 2\pi$  has elapsed.

## Classification of Orbits of an ODE.

- (1) If  $g^t a = a$  for all  $t \in \mathbb{R}$ , then  $\gamma(a) = \{a\}$  and it is called a *point orbit*. Point orbits correspond to equilibrium points.
- (2) If there exists a  $T > 0$  such that  $g^T a = a$ , then  $\gamma(a)$  is called a *periodic orbit*. Periodic orbits describe a system that evolves periodically in time.
- (3) If  $g^t a \neq a$  for all  $t \neq 0$ , then  $\gamma(a)$  is called a *non-periodic orbit*.

Note that:

1. Non-periodic orbits can be of great complexity even for linear ODEs if  $n > 3$  (for nonlinear ODEs if  $n > 2$ ).

2. A *solution curve* of an ODE is a parameterized curve and hence contains information about the flow of time  $t$ . The *orbits* are paths in state-space (or subsets of state space). Orbits which are not point orbits are *directed paths* with the direction defined by increasing time. The orbits thus do not provide detailed information about the flow of time.

For an autonomous ODE, the slope of the solution curves depend only on  $x$  and hence the tangent vectors to the solution curves define a vector-field  $f(x)$  in  $x$ -space. Infinitely many solution curves may correspond to a single orbit. On the other hand, a non-autonomous ODE does not define a flow or a family of orbits.

### 2.2.2.2 Canonical Linear Flows in $\mathbb{R}^2$

**Jordan Canonical Forms.** For any  $2 \times 2$  real matrix  $A$ , there exists a non-singular matrix  $P$  such that

$$J = P^{-1}AP,$$

and  $J$  is one of the following matrices:

$$\begin{pmatrix} \lambda_1 & 0 \\ 0 & \lambda_2 \end{pmatrix}, \quad \begin{pmatrix} \lambda & 1 \\ 0 & \lambda \end{pmatrix}, \quad \begin{pmatrix} \alpha & \beta \\ -\beta & \alpha \end{pmatrix}.$$

Two linear ODEs,  $\dot{x} = Ax$  and  $\dot{x} = Bx$ , are linearly equivalent iff there exists a non-singular matrix  $P$  and a positive constant  $k$  such that

$$A = kP^{-1}BP.$$

In other words, the linear ODEs,  $\dot{x} = Ax$  and  $\dot{x} = Bx$  are *linearly equivalent* iff there exists an invertible matrix  $P$  and a positive constant  $k$  such that

$$Pe^{tA} = e^{ktB}P, \quad \text{for all } t \in \mathbb{R}.$$

**Case I: two eigendirections.** *Jordan canonical form* is

$$J = \begin{pmatrix} \lambda_1 & 0 \\ 0 & \lambda_2 \end{pmatrix}.$$

The flow is

$$e^{tJ} = \begin{pmatrix} e^{\lambda_1 t} & 0 \\ 0 & e^{\lambda_2 t} \end{pmatrix},$$

and the eigenvectors are  $e_1 = \begin{pmatrix} 1 \\ 0 \end{pmatrix}$  and  $e_2 = \begin{pmatrix} 0 \\ 1 \end{pmatrix}$ . The solutions are  $y(t) = e^{tJ}b$  for all  $b \in \mathbb{R}^2$ , i.e.,  $y_1 = e^{\lambda_1 t}b_1$  and  $y_2 = e^{\lambda_2 t}b_2$ .

- Ia.**  $\lambda_1 = \lambda_2 < 0$  : *attracting focus*;
- Ib.**  $\lambda_1 < \lambda_2 < 0$  : *attracting node*;
- Ic.**  $\lambda_1 < \lambda_2 = 0$  : *attracting line*;
- Id.**  $\lambda_1 < 0 < \lambda_2$  : *saddle*;
- Ie.**  $\lambda_1 = 0 < \lambda_2$  : *repelling line*;
- If.**  $0 < \lambda_1 < \lambda_2$  : *repelling node*;
- Ig.**  $0 < \lambda_1 = \lambda_2$  : *repelling focus*.

**Case II: one eigendirection.** *Jordan canonical form* is

$$J = \begin{pmatrix} \lambda & 1 \\ 0 & \lambda \end{pmatrix}.$$

The flow is

$$e^{tJ} = e^{\lambda t} \begin{pmatrix} 1 & t \\ 0 & 1 \end{pmatrix},$$

and the single eigenvector is  $e = \begin{pmatrix} 1 \\ 0 \end{pmatrix}$ .

- IIa.**  $\lambda < 0$  : *attracting Jordan node*;
- IIb.**  $\lambda = 0$  : *neutral line*;
- IIc.**  $\lambda > 0$  : *repelling Jordan node*.

**Case III: no eigendirections.** *Jordan canonical form* is

$$J = \begin{pmatrix} \alpha & \beta \\ -\beta & \alpha \end{pmatrix}.$$

The given ODE is linearly equivalent to  $\dot{y} = Jy$ .

- IIIa.**  $\alpha < 0$  : *attracting spiral*;  
**IIIb.**  $\alpha = 0$  : *center*;  
**IIIc.**  $\alpha > 0$  : *repelling spiral*.

In terms of the Jordan canonical form of two matrices  $A$  and  $B$ , the corresponding ODEs are linearly equivalent iff:

- (1)  $A$  and  $B$  have the same number of eigendirections, and
- (2) The eigenvalues of  $A$  are multiple ( $k$ ) of the eigenvalues of  $B$ .

### 2.2.2.3 Topological Equivalence

Now, cases **Ia**, **Ib**, **IIa**, and **IIIa** have common characteristic that all orbits approach the origin (an equilibrium point) as  $t \rightarrow \infty$ . We would like these flows to be 'equivalent' in some sense. In fact, it can be shown, that for all flows of these types, *the orbits of one flow can be mapped onto the orbits of the simplest flow Ia*, using a (nonlinear) map  $h : \mathbb{R}^2 \rightarrow \mathbb{R}^2$ , which is a *homeomorphism* on  $\mathbb{R}^2$ .

Recall (see section (2.1.1) above) that map  $h : \mathbb{R}^n \rightarrow \mathbb{R}^n$  is a *homeomorphism* on  $\mathbb{R}^n$  iff (i)  $h$  is one-to-one and onto, (ii)  $h$  is continuous, and (iii)  $h^{-1}$  is continuous. Two linear flows  $e^{tA}$  and  $e^{tB}$  on  $\mathbb{R}^n$  are said to be *topologically equivalent* if there exists a homeomorphism  $h$  on  $\mathbb{R}^n$  and a positive constant  $k$  such that

$$h(e^{tA}x) = e^{ktB}h(x), \quad \text{for all } x \in \mathbb{R}^n, \text{ and for all } t \in \mathbb{R}.$$

A *hyperbolic* linear flow in  $\mathbb{R}^2$  is one in which the real parts of the eigenvalues are all non-zero (i.e.,  $\operatorname{Re}(\lambda_i) \neq 0$ , for  $i = 1, 2$ .)

Any hyperbolic linear flow in  $\mathbb{R}^2$  is topologically equivalent to the linear flow  $e^{tA}$ , where  $A$  is one of the following matrices:

1.  $A = \begin{pmatrix} -1 & 0 \\ 0 & -1 \end{pmatrix}$ , *standard sink*.
2.  $A = \begin{pmatrix} 1 & 0 \\ 0 & 1 \end{pmatrix}$ , *standard source*.
3.  $A = \begin{pmatrix} -1 & 0 \\ 0 & 1 \end{pmatrix}$ , *standard saddle*.

Any non-hyperbolic linear flow in  $\mathbb{R}^2$  is linearly (and hence topologi-

cally) equivalent to the flow  $e^{tA}$ , where  $A$  is one of the following matrices:

$$\begin{pmatrix} 0 & 0 \\ 0 & 0 \end{pmatrix}, \quad \begin{pmatrix} 0 & -1 \\ 1 & 0 \end{pmatrix}, \quad \begin{pmatrix} 0 & 1 \\ 0 & 0 \end{pmatrix}, \quad \begin{pmatrix} -1 & 0 \\ 0 & 0 \end{pmatrix}, \quad \begin{pmatrix} 1 & 0 \\ 0 & 0 \end{pmatrix}.$$

These five flows are topologically equivalent.

To extend the dynamical language to the much more natural, *nonlinear dynamics*, we need the geometric framework of smooth manifolds (see (3.4.4) below).

### 2.3 Chaos and Synergetics in Biodynamics

In this section we present the basics of the *chaos theory*, as well as the most powerful tool for high-dimensional chaos control, which is the *synergetics*. These two scientific theories, coupled with the *self-organizing learning dynamics*, will represent our main tools for discovering *diversity in unity*, biodynamic diversity in natural mathematical unity.

Mathematical term *deterministic chaos* depicts an *irregular and unpredictable* time evolution of many simple deterministic dynamical systems characterized by nonlinear coupling of its variables (see e.g., [Yorke *et al.* (1996); Grebogi *et al.* (1987); Baker and Gollub (1996)]). The unique character of chaotic dynamics may be seen most clearly by imagining the system to be started twice, but from slightly different initial conditions (in case of human motion, these are initial joint angles and angular velocities). We can think of this small initial difference as resulting from measurement error. For non-chaotic systems, this uncertainty leads only to an error in prediction that *grows linearly* with time. For chaotic systems, on the other hand, the error *grows exponentially* in time, so that the state of the system is essentially unknown after very short time. This phenomenon, firstly recognized by H. Poincaré, the father of topology, in 1913, which occurs only when the governing equations are nonlinear, with nonlinearly coupled variables, is known as *sensitivity to initial conditions*. Another type of sensitivity of chaotic systems is *sensitivity to parameters*: a small variation of system parameters (e.g., mass, length and moment of inertia of human body segments) results in great change of system output (dynamics of human movement).

If prediction becomes impossible, it is evident that a chaotic system can resemble a stochastic system, say a Brownian motion. However, the source of the irregularity is quite different. For chaos, the irregularity is

part of the intrinsic dynamics of the system, not random external influences (for example, random muscular contractions in human motion). Usually, though, chaotic systems are predictable in the short-term. This *short-term predictability* is useful in various domains ranging from weather forecasting to economic forecasting.

Some aspects of chaos have been known for over a hundred years. Isaac Newton was said to get headaches thinking about the 3-body problem (Sun, Moon, and Earth). In 1890, King Oscar II of Sweden announced a prize for anyone who could solve the  $n$ -body problem and hence demonstrate stability of the solar system. The prize was awarded to Henri Poincaré who showed that even the 3-body problem has no analytical solution [Peterson (1993); BG79]. He went on to deduce many of the properties of chaotic systems including the sensitive dependence on initial conditions. With the successes of linear models in the sciences and the lack of powerful computers, the work of these early nonlinear dynamists went largely unnoticed and undeveloped for many decades. In 1963, E. Lorenz from MIT published a seminal paper [Lorenz (1963)] in which he showed that chaos can occur in systems of autonomous (no explicit time dependence) ordinary differential equations (ODEs) with as few as three variables and two quadratic nonlinearities. For continuous flows, the *Poincaré-Bendixson theorem* [Hirsch and Smale (1974)] implies the necessity of three variables, and chaos requires at least one nonlinearity. More explicitly, the theorem states that the long-time limit of any 'smooth' two-dimensional flow is either a fixed point or a periodic solution. With the growing availability of powerful computers, many other examples of chaos were subsequently discovered in algebraically simple ODEs. Yet the sufficient conditions for chaos in a system of ODEs remain unknown [Sprott and Linz (2000)].

So, *necessary condition for existence of chaos* satisfies any autonomous continuous-time dynamical system (a vector-field) of dimension three or higher, with at least two nonlinearly coupled variables (e.g., a single human swivel joint like a shoulder or hip, determined by three joint angles and three angular momenta). In case of non-autonomous continuous-time systems, chaos can happen in dimension two, while in case of discrete-time systems — even in dimension one. Now, whether the behavior (a flow), of any such system will actually be chaotic or not depends upon the values of its parameters and/or initial conditions. Usually, for some values of involved parameters, the system behavior is oscillating in a stable regime, while for another values of the parameters the behavior becomes chaotic, showing a *bifurcation*, or a *phase transition* — from one regime/phase to a totally

different one. If a change in the system's behavior at the bifurcation point is really sharp, we could probably be able to recognize one of the celebrated polynomial *catastrophes* of R. Thom (see [Thom (1975); Arnold (1992)]). A series of such bifurcations usually depicts a *route to chaos*.

Chaos theory has developed special mathematical procedures to *understand* irregularity and unpredictability of low-dimensional nonlinear systems, including Poincaré sections, bifurcation diagrams, power spectra, Lyapunov exponents, period doubling, fractal dimension, stretching and folding, special identification and estimation techniques, etc. (see e.g., [Arnold (1989); Arnold (1978); Arnold (1988); Arnold (1993); Yorke *et al.* (1996); Baker and Gollub (1996)]). Understanding these phenomena has enabled science to *control* the chaos (see [Ott *et al.* (1990); Chen and Dong (1998)]).

There are many practical reasons for *controlling or ordering chaos*. For example, in case of a distributed artificial intelligence system, which is usually characterized by a massive collection of decision-making agents, the fact that an agent's decision also depends on decisions made by other agents — leads to extreme complexity and nonlinearity of the overall system. More often than not, the information received by agents about the 'state' of the system may be 'tainted'. When the system contains imperfect information, its agents tend to make poor decisions concerning choosing an optimal problem-solving strategy or cooperating with other agents. This can result in certain chaotic behavior of the agents, thereby downgrading the performance of the entire system. Naturally, chaos should be reduced as much as possible, or totally suppressed, in these situations [Chen and Dong (1998)].

In contrast, recent research has shown that chaos may actually be useful under certain circumstances, and there is growing interest in utilizing the richness of chaos [Gleick (1997); Mosekilde (1996); Ding *et al.* (1997)]. Since a chaotic attractor usually has embedded within it a dense set of unstable limit cycles, if any of these limit cycles can be stabilized, it may be desirable to stabilize one that characterizes certain maximal system performance [Ott *et al.* (1990)]. The key is, in a situation where a system is meant for multiple purposes, switching among different limit cycles may be sufficient for achieving these goals. If, on the other hand the attractor is not chaotic, then changing the original system configuration may be necessary to accommodate different purposes. Thus, when designing a system intended for multiple uses, purposely building chaotic dynamics into the system may allow for the desired flexibilities [Ott *et al.* (1990)].

Within the context of *brain dynamics*, there are suggestions that 'the controlled chaos of the brain is more than an accidental by-product of the brain complexity, including its myriad connections' and that 'it may be the chief property that makes the brain different from an artificial-intelligence machine [Freeman and Skapura (1992)]. The so-called *anticontrol of chaos* has been proposed for solving the problem of driving the system trajectories of a human brain model away from the stable direction and, hence, away from the stable equilibrium (in the case of a saddle type equilibrium), thereby preventing the periodic behavior of neuronal population bursting. Namely, in a spontaneously bursting neuronal network in vitro, chaos can be demonstrated by the presence of unstable fixed-point behavior. Chaos control techniques can increase the periodicity of such neuronal population bursting behavior. Periodic pacing is also effective in entraining such systems, although in a qualitatively different fashion. Using a strategy of anticontrol such systems can be made less periodic. These techniques may be applicable to in vivo epileptic foci [Schiff *et al.* (1994)].

Within the context of *heart dynamics*, traditionally in physiology, healthy dynamics has been regarded as regular and predictable, whereas disease, such as fatal arrhythmias, aging, and drug toxicity, are commonly assumed to produce disorder and even chaos [Goldberger (1999); Amaral *et al.* (1998); Ivanov *et al.* (1999); Kaplan *et al.* (1991)]. However, in the last two decades, laboratory studies produced evidence to show that:

- (1) The complex variability of healthy dynamics in a variety of physiological systems has features reminiscent of deterministic chaos; and
- (2) A wide class of disease processes (including drug toxicities and aging) may actually decrease, yet not completely eliminate, the amount of chaos or complexity in physiological systems (decomplexification).

These postulates have implications both for basic mechanisms in physiology as well as for clinical monitoring, including the problem of anticipating sudden cardiac death. In contrast to the prevalent belief of clinicians that healthy heart beats are regular, recent research on the interbeat interval variations in healthy individuals shows that a normal heart rate apparently fluctuates in a highly erratic fashion. This turns out to be consistent with deterministic chaos [Goldberger (1999); Amaral *et al.* (1998); Ivanov *et al.* (1999); Kaplan *et al.* (1991)].

Similar to the brain (and heart) dynamics, human biodynamics represents a highly nonlinear dynamics with several hundreds of degrees of free-



dom, many of which are naturally and nonlinearly coupled [Ivancevic and Snoswell (2001); Ivancevic (2002); Ivancevic (2004); Ivancevic and Pearce (2001b); Ivancevic (2005); Ivancevic (1991); Ivancevic and Pearce (2001a)]. Its hierarchical control system, neural motor controller, necessarily has to cope with the high-dimensional chaos.

Nevertheless, whether the purpose is to reduce 'bad' chaos or to induce 'good' ones, researchers felt strongly the necessity for chaos control [Chen and Dong (1998)].

On the other hand, the most powerful scientific tool to *extract order from chaos* has been developed outside of chaos theory, with intention to deal with much more complex, high-dimensional, hierarchical systems, in the realm of *synergetics*. Synergetics is an interdisciplinary field of research that was founded by H. Haken in 1969 (see [Haken (1983); Haken (1993); Haken (1996); Haken (2000)]). Synergetics deals with complex systems that are composed of many individual parts (components, elements) that interact with each other and are able to produce spatial, temporal or functional structures by self-organization. In particular, synergetics searches for general principles governing self-organization irrespective of the nature of the individual parts of the systems that may belong to a variety of disciplines such as physics (lasers, fluids, plasmas), meteorology, chemistry (pattern formation by chemical reactions, including flames), biology (morphogenesis, evolution theory) movement science, brain activities, computer sciences (synergetic computer), sociology (e.g., city growth) psychology and psychiatry (including Gestalt psychology).

The aim of synergetics has been to describe processes of *spontaneous self-organization and cooperation* in complex systems built from many subsystems which themselves can be complicated nonlinear objects (like many individual neuro-muscular components of the human motion system, having their own excitation and contraction dynamics, embedded in a synergistic way to produce coordinated human movement). General properties of the subsystems are their own nonlinear/chaotic dynamics as well as mutual nonlinear/chaotic interactions. Furthermore, the systems of synergetics are *open*. The influence from outside is measured by a certain set of *control parameters*  $\{\sigma\}$  (like amplitudes, frequencies and time characteristics of neuro-muscular driving forces). Processes of self-organization in synergetics, (like musculo-skeletal coordination in human motion dynamics) are observed as temporal macroscopic patterns. They are described by a small set of *order parameters*  $\{o\}$ , similar to those in Landau's *phase-transition*

theory (named after Nobel Laureate Lev D. Landau) of physical systems in thermal equilibrium [Haken (1983)].

The power of synergetics as a way to control the high-dimensional chaos can be increased by the help of modern geometric nonlinear control (see chapter 6), as well as robust neuro-fuzzy control (see chapter 7).

### 2.3.1 Prototype of Chaotic and Synergetic Systems

In 1963, E. Lorenz from MIT (see [Lorenz (1963); Sparrow (1982)]) reduced the Navier–Stokes equations for convective fluid flow into three first order coupled nonlinear differential equations and demonstrated with these the idea of sensitive dependence upon initial conditions and chaos.

$$\dot{x} = a(y - x), \quad \dot{y} = bx - y - xz, \quad \dot{z} = xy - cz, \quad (2.8)$$

where  $x$ ,  $y$  and  $z$  are dynamical variables, constituting the 3D *phase-space* of the *Lorenz system*; and  $a$ ,  $b$  and  $c$  are the parameters of the system. Originally, Lorenz used this model to describe the unpredictable behavior of the weather, where  $x$  is the rate of convective overturning (convection is the process by which heat is transferred by a moving fluid),  $y$  is the horizontal temperature overturning, and  $z$  is the vertical temperature overturning; the parameters are:  $a \equiv P$ —proportional to the Prandtl number (ratio of the fluid viscosity of a substance to its thermal conductivity, usually set at 10),  $b \equiv R$ —proportional to the Rayleigh number (difference in temperature between the top and bottom of the system, usually set at 28), and  $c \equiv K$ —a number proportional to the physical proportions of the region under consideration (width to height ratio of the box which holds the system, usually set at 8/3). The Lorenz system (2.8) has the properties:

- (1) *symmetry*:  $(x, y, z) \rightarrow (-x, -y, z)$  for all values of the parameters, and
- (2) the  $z$ -axis ( $x = y = 0$ ) is *invariant* (i.e., all trajectories that start on it also end on it).

Nowadays it is well-known that the Lorenz model is a paradigm for low-dimensional chaos in dynamical systems in synergetics and this model or its modifications are widely investigated in connection with modelling purposes in meteorology, hydrodynamics, laser physics, superconductivity, electronics, oil industry, chemical and biological kinetics, etc.

The 3D *phase-portrait* of the Lorenz system (2.2) shows the celebrated '*Lorenz mask*', a special type of (*fractal*, or '*strange*') chaotic *Lorenz attractor* (see Figure 2.2). It depicts the famous '*butterfly effect*', (i.e., sensitive

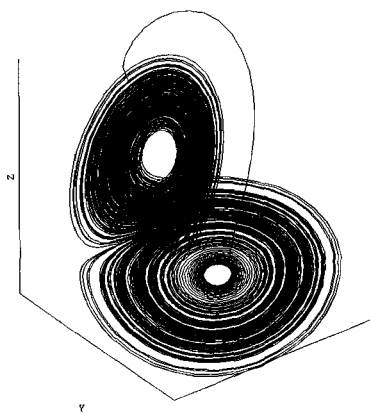


Fig. 2.2 The celebrated 'Lorenz-mask' strange attractor, as simulated in *Matlab*<sup>TM</sup>.

dependence on initial conditions) – the idea in meteorology that the flapping of a butterfly's wing will create a disturbance that in the chaotic motion of the atmosphere will become amplified eventually to change the large scale atmospheric motion, so that the long term behavior becomes impossible to forecast. The Lorenz mask has the following characteristics:

- (1) Trajectory does not intersect itself in three dimensions,
- (2) Trajectory is not periodic or transient,
- (3) General form of the shape does not depend on initial conditions, and
- (4) Exact sequence of loops is very sensitive to the initial conditions.

In 1975, H. Haken showed [Haken (1983)] that the Lorenz equations (2.2) were isomorphic to the *Maxwell-Haken laser equations*

$$\dot{E} = \sigma(P - E), \quad \dot{P} = \beta(ED - P), \quad \dot{D} = \gamma(\sigma - 1 - D - \sigma EP),$$

Here, the variables in the Lorenz equations, namely  $x, y$  and  $z$  correspond to the slowly varying amplitudes of the electric field  $E$  and polarization  $P$  and the inversion  $D$  respectively in the Lorenz-Haken equations. The parameters are related via  $c = \frac{\gamma}{\beta}$ ,  $a = \frac{\sigma}{\beta}$  and  $b = \sigma + 1$ , where  $\gamma$  is the relaxation rate of the inversion,  $\beta$  is the relaxation rate of the polarization,  $\sigma$  is the field relaxation rate, and  $\sigma$  represents the normalized pump power.

### 2.3.2 Chaotic Systems and Biomorphs

In this subsection we present some other well-known chaotic and fractal systems, as well as biologically inspired complex-plane biomorphs.

#### 2.3.2.1 Simulation Examples: Chaotic Systems

Here we present numerical simulations of several popular chaotic systems (see, e.g., [Wiggins (1990); Borelli *et al.* (1992); Acheson (1997)]). Generally, to observe chaos in continuous time system, it is known that the dimension of the equation must be three or higher. On the other hand, in discrete-time systems like logistic map or Hénon map, we can see chaos even if the dimension is one.

**Van der Pol Equation.** The unforced *Van der Pol's oscillator* has the form of a second order ODE

$$\ddot{x} = \alpha(1 - x^2)\dot{x} - \omega^2 x. \quad (2.9)$$

Its celebrated *limit cycle* is given in Figure 2.3. The simulation is performed with zero initial conditions and parameters  $\alpha = \text{random}(0,3)$ , and  $\omega = 1$ . The Van der Pol oscillator was the first *relaxation oscillator*, used in 1928 as a model of human heartbeat ( $\omega$  controls how much voltage is injected into the system, and  $\alpha$  controls the way in which voltage flows through the system). The oscillator was also used as a model of an electronic circuit that appeared in very early radios in the days of vacuum tubes. The tube acts like a normal resistor when current is high, but acts like a negative resistor if the current is low. So this circuit pumps up small oscillations, but drags down large oscillations.  $\alpha$  is a constant that affects how nonlinear the system is. For  $\alpha$  equal to zero, the system is actually just a linear oscillator. As  $\alpha$  grows the nonlinearity of the system becomes considerable.

The *sinusoidally-forced Van der Pol oscillator* is given by equation

$$\ddot{x} - \alpha(1 - x^2)\dot{x} + \omega^2 x = \gamma \sin(\phi t), \quad (2.10)$$

where  $\phi$  is the forcing frequency and  $\gamma$  is the amplitude of the forcing sinusoid.

**Duffing Equation.** The forced *Duffing oscillator* has the form similar to (2.10),

$$\ddot{x} + b\dot{x} - ax(1 - x^2) = \gamma \cos(\phi t).$$

Stroboscopic *Poincaré sections* of a *strange attractor* can be seen (Figure

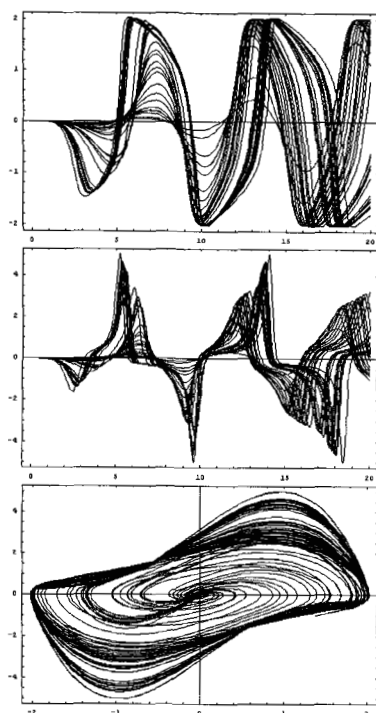


Fig. 2.3 Cascade of 30 unforced Van der Pol oscillators, simulated using *Mathematica*<sup>TM</sup>; top-down: displacements, velocities and phase-plot (showing the celebrated limit cycle).

2.4), with the *stretch-and-fold* action at work. The simulation is performed with parameters:  $a = 1$ ,  $b = 0.2$ , and  $\gamma = 0.3$ ,  $\phi = 1$ . The Duffing equation is used to model a double well oscillator such as the magneto-elastic mechanical system. This system consists of a beam positioned vertically between two magnets, with the top end fixed, and the bottom end free to swing. The beam will be attracted to one of the two magnets, and given some velocity will oscillate about that magnet until friction stops it. Each of the magnets creates a fixed point where the beam may come to rest above that magnet and remain there in equilibrium. However, when this whole system is shaken by a periodic forcing term, the beam may jump back and forth from one magnet to the other in a seemingly random manner. Depending on how big the shaking term is, there may be no stable fixed points and no stable fixed cycles in the system.

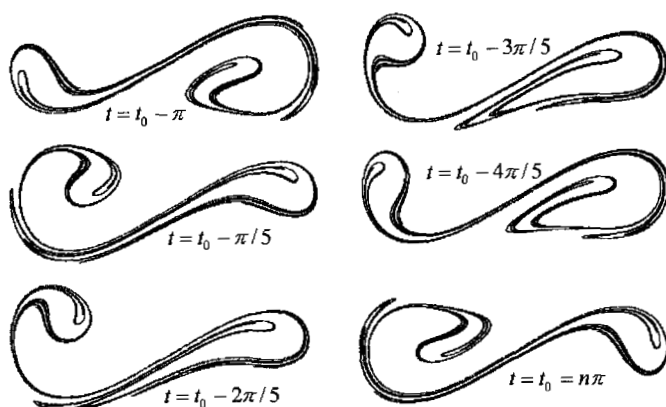


Fig. 2.4 Duffing strange attractor, showing stroboscopic Poincaré sections; simulated using *Dynamics Solver*<sup>TM</sup>.

**Rossler System.** Classical *Rossler system* is given by equations

$$\dot{x} = -y - z, \quad \dot{y} = x + by, \quad \dot{z} = b + z(x - a). \quad (2.11)$$

Using the parameter values  $a = 4$  and  $b = 0.2$ , the phase-portrait is produced (see Figure 2.5), showing the celebrated attractor. The system is credited to O. Rossler and arose from work in chemical kinetics.

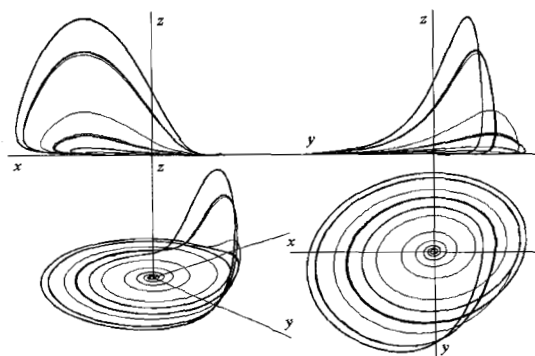


Fig. 2.5 The celebrated Rossler attractor, simulated using *Dynamics Solver*<sup>TM</sup>.

**Inverted Pendulum.** Stability of the *inverted driven pendulum* given by equation

$$\ddot{\theta} + k\dot{\theta} + (1 + a\sqrt{\phi}\cos(\phi t))\sin\theta = 0,$$

where  $\theta$  is the angle, is simulated in Figure 2.6, using the parameter  $a = 0.33$ . It is possible to stabilize a mathematical pendulum around the upper vertical position by moving sinusoidally the suspension point in the vertical direction. Furthermore, the perturbed solution may be of two kinds: one goes to the vertical position while the other becomes periodic (see, e.g., [Acheson (1997)]).

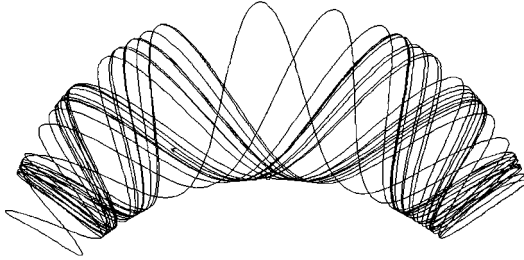


Fig. 2.6 Duffing strange attractor, showing stroboscopic Poincaré sections; simulated using *Dynamics Solver<sup>TM</sup>*.

**Elastic Pendulum.** Elastic pendulum (Figure 2.7) of proper length  $l$ , mass  $m$  and elastic constant  $k$  is given by equation

$$\ddot{x} = x\sqrt{\dot{y}} + \cos y - a(x-1), \quad \ddot{y} = -(2\dot{x}\dot{y} + \sin y)/x,$$

where the parameter  $a = kl/mg = 0.4$ . High values of  $a$  give rise to a simple pendulum.

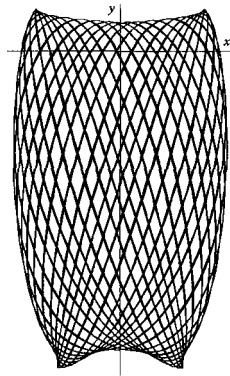


Fig. 2.7 Phase-portrait of an elastic pendulum showing *Lissajous curves*; simulated using *Dynamics Solver<sup>TM</sup>*.

**Autocatalator System.** This 4D *autocatalator* system from *chemical kinetics* (see Figure 2.8) is defined as (see, e.g., [Borelli *et al.* (1992)])

$$\dot{x}_1 = -a x_1, \quad \dot{x}_2 = a x_1 - b x_2 - x_2 x_3^2, \quad \dot{x}_3 = b x_2 - x_3 + x_2 x_3^2, \quad \dot{x}_4 = x_3.$$

The simulation is performed with parameters:  $a = 0.002$ , and  $b = 0.08$ .

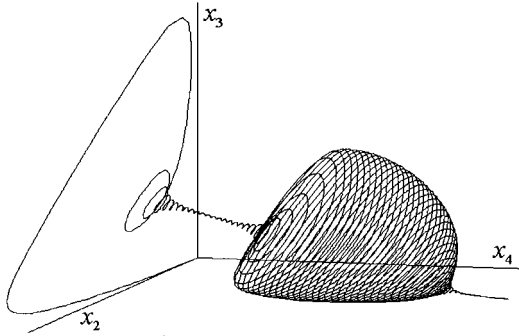


Fig. 2.8 3D phase-portrait of the four-dimensional autocatalator system, simulated using *Dynamics Solver<sup>TM</sup>*.

**Logistic Map.** May's classical *logistic map* [May (1976)] (see Figure 2.9) has the form

$$x_{n+1} = r x_n (1 - x_n), \quad (2.12)$$

where  $r$  is a parameter which varies between 0 and 4, and the initial value of  $x$  is restricted to be between 0 and 1. For  $r < 3$ , the  $x_n$  have a single value. For  $3 < r < 3.4$ , the  $x_n$  oscillate between two values. As  $r$  increases, bifurcations occur where the number of iterates doubles. These *period doubling bifurcations* continue to a limit point at  $r_{lim} = 3.569944$  at which the period is  $2^\infty$  and the dynamics become chaotic. The  $r$  values for the first two bifurcations can be found analytically, they are  $r_1 = 3$  and  $r_2 = 1 + \sqrt{6}$ . We can label the successive values of  $r$  at which bifurcations occur as  $r_1, r_2, \dots$ . The universal number associated with such period doubling sequences is called the *Feigenbaum number*,

$$\delta = \lim_{k \rightarrow \infty} \frac{r_k - r_{k-1}}{r_{k+1} - r_k} \approx 4.669.$$

This says that close enough to  $r_{lim}$  the distance between bifurcation points decreases by a factor of  $\delta$  for each bifurcation.



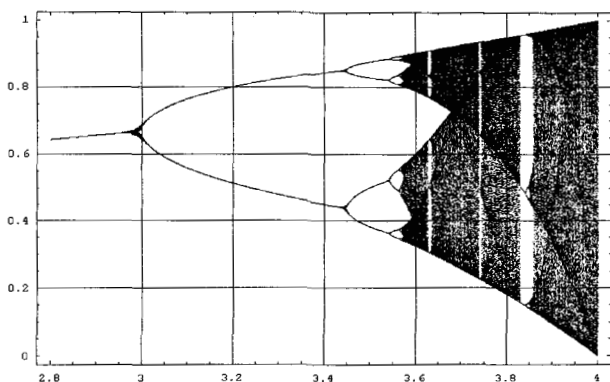


Fig. 2.9 Bifurcation diagram for the logistic map, simulated using *Mathematica*<sup>TM</sup>.

**Hénon Map.** *Hénon map* (see Figure 2.10) is an extension of the logistic map, defined by equations

$$x_{n+1} = c x_n - z (y_n - x_n^2), \quad y_{n+1} = z x_n + c (y_n - x_n^2), \quad z_{n+1} = z_n,$$

where  $c = 0.24$  is a parameter. It is an *area-preserving map*, and simulates the Poincaré map of period orbits in Hamiltonian systems. Repeated random initial conditions are used in the simulation and their gray-scale color is selected at random.

**Mandelbrot and Julia Sets.** *Mandelbrot and Julia sets* are celebrated *fractals* (see Figure 2.11), defined either by a quadratic *conformal z-map*

$$z_{n+1} = z_n^2 + c,$$

or by a real  $(x, y)$ -map

$$x_{n+1} = \sqrt{x_n} - \sqrt{y_n} + c_1, \quad y_{n+1} = 2 x_n y_n + c_2,$$

where  $c, c_1$  and  $c_2$  are parameters. For almost every  $c$ , this conformal transformation generates a fractal (probably, only for  $c = -2$  it is not a fractal). Julia set  $J_c$  with  $c \ll 1$ , the *capacity dimension* is

$$d_{cap} = 1 + \frac{|c|^2}{4 \ln 2} + O(|c|^3).$$

The set of all points for which  $J_c$  is connected is the Mandelbrot set.

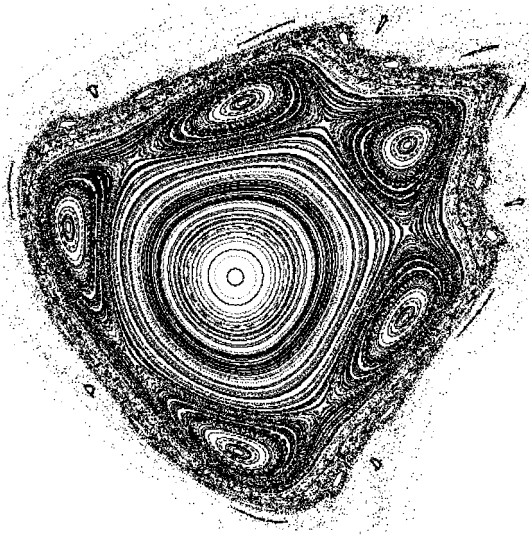


Fig. 2.10 Phase-plot of the area-preserving Hénon map, simulated using *Dynamics Solver<sup>TM</sup>*.

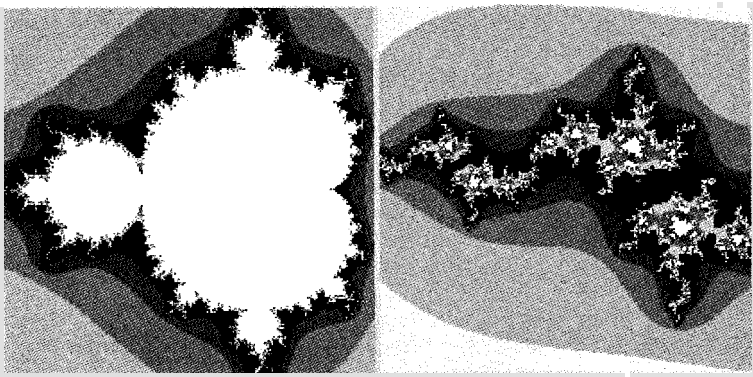


Fig. 2.11 The celebrated conformal Mandelbrot (left) and Julia (right) sets, simulated using *Dynamics Solver<sup>TM</sup>*.

### 2.3.2.2 Simulation Examples: Biomorphic Systems

Closely related to the Mandelbrot and Julia sets are *biomorphic systems*, which look like one-celled organisms. The term '*biomorph*' was proposed by C. Pickover from IBM [Pickover (1986); Pickover (1987)]. Pickover's biomorphs inhabit the complex plane like the the Mandelbrot and Julia

sets and exhibit a *protozoan morphology*. Biomorphs began for Pickover as a ‘bug’ in a program intended to probe the fractal properties of various formulas. He accidentally used an OR logical operator instead of an AND operator in the conditional test for the size of  $z$ ’s real and imaginary parts. The cilia that project from the biomorphs are a consequence of this ‘error’. Each biomorph is generated by multiple iterations of a particular conformal map,

$$z_{n+1} = f(z_n, c),$$

where  $c$  is a parameter. Each iteration takes the output of the previous operations as the input of the next iteration. To generate a biomorph, one first needs to lay out a grid of points on a rectangle in the complex plane [Andreut (2001)]. The coordinate of each point constitutes the real and imaginary parts of an initial value,  $z_0$ , for the iterative process. Each point is also assigned a pixel on the computer screen. Depending on the outcome of a simple test on the ‘size’ of the real and imaginary parts of the final value, the pixel is colored either black or white. The biomorphs presented in Figure 2.12 are generated using the following conformal functions:

- (1)  $f(z, c) = z^3$ ,
- (2)  $f(z, c) = z^3 + c$ ,  $c = 10$ ,
- (3)  $f(z, c) = z^3 + c$ ,  $c = 10 - 10i$ ,
- (4)  $f(z, c) = z^5 + c$ ,  $c = 0.77 - 0.77i$ ,
- (5)  $f(z, c) = z^3 + \sin z + c$ ,  $c = 1 - i$ ,
- (6)  $f(z, c) = z^6 + \sin z + c$ ,  $c = 0.5 - 0.5i$ ,
- (7)  $f(z, c) = z^2 \sin z + c$ ,  $c = 0.78 - 0.78i$ ,
- (8)  $f(z, c) = z^c$ ,  $c = 5 - i$ ,
- (9)  $f(z, c) = |z|^c \sin z$ ,  $c = 4$ ,
- (10)  $f(z, c) = |z|^c \cos z + c$ ,  $c = 3 + 3i$ ,
- (11)  $f(z, c) = |z|^c (\cos z + z) + c$ ,  $c = 3 + 2i$ .

### 2.3.3 Controlling Chaos within the Chaos Theory

#### 2.3.3.1 Exploiting Critical Sensitivity

The fact that some dynamical systems showing the necessary conditions for chaotic behavior possess such a critical dependence on the initial conditions was known since the end of the last century. However, only in the last thirty years, experimental observations have pointed out that, in

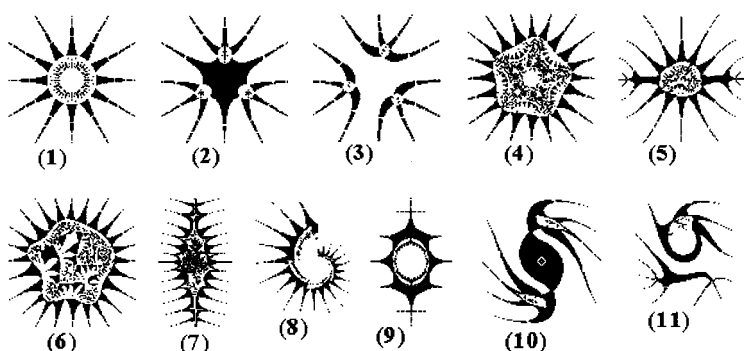


Fig. 2.12 *Pickover's biomorphs* (see text for details).

fact, chaotic systems are common in nature. They can be found, e.g., in chemistry (*Belousov–Zhabotinski reaction*), in nonlinear optics (lasers), in electronics (*Chua–Matsumoto circuit*), in fluid dynamics (*Rayleigh–Bernard convection*), etc. Many natural phenomena can also be characterized as being chaotic. They can be found in meteorology, solar system, heart and brain of living organisms and so on.

Due to their critical dependence on the initial conditions, and due to the fact that, in general, experimental initial conditions are never known perfectly, these systems are intrinsically unpredictable. Indeed, the prediction trajectory emerging from an initial condition and the real trajectory emerging from the real initial condition diverge exponentially in course of time, so that the error in the prediction (the distance between prediction and real trajectories) grows exponentially in time, until making the system's real trajectory completely different from the predicted one at long times.

For many years, this feature made chaos undesirable, and most experimentalists considered such characteristic as something to be strongly avoided. Besides their critical sensitivity to initial conditions, chaotic systems exhibit two other important properties. Firstly, there is an infinite number of unstable periodic orbits embedded in the underlying chaotic set. In other words, the skeleton of a chaotic attractor is a collection of an infinite number of periodic orbits, each one being unstable. Secondly, the dynamics in the chaotic attractor is *ergodic*, which implies that during its temporal evolution the system ergodically visits small neighborhood of every point in each one of the unstable periodic orbits embedded within the

chaotic attractor.

A relevant consequence of these properties is that a chaotic dynamics can be seen as shadowing some periodic behavior at a given time, and erratically jumping from one to another periodic orbit. The idea of controlling chaos is then when a trajectory approaches ergodically a desired periodic orbit embedded in the attractor, one applies small perturbations to stabilize such an orbit. If one switches on the stabilizing perturbations, the trajectory moves to the neighborhood of the desired periodic orbit that can now be stabilized. This fact has suggested the idea that the critical sensitivity of a chaotic system to changes (perturbations) in its initial conditions may be, in fact, very desirable in practical experimental situations. Indeed, if it is true that a small perturbation can give rise to a very large response in the course of time, it is also true that a judicious choice of such a perturbation can direct the trajectory to wherever one wants in the attractor, and to produce a series of desired dynamical states. This is exactly the idea of targeting [Boccaletti *et al.* (2000)].

The important point here is that, because of chaos, one is able to produce an infinite number of desired dynamical behaviors (either periodic and not periodic) using the same chaotic system, with the only help of tiny perturbations chosen properly. We stress that this is not the case for a nonchaotic dynamics, wherein the perturbations to be done for producing a desired behavior must, in general, be of the same order of magnitude as the unperturbed evolution of the dynamical variables.

The *idea of chaos control* was enunciated in 1990 at the University of Maryland, by E. Ott, C. Grebogi and J.A. Yorke [Ott *et al.* (1990)], widely referred to as Ott-Grebogi-Yorke (OGY, for short). In OGY-paper [Ott *et al.* (1990)], the ideas for controlling chaos were outlined and a method for stabilizing an unstable periodic orbit was suggested, as a proof of principle. The main idea consisted in waiting for a natural passage of the chaotic orbit close to the desired periodic behavior, and then applying a small judiciously chosen perturbation, in order to stabilize such periodic dynamics (which would be, in fact, unstable for the unperturbed system). Through this mechanism, one can use a given laboratory system for producing an infinite number of different periodic behavior (the infinite number of its unstable periodic orbits), with a great flexibility in switching from one to another behavior. Much more, by constructing appropriate goal dynamics, compatible with the chaotic attractor, an operator may apply small perturbations to produce any kind of desired dynamics, even not periodic, with practical application in the coding process of signals.

A branch of the theory of dynamical systems has been developed with the aim of formalizing and quantitatively characterizing the sensitivity to initial conditions. The *largest Lyapunov exponent*  $\lambda$  (together with the related *Kaplan–Yorke dimension*  $d_{KY}$ ) and the *Kolmogorov–Sinai entropy*  $h_{KS}$  are the two indicators for measuring the *rate of error growth and information* produced by the dynamical system [Eckmann and Ruelle (1985)].

### 2.3.3.2 Lyapunov exponents and KY–dimension

The characteristic Lyapunov exponents are somehow an extension of the linear stability analysis to the case of aperiodic motions. Roughly speaking, they measure the typical rate of exponential divergence of nearby trajectories. In this sense they give information on the rate of growth of a very small error on the initial state of a system [Boffetta *et al.* (2002)].

Consider an  $n$ D dynamical system given by the set of ODEs of the form

$$\dot{x} = f(x), \quad (2.13)$$

where  $x = (x_1, \dots, x_n) \in \mathbb{R}^n$  and  $f : \mathbb{R}^n \rightarrow \mathbb{R}^n$ . Recall that since the r.h.s of equation (2.13) does not depend on  $t$  explicitly, the system is called *autonomous*. We assume that  $f$  is smooth enough that the evolution is well-defined for time intervals of arbitrary extension, and that the motion occurs in a bounded region  $R$  of the system phase space  $M$ . We intend to study the separation between two trajectories in  $M$ ,  $x(t)$  and  $x'(t)$ , starting from two close initial conditions,  $x(0)$  and  $x'(0) = x(0) + \delta x(0)$  in  $R_0 \subset M$ , respectively.

As long as the difference between the trajectories,  $\delta x(t) = x'(t) - x(t)$ , remains infinitesimal, it can be regarded as a vector,  $z(t)$ , in the tangent space  $T_x M$  of  $M$ . The time evolution of  $z(t)$  is given by the linearized differential equations:

$$\dot{z}_i(t) = \left. \frac{\partial f_i}{\partial x_j} \right|_{x(t)} z_j(t).$$

Under rather general hypothesis, Oseledets [Oseledets (1968)] proved that for almost all initial conditions  $x(0) \in R$ , there exists an orthonormal basis  $\{e_i\}$  in the tangent space  $T_x M$  such that, for large times,

$$z(t) = c_i e_i \exp(\lambda_i t), \quad (2.14)$$

where the coefficients  $\{c_i\}$  depend on  $z(0)$ . The exponents  $\lambda_1 \geq \lambda_2 \geq \dots \geq \lambda_d$  are called *characteristic Lyapunov exponents*. If the dynamical system

has an ergodic invariant measure on  $M$ , the spectrum of LEs  $\{\lambda_i\}$  does not depend on the initial conditions, except for a set of measure zero with respect to the natural invariant measure.

Equation (2.14) describes how a  $dD$  spherical region  $R = S^n \subset M$ , with radius  $\epsilon$  centered in  $x(0)$ , deforms, with time, into an ellipsoid of semi-axes  $\epsilon_i(t) = \epsilon \exp(\lambda_i t)$ , directed along the  $e_i$  vectors. Furthermore, for a generic small perturbation  $\delta x(0)$ , the distance between the reference and the perturbed trajectory behaves as

$$|\delta x(t)| \sim |\delta x(0)| \exp(\lambda_1 t) [1 + O(\exp -(\lambda_1 - \lambda_2)t)].$$

If  $\lambda_1 > 0$  we have a rapid (exponential) amplification of an error on the initial condition. In such a case, the system is chaotic and, unpredictable on the long times. Indeed, if the initial error amounts to  $\delta_0 = |\delta x(0)|$ , and we purpose to predict the states of the system with a certain tolerance  $\Delta$ , then the prediction is reliable just up to a *predictability time* given by

$$T_p \sim \frac{1}{\lambda_1} \ln \left( \frac{\Delta}{\delta_0} \right).$$

This equation shows that  $T_p$  is basically determined by the *positive leading Lyapunov exponent*, since its dependence on  $\delta_0$  and  $\Delta$  is logarithmically weak. Because of its preeminent role,  $\lambda_1$  is often referred as ‘the leading positive Lyapunov exponent’, and denoted by  $\lambda$ .

Therefore, Lyapunov exponents are average rates of expansion or contraction along the principal axes. For the  $i$ th principal axis, the corresponding Lyapunov exponent is defined as (compare with (5.13) in chapter 5)

$$\lambda_i = \lim_{t \rightarrow \infty} \{(1/t) \ln [L_i(t)/L_i(0)]\}, \quad (2.15)$$

where  $L_i(t)$  is the radius of the ellipsoid along the  $i$ th principal axis at time  $t$ . For technical details on calculating Lyapunov exponents from any time series data, see [Wolf *et al.* (1985)].

An initial volume  $V_0$  of the phase-space region  $R_0$  evolves on average as

$$V(t) = V_0 e^{(\lambda_1 + \lambda_2 + \dots + \lambda_{2n})t}, \quad (2.16)$$

and therefore the rate of change of  $V(t)$  is simply

$$\dot{V}(t) = \sum_{i=1}^{2n} \lambda_i V(t).$$

In the case of a 2D phase area  $A$ , evolving as  $A(t) = A_0 e^{(\lambda_1 + \lambda_2)t}$ , a *Lyapunov dimension*  $d_L$  is defined as

$$d_L = \lim_{\epsilon \rightarrow 0} \left[ \frac{d(\ln(N(\epsilon)))}{d(\ln(1/\epsilon))} \right],$$

where  $N(\epsilon)$  is the number of squares with sides of length  $\epsilon$  required to cover  $A(t)$ , and  $d$  represents an ordinary *capacity dimension*,

$$d_c = \lim_{\epsilon \rightarrow 0} \left( \frac{\ln N}{\ln(1/\epsilon)} \right).$$

Lyapunov dimension can be extended to the case of  $n$ D phase-space by means of the *Kaplan-Yorke dimension* [Kaplan and Yorke (1979); Yorke *et al.* (1996); Ott *et al.* (1990)] as

$$d_{KY} = j + \frac{\lambda_1 + \lambda_2 + \cdots + \lambda_j}{|\lambda_{j+1}|},$$

where the  $\lambda_i$  are ordered ( $\lambda_1$  being the largest) and  $j$  is the index of the smallest nonnegative Lyapunov exponent.

### 2.3.3.3 Kolmogorov-Sinai entropy

The LE,  $\lambda$ , gives a first quantitative information on how rapidly we loose the ability of predicting the evolution of a system [Boffetta *et al.* (2002)]. A state, initially determined with an error  $\delta x(0)$ , after a time enough larger than  $1/\lambda$ , may be found almost everywhere in the region of motion  $R \in M$ . In this respect, the *Kolmogorov-Sinai* (KS) *entropy*,  $h_{KS}$ , supplies a more refined information. The error on the initial state is due to the maximal resolution we use for observing the system. For simplicity, let us assume the same resolution  $\epsilon$  for each degree of freedom. We build a partition of the phase space  $M$  with cells of volume  $\epsilon^d$ , so that the state of the system at  $t = t_0$  is found in a region  $R_0$  of volume  $V_0 = \epsilon^d$  around  $x(t_0)$ . Now we consider the trajectories starting from  $V_0$  at  $t_0$  and sampled at discrete times  $t_j = j\tau$  ( $j = 1, 2, 3, \dots, t$ ). Since we are considering motions that evolve in a bounded region  $R \subset M$ , all the trajectories visit a finite number of different cells, each one identified by a symbol. In this



way a unique sequence of symbols  $\{s(0), s(1), s(2), \dots\}$  is associated with a given trajectory  $x(t)$ . In a chaotic system, although each evolution  $x(t)$  is univocally determined by  $x(t_0)$ , a great number of different symbolic sequences originates by the same initial cell, because of the divergence of nearby trajectories. The total number of the admissible symbolic sequences,  $\tilde{N}(\epsilon, t)$ , increases exponentially with a rate given by the topological entropy

$$h_T = \lim_{\epsilon \rightarrow 0} \lim_{t \rightarrow \infty} \frac{1}{t} \ln \tilde{N}(\epsilon, t).$$

However, if we consider only the number of sequences  $N_{eff}(\epsilon, t) \leq \tilde{N}(\epsilon, t)$  which appear with very high probability in the long time limit – those that can be numerically or experimentally detected and that are associated with the natural measure – we arrive at a more physical quantity called the Kolmogorov–Sinai (or metric) entropy [Eckmann and Ruelle (1985)]:

$$h_{KS} = \lim_{\epsilon \rightarrow 0} \lim_{t \rightarrow \infty} \frac{1}{t} \ln N_{eff}(\epsilon, t) \leq h_T. \quad (2.17)$$

$h_{KS}$  quantifies the long time exponential rate of growth of the number of the effective coarse-grained trajectories of a system. This suggests a link with information theory where the Shannon entropy measures the mean asymptotic growth of the number of the typical sequences – the ensemble of which has probability almost one – emitted by a source.

We may wonder what is the number of cells where, at a time  $t > t_0$ , the points that evolved from  $R_0$  can be found, i.e., we wish to know how big is the coarse-grained volume  $V(\epsilon, t)$ , occupied by the states evolved from the volume  $V_0$  of the region  $R_0$ , if the minimum volume we can observe is  $V_{min} = \epsilon^d$ . As stated above (2.16), we have

$$V(t) \sim V_0 \exp\left(t \sum_{i=1}^d \lambda_i\right).$$

However, this is true only in the limit  $\epsilon \rightarrow 0$ . In this (unrealistic) limit,  $V(t) = V_0$  for a conservative system (where  $\sum_{i=1}^d \lambda_i = 0$ ) and  $V(t) < V_0$  for a dissipative system (where  $\sum_{i=1}^d \lambda_i < 0$ ). As a consequence of limited resolution power, in the evolution of the volume  $V_0 = \epsilon^d$  the effect of the contracting directions (associated with the negative Lyapunov exponents) is completely lost. We can experience only the effect of the expanding directions, associated with the positive Lyapunov exponents. As a consequence,

in the typical case, the coarse grained volume behaves as

$$V(\epsilon, t) \sim V_0 e^{(\sum_{\lambda_i > 0} \lambda_i) t},$$

when  $V_0$  is small enough. Since  $N_{eff}(\epsilon, t) \propto V(\epsilon, t)/V_0$ , one has

$$h_{KS} = \sum_{\lambda_i > 0} \lambda_i.$$

This argument can be made more rigorous with a proper mathematical definition of the metric entropy. In this case one derives the Pesin relation [Pesin (1977); Eckmann and Ruelle (1985)]

$$h_{KS} \leq \sum_{\lambda_i > 0} \lambda_i. \quad (2.18)$$

Because of its relation with the Lyapunov exponents – or by the definition (2.17) – it is clear that also  $h_{KS}$  is a fine-grained and global characterization of a dynamical system.

The metric entropy is an invariant characteristic quantity of a dynamical system, i.e., given two systems with invariant measures, their KS-entropies exist and they are equal iff the systems are isomorphic [Billingsley (1965)].

#### 2.3.3.4 Chaos Control by Ott, Grebogi and Yorke

Besides the occurrence of chaos in a large variety of natural processes, chaos may also occur because one may wish to design a physical, biological or chemical experiment, or to project an industrial plant to behave in a chaotic manner. The OGY-idea is that chaos may indeed be desirable since it can be controlled by using small perturbation to some accessible parameter.

The major key ingredient for the OGY-control of chaos is the observation that a chaotic set, on which the trajectory of the chaotic process lives, has embedded within it a large number of unstable low-period periodic orbits. In addition, because of ergodicity, the trajectory visits or accesses the neighborhood of each one of these periodic orbits. Some of these periodic orbits may correspond to a desired system's performance according to some criterion. The second ingredient is the realization that chaos, while signifying sensitive dependence on small changes to the current state and henceforth rendering unpredictable the system state in the long time, also

implies that the system's behavior can be altered by using small perturbations. Then, the accessibility of the chaotic systems to many different periodic orbits combined with its sensitivity to small perturbations allows for the control and the manipulation of the chaotic process. Specifically, the OGY approach is then as follows. One first determines some of the unstable low-period periodic orbits that are embedded in the chaotic set. One then examines the location and the stability of these orbits and chooses one which yields the desired system performance. Finally, one applies small control to stabilize this desired periodic orbit. However, all this can be done from data by using nonlinear time series analysis for the observation, understanding and control of the system. This is particularly important since chaotic systems are rather complicated and the detailed knowledge of the equations of the process is often unknown [Boccaletti *et al.* (2000)].

**Simple Example of Chaos Control: a 1D Map.** The basic idea of controlling chaos can be understood [Lai (1994)] by considering May's classical *logistic map* [May (1976)] (2.12)

$$x_{n+1} = f(x_n, r) = rx_n(1 - x_n),$$

where  $x$  is restricted to the unit interval  $[0, 1]$ , and  $r$  is a control parameter. It is known that this map develops chaos via the *period-doubling bifurcation* route. For  $0 < r < 1$ , the asymptotic state of the map (or the attractor of the map) is  $x = 0$ ; for  $1 < r < 3$ , the attractor is a nonzero fixed point  $x_F = 1 - 1/r$ ; for  $3 < r < 1 + \sqrt{6}$ , this fixed point is unstable and the attractor is a stable period-2 orbit. As  $r$  is increased further, a sequence of period-doubling bifurcations occurs in which successive period-doubled orbits become stable. The period-doubling cascade accumulates at  $r = r_\infty \approx 3.57$ , after which chaos can arise.

Consider the case  $r = 3.8$  for which the system is apparently chaotic. An important characteristic of a chaotic attractor is that there exists an infinite number of unstable periodic orbits embedded within it. For example, there are a fixed point  $x_F \approx 0.7368$  and a period-2 orbit with components  $x(1) \approx 0.3737$  and  $x(2) = 0.8894$ , where  $x(1) = f(x(2))$  and  $x(2) = f(x(1))$ .

Now suppose we want to avoid chaos at  $r = 3.8$ . In particular, we want trajectories resulting from a randomly chosen initial condition  $x_0$  to be as close as possible to the period-2 orbit, assuming that this period-2 orbit gives the best system performance. Of course, we can choose the desired asymptotic state of the map to be any of the infinite number of unstable periodic orbits. Suppose that the parameter  $r$  can be finely tuned in a small range around the value  $r_0 = 3.8$ , i.e.,  $r$  is allowed to vary in the

range  $[r_0 - \delta, r_0 + \delta]$ , where  $\delta \ll 1$ . Due to the nature of the chaotic attractor, a trajectory that begins from an arbitrary value of  $x_0$  will fall, with probability one, into the neighborhood of the desired period-2 orbit at some later time. The trajectory would diverge quickly from the period-2 orbit if we do not intervene. Our task is to program the variation of the control parameter so that the trajectory stays in the neighborhood of the period-2 orbit as long as the control is present. In general, the small parameter perturbations will be time dependent [Boccaletti *et al.* (2000)].

The logistic map in the neighborhood of a periodic orbit can be approximated by a linear equation expanded around the periodic orbit. Denote the target period- $m$  orbit to be controlled as  $x(i)$ ,  $i = 1, \dots, m$ , where  $x(i+1) = f(x(i))$  and  $x(m+1) = x(1)$ . Assume that at time  $n$ , the trajectory falls into the neighborhood of component  $i$  of the period- $m$  orbit. The linearized dynamics in the neighborhood of component  $i+1$  is then

$$\begin{aligned} x_{n+1} - x(i+1) &= \frac{\partial f}{\partial x}[x_n - x(i)] + \frac{\partial f}{\partial r} \Delta r_n \\ &= r_0[1 - 2x(i)][x_n - x(i)] + x(i)[1 - x(i)]\Delta r_n, \end{aligned}$$

where the partial derivatives are evaluated at  $x = x(i)$  and  $r = r_0$ . We require  $x_{n+1}$  to stay in the neighborhood of  $m$ . Hence, we set  $x_{n+1} - x(i+1) = 0$ , which gives

$$\Delta r_n = r_0 \frac{[2x(i) - 1][x_n - x(i)]}{x(i)[1 - x(i)]}. \quad (2.19)$$

Equation (2.19) holds only when the trajectory  $x_n$  enters a small neighborhood of the period- $m$  orbit, i.e., when  $|x_n - x(i)| \ll 1$ , and hence the required parameter perturbation  $\Delta r_n$  is small. Let the length of a small interval defining the neighborhood around each component of the period- $m$  orbit be  $2\varepsilon$ . In general, the required maximum parameter perturbation  $\delta$  is proportional to  $\varepsilon$ . Since  $\varepsilon$  can be chosen to be arbitrarily small,  $\delta$  also can be made arbitrarily small. The average transient time before a trajectory enters the neighborhood of the target periodic orbit depends on  $\varepsilon$  (or  $\delta$ ). When the trajectory is outside the neighborhood of the target periodic orbit, we do not apply any parameter perturbation, so the system evolves at its nominal parameter value  $r_0$ . Hence we set  $\Delta r_n = 0$  when  $\Delta r_n > \delta$ . The parameter perturbation  $\Delta r_n$  depends on  $x_n$  and is time-dependent.

The above strategy for controlling the orbit is very flexible for stabilizing different periodic orbits at different times. Suppose we first stabilize a chaotic trajectory around a period-2 orbit. Then we might wish to stabilize

the fixed point of the logistic map, assuming that the fixed point would correspond to a better system performance at a later time. To achieve this change of control, we simply turn off the parameter control with respect to the period-2 orbit. Without control, the trajectory will diverge from the period-2 orbit exponentially. We let the system evolve at the parameter value  $r_0$ . Due to the nature of chaos, there comes a time when the chaotic trajectory enters a small neighborhood of the fixed point. At this time we turn on a new set of parameter perturbations calculated with respect to the fixed point. The trajectory can then be stabilized around the fixed point [Lai (1994)].

In the presence of external noise, a controlled trajectory will occasionally be 'kicked' out of the neighborhood of the periodic orbit. If this behavior occurs, we turn off the parameter perturbation and let the system evolve by itself. With probability one the chaotic trajectory will enter the neighborhood of the target periodic orbit and be controlled again. The effect of the noise is to turn a controlled periodic trajectory into an intermittent one in which chaotic phases (uncontrolled trajectories) are interspersed with laminar phases (controlled periodic trajectories). It is easy to verify that the averaged length of the laminar phase increases as the noise amplitude decreases [Lai (1994)].

### 2.3.3.5 Floquet Stability Analysis and OGY Control

Controlling chaos, or stabilization of unstable periodic orbits of chaotic systems, has established to a field of large interest since the seed paper of Ott, Grebogi, Yorke [Ott *et al.* (1990)]. The idea is to stabilize by a feedback calculated at each *Poincaré section*, which reduces the control problem to stabilization of an unstable fixed point of an iterated map. The feedback can, as in OGY scheme, be chosen proportional to the distance to the desired fixed point, or proportional to the difference in phase-space position between actual and last but one Poincaré section. This difference control scheme [Bielawski *et al.* (1993)], being a time-discrete counterpart of the Pyragas approach [Pyragas (1992); Pyragas (1995)], allows for stabilization of inaccurately known fixed points, and can be extended by a memory term to overcome stability restrictions and to allow for tracking of drifting fixed points [Claussen *et al.* (1998a)].

In this section the stability of perturbations  $x(t)$  around an unstable periodic orbit being subject to a Poincaré-based control scheme is analyzed by means of *Floquet theory* [Hale and Lunel (1993)]. This approach allows

to investigate viewpoints that have not been accessible by considering only the iteration dynamics between the Poincaré sections. Among these are primary the discussion of small measurement delays and variable impulse lengths. The impulse length is for both OGY and difference control usually a fixed parameter; and the iterated dynamics is uniquely defined only as long as this impulse length is not varied. The influence of the impulse length has not been point of consideration before; if reported at all, usually for both OGY and difference control a relative length of approximately  $1/3$  is chosen without any reported sensitivity [Claussen (2002b)].

The linearized ODEs of both schemes are invariant under translation in time,  $t \rightarrow t + T$ . Therefore we can expand the solutions after periodic solutions  $u(t + T) = u(t)$  according to

$$x(t) = e^{\gamma T} u_\gamma(t).$$

The necessary condition for stability of the solution is  $\text{Re}(\gamma) < 0$ ; and  $x(t) \equiv 0$  refers to motion along the orbit.

Whereas for the *Pyragas control* method (in which the delayed state feedback enforces a time-continuous description) a *Floquet stability analysis* is known [Just *et al.* (1997)], here the focus is on the time-discrete control schemes.

**Time-Continuous Stability Analysis of OGY Control.** Due to the mathematically elegant and practical convenient description and application of OGY control in the Poincaré section up to now there seems to have been no need to calculate explicitly the *Floquet multiplier* for a stability analysis. However, this allows a novel viewpoint on the differences between the local dynamics around an instable periodic orbit of a dynamical system being subject to Pyragas and OGY control.

For the 1D case, one has the dynamical system [Claussen (2002b)]

$$\dot{x}(t) = \lambda x(t) + \mu \varepsilon x(t - (t \bmod T)).$$

In the first time interval between  $t = 0$  and  $t = T$  the differential equation reads

$$\dot{x}(t) = \lambda x(t) - \mu \varepsilon x(0), \quad \text{for} \quad 0 < t < T.$$

Integration of this differential equation yields

$$x(t) = \left( \left( 1 - \frac{\mu \varepsilon}{\lambda} \right) e^{\lambda t} + \frac{\mu \varepsilon}{\lambda} \right) x(0).$$

This gives us an iterated dynamics (here we label the beginning of the time period again with  $t$ )

$$x(t+T) = \left( \left(1 - \frac{\mu\varepsilon}{\lambda}\right)e^{\lambda T} + \frac{\mu\varepsilon}{\lambda} \right) x(t).$$

The Floquet multiplier of an orbit therefore is

$$e^{\gamma T} = \left(1 - \frac{\mu\varepsilon}{\lambda}\right)e^{\lambda T} + \frac{\mu\varepsilon}{\lambda}.$$

**Influence of the Duration of the Control Impulse on OGY Control.** The time-discrete viewpoint now allows to investigate the influence of timing questions on control. First we consider the case that the control impulse is applied timely in the Poincaré section, but only for a finite period  $T \cdot p$  within the orbit period ( $0 < p < 1$ ).

This situation is described by the differential equation [Claussen (2002b)]

$$\dot{x}(t) = \lambda x(t) \mu \varepsilon x(t - (t \bmod T)) \cdot \Theta((t \bmod T) - p).$$

Here  $\Theta$  is a step function ( $\Theta(x) = 1$  for  $x > 0$  and  $\Theta(x) = 0$  elsewhere). In the first time interval between  $t = 0$  and  $t = T \cdot p$  the differential equation reads

$$\dot{x}(t) = \lambda x(t) + \mu \varepsilon x(0), \quad \text{for} \quad 0 < t < T \cdot p.$$

Integration of this differential equation yields

$$x(t) = \left( \left(1 + \frac{\mu\varepsilon}{\lambda}\right)e^{\lambda t} - \frac{\mu\varepsilon}{\lambda} \right) x(0), \quad x(T \cdot p) = \left( \left(1 + \frac{\mu\varepsilon}{\lambda}\right)e^{\lambda T \cdot p} - \frac{\mu\varepsilon}{\lambda} \right) x(0).$$

In the second interval between  $t = T \cdot p$  and  $t = T$  the differential equation is the same as without control,

$$\dot{x}(t) = \lambda x(t), \quad \text{for} \quad T \cdot p < t < T.$$

From this one has immediately

$$x(t) = e^{\lambda(t-T \cdot p)} x(T \cdot p).$$

If the beginning of the integration period again is denoted by  $t$ , this defines an iteration dynamics,

$$x(t+T) = e^{\lambda(1-p)T} \left( \left(1 + \frac{\mu\varepsilon}{\lambda}\right)e^{\lambda T \cdot p} - \frac{\mu\varepsilon}{\lambda} \right) x(t) = \left( \left(1 + \frac{\mu\varepsilon}{\lambda}\right)e^{\lambda T} - \frac{\mu\varepsilon}{\lambda} e^{\lambda(1-p)T} \right),$$

and the Floquet multiplier of an orbit is given by

$$e^{\gamma T} = \left(1 - \frac{\mu\varepsilon}{\lambda}\right)e^{\lambda T} + \frac{\mu\varepsilon}{\lambda}e^{\lambda(1-p)T} = e^{\lambda T} \left(1 - \frac{\mu\varepsilon}{\lambda}(1 - e^{-\lambda p T})\right). \quad (2.20)$$

One finds that in zero order the ‘strength’ of control is given by the product  $p \cdot \mu\varepsilon$ ; in fact there is a weak linear correction in  $p$ . For  $\lambda p T \leq 1$  one has

$$e^{\gamma T} = e^{\lambda T} \left(1 + \mu\varepsilon p T + \frac{1}{2} \mu\varepsilon \lambda p^2 T^2 + o(p^3)\right) = e^{\lambda T} \left(1 + \mu\varepsilon p T \left(1 - \frac{1}{2} \lambda p T + o(p^2)\right)\right),$$

i.e., to obtain a constant strength of control, one has to fulfill the condition

$$\mu\varepsilon p T = \frac{1}{1 - \frac{\lambda T}{2} p} = 1 + \frac{\lambda T}{2} p + o(p^2).$$

The result is, apart from a weak linear correction for OGY control the length of the impulse can be chosen arbitrarily, and the ‘strength’ of control in zero order is given by the time integral over the control impulse.

**Floquet Stability Analysis of Difference Control.** Again the starting point is the linearized equation of motion around the periodic orbit when control is applied. For difference control now there is a dependency on two past time steps,

$$\dot{x}(t) = \lambda x(t) + \mu\varepsilon x(t - (t \bmod T)) - \mu\varepsilon x(t - T - (t \bmod T)). \quad (2.21)$$

Although the r.h.s of (2.21) depends on  $x$  at three different times, it can be nevertheless integrated exactly, which is mainly due to the fact that the two past times (of the two last Poincaré crossings) have a fixed time difference being equal to the orbit length. This allows not only for an exact solution, but also offers a correspondence to the time-discrete dynamics and the matrix picture used in time-delayed coordinates [Claussen *et al.* (1998a); Claussen and Schuster (1998); Claussen *et al.* (1998b)].

**Stability Analysis of Difference Control.** Now also for difference control the experimentally more common situation of a finite but small measurement delay  $T \cdot s$  is considered, together with a finite impulse length  $T \cdot p$  (here  $0 < p < 1$  and  $0 < (s + p) < 1$ ) [Claussen (2002b)].

In the first time interval between  $t = 0$  and  $t = T \cdot s$  the ODE reads

$$\dot{x}(t) = \lambda x(t), \quad \text{for} \quad 0 < t < T \cdot s.$$

The integration gives  $x(T \cdot s) = e^{\lambda T \cdot s} x(0)$ .

For the second interval between  $t = T \cdot s$  and  $t = T \cdot (s + p)$  we have

$$\dot{x}(t) = \lambda x(t) - \mu\varepsilon x(0) = \lambda x(t) + \mu\varepsilon (x(0) - x(-T)), \quad \text{for} \quad T \cdot s < t < T \cdot (s + p).$$



Integration of this ODE yields

$$x(t) = -\frac{\mu\varepsilon}{\lambda}(x(0) - x(-T)) + \frac{\mu\varepsilon}{\lambda}(x(0) - x(-T)) + e^{\lambda s T} x(0) e^{\lambda(t-sT)}$$

$$x(T(s+p)) = -\frac{\mu\varepsilon}{\lambda}(x(0) - x(-T)) \frac{\mu\varepsilon}{\lambda}(x(0) - x(-T)) + e^{\lambda p T} + e^{\lambda(s+p)T} x(0).$$

For the third interval, the ODE is homogeneous again and one has

$$x(t) = e^{\lambda(t-(s+p)T)} x(T \cdot (s+p)), \quad \text{for} \quad T \cdot (s+p) < t < T.$$

Insertion gives

$$x(T) = x(0)e^{\lambda T} \left(1 + \frac{\mu\varepsilon}{\lambda} e^{-\lambda s T} (1 - e^{-\lambda p T})\right) - x(-T)e^{\lambda T} \frac{\mu\varepsilon}{\lambda} e^{-\lambda s T} (1 - e^{-\lambda p T})$$

or, in time-delayed coordinates of the last and last but one Poincaré crossing [Claussen (2002b)]

$$\begin{pmatrix} x_{n+1} \\ x_n \end{pmatrix} = \begin{pmatrix} e^{\lambda T} \left(1 + \frac{\mu\varepsilon(1-e^{-\lambda p T})}{\lambda e^{\lambda s T}}\right) & -e^{\lambda T} \frac{\mu\varepsilon(1-e^{-\lambda p T})}{\lambda e^{\lambda s T}} \\ 1 & 0 \end{pmatrix} \begin{pmatrix} x_n \\ x_{n-1} \end{pmatrix}.$$

If we identify with the coefficients of the time-discrete case,  $\lambda_d = e^{\lambda T}$  and  $\mu_d \varepsilon_d = e^{-\lambda s T} (1 - e^{\lambda p T}) \frac{\mu\varepsilon}{\lambda}$ , the dynamics in the Poincaré iteration  $t = nT$  becomes identical with the pure discrete description; this again illustrates the power of the concept of the Poincaré map. Due to the low degree of the characteristic polynomial, one in principle can explicitly diagonalize the iteration matrix, allowing for a closed expression for the  $n$ th power of the iteration matrix. As for the stability analysis only the eigenvalues are needed, this straightforward calculation is excluded here.

For the Floquet multiplier one has [Claussen (2002b)]

$$e^{2\gamma T} = e^{\gamma T} e^{\lambda T} \left(1 + \frac{\mu\varepsilon}{\lambda} e^{-\lambda s T} (1 - e^{-\lambda p T})\right) - e^{\lambda T} \frac{\mu\varepsilon}{\lambda} e^{-\lambda s T} (1 - e^{-\lambda p T}).$$

This quadratic equation yields two Floquet multipliers,

$$e^{\gamma T} = \frac{1}{2} e^{\lambda T} \left(1 + \frac{\mu\varepsilon}{\lambda} e^{-\lambda s T} (1 - e^{-\lambda p T})\right) \pm \frac{1}{2} \sqrt{\left(e^{\lambda T} \left(1 + \frac{\mu\varepsilon}{\lambda} e^{-\lambda s T} (1 - e^{-\lambda p T})\right)\right)^2 + 4e^{\lambda T} \frac{\mu\varepsilon}{\lambda} e^{-\lambda s T} (1 - e^{-\lambda p T})}.$$

For  $s = 0$  one obtains the special cases discussed above.

### 2.3.3.6 Jerk Functions of Simple Chaotic Flows

Recall that the celebrated *Lorenz equations* (2.8) can be rewritten as

$$\dot{x} = -ax + ay, \quad \dot{y} = -xz + bx - y, \quad \dot{z} = xy - cz. \quad (2.22)$$

Note that there are seven terms in the phase-flow of these equations, two of which are nonlinear ( $xz$  and  $xy$ ); also, there are three parameters, for which Lorenz found chaos with  $a = 10$ ,  $b = 28$ , and  $c = 8/3$ . The number of independent parameters is generally  $d + 1$  less than the number of terms for a  $d$ -dimensional system, since each of the variables ( $x$ ,  $y$ , and  $z$  in this case) and time ( $t$ ) can be arbitrarily rescaled [Sprott and Linz (2000)]. The Lorenz system has been extensively studied, and there is an entire book [Sparrow (1982)] devoted to it.

Although the Lorenz system is often taken as the prototypical chaotic flow, it is not the algebraically simplest such system [Sprott and Linz (2000)]. Recall that in 1976, *Rössler* [Rössler (1976)] proposed his equations (2.11), rewritten here as

$$\dot{x} = -y - z, \quad \dot{y} = x + ay, \quad \dot{z} = b + xz - cz. \quad (2.23)$$

Rössler phase-flow also has seven terms and two parameters, which Rössler took as  $a = b = 0.2$  and  $b = 5.7$ , but only a single quadratic nonlinearity ( $xz$ ).

In 1994, Sprott [Sprott (1994)] embarked on an extensive search for autonomous three-dimensional chaotic systems with fewer than seven terms and a single quadratic nonlinearity and systems with fewer than six terms and two quadratic nonlinearities. The *brute-force* method [Sprott (1993a); Sprott (1993b)] involved the numerical solution of a huge number (about  $10^8$ ) systems of autonomous ODEs with randomly chosen real coefficients and initial conditions. The criterion for chaos was the existence of a leading Lyapunov exponent. He found fourteen algebraically distinct cases with six terms and one nonlinearity, and five cases with five terms and two nonlinearities. One case was volume conserving (conservative), and all the others were volume-contracting (dissipative), implying the existence of a strange attractor. Sprott provided a table of the spectrum of Lyapunov exponents, the related Kaplan-Yorke dimension, and the types and eigenvalues of the unstable fixed points for each of the nineteen cases [Sprott and Linz (2000)].

Subsequently, Hoover [Hoover (1995)] pointed out that the conservative case found by Sprott in [Sprott (1994)]

$$\dot{x} = y, \quad \dot{y} = -x + yz, \quad \dot{z} = 1 - y^2, \quad (2.24)$$

is a special case of the Nosé–Hoover thermostated dynamic system that had earlier been shown [Posch *et al.* (1986)] to exhibit time-reversible *Hamiltonian chaos*.

In response to Sprott's work, Gottlieb [Gottlieb (1996)] pointed out that the conservative system (2.24) could be recast in the *explicit third-order form*

$$\ddot{x} = -\dot{x} + \ddot{x}(x + \ddot{x})/\dot{x},$$

which he called a '*jerk function*' since it involves a third derivative of  $\ddot{x}$ , which in a mechanical system is the time rate of change of the acceleration, also called the '*jerk*' [Schot (1978)]. It is known that any explicit ODE can be cast in the form of a system of coupled first-order ODEs, but the converse does not hold in general. Even if one can reduce the dynamical system to a jerk form for each of the phase-space variables, the resulting differential equations may look quite different. Gottlieb asked the provocative question 'What is the simplest jerk function that gives chaos?'

One response was provided by Linz [Linz (1997)] who showed that both the original Rössler model and the Lorenz model can be reduced to jerk forms. The Rössler model (2.23) can be rewritten (in a slightly modified form) as

$$\ddot{x} + (c - \varepsilon + \varepsilon x - \dot{x})\ddot{x} + [1 - \varepsilon c - (1 + \varepsilon^2)x + \varepsilon\dot{x}]\dot{x} + (\varepsilon x + c)x + \varepsilon = 0,$$

where  $\varepsilon = 0.2$  and  $c = 5.7$  gives chaos. Note that the jerk form of the Rössler equation is a rather complicated quadratic polynomial with 10 terms.

The Lorenz model in (2.22) can be written as

$$\ddot{x} + (1 + \sigma + b - \dot{x}/x)\ddot{x} + [b(1 + \sigma + x^2) - (1 + \sigma)\dot{x}/x]\dot{x} - b\sigma(r - 1 - x^2)x = 0.$$

The jerk form of the Lorenz equation is not a polynomial since it contains terms proportional to  $\dot{x}/x$  as is typical of dynamical systems with multiple nonlinearities. Its jerk form contains eight terms.

Linz [Linz (1997)] showed that Sprott's case R model (see [Sprott (1994)]) can be written as a polynomial with only five terms and a single quadratic nonlinearity

$$\ddot{x} + \ddot{x} - x\dot{x} + ax + b = 0,$$

with chaos for  $a = 0.9$  and  $b = 0.4$ .

Sprott [Sprott (1997)] also took up Gottlieb's challenge and embarked on an extensive numerical search for chaos in systems of the explicit form

$$\ddot{x} = J(\ddot{x}, \dot{x}, x),$$

where the jerk function  $J$  is a simple quadratic or cubic polynomial. He found a variety of cases, including two with three terms and two quadratic nonlinearities in their jerk function,

$$\ddot{x} + ax\ddot{x} - \dot{x}^2 + x = 0,$$

with  $a = 0.645$  and

$$\ddot{x} + ax\ddot{x} - x\dot{x} + x = 0,$$

with  $a = -0.113$ , and a particularly simple case with three terms and a single quadratic nonlinearity

$$\ddot{x} + a\ddot{x} \pm \dot{x}^2 + x = 0, \tag{2.25}$$

with  $a = 2.017$ . For this value of  $a$ , the Lyapunov exponents are  $(0.0550, 0, -2.0720)$  and the Kaplan–Yorke dimension is  $d_{KY} = 2.0265$ .

Equation (2.25) is simpler than any previously discovered case. The range of the parameter  $a$  over which chaos occurs is quite narrow  $(2.0168... < a < 2.0577...)$ . It also has a relatively small basin of attraction, so that initial conditions must be chosen carefully. One choice of initial conditions that lies in the basin of attraction is  $(x, y, z) = (0, 0, \pm 1)$ , where the sign is chosen according to the sign of the  $\pm \dot{x}^2$  term.

All above systems share a common *route to chaos*. The control parameter  $a$  can be considered a *damping rate* for the nonlinear oscillator. For large values of  $a$ , there are one or more stable equilibrium points. As  $a$  decreases, a *Hopf bifurcation* (see [Chen and Dong (1998)]) occurs in which the equilibrium becomes unstable, and a stable limit cycle is born. The limit cycle grows in size until it bifurcates into a more complicated limit cycle with two loops, which then bifurcates into four loops, and so forth, in a *sequence of period doublings* until chaos finally onsets. A further decrease in  $a$  causes the *chaotic attractor* to grow in size, passing through infinitely many periodic windows, and finally becoming unbounded when the attractor grows to touch the boundary of its *basin of attraction* (a 'crisis').

Recently, Malasoma [Malasoma (2000)] joined the search for simple chaotic jerk functions and found a cubic case as simple as (2.25) but of

a different form

$$\ddot{x} + a\dot{x} - x\dot{x}^2 + x = 0,$$

which exhibits chaos for  $a = 2.05$ . For this value of  $a$ , the Lyapunov exponents are  $(0.0541, 0, -2.1041)$ , and the Kaplan–Yorke dimension is  $d_{KY} = 2.0257$ . This case follows the usual period-doubling route to chaos, culminating in a boundary crisis and unbounded solutions as  $a$  is lowered. The range of  $a$  over which chaos occurs is very narrow,  $(2.0278 \dots < a < 2.0840 \dots)$ . There is also a second extraordinarily small window of chaos for  $(0.0753514 \dots < a < 0.0753624 \dots)$ , which is five thousand times smaller than the previous case. Malasoma points out that this system is invariant under the parity transformation  $x \rightarrow -x$  and speculates that this system is the simplest such example.

Both Linz and Sprott pointed out that if the jerk function is considered the time derivative of an acceleration of a particle of mass  $m$ , then *Newton's second law* implies a force  $F$  whose time derivative is  $\dot{F} = mJ$ . If the force has an explicit dependence on only  $\dot{x}$ ,  $x$ , and time, it is considered to be 'Newtonian jerk'. The condition for  $F = F(\dot{x}, x, t)$  is that  $J$  depends only linearly on  $\ddot{x}$ . In such a case the force in general includes a *memory term* of the form

$$M = \int_0^t G(x(\tau)) d\tau,$$

which depends on the dynamical history of the motion.

The jerk papers by Linz [Linz (1997)] and Sprott [Sprott (1997)] appeared in the same issue of the American Journal of Physics and prompted von Baeyer [von Baeyer (1998)] to comment: "The articles with those funny titles are not only perfectly serious, but they also illustrate in a particularly vivid way the revolution that is transforming the ancient study of mechanics into a new science — one that is not just narrowly concerned with the motion of physical bodies, but that deals with changes of all kinds." He goes on to say that the method of searching for chaos in a large class of systems "is not just empty mathematical formalism. Rather it illustrates the arrival of a new level of abstraction in physical science. . . . At that higher level of abstraction, dynamics has returned to the classical Aristotelian goal of trying to understand all change."

We will use the jerk functions in chapter 4 below as a *natural measure for the risk of spinal injuries*.

### 2.3.4 The Basic Hamiltonian Model of Biodynamics

Now, we return to biodynamics. To describe the biodynamics of human-like movement, namely our *covariant force law*,  $F_i = mg_{ij}a^j$ , we can also start from generalized Hamiltonian vector-field  $X_H$  describing the behavior of the *human-like locomotor system* (see [Ivancevic and Snoswell (2001); Ivancevic (2002); Ivancevic and Pearce (2001b); Ivancevic (2005)])

$$\dot{q}^i = \frac{\partial H}{\partial p_i} + \frac{\partial R}{\partial p_i}, \quad (2.26)$$

$$\dot{p}_i = F_i - \frac{\partial H}{\partial q^i} + \frac{\partial R}{\partial q^i}, \quad (2.27)$$

where the vector-field  $X_H$  is generating time evolution, or *phase-flow*, of  $2n$  system variables:  $n$  generalized coordinates (joint angles  $q^i$ ) and  $n$  generalized momenta (joint angular momenta  $p_i$ ),  $H = H(q, p)$  represents the system's conservative energy: kinetic energy + various mechano-chemical potentials,  $R = R(q, p)$  denotes the nonlinear dissipation of energy, and  $F_i = F_i(t, q, p, \sigma)$  are external control forces (biochemical energy inputs). The *system parameters* include inertia tensor with mass distribution of all body segments, stiffness and damping tensors for all joints (labelled by index  $i$ , which is, for geometric reasons, written as a subscript on angle variables, and as a superscript on momentum variables), as well as amplitudes, frequencies and time characteristics of all active muscular forces (supposed to be acting in all the joints; if some of the joints are inactive, we have the affine Hamiltonian control system, see chapter 6).

The equation (2.26) is called the *velocity equation*, representing the *flow* of the system (analogous to current in electrodynamics), while the equation (2.27) is a Newton-like *force equation*, representing the *effort* of the system (analogous to voltage). Together, these two functions represent Hamiltonian formulation of the *biomechanical force-velocity relation* of A.V. Hill [Hill (1938)]. From engineering perspective, their (inner) product, *flow · effort*, represents the total system's *power*, equal to the time-rate-of-change of the total system's energy (included in  $H, R$  and  $F_i$  functions). And energy itself is transformed into the *work* done by the system.

Now, the reasonably accurate musculo-skeletal biodynamics would include say a hundred DOF, which means a hundred of joint angles and a hundred of joint momenta, which further means a hundred of coupled equations of the form of (2.26–2.27). And the *full coupling* means that each angle (and momentum) includes the information of all the other an-

gles (and momenta), the *chain coupling* means that each angle (and momentum) includes the information of all the previous (i.e., children) angles (and momenta), the *nearest neighbor coupling* includes the information of the nearest neighbors, etc.

No matter which coupling we use for modelling the dynamics of human motion, one thing is certain: the *coupling is nonlinear*. And we obviously have to fight chaos within several hundreds of variables.

Wouldn't it be better if we could somehow be able to obtain a synthetic information about the whole musculo-skeletal dynamics, synthesizing the hundreds of equations of motion of type (2.26–2.27) into a small number of equations describing the time evolution of the so-called *order parameters*? If we could do something similar to principal component analysis in multivariate statistics and neural networks, to get something like 'nonlinear factor dynamics'?

Starting from the basic system (2.26–2.27), on the lowest, *microscopic level of human movement organization*, the *order parameter equations of macroscopic synergetics* can be (at least theoretically), either exactly derived along the lines of *mezoscopic synergetics*, or phenomenologically stated by the use of the certain biophysical analogies and nonlinear identification and control techniques (a highly complex nonlinear system like human locomotor apparatus could be neither identified nor controlled by means of standard linear engineering techniques).

### 2.3.5 The Basics of Haken's Synergetics

The *measure for the degree of disorder* in any isolated, or conservative, system (such a system that does not interact with its surrounding, i.e., does neither dissipate nor gain energy) is *entropy*. The *second law of thermodynamics*<sup>3</sup> states that in every conservative irreversible system the entropy ever increases to its maximal value, i.e., to the total disorder of the system (or remains constant for a reversible system).

Example of such a system is conservative Hamiltonian dynamics of human skeleton in the phase-space  $\Gamma$  defined by all joint angles  $q^i$  and momenta  $p_i$ <sup>4</sup>, defined by ordinary (conservative) Hamilton's equations

$$\dot{q}^i = \partial_{p_i} H, \quad \dot{p}_i = -\partial_{q^i} H. \quad (2.28)$$

<sup>3</sup>This is the only physical law that implies the arrow of time.

<sup>4</sup>If we neglect joints dissipation and muscular driving forces, we are dealing with pure skeleton conservative dynamics.

The basic fact of the conservative Hamiltonian system is that its phase-flow, the time evolution of equations (2.28), preserves the phase-space volume (the so-called *Liouville measure*), as proposed by the *Liouville theorem*. This might look fine at first sight, however, the preservation of phase-space volume causes *structural instability* of the conservative Hamiltonian system, i.e., the phase-space spreading effect, by which small phase regions  $R_t$  will tend to get distorted from the initial one  $R_0$  during the system evolution. The problem is much more serious in higher dimensions than in lower dimensions, since there are so many 'directions' in which the region can locally spread. Here we see the work of the second law of thermodynamics on an irreversible process: the increase of entropy towards the total disorder/chaos [Penrose (1989)]. In this way, the conservative Hamiltonian systems of the form (2.28) cover the wide range of dynamics, from completely integrable, to completely ergodic. Biodynamics of human-like movement is probably somewhere in the middle of this range, the more DOF included in the model, the closer to the ergodic case. One can easily imagine that the conservative skeleton-like system with 300 DOF, which means 600-D system of the form (2.28), which is full of trigonometry (coming from its noncommutative rotational matrices), is probably closer to the ergodic than to the completely integrable case.

On the other hand, when we manipulate a system from the outside, by the use of certain *control parameters*  $\{\sigma\}$ , we can change its *degree of order* (see [Haken (1983); Haken (1993)]). Consider for example *water vapor*. At elevated temperature its molecules move freely without mutual correlation. When temperature is lowered, a liquid drop is formed, the molecules now keep a mean distance between each other. Their motion is thus highly correlated. Finally, at still lower temperature, at the freezing point, water is transformed into ice crystals. The transitions between the different aggregate states, also called phases, are quite abrupt. Though the same kind of molecules are involved all the time, the macroscopic features of the three phases differ drastically.

Similar type of ordering, but not related to the thermal equilibrium conditions, occurs in *lasers*, mathematically given by Lorenz-like attractor equations. Lasers are certain types of lamps which are capable of emitting coherent light. A typical laser consists of a crystal rod filled with gas, with the following features important from the synergetics point of view: when the atoms the laser material consists of are excited or 'pumped' from the outside, they emit light waves. So, the pump power, or pump rate represents the control parameter  $\sigma$ . At low pump power, the waves are



entirely uncorrelated as in a usual lamp. Could we hear light, it would sound like noise to us [Haken (1983)].

When we increase the pump rate to a critical value  $\sigma_c$ , the noise disappears and is replaced by a pure tone. This means that the atoms emit a pure sinusoidal light wave which in turn means that the individual atoms act in a perfectly correlated way – they become self-organized. When the pump rate is increased beyond a second critical value, the laser may periodically emit very intense and short pulses. In this way the following *instability sequence* occurs [Haken (1983)]:

noise  $\mapsto$  {coherent oscillation at frequency  $\omega_1$ }  $\mapsto$

periodic pulses at frequency  $\omega_2$  which modulate oscillation at frequency  $\omega_1$

i.e., no oscillation  $\mapsto$  first frequency  $\mapsto$  second frequency.

Under different conditions the light emission may become *chaotic* or even *turbulent*. The frequency spectrum becomes broadened.

The laser played a crucial role in the development of synergetics for various reasons [Haken (1983)]. In particular, it allowed detailed theoretical and experimental study of the phenomena occurring within the transition region: *lamp*  $\leftrightarrow$  *laser*, where a surprising and far-reaching analogy with phase transitions of systems in thermal equilibrium was discovered. This analogy includes all basic *phase-transition effects*: a *symmetry breaking instability*, *critical slowing down* and *hysteresis effect*.

### 2.3.5.1 Phase Transitions

Besides water vapor, a typical example is a *ferromagnet* [Haken (1983)]. When a ferromagnet is heated, it suddenly loses its magnetization. When temperature is lowered, the magnet suddenly regains its magnetization. What happens on a microscopic, atomic level, is this: We may visualize the magnet as being composed of many, elementary (atomic) magnets (called spins). At elevated temperature, the elementary magnets point in random directions. Their magnetic moments, when added up, cancel each other and no macroscopic magnetization results. Below a critical value of temperature  $T_c$ , the elementary magnets are lined up, giving rise to a macroscopic magnetization. Thus the *order on the microscopic level* is a cause of a *new feature* of the material *on the macroscopic level*. The change of one phase to the other one is called *phase transition*.

A thermodynamical description of ferromagnet is based on analysis of its *free energy potential* (in thermal equilibrium conditions). The free en-

ergy  $\mathcal{F}$ , depends on the *control parameter*  $\sigma = T$ , the temperature. We seek the minimum of the potential  $\mathcal{F}$  for a fixed value of magnetization  $o$ , which is called *order parameter* in Landau's theory of phase transitions (see Appendix).

This phenomenon is called a *phase transition of second order* because the second derivative (specific heat) of the free energy potential  $\mathcal{F}$  is discontinuous. On the other hand, the entropy  $S$  (the first derivative of  $\mathcal{F}$ ) itself is continuous so that this transition is also referred to as a *continuous phase transition*.

In statistical physics one also investigates the temporal change of the order parameter – magnetization  $o$ . Usually, in a more or less phenomenological manner, one assumes that  $o$  obeys an equation of the form

$$\dot{o} = -\frac{\partial \mathcal{F}}{\partial o} = -\sigma o - \beta o^3. \quad (2.29)$$

For  $\sigma \rightarrow 0$  we observe a phenomenon called *critical slowing down*, because the 'particle' with coordinate  $o$  falls down the slope of the 'potential well' more and more slowly. Simple relation (2.29) is called *order parameter equation*.

We now turn to the case where the free energy potential has the form

$$\mathcal{F}(o, T) = \frac{\sigma}{2}o^2 + \frac{\gamma}{3}o^3 + \frac{\beta}{4}o^4, \quad (2.30)$$

( $\beta$  and  $\gamma$  – positive but  $\sigma$  may change its sign according to  $\sigma = a(T - T_c)$ , ( $a > 0$ )). When we change the control parameter – temperature  $T$ , i.e., the parameter  $\sigma$ , we pass through a sequence of deformations of the potential curve.

When lowering temperature, the local minimum first remains at  $o_0 = 0$ . When lowering temperature, the 'particle' may fall down from  $o_0$  to the new (global) minimum of  $\mathcal{F}$  at  $o_1$ . The entropies of the two states,  $o_0$  and  $o_1$ , differ. This phenomenon is called a *phase transition of first order* because the first derivative of the potential  $\mathcal{F}$  with respect to the control parameter  $T$  is discontinuous. Since the entropy  $S$  is discontinuous this transition is also referred to as a *discontinuous phase transition*. When we now increase the temperature, is apparent that the system stays at  $o_1$  longer than it had been before when lowering the control parameter. This represents *hysteresis effect*.

In the case of the potential (2.30) the order parameter equation obtains

the form

$$\dot{o} = -\sigma o - \gamma o^2 - \beta o^3.$$

Similar *disorder*  $\Rightarrow$  *order* transitions occur also in various nonequilibrium systems of physics, chemistry, biology, psychology, sociology, as well as in human motion dynamics. The analogy is subsumed in Table 1.

**Table 1. Phase transition analogy**

System in thermal equilibrium	Nonequilibrium system
Free energy potential $\mathcal{F}$	Generalized potential $V$
Order parameters $o_i$	Order parameters $o_i$
$\dot{o}_i = -\frac{\partial \mathcal{F}}{\partial o_i}$	$\dot{o}_i = -\frac{\partial V}{\partial o_i}$
Temperature $T$	Control input $u$
Entropy $S$	System output $y$
Specific Heat $c$	System efficiency $e$

In the case of human motion dynamics, natural control inputs  $u_i$  are muscular torques  $F_i$ , natural system outputs  $y_i$  are joint coordinates  $q^i$  and momenta  $p_i$ , while the system efficiencies  $e_i$  represent the changes of coordinates and momenta with changes of corresponding muscular torques for the  $i$ th joint,

$$e_i^q = \frac{\partial q^i}{\partial F_i}, \quad e_i^p = \frac{\partial p_i}{\partial F_i}.$$

Order parameters  $o_i$  represent certain important qualities of the human motion system, depending on muscular torques as control inputs, similar to *magnetization*, and usually defined by equations similar to (2.29) or

$$\dot{o}_i = -\sigma o - \gamma o^2 - \beta o^3,$$

with nonnegative parameters  $\sigma, \beta, \gamma$ , and corresponding to the second and first order phase transitions, respectively. The choice of actual order parameters is a matter of *expert knowledge* and *purpose of macroscopic system modelling* [Haken (1983)].

### 2.3.5.2 Mezosopic Derivation of Order Parameters

Basic Hamiltonian equations (2.26–2.27) are in general quite complicated and can hardly be solved completely in the whole locomotor phase-space

$\Gamma$ , spanned by the set of possible joint vectors  $\{q^i(t), p_i(t)\}$ . We therefore have to restrict ourselves to local concepts for analyzing the behavior of our locomotor system. To this end we shall consider a reference musculo-skeletal state  $\{q_0, p_0\}$  and its neighborhood. Following the procedures of the mezosopic synergetics (see [Haken (1983); Haken (1993)]), we assume that the reference state has the properties of an attractor and is a comparably low-dimensional object in  $\Gamma$ . In order to explore the behavior of our locomotor system (dependent on the set of control parameters  $\sigma$ ) in the neighborhood of  $\{q_0, p_0\}$  we look for the time development of small deviations from the reference state (to make the formalism as simple as possible, we drop the joint index in this section)

$$q(t) = q_0 + \delta q(t), \quad p(t) = p_0 + \delta p(t),$$

and consider  $\delta q(t)$  and  $\delta p(t)$  as small entities. As a result we may linearize the equations of  $\delta q$  and  $\delta p$  in the vicinity of the reference state  $\{q_0, p_0\}$ . We obtain

$$\partial_t \delta q(t) = L[q_0, p_0, \sigma] \delta q(t), \quad \partial_t \delta p(t) = K[q_0, p_0, \sigma] \delta p(t),$$

where  $L[\cdot]$  and  $K[\cdot]$  are linear matrices independent of  $\delta q(t)$  and  $\delta p(t)$ , which can be derived from the basic Hamiltonian vector-field (2.26–2.27) by standard synergetics methods [Haken (1983); Haken (1993); Haken (1996); Haken (2000)]. We now assume that we can construct a complete set of eigenvectors  $\{l^{(j)}(t), k^{(j)}(t)\}$  corresponding to (2.29). These eigenvectors allow us to decompose arbitrary deviations  $\delta q(t)$  and  $\delta p(t)$  into elementary collective deviations along the directions of the eigenvectors

$$\delta q(t) = \xi_j(t) l^j(t), \quad \delta p(t) = \zeta_j(t) k^j(t), \quad (2.31)$$

where  $\xi_j(t)$  and  $\zeta_j(t)$  represent the excitations of the system along the directions in the phase-space  $\Gamma$  prescribed by the eigenvectors  $l^j(t)$  and  $k^j(t)$ , respectively. These amplitudes are still dependent on the set of control parameters  $\{\sigma\}$ . We note that the introduction of the eigenvectors  $\{l^j(t), k^j(t)\}$  is of crucial importance. In the realm of synergetics they are considered as the *collective modes or patterns* of the system. Whereas the basic Hamiltonian equation (2.26–2.27) is formulated on the basis of the human locomotor-system variables (coordinates and momenta) of the single subsystems (joints), we can now give a new formulation which is based on these collective patterns and describes the dynamical behavior of the locomotor system in terms of these different collective patterns. Inserting

relations (2.31) into the basic system (2.26–2.27) we get equations for the amplitudes  $\xi_j(t)$  and  $\zeta_j(t)$ ,

$$\dot{\xi}_i(t) = A_{ij} \cdot \xi_j(t) + \text{nonlinear terms}, \quad \dot{\zeta}_j(t) = B_{ij} \cdot \zeta_j(t) + \text{nonlinear terms},$$

where  $\cdot$  denotes the scalar product, and it is assumed that the time dependence of the linear matrices  $L$  and  $K$  is carried out by the eigenvectors leaving us with constant matrices  $A$  and  $B$ .

We now summarize the results by discussing the following time-evolution formulas for joint coordinates  $q(t)$  and momenta  $p(t)$ ,

$$q(t) = q_0 + \xi_j(t) l^j(t), \quad p(t) = p_0 + \zeta_j(t) k^j(t), \quad (2.32)$$

which describes the time dependence of the phase vectors  $q(t)$  and  $p(t)$  through the evolution of the collective patterns. Obviously, the reference musculo-skeletal state  $\{q_0(t), p_0(t)\}$  can be called stable when all the possible excitations  $\{\xi_j(t), \zeta_j(t)\}$  decay during the course of time. When we now change the control parameters  $\{\sigma\}$  some of the  $\{\xi_j(t), \zeta_j(t)\}$  can become unstable and start to grow in time. The border between decay and growth in parameter space is called a Tablecritical region. Haken has shown that the few unstable amplitudes, denoted by  $u_q$  and  $u_p$ , change very slowly in the vicinity of a critical region, whereas the damped amplitudes, denoted by  $s_q$  and  $s_p$ , quickly decay to values which are completely prescribed by the unstable modes. This fact is expressed as the Tableslaving principle of synergetics [Haken (1983); Haken (1993); Haken (1996); Haken (2000)], in our case reading as

$$s_q = s_q(u_q), \quad s_p = s_p(u_p).$$

These relations allow us to eliminate the stable modes in (2.32), and leave us with a low-dimensional set of equations for the unstable modes which play the role of the order parameters. These Tableorder parameter equations then completely rule the behavior of our microscopic  $nD$  musculo-skeletal system on macroscopic scales near an instability.

The fundamental result of synergetics consists in the observation that on macroscopic scales new laws can be discovered which exist in their own right [Haken (1983)]. These laws which are expressed by the order parameter equations turn out to be independent of the detailed nature of the subsystems and their interactions. As a consequence this allows us to introduce the concept of Tablenormal forms [Arnold (1988)] as a method to discuss instabilities and qualitative dynamics in the neighborhood of the

critical regions. This method of phenomenological synergetics allows us to start qualitative analysis from purely macroscopic considerations.

Using the so-called Tableadiabatic elimination of fast variables [Haken (1983)], one tries to identify macroscopic quantities related to global musculo-skeletal dynamics (similar but different from the *mean-field* center-of-mass dynamics) – from experience and classifies them according to time-scale arguments. The slowest variables are usually identified with the control parameters which are assumed to be quasi static quantities. The slow macroscopic dynamics of the system has to be attributed to the order parameters. Very quickly relaxing variables have to be considered as enslaved modes.

### 2.3.6 Macro-Synergetic Control of Biodynamics

The basic microscopic synergetic level of human musculo-skeletal dynamics (2.26–2.27), can be viewed on the highest, *macroscopic synergetic center-of-mass organization level* of human motion dynamics as a simple *Hamilton oscillator*, physically representing the damped, sinusoidally driven pendulum of the unit mass and length  $l$

$$l^2\ddot{q} + \gamma\dot{q} + lg \sin q = A \cos(p_D t).$$

This equation expresses Newtonian second law of motion with the various terms on the left representing acceleration, damping, and gravitation. The angular momentum of the forcing  $p_D$ , may be different from the natural frequency of the pendulum. In order to minimize the number of adjustable parameters the equation may be rewritten in dimensionless form as

$$\ddot{q} + (1/\nu)\dot{q} + \sin q = \epsilon \cos(p_D t),$$

where  $\nu$  is the damping or quality parameter,  $\epsilon$  is the forcing amplitude, and  $p_D$  is the drive frequency. The low-amplitude natural angular frequency of the pendulum is unity, and time is regarded as dimensionless. This equation satisfies the necessary conditions for chaos when it is written as an extended Hamiltonian system

$$\dot{q} = p, \quad \dot{p} = -(1/\nu)p - \sin q + \epsilon \cos \phi, \quad \dot{\phi} = p_D. \quad (2.33)$$

The variable  $\phi$  is introduced as the phase of the drive term. Three variables are evident and also two nonlinear coupling terms. Whether the motion is chaotic depends upon the values of the three parameters: damping, forcing amplitude and drive frequency. For some values the pendulum locks onto

the driving force, oscillating in a periodic motion whose frequency is the driving frequency, possibly with some harmonics or subharmonics. But for other choices of the parameters the pendulum motion is chaotic. One may view the chaos as resulting from a subtle interplay between the tendency of the pendulum to oscillate at its 'natural' frequency and the action of the forcing term. The transitions between non-chaotic and chaotic states, due to changes in the parameters, occur in several ways and depend delicately upon the values of the parameters.

To include (in the simplest possible way) the muscle excitation-contraction dynamics, and thus make the damped, driven Hamilton oscillator (2.33) a more realistic macroscopic model for human motion dynamics, we assume that the time-dependent forcing amplitude  $\epsilon = \epsilon(t)$  has the form of a low pass filter, a characteristic feature of biological systems, given by first-order transfer function  $\frac{K}{Ts+1}$ . Here  $K$  denotes gain of the filter and  $T$  its time constant.

Therefore, macroscopic mechanical model of human motion dynamics obtains the fully-functional form

$$\ddot{q} + (1/\nu)\dot{q} + \sin q = K(1 - e^{-t/T}) \cos(p_D t),$$

which can be rewritten in the form of *extended Hamilton oscillator*

$$\dot{q} = p, \quad \dot{p} = -(1/\nu)p - \sin q + K(1 - e^{-t/T}) \cos \phi, \quad \dot{\phi} = p_D. \quad (2.34)$$

Now, to effectively control the macroscopic HML model (2.34), we can use two standard nonlinear-control techniques:

- (1) Adaptive Lie-derivative based geometric control (see chapter 6); and
- (2) Adaptive fuzzy-logic based AI control (see chapter 7).

## Chapter 3

# Natural Geometry of Biodynamics

In this second part, we present lower, mechanical biodynamics, enveloped in its natural, functorial language. This part of biodynamics is fully elaborated today and can be written in a mathematically rigorous form of *unity in diversity*. The exception of these mathematical approaches are medical subsections, which are necessarily written in 'plain English with lots of figures'.

As a motivation for geometric mechanics, we cite here an extract from the *Nobel Lecture of Albert Einstein*: "...The whole development of the theory turns on the question of whether there are physically preferred states of motion in *Nature* (physical relativity problem). Also, concepts and distinctions are only admissible to the extent that observable facts can be assigned to them without ambiguity (stipulation that concepts and distinctions should have meaning). This postulate, pertaining to epistemology, proves to be of fundamental importance.

These two aspects become clear when applied to a special case, to classical mechanics. Firstly we see that at any point filled with matter there exists a preferred state of motion, namely that of the substance at the point considered. Our problem starts however with the question whether physically preferred states of motion exist in reference to extensive regions. From the viewpoint of classical mechanics the answer is in the affirmative; the physically preferred states of motion from the viewpoint of mechanics are those of the inertial frames.

This assertion, in common with the basis of the whole of mechanics as it generally used to be described before the relativity theory, far from meets the above 'stipulation of meaning'. Motion can only be conceived as the relative motion of bodies. In mechanics, motion relative to the system of coordinates is implied when merely motion is referred to. Nevertheless



this interpretation does not comply with the 'stipulation of meaning' if the coordinate system is considered as something purely imaginary. If we turn our attention to experimental physics we see that there the coordinate system is invariably represented by a *practically rigid body*. Furthermore it is assumed that such rigid bodies can be positioned in rest relative to one another in common with the bodies of Euclidian geometry. Insofar as we may think of the rigid measuring body as existing as an object which can be experienced, the *system of coordinates* concept as well as the concept of the motion of matter relative thereto can be accepted in the sense of the 'stipulation of meaning'.

In classical mechanics the inertial frame and time are best defined together by a suitable formulation of the law of inertia: It is possible to fix the time and assign a state of motion to the system of coordinates (inertial frame) such that, with reference to the latter, force-free material points undergo no acceleration; furthermore it is assumed that this time can be measured without disagreement by identical clocks (systems which run down periodically) in any arbitrary state of motion. There are then an infinite number of inertial frames which are in uniform translational motion relative to each other, and hence there is also an infinite number of mutually equivalent, physically preferred states of motion. Time is absolute, i.e. independent of the choice of the particular inertial frame; it is defined by more characteristics than logically necessary, although – as implied by mechanics – this should not lead to contradictions with experience. Note in passing that the logical weakness of this exposition from the point of view of the stipulation of meaning is the lack of an experimental criterion for whether a material point is force-free or not; therefore the concept of the inertial frame remains rather problematical. This deficiency leads to the general theory of relativity.

The concept of the rigid body (and that of the clock) has a key bearing on the foregoing consideration of the fundamentals of mechanics, a bearing which there is some justification for challenging. The rigid body is only approximately achieved in *Nature*, not even with desired approximation; this concept does not therefore strictly satisfy the 'stipulation of meaning'. It is also logically unjustifiable to base all physical consideration on the rigid or solid body and then finally reconstruct that body atomically by means of elementary physical laws which in turn have been determined by means of the rigid measuring body. I am mentioning these deficiencies of method because in the same sense they are also a feature of the relativity theory in the schematic exposition which I am advocating here. Certainly it would be

logically more correct to begin with the whole of the laws and to apply the 'stipulation of meaning' to this whole first, i.e., to put the unambiguous relation to the world of experience last instead of already fulfilling it in an imperfect form for an artificially isolated part, namely the space-time metric. We are not, however, sufficiently advanced in our knowledge of *Nature's* elementary laws to adopt this more perfect method without going out of our depth. At the close of our considerations we shall see that in the most recent studies there is an attempt, based on ideas by Levi-Civita, Weyl, and Eddington, to implement that logically purer method.

It more clearly follows from the above what is implied by 'preferred states of motion'. They are preferred as regards the laws of *Nature*. States of motion are preferred when, relative to the formulation of the laws of *Nature*, coordinate systems within them are distinguished in that with respect to them those laws assume a form preferred by simplicity. According to classical mechanics the states of motion of the inertial frames in this sense are physically preferred. Classical mechanics permits a distinction to be made between (absolutely) unaccelerated and accelerated motions; it also claims that velocities have only a relative existence (dependent on the selection of the inertial frame), while accelerations and rotations have an absolute existence (independent of the selection of the inertial frame). This state of affairs can be expressed thus: According to classical mechanics 'velocity relativity' exists, but not 'acceleration relativity'. After these preliminary considerations we can pass to the actual topic of our contemplations, the relativity theory, by characterizing its development so far in terms of principles..."

The purpose of the present chapter is to introduce just enough differential geometry necessary to properly describe our *covariant force law*,  $F_i = mg_{ij}a^j$ . It is based on the *concept of biodynamic manifold*, a natural tool for *understanding the manifoldness of natural biodynamics*. The chapter starts with manifold and bundle theory. Then it moves on to Lie groups and algebras. After that it presents Riemannian and symplectic geometries as foundations for Lagrangian and Hamiltonian formalisms, respectively. Finally it gives some modern geometric aspects from the field theory and computer graphics. It is assumed that the reader has advanced calculus in his background.

### 3.1 Motivation for Geometry in Biodynamics

In this section we describe our motivation for modern geometric approach in studying biodynamics. Briefly, as it is pointed out in Appendix, the acceleration vector *is not* an ordinary time derivative of the velocity vector; ‘even worse’, the force, which is a paradigm of a vector in statics and engineering vector mechanics, *is not* a vector at all. The acceleration vector is the absolute time derivative of the velocity vector, while the force is a differential one-form. Proper description of these ideas is called *geometrodynamics*.<sup>1</sup> In particular, the objective here is to introduce our *covariant force law*,  $F_i = mg_{ij}a^j$ .

Let us start from the beginning – biodynamics is all about motion: *causes of motion* (like neuro-muscular patterns), *effects of motion* (like musculo-skeletal injuries), and *control of motion* (to perform some task and prevent injuries). The simplistic form of motion takes place in an Euclidean space  $\mathbb{R}^n$ , defined as a  $C^k$ -map  $x : I \in \mathbb{R} \rightarrow \mathbb{R}^n$ . Its time derivative

$$\dot{x}(t_0) = \left. \frac{dx}{dt} \right|_{t=t_0} = \lim_{h \rightarrow 0} \frac{x(t_0 + h) - x(t_0)}{h}$$

is called the *velocity vector* at the point  $t_0 \in I$ . Its second derivative

$$\ddot{x}(t_0) = \left. \frac{d^2x}{dt^2} \right|_{t=t_0}$$

is called the *acceleration vector* at the point  $t_0$ . The image of a map  $x : I \rightarrow \mathbb{R}^n$  is called a *trajectory* or *curve* in  $\mathbb{R}^n$  [Arnold (1989)].

Now, to be able to describe *realistic motion*, *dynamics* and *control* of a complex biodynamic system  $\Xi$ , with  $n$  actuated DOF and hierarchical neural-like control, we need firstly, to construct its *configuration manifold*  $M$  and derive two higher geometric structures from it:

- The velocity phase-space, defined as a *tangent bundle*  $TM$ ; and
- The momentum phase-space, defined as a *cotangent bundle*  $T^*M$ .

The sections of  $TM$  are the *vector-fields*  $v$ , which can be expanded in terms of the basis vector-fields  $\{e_\mu \equiv \frac{\partial}{\partial x^\mu}\}$ . Similarly, the sections of  $T^*M$  are the 1-forms  $\alpha$ , which can be expanded in terms of the basis 1-forms  $\{\omega^\mu \equiv dx^\mu\}$ . Here  $d$  denotes the *exterior derivative* (antisymmetric differential, an inverse of the definite integral), such that  $dd = 0$ . In particular,

---

<sup>1</sup>Term *geometrodynamics* was coined by John A. Wheeler from Princeton.

the velocity vector-fields  $\dot{x}$  are defined on  $TM$  as  $\dot{x} = \dot{x}^\mu e_\mu$ , while the momentum 1-forms  $\pi$  are defined on  $T^*M$  as  $\pi = \pi_\mu \omega^\mu$ .

Also, the system's configuration manifold  $M$  is *Riemannian*, admitting the metric  $g = \langle \omega^\mu, \omega^\eta \rangle$ , determined by the system's kinetic energy  $T = \langle \dot{x}^\mu, \dot{x}^\eta \rangle$ , with the metric tensor  $g = g_{\mu\eta} \omega^\mu \otimes \omega^\eta$ . This implies that vector-fields  $v$  and 1-forms  $\alpha$  are related by  $g$ -induced scalar products  $\langle \omega^\mu, e_\eta \rangle = \delta_\eta^\mu$ .

The *Riemannian metric*  $g = \langle, \rangle$  on  $M$  is the positive-definite quadratic form  $g : TM \rightarrow \mathbb{R}$ , in local curvilinear coordinates  $x^i$  in an open chart  $U$  on  $M$ , given by

$$g_{ij} \mapsto g_{ij}(x) dx^i dx^j,$$

where  $g_{ij}(x)$  denotes the covariant metric tensor defined as (see Appendix)

$$g_{ij}(x) = \delta_{rs} \frac{\partial y^r}{\partial x^i} \frac{\partial y^s}{\partial x^j},$$

where  $\delta_{rs}$  denotes the Kronecker symbol, and  $(y^r)$ ,  $r = 1, \dots, n$  are Cartesian coordinates.

*Nonlinear dynamics* of the biodynamic system  $\Xi$  is usually described using either *Lagrangian formalism* or *Hamiltonian formalism* on the configuration manifold  $M$ .

Lagrangian mechanics describes motion in a mechanical system  $\Xi$  by means of the configuration space  $M$ , which has the structure of a  $C^k$ -manifold. The one-parametric group of diffeomorphisms  $F_t$  acts on  $M$ . A system  $\Xi$  is given by a configuration manifold  $M$  and the Lagrangian function  $L$  on its tangent bundle  $TM$ . Every one-parametric group of diffeomorphisms  $F_t$  of  $M$  which fixes the Lagrangian function  $L$  defines a conservation law, i.e., a first integral of the equations of motion. A Newtonian potential system is a particular case of a Lagrangian system, in which  $M = \mathbb{R}^n$ , and the Lagrangian function  $L$  is kinetic minus potential energy [Arnold (1989)].

The system's Lagrangian function on  $M$  is defined as a velocity  $v$ -dependent quadratic form  $L : TM \rightarrow \mathbb{R}$ , such that  $L(v) = \frac{1}{2} \langle v, v \rangle$ , in local internal coordinates  $x^i$ ,  $v^i = \dot{x}^i \in U_v$ ,  $U_v$  open in  $TM$ , given by

$$L(v) = \frac{1}{2} g_{ij}(x) v^i v^j.$$

Hamiltonian mechanics is geometry in phase-space  $P$ , which has the structure of a symplectic manifold. The one-parametric group of symplec-

tic diffeomorphisms acts on phase-space. The basic concepts and theorems of Hamiltonian mechanics are invariant under this group. Lagrangian mechanics is contained in Hamiltonian mechanics as a special case, in which the phase space  $P$  is the cotangent bundle  $T^*M$  of the configuration space  $M$ , and the Hamiltonian function  $H$  on  $T^*M$  is the Legendre transformation of the Lagrangian function  $L$  [Arnold (1989)].

The system's Hamiltonian function (its total energy) is defined as a momentum  $p$ -dependent quadratic form  $H : T^*M \rightarrow \mathbb{R}$ , such that  $H(p) = \frac{1}{2}\langle p, p \rangle$ , in local canonical coordinates  $x^i$ ,  $p_i \in U_p$ ,  $U_p$  open in  $T^*M$ , given by

$$H(p) = \frac{1}{2}g^{ij}(x)p_ip_j,$$

where  $g^{ij}(x)$  denotes the inverse or contravariant metric tensor

$$g^{ij}(x) = \delta^{rs} \frac{\partial x^i}{\partial y^r} \frac{\partial x^j}{\partial y^s}.$$

*Nonlinear control* of the biodynamic system  $\Xi$  is in a most sophisticated manner described using *Lie derivative formalism*. Let  $C^k(M, \mathbb{R})$  denote the set of all smooth real valued functions  $f : M \rightarrow \mathbb{R}$  on  $M$ ,  $\mathcal{X}^k(M)$  – the set of all smooth vector-fields on  $M$ , and  $\Omega^1(M)$  – the set of all 1-forms on  $M$ . Also, let the vector-field  $X \in \mathcal{X}^k(M)$  be given with its local flow  $F_t : M \rightarrow M$  such that at a point  $m \in M$ ,  $\frac{d}{dt}|_{t=0} F_t m = X(m)$ , and  $\varphi_t^*$  representing the *pull-back* by  $F_t$ . The Lie derivative differential operator  $\mathcal{L}_X$  is defined:

(1) On a function  $f \in C^k(M, \mathbb{R})$  as

$$\mathcal{L}_X : C^k(M, \mathbb{R}) \rightarrow C^k(M, \mathbb{R}), \quad \mathcal{L}_X f = \frac{d}{dt}(\varphi_t^* f)|_{t=0};$$

(2) On a vector-field  $Y \in V(M)$  as

$$\mathcal{L}_X : \mathcal{X}^k(M) \rightarrow \mathcal{X}^k(M), \quad \mathcal{L}_X Y = \frac{d}{dt}(\varphi_t^* Y)|_{t=0} \equiv [X, Y]$$

– the so-called Lie bracket; and

(3) On a covector-field (1-form)  $\alpha \in \Lambda(M)$  as

$$\mathcal{L}_X : \Omega^1(M) \rightarrow \Omega^1(M), \quad \mathcal{L}_X \alpha = \frac{d}{dt}(\varphi_t^* \alpha)|_{t=0}.$$

In general, for any smooth tensor-field  $\tau$  on  $M$ , the Lie derivative (or, Liouville operator)  $\mathcal{L}_X \tau$  geometrically represents a directional derivative

of  $\tau$  along the flow  $F_t$  of the vector-field  $X \in M$ .  $\mathcal{L}_X \tau$  is a tensor of the same variance as  $\tau$ , and it is used for the so-called ‘Lie dragging’, or ‘Lie transport’ of a tensor-field  $\tau$  along the flow of  $X$ . This reduces to classical directional derivative in a special case when  $\tau$  is a scalar function and a vector-field  $X$  is constant.

For example, if we have two vector-fields  $X_1$  and  $X_2$  on  $M$

$$X_1 = X_{1,h}^i(x, v) \partial_{x^i} + X_{1,v}^i(x, v) \partial_{v^i}, \quad X_2 = X_{2,h}^i(x, v) \partial_{x^i} + X_{2,v}^i(x, v) \partial_{v^i},$$

their Lie bracket can be (roughly) represented by

$$[X_1, X_2] \sim \left[ \begin{array}{cc} \frac{\partial X_{2,h}^i}{\partial x^j} & \frac{\partial X_{2,h}^i}{\partial v^j} \\ \frac{\partial X_{2,v}^i}{\partial x^j} & \frac{\partial X_{2,v}^i}{\partial v^j} \end{array} \right] \begin{pmatrix} X_{1,h}^j \\ X_{1,v}^j \end{pmatrix} - \left[ \begin{array}{cc} \frac{\partial X_{1,h}^i}{\partial x^j} & \frac{\partial X_{1,h}^i}{\partial v^j} \\ \frac{\partial X_{1,v}^i}{\partial x^j} & \frac{\partial X_{1,v}^i}{\partial v^j} \end{array} \right] \begin{pmatrix} X_{2,h}^j \\ X_{2,v}^j \end{pmatrix}.$$

### 3.2 Biodynamic Manifold $M$

In this section we introduce our essential tool for understanding the *manifoldness of natural biodynamics*, namely the concept of *biodynamic manifold*. The basic idea of a manifold is to introduce a local object that will support differentiation processes and then to patch these local objects together smoothly. Intuitively, an  $n$ D manifold is a subset of some Euclidean space  $\mathbb{R}^n$  that is locally Euclidean of dimension  $n$ , i.e., an  $n$ -manifold is an object modelled locally on  $\mathbb{R}^n$ . This means that it takes exactly  $n$  numbers to specify a point, at least if we do not stray too far from a given starting point. A physicist would say that an  $n$ D manifold is an object with  $n$  DOF. Manifolds of dimension 1 are commonly called *curves*, e.g., space curves, which are often described parametrically by equations such as  $(x, y, z) = (\varphi(t), g(t), h(t))$  for some continuous functions  $\varphi, g, h$ . Manifolds of dimension 2 are surfaces. The only higher-dimensional manifold that we can visualize is Euclidean 3-space. In general, a subset  $M$  of some Euclidean space  $\mathbb{R}^n$  is locally Euclidean of dimension  $n$  if every point of  $M$  has a neighborhood in  $M$  that is topologically equivalent to a ball in  $\mathbb{R}^n$  (see [Lee (2000)]). For example in mechanics, the set of possible positions of a rigid body moving through space under the influence of gravity is a certain 6D manifold  $M \subset \mathbb{R}^9$  (describing its 3D translations and rotations).

More precisely, a *topological manifold* is a separable Hausdorff space  $M$  which is locally homeomorphic to  $\mathbb{R}^n$ . So, a topological manifold has the following properties [Lee (2000); Lee (2002)]:

- (1)  $M$  is a *Hausdorff space*: For every pair of points  $m_1, m_2 \in M$ , there are disjoint open subsets  $U, V \subset M$  such that  $m_1 \in U$  and  $m_2 \in V$ .
- (2)  $M$  is *second countable*: There exists a countable basis for the topology of  $M$ .
- (3)  $M$  is *locally Euclidean of dimension  $n$* : Every point of  $M$  has a neighborhood that is homeomorphic to an open subset of  $\mathbb{R}^n$ .

This further implies that for any point  $m \in M$  there is a homeomorphism  $\phi : U \rightarrow \phi(U) \subseteq \mathbb{R}^n$ , where  $U$  is an open neighborhood of  $m$  in  $M$  and  $\phi(U)$  is an open subset in  $\mathbb{R}^n$ . The pair  $(U, \phi)$  is called a *coordinate chart* at a point  $m \in M$  (see [Lee (2002); Kolar et al. (1993)]).

### 3.2.1 Definition of the Manifold $M$

Given a chart  $(U, \phi)$ , we call the set  $U$  a *coordinate domain*, or a coordinate neighborhood of each of its points. If in addition  $\phi(U)$  is an open ball in  $\mathbb{R}^n$ , then  $U$  is called a *coordinate ball*. The map  $\phi$  is called a (*local*) *coordinate map*, and the component functions  $(x^1, \dots, x^n)$  of  $\phi$ , defined by  $\phi(m) = (x^1(m), \dots, x^n(m))$ , are called *local coordinates* on  $U$ .

Two charts  $(U_1, \phi_1)$  and  $(U_2, \phi_2)$  such that  $U_1 \cap U_2 \neq \emptyset$  are called *compatible* if  $\phi_1(U_1 \cap U_2)$  and  $\phi_2(U_2 \cap U_1)$  are open subsets of  $\mathbb{R}^n$  [Marsden and Ratiu (1999)]. A family  $(U_\alpha, \phi_\alpha)_{\alpha \in A}$  of compatible charts on  $M$  such that the  $U_\alpha$  form a *cover* of  $M$  is called an *atlas*. The maps  $\phi_{\alpha\beta} = \phi_\beta \circ \phi_\alpha^{-1} : \phi_\alpha(U_{\alpha\beta}) \rightarrow \phi_\beta(U_{\alpha\beta})$  are called the *chart changings*, or *transition maps*, for the atlas  $(U_\alpha, \phi_\alpha)_{\alpha \in A}$ , where  $U_{\alpha\beta} = U_\alpha \cap U_\beta$ , so that we have a commutative triangle:

$$\begin{array}{ccc}
 & U_{\alpha\beta} \subseteq M & \\
 \phi_\alpha \swarrow & & \searrow \phi_\beta \\
 \phi_\alpha(U_{\alpha\beta}) & \xrightarrow{\phi_{\alpha\beta}} & \phi_\beta(U_{\alpha\beta})
 \end{array}$$

An atlas  $(U_\alpha, \phi_\alpha)_{\alpha \in A}$  for a manifold  $M$  is said to be a  $C^k$ -*atlas*, if all transition maps  $\phi_{\alpha\beta} : \phi_\alpha(U_{\alpha\beta}) \rightarrow \phi_\beta(U_{\alpha\beta})$  are differentiable of class  $C^k$ . Two  $C^k$  atlases are called  $C^k$ -*equivalent*, if their union is again a  $C^k$ -atlas for  $M$ . An equivalence class of  $C^k$ -atlases is called a  $C^k$ -*structure* on  $M$ . In other words, a smooth structure on  $M$  is a *maximal* smooth atlas on  $M$ , i.e., such an atlas that is not contained in any strictly larger smooth atlas. By a  $C^k$ -*manifold*  $M$ , we mean a topological manifold together

with a  $C^k$ -structure and a chart on  $M$  will be a chart belonging to some atlas of the  $C^k$ -structure. Smooth manifold means  $C^\infty$ -manifold, and the word 'smooth' is used synonymously for  $C^\infty$ . However, for most of our biodynamic needs, the weaker requirement,  $C^k$  would be sufficient. In case of any doubt, we can simply replace  $C^k$  with  $C^\infty$ .

Sometimes the terms 'local coordinate system' or 'parametrization' are used instead of charts. That  $M$  is not defined with any particular atlas, but with an equivalence class of atlases, is a mathematical formulation of the *general covariance* principle. Every suitable coordinate system is equally good. A Euclidean chart may well suffice for an open subset of  $\mathbb{R}^n$ , but this coordinate system is not to be preferred to the others, which may require many charts (as with polar coordinates), but are more convenient in other respects.

For example, the atlas of a  $n$ -sphere  $S^n$  has two charts. If  $N = (1, 0, \dots, 0)$  and  $S = (-1, \dots, 0, 0)$  are the north and south poles of  $S^n$  respectively, then the two charts are given by the stereographic projections from  $N$  and  $S$ :

$$\phi_1 : S^n \setminus \{N\} \rightarrow \mathbb{R}^n, \phi_1(x^1, \dots, x^{n+1}) = (x^2/(1-x^1), \dots, x^{n+1}/(1-x^1)),$$

and

$$\phi_2 : S^n \setminus \{S\} \rightarrow \mathbb{R}^n, \phi_2(x^1, \dots, x^{n+1}) = (x^2/(1+x^1), \dots, x^{n+1}/(1+x^1)),$$

and the overlap map  $\phi_2 \circ \phi_1^{-1} : \mathbb{R}^n \setminus \{0\} \rightarrow \mathbb{R}^n \setminus \{0\}$  is given by the diffeomorphism  $(\phi_2 \circ \phi_1^{-1})(z) = z/\|z\|^2$ , for  $z$  in  $\mathbb{R}^n \setminus \{0\}$ , from  $\mathbb{R}^n \setminus \{0\}$  to itself.

Various *additional structures* can be imposed on  $\mathbb{R}^n$ , and the corresponding manifold  $M$  will inherit them through its covering by charts. For example, if a covering by charts takes their values in a *Banach space*  $E$ , then  $E$  is called the *model space* and  $M$  is referred to as a  $C^k$ -*Banach manifold* modelled on  $E$ . Similarly, if a covering by charts takes their values in a *Hilbert space*  $\mathcal{H}$ , then  $\mathcal{H}$  is called the *model space* and  $M$  is referred to as a  $C^k$ -*Hilbert manifold* modelled on  $\mathcal{H}$ . If not otherwise specified, we will consider  $M$  to be an Euclidean manifold, with its covering by charts taking their values in  $\mathbb{R}^n$ .

For a Hausdorff  $C^k$ -manifold the following properties are equivalent [Kolar *et al.* (1993)]:

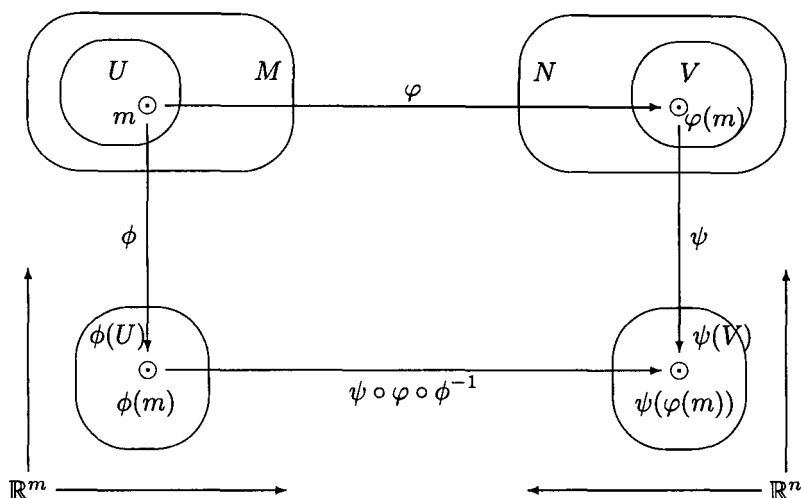
- (1) It is paracompact.
- (2) It is metrizable.



- (3) It admits a Riemannian metric.
- (4) Each connected component is separable.

### 3.2.2 Smooth Maps Between Manifolds

A map  $\varphi : M \rightarrow N$  between two manifolds  $M$  and  $N$ , with  $M \ni m \mapsto \varphi(m) \in N$ , is called a *smooth map*, or  $C^k$ -map, if we have the following charting:



This means that for each  $m \in M$  and each chart  $(V, \psi)$  on  $N$  with  $\varphi(m) \in V$  there is a chart  $(U, \phi)$  on  $M$  with  $m \in U$ ,  $\varphi(U) \subseteq V$ , and  $\Phi = \psi \circ \varphi \circ \phi^{-1}$  is  $C^k$ , that is, the following diagram commutes:

$$\begin{array}{ccc}
 M \supseteq U & \xrightarrow{\varphi} & V \subseteq N \\
 \downarrow \phi & & \downarrow \psi \\
 \phi(U) & \xrightarrow{\Phi} & \psi(V)
 \end{array}$$

Let  $M$  and  $N$  be smooth manifolds and let  $\varphi : M \rightarrow N$  be a smooth map. The map  $\varphi$  is called a *covering*, or equivalently,  $M$  is said to *cover*  $N$ , if  $\varphi$  is surjective and each point  $n \in N$  admits an open neighborhood  $V$  such that  $\varphi^{-1}(V)$  is a union of disjoint open sets, each diffeomorphic via  $\varphi$  to  $V$ .

A  $C^k$ -map  $\varphi : M \rightarrow N$  is called a  $C^k$ -diffeomorphism if  $\varphi$  is a bijection,  $\varphi^{-1} : N \rightarrow M$  exists and is also  $C^k$ . Two manifolds are called diffeomorphic if there exists a diffeomorphism between them.

All smooth manifolds and smooth maps between them form the category  $\mathcal{M}$ .

The most important examples of biodynamic manifolds have an additional group structure and thus belong to the category of Lie groups  $\mathcal{G}$ .

### 3.3 Biodynamic Bundles

In this section we introduce secondary concepts of *biodynamic bundles*, derived from the primary concept of the manifold.

#### 3.3.1 The Tangent Bundle of the Manifold $M$

Recall that if  $[a, b]$  is a closed interval, a  $C^0$ -map  $\gamma : [a, b] \rightarrow M$  is said to be *differentiable* at the endpoint  $a$  if there is a chart  $(U, \phi)$  at  $\gamma(a)$  such that the following limit exists and is finite [Abraham et al. (1988)]:

$$\frac{d}{dt}(\phi \circ \gamma)(a) \equiv (\phi \circ \gamma)'(a) = \lim_{t \rightarrow a} \frac{(\phi \circ \gamma)(t) - (\phi \circ \gamma)(a)}{t - a}. \quad (3.1)$$

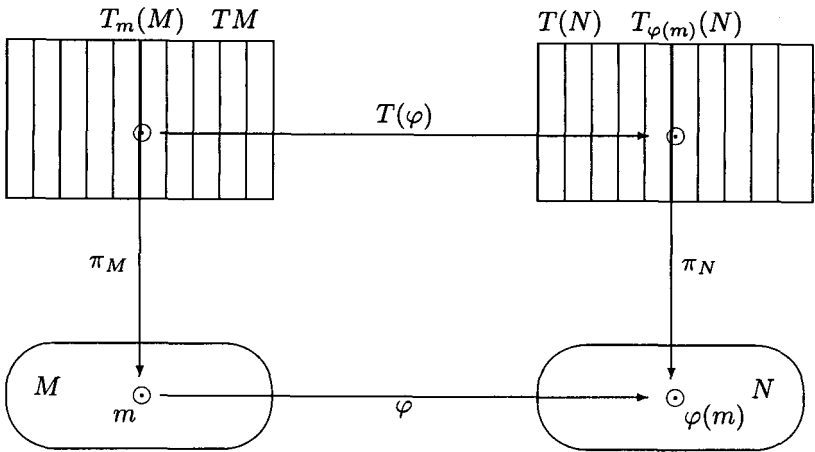
Generalizing (3.1), we get the notion of the *curve on a manifold*. For a smooth manifold  $M$  and a point  $m \in M$  a curve at  $m$  is a  $C^0$ -map  $\gamma : I \rightarrow M$  from an interval  $I \subset \mathbb{R}$  into  $M$  with  $0 \in I$  and  $\gamma(0) = m$ .

Two curves  $\gamma_1$  and  $\gamma_2$  passing through a point  $m \in U$  are *tangent at  $m$*  with respect to the chart  $(U, \phi)$  if  $(\phi \circ \gamma_1)'(0) = (\phi \circ \gamma_2)'(0)$ . Thus, two curves are tangent if they have identical tangent vectors (same direction and speed) in a local chart on a manifold.

For a smooth manifold  $M$  and a point  $m \in M$ , the *tangent space*  $T_m M$  to  $M$  at  $m$  is the *set of equivalence classes* of curves at  $m$ :

$$T_m M = \{[\gamma]_m : \gamma \text{ is a curve at a point } m \in M\}.$$

A  $C^k$ -map  $\varphi : M \ni m \mapsto \varphi(m) \in N$  between two manifolds  $M$  and  $N$  induces a linear map  $T_m \varphi : T_m M \rightarrow T_{\varphi(m)} N$  for each point  $m \in M$ , called a *tangent map*, if we have:



i.e., the following diagram commutes:

$$\begin{array}{ccc}
 T_m M & \xrightarrow{T_m \varphi} & T_{\varphi(m)} N \\
 \pi_M \downarrow & & \downarrow \pi_N \\
 M \ni m & \xrightarrow{\varphi} & \varphi(m) \in N
 \end{array}$$

with the *natural projection*, or *tangent bundle projection*,  $\pi_M : TM \rightarrow M$ , given by  $\pi_M(T_m M) = m$ , that takes a tangent vector  $v$  to the point  $m \in M$  at which the vector  $v$  is attached i.e.,  $v \in T_m M$ .

For a smooth manifold  $M$  of dimension  $n$ , its *tangent bundle*  $TM$  is the disjoint union of all its tangent spaces  $T_m M$  at all points  $m \in M$ , i.e.,  $TM = \bigsqcup_{m \in M} T_m M$ .

If  $M$  is an  $n$ -manifold, then  $TM$  is a  $2n$ -manifold. To define the smooth structure on  $TM$ , we need to specify how to construct local coordinates on  $TM$ . To do this, let  $(x^1(m), \dots, x^n(m))$  be local coordinates of a point  $m$  on  $M$  and let  $(v^1(m), \dots, v^n(m))$  be components of a tangent vector in this coordinate system. Then the  $2n$  numbers  $(x^1(m), \dots, x^n(m), v^1(m), \dots, v^n(m))$  give a local coordinate system on  $TM$ . This is the basic idea one uses to prove that indeed  $TM$  is a  $2n$ -manifold [Marsden and Ratiu (1999)].

$TM = \bigsqcup_{m \in M} T_m M$  defines a family of vector spaces parameterized by  $M$ .

The inverse image  $\pi_M^{-1}(m)$  of a point  $m \in M$  under the natural projection

$\pi_M$  is the tangent space  $T_m M$ . This space is called the *fibre* of the tangent bundle over the point  $m \in M$  [Steenrod (1951)].

A  $C^k$ -map  $\varphi : M \rightarrow N$  between two manifolds  $M$  and  $N$  induces a linear *tangent map*  $T\varphi : TM \rightarrow TN$  between their tangent bundles, i.e., the following diagram commutes:

$$\begin{array}{ccc} TM & \xrightarrow{T\varphi} & TN \\ \pi_M \downarrow & & \downarrow \pi_N \\ M & \xrightarrow{\varphi} & N \end{array}$$

All tangent bundles and their tangent maps form the category  $\mathcal{TB}$ . The category  $\mathcal{TB}$  is the natural framework for *Lagrangian biodynamics*.

Now, we can formulate the *global version of the chain rule*. If  $\varphi : M \rightarrow N$  and  $\psi : N \rightarrow P$  are two smooth maps, then we have  $T(\psi \circ \varphi) = T\psi \circ T\varphi$  (see [Kolar *et al.* (1993)]). In other words, we have a functor  $T : \mathcal{M} \Rightarrow \mathcal{TB}$  from the category  $\mathcal{M}$  of smooth manifolds to the category  $\mathcal{TB}$  of their tangent bundles:

$$\begin{array}{ccc} M & & \\ \varphi \swarrow & & \searrow (\psi \circ \varphi) \\ N & \xrightarrow{\psi} & P \end{array} \quad \xRightarrow{T} \quad \begin{array}{ccc} TM & & \\ T\varphi \swarrow & & \searrow T(\psi \circ \varphi) \\ TN & \xrightarrow{T\psi} & TP \end{array}$$

### 3.3.2 The Cotangent Bundle of the Manifold $M$

The *dual* notion to the tangent space  $T_m M$  to a smooth manifold  $M$  at a point  $m$  is its *cotangent space*  $T_m^* M$  at the same point  $m$ . Similarly to the tangent bundle, for a smooth manifold  $M$  of dimension  $n$ , its *cotangent bundle*  $T^* M$  is the disjoint union of all its cotangent spaces  $T_m^* M$  at all points  $m \in M$ , i.e.,  $T^* M = \bigsqcup_{m \in M} T_m^* M$ . Therefore, the cotangent bundle

of an  $n$ -manifold  $M$  is the vector bundle  $T^* M = (TM)^*$ , the (real) dual of the tangent bundle  $TM$ .

If  $M$  is an  $n$ -manifold, then  $T^* M$  is a  $2n$ -manifold. To define the smooth structure on  $T^* M$ , we need to specify how to construct local coordinates on  $T^* M$ . To do this, let  $(x^1(m), \dots, x^n(m))$  be local coordinates of a point  $m$  on  $M$  and let  $(p_1(m), \dots, p_n(m))$  be components of a covector in this coordinate system. Then the  $2n$  num-

bers  $(x^1(m), \dots, x^n(m), p_1(m), \dots, p_n(m))$  give a local coordinate system on  $T^*M$ . This is the basic idea one uses to prove that indeed  $T^*M$  is a  $2n$ -manifold.

$T^*M = \bigsqcup_{m \in M} T_m^*M$  defines a family of vector spaces parameterized by

$M$ , with the *conatural projection*, or *cotangent bundle projection*,  $\pi_M^* : T^*M \rightarrow M$ , given by  $\pi_M^*(T_m^*M) = m$ , that takes a covector  $p$  to the point  $m \in M$  at which the covector  $p$  is attached i.e.,  $p \in T_m^*M$ . The inverse image  $\pi_M^{-1}(m)$  of a point  $m \in M$  under the conatural projection  $\pi_M^*$  is the cotangent space  $T_m^*M$ . This space is called the *fibre* of the cotangent bundle over the point  $m \in M$ .

In a similar way, a  $C^k$ -map  $\varphi : M \rightarrow N$  between two manifolds  $M$  and  $N$  induces a linear *cotangent map*  $T^*\varphi : T^*M \rightarrow T^*N$  between their cotangent bundles, i.e., the following diagram commutes:

$$\begin{array}{ccc} T^*M & \xrightarrow{T^*\varphi} & T^*N \\ \pi_M^* \downarrow & & \downarrow \pi_N^* \\ M & \xrightarrow{\varphi} & N \end{array}$$

All cotangent bundles and their cotangent maps form the category  $T^*\mathcal{B}$ . The category  $T^*\mathcal{B}$  is the natural stage for *Hamiltonian biodynamics*.

Now, we can formulate the *dual version of the global chain rule*. If  $\varphi : M \rightarrow N$  and  $\psi : N \rightarrow P$  are two smooth maps, then we have  $T^*(\psi \circ \varphi) = T^*\psi \circ T^*\varphi$ . In other words, we have a cofunctor  $T^* : \mathcal{M} \Rightarrow T^*\mathcal{B}$  from the category  $\mathcal{M}$  of smooth manifolds to the category  $T^*\mathcal{B}$  of their cotangent bundles:

$$\begin{array}{ccc} & M & \\ \varphi \swarrow & & \searrow (\psi \circ \varphi) \\ N & \xrightarrow{\psi} & P \end{array} \quad \xRightarrow{T^*} \quad \begin{array}{ccc} & T^*M & \\ T^*\varphi \swarrow & & \searrow T^*(\psi \circ \varphi) \\ T^*N & \xleftarrow{T^*\psi} & T^*P \end{array}$$

### 3.4 Sections of Biodynamic Bundles

In this section we introduce *sections of biodynamic bundles*, including vector (and tensor) fields and their flows, as well as differential forms of various degree.

### 3.4.1 Biodynamic Evolution and Flow

As a motivational example, consider a biodynamic system that is capable of assuming various states described by points in a set  $U$ . For example,  $U$  might be  $\mathbb{R}^3 \times \mathbb{R}^3$  and a state might be the positions and momenta  $(x^i, p_i)$  of a particle moving under the influence of the central force field, with  $i = 1, 2, 3$ . As time passes, the state evolves. If the state is  $\gamma_0 \in U$  at time  $s$  and this changes to  $\gamma$  at a later time  $t$ , we set

$$F_{t,s}(\gamma_0) = \gamma,$$

and call  $F_{t,s}$  the *evolution operator*; it maps a state at time  $s$  to what the state would be at time  $t$ ; that is, after time  $t - s$ , has elapsed. Determinism is expressed by the *Chapman-Kolmogorov law* [Abraham *et al.* (1988)]:

$$F_{\tau,t} \circ F_{t,s} = F_{\tau,s}, \quad F_{t,t} = \text{identity}. \quad (3.2)$$

The evolution laws are called *time independent*, or *autonomous*, when  $F_{t,s}$  depends only on  $t - s$ . In this case the preceding law (3.2) becomes the *group property*:

$$F_t \circ F_s = F_{t+s}, \quad F_0 = \text{identity}. \quad (3.3)$$

We call such an  $F_t$  a *flow* and  $F_{t,s}$  a *time-dependent flow*, or an evolution operator. If the system is irreversible, that is, defined only for  $t \geq s$ , we speak of a *semi-flow* [Abraham *et al.* (1988)].

Usually, instead of  $F_{t,s}$  the *laws of motion* are given in the form of ODEs that we must solve to find the flow. These equations of motion read:

$$\dot{\gamma} = X(\gamma), \quad \gamma(0) = \gamma_0,$$

where  $X$  is a (possibly time-dependent) vector-field on  $U$ .

As a continuation of the previous example, consider the motion of a particle of mass  $m$  under the influence of the central force field (like gravity, or Coulombic potential)  $F^i$  ( $i = 1, 2, 3$ ), described by the Newtonian equation of motion:

$$m\ddot{x}^i = F^i(x). \quad (3.4)$$

By introducing momenta  $p_i = m\dot{x}^i$ , equation (7.140) splits into two Hamiltonian equations:

$$\dot{x}^i = p_i/m, \quad \dot{p}_i = F_i(x). \quad (3.5)$$

(in Euclidean space we can interchange subscripts and superscripts) The phase-space here is the manifold  $(\mathbb{R}^3 \setminus \{0\}) \times \mathbb{R}^3$ , that is, the cotangent bundle of  $\mathbb{R}^3 \setminus \{0\}$ , which is itself the manifold for the central force field. The r.h.s of equations (3.5) define a Hamiltonian vector-field on this 6D manifold by

$$X(x, p) = ((x^i, p_i), (p_i/m, F_i(x))) . \quad (3.6)$$

Integration of equations (3.5) produces trajectories (in this particular case, planar conic sections). These trajectories comprise the flow  $F_t$  of the vector-field  $X(x, p)$  defined in (3.6).

### 3.4.2 Vector-Fields and Their Flows

#### 3.4.2.1 Vector-Fields on $M$

A *vector-field*  $X$  on  $U$ , where  $U$  is an open chart in  $n$ -manifold  $M$ , is a *smooth function* from  $U$  to  $M$  assigning to each point  $m \in U$  a vector at that point, i.e.,  $X(m) = (m, X(m))$ . If  $X(m)$  is tangent to  $M$  for each  $m \in M$ ,  $X$  is said to be a *tangent vector-field* on  $M$ . If  $X(m)$  is orthogonal to  $M$  (i.e.,  $X(p) \in M_m^\perp$ ) for each  $X(m) \in M$ ,  $X$  is said to be a *normal vector-field* on  $M$ .

In other words, let  $M$  be a  $C^k$ -manifold. A  $C^k$ -vector-field on  $M$  is a  $C^k$ -section of the tangent bundle  $TM$  of  $M$ . Thus a vector-field  $X$  on a manifold  $M$  is a  $C^k$ -map  $X : M \rightarrow TM$  such that  $X(m) \in T_m M$  for all points  $m \in M$ , and  $\pi_M \circ X = Id_M$ . Therefore, a vector-field assigns to each point  $m$  of  $M$  a vector based (i.e., bound) at that point. The set of all  $C^k$  vector-fields on  $M$  is denoted by  $\mathcal{X}^k(M)$ .

A vector-field  $X \in \mathcal{X}^k(M)$  represents a field of direction indicators [Thirring (1979)]: to every point  $m$  of  $M$  it assigns a vector in the tangent space  $T_m M$  at that point. If  $X$  is a vector-field on  $M$  and  $(U, \phi)$  is a chart on  $M$  and  $m \in U$ , then we have  $X(m) = X(m) \phi^i \frac{\partial}{\partial \phi^i}$ . Following [Kolar *et al.* (1993)], we write  $X|_U = X \phi^i \frac{\partial}{\partial \phi^i}$ .

Let  $M$  be a connected  $n$ -manifold, and let  $f : U \rightarrow \mathbb{R}$  ( $U$  an open set in  $M$ ) and  $c \in \mathbb{R}$  be such that  $M = f^{-1}(c)$  (i.e.,  $M$  is the *level set* of the function  $f$  at *height*  $c$ ) and  $\nabla f(m) \neq 0$  for all  $m \in M$ . Then there exist on  $M$  exactly two smooth unit normal vector-fields  $N_{1,2}(m) = \pm \frac{\nabla f(m)}{|\nabla f(m)|}$  (here  $|X| = (X \cdot X)^{1/2}$  denotes the norm or length of a vector  $X$ , and  $(\cdot)$  denotes the scalar product on  $M$ ) for all  $m \in M$ , called *orientations* on  $M$ .

Let  $\varphi : M \rightarrow N$  be a smooth map. Recall that two vector-fields  $X \in$

$\mathcal{X}^k(M)$  and  $Y \in \mathcal{X}(N)$  are called  $\varphi$ -related, if  $T\varphi \circ X = Y \circ \varphi$  holds, i.e., if the following diagram commutes:

$$\begin{array}{ccc} TM & \xrightarrow{T\varphi} & TN \\ \uparrow X & & \uparrow Y \\ M & \xrightarrow{\varphi} & N \end{array}$$

In particular, a diffeomorphism  $\varphi : M \rightarrow N$  induces a linear map between vector-fields on two manifolds,  $\varphi^* : \mathcal{X}^k(M) \rightarrow \mathcal{X}(N)$ , such that  $\varphi^*X = T\varphi \circ X \circ \varphi^{-1} : N \rightarrow TN$ , i.e., the following diagram commutes:

$$\begin{array}{ccc} TM & \xrightarrow{T\varphi} & TN \\ \uparrow X & & \uparrow \varphi^*X \\ M & \xrightarrow{\varphi} & N \end{array}$$

The correspondences  $M \rightarrow TM$  and  $\varphi \rightarrow T\varphi$  obviously define a functor  $T : \mathcal{M} \Rightarrow \mathcal{M}$  from the category of smooth manifolds to itself.  $T$  is closely related to the tangent bundle functor (3.3.1).

A  $C^k$  time-dependent vector-field is a  $C^k$ -map  $X : \mathbb{R} \times M \rightarrow TM$  such that  $X(t, m) \in T_m M$  for all  $(t, m) \in \mathbb{R} \times M$ , i.e.,  $X_t(m) = X(t, m)$ .

### 3.4.2.2 Integral Curves as Biodynamic Trajectories

Recall (3.3.1) that a curve  $\gamma$  at a point  $m$  of an  $n$ -manifold  $M$  is a  $C^0$ -map from an open interval  $I$  of  $\mathbb{R}$  into  $M$  such that  $0 \in I$  and  $\gamma(0) = m$ . For such a curve we may assign a tangent vector at each point  $\gamma(t)$ ,  $t \in I$ , by  $\dot{\gamma}(t) = T_t\gamma(1)$ .

Let  $X$  be a smooth tangent vector-field on the smooth  $n$ -manifold  $M$ , and let  $m \in M$ . Then there exists an open interval  $I \subset \mathbb{R}$  containing 0 and a parameterized curve  $\gamma : I \rightarrow M$  such that:

- (1)  $\gamma(0) = m$ ;
- (2)  $\dot{\gamma}(t) = X(\gamma(t))$  for all  $t \in I$ ; and
- (3) If  $\beta : \tilde{I} \rightarrow M$  is any other parameterized curve in  $M$  satisfying (1) and (2), then  $\tilde{I} \subset I$  and  $\beta(t) = \gamma(t)$  for all  $t \in \tilde{I}$ .

A parameterized curve  $\gamma : I \rightarrow M$  satisfying condition (2) is called an *integral curve* of the tangent vector-field  $X$ . The unique  $\gamma$  satisfying conditions



(1)–(3) is the *maximal integral curve* of  $X$  through  $m \in M$ .

In other words, let  $\gamma : I \rightarrow M$ ,  $t \mapsto \gamma(t)$  be a smooth curve in a manifold  $M$  defined on an interval  $I \subseteq \mathbb{R}$ .  $\dot{\gamma}(t) = \frac{d}{dt}\gamma(t)$  defines a smooth vector-field along  $\gamma$  since we have  $\pi_M \circ \dot{\gamma} = \gamma$ . Curve  $\gamma$  is called an *integral curve* or *flow line* of a vector-field  $X \in \mathcal{X}^k(M)$  if the tangent vector determined by  $\gamma$  equals  $X$  at every point  $m \in M$ , i.e.,

$$\dot{\gamma} = X \circ \gamma,$$

or, if the following diagram commutes:

$$\begin{array}{ccc} TI & \xrightarrow{T\gamma} & TM \\ \uparrow 1 & \nearrow \dot{\gamma} & \uparrow X \\ I & \xrightarrow{\gamma} & M \end{array}$$

On a chart  $(U, \phi)$  with coordinates  $\phi(m) = (x^1(m), \dots, x^n(m))$ , for which  $\varphi \circ \gamma : t \mapsto \gamma_i(t)$  and  $T\varphi \circ X \circ \varphi^{-1} : x^i \mapsto (x^i, X_i(m))$ , this is written

$$\dot{\gamma}_i(t) = X_i(\gamma(t)), \text{ for all } t \in I \subseteq \mathbb{R}, \quad (3.7)$$

which is an ordinary differential equation of first order in  $n$  dimensions.

The *velocity*  $\dot{\gamma}$  of the parameterized curve  $\gamma(t)$  is a vector-field along  $\gamma$  defined by

$$\dot{\gamma}(t) = (\gamma(t), \dot{x}^1(t), \dots, \dot{x}^n(t)).$$

Its length  $|\dot{\gamma}| : I \rightarrow \mathbb{R}$ , defined by  $|\dot{\gamma}|(t) = |\dot{\gamma}(t)|$  for all  $t \in I$ , is a function along  $\alpha$ .  $|\dot{\gamma}|$  is called *speed* of  $\gamma$  [Arnold (1989)].

Each vector-field  $X$  along  $\gamma$  is of the form  $X(t) = (\gamma(t), X_1(t), \dots, X_n(t))$ , where each component  $X_i$  is a function along  $\gamma$ .  $X$  is *smooth* if each  $X_i : I \rightarrow M$  is smooth. The *derivative* of a smooth vector-field  $X$  along a curve  $\gamma(t)$  is the vector-field  $\dot{X}$  along  $\gamma$  defined by

$$\dot{X}(t) = (\gamma(t), \dot{X}_1(t), \dots, \dot{X}_n(t)).$$

$\dot{X}(t)$  measures the *rate of change of the vector part*  $(X_1(t), \dots, X_n(t))$  of  $X(t)$  *along*  $\gamma$ . Thus, the *acceleration*  $\ddot{\gamma}(t)$  of a parameterized curve  $\gamma(t)$  is the vector-field along  $\gamma$  obtained by differentiating the velocity field  $\dot{\gamma}(t)$ .

Differentiation of vector-fields along parameterized curves has the following properties. For  $X$  and  $Y$  smooth vector-fields on  $M$  along the parameterized curve  $\gamma : I \rightarrow M$  and  $f$  a smooth function along  $\gamma$ , we have:

- (1)  $\frac{d}{dt}(X + Y) = \dot{X} + \dot{Y}$ ;
- (2)  $\frac{d}{dt}(fX) = \dot{f}X + f\dot{X}$ ; and
- (3)  $\frac{d}{dt}(X \cdot Y) = \dot{X}Y + X\dot{Y}$ .

A *geodesic* in  $M$  is a parameterized curve  $\gamma : I \rightarrow M$  whose acceleration  $\ddot{\gamma}$  is everywhere orthogonal to  $M$ ; that is,  $\ddot{\gamma}(t) \in M_{\alpha(t)}^\perp$  for all  $t \in I \subset \mathbb{R}$ . Thus a geodesic is a curve in  $M$  which always goes 'straight ahead' in the surface. Its acceleration serves only to keep it in the surface. It has no component of acceleration tangent to the surface. Therefore, it also has a constant speed  $\dot{\gamma}(t)$ .

Let  $v \in M_m$  be a vector on  $M$ . Then there exists an open interval  $I \subset \mathbb{R}$  containing 0 and a geodesic  $\gamma : I \rightarrow M$  such that:

- (1)  $\gamma(0) = m$  and  $\dot{\gamma}(0) = v$ ; and
- (2) If  $\beta : \tilde{I} \rightarrow M$  is any other geodesic in  $M$  with  $\beta(0) = m$  and  $\dot{\beta}(0) = v$ , then  $\tilde{I} \subset I$  and  $\beta(t) = \gamma(t)$  for all  $t \in \tilde{I}$ .

The geodesic  $\gamma$  is now called the *maximal geodesic* in  $M$  passing through  $m$  with initial velocity  $v$  (see section 3.6).

By definition, a parameterized curve  $\gamma : I \rightarrow M$  is a geodesic of  $M$  iff its acceleration is everywhere perpendicular to  $M$ , i.e., iff  $\ddot{\gamma}(t)$  is a multiple of the orientation  $N(\gamma(t))$  for all  $t \in I$ , i.e.,  $\ddot{\gamma}(t) = g(t)N(\gamma(t))$ , where  $g : I \rightarrow \mathbb{R}$ . Taking the scalar product of both sides of this equation with  $N(\gamma(t))$  we find  $g = -\dot{\gamma}\dot{N}(\gamma(t))$ . Thus  $\gamma : I \rightarrow M$  is geodesic iff it satisfies the differential equation

$$\ddot{\gamma}(t) + \dot{N}(\gamma(t))N(\gamma(t)) = 0.$$

This vector equation represents the system of second order component ODEs

$$\ddot{x}^i + N_i(x + 1, \dots, x^n) \frac{\partial N_j}{\partial x^k}(x + 1, \dots, x^n) \dot{x}^j \dot{x}^k = 0.$$

The substitution  $u^i = \dot{x}^i$  reduces this second order differential system (in  $n$  variables  $x^i$ ) to the first order differential system

$$\dot{x}^i = u^i, \quad \dot{u}^i = -N_i(x + 1, \dots, x^n) \frac{\partial N_j}{\partial x^k}(x + 1, \dots, x^n) \dot{x}^j \dot{x}^k$$

(in  $2n$  variables  $x^i$  and  $u^i$ ). This first order system is just the differential equation for the integral curves of the vector-field  $X$  in  $U \times \mathbb{R}$  ( $U$  open chart in  $M$ ), in which case  $X$  is called a *geodesic spray*.

Now, when an integral curve  $\gamma(t)$  is the path a biodynamic system  $\Xi$  follows, i.e., the solution of the equations of motion, it is called a *trajectory*. In this case the parameter  $t$  represents time, so that (3.7) describes motion of the system  $\Xi$  on its configuration manifold  $M$ .

If  $X_i(m)$  is  $C^0$  the existence of a local solution is guaranteed, and a *Lipschitz condition* would imply that it is unique. Therefore, exactly one integral curve passes through every point, and different integral curves can never cross. As  $X \in \mathcal{X}^k(M)$  is  $C^k$ , the following statement about the solution with arbitrary initial conditions holds [Thirring (1979); Arnold (1989)]:

**Theorem.** Given a vector-field  $X \in \mathcal{X}(M)$ , for all points  $p \in M$ , there exist  $\eta > 0$ , a neighborhood  $V$  of  $p$ , and a function  $\gamma : (-\eta, \eta) \times V \rightarrow M$ ,  $(t, x^i(0)) \mapsto \gamma(t, x^i(0))$  such that

$$\dot{\gamma} = X \circ \gamma, \quad \gamma(0, x^i(0)) = x^i(0) \quad \text{for all } x^i(0) \in V \subseteq M.$$

For all  $|t| < \eta$ , the map  $x^i(0) \mapsto \gamma(t, x^i(0))$  is a diffeomorphism  $f_t^X$  between  $V$  and some open set of  $M$ . For proof, see [Dieudonne (1969)], I, 10.7.4 and 10.8.

This theorem states that trajectories that are near neighbors cannot suddenly be separated. There is a well-known estimate (see [Dieudonne (1969)], I, 10.5) according to which points cannot diverge faster than exponentially in time if the derivative of  $X$  is uniformly bounded.

An integral curve  $\gamma(t)$  is said to be *maximal* if it is not a restriction of an integral curve defined on a larger interval  $I \subseteq \mathbb{R}$ . It follows from the existence and uniqueness theorems for ODEs with smooth r.h.s and from elementary properties of Hausdorff spaces that for any point  $m \in M$  there exists a maximal integral curve  $\gamma_m$  of  $X$ , passing for  $t = 0$  through point  $m$ , i.e.,  $\gamma(0) = m$ .

**Theorem** (Local Existence, Uniqueness, and Smoothness) [Abraham *et al.* (1988)]. Let  $E$  be a Banach space,  $U \subset E$  be open, and suppose  $X : U \subset E \rightarrow E$  is of class  $C^k$ ,  $k \geq 1$ . Then

1. For each  $x_0 \in U$ , there is a curve  $\gamma : I \rightarrow U$  at  $x_0$  such that  $\dot{\gamma}(t) = X(\gamma(t))$  for all  $t \in I$ .
2. Any two such curves are equal on the intersection of their domains.
3. There is a neighborhood  $U_0$  of the point  $x_0 \in U$ , a real number  $a > 0$ ,

and a  $C^k$  map  $F : U_0 \times I \rightarrow E$ , where  $I$  is the open interval  $] -a, a[$ , such that the curve  $\gamma_u : I \rightarrow E$ , defined by  $\gamma_u(t) = F(u, t)$  is a curve at  $u \in E$  satisfying the ODEs  $\dot{\gamma}_u(t) = X(\gamma_u(t))$  for all  $t \in I$ .

**Proposition** (Global Uniqueness). Suppose  $\gamma_1$  and  $\gamma_2$  are two integral curves of a vector-field  $X$  at a point  $m \in M$ . Then  $\gamma_1 = \gamma_2$  on the intersection of their domains [Abraham *et al.* (1988)].

If for every point  $m \in M$  the curve  $\gamma_m$  is defined on the entire real axis  $\mathbb{R}$ , then the vector-field  $X$  is said to be *complete*.

The *support* of a vector-field  $X$  defined on a manifold  $M$  is defined to be the closure of the set  $\{m \in M | X(m) = 0\}$ . A  $C^k$  vector-field with compact support on a manifold  $M$  is complete. In particular, a  $C^k$  vector-field on a compact manifold is complete. Completeness corresponds to well-defined dynamics persisting eternally.

Now, following [Abraham *et al.* (1988)], for the *derivative* of a  $C^k$  function  $f : E \rightarrow \mathbb{R}$  in the direction  $X$  we use the notation  $X[f] = df \cdot X$ , where  $df$  stands for the *derivative map*. In standard coordinates on  $\mathbb{R}^n$  this is a standard *gradient*

$$df(x) = \nabla f = \left( \frac{\partial f}{\partial x^1}, \dots, \frac{\partial f}{\partial x^n} \right) \quad \text{and} \quad X[f] = X^i \frac{\partial f}{\partial x^i}.$$

Let  $F_t$  be the flow of  $X$ . Then  $f(F_t(x)) = f(F_s(x))$  if  $t \geq s$ .

For example, Newtonian equations for a moving particle of mass  $m$  in a potential field  $V$  in  $\mathbb{R}^n$  are given by  $\ddot{q}^i(t) = -(1/m)\nabla V(q^i(t))$ , for a smooth function  $V : \mathbb{R}^n \rightarrow \mathbb{R}$ . If there are constants  $a, b \in \mathbb{R}$ ,  $b \geq 0$  such that  $(1/m)V(q^i) \geq a - b\|q^i\|^2$ , then *every solution exists for all time*. To show this, rewrite the second order equations as a first order system  $\dot{q}^i = (1/m)p_i$ ,  $\dot{p}_i = -V(q^i)$  and note that the energy  $E(q^i, p_i) = (1/2m)\|p_i\|^2 + V(q)$  is a *first integral* of the motion. Thus, for any solution  $(q^i(t), p_i(t))$  we have  $E(q^i(t), p_i(t)) = E(q^i(0), p_i(0)) = V(q(0))$ .

Let  $X_t$  be a  $C^k$  time-dependent vector-field on an  $n$ -manifold  $M$ ,  $k \geq 1$ , and let  $m_0$  be an *equilibrium* of  $X_t$ , that is,  $X_t(m_0) = 0$  for all  $t$ . Then for any  $T$  there exists a neighborhood  $V$  of  $m_0$  such that any  $m \in V$  has integral curve existing for time  $t \in [-T, T]$ .

### 3.4.2.3 Biodynamic Flows on $M$

Recall (3.4.1) that the flow  $F_t$  of a  $C^k$  vector-field  $X \in \mathcal{X}^k(M)$  is the *one-parameter group of diffeomorphisms*  $F_t : M \rightarrow M$  such that  $t \mapsto F_t(m)$

is the integral curve of  $X$  with initial condition  $m$  for all  $m \in M$  and  $t \in I \subseteq \mathbb{R}$ . The flow  $F_t(m)$  is  $C^k$  by induction on  $k$ . It is defined as [Abraham *et al.* (1988)]:

$$\frac{d}{dt} F_t(x) = X(F_t(x)).$$

Existence and uniqueness theorems for ODEs guarantee that  $F_t$  is smooth in  $m$  and  $t$ . From uniqueness, we get the *flow property*:

$$F_{t+s} = F_t \circ F_s,$$

along with the initial conditions  $F_0 = \text{identity}$ . The flow property generalizes the situation where  $M = V$  is a linear space,  $X(x) = Ax$  for a (bounded) linear operator  $A$ , and where  $F_t(x) = e^{tA}x$  – to the nonlinear case. Therefore, the flow  $F_t(m)$  can be defined as a *formal exponential*

$$F_t(m) = \exp(tX) = (I + tX + \frac{t^2}{2}X^2 + \dots) = \sum_{k=0}^{\infty} \frac{X^k t^k}{k!}.$$

A *time-dependent vector-field* is a map  $X : M \times \mathbb{R} \rightarrow TM$  such that  $X(m, t) \in T_m M$  for each point  $m \in M$  and  $t \in \mathbb{R}$ . An *integral curve* of  $X$  is a curve  $\gamma(t)$  in  $M$  such that

$$\dot{\gamma}(t) = X(\gamma(t), t), \quad \text{for all } t \in I \subseteq \mathbb{R}.$$

In this case, the flow is the one-parameter group of diffeomorphisms  $F_{t,s} : M \rightarrow M$  such that  $t \mapsto F_{t,s}(m)$  is the integral curve  $\gamma(t)$  with initial condition  $\gamma(s) = m$  at  $t = s$ . Again, the existence and uniqueness theorem from ODE-theory applies here, and in particular, uniqueness gives the time-dependent flow property, i.e., the *Chapman-Kolmogorov law*

$$F_{t,r} = F_{t,s} \circ F_{s,r}.$$

If  $X$  happens to be time independent, the two notions of flows are related by  $F_{t,s} = F_{t-s}$  (see [Marsden and Ratiu (1999)]).

#### 3.4.2.4 Categories of ODEs

Ordinary differential equations are naturally organized into their categories (see [Kock (1981)]). First order ODEs are organized into a category  $ODE_1$ . A first order ODE on a manifold-like object  $M$  is a vector-field  $X : M \rightarrow$

$TM$ , and a *morphism of vector-fields*  $(M_1, X_1) \rightarrow (M_2, X_2)$  is a map  $f : M_1 \rightarrow M_2$  such that the following diagram commutes

$$\begin{array}{ccc} TM_1 & \xrightarrow{Tf} & TM_2 \\ X_1 \uparrow & & \uparrow X_2 \\ M_1 & \xrightarrow{f} & M_2 \end{array}$$

A *global solution* of the differential equation  $(M, X)$ , or a *flow line* of a vector-field  $X$ , is a morphism from  $(\mathbb{R}, \frac{\partial}{\partial x})$  to  $(M, X)$ .

Similarly, second order ODEs are organized into a category  $ODE_2$ . A second order ODE on  $M$  is usually constructed as a vector-field on  $TM$ ,  $\xi : TM \rightarrow TTM$ , and a morphism of vector-fields  $(M_1, \xi_1) \rightarrow (M_2, \xi_2)$  is a map  $f : M_1 \rightarrow M_2$  such that the following diagram commutes

$$\begin{array}{ccc} TTM_1 & \xrightarrow{TTf} & TTM_2 \\ \xi_1 \uparrow & & \uparrow \xi_2 \\ TM_1 & \xrightarrow{Tf} & TM_2 \end{array}$$

Unlike solutions for first order ODEs, solutions for second order ODEs are not in general homomorphisms from  $\mathbb{R}$ , unless the second order ODE is a *spray* [Kock and Reyes (2003)].

### 3.4.3 Differential Forms on $M$

Differential  $k$ -forms are tensor-fields of type  $(0, k)$  that are completely antisymmetric. Such tensor-fields arise in many applications in physics, engineering, and differential geometry. The reason for this is the fact that the classical vector operations of **grad**, **div**, and **curl** as well as the theorems of Green, Gauss, and Stokes can all be expressed concisely in terms of differential forms and the main operator acting on them, the exterior derivative  $d$ . We start with 1-forms, which are dual to vector-fields, and after that introduce general  $k$ -forms.

### 3.4.3.1 1-Forms on $M$

Dual to the notion of a  $C^k$  vector-field  $X$  on an  $n$ -manifold  $M$  is a  $C^k$  *covector-field*, or a  $C^k$  1-form  $\alpha$ , which is defined as a  $C^k$ -section of the cotangent bundle  $T^*M$ , i.e.,  $\alpha : M \rightarrow T^*M$  is smooth and  $\pi_M^* \circ \alpha = Id_M$ . We denote the set of all  $C^k$  1-forms by  $\Omega^1(M)$ . A basic example of a 1-form is the differential  $df$  of a real-valued function  $f \in C^k(M, \mathbb{R})$ . With point wise addition and scalar multiplication  $\Omega^1(M)$  becomes a vector space.

In other words, a  $C^k$  1-form  $\alpha$  on a  $C^k$  manifold  $M$  is a real-valued function on the set of all tangent vectors to  $M$ , i.e.,  $\alpha : TM \rightarrow \mathbb{R}$  with the following properties:

- (1)  $\alpha$  is linear on the tangent space  $T_m M$  for each  $m \in M$ ;
- (2) For any  $C^k$  vector-field  $X \in \mathcal{X}^k(M)$ , the function  $f : M \rightarrow \mathbb{R}$  is  $C^k$ .

Given a 1-form  $\alpha$ , for each point  $m \in M$  the map  $\alpha(m) : T_m M \rightarrow \mathbb{R}$  is an element of the dual space  $T_m^* M$ . Therefore, the space of 1-forms  $\Omega^1(M)$  is dual to the space of vector-fields  $\mathcal{X}^k(M)$ .

In particular, the *coordinate 1-forms*  $dx^1, \dots, dx^n$  are locally defined at any point  $m \in M$  by the property that for any vector-field  $X = (X^1, \dots, X^n) \in \mathcal{X}^k(M)$ ,

$$dx^i(X) = X^i.$$

The  $dx^i$ 's form a *basis* for the 1-forms at any point  $m \in M$ , with local coordinates  $(x^1, \dots, x^n)$ , so any other 1-form  $\alpha$  may be expressed in the form

$$\alpha = f_i(m) dx^i.$$

If a vector-field  $X$  on  $M$  has the form  $X(m) = (X^1(m), \dots, X^n(m))$ , then at any point  $m \in M$ ,

$$\alpha_m(X) = f_i(m) X^i(m),$$

where  $f \in C^k(M, \mathbb{R})$ .

The 1-forms on  $M$  are part of an algebra, called the *exterior algebra*, or *Grassmann algebra* on  $M$ . The multiplication  $\wedge$  in this algebra is called *wedge product* (see (3.8) below), and it is skew-symmetric,

$$dx^i \wedge dx^j = -dx^j \wedge dx^i.$$

One consequence of this is that  $dx^i \wedge dx^i = 0$ .

### 3.4.3.2 $k$ -Forms on $M$

A differential form, or an exterior form  $\alpha$  of degree  $k$ , or a  $k$ -form for short, is a section of the vector bundle  $\Lambda^k T^*M$ , i.e.,  $\alpha : M \rightarrow \Lambda^k T^*M$ . In other words,  $\alpha(m) : T_m M \times \dots \times T_m M \rightarrow \mathbb{R}$  (with  $k$  factors  $T_m M$ ) is a function that assigns to each point  $m \in M$  a skew-symmetric  $k$ -multilinear map on the tangent space  $T_m M$  to  $M$  at  $m$ . Without the skew-symmetry assumption,  $\alpha$  would be called a  $(0, k)$ -tensor-field. The space of all  $k$ -forms is denoted by  $\Omega^k(M)$ . It may also be viewed as the space of all skew symmetric  $(0, k)$ -tensor-fields, the space of all maps

$$\Phi : \mathcal{X}^k(M) \times \dots \times \mathcal{X}^k(M) \rightarrow C^k(M, \mathbb{R}),$$

which are  $k$ -linear and skew-symmetric (see (3.8) below). We put  $\Omega^k(M) = C^k(M, \mathbb{R})$ .

In particular, a 2-form  $\omega$  on an  $n$ -manifold  $M$  is a section of the vector bundle  $\Lambda^2 T^*M$ . If  $(U, \phi)$  is a chart at a point  $m \in M$  with local coordinates  $(x^1, \dots, x^n)$  let

$$\{e_1, \dots, e_n\} = \{\partial_{x^1}, \dots, \partial_{x^n}\}, \quad \left( \text{remember, } \partial_{x^i} \equiv \frac{\partial}{\partial x^i} \right)$$

be the corresponding basis for  $T_m M$ , and let

$$\{e^1, \dots, e^n\} = \{dx^1, \dots, dx^n\}$$

be the dual basis for  $T_m^* M$ . Then at each point  $m \in M$ , we can write a 2-form  $\omega$  as

$$\omega_m(v, u) = \omega_{ij}(m) v^i u^j, \quad \text{where } \omega_{ij}(m) = \omega_m(\partial_{x^i}, \partial_{x^j}).$$

If each summand of a differential form  $\alpha \in \Omega^k(M)$  contains  $k$  basis 1-forms  $dx^i$ 's, the form is called a  $k$ -form. Functions  $f \in C^k(M, \mathbb{R})$  are considered to be 0-forms, and any form on an  $n$ -manifold  $M$  of degree  $k > n$  must be zero due to the skew-symmetry.

Any  $k$ -form  $\alpha \in \Omega^k(M)$  may be expressed in the form

$$\alpha = f_I dx^{i_1} \wedge \dots \wedge dx^{i_k} = f_I dx^I,$$

where  $I$  is a multiindex  $I = (i_1, \dots, i_k)$  of length  $k$ , and  $\wedge$  is the wedge product which is associative, bilinear and anticommutative.

Just as 1-forms act on vector-fields to give real-valued functions, so  $k$ -forms act on  $k$ -tuples of vector-fields to give real-valued functions.



The *wedge product* of two differential forms, a  $k$ -form  $\alpha \in \Omega^k(M)$  and an  $l$ -form  $\beta \in \Omega^l(M)$  is a  $(k+l)$ -form  $\alpha \wedge \beta$  defined as:

$$\alpha \wedge \beta = \frac{(k+l)!}{k!l!} \mathbf{A}(\alpha \otimes \beta), \quad (3.8)$$

where  $\mathbf{A} : \Omega^k(M) \rightarrow \Omega^k(M)$ ,

$$\mathbf{A}\tau(e_1, \dots, e_k) = \frac{1}{k!} \sum_{\sigma \in S_k} (\text{sign } \sigma) \tau(e_{\sigma(1)}, \dots, e_{\sigma(k)}),$$

where  $S_k$  is the permutation group on  $k$  elements consisting of all bijections  $\sigma : \{1, \dots, k\} \rightarrow \{1, \dots, k\}$ .

For any  $k$ -form  $\alpha \in \Omega^k(M)$  and  $l$ -form  $\beta \in \Omega^l(M)$ , the wedge product is defined fiberwise, i.e.,  $(\alpha \wedge \beta)_m = \alpha_x \wedge \beta_m$  for each point  $m \in M$ . It is also associative, i.e.,  $(\alpha \wedge \beta) \wedge \gamma = \alpha \wedge (\beta \wedge \gamma)$ , and graded commutative, i.e.,  $\alpha \wedge \beta = (-1)^{kl} \beta \wedge \alpha$ . These properties are proved in multilinear algebra. So  $M \Rightarrow \Omega^k(M)$  is a contravariant functor from the category  $\mathcal{M}$  into the category of real graded commutative algebras [Kolar *et al.* (1993)].

Let  $M$  be an  $n$ -manifold,  $X \in \mathcal{X}^k(M)$ , and  $\alpha \in \Omega^{k+1}(M)$ . The *interior product*, or *contraction*,  $i_X \alpha = X \lrcorner \alpha \in \Omega^k(M)$  of  $X$  and  $\alpha$  (with *insertion operator*  $i_X$ ) is defined as

$$i_X \alpha(X^1, \dots, X^k) = \alpha(X, X^1, \dots, X^k).$$

Insertion operator  $i_X$  of a vector-field  $X \in \mathcal{X}^k(M)$  is natural with respect to the pull-back  $F^*$  of a diffeomorphism  $F : M \rightarrow N$  between two manifolds, i.e., the following diagram commutes:

$$\begin{array}{ccc} \Omega^k(N) & \xrightarrow{F^*} & \Omega^k(M) \\ i_X \downarrow & & \downarrow i_{F^*X} \\ \Omega^{k-1}(N) & \xrightarrow{F^*} & \Omega^{k-1}(M) \end{array}$$

Similarly, insertion operator  $i_X$  of a vector-field  $X \in \mathcal{Y}^k(M)$  is natural with respect to the push-forward  $F_*$  of a diffeomorphism  $F : M \rightarrow N$ , i.e.,

the following diagram commutes:

$$\begin{array}{ccc}
 \Omega^k(M) & \xrightarrow{F_*} & \Omega^k(N) \\
 i_Y \downarrow & & \downarrow i_{F_*Y} \\
 \Omega^{k-1}(M) & \xrightarrow{F_*} & \Omega^{k-1}(N)
 \end{array}$$

In case of *Riemannian manifolds* there is another exterior operation. Let  $M$  be a smooth  $n$ -manifold with Riemannian metric  $g \approx \langle, \rangle$  and the corresponding volume element  $\mu$  (see section (3.6) below). *Hodge star operator*  $*$  :  $\Omega^k(M) \rightarrow \Omega^{n-k}(M)$  on  $M$  is defined as

$$\alpha \wedge * \beta = \langle \alpha, \beta \rangle \mu \quad \text{for } \alpha, \beta \in \Omega^k(M).$$

The Hodge star operator satisfies the following properties for  $\alpha, \beta \in \Omega^k(M)$  [Abraham *et al.* (1988)]:

- (1)  $\alpha \wedge * \beta = \langle \alpha, \beta \rangle \mu = \beta \wedge * \alpha$ ;
- (2)  $*1 = \mu, \quad * \mu = (-1)^{Ind(g)}$ ;
- (3)  $** \alpha = (-1)^{Ind(g)} (-1)^{k(n-k)} \alpha$ ;
- (4)  $\langle \alpha, \beta \rangle = (-1)^{Ind(g)} \langle * \alpha, * \beta \rangle$ , where  $Ind(g)$  is the *index* of the metric  $g$ .

### 3.4.3.3 Exterior Differential Systems

Here we give an informal introduction to *exterior differential systems* (EDS, for short), which are expressions involving differential forms related to any manifold  $M$  (for a rigorous treatment, see [Bryant *et al.* (2003)]).

Central in the language of EDS is the notion of *coframing*, which is a real finite-dimensional smooth manifold  $M$  with a given global *cobasis* and coordinates, but without requirement for a proper topological and differential structures. For example,  $M = \mathbb{R}^3$  is a coframing with cobasis  $\{dx, dy, dz\}$  and coordinates  $\{x, y, z\}$ . In addition to the cobasis and coordinates, a coframing can be given structure equations and restrictions. For example,  $M = \mathbb{R}^2 \setminus \{0\}$  is a coframing with cobasis  $\{e^1, e^2\}$ , a single coordinate  $\{r\}$ , structure equations  $\{dr = e^1, de^1 = 0, de^2 = e^1 \wedge e^2 / r\}$  and restrictions  $\{r \neq 0\}$ .

A *system*  $S$  on  $M$  in EDS terminology is a list of expressions including differential forms (e.g.,  $S = \{dz - ydx\}$ ).

Now, a simple EDS is a triple  $(S, \Omega, M)$ , where  $S$  is a system on  $M$ , and  $\Omega$  is an *independence condition*: either a decomposable  $k$ -form or a

system of  $k$ -forms on  $M$ . An EDS is a list of simple EDS objects where the various coframings are all disjoint.

An *integral element* of an exterior system  $(S, \Omega, M)$  is a subspace  $P \subset T_m M$  of the tangent space at some point  $m \in M$  such that all forms in  $S$  vanish when evaluated on vectors from  $P$ . Alternatively, an integral element  $P \subset T_m M$  can be represented by its annihilator  $P^\perp \subset T_m^* M$ , comprising those 1-forms at  $m$  which annul every vector in  $P$ . For example, with  $M = \mathbb{R}^3 = \{(x, y, z)\}$ ,  $S = \{dx \wedge dz\}$  and  $\Omega = \{dx, dz\}$ , the integral element  $P = \{\partial_x + \partial_z, \partial_y\}$  is equally determined by its annihilator  $P^\perp = \{dz - dx\}$ . Again, for  $S = \{dz - ydx\}$  and  $\Omega = \{dx\}$ , the integral element  $P = \{\partial_x + y\partial_z\}$  can be specified simply as  $\{dy\}$ .

#### 3.4.3.4 Exterior Derivative on $M$

The *exterior derivative* is an operation that takes  $k$ -forms to  $(k+1)$ -forms on a smooth manifold  $M$ . It defines a unique family of maps  $d : \Omega^k(U) \rightarrow \Omega^{k+1}(U)$ ,  $U$  open in  $M$ , such that (see [Abraham *et al.* (1988)]):

- (1)  $d$  is a  $\wedge$ -*antiderivation*; that is,  $d$  is  $\mathbb{R}$ -linear and for two forms  $\alpha \in \Omega^k(U)$ ,  $\beta \in \Omega^l(U)$ ,

$$d(\alpha \wedge \beta) = d\alpha \wedge \beta + (-1)^k \alpha \wedge d\beta.$$

- (2) If  $f \in C^k(U, \mathbb{R})$  is a function on  $M$ , then  $df = \frac{\partial f}{\partial x^i} dx^i : M \rightarrow T^*M$  is the differential of  $f$ , such that  $df(X) = i_X df = \mathcal{L}_X f - di_X f = \mathcal{L}_X f = X[f]$  for any  $X \in \mathcal{X}^k(M)$ .
- (3)  $d^2 = d \circ d = 0$  (that is,  $d^{k+1}(U) \circ d^k(U) = 0$ ).
- (4)  $d$  is natural with respect to restrictions  $|U$ ; that is, if  $U \subset V \subset M$  are open and  $\alpha \in \Omega^k(V)$ , then  $d(\alpha|U) = (d\alpha)|U$ , or the following diagram commutes:

$$\begin{array}{ccc} \Omega^k(V) & \xrightarrow{|U} & \Omega^k(U) \\ d \downarrow & & \downarrow d \\ \Omega^{k+1}(V) & \xrightarrow{|U} & \Omega^{k+1}(U) \end{array}$$

- (5)  $d$  is natural with respect to the Lie derivative  $\mathcal{L}_X$  along any vector-field  $X \in \mathcal{X}^k(M)$ ; that is, for  $\omega \in \Omega^k(M)$  we have  $\mathcal{L}_X \omega \in \Omega^k(M)$  and

$d\mathcal{L}_X\omega = \mathcal{L}_Xd\omega$ , or the following diagram commutes:

$$\begin{array}{ccc} \Omega^k(M) & \xrightarrow{\mathcal{L}_X} & \Omega^k(M) \\ d \downarrow & & \downarrow d \\ \Omega^{k+1}(M) & \xrightarrow{\mathcal{L}_X} & \Omega^{k+1}(M) \end{array}$$

- (6) Let  $\varphi : M \rightarrow N$  be a  $C^k$  map of manifolds. Then  $\varphi^* : \Omega^k(N) \rightarrow \Omega^k(M)$  is a homomorphism of differential algebras (with  $\wedge$  and  $d$ ) and  $d$  is natural with respect to  $\varphi^* = F^*$ ; that is,  $\varphi^*d\omega = d\varphi^*\omega$ , or the following diagram commutes:

$$\begin{array}{ccc} \Omega^k(N) & \xrightarrow{\varphi^*} & \Omega^k(M) \\ d \downarrow & & \downarrow d \\ \Omega^{k+1}(N) & \xrightarrow{\varphi^*} & \Omega^{k+1}(M) \end{array}$$

- (7) Analogously,  $d$  is natural with respect to diffeomorphism  $\varphi_* = (F^*)^{-1}$ ; that is,  $\varphi_*d\omega = d\varphi_*\omega$ , or the following diagram commutes:

$$\begin{array}{ccc} \Omega^k(N) & \xrightarrow{\varphi_*} & \Omega^k(M) \\ d \downarrow & & \downarrow d \\ \Omega^{k+1}(N) & \xrightarrow{\varphi_*} & \Omega^{k+1}(M) \end{array}$$

- (8)  $\mathcal{L}_X = i_X \circ d + d \circ i_X$  for any  $X \in \mathcal{X}^k(M)$  (a ‘magic’ formula of Cartan).  
 (9)  $\mathcal{L}_X \circ d = d \circ \mathcal{L}_X$ , i.e.,  $[\mathcal{L}_X, d] = 0$  for any  $X \in \mathcal{X}^k(M)$ .  
 (10)  $[\mathcal{L}_X, i_Y] = i_{[X, Y]}$ ; in particular,  $i_X \circ \mathcal{L}_X = \mathcal{L}_X \circ i_X$  for all  $X, Y \in \mathcal{X}^k(M)$ .

Given a  $k$ -form  $\alpha = f_I dx^I \in \Omega^k(M)$ , the exterior derivative is defined in local coordinates  $(x^1, \dots, x^n)$  of a point  $m \in M$  as

$$d\alpha = d(f_I dx^I) = \frac{\partial f_I}{\partial x^{i_k}} dx^{i_k} \wedge dx^I = df_I \wedge dx^{i_1} \wedge \dots \wedge dx^{i_k}.$$

In particular, the exterior derivative of a function  $f \in C^k(M, \mathbb{R})$  is a 1-form  $df \in \Omega^1(M)$ , with the property that for any  $m \in M$ , and  $X \in \mathcal{X}^k(M)$ ,

$$df_m(X) = X(f),$$

i.e.,  $df_m(X)$  is a Lie derivative of  $f$  at  $m$  in the direction of  $X$ . Therefore, in local coordinates  $(x^1, \dots, x^n)$  of a point  $m \in M$  we have

$$df = \frac{\partial f}{\partial x^i} dx^i.$$

For any two functions  $f, g \in C^k(M, \mathbb{R})$ , exterior derivative obeys the *Leibniz rule*:

$$d(fg) = g df + f dg$$

and the *chain rule*:

$$d(g(f)) = g'(f) df.$$

A  $k$ -form  $\alpha \in \Omega^k(M)$  is called *closed form* if  $d\alpha = 0$ , and it is called *exact form* if there exists a  $(k-1)$ -form  $\beta \in \Omega^{k-1}(M)$  such that  $\alpha = d\beta$ . Since  $d^2 = 0$ , every exact form is closed. The converse is only partially true (Poincaré Lemma): every closed form is *locally exact*. This means that given a closed  $k$ -form  $\alpha \in \Omega^k(M)$  on an open set  $U \subset M$ , any point  $m \in U$  has a neighborhood on which there exists a  $(k-1)$ -form  $\beta \in \Omega^{k-1}(U)$  such that  $d\beta = \alpha|_U$ .

The Poincaré lemma is a generalization and unification of two well-known facts in vector calculus:

- (1) If  $\text{curl } F = 0$ , then locally  $F = \text{grad } f$ ;
- (2) If  $\text{div } F = 0$ , then locally  $F = \text{curl } G$ .

*Poincaré lemma* for contractible manifolds: Any closed form on a smoothly contractible manifold is exact.

### 3.4.3.5 De Rham Complex and Homotopy Operators

Given a biodynamic manifold  $M$ , let  $\Omega^p(M)$  denote the space of all smooth  $p$ -forms on  $M$ . The differential  $d$ , mapping  $p$ -forms to  $(p+1)$ -forms, serves to define the *De Rham complex* on  $M$ ,

$$0 \rightarrow \Omega^0(M) \xrightarrow{d^0} \Omega^1(M) \xrightarrow{d^1} \dots \xrightarrow{d^{n-1}} \Omega^n(M) \rightarrow 0. \quad (3.9)$$

In general, a *complex* (see subsection (2.1.8) above) is defined as a sequence of vector spaces, and linear maps between successive spaces, with the property that the composition of any pair of successive maps is identically 0. In the case of the de Rham complex (3.9), this requirement is a restatement of the closure property for the exterior differential:  $d \circ d = 0$ .

In particular, for  $n = 3$ , the De Rham complex on a biodynamic manifold  $M$  reads

$$0 \rightarrow \Omega^0(M) \xrightarrow{d^0} \Omega^1(M) \xrightarrow{d^1} \Omega^2(M) \xrightarrow{d^2} \Omega^3(M) \rightarrow 0. \quad (3.10)$$

If  $\omega \equiv f(x, y, z) \in \Omega^0(M)$ , then

$$d^0\omega \equiv d^0f = \frac{\partial f}{\partial x}dx + \frac{\partial f}{\partial y}dy + \frac{\partial f}{\partial z}dz = \text{grad } \omega.$$

If  $\omega \equiv fdx + gdy + hdz \in \Omega^1(M)$ , then

$$d^1\omega \equiv \left( \frac{\partial g}{\partial x} - \frac{\partial f}{\partial y} \right) dx \wedge dy + \left( \frac{\partial h}{\partial y} - \frac{\partial g}{\partial z} \right) dy \wedge dz + \left( \frac{\partial f}{\partial z} - \frac{\partial h}{\partial x} \right) dz \wedge dx = \text{curl } \omega.$$

If  $\omega \equiv Fdy \wedge dz + Gdz \wedge dx + Hdx \wedge dy \in \Omega^2(M)$ , then

$$d^2\omega \equiv \frac{\partial F}{\partial x} + \frac{\partial G}{\partial y} + \frac{\partial H}{\partial z} = \text{div } \omega.$$

Therefore, the De Rham complex (3.10) can be written as

$$0 \rightarrow \Omega^0(M) \xrightarrow{\text{grad}} \Omega^1(M) \xrightarrow{\text{curl}} \Omega^2(M) \xrightarrow{\text{div}} \Omega^3(M) \rightarrow 0.$$

Using the closure property for the exterior differential,  $d \circ d = 0$ , we get the standard identities from vector calculus

$$\text{curl} \cdot \text{grad} = 0 \quad \text{and} \quad \text{div} \cdot \text{curl} = 0.$$

The definition of the complex requires that the kernel of one of the linear maps contains the image of the preceding map. The complex is *exact* if this containment is *equality*. In the case of the De Rham complex (3.9), exactness means that a closed  $p$ -form  $\omega$ , meaning that  $d\omega = 0$ , is necessarily an exact  $p$ -form, meaning that there exists a  $(p-1)$ -form  $\theta$  such that  $\omega = d\theta$ . (For  $p = 0$ , it says that a smooth function  $f$  is closed,  $df = 0$ , iff it is constant). Clearly, any exact form is closed, but the converse need not hold. Thus the De Rham complex is *not* in general exact. The celebrated *De Rham theorem* states that the extent to which this complex fails to be exact measures purely topological information about the manifold  $M$ , its cohomology group.

On the local side, for special types of domains in Euclidean space  $\mathbb{R}^m$ , there is only trivial topology and we do have exactness of the De Rham

complex (3.9). This result, known as the *Poincaré lemma*, holds for *star-shaped* domains  $M \subset \mathbb{R}^m$ : Let  $M \subset \mathbb{R}^m$  be a star-shaped domain. Then the De Rham complex over  $M$  is exact.

The key to the proof of exactness of the De Rham complex lies in the construction of suitable *homotopy operators*. By definition, these are linear operators  $h : \Omega^p \rightarrow \Omega^{p-1}$ , taking differential  $p$ -forms into  $(p-1)$ -forms, and satisfying the basic identity [Olver (1986)]

$$\omega = dh(\omega) + h(d\omega), \quad (3.11)$$

for all  $p$ -forms  $\omega \in \Omega^p$ . The discovery of such a set of operators immediately implies exactness of the complex. For if  $\omega$  is closed,  $d\omega = 0$ , then (3.11) reduces to  $\omega = d\theta$  where  $\theta = h(\omega)$ , so  $\omega$  is exact.

### 3.4.3.6 Stokes Theorem and De Rham Cohomology

Stokes theorem states that if  $\alpha$  is an  $(n-1)$ -form on an orientable  $n$ -manifold  $M$ , then the integral of  $d\alpha$  over  $M$  equals the integral of  $\alpha$  over  $\partial M$ , the boundary of  $M$ . The classical theorems of Gauss, Green, and Stokes are special cases of this result.

A *manifold with boundary* is a set  $M$  together with an atlas of charts  $(U, \phi)$  with boundary on  $M$ . Define (see [Abraham *et al.* (1988)]) the *interior* and *boundary* of  $M$  respectively as

$$\text{Int } M = \bigcup_U \phi^{-1}(\text{Int}(\phi(U))) \quad \text{and} \quad \partial M = \bigcup_U \phi^{-1}(\partial(\phi(U))).$$

If  $M$  is a manifold with boundary, then its interior  $\text{Int } M$  and its boundary  $\partial M$  are smooth manifolds without boundary. Moreover, if  $f : M \rightarrow N$  is a diffeomorphism,  $N$  being another manifold with boundary, then  $f$  induces, by restriction, two diffeomorphisms

$$\text{Int } f : \text{Int } M \rightarrow \text{Int } N \quad \text{and} \quad \partial f : \partial M \rightarrow \partial N.$$

If  $n = \dim M$ , then  $\dim(\text{Int } M) = n$  and  $\dim(\partial M) = n-1$ .

To integrate a differential  $n$ -form over an  $n$ -manifold  $M$ ,  $M$  must be oriented. If  $\text{Int } M$  is oriented, we want to choose an *orientation* on  $\partial M$  compatible with it. As for manifolds without boundary a volume form on an  $n$ -manifold with boundary  $M$  is a nowhere vanishing  $n$ -form on  $M$ . Fix an orientation on  $\mathbb{R}^n$ . Then a chart  $(U, \phi)$  is called *positively oriented* if the map  $T_m \phi : T_m M \rightarrow \mathbb{R}^n$  is orientation preserving for all  $m \in U$ .

Let  $M$  be a compact, oriented  $k$ D smooth manifold with boundary  $\partial M$ . Let  $\alpha$  be a smooth  $(k-1)$ -form on  $M$ . Then the classical *Stokes formula* holds

$$\int_M d\alpha = \int_{\partial M} \alpha.$$

If  $\partial M = \emptyset$  then  $\int_M d\alpha = 0$ .

The quotient space

$$H^k(M) = \frac{\text{Ker}(d : \Omega^k(M) \rightarrow \Omega^{k+1}(M))}{\text{Im}(d : \Omega^{k-1}(M) \rightarrow \Omega^k(M))}$$

is called the  $k$ th *De Rham cohomology group* of a manifold  $M$ . The *De Rham theorem* states that these Abelian groups are isomorphic to the so-called singular cohomology groups of  $M$  defined in algebraic topology in terms of simplices and that depend only on the topological structure of  $M$  and not on its differentiable structure. The isomorphism is provided by integration; the fact that the integration map drops to the preceding quotient is guaranteed by Stokes' theorem.

The exterior derivative commutes with the pull-back of differential forms. That means that the vector bundle  $\Lambda^k T^*M$  is in fact the value of a functor, which associates a bundle over  $M$  to each manifold  $M$  and a vector bundle homomorphism over  $\varphi$  to each (local) diffeomorphism  $\varphi$  between manifolds of the same dimension. This is a simple example of the concept of a natural bundle. The fact that the exterior derivative  $d$  transforms sections of  $\Lambda^k T^*M$  into sections of  $\Lambda^{k+1} T^*M$  for every manifold  $M$  can be expressed by saying that  $d$  is an operator from  $\Lambda^k T^*M$  into  $\Lambda^{k+1} T^*M$ . That the exterior derivative  $d$  commutes with (local) diffeomorphisms now means, that  $d$  is a natural operator from the functor  $\Lambda^k T^*$  into functor  $\Lambda^{k+1} T^*$ . If  $k > 0$ , one can show that  $d$  is the unique natural operator between these two natural bundles up to a constant. So even linearity is a consequence of naturality [Kolar *et al.* (1993)].

#### 3.4.3.7 Euler–Poincaré Characteristics of $M$

The *Euler–Poincaré characteristics* of a manifold  $M$  equals the sum of its *Betti numbers*

$$\chi(M) = (-1)^p b_p, \quad (\text{summing from } 0 \text{ to } n).$$

In case of  $2n$ D oriented compact Riemannian manifold  $M$  (*Gauss–*



*Bonnet theorem*) its Euler–Poincaré characteristics is equal

$$\chi(M) = \int_M \gamma,$$

where  $\gamma$  is a closed  $2n$  form on  $M$ , given by

$$\gamma = \frac{(-1)^n}{(4\pi)^n n!} \epsilon_{i_1 \dots i_{2n}}^{1 \dots 2n} \Omega_{i_2}^{i_1} \wedge \Omega_{i_{2n}}^{i_{2n-1}},$$

where  $\Omega_j^i$  is the curvature 2-form of a Riemannian connection on  $M$  (see chapter 5 for more details).

*Poincaré–Hopf theorem*: The Euler–Poincaré characteristics  $\chi(M)$  of a compact manifold  $M$  equals the sum of indices of zeros of any vector-field on  $M$  which has only isolated zeros.

### 3.4.3.8 Duality of Chains and Forms on $M$

In topology of finite-dimensional smooth (i.e.,  $C^{p+1}$  with  $p \geq 0$ ) manifolds, a fundamental notion is the *duality* between  $p$ -chains  $C$  and  $p$ -forms (i.e.,  $p$ -cochains)  $\omega$  on the smooth manifold  $M$ , or domains of integration and integrands – as an integral on  $M$  represents a bilinear functional (see [Choquet-Bruhat and DeWitt-Morete (1982); Dodson and Parker (1997)])

$$\int_C \omega \equiv \langle C, \omega \rangle, \quad (3.12)$$

where the integral is called the *period* of  $\omega$ . Period depends only on the cohomology class of  $\omega$  and the homology class of  $C$ . A closed form (cocycle) is exact (coboundary) if all its periods vanish, i.e.,  $d\omega = 0$  implies  $\omega = d\theta$ . The duality (3.12) is based on the classical Stokes formula

$$\int_C d\omega = \int_{\partial C} \omega.$$

This is written in terms of scalar products on  $M$  as

$$\langle C, d\omega \rangle = \langle \partial C, \omega \rangle,$$

where  $\partial C$  is the boundary of the  $p$ -chain  $C$  oriented coherently with  $C$ . While the boundary operator  $\partial$  is a global operator, the coboundary operator, that is, the exterior derivative  $d$ , is local, and thus more suitable for applications. The main property of the exterior differential,

$$d^2 = 0 \quad \text{implies} \quad \partial^2 = 0,$$

can be easily proved by the use of Stokes' formula

$$\langle \partial^2 C, \omega \rangle = \langle \partial C, d\omega \rangle = \langle C, d^2 \omega \rangle = 0.$$

The analysis of  $p$ -chains and  $p$ -forms on the finite-dimensional biodynamic manifold  $M$  is usually performed in (co)homology categories (see [Dodson and Parker (1997); Dieudonne (1988)]) related to  $M$ .

Let  $\mathcal{M}^\bullet$  denote the category of cochains, (i.e.,  $p$ -forms) on the smooth manifold  $M$ . When  $\mathcal{C} = \mathcal{M}^\bullet$ , we have the category  $\mathcal{S}^\bullet(\mathcal{M}^\bullet)$  of generalized cochain complexes  $A^\bullet$  in  $\mathcal{M}^\bullet$ , and if  $A' = 0$  for  $n < 0$  we have a subcategory  $\mathcal{S}_{DR}^\bullet(\mathcal{M}^\bullet)$  of the De Rham differential complexes in  $\mathcal{M}^\bullet$

$$\begin{aligned} A_{DR}^\bullet : 0 \rightarrow \Omega^0(M) \xrightarrow{d} \Omega^1(M) \xrightarrow{d} \Omega^2(M) \cdots \\ \cdots \xrightarrow{d} \Omega^n(M) \xrightarrow{d} \cdots \end{aligned} \quad (3.13)$$

Here  $A' = \Omega^n(M)$  is the vector space over  $\mathbb{R}$  of all  $p$ -forms  $\omega$  on  $M$  (for  $p = 0$  the smooth functions on  $M$ ) and  $d_n = d : \Omega^{n-1}(M) \rightarrow \Omega^n(M)$  is the exterior differential. A form  $\omega \in \Omega^n(M)$  such that  $d\omega = 0$  is a closed form or  $n$ -cocycle. A form  $\omega \in \Omega^n(M)$  such that  $\omega = d\theta$ , where  $\theta \in \Omega^{n-1}(M)$ , is an exact form or  $n$ -coboundary. Let  $Z^n(M) = \text{Ker}(d)$  (resp.  $B^n(M) = \text{Im}(d)$ ) denote a real vector space of cocycles (resp. coboundaries) of degree  $n$ . Since  $d_{n+1}d_n = d^2 = 0$ , we have  $B^n(M) \subset Z^n(M)$ . The quotient vector space

$$H_{DR}^n(M) = \text{Ker}(d) / \text{Im}(d) = Z^n(M) / B^n(M)$$

is the De Rham cohomology group. The elements of  $H_{DR}^n(M)$  represent equivalence sets of cocycles. Two cocycles  $\omega_1, \omega_2$  belong to the same equivalence set, or are cohomologous (written  $\omega_1 \sim \omega_2$ ) iff they differ by a coboundary  $\omega_1 - \omega_2 = d\theta$ . The De Rham cohomology class of any form  $\omega \in \Omega^n(M)$  is  $[\omega] \in H_{DR}^n(M)$ . The De Rham differential complex (3.13) can be considered as a system of second-order ODEs  $d^2\theta = 0$ ,  $\theta \in \Omega^{n-1}(M)$  having a solution represented by  $Z^n(M) = \text{Ker}(d)$ .

Analogously let  $\mathcal{M}_\bullet$  denote the category of chains on the smooth manifold  $M$ . When  $\mathcal{C} = \mathcal{M}_\bullet$ , we have the category  $\mathcal{S}_\bullet(\mathcal{M}_\bullet)$  of generalized chain complexes  $A_\bullet$  in  $\mathcal{M}_\bullet$ , and if  $A_n = 0$  for  $n < 0$  we have a subcategory  $\mathcal{S}_\bullet^\mathcal{C}(\mathcal{M}_\bullet)$  of chain complexes in  $\mathcal{M}_\bullet$ .

$$A_\bullet : 0 \leftarrow C^0(M) \xleftarrow{\partial} C^1(M) \xleftarrow{\partial} C^2(M) \cdots \xleftarrow{\partial} C^n(M) \xleftarrow{\partial} \cdots$$

Here  $A_n = C^n(M)$  is the vector space over  $\mathbb{R}$  of all finite chains  $C$  on the manifold  $M$  and  $\partial_n = \partial : C^{n+1}(M) \rightarrow C^n(M)$ . A finite chain  $C$  such that  $\partial C = 0$  is an  $n$ -cycle. A finite chain  $C$  such that  $C = \partial B$  is an  $n$ -boundary. Let  $Z_n(M) = \text{Ker}(\partial)$  (resp.  $B_n(M) = \text{Im}(\partial)$ ) denote a real vector space of cycles (resp. boundaries) of degree  $n$ . Since  $\partial_{n+1}\partial_n = \partial^2 = 0$ , we have  $B_n(M) \subset Z_n(M)$ . The quotient vector space

$$H_n^C(M) = \text{Ker}(\partial)/\text{Im}(\partial) = Z_n(M)/B_n(M)$$

is the  $n$ -homology group. The elements of  $H_n^C(M)$  are equivalence sets of cycles. Two cycles  $C_1, C_2$  belong to the same equivalence set, or are homologous (written  $C_1 \sim C_2$ ), iff they differ by a boundary  $C_1 - C_2 = \partial B$ . The homology class of a finite chain  $C \in C^n(M)$  is  $[C] \in H_n^C(M)$ .

The dimension of the  $n$ -cohomology (resp.  $n$ -homology) group equals the  $n$ th Betti number  $b^n$  (resp.  $b_n$ ) of the manifold  $M$ . *Poincaré lemma* says that on an open set  $U \in M$  diffeomorphic to  $\mathbb{R}^N$ , all closed forms (cycles) of degree  $p \geq 1$  are exact (boundaries). That is, the Betti numbers satisfy  $b^p = 0$  (resp.  $b_p = 0$ ) for  $p = 1, \dots, n$ .

The *De Rham theorem* states the following. The map  $\Phi: H_n \times H^n \rightarrow \mathbb{R}$  given by  $([C], [\omega]) \rightarrow \langle C, \omega \rangle$  for  $C \in Z_n, \omega \in Z^n$  is a bilinear nondegenerate map which establishes the duality of the groups (vector spaces)  $H_n$  and  $H^n$  and the equality  $b_n = b^n$ .

### 3.4.3.9 Other Exterior Operators on $M$

As the configuration manifold  $M$  is an oriented  $ND$  Riemannian manifold, we may select an orientation on all tangent spaces  $T_m M$  and all cotangent spaces  $T_m^* M$ , with the local coordinates  $x^i = (q^i, p_i)$  at a point  $m \in M$ , in a consistent manner. The simplest way to do that is to choose the Euclidean orthonormal basis  $\partial_1, \dots, \partial_N$  of  $\mathbb{R}^N$  as being positive.

Since the manifold  $M$  carries a Riemannian structure  $g = \langle \cdot, \cdot \rangle$ , we have a scalar product on each  $T_m^* M$ . We define the linear *Hodge star operator*

$$*: \Lambda^p(T_m^* M) \rightarrow \Lambda^{N-p}(T_m^* M),$$

i.e., a base point preserving operator

$$*: \Omega^p(M) \rightarrow \Omega^{N-p}(M), \quad (\Omega^p(M) = \Gamma(\Lambda^p(M)))$$

(here  $\Lambda^p(V)$  denotes the  $p$ -fold exterior product of any vector space  $V$ ,  $\Omega^p(M)$  is a space of all  $p$ -forms on  $M$ , and  $\Gamma(E)$  denotes the space of

sections of the vector bundle  $E$ ). Also,

$$** = (-1)^{p(N-p)} : \Lambda^p(T_x^*M) \rightarrow \Lambda^p(T_m^*M).$$

As the metric on  $T_m^*M$  is given by  $g^{ij}(x) = (g_{ij}(x))^{-1}$ , we have the *volume form* defined in local coordinates as

$$*(1) = \sqrt{\det(g_{ij})} dx^1 \wedge \dots \wedge dx^n,$$

and

$$\text{vol}(M) = \int_M *(1).$$

For any to  $p$ -forms  $\alpha, \beta \in \Omega^p(M)$  with compact support, we define the (bilinear and positive definite)  $L^2$ -product as

$$(\alpha, \beta) = \int_M \langle \alpha, \beta \rangle * (1) = \int_M \alpha \wedge *\beta.$$

We can extend the product  $(\cdot, \cdot)$  to  $L^2(\Omega^p(M))$ ; it remains bilinear and positive definite, because as usual, in the definition of  $L^2$ , functions that differ only on a set of measure zero are identified.

Using the Hodge star operator  $*$ , we can introduce the *codifferential* operator  $\delta$ , which is formally adjoint to the exterior derivative  $d : \Omega^p(M) \rightarrow \Omega^{p+1}(M)$  on  $\oplus_{p=0}^N \Omega^p(M)$  w.r.t.  $(\cdot, \cdot)$ . This means that for  $\alpha \in \Omega^{p-1}(M), \beta \in \Omega^p(M)$

$$(d\alpha, \beta) = (\alpha, \delta\beta).$$

Therefore, we have  $\delta : \Omega^p(M) \rightarrow \Omega^{p-1}(M)$  and

$$\delta = (-1)^{N(p+1)+1} * d *.$$

Now, the Laplace–Beltrami operator (or, *Hodge Laplacian*),  $\Delta$  on  $\Omega^p(M)$ , is defined by relation similar to (3.11) above

$$\Delta = d\delta + \delta d : \Omega^p(M) \rightarrow \Omega^p(M) \quad (3.14)$$

and  $\alpha \in \Omega^p(M)$  is called *harmonic* if

$$\Delta\alpha = 0.$$

### 3.4.4 Geometry of Nonlinear Dynamics

Now we have enough geometric background to extend our language of linear dynamics (2.2) to the real world situations. The basic form of nonlinear ODEs is

$$\dot{x} = f(x, t), \quad (3.15)$$

where  $x \in \mathcal{P} \subset \mathbb{R}^n$  and  $f$  is a  $C^r$  (i.e., sufficiently smooth) vector-field defined on  $\mathcal{P} \times \mathbb{R}$ . The set  $\mathcal{P}$  is called the *phase-space* for the ODE (3.15), while  $\mathcal{P} \times \mathbb{R}$  is called its *extended phase-space*. An equivalent formulation for (3.15) is the integral equation

$$x(t) = x_0 + \int_{t_0}^t f(x(\tau), \tau) d\tau$$

for the unknown function  $x(t)$ .

A *one-parameter family of maps*  $F^t : \mathcal{P} \rightarrow \mathcal{P}$  with  $t \in \mathbb{R}$  is called a *flow* if  $F^0(x) = x$  for all  $x \in \mathcal{P}$  and  $F^{t+s} = F^t \circ F^s$  for all  $t, s \in \mathbb{R}$ . These two properties imply that  $F^t$  is invertible with inverse  $F^{-t}$ . The pairing  $(\mathcal{P}, F^t)$  is called a *dynamical system* on  $\mathcal{P}$ .

An ODE is called *autonomous ODE* if  $f$  has no explicit time dependence, i.e.,  $f(x, t) \equiv f(x)$ . The flow associated with an autonomous equation<sup>2</sup> is given as

$$F^t : \mathcal{P} \rightarrow \mathbb{R}^n, \quad x_0 \mapsto x(t, x_0),$$

where  $x_0$  denotes the initial condition for the solution  $x(t)$ , i.e.,  $x(0) = x_0$ . The function  $F^t$  is as smooth as the r.h.s of (3.15) and also depends smoothly on  $t$ . If  $f$  depends on parameters in a  $C^r$  fashion, then  $F^t$  is also of class  $C^r$  with respect to those parameters.

The *orbit* through the point  $x$  is the set  $\gamma(x) = \cup_{t \in \mathbb{R}} F^t(x)$ . A *fixed point* of the flow is a point  $x$  with  $F^t(x) = x$  for all  $t \in \mathbb{R}$ . A *periodic orbit* for the flow is an orbit through a point  $x$  for which there exists  $T > 0$  with  $F^T(x) = x$ . The  $\omega$ -*limit set* of a point  $x \in \mathcal{P}$  is defined as

$$\omega(x) = \{q \in \mathcal{P} : \lim_{t \rightarrow \infty} f(x, t) \rightarrow q\}.$$

---

<sup>2</sup>Nonautonomous ODEs do not generate flows, as the evolution of the solution  $x(t; x_0, t_0)$  depends explicitly on the initial time  $t_0$  for which  $x(t; x_0, t_0) = x_0$ ; therefore, we have

$$x(t + s; x_0, t_0) \neq x(s; x(t; x_0, t_0), t_0).$$

If  $f$  is invertible, the  $\alpha$ -limit set of  $x$  is defined as the  $\omega$ -limit set of  $x$  with respect to  $f^{-1}$ .

A 'stroboscopic picture' of a flow gives its *Poincaré map*, which is constructed as follows. Assume that  $\mathcal{P}$  is an open set in  $\mathbb{R}^n$  and  $\Sigma$  is a  $C^r$  submanifold in  $\mathcal{P}$ , called the *Poincaré section*. Suppose that any orbit  $\gamma(x)$  with  $x \in \Sigma$  intersects  $\Sigma$  transversely in a point that is different from  $x$ . Then the *first return time*  $\tau(x)$  is well-defined for any  $x \in \Sigma$  as

$$\tau(x) = \min\{t > 0 : F^t(x) \in \Sigma\}.$$

The Poincaré map associated with the flow  $F^t$  is defined as

$$P : \Sigma \rightarrow \Sigma, \quad x \mapsto F^{\tau(x)}(x).$$

Both  $P$  and  $\Sigma$  are as smooth (i.e.,  $C^r$ ) as the underlying flow  $F^t$ .

An important feature of the flow of an autonomous ODE

$$\dot{x} = f(x), \tag{3.16}$$

is its effect on volume elements, i.e., it *compresses*, *expands*, or *preserves* the volume of a set of initial conditions. If  $V(t)$  denotes the volume of the set  $F^t(U)$  for an open set of initial conditions  $U \subset \mathbb{R}^n$ , then the *Liouville theorem* states

$$\dot{V}(t)|_{t=0} = \int_U \operatorname{div} f \, dx.$$

This formula shows that divergence-free vector-fields generate volume-preserving flows on  $\mathbb{R}^n$ . Also, 'damped' systems with  $\operatorname{div} f < 0$  compress phase-space volume, while 'forced systems' with  $\operatorname{div} f > 0$  expand phase-space volume.

The Liouville theorem has the following form. Let  $\Omega$  be a volume 1-form on a manifold  $M$  and let  $f$  be a vector-field on  $M$ . The divergence on  $f$  with respect to  $\Omega$  is defined by

$$\frac{d}{dt}[(F^t)^*\Omega]|_{t=0} = (\operatorname{div}_\Omega f) \Omega,$$

where  $(F^t)^*\Omega$  denotes the pull-back of  $\Omega$  under  $F^t$ . If  $V(t)$  denotes the  $\Omega$ -volume of  $F^t(U)$ , then we have

$$\dot{V}(t)|_{t=0} = \int_U (\operatorname{div}_\Omega f) \Omega.$$

Consider two vector-fields  $f$  and  $g$  defined on a manifold  $M$  with boundary. The vector-fields are said to be *topologically equivalent* on  $M$  if there

exists a homeomorphism  $h : M \rightarrow M$  that takes the orbits of  $f$  to the orbits of  $g$  preserving their orientation. On a compact manifold  $M$ , a class  $C^r$  vector-field  $f$  is called structurally stable if it is topologically equivalent to any other vector-field on  $M$  that is sufficiently close to  $f$  in the  $C^0$  norm. Loosely speaking, a vector-field is *structurally stable* if small deformations do not change its orbit structure qualitatively.

A vector-field  $u$  in the space of class  $C^r$  vector-fields defined on  $M$  is said to be a *bifurcation point* if it is not structurally stable. By a *bifurcation* we mean a passage through a bifurcation point as the parameters are varied in a parameterized family of vector-fields. Qualitative changes in the vicinity of an invariant set are usually referred to as *local bifurcations*, whereas qualitative changes involving extended structures in the phase-space are called *global bifurcations*.

For a vector-field  $v$  defined on the phase-space  $\mathcal{P}$  and generating the flow  $F^t$ , an *invariant manifold* is a manifold  $M \subset \mathcal{P}$  such that  $F^t(M) \subset M$  for all  $t \in \mathbb{R}$ .<sup>3</sup> A positively (negatively) *invariant manifold* is a manifold  $M$  for which  $F^t(M) \subset M$  holds for all  $t > 0$  ( $t < 0$ ). By definition, invariant manifolds are both positively and negatively invariant. If  $M$  is a manifold with a boundary  $\partial M$ , then  $M$  is called locally invariant if solutions of the autonomous ODE (3.16) starting in  $M$  can leave  $M$  only through  $\partial M$  in either time direction.

Let  $M$  be an invariant manifold for a flow  $F^t : \mathcal{P} \rightarrow \mathcal{P}$ . The *stable set*  $W^s(M)$  associated with  $M$  is defined as

$$W^s(M) = \{x \in \mathcal{P} : \lim_{t \rightarrow \infty} F^t(x) \rightarrow M\},$$

while *unstable set*  $W^u(M)$  is defined as

$$W^u(M) = \{x \in \mathcal{P} : \lim_{t \rightarrow -\infty} F^t(x) \rightarrow M\}.$$

Let  $S$  be an invariant manifold for a flow  $F^t : \mathcal{P} \rightarrow \mathcal{P}$ . If  $F^t(x)$  tends to  $S$  in both forward and backward time, then the orbit through the point  $x$  is said to be *homoclinic orbit* to  $S$ . In the simplest case  $S \equiv p$  is just a fixed point. If  $p$  is a hyperbolic fixed point in an  $n$ D phase-space, then any homoclinic orbit is structurally unstable.

Let  $P$  and  $S$  be two invariant manifolds for  $F^t$ . A heteroclinic orbit between  $P$  and  $S$  is an orbit through a point  $x$  for which  $F^t(x)$  tends to  $S$  in forward time and to  $P$  in backward time. An orbit can be at the same time a homoclinic relative to one set and heteroclinic relative to another

---

<sup>3</sup>This is possible only if  $v(x) \in T_x M$  for all  $x \in M$ .

set. A *homoclinic (heteroclinic) manifold* is a manifold of orbits homoclinic (heteroclinic) to an invariant manifold  $S$ .

The subject of *singular perturbation theory* (SPT) is a dynamical system that exhibits at least two different time scales. It is typically expressed by splitting the system as

$$\dot{x} = f(x, y; \epsilon), \quad \epsilon \dot{y} = g(x, y; \epsilon),$$

where  $x \in \mathbb{R}^n$ ,  $y \in \mathbb{R}^m$ , and  $0 \leq \epsilon \ll 1$ . Here  $x$  is referred to as the *slow variable*, and  $y$  is called the *fast variable*. In  $\epsilon = 0$  limit the  $g(x, y; 0) = 0$  equation yields a constraint between fast and slow variables, which shows that in the singular limit  $\epsilon = 0$ , the fast variables are ‘enslaved’ to the slow variables. The fundamental question of SPT is whether this enslaved state has any meaning for  $\epsilon > 0$ . In particular, is there a smooth invariant set for  $\epsilon > 0$  near the set determined by  $g(x, y; 0) = 0$ ? Finally, if solutions are attracted to the invariant set, what is their exact asymptotic behavior? If such an invariant set exists for  $\epsilon > 0$ , it is called the *slow manifold*, since both  $x$  and  $y$  can vary only at a rate of  $O(\epsilon)$  on it. It governs the fate of all nearby initial conditions if it is stable as a set.

In physical problems one often seeks special solutions connecting slow manifolds. Perhaps the best known example with orbits connecting slow manifolds is the travelling wave solution of the 3D *FitzHugh–Nagumo model* [FitzHugh (1961); Nagumo *et al.* (1960)]

$$\dot{u} = v, \quad \dot{v} = -cv - f(u) + w, \quad \dot{w} = \epsilon \frac{1}{c}(\gamma v - u), \quad (3.17)$$

where  $f$  is a cubic polynomial,  $c$  is the wave speed, and  $\gamma$  is a parameter (for details on the FitzHugh–Nagumo neuron model, see section 7.5 below).

Loosely speaking, the *normal form of a vector-field* is its simplest possible form after a coordinate transformation. *Normalization* is typically carried out near an invariant set that one wants to study. This set may be an equilibrium, a period orbit, an invariant torus, or a general invariant manifold.

*Chaotic sets* typically admit a *hyperbolic structure*, i.e., each orbit in the set displays a saddle-type behavior: It attracts a set of initial conditions and repels another. An invariant property of *hyperbolic sets* is their persistence under small perturbations. Their robustness, however, does not necessarily imply that they can be observed directly. For instance, Smale horseshoes are chaotic hyperbolic sets, but they do not attract open sets of initial conditions. In fact, there is only a measure zero set of initial conditions that



will approach a hyperbolic set  $\Lambda$  in forward or backward time, and hence will exhibit chaotic behavior. Nevertheless, nearby initial conditions are greatly influenced by the stretching, contraction, and folding that are responsible for the creation of the chaotic invariant set. Specifically, an open set of initial conditions stays near horseshoes for long times, exhibiting *transient chaos*, i.e., seemingly irregular behavior for finite times. This is particularly true in Hamiltonian (conservative) systems in which no attractor can exist due to the preservation of phase-space volume.

There are different definitions for chaotic attractors. According to one of them, a *chaotic (strange) attractor* is a compact set that is the  $\omega$ -limit set for all points in an open set  $U$ , and all but a measure zero set of initial conditions in  $U$  give rise to chaotic orbits. Here the exceptional nonchaotic set is reserved for initial conditions that, for instance, approach unstable periodic orbits. Other definitions may differ slightly, but they all agree that a strange attractor should be a chaotic  $\omega$ -limit set for initial conditions of nonzero measure.

### 3.5 Lie Categories in Biodynamics

In this section we introduce *Lie categories in biodynamics*, as a unique framework for the concepts of Lie derivative, Lie groups and their associated algebras, as well as Lie symmetries of main biodynamic equations. For some classical Lie theory, see Appendix.

#### 3.5.1 Lie Derivative in Biodynamics

Lie derivative is popularly called *fisherman's derivative*. In continuum mechanics it is called Liouville operator. This is a central differential operator in modern differential geometry and its physical and control applications.

##### 3.5.1.1 Lie Derivative on Functions

To define how vector-fields operate on functions on an  $m$ -manifold  $M$ , we will use the *directional derivative* or *Lie derivative*. Let  $f : M \rightarrow \mathbb{R}$  so  $Tf : TM \rightarrow T\mathbb{R} = \mathbb{R} \times \mathbb{R}$ . Following [Abraham *et al.* (1988)] we write  $Tf$  acting on a vector  $v \in T_m M$  in the form

$$Tf \cdot v = (f(m), df(m) \cdot v).$$

This defines, for each point  $m \in M$ , the element  $df(m) \in T_m^*M$ . Thus  $df$  is a section of the cotangent bundle  $T^*M$ , i.e., a 1-form. The 1-form  $df : M \rightarrow T^*M$  defined this way is called the *differential* of  $f$ . If  $f$  is  $C^k$ , then  $df$  is  $C^{k-1}$ .

If  $\phi : U \subset M \rightarrow V \subset E$  is a local chart for  $M$ , then the local representative of  $f \in C^k(M, \mathbb{R})$  is the map  $f : V \rightarrow \mathbb{R}$  defined by  $f = f \circ \phi^{-1}$ . The local representative of  $Tf$  is the tangent map for local manifolds,

$$Tf(x, v) = (f(x), Df(x) \cdot v).$$

Thus the local representative of  $df$  is the derivative of the local representative of  $f$ . In particular, if  $(x^1, \dots, x^n)$  are local coordinates on  $M$ , then the local components of  $df$  are

$$(df)^i = \partial_{x^i} f.$$

The introduction of  $df$  leads to the following definition of the Lie derivative. The *directional* or *Lie derivative*  $\mathcal{L}_X : C^k(M, \mathbb{R}) \rightarrow C^{k-1}(M, \mathbb{R})$  of a function  $f \in C^k(M, \mathbb{R})$  along a vector-field  $X$  is defined by

$$\mathcal{L}_X f(m) = X[f](m) = df(m) \cdot X(m),$$

for any  $m \in M$ . Denote by  $X[f] = df(X)$  the map  $M \ni m \mapsto X[f](m) \in \mathbb{R}$ . If  $f$  is  $F$ -valued, the same definition is used, but now  $X[f]$  is  $F$ -valued.

If a local chart  $(U, \phi)$  on an  $n$ -manifold  $M$  has local coordinates  $(x^1, \dots, x^n)$ , the local representative of  $X[f]$  is given by the function

$$\mathcal{L}_X f = X[f] = X^i \partial_{x^i} f.$$

Evidently if  $f$  is  $C^k$  and  $X$  is  $C^{k-1}$  then  $X[f]$  is  $C^{k-1}$ .

Let  $\varphi : M \rightarrow N$  be a diffeomorphism. Then  $\mathcal{L}_X$  is natural with respect to push-forward by  $\varphi$ . That is, for each  $f \in C^k(M, \mathbb{R})$ ,

$$\mathcal{L}_{\varphi_* X}(\varphi_* f) = \varphi_* \mathcal{L}_X f,$$

i.e., the following diagram commutes:

$$\begin{array}{ccc} C^k(M, \mathbb{R}) & \xrightarrow{\varphi_*} & C^k(N, \mathbb{R}) \\ \mathcal{L}_X \downarrow & & \downarrow \mathcal{L}_{\varphi_* X} \\ C^k(M, \mathbb{R}) & \xrightarrow{\varphi_*} & C^k(N, \mathbb{R}) \end{array}$$

Also,  $\mathcal{L}_X$  is natural with respect to restrictions. That is, for  $U$  open in  $M$  and  $f \in C^k(M, \mathbb{R})$ ,

$$\mathcal{L}_{X|U}(f|U) = (\mathcal{L}_X f)|U,$$

where  $|U : C^k(M, \mathbb{R}) \rightarrow C^k(U, \mathbb{R})$  denotes restriction to  $U$ , i.e., the following diagram commutes:

$$\begin{array}{ccc} C^k(M, \mathbb{R}) & \xrightarrow{|U} & C^k(U, \mathbb{R}) \\ \mathcal{L}_X \downarrow & & \downarrow \mathcal{L}_{X|U} \\ C^k(M, \mathbb{R}) & \xrightarrow{|U} & C^k(U, \mathbb{R}) \end{array}$$

Since  $\varphi^* = (\varphi^{-1})_*$  the Lie derivative is also natural with respect to pull-back by  $\varphi$ . This has a generalization to  $\varphi$ -related vector-fields as follows: Let  $\varphi : M \rightarrow N$  be a  $C^k$ -map,  $X \in \mathcal{X}^{k-1}(M)$  and  $Y \in \mathcal{X}^{k-1}(N)$ ,  $k \geq 1$ . If  $X \sim_\varphi Y$ , then

$$\mathcal{L}_X(\varphi^* f) = \varphi^* \mathcal{L}_Y f$$

for all  $f \in C^k(N, \mathbb{R})$ , i.e., the following diagram commutes:

$$\begin{array}{ccc} C^k(N, \mathbb{R}) & \xrightarrow{\varphi^*} & C^k(M, \mathbb{R}) \\ \mathcal{L}_Y \downarrow & & \downarrow \mathcal{L}_X \\ C^k(N, \mathbb{R}) & \xrightarrow{\varphi^*} & C^k(M, \mathbb{R}) \end{array}$$

The Lie derivative map  $\mathcal{L}_X : C^k(M, \mathbb{R}) \rightarrow C^{k-1}(M, \mathbb{R})$  is a *derivation*, i.e., for two functions  $f, g \in C^k(M, \mathbb{R})$  the *Leibniz rule* is satisfied

$$\mathcal{L}_X(fg) = g\mathcal{L}_X f + f\mathcal{L}_X g;$$

Also, Lie derivative of a constant function is zero,  $\mathcal{L}_X(\text{const}) = 0$ .

The connection between the Lie derivative  $\mathcal{L}_X f$  of a function  $f \in C^k(M, \mathbb{R})$  and the flow  $F_t$  of a vector-field  $X \in \mathcal{X}^{k-1}(M)$  is given as:

$$\frac{d}{dt}(F_t^* f) = F_t^*(\mathcal{L}_X f).$$

### 3.5.1.2 Lie Derivative of Vector Fields

If  $X, Y \in \mathcal{X}^k(M)$ ,  $k \geq 1$  are two vector-fields on  $M$ , then

$$[\mathcal{L}_X, \mathcal{L}_Y] = \mathcal{L}_X \circ \mathcal{L}_Y - \mathcal{L}_Y \circ \mathcal{L}_X$$

is a derivation map from  $C^{k+1}(M, \mathbb{R})$  to  $C^{k-1}(M, \mathbb{R})$ . Then there is a unique vector-field,  $[X, Y] \in \mathcal{X}^k(M)$  of  $X$  and  $Y$  such that  $\mathcal{L}_{[X, Y]} = [\mathcal{L}_X, \mathcal{L}_Y]$  and  $[X, Y](f) = X(Y(f)) - Y(X(f))$  holds for all functions  $f \in C^k(M, \mathbb{R})$ . This vector-field is also denoted  $\mathcal{L}_X Y$  and is called the Lie derivative of  $Y$  with respect to  $X$ , or the *Lie bracket* of  $X$  and  $Y$ . In a local chart  $(U, \phi)$  at a point  $m \in M$  with coordinates  $(x^1, \dots, x^n)$ , for  $X|_U = X^i \partial_{x^i}$  and  $Y|_U = Y^j \partial_{x^j}$  we have

$$[X^i \partial_{x^i}, Y^j \partial_{x^j}] = (X^i (\partial_{x^i} Y^j) - Y^j (\partial_{x^i} X^j)) \partial_{x^j},$$

since second partials commute. If, also  $X$  has flow  $F_t$ , then [Abraham *et al.* (1988)]

$$\frac{d}{dt} (F_t^* Y) = F_t^* (\mathcal{L}_X Y).$$

In particular, if  $t = 0$ , this formula becomes

$$\frac{d}{dt} \big|_{t=0} (F_t^* Y) = \mathcal{L}_X Y.$$

Then the unique  $C^{k-1}$  vector-field  $\mathcal{L}_X Y = [X, Y]$  on  $M$  defined by

$$[X, Y] = \frac{d}{dt} \big|_{t=0} (F_t^* Y),$$

is called the Lie derivative of  $Y$  with respect to  $X$ , or the Lie bracket of  $X$  and  $Y$ , and can be interpreted as the leading order term that results from the sequence of flows

$$F_t^{-Y} \circ F_t^{-X} \circ F_t^Y \circ F_t^{-X}(m) = \epsilon^2 [X, Y](m) + \mathcal{O}(\epsilon^3), \quad (3.18)$$

for some real  $\epsilon > 0$ . Therefore a Lie bracket can be interpreted as a ‘new direction’ in which the system can flow, by executing the sequence of flows (3.18).

Lie bracket satisfies the following property:

$$[X, Y][f] = X[Y[f]] - Y[X[f]],$$

for all  $f \in C^{k+1}(U, \mathbb{R})$ , where  $U$  is open in  $M$ .

An important relationship between flows of vector-fields is given by the *Campbell-Baker-Hausdorff* formula:

$$F_t^Y \circ F_t^X = F_t^{X+Y+\frac{1}{2}[X,Y]+\frac{1}{12}([X,[X,Y]]-[Y,[X,Y]])+\dots} \quad (3.19)$$

Essentially, if given the composition of multiple flows along multiple vector-fields, this formula gives the one flow along one vector-field which results in the same net flow. One way to prove the Campbell-Baker-Hausdorff formula (3.19) is to expand the product of two formal exponentials and equate terms in the resulting formal power series.

Lie bracket is the  $\mathbb{R}$ -bilinear map  $[\cdot, \cdot] : \mathcal{X}^k(M) \times \mathcal{X}^k(M) \rightarrow \mathcal{X}^k(M)$  with the following properties:

- (1)  $[X, Y] = -[Y, X]$ , i.e.,  $\mathcal{L}_X Y = -\mathcal{L}_Y X$  for all  $X, Y \in \mathcal{X}^k(M)$  - skew-symmetry;
- (2)  $[X, X] = 0$  for all  $X \in \mathcal{X}^k(M)$ ;
- (3)  $[X, [Y, Z]] + [Y, [Z, X]] + [Z, [X, Y]] = 0$  for all  $X, Y, Z \in \mathcal{X}^k(M)$  - the Jacobi identity;
- (4)  $[fX, Y] = f[X, Y] - (Yf)X$ , i.e.,  $\mathcal{L}_{fX}(Y) = f(\mathcal{L}_X Y) - (\mathcal{L}_Y f)X$  for all  $X, Y \in \mathcal{X}^k(M)$  and  $f \in C^k(M, \mathbb{R})$ ;
- (5)  $[X, fY] = f[X, Y] + (Xf)Y$ , i.e.,  $\mathcal{L}_X(fY) = f(\mathcal{L}_X Y) + (\mathcal{L}_X f)Y$  for all  $X, Y \in \mathcal{X}^k(M)$  and  $f \in C^k(M, \mathbb{R})$ ;
- (6)  $[\mathcal{L}_X, \mathcal{L}_Y] = \mathcal{L}_{[X, Y]}$  for all  $X, Y \in \mathcal{X}^k(M)$ .

The pair  $(\mathcal{X}^k(M), [\cdot, \cdot])$  is the prototype of a *Lie algebra* [Kolar *et al.* (1993)]. In more general case of a *general linear Lie algebra*  $\mathfrak{gl}(n)$ , which is the Lie algebra associated to the Lie group  $GL(n)$ , Lie bracket is given by a *matrix commutator*

$$[A, B] = AB - BA,$$

for any two matrices  $A, B \in \mathfrak{gl}(n)$ .

Let  $\varphi : M \rightarrow N$  be a diffeomorphism. Then  $\mathcal{L}_X : \mathcal{X}^k(M) \rightarrow \mathcal{X}^k(M)$  is natural with respect to push-forward by  $\varphi$ . That is, for each  $f \in C^k(M, \mathbb{R})$ ,

$$\mathcal{L}_{\varphi_* X}(\varphi_* Y) = \varphi_* \mathcal{L}_X Y,$$

i.e., the following diagram commutes:

$$\begin{array}{ccc} \mathcal{X}^k(M) & \xrightarrow{\varphi_*} & \mathcal{X}^k(N) \\ \mathcal{L}_X \downarrow & & \downarrow \mathcal{L}_{\varphi_* X} \\ \mathcal{X}^k(M) & \xrightarrow{\varphi_*} & \mathcal{X}^k(N) \end{array}$$

Also,  $\mathcal{L}_X$  is natural with respect to restrictions. That is, for  $U$  open in  $M$  and  $f \in C^k(M, \mathbb{R})$ ,

$$[X|U, Y|U] = [X, Y]|U,$$

where  $|U : C^k(M, \mathbb{R}) \rightarrow C^k(U, \mathbb{R})$  denotes restriction to  $U$ , i.e., the following diagram commutes [Abraham *et al.* (1988)]:

$$\begin{array}{ccc} \mathcal{X}^k(M) & \xrightarrow{|U} & \mathcal{X}^k(U) \\ \mathcal{L}_X \downarrow & & \downarrow \mathcal{L}_{X|U} \\ \mathcal{X}^k(M) & \xrightarrow{|U} & \mathcal{X}^k(U) \end{array}$$

If a local chart  $(U, \phi)$  on an  $n$ -manifold  $M$  has local coordinates  $(x^1, \dots, x^n)$ , then the local components of a Lie bracket are

$$[X, Y]^j = X^i \partial_{x^i} Y^j - Y^i \partial_{x^i} X^j,$$

that is,  $[X, Y] = (X \cdot \nabla)Y - (Y \cdot \nabla)X$ .

Let  $\varphi : M \rightarrow N$  be a  $C^k$ -map,  $X \in \mathcal{X}^{k-1}(M)$  and  $Y \in \mathcal{X}^{k-1}(N)$ ,  $k \geq 1$ . Then  $X \sim_\varphi Y$ , iff

$$(Y[f]) \circ \varphi = X[f \circ \varphi]$$

for all  $f \in C^k(V, \mathbb{R})$ , where  $V$  is open in  $N$ .

For every  $X \in \mathcal{X}^k(M)$ , the operator  $\mathcal{L}_X$  is a derivation on  $(C^k(M, \mathbb{R}), \mathcal{X}^k(M))$ , i.e.,  $\mathcal{L}_X$  is  $\mathbb{R}$ -linear.

For any two vector-fields  $X \in \mathcal{X}^k(M)$  and  $Y \in \mathcal{X}^k(N)$ ,  $k \geq 1$  with flows  $F_t$  and  $G_t$ , respectively, if  $[X, Y] = 0$  then  $F_t^* Y = Y$  and  $G_t^* X = X$ .

### 3.5.1.3 Derivative of the Evolution Operator

Recall (3.4.1) that the time-dependent flow or evolution operator  $F_{t,s}$  of a vector-field  $X \in \mathcal{X}^k(M)$  is defined by the requirement that  $t \mapsto F_{t,s}(m)$  be

the integral curve of  $X$  starting at a point  $m \in M$  at time  $t = s$ , i.e.,

$$\frac{d}{dt}F_{t,s}(m) = X(t, F_{t,s}(m)) \quad \text{and} \quad F_{t,t}(m) = m.$$

By uniqueness of integral curves we have  $F_{t,s} \circ F_{s,r} = F_{t,r}$  (replacing the flow property  $F_{t+s} = F_t + F_s$ ) and  $F_{t,t} = \text{identity}$ .

Let  $X_t \in \mathcal{X}^k(M)$ ,  $k \geq 1$  for each  $t$  and suppose  $X(t, m)$  is continuous in  $(t, m) \in \mathbb{R} \times M$ . Then  $F_{t,s}$  is of class  $C^k$  and for  $f \in C^{k+1}(M, \mathbb{R})$  [Abraham *et al.* (1988)], and  $Y \in \mathcal{X}^k(M)$ , we have

- (1)  $\frac{d}{dt}F_{t,s}^* f = F_{t,s}^*(\mathcal{L}_{X_t} f)$ , and
- (2)  $\frac{d}{dt}F_{t,s}^* f = F_{t,s}^*([X_t, Y]) = F_{t,s}^*(\mathcal{L}_{X_t} Y)$ .

From the above theorem, the following identity holds:

$$\frac{d}{dt}F_{t,s}^* f = -X_t[F_{t,s}^* f].$$

#### 3.5.1.4 Lie Derivative of Differential Forms

Since  $\mathcal{F} : M \Rightarrow \Lambda^k T^*M$  is a vector bundle functor on  $\mathcal{M}$ , the Lie derivative of a  $k$ -form  $\alpha \in \Omega^k(M)$  along a vector-field  $X \in \mathcal{X}^k(M)$  is defined by

$$\mathcal{L}_X \alpha = \frac{d}{dt} \Big|_{t=0} F_t^* \alpha.$$

It has the following properties:

- (1)  $\mathcal{L}_X(\alpha \wedge \beta) = \mathcal{L}_X \alpha \wedge \beta + \alpha \wedge \mathcal{L}_X \beta$ , so  $\mathcal{L}_X$  is a derivation.
- (2)  $[\mathcal{L}_X, \mathcal{L}_Y] \alpha = \mathcal{L}_{[X, Y]} \alpha$ .
- (3)  $\frac{d}{dt}F_t^* \alpha = F_t^* \mathcal{L}_X \alpha = \mathcal{L}_X(F_t^* \alpha)$ .

Formula (3) holds also for time-dependent vector-fields in the sense that  $\frac{d}{dt}F_{t,s}^* \alpha = F_{t,s}^* \mathcal{L}_X \alpha = \mathcal{L}_X(F_{t,s}^* \alpha)$  and in the expression  $\mathcal{L}_X \alpha$  the vector-field  $X$  is evaluated at time  $t$ .

*Cartan's magic formula* (see [Marsden and Ratiu (1999)]) states: the Lie derivative of a  $k$ -form  $\alpha \in \Omega^k(M)$  along a vector-field  $X \in \mathcal{X}^k(M)$  on a smooth manifold  $M$  is defined as

$$\mathcal{L}_X \alpha = di_X \alpha + i_X d\alpha = d(X \lrcorner \alpha) + X \lrcorner d\alpha.$$

Also, the following identities hold [Marsden and Ratiu (1999); Kolar *et al.* (1993)]:

- (1)  $\mathcal{L}_f X \alpha = f \mathcal{L}_X \alpha + df \wedge i_X \alpha$ .

- (2)  $\mathcal{L}_{[X,Y]}\alpha = \mathcal{L}_X\mathcal{L}_Y\alpha - \mathcal{L}_Y\mathcal{L}_X\alpha.$
- (3)  $i_{[X,Y]}\alpha = \mathcal{L}_Xi_Y\alpha - i_Y\mathcal{L}_X\alpha.$
- (4)  $\mathcal{L}_Xd\alpha = d\mathcal{L}_X\alpha$ , i.e.,  $[\mathcal{L}_X, d] = 0.$
- (5)  $\mathcal{L}_Xi_X\alpha = i_X\mathcal{L}_X\alpha$ , i.e.,  $[\mathcal{L}_X, i_X] = 0.$
- (6)  $\mathcal{L}_X(\alpha \wedge \beta) = \mathcal{L}_X\alpha \wedge \beta + \alpha \wedge \mathcal{L}_X\beta.$

### 3.5.1.5 Lie Derivative of Various Tensor Fields

In this subsection, we use local coordinates  $x^i$  ( $i = 1, \dots, n$ ) on a biodynamic  $n$ -manifold  $M$ , to calculate the Lie derivative  $\mathcal{L}_{X^i}$  with respect to a generic vector-field  $X^i$ . (As always,  $\partial_{x^i} \equiv \frac{\partial}{\partial x^i}$ ).

*Lie Derivative of a Scalar Field.* Given the scalar field  $\phi$ , its Lie derivative  $\mathcal{L}_{X^i}\phi$  is given as

$$\mathcal{L}_{X^i}\phi = X^i\partial_{x^i}\phi = X^1\partial_{x^1}\phi + X^2\partial_{x^2}\phi + \dots + X^n\partial_{x^n}\phi.$$

*Lie Derivative of Vector and Covector-Fields.* Given a contravariant vector-field  $V^i$ , its Lie derivative  $\mathcal{L}_{X^i}V^i$  is given as

$$\mathcal{L}_{X^i}V^i = X^k\partial_{x^k}V^i - V^k\partial_{x^k}X^i \equiv [X^i, V^i] - \text{the Lie bracket.}$$

Given a covariant vector-field (i.e., a one-form)  $\omega_i$ , its Lie derivative  $\mathcal{L}_{X^i}\omega_i$  is given as

$$\mathcal{L}_{X^i}\omega_i = X^k\partial_{x^k}\omega_i + \omega_k\partial_{x^i}X^k.$$

*Lie Derivative of a Second-Order Tensor-Field.* Given a  $(2, 0)$  tensor-field  $S^{ij}$ , its Lie derivative  $\mathcal{L}_{X^i}S^{ij}$  is given as

$$\mathcal{L}_{X^i}S^{ij} = X^i\partial_{x^i}S^{ij} - S^{ij}\partial_{x^i}X^i - S^{ii}\partial_{x^i}X^j.$$

Given a  $(1, 1)$  tensor-field  $S_j^i$ , its Lie derivative  $\mathcal{L}_{X^i}S_j^i$  is given as

$$\mathcal{L}_{X^i}S_j^i = X^i\partial_{x^i}S_j^i - S_j^i\partial_{x^i}X^i + S_i^i\partial_{x^j}X^i.$$

Given a  $(0, 2)$  tensor-field  $S_{ij}$ , its Lie derivative  $\mathcal{L}_{X^i}S_{ij}$  is given as

$$\mathcal{L}_{X^i}S_{ij} = X^i\partial_{x^i}S_{ij} + S_{ij}\partial_{x^i}X^i + S_{ii}\partial_{x^j}X^i.$$

*Lie Derivative of a Third-Order Tensor-Field.* Given a  $(3, 0)$  tensor-field  $T^{ijk}$ , its Lie derivative  $\mathcal{L}_{X^i}T^{ijk}$  is given as

$$\mathcal{L}_{X^i}T^{ijk} = X^i\partial_{x^i}T^{ijk} - T^{ijk}\partial_{x^i}X^i - T^{iik}\partial_{x^i}X^j - T^{ijj}\partial_{x^i}X^k.$$



Given a (2, 1) tensor-field  $T_k^{ij}$ , its Lie derivative  $\mathcal{L}_X T_k^{ij}$  is given as

$$\mathcal{L}_X T_k^{ij} = X^i \partial_x T_k^{ij} - T_k^{ij} \partial_x X^i + T_i^{ij} \partial_{x^k} X^i - T_k^{ii} \partial_{x^i} X^j.$$

Given a (1, 2) tensor-field  $T_{jk}^i$ , its Lie derivative  $\mathcal{L}_X T_{jk}^i$  is given as

$$\mathcal{L}_X T_{jk}^i = X^i \partial_x T_{jk}^i - T_{jk}^i \partial_x X^i + T_{ik}^i \partial_{x^j} X^i + T_{ji}^i \partial_{x^k} X^i.$$

Given a (0, 3) tensor-field  $T_{ijk}$ , its Lie derivative  $\mathcal{L}_X T_{ijk}$  is given as

$$\mathcal{L}_X T_{ijk} = X^i \partial_x T_{ijk} + T_{ijk} \partial_x X^i + T_{ik} \partial_{x^j} X^i + T_{ij} \partial_{x^k} X^i.$$

*Lie Derivative of a Fourth-Order Tensor-Field.* Given a (4, 0) tensor-field  $R^{ijkl}$ , its Lie derivative  $\mathcal{L}_X R^{ijkl}$  is given as

$$\mathcal{L}_X R^{ijkl} = X^i \partial_x R^{ijkl} - R^{ijkl} \partial_x X^i - R^{iikl} \partial_{x^i} X^j - R^{ijil} \partial_{x^i} X^k - R^{ijk i} \partial_{x^i} X^l.$$

Given a (3, 1) tensor-field  $R_l^{ijk}$ , its Lie derivative  $\mathcal{L}_X R_l^{ijk}$  is given as

$$\mathcal{L}_X R_l^{ijk} = X^i \partial_x R_l^{ijk} - R_l^{ijk} \partial_x X^i + R_i^{ijk} \partial_{x^i} X^i - R_l^{ik} \partial_{x^i} X^j - R_l^{ij} \partial_{x^i} X^k.$$

Given a (2, 2) tensor-field  $R_{kl}^{ij}$ , its Lie derivative  $\mathcal{L}_X R_{kl}^{ij}$  is given as

$$\mathcal{L}_X R_{kl}^{ij} = X^i \partial_x R_{kl}^{ij} - R_{kl}^{ij} \partial_x X^i + R_{il}^{ij} \partial_{x^k} X^i + R_{ki}^{ij} \partial_{x^l} X^i - R_{kl}^{ii} \partial_{x^i} X^j.$$

Given a (1, 3) tensor-field  $R_{jkl}^i$ , its Lie derivative  $\mathcal{L}_X R_{jkl}^i$  is given as

$$\mathcal{L}_X R_{jkl}^i = X^i \partial_x R_{jkl}^i - R_{jkl}^i \partial_x X^i + R_{ikl}^i \partial_{x^j} X^i + R_{jil}^i \partial_{x^k} X^i + R_{jki}^i \partial_{x^l} X^i.$$

Given a (0, 4) tensor-field  $R_{ijkl}$ , its Lie derivative  $\mathcal{L}_X R_{ijkl}$  is given as

$$\mathcal{L}_X R_{ijkl} = X^i \partial_x R_{ijkl} + R_{ijkl} \partial_x X^i + R_{iikl} \partial_{x^j} X^i + R_{ijil} \partial_{x^k} X^i + R_{ijk i} \partial_{x^l} X^i.$$

Finally, recall that a *spinor* is a two-component complex column vector. Physically, spinors can describe both bosons and fermions, while tensors can describe only bosons. The Lie derivative of a spinor  $\phi$  is defined by

$$\mathcal{L}_X \phi(x) = \lim_{t \rightarrow 0} \frac{\bar{\phi}_t(x) - \phi(x)}{t},$$

where  $\bar{\phi}_t$  is the image of  $\phi$  by a one-parameter group of isometries with  $X$  its generator. For a vector field  $X^a$  and a covariant derivative  $\nabla_a$ , the Lie derivative of  $\phi$  is given explicitly by

$$\mathcal{L}_X \phi = X^a \nabla_a \phi - \frac{1}{8} (\nabla_a X_b - \nabla_b X_a) \gamma^a \gamma^b \phi,$$

where  $\gamma^a$  and  $\gamma^b$  are *Dirac matrices* (see, e.g., [Choquet-Bruhat and DeWitt-Morete (2000)]).

### 3.5.1.6 Lie Algebras

Recall from chapter 2 that an *algebra*  $A$  is a vector space with a product. The product must have the property that

$$a(uv) = (au)v = u(av),$$

for every  $a \in \mathbb{R}$  and  $u, v \in A$ . A map  $\phi : A \rightarrow A'$  between algebras is called an *algebra homomorphism* if  $\phi(u \cdot v) = \phi(u) \cdot \phi(v)$ . A vector subspace  $\mathcal{I}$  of an algebra  $A$  is called a *left ideal* (resp. *right ideal*) if it is closed under algebra multiplication and if  $u \in A$  and  $i \in \mathcal{I}$  implies that  $ui \in \mathcal{I}$  (resp.  $iu \in \mathcal{I}$ ). A subspace  $\mathcal{I}$  is said to be a *two-sided ideal* if it is both a left and right ideal. An ideal may not be an algebra itself, but the quotient of an algebra by a two-sided ideal inherits an algebra structure from  $A$ .

A *Lie algebra* is an algebra  $A$  where the multiplication, i.e., the *Lie bracket*  $(u, v) \mapsto [u, v]$ , has the following properties:

LA 1.  $[u, u] = 0$  for every  $u \in A$ , and

LA 2.  $[u, [v, w]] + [w, [u, v]] + [v, [w, u]] = 0$  for all  $u, v, w \in A$ .

The condition LA 2 is usually called *Jacobi identity*. A subspace  $E \subset A$  of a Lie algebra is called a *Lie subalgebra* if  $[u, v] \in E$  for every  $u, v \in E$ . A map  $\phi : A \rightarrow A'$  between Lie algebras is called a *Lie algebra homomorphism* if  $\phi([u, v]) = [\phi(u), \phi(v)]$  for each  $u, v \in A$ .

All Lie algebras (over a given field  $\mathbb{K}$ ) and all smooth homomorphisms between them form the category  $\mathcal{LAL}$ , which is itself a complete subcategory of the category  $\mathcal{AL}$  of all algebras and their homomorphisms.

**Hamiltonian Equations in the Lie-Bracket Form.** *Hamiltonian function* (kinetic energy) on a Lie algebra  $\mathfrak{g}$  associated to a Lie group  $G$  is given by

$$H(q, p) = \frac{1}{2} \| [p, q] \|^2,$$

where  $\| \cdot \| = \langle \cdot, \cdot \rangle^{1/2}$  denotes the metric-induced *norm* on  $\mathfrak{g}$ ,  $q \in G$  is a coordinate variable and  $p$  is a *momentum* variable viewed as lying in  $\mathfrak{g}$  by identifying  $\mathfrak{g}$  with its dual  $\mathfrak{g}^*$ .

*Hamiltonian equations of motion* are defined in the symmetric Lie-bracket form as

$$\dot{q} = [q, [p, q]], \quad \dot{p} = [p, [p, q]],$$

representing *geodesic equations* on  $\mathfrak{g}$ .

### 3.5.2 Lie Groups in Biodynamics

In the middle of the 19th century S. Lie made a far reaching discovery that techniques designed to solve particular unrelated types of ODEs, such as separable, homogeneous and exact equations, were in fact all special cases of a general form of integration procedure based on the invariance of the differential equation under a continuous group of symmetries. Roughly speaking a symmetry group of a system of differential equations is a group that transforms solutions of the system to other solutions. Once the symmetry group has been identified a number of techniques to solve and classify these differential equations becomes possible. In the classical framework of Lie, these groups were local groups and arose locally as groups of transformations on some Euclidean space. The passage from the local Lie group to the present day definition using manifolds was accomplished by E. Cartan at the end of the 19th century, whose work is a striking synthesis of Lie theory, classical geometry, differential geometry and topology.

These continuous groups, which originally appeared as symmetry groups of differential equations, have over the years had a profound impact on diverse areas such as algebraic topology, differential geometry, numerical analysis, control theory, classical mechanics, quantum mechanics etc. They are now universally known as Lie groups.

#### 3.5.2.1 Lie Groups and Their Lie Algebras

Recall that a *Lie group* is a smooth (Banach) manifold  $M$  that has at the same time a group  $G$ -structure consistent with its manifold  $M$ -structure in the sense that group multiplication

$$\mu : G \times G \rightarrow G, \quad (g, h) \mapsto gh, \quad (3.20)$$

and the inversion

$$\nu : G \rightarrow G, \quad g \mapsto g^{-1} \quad (3.21)$$

– are  $C^k$ -maps [Chevalley (1955); Abraham *et al.* (1988); Marsden and Ratiu (1999); Puta (1993)]. A point  $e \in G$  is called the group *identity* element.

For example, any finite-dimensional Banach vector space  $V$  is an Abelian Lie group with group operations  $\mu : V \times V \rightarrow V$ ,  $\mu(x, y) = x + y$ ,

and  $\nu : V \rightarrow V$ ,  $\nu(x) = -x$ . The identity is just the zero vector. We call such a Lie group a *vector group*.

Let  $G$  and  $H$  be two Lie groups. A map  $G \rightarrow H$  is said to be a *morphism* of Lie groups (or their *smooth homomorphism*) if it is their homomorphism as abstract groups and their smooth map as manifolds [Postnikov (1986)].

All Lie groups and all their morphisms form the category  $\mathcal{LG}$  (more precisely, there is a countable family of categories  $\mathcal{LG}$  depending on  $C^k$ -smoothness of the corresponding manifolds).

Similarly, a group  $G$  which is at the same time a topological space is said to be a *topological group* if maps (3.20–3.21) are continuous, i.e.,  $C^0$ -maps for it. The homomorphism  $G \rightarrow H$  of topological groups is said to be continuous if it is a continuous map. Topological groups and their continuous homomorphisms form the category  $\mathcal{TG}$ .

A topological group (as well as a smooth manifold) is not necessarily Hausdorff. A topological group  $G$  is Hausdorff iff its identity is closed. As a corollary we have that every Lie group is a Hausdorff topological group (see [Postnikov (1986)]).

For every  $g$  in a Lie group  $G$ , the two maps,

$$\begin{aligned} L_g : G &\rightarrow G, & h &\mapsto gh, & \text{and} \\ R_h : G &\rightarrow G, & g &\mapsto gh, \end{aligned}$$

are called *left* and *right translation* maps. Since  $L_g \circ L_h = L_{gh}$ , and  $R_g \circ R_h = R_{gh}$ , it follows that  $(L_g)^{-1} = L_{g^{-1}}$  and  $(R_g)^{-1} = R_{g^{-1}}$ , so both  $L_g$  and  $R_g$  are diffeomorphisms. Moreover  $L_g \circ R_h = R_h \circ L_g$ , i.e., left and right translation commute.

A vector-field  $X$  on  $G$  is called *left invariant vector-field* if for every  $g \in G$ ,  $L_g^* X = X$ , that is, if  $(T_h L_g)X(h) = X(gh)$  for all  $h \in G$ , i.e., the following diagram commutes:

$$\begin{array}{ccc} TG & \xrightarrow{TL_g} & TG \\ \uparrow X & & \uparrow X \\ G & \xrightarrow{L_g} & G \end{array}$$

The correspondences  $G \rightarrow TG$  and  $L_g \rightarrow TL_g$  obviously define a functor  $\mathcal{F} : \mathcal{LG} \Rightarrow \mathcal{LG}$  from the category  $G$  of Lie groups to itself.

Let  $\mathcal{X}_L(G)$  denote the set of left invariant vector-fields on  $G$ ; it is a Lie subalgebra of  $\mathcal{X}(G)$ , the set of all vector-fields on  $G$ , since  $L_g^*[X, Y] =$

$[L_g^*X, L_g^*Y] = [X, Y]$ , so the Lie bracket  $[X, Y] \in \mathcal{X}_L(G)$ .

Let  $e$  be the identity element of  $G$ . Then for each  $\xi$  on the tangent space  $T_eG$  we define a vector-field  $X_\xi$  on  $G$  by

$$X_\xi(g) = T_eL_g(\xi).$$

$\mathcal{X}_L(G)$  and  $T_eG$  are isomorphic as vector spaces. Define the Lie bracket on  $T_eG$  by

$$[\xi, \eta] = [X_\xi, X_\eta](e),$$

for all  $\xi, \eta \in T_eG$ . This makes  $T_eG$  into a Lie algebra. Also, by construction, we have

$$[X_\xi, X_\eta] = X_{[\xi, \eta]},$$

this defines a bracket in  $T_eG$  via *left extension*. The vector space  $T_eG$  with the above algebra structure is called the Lie algebra of the Lie group  $G$  and is denoted  $\mathfrak{g}$ .

For example, let  $V$  be a finite-dimensional vector space. Then  $T_eV \simeq V$  and the left invariant vector-field defined by  $\xi \in T_eV$  is the constant vector-field  $X_\xi(\eta) = \xi$ , for all  $\eta \in V$ . The Lie algebra of  $V$  is  $V$  itself.

Since any two elements of an Abelian Lie group  $G$  commute, it follows that all adjoint operators  $Ad_g$ ,  $g \in G$ , equal the identity. Therefore, the Lie algebra  $\mathfrak{g}$  is Abelian; that is,  $[\xi, \eta] = 0$  for all  $\xi, \eta \in \mathfrak{g}$  [Marsden and Ratiu (1999)].

Recall (3.5.1.6) that Lie algebras and their smooth homomorphisms form the category  $\mathcal{LAL}$ . We can now introduce the fundamental *Lie functor*,  $\mathcal{F}: \mathcal{LG} \Rightarrow \mathcal{LAL}$ , from the category of Lie groups to the category of Lie algebras [Postnikov (1986)].

Let  $X_\xi$  be a left invariant vector-field on  $G$  corresponding to  $\xi$  in  $\mathfrak{g}$ . Then there is a unique integral curve  $\gamma_\xi: \mathbb{R} \rightarrow G$  of  $X_\xi$  starting at  $e$ , i.e.,

$$\dot{\gamma}_\xi(t) = X_\xi(\gamma_\xi(t)), \quad \gamma_\xi(0) = e.$$

$\gamma_\xi(t)$  is a smooth *one parameter subgroup* of  $G$ , i.e.,

$$\gamma_\xi(t+s) = \gamma_\xi(t) \cdot \gamma_\xi(s),$$

since, as functions of  $t$  both sides equal  $\gamma_\xi(s)$  at  $t = 0$  and both satisfy differential equation

$$\dot{\gamma}(t) = X_\xi(\gamma_\xi(t))$$

by left invariance of  $X_\xi$ , so they are equal. Left invariance can be also used to show that  $\gamma_\xi(t)$  is defined for all  $t \in \mathbb{R}$ . Moreover, if  $\phi : \mathbb{R} \rightarrow G$  is a one parameter subgroup of  $G$ , i.e., a *smooth homomorphism* of the additive group  $\mathbb{R}$  into  $G$ , then  $\phi = \gamma_\xi$  with  $\xi = \dot{\phi}(0)$ , since taking derivative at  $s = 0$  in the relation

$$\phi(t+s) = \phi(t) \cdot \phi(s)$$

gives

$$\dot{\phi}(t) = X_{\dot{\phi}(0)}(\phi(t)),$$

so  $\phi = \gamma_\xi$  since both equal  $e$  at  $t = 0$ . Therefore, all one parameter subgroups of  $G$  are of the form  $\gamma_\xi(t)$  for some  $\xi \in \mathfrak{g}$ .

The map  $\exp : \mathfrak{g} \rightarrow G$ , given by

$$\exp(\xi) = \gamma_\xi(1), \quad \exp(0) = e, \quad (3.22)$$

is called the *exponential map* of the Lie algebra  $\mathfrak{g}$  of  $G$  into  $G$ .  $\exp$  is a  $C^k$ -map, similar to the projection  $\pi$  of tangent and cotangent bundles;  $\exp$  is locally a diffeomorphism from a neighborhood of zero in  $\mathfrak{g}$  onto a neighborhood of  $e$  in  $G$ ; if  $f : G \rightarrow H$  is a smooth homomorphism of Lie groups, then

$$f \circ \exp_G = \exp_H \circ T_e f.$$

Also, in this case (see [Chevalley (1955); Marsden and Ratiu (1999); Postnikov (1986)])

$$\exp(s\xi) = \gamma_\xi(s).$$

Indeed, for fixed  $s \in \mathbb{R}$ , the curve  $t \mapsto \gamma_\xi(ts)$ , which at  $t = 0$  passes through  $e$ , satisfies the differential equation

$$\frac{d}{dt} \gamma_\xi(ts) = sX_\xi(\gamma_\xi(ts)) = X_{s\xi}(\gamma_\xi(ts)).$$

Since  $\gamma_{s\xi}(t)$  satisfies the same differential equation and passes through  $e$  at  $t = 0$ , it follows that  $\gamma_{s\xi}(t) = \gamma_\xi(st)$ . Putting  $t = 1$  yields  $\exp(s\xi) = \gamma_\xi(s)$  [Marsden and Ratiu (1999)].

Hence  $\exp$  maps the line  $s\xi$  in  $\mathfrak{g}$  onto the one-parameter subgroup  $\gamma_\xi(s)$  of  $G$ , which is tangent to  $\xi$  at  $e$ . It follows from left invariance that the flow  $F_t^\xi$  of  $X$  satisfies  $F_t^\xi(g) = g \exp(s\xi)$ .

Globally, the exponential map  $\exp$ , as given by (3.22), is a natural operation, i.e., for any morphism  $\varphi : G \rightarrow H$  of Lie groups  $G$  and  $H$  and a Lie functor  $\mathcal{F}$ , the following diagram commutes [Postnikov (1986)]:

$$\begin{array}{ccc} \mathcal{F}(G) & \xrightarrow{\mathcal{F}(\varphi)} & \mathcal{F}(H) \\ \exp \downarrow & & \downarrow \exp \\ G & \xrightarrow{\varphi} & H \end{array}$$

Let  $G_1$  and  $G_2$  be Lie groups with Lie algebras  $\mathfrak{g}_1$  and  $\mathfrak{g}_2$ . Then  $G_1 \times G_2$  is a Lie group with Lie algebra  $\mathfrak{g}_1 \times \mathfrak{g}_2$ , and the exponential map is given by [Marsden and Ratiu (1999)].

$$\exp : \mathfrak{g}_1 \times \mathfrak{g}_2 \rightarrow G_1 \times G_2, \quad (\xi_1, \xi_2) \mapsto (\exp_1(\xi_1), \exp_2(\xi_2)).$$

For example, in case of a finite-dimensional vector space, or infinite-dimensional Banach space, the exponential map is the identity.

The unit circle in the complex plane  $S^1 = \{z \in \mathbb{C} : |z| = 1\}$  is an Abelian Lie group under multiplication. The tangent space  $T_e S^1$  is the imaginary axis, and we identify  $\mathbb{R}$  with  $T_e S^1$  by  $t \mapsto 2\pi i t$ . With this identification, the exponential map  $\exp : \mathbb{R} \rightarrow S^1$  is given by  $\exp(t) = e^{2\pi i t}$ .

The  $n$ D torus  $T^n = S^1 \times \dots \times S^1$  ( $n$  times) is an Abelian Lie group. The exponential map  $\exp : \mathbb{R}^n \rightarrow T^n$  is given by

$$\exp(t_1, \dots, t_n) = (e^{2\pi i t_1}, \dots, e^{2\pi i t_n}).$$

Since  $S^1 = \mathbb{R}/\mathbb{Z}$ , it follows that

$$T^n = \mathbb{R}^n / \mathbb{Z}^n,$$

the projection  $\mathbb{R}^n \rightarrow T^n$  being given by the  $\exp$  map (see [Marsden and Ratiu (1999); Postnikov (1986)]).

For every  $g \in G$ , the map

$$Ad_g = T_e (R_{g^{-1}} \circ L_g) : \mathfrak{g} \rightarrow \mathfrak{g}$$

is called the *adjoint map* (or *operator*) associated with  $g$ .

For each  $\xi \in \mathfrak{g}$  and  $g \in G$  we have

$$\exp(Ad_g \xi) = g(\exp \xi)g^{-1}.$$

The relation between the adjoint map and the Lie bracket is the following: For all  $\xi, \eta \in \mathfrak{g}$  we have

$$\left. \frac{d}{dt} \right|_{t=0} \text{Ad}_{\exp(t\xi)} \eta = [\xi, \eta].$$

A Lie subgroup  $H$  of  $G$  is a subgroup  $H$  of  $G$  which is also a submanifold of  $G$ . Then  $\mathfrak{h}$  is a Lie subalgebra of  $\mathfrak{g}$  and moreover  $\mathfrak{h} = \{\xi \in \mathfrak{g} | \exp(t\xi) \in H, \text{ for all } t \in \mathbb{R}\}$ .

One can characterize Lebesgue measure up to a multiplicative constant on  $\mathbb{R}^n$  by its invariance under translations. Similarly, on a locally compact group there is a unique (up to a nonzero multiplicative constant) left-invariant measure, called *Haar measure*. For Lie groups the existence of such measures is especially simple [Marsden and Ratiu (1999)]: Let  $G$  be a Lie group. Then there is a volume form  $Ub5$ , unique up to nonzero multiplicative constants, that is left invariant. If  $G$  is compact,  $Ub5$  is right invariant as well.

### 3.5.2.2 Actions of Lie Groups on $M$

Let  $M$  be a smooth manifold. An action of a Lie group  $G$  (with the unit element  $e$ ) on  $M$  is a smooth map  $\phi : G \times M \rightarrow M$ , such that for all  $x \in M$  and  $g, h \in G$ , (i)  $\phi(e, x) = x$  and (ii)  $\phi(g, \phi(h, x)) = \phi(gh, x)$ . In other words, letting  $\phi_g : x \in M \mapsto \phi_g(x) = \phi(g, x) \in M$ , we have (i')  $\phi_e = id_M$  and (ii')  $\phi_g \circ \phi_h = \phi_{gh}$ .  $\phi_g$  is a diffeomorphism, since  $(\phi_g)^{-1} = \phi_{g^{-1}}$ . We say that the map  $g \in G \mapsto \phi_g \in Diff(M)$  is a homomorphism of  $G$  into the group of diffeomorphisms of  $M$ . In case that  $M$  is a vector space and each  $\phi_g$  is a linear operator, the function of  $G$  on  $M$  is called a representation of  $G$  on  $M$  [Putz (1993)]

An action  $\phi$  of  $G$  on  $M$  is said to be *transitive action*, if for every  $x, y \in M$ , there is  $g \in G$  such that  $\phi(g, x) = y$ ; *effective action*, if  $\phi_g = id_M$  implies  $g = e$ , that is  $g \mapsto \phi_g$  is one-to-one; and *free action*, if for each  $x \in M$ ,  $g \mapsto \phi_g(x)$  is one-to-one.

For example,

- (1)  $G = \mathbb{R}$  acts on  $M = \mathbb{R}$  by translations; explicitly,

$$\phi : G \times M \rightarrow M, \quad \phi(s, x) = x + s.$$

Then for  $x \in \mathbb{R}$ ,  $O_x = \mathbb{R}$ . Hence  $M/G$  is a single point, and the action is transitive and free.



- (2) A complete flow  $\phi_t$  of a vector-field  $X$  on  $M$  gives an action of  $\mathbb{R}$  on  $M$ , namely

$$(t, x) \in \mathbb{R} \times M \mapsto \phi_t(x) \in M.$$

- (3) Left translation  $L_g : G \rightarrow G$  defines an effective action of  $G$  on itself. It is also transitive.
- (4) The coadjoint action of  $G$  on  $\mathfrak{g}^*$  is given by

$$Ad^* : (g, \alpha) \in G \times \mathfrak{g}^* \mapsto Ad_{g^{-1}}^*(\alpha) = (T_e(R_{g^{-1}} \circ L_g))^* \alpha \in \mathfrak{g}^*.$$

Let  $\phi$  be an action of  $G$  on  $M$ . For  $x \in M$  the *orbit* of  $x$  is defined by

$$O_x = \{\phi_g(x) | g \in G\} \subset M$$

and the *isotropy group* of  $\phi$  at  $x$  is given by

$$G_x = \{g \in G | \phi(g, x) = x\} \subset G.$$

An action  $\phi$  of  $G$  on a manifold  $M$  defines an equivalence relation on  $M$  by the relation belonging to the same orbit; explicitly, for  $x, y \in M$ , we write  $x \sim y$  if there exists a  $g \in G$  such that  $\phi(g, x) = y$ , that is, if  $y \in O_x$ . The set of all orbits  $M/G$  is called the *orbit space*.

For example, let  $M = \mathbb{R}^2 \setminus \{0\}$ ,  $G = SO(2)$ , the group of rotations in plane, and the action of  $G$  on  $M$  given by

$$\left( \begin{bmatrix} \cos \theta & -\sin \theta \\ \sin \theta & \cos \theta \end{bmatrix}, (x, y) \right) \mapsto (x \cos \theta - y \sin \theta, x \sin \theta + y \cos \theta).$$

The action is always free and effective, and the orbits are concentric circles, thus the orbit space is  $M/G \simeq \mathbb{R}_+^*$ .

A crucial concept in mechanics is the infinitesimal description of an action. Let  $\phi : G \times M \rightarrow M$  be an action of a Lie group  $G$  on a smooth manifold  $M$ . For each  $\xi \in \mathfrak{g}$ ,

$$\phi_\xi : \mathbb{R} \times M \rightarrow M, \quad \phi_\xi(t, x) = \phi(\exp(t\xi), x)$$

is an  $\mathbb{R}$ -action on  $M$ . Therefore,  $\phi_{\exp(t\xi)} : M \rightarrow M$  is a flow on  $M$ ; the corresponding vector-field on  $M$ , given by

$$\xi_M(x) = \left. \frac{d}{dt} \right|_{t=0} \phi_{\exp(t\xi)}(x)$$

is called the *infinitesimal generator of the action*, corresponding to  $\xi$  in  $\mathfrak{g}$ .

The tangent space at  $x$  to an orbit  $O_x$  is given by

$$T_x O_x = \{\xi_M(x) | \xi \in \mathfrak{g}\}.$$

Let  $\phi : G \times M \rightarrow M$  be a smooth  $G$ -action. For all  $g \in G$ , all  $\xi, \eta \in \mathfrak{g}$  and all  $\alpha, \beta \in \mathbb{R}$ , we have:

$$(Ad_g \xi)_M = \phi_{g^{-1}}^* \xi_M, [\xi_M, \eta_M] = -[\xi, \eta]_M, \text{ and } (\alpha\xi + \beta\eta)_M = \alpha\xi_M + \beta\eta_M.$$

Let  $M$  be a smooth manifold,  $G$  a Lie group and  $\phi : G \times M \rightarrow M$  a  $G$ -action on  $M$ . We say that a smooth map  $f : M \rightarrow M$  is with respect to this action if for all  $g \in G$ ,

$$f \circ \phi_g = \phi_g \circ f.$$

Let  $f : M \rightarrow M$  be an equivariant smooth map. Then for any  $\xi \in \mathfrak{g}$  we have

$$Tf \circ \xi_M = \xi_M \circ f.$$

### 3.5.2.3 Basic Biodynamic Groups

**General Linear Group.** The group of linear isomorphisms of  $\mathbb{R}^n$  to  $\mathbb{R}^n$  is a Lie group of dimension  $n^2$ , called the general linear group and denoted  $Gl(n, \mathbb{R})$ . It is a smooth manifold, since it is a subset of the vector space  $L(\mathbb{R}^n, \mathbb{R}^n)$  of all linear maps of  $\mathbb{R}^n$  to  $\mathbb{R}^n$ , as  $Gl(n, \mathbb{R})$  is the inverse image of  $\mathbb{R} \setminus \{0\}$  under the continuous map  $A \mapsto \det A$  of  $L(\mathbb{R}^n, \mathbb{R}^n)$  to  $\mathbb{R}$ . The group operation is composition

$$(A, B) \in Gl(n, \mathbb{R}) \times Gl(n, \mathbb{R}) \mapsto A \circ B \in Gl(n, \mathbb{R})$$

and the inverse map is

$$A \in Gl(n, \mathbb{R}) \mapsto A^{-1} \in Gl(n, \mathbb{R}).$$

If we choose a basis in  $\mathbb{R}^n$ , we can represent each element  $A \in Gl(n, \mathbb{R})$  by an invertible  $(n \times n)$ -matrix. The group operation is then matrix multiplication and the inversion is matrix inversion. The identity is the identity matrix  $I_n$ . The group operations are smooth since the formulas for the product and inverse of matrices are smooth in the matrix components.

The Lie algebra of  $Gl(n, \mathbb{R})$  is  $\mathfrak{gl}(n)$ , the vector space  $L(\mathbb{R}^n, \mathbb{R}^n)$  of all linear transformations of  $\mathbb{R}^n$ , with the commutator bracket

$$[A, B] = AB - BA.$$

For every  $A \in L(\mathbb{R}^n, \mathbb{R}^n)$ ,

$$\gamma_A : t \in \mathbb{R} \mapsto \gamma_A(t) = \sum_{i=0}^{\infty} \frac{t^i}{i!} A^i \in Gl(n, \mathbb{R})$$

is a one parameter subgroup of  $Gl(n, \mathbb{R})$ , because

$$\gamma_A(0) = I$$

and

$$\dot{\gamma}_A(t) = \sum_{i=0}^{\infty} \frac{t^{i-1}}{(i-1)!} A^i = \gamma_A(t) A.$$

Hence  $\gamma_A$  is an integral curve of the left invariant vector-field  $X_A$ . Therefore, the exponential map is given by

$$\exp : A \in L(\mathbb{R}^n, \mathbb{R}^n) \mapsto \exp(A) \equiv e^A = \gamma_A(1) = \sum_{i=0}^{\infty} \frac{A^i}{i!} \in Gl(n, \mathbb{R}).$$

For each  $A \in Gl(n, \mathbb{R})$  the corresponding adjoint map

$$Ad_A : L(\mathbb{R}^n, \mathbb{R}^n) \rightarrow L(\mathbb{R}^n, \mathbb{R}^n)$$

is given by

$$Ad_A B = A \cdot B \cdot A^{-1}.$$

**Galilean Group of Transformations.** We introduced this group in the Introduction (see (1.3.1)). As a different point of view, consider the (closed) subgroup  $G$  of  $GL(5, \mathbb{R})$  that consists of matrices with the following block structure:

$$\{R, v, a, \tau\} = \begin{bmatrix} R & v & a \\ 0 & 1 & \tau \\ 0 & 0 & 1 \end{bmatrix},$$

where  $R \in SO(3)$ ,  $v, a \in \mathbb{R}^3$ , and  $\tau \in \mathbb{R}$ . This group is called the *Galilean group*. Its Lie algebra is a subalgebra of  $L(\mathbb{R}^5, \mathbb{R}^5)$  given by the set of matrices of the form [Marsden and Ratiu (1999)]

$$\{\omega, u, \alpha, \theta\} = \begin{bmatrix} \omega & u & \alpha \\ 0 & 0 & \theta \\ 0 & 0 & 0 \end{bmatrix},$$

where  $\omega, u, \alpha \in \mathbb{R}^3$  and  $\theta \in \mathbb{R}$ . Clearly, the Galilean group acts naturally on  $\mathbb{R}^5$ ; moreover, it acts naturally on  $\mathbb{R}^4$ , embedded as the following  $G$ -invariant subset of  $\mathbb{R}^5$

$$\begin{bmatrix} x \\ t \end{bmatrix} \mapsto \begin{bmatrix} x \\ t \\ 1 \end{bmatrix},$$

where  $x \in \mathbb{R}^3$  and  $t \in \mathbb{R}$ . Concretely, the action of  $\{R, v, a, \tau\}$  on  $(x, t)$  is given by

$$(x, t) \mapsto (Rx + tv + a, t + \tau).$$

Thus, the Galilean group gives a change of frame of reference by rotations ( $R$ ), space translations ( $a$ ), time translations ( $\tau$ ), and going to a moving frame, or boosts ( $v$ ) [Marsden and Ratiu (1999)].

#### 3.5.2.4 Groups of Joint Rotations

Local kinematics at each rotational robot or (synovial) human joint, is defined as a *group action* of an  $n$ D constrained rotational Lie group  $SO(n)$  on the Euclidean space  $\mathbb{R}^n$ . In particular, there is an action of  $SO(2)$ -group in uniaxial humanoid joints (cylindrical, or *hinge joints*, like knee and elbow) and an action of  $SO(3)$ -group in three-axial humanoid joints (spherical, or *ball-and-socket joints*, like hip, shoulder, neck, wrist and ankle). In both cases,  $SO(n)$  acts, with its operators of rotation, on the vector  $x = \{x^\mu\}$ , ( $i = 1, 2, 3$ ) of external, Cartesian coordinates of the parent body-segment, depending, at the same time, on the vector  $q = \{q^s\}$ , ( $s = 1, \dots, n$ ) on  $n$  group-parameters, i.e., joint angles.

Each joint rotation  $R \in SO(n)$  defines a map

$$R : x^\mu \mapsto \dot{x}^\mu, \quad R(x^\mu, q^s) = R_{q^s} x^\mu,$$

where  $R_{q^s} \in SO(n)$  are joint group operators. The vector  $v = \{v_s\}$ , ( $s = 1, \dots, n$ ) of  $n$  infinitesimal generators of these rotations, i.e., joint angular velocities, given by

$$v_s = -\left[\frac{\partial R(x^\mu, q^s)}{\partial q^s}\right]_{q=0} \frac{\partial}{\partial x^\mu},$$

constitute an  $n$ D Lie algebra  $\mathfrak{so}(n)$  corresponding to the joint rotation group  $SO(n)$ . Conversely, each joint group operator  $R_{q^s}$ , representing a one-

parameter subgroup of  $SO(n)$ , is defined as the exponential map of the corresponding joint group generator  $v_s$

$$R_{q^s} = \exp(q^s v_s). \quad (3.23)$$

The exponential map (3.23) represents a solution of the joint operator differential equation in the joint group-parameter space  $\{q^s\}$

$$\frac{dR_{q^s}}{dq^s} = v_s R_{q^s}.$$

**Uniaxial Group of Joint Rotations.** The uniaxial joint rotation in a single Cartesian plane around a perpendicular axis, e.g.,  $xy$ -plane about the  $z$  axis, by an internal joint angle  $\theta$ , leads to the following transformation of the joint coordinates

$$\dot{x} = x \cos \theta - y \sin \theta, \quad \dot{y} = x \sin \theta + y \cos \theta.$$

In this way, the joint  $SO(2)$ -group, given by

$$SO(2) = \left\{ R_\theta = \begin{pmatrix} \cos \theta & -\sin \theta \\ \sin \theta & \cos \theta \end{pmatrix} \mid \theta \in [0, 2\pi] \right\},$$

acts in a canonical way on the Euclidean plane  $\mathbb{R}^2$  by

$$SO(2) = \left( \begin{pmatrix} \cos \theta & -\sin \theta \\ \sin \theta & \cos \theta \end{pmatrix}, \begin{pmatrix} x \\ w \end{pmatrix} \right) \mapsto \begin{pmatrix} x \cos \theta - y \sin \theta \\ x \sin \theta + y \cos \theta \end{pmatrix}.$$

Its associated Lie algebra  $\mathfrak{so}(2)$  is given by

$$\mathfrak{so}(2) = \left\{ \begin{pmatrix} 0 & -t \\ t & 0 \end{pmatrix} \mid t \in \mathbb{R} \right\},$$

since the curve  $\gamma_\theta \in SO(2)$  given by

$$\gamma_\theta : t \in \mathbb{R} \mapsto \gamma_\theta(t) = \begin{pmatrix} \cos t\theta & -\sin t\theta \\ \sin t\theta & \cos t\theta \end{pmatrix} \in SO(2),$$

passes through the identity  $I_2 = \begin{pmatrix} 1 & 0 \\ 0 & 1 \end{pmatrix}$  and then

$$\left. \frac{d}{dt} \right|_{t=0} \gamma_\theta(t) = \begin{pmatrix} 0 & -\theta \\ \theta & 0 \end{pmatrix},$$

so that  $I_2$  is a basis of  $\mathfrak{so}(2)$ , since  $\dim(SO(2)) = 1$ .

The exponential map  $\exp : \mathfrak{so}(2) \rightarrow SO(2)$  is given by

$$\exp \begin{pmatrix} 0 & -\theta \\ \theta & 0 \end{pmatrix} = \gamma_\theta(1) = \begin{pmatrix} \cos \theta & -\sin \theta \\ \sin \theta & \cos \theta \end{pmatrix}.$$

The infinitesimal generator of the action of  $SO(2)$  on  $\mathbb{R}^2$ , i.e., joint angular velocity  $v$ , is given by

$$v = -y \frac{\partial}{\partial x} + x \frac{\partial}{\partial y},$$

since

$$\begin{aligned} v_{\mathbb{R}^2}(x, y) &= \left. \frac{d}{dt} \right|_{t=0} \exp(tv)(x, y) \\ &= \left. \frac{d}{dt} \right|_{t=0} \begin{pmatrix} \cos tv & -\sin tv \\ \sin tv & \cos tv \end{pmatrix} \begin{pmatrix} x \\ y \end{pmatrix}. \end{aligned}$$

The momentum map  $J : T^*\mathbb{R}^2 \rightarrow \mathbb{R}$  associated to the lifted action of  $SO(2)$  on  $T^*\mathbb{R}^2 \simeq \mathbb{R}^4$  is given by

$$\begin{aligned} J(x, y, p_1, p_2) &= xp_y - yp_x, \quad \text{since} \\ J(x, y, p_x, p_y)(\xi) &= (p_x dx + p_y dy)(v_{\mathbb{R}^2}) = -vp_x y + -vp_y x. \end{aligned}$$

The Lie group  $SO(2)$  acts on the symplectic manifold  $(\mathbb{R}^4, \omega = dp_x \wedge dx + dp_y \wedge dy)$  by

$$\begin{aligned} &\phi \left( \begin{pmatrix} \cos \theta & -\sin \theta \\ \sin \theta & \cos \theta \end{pmatrix}, (x, y, p_x, p_y) \right) \\ &= (x \cos \theta - y \sin \theta, x \sin \theta + y \cos \theta, p_x \cos \theta - p_y \sin \theta, p_x \sin \theta + p_y \cos \theta). \end{aligned}$$

**Three-Axial Group of Joint Rotations.** The three-axial  $SO(3)$ -group of human-like joint rotations depends on three parameters, Euler joint angles  $q^i = (\varphi, \psi, \theta)$ , defining the rotations about the Cartesian coordinate triad  $(x, y, z)$  placed at the joint pivot point. Each of the Euler angles are defined in the constrained range  $(-\pi, \pi)$ , so the joint group space is a constrained sphere of radius  $\pi$ .

Let  $G = SO(3) = \{A \in \mathcal{M}_{3 \times 3}(\mathbb{R}) : A^t A = I_3, \det(A) = 1\}$  be the group of rotations in  $\mathbb{R}^3$ . It is a Lie group and  $\dim(G) = 3$ . Let us isolate its one-parameter joint subgroups, i.e., consider the three operators of the

finite joint rotations  $R_\varphi, R_\psi, R_\theta \in SO(3)$ , given by

$$R_\varphi = \begin{bmatrix} 1 & 0 & 0 \\ 0 & \cos \varphi & -\sin \varphi \\ 0 & \sin \varphi & \cos \varphi \end{bmatrix}, \quad R_\psi = \begin{bmatrix} \cos \psi & 0 & \sin \psi \\ 0 & 1 & 0 \\ -\sin \psi & 0 & \cos \psi \end{bmatrix}, \quad R_\theta = \begin{bmatrix} \cos \theta & -\sin \theta & 0 \\ \sin \theta & \cos \theta & 0 \\ 0 & 0 & 1 \end{bmatrix}$$

corresponding respectively to rotations about  $x$ -axis by an angle  $\varphi$ , about  $y$ -axis by an angle  $\psi$ , and about  $z$ -axis by an angle  $\theta$ .

The total three-axial joint rotation  $A$  is defined as the product of above one-parameter rotations  $R_\varphi, R_\psi, R_\theta$ , i.e.,  $A = R_\varphi \cdot R_\psi \cdot R_\theta$  is equal

$$A = \begin{bmatrix} \cos \psi \cos \varphi - \cos \theta \sin \varphi \sin \psi & \cos \psi \cos \varphi + \cos \theta \cos \varphi \sin \psi & \sin \theta \sin \psi \\ -\sin \psi \cos \varphi - \cos \theta \sin \varphi \sin \psi & -\sin \psi \sin \varphi + \cos \theta \cos \varphi \cos \psi & \sin \theta \cos \psi \\ \sin \theta \sin \varphi & -\sin \theta \cos \varphi & \cos \theta \end{bmatrix}.$$

$R_\varphi, R_\psi$  and  $R_\theta$  are curves in  $SO(3)$  starting from  $I_3 = \begin{pmatrix} 1 & 0 & 0 \\ 0 & 1 & 0 \\ 0 & 0 & 1 \end{pmatrix}$ . Their

derivatives in  $\varphi = 0, \psi = 0$  and  $\theta = 0$  belong to the associated *tangent Lie algebra*  $\mathfrak{so}(3)$ . That is the corresponding infinitesimal generators of joint rotations – joint angular velocities  $v_\varphi, v_\psi, v_\theta \in \mathfrak{so}(3)$  – are respectively given by

$$v_\varphi = \begin{bmatrix} 0 & 0 & 0 \\ 0 & 0 & -1 \\ 0 & 1 & 0 \end{bmatrix} = -y \frac{\partial}{\partial z} + z \frac{\partial}{\partial y}, \quad v_\psi = \begin{bmatrix} 0 & 0 & 1 \\ 0 & 0 & 0 \\ -1 & 0 & 0 \end{bmatrix} = -z \frac{\partial}{\partial x} + x \frac{\partial}{\partial z},$$

$$v_\theta = \begin{bmatrix} 0 & -1 & 0 \\ 1 & 1 & 0 \\ 0 & 0 & 0 \end{bmatrix} = -x \frac{\partial}{\partial y} + y \frac{\partial}{\partial x}.$$

Moreover, the elements are linearly independent and so

$$\mathfrak{so}(3) = \left\{ \begin{bmatrix} 0 & -a & b \\ a & 0 & -\gamma \\ -b & \gamma & 0 \end{bmatrix} \mid a, b, \gamma \in \mathbb{R} \right\}.$$

the Lie algebra  $\mathfrak{so}(3)$  is identified with  $\mathbb{R}^3$  by associating to each  $v =$

$(v_\varphi, v_\psi, v_\theta) \in \mathbb{R}^3$  the matrix  $v \in \mathfrak{so}(3)$  given by  $v = \begin{bmatrix} 0 & -a & b \\ a & 0 & -\gamma \\ -b & \gamma & 0 \end{bmatrix}$ . Then we

have following identities:

- (1)  $\widehat{u \times v} = [\hat{u}, \hat{v}]$ ; and
- (2)  $u \cdot v = -\frac{1}{2} \text{Tr}(\hat{u} \cdot \hat{v})$ .

The exponential map  $\exp : \mathfrak{so}(3) \rightarrow SO(3)$  is given by *Rodrigues relation*

$$\exp(v) = I + \frac{\sin \|v\|}{\|v\|} v + \frac{1}{2} \left( \frac{\sin \frac{\|v\|}{2}}{\frac{\|v\|}{2}} \right)^2 v^2,$$

where the norm  $\|v\|$  is given by

$$\|v\| = \sqrt{(v^1)^2 + (v^2)^2 + (v^3)^2}.$$

The dual, *cotangent Lie algebra*  $\mathfrak{so}(3)^*$ , includes the three joint angular momenta  $p_\varphi, p_\psi, p_\theta \in \mathfrak{so}(3)^*$ , derived from the joint velocities  $v$  by multiplying them with corresponding moments of inertia.

### 3.5.2.5 Special Euclidean Groups of Joint Motions

Biomechanically realistic joint movement is predominantly rotational, plus restricted translational (translational motion in human joints is observed after reaching the limit of rotational amplitude). Gross translation in any human joint means joint dislocation, which is a severe injury. Obvious models for uniaxial and triaxial joint motions are *special Euclidean groups of rigid body motions*,  $SE(2)$  and  $SE(3)$ , respectively.

**Special Euclidean Group in the Plane.** The motion in uniaxial human joints is naturally modelled by the *special Euclidean group in the plane*,  $SE(2)$ . It consists of all transformations of  $\mathbb{R}^2$  of the form  $Az + a$ , where  $z, a \in \mathbb{R}^2$ , and

$$A \in SO(2) = \left\{ \text{matrices of the form } \begin{pmatrix} \cos \theta & -\sin \theta \\ \sin \theta & \cos \theta \end{pmatrix} \right\}.$$

In other words [Marsden and Ratiu (1999)], group  $SE(2)$  consists of matrices of the form:

$$(R_\theta, a) = \begin{pmatrix} R_\theta & a \\ 0 & I \end{pmatrix}, \text{ where } a \in \mathbb{R}^2 \text{ and } R_\theta \text{ is the rotation matrix:}$$

$$R_\theta = \begin{pmatrix} \cos \theta & -\sin \theta \\ \sin \theta & \cos \theta \end{pmatrix}, \text{ while } I \text{ is the } 2 \times 2 \text{ identity matrix. The inverse } (R_\theta, a)^{-1} \text{ is given by}$$

$$(R_\theta, a)^{-1} = \begin{pmatrix} R_\theta & a \\ 0 & I \end{pmatrix}^{-1} = \begin{pmatrix} R_{-\theta} & -R_{-\theta}a \\ 0 & I \end{pmatrix}.$$



The Lie algebra  $\mathfrak{se}(2)$  of  $SE(2)$  consists of  $3 \times 3$  block matrices of the form

$$\begin{pmatrix} -\xi J & v \\ 0 & 0 \end{pmatrix}, \quad \text{where} \quad J = \begin{pmatrix} 0 & 1 \\ -1 & 0 \end{pmatrix}, \quad (J^T = J^{-1} = -J),$$

with the usual commutator bracket. If we identify  $\mathfrak{se}(2)$  with  $\mathbb{R}^3$  by the isomorphism

$$\begin{pmatrix} -\xi J & v \\ 0 & 0 \end{pmatrix} \in \mathfrak{se}(2) \longmapsto (\xi, v) \in \mathbb{R}^3,$$

then the expression for the Lie algebra bracket becomes

$$[(\xi, v_1, v_2), (\zeta, w_1, w_2)] = (0, \zeta v_2 - \xi w_2, \xi w_1 - \zeta v_1) = (0, \xi J^T w - \zeta J^T v),$$

where  $v = (v_1, v_2)$  and  $w = (w_1, w_2)$ .

The *adjoint group action* of

$$(R_\theta, a) \begin{pmatrix} R_\theta & a \\ 0 & I \end{pmatrix} \quad \text{on} \quad (\xi, v) = \begin{pmatrix} -\xi J & v \\ 0 & 0 \end{pmatrix}$$

is given by the *group conjugation*,

$$\begin{pmatrix} R_\theta & a \\ 0 & I \end{pmatrix} \begin{pmatrix} -\xi J & v \\ 0 & 0 \end{pmatrix} \begin{pmatrix} R_{-\theta} & -R_{-\theta}a \\ 0 & I \end{pmatrix} = \begin{pmatrix} -\xi J & \xi Ja + R_\theta v \\ 0 & 0 \end{pmatrix},$$

or, in coordinates [Marsden and Ratiu (1999)],

$$Ad_{(R_\theta, a)}(\xi, v) = (\xi, \xi Ja + R_\theta v). \quad (3.24)$$

In proving (3.24) we used the identity  $R_\theta J = J R_\theta$ . Identify the dual algebra,  $\mathfrak{se}(2)^*$ , with matrices of the form  $\begin{pmatrix} \frac{\mu}{2} J & 0 \\ \alpha & 0 \end{pmatrix}$ , via the nondegenerate pairing given by the trace of the product. Thus,  $\mathfrak{se}(2)^*$  is isomorphic to  $\mathbb{R}^3$  via

$$\begin{pmatrix} \frac{\mu}{2} J & 0 \\ \alpha & 0 \end{pmatrix} \in \mathfrak{se}(2)^* \longmapsto (\mu, \alpha) \in \mathbb{R}^3,$$

so that in these coordinates, the pairing between  $\mathfrak{se}(2)^*$  and  $\mathfrak{se}(2)$  becomes

$$\langle (\mu, \alpha), (\xi, v) \rangle = \mu \xi + \alpha \cdot v,$$

that is, the usual dot product in  $\mathbb{R}^3$ . The *coadjoint group action* is thus given by

$$Ad_{(R_\theta, a)}^*(\mu, \alpha) = (\mu - R_\theta \alpha \cdot Ja + R_\theta \alpha). \quad (3.25)$$

Formula (3.25) shows that the coadjoint orbits are the cylinders  $T^*S_\alpha^1 = \{(\mu, \alpha) \mid \|\alpha\| = \text{const}\}$  if  $\alpha \neq 0$  together with the points are on the  $\mu$ -axis. The canonical cotangent bundle projection  $\pi : T^*S_\alpha^1 \rightarrow S_\alpha^1$  is defined as  $\pi(\mu, \alpha) = \alpha$ .

**Special Euclidean Group in the 3D Space.** The most common group structure in biodynamics is the *special Euclidean group in 3D space*,  $SE(3)$ . It is defined as a semidirect (noncommutative) product of 3D rotations and 3D translations,  $SO(3) \triangleright \mathbb{R}^3$ .

**The Heavy Top.** As a starting point consider a rigid body (see (4.2.1.3) below) moving with a fixed point but under the influence of gravity. This problem still has a configuration space  $SO(3)$ , but the symmetry group is only the circle group  $S^1$ , consisting of rotations about the direction of gravity. One says that gravity has broken the symmetry from  $SO(3)$  to  $S^1$ . This time, eliminating the  $S^1$  symmetry mysteriously leads one to the larger Euclidean group  $SE(3)$  of rigid motion of  $\mathbb{R}^3$ . Conversely, we can start with  $SE(3)$  as the configuration space for the rigid-body and ‘reduce out’ translations to arrive at  $SO(3)$  as the configuration space (see [Marsden and Ratiu (1999)]).

The equations of motion for a rigid body with a fixed point in a gravitational field provide an interesting example of a system that is Hamiltonian (see (4.2.1.3)) relative to a *Lie-Poisson bracket* (see (4.2.3.1)). The underlying Lie algebra consists of the algebra of infinitesimal Euclidean motions in  $\mathbb{R}^3$ .

The basic phase-space we start with is again  $T^*SO(3)$ , parameterized by Euler angles and their conjugate momenta. In these variables, the equations are in canonical Hamiltonian form; however, the presence of gravity breaks the symmetry, and the system is no longer  $SO(3)$  invariant, so it cannot be written entirely in terms of the body angular momentum  $p$ . One also needs to keep track of  $\Gamma$ , the ‘direction of gravity’ as seen from the body. This is defined by  $\Gamma = A^{-1}k$ , where  $k$  points upward and  $A$  is the element of  $SO(3)$  describing the current configuration of the body. The equations

of motion are

$$\begin{aligned}\dot{p}_1 &= \frac{I_2 - I_3}{I_2 I_3} p_2 p_3 + Mgl(\Gamma^2 \chi^3 - \Gamma^3 \chi^2), \\ \dot{p}_2 &= \frac{I_3 - I_1}{I_3 I_1} p_3 p_1 + Mgl(\Gamma^3 \chi^1 - \Gamma^1 \chi^3), \\ \dot{p}_3 &= \frac{I_1 - I_2}{I_1 I_2} p_1 p_2 + Mgl(\Gamma^1 \chi^2 - \Gamma^2 \chi^1),\end{aligned}$$

and

$$\dot{\Gamma} = \Gamma \times \Omega,$$

where  $\Omega$  is the body angular velocity vector,  $I_1, I_2, I_3$  are the body's principal moments of inertia,  $M$  is the body's mass,  $g$  is the acceleration of gravity,  $\chi$  is the body fixed unit vector on the line segment connecting the fixed point with the body's center of mass, and  $l$  is the length of this segment.

**The Euclidean Group and Its Lie Algebra.** An element of  $SE(3)$  is a pair  $(A, a)$  where  $A \in SO(3)$  and  $a \in \mathbb{R}^3$ . The action of  $SE(3)$  on  $\mathbb{R}^3$  is the rotation  $A$  followed by translation by the vector  $a$  and has the expression

$$(A, a) \cdot x = Ax + a.$$

Using this formula, one sees that multiplication and inversion in  $SE(3)$  are given by

$$(A, a)(B, b) = (AB, Ab + a) \quad \text{and} \quad (A, a)^{-1} = (A^{-1}, -A^{-1}a),$$

for  $A, B \in SO(3)$  and  $a, b \in \mathbb{R}^3$ . The identity element is  $(I, 0)$ .

The Lie algebra of the Euclidean group  $SE(3)$  is  $\mathfrak{se}(3) = \mathbb{R}^3 \times \mathbb{R}^3$  with the Lie bracket

$$[(\xi, u), (\eta, v)] = (\xi \times \eta, \xi \times v - \eta \times u). \quad (3.26)$$

The Lie algebra of the Euclidean group has a structure that is a special case of what is called a *semidirect product*. Here it is the *product of the group of rotations with the corresponding group of translations*. It turns out that semidirect products occur under rather general circumstances when the symmetry in  $T^*G$  is broken.

The dual Lie algebra of the Euclidean group  $SE(3)$  is  $\mathfrak{se}(3)^* = \mathbb{R}^3 \times \mathbb{R}^3$  with the same Lie bracket (3.26). For the further details on adjoint orbits in  $\mathfrak{se}(3)$  as well as coadjoint orbits in  $\mathfrak{se}(3)^*$  see [Marsden and Ratiu (1999)].

**Symplectic Group in Hamiltonian Mechanics.** Let

$$J = \begin{pmatrix} 0 & I \\ -I & 0 \end{pmatrix},$$

with  $I$  the  $n \times n$  identity matrix. Now,  $A \in L(\mathbb{R}^{2n}, \mathbb{R}^{2n})$  is called a *symplectic matrix* if  $A^T J A = J$ . Let  $Sp(2n, \mathbb{R})$  be the set of  $2n \times 2n$  symplectic matrices. Taking determinants of the condition  $A^T J A = J$  gives  $\det A = \pm 1$ , and so  $A \in GL(2n, \mathbb{R})$ . Furthermore, if  $A, B \in Sp(2n, \mathbb{R})$ , then  $(AB)^T J (AB) = B^T A^T J AB = J$ . Hence,  $AB \in Sp(2n, \mathbb{R})$ , and if  $A^T J A = J$ , then  $JA = (A^T)^{-1} J = (A^{-1})^T J$ , so  $J = (A - 1)^T J A^{-1}$ , or  $A^{-1} \in Sp(2n, \mathbb{R})$ . Thus,  $Sp(2n, \mathbb{R})$  is a group [Marsden and Ratiu (1999)].

The *symplectic Lie group*

$$Sp(2n, \mathbb{R}) = \{A \in GL(2n, \mathbb{R}) : A^T J A = J\}$$

is a noncompact, connected Lie group of dimension  $2n^2 + n$ . Its Lie algebra

$$\mathfrak{sp}(2n, \mathbb{R}) = \{A \in L(\mathbb{R}^{2n}, \mathbb{R}^{2n}) : A^T J A = J = 0\},$$

called the *symplectic Lie algebra*, consists of the  $2n \times 2n$  matrices  $A$  satisfying  $A^T J A = 0$  [Marsden and Ratiu (1999)].

Consider a particle of mass  $m$  moving in a potential  $V(q)$ , where  $q^i = (q^1, q^2, q^3) \in \mathbb{R}^3$ . Newtonian second law states that the particle moves along a curve  $q(t)$  in  $\mathbb{R}^3$  in such a way that  $m\ddot{q}^i = -\text{grad } V(q^i)$ . Introduce the momentum  $p_i = m\dot{q}^i$ , and the energy

$$H(q, p) = \frac{1}{2m} \sum_{i=1}^3 p_i^2 + V(q).$$

Then

$$\begin{aligned} \frac{\partial H}{\partial q^i} &= \frac{\partial V}{\partial q^i} = -m\ddot{q}^i = -\dot{p}_i, \quad \text{and} \\ \frac{\partial H}{\partial p_i} &= \frac{1}{m} p_i = \dot{q}^i, \quad (i = 1, 2, 3), \end{aligned}$$

and hence Newtonian law  $F = m\ddot{q}^i$  is equivalent to Hamilton's equations

$$\dot{q}^i = \frac{\partial H}{\partial p_i}, \quad \dot{p}_i = -\frac{\partial H}{\partial q^i}, \quad (i = 1, 2, 3).$$

Now, writing  $z = (q^i, p_i)$  [Marsden and Ratiu (1999)],

$$J \operatorname{grad} H(z) = \begin{pmatrix} 0 & I \\ -I & 0 \end{pmatrix} \begin{pmatrix} \frac{\partial H}{\partial q^i} \\ \frac{\partial H}{\partial p_i} \end{pmatrix} = (\dot{q}^i, \dot{p}_i) = \dot{z},$$

so Hamilton's equations read

$$\dot{z} = J \operatorname{grad} H(z). \quad (3.27)$$

Now let  $f : \mathbb{R}^3 \times \mathbb{R}^3 \rightarrow \mathbb{R}^3 \times \mathbb{R}^3$  and write  $w = f(z)$ . If  $z(t)$  satisfies Hamilton's equations (3.27) then  $w(t) = f(z(t))$  satisfies  $\dot{w} = A^T \dot{z}$ , where  $A^T = [\partial w^i / \partial z^j]$  is the Jacobian matrix of  $f$ . By the chain rule,

$$\dot{w} = A^T \underset{z}{J \operatorname{grad} H(z)} = A^T \underset{w}{J A \operatorname{grad} H(z(w))}.$$

Thus, the equations for  $w(t)$  have the form of Hamilton's equations with energy  $K(w) = H(z(w))$  iff  $A^T J A = J$ , that is, iff  $A$  is symplectic. A nonlinear transformation  $f$  is canonical iff its Jacobian matrix is symplectic.  $Sp(2n, \mathbb{R})$  is the linear invariance group of classical mechanics [Marsden and Ratiu (1999)].

### 3.5.3 Group Structure of the Biodynamic Manifold $M$

#### 3.5.3.1 Purely Rotational Biodynamic Manifold

Kinematics of an  $n$ -segment humanoid chain is usually defined as a map between *external coordinates* (usually, end-effector coordinates)  $x^r$  ( $r = 1, \dots, n$ ) and *internal joint coordinates*  $q^i$  ( $i = 1, \dots, N$ ) (see [Ivancevic and Snoswell (2001); Ivancevic (2002); Ivancevic and Pearce (2001b); Ivancevic and Pearce (2001b); Ivancevic (2005)]). The *forward kinematics* are defined as a nonlinear map  $x^r = x^r(q^i)$  with a corresponding linear vector functions  $dx^r = \partial x^r / \partial q^i dq^i$  of differentials: and  $\dot{x}^r = \partial x^r / \partial q^i \dot{q}^i$  of velocities. When the rank of the configuration-dependent Jacobian matrix  $J \equiv \partial x^r / \partial q^i$  is less than  $n$  the *kinematic singularities* occur; the onset of this condition could be detected by the *manipulability measure*. The *inverse kinematics* are defined conversely by a nonlinear map  $q^i = q^i(x^r)$  with a corresponding linear vector functions  $dq^i = \partial q^i / \partial x^r dx^r$  of differentials and  $\dot{q}^i = \partial q^i / \partial x^r \dot{x}^r$  of velocities. Again, in the case of *redundancy* ( $n < N$ ), the inverse kinematic problem admits infinite solutions; often the 'pseudoinverse' configuration-control is used instead:  $\dot{q}^i = J^* \dot{x}^r$ , where

$J^* = J^T(JJ^T)^{-1}$  denotes the *Moore–Penrose pseudoinverse* of the Jacobian matrix  $J$ .

Humanoid joints, that is, internal coordinates  $q^i$  ( $i = 1, \dots, N$ ), constitute a smooth configuration manifold  $M$ , described as follows. Uniaxial, ‘hinge’ joints represent constrained, rotational Lie groups  $SO(2)_{cnstr}^i$ , parameterized by constrained angles  $q_{cnstr}^i \equiv q^i \in [q_{\min}^i, q_{\max}^i]$ . Three-axial, ‘ball-and-socket’ joints represent constrained rotational Lie groups  $SO(3)_{cnstr}^i$ , parameterized by constrained Euler angles  $q^i = q_{cnstr}^{\phi_i}$  (in the following text, the subscript ‘cnstr’ will be omitted, for the sake of simplicity, and always assumed in relation to internal coordinates  $q^i$ ).

All  $SO(n)$ -joints are Hausdorff  $C^k$ -manifolds with atlases  $(U_\alpha, u_\alpha)$ ; in other words, they are paracompact and metrizable smooth manifolds, admitting Riemannian metric.

Let  $A$  and  $B$  be two smooth manifolds described by smooth atlases  $(U_\alpha, u_\alpha)$  and  $(V_\beta, v_\beta)$ , respectively. Then the family  $(U_\alpha \times V_\beta, u_\alpha \times v_\beta : U_\alpha \times V_\beta \rightarrow \mathbb{R}^m \times \mathbb{R}^n)_{(\alpha, \beta) \in A \times B}$  is a smooth atlas for the direct product  $A \times B$ . Now, if  $A$  and  $B$  are two Lie groups (say,  $SO(n)$ ), then their *direct product*  $G = A \times B$  is at the same time their direct product as smooth manifolds and their direct product as algebraic groups, with the product law

$$(a_1, b_1)(a_2, b_2) = (a_1a_2, b_1b_2), \quad a_{1,2} \in A, b_{1,2} \in B.$$

Generalizing the direct product to  $N$  rotational joint groups, we can draw an *anthropomorphic product-tree* (see Figure 3.1) using a line segment ‘—’ to represent direct products of humanoid’s  $SO(n)$ -joints. This is our basic model of the humanoid configuration manifold  $M$  (see (4.2.1.3) below).

Let  $T_qM$  be a tangent space to  $M$  at the point  $q$ . The *tangent bundle*  $TM$  represents a union  $\cup_{q \in M} T_qM$ , together with the standard topology on  $TM$  and a natural smooth manifold structure, the dimension of which is twice the dimension of  $M$ . A vector-field  $X$  on  $M$  represents a section  $X : M \rightarrow TM$  of the tangent bundle  $TM$ .

Analogously let  $T_q^*M$  be a cotangent space to  $M$  at  $q$ , the dual to its tangent space  $T_qM$ . The *cotangent bundle*  $T^*M$  represents a union  $\cup_{q \in M} T_q^*M$ , together with the standard topology on  $T^*M$  and a natural smooth manifold structure, the dimension of which is twice the dimension of  $M$ . A 1-form  $\theta$  on  $M$  represents a section  $\theta : M \rightarrow T^*M$  of the cotangent bundle  $T^*M$ .

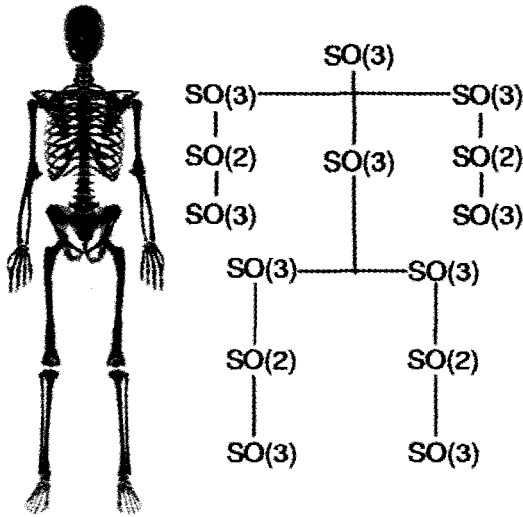


Fig. 3.1 Purely rotational, whole-body biodynamic manifold, with a single  $SO(3)$ -joint representing the whole spinal movability.

We refer to the tangent bundle  $TM$  of biodynamics configuration manifold  $M$  as the *velocity phase-space* manifold, and to its cotangent bundle  $T^*M$  as the *momentum phase-space* manifold.

### 3.5.3.2 Reduction of the Rotational Manifold

The biodynamics configuration manifold  $M$  (Figure 3.1) can be (for the sake of the brain-like motor control, see chapter 7) reduced to  $N$ -torus  $T^N$ , in three steps, as follows.

First, a single three-axial  $SO(3)$ -joint can be reduced to the direct product of three uniaxial  $SO(2)$ -joints, in the sense that three hinge joints can produce any orientation in space, just as a ball-joint can. Algebraically, this means reduction (using symbol ' $\gtrsim$ ') of each of the three  $SO(3)$  rotation matrices to the corresponding  $SO(2)$  rotation matrices

$$\begin{pmatrix} 1 & 0 & 0 \\ 0 & \cos \phi & -\sin \phi \\ 0 & \sin \phi & \cos \phi \end{pmatrix} \gtrsim \begin{pmatrix} \cos \phi & -\sin \phi \\ \sin \phi & \cos \phi \end{pmatrix},$$

$$\begin{pmatrix} \cos \psi & 0 & \sin \psi \\ 0 & 1 & 0 \\ -\sin \psi & 0 & \cos \psi \end{pmatrix} \gtrsim \begin{pmatrix} \cos \psi & \sin \psi \\ -\sin \psi & \cos \psi \end{pmatrix},$$

$$\begin{pmatrix} \cos \theta & -\sin \theta & 0 \\ \sin \theta & \cos \theta & 0 \\ 0 & 0 & 1 \end{pmatrix} \gtrsim \begin{pmatrix} \cos \theta & -\sin \theta \\ \sin \theta & \cos \theta \end{pmatrix}.$$

In this way we can set the *reduction equivalence relation*  $SO(3) \gtrsim SO(2) \triangleright SO(2) \triangleright SO(2)$ , where ' $\triangleright$ ' denotes the noncommutative *semidirect product* (see (3.5.2.5) above).

Second, we have a homeomorphism:  $SO(2) \sim S^1$ , where  $S^1$  denotes the constrained unit circle in the complex plane, which is an Abelian Lie group.

Third, let  $I^N$  be the unit cube  $[0, 1]^N$  in  $\mathbb{R}^N$  and ' $\sim$ ' an equivalence relation on  $\mathbb{R}^N$  obtained by 'gluing' together the opposite sides of  $I^N$ , preserving their orientation. The manifold of humanoid configurations (Figure 3.1) can be represented as the *quotient space* of  $\mathbb{R}^N$  by the space of the integral lattice points in  $\mathbb{R}^N$ , that is a constrained  $ND$  torus  $T^N$  (5.2),

$$\mathbb{R}^N / \mathbb{Z}^N = I^N / \sim \cong \prod_{i=1}^N S_i^1 \equiv \{(q^i, i = 1, \dots, N) : \text{mod } 2\pi\} = T^N. \quad (3.28)$$

Since  $S^1$  is an Abelian Lie group, its  $N$ -fold tensor product  $T^N$  is also an Abelian Lie group, the toral group, of all nondegenerate diagonal  $N \times N$  matrices. As a Lie group, the biodynamics configuration space  $M \equiv T^N$  has a natural Banach manifold structure with local internal coordinates  $q^i \in U$ ,  $U$  being an open set (chart) in  $T^N$ .

Conversely by 'ungluing' the configuration space we get the primary unit cube. Let ' $\sim^*$ ' denote an equivalent decomposition or 'ungluing' relation. By the Tychonoff product-topology theorem, for every such quotient space there exists a 'selector' such that their quotient models are homeomorphic, that is,  $T^N / \sim^* \approx A^N / \sim^*$ . Therefore  $I^N$  represents a 'selector' for the configuration torus  $T^N$  and can be used as an  $N$ -directional 'command-space' for the topological control of humanoid motion. Any subset of DOF on the configuration torus  $T^N$  representing the joints included in humanoid motion has its simple, rectangular image in the command space – selector  $I^N$ . Operationally, this resembles what the *brain-motor-controller*, the *cerebellum*, actually performs on the highest level of human motor control (see chapter 7).



### 3.5.3.3 The Complete Biodynamic Manifold

The full kinematics of a whole human-like body can be split down into *five kinematic chains*: one for each leg and arm, plus one for spine with the head. In all five chains internal joint coordinates, namely  $n_1$  constrained rotations  $x_{rt}^k$  together with  $n_2$  of even more constrained translations  $x_{tr}^j$  (see Figure 3.2), constitute a smooth  $nD$  anthropomorphic configuration manifold  $M$ , with local coordinates  $x^i$ , ( $i = 1, \dots, n$ ). That is, the motion space in each joint is defined as a semidirect (noncommutative) product of the Lie group  $SO(n)$  of constrained rotations and a corresponding Lie group  $\mathbb{R}^n$  of even more restricted translations. More precisely, in each movable human-like joint we have an action of the constrained special Euclidean  $SE(3)$  group (see (3.5.2.5) above). The joints themselves are linked by direct (commutative) products.

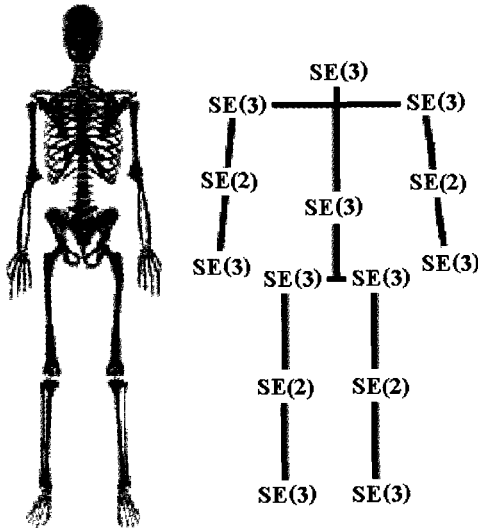


Fig. 3.2 A medium-resolution, whole-body biodynamic manifold, with just a single  $SE(3)$ -joint representing the spinal movability.

### 3.5.3.4 Realistic Human Spine Manifold

The high-resolution human spine manifold is a dynamical chain consisting of 25 constrained  $SE(3)$ -joints. Each movable spinal joint has 6 DOF: 3 dominant rotations, (performed first in any free spinal movement), re-

stricted to about 7 angular degrees and 3 secondary translations (performed after reaching the limit of rotational amplitude), restricted to about 5 mm (see Figure 3.3).

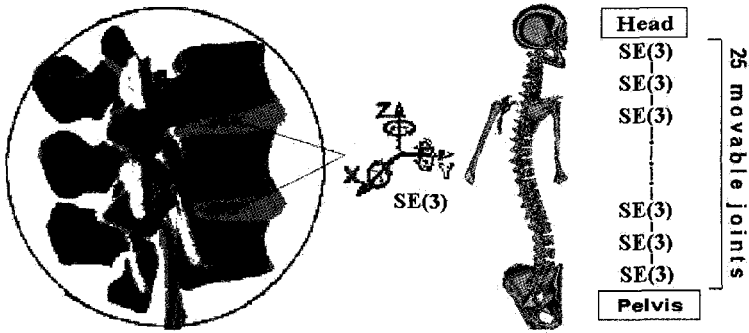


Fig. 3.3 The high-resolution human spine manifold is a dynamical chain consisting of 25 constrained  $SE(3)$ -joints.

Now,  $SE(3) = SO(3) \supset \mathbb{R}^3$  is a non-compact group, so there is no any natural metric given by the kinetic energy on  $SE(3)$ , and consequently, no natural controls in the sense of geodesics on  $SE(3)$ . However, both of its subgroups,  $SO(3)$  and  $\mathbb{R}^3$ , are compact with quadratic metric forms defined by standard line element  $g_{ij}dq^i dq^j$ , and therefore admit optimal muscular-like controls in the sense of geodesics (see section (3.6.1.2) below).

### 3.5.4 Lie Symmetries in Biodynamics

#### 3.5.4.1 Lie Symmetry Groups

**Exponentiation of Vector Fields on  $M$ .** Let  $x = (x^1, \dots, x^r)$  be local coordinates at a point  $m$  on a smooth  $n$ -manifold  $M$ . Recall that the flow generated by the vector-field

$$v = \xi^i(x) \partial_{x^i} \in M,$$

is a solution of the system of ODEs

$$\frac{dx^i}{d\varepsilon} = \xi^i(x^1, \dots, x^m), \quad i = 1, \dots, r.$$

The computation of the flow, or one-parameter group of diffeomorphisms, generated by a given vector-field  $v$  (i.e., solving the system of ODEs) is

often referred to as *exponentiation* of the vector-field, denoted by  $\exp(\varepsilon v) x$  (see [Olver (1986)]).

If  $v, w \in M$  are two vectors defined by

$$v = \xi^i(x) \partial_{x^i} \quad \text{and} \quad w = \eta^i(x) \partial_{x^i},$$

then

$$\exp(\varepsilon v) \exp(\theta w) x = \exp(\theta w) \exp(\varepsilon v) x,$$

for all  $\varepsilon, \theta \in \mathbb{R}, x \in M$ , such that both sides are defined, iff they commute, i.e.,  $[v, w] = 0$  everywhere [Olver (1986)].

A system of vector-fields  $\{v_1, \dots, v_r\}$  on a smooth manifold  $M$  is in *involution* if there exist smooth real-valued functions  $h_{ij}^k(x)$ ,  $x \in M$ ,  $i, j, k = 1, \dots, r$ , such that for each  $i, j$ ,

$$[v_i, v_j] = h_{ij}^k \cdot v_k.$$

Let  $v \neq 0$  be a right-invariant vector-field on a Lie group  $G$ . Then the flow generated by  $v$  through the identity  $e$ , namely

$$g_\varepsilon = \exp(\varepsilon v) e \equiv \exp(\varepsilon v),$$

is defined for all  $\varepsilon \in \mathbb{R}$  and forms a one-parameter subgroup of  $G$ , with

$$g_{\varepsilon+\delta} = g_\varepsilon \cdot g_\delta, \quad g_0 = e, \quad g_\varepsilon^{-1} = g_{-\varepsilon},$$

isomorphic to either  $\mathbb{R}$  itself or the circle group  $SO(2)$ . Conversely, any connected 1D subgroup of  $G$  is generated by such a right-invariant vector-field in the above manner [Olver (1986)].

For example, let  $G = GL(n)$  with Lie algebra  $\mathfrak{gl}(n)$ , the space of all  $n \times n$  matrices with commutator as the Lie bracket. If  $A \in \mathfrak{gl}(n)$ , then the corresponding right-invariant vector-field  $v_A$  on  $GL(n)$  has the expression [Olver (1986)]

$$v_A = a_k^i x_j^k \partial_{x_j^i}.$$

The one-parameter subgroup  $\exp(\varepsilon v_A) e$  is found by integrating the system of  $n^2$  ordinary differential equations

$$\frac{dx_j^i}{d\varepsilon} = a_k^i x_j^k, \quad x_j^i(0) = \delta_j^i, \quad i, j = 1, \dots, n,$$

involving matrix entries of  $A$ . The solution is just the matrix exponential  $X(\varepsilon) = e^{\varepsilon A}$ , which is the one-parameter subgroup of  $GL(n)$  generated by a matrix  $A$  in  $\mathfrak{gl}(n)$ .

Recall that the *exponential map*  $\exp : \mathfrak{g} \rightarrow G$  is obtained by setting  $\varepsilon = 1$  in the one-parameter subgroup generated by vector-field  $v$  :

$$\exp(v) \equiv \exp(v) e.$$

Its differential at 0,

$$d\exp : T\mathfrak{g}|_0 \simeq \mathfrak{g} \rightarrow TG|_e \simeq \mathfrak{g}$$

is the identity map.

### Lie Symmetry Groups and General Differential Equations.

Consider a system  $S$  of general differential equations (DEs, to be distinguished from ODEs) involving  $p$  independent variables  $x = (x^1, \dots, x^p)$ , and  $q$  dependent variables  $u = (u^1, \dots, u^q)$ . The solution of the system will be of the form  $u = f(x)$ , or, in components,  $u^\alpha = f^\alpha(x^1, \dots, x^p)$ ,  $\alpha = 1, \dots, q$  (so that Latin indices refer to independent variables while Greek indices refer to dependent variables). Let  $X = \mathbb{R}^p$ , with coordinates  $x = (x^1, \dots, x^p)$ , be the space representing the independent variables, and let  $U = \mathbb{R}^q$ , with coordinates  $u = (u^1, \dots, u^q)$ , represent dependent variables. A Lie symmetry group  $G$  of the system  $S$  will be a local group of transformations acting on some open subset  $M \subset X \times U$  in such way that  $G$  transforms solutions of  $S$  to other solutions of  $S$  [Olver (1986)].

More precisely, we need to explain exactly how a given transformation  $g \in G$ , where  $G$  is a Lie group, transforms a function  $u = f(x)$ . We firstly identify the function  $u = f(x)$  with its graph

$$\Gamma_f \equiv \{(x, f(x)) : x \in \text{dom } f \equiv \Omega\} \subset X \times U,$$

where  $\Gamma_f$  is a submanifold of  $X \times U$ . If  $\Gamma_f \subset M_g \equiv \text{dom } g$ , then the transform of  $\Gamma_f$  by  $g$  is defined as

$$g \cdot \Gamma_f = \{(\tilde{x}, \tilde{u}) = g \cdot (x, u) : (x, u) \in \Gamma_f\}.$$

We write  $\tilde{f} = g \cdot f$  and call the function  $\tilde{f}$  the *transform* of  $f$  by  $g$ .

For example, let  $p = 1$  and  $q = 1$ , so  $X = \mathbb{R}$  with a single independent variable  $x$ , and  $U = \mathbb{R}$  with a single dependent variable  $u$ , so we have a single ODE involving a single function  $u = f(x)$ . Let  $G = SO(2)$  be the rotation group acting on  $X \times U \simeq \mathbb{R}^2$ . The transformations in  $G$  are given

by

$$(\tilde{x}, \tilde{u}) = \theta \cdot (x, u) = (x \cos \theta - u \sin \theta, x \sin \theta + u \cos \theta).$$

Let  $u = f(x)$  be a function whose graph is a subset  $\Gamma_f \subset X \times U$ . The group  $SO(2)$  acts on  $f$  by rotating its graph.

In general, the procedure for finding the transformed function  $\tilde{f} = g \cdot f$  is given by [Olver (1986)]:

$$g \cdot f = [\Phi_g \circ (1 \times f)] \circ [\Xi_g \circ (1 \times f)]^{-1}, \quad (3.29)$$

where  $\Xi_g = \Xi_g(x, u)$ ,  $\Phi_g = \Phi_g(x, u)$  are smooth functions such that

$$(\tilde{x}, \tilde{u}) = g \cdot (x, u) = (\Xi_g(x, u), \Phi_g(x, u)),$$

while 1 denotes the identity function of  $X$ , so  $1(x) = x$ . Formula (3.29) holds whenever the second factor is invertible.

Let  $\mathcal{S}$  be a system of DEs. A *symmetry group* of the system  $\mathcal{S}$  is a local Lie group of transformations  $G$  acting on an open subset  $M \subset X \times U$  of the space  $X \times U$  of independent and dependent variables of the system with the property that whenever  $u = f(x)$  is a solution of  $\mathcal{S}$ , and whenever  $g \cdot f$  is defined for  $g \in G$ , then  $u = g \cdot f(x)$  is also a solution of the system.

For example, in the case of the ODE  $u_{xx} = 0$ , the rotation group  $SO(2)$  is obviously a symmetry group, since the solutions are all linear functions and  $SO(2)$  takes any linear function to another linear function. Another easy example is given by the classical *heat equation*  $u_t = u_{xx}$ . Here the group of translations

$$(x, t, u) \mapsto (x + \varepsilon a, t + \varepsilon b, u), \quad \varepsilon \in \mathbb{R},$$

is a symmetry group since  $u = f(x - \varepsilon a, t - \varepsilon b)$  is a solution to the heat equation whenever  $u = f(x, t)$  is.

### 3.5.4.2 Prolongations

**Prolongations of Functions.** Given a smooth real-valued function  $u = f(x) = f(x^1, \dots, x^p)$  of  $p$  independent variables, there is an induced function  $u^{(n)} = \mathbf{pr}^{(n)} f(x)$ , called the *n*th *prolongation* of  $f$  [Olver (1986)], which is defined by the equations

$$u_J = \partial_J f(x) = \frac{\partial^k f(x)}{\partial x^{j_1} \partial x^{j_2} \dots \partial x^{j_k}},$$

where the multi-index  $J = (j_1, \dots, j_k)$  is an unordered  $k$ -tuple of integers, with entries  $1 \leq j_k \leq p$  indicating which derivatives are being taken. More generally, if  $f : X \rightarrow U$  is a smooth function from  $X \simeq \mathbb{R}^p$  to  $U \simeq \mathbb{R}^q$ , so  $u = f(x) = (f^1(x), \dots, f^q(x))$ , there are  $q \cdot p_k$  numbers

$$u_J^\alpha = \partial_J f^\alpha(x) = \frac{\partial^k f^\alpha(x)}{\partial x^{j_1} \partial x^{j_2} \dots \partial x^{j_k}},$$

needed to represent all the different  $k$ th order derivatives of the components of  $f$  at a point  $x$ . Thus  $\mathbf{pr}^{(n)} f : X \rightarrow U^{(n)}$  is a function from  $X$  to the space  $U^{(n)}$ , and for each  $x \in X$ ,  $\mathbf{pr}^{(n)} f(x)$  is a vector whose  $q \cdot p^{(n)}$  entries represent the values of  $f$  and all its derivatives up to order  $n$  at the point  $x$ .

For example, in the case  $p = 2$ ,  $q = 1$  we have  $X \simeq \mathbb{R}^2$  with coordinates  $(x^1, x^2) = (x, y)$ , and  $U \simeq \mathbb{R}$  with the single coordinate  $u = f(x, y)$ . The second prolongation  $u^{(2)} = \mathbf{pr}^{(2)} f(x, y)$  is given by [Olver (1986)]

$$(u; u_x, u_y; u_{xx}, u_{xy}, u_{yy}) = \left( f; \frac{\partial f}{\partial x}, \frac{\partial f}{\partial y}; \frac{\partial^2 f}{\partial x^2}, \frac{\partial^2 f}{\partial x \partial y}, \frac{\partial^2 f}{\partial y^2} \right), \quad (3.30)$$

all evaluated at  $(x, y)$ .

The  $n$ th prolongation  $\mathbf{pr}^{(n)} f(x)$  is also known as the  $n$ -jet of  $f$ . In other words, the  $n$ th prolongation  $\mathbf{pr}^{(n)} f(x)$  represents the Taylor polynomial of degree  $n$  for  $f$  at the point  $x$ , since the derivatives of order  $\leq n$  determine the Taylor polynomial and vice versa.

**Prolongations of Differential Equations.** A system  $S$  of  $n$ th order DEs in  $p$  independent and  $q$  dependent variables is given as a system of equations [Olver (1986)]

$$\Delta_r(x, u^{(n)}) = 0, \quad r = 1, \dots, l \quad (3.31)$$

involving  $x = (x^1, \dots, x^p)$ ,  $u = (u^1, \dots, u^q)$  and the derivatives of  $u$  with respect to  $x$  up to order  $n$ . The functions  $\Delta(x, u^{(n)}) = (\Delta_1(x, u^{(n)}), \dots, \Delta_l(x, u^{(n)}))$  are assumed to be smooth in their arguments, so  $\Delta : X \times U^{(n)} \rightarrow \mathbb{R}^l$  represents a smooth map from the *jet space*  $X \times U^{(n)}$  to some  $l$ D Euclidean space. The DEs themselves tell where the given map  $\Delta$  vanishes on the jet space  $X \times U^{(n)}$ , and thus determine a submanifold

$$S_\Delta = \left\{ (x, u^{(n)}) : \Delta(x, u^{(n)}) = 0 \right\} \subset X \times U^{(n)} \quad (3.32)$$

of the total the jet space  $X \times U^{(n)}$ .

We can identify the system of DEs (3.31) with its corresponding submanifold  $S_\Delta$  (3.32). From this point of view, a smooth *solution* of the given

system of DEs is a smooth function  $u = f(x)$  such that [Olver (1986)]

$$\Delta_r(x, \mathbf{pr}^{(n)}f(x)) = 0, \quad r = 1, \dots, l,$$

whenever  $x$  lies in the domain of  $f$ . This is just a restatement of the fact that the derivatives  $\partial_J f^\alpha(x)$  of  $f$  must satisfy the algebraic constraints imposed by the system of DEs. This condition is equivalent to the statement that the graph of the prolongation  $\mathbf{pr}^{(n)}f(x)$  must lie entirely within the submanifold  $S_\Delta$  determined by the system:

$$\Gamma_f^{(n)} \equiv \left\{ (x, \mathbf{pr}^{(n)}f(x)) \right\} \subset S_\Delta = \left\{ \Delta(x, u^{(n)}) = 0 \right\}.$$

We can thus take an  $n$ th order system of DEs to be a submanifold  $S_\Delta$  in the  $n$ -jet space  $X \times U^{(n)}$  and a solution to be a function  $u = f(x)$  such that the graph of the  $n$ th prolongation  $\mathbf{pr}^{(n)}f(x)$  is contained in the submanifold  $S_\Delta$ .

For example, consider the case of *Laplace equation* in the plane

$$u_{xx} + u_{yy} = 0 \quad (u_x \equiv \partial_x u).$$

Here  $p = 2$  since there are two independent variables  $x$  and  $y$ , and  $q = 1$  since there is one dependent variable  $u$ . Also  $n = 2$  since the equation is second order, so  $S_\Delta \subset X \times U^{(2)}$  is given by (3.30). A solution  $u = f(x, y)$  must satisfy

$$\frac{\partial^2 f}{\partial x^2} + \frac{\partial^2 f}{\partial y^2} = 0$$

for all  $(x, y)$ . This is the same as requiring that the graph of the second prolongation  $\mathbf{pr}^{(2)}f$  lie in  $S_\Delta$ .

**Prolongations of Group Actions.** Let  $G$  be a local group of transformations acting on an open subset  $M \subset X \times U$  of the space of independent and dependent variables. There is an induced local action of  $G$  on the  $n$ -jet space  $M^{(n)}$ , called the  $n$ th prolongation  $\mathbf{pr}^{(n)}G$  of the action of  $G$  on  $M$ . This prolongation is defined so that it transforms the derivatives of functions  $u = f(x)$  into the corresponding derivatives of the transformed function  $\tilde{u} = \tilde{f}(\tilde{x})$  [Olver (1986)].

More precisely, suppose  $(x_0, u_0^{(n)})$  is a given point in  $M^{(n)}$ . Choose any smooth function  $u = f(x)$  defined in a neighborhood of  $x_0$ , whose graph  $\Gamma_f$  lies in  $M$ , and has the given derivatives at  $x_0$ :

$$u_0^{(n)} = \mathbf{pr}^{(n)}f(x_0), \quad \text{i.e.,} \quad u_{j_0}^\alpha = \partial_J f^\alpha(x_0).$$

If  $g$  is an element of  $G$  sufficiently near the identity, the transformed function  $g \cdot f$  as given by (3.29) is defined in a neighborhood of the corresponding point  $(\tilde{x}_0, \tilde{u}_0) = g \cdot (x_0, u_0)$ , with  $u_0 = f(x_0)$  being the zeroth order components of  $u_0^{(n)}$ . We then determine the action of the prolonged group of transformations  $\mathbf{pr}^{(n)}g$  on the point  $(x_0, u_0^{(n)})$  by evaluating the derivatives of the transformed function  $g \cdot f$  at  $\tilde{x}_0$ ; explicitly [Olver (1986)]

$$\mathbf{pr}^{(n)}g \cdot (x_0, u_0^{(n)}) = (\tilde{x}_0, \tilde{u}_0^{(n)}),$$

where

$$\tilde{u}_0^{(n)} \equiv \mathbf{pr}^{(n)}(g \cdot f)(\tilde{x}_0).$$

For example, let  $p = q = 1$ , so  $X \times U \simeq \mathbb{R}^2$ , and consider the action of the rotation group  $SO(2)$ . To calculate its first prolongation  $\mathbf{pr}^{(1)}SO(2)$ , first note that  $X \times U^{(1)} \simeq \mathbb{R}^3$ , with coordinates  $(x, u, u_x)$ . Given a function  $u = f(x)$ , the first prolongation is [Olver (1986)]

$$\mathbf{pr}^{(1)}f(x) = (f(x), f'(x)).$$

Now, given a point  $(x^0, u^0, u_x^0) \in X \times U^{(1)}$ , and a rotation in  $SO(2)$  characterized by the angle  $\theta$  as given above, the corresponding transformed point

$$\mathbf{pr}^{(1)}\theta \cdot (x^0, u^0, u_x^0) = (\tilde{x}^0, \tilde{u}^0, \tilde{u}_x^0)$$

(provided it exists). As for the first order derivative, we find

$$\tilde{u}_x^0 = \frac{\sin \theta + u_x \cos \theta}{\cos \theta - u_x \sin \theta}.$$

Now, applying the group transformations given above, and dropping the 0-indices, we find that the prolonged action  $\mathbf{pr}^{(1)}SO(2)$  on  $X \times U^{(1)}$  is given by

$$\mathbf{pr}^{(1)}\theta \cdot (x, u, u_x) = \left( x \cos \theta - u \sin \theta, x \sin \theta + u \cos \theta, \frac{\sin \theta + u_x \cos \theta}{\cos \theta - u_x \sin \theta} \right),$$

which is defined for  $|\theta| < |\operatorname{arccot} u_x|$ . Note that even though  $SO(2)$  is a linear, globally defined group of transformations, its first prolongation  $\mathbf{pr}^{(1)}SO(2)$  is both nonlinear and only locally defined. This fact demonstrates the complexity of the operation of prolonging a group of transformations.

In general, for any Lie group  $G$ , the first prolongation  $\mathbf{pr}^{(1)}G$  acts on the original variables  $(x, u)$  exactly the same way that  $G$  itself does; only



the action on the derivative  $u_x$  provides an new information. Therefore,  $\mathbf{pr}^{(0)}G$  agrees with  $G$  itself, acting on  $M^{(0)} = M$ .

**Prolongations of Vector Fields.** Prolongation of the infinitesimal generators of the group action turn out to be the *infinitesimal generators* of the *prolonged group action* [Olver (1986)]. Let  $M \subset X \times U$  be open and suppose  $v$  is a vector-field on  $M$ , with corresponding local one-parameter group  $\exp(\varepsilon v)$ . The  $n$ th prolongation of  $v$ , denoted  $\mathbf{pr}^{(n)}v$ , will be a vector-field on the  $n$ -jet space  $M^{(n)}$ , and is defined to be the infinitesimal generator of the corresponding prolonged on-parameter group  $\mathbf{pr}^{(n)}[\exp(\varepsilon v)]$ . In other words,

$$\mathbf{pr}^{(n)}v|_{(x, u^{(n)})} = \left. \frac{d}{d\varepsilon} \right|_{\varepsilon=0} \mathbf{pr}^{(n)}[\exp(\varepsilon v)](x, u^{(n)}) \quad (3.33)$$

for any  $(x, u^{(n)}) \in M^{(n)}$ .

For a vector-field  $v$  on  $M$ , given by

$$v = \xi^i(x, u) \frac{\partial}{\partial x^i} + \phi^\alpha(x, u) \frac{\partial}{\partial u^\alpha}, \quad i = 1, \dots, p, \alpha = 1, \dots, q,$$

the  $n$ th prolongation  $\mathbf{pr}^{(n)}v$  is given by [Olver (1986)]

$$\mathbf{pr}^{(n)}v = \xi^i(x, u) \frac{\partial}{\partial x^i} + \phi_J^\alpha(x, u^{(n)}) \frac{\partial}{\partial u_J^\alpha},$$

with  $\phi_0^\alpha = \phi^\alpha$ , and  $J$  a multiindex defined above.

For example, in the case of  $SO(2)$  group, the corresponding infinitesimal generator is

$$v = -u \frac{\partial}{\partial x} + x \frac{\partial}{\partial u}, \quad \text{with} \\ \exp(\varepsilon v)(x, u) = (x \cos \varepsilon - u \sin \varepsilon, x \sin \varepsilon + u \cos \varepsilon),$$

being the rotation through angle  $\varepsilon$ . The first prolongation takes the form

$$\mathbf{pr}^{(1)}[\exp(\varepsilon v)](x, u, u_x) = \left( x \cos \varepsilon - u \sin \varepsilon, x \sin \varepsilon + u \cos \varepsilon, \frac{\sin \varepsilon + u_x \cos \varepsilon}{\cos \varepsilon - u_x \sin \varepsilon} \right).$$

According to (3.33), the first prolongation of  $v$  is obtained by differentiating these expressions with respect to  $\varepsilon$  and setting  $\varepsilon = 0$ , which gives

$$\mathbf{pr}^{(1)}v = -u \frac{\partial}{\partial x} + x \frac{\partial}{\partial u} + (1 + u_x^2) \frac{\partial}{\partial u_x}.$$

**General Prolongation Formula.** Let

$$v = \xi^i(x, u) \frac{\partial}{\partial x^i} + \phi^\alpha(x, u) \frac{\partial}{\partial u^\alpha}, \quad i = 1, \dots, p, \alpha = 1, \dots, q \quad (3.34)$$

be a vector-field defined on an open subset  $M \subset X \times U$ . The  $n$ th prolongation of  $v$  is the vector-field [Olver (1986)]

$$\mathbf{pr}^{(n)}v = v + \phi_J^\alpha(x, u^{(n)}) \frac{\partial}{\partial u_J^\alpha}, \quad (3.35)$$

defined on the corresponding jet space  $M^{(n)} \subset X \times U^{(n)}$ . The coefficient functions  $\phi_J^\alpha$  are given by the following formula:

$$\phi_J^\alpha = D_J (\phi^\alpha - \xi^i u_i^\alpha) + \xi^i u_{J,i}^\alpha, \quad (3.36)$$

where  $u_i^\alpha = \partial u^\alpha / \partial x^i$ , and  $u_{J,i}^\alpha = \partial u_J^\alpha / \partial x^i$ .  $D_J$  is the *total derivative* with respect to the multiindex  $J$ , i.e.,

$$D_J = D_{j_1} D_{j_2} \dots D_{j_k},$$

while the total derivative with respect to the ordinary index,  $D_i$ , is defined as follows. Let  $P(x, u^{(n)})$  be a smooth function of  $x, u$  and derivatives of  $u$  up to order  $n$ , defined on an open subset  $M^{(n)} \subset X \times U^{(n)}$ . the total derivative of  $P$  with respect to  $x^i$  is the unique smooth function  $D_i P(x, u^{(n)})$  defined on  $M^{(n+1)}$  and depending on derivatives of  $u$  up to order  $n+1$ , with the *recursive property* that if  $u = f(x)$  is any smooth function then

$$D_i P(x, \mathbf{pr}^{(n+1)} f(x)) = \partial_{x^i} \{P(x, \mathbf{pr}^{(n)} f(x))\}.$$

For example, in the case of  $SO(2)$  group, with the infinitesimal generator

$$v = -u \frac{\partial}{\partial x} + x \frac{\partial}{\partial u},$$

the first prolongation is (as calculated above)

$$\mathbf{pr}^{(1)}v = -u \frac{\partial}{\partial x} + x \frac{\partial}{\partial u} + \phi^x \frac{\partial}{\partial u_x},$$

where

$$\phi^x = D_x(\phi - \xi u_x) + \xi u_{xx} = 1 + u_x^2.$$

Also,

$$\phi^{xx} = D_x \phi^x - u_{xx} D_x \xi = 3u_x u_{xx},$$

thus the infinitesimal generator of the second prolongation  $\mathbf{pr}^{(2)}SO(2)$  acting on  $X \times U^{(2)}$  is

$$\mathbf{pr}^{(2)}v = -u \frac{\partial}{\partial x} + x \frac{\partial}{\partial u} + (1 + u_x^2) \frac{\partial}{\partial u_x} + 3u_x u_{xx} \frac{\partial}{\partial u_{xx}}.$$

Let  $v$  and  $w$  be two smooth vector-fields on  $M \subset X \times U$ . Then their  $n$ th prolongations,  $\mathbf{pr}^{(n)}v$  and  $\mathbf{pr}^{(n)}w$  respectively, have the *linearity property*

$$\mathbf{pr}^{(n)}(c_1 v + c_2 w) = c_1 \mathbf{pr}^{(n)}v + c_2 \mathbf{pr}^{(n)}w, \quad (c_1, c_2 = \text{constant}),$$

and the *Lie bracket property*

$$\mathbf{pr}^{(n)}[v, w] = [\mathbf{pr}^{(n)}v, \mathbf{pr}^{(n)}w].$$

### 3.5.4.3 Special Biodynamic Equations

Here we consider two most important equations for human-like biodynamics:

- (1) The heat equation, which has been analyzed in muscular mechanics since the early works of A.V. Hill ([Hill (1938)]); and
- (2) The Korteweg-De Vries equation, the basic equation for solitary models of muscular excitation-contraction dynamics (see subsection (4.2.3.1) below).

Suppose

$$\mathcal{S} : \Delta_r(x, u^{(n)}) = 0, \quad (r = 1, \dots, l)$$

is a system of DEs of maximal rank defined over  $M \subset X \times U$ . If  $G$  is a local group of transformations acting on  $M$ , and

$$\mathbf{pr}^{(n)}v[\Delta_r(x, u^{(n)})] = 0, \quad \text{whenever} \quad \Delta(x, u^{(n)}) = 0, \quad (3.37)$$

(with  $r = 1, \dots, l$ ) for every infinitesimal generator  $v$  of  $G$ , then  $G$  is a symmetry group of the system  $\mathcal{S}$  [Olver (1986)].

**The Heat Equation.** The  $(1+1)$ D *heat equation* (with the thermal diffusivity normalized to unity)

$$u_t = u_{xx} \quad (3.38)$$

has two independent variables  $x$  and  $t$ , and one dependent variable  $u$ , so  $p = 2$  and  $q = 1$ . Equation (3.38) has the second order,  $n = 2$ , and can be identified with the linear submanifold  $M^{(2)} \subset X \times U^{(2)}$  determined by the vanishing of  $\Delta(x, t, u^{(2)}) = u_t - u_{xx}$ .

Let

$$v = \xi(x, t, u) \frac{\partial}{\partial x} + \tau(x, t, u) \frac{\partial}{\partial t} + \phi(x, t, u) \frac{\partial}{\partial u}.$$

be a vector-field on  $X \times U$ . According to (3.37) we need to now the second prolongation

$$\mathbf{pr}^{(2)}v = v + \phi^x \frac{\partial}{\partial u_x} + \phi^t \frac{\partial}{\partial u_t} + \phi^{xx} \frac{\partial}{\partial u_{xx}} + \phi^{xt} \frac{\partial}{\partial u_{xt}} + \phi^{tt} \frac{\partial}{\partial u_{tt}}$$

of  $v$ . Applying  $\mathbf{pr}^{(2)}v$  to (3.38) we find the criterion (3.37) to be

$$\phi^t = \phi^{xx},$$

which must be satisfied whenever  $u_t = u_{xx}$ .

**The Korteveg–De Vries Equation.** The Korteveg–De Vries equation

$$u_t + u_{xxx} + uu_x = 0 \quad (3.39)$$

arises in physical systems in which both nonlinear and dispersive effects are relevant. A vector-field

$$v = \xi(x, t, u) \frac{\partial}{\partial x} + \tau(x, t, u) \frac{\partial}{\partial t} + \phi(x, t, u) \frac{\partial}{\partial u}$$

generates a one-parameter symmetry group iff

$$\phi^t + \phi^{xxx} + u\phi^x + u_x\phi = 0,$$

whenever  $u$  satisfies (3.39), etc.

### 3.6 Riemannian Geometry in Biodynamics

In this section we develop the basic techniques of Riemannian geometry on the biodynamic manifold  $M$ , from both local and global perspective. We start with the local Riemannian notions of metric, geodesics and curvature on  $M$ , including the first variation formula and parallel transport along the vector-fields on  $M$ . After that we move to the global Riemannian notions on  $M$ , including the second variation and Gauss–Bonnet formulae, as well as the global Ricci flow on  $M$ . The last part of the section presents the structure equations on  $M$ , the basics of Morse theory (as a preparation for the next chapter), and the basics of (co)bordism theory.

### 3.6.1 Local Riemannian Geometry on $M$

An important class of problems in Riemannian geometry is to understand the interaction between the curvature and topology on a differentiable manifold [Cao and Chow (1999)]. A prime example of this interaction is the *Gauss–Bonnet formula* on a closed surface  $M^2$ , which says

$$\int_M K \, dA = 2\pi \chi(M), \quad (3.40)$$

where  $dA$  is the area element of a metric  $g$  on  $M$ ,  $K$  is the Gaussian curvature of  $g$ , and  $\chi(M)$  is the Euler characteristic of  $M$ .

To study the geometry of a differentiable manifold we need an additional structure: the *Riemannian metric*. The metric is an inner product on each of the tangent spaces and tells us how to measure angles and distances infinitesimally. In local coordinates  $(x^1, x^2, \dots, x^n)$ , the metric  $g$  is given by  $g_{ij}(x) \, dx^i \otimes dx^j$ , where  $(g_{ij}(x))$  is a positive definite symmetric matrix at each point  $x$ . For a differentiable manifold one can differentiate functions. A Riemannian metric defines a natural way of differentiating vector-fields: *covariant differentiation*. In Euclidean space, one can change the order of differentiation. On a Riemannian manifold the commutator of twice covariant differentiating vector-fields is in general nonzero and is called the *Riemann curvature tensor*, which is a 4-tensor-field on the manifold.

For surfaces, the Riemann curvature tensor is equivalent to the *Gauss curvature*  $K$ , a scalar function. In dimensions 3 or more, the Riemann curvature tensor is inherently a tensor-field. In local coordinates, it is denoted by  $R_{ijkl}$ , which is anti-symmetric in  $i$  and  $k$  and in  $j$  and  $l$ , and symmetric in the pairs  $\{ij\}$  and  $\{kl\}$ . Thus, it can be considered as a bilinear form on 2-forms which is called the *curvature operator*. We now describe heuristically the various curvatures associated to the *Riemann curvature tensor*. Given a point  $x \in M^n$  and 2-plane  $\Pi$  in the tangent space of  $M$  at  $x$ , we can define a surface  $S$  in  $M$  to be the union of all geodesics passing through  $x$  and tangent to  $\Pi$ . In a neighborhood of  $x$ ,  $S$  is a smooth 2D submanifold of  $M$ . We define the *sectional curvature*  $K(\Pi)$  of the 2-plane to be the Gauss curvature of  $S$  at  $x$ :

$$K(\Pi) = K_S(x).$$

Thus the sectional curvature  $K$  of a Riemannian manifold associates to each 2-plane in a tangent space a real number. Given a line  $L$  in a tangent space, we can average the sectional curvatures of all planes through  $L$  to

get the *Ricci curvature*  $Rc(L)$ . Likewise, given a point  $x \in M$ , we can average the Ricci curvatures of all lines in the tangent space of  $x$  to get the *scalar curvature*  $R(x)$ . In local coordinates, the *Ricci tensor* is given by  $R_{ik} = g^{jl} R_{ijkl}$  and the scalar curvature is given by  $R = g^{ik} R_{ik}$ , where  $(g^{ij}) = (g_{ij})^{-1}$  is the inverse of the metric tensor  $(g_{ij})$ .

### 3.6.1.1 Riemannian Metric on $M$

In this subsection we mainly follow [Petersen (1999); Petersen (1998)].

Riemann in 1854 observed that around each point  $m \in M$  one can pick a *special* coordinate system  $(x^1, \dots, x^n)$  such that there is a symmetric  $(0, 2)$ -tensor-field  $g_{ij}(m)$  called the *metric tensor* defined as

$$g_{ij}(m) = g(\partial_{x^i}, \partial_{x^j}) = \delta_{ij}, \quad \partial_{x^k} g_{ij}(m) = 0.$$

Thus the metric, at the specified point  $m \in M$ , in the coordinates  $(x^1, \dots, x^n)$  looks like the Euclidean metric on  $\mathbb{R}^n$ . We emphasize that these conditions only hold at the specified point  $m \in M$ . When passing to different points it is necessary to pick different coordinates. If a curve  $\gamma$  passes through  $m$ , say,  $\gamma(0) = m$ , then the acceleration at 0 is simply defined by firstly, writing the curve out in our special coordinates

$$\gamma(t) = (\gamma^1(t), \dots, \gamma^n(t)),$$

secondly, defining the tangent, *velocity* vector-field, as

$$\dot{\gamma} = \dot{\gamma}^i(t) \cdot \partial_{x^i},$$

and finally, the *acceleration* vector-field as

$$\ddot{\gamma}(0) = \ddot{\gamma}^i(0) \cdot \partial_{x^i}.$$

Here, the background idea is that we have a *connection*.

A vector-field  $X$  along a parameterized curve  $\alpha : I \rightarrow M$  in  $M$  is *tangent to  $M$  along  $\alpha$*  if  $X(t) \in M_{\alpha(t)}$  for all for  $t \in I \subset \mathbb{R}$ . The derivative  $\dot{X}$  of such a vector-field is, however, generally not tangent to  $M$ . We can, nevertheless, get a vector-field tangent to  $M$  by projecting  $\dot{X}(t)$  orthogonally onto  $M_{\alpha(t)}$  for each  $t \in I$ . This process of differentiating and then projecting onto the tangent space to  $M$  defines an operation with the same properties as differentiation, except that now differentiation of vector-fields tangent to  $M$  yields vector-fields tangent to  $M$ . This operation is called *covariant differentiation*.

Let  $\gamma : I \rightarrow M$  be a parameterized curve in  $M$ , and let  $X$  be a smooth vector-field tangent to  $M$  along  $\alpha$ . The *absolute covariant derivative* of  $X$  is the vector-field  $\dot{X}$  tangent to  $M$  along  $\alpha$ , defined by  $\dot{X} = \dot{X}(t) - [\dot{X}(t) \cdot N(\alpha(t))] N(\alpha(t))$ , where  $N$  is an orientation on  $M$ . Note that  $\dot{X}$  is independent of the choice of  $N$  since replacing  $N$  by  $-N$  has no effect on the above formula.

Lie bracket (3.5.1.2) defines a *symmetric affine connection*  $\nabla$  on any manifold  $M$ :

$$[X, Y] = \nabla_X Y - \nabla_Y X.$$

In case of a Riemannian manifold  $M$ , the connection  $\nabla$  is also compatible with the Riemannian metrics  $g$  on  $M$  and is called the *Levi-Civita connection* on  $TM$ .

For a function  $f \in C^k(M, \mathbb{R})$  and a vector a vector-field  $X \in \mathcal{X}^k(M)$  we always have the Lie derivative (3.5.1)

$$\mathcal{L}_X f = \nabla_X f = df(X).$$

But there is no natural definition for  $\nabla_X Y$ , where  $Y \in \mathcal{X}^k(M)$ , unless one also has a Riemannian metric. Given the tangent field  $\dot{\gamma}$ , the acceleration can then be computed by using a Leibniz rule on the r.h.s, if we can make sense of the derivative of  $\partial_{x^i}$  in the direction of  $\dot{\gamma}$ . This is exactly what the *covariant derivative*  $\nabla_X Y$  does. If  $Y \in T_m M$  then we can simply write  $Y = a^i \partial_{x^i}$ , and therefore

$$\nabla_X Y = \mathcal{L}_X a^i \partial_{x^i}. \quad (3.41)$$

Since there are several ways of choosing these coordinates, one must check that the definition does not depend on the choice. Note that for two vector-fields we define  $(\nabla_Y X)(m) = \nabla_{Y(m)} X$ . In the end we get a *connection*

$$\nabla : \mathcal{X}^k(M) \times \mathcal{X}^k(M) \rightarrow \mathcal{X}^k(M),$$

which satisfies (for all  $f \in C^k(M, \mathbb{R})$  and  $X, Y, Z \in \mathcal{X}^k(M)$ ):

- (1)  $Y \rightarrow \nabla_Y X$  is tensorial, i.e., linear and  $\nabla_{fY} X = f \nabla_Y X$ .
- (2)  $X \rightarrow \nabla_Y X$  is linear.
- (3)  $\nabla_X (fY) = (\nabla_X f)Y(m) + f(m) \nabla_X Y$ .
- (4)  $\nabla_X Y - \nabla_Y X = [X, Y]$ .
- (5)  $\mathcal{L}_X g(Z, Y) = g(\nabla_X Z, Y) + g(Z, \nabla_X Y)$ .

A semicolon is commonly used to denote covariant differentiation with respect to a natural basis vector. If  $X = \partial_{x^i}$ , then the components of  $\nabla_X Y$  in (3.41) are denoted

$$Y^k_{;i} = \partial_{x^i} Y^k + \Gamma^k_{ij} Y^j, \quad (3.42)$$

where  $\Gamma^k_{ij}$  are *Christoffel symbols* defined in (3.43) below. Similar relations hold for higher-order tensor-fields (with as many terms with Christoffel symbols as is the tensor valence).

Therefore, no matter which coordinates we use, we can now define the acceleration of a curve in the following way:

$$\begin{aligned} \gamma(t) &= (\gamma^1(t), \dots, \gamma^n(t)), \\ \dot{\gamma}(t) &= \dot{\gamma}^i(t) \partial_{x^i}, \\ \ddot{\gamma}(t) &= \ddot{\gamma}^i(t) \partial_{x^i} + \dot{\gamma}^i(t) \nabla_{\dot{\gamma}(t)} \partial_{x^i}. \end{aligned}$$

We call  $\gamma$  a *geodesic* if  $\ddot{\gamma}(t) = 0$ . This is a second order nonlinear ODE in a fixed coordinate system  $(x^1, \dots, x^n)$  at the specified point  $m \in M$ . Thus we see that given any tangent vector  $X \in T_m M$ , there is a unique geodesic  $\gamma_X(t)$  with  $\dot{\gamma}_X(0) = X$ . If the manifold  $M$  is closed, the geodesic must exist for all time, but in case the manifold  $M$  is open this might not be so. To see this, simply take as  $M$  any open subset of Euclidean space with the induced metric.

Given an arbitrary vector-field  $Y(t)$  along  $\gamma$ , i.e.,  $Y(t) \in T_{\gamma(t)} M$  for all  $t$ , we can also define the derivative  $\dot{Y} \equiv \frac{dY}{dt}$  in the direction of  $\dot{\gamma}$  by writing

$$\begin{aligned} Y(t) &= a^i(t) \partial_{x^i}, \\ \dot{Y}(t) &= \dot{a}^i(t) \partial_{x^i} + a^i(t) \nabla_{\dot{\gamma}(t)} \partial_{x^i}. \end{aligned}$$

Here the derivative of the tangent field  $\dot{\gamma}$  is simply the acceleration  $\ddot{\gamma}$ . The field  $Y$  is said to be *parallel* iff  $\dot{Y} = 0$ . The equation for a field to be parallel is a first order linear ODE, so we see that for any  $X \in T_{\gamma(t_0)} M$  there is a unique parallel field  $Y(t)$  defined on the entire domain of  $\gamma$  with the property that  $Y(t_0) = X$ . Given two such parallel fields  $Y, Z \in \mathcal{X}^k(M)$ , we have that

$$\dot{g}(Y, Z) = D_{\dot{\gamma}} g(Y, Z) = g(\dot{Y}, Z) + g(Y, \dot{Z}) = 0.$$

Thus  $X$  and  $Y$  are both of constant length and form constant angles along  $\gamma$ . Hence, ‘parallel translation’ along a curve defines an orthogonal transformation between the tangent spaces to the manifold along the curve. However,



in contrast to Euclidean space, this parallel translation will depend on the choice of curve.

An infinitesimal distance between the two nearby local points  $m$  and  $n$  on  $M$  is defined by an *arc-element*

$$ds^2 = g_{ij} dx^i dx^j,$$

and realized by the curves  $x^i(s)$  of shortest distance, called *geodesics*, addressed by the *Hilbert 4th problem*. In local coordinates  $(x^1(s), \dots, x^n(s))$  at a point  $m \in M$ , the geodesic defining equation is a second order ODE,

$$\ddot{x}^i + \Gamma_{jk}^i \dot{x}^j \dot{x}^k = 0,$$

where the overdot denotes the derivative with respect to the affine parameter  $s$ ,  $\dot{x}^i(s) = \frac{d}{ds} x^i(s)$  is the tangent vector to the base geodesic, while the *Christoffel symbols*  $\Gamma_{jk}^i = \Gamma_{jk}^i(m)$  (see Appendix) of the *affine connection* (Levi-Civita)  $\nabla$  at the point  $m \in M$  are defined as

$$\begin{aligned} \Gamma_{ij}^k &= g^{kl} \Gamma_{ijl}, \quad \text{with} \quad g^{ij} = (g_{ij})^{-1} \quad \text{and} \quad (3.43) \\ \Gamma_{ijk} &= \frac{1}{2} (\partial_{x^i} g_{jk} - \partial_{x^j} g_{ki} + \partial_{x^k} g_{ij}). \end{aligned}$$

The *torsion* tensor-field  $T$  of the connection  $\nabla$  is the function  $T : \mathcal{X}^k(M) \times \mathcal{X}^k(M) \rightarrow \mathcal{X}^k(M)$  given by

$$T(X, Y) = \nabla_X Y - \nabla_Y X - [X, Y].$$

From the skew symmetry ( $[X, Y] = -[Y, X]$ ) of the Lie bracket, follows the skew symmetry ( $T(X, Y) = -T(Y, X)$ ) of the torsion tensor. The mapping  $T$  is said to be  $f$ -bilinear since it is linear in both arguments and also satisfies  $T(fX, Y) = fT(X, Y)$  for smooth functions  $f$ . Since  $[\partial_{x^i}, \partial_{x^j}] = 0$  for all  $1 \leq i, j \leq n$ , it follows that

$$T(\partial_{x^i}, \partial_{x^j}) = (\Gamma_{ij}^k - \Gamma_{ji}^k) \partial_{x^k}. \quad (3.44)$$

Consequently, torsion  $T$  is a  $(1, 2)$  tensor-field which is given in local coordinates by

$$T = T_{ij}^k dx^i \otimes \partial_{x^k} \otimes dx^j, \quad (3.45)$$

where the torsion components  $T_{ij}^k$  are given by

$$T_{ij}^k = \Gamma_{ij}^k - \Gamma_{ji}^k. \quad (3.46)$$

Therefore, the torsion tensor provides a measure of the nonsymmetry of the connection coefficients. Hence,  $T = 0$  if and only if these coefficients are symmetric in their subscripts. A connection  $\nabla$  with  $T = 0$  is said to be *torsion free* or *symmetric*.

The connection also enables us to define many other classical concepts from calculus in the setting of Riemannian manifolds. Suppose we have a function  $f \in C^k(M, \mathbb{R})$ . If the manifold is not equipped with a Riemannian metric, then we have the differential of  $f$  defined by  $df(X) = \mathcal{L}_X f$ , which is a 1-form. The dual concept, the *gradient* of  $f$ , is supposed to be a vector-field. But we need a metric  $g$  to define it. Namely,  $\nabla f$  is defined by the relationship

$$g(\nabla f, X) = df(X).$$

Having defined the gradient of a function on a Riemannian manifold, we can then use the connection to define the *Hessian* as the linear map

$$\nabla^2 f : TM \rightarrow TM, \quad \nabla^2 f(X) = \nabla_X \nabla f.$$

The corresponding bilinear map is then defined as

$$\nabla^2 f(X, Y) = g(\nabla^2 f(X), Y).$$

One easily checks that this is a symmetric bilinear form. The *Laplacian* of  $f$ ,  $\Delta f$ , is now defined as the trace of the Hessian

$$\Delta f = \text{Tr}(\nabla^2 f(X)) = \text{Tr}(\nabla_X \nabla f),$$

which is a linear map. It is also called the *Laplace–Beltrami operator*, since Beltrami first considered this operator on Riemannian manifolds.

### 3.6.1.2 Geodesics on $M$

For a  $C^k$ ,  $k \geq 2$  curve  $\gamma : I \rightarrow M$ , we define its *length* on  $I$  as

$$L(\gamma, I) = \int_I |\dot{\gamma}| \, dt = \int_I \sqrt{g(\dot{\gamma}, \dot{\gamma})} \, dt.$$

This length is independent of our parametrization of the curve  $\gamma$ . Thus the curve  $\gamma$  can be reparameterized, in such a way that it has unit velocity. The *distance between two points*  $m_1$  and  $m_2$  on  $M$ ,  $d(m_1, m_2)$ , can now be defined as the infimum of the lengths of all curves from  $m_1$  to  $m_2$ , i.e.,

$$L(\gamma, I) \rightarrow \min.$$

This means that the distance measures the shortest way one can travel from  $m_1$  to  $m_2$ .

If we take a variation  $V(s, t) : (-\varepsilon, \varepsilon) \times [0, \ell] \rightarrow M$  of a smooth curve  $\gamma(t) = V(0, t)$  parameterized by arc-length  $L$  and of length  $\ell$ , then the first derivative of the arc-length function

$$L(s) = \int_0^\ell |\dot{V}| dt, \quad \text{is given by}$$

$$\frac{dL(0)}{ds} \equiv \dot{L}(0) = g(\dot{\gamma}, X)|_0^\ell - \int_0^\ell g(\gamma, X) dt, \quad (3.47)$$

where  $X(t) = \frac{\partial V}{\partial s}(0, t)$  is the so-called *variation vector-field*. Equation (3.47) is called the *first variation formula*. Given any vector-field  $X$  along  $\gamma$ , one can produce a variation whose variational field is  $X$ . If the variation fixes the endpoints,  $X(a) = X(b) = 0$ , then the second term in the formula drops out, and we note that the length of  $\gamma$  can always be decreased as long as the acceleration of  $\gamma$  is not everywhere zero. Thus the *Euler-Lagrange equation* for the arc-length functional is simply the equation for a curve to be a *geodesic*.

In local coordinates  $x^i \in U$ , where  $U$  is an open subset in the Riemannian manifold  $M$ , the geodesics are defined by the *geodesic equation* (see Appendix)

$$\ddot{x}^i + \Gamma_{jk}^i \dot{x}^j \dot{x}^k = 0, \quad (3.48)$$

where overdot means derivative upon the line parameter  $s$ , while  $\Gamma_{jk}^i$  are Christoffel symbols of the affine Levi-Civita connection  $\nabla$  on  $M$ . From (3.48) it follows that the linear *connection homotopy*,

$$\bar{\Gamma}_{jk}^i = s\Gamma_{jk}^i + (1-s)\Gamma_{jk}^i, \quad (0 \leq s \leq 1),$$

determines the same geodesics as the original  $\Gamma_{jk}^i$ .

### 3.6.1.3 Riemannian Curvature on $M$

The *Riemann curvature tensor* is a rather ominous tensor of type  $(1, 3)$ ; i.e., it has three vector variables and its value is a vector as well. It is defined through the Lie bracket (3.5.1.2) as

$$R(X, Y)Z = (\nabla_{[X, Y]} - [\nabla_X, \nabla_Y])Z = \nabla_{[X, Y]}Z - \nabla_X \nabla_Y Z + \nabla_Y \nabla_X Z.$$

This turns out to be a vector valued  $(1, 3)$ -tensor-field in the three variables  $X, Y, Z \in \mathcal{X}^k(M)$ . We can then create a  $(0, 4)$ -tensor with scalar values as

follows

$$R(X, Y, Z, W) = g(\nabla_{[X, Y]}Z - \nabla_X \nabla_Y Z + \nabla_Y \nabla_X Z, W).$$

Clearly this tensor is skew-symmetric in  $X$  and  $Y$ , and also in  $Z$  and  $W \in \mathcal{X}^k(M)$ . This was already known to Riemann, but there are some further, more subtle properties that were discovered a little later by Bianchi. The *Bianchi symmetry condition* reads

$$R(X, Y, Z, W) = R(Z, W, X, Y).$$

Thus the Riemannian curvature tensor can be thought of as a symmetric operator

$$\mathfrak{R} : \Lambda^2 TM \rightarrow \Lambda^2 TM,$$

also known as the *curvature operator*.

The *Ricci tensor* is the  $(1, 1)$ - or  $(0, 2)$ -tensor defined by

$$\text{Ric}(X) = R(\partial_{x^i}, X)\partial_{x^i}, \quad \text{Ric}(X, Y) = g(R(\partial_{x^i}, X)\partial_{x^i}, Y),$$

for any orthonormal basis  $(\partial_{x^i})$ . In other words, the Ricci curvature is simply a trace of the curvature tensor. Similarly one can define the *scalar curvature* as the trace

$$\text{scal}(m) = \text{Tr}(\text{Ric}) = \text{Ric}(\partial_{x^i}, \partial_{x^i}).$$

When the Riemannian manifold has dimension 2, all of these curvatures are essentially the same. Since  $\dim \Lambda^2 TM = 1$  and is spanned by  $X \wedge Y$  where  $X, Y \in \mathcal{X}^k(M)$  form an orthonormal basis for  $T_m M$ , we see that the curvature tensor depends only on the scalar value

$$K(m) = R(X, Y, X, Y),$$

which also turns out to be the *Gaussian curvature*. The Ricci tensor is a *homothety*

$$\text{Ric}(X) = K(m)X, \quad \text{Ric}(Y) = K(m)Y,$$

and the scalar curvature is twice the Gauss curvature. In dimension 3 there are also some redundancies as  $\dim TM = \dim \Lambda^2 TM = 3$ . In particular, the Ricci tensor and the curvature tensor contain the same amount of information.

The *sectional curvature* is a kind of generalization of the Gauss curvature whose importance Riemann was already aware of. Given a 2-plane  $\pi \subset T_m M$  spanned by an orthonormal basis  $X, Y \in \mathcal{X}^k(M)$  it is defined as

$$\sec(\pi) = R(X, Y, X, Y).$$

The remarkable observation by Riemann was that the *curvature operator* is a *homothety*, i.e., looks like  $\mathfrak{R} = kI$  on  $\Lambda^2 T_m M$  iff all sectional curvatures of planes in  $T_m M$  are equal to  $k$ . This result is not completely trivial, as the sectional curvature is not the entire quadratic form associated to the symmetric operator  $\mathfrak{R}$ . In fact, it is not true that  $\sec \geq 0$  implies that the curvature operator is nonnegative in the sense that all its eigenvalues are nonnegative. What Riemann did was to show that our special coordinates  $(x^1, \dots, x^n)$  at  $m$  can be chosen to be *normal* at  $m$ , i.e., satisfy the stronger condition

$$x^i = \delta_j^i x^j, \quad (\delta_j^i x^j = g_{ij})$$

on a neighborhood of  $m$ . One can easily show that such coordinates are actually exponential coordinates together with a choice of an orthonormal basis for  $T_m M$  so as to identify  $T_m M$  with  $\mathbb{R}^n$ . In these coordinates one can then expand the metric as follows:

$$g_{ij} = \delta_{ij} - \frac{1}{3} R_{ikjl} x^k x^l + O(r^3).$$

Now the equations  $x^i = g_{ij} x^j$  evidently give conditions on the curvatures  $R_{ijkl}$  at  $m$ .

If  $\Gamma_{jk}^i(m) = 0$ , the manifold  $M$  is flat at the point  $m$ . This means that the  $(1, 3)$  curvature tensor, defined locally at  $m \in M$  as

$$R_{ijk}^l = \partial_{x^j} \Gamma_{ik}^l - \partial_{x^k} \Gamma_{ij}^l + \Gamma_{rj}^l \Gamma_{ik}^r - \Gamma_{rk}^l \Gamma_{ij}^r,$$

also vanishes at that point, i.e.,  $R_{ijk}^l(m) = 0$ .

Now, the rate of change of a vector-field  $A^k$  on the manifold  $M$  along the curve  $x^i(s)$  is properly defined by the *absolute covariant derivative*

$$\frac{D}{ds} A^k = \dot{x}^i \nabla_i A^k = \dot{x}^i (\partial_{x^i} A^k + \Gamma_{ij}^k A^j) = \dot{A}^k + \Gamma_{ij}^k \dot{x}^i A^j.$$

By applying this result to itself, we can get an expression for the second covariant derivative of the vector-field  $A^k$  along the curve  $x^i(s)$ :

$$\frac{D^2}{ds^2} A^k = \frac{d}{ds} \left( \dot{A}^k + \Gamma_{ij}^k \dot{x}^i A^j \right) + \Gamma_{ij}^k \dot{x}^i (\dot{A}^j + \Gamma_{mn}^j \dot{x}^m A^n).$$

In the local coordinates  $(x^1(s), \dots, x^n(s))$  at a point  $m \in M$ , if  $\delta x^i = \delta x^i(s)$  denotes the *geodesic deviation*, i.e., the infinitesimal vector describing perpendicular separation between the two neighboring geodesics, passing through two neighboring points  $m, n \in M$ , then the *Jacobi equation of geodesic deviation* on the manifold  $M$  holds:

$$\frac{D^2 \delta x^i}{ds^2} + R_{jkl}^i \dot{x}^j \delta x^k \dot{x}^l = 0. \quad (3.49)$$

This equation describes the *relative acceleration* between two infinitesimally close facial geodesics, which is proportional to the facial curvature (measured by the Riemann tensor  $R_{jkl}^i$  at a point  $m \in M$ ), and to the geodesic deviation  $\delta x^i$ . Solutions of equation (3.49) are called *Jacobi fields*.

In particular, if the manifold  $M$  is a 2D-surface in  $\mathbb{R}^3$ , the Riemann curvature tensor simplifies into

$$R_{jmn}^i = \frac{1}{2} R g^{ik} (g_{km} g_{jn} - g_{kn} g_{jm}),$$

where  $R$  denotes the *scalar curvature*. Consequently the equation of geodesic deviation (3.49) also simplifies into

$$\frac{D^2}{ds^2} \delta x^i + \frac{R}{2} \delta x^i - \frac{R}{2} \dot{x}^i (g_{jk} \dot{x}^j \delta x^k) = 0. \quad (3.50)$$

This simplifies even more if we work in a locally Cartesian coordinate system; in this case the covariant derivative  $\frac{D^2}{ds^2}$  reduces to an ordinary derivative  $\frac{d^2}{ds^2}$  and the metric tensor  $g_{ij}$  reduces to identity matrix  $I_{ij}$ , so our 2D equation of geodesic deviation (3.50) reduces into a simple second order ODE in just two coordinates  $x^i$  ( $i = 1, 2$ )

$$\ddot{x}^i + \frac{R}{2} \delta x^i - \frac{R}{2} \dot{x}^i (I_{jk} \dot{x}^j \delta x^k) = 0.$$

### 3.6.2 Global Riemannian Geometry on $M$

#### 3.6.2.1 The Second Variation Formula

Cartan also establishes another important property of manifolds with non-positive curvature. First he observes that all spaces of constant zero curvature have torsion-free fundamental groups. This is because any isometry of finite order on Euclidean space must have a fixed point (the center of mass of any orbit is necessarily a fixed point). Then he notices that one can geometrically describe the  $L^\infty$  center of mass of finitely many points

$\{m_1, \dots, m_k\}$  in Euclidean space as the unique minimum for the strictly convex function

$$x \rightarrow \max_{i=1, \dots, k} \frac{1}{2} \left\{ (d(m_i, x))^2 \right\}.$$

In other words, the center of mass is the center of the ball of smallest radius containing  $\{m_1, \dots, m_k\}$ . Now Cartan's observation from above was that the exponential map is expanding and globally distance nondecreasing as a map:

$$(T_m M, \text{Euclidean metric}) \rightarrow (T_m M, \text{with pull-back metric}).$$

Thus distance functions are convex in nonpositive curvature as well as in Euclidean space. Hence the above argument can in fact be used to conclude that any Riemannian manifold of nonpositive curvature must also have torsion free fundamental group.

Now, let us set up the *second variation formula* and explain how it is used. We have already seen the first variation formula and how it can be used to characterize geodesics. Now suppose that we have a unit speed geodesic  $\gamma(t)$  parameterized on  $[0, \ell]$  and consider a variation  $V(s, t)$ , where  $V(0, t) = \gamma(t)$ . Synge then shows that ( $\ddot{L} \equiv \frac{d^2 L}{ds^2}$ )

$$\ddot{L}(0) = \int_0^\ell \{g(\dot{X}, \dot{X}) - (g(\dot{X}, \dot{\gamma}))^2 - g(R(X, \dot{\gamma})X, \dot{\gamma})\} dt + g(\dot{\gamma}, A)|_0^\ell,$$

where  $X(t) = \frac{\partial V}{\partial s}(0, t)$  is the variational vector-field,  $\dot{X} = \nabla_{\dot{\gamma}} X$ , and  $A(t) = \nabla_{\frac{\partial V}{\partial s}} X$ . In the special case where the variation fixes the endpoints, i.e.,  $s \rightarrow V(s, a)$  and  $s \rightarrow V(s, b)$  are constant, the term with  $A$  in it falls out. We can also assume that the variation is perpendicular to the geodesic and then drop the term  $g(\dot{X}, \dot{\gamma})$ . Thus, we arrive at the following simple form:

$$\ddot{L}(0) = \int_0^\ell \{g(\dot{X}, \dot{X}) - g(R(X, \dot{\gamma})X, \dot{\gamma})\} dt = \int_0^\ell \{|\dot{X}|^2 - \sec(\dot{\gamma}, X)|X|^2\} dt.$$

Therefore, if the sectional curvature is nonpositive, we immediately observe that any geodesic locally minimizes length (that is, among close-by curves), even if it does not minimize globally (for instance  $\gamma$  could be a closed geodesic). On the other hand, in positive curvature we can see that if a geodesic is too long, then it cannot minimize even locally. The motivation for this result comes from the unit sphere, where we can consider geodesics of length  $> \pi$ . Globally, we of course know that it would be shorter to go in

the opposite direction. However, if we consider a variation of  $\gamma$  where the variational field looks like  $X = \sin\left(t \cdot \frac{\pi}{\ell}\right) E$  and  $E$  is a unit length parallel field along  $\gamma$  which is also perpendicular to  $\gamma$ , then we get

$$\begin{aligned}\ddot{L}(0) &= \int_0^\ell \left\{ \left| \dot{X} \right|^2 - \sec(\dot{\gamma}, X) |X|^2 \right\} dt \\ &= \int_0^\ell \left\{ \left( \frac{\pi}{\ell} \right)^2 \cdot \cos^2 \left( t \cdot \frac{\pi}{\ell} \right) - \sec(\dot{\gamma}, X) \sin^2 \left( t \cdot \frac{\pi}{\ell} \right) \right\} dt \\ &= \int_0^\ell \left( \left( \frac{\pi}{\ell} \right)^2 \cdot \cos^2 \left( t \cdot \frac{\pi}{\ell} \right) - \sin^2 \left( t \cdot \frac{\pi}{\ell} \right) \right) dt = -\frac{1}{2\ell} (\ell^2 - \pi^2),\end{aligned}$$

which is negative if the length  $\ell$  of the geodesic is greater than  $\pi$ . Therefore, the variation gives a family of curves that are both close to and shorter than  $\gamma$ . In the general case, we can then observe that if  $\sec \geq 1$ , then for the same type of variation we get

$$\ddot{L}(0) \leq -\frac{1}{2\ell} (\ell^2 - \pi^2).$$

Thus we can conclude that, if the space is complete, then the diameter must be  $\leq \pi$  because in this case any two points are joined by a segment, which cannot minimize if it has length  $> \pi$ . With some minor modifications one can now conclude that any complete Riemannian manifold  $(M, g)$  with  $\sec \geq k^2 > 0$  must satisfy  $\text{diam}(M, g) \leq \pi \cdot k^{-1}$ . In particular,  $M$  must be compact. Since the universal covering of  $M$  satisfies the same curvature hypothesis, the conclusion must also hold for this space; hence  $M$  must have compact universal covering space and finite fundamental group.

In odd dimensions all spaces of constant positive curvature must be orientable, as orientation reversing orthogonal transformation on odd-dimensional spheres have fixed points. This can now be generalized to manifolds of varying positive curvature. Synge did it in the following way: Suppose  $M$  is not simply connected (or not orientable), and use this to find a shortest closed geodesic in a free homotopy class of curves (that reverses orientation). Now consider parallel translation around this geodesic. As the tangent field to the geodesic is itself a parallel field, we see that parallel translation preserves the orthogonal complement to the geodesic. This complement is now odd dimensional (even dimensional), and by assumption parallel translation preserves (reverses) the orientation; thus it must have a fixed point. In other words, there must exist a closed parallel field  $X$  perpendicular to the closed geodesic  $\gamma$ . We can now use the above second



variation formula

$$\ddot{L}(0) = \int_0^\ell \{ |\dot{X}|^2 - |X|^2 \sec(\dot{\gamma}, X) \} dt + g(\dot{\gamma}, A)|_0^\ell = - \int_0^\ell |X|^2 \sec(\dot{\gamma}, X) dt.$$

Here the boundary term drops out because the variation closes up at the endpoints, and  $\dot{X} = 0$  since we used a parallel field. In case the sectional curvature is always positive we then see that the above quantity is negative. But this means that the closed geodesic has nearby closed curves which are shorter. This is, however, in contradiction with the fact that the geodesic was constructed as a length minimizing curve in a free homotopy class.

In 1941 Myers generalized the diameter bound to the situation where one only has a lower bound for the Ricci curvature. The idea is simply that  $\text{Ric}(\dot{\gamma}, \dot{\gamma}) = \sum_{i=1}^{n-1} \sec(E_i, \dot{\gamma})$  for any set of vector-fields  $E_i$  along  $\gamma$  such that  $\dot{\gamma}, E_1, \dots, E_{n-1}$  forms an orthonormal frame. Now assume that the fields are parallel and consider the  $n-1$  variations coming from the variational vector-fields  $\sin(t \cdot \frac{\pi}{\ell}) E_i$ . Adding up the contributions from the variational formula applied to these fields then yields

$$\begin{aligned} \sum_{i=1}^{n-1} \ddot{L}(0) &= \sum_{i=1}^{n-1} \int_0^\ell \left\{ \left( \frac{\pi}{\ell} \right)^2 \cdot \cos^2 \left( t \cdot \frac{\pi}{\ell} \right) - \sec(\dot{\gamma}, E_i) \sin^2 \left( t \cdot \frac{\pi}{\ell} \right) \right\} dt \\ &= \int_0^\ell \left\{ (n-1) \left( \frac{\pi}{\ell} \right)^2 \cdot \cos^2 \left( t \cdot \frac{\pi}{\ell} \right) - \text{Ric}(\dot{\gamma}, \dot{\gamma}) \sin^2 \left( t \cdot \frac{\pi}{\ell} \right) \right\} dt. \end{aligned}$$

Therefore, if  $\text{Ric}(\dot{\gamma}, \dot{\gamma}) \geq (n-1)k^2$  (this is the Ricci curvature of  $S_k^n$ ), then we get

$$\begin{aligned} \sum_{i=1}^{n-1} \ddot{L}(0) &\leq (n-1) \int_0^\ell \left\{ \left( \frac{\pi}{\ell} \right)^2 \cdot \cos^2 \left( t \cdot \frac{\pi}{\ell} \right) - k^2 \sin^2 \left( t \cdot \frac{\pi}{\ell} \right) \right\} dt \\ &= -(n-1) \frac{1}{2\ell} (\ell^2 k^2 - \pi^2), \end{aligned}$$

which is negative when  $\ell > \pi \cdot k^{-1}$  (the diameter of  $S_k^n$ ). Thus at least one of the contributions  $\frac{d^2 L_i}{ds^2}(0)$  must be negative as well, implying that the geodesic cannot be a segment in this situation.

### 3.6.2.2 Gauss-Bonnet Formula

In 1926 Hopf proved that in fact there is a Gauss-Bonnet formula for all even-dimensional hypersurfaces  $H^{2n} \subset \mathbb{R}^{2n+1}$ . The idea is simply that the determinant of the differential of the Gauss map  $G : H^{2n} \rightarrow S^{2n}$  is the

Gaussian curvature of the hypersurface. Moreover, this is an intrinsically computable quantity. If we integrate this over the hypersurface, we get, as Kronecker did for surfaces,

$$\frac{1}{\text{vol } S^{2n}} \int_H \det(DG) = \deg(G),$$

where  $\deg(G)$  is the *Brouwer degree of the Gauss map*. Note that this can also be done for odd-dimensional surfaces, in particular curves, but in this case the degree of the Gauss map will depend on the embedding or immersion of the hypersurface. Instead one gets the so-called winding number. Hopf then showed, as Dyck had earlier done for surfaces, that  $\deg(G)$  is always half the *Euler characteristic* of  $H$ , thus yielding

$$\frac{2}{\text{vol } S^{2n}} \int_H \det(DG) = \chi(H). \quad (3.51)$$

Since the l.h.s of this formula is in fact intrinsic, it is natural to conjecture that such a formula should hold for all manifolds.

### 3.6.2.3 Ricci Flow on $M$

*Ricci flow*, or the *parabolic Einstein equation*, was introduced by R. Hamilton in 1982 [Hamilton (1982)] in the form

$$\partial_t g_{ij} = -2R_{ij}. \quad (3.52)$$

Now, because of the minus sign in the front of the Ricci tensor  $R_{ij}$  in this equation, the solution metric  $g_{ij}$  to the Ricci flow shrinks in positive Ricci curvature direction while it expands in the negative Ricci curvature direction. For example, on the 2-sphere  $S^2$ , any metric of positive Gaussian curvature will shrink to a point in finite time. Since the Ricci flow (3.52) does not preserve volume in general, one often considers the *normalized Ricci flow* defined by

$$\partial_t g_{ij} = -2R_{ij} + \frac{2}{n} r g_{ij}, \quad (3.53)$$

where  $r = \int R dV / \int dV$  is the average scalar curvature. Under this normalized flow, which is equivalent to the (unnormalized) Ricci flow (3.52) by reparameterizing in time  $t$  and scaling the metric in space by a function of  $t$ , the volume of the solution metric is constant in time. Also that Einstein metrics (i.e.,  $R_{ij} = c g_{ij}$ ) are fixed points of (3.53).

Hamilton [Hamilton (1982)] showed that on a closed Riemannian 3-manifold  $M^3$  with initial metric of positive Ricci curvature, the solution  $g(t)$  to the normalized Ricci flow (3.53) exists for all time and the metrics  $g(t)$  converge exponentially fast, as time  $t$  tends to the infinity, to a constant positive sectional curvature metric  $g_\infty$  on  $M^3$ . In particular, such a  $M^3$  is necessarily diffeomorphic to a quotient of the 3-sphere  $S^3$  by a finite group of isometries.

Since the Ricci flow lies in the realm of parabolic partial differential equations, where the prototype is the heat equation, here is a brief review of the heat equation [Cao and Chow (1999)].

Let  $(M^n, g)$  be a Riemannian manifold. Given a  $C^2$  function  $u : M \rightarrow \mathbb{R}$ , its Laplacian is defined in local coordinates  $\{x^i\}$  to be

$$\Delta u = \text{Tr} (\nabla^2 u) = g^{ij} \nabla_i \nabla_j u,$$

where  $\nabla_i = \nabla_{\partial_{x^i}}$  is its associated covariant derivative (Levi-Civita connection). We say that a  $C^2$  function  $u : M^n \times [0, T) \rightarrow \mathbb{R}$ , where  $T \in (0, \infty]$ , is a solution to the heat equation if

$$\partial_t u = \Delta u.$$

One of the most important properties satisfied by the heat equation is the maximum principle, which says that for any smooth solution to the heat equation, whatever pointwise bounds hold at  $t = 0$  also hold for  $t > 0$ . Let  $u : M^n \times [0, T) \rightarrow \mathbb{R}$  be a  $C^2$  solution to the heat equation on a complete Riemannian manifold. If  $C_1 \leq u(x, 0) \leq C_2$  for all  $x \in M$ , for some constants  $C_1, C_2 \in \mathbb{R}$ , then  $C_1 \leq u(x, t) \leq C_2$  for all  $x \in M$  and  $t \in [0, T)$  [Cao and Chow (1999)].

Now, given a differentiable manifold  $M$ , a one-parameter family of metrics  $g(t)$ , where  $t \in [0, T)$  for some  $T > 0$ , is a solution to the Ricci flow if (3.52) is valid at all  $x \in M$  and  $t \in [0, T)$ . The minus sign in the equation (3.52) makes the Ricci flow a *forward* heat equation [Cao and Chow (1999)] (with the normalization factor 2).

In local geodesic coordinates  $\{x^i\}$ , we have [Cao and Chow (1999)]

$$g_{ij}(x) = \delta_{ij} - \frac{1}{3} R_{ipjq} x^p x^q + O(|x|^3); \quad \text{therefore,}$$

$$\Delta g_{ij}(0) = -\frac{1}{3} R_{ij},$$

where  $\Delta$  is the standard Euclidean Laplacian. Hence the Ricci flow is like

the heat equation for a Riemannian metric

$$\partial_t g_{ij} = 6\Delta g_{ij}.$$

The practical study of the Ricci flow is made possible by the following short-time existence result: Given any smooth compact Riemannian manifold  $(M, g_o)$ , there exists a unique smooth solution  $g(t)$  to the Ricci flow defined on some time interval  $t \in [0, \epsilon)$  such that  $g(0) = g_o$  [Cao and Chow (1999)].

Now, given that short-time existence holds for any smooth initial metric, one of the main problems concerning the Ricci flow is to determine under what conditions the solution to the normalized equation exists for all time and converges to a constant curvature metric. Results in this direction have been established under various curvature assumptions, most of them being some sort of positive curvature. Since the Ricci flow (3.52) does not preserve volume in general, one often considers, as we mentioned in the Introduction, the normalized Ricci flow (3.53). Under this flow, the volume of the solution  $g(t)$  is independent of time.

To study the long-time existence of the normalized Ricci flow, it is important to know what kind of curvature conditions are preserved under the equation. In general, the Ricci flow tends to preserve some kind of positivity of curvatures. For example, positive scalar curvature is preserved in all dimensions. This follows from applying the maximum principle to the evolution equation for scalar curvature  $R$ , which is

$$\partial_t R = \Delta R + 2|R_{ij}|^2.$$

In dimension 3, positive Ricci curvature is preserved under the Ricci flow. This is a special feature of dimension 3 and is related to the fact that the Riemann curvature tensor may be recovered algebraically from the Ricci tensor and the metric in dimension 3. Positivity of sectional curvature is not preserved in general. However, the stronger condition of positive curvature operator is preserved under the Ricci flow. Recall that the Riemann curvature tensor may be considered as a self-adjoint map  $Rm : \wedge^2 M \rightarrow \wedge^2 M$ . We say that a metric  $g$  has positive (non-negative) curvature operator if the eigenvalues of  $Rm$  are positive (non-negative). We remark that positivity of curvature operator implies the positivity of the sectional curvature (and in dimension 3, the two conditions are equivalent).

Although the condition of positive scalar curvature is preserved in all dimensions, no convergence results are known for metrics satisfying this

condition except in dimension 2.

### 3.6.2.4 Structure Equations on $M$

Let  $\{X_a\}_{a=1}^m$ ,  $\{Y_i\}_{i=1}^n$  be local orthonormal framings on  $M$ ,  $N$  respectively and  $\{e_i\}_{i=1}^n$  be the induced framing on  $E$  defined by  $e_i = Y_i \circ \phi$ , then there exist smooth local coframings  $\{\omega_a\}_{a=1}^m$ ,  $\{\eta_i\}_{i=1}^n$  and  $\{\phi^*\eta_i\}_{i=1}^n$  on  $TM$ ,  $TN$  and  $E$  respectively such that (locally)

$$g = \sum_{a=1}^m \omega_a^2 \quad \text{and} \quad h = \sum_{i=1}^n \eta_i^2.$$

The corresponding first *structure equations* are (see [Mustafa (1999)]):

$$\begin{aligned} d\omega_a &= \omega_b \wedge \omega_{ba}, & \omega_{ab} &= -\omega_{ba}, \\ d\eta_i &= \eta_j \wedge \eta_{ji}, & \eta_{ij} &= -\eta_{ji}, \\ d(\phi^*\eta_i) &= \phi^*\eta_j \wedge \phi^*\eta_{ji}, & \phi^*\eta_{ij} &= -\phi^*\eta_{ji}, \end{aligned}$$

where the unique 1-forms  $\omega_{ab}$ ,  $\eta_{ij}$ ,  $\phi^*\eta_{ij}$  are the respective connection forms. The second structure equations are

$$\begin{aligned} d\omega_{ab} &= \omega_{ac} \wedge \omega_{cb} + \Omega_{ab}^M, & d\eta_{ij} &= \eta_{ik} \wedge \eta_{kj} + \Omega_{ij}^N, \\ d(\phi^*\eta_{ij}) &= \phi^*\eta_{ik} \wedge \phi^*\eta_{kj} + \phi^*\Omega_{ij}^N, \end{aligned}$$

where the curvature 2-forms are given by

$$\Omega_{ab}^M = -\frac{1}{2} R_{abcd}^M \omega_c \wedge \omega_d \quad \text{and} \quad \Omega_{ij}^N = -\frac{1}{2} R_{ijkl}^N \eta_k \wedge \eta_l.$$

The pull back map  $\phi^*$  and the push forward map  $\phi_*$  can be written as [Mustafa (1999)]

$$\phi^*\eta_i = f_{ia}\omega_a$$

for unique functions  $f_{ia}$  on  $U \subset M$ , so that

$$\phi_* = e_i \otimes \phi^*\eta_i = f_{ia}e_i \otimes \omega_a.$$

Note that  $\phi_*$  is a section of the vector bundle  $\phi^{-1}TN \otimes T^*M$ .

The covariant differential operators are represented as

$$\nabla^M X_a = \omega_{ab} \otimes X_b, \quad \nabla^N Y_i = \eta_{ij} \otimes Y_j, \quad \nabla^* \omega_a = -\omega_{ca} \otimes \omega_c,$$

where  $\nabla^*$  is the dual connection on the cotangent bundle  $T^*M$ .

The Laplacian of a function  $f$  on  $M$  is given by

$$\Delta f = -\text{Tr}(\nabla df)$$

that is, negative of the usual Laplacian on functions.

### 3.6.2.5 Basics of Morse Theory

At the same time the variational formulae were discovered, a related technique, called *Morse theory*, was introduced into Riemannian geometry. This theory was developed by Morse, first for functions on manifolds in 1925, and then in 1934, for the loop space. The latter theory, as we shall see, sets up a very nice connection between the first and second variation formulae from the previous section and the topology of  $M$ . It is this relationship that we shall explore at a general level here. In section 5 we shall then see how this theory was applied in various specific settings.

If we have a *proper function*  $f : M \rightarrow \mathbb{R}$ , then its Hessian (as a quadratic form) is in fact well defined at its *critical points* without specifying an underlying Riemannian metric. The *nullity* of  $f$  at a *critical point* is defined as the dimension of the *kernel* of  $\nabla^2 f$ , while the *index* is the number of negative eigenvalues counted with multiplicity. A function is said to be a *Morse function* if the nullity at any of its critical points is zero. Note that this guarantees in particular that all critical points are isolated. The first fundamental theorem of Morse theory is that one can determine the topological structure of a manifold from a Morse function. More specifically, if one can order the critical points  $x_1, \dots, x_k$  so that  $f(x_1) < \dots < f(x_k)$  and the index of  $x_i$  is denoted  $\lambda_i$ , then  $M$  has the structure of a CW complex with a cell of dimension  $\lambda_i$  for each  $i$ . Note that in case  $M$  is closed then  $x_1$  must be a minimum and so  $\lambda_1 = 0$ , while  $x_k$  is a maximum and  $\lambda_k = n$ . The classical example of Milnor of this theorem in action is a torus in 3-space and  $f$  the height function.

We are now left with the problem of trying to find appropriate Morse functions. While there are always plenty of such functions, there does not seem to be a natural way of finding one. However, there are natural choices for Morse functions on the loop space to a Riemannian manifold. This is, somewhat inconveniently, infinite-dimensional. Still, one can develop Morse theory as above for suitable functions, and moreover *the loop space of a manifold determines the topology of the underlying manifold*.

If  $m, p \in M$ , then we denote by  $\Omega_{mp}$  the space of all  $C^k$  paths from  $m$

to  $p$ . The first observation about this space is that

$$\pi_{i+1}(M) = \pi_i(\Omega_{mp}).$$

To see this, just fix a path from  $m$  to  $q$  and then join this path to every curve in  $\Omega_{mp}$ . In this way  $\Omega_{mp}$  is identified with  $\Omega_m$ , the space of loops fixed at  $m$ . For this space the above relationship between the homotopy groups is almost self-evident.

On the space  $\Omega_{mp}$  we have two naturally defined functions, the *arc-length* and *energy functionals*:

$$L(\gamma, I) = \int_I |\dot{\gamma}| dt, \quad \text{and} \quad E(\gamma, I) = \frac{1}{2} \int_I |\dot{\gamma}|^2 dt.$$

While the energy functional is easier to work with, it is of course the arc-length functional that we are really interested in. In order to make things work out nicely for the arc-length functional, it is convenient to parameterize all curves on  $[0, 1]$  and proportionally to arc-length. We shall think of  $\Omega_{mp}$  as an *infinite-dimensional manifold*. For each curve  $\gamma \in \Omega_{mp}$  the natural choice for the tangent space consists of the vector-fields along  $\gamma$  which vanish at the endpoints of  $\gamma$ . This is because these vector-fields are exactly the variational fields for curves through  $\gamma$  in  $\Omega_{mp}$ , i.e., fixed endpoint variations of  $\gamma$ . An inner product on the tangent space is then naturally defined by

$$(X, Y) = \int_0^1 g(X, Y) dt.$$

Now the first variation formula for arc-length tells us that the gradient for  $L$  at  $\gamma$  is  $-\nabla_{\dot{\gamma}} \dot{\gamma}$ . Actually this cannot be quite right, as  $-\nabla_{\dot{\gamma}} \dot{\gamma}$  does not vanish at the endpoints. The real gradient is gotten in the same way we find the gradient for a function on a surface in space, namely, by projecting it down into the correct tangent space. In any case we note that the critical points for  $L$  are exactly the geodesics from  $m$  to  $p$ . The second variation formula tells us that the Hessian of  $L$  at these critical points is given by

$$\nabla^2 L(X) = \ddot{X} + R(X, \dot{\gamma}) \dot{\gamma},$$

at least for vector-fields  $X$  which are perpendicular to  $\gamma$ . Again we ignore the fact that we have the same trouble with endpoint conditions as above. We now need to impose the Morse condition that this Hessian is not allowed to have any kernel. The vector-fields  $J$  for which  $\ddot{J} + R(J, \dot{\gamma}) \dot{\gamma} = 0$  are called *Jacobi fields*. Thus we have to figure out whether there are any

Jacobi fields which vanish at the endpoints of  $\gamma$ . The first observation is that Jacobi fields must always come from geodesic variations. The Jacobi fields which vanish at  $m$  can therefore be found using the exponential map  $\exp_m$ . If the Jacobi field also has to vanish at  $p$ , then  $p$  must be a critical value for  $\exp_m$ . Now Sard's theorem asserts that the set of critical values has measure zero. For given  $m \in M$  it will therefore be true that the arc-length functional on  $\Omega_{mp}$  is a Morse function for almost all  $p \in M$ . Note that it may not be possible to choose  $p = m$ , the simplest example being the standard sphere. We are now left with trying to decide what the *index* should be. This is of course the dimension of the largest subspace on which the Hessian is negative definite. It turns out that this index can also be computed using Jacobi fields and is in fact always finite. Thus one can compute the topology of  $\Omega_{mp}$ , and hence  $M$ , by finding all the geodesics from  $m$  to  $p$  and then computing their index.

In geometric situations it is often unrealistic to suppose that one can compute the index precisely, but as we shall see it is often possible to given lower bounds for the index. As an example, note that if  $M$  is not simply connected, then  $\Omega_{mp}$  is not connected. Each curve of minimal length in the path components is a geodesic from  $m$  to  $p$  which is a local minimum for the arc-length functional. Such geodesics evidently have index zero. In particular, if one can show that all geodesics, except for the minimal ones from  $m$  to  $p$ , have index  $> 0$ , then the manifold must be simply connected.

### 3.6.2.6 Basics of (Co)Bordism Theory

(Co)bordism appeared as a revival of Poincaré's unsuccessful 1895 attempts to define homology using only manifolds. Smooth manifolds (without boundary) are again considered as 'negligible' when they are *boundaries* of smooth manifolds-with-boundary. But there is a big difference, which keeps definition of 'addition' of manifolds from running into the difficulties encountered by Poincaré; it is now the disjoint union. The (unoriented) (co)bordism relation between two compact smooth manifolds  $M_1, M_2$  of same dimension  $n$  simply means that their disjoint union  $\partial W = M_1 \cup M_2$  is the boundary  $\partial W$  of an  $(n+1)$ D smooth manifold-with-boundary  $W$ . This is an *equivalence relation*, and the classes for that relation of  $n$ D manifolds form a *commutative group*  $\mathfrak{N}_n$  in which every element has order 2. The direct sum  $\mathfrak{N}_\bullet = \bigoplus_{n \geq 0} \mathfrak{N}_n$  is a ring for the multiplication of classes deduced from the Cartesian product of manifolds.

More precisely, a manifold  $M$  is said to be a (co)bordism from  $A$  to  $B$



if exists a diffeomorphism from a disjoint sum,  $\varphi \in \text{diff}(A^* \cup B, \partial M)$ . Two (co)bordisms  $M(\varphi)$  and  $M'(\varphi')$  are equivalent if there is a  $\Phi \in \text{diff}(M, M')$  such that  $\varphi' = \Phi \circ \varphi$ . The equivalence class of (co)bordisms is denoted by  $M(A, B) \in \text{Cob}(A, B)$  [Stong (1968)].

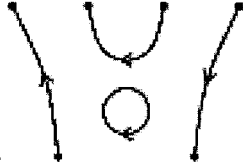
Composition  $c_{\text{Cob}}$  of (co)bordisms comes from gluing of manifolds [Baez and Dolan (1995)]. Let  $\varphi' \in \text{diff}(C^* \cup D, \partial N)$ . One can glue (co)bordism  $M$  with  $N$  by identifying  $B$  with  $C^*$ ,  $(\varphi')^{-1} \circ \varphi \in \text{diff}(B, C^*)$ . We obtain the glued (co)bordism  $(M \circ N)(A, D)$  and a semigroup operation,

$$c(A, B, D) : \text{Cob}(A, B) \times \text{Cob}(B, D) \longrightarrow \text{Cob}(A, D).$$

A *surgery* is an operation of cutting a manifold  $M$  and gluing to cylinders. A surgery gives new (co)bordism: from  $M(A, B)$  into  $N(A, B)$ . The disjoint sum of  $M(A, B)$  with  $N(C, D)$  is a (co)bordism  $(M \cup N)(A \cup C, B \cup D)$ . We got a 2-graph of (co)bordism  $\text{Cob}$  with  $\text{Cob}_0 = \text{Man}_d$ ,  $\text{Cob}_1 = \text{Man}_{d+1}$ , whose 2-cells from  $\text{Cob}_2$  are surgery operations.

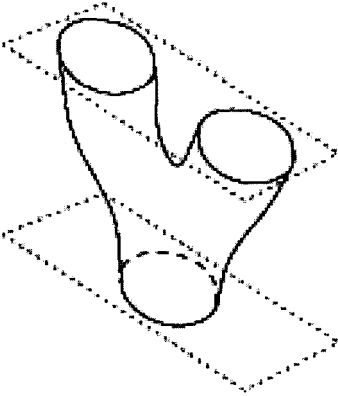
There is an  $n$ -category of (co)bordisms  $\mathcal{BO}$  [Leinster (2003)] with:

- 0-cells: 0-manifolds, where ‘manifold’ means ‘compact, smooth, oriented manifold’. A typical 0-cell is . . . .
- 1-cells: 1-manifolds with corners, i.e., (co)bordisms between



0-manifolds, such as (this being a 1-cell from the 4-point manifold to the 2-point 0-manifold).

- 2-cells: 2-manifolds with corners, such as



- 3-cells, 4-cells,... are defined similarly;
- Composition is gluing of manifolds.

The (co)bordisms theme was taken a step further by Baez and Dolan in [Baez and Dolan (1995)], when they started a programme to understand the subtle relations between certain TMFT models for manifolds of different dimensions, frequently referred to as the dimensional ladder. This programme is based on higher-dimensional algebra, a generalization of the theory of categories and functors to  $n$ -categories and  $n$ -functors. In this framework a topological quantum field theory (TMFT) becomes an  $n$ -functor from the  $n$ -category  $\mathcal{BO}$  of  $n$ -cobordisms to the  $n$ -category of  $n$ -Hilbert spaces.

### 3.7 Symplectic Geometry in Biodynamics

In this section we develop the basic techniques of symplectic geometry on the biodynamic manifold  $M$  [Ivancevic (2004)].

#### 3.7.1 Symplectic Algebra

Symplectic algebra works in the category of symplectic vector spaces  $V_i$  and linear symplectic mappings  $t \in L(V_i, V_j)$  [Putz (1993)].

Let  $V$  be a  $n$ D real vector space and  $L^2(V, \mathbb{R})$  the space of all bilinear maps from  $V \times V$  to  $\mathbb{R}$ . We say that a *bilinear map*  $\omega \in L^2(V, \mathbb{R})$  is *nondegenerate*, i.e., if  $\omega(v_1, v_2) = 0$  for all  $v_2 \in V$  implies  $v_1 = 0$ .

If  $\{e_1, \dots, e_n\}$  is a basis of  $V$  and  $\{e^1, \dots, e^n\}$  is the dual basis,  $\omega_{ij} = \omega(e_i, e_j)$  is the matrix of  $\omega$ . A bilinear map  $\omega \in L^2(V, \mathbb{R})$  is nondegenerate iff its matrix  $\omega_{ij}$  is nonsingular. The transpose  $\omega^t$  of  $\omega$  is defined by  $\omega^t(e_i, e_j) = \omega(e_j, e_i)$ .  $\omega$  is *symmetric* if  $\omega^t = \omega$ , and *skew-symmetric* if  $\omega^t = -\omega$ .

Let  $A^2(V)$  denote the space of skew-symmetric bilinear maps on  $V$ . An element  $\omega \in A^2(V)$  is called a 2-form on  $V$ . If  $\omega \in A^2(V)$  is nondegenerate then in the basis  $\{e_1, \dots, e_n\}$  its matrix  $\omega(e_i, e_j)$  has the form

$$J = \begin{pmatrix} 0 & I_n \\ -I_n & 0 \end{pmatrix}.$$

A *symplectic form* on a real vector space  $V$  of dimension  $2n$  is a nondegenerate 2-form  $\omega \in A^2(V)$ . The pair  $(V, \omega)$  is called a symplectic vector space. If  $(V_1, \omega_1)$  and  $(V_2, \omega_2)$  are symplectic vector spaces, a linear map  $t \in L(V_1, V_2)$  is a *symplectomorphism* (i.e., a symplectic mapping) iff

$t^*\omega_2 = \omega_1$ . If  $(V, \omega)$  is a symplectic vector space, we have an orientation  $\Omega_\omega$  on  $V$  given by

$$\Omega_\omega = \frac{(-1)^{\frac{n(n-1)}{2}}}{n!} \omega^n.$$

Let  $(V, \omega)$  be a  $2n$ D symplectic vector space and  $t \in L(V, V)$  a symplectomorphism. Then  $t$  is volume preserving, i.e.,  $t^*(\Omega_\omega) = \Omega_\omega$ , and  $\det_{\Omega_\omega}(t) = 1$ .

The set of all symplectomorphisms  $t : V \rightarrow V$  of a  $2n$ D symplectic vector space  $(V, \omega)$  forms a group under composition, called the *symplectic group*, denoted by  $Sp(V, \omega)$ .

In matrix notation, there is a basis of  $V$  in which the matrix of  $\omega$  is  $J = \begin{pmatrix} 0 & I_n \\ -I_n & 0 \end{pmatrix}$ , such that  $J^{-1} = J^t = -J$ , and  $J^2 = -I$ . For  $t \in L(V, V)$  with matrix  $T = [T_j^i]$  relative to this basis, the condition  $t \in Sp(V, \omega)$ , i.e.,  $t^*\omega = \omega$ , becomes

$$T^t J T = J.$$

In general, by definition a matrix  $A \in M_{2n \times 2n}(\mathbb{R})$  is symplectic iff  $A^t J A = J$ .

Let  $(V, \omega)$  be a symplectic vector space,  $t \in Sp(V, \omega)$  and  $\lambda \in \mathbb{C}$  an eigenvalue of  $t$ . Then  $\lambda^{-1}$ ,  $\bar{\lambda}$  and  $\bar{\lambda}^{-1}$  are eigenvalues of  $t$ .

### 3.7.2 Symplectic Geometry on $M$

Symplectic geometry is a globalization of symplectic algebra [Putz (1993)]; it works in the category **Symplec** of symplectic manifolds  $M$  and symplectic diffeomorphisms  $f$ . The phase-space of a conservative dynamical system is a symplectic manifold, and its time evolution is a one-parameter family of symplectic diffeomorphisms.

A *symplectic form* or a symplectic structure on a smooth (i.e.,  $C^k$ ) manifold  $M$  is a nondegenerate closed 2-form  $\omega$  on  $M$ , i.e., for each  $x \in M$   $\omega(x)$  is nondegenerate, and  $d\omega = 0$ . A *symplectic manifold* is a pair  $(M, \omega)$  where  $M$  is a smooth  $2n$ D manifold and  $\omega$  is a symplectic form on it. If  $(M_1, \omega_1)$  and  $(M_2, \omega_2)$  are symplectic manifolds then a smooth map  $f : M_1 \rightarrow M_2$  is called *symplectic map* or *canonical transformation* if  $f^*\omega_2 = \omega_1$ .

For example, any symplectic vector space  $(V, \omega)$  is also a symplectic manifold; the requirement  $d\omega = 0$  is automatically satisfied since  $\omega$  is a

constant map. Also, any orientable, compact surface  $\Sigma$  is a symplectic manifold; any nonvanishing 2-form (volume element)  $\omega$  on  $\Sigma$  is a symplectic form on  $\Sigma$ .

If  $(M, \omega)$  is a symplectic manifold then it is orientable with the standard volume form

$$\Omega_\omega = \frac{(-1)^{\frac{n(n-1)}{2}}}{n!} \omega^n,$$

If  $f : M \rightarrow M$  is a symplectic map, then  $f$  is volume preserving,  $\det_{\Omega_\omega}(f) = 1$  and  $f$  is a local diffeomorphism.

In general, if  $(M, \omega)$  is a  $2n$ D compact symplectic manifold then  $\omega^n$  is a volume element on  $M$ , so the De Rham cohomology class  $[\omega^n] \in H^{2n}(M, \mathbb{R})$  is nonzero. Since  $[\omega^n] = [\omega]^n$ ,  $[\omega] \in H^2(M, \mathbb{R})$  and all of its powers through the  $n$ th must be nonzero as well. The existence of such an element of  $H^2(M, \mathbb{R})$  is a *necessary condition* for the compact manifold to admit a symplectic structure.

However, if  $M$  is a  $2n$ D compact manifold without boundary, then there does not exist any exact symplectic structure,  $\omega = d\theta$  on  $M$ , as its total volume is zero (by Stokes' theorem),

$$\int_M \Omega_\omega = \frac{(-1)^{\frac{n(n-1)}{2}}}{n!} \int_M \omega^n = \frac{(-1)^{\frac{n(n-1)}{2}}}{n!} \int_M d(\theta \wedge \omega^{n-1}) = 0.$$

For example, spheres  $S^{2n}$  do not admit a symplectic structure for  $n \geq 2$ , since the second De Rham group vanishes, i.e.,  $H^2(S^{2n}, \mathbb{R}) = 0$ . This argument applies to any compact manifold without boundary and having  $H^2(M, \mathbb{R}) = 0$ .

In mechanics, the phase-space is the cotangent bundle  $T^*M$  of a configuration space  $M$ . There is a natural symplectic structure on  $T^*M$  that is usually defined as follows. Let  $M$  be a smooth  $n$ D manifold and pick local coordinates  $\{dq^1, \dots, dq^n\}$ . Then  $\{dq^1, \dots, dq^n\}$  defines a basis of the tangent space  $T_q^*M$ , and by writing  $\theta \in T_q^*M$  as  $\theta = p_i dq^i$  we get local coordinates  $\{q^1, \dots, q^n, p_1, \dots, p_n\}$  on  $T^*M$ . Define the canonical symplectic form  $\omega$  on  $T^*M$  by

$$\omega = dp_i \wedge dq^i.$$

This 2-form  $\omega$  is obviously independent of the choice of coordinates  $\{q^1, \dots, q^n\}$  and independent of the base point  $\{q^1, \dots, q^n, p_1, \dots, p_n\} \in T_q^*M$ ; therefore, it is locally constant, and so  $d\omega = 0$ .

The canonical 1-form  $\theta$  on  $T^*M$  is the unique 1-form with the property that, for any 1-form  $\beta$  which is a section of  $T^*M$  we have  $\beta^*\theta = \theta$ .

Let  $f : M \rightarrow M$  be a diffeomorphism. Then  $T^*f$  preserves the canonical 1-form  $\theta$  on  $T^*M$ , i.e.,  $(T^*f)^*\theta = \theta$ . Thus  $T^*f$  is symplectic diffeomorphism.

If  $(M, \omega)$  is a  $2n$ D symplectic manifold then about each point  $x \in M$  there are local coordinates  $\{q^1, \dots, q^n, p_1, \dots, p_n\}$  such that  $\omega = dp_i \wedge dq^i$ . These coordinates are called canonical or symplectic. By the Darboux theorem,  $\omega$  is constant in this local chart, i.e.,  $d\omega = 0$ .

A large class of symplectic manifolds is given by the *Kähler manifolds*. Let  $M$  be a smooth manifold and  $g$  a Riemannian metric on  $M$ . Let  $J$  be a complex structure on  $M$ , that is,  $J : TM \rightarrow TM$ ,  $J^2 = -\text{Id}$  and  $J$  is  $g$ -orthogonal.  $M$  is called a *Kähler manifold* if  $\nabla J = 0$ , where  $\nabla$  is the Levi-Civita connection of  $g$  and  $J$  is regarded as a  $(1, 1)$ -tensor-field. Define a 2-form  $\omega$  on  $M$  by  $\omega(X, Y) = g(JX, Y)$ , for each vector-field  $X, Y$  on  $M$ . Then  $(M, \omega)$  is a symplectic manifold.

### 3.8 Impulse Biodynamics and Synthetic Geometry

In this section we present both classical and modern view on Dirac's  $\delta$ -function, together with its generalizations and biodynamic applications.

#### 3.8.1 Delta Spikes

Recall that the *Dirac delta function*, or *delta distribution*<sup>4</sup>, represents a *limit* of the *Gaussian bell-shaped curve*

$$g(t, \alpha) = \frac{1}{\sqrt{\pi\alpha}} e^{-t^2/\alpha} \quad (\text{with parameter } \alpha \rightarrow 0) \quad (3.54)$$

(where the factor  $1/\sqrt{\pi\alpha}$  serves for the *normalization* of (3.54)),

$$\int_{-\infty}^{+\infty} \frac{dt}{\sqrt{\pi\alpha}} e^{-t^2/\alpha} = 1, \quad (3.55)$$

i.e., the *area* under the *pulse* is equal to *unity*. In (3.54), the smaller  $\alpha$  the higher the peak. In other words,

$$\delta(t) = \lim_{\alpha \rightarrow 0} \frac{1}{\sqrt{\pi\alpha}} e^{-t^2/\alpha}, \quad (3.56)$$

---

<sup>4</sup>also called the *impulse function* in the systems and signals theory

which is a pulse so short that outside of  $t = 0$  it vanishes, whereas at  $t = 0$  it still remains normalized according to (3.55). Therefore, we get the usual definition of the  $\delta$ -function:

$$\begin{aligned} \delta(t) &= 0 \quad \text{for } t \neq 0, \\ \int_{-\epsilon}^{+\epsilon} \delta(t) dt &= 1, \end{aligned} \quad (3.57)$$

where  $\epsilon$  may be arbitrarily small. Instead of centering the  $\delta$ -pulse around  $t = 0$ , we can center it around any other time  $t_0$  so that (3.57) is transformed into

$$\begin{aligned} \delta(t - t_0) &= 0 \quad \text{for } t \neq t_0, \\ \int_{t_0-\epsilon}^{t_0+\epsilon} \delta(t - t_0) dt &= 1. \end{aligned} \quad (3.58)$$

Another well-known fact is that the integral of the  $\delta$ -function is the *Heaviside's step function*

$$H(T) = \int_{-\infty}^T \delta(t) dt = \begin{cases} 0 & \text{for } T < 0 \\ 1 & \text{for } T > 0 \\ (\frac{1}{2}) & \text{for } T = 0 \end{cases}. \quad (3.59)$$

Now we can perform several generalizations of the relation (3.59). First, we have

$$\int_{-\infty}^T \delta(ct - t_0) dt = \begin{cases} 0 & \text{for } T < t_0/c \\ 1/c & \text{for } T > t_0/c \\ \frac{1}{2c} & \text{for } T = t_0/c \end{cases}.$$

More generally, we can introduce the so-called *phase function*  $\phi(t)$ , (e.g.,  $\phi(t) = ct - t_0$ ) which is continuous at  $t = t_0$  but its time derivative  $\dot{\phi}(t) \equiv \frac{d\phi(t)}{dt}$  is discontinuous at  $t = t_0$  (yet positive,  $\dot{\phi}(t) > 0$ ), and such that

$$\int_{-\infty}^T \delta(\phi(t)) dt = \begin{cases} 0 & \text{for } T < t_0 \\ 1/\dot{\phi}(t_0) & \text{for } T > t_0 \\ \frac{1}{\dot{\phi}(t_0)} & \text{for } T = t_0 \end{cases}.$$

Finally, we come to the *spike function*  $\delta(\phi(t))\dot{\phi}(t)$ , which like  $\delta$ -function represents a *spike* at  $t = t_0$ , such that the normalization criterion (3.58) is still valid,

$$\int_{t_0-\epsilon}^{t_0+\epsilon} \delta(\phi(t))\dot{\phi}(t) dt = 1.$$

Below, we give modern ‘synthetic geometric’ treatment of  $\delta$ -functions, but first we consider both deterministic and stochastic ‘kick dynamics’.

### 3.8.2 Kick Dynamics

#### 3.8.2.1 Deterministic Delayed Kicks

Following Haken [Haken (2002)], we consider the mechanical example of a soccer ball that is kicked by a soccer player and rolls over grass, whereby its motion will be slowed down. We start with the Newton’s (second) law of motion,  $m\dot{v} = \text{force}$ , and in order to get rid of superfluous constants, we put temporarily  $m = 1$ . The *force* on the r.h.s. consists of the damping force  $-\gamma v(t)$  of the grass (where  $\gamma$  is the damping constant) and the sharp force  $F(t) = s\delta(t - \sigma)$  of the individual kick occurring at time  $t = \sigma$  (where  $s$  is the strength of the kick, and  $\delta$  is the Dirac’s ‘delta’ function). In this way, the (single) *kick equation* of the ball motion becomes

$$\dot{v} = -\gamma v(t) + s\delta(t - \sigma), \quad (3.60)$$

with the general solution

$$v(t) = sG(t - \sigma),$$

where  $G(t - \sigma)$  is the *Green’s function*<sup>5</sup>

$$G(t - \sigma) = \begin{cases} 0 & \text{for } t < \sigma \\ e^{-\gamma(t-\sigma)} & \text{for } t \geq \sigma \end{cases}.$$

Now, we can generalize the above to  $N$  kicks with individual strengths  $s_j$ , occurring at a sequence of times  $\{\sigma_j\}$ , so that the total kicking force becomes

$$F(t) = \sum_{j=1}^N s_j \delta(t - \sigma_j).$$

---

<sup>5</sup>This is the Green’s function of the first order system (3.60). Similarly, the Green’s function

$$G(t - \sigma) = \begin{cases} 0 & \text{for } t < \sigma \\ (t - \sigma)e^{-\gamma(t-\sigma)} & \text{for } t \geq \sigma \end{cases}$$

corresponds to the second order system

$$\left(\frac{d}{dt} + \gamma\right)^2 G(t - \sigma) = \delta(t - \sigma).$$

In this way, we get the *multi-kick equation* of the ball motion

$$\dot{v} = -\gamma v(t) + \sum_{j=1}^N s_j \delta(t - \sigma_j),$$

with the general solution

$$v(t) = \sum_{j=1}^N s_j G(t - \sigma_j). \quad (3.61)$$

As a final generalization, we would imagine that the kicks are continuously exerted on the ball, so that kicking force becomes

$$F(t) = \int_{t_0}^T s(\sigma) \delta(t - \sigma) d\sigma \equiv \int_{t_0}^T d\sigma F(\sigma) \delta(t - \sigma),$$

so that the continuous multi-kick equation of the ball motion becomes

$$\dot{v} = -\gamma v(t) + \int_{t_0}^T s(\sigma) \delta(t - \sigma) d\sigma \equiv -\gamma v(t) + \int_{t_0}^T d\sigma F(\sigma) \delta(t - \sigma),$$

with the general solution

$$v(t) = \int_{t_0}^T d\sigma F(\sigma) G(t - \sigma) = \int_{t_0}^T d\sigma F(\sigma) e^{-\gamma(t-\sigma)}. \quad (3.62)$$

### 3.8.2.2 Random Kicks and Langevin Equation

We now denote the times at which kicks occur by  $t_j$  and indicate their direction in a one-dimensional game by  $(\pm 1)_j$ , where the choice of the plus or minus sign is random (e.g., throwing a coin). Thus the kicking force can be written in the form [Haken (2002)]

$$F(t) = s \sum_{j=1}^N \delta(t - t_j) (\pm 1)_j, \quad (3.63)$$

where for simplicity we assume that all kicks have the same strength  $s$ . When we observe many games, then we may perform an average  $\langle \dots \rangle$  over all these different *performances*,

$$\langle F(t) \rangle = s \langle \sum_{j=1}^N \delta(t - t_j) (\pm 1)_j \rangle. \quad (3.64)$$



Since the direction of the kicks is assumed to be independent of the time at which the kicks happen, we may split (3.64) into the product

$$\langle F(t) \rangle = s \langle \sum_{j=1}^N \delta(t - t_j) \rangle \langle (\pm 1)_j \rangle.$$

As the kicks are assumed to happen with equal frequency in both directions, we get the cancellation

$$\langle (\pm 1)_j \rangle = 0,$$

which implies that the average kicking force also vanishes,

$$\langle F(t) \rangle = 0.$$

In order to characterize the strength of the force (3.63), we consider a quadratic expression in  $F$ , e.g., by calculating the *correlation function* for two times  $t, t'$ ,

$$\langle F(t)F(t') \rangle = s^2 \langle \sum_j \delta(t - t_j)(\pm 1)_j \sum_k \delta(t' - t_k)(\pm 1)_k \rangle.$$

As the ones for  $j \neq k$  will cancel each other and for  $j = k$  will become 1, the correlation function becomes a single sum

$$\langle F(t)F(t') \rangle = s^2 \langle \sum_j \delta(t - t_j)\delta(t' - t_k) \rangle, \quad (3.65)$$

which is usually evaluated by assuming the *Poisson process* for the times of the kicks.

Now, proper description of random motion is given by *Langevin rate equation*, which describes the *Brownian motion*: when a particle is immersed in a fluid, the velocity of this particle is slowed down by a force proportional to its velocity and the particle undergoes a zig-zag motion (the particle is steadily pushed by much smaller particles of the liquid in a random way). In physical terminology, we deal with the behavior of a system (particle) which is coupled to a *heat bath* or reservoir (namely the liquid). The heat bath has two effects [Haken (2002)]:

- (1) It decelerates the mean motion of the particle; and
- (2) It causes statistical fluctuation.

The standard Langevin equation has the form

$$\dot{v} = -\gamma v(t) + F(t), \quad (3.66)$$

where  $F(t)$  is a *fluctuating force* with the following properties:

- (1) Its statistical average (3.64) vanishes; and
- (2) Its correlation function (3.65) is given by

$$\langle F(t)F(t') \rangle = Q\delta(t - t_0), \quad (3.67)$$

where  $t_0 = T/N$  denotes the mean free time between kicks, and  $Q = s^2/t_0$  is the *random fluctuation*.

The general solution of the Langevin equation (3.66) is given by (3.62).

The average velocity vanishes,  $\langle v(t) \rangle = 0$ , as both directions are possible and cancel each other. Using the integral solution (3.62) we get

$$\langle v(t)v(t') \rangle = \left\langle \int_{t_0}^t d\sigma \int_{t_0}^{t'} d\sigma' F(\sigma)F(\sigma')e^{-\gamma(t-\sigma)}e^{-\gamma(t'-\sigma')} \right\rangle,$$

which, in the steady-state, reduces to

$$\langle v(t)v(t') \rangle = \frac{Q}{2\gamma}e^{-\gamma(t-\sigma)},$$

and for equal times

$$\langle v(t)^2 \rangle = \frac{Q}{2\gamma}.$$

If we now repeat all the steps performed so far with  $m \neq 1$ , the final result reads

$$\langle v(t)^2 \rangle = \frac{Q}{2\gamma m}. \quad (3.68)$$

Now, according to thermodynamics, the *mean kinetic energy* of a particle is given by

$$\frac{m}{2} \langle v(t)^2 \rangle = \frac{1}{2}k_B T, \quad (3.69)$$

where  $T$  is the (absolute) temperature, and  $k_B$  is the Boltzman's constant. Comparing (3.68) and (3.69), we get the important Einstein's result

$$Q = 2\gamma k_B T,$$

which says that whenever there is damping, i.e.,  $\gamma \neq 0$ , then there are random fluctuations (or noise)  $Q$ . In other words, fluctuations or noise are inevitable in any physical system. For example, in a resistor (with

the resistance  $R$ ) the electric field  $E$  fluctuates with a correlation function (similar to (3.67))

$$\langle E(t)E(t') \rangle = 2Rk_B T \delta(t - t_0).$$

This is the simplest example of the *dissipation-fluctuation theorem*.

### 3.8.3 Distributions and Synthetic Differential Geometry

The sense in which we understand ‘synthetic’ in this context is that we place ourselves in the certain category  $\mathbf{E}$  of manifold-like objects where everything is smooth. A main assumption about our category  $\mathbf{E}$  is that it is cartesian closed, meaning that functional spaces as well as methods of classical functional analysis are available.

Recall that *distributions* are usually thought of as very non-smooth functions, like the Heaviside function, or the Dirac  $\delta$ -function. These so-called *generalized functions* are commonly presented following the *Sobolev-Schwartz* concept of functional analysis, usually including the integral transforms of Fourier, Laplace, Mellin, Hilbert, Cauchy-Bochner and Poisson. The main application of the theory of generalized functions is the solution of classical *equations of mathematical physics* (see e.g., [Vladimirov (1971); Vladimirov (1986)]).

On the other hand, there is a viewpoint, firstly stressed by Lawvere [Lawvere (1979)], and fully elaborated by Kock [Kock (1981); Kock and Reyes (2003)], that distributions are *extensive quantities*, where functions are *intensive quantities*. This viewpoint also makes it quite natural to formulate partial equations of mathematical physics (like classical wave and heat equations) – as ODEs describing the evolution over time of any initial distributions. For example, the main construction in the theory of the wave equation is the construction of the fundamental solution: the description of the evolution of a point  $\delta$ -distribution over time.

To say that *distributions* are extensive quantities implies that they transform *covariantly* (in a categorical sense). To say that *functions* are intensive quantities implies that they transform *contravariantly*. Distributions are here construed, as linear functionals on the space of (smooth) functions. However, since all functions in the synthetic context are smooth, as well as continuous, there is no distinction between distributions and Radon measures.

In the category  $\mathbf{E}$  one can define the vector space  $\mathcal{D}'_c(M)$  of distributions of compact support on  $M$ , for each manifold-like object  $M \in \mathbf{E}$ , namely

the object of  $\mathbb{R}$ -linear maps  $\mathbb{R}^M \rightarrow \mathbb{R}$ . We shall assume that elementary differential calculus for functions  $\mathbb{R} \rightarrow \mathbb{R}$  is available, as in all models of *synthetic differential geometry* (SDG, see [Kock (1981); Moerdijk and Reyes (1991); Lavendhomme (1996)]). Following Kock [Kock (1981)], we shall also assume some integral calculus, but only in the weakest possible sense, namely we assume that for every  $\psi : \mathbb{R} \rightarrow \mathbb{R}$ , there is a unique  $\Psi : \mathbb{R} \rightarrow \mathbb{R}$  with  $\Psi' = \psi$  and with  $\Psi(0) = 0$ . Using this result, *intervals* will be construed as *distributions*: for  $a, b \in \mathbb{R}$ ,  $[a, b]$  denotes the distribution

$$\psi \mapsto \int_a^b \psi(x) dx = \Psi(b) - \Psi(a).$$

### 3.8.3.1 Distributions

Let us make the formula for covariant functoriality  $\mathcal{D}'_c$  explicit. Let  $f : M \rightarrow N$  be a map. Then the corresponding map  $f_* = \mathcal{D}'_c(f) : \mathcal{D}'_c(M) \rightarrow \mathcal{D}'_c(N)$  is described by declaring

$$\langle f_*(T), \phi \rangle = \langle T, \phi \circ f \rangle, \quad (3.70)$$

where  $T$  is a distribution on  $M$ , and  $\phi$  is a function on  $N$ . The brackets denote evaluation of distributions on functions. If we similarly denote the value of the contravariant functor  $M \mapsto \mathbb{R}^M$  on a map  $f$  by  $f^*$ , the defining equation for  $f_*$  reads

$$\langle f_*(T), \phi \rangle = \langle T, f^*(\phi) \rangle.$$

$\mathcal{D}'_c(M)$  is an  $\mathbb{R}$ -linear space, and all maps  $f_* : \mathcal{D}'_c(M) \rightarrow \mathcal{D}'_c(N)$  are  $\mathbb{R}$ -linear. Also  $\mathcal{D}'_c(M)$  is a *Euclidean* vector space  $V$ , meaning that the basic differential calculus is available.

For any distribution  $T$  of compact support on  $M$ , one has its *Total*, which is just the number  $\langle T, 1 \rangle \in \mathbb{R}$ , where  $1$  denotes the function on  $M$  with constant value 1. Since  $f^*(1) = 1$  for any map  $f$ , it follows that  $f_*$  preserves Totals.

Recall that a distribution  $T$  on  $M$  may be multiplied by any function  $g : M \rightarrow \mathbb{R}$ , by the rule

$$\langle g \cdot T, \phi \rangle = \langle T, g \cdot \phi \rangle. \quad (3.71)$$

A basic result from single-variable calculus, ‘integration by substitution’, in a pure ‘distribution’ form reads: Given any function  $g : \mathbb{R} \rightarrow \mathbb{R}$ ,

and given  $a, b \in \mathbb{R}$ , we have

$$g_*(g' \cdot [a, b]) = [g(a), g(b)].$$

Let  $\psi$  be a test function, and let  $\Psi$  be a primitive of it,  $\Psi' = \psi$ . Then

$$\langle [g(a), g(b)], \psi \rangle = \Psi(g(b)) - \Psi(g(a)).$$

On the other hand, by the chain rule,  $\Psi \circ g$  is a primitive of  $g' \cdot (\psi \circ g)$ , and so

$$\Psi(g(a)) - \Psi(g(b)) = \langle [a, b], g' \cdot (\psi \circ g) \rangle = \langle g' \cdot [a, b], \psi \circ g \rangle = \langle g_*(g' \cdot [a, b]), \psi \rangle.$$

The external product of distributions of compact support is defined as follows. If  $P$  is a distribution on  $M$ , and  $Q$  a distribution on  $N$ , we get a distribution  $P \times Q$  on  $M \times N$ , by

$$\langle P \times Q, \psi \rangle = \langle P, [m \mapsto \langle Q, \psi(m, -) \rangle] \rangle.$$

However, if  $[a, b]$  and  $[c, d]$  are intervals (viewed as distributions on  $\mathbb{R}$ , as described above),  $[a, b] \times [c, d] = [a, b] \overline{\times} [c, d]$ , as distributions on  $\mathbb{R}^2$ , by an application of Fubini's theorem, (which holds in our context here as a consequence of equality of mixed partial derivatives). Distributions arising in this way on  $\mathbb{R}^2$ , are called *rectangles*. The obvious generalizations to higher dimensions are called *boxes*. We have

$$\langle [a, b] \times [c, d], \psi \rangle = \int_a^b \int_c^d \psi(x, y) \, dy \, dx,$$

in traditional notation. Here, we can define *the boundary* of the box  $[a, b] \times [c, d]$  as the obvious distribution on  $\mathbb{R}^2$ ,

$$(p_c^2)_*[a, b] + (p_b^1)_*[c, d] - (p_d^2)_*[a, b] - (p_a^1)_*[c, d],$$

where  $p_c^2(x) = (x, c)$ ,  $p_b^1(y) = (b, y)$ , etc.

By a *singular box* in a manifold-like object  $M$ , we understand the data of a map  $\gamma : \mathbb{R}^2 \rightarrow M$  and a box  $[a, b] \times [c, d]$  in  $\mathbb{R}^2$ , and similarly for singular intervals and singular rectangles. Such a singular box gives rise to a distribution on  $M$ , namely  $g_*([a, b] \times [c, d])$ .

By *differential operator* on an object  $M$ , we here understand just an  $\mathbb{R}$ -linear map  $D : \mathbb{R}^M \rightarrow \mathbb{R}^M$ . If  $D$  is such an operator, and  $T$  is a distribution on  $M$ , we define  $D(T)$  by

$$\langle D(T), \psi \rangle = \langle T, D(\psi) \rangle,$$

and in this way,  $D$  becomes a linear operator  $\mathcal{D}'_c(M) \rightarrow \mathcal{D}'_c(M)$ .

In particular, if  $X$  is a vector-field on  $M$ , one defines the *directional* (i.e., *Lie*) derivative  $D_X(T)$  of a distribution  $T$  on  $M$  by the formula

$$\langle D_X(T), \psi \rangle = \langle T, D_X(\psi) \rangle. \quad (3.72)$$

This in particular applies to the vector-field  $\partial/\partial x$  on  $\mathbb{R}$ , and reads here

$$\langle T', \psi \rangle = \langle T, \psi' \rangle,$$

where  $\psi'$  denotes the ordinary derivative of the function  $\psi$ .

The following Proposition is an application of the covariant functoriality of the functor  $\mathcal{D}'_c$ , which will be used in connection with the wave (and heat) equations in dimension 2. We consider the (orthogonal) projection  $p: \mathbb{R}^3 \rightarrow \mathbb{R}^2$  onto the  $xy$ -plane;  $\Delta$  denotes the Laplace operator in the relevant  $\mathbb{R}^n$ , so for  $\mathbb{R}^3$ ,  $\Delta$  is  $\partial^2/\partial x^2 + \partial^2/\partial y^2 + \partial^2/\partial z^2$ . For any distribution  $S$  (of compact support) on  $\mathbb{R}^3$ ,

$$p_*(\Delta(S)) = \Delta(p_*(S)).$$

This follows from the fact that for any  $\psi: \mathbb{R}^2 \rightarrow \mathbb{R}$ ,

$$\Delta(p^*\psi) = p^*(\Delta(\psi)),$$

namely,  $\partial^2\psi/\partial x^2 + \partial^2\psi/\partial y^2$ .

### 3.8.3.2 Synthetic Calculus in Euclidean Spaces

Recall that a *vector space*  $E$  (which in the present context means an  $\mathbb{R}$ -module) is called *Euclidean* if differential and integral calculus for functions  $\mathbb{R} \rightarrow E$  is available (see [Kock (1981); Moerdijk and Reyes (1991); Lavendhomme (1996)]). The coordinate vector spaces are Euclidean, but so are also the vector spaces  $\mathbb{R}^M$ , and  $\mathcal{D}'_c(M)$  for any  $M$ . To describe for instance the 'time-derivative'  $\dot{f}$  of a function  $f: \mathbb{R} \rightarrow \mathcal{D}'_c(M)$ , we put

$$\langle \dot{f}(t), \psi \rangle = \frac{d}{dt} \langle f(t), \psi \rangle.$$

Similarly, from the integration axiom for  $\mathbb{R}$ , one immediately proves that  $\mathcal{D}'_c(M)$  satisfies the integration axiom, in the sense that for any  $h: \mathbb{R} \rightarrow \mathcal{D}'_c(M)$ , there exists a unique  $H: \mathbb{R} \rightarrow \mathcal{D}'_c(M)$  satisfying  $H(0) = 0$  and  $H'(t) = h(t)$  for all  $t$ . In particular, if  $h: \mathbb{R} \rightarrow \mathcal{D}'_c(M)$ , the 'integral'  $\int_a^b h(u) du = H(b) - H(a)$  makes sense, and the Fundamental Theorem of Calculus holds.

As a particular case of special importance, we consider a *linear* vector-field on a Euclidean  $\mathbb{R}$ -module  $V$ . To say that the vector field is *linear* is to say that its principal-part formation  $V \rightarrow V$  is a linear map,  $\Gamma$ , say. We have then the following version of a classical result. By a *formal* solution for an ordinary differential equation, we mean a solution defined on the set  $D_\infty$  of nilpotent elements in  $\mathbb{R}$  (these form a subgroup of  $(\mathbb{R}, +)$ ).

Let a linear vector-field on a Euclidean vector space  $V$  be given by the linear map  $\Gamma : V \rightarrow V$ . Then the unique formal solution of the corresponding differential equation,

$$\dot{F}(t) = \Gamma(F(t)),$$

with initial position  $v$ , is the map  $D_\infty \times V \rightarrow V$  given by [Kock (1981); Kock and Reyes (2003)]

$$(t, v) \mapsto e^{t \cdot \Gamma}(v), \quad (3.73)$$

where the r.h.s here means the sum of the following ‘series’ (which has only finitely many non-vanishing terms, since  $t$  is assumed nilpotent):

$$v + t\Gamma(v) + \frac{t^2}{2!}\Gamma^2(v) + \frac{t^3}{3!}\Gamma^3(v) + \dots$$

where  $\Gamma^2(v)$  means  $\Gamma(\Gamma(v))$ , etc.

There is an analogous result for second order differential equations of the form

$$\ddot{F}(t) = \Gamma(F(t)).$$

The formal solution of this second order differential equation with initial position  $v$  and initial velocity  $w$ , is given by [Kock (1981); Kock and Reyes (2003)]

$$F(t) = v + t \cdot w + \frac{t^2}{2!}\Gamma(v) + \frac{t^3}{3!}\Gamma(w) + \frac{t^4}{4!}\Gamma^2(v) + \frac{t^5}{5!}\Gamma^2(w) + \dots$$

Also, given  $f : \mathbb{R} \rightarrow V$ , where  $V$  is a Euclidean vector space, and given  $g : \mathbb{R} \rightarrow \mathbb{R}$ . Then for any  $a, b \in \mathbb{R}$ ,

$$\int_a^b f(g(x)) \cdot g'(x) dx = \int_{g(a)}^{g(b)} f(u) du.$$

Linear maps between Euclidean vector spaces preserve differentiation and integration of functions  $\mathbb{R} \rightarrow V$ ; we shall explicitly need the following particular assertion: Let  $F : V \rightarrow W$  be a linear map between Euclidean vector spaces. Then for any  $f : \mathbb{R} \rightarrow V$ ,

$$F\left(\int_a^b f(t) dt\right) = \int_a^b F(f(t)) dt.$$

### 3.8.3.3 Spheres and Balls as Distributions

For  $a, b \in \mathbb{R}$ , we let  $[a, b]$  denote the distribution  $f \mapsto \int_a^b f(x) dx$ . Recall that such distributions on the line we call *intervals*; the *length* of an interval  $[a, b]$  is defined to be  $b - a$ . Let  $[a_1, b_1]$  and  $[a_2, b_2]$  be two such intervals. They are equal as distributions if and only if they have same length,  $b_1 - a_1 = b_2 - a_2 (= l, \text{ say})$ , and  $l \cdot (a_1 - a_2) = 0$  (this then also implies  $l \cdot (b_1 - b_2) = 0$ ).

We shall also consider such ‘balls’ in dimension 2 and 3, where, however,  $t$  cannot in general be recovered from the distribution, unless  $t$  is strictly positive.

We fix a positive integer  $n$ . We shall consider the sphere  $S_t$  of radius  $t$ , and the ball  $B_t$  of radius  $t$ , for any  $t \in \mathbb{R}$ , as distributions on  $\mathbb{R}^n$  (of compact support), in the following sense:

$$\begin{aligned} \langle S_t, \psi \rangle &= \int_{S_t} \psi(x) dx = t^{n-1} \int_{S_1} \psi(t \cdot u) du, \\ \langle B_t, \psi \rangle &= \int_{B_t} \psi(x) dx = t^n \int_{B_1} \psi(t \cdot u) du, \end{aligned}$$

where  $du$  refers to the surface element of the unit sphere  $S_1$  in the first equation and to the volume element of the unit ball  $B_1$  in the second. The expressions involving  $\int_{S_t}$  and  $\int_{B_t}$  are to be understood symbolically, unless  $t > 0$ ; if  $t > 0$ , they make sense literally as integrals over sphere and ball, respectively, of radius  $t$ , with  $dx$  denoting surface-, resp. volume element. The expression on the right in both equations makes sense for any  $t$ , and so the distributions  $S_t$  and  $B_t$  are defined for all  $t$ ; in particular, for nilpotent ones.

It is natural to consider also the following distributions  $S^t$  and  $B^t$  on  $\mathbb{R}^n$  (again of compact support):

$$\langle S^t, \psi \rangle = \int_{S_1} \psi(t \cdot u) du,$$



$$\langle B^t, \psi \rangle = \int_{B_1} \psi(t \cdot u) \, du.$$

For  $t > 0$ , they may, modulo factors of the type  $4\pi$ , be considered as 'average over  $S_t$ ' and 'average over  $B_t$ ', respectively, since  $S^t$  differs from  $S_t$  by a factor  $t^{n-1}$ , which is just the surface area of  $S_t$  (modulo the factor of type  $4\pi$ ), and similarly for  $B^t$ .

Note that  $S^1 = S_1$  and  $B^1 = B_1$ . And also note that the definition of  $S^t$  and  $B^t$  can be formulated as

$$S^t = H_t(S_1), \quad B^t = H_t(B_1),$$

where  $H_t : \mathbb{R}^n \rightarrow \mathbb{R}^n$  is the homothetic transformation  $u \mapsto t \cdot u$ , and where we are using the covariant functoriality of distributions of compact support.

For low dimensions, we shall describe the distributions  $S_t$ ,  $B_t$ ,  $S^t$  and  $B^t$  explicitly:

Dimension 1:

$$\begin{aligned} \langle S_t, \psi \rangle &= \psi(-t) + \psi(t), & \langle B_t, \psi \rangle &= \int_{-t}^t \psi(s) \, ds, \\ \langle S^t, \psi \rangle &= \psi(-t) + \psi(t), & \langle B^t, \psi \rangle &= \int_{-1}^1 \psi(t \cdot s) \, ds. \end{aligned}$$

Dimension 2:

$$\begin{aligned} \langle S_t, \psi \rangle &= \int_0^{2\pi} \psi(t \cos \theta, t \sin \theta) \, t \, d\theta, \\ \langle B_t, \psi \rangle &= \int_0^t \int_0^{2\pi} \psi(s \cos \theta, s \sin \theta) \, s \, d\theta \, ds, \\ \langle S^t, \psi \rangle &= \int_0^{2\pi} \psi(t \cos \theta, t \sin \theta) \, d\theta, \\ \langle B^t, \psi \rangle &= \int_0^1 \int_0^{2\pi} \psi(ts \cos \theta, ts \sin \theta) \, s \, d\theta \, ds. \end{aligned}$$

Dimension 3:

$$\begin{aligned} \langle S_t, \psi \rangle &= \int_0^\pi \int_0^{2\pi} \psi(t \cos \theta \sin \phi, t \sin \theta \sin \phi, t \cos \phi) t^2 \sin \phi \, d\theta \, d\phi, \\ \langle B_t, \psi \rangle &= \int_0^t \int_0^\pi \int_0^{2\pi} \psi(s \cos \theta \sin \phi, s \sin \theta \sin \phi, s \cos \phi) s^2 \sin \phi \, d\theta \, d\phi \, ds, \end{aligned}$$

$$\begin{aligned} \langle S^t, \psi \rangle &= \int_0^\pi \int_0^{2\pi} \psi(t \cos \theta \sin \phi, t \sin \theta \sin \phi, t \cos \phi) \sin \phi \, d\theta \, d\phi, \\ \langle B^t, \psi \rangle &= \int_0^1 \int_0^\pi \int_0^{2\pi} \psi(ts \cos \theta \sin \phi, ts \sin \theta \sin \phi, ts \cos \phi) s^2 \sin \phi \, d\theta \, d\phi \, ds. \end{aligned}$$

These formulas make sense for all  $t$ , whereas set-theoretically  $S_t$  and  $B_t$  (as point sets) only make good sense for  $t > 0$ .

### 3.8.3.4 Stokes Theorem for Unit Sphere

Recall that the main theorem of vector calculus is the *Stokes theorem*:

$$\int_{\partial\gamma} \omega = \int_{\gamma} d\omega,$$

for  $\omega$  an  $(n-1)$ -form,  $\gamma$  a suitable  $n$ -dimensional figure (with appropriate measure on it) and  $\partial\gamma$  its geometric boundary. In the synthetic context, the theorem holds at least for any singular cubical chain  $\gamma : I^n \rightarrow M$  ( $I^n$  the  $n$ -dimensional coordinate cube), because the theorem may then be reduced to the fundamental theorem of calculus, which is the only way integration enters in the elementary synthetic context; measure theory not being available therein (see [Moerdijk and Reyes (1991)] for details). Below, we shall apply the result not only for singular *cubes*, but also for singular *boxes*, like the usual  $(\gamma : \mathbb{R}^2 \rightarrow \mathbb{R}^2, [0, 2\pi] \times [0, 1])$ , ‘parameterizing the unit disk  $B$  by polar coordinates’,

$$\gamma(\theta, r) = (r \cos \theta, r \sin \theta). \quad (3.74)$$

We shall need from vector calculus the *Green–Gauss–Ostrogradsky Divergence theorem*

$$\text{flux of } \mathbf{F} \text{ over } \partial\gamma = \int_{\gamma} (\text{divergence of } \mathbf{F}),$$

with  $\mathbf{F}$  a vector-field, for the geometric ‘figure’  $\gamma$  = the unit ball in  $\mathbb{R}^n$ . For the case of the unit ball in  $\mathbb{R}^n$ , the reduction of the Divergence theorem to Stokes’ theorem is a matter of the *differential* calculus of vector fields and differential forms. For the convenience of the reader, we recall the case  $n = 2$ .

Given a vector-field  $\mathbf{F}(x, y) = (F(x, y), G(x, y))$  in  $\mathbb{R}^2$ , apply Stokes’ theorem to the differential form

$$\omega = -G(x, y)dx + F(x, y)dy$$

for the singular rectangle  $\gamma$  given by (3.74) above.

We also need that the trigonometric functions  $\cos$  and  $\sin$  should be present. We assume that they are given as part of the data, and that they satisfy  $\cos^2 + \sin^2 = 1$ , and  $\cos' = -\sin$ ,  $\sin' = \cos$ . Also as part of the data, we need specified an element  $\pi \in \mathbb{R}$  so that  $\cos \pi = -1$ ,  $\cos 0 = 1$ . Then we have

$$\begin{cases} \gamma^*(dx) = \cos \theta dr - r \sin \theta d\theta \\ \gamma^*(dy) = \sin \theta dr + r \cos \theta d\theta \\ \gamma^*(dx \wedge dy) = r (dr \wedge d\theta) \end{cases}.$$

Since  $d\omega = (\partial G/\partial y + \partial F/\partial x) dx \wedge dy = \operatorname{div}(\mathbf{F}) dx \wedge dy$ , then

$$\gamma^*(d\omega) = \operatorname{div}(\mathbf{F}) r (dr \wedge d\theta).$$

On the other hand,

$$\gamma^*\omega = (F \sin \theta - G \cos \theta)dr + (F r \cos \theta + G r \sin \theta) d\theta, \quad (3.75)$$

(all  $F$ ,  $G$ , and  $\mathbf{F}$  to be evaluated at  $(r \cos \theta, r \sin \theta)$ ). Therefore

$$\int_{\gamma} d\omega = \int_0^{2\pi} \int_0^1 \operatorname{div}(\mathbf{F}) r dr d\theta;$$

this is  $\int_{B_1} \operatorname{div}(\mathbf{F}) dA$ . On the other hand, by Stokes' theorem  $\int_{\gamma} d\omega = \int_{\partial\gamma} \omega$ , which is a curve integral of the 1-form (3.75) around the boundary of the rectangle  $[0, 2\pi] \times [0, 1]$ . This curve integral is a sum of four terms corresponding to the four sides of the rectangle. Two of these (corresponding to the sides  $\theta = 0$  and  $\theta = 2\pi$ ) cancel, and the term corresponding to the side where  $r = 0$  vanishes because of the  $r$  in  $r (dr \wedge d\theta)$ , so only the side with  $r = 1$  remains, and its contribution is, with the correct orientation,

$$\int_0^{2\pi} (F(\cos \theta, \sin \theta) \cos \theta + G(\cos \theta, \sin \theta) \sin \theta) d\theta = \int_{S_1} \mathbf{F} \cdot \mathbf{n} ds,$$

where  $\mathbf{n}$  is the outward unit normal of the unit circle. This expression is the flux of  $\mathbf{F}$  over the unit circle, which thus equals the divergence integral calculated above.

### 3.8.3.5 Time Derivatives of Expanding Spheres

We now combine vector calculus with the calculus of the basic ball- and sphere-distributions, to get the following result [Kock and Reyes (2003)]:

In  $\mathbb{R}^n$  (for any  $n$ ), we have, for any  $t$ ,

$$\frac{d}{dt}S^t = t \cdot \Delta(B^t),$$

where  $\Delta$  denotes the *Laplacian operator* (see [Kock (2001)] for ‘synthetic’ analysis of the Laplacian).

We collect some further information about  $t$ -derivatives of some of the  $t$ -parameterized distributions considered:

$$\frac{d}{dt}(B_t) = S_t. \quad (3.76)$$

In dimension 1, we have

$$\frac{d}{dt}(S_t) = \Delta(B_t); \quad (3.77)$$

for,

$$\frac{d}{dt} \langle S_t, \psi \rangle = \frac{d}{dt} \langle \psi(t) + \psi(-t) \rangle = \psi'(t) - \psi'(-t),$$

whereas

$$\langle \Delta B_t, \psi \rangle = \langle B_t, \psi'' \rangle = \int_{-t}^t \psi''(t) dt,$$

and the result follows from the *Fundamental theorem of calculus*.

The equation (3.77) implies the following equation if  $n = 1$ , while in [Kock and Reyes (2003)] it was proved that it also holds if  $n \geq 2$ :

$$t \cdot \frac{d}{dt}(S_t) = (n-1)S_t + t \cdot \Delta(B_t). \quad (3.78)$$

### 3.8.3.6 The Wave Equation

Let  $\Delta$  denote the Laplacian operator  $\sum \partial^2 / \partial x_i^2$  on  $\mathbb{R}^n$  (see [Kock (2001)]). We shall consider the wave equation (WE) in  $\mathbb{R}^n$ , (for  $n = 1, 2, 3$ ),

$$\frac{d^2}{dt^2}Q(t) = \Delta Q(t) \quad (3.79)$$

as a second order ordinary differential equation on the Euclidean vector space  $\mathcal{D}'_c(\mathbb{R}^n)$  of distributions of compact support; in other words, we are looking for functions

$$Q : \mathbb{R} \rightarrow \mathcal{D}'_c(\mathbb{R}^n),$$

so that for all  $t \in \mathbb{R}$ ,  $\ddot{Q}(t) = \Delta(Q(t))$ , viewing  $\Delta$  as a map  $\mathcal{D}'_c(\mathbb{R}^n) \rightarrow \mathcal{D}'_c(\mathbb{R}^n)$  [Kock and Reyes (2003)].

Consider a function  $f : \mathbb{R} \rightarrow V$ , where  $V$  is a Euclidean vector space (we are interested in  $V = \mathcal{D}'_c(\mathbb{R}^n)$ ). Then we call the pair of vectors in  $V$  consisting of  $f(0)$  and  $\dot{f}(0)$  the *initial state* of  $f$ . We can now, for each of the cases  $n = 1$ ,  $n = 3$ , and  $n = 2$  describe fundamental solutions to the wave equations. By *fundamental solutions*, we mean solutions whose initial state is either a constant times  $(\delta(\underline{0}), 0)$ , or a constant times  $(0, \delta(\underline{0}))$ .

In dimension 1 : The function  $\mathbb{R} \rightarrow \mathcal{D}'_c(\mathbb{R})$  given by

$$t \mapsto S^t (= S_t)$$

is a solution of the WE; its initial state is  $2(\delta(\underline{0}), 0)$ .

The function  $\mathbb{R} \rightarrow \mathcal{D}'_c(\mathbb{R})$  given by

$$t \mapsto B_t$$

is a solution of the WE with initial state  $2(0, \delta(\underline{0}))$ .

In dimension 3: The function  $\mathbb{R} \rightarrow \mathcal{D}'_c(\mathbb{R}^3)$  given by

$$t \mapsto S^t + t^2 \Delta(B^t)$$

is a solution of the WE with initial state  $4\pi\delta(\underline{0}), 0)$ . The function  $\mathbb{R} \rightarrow \mathcal{D}'_c(\mathbb{R}^3)$  given by

$$t \mapsto t \cdot S^t$$

is a solution of the WE with initial state  $4\pi(0, \delta(\underline{0}))$ .

In dimension 2: The function  $\mathbb{R} \rightarrow \mathcal{D}'_c(\mathbb{R}^2)$  given by

$$t \mapsto p_*(S^t + t^2 \Delta(B^t))$$

is a fundamental solution of the WE in dimension 2; its initial state is  $4\pi(\delta(\underline{0}), 0)$ . The function  $\mathbb{R} \rightarrow \mathcal{D}'_c(\mathbb{R}^2)$  given by

$$t \mapsto p_*(t \cdot S^t)$$

is a fundamental solution of the WE in dimension 2; its initial state is  $4\pi(0, \delta(\underline{0}))$ .

### 3.9 A Quick Look at Modern Geometrodynamics

Although not actually used in current biodynamics, the geometric machinery developed so far enables us to have a quick look at modern geometrodynamics, as used by mathematical physics of the last three decades.

#### 3.9.1 Einstein Equations

The most elegant physical theory of the 20th century was Einstein gravity theory. Here we give a bird-view on *Einstein equations*, as derived from *Hilbert action principle*, starting from the space-time manifold  $M$  (see [Misner *et al.* (1973)]), and following J. Wheeler's slogan: "Space tells matter how to move, matter tells space how to curve."

$$\begin{aligned}
 M & \quad \dots \text{ manifold } M \text{ (with tensor-fields defined on it)} \\
 g_{ij} &= g_{ij}(x^i) \in T_p M \quad \dots \text{ metric tensor on } M \\
 g^{ij} &= (g_{ij})^{-1} \quad \dots \text{ inverse metric tensor} \\
 \Gamma_{ijk} &= \frac{1}{2}(\partial_{x^i} g_{jk} - \partial_{x^j} g_{ki} + \partial_{x^k} g_{ij}) \quad \dots \text{ Christoffel symbols} \\
 R^l_{ijk} &= \partial_{x^j} \Gamma^l_{ik} - \partial_{x^k} \Gamma^l_{ij} + \Gamma^l_{rj} \Gamma^r_{ik} - \Gamma^l_{rk} \Gamma^r_{ij} \quad \dots \text{ Riemann tensor} \\
 R_{ij} &= R^l_{ijl} \quad \dots \text{ Ricci is the trace of Riemann} \\
 R &= g^{ij} R_{ij} \quad \dots \text{ scalar curvature is the trace of Ricci} \\
 G_{ij} &= R_{ij} - \frac{1}{2} R g_{ij} \quad \dots \text{ Einstein is trace-reversed Ricci} \\
 T_{ij} &= -2 \frac{\delta L_{Hilb}}{\delta g^{ij}} + g_{ij} L_{Hilb} \quad \dots \text{ deriving stress-energy tensor} \\
 L_{Hilb} &= \frac{1}{16\pi} g^{ij} R_{ij} (-g)^{1/2} \quad \dots \text{ from Hilbert Lagrangian} \\
 \delta S &= \delta \int L_{Hilb} (-g)^{1/2} d^4 x = 0 \quad \dots \text{ Hilbert action principle gives} \\
 G_{ij} &= 8\pi T_{ij} \quad \dots \text{ Einstein equations.}
 \end{aligned}$$

#### 3.9.2 $n$ -Categories in Physics

Now, recall that in the 19th century Maxwell unified Faraday's electric and magnetic fields. Maxwell's theory led to Einstein's special relativity where this unification becomes a spin-off of the unification of space and time in

the form of the *Faraday tensor* [Misner *et al.* (1973); Baez (2002)]

$$F = E \wedge dt + B,$$

where  $F$  is electromagnetic 2-form on space-time,  $E$  is electric 1-form on space, and  $B$  is magnetic 2-form on space. Gauge theory considers  $F$  as secondary object to a connection-potential 1-form  $A$ . This makes half of *Maxwell's equations* into tautologies [Baez (2002)], i.e.,

$$F = dA$$

implies Bianchi relation

$$dF = 0,$$

but does not imply the *dual Bianchi relation*, which is a second half of Maxwell's equations,

$$*d * F = J,$$

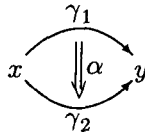
where  $*$  is the *dual Hodge star operator* and  $J$  is current 1-form.

To understand the deeper meaning of the connection-potential 1-form  $A$ , we can integrate it along a path  $\gamma$  in space-time

$$x \xrightarrow{\gamma} y$$

Classically, the integral  $\int_{\gamma} A$  represents an *action* for a charged point particle to move along the path  $\gamma$  (see section 4.4 below). Quantum-mechanically,  $\exp\left(i \int_{\gamma} A\right)$  represents a *phase* (within the unitary group  $U(1)$ ) by which the particle's wavefunction changes as it moves along the path  $\gamma$ , so  $A$  is a  $U(1)$ -connection.

The only thing that matters here is the *difference*  $\alpha$  between two paths  $\gamma_1$  and  $\gamma_2$  in the action  $\int_{\gamma} A$  [Baez (2002)], which is a two-morphism



To generalize this construction, consider any compact Lie group  $G$ . A connection  $A$  on a trivial  $G$ -bundle is a  $\gamma$ -valued 1-form.  $A$  assigns a

holonomy  $P \exp \left( i \int_{\gamma} A \right) \in G$  along any path

$$x \xrightarrow{\gamma} y$$

and has a curvature  $F$  given by

$$F = dA + A \wedge A.$$

The curvature  $F$  implies the extended *Bianchi relation*

$$dF + A \wedge F = 0,$$

but does not imply the dual Bianchi relation, i.e., *Yang-Mills relation*

$$*(d * F + A \wedge * F) = J.$$

Further generalization is performed with string theory. Just as point particles naturally interact with a 1-form  $A$ , strings naturally interact with a 2-form  $B$ , such that [Baez (2002)]

$$\text{action} = \int_{\Sigma} B, \quad \text{and} \quad \text{phase} = \exp \left( i \int_{\Sigma} B \right).$$

This 2-form connection  $B$  has a 3-form curvature  $G = dB$  which satisfies Maxwell-like equations, i.e.,

$$G = dB$$

implies Bianchi-like relation

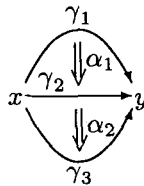
$$dG = 0,$$

but does not imply the dual, current relation

$$*d * G = J,$$

with the current 2-form  $J$ .

In this way, the ‘higher Yang-Mills theory’ assigns holonomies to paths and also to paths of paths, so that we have a 3-morphism





allowing us to ask not merely whether holonomies along paths are equal, but whether and how they are isomorphic.

This generalization actually proposes *categorification* of the basic geometric concepts of manifold, group, Lie group and Lie algebra [Baez (2002)]. Replacing the words *set* and *function* by *smooth manifold* and *smooth map* we get the concept of *smooth category*. Replacing them by *group* and *homomorphism* we get the concept of *2-group*. Replacing them by *Lie group* and *smooth homomorphism* we get the concept of *Lie 2-group*. Replacing them by *Lie algebra* and *Lie algebra homomorphism* we get the concept of *Lie 2-algebra*. Examples of the smooth categories are the following:

- (1) A smooth category with only identity morphisms is a smooth manifold.
- (2) A smooth category with one object and all morphisms invertible is a Lie group.
- (3) Any Lie groupoid gives a smooth category with all morphisms invertible.
- (4) A generalization of a vector bundle  $(E, M, \pi)$ , where  $E$  and  $M$  are smooth manifolds and projection  $\pi : E \rightarrow M$  is a smooth map, gives a a vector 2-bundle  $(E, M, \pi)$  where  $E$  and  $M$  are smooth categories and projection  $\pi : E \rightarrow M$  is a smooth functor.

3.9.3 Quantum Geometry Framework

Finally, although the quantum formalism is developed in the next chapter, here we give an introductory bird-view on the quantum stringy geometry of the 21st century (see e.g., [Witten (1998)]), which is supposed to be an ultimate form of geometrodynamics.

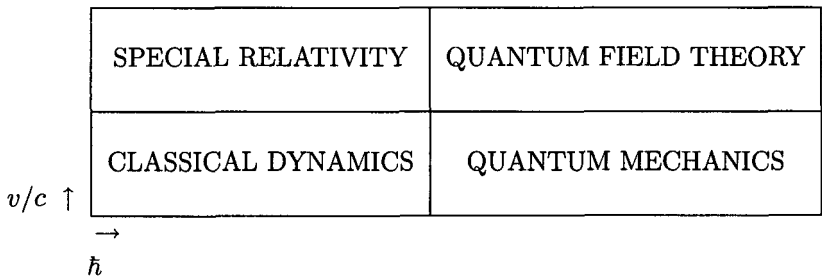


Fig. 3.4 The deformation from classical dynamics to quantum field theory (see text for explanation).

The relationship between non-relativistic classical mechanics and quantum field theory (see [Coleman (1988)]) is summarized in Figure 3.4. We see that the horizontal axis corresponds to the *Planck constant* (named after *Nobel Laureate Max Planck*)  $\hbar$  (divided by the typical action of the system being studied), while the vertical axis corresponds to  $v/c$ , the ration of motion velocity and light velocity.

Similarly, in modern superstring theory ('a theory of everything', see [Greene (2000)])<sup>6</sup>, there are also two relevant expansion parameters, as shown in Figure 3.5. Here we see that the horizontal axis corresponds to the value of the *string coupling constant*,  $g_s$ , while the vertical axis corresponds to the value of the dimensionless *sigma model coupling*  $\alpha'/R^2$  with  $R$  being a typical radius of a compactified portion of space). In the extreme  $\alpha' = g_s = 0$  limit, for instance, we recover relativistic particle dynamics. For nonzero  $g_s$  we recover point particle quantum field theory. For  $g_s = 0$  and nonzero  $\alpha'$  we are studying classical string theory. In general though, we need to understand the theory for arbitrary values of these parameters (see [Greene (1996)]).

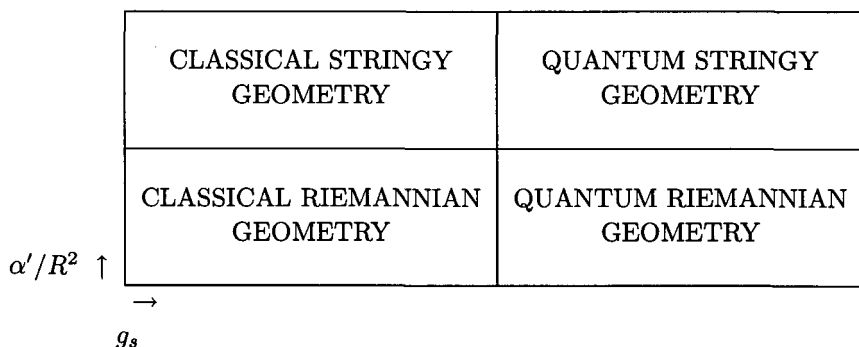


Fig. 3.5 The deformation from classical Riemannian geometry to *quantum stringy geometry* (see text for explanation).

<sup>6</sup>String theory proclaims, for instance, that the observed particle properties – that is, the different masses and other properties of both the fundamental particles and the force particles associated with the four forces of nature (the strong and weak nuclear forces, electromagnetism, and gravity) – are a reflection of the various ways in which a string can vibrate. Just as the strings on a violin or on a piano have resonant frequencies at which they prefer to vibrate – patterns that our ears sense as various musical notes and their higher harmonics – the same holds true for the loops of string theory. But rather than producing musical notes, each of the preferred mass and force charges are determined by the string's oscillatory pattern. The electron is a string vibrating one way, the up-quark is a string vibrating another way, and so on.

Quantum stringy geometry postulates the existence of 6D *Calabi–Yau manifolds* at every point of the space–time. These curled–up local manifolds transform according to the *orbifolding* procedure (see [Greene (1996)]).

For more details on quantum mechanics see next chapter as well as Appendix.

### 3.10 3D Modelling and Animation in Biodynamics

In this section we switch from ‘hard’ to ‘soft’ geometry and present some basic *3D–graphics* techniques of *human animation* and *geometric modelling*, as used in contemporary biodynamics. Recall that a related technique, called *stereolithography* (also known as *3D–layering* or *3D–printing*), gives a fast, easy way to turn CAD drawings into real 3D–objects. It is currently one of the most advanced techniques in medical surgery.

#### 3.10.1 *Essentials of Human Animation*

Human animation is a modern, computer graphics based technique of 3D geometric modelling of human body in motion. It uses specialized computer hardware (powerful graphical work–stations) and software (3D–graphics packages) to create virtual human motion.

Now, automatically animating virtual humans with actions that reflect real human motions is still a challenge. Skilled animators are able to create effective and compelling human characters through labor–intensive scripting of every subtlety of motion.

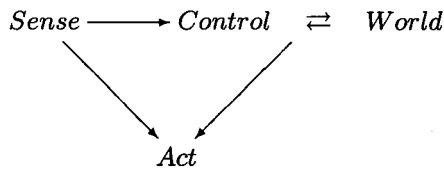
Classical techniques of human animation included:

- (1) Manual *key–frame animation*, and
- (2) Automatic *motion capture* based animation.

The recent trend in human animation is the so–called *physically based geometric modelling*, which attempts to go beyond the computer illusion created by above two classical techniques, including realistic physical forces (whose action human eye cannot really see on the screen). This new physical approach has two main branches, namely controller based whole body animation, and local muscular dynamics.

Another new trend in human animation involves the use of *autonomous* or *reactive agents* (like popular *Jack* and *DI–Guy* agents). The so–called *smart avatars* are virtual human representations controlled by real people.

Given instructions interactively, smart avatars can act as reactive agents. During a real-time simulation, a user should be able to dynamically refine his or her avatar's behavior in reaction to simulated stimuli without having to undertake a lengthy off-line programming session. The *agent action cycle* works according to the diagram



and has a bilateral relation with external world. The avatars can also appear in the form of virtual humanoids (see Figure 3.6).

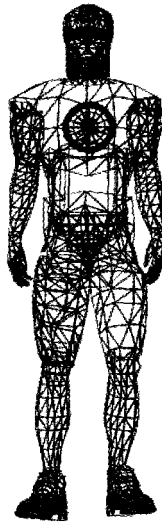


Fig. 3.6 A virtual humanoid.

#### 3.10.1.1 Motion Capture-Based Human Animation

Human animation classically starts with the process of *motion capture* (MC). The MC is the kinematic recording technique, usually performed in indoor studios equipped with several high-speed digital video cameras. It provides us with the data collected from an individual performing the

task that we would like to animate. The raw MC-data are then converted into joint angle data, i.e., discrete angular trajectories, for each joint of the virtual human body that we wish to animate.

A simulated PD *servomechanism* is frequently used to compute joint torques that will move a virtual human limb along a desired trajectory defined by the *captured motion*. The servomechanism works by monitoring the actual and goal joint angle *pos* and velocity *vel* and computing a torque to reduce the error between the two based on the following relation:

$$torque = -k \cdot (pos - pos_{goal}) - b \cdot (vel - vel_{goal}),$$

where  $k$  is the position gain for the PD servo on the specified joint (this corresponds to a spring constant, and has units of Newton-meters per radian);  $b$  is the velocity gain for the PD servo on the specified joint (this corresponds to a damping constant, and has units of Newton-meters per radian/second).

These PD servomechanisms are used at each internal joint of the virtual human. The servo parameters  $k$  and  $b$  need to be tuned to the joint and the behavior and will depend upon the mass, inertia, and configuration of the limbs.

### 3.10.1.2 Virtual Muscular Dynamics in 3D-Graphics

Inside the common 3D-Graphics environment, like Discreet's 3DS MAX, the contraction of a virtual skeletal muscle is animated by interaction of muscular 3D-vertices obeying the second Newton law. In vector form of the MAX *point-3*-class it reads:

$$\mathbf{F} = \dot{\mathbf{p}},$$

where  $\mathbf{F}$  represents the force vector (the cause of motion of a single vertex) and  $\mathbf{p}$  represents the momentum vector (the measure of motion of a vertex).

The momentum vector  $\mathbf{p}$  of each muscular vertex equals the product  $m\dot{\mathbf{r}}$  of its scalar mass  $m$  and its velocity vector  $\dot{\mathbf{r}}$ , where  $\mathbf{r}$  denotes the position vector of a vertex.

*Interaction of two vertices with masses  $m_1$  and  $m_2$*

$$\mathbf{F}_{12} \longleftarrow \bigcirc_{m_1} \blacktriangleleft \blacktriangleright \bigcirc_{m_2} \longrightarrow \mathbf{F}_{21}$$

caused by attractive force  $\mathbf{F}_{12} = -\mathbf{F}_{21}$ , in the absence of external forces,

obeys the third Newtonian law

$$\dot{\mathbf{p}}_1 + \dot{\mathbf{p}}_2 = \mathbf{F}_{12} + \mathbf{F}_{21} = 0.$$

The *ideal muscle* has  $N$  vertices with masses  $m_i$  which are interacting with each other through forces  $\mathbf{F}_{ij}$  ( $i \neq j$ )

$$\sum_{i=1}^N \dot{\mathbf{p}}_i = \sum_{i \neq j} \mathbf{F}_{ij} = 0,$$

which means that its total momentum

$$\sum_{i=1}^N \mathbf{p}_i = \sum_{i=1}^N m_i \dot{\mathbf{R}}$$

is conserved during the contraction. Here,  $\mathbf{R} = \frac{\sum_i m_i \mathbf{r}_i}{\sum_i m_i}$  represents the position vector of the center of mass of the muscle. Therefore, both the total mass of the muscle  $\sum_i m_i$  and velocity of its center of mass  $\dot{\mathbf{R}}$  are also conserved quantities during the muscular contraction.

The *real muscle* has also certain amount of elasticity ( $c_i$ -coefficients) as well as viscosity ( $b_i$ -coefficients) distributed among the vertices, thus obeying the following *contraction law*

$$\sum_{i=1}^N \dot{\mathbf{p}}_i + b_i \mathbf{p}_i + c_i \int \mathbf{p}_i dt = \sum_{i \neq j} \mathbf{F}_{ij} = 0.$$

### 3.10.2 Curves and Surfaces in Geometric Modelling

The two most common methods of representing curves and surfaces in geometric modelling are implicit equations and parametric functions [Piegl and Tiller (1997)]. In this subsection, summing over repeated indices from 0 to  $n$  (and  $m$  in the surface case) is assumed, unless otherwise stated.

The implicit equation of a curve lying in the  $xy$  plane has the form  $f(x, y) = 0$ . This equation describes an implicit relationship between the  $x$  and  $y$  coordinates of the points lying on the curve. For a given curve the equation is unique up to a multiplicative constant.

In parametric form, each of the coordinates of a point on the curve is represented separately as an explicit function of an independent parameter

$$\mathbf{C}(u) = (x(u), y(u)), \quad a \leq u \leq b.$$

Thus,  $\mathbf{C}(u)$  is a vector-valued function of the independent variable,  $u$ . Although the interval  $[a, b]$  is arbitrary, it is usually normalized to  $[0, 1]$ .

The parametric representation of a curve is not unique [Piegl and Tiller (1997)].

It is instructive to think of  $\mathbf{C}(u) = (x(u), y(u))$  as the path traced out by a particle as a function of time;  $u$  is the time variable, and  $[a, b]$  is the time interval. The first and second derivatives of  $\mathbf{C}(u)$  are the velocity,  $\mathbf{C}'(u) = (\dot{x}(u), \dot{y}(u))$ , and acceleration,  $\mathbf{C}''(u) = (\ddot{x}(u), \ddot{y}(u))$ , of the particle, respectively. Velocity vectors represent tangent vectors to the curve at certain time points.

By adding a  $z$  coordinate, the parametric method is easily extended to represent arbitrary curves in 3D space,  $\mathbf{C}(u) = (x(u), y(u), z(u))$ .

A surface is defined by an implicit equation of the form  $f(x, y, z) = 0$ . A parametric representation (not unique) of the same surface is given by  $\mathbf{S}(u, v) = (x(u, v), y(u, v), z(u, v))$ . Thus two parameters  $(u, v)$  are required to define a surface. In case of sphere, holding  $u$  fixed and varying  $v$  generates the latitudinal lines of the sphere; holding  $v$  fixed and varying  $u$  generates the longitudinal lines. In case of arbitrary surface we have *isoparametric curves* (or *isocurves*).

Given the first partial derivatives  $\mathbf{S}_u(u, v)$  and  $\mathbf{S}_v(u, v)$ , (the velocities along latitudinal and longitudinal lines in case of sphere), at any point on the surface  $\mathbf{S}(u, v)$  where the vector cross product  $\mathbf{S}_u \times \mathbf{S}_v$  does not vanish, the unit normal vector,  $\mathbf{N}$ , is given by [Piegl and Tiller (1997)]

$$\mathbf{N} = \frac{\mathbf{S}_u \times \mathbf{S}_v}{|\mathbf{S}_u \times \mathbf{S}_v|}.$$

The existence of a normal vector at a point, and the corresponding tangent plane, is a geometric property of the surface independent of the parametrization.

### 3.10.2.1 Power Basis Form of a Curve

An  $n$ th degree power basis curve is given by

$$\mathbf{C}(u) = (x(u), y(u), z(u)) = \mathbf{a}_i u^i, \quad 0 \leq u \leq 1.$$

The  $\mathbf{a}_i = (x_i, y_i, z_i)$  are vectors, hence

$$x(u) = x_i u^i, \quad y(u) = y_i u^i, \quad z(u) = z_i u^i.$$

- $n = 1$ .  $\mathbf{C}(u) = \mathbf{a}_0 + \mathbf{a}_1 u$ ,  $0 \leq u \leq 1$ , is a straight line segment between points  $\mathbf{a}_0$  and  $\mathbf{a}_0 + \mathbf{a}_1$ . The constant  $\mathbf{C}'(u) = \mathbf{a}_1$  gives the direction of the line [Piegl and Tiller (1997)].
- $n = 2$ . In general,  $\mathbf{C}(u) = \mathbf{a}_0 + \mathbf{a}_1 u + \mathbf{a}_2 u^2$ ,  $0 \leq u \leq 1$ , is a parabolic arc between the points  $\mathbf{a}_0$  and  $\mathbf{a}_0 + \mathbf{a}_1$ . The acceleration vector,  $\mathbf{C}''(u) = 2\mathbf{a}_2$ , is a constant.
- $n = 3$ . The cubic,  $\mathbf{C}(u) = \mathbf{a}_0 + \mathbf{a}_1 u + \mathbf{a}_2 u^2 + \mathbf{a}_3 u^3$ ,  $0 \leq u \leq 1$ , is a very general curve; it can be a truly *twisted* 3D curve, not lying in a single plane; it can have an inflection point, a cusp, or a loop (see Figure 7.45 below). A twisted curve results if  $\mathbf{a}_0, \mathbf{a}_1, \mathbf{a}_2, \mathbf{a}_3$  do not lie in a unique plane. An inflection point on a planar curve is defined as a point where the curve is smooth (no cusp) and the tangent line at the point passes through the curve. This implies a change in the turning direction of the curve. At an inflection point, either  $\mathbf{C}''(u) = 0$ , or  $\mathbf{C}'(u)$  is parallel to  $\mathbf{C}''(u)$ . A necessary (but not sufficient) condition for a cusp at  $u = u_0$  is  $\mathbf{C}'(u_0) = 0$  (zero velocity).

### 3.10.2.2 Bezier Curves

Another parametric polynomial curve is the Bezier curve. The power basis and Bezier forms are mathematically equivalent, since they both use polynomials for their coordinate functions; i.e., any curve that can be represented in one form can also be represented in the other form. However, the Bezier method is superior for geometric modelling [Piegl and Tiller (1997)].

An  $n$ th degree Bezier curve is defined by

$$\mathbf{C}(u) = B_{i,n}(u)\mathbf{P}_i, \quad 0 \leq u \leq 1.$$

The basis (blending) functions,  $\{B_{i,n}(u)\}$ , are the classical  $n$ th degree Bernstein polynomials given by

$$B_{i,n}(u) = \frac{n!}{i!(n-i)!} u^i (1-u)^{n-i}.$$

The geometric coefficients of this form,  $\{\mathbf{P}_i\}$ , are called *control points*.

Case  $n = 3$ :

- the control polygons approximate the shapes of the curves;
- $\mathbf{P}_0 = \mathbf{C}(0)$  and  $\mathbf{P}_3 = \mathbf{C}(1)$ ;
- the endpoint tangent directions are parallel to  $\mathbf{P}_1 - \mathbf{P}_0$  and  $\mathbf{P}_3 - \mathbf{P}_2$ ;



- convex hull property: the curves are contained in the convex hulls of their defining control points;
- variation diminishing property: no straight line (plane in the 3D case) intersects a curve more times than it intersects the curve's control polygon. This expresses the property that a Bezier curve follows its control polygon rather closely and does not wiggle more than its control polygon.
- initially (at  $u = 0$ ) the curve is turning in the same direction as  $\mathbf{P}_0\mathbf{P}_1\mathbf{P}_2$ . At  $u = 1$  it is turning in the direction  $\mathbf{P}_1\mathbf{P}_2\mathbf{P}_3$ ;
- a loop in the control polygon may or may not imply a loop in the curve.

Bezier curves are invariant under the usual transformations such as rotations, translations, and scalings; that is, one applies the transformation to the curve by applying it to the control polygon [Piegl and Tiller (1997)].

The general expression for the derivative of a Bezier curve is

$$\mathbf{C}'(u) = B'_{i,n}(u)\mathbf{P}_i = n \sum_{i=0}^{n-1} B_{i,n-1}(u)(\mathbf{P}_{i+1} - \mathbf{P}_i). \quad (3.80)$$

From (3.80) it follows that:

- the derivative of an  $n$ th degree Bezier curve is an  $(n-1)$ th degree Bezier curve;
- the expressions for the end derivatives at  $u = 0$  and  $u = 1$  are symmetric (due to the symmetry of the basis functions);
- the  $k$ th derivative at an endpoint depends solely on the  $k + 1$  control points at that end.

A general  $n$ th degree Bezier curve is recursively given by [Piegl and Tiller (1997)]

$$\mathbf{C}_n(\mathbf{P}_0, \dots, \mathbf{P}_n) = (1 - u)\mathbf{C}_{n-1}(\mathbf{P}_0, \dots, \mathbf{P}_{n-1}) + u\mathbf{C}_{n-1}(\mathbf{P}_1, \dots, \mathbf{P}_n).$$

This follows from the recursive definition of the basis functions. Fixing  $u = u_0$  and denoting  $\mathbf{P}_i$  by  $\mathbf{P}_{0,i}$  we get a recursive *de Casteljau Algorithm* for computing the point  $\mathbf{C}(u_0) = \mathbf{P}_{n,0}(u_0)$  of an  $n$ th degree Bezier curve

$$\begin{aligned} \mathbf{P}_{k,i}(u_0) &= (1 - u_0)\mathbf{P}_{k-1,i}(u_0) + u_0\mathbf{P}_{k-1,i+1}(u_0), \\ &\quad (k = 1, \dots, n; \quad i = 0, \dots, n - k). \end{aligned}$$

### 3.10.2.3 Rational Bezier Curves

Although polynomials offer many advantages, there exist a number of important curve and surface types which cannot be represented precisely using polynomials, e.g., circles, ellipses, hyperbolas, cylinders, cones, spheres, etc. All conic curves, including the circle, can be represented using *rational functions*, which are defined as the ratio of two polynomials. In fact, they are represented with rational functions of the form

$$x(u) = \frac{X(u)}{W(u)}, \quad y(u) = \frac{Y(u)}{W(u)},$$

where  $X(u)$ ,  $Y(u)$ , and  $W(u)$  are polynomials, that is, each of the coordinate functions has the same denominator.

An  $n$ th degree *rational Bezier curve* is defined as [Piegl and Tiller (1997)]

$$C(u) = R_{i,n}(u)P_i, \quad 0 \leq u \leq 1,$$

where

$$R_{i,n}(u) = \frac{B_{i,n}(u)w_i}{B_{j,n}(u)w_j}$$

are the rational basis functions for this curve form.

### 3.10.3 B-Spline Basis Functions

Curves consisting of just one polynomial or rational segment are often inadequate. Their shortcomings are:

- a high degree is required to satisfy a large number of constraints; e.g.,  $(n - 1)$ -degree is needed to pass a polynomial Bezier curve through  $n$  data points. However, high degree curves are inefficient to process and are numerically unstable;
- a high degree is required to accurately fit some complex shapes;
- single-segment curves (surfaces) are not well-suited to interactive shape design; although Bezier curves can be shaped by means of their control points (and weights), the control is not sufficiently local.

The solution is to use curves (surfaces) which are *piecewise polynomial*, or *piecewise rational*. We want a curve representation of the form

$$C(u) = f_i(u)P_i, \quad (3.81)$$

where the  $\mathbf{P}_i$  are *control points*, and the  $\{f_i(u), i = 0, \dots, n\}$  are *piecewise polynomial functions* forming a basis for the vector space of all piecewise polynomial functions of the desired degree and continuity (for a fixed break-point sequence,  $U = \{u_i\}, 0 \leq i \leq m$ ). Note that continuity is determined by the basis functions, hence the control points can be modified without altering the curve's continuity. Furthermore, the  $\{f_i\}$  should have the 'usual' nice analytic properties, which insures that the curves defined by (3.81) have nice geometric properties similar to Bezier curves, e.g., convex hull, variation diminishing, transformation invariance. Another important property that we seek in our basis functions is that of *local support*; this implies that each  $\{f_i(u)\}$  is nonzero only on a limited number of subintervals, not the entire domain,  $[u_0, u_m]$ . Since  $\mathbf{P}_i$  is multiplied by  $\{f_i(u)\}$ , moving  $\mathbf{P}_i$  affects curve shape only on the subintervals where  $\{f_i(u)\}$  are zero [Piegl and Tiller (1997)].

Finally, given appropriate piecewise polynomial basis functions, we can construct piecewise rational curves

$$\mathbf{C}^w(u) = f_i(u)\mathbf{P}_i^w$$

and nonrational and rational tensor-product surfaces, respectively

$$\mathbf{S}(u, v) = f_i(u)g_j(v)\mathbf{P}_{i,j} \quad \text{and} \quad \mathbf{S}^w(u, v) = f_i(u)g_j(v)\mathbf{P}_{i,j}^w.$$

### 3.10.3.1 DeBoor-Cox Recursive Definition

Let  $U = \{u_0, \dots, u_m\}$  be a nondecreasing sequence of real numbers, i.e.,  $u_i \leq u_{i+1}, i = 0, \dots, m-1$ . The  $u_i$  are called *knots*, and  $U$  is the *knot vector*. The  $i$ th B-spline basis function of  $p$ -degree (order  $p+1$ ), denoted by  $N_{i,p}(u)$ , is defined as

$$N_{i,0}(u) = \begin{cases} 1 & : \text{ if } u_i \leq u \leq u_{i+1}, \\ 0 & : \text{ otherwise.} \end{cases}$$

$$N_{i,p}(u) = \frac{u - u_i}{u_{i+p} - u_i} N_{i,p-1}(u) + \frac{u_{i+p+1} - u}{u_{i+p+1} - u_{i+1}} N_{i+1,p-1}(u).$$

### 3.10.3.2 Derivatives of B-Spline Basis Functions

The derivative of a basis function is recursively defined by

$$N'_{i,p}(u) = \frac{p}{u_{i+p} - u_i} N_{i,p-1}(u) - \frac{p}{u_{i+p+1} - u_{i+1}} N_{i+1,p-1}(u). \quad (3.82)$$

Repeated differentiation of (3.82) produces the general formula for the  $k$ th derivative of  $N_{i,p}(u)$

$$N_{i,p}^{(k)}(u) = p \left( \frac{N_{i,p-1}^{(k-1)}(u)}{u_{i+p} - u_i} - \frac{N_{i+1,p-1}^{(k-1)}(u)}{u_{i+p+1} - u_{i+1}} \right).$$

### 3.10.4 *B-Spline Curves and Surfaces in Geometric Modelling*

#### 3.10.4.1 *Definition of B-Spline Curves*

A  $p$ th degree— *B-spline curve* is defined by [Piegl and Tiller (1997)]

$$\mathbf{C}(u) = N_{i,p}(u)\mathbf{P}_i, \quad a \leq u \leq b,$$

where the  $\{\mathbf{P}_i\}$  are *control points*, and the  $\{N_{i,p}(u)\}$  are the  $p$ th degree B-spline basis functions (3.82) defined on the nonperiodic (and nonuniform) knot vector

$$U = \{\underbrace{a, \dots, a}_{p+1}, u_{p+1}, \dots, u_{m-p-1}, \underbrace{b, \dots, b}_{p+1}\}.$$

The polygon formed by the  $\{\mathbf{P}_i\}$  is called the *control polygon*.

#### 3.10.4.2 *Properties of B-Spline Curves*

- If  $n = p$  and  $U = \{0, \dots, 0, 1, \dots, 1\}$ , then  $\mathbf{C}(u)$  is a Bezier curve.
- $\mathbf{C}(u)$  is a piecewise polynomial curve (since the  $N_{i,p}(u)$  are piecewise polynomials); the degree,  $p$ , number of control points,  $n+1$ , and number of knots,  $m+1$ , are related by:  $m = n + p + 1$ .
- Endpoint interpolation:  $\mathbf{C}(0) = \mathbf{P}_0$  and  $\mathbf{C}(1) = \mathbf{P}_n$ .
- Affine invariance: an affine transformation is applied to the curve by applying it to the control points. Let  $\mathbf{r}$  be a point in  $\mathbb{R}^3$ . An *affine transformation*  $\Phi: \mathbb{R}^3 \rightarrow \mathbb{R}^3$  has the form:  $\Phi(\mathbf{r}) = \mathbf{A}\mathbf{r} + \mathbf{v}$ , where  $\mathbf{A}$  is a  $3 \times 3$  matrix and  $\mathbf{v}$  is a vector. Affine transformations include translations, rotations, scalings, and shears. The affine invariance property for B-spline curves follows from the partition of unity property of the  $N_{i,p}(u)$ .
- Strong convex hull property: the curve is contained in the convex hull of its control polygon; in fact, if  $u \in [u_i, u_{i+1}]$ ,  $p \leq i \leq m - p - 1$ , then  $\mathbf{C}(u)$  is in the convex hull of the control points  $\mathbf{P}_{i-p}, \dots, \mathbf{P}_i$ .

- Local modification scheme: moving  $\mathbf{P}_i$  changes  $\mathbf{C}(u)$  only in the interval  $u \in [u_i, u_{i+p+1})$ .
- The control polygon represents a piecewise linear approximation to the curve; this approximation is improved by knot insertion or degree elevation. As a general rule, the lower the degree, the closer a B-spline curve follows its control polygon. The extreme case is  $p = 1$ , for which every point  $\mathbf{C}(u)$  is just a linear interpolation between two control points. In this case, the curve is the control polygon itself [Piegl and Tiller (1997)].
- Moving along the curve  $\mathbf{C}(u)$  from  $u = 0$  to  $u = 1$ , the  $N_{i,p}(u)$  functions act like switches; as  $u$  moves past a knot, one  $N_{i,p}(u)$  (and hence the corresponding  $\mathbf{P}_i$ ) switches off, and the next one switches on.
- Variation diminishing property: no plane (resp. line) has more intersections with the curve than with the control polygon.
- The continuity and differentiability of  $\mathbf{C}(u)$  follow from that of the  $N_{i,p}(u)$  (since  $\mathbf{C}(u)$  is just a linear combination of the  $N_{i,p}(u)$ ). Thus,  $\mathbf{C}(u)$  is infinitely differentiable in the interior of knot intervals, and it is at least  $p - k$  times continuously differentiable at knot of multiplicity  $k$ .
- It is possible (and sometimes useful) to use multiple (coincident) control points.

### 3.10.4.3 Derivatives of a B-Spline Curve

$\mathbf{C}^{(k)}(u)$ , the  $k$ th derivative of  $\mathbf{C}(u)$  is, for fixed  $u$  obtained by computing the  $k$ th derivatives of the basis functions, given by [Piegl and Tiller (1997)]

$$\mathbf{C}^{(k)}(u) = N_{i,p}^{(k)}(u)\mathbf{P}_i.$$

If  $u$  is not fixed, the first derivative is defined as

$$\mathbf{C}'(u) = \sum_{i=0}^{n-1} N_{i,p-1}(u)\mathbf{Q}_i, \quad (3.83)$$

where

$$\mathbf{Q}_i = p \frac{\mathbf{P}_{i+1} - \mathbf{P}_i}{u_{i+p+1} - u_{i+1}}.$$

Recursively applying (3.83) through (3.81) the higher derivatives are ob-

tained

$$\mathbf{C}^{(k)}(u) = \sum_{i=0}^{n-1} N_{i,p-k}(u) \mathbf{P}_i^{(k)},$$

with

$$\mathbf{P}_i^{(k)} = \begin{cases} \mathbf{P}_i & : k = 0 \\ \frac{p-k+1}{u_{i+p+1}-u_{i+k}} \left( \mathbf{P}_{i+1}^{(k-1)} - \mathbf{P}_i^{(k-1)} \right) & : k > 0 \end{cases}$$

and

$$U^{(k)} = \{ \underbrace{0, \dots, 0}_{p-k+1}, u_{p+1}, \dots, u_{m-p-1}, \underbrace{1, \dots, 1}_{p-k+1} \}.$$

#### 3.10.4.4 Definition of B-Spline Surfaces

A B-spline surface is obtained by taking a bidirectional net of control points, two knot vectors, and the products of the univariate B-spline functions [Piegl and Tiller (1997)]

$$\mathbf{S}(u, v) = N_{i,p}(u) N_{j,q}(v) \mathbf{P}_{i,j},$$

with

$$U = \{ \underbrace{0, \dots, 0}_{p+1}, u_{p+1}, \dots, u_{r-p-1}, \underbrace{1, \dots, 1}_{p+1} \},$$

$$V = \{ \underbrace{0, \dots, 0}_{q+1}, v_{q+1}, \dots, v_{s-q-1}, \underbrace{1, \dots, 1}_{q+1} \}.$$

(where  $r = n + p + 1$  and  $s = m + q + 1$ ).

#### 3.10.4.5 Properties of B-Spline Surfaces

- If  $n = p$ ,  $m = q$ ,  $U = \{0, \dots, 0, 1, \dots, 1\}$ ,  $V = \{0, \dots, 0, 1, \dots, 1\}$ , then  $\mathbf{S}(u, v)$  is a Bezier surface.
- The surface interpolates the four corner control points:  
 $\mathbf{S}(0, 0) = \mathbf{P}_{0,0}$ ,  $\mathbf{S}(1, 0) = \mathbf{P}_{n,0}$ ,  $\mathbf{S}(0, 1) = \mathbf{P}_{0,m}$ ,  $\mathbf{S}(1, 1) = \mathbf{P}_{n,m}$ .
- Affine invariance: an affine transformation is applied to the surface by applying it to the control points.
- Strong convex hull property: if  $(u, v) \in [u_{i_0}, u_{i_0+1}] \times [v_{j_0}, v_{j_0+1}]$ , then  $\mathbf{S}(u, v)$  is in the convex hull of the control points  $\mathbf{P}_{i,j}$ ,  $i_0 - p \leq i \leq i_0$  and  $j_0 - q \leq j \leq j_0$ .

- If triangulated, the control net forms a piecewise planar approximation to the surface; as in the case of curves, the lower the degree the better the approximation.
- Local modification scheme: if  $\mathbf{P}_{i,j}$  is moved it affects the surface only in the rectangle  $[u_{i_0}, u_{i_0+1}] \times [v_{j_0}, v_{j_0+1}]$ .
- The continuity and differentiability of  $\mathbf{S}(u, v)$  follows from that of the basis functions [Piegl and Tiller (1997)].

### 3.10.4.6 Derivatives of a B-Spline Surface

Let  $(u, v)$  be fixed. As for curves, we get these derivatives by computing derivatives of the basis functions. In particular

$$\frac{\partial^{k+l}}{\partial^k u \partial^l v} \mathbf{S}(u, v) = N_{i,p}^{(k)}(u) N_{j,q}^{(l)}(v) \mathbf{P}_{i,j}.$$

Now, let us formally differentiate  $\mathbf{S}(u, v)$ . With respect to  $u$  we have

$$\mathbf{S}_u(u, v) = \frac{\partial}{\partial u} \mathbf{S}(u, v) = \sum_{i=0}^{n-1} \sum_{j=0}^m N_{i,p-1}(u) N_{j,q}(v) \mathbf{P}_{i,j}^{(1,0)}, \quad (3.84)$$

where

$$\mathbf{P}_{i,j}^{(1,0)} = p \frac{\mathbf{P}_{i+1,j} - \mathbf{P}_{i,j}}{u_{i+p+1} - u_{i+1}}, \quad (3.85)$$

$$U^{(1)} = \{\overbrace{0, \dots, 0}^p, u_{p+1}, \dots, u_{r-p-1}, \overbrace{1, \dots, 1}^p\}, \quad V^{(0)} = V$$

Analogously, with respect to  $v$  we have

$$\mathbf{S}_v(u, v) = \frac{\partial}{\partial v} \mathbf{S}(u, v) = \sum_{i=0}^n \sum_{j=0}^{m-1} N_{i,p}(u) N_{j,q-1}(v) \mathbf{P}_{i,j}^{(0,1)}, \quad (3.86)$$

where

$$\mathbf{P}_{i,j}^{(0,1)} = q \frac{\mathbf{P}_{i,j+1} - \mathbf{P}_{i,j}}{v_{j+q+1} - v_{j+1}}, \quad (3.87)$$

$$U^{(0)} = U, \quad V^{(1)} = \{0, \dots, 0, \overbrace{v_{q+1}, \dots, v_{s-q-1}}^q, \overbrace{1, \dots, 1}^q\}.$$

Applying first (3.84, 3.85), then (3.86, 3.87) yields

$$\mathbf{S}_{uv}(u, v) = \frac{\partial^2}{\partial u \partial v} \mathbf{S}(u, v) = \sum_{i=0}^{n-1} \sum_{j=0}^{m-1} N_{i,p-1}(u) N_{j,q-1}(v) \mathbf{P}_{i,j}^{(1,1)},$$

where

$$\mathbf{P}_{i,j}^{(1,1)} = q \frac{\mathbf{P}_{i,j+1}^{(1,0)} - \mathbf{P}_{i,j}^{(1,0)}}{v_{j+q+1} - v_{j+1}},$$

and  $U^{(1)}$  and  $V^{(1)}$  are as defined previously.

In general

$$\frac{\partial^{k+l}}{\partial^k u \partial^l v} \mathbf{S}(u, v) = N_{i,p-k}(u) N_{j,q-l}(v) \mathbf{P}_{i,j}^{(k,l)},$$

where

$$\mathbf{P}_{i,j}^{(k,l)} = (q-l+1) \frac{\mathbf{P}_{i,j+1}^{(k,l-1)} - \mathbf{P}_{i,j}^{(k,l-1)}}{v_{j+q+1} - v_{j+1}}.$$

### 3.10.5 NURBS Curves and Surfaces

The most important tools in GM are non-uniform rational B-splines (popular NURBS, for short).

#### 3.10.5.1 Definition of NURBS Curves

A  $p$ th degree NURBS curve is defined by [Piegl and Tiller (1997)]

$$\mathbf{C}(u) = R_{i,p}(u) \mathbf{P}_i,$$

where  $\{R_{i,p}(u)\}$  are the *rational basis functions*; they are piecewise rational functions defined on  $u \in [a, b]$  as

$$R_{i,p}(u) = \frac{N_{i,p}(u)w_i}{N_{j,p}(u)w_j}.$$

#### 3.10.5.2 Properties of NURBS Curves

- $\mathbf{C}(0) = \mathbf{P}_0$  and  $\mathbf{C}(1) = \mathbf{P}_n$ .
- Affine invariance: an affine transformation is applied to the curve by applying it to the control points; NURBS curves are also invariant under perspective projections, a fact which is important in computer graphics.
- Strong convex hull property: if  $u \in [u_i, u_{i+1}]$ , then  $\mathbf{C}(u)$  lies within the convex hull of the control points  $\mathbf{P}_{i-p}, \dots, \mathbf{P}_i$ .
- $\mathbf{C}(u)$  is infinitely differentiable on the interior of knot spans and is  $p-k$  times differentiable at a knot of multiplicity  $k$ .



- Variation diminishing property: no plane (line) has more intersections with the curve than with the control polygon.
- A NURBS curve with no interior knots is a rational Bezier curve, since the  $N_{i,p}(u)$  reduce to the  $B_{i,n}(u)$ . NURBS curves contain nonrational B-spline and rational and nonrational Bezier curves as special cases.
- Local approximation: if the control point  $\mathbf{P}_i$  is moved, or the weight  $w_i$  is changed, it affects only that portion of the curve on the interval  $u \in [u_i, u_{i+p+1})$ .

The last property is very important for interactive shape design. Using NURBS curves, we can utilize both control point movement and weight modification to attain local shape control. Qualitatively the effect is: Assume  $u \in [u_i, u_{i+p+1})$ ; then if  $w_i$  increases (decreases), the point  $\mathbf{C}(u)$  moves closer to (farther from)  $\mathbf{P}_i$ , and hence the curve is pulled toward (pushed away from)  $\mathbf{P}_i$ . Furthermore, the movement of  $\mathbf{C}(u)$  for fixed  $u$  is along a straight line.

### 3.10.5.3 Definition of NURBS Surfaces

A NURBS surface of degree  $p$  in the  $u$  direction and degree  $q$  in the  $v$  direction is a bivariate vector-valued piecewise rational function of the form [Piegl and Tiller (1997)]

$$\mathbf{S}(u, v) = R_{i,j}(u, v)\mathbf{P}_{i,j},$$

with piecewise rational basis functions

$$R_{i,j}(u, v) = \frac{N_{i,p}(u)N_{j,q}(v)w_{i,j}}{N_{k,p}(u)N_{l,q}(v)w_{k,l}}.$$

The  $\{\mathbf{P}_{i,j}\}$  form a bidirectional control net, the  $\{w_{i,j}\}$  are the weights, and the  $\{N_{i,p}(u)\}$  and  $\{N_{j,q}(v)\}$  are the nonrational B-spline basis functions defined on the knot vectors

$$U = \{\underbrace{0, \dots, 0}_{p+1}, u_{p+1}, \dots, u_{r-p-1}, \underbrace{1, \dots, 1}_{p+1}\},$$

$$V = \{\underbrace{0, \dots, 0}_{q+1}, v_{q+1}, \dots, v_{s-q-1}, \underbrace{1, \dots, 1}_{q+1}\},$$

(where  $r = n + p + 1$  and  $s = m + q + 1$ ).

### 3.10.5.4 Properties of NURBS Surfaces

- Corner point interpolation:  $\mathbf{S}(0, 0) = \mathbf{P}_{0,0}$ ,  $\mathbf{S}(1, 0) = \mathbf{P}_{n,0}$ ,  $\mathbf{S}(0, 1) = \mathbf{P}_{0,m}$ ,  $\mathbf{S}(1, 1) = \mathbf{P}_{n,m}$ .
- Affine invariance: an affine transformation is applied to the surface by applying it to the control points.
- Strong convex hull property: assume  $w_{i,j} \geq 0$  for all  $i, j$ . If  $(u, v) \in [u_{i_0}, u_{i_0+1}) \times [v_{j_0}, v_{j_0+1})$ , then  $\mathbf{S}(u, v)$  is in the convex hull of the control points  $\mathbf{P}_{i,j}$ ,  $i_0 - p \leq i \leq i_0$  and  $j_0 - q \leq j \leq j_0$ .
- Local modification: if  $\mathbf{P}_{i,j}$  is moved, or  $w_{i,j}$  is changed, it affects the surface shape only in the rectangle  $[u_i, u_{i+p+1}) \times [v_j, v_{j+q+1})$ .
- Nonrational B-spline and Bezier and rational Bezier surfaces are special cases of NURBS surfaces.
- Differentiability:  $(u, v)$  is  $p - k(q - k)$  times differentiable with respect to  $u(v)$  at a  $u$  knot ( $v$  knot) of multiplicity  $k$ .

There is *no* known variation diminishing property for NURBS surfaces [Piegl and Tiller (1997)].

We can use both control point movement and weight modification to locally change the shape of NURBS surfaces. Qualitatively the effect on the surface is: Assume  $(u, v) \in [u_i, u_{i+p+1}) \times [v_j, v_{j+q+1})$ ; then if  $w_{i,j}$  increases (decreases), the point  $\mathbf{S}(u, v)$  moves closer to (farther from)  $\mathbf{P}_{i,j}$ , and hence the surface is pulled toward (pushed away from)  $\mathbf{P}_{i,j}$ . As in the case for curves, the movement of  $\mathbf{S}(u, v)$  is along a straight line.

## 3.11 Kinematics of Biomechanical Chains

### 3.11.1 3D Transformation Matrix

Recall that the position of a local Cartesian coordinate system  $\{x, y, z\}$  attached to a rigid body, with respect to the global coordinate system  $\{X, Y, Z\}$ , can be expressed as the sequence of  $\{X, Y, Z\}$  translations, i.e., a translation vector  $\{L_X, L_Y, L_Z\}^T$ , and nine Euler rotations, described by the standard  $SO(3)$ -rotation matrix  $R$ , rewritten here in terms of *direction cosines*,

$$R = \begin{bmatrix} \cos X_x & \cos X_y & \cos X_z \\ \cos Y_x & \cos Y_y & \cos Y_z \\ \cos Z_x & \cos Z_y & \cos Z_z \end{bmatrix},$$

where columns denote axes of the local system, while rows denote axes of the global system. Together, 3D translations and rotations form a *biomechanical transformation matrix*  $T$  (with added row  $\{1, 0, 0, 0\}$  on the top),

$$T = \begin{bmatrix} 1 & 0 & 0 & 0 \\ L_X & \cos X_x & \cos X_y & \cos X_z \\ L_Y & \cos Y_x & \cos Y_y & \cos Y_z \\ L_Z & \cos Z_x & \cos Z_y & \cos Z_z \end{bmatrix}. \quad (3.88)$$

It is obvious that  $T$  actually gives a *practical biomechanical representation* of the Special Euclidean group  $SE(3)$  of rigid body motions (see subsection 3.5.2 above).

### 3.11.2 A Multilink Kinematic Chain

Now, consider an open kinematic chain of  $N \geq 2$  rigid bodies, in which local coordinate systems  $\{x, y, z\}_i = \{x_i, y_i, z_i\}$  are attached to each link  $i = 1, \dots, N$ . The position of each link can also be represented in the global frame  $\{X, Y, Z\}$ . Here, we discuss the direct kinematic problem, as the inverse kinematic problem in biomechanics does not have a unique solution, due to the chain's redundancy (see, [van der Helm *et al.* (1995); Cole *et al.* (1993); Zatsiorsky (1998)]).

The position of frame  $i$  relative to the the previous frame  $(i - 1)$  can be described by the  $4 \times 4$  *transformation matrix*  $T_{(i-1),i}$ . The matrices of the local transformations are assumed to be known. The end-effector position is then defined as the composition of sequential coordinate transformations  $T_{(i-1),i}$ . Because the composition of several displacements is given by matrix multiplication of the corresponding transformation matrices, the end-effector position in the global space is defined by the *kinematic structure equation for the chain*,

$$T_{0,N} = T_{0,1}T_{1,2}\dots T_{(N-1),N},$$

where  $T_{0,N}$  is the transformation matrix of the *homogenous transformation*, defining the position of the end-effector  $N$ , in terms of the relative positions of each link  $i$  in the chain. The  $4 \times 4$  matrix  $T_{0,N}$  comprises a position vector of the origin of the local end-effector coordinate frame as well as a  $3 \times 3$  rotation matrix.

### 3.11.3 CNS Representation of the Body Posture

Recall that the kinematics problem of end-effector positioning (see, e.g., VukSpringer) is usually done in two steps:

- (1) the (real or desired) position of the end-effector is given in an external reference system, and then
- (2) the inverse kinematics solution is sought to define the appropriate joint angular coordinates.

Hence, the position of the robot's hand is given first in the extrinsic coordinates, and then the intrinsic coordinates of the joint angles are found. However, in a general case of a multilink chain with many DOF, there is no unique solution to the inverse kinematics problem, and an optimal solution is the only option based on the *Moore-Penrose pseudoinverse* least squares method.

This robotics approach, where the end-effector position is described by a composition of several joint transformations, inevitably leads to the accumulation of errors from various joints. The positioning accuracy of the terminal point in the chain is less than the accuracy of individual joint positioning.

Surprisingly (see [Zatsiorsky (1998)] joint), joint errors are not accumulated in human movements: the accuracy of the end-effector positioning does not depend on the length of the chain. To illustrate this, we can conduct a simple experiment. With any finger of one hand, most people can easily touch the same finger of the opposite hand behind our back. To formally describe this motor task, suppose that an internal global coordinate system is fixed somewhere in the shoulder girdle. In this experiment, each arm chain includes at least six joints: shoulder (glenohumeral) elbow, wrist, and the three finger joints (carpometacarpal, metacarpophalangeal and interphalangeal). Therefore, for each arm the following kinematic structure equation can be written

$$P = T_{sh}T_{el}T_{wr}T_{f1}T_{f2}T_{f3}L_N,$$

where  $P$  is a 3D vector of the position of the terminal point in the global reference frame, the  $T$ s are transformation matrices (3.88) corresponding respectively to shoulder, elbow, wrist, and the three finger joints, while  $L_N$  is the position of the tip in the local joint coordinates of the  $N$ th joint. Each transformation matrix contains certain 'errors of measurement' (i.e., people reproduce a joint angular position with some variation). Despite

these errors, and the involvement of 12 joints totally, the final accuracy of the two chains is very high. When the same movement is performed several times, the variability of the end-effector trajectory is less than that of the individual joints.

The complexity and robustness of strategies used by animal species for positioning their limbs are confirmed by classic physiological experiments with *spinal frogs* (frogs with dissected brains and intact spinal cords). When a piece of paper soaked in acid is applied to a frog's skin, the frog wipes the paper away from the body. This multijoint movement is performed in a coordinated manner, disregarding all attempts to fool the spinal frog (e.g., to place the stimulus at different locations, like on the ipsilateral forelimb, to change the limb position, to load the limb, to introduce mechanical obstacles to the movement, etc.) If the task is solvable, the spinal frogs solve it, and usually on the first trial. These experiments have led to the conclusion that a *body scheme* is somehow represented in the CNS [Zatsiorsky (1998)]. A brain-like motor control is fully described in chapters 6 and 7.

### 3.11.4 Transformation Matrix Used in Computer Graphics

In 3D computer graphics, biomechanical transformation matrix (3.88) is slightly modified so to include the 3D scale vector  $\{S_X, S_Y, S_Z\}$ ,

$$T = \begin{bmatrix} 1 & S_X & S_Y & S_Z \\ L_X \cos X_x & \cos X_y & \cos X_z \\ L_Y \cos Y_x & \cos Y_y & \cos Y_z \\ L_Z \cos Z_x & \cos Z_y & \cos Z_z \end{bmatrix}. \quad (3.89)$$

The matrix (3.89) lies in the core of many powerful 3D animation software packages, like *3DS Max* and *Maya*.

## Chapter 4

# Natural Mechanics of Biodynamics

This chapter studies various aspects of modern mechanics as is currently used in biodynamics, or has a potential for the future use in biodynamics. It includes both Lagrangian and Hamiltonian variations on the central theme of our *covariant force law*,  $F_i = mg_{ij}a^j$ . We start with the basics of Lagrangian and Hamiltonian formalisms. Then we present the basics of modern quantum biodynamics. After that we move on to the general variational principles of holonomic mechanics, both classical and quantum. Next we depart to nonholonomic and stochastic mechanics. Then we include the essential biology in the form of muscular contraction dynamics. Finally we present the current research in mechanical biodynamics given in the framework of Lie–Lagrangian and Lie–Hamiltonian functors.

### 4.1 Lagrangian Formalism in Biodynamics

In this section we present classical Lagrangian formalism, as has been used in human-like biodynamics for over fifty years now (see the History section in the first chapter). It describes the motion of mechanical systems by the use of the *configuration space*. The configuration space of the mechanical system has the structure of the *Riemannian manifold*. On the smooth manifold there acts a group of diffeomorphisms. Essential terms and theorems of Lagrangian mechanics (even if formulated in local coordinates) are invariant with respect to this group, as well as to the extended Riemannian space–time group.

Lagrangian mechanical system is given by its configuration manifold and the ‘Lagrange’s energetic function’ on its tangent bundle.

Each one-parameter group of diffeomorphisms of the configuration space, preserving the Lagrange’s function, determines the conservation law

(i.e., the first integral of the equation of motion).

Newtonian potential system is the particular case of the Lagrangian one (here, the configuration space is Euclidean, and Lagrange's function equals the difference between kinetic and potential energy).

Lagrangian mechanics enables us to analyze up to the end a series of important mechanical problems, e.g., in the theory of small oscillations and rigid body dynamics.

Consider our  $n$ D configuration manifold  $M$  and its tangent bundle  $TM$ . We denote coordinates on  $M$  by  $q^i$  and those on  $TM$  by  $(q^i, \dot{q}^i)$ . Consider a Lagrangian  $L : TM \rightarrow \mathbb{R}$ . Construct the corresponding action functional  $S$  on  $C^2$  curves  $q(t)$  in  $M$  by integration of  $L$  along the tangent to the curve. In coordinate notation, this reads [Marsden and Ratiu (1999)]

$$S(q(t)) \equiv \int_a^b L\left(q^i(t), \frac{dq^i}{dt}(t)\right) dt. \quad (4.1)$$

The action functional (4.1) depends on  $a$  and  $b$ , but this is not explicit in the notation. *Hamilton's principle* seeks the curves  $q(t)$  for which the functional  $S$  is stationary under variations of  $q(t)$  with fixed endpoints; namely, we seek curves  $q(t)$  which satisfy

$$dS(q(t)) \cdot \delta q(t) \equiv \left. \frac{d}{d\epsilon} \right|_{\epsilon=0} S(q_\epsilon(t)) = 0 \quad (4.2)$$

for all  $\delta q(t)$  with  $\delta q(a) = \delta q(b) = 0$ , where  $q_\epsilon$  is a smooth family of curves with  $q_0 = q$  and  $(d/d\epsilon)|_{\epsilon=0} q_\epsilon = \delta q$ . Using integration by parts, the calculation for this is simply

$$\begin{aligned} dS(q(t)) \cdot \delta q(t) &= \left. \frac{d}{d\epsilon} \right|_{\epsilon=0} \int_a^b L\left(q_\epsilon^i(t), \frac{dq_\epsilon^i}{dt}(t)\right) dt \\ &= \int_a^b \delta q^i \left( \frac{\partial L}{\partial q^i} - \frac{d}{dt} \frac{\partial L}{\partial \dot{q}^i} \right) dt + \left. \frac{\partial L}{\partial \dot{q}^i} \delta q^i \right|_a^b. \end{aligned} \quad (4.3)$$

The last term in (4.3) vanishes since  $\delta q(a) = \delta q(b) = 0$ , so that the requirement (4.2) for  $S$  to be stationary yields the *Euler-Lagrange equation*

$$\frac{\partial L}{\partial q^i} - \frac{d}{dt} \frac{\partial L}{\partial \dot{q}^i} = 0. \quad (4.4)$$

Recall that  $L$  is called *regular* when the symmetric matrix  $[\partial^2 L / \partial \dot{q}^i \partial \dot{q}^j]$  is everywhere nonsingular. If  $L$  is regular, the Euler-Lagrange equations (4.4) are second order ODEs for the required curves. The action principle is further developed in the section (4.4) below.

In particular, for a system of  $N$  particles moving in Euclidean 3-space, we choose the configuration space to be  $M = \mathbb{R}^{3N} = \mathbb{R}^3 \times \dots \times \mathbb{R}^3$  ( $N$  times), and in the case of *simple mechanical systems*  $L$  has the form of kinetic minus potential energy (see [Abraham and Marsden (1978); Arnold (1989); Marsden and Ratiu (1999)])

$$L(y^i, \dot{y}^i, t) = \frac{1}{2} m_i \|\dot{y}^i\|^2 - V(y).$$

where we write points in  $M$  as  $y^1, \dots, y^N$ , where  $y^i \in \mathbb{R}^3$ . In this case the Euler–Lagrange equations (4.4) reduce to Newtonian second law

$$\frac{d}{dt}(m_i \dot{y}^i) = -\frac{\partial V}{\partial y^i}, \quad i = 1, \dots, N,$$

that is,  $\mathbf{F} = m\mathbf{a}$ , for the motion of particles in the potential field  $V = V(y)$ .

In general, one identifies the  $2nD$  *velocity phase-space* with the tangent bundle  $TM$ , using local coordinates  $(q^i, \dot{q}^i, i = 1, \dots, n)$  in an open chart  $U \subset TM$ .

Recall that the biodynamic manifold  $M$  is Riemannian, with the metric tensor  $g_{ij}(q)$  (see (3.6.1.1)) which is now material, also called the *inertia matrix*. If we consider the kinetic energy Lagrangian

$$L(q^i, \dot{q}^i) = \frac{1}{2} g_{ij}(q) \dot{q}^i \dot{q}^j,$$

then the Euler–Lagrange equations are equivalent to the equations of geodesic motion (3.47).

The Riemannian metric  $g = \langle, \rangle$  on the configuration manifold  $M$  is a positive-definite quadratic form  $g : TM \rightarrow \mathbb{R}$ , given in local coordinates  $q^i \in U$  ( $U$  open in  $M$ ) as

$$g_{ij} \mapsto g_{ij}(q, m) dq^i dq^j. \quad (4.5)$$

Here

$$g_{ij}(q, m) = \sum_{\mu=1}^n m_{\mu} \delta_{rs} \frac{\partial x^r}{\partial q^i} \frac{\partial x^s}{\partial q^j} \quad (4.6)$$

is the covariant material metric tensor defining a relation between internal and external coordinates and including  $n$  segmental masses  $m_{\mu}$ . The quantities  $x^r$  are external coordinates ( $r, s = 1, \dots, 6n$ ) and  $i, j = 1, \dots, N \equiv 6n - h$ , where  $h$  denotes the number of holonomic constraints.



The *Lagrangian* of the system is a quadratic form  $L : TM \rightarrow \mathbb{R}$  dependent on velocity  $v$  and such that  $L(v) = \frac{1}{2} \langle v, v \rangle$ . It is given by

$$L(v) = \frac{1}{2} g_{ij}(q, m) v^i v^j,$$

in local coordinates  $q^i$ ,  $v^i = \dot{q}^i \in U_v$  ( $U_v$  open in  $TM$ ).

On the velocity phase-space manifold  $TM$  exists:

- (1) A unique 1-form  $\theta_L$ , defined in local coordinates  $q^i$ ,  $v^i = \dot{q}^i \in U_v$  ( $U_v$  open in  $TM$ ) by  $\theta_L = L_{v^i} dq^i$ , where  $L_{v^i} \equiv \partial L / \partial v^i$ .
- (2) A unique nondegenerate Lagrangian symplectic 2-form  $\omega_L$ , which is closed ( $d\omega_L = 0$ ) and exact ( $\omega_L = d\theta_L = dL_{v^i} \wedge dq^i$ ).

$TM$  is an orientable manifold, admitting the standard volume given by

$$\Omega_{\omega_L} = \frac{(-1)^{\frac{N(N+1)}{2}}}{N!} \omega_L^N,$$

in local coordinates  $q^i$ ,  $v^i = \dot{q}^i \in U_v$  ( $U_v$  open in  $TM$ ) it is given by

$$\Omega_L = dq^1 \wedge \cdots \wedge dq^N \wedge dv^1 \wedge \cdots \wedge dv^N.$$

On the velocity phase-space manifold  $TM$  we can also define the *action*  $A : TM \rightarrow \mathbb{R}$  in local coordinates  $q^i$ ,  $v^i = \dot{q}^i \in U_v$  ( $U_v$  open in  $TM$ ) given by  $A = v^i L_{v^i}$ , so  $E = v^i L_{v^i} - L$ . The Lagrangian vector-field  $X_L$  on  $TM$  is determined by the condition  $i_{X_L} \omega_L = dE$ . Classically, it is given by the second-order Lagrange equations (compare with (4.4))

$$\frac{d}{dt} \frac{\partial L}{\partial v^i} = \frac{\partial L}{\partial q^i}. \quad (4.7)$$

For a Lagrangian vector-field  $X_L$  on  $M$ , there is a base integral curve  $\gamma_0(t) = (q^i(t), v^i(t))$  iff  $\gamma_0(t)$  is a geodesic. This is given by the contravariant velocity equation

$$\dot{q}^i = v^i, \quad \dot{v}^i + \Gamma_{jk}^i v^j v^k = 0. \quad (4.8)$$

Here  $\Gamma_{jk}^i$  denote the Christoffel symbols of the Levi-Civita affine connection  $\nabla$  in an open chart  $U$  on  $M$ , defined on the Riemannian metric  $g = \langle, \rangle$  by (see Appendix, as well as section 3.6.1.1 above)

$$\Gamma_{jk}^i = g^{il} \Gamma_{jkl}, \quad \Gamma_{ijk} = \frac{1}{2} (\partial_{x^i} g_{jk} + \partial_{x^j} g_{ki} + \partial_{x^k} g_{ij}). \quad (4.9)$$

The l.h.s  $\dot{v}^i = v^i + \Gamma_{jk}^i v^j v^k$  in the second part of (4.8) represents the *Bianchi covariant derivative* of the velocity with respect to  $t$ . *Parallel*

transport on  $M$  is defined by  $\dot{v}^i = 0$ . When this applies,  $X_L$  is called the *geodesic spray* and its flow the *geodesic flow*.

For the dynamics in the gravitational potential field  $V : M \rightarrow \mathbb{R}$ , the Lagrangian  $L : TM \rightarrow \mathbb{R}$  has an extended form

$$L(v, q) = \frac{1}{2} g_{ij} v^i v^j - V(q),$$

A Lagrangian vector-field  $X_L$  is still defined by the second-order Lagrangian equations (4.7, 4.8).

A general form of the forced, non-conservative Lagrange's equations is given as

$$\frac{d}{dt} \frac{\partial L}{\partial v^i} - \frac{\partial L}{\partial q^i} = F_i(t, q^i, v^i).$$

Here the  $F_i(t, q^i, v^i)$  represent any kind of *covariant forces*, including dissipative and elastic joint forces, as well as muscular-like actuator drives and neural-like control forces, as a function of time, coordinates and momenta. In covariant form we have

$$\dot{q}^i = v^i, \quad g_{ij}(\dot{v}^i + \Gamma_{jk}^i v^j v^k) = F_j(t, q^i, v^i).$$

## 4.2 Hamiltonian Formalism in Biodynamics

In this section we present classical Hamiltonian formalism, as is used in contemporary biodynamics. Let  $(M, \omega)$  be a *symplectic manifold* and  $H \in C^k(M, \mathbb{R})$  a smooth real valued function on  $M$ . The vector-field  $X_H$  determined by the condition

$$i_{X_H} \omega + dH = 0,$$

is called *Hamiltonian vector-field* with *Hamiltonian energy function*  $H$ . A triple  $(M, \omega, H)$  is called a *Hamiltonian mechanical system* [Marsden and Ratiu (1999); Puta (1993)].

Nondegeneracy of  $\omega$  guarantees that  $X_H$  exists, but only in the finite-dimensional case.

Let  $\{q^1, \dots, q^n, p_1, \dots, p_n\}$  be *canonical coordinates* on  $M$ , i.e.,  $\omega = dp_i \wedge dq^i$ . Then in these coordinates

$$X_H = \left( \frac{\partial H}{\partial p_i} \frac{\partial}{\partial q^i} - \frac{\partial H}{\partial q^i} \frac{\partial}{\partial p_i} \right).$$

As a consequence,  $((q^i(t)), (p_i(t)))$  is an integral curve of  $X_H$  (for  $i = 1, \dots, n$ ) iff *Hamilton's equations* hold,

$$\dot{q}^i = \partial_{p_i} H, \quad \dot{p}_i = -\partial_{q^i} H. \quad (4.10)$$

Let  $(M, \omega, H)$  be a Hamiltonian mechanical system and let  $\gamma(t)$  be an integral curve of  $X_H$ . Then  $H(\gamma(t))$  is constant in  $t$ . Moreover, if  $\phi_t$  is the flow of  $X_H$ , then  $H \circ \phi_t = H$  for each  $t$ .

Let  $(M, \omega, H)$  be a Hamiltonian mechanical system and  $\phi_t$  be the flow of  $X_H$ . Then, by the Liouville theorem, for each  $t$ ,  $\phi_t^* \omega = \omega$ ,  $(\frac{d}{dt} \phi_t^* \omega = 0$ , so  $\phi_t^* \omega$  is constant in  $t$ ), that is,  $\phi_t$  is symplectic, and it preserves the volume  $\Omega_\omega$ .

A convenient criterion for symplectomorphisms is that they preserve the form of Hamilton's equations. More precisely, let  $(M, \omega)$  be a symplectic manifold and  $f : M \rightarrow M$  a diffeomorphism. Then  $f$  is symplectic iff for all  $H \in C^k(M, \mathbb{R})$  we have  $f^*(X_H) = X_{H \circ f}$ .

A vector-field  $X \in \mathcal{X}(M)$  on a symplectic manifold  $(M, \omega)$  is called locally Hamiltonian iff  $\mathcal{L}_X \omega = 0$ , where  $L$  denotes the *Lie derivative*. From the equality  $L_{[X, Y]} \omega = \mathcal{L}_X L_Y \omega - L_Y \mathcal{L}_X \omega$ , it follows that the locally Hamiltonian vector-fields on  $M$  form a Lie subalgebra of  $\mathcal{X}(M)$ .

Let  $(M, \omega)$  be a symplectic manifold and  $f, g \in C^k(M, \mathbb{R})$ . The *Poisson bracket* of  $f$  and  $g$  is the function

$$\{f, g\}_\omega = -\omega(X_f, X_g) = -\mathcal{L}_{X_f} g = \mathcal{L}_{X_g} f.$$

Also, for  $f_0 \in C^k(M, \mathbb{R})$ , the map  $g \mapsto \{f_0, g\}_\omega$  is a derivation. The connection between the Lie bracket and the Poisson bracket is

$$[X_f, X_g] = -X_{\{f, g\}_\omega} \quad \Longleftrightarrow \quad d\omega = 0.$$

The real vector space  $C^k(M, \mathbb{R})$  together with the Poisson bracket on it forms an infinite-dimensional Lie algebra called the *algebra of classical observables*.

In canonical coordinates  $\{q^1, \dots, q^n, p_1, \dots, p_n\}$  on  $(M, \omega)$  the Poisson bracket of two functions  $f, g \in C^k(M, \mathbb{R})$  is given by

$$\{f, g\}_\omega = \sum_{i=1}^n \left( \frac{\partial f}{\partial q^i} \frac{\partial g}{\partial p_i} - \frac{\partial f}{\partial p_i} \frac{\partial g}{\partial q^i} \right).$$

From this definition follows:

$$\{q^i, q^j\}_\omega = 0, \quad \{p_i, p_j\}_\omega = 0, \quad \{q^i, p_j\}_\omega = \delta_j^i.$$

Let  $(M, \omega)$  be a symplectic manifold and  $f : M \rightarrow \mathbb{R}$  a function. Then  $f$  is symplectic iff it preserves the Poisson bracket.

Let  $(M, \omega, H)$  be a Hamiltonian mechanical system and  $\phi_t$  the flow of  $X_H$ . Then for each function  $f \in C^k(M, \mathbb{R})$  we have the equations of motion in the Poisson bracket notation:

$$\frac{d}{dt}(f \circ \phi_t) = \{f \circ \phi_t, H\}_\omega = \{f, H\}_\omega \circ \phi_t.$$

Also,  $f$  is called a *constant of motion*, or a *first integral*, if it satisfies the following condition

$$\{f, H\}_\omega = 0.$$

If  $f$  and  $g$  are constants of motion then their Poisson bracket is also a constant of motion.

A Hamiltonian mechanical system  $(M, \omega, H)$  is said to be integrable if there exists  $n = \frac{1}{2} \dim(M)$  linearly-independent functions  $K_1 = H, K_2, \dots, K_n$  such that for each  $i, j = 1, 2, \dots, n$ :

$$\{K_i, H\}_\omega = 0, \quad \{K_i, K_j\}_\omega = 0.$$

#### 4.2.1 Nonlinear Dynamics in Hamiltonian Form

Here we continue our exposition on the language of nonlinear dynamics in biodynamics (see (3.4.4)), by putting it into the most convenient Hamiltonian form. In this way we will gradually approach the basic biodynamics model (2.26–2.27).

##### 4.2.1.1 Real 1-DOF Hamiltonian Dynamics

The basic structural unit of the biodynamics is a *uniaxial rotational joint*, geometrically representing a *constrained  $SO(2)$  group of plane rotations*. In other words, this is a one-DOF dynamical system, represented in a differential formulation as a *vector-field*, or in an integral form as a *phase-flow*, on a 2D phase-space manifold  $M$ , *cylinder  $\mathbb{R} \times S^1$* , being itself a *cotangent bundle  $T^*M$*  of the joint  *$SO(2)$ -configuration manifold, circle  $S^1$* .

A vector-field  $X(t)$  on the momentum phase-space manifold  $M$  can be given by a system of *canonical equations of motion*

$$\dot{q} = f(q, p, t, \mu), \quad \dot{p} = g(q, p, t, \mu), \quad (4.11)$$

where  $t$  is time,  $\mu$  is a parameter,  $q \in S^1$ ,  $p \in \mathbb{R} \times S^1$  are *coordinates* and *momenta*, respectively, while  $f$  and  $g$  are smooth functions on the phase-space  $\mathbb{R} \times S^1$ .

If time  $t$  does not explicitly appear in the functions  $f$  and  $g$ , the vector-field  $X$  is called *autonomous*. In this case equation (4.11) simplifies as

$$\dot{q} = f(q, p, \mu), \quad \dot{p} = g(q, p, \mu). \quad (4.12)$$

By a *solution curve* of the vector-field  $X$  we mean a map  $x = (q, p)$ , from some interval  $I \subset \mathbb{R}$  into the phase-space manifold  $M$ , such that  $t \mapsto x(t)$ . The map  $x(t) = (q(t), p(t))$  geometrically represents a curve in  $M$ , and equations (4.11) or (4.12) give the tangent vector at each point of the curve.

To specify an *initial condition* on the vector-field  $X$ , by

$$x(t, t_0, x_0) = (q(t, t_0, q_0), p(t, t_0, p_0)),$$

geometrically means to distinguish a solution curve by a particular point  $x(t_0) = x_0$  in the phase-space manifold  $M$ . Similarly, it may be useful to explicitly display the parametric dependence of solution curves, as  $x(t, t_0, x_0, \mu) = (q(t, t_0, q_0, \mu_q), p(t, t_0, p_0, \mu_p))$ , where  $\mu_q, \mu_p$  denote  $q$ -dependent and  $p$ -dependent parameters, respectively.

The solution curve  $x(t, t_0, x_0)$  of the vector-field  $X$ , may be also referred as the *phase trajectory* through the point  $x_0$  at  $t = t_0$ . Its graph over  $t$  is referred to as an *integral curve*; more precisely, *graph*

$$x(t, t_0, x_0) \equiv \{(x, t) \in M \times \mathbb{R} : x = x(t, t_0, x_0), t \in I \subset \mathbb{R}\}.$$

Let  $x_0 = (q_0, p_0)$  be a point on  $M$ . By the *orbit through*  $x_0$ , denoted  $O(x_0)$ , we mean the set of points in  $M$  that lie on a trajectory passing through  $x_0$ ; more precisely, for  $x_0 \in U$ ,  $U$  open in  $M$ , the orbit through  $x_0$  is given by  $O(x_0) = \{x \in \mathbb{R} \times S^1 : x = x(t, t_0, x_0), t \in I \subset \mathbb{R}\}$ .

Consider a general autonomous vector-field  $X$  on the phase-space manifold  $M$ , given by equation  $\dot{x} = f(x)$ ,  $x = (q, p) \in M$ . An *equilibrium solution*, *singularity*, or *fixed point* of  $X$  is a point  $\bar{x} \in M$  such that  $f(\bar{x}) = 0$ , i.e., a solution which does not change in time.

Any solution  $\bar{x}(t)$  of an autonomous vector-field  $X$  on  $M$  is *stable* if solutions starting 'close' to  $\bar{x}(t)$  at a given time remain close to  $\bar{x}(t)$  for all later times. It is *asymptotically stable* if nearby solutions actually converge to  $\bar{x}(t)$  as  $t \rightarrow \infty$ . In order to determine the stability of  $\bar{x}(t)$  we must understand the nature of solutions near  $\bar{x}(t)$ , which is done by *linearization* of the vector-field  $X$ . The solution of the linearized vector-field  $Y$

is asymptotically stable if all eigenvalues have negative real parts. In that case the fixed point  $x = \bar{x}$  of associated nonlinear vector-field  $X$  is also asymptotically stable. A fixed point  $\bar{x}$  is called *hyperbolic point* if none of the eigenvalues of  $Y$  have zero real part; in that case the orbit structure near  $\bar{x}$  is essentially the same for  $X$  and  $Y$ .

In the case of autonomous vector-fields on  $M$  we have also an important property of *Hamiltonian flow*. If  $x(t) = (q(t), p(t))$  is a solution of  $\dot{x} = f(x)$ ,  $x \in M$ , then so is  $x(t + \tau)$  for any  $\tau \in \mathbb{R}$ . Also, for any  $x_0 \in M$  there exists only one solution of an autonomous vector-field passing through this point. The autonomous vector-field

$$\dot{x} = f(x)$$

has the following properties (compare with the section (3.4.1) above):

- (1)  $x(t, x_0)$  is  $C^k$ ;
- (2)  $x(0, x_0) = x_0$ ; and
- (3)  $x(t + s, x_0) = x(t, x(s, x_0))$ .

These properties show that the solutions of an autonomous vector-field form a *one-parameter family of diffeomorphisms* of the phase-space manifold  $M$ . This is referred to as a *phase-flow* and denoted by  $\phi_t(x)$  or  $\phi(t, x)$ .

Consider a flow  $\phi(t, x)$  generated by vector-field  $\dot{x} = f(x)$ . A point  $x_0 = (q_0, p_0)$  on  $M$  is called an  $\omega$ -*limit point* of  $x = (q, p) \in M$ , denoted  $\omega(x)$ , if there exists a sequence  $\{t_i\}$ ,  $t_i \mapsto \infty$ , such that  $\phi(t_i, x) \mapsto x_0$ . Similarly,  $\alpha$ -*limit points* are defined by taking a sequence  $\{t_i\}$ ,  $t_i \mapsto -\infty$ . The set of all  $\omega$ -limit points of a flow is called the  $\omega$ -*limit set*. The  $\alpha$ -limit set is similarly defined.

A point  $x_0 = (q_0, p_0)$  on  $M$  is called *nonwandering* if for any open neighborhood  $U \subset M$  of  $x_0$ , there exists some  $t \neq 0$  such that  $\phi(t, U) \cap U \neq \emptyset$ . The set of all nonwandering points of a flow is called the *nonwandering set* of that particular map or flow.

A closed invariant subset  $A \subset M$  is called an *attracting set* if there is some open neighborhood  $U \subset M$  of  $A$  such that  $\phi(t, x) \in U$  and  $\phi(t, x) \mapsto A$  for any  $x \in U$  and  $t \geq 0$ . The *domain* or *basin of attraction* of  $A$  is given by  $\cup_{t \geq 0} \phi(t, U)$ . In practice, a way of locating attracting sets is to first find a *trapping region*, i.e., a closed, connected subset  $V \subset M$  such that for any  $t \geq 0$   $\phi(t, V) \subset V$ . Then  $\cap_{t \geq 0} \phi(t, V) = A$  is an *attracting set*.

As a first example of one-DOF dynamical systems, let us consider a vector-field  $x = (q, p) \in \mathbb{R} \times \mathbb{R}$  of a simple harmonic oscillator, given by

equations

$$\dot{q} = p, \quad \dot{p} = -q. \quad (4.13)$$

Here, the *solution* passing through the point  $(q, p) = (1, 0)$  at  $t = 0$  is given by  $(q(t), p(t)) = (\cos t, -\sin t)$ ; the *integral curve* passing through  $(q, p) = (1, 0)$  at  $t = 0$  is given by  $\{(q, p, t) \in \mathbb{R} \times \mathbb{R} \times \mathbb{R} : (q(t), p(t)) = (\cos t, -\sin t)\}$ , for all  $t \in \mathbb{R}$ ; the *orbit* passing through  $(q, p) = (1, 0)$  is given by the circle  $q^2 + p^2 = 1$ .

A one-DOF dynamical system is called *Hamiltonian system* if there exists a *first integral* or a function of the dependent variables  $(q, p)$  whose level curves give the orbits of the vector-field  $X = X_H$ , i.e., a total-energy *Hamiltonian function*  $H = H(q, p) : U \rightarrow \mathbb{R}$ , ( $U$  open set on the phase-space manifold  $M$ ), such that the vector-field  $X_H$  is given by *Hamilton's canonical equations* (4.10). In (4.10), the first,  $\dot{q}$ -equation, is called the *velocity equation* and serves as a definition of the *momentum*, while the second,  $\dot{p}$ -equation is called the *force equation*, and represents the *Newtonian second law of motion*.

The simple harmonic oscillator (4.13) is a Hamiltonian system with a Hamiltonian function  $H = \frac{p^2}{2} + \frac{q^2}{2}$ . It has a *fixed point - center* (having purely imaginary eigenvalues) at  $(q, p) = (0, 0)$  and is surrounded by a one-parameter family of periodic orbits given by the Hamiltonian  $H$ .

A nice example of one-DOF dynamical system with a Hamiltonian structure is a *damped Duffing oscillator* (see, e.g., [Wiggins (1990)]). This is a *plane* Hamiltonian vector-field  $x = (q, p) \in \mathbb{R}^2$ , given by Hamilton's equations

$$\dot{q} = p \equiv f(q, p), \quad \dot{p} = q - q^3 - \delta p \equiv g(q, p, \delta), \quad \delta \geq 0. \quad (4.14)$$

For the special parameter value  $\delta = 0$ , we have an *undamped* Duffing oscillator with a *first integral* represented by Hamiltonian function  $H = \frac{p^2}{2} - \frac{q^2}{2} + \frac{q^4}{4}$ , where  $\frac{p^2}{2}$  corresponds to the *kinetic energy* (with a mass scaled to unity), and  $-\frac{q^2}{2} + \frac{q^4}{4} \equiv V(x)$  corresponds to the *potential energy* of the oscillator.

In general, if the first integral, i.e., a Hamiltonian function  $H$ , is defined by  $H = \frac{p^2}{2} + V(x)$ , then the momentum is given by  $p = \pm\sqrt{2}\sqrt{H - V(x)}$ . All one-DOF Hamiltonian systems are *integrable* and all the solutions lie on *level curves* of the Hamiltonian function, which are topologically equivalent with the circle  $S^1$ . This is actually a general characteristic of all  $n$ -DOF integrable Hamiltonian systems: their bounded motions lie on  $nD$  *invariant*

tori  $T^n = S^1 \times \cdots \times S^1$ , or *homoclinic orbits*. The homoclinic orbit is sometimes called a *separatrix* because it is the boundary between two distinctly different types of motion.

For example, in case of a damped Duffing oscillator (4.14) with  $\delta \neq 0$ , we have

$$\partial_q f + \partial_p g = -\delta,$$

and according to the *Bendixon's criterion* for  $\delta > 0$  it has no closed orbits.

The vector-field  $X$  given by equations (4.14) has three fixed points given by  $(q, p) = (0, 0)$ ,  $(\pm 1, 0)$ . The *eigenvalues*  $\lambda_{1,2}$  of the associated linearized vector-field are given by  $\lambda_{1,2} = -\delta/2 \pm \frac{1}{2}\sqrt{\delta^2 + 4}$ , for the fixed point  $(0, 0)$ , and by  $\lambda_{1,2} = -\delta/2 \pm \frac{1}{2}\sqrt{\delta^2 - 8}$ , for the fixed point  $(\pm 1, 0)$ . Hence, for  $\delta > 0$ ,  $(0, 0)$  is *unstable* and  $(\pm 1, 0)$  are *asymptotically stable*; for  $\delta = 0$ ,  $(\pm 1, 0)$  are *stable in the linear approximation* (see, e.g., [Wiggins (1990)]).

Another example of one-DOF Hamiltonian systems, representing the actual basis of the human  $SO(2)$ -joint dynamics, is a *simple pendulum* (again, all physical constants are scaled to unity), given by Hamiltonian function  $H = \frac{p^2}{2} - \cos q$ . This is the first integral of the *cylindrical* Hamiltonian vector-field  $(q, p) \in S^1 \times \mathbb{R}$ , defined by canonical equations

$$\dot{q} = p, \quad \dot{p} = -\sin q.$$

This vector-field has fixed points at  $(0, 0)$ , which is a center (i.e., the eigenvalues are purely imaginary), and at  $(\pm\pi, 0)$ , which are saddles, but since the phase-space manifold is the cylinder, these are really the same point.

The basis of human arm and leg dynamics represents the *coupling* of two uniaxial,  $SO(2)$ -joints. The study of two DOF Hamiltonian dynamics we shall start with the most simple case of two linearly coupled linear undamped oscillators with parameters scaled to unity. Under general conditions we can perform a change of variables to canonical coordinates (the 'normal modes')  $(q^i, p_i)$ ,  $i = 1, 2$ , so that the vector-field  $X_H$  is given by

$$\dot{q}^1 = p_1, \quad \dot{q}^2 = p_2, \quad \dot{p}_1 = -\omega_1^2 q^1, \quad \dot{p}_2 = -\omega_2^2 q^2.$$

This system is integrable, since we have two independent functions of  $(q^i, p_i)$ , i.e., Hamiltonians

$$H_1 = \frac{p_1^2}{2} + \frac{\omega_1^2 (q^1)^2}{2}, \quad H_2 = \frac{p_2^2}{2} + \frac{\omega_2^2 (q^2)^2}{2}.$$



The level curves of these functions are compact sets (topological circles); therefore, the orbits in the 4D phase-space  $\mathbb{R}^4$  actually lie on the two-torus  $T^2$ . By making the appropriate change of variables, it can be shown (see, e.g., [Wiggins (1990)]) that the whole dynamics of the two linearly coupled linear undamped oscillators is actually contained in the equations

$$\dot{\theta}_1 = \omega_1, \quad \dot{\theta}_2 = \omega_2, \quad (\theta_1, \theta_2) \in S^1 \times S^1 \equiv T^2. \quad (4.15)$$

The flow on the two-torus  $T^2$ , generated by (4.15), is simple to compute and is given by

$$\theta_1(t) = \omega_1 t + \theta_{10}, \quad \theta_2(t) = \omega_2 t + \theta_{20}, \quad (\text{mod } 2\pi),$$

and  $\theta_1$  and  $\theta_2$  are called the longitude and latitude. However, orbits under this flow will depend on how  $\omega_1$  and  $\omega_2$  are related. If  $\omega_1$  and  $\omega_2$  are *commensurate* (i.e., the equation  $m\omega_1 + n\omega_2 = 0$ ,  $(n, m) \in \mathbb{Z}$  has solutions), then every phase curve of (4.15) is closed. However, if  $\omega_1$  and  $\omega_2$  are *incommensurate* i.e., upper equation has no solutions), then every phase curve of (4.15) is everywhere dense on  $T^2$ .

Somewhat deeper understanding of Hamiltonian dynamics is related to the method of *action-angle variables*. The easiest way to introduce this idea is to consider again a simple harmonic oscillator (4.13). If we transform equations (4.13) into polar coordinates using  $q = r \sin \theta$ ,  $p = r \cos \theta$ , then the equations of the vector-field become  $\dot{r} = 0$ ,  $\dot{\theta} = 1$ , having the obvious solution  $r = \text{const}$ ,  $\theta = t + \theta_0$ . For this example polar coordinates work nicely because the system (4.13) is linear and, therefore, all of the periodic orbits have the same period.

For the general, nonlinear one-DOF Hamiltonian system (4.10) we will seek a coordinate transformation that has the same effect. Namely, we will seek a coordinate transformation  $(q, p) \mapsto (\theta(q, p), I(q, p))$  with inverse transformation  $(\theta, I) \mapsto (q(I, \theta), p(I, \theta))$  such that the vector-field (4.10) in the action-angle  $(\theta, I)$  coordinates satisfies the following conditions: (i)  $\dot{I} = 0$ ; (ii)  $\theta$  changes linearly in time on the closed orbits with  $\dot{\theta} = \Omega(I)$ . We might even think of  $I$  and  $\theta$  heuristically as 'nonlinear polar coordinates'. In such a coordinate system Hamiltonian function takes the form  $H = H(I)$ , and also,  $\Omega(I) = \partial_I H$ , i.e., specifying  $I$  specifies a periodic orbit.

The action variable  $I(q, p)$  geometrically represents an area enclosed by any closed curve, which is constant in time. It is defined as an integral  $I = \frac{1}{2\pi} \int_H p dq$ , where  $H$  denotes the periodic orbit defined by  $H(q, p) = H = \text{const}$ . If the period of each periodic orbit defined by  $H(q, p) = H = \text{const}$

is denoted by  $T(H)$ , the angle variable  $\theta(q, p)$  is defined by

$$\theta(q, p) = \frac{2\pi}{T(H)} t(q, p),$$

where  $t = t(q, p)$  represents the time taken for the solution starting from  $(q_0, p_0)$  to reach  $(q, p)$ .

For the system with Hamiltonian  $H = \frac{p^2}{2} + V(x)$  and momentum  $p = \pm\sqrt{2}\sqrt{H - V(x)}$  the action is given by  $I = \frac{\sqrt{2}}{\pi} \int_{q_{\min}}^{q_{\max}} \sqrt{H - V(q)} dq$ , and the angle is given by  $\theta(q, p) = \frac{2\pi}{T(H)} \int_{q_{\min}}^{q_{\max}} \frac{dq}{\sqrt{2}\sqrt{H - V(q)}}$ .

Closely related to the action-angle variables is the *perturbation theory* (see [Nay73]). To explain the main idea of this theory, let us consider an  $\epsilon$ -perturbed vector-field periodic in  $t$  which can be in component form given as (with  $(q, p) \in \mathbb{R}^2$ )

$$\dot{q} = f_1(q, p) + \epsilon g_1(q, p, t, \epsilon), \quad \dot{p} = f_2(q, p) + \epsilon g_2(q, p, t, \epsilon). \quad (4.16)$$

Setting  $\epsilon = 0$  we get the *unperturbed* Hamiltonian system with a smooth scalar-valued function  $H(q, p)$  for which holds

$$f_1(q, p) = \frac{\partial H(q, p)}{\partial p}, \quad f_2(q, p) = -\frac{\partial H(q, p)}{\partial q},$$

so, the perturbed system (4.16) obtains the symmetric canonical form

$$\dot{q} = \frac{\partial H(q, p)}{\partial p} + \epsilon g_1(q, p, t, \epsilon), \quad \dot{p} = -\frac{\partial H(q, p)}{\partial q} + \epsilon g_2(q, p, t, \epsilon).$$

The perturbation  $(g_1, g_2)$  need not be Hamiltonian, although in the case where perturbation is Hamiltonian versus the case where it is not, the dynamics are very different.

Now, if we transform the coordinates of the perturbed vector-field using the action-angle transformation for the unperturbed Hamiltonian vector-field, we get

$$\dot{I} = \epsilon \left( \frac{\partial I}{\partial q} g_1 + \frac{\partial I}{\partial p} g_2 \right) \equiv \epsilon F(I, \theta, t, \epsilon), \quad (4.17)$$

$$\dot{\theta} = \Omega(I) + \epsilon \left( \frac{\partial \theta}{\partial q} g_1 + \frac{\partial \theta}{\partial p} g_2 \right) \equiv \Omega(I) + \epsilon G(I, \theta, t, \epsilon),$$

where

$$\begin{aligned}
 F(I, \theta, t, \epsilon) &= \frac{\partial I}{\partial q}(q(I, \theta), p(I, \theta)) g_1((q(I, \theta), p(I, \theta), t, \epsilon) \\
 &\quad + \frac{\partial I}{\partial p}(q(I, \theta), p(I, \theta)) g_2((q(I, \theta), p(I, \theta), t, \epsilon), \\
 G(I, \theta, t, \epsilon) &= \frac{\partial \theta}{\partial q}(q(I, \theta), p(I, \theta)) g_1((q(I, \theta), p(I, \theta), t, \epsilon) \\
 &\quad + \frac{\partial \theta}{\partial p}(q(I, \theta), p(I, \theta)) g_2((q(I, \theta), p(I, \theta), t, \epsilon).
 \end{aligned}$$

Here,  $F$  and  $G$  are  $2\pi$  periodic in  $\theta$  and  $T = 2\pi/\omega$  periodic in  $t$ .

Finally, we shall explain in brief the most important idea in the dynamical systems theory, the idea of *Poincaré maps*. The idea of reducing the study of continuous time systems (flows) to the study of an *associated discrete time system (map)* is due to Poincaré who first utilized it in the end of the last century in his studies of the three body problem in celestial mechanics. Nowadays virtually any discrete time system that is associated with an ordinary differential equation is refereed to as a Poincaré map [Wiggins (1990)]. This technique offers several advantages in the study of dynamical systems, including dimensional reduction, global dynamics and conceptual clarity. However, construction of a Poincaré map requires some knowledge of the phase-space of a dynamical system. One of the techniques which can be used for construction of Poincaré maps is the perturbation method.

To construct the Poincaré map for the system (4.17), we have to rewrite it as an autonomous system

$$\dot{I} = \epsilon F(I, \theta, \phi, \epsilon), \quad \dot{\theta} = \Omega(I) + \epsilon G(I, \theta, \phi, \epsilon), \quad \dot{\phi} = \omega, \quad (4.18)$$

(where  $(I, \theta, \phi) \in \mathbb{R}^+ \times S^1 \times S^1$ ). We construct a global *cross-section*  $\Sigma$  to this vector-field defined as  $\Sigma^{\phi_0} = \{(I, \theta, \phi) | \phi = \phi_0\}$ . If we denote the  $(I, \theta)$  components of solutions of (4.18) by  $(I_\epsilon(t), \theta_\epsilon(t))$  and the  $(I, \theta)$  components of solutions of (4.18) for  $\epsilon = 0$  by  $(I_0, \Omega(I_0)t + \theta_0)$ , then the perturbed Poincaré map is given by

$$P_\epsilon : \Sigma^{\phi_0} \rightarrow \Sigma^{\phi_0}, \quad (I_\epsilon(0), \theta_\epsilon(0)) \mapsto (I_\epsilon(T), \theta_\epsilon(T)),$$

and the  $m$ th *iterate* of the Poincaré map is given by

$$P_\epsilon^m : \Sigma^{\phi_0} \rightarrow \Sigma^{\phi_0}, \quad (I_\epsilon(0), \theta_\epsilon(0)) \mapsto (I_\epsilon(mT), \theta_\epsilon(mT)).$$

Now we can approximate the solutions to the perturbed problem as linear, constant-coefficient approximation

$$I_\epsilon(t) = I_0 + \epsilon I_1(t) + O(\epsilon^2), \quad \theta_\epsilon(t) = \theta_0 + \Omega(I_0)t + \epsilon \theta_1(t) + O(\epsilon^2),$$

where we have chosen  $I_\epsilon(0) = I_0$ ,  $\theta_\epsilon(0) = \theta_0$ .

As a last example of one-DOF Hamiltonian dynamics we shall analyze a *damped, forced Duffing oscillator*, given by canonical equations [Wiggins (1990)]

$$\dot{q} = p, \quad \dot{p} = q - q^3 - \delta p + \gamma \cos \omega t, \quad \delta, \gamma, \omega \geq 0, \quad (q, p) \in \mathbb{R}^2. \quad (4.19)$$

where  $\delta, \gamma$ , and  $\omega$  are real parameters physically meaning *dissipation*, *amplitude of forcing* and *frequency*, respectively.

The *perturbed* system (4.19) is given by

$$\dot{q} = p, \quad \dot{p} = q - q^3 + \epsilon(\gamma \cos \omega t - \delta p), \quad (4.20)$$

where  $\epsilon$ -perturbation is assumed small. Then the *unperturbed* system is given by

$$\dot{q} = p, \quad \dot{p} = q - q^3,$$

and is conservative with Hamiltonian function

$$H(q, p) = \frac{p^2}{2} - \frac{q^2}{2} + \frac{q^4}{4}. \quad (4.21)$$

In the unperturbed phase-space all orbits are given by the level sets of the Hamiltonian (4.21). There are three equilibrium points at the following coordinates:  $(q, p) = (\pm 1, 0)$  – centers, and  $(q, p) = (0, 0)$  – saddle. The saddle point is connected to itself by two homoclinic orbits given by

$$q_+^0(t) = (\sqrt{2}(\cosh t)^{-1}, -\sqrt{2}(\cosh t)^{-1} \tanh t), \quad q_-^0(t) = -q_+^0(t).$$

There are two families of *periodic orbits*  $q_\pm^k(t)$ , where  $k$  represents the *elliptic modulus* related to the Hamiltonian by  $H(q_\pm^k(t)) \equiv H(k) = \frac{k^2-1}{(2-k^2)^2}$ , inside the corresponding homoclinic orbits  $q_\pm^0(t)$ , with the period  $T(k) = 2K(k)\sqrt{2-k^2}$  ( $K(k)$  is the complete elliptic integral of the first kind).

Also, there exists a family of periodic orbits outside the homoclinic orbits with the period  $T(k) = 4K(k)\sqrt{k^2-1}$ .

The perturbed system (4.20) can be rewritten as a third-order autonomous system

$$\dot{q} = p, \quad \dot{p} = q - q^3 + \epsilon(\gamma \cos \phi - \delta p), \quad \dot{\phi} = \omega,$$

where  $(q, p, \phi) \in \mathbb{R}^2 \times S^1$ ,  $S^1$  is the circle of length  $2\pi/\omega$  and  $\phi(t) = \omega t + \phi_0$ . We form the global cross-section to the flow

$$\Sigma^{\phi_0} = \{(q, p, \phi) | \phi = \phi_0 \in [0, 2\pi/\omega]\}$$

and the associated Poincaré map is given by

$$P : \Sigma^{\phi_0} \rightarrow \Sigma^{\phi_0}, \quad (q(0), p(0)) \mapsto (q(2\pi/\omega), p(2\pi/\omega)).$$

A detailed analysis of the perturbed Poincaré map for the damped, forced Duffing oscillator is related to the *Melnikov function* and can be found in [Wiggins (1990)].

#### 4.2.1.2 Complex One-DOF Hamiltonian Dynamics

*Global complex analysis* (see Appendix, for technical details on complex functions and manifolds) represents another powerful tool for analyzing the uniaxial joint dynamics, which can be easily generalized to  $n$ -DOF human-like musculo-skeletal chains. Setting  $z = q + ip$ ,  $z \in \mathbb{C}$ ,  $i = \sqrt{-1}$ , Hamilton's equations  $\dot{q} = \partial H / \partial p$ ,  $\dot{p} = -\partial H / \partial q$  may be written in *complex notation* as [Abraham and Marsden (1978); Marsden and Ratiu (1999); Wiggins (1990)]

$$\dot{z} = -2i \frac{\partial H}{\partial \bar{z}}. \quad (4.22)$$

Let  $U$  be an open set in the *complex phase-space manifold*  $M_C$  (i.e., manifold  $M$  modelled on  $\mathbb{C}$ ). A  $C^0$  function  $\gamma : [a, b] \rightarrow U \subset M_C$ ,  $t \mapsto \gamma(t)$  represents a *solution curve*  $\gamma(t) = q(t) + ip(t)$  of a complex Hamiltonian system (4.22). For instance, the curve  $\gamma(\theta) = \cos \theta + i \sin \theta$ ,  $0 \leq \theta \leq 2\pi$  is the unit circle.  $\gamma(t)$  is a *parameterized curve*. We call  $\gamma(a)$  the *beginning point*, and  $\gamma(b)$  the *end point* of the curve. By a *point on the curve* we mean a point  $w$  such that  $w = \gamma(t)$  for some  $t \in [a, b]$ .

The derivative  $\dot{\gamma}(t)$  is defined in the usual way, namely

$$\dot{\gamma}(t) = \dot{q}(t) + i\dot{p}(t),$$

so that the usual rules for the derivative of a sum, product, quotient, and chain rule are valid. The *speed* is defined as usual to be  $|\dot{\gamma}(t)|$ . Also, if  $f : U \rightarrow M_C$  represents a *holomorphic*, or *analytic* (i.e., complex-differentiable, see Appendix) function, then the composite  $f \circ \gamma$  is differentiable (as a function of the real variable  $t$ ) and  $(f \circ \gamma)'(t) = f'(\gamma(t)) \dot{\gamma}(t)$ .

A *path* represents a sequence of  $C^1$ -curves,

$$\gamma = \{\gamma_1, \gamma_2, \dots, \gamma_n\},$$

such that the end point of  $\gamma_j$ , ( $j = 1, \dots, n$ ) is equal to the beginning point of  $\gamma_{j+1}$ . If  $\gamma_j$  is defined on the interval  $[a_j, b_j]$ , this means that

$$\gamma_j(b_j) = \gamma_{j+1}(a_{j+1}).$$

We call  $\gamma_1(a_1)$  the *beginning point* of  $\gamma_j$ , and  $\gamma_n(b_n)$  the *end point* of  $\gamma_j$ . The path is said to *lie in an open set*  $U \subset M_C$  if each curve  $\gamma_j$  lies in  $U$ , i.e., for each  $t$ , the point  $\gamma_j(t)$  lies in  $U$ .

An open set  $U$  is *connected* if given two points  $\alpha$  and  $\beta$  in  $U$ , there exists a path  $\gamma = \gamma_1, \gamma_2, \dots, \gamma_n$  in  $U$  such that  $\alpha$  is the beginning point of  $\gamma_1$  and  $\beta$  is the end point of  $\gamma_n$ ; in other words, if there is a path  $\gamma$  in  $U$  which joins  $\alpha$  to  $\beta$ . If  $U$  is a connected open set and  $f$  a holomorphic function on  $U$  such that  $f' = 0$ , then  $f$  is a constant. If  $g$  is a function on  $U$  such that  $f' = g$ , then  $f$  is called a *primitive* of  $g$  on  $U$ . Primitives can be either find out by integration or written down directly.

Let  $f$  be a  $C^0$ -function on an open set  $U$ , and suppose that  $\gamma$  is a curve in  $U$ , meaning that all values  $\gamma(t)$  lie in  $U$  for  $a \leq t \leq b$ . The *integral of  $f$  along  $\gamma$*  is defined as

$$\int_{\gamma} f = \int_{\gamma} f(z) = \int_a^b f(\gamma(t)) \dot{\gamma}(t) dt.$$

For example, let  $f(z) = 1/z$ , and  $\gamma(\theta) = e^{i\theta}$ . Then  $\dot{\gamma}(\theta) = ie^{i\theta}$ . We want to find the value of the integral of  $f$  over the circle,  $\int_{\gamma} dz/z$ , so  $0 \leq \theta \leq 2\pi$ . By definition, this integral is equal to  $\int_0^{2\pi} ie^{i\theta}/e^{i\theta} d\theta = i \int_0^{2\pi} d\theta = 2\pi i$ .

The *length*  $L(\gamma)$  is defined to be the integral of the speed,  $L(\gamma) = \int_a^b |\dot{\gamma}(t)| dt$ .

If  $\gamma = \gamma_1, \gamma_2, \dots, \gamma_n$  is a path, then the integral of a  $C^0$ -function  $f$  on an open set  $U$  is defined as  $\int_{\gamma} f = \sum_{i=1}^n \int_{\gamma_i} f$ , i.e., the sum of the integrals of  $f$  over each curve  $\gamma_i$  ( $i = 1, \dots, n$ ) of the path  $\gamma$ . The *length of a path* is defined as  $L(\gamma) = \sum_{i=1}^n L(\gamma_i)$ .

Let  $f$  be continuous on an open set  $U \subset M_C$ , and suppose that  $f$  has a primitive  $g$ , that is,  $g$  is holomorphic and  $g' = f$ . Let  $\alpha, \beta$  be two points in  $U$ , and let  $\gamma$  be a path in  $U$  joining  $\alpha$  to  $\beta$ . Then  $\int_{\gamma} f = g(\beta) - g(\alpha)$ ; this integral is independent of the path and depends only on the beginning and end point of the path.

A *closed path* is a path whose beginning point is equal to its end point. If  $f$  is a  $C^0$ -function on an open set  $U \subset M_C$  admitting a holomorphic primitive  $g$ , and  $\gamma$  is any closed path in  $U$ , then  $\int_\gamma f = 0$ .

Let  $\gamma, \eta$  be two paths defined over the same interval  $[a, b]$  in an open set  $U \subset M_C$ . Recall (see section on categorical language) that  $\gamma$  is *homotopic* to  $\eta$  if there exists a  $C^0$ -function  $\psi : [a, b] \times [c, d] \rightarrow U$  defined on a rectangle  $[a, b] \times [c, d] \subset U$ , such that  $\psi(t, c) = \gamma(t)$  and  $\psi(t, d) = \eta(t)$  for all  $t \in [a, b]$ . For each number  $s \in [c, d]$  we may view the function  $|\psi|_s(t) = \psi(t, s)$  as a continuous curve defined on  $[a, b]$ , and we may view the family of continuous curves  $\psi_s$  as a *deformation* of the path  $\gamma$  to the path  $\eta$ . It is said that the homotopy  $\psi$  *leaves the end points fixed* if we have  $\psi(a, s) = \gamma(a)$  and  $\psi(b, s) = \gamma(b)$  for all values of  $s \in [c, d]$ . Similarly, when we speak of a homotopy of closed paths, we assume that each path  $\psi_s$  is a closed path.

Let  $\gamma, \eta$  be paths in an open set  $U \subset M_C$  having the same beginning and end points. Assume that they are homotopic in  $U$ . Let  $f$  be holomorphic on  $U$ . Then  $\int_\gamma f = \int_\eta f$ . The same holds for closed homotopic paths in  $U$ . In particular, if  $\gamma$  is homotopic to a point in  $U$ , then  $\int_\gamma f = 0$ . Also, it is said that an open set  $U \subset M_C$  is *simply connected* if it is connected and if every closed path in  $U$  is homotopic to a point.

In the previous example we found that

$$\frac{1}{2\pi i} \int_\gamma \frac{1}{z} dz = 1,$$

if  $\gamma$  is a circle around the origin, oriented counterclockwise. Now we define for any closed path  $\gamma$  its *winding number* with respect to a point  $\alpha$  to be

$$W(\gamma, \alpha) = \frac{1}{2\pi i} \int_\gamma \frac{1}{z - \alpha} dz,$$

provided the path does not pass through  $\alpha$ . If  $\gamma$  is a closed path, then  $W(\gamma, \alpha)$  is an integer.

A closed path  $\gamma \in U \subset M_C$  is *homologous to 0* in  $U$  if

$$\int_\gamma \frac{1}{z - \alpha} dz = 0,$$

for every point  $\alpha$  not in  $U$ , or in other words,  $W(\gamma, \alpha) = 0$  for every such point.

Similarly, let  $\gamma, \eta$  be closed paths in an open set  $U \subset M_C$ . We say that they are *homologous* in  $U$ , and write  $\gamma \sim \eta$ , if  $W(\gamma, \alpha) = W(\eta, \alpha)$  for every

point  $\alpha$  in the complement of  $U$ . We say that  $\gamma$  is *homologous to 0 in  $U$* , and write  $\gamma \sim 0$ , if  $W(\gamma, \alpha) = 0$  for every point  $\alpha$  in the complement of  $U$ .

If  $\gamma$  and  $\eta$  are closed paths in  $U$  and are homotopic, then they are homologous. If  $\gamma$  and  $\eta$  are closed paths in  $U$  and are close together, then they are homologous.

Let  $\gamma_1, \dots, \gamma_n$  be curves in an open set  $U \subset M_C$ , and let  $m_1, \dots, m_n$  be integers. A formal sum  $\gamma = m_1\gamma_1 + \dots + m_n\gamma_n = \sum_{i=1}^n m_i\gamma_i$  is called a *chain in  $U$* . The chain is called *closed* if it is a finite sum of closed paths. If  $\gamma$  is the chain as above, then  $\int_\gamma f = \sum_i m_i \int_{\gamma_i} f$ . If  $\gamma$  and  $\eta$  are closed chains in  $U$ , then  $W(\gamma + \eta, \alpha) = W(\gamma, \alpha) + W(\eta, \alpha)$ . We say that  $\gamma$  and  $\eta$  are *homologous in  $U$* , and write  $\gamma \sim \eta$ , if  $W(\gamma, \alpha) = W(\eta, \alpha)$  for every point  $\alpha$  in the complement of  $U$ . We say that  $\gamma$  is *homologous to 0 in  $U$* , and write  $\gamma \sim 0$ , if  $W(\gamma, \alpha) = 0$  for every point  $\alpha$  in the complement of  $U$ .

*Cauchy's theorem* states that if  $\gamma$  is a closed chain in an open set  $U \subset M_C$ , and  $\gamma$  is homologous to 0 in  $U$ , then  $\int_\gamma f = 0$ . If  $\gamma$  and  $\eta$  are closed chains in  $U$ , and  $\gamma \sim \eta$  in  $U$ , then  $\int_\gamma f = \int_\eta f$ .

It follows from Cauchy's theorem that if  $\gamma$  and  $\eta$  are homologous, then  $\int_\gamma f = \int_\eta f$  for all holomorphic functions  $f$  on  $U$  [Abraham and Marsden (1978); Wiggins (1990)].

#### 4.2.1.3 Library of Basic Hamiltonian Systems

In this subsection, mainly following [Putz (1993)], we present some basic Hamiltonian biodynamic systems.

**1D Harmonic Oscillator.** In this case we have  $\{p, q\}$  as canonical coordinates on  $\mathbb{R}^2$

$$\begin{aligned} M &= T^*\mathbb{R} \simeq \mathbb{R}^2, & \omega &= dp \wedge dq, \\ H &= \frac{1}{2}(p^2 + q^2), & X_H &= p \frac{\partial}{\partial q} - q \frac{\partial}{\partial p}, \end{aligned}$$

and Hamilton's equations read

$$\dot{q} = p, \quad \dot{p} = -q.$$

For each  $f, g \in C^k(\mathbb{R}^2, \mathbb{R})$  the Poisson bracket is given by

$$\{f, g\}_\omega = \frac{\partial f}{\partial q} \frac{\partial g}{\partial p} - \frac{\partial f}{\partial p} \frac{\partial g}{\partial q}.$$

**Complex Plane.** Let  $T^*\mathbb{R} \simeq \mathbb{R}^2$  have the canonical symplectic struc-



ture  $\omega = dp \wedge dq$ . Writing  $z = q + ip$ , we have

$$\omega = \frac{1}{2i} dz \wedge d\bar{z}, \quad X_H = i \left( \frac{\partial H}{\partial z} \frac{\partial}{\partial \bar{z}} - \frac{\partial H}{\partial \bar{z}} \frac{\partial}{\partial z} \right),$$

$$\{f, g\}_\omega = \frac{i}{2} \left( \frac{\partial f}{\partial z} \frac{\partial g}{\partial \bar{z}} - \frac{\partial f}{\partial \bar{z}} \frac{\partial g}{\partial z} \right),$$

so, the Hamilton's equations,  $\dot{q} = \partial_p H$ ,  $\dot{p} = -\partial_q H$ , become

$$\dot{z} = -2i \frac{\partial H}{\partial \bar{z}}.$$

**2D Harmonic Oscillator.** In this case we have  $\{q^1, y, p_1, p_2\}$  as canonical coordinates on  $\mathbb{R}^4$

$$M = T^*\mathbb{R}^2 \simeq \mathbb{R}^4, \quad \omega = dp_1 \wedge dq^1 + dp_2 \wedge dq^2,$$

$$H = \frac{1}{2} [p_1^2 + p_2^2 + (q^1)^2 + (y)^2].$$

The functions  $f = p_i p_j + q^i q^j$  and  $g = p_i q^j + p_j q^i$ , (for  $i, j = 1, 2$ ), are constants of motion.

**$n$ D Harmonic Oscillator.** In this case we have ( $i = 1, \dots, n$ )

$$M = T^*\mathbb{R}^n \simeq \mathbb{R}^{2n}, \quad \omega = dp_i \wedge dq^i,$$

$$H = \frac{1}{2} \sum_{i=1}^n [p_i^2 + (q^i)^2].$$

The system is integrable in an open set of  $T^*\mathbb{R}^n$  with:

$$K_1 = H, \quad K_2 = p_2^2 + (y)^2, \quad \dots, \quad K_n = p_n^2 + (q^n)^2.$$

**Toda Molecule.** Consider three mass-points on the line with coordinates  $q^i$ , ( $i = 1, 2, 3$ ), and satisfying the ODEs:

$$\ddot{q}^i = -\partial_{q^i} U, \quad \text{where} \quad U = e^{q^1 - q^2} + e^{q^2 - q^3} - e^{q^3 - q^1}.$$

This is a Hamiltonian system with  $\{q^i, p_i\}$  as canonical coordinates on  $\mathbb{R}^6$ ,

$$M = T^*\mathbb{R}^3 \simeq \mathbb{R}^6, \quad \omega = dp_i \wedge dq^i,$$

$$H = \frac{1}{2} (p_1^2 + p_2^2 + p_3^2) + U.$$

The Toda molecule (4.2.1.3) is an integrable Hamiltonian system in an open set of  $T^*\mathbb{R}^3$  with:

$$\begin{aligned} K_1 &= H, & K_2 &= p_1 + p_2 + p_3, \\ K_3 &= \frac{1}{9} (p_1 + p_2 + p_3) (p_2 + p_3 - 2p_1) (p_3 + p_1 - 2p_2) - (p_1 + p_2 - 2p_3) e^{q^1 - q^2} \\ &\quad - (p_2 + p_3 - 2p_1) e^{q^2 - q^3} - (p_3 + p_1 - 2p_2) e^{q^3 - q^1}. \end{aligned}$$

**3-Point Vortex Problem.** The motion of three-point vortices for an ideal incompressible fluid in the plane is given by the equations:

$$\begin{aligned} \dot{q}^j &= -\frac{1}{2\pi} \sum_{i \neq j} \Gamma_i (p_j - p_i) / r_{ij}^2, \\ \dot{p}_j &= \frac{1}{2\pi} \sum_{i \neq j} \Gamma_i (q^i - q^j) / r_{ij}^2, \\ r_{ij}^2 &= (q^i - q^j)^2 + (p_j - p_i)^2, \end{aligned}$$

where  $i, j = 1, 2, 3$ , and  $\Gamma_i$  are three nonzero constants. This mechanical system is Hamiltonian if we take:

$$\begin{aligned} M &= T^*\mathbb{R}^3 \simeq \mathbb{R}^6, & \omega &= dp_i \wedge dq^i, & (i = 1, \dots, 3), \\ H &= -\frac{1}{4\pi} \sum_{i,j=1}^3 \Gamma_i \Gamma_j \ln(r_{ij}). \end{aligned}$$

Moreover, it is integrable in an open set of  $T^*\mathbb{R}^3$  with:

$$\begin{aligned} K_1 &= H, & K_2 &= \sum_{i=1}^3 \Gamma_i \left[ (q^i)^2 + p_i^2 \right], \\ K_3 &= \left( \sum_{i=1}^3 \Gamma_i q^i \right)^2 + K_2^2. \end{aligned}$$

**The Newton's Second Law as a Hamiltonian System.** In the case of conservative forces, Newton's law of motion can be written on  $\mathbb{R}^{3n}$  as

$$m_i \ddot{q}^i = -\partial_{q^i} U, \quad (i = 1, 2, \dots, 3n).$$

Its symplectic formulation reads:

$$M = T^*\mathbb{R}^3 \simeq \mathbb{R}^6, \quad \omega = dp_i \wedge dq^i,$$

$$H = \sum_{i=1}^{3n} \frac{p_i^2}{2m_i} + U.$$

The Hamiltonian vector-field  $X_H$  is

$$X_H = \left( \frac{p_i}{m_i} \partial_{q^i} - \partial_{q^i} U \partial_{p_i} \right),$$

giving the Hamilton's equations

$$\dot{q}^i = \frac{p_i}{m_i}, \quad \dot{p}_i = -\partial_{q^i} U.$$

**Rigid Body.** A *rigid body with a fixed point* is a basic model of a single segment of the human (or robot) body. This is a left-invariant Hamiltonian mechanical system on the phase-space  $T^*SO(3)$ . The differentiable structure on  $SO(3)$  is defined using the traditional Euler angles  $\{\varphi, \psi, \theta\}$ .

More precisely, a local chart is given by [Puta (1993)]

$$(\varphi, \psi, \theta) \in \mathbb{R}^3 \longmapsto A \in SO(3), \quad 0 < \varphi, \psi < 2\pi; \quad 0 < \theta < \pi,$$

where  $A =$

$$\begin{bmatrix} \cos \psi \cos \varphi - \cos \theta \sin \varphi \sin \psi & \cos \psi \cos \varphi + \cos \theta \cos \varphi \sin \psi & \sin \theta \sin \psi \\ -\sin \psi \cos \varphi - \cos \theta \sin \varphi \sin \psi & -\sin \psi \sin \varphi + \cos \theta \cos \varphi \cos \psi & \sin \theta \cos \psi \\ \sin \theta \sin \varphi & -\sin \theta \cos \varphi & \cos \theta \end{bmatrix}$$

The corresponding conjugate momenta are denoted by  $p_\varphi, p_\psi, p_\theta$ , so  $\{\varphi, \psi, \theta, p_\varphi, p_\psi, p_\theta\}$  is the phase-space  $T^*SO(3)$ . Thus, we have

$$M = T^*SO(3), \quad \omega = dp_\varphi \wedge d\varphi + dp_\psi \wedge d\psi + dp_\theta \wedge d\theta, \quad H = \frac{1}{2}K,$$

$$K = \frac{[(p_\varphi - p_\psi \cos \theta) \sin \psi + p_\theta \sin \theta \cos \psi]^2}{I_1 \sin^2 \theta}$$

$$+ \frac{[(p_\varphi - p_\psi \cos \theta) \cos \psi - p_\theta \sin \theta \sin \psi]^2}{I_2 \sin^2 \theta} + \frac{p_\psi^2}{I_3},$$

where  $I_1, I_2, I_3$  are the moments of inertia, diagonalizing the inertia tensor of the body.

The Hamilton's equations are

$$\begin{aligned}\dot{\varphi} &= \frac{\partial H}{\partial p_{\varphi}}, & \dot{\psi} &= \frac{\partial H}{\partial p_{\psi}}, & \dot{\theta} &= \frac{\partial H}{\partial p_{\theta}}, \\ \dot{p}_{\varphi} &= -\frac{\partial H}{\partial \varphi}, & \dot{p}_{\psi} &= -\frac{\partial H}{\partial \psi}, & \dot{p}_{\theta} &= -\frac{\partial H}{\partial \theta}.\end{aligned}$$

For each  $f, g \in C^k(T^*SO(3), \mathbb{R})$  the Poisson bracket is given by

$$\begin{aligned}\{f, g\}_{\omega} &= \frac{\partial f}{\partial \varphi} \frac{\partial g}{\partial p_{\varphi}} - \frac{\partial f}{\partial p_{\varphi}} \frac{\partial g}{\partial \varphi} + \frac{\partial f}{\partial \psi} \frac{\partial g}{\partial p_{\psi}} - \frac{\partial f}{\partial p_{\psi}} \frac{\partial g}{\partial \psi} \\ &+ \frac{\partial f}{\partial \theta} \frac{\partial g}{\partial p_{\theta}} - \frac{\partial f}{\partial p_{\theta}} \frac{\partial g}{\partial \theta}.\end{aligned}$$

**The Heavy Top – Continued.** Recall (see (7.153) above) that the heavy top is by definition a rigid body moving about a fixed point in a 3D space [Putz (1993)]. The rigidity of the top means that the distances between points of the body are fixed as the body moves. In this case we have

$$\begin{aligned}M &= T^*SO(3), \\ \omega &= dp_{\varphi} \wedge d\varphi + dp_{\psi} \wedge d\psi + dp_{\theta} \wedge d\theta, \\ H &= \frac{1}{2}K + mgl \cos \theta, \\ K &= \frac{[(p_{\varphi} - p_{\psi} \cos \theta) \sin \psi + p_{\theta} \sin \theta \cos \psi]^2}{I_1 \sin^2 \theta} \\ &+ \frac{[(p_{\varphi} - p_{\psi} \cos \theta) \cos \psi - p_{\theta} \sin \theta \sin \psi]^2}{I_2 \sin^2 \theta} + \frac{p_{\psi}^2}{I_3},\end{aligned}$$

where  $I_1, I_2, I_3$  are the moments of inertia,  $m$  is the total mass,  $g$  is the gravitational acceleration and  $l$  is the length of the vector determining the center of mass at  $t = 0$ .

The Hamilton's equations are

$$\begin{aligned}\dot{\varphi} &= \frac{\partial H}{\partial p_{\varphi}}, & \dot{\psi} &= \frac{\partial H}{\partial p_{\psi}}, & \dot{\theta} &= \frac{\partial H}{\partial p_{\theta}}, \\ \dot{p}_{\varphi} &= -\frac{\partial H}{\partial \varphi}, & \dot{p}_{\psi} &= -\frac{\partial H}{\partial \psi}, & \dot{p}_{\theta} &= -\frac{\partial H}{\partial \theta}.\end{aligned}$$

For each  $f, g \in C^k(T^*SO(3), \mathbb{R})$  the Poisson bracket is given by

$$\begin{aligned}\{f, g\}_\omega &= \frac{\partial f}{\partial \varphi} \frac{\partial g}{\partial p_\varphi} - \frac{\partial f}{\partial p_\varphi} \frac{\partial g}{\partial \varphi} + \frac{\partial f}{\partial \psi} \frac{\partial g}{\partial p_\psi} - \frac{\partial f}{\partial p_\psi} \frac{\partial g}{\partial \psi} \\ &+ \frac{\partial f}{\partial \theta} \frac{\partial g}{\partial p_\theta} - \frac{\partial f}{\partial p_\theta} \frac{\partial g}{\partial \theta}.\end{aligned}$$

The Hamiltonian  $H$  is invariant under rotations about the  $z$ -axis, i.e.,  $\varphi$  is a cyclic variable, so  $p_\varphi$  is a constant of motion. The momentum map for this  $S^1$ -action is  $J(\varphi, \psi, \theta, p_\varphi, p_\psi, p_\theta) = p_\varphi$ . The reduced phase-space  $J^{-1}(p_\varphi)/S^1$  can be identified with  $T^*S^2$  and it is parameterized by  $\{\psi, \theta, p_\psi, p_\theta\}$ . The equations of motion for  $\psi, \theta$  are just Hamilton's equations for  $H$  with  $p_\varphi$  held constant.

**Two Coupled Pendula.** The configuration space of the system of two coupled pendula in the plane is  $T^2 = \{(\theta_1, \theta_2)\}$ , where the  $\theta$ s are the two pendulum angles, the phase-space is  $T^*T^2$  with its canonical symplectic structure and the Hamiltonian  $H$  is given by [Puta (1993)]

$$H = \frac{1}{2}(p_\varphi^2 + p_\psi^2) + V(\sqrt{2}\psi),$$

where

$$\varphi = \frac{\theta_1 + \theta_2}{\sqrt{2}}, \quad \psi = \frac{\theta_1 - \theta_2}{\sqrt{2}}.$$

The group  $S^1$  acts on  $T^2$  by

$$\theta \cdot (\theta_1 + \theta_2) = (\theta + \theta_1, \theta + \theta_2)$$

and hence the induced momentum map for the lifted action to  $T^*T^2$  is given by

$$J(\varphi, \psi, p_\varphi, p_\psi) = p_\varphi.$$

Therefore, the reduced phase-space  $J^{-1}(p_\varphi)/S^1$  is symplectically diffeomorphic to  $T^*S^1$  with its canonical symplectic structure  $\omega_\mu = dp_\psi \wedge d\psi$ . The reduced Hamiltonian  $H_\mu$  is

$$H_\mu = \frac{1}{2}p_\psi^2 + V(\sqrt{2}\psi),$$

and Hamilton's equations for  $H_\mu$  are

$$\dot{\psi} = p_\psi, \quad \dot{p}_\psi = -\sqrt{2}\dot{V}(\sqrt{2}\psi).$$

**The Plane 2-Body Problem.** The plane two body problem can be formulated as the triple  $(M, \omega, H)$  where [Putz (1993)]

$$M = T^*((0, \infty) \times S^1), \quad \omega = dp_r \wedge dr + dp_\theta \wedge d\theta, \\ H = (p_r^2 + p_\theta^2)/r^2 - 1/r.$$

The Lie group  $G = SO(2) \simeq S^1$  acts on the configuration space  $M = (0, \infty) \times S^1$  by rotations, i.e., if  $R_\varphi \in SO(2)$  then

$$\phi : (R_\varphi, (r, \theta)) \mapsto (r, \theta + \varphi, p_r, p_\theta).$$

The corresponding momentum map is

$$J(r, \theta, p_r, p_\theta) = p_\theta.$$

**The 3-Body Problem.** There is a vast literature on the *restricted three-body problem* (see [Meyer and Hall (1992)]). Among other things, there are investigations of the equilibria points and their stability, investigations of the existence, stability and bifurcation of periodic orbits, and investigations of collisions and ejection orbits. The restricted problem is said to be a limit of the *full three-body problem* as one of the masses tends to zero, and so to each result for the restricted problem there should be a corresponding result for the full three-body problem.

The restricted three-body problem is a Hamiltonian system of differential equations which describes the motion of an infinitesimal particle (the *satellite*) moving under the gravitational influence of two particles of finite mass (the *primaries*) which are moving on a circular orbit of the Kepler problem [Meyer and Schmidt (2000)].

Since the motion of the primaries is given, the restricted problem has two DOF for the planar problem and three DOF for the spatial problem. However, the full problem has six DOF in the planar case and nine DOF in the spatial case. Thus, at first the restricted problem seems too small to reflect the full complexity of the full problem; but when the symmetries of the full problem are taken into account the dimension gap narrows considerably.

The Hamiltonian of the full problem is invariant under Euclidean motions, i.e., translations and rotations, which begets the integrals of linear and angular momentum. Translations and rotations give rise to ignorable coordinates. Holding the integrals fixed and dropping the ignorable coordinates reduces the full problem from six to three DOF in the planar case and from nine to four DOF in the spatial case. Thus the full problem on

the reduced space is only one DOF larger than the restricted problem in either the planar or the spatial case [Meyer and Schmidt (2000)].

The full 3-body problem in 3D space has 9 DOF. By placing the center of mass at the origin and setting linear momentum equal to zero the problem reduces one with six DOF. This is easily done using Jacobi coordinates. The Hamiltonian of the full 3-body problem in rotating (about the  $z$ -axis) Jacobi coordinates  $(u_0, u_1, u_2, v_0, v_1, v_2)$  is

$$H = \frac{\|v_0\|^2}{2M_0} - u_0^T J v_0 + \frac{\|v_1\|^2}{2M_1} - u_1^T J v_1 - \frac{m_0 m_1}{\|u_1\|} \\ + \frac{\|v_2\|^2}{2M_2} - u_2^T J v_2 - \frac{m_1 m_2}{\|u_2 - \alpha_0 u_1\|} - \frac{m_2 m_0}{\|u_2 + \alpha_1 u_1\|}$$

where  $u_i, v_i \in \mathbb{R}^3$ ,

$$M_0 = m_0 + m_1 + m_2, \quad M_1 = m_0 m_1 / (m_0 + m_1), \\ M_2 = m_2 (m_0 + m_1) / (m_0 + m_1 + m_2), \\ \alpha_0 = m_0 / (m_0 + m_1), \quad \alpha_1 = m_1 / (m_0 + m_1),$$

and  $J = \begin{pmatrix} 0 & 1 & 0 \\ -1 & 0 & 0 \\ 0 & 0 & 0 \end{pmatrix}$ . In these coordinates  $u_0$  is the center of mass,  $v_0$  is total linear momentum, and total angular momentum is

$$A = u_0 \times v_0 + u_1 \times v_1 + u_2 \times v_2.$$

See [Meyer and Hall (1992)] for further details.

#### 4.2.1.4 $n$ -DOF Hamiltonian Dynamics

Classically,  $n$ -DOF Hamiltonian dynamics combines the ideas of differential equations and variational principles (see [Abraham and Marsden (1978); Arnold (1989); Marsden and Ratiu (1999); Wiggins (1990)]). As Hamilton first realized, many of the systems of mechanics and optics can be put into the special form (compare (4.10))

$$\dot{q}^i = \frac{\partial H}{\partial p_i}(q^i, p_i, t), \quad \dot{p}_i = -\frac{\partial H}{\partial q^i}(q^i, p_i, t), \quad (i = 1, \dots, n),$$

or an associated variational form (summing upon the repeated index is used in the following text)

$$\delta \int (p_i dq^i - H) dt = 0.$$

Here the state of the system is given as a point  $(q^1, \dots, q^n, p_1, \dots, p_n)$  in *phase-space*, the  $q$ 's are the configuration coordinates, the  $p$ 's are the momenta,  $t$  is time, and  $H = H(q^i, p_i, t)$  is a total-energy function called Hamiltonian. The variables  $(q^i, p_i)$  are called *canonical* coordinates.

If  $H = H(q^i, p_i)$  does not depend explicitly on time, the system is said to be *autonomous*. In this case, it is easy to verify that  $H$  is conserved. The search for other conserved quantities led to a new notion of solving Hamiltonian systems. Instead of finding formulae for the coordinates as a function of time, one searches for constants of the motion (*integrals*). If one can find  $n$  integrals  $I_i(q^i, p_i)$  which are in *involution*:

$$[I_i, I_j] = \frac{\partial I_i}{\partial q^k} \frac{\partial I_j}{\partial p_k} - \frac{\partial I_i}{\partial p_k} \frac{\partial I_j}{\partial q^k} = 0, \quad (i \neq j),$$

(here the square brackets denote the Poisson bracket) and *independent* (the vectors  $\nabla I_i$  are independent 'almost everywhere'), then associated variables  $\phi_i$  can be derived which evolve linearly in time:  $\dot{\phi}^i = \frac{\partial H}{\partial I_i}(I_i)$ .

Such a system is *integrable* in the sense of Liouville [Arnold (1989)]. If the sets  $I = \text{const}$  are bounded, then they are  $nD$  *tori*  $T^n$  in phase-space. Choosing irreducible cycles,  $\gamma_i$ , on the tori, one can define a preferred set of integrals  $J_i = \int_{\gamma_i} p_i dq^i$ , called *action variables*, for which the corresponding  $\phi_i$  are *angle variables* mod 1 on  $T^n$ . The quantities  $\omega^i(J) = \frac{\partial H}{\partial J_i}(J_i)$  are called the *frequencies* on  $T^n$ .

Another feature of Hamiltonian systems noticed by Liouville is the preservation of phase-space volume  $\int (dq)^n (dp)^n$ . A more general result is that Poincaré's integral  $\int p_i dq^i$  is conserved around any loop following the flow [Arnold (1989)]. This is the property that really distinguishes Hamiltonian differential equations from general ones.

The major problem with the notion of integrability is that *most systems are not integrable*. This was first appreciated when Poincaré proved that the *circular restricted three-body problem has no integral analytic in the mass ratio*. The perturbation expansions which gave excellent predictions of motion of the planets do not converge. The basic reason is that among the invariant tori of integrable systems is a dense subset on which the frequencies  $\omega^i$  are *commensurate*, i.e.,  $m_i \omega^i = 0$  for some non-zero integer vector  $m_i$ ; however, most systems have no commensurate tori, because they can be destroyed by arbitrarily small perturbation.

Poincaré went on to examine what really does happen. The key technique he used was geometric analysis: instead of manipulating formulae for



canonical transformations as Jacobi and others did, he pictured the *orbits* in phase-space. An important step in this *qualitative theory* of differential equations was the idea of *surface of section*. If  $\Sigma$  is a *codimension-one* surface (i.e., of dimension one less than that of the phase-space) transverse to a *flow*, then the sequence  $\{x_j\}$  of successive intersections of an orbit with  $\Sigma$  provides a lot of information about that orbit. For example, if  $\{x_j\}$  is periodic then it corresponds to a periodic orbit. If  $\{x_j\}$  is confined to a subset of codimension  $m$  on  $\Sigma$  then so is the orbit of the flow, etc.. The flow induces a mapping of  $\Sigma$  to itself; the map takes a point in  $\Sigma$  to the point at which it first returns to  $\Sigma$  (assuming there is one). Since the surface of section has one dimension less than the phase-space it is easier to picture the dynamics of the return map than the flow. In fact, for Hamiltonian systems one can do even better; since  $H$  is conserved,  $\Sigma$  decomposes into a one-parameter family of codimension two surfaces parameterized by the value of the energy, a reduction of two dimensions.

This led Poincaré to the ideas of *stable* and *unstable manifolds* for *hyperbolic* periodic orbits, which are extensions of the stable and unstable *eigenspaces* for associated linear systems, and their intersections, known as *hetero- and homo-clinic points*, whose orbits converge to one periodic orbit in the past and to another (or the same) in the future. He showed that having intersected once, the invariant manifolds must intersect infinitely often. Moreover the existence of one heteroclinic orbit implies the existence of an infinity of others.

The distance between the stable and unstable manifolds can be quantified by Melnikov's integral. This leads to a technique for proving the non-existence of integrals for a slightly perturbed, integrable Hamiltonian.

For integrable systems, nearby orbits separate linearly in time; however, dynamical systems can have exponentially separating orbits. Let  $\delta x$  be a tangent vector at the phase-space point  $x$  and  $\delta x_t$  be the evolved vector following the orbit of  $x$ . Then, recall from section 2.3 above, the average rate of exponentiation of  $\delta x_t$  is the *Lyapunov exponent*  $\lambda$ ,

$$\lambda(x, \delta x) = \lim_{t \rightarrow \infty} 1/t \ln |\delta x_t|.$$

If  $\lambda$  is nonzero, then the predictions one can make will be valid for a time only logarithmic in the precision. Therefore, although deterministic in principle, a system need not be predictable in practice.

A concrete example of the complexity of behavior of typical Hamiltonian systems is provided by the 'horseshoe', a type of invariant set found near

homoclinic orbits. Its points can be labelled by doubly infinite sequences of 0's and 1's corresponding to which half of a horseshoe shaped set the orbit is in at successive times. For every sequence, no matter how complicated, there is an orbit which has that symbol sequence. This implies, e.g., that a simple pendulum in a sufficiently strongly modulated time-periodic gravitational field has an initial condition such that the pendulum will turn over once each period when there is 1 in the sequence and not if there is a 0 for any sequence of 0's and 1's.

#### 4.2.2 Hamiltonian Geometry in Biodynamics

We will develop our Hamiltonian geometry on the configuration biodynamics manifold  $M$  in three steps, as follows (compare with section (3.7) above):  
**Step A** Find a symplectic momentum phase-space  $(P, \omega)$ .

Recall that a symplectic structure on a smooth manifold  $M$  is a nondegenerate closed 2-form  $\omega$  on  $M$ , i.e., for each  $x \in M$ ,  $\omega(x)$  is nondegenerate, and  $d\omega = 0$ .

Let  $T_x^*M$  be a cotangent space to  $M$  at  $m$ . The cotangent bundle  $T^*M$  represents a union  $\cup_{m \in M} T_x^*M$ , together with the standard topology on  $T^*M$  and a natural smooth manifold structure, the dimension of which is twice the dimension of  $M$ . A 1-form  $\theta$  on  $M$  represents a section  $\theta : M \rightarrow T^*M$  of the cotangent bundle  $T^*M$ .

$P = T^*M$  is our momentum phase-space. On  $P$  there is a nondegenerate symplectic 2-form  $\omega$  is defined in local joint coordinates  $q^i, p_i \in U$ ,  $U$  open in  $P$ , as  $\omega = dq^i \wedge dp_i$  ( $\wedge$  denotes the wedge or exterior product). In that case the coordinates  $q^i, p_i \in U$  are called canonical. In a usual procedure the canonical 1-form  $\theta$  is first defined as  $\theta = p_i dq^i$ , and then the canonical 2-form  $\omega$  is defined as  $\omega = -d\theta$ .

A symplectic phase-space manifold is a pair  $(P, \omega)$ .

**Step B** Find a Hamiltonian vector-field  $X_H$  on  $(P, \omega)$ .

Let  $(P, \omega)$  be a symplectic manifold. A vector-field  $X : P \rightarrow TP$  is called Hamiltonian if there is a smooth function  $F : P \rightarrow \mathbb{R}$  such that  $i_X \omega = dF$  ( $i_X \omega$  denotes the interior product or contraction of the vector-field  $X$  and the 2-form  $\omega$ ).  $X$  is locally Hamiltonian if  $i_X \omega$  is closed.

Let the smooth real-valued Hamiltonian function  $H : P \rightarrow \mathbb{R}$ , representing the total biomechanical energy  $H(q, p) = T(p) + V(q)$  ( $T$  and  $V$  denote kinetic and potential energy of the system, respectively), be given in local canonical coordinates  $q^i, p_i \in U$ ,  $U$  open in  $P$ . The Hamiltonian vector-field  $X_H$ , condition by  $i_{X_H} \omega = dH$ , is actually defined via sym-

plectic matrix  $J$ , in a local chart  $U$ , as

$$X_H = J\nabla H = (\partial_{p_i} H, -\partial_{q^i} H), \quad J = \begin{pmatrix} 0 & I \\ -I & 0 \end{pmatrix},$$

where  $I$  denotes the  $n \times n$  identity matrix and  $\nabla$  is the gradient operator.

**Step C** Find a *Hamiltonian phase-flow*  $\phi_t$  of  $X_H$ .

Let  $(P, \omega)$  be a symplectic phase-space manifold and  $X_H = J\nabla H$  a Hamiltonian vector-field corresponding to a smooth real-valued Hamiltonian function  $H : P \rightarrow \mathbb{R}$ , on it. If a unique one-parameter group of diffeomorphisms  $\phi_t : P \rightarrow P$  exists so that  $\frac{d}{dt}|_{t=0} \phi_t x = J\nabla H(x)$ , it is called the *Hamiltonian phase-flow*.

A smooth curve  $t \mapsto (q^i(t), p_i(t))$  on  $(P, \omega)$  represents an *integral curve* of the Hamiltonian vector-field  $X_H = J\nabla H$ , if in the local canonical coordinates  $q^i, p_i \in U$ ,  $U$  open in  $P$ , *Hamilton's canonical equations* (4.10) hold.

An integral curve is said to be *maximal* if it is not a restriction of an integral curve defined on a larger interval of  $\mathbb{R}$ . It follows from the standard theorem on the *existence* and *uniqueness* of the solution of a system of ODEs with smooth r.h.s, that if the manifold  $(P, \omega)$  is Hausdorff, then for any point  $x = (q^i, p_i) \in U$ ,  $U$  open in  $P$ , there exists a maximal integral curve of  $X_H = J\nabla H$ , passing for  $t = 0$ , through point  $x$ . In case  $X_H$  is complete, i.e.,  $X_H$  is  $C^p$  and  $(P, \omega)$  is compact, the maximal integral curve of  $X_H$  is the Hamiltonian phase-flow  $\phi_t : U \rightarrow U$ .

The phase-flow  $\phi_t$  is *symplectic* if  $\omega$  is constant along  $\phi_t$ , i.e.,  $\phi_t^* \omega = \omega$  ( $\phi_t^* \omega$  denotes the *pull-back* of  $\omega$  by  $\phi_t$ ),

iff  $\mathcal{L}_{X_H} \omega = 0$

( $\mathcal{L}_{X_H} \omega$  denotes the *Lie derivative* of  $\omega$  upon  $X_H$ ).

Symplectic phase-flow  $\phi_t$  consists of canonical transformations on  $(P, \omega)$ , i.e., diffeomorphisms in canonical coordinates  $q^i, p_i \in U$ ,  $U$  open on all  $(P, \omega)$  which leave  $\omega$  invariant. In this case the *Liouville theorem* is valid:  $\phi_t$  *preserves* the *phase volume* on  $(P, \omega)$ . Also, the system's total energy  $H$  is conserved along  $\phi_t$ , i.e.,  $H \circ \phi_t = H$ .

Recall that the Riemannian metrics  $g = \langle, \rangle$  on the configuration manifold  $M$  is a positive-definite quadratic form  $g : TM \rightarrow \mathbb{R}$ , in local coordinates  $q^i \in U$ ,  $U$  open in  $M$ , given by (4.5–4.6) above. Given the metrics  $g_{ij}$ , the system's Hamiltonian function represents a momentum  $p$ -dependent quadratic form  $H : T^*M \rightarrow \mathbb{R}$  – the system's kinetic energy  $H(p) = T(p) = \frac{1}{2} \langle p, p \rangle$ , in local canonical coordinates  $q^i, p_i \in U_p$ ,  $U_p$

open in  $T^*M$ , given by

$$H(p) = \frac{1}{2} g^{ij}(q, m) p_i p_j, \quad (4.23)$$

where  $g^{ij}(q, m) = g_{ij}^{-1}(q, m)$  denotes the *inverse* (contravariant) material metric tensor

$$g^{ij}(q, m) = \sum_{\chi=1}^n m_{\chi} \delta_{rs} \frac{\partial q^i}{\partial x^r} \frac{\partial q^j}{\partial x^s}.$$

$T^*M$  is an *orientable* manifold, admitting the standard volume form

$$\Omega_{\omega_H} = \frac{(-1)^{\frac{N(N+1)}{2}}}{N!} \omega_H^N.$$

For Hamiltonian vector-field,  $X_H$  on  $M$ , there is a base integral curve  $\gamma_0(t) = (q^i(t), p_i(t))$  iff  $\gamma_0(t)$  is a *geodesic*, given by the one-form force equation

$$\dot{\tilde{p}}_i \equiv \dot{p}_i + \Gamma_{jk}^i g^{jl} g^{km} p_l p_m = 0, \quad \text{with} \quad \dot{q}^k = g^{ki} p_i, \quad (4.24)$$

where  $\Gamma_{jk}^i$  denote *Christoffel symbols* of an affine *Levi-Civita connection* on  $M$ , defined upon the *Riemannian metric*  $g = \langle, \rangle$  by (4.9).

The l.h.s  $\dot{\tilde{p}}_i$  of the covariant momentum equation (4.24) represents the *intrinsic* or *Bianchi covariant derivative* of the momentum with respect to time  $t$ . Basic relation  $\dot{\tilde{p}}_i = 0$  defines the *parallel transport* on  $T^N$ , the simplest form of humanoid dynamics. In that case Hamiltonian vector-field  $X_H$  is called the *geodesic spray* and its phase-flow is called the *geodesic flow*.

For Earthly dynamics in the gravitational *potential* field  $V : M \rightarrow \mathbb{R}$ , the Hamiltonian  $H : T^*M \rightarrow \mathbb{R}$  (4.23) extends into potential form

$$H(p, q) = \frac{1}{2} g^{ij} p_i p_j + V(q),$$

with Hamiltonian vector-field  $X_H = J \nabla H$  still defined by canonical equations (4.10).

A general form of a *driven*, non-conservative Hamilton's equations reads:

$$\dot{q}^i = \partial_{p_i} H, \quad \dot{p}_i = F_i - \partial_{q^i} H, \quad (4.25)$$

where  $F_i = F_i(t, q, p)$  represent any kind of joint-driving *covariant torques*, including active neuro-muscular-like controls, as functions of time, angles

and momenta, as well as passive dissipative and elastic joint torques. In the covariant momentum formulation (4.24), the non-conservative Hamilton's equations (4.25) become

$$\dot{p}_i \equiv \dot{p}_i + \Gamma_{jk}^i g^{jl} g^{km} p_l p_m = F_i, \quad \text{with} \quad \dot{q}^k = g^{ki} p_i.$$

#### 4.2.3 Hamilton–Poisson Geometry in Biodynamics

Now, instead of using symplectic structures arising in Hamiltonian biodynamics, we propose the more general *Poisson manifold*  $(\mathfrak{g}^*, \{F, G\})$ . Here  $\mathfrak{g}^*$  is a chosen Lie algebra with a  $(\pm)$  *Lie–Poisson bracket*  $\{F, G\}_{\pm}(\mu)$  and carries an abstract *Poisson evolution equation*  $\dot{F} = \{F, H\}$ . This approach is well-defined in both the finite- and the infinite-dimensional case. It is equivalent to the strong symplectic approach when this exists and offers a viable formulation for Poisson manifolds which are not symplectic (for technical details, see [Weinstein (1990); Abraham *et al.* (1988); Marsden and Ratiu (1999); Puta (1993); Ivancevic and Pearce (2001a)]).

Let  $E_1$  and  $E_2$  be Banach spaces. A continuous bilinear functional  $\langle, \rangle: E_1 \times E_2 \rightarrow \mathbb{R}$  is nondegenerate if  $\langle x, y \rangle = 0$  implies  $x = 0$  and  $y = 0$  for all  $x \in E_1$  and  $y \in E_2$ . We say  $E_1$  and  $E_2$  are in *duality* if there is a nondegenerate bilinear functional  $\langle, \rangle: E_1 \times E_2 \rightarrow \mathbb{R}$ . This functional is also referred to as an  $L^2$ -pairing of  $E_1$  with  $E_2$ .

Recall that a *Lie algebra* consists of a vector space  $\mathfrak{g}$  (usually a Banach space) carrying a bilinear skew-symmetric operation  $[\cdot, \cdot]: \mathfrak{g} \times \mathfrak{g} \rightarrow \mathfrak{g}$ , called the *commutator* or *Lie bracket*. This represents a pairing  $[\xi, \eta] = \xi\eta - \eta\xi$  of elements  $\xi, \eta \in \mathfrak{g}$  and satisfies *Jacobi identity*

$$[[\xi, \eta], \mu] + [[\eta, \mu], \xi] + [[\mu, \xi], \eta] = 0.$$

Let  $\mathfrak{g}$  be a (finite- or infinite-dimensional) Lie algebra and  $\mathfrak{g}^*$  its dual Lie algebra, that is, the vector space  $L^2$  paired with  $\mathfrak{g}$  via the inner product  $\langle, \rangle: \mathfrak{g}^* \times \mathfrak{g} \rightarrow \mathbb{R}$ . If  $\mathfrak{g}$  is finite-dimensional, this pairing reduces to the usual action (interior product) of forms on vectors. The standard way of describing any finite-dimensional Lie algebra  $\mathfrak{g}$  is to provide its  $n^3$  *structural constants*  $\gamma_{ij}^k$ , defined by  $[\xi_i, \xi_j] = \gamma_{ij}^k \xi_k$ , in some basis  $\xi_i$ , ( $i = 1, \dots, n$ )

For any two smooth functions  $F: \mathfrak{g}^* \rightarrow \mathbb{R}$ , we define the *Fréchet derivative*  $D$  on the space  $L(\mathfrak{g}^*, \mathbb{R})$  of all linear diffeomorphisms from  $\mathfrak{g}^*$  to  $\mathbb{R}$  as a map  $DF: \mathfrak{g}^* \rightarrow L(\mathfrak{g}^*, \mathbb{R})$ ;  $\mu \mapsto DF(\mu)$ . Further, we define the *functional*

derivative  $\delta F/\delta\mu \in \mathfrak{g}$  by

$$DF(\mu) \cdot \delta\mu = \langle \delta\mu, \frac{\delta F}{\delta\mu} \rangle$$

with arbitrary 'variations'  $\delta\mu \in \mathfrak{g}^*$ .

For any two smooth functions  $F, G : \mathfrak{g}^* \rightarrow \mathbb{R}$ , we define the  $(\pm)$  Lie-Poisson bracket by

$$\{F, G\}_{\pm}(\mu) = \pm \langle \mu, \left[ \frac{\delta F}{\delta\mu}, \frac{\delta G}{\delta\mu} \right] \rangle. \quad (3.1)$$

Here  $\mu \in \mathfrak{g}^*$ ,  $[\xi, \mu]$  is the Lie bracket in  $\mathfrak{g}$  and  $\delta F/\delta\mu, \delta G/\delta\mu \in \mathfrak{g}$  are the functional derivatives of  $F$  and  $G$ .

The  $(\pm)$  Lie-Poisson bracket (3.1) is clearly a bilinear and skew-symmetric operation. It also satisfies the Jacobi identity

$$\{\{F, G\}, H\}_{\pm}(\mu) + \{\{G, H\}, F\}_{\pm}(\mu) + \{\{H, F\}, G\}_{\pm}(\mu) = 0$$

thus confirming that  $\mathfrak{g}^*$  is a Lie algebra, as well as Leibniz' rule

$$\{FG, H\}_{\pm}(\mu) = F\{G, H\}_{\pm}(\mu) + G\{F, H\}_{\pm}(\mu). \quad (4.26)$$

If  $\mathfrak{g}$  is a finite-dimensional phase-space manifold with structure constants  $\gamma_{ij}^k$ , the  $(\pm)$  Lie-Poisson bracket (4.26) becomes

$$\{F, G\}_{\pm}(\mu) = \pm \mu_k \gamma_{ij}^k \frac{\delta F}{\delta \mu_i} \frac{\delta G}{\delta \mu_j}. \quad (4.27)$$

The  $(\pm)$  Lie-Poisson bracket represents a Lie-algebra generalization of the classical finite-dimensional Poisson bracket  $\{F, G\} = \omega(X_f, X_g)$  on the symplectic phase-space manifold  $(P, \omega)$  for any two real-valued smooth functions  $F, G : P \rightarrow \mathbb{R}$ .

As in the classical case, any two smooth functions  $F, G : \mathfrak{g}^* \rightarrow \mathbb{R}$  are in involution if  $\{F, G\}_{\pm}(\mu) = 0$ .

The Lie-Poisson theorem states that a Lie algebra  $\mathfrak{g}^*$  with a  $\pm$  Lie-Poisson bracket  $\{F, G\}_{\pm}(\mu)$  represents a Poisson manifold  $(\mathfrak{g}^*, \{F, G\}_{\pm}(\mu))$ .

Given a smooth Hamiltonian function  $H : \mathfrak{g}^* \rightarrow \mathbb{R}$  on the Poisson manifold  $(\mathfrak{g}^*, \{F, G\}_{\pm}(\mu))$ , the time evolution of any smooth function  $F : \mathfrak{g}^* \rightarrow \mathbb{R}$  is given by the abstract Poisson evolution equation

$$\dot{F} = \{F, H\}. \quad (4.28)$$

#### 4.2.3.1 Hamilton–Poisson Biodynamic Systems

Let  $(P, \{\})$  be a Poisson manifold and  $H \in C^k(P, \mathbb{R})$  a smooth real valued function on  $P$ . The vector-field  $X_H$  defined by

$$X_H(F) = \{F, H\},$$

is the Hamiltonian vector-field with energy function  $H$ . The triple  $(P, \{\}, H)$  we call the *Hamilton–Poisson biodynamic system* (HPBS) [Marsden and Ratiu (1999); Puta (1993); Ivancevic and Pearce (2001a)]. The map  $F \mapsto \{F, H\}$  is a derivation on the space  $C^k(P, \mathbb{R})$ , hence it defines a vector-field on  $P$ . The map  $F \in C^k(P, \mathbb{R}) \mapsto X_F \in \mathcal{X}(P)$  is a Lie algebra anti-homomorphism, i.e.,  $[X_F, X_g] = -X_{\{F, g\}}$ .

Let  $(P, \{\}, H)$  be a HPBS and  $\phi_t$  the flow of  $X_H$ . Then for all  $F \in C^k(P, \mathbb{R})$  we have the *conservation of energy*:

$$H \circ \phi_t = H,$$

and the *equations of motion in Poisson bracket form*,

$$\frac{d}{dt}(F \circ \phi_t) = \{F, H\} \circ \phi_t = \{F \circ \phi_t, H\},$$

that is, the above Poisson evolution equation (4.28) holds. Now, the function  $F$  is constant along the integral curves of the Hamiltonian vector-field  $X_H$  iff

$$\{F, H\} = 0.$$

$\phi_t$  preserves the Poisson structure.

Next we present two main examples of HPBS.

**‘Ball-and-Socket’ Joint Dynamics in Euler Vector Form.** The dynamics of human body-segments, classically modelled *via* Lagrangian formalism (see [Hatze (1977b); Ivancevic (1991)]), may be also prescribed by Euler’s equations of rigid body dynamics. The equations of motion for a free rigid body, described by an observer fixed on the moving body, are usually given by *Euler’s vector equation*

$$\dot{p} = p \times w. \quad (4.29)$$

Here  $p, w \in \mathbb{R}^3$ ,  $p_i = I_i w_i$  and  $I_i$  ( $i = 1, 2, 3$ ) are the principal moments of inertia, the coordinate system in the segment is chosen so that the axes are principal axes,  $w$  is the angular velocity of the body and  $p$  is the corresponding angular momentum.

The kinetic energy of the segment is the Hamiltonian function  $H : \mathbb{R}^3 \rightarrow \mathbb{R}$  given by [Ivancevic and Pearce (2001a)]

$$H(p) = \frac{1}{2} p \cdot w$$

and is a conserved quantity for (4.29).

The vector space  $\mathbb{R}^3$  is a Lie algebra with respect to the bracket operation given by the usual cross product. The space  $\mathbb{R}^3$  is paired with itself *via* the usual dot product. So if  $F : \mathbb{R}^3 \rightarrow \mathbb{R}$ , then  $\delta F / \delta p = \nabla F(p)$  and the  $(-)$  Lie–Poisson bracket  $\{F, G\}_-(p)$  is given *via* (4.27) by the triple product

$$\{F, G\}_-(p) = -p \cdot (\nabla F(p) \times \nabla G(p)).$$

Euler’s vector equation (4.29) represents a generalized Hamiltonian system in  $\mathbb{R}^3$  relative to the Hamiltonian function  $H(p)$  and the  $(-)$  Lie–Poisson bracket  $\{F, G\}_-(p)$ . Thus the Poisson manifold  $(\mathbb{R}^3, \{F, G\}_-(p))$  is defined and the abstract Poisson equation is equivalent to Euler’s equation (4.29) for a body segment and associated joint.

**Solitary Model of Muscular Contraction.** The basis of the molecular model of muscular contraction is oscillations of Amid I peptide groups with associated dipole electric momentum inside a spiral structure of myosin filament molecules (see 4.7.3 and 4.7.2 below, as well as [Davydov (1981); Davydov (1991)]).

There is a simultaneous resonant interaction and strain interaction generating a collective interaction directed along the axis of the spiral. The resonance excitation jumping from one peptide group to another can be represented as an exciton, the local molecule strain caused by the static effect of excitation as a phonon and the resultant collective interaction as a *soliton*.

The simplest model of Davydov’s solitary particle–waves is given by the *nonlinear Schrödinger equation* (named after *Nobel Laureate Erwin Schrödinger*) [Ivancevic and Pearce (2001a)]

$$i\partial_t \psi = -\partial_{x^2} \psi + 2\chi |\psi|^2 \psi \quad (4.30)$$

for  $-\infty < x < +\infty$ . Here  $\psi(x, t)$  is a smooth complex–valued wave function with initial condition  $\psi(x, t)|_{t=0} = \psi(x)$  and  $\chi$  is a nonlinear parameter. In the linear limit ( $\chi = 0$ ) (4.30) becomes the ordinary Schrödinger equation for the wave function of the free 1D particle with mass  $m = 1/2$  (see section 4.3 below).



We may define the infinite-dimensional phase-space manifold  $\mathcal{P} = \{(\psi, \bar{\psi}) \in S(\mathbb{R}, \mathbb{C})\}$ , where  $S(\mathbb{R}, \mathbb{C})$  is the Schwartz space of rapidly-decreasing complex-valued functions defined on  $\mathbb{R}$ ). We define also the algebra  $\chi(\mathcal{P})$  of observables on  $\mathcal{P}$  consisting of real-analytic functional derivatives  $\delta F/\delta\psi, \delta F/\delta\bar{\psi} \in S(\mathbb{R}, \mathbb{C})$ .

The Hamiltonian function  $H : \mathcal{P} \rightarrow \mathbb{R}$  is given by

$$H(\psi) = \int_{-\infty}^{+\infty} \left( \left| \frac{\partial \psi}{\partial x} \right|^2 + \chi |\psi|^4 \right) dx$$

and is equal to the total energy of the soliton. It is a conserved quantity for (4.3) (see [Seiler (1995)]).

The Poisson bracket on  $\chi(\mathcal{P})$  represents a direct generalization of the classical finite-dimensional Poisson bracket

$$\{F, G\}_+(\psi) = i \int_{-\infty}^{+\infty} \left( \frac{\delta F}{\delta \psi} \frac{\delta G}{\delta \bar{\psi}} - \frac{\delta F}{\delta \bar{\psi}} \frac{\delta G}{\delta \psi} \right) dx. \quad (4.31)$$

It manifestly exhibits skew-symmetry and satisfies Jacobi identity. The functionals are given by  $\delta F/\delta\psi = -i\{F, \psi\}$  and  $\delta F/\delta\bar{\psi} = i\{F, \psi\}$ . Therefore the algebra of observables  $\chi(\mathcal{P})$  represents the Lie algebra and the Poisson bracket is the (+) Lie-Poisson bracket  $\{F, G\}_+(\psi)$ .

The nonlinear Schrödinger equation (4.30) for the solitary particle-wave is a Hamiltonian system on the Lie algebra  $\chi(\mathcal{P})$  relative to the (+) Lie-Poisson bracket  $\{F, G\}_+(\psi)$  and Hamiltonian function  $H(\psi)$ . Therefore the Poisson manifold  $(\chi(\mathcal{P}), \{F, G\}_+(\psi))$  is defined and the abstract Poisson evolution equation (4.28), which holds for any smooth function  $F : \chi(\mathcal{P}) \rightarrow \mathbb{R}$ , is equivalent to equation (4.30).

A more subtle model of soliton dynamics is provided by the *Korteweg-De Vries equation* [Ivancevic and Pearce (2001a)]

$$f_t - 6ff_x + f_{xxx} = 0, \quad (f_x = \partial_x f) \quad (4.32)$$

where  $x \in \mathbb{R}$  and  $f$  is a real-valued smooth function defined on  $\mathbb{R}$  (compare with (3.39) above). This equation is related to the ordinary Schrödinger equation by the inverse scattering method [Seiler (1995); Ivancevic and Pearce (2001a)].

We may define the infinite-dimensional phase-space manifold  $\mathcal{V} = \{f \in S(\mathbb{R})\}$ , where  $S(\mathbb{R})$  is the Schwartz space of rapidly-decreasing real-valued functions  $\mathbb{R}$ . We define further  $\chi(\mathcal{V})$  to be the algebra of observables consisting of functional derivatives  $\delta F/\delta f \in S(\mathbb{R})$ .

The Hamiltonian  $H : \mathcal{V} \rightarrow \mathbb{R}$  is given by

$$H(f) = \int_{-\infty}^{+\infty} \left( f^3 + \frac{1}{2} f_x^2 \right) dx$$

and provides the total energy of the soliton. It is a conserved quantity for (4.32) (see [Seiler (1995)]).

As a real-valued analogue to (4.31), the (+) Lie-Poisson bracket on  $\chi(\mathcal{V})$  is given *via* (4.26) by

$$\{F, G\}_+(f) = \int_{-\infty}^{+\infty} \frac{\delta F}{\delta f} \frac{d}{dx} \frac{\delta G}{\delta f} dx.$$

Again it possesses skew-symmetry and satisfies Jacobi identity. The functionals are given by  $\delta F / \delta f = \{F, f\}$ .

The Korteweg-De Vries equation (KdV1), describing the behaviour of the molecular solitary particle-wave, is a Hamiltonian system on the Lie algebra  $\chi(\mathcal{V})$  relative to the (+) Lie-Poisson bracket  $\{F, G\}_+(f)$  and the Hamiltonian function  $H(f)$ . Therefore, the Poisson manifold  $(\chi(\mathcal{V}), \{F, G\}_+(f))$  is defined and the abstract Poisson evolution equation (4.28), which holds for any smooth function  $F : \chi(\mathcal{V}) \rightarrow \mathbb{R}$ , is equivalent to (4.32).

Finally, it is clear that the two solitary equations, (4.32) and (4.30), have a quantum-mechanical origin. By the use of the first quantization method, every classical biodynamic observable  $F$  is represented in the Hilbert space  $L^2(\psi)$  of square-integrable complex  $\psi$ -functions by a Hermitian (self-adjoint) linear operator  $\hat{F}$  with real eigenvalues. The classical Poisson bracket  $\{F, G\} = K$  corresponds to the *quantum commutator*  $[\hat{F}, \hat{G}] = i\hbar \hat{K}$ . Therefore the classical evolution equation (4.28) corresponds, in the *Heisenberg picture* (named after *Nobel Laureate Werner Heisenberg*), to the *quantum evolution equation* (see section (4.3.1) below)

$$i\hbar \dot{\hat{F}} = [\hat{F}, \hat{H}],$$

for any representative operator  $\hat{F}$  and quantum Hamiltonian  $\hat{H}$ . By Ehrenfest's theorem, this equation is also valid for expectation values  $\langle \cdot \rangle$  of observables, that is,

$$i\hbar \langle \dot{\hat{F}} \rangle = \langle [\hat{F}, \hat{H}] \rangle.$$

### 4.2.4 Completely Integrable Hamiltonian Systems

In order to integrate a system of  $2n$  ODEs, we must know  $2n$  first integrals. It turns out that if we are given a canonical system of ODEs, it is often sufficient to know only  $n$  first integrals [Arnold (1989)].

#### 4.2.4.1 Liouville Theorem

Recall that a function  $F$  is a first integral of a system  $\Xi$  with Hamiltonian function  $H$  iff  $H$  and  $F$  are in involution on the system's phase-space  $P$  (which is the cotangent bundle of the system's configuration manifold  $T^*M$ ), i.e., iff the Poisson bracket of  $H$  and  $F$  is identically equal to zero on  $P$ ,  $\{H, F\} \equiv 0$ .

Liouville proved that if, in a system  $\Xi$  with  $n$  DOF (i.e., with a  $2n$ D phase-space  $P = T^*M$ ),  $n$  independent first integrals in involution are known, then the system is integrable by quadratures.

Here is the exact formulation of the *Liouville theorem* [Arnold (1989)]: Suppose that we are given  $n$  functions in involution on a symplectic  $2n$ D manifold:

$$F_1, \dots, F_n; \quad \{F_i, F_j\} \equiv 0, \quad (i, j = 1, \dots, n).$$

Consider a level set of the functions  $F_i$ :

$$M_f = \{x : F_i(x) = f_i\}, \quad (i = 1, \dots, n).$$

Assume that the  $n$  functions  $F_i$  are independent on  $M_f$  (i.e., the  $n$  1-forms  $dF_i$  are linearly independent at each point of  $M_f$ ). Then

1.  $M_f$  is a smooth manifold, invariant under the phase-flow with Hamiltonian function  $H = F_1$ .

2. If the manifold  $M_f$  is compact and connected, then it is diffeomorphic to the  $n$ -torus

$$T^n = \{(\varphi^1, \dots, \varphi^n) \bmod 2\pi\}.$$

3. The phase-flow with Hamiltonian function  $H$  determines a conditionally periodic motion on  $M_f$ , i.e., in angular coordinates  $\varphi^i = (\varphi^1, \dots, \varphi^n)$  we have

$$\dot{\varphi}^i = \omega^i, \quad \omega^i = \omega^i(f_i), \quad (i = 1, \dots, n).$$

4. The canonical equations with Hamiltonian function  $H$  can be integrated by quadratures.

For the proof of this theorem see [Arnold (1989)].

As an example with 3 DOF, we consider a heavy symmetrical Lagrange top fixed at a point on its axis. Three first integrals are immediately obvious:  $H$ ,  $M_z$  and  $M_3$ . It is easy to verify that the integrals  $M_z$  and  $M_3$  are in involution. Furthermore, the manifold  $H = h$  in the phase-space is compact. Therefore, we can say without any calculations that the motion of the top is conditionally periodic: the phase trajectories fill up the 3D torus  $T^3$ , given by:  $H = c_1$ ,  $M_z = c_2$ ,  $M_3 = c_3$ . The corresponding three frequencies are called frequencies of fundamental rotation, precession, and nutation.

Other examples arise from the following observation: *if a canonical system can be integrated by the method of Hamilton-Jacobi, then it has  $n$  first integrals in involution.* The method consists of a canonical transformation  $(p_i, q^i) \rightarrow (P_i, Q^i)$  such that the  $Q^i$  are first integrals, while the functions  $Q^i$  and  $Q^i$  are in involution.

The Liouville theorem, as formulated above, covers all the problems of dynamics which have been integrated to the present day [Arnold (1989)].

#### 4.2.4.2 Action-Angle Variables

Under the hypothesis of the Liouville theorem, we can find symplectic coordinates  $(I_i, \varphi^i)$  such that the first integrals  $F_i$  depend only on  $I_i$  and  $\varphi^i$  (for  $i = 1, \dots, n$ ) are angular coordinates on the  $n$ -torus  $T^n \simeq M_f = \{x : F_i(x) = f_i\}$ , which is invariant with respect to the phase-flow. We choose angular coordinates  $\varphi^i$  on  $M_f$  so that the phase-flow with Hamiltonian function  $H = F_1$  takes an especially simple form [Arnold (1989)]:

$$\dot{\varphi}^i = \omega^i(f_i), \quad \varphi^i(t) = \varphi^i(0) + \omega^i t.$$

Now we look at a neighborhood of the  $n$ -manifold  $M_f = T^n$  in the system's  $2n$ D phase-space  $P$ .

In the coordinates  $(F_i, \varphi^i)$  the phase-flow with Hamiltonian function  $H = F_1$  can be written in the form of the simple system of  $2n$  ODEs

$$\dot{F}_i = 0, \quad \dot{\varphi}^i = \omega^i(F_i), \quad (i = 1, \dots, n), \quad (4.33)$$

which is easily integrated:  $F_i(t) = F_i(0)$ ,  $\varphi^i(t) = \varphi^i(0) + \omega^i(F_i(0))t$ .

Thus, in order to integrate explicitly the original canonical system of ODEs, it is sufficient to find the variables  $\varphi^i$  in explicit form. It turns out that this can be done using only quadratures. A construction of the variables  $\varphi^i$  is given below [Arnold (1989)].

In general, the variables  $(F_i, \varphi^i)$  are not symplectic coordinates. However, there are functions of  $F_i$ , which we denote by  $I_i = I_i(F_i)$ ,  $(i = 1, \dots, n)$ , such that the variables  $(I_i, \varphi^i)$  are symplectic coordinates: the original symplectic structure  $dp_i \wedge dq^i$  is expressed in them as  $dI_i \wedge d\varphi^i$ . The variables  $I_i$  have physical dimensions of action and are called action variables; together with the angle variables  $\varphi^i$  they form the *action-angle system of canonical coordinates* in a neighborhood of  $M_f = T^n$ .

The quantities  $I_i$  are first integrals of the system with Hamiltonian function  $H = F_1$ , since they are functions of the first integrals  $F_i$ . In turn, the variables  $F_i$  can be expressed in terms of  $I_i$  and, in particular,  $H = F_1 = H(I_i)$ . In action-angle variables, the ODEs of our flow (4.33) have the form

$$\dot{I}_i = 0, \quad \dot{\varphi}^i = \omega^i(I_i), \quad (i = 1, \dots, n).$$

A system with one DOF in the phase plane  $(p, q)$  is given by the Hamiltonian function  $H(p, q)$ . In order to construct the action-angle variables, we look for a canonical transformation  $(p, q) \rightarrow (I, \varphi)$  satisfying the two conditions:

$$I = I(h), \quad \oint_{M_h} d\varphi = 2\pi. \quad (4.34)$$

The *action variable* in the system with one DOF given by the Hamiltonian function  $H(p, q)$  is the quantity

$$I(h) = \frac{1}{2\pi} \Pi(h) = \frac{1}{2\pi} \oint_{M_h} pdq,$$

which is the area bounded by the phase curve  $H = h$  [Arnold (1989)]. Arnold states the following theorem: Set  $S(I, q) = \int_{q_0}^q pdq|_{H=h(I)}$  is a *generating function*. Then a canonical transformation  $(p, q) \rightarrow (I, \varphi)$  satisfying conditions (4.34) is given by

$$p = \frac{\partial S(I, q)}{\partial q}, \quad \varphi = \frac{\partial S(I, q)}{\partial I}, \quad H\left(\frac{\partial S(I, q)}{\partial q}, q\right) = h(I).$$

We turn now to systems with  $n$  DOF given in  $\mathbb{R}^{2n} = \{(p_i, q^i), i = 1, \dots, n\}$  by a Hamiltonian function  $H(p_i, q^i)$  and having  $n$  first integrals in involution  $F_1 = H, F_2, \dots, F_n$ . Let  $\gamma_1, \dots, \gamma_n$  be a basis for the 1D cycles on the torus  $M_f = T^n$  (the increase of the coordinate  $\varphi^i$  on the cycle  $\gamma_j$  is

equal to  $2\pi$  if  $i = j$  and 0 if  $i \neq j$ ). We set

$$I_i(f_i) = \frac{1}{2\pi} \oint_{M_h} p_i dq^i, \quad (i = 1, \dots, n). \quad (4.35)$$

The  $n$  quantities  $I_i(f_i)$  given by formula (4.35) are called the *action variables* [Arnold (1989)].

We assume now that, for the given values  $f_i$  of the  $n$  integrals  $F_i$ , the  $n$  quantities  $I_i$  are independent,  $\det(\partial I_i / \partial f_i)|_{f_i} \neq 0$ . Then in a neighborhood of the torus  $M_f = T^n$  we can take the variables  $I_i, \varphi^i$  as symplectic coordinates, i.e., the transformation  $(p_i, q^i) \rightarrow (I_i, \varphi^i)$  is canonical, or [Arnold (1989)]

$$dp_i \wedge dq^i = dI_i \wedge d\varphi^i, \quad (i = 1, \dots, n).$$

Now, let  $m$  be a point on  $M_f$ , in a neighborhood of which the  $n$  variables  $q^i$  are coordinates of  $M_f$ , such that the submanifold  $M_f \subset \mathbb{R}^{2n}$  is given by  $n$  equations of the form  $p_i = p_i(I_i, q^i)$ ,  $q^i(m) = q_0^i$ . In a simply connected neighborhood of the point  $q_0^i$  a single-valued function is defined,

$$S(I_i, q^i) = \int_{q_0}^q p_i(I_i, q^i) dq^i,$$

and we can use it as the generating function of a canonical transformation  $(p_i, q^i) \rightarrow (I_i, \varphi^i)$ :

$$p_i = \frac{\partial S}{\partial q^i}, \quad \varphi^i = \frac{\partial S}{\partial I_i}.$$

## 4.2.5 Ergodicity

### 4.2.5.1 Ergodicity in Hamiltonian Systems

The notion of *ergodicity* was introduced by Boltzman as a *property satisfied by a Hamiltonian flow on its energy manifold*. The emergence of the *Kolmogorov–Arnold–Moser (KAM) theory of quasiperiodic motions* made it clear that very few Hamiltonian systems are actually ergodic. Moreover, those systems which seem to be ergodic do not lend themselves easily to rigorous methods [Liverani and Wojtkowski (1995)].

Ergodicity is a rather weak property in the hierarchy of stochastic behavior of a dynamical system. The study of strong properties (mixing, K-property and Bernoulliness) in smooth dynamical systems began from the geodesic flows on surfaces of negative curvature. In particular, Hopf

[Hopf (1939)] invented a method of proving ergodicity, using horocycles, which turned out to be so versatile that it endured a lot of generalizations. It was developed by Anosov and Sinai [Anosov and Sinai (1982)] and applied to Anosov systems with a smooth invariant measure.

The key role in this approach is played by the hyperbolic behavior in a dynamical system. By the hyperbolic behavior we mean the property of exponential divergence of nearby orbits. In the strongest form it is present in Anosov systems and Smale systems. It leads there to a rigid topological behavior. In weaker forms it seems to be a common phenomenon.

In his pioneering work on billiard systems Sinai [Sinai (1970)] showed that already weak hyperbolic properties are sufficient to establish the strong mixing properties. Even the discontinuity of the system can be accommodated.

The Multiplicative Ergodic theorem of Oseledets [Oseledets (1968)] makes Lyapunov exponents a natural tool to describe the hyperbolic behavior of a dynamical system with a smooth invariant measure.

Pesin [Pesin (1977)] made the nonvanishing of Lyapunov exponents the starting point for the study of hyperbolic behavior. He showed that, if a diffeomorphism preserving a smooth measure has only nonvanishing Lyapunov exponents, then it has at most countably many ergodic components and (roughly speaking) on each component it has the Bernoulli property.

Pesin's work raised the question of sufficient conditions for ergodicity or, more modestly, for the openness (modulo sets of measure zero) of the ergodic components.

In his work, spanning two decades, on the system of colliding balls (gas of hard balls) Sinai developed a method of proving (local) ergodicity in discontinuous systems with nonuniform hyperbolic behavior [Sinai (1970)].

#### 4.2.5.2 *Dynamical Systems and Hyperbolicity*

Smooth ergodic theory [Barreira and Pesin (2002)] studies the ergodic properties of smooth dynamical systems on Riemannian manifolds with respect to natural invariant measures. Among these measures most important are smooth measures, i.e., measures that are equivalent to the Riemannian volume. There are various classes of smooth dynamical systems whose study requires different techniques. In this book we concentrate on systems whose trajectories are hyperbolic in some sense. Roughly speaking, this means that the behavior of trajectories near a given orbit resembles the behavior of trajectories near a saddle point. In particular, to every hyperbolic trajec-

tory one can associate two complementary subspaces such that the system acts as a contraction along one of them (called the *stable submanifold*) and as an expansion along the other (called the *unstable submanifold*).

A hyperbolic trajectory is unstable – almost every nearby trajectory moves away from it with time. If the set of hyperbolic trajectories is sufficiently large (e.g., has positive or full measure), this instability forces trajectories to become separated. If the phase-space of the system is compact, the trajectories mix together because there is not enough room to separate them. This is one of the main reasons why systems with hyperbolic trajectories on compact phase-spaces exhibit chaotic behavior. Indeed, hyperbolic theory provides a mathematical foundation for the paradigm that is widely known as *deterministic chaos* – the appearance of irregular chaotic motions in purely deterministic dynamical systems (see chapter 2). This paradigm asserts that conclusions about global properties of a nonlinear dynamical system with sufficiently strong hyperbolic behavior can be deduced from studying the linearized systems along its trajectories [Barreira and Pesin (2002)].

One of the paradigms of the theory of dynamical systems is that the local instability of trajectories influences the global behavior of the system and opens the way to the existence of stochastic behavior. Mathematically, the instability of trajectories corresponds to some degree of hyperbolicity [Barreira and Pesin (2002)].

Let  $f: M \rightarrow M$  be a diffeomorphism and  $\Lambda \subset M$  an  $f$ -invariant set, i.e., a set such that  $f^{-1}\Lambda = \Lambda$ . We say that  $\Lambda$  is a *hyperbolic set* for  $f$  if for every point  $x \in \Lambda$  there exists a decomposition of the tangent space

$$T_x M = E^s(x) \oplus E^u(x) \quad (4.36)$$

varying continuously with  $x$  that satisfies

$$d_x f E^s(x) = E^s(fx) \quad \text{and} \quad d_x f E^u(x) = E^u(fx),$$

and there exist constants  $\lambda \in (0, 1)$  and  $c > 0$  such that

$$\|d_x f^n|E^s(x)\| \leq c\lambda^n \quad \text{and} \quad \|d_x f^{-n}|E^u(x)\| \leq c\lambda^n$$

for each  $x \in \Lambda$  and  $n \in \mathbb{N}$ .

Given  $\varepsilon > 0$ , for each  $x \in M$  we consider the sets

$$V_\varepsilon^s(x) = \{y \in B(x, \varepsilon) : d(f^n y, f^n x) < \varepsilon \text{ for every } n > 0\}$$



and

$$V_\varepsilon^u(x) = \{y \in B(x, \varepsilon) : d(f^n y, f^n x) < \varepsilon \text{ for every } n < 0\},$$

where  $d$  is the distance on  $M$  and  $B(x, \varepsilon) \subset M$  is the open ball centered at  $x$  of radius  $\varepsilon$  [Barreira and Pesin (2002)].

A hyperbolic set possesses a very rich structure. The Hadamard–Perron theorem (see e.g., [Anosov (1969)]) states that if  $\Lambda$  is a compact hyperbolic set for a  $C^1$ –diffeomorphism then there exists  $\varepsilon > 0$  such that for each  $x \in \Lambda$  the sets  $V_\varepsilon^s(x)$  and  $V_\varepsilon^u(x)$  are manifolds containing  $x$  and satisfying

$$T_x V_\varepsilon^s(x) = E^s(x) \quad \text{and} \quad T_x V_\varepsilon^u(x) = E^u(x). \quad (4.37)$$

The manifolds  $V_\varepsilon^s(x)$  and  $V_\varepsilon^u(x)$  are called respectively *local stable manifold* and *local unstable manifold* at  $x$  (of size  $\varepsilon$ ). It follows from (4.36) and (4.37) that these manifolds are transverse. Furthermore, under the assumptions of the Hadamard–Perron theorem one can show that the sizes of  $V_\varepsilon^s(x)$  and  $V_\varepsilon^u(x)$  are uniformly bounded away from zero, i.e., there exists  $\gamma = \gamma(\varepsilon) > 0$  such that

$$V_\varepsilon^s(x) \supset B_\gamma^s(x) \quad \text{and} \quad V_\varepsilon^u(x) \supset B_\gamma^u(x)$$

for every point  $x \in \Lambda$ , where  $B_\gamma^s(x)$  and  $B_\gamma^u(x)$  are the open balls centered at  $x$  of radius  $\gamma$  with respect to the distances induced by  $d$  respectively on  $V_\varepsilon^s(x)$  and  $V_\varepsilon^u(x)$ . The continuous dependence of the spaces  $E^s(x)$  and  $E^u(x)$  in  $x \in \Lambda$  guarantees that there exists  $\delta = \delta(\varepsilon) > 0$  such that if  $d(x, y) < \delta$  for two given points  $x, y \in \Lambda$  then the intersection  $V_\varepsilon^s(x) \cap V_\varepsilon^u(y)$  is composed of exactly one point. We call *product structure* to the function

$$[\cdot, \cdot]: \{(x, y) \in \Lambda \times \Lambda : d(x, y) < \delta\} \rightarrow M$$

defined by  $[x, y] = V_\varepsilon^s(x) \cap V_\varepsilon^u(y)$  [Barreira and Pesin (2002)].

When the whole manifold  $M$  is a hyperbolic set for  $f$  we say that  $f$  is an *Anosov diffeomorphism*. This class of diffeomorphisms was introduced and studied by Anosov in [Anosov (1969)]. The notion of hyperbolic set was introduced by Smale in his seminal paper [Smale (1967)]. Anosov diffeomorphisms and more generally the diffeomorphisms with hyperbolic sets constitute in a certain sense the class of transformations with the ‘strongest possible’ hyperbolicity. Moreover, hyperbolicity is one of the main mechanisms responsible for the stochastic behavior in natural phenomena, even though not always with the presence of (uniformly) hyperbolic sets as defined above. These considerations justify the search for a ‘weaker’ concept

of hyperbolicity, present in a much more general class of dynamical systems that we will call *nonuniformly hyperbolic dynamical systems*. The study of these systems is much more delicate than the study of diffeomorphisms with hyperbolic sets and namely of Anosov diffeomorphisms. However, it is still possible to establish the presence of a very rich structure and in particular the existence of families of stable and unstable manifolds.

#### 4.2.5.3 Ergodic Theory and Nontrivial Recurrence

We now introduce the concept of invariant measure, which constitutes another fundamental departure point for the study of stochastic behavior. Namely, the existence of a finite invariant measure causes the existence of a *nontrivial recurrence*, that is proper of stochastic behavior.

If  $T: X \rightarrow X$  is a measurable transformation, we say that a measure  $\mu$  on  $X$  is  $T$ -invariant if

$$\mu(T^{-1}A) = \mu(A),$$

for every measurable set  $A \subset X$ . The study of transformations with invariant measures is the main theme of ergodic theory.

In order to describe rigorously the concept of nontrivial recurrence, we recall one of the basic but fundamental results of ergodic theory—the Poincaré recurrence theorem. This result states that any dynamical system preserving a finite measure exhibits a nontrivial recurrence in any set  $A$  with positive measure, in the sense that the orbit of almost every point in  $A$  returns infinitely often to  $A$ .

Poincaré Recurrence theorem states: Let  $T: X \rightarrow X$  be a measurable transformation and  $\mu$  a  $T$ -invariant finite measure on  $X$ . If  $A \subset X$  is a measurable set with positive measure then

$$\text{card}\{n \in \mathbb{N} : T^n x \in A\} = \infty,$$

for  $\mu$ -almost every point  $x \in A$  [Poincaré (1890)].

The simultaneous existence of *hyperbolicity* and *nontrivial recurrence* ensures the existence of a very rich orbit structure. Roughly speaking, the nontrivial recurrence allows us to conclude that there exist orbits that return as close to themselves as desired. On the other hand, the existence of stable and unstable manifolds at these points and their transversality guarantees the existence of transverse homoclinic points, thus causing an enormous complexity through the occurrence of Smale horseshoes. As such,

hyperbolicity and nontrivial recurrence are two of the main mechanisms responsible for the existence of stochastic behavior in natural phenomena.

#### 4.2.5.4 Nonuniformly Hyperbolic Trajectories

The concept of *nonuniform hyperbolicity* originated in the fundamental work of Pesin [Pesin (1977)], in particular with the study of smooth ergodic theory that today is clearly recognized as a fundamental step in the study of stochastic behavior.

Let  $f: M \rightarrow M$  be a diffeomorphism. The trajectory  $\{f^n x : n \in \mathbb{Z}\}$  of a point  $x \in M$  is called *nonuniformly hyperbolic* if there exist decompositions

$$T_{f^n x} M = E_{f^n x}^s \oplus E_{f^n x}^u$$

for each  $n \in \mathbb{Z}$ , a constant  $\lambda \in (0, 1)$ , and for each sufficiently small  $\varepsilon > 0$  a positive function  $C_\varepsilon$  defined on the trajectory of  $x$  such that if  $k \in \mathbb{Z}$  then:

- (1)  $C_\varepsilon(f^k x) \leq e^{\varepsilon|k|} C_\varepsilon(x)$ ;
- (2)  $d_x f^k E_x^s = E_{f^k x}^s$  and  $d_x f^k E_x^u = E_{f^k x}^u$ ;
- (3) if  $v \in E_{f^k x}^s$  and  $m > 0$  then

$$\|d_{f^k x} f^m v\| \leq C_\varepsilon(f^k x) \lambda^m e^{\varepsilon m} \|v\|;$$

- (4) if  $v \in E_{f^k x}^u$  and  $m < 0$  then

$$\|d_{f^k x} f^m v\| \leq C_\varepsilon(f^k x) \lambda^{|m|} e^{\varepsilon|m|} \|v\|;$$

- (5)  $\angle(E_{f^k x}^u, E_{f^k x}^s) \geq C_\varepsilon(f^k x)^{-1}$ .

The expression ‘nonuniform’ refers to the estimates in conditions 3. and 4. that can differ from the ‘uniform’ estimate  $\lambda^m$  by multiplicative terms that may grow along the orbit, although the exponential rate  $\varepsilon$  in 1. is small when compared to the constant  $-\log \lambda$ . It is immediate that any trajectory in a hyperbolic set is nonuniformly hyperbolic.

Among the most important properties due to nonuniform hyperbolicity is the existence of stable and unstable manifolds (with an appropriate version of Hadamard–Perron theorem), and their ‘absolute continuity’ established by Pesin [Pesin (1977)]. The theory also describes the ergodic properties of dynamical systems with an invariant measure absolutely continuous with respect to the volume. Also of importance is the Pesin entropy formula for the Kolmogorov–Sinai entropy (2.17) in terms of the Lyapunov

exponents (2.18). Combining the *nonuniform hyperbolicity* with the *non-trivial recurrence* guaranteed by the existence of a finite invariant measure, the fundamental work of Katok [Katok (1980)] revealed a very rich and complicated orbit structure.

If  $\{f^n x : n \in \mathbb{Z}\}$  is a nonuniformly hyperbolic trajectory of a  $C^{1+\alpha}$ -diffeo-morphism, for some  $\alpha > 0$ , then for each sufficiently small  $\varepsilon > 0$  there exist manifolds  $V^s(x)$  and  $V^u(x)$  containing  $x$ , and a function  $D_\varepsilon$  defined on the trajectory of  $x$  such that [Barreira (1996)]:

- (1)  $T_x V^s(x) = E_x^s$  and  $T_x V^u(x) = E_x^u$ ;
- (2)  $D_\varepsilon(f^k x) \leq e^{2\varepsilon|k|} D_\varepsilon(x)$  for each  $k \in \mathbb{Z}$ ;
- (3) If  $y \in V^s(x)$ ,  $m > 0$  and  $k \in \mathbb{Z}$  then

$$d(f^{m+k} x, f^{m+k} y) \leq D_\varepsilon(f^k x) \lambda^m e^{\varepsilon m} d(f^k x, f^k y); \quad (4.38)$$

- (4) If  $y \in V^u(x)$ ,  $m < 0$  and  $k \in \mathbb{Z}$  then

$$d(f^{m+k} x, f^{m+k} y) \leq D_\varepsilon(f^k x) \lambda^{|m|} e^{\varepsilon|m|} d(f^k x, f^k y). \quad (4.39)$$

The manifolds  $V^s(x)$  and  $V^u(x)$  are called respectively *local stable manifold* and *local unstable manifold* at  $x$ . Contrarily to what happens with hyperbolic sets, in the case of nonuniformly hyperbolic trajectories the ‘size’ of these manifolds may not be bounded from below along the orbit (although they may decrease at most with an exponentially small speed when compared to the speeds in (4.38) and (4.39). This makes their study more complicated.

#### 4.2.5.5 Systems with Nonzero Lyapunov Exponents

The concept of hyperbolicity is closely related to the study of Lyapunov exponents. These numbers measure the asymptotic exponential rates of contraction and expansion in the neighborhood of each given trajectory.

Let  $f: M \rightarrow M$  be a diffeomorphism. Given  $x \in M$  and  $v \in T_x M$ , we define the *forward Lyapunov exponent* of  $(x, v)$  by

$$\chi(x, v) = \limsup_{n \rightarrow +\infty} \frac{1}{n} \log \|d_x f^n v\|,$$

with the convention that  $\log 0 = -\infty$ . The abstract theory of Lyapunov exponents (see [Barreira and Pesin (2002)]), guarantees that for each  $x \in M$  there exist a positive integer  $s(x) \leq \dim M$ , numbers

$$\chi_1(x) < \cdots < \chi_{s(x)}(x),$$

and linear spaces

$$\{0\} = E_0(x) \subset E_1(x) \subset \cdots \subset E_{s(x)}(x) = T_x M$$

such that if  $i = 1, \dots, s(x)$  then

$$E_i(x) = \{v \in T_x M : \chi(x, v) \leq \chi_i(x)\},$$

and  $\chi(x, v) = \chi_i(x)$  whenever  $v \in E_i(x) \setminus E_{i-1}(x)$ . Considering negative time, we can also define for each  $x \in M$  and  $v \in T_x M$  the *backward Lyapunov exponent* of  $(x, v)$  by

$$\chi^-(x, v) = \limsup_{n \rightarrow -\infty} \frac{1}{|n|} \log \|d_x f^n v\|.$$

Again, the *abstract theory of Lyapunov exponents* guarantees that for each  $x \in M$  there exist a positive integer  $s^-(x) \leq \dim M$ , numbers

$$\chi_1^-(x) > \cdots > \chi_{s^-(x)}^-(x),$$

and linear spaces

$$T_x M = E_1^-(x) \supset \cdots \supset E_{s^-(x)}^-(x) \supset E_{s^-(x)+1}^-(x) = \{0\}$$

such that if  $i = 1, \dots, s^-(x)$  then

$$E_i^-(x) = \{v \in T_x M : \chi^-(x, v) \leq \chi_i^-(x)\},$$

and  $\chi^-(x, v) = \chi_i^-(x)$  whenever  $v \in E_i^-(x) \setminus E_{i+1}^-(x)$ . A priori these two structures (for positive and negative time) could be totally unrelated. The following result of Oseledets [Oseledets (1968)] shows that the two structures are indeed related, in a very strong manner, in sets of full measure with respect to any finite invariant measure.

Let  $f: M \rightarrow M$  be a  $C^1$ -diffeomorphism and  $\mu$  an  $f$ -invariant finite measure on  $M$  such that  $\log^+ \|df\|$  and  $\log^+ \|df^{-1}\|$  are  $\mu$ -integrable. Then for  $\mu$ -almost every point  $x \in \Lambda$  there exist subspaces  $H_j(x) \subset T_x M$  for  $j = 1, \dots, s(x)$  such that [Barreira and Pesin (2002)]:

(1) If  $i = 1, \dots, s(x)$  then  $E_i(x) = \bigoplus_{j=1}^i H_j(x)$  and

$$\lim_{n \rightarrow \pm\infty} \frac{1}{n} \log \|d_x f^n v\| = \chi_i(x),$$

with uniform convergence for  $v$  on  $\{v \in H_i(x) : \|v\| = 1\}$ ;

(2) If  $i \neq j$  then

$$\lim_{n \rightarrow \pm\infty} \frac{1}{n} \log |\angle(H_i(f^n x), H_j(f^n x))| = 0.$$

We note that if  $M$  is a compact manifold then the functions  $\log^+ \|df\|$  and  $\log^+ \|df^{-1}\|$  are  $\mu$ -integrable for any finite measure  $\mu$  on  $M$ . This statement also holds in the more general case of cocycles over a measurable transformation.

Let  $f: M \rightarrow M$  be a  $C^1$ -diffeomorphism on a compact manifold and  $\mu$  an  $f$ -invariant finite Borel measure on  $M$ . We say that  $f$  is *nonuniformly hyperbolic* with respect to  $\mu$  if the set  $\Lambda \subset M$  of points whose trajectories are nonuniformly hyperbolic has measure  $\mu(\Lambda) > 0$ . In this case the constants  $\lambda$  and  $\varepsilon$  in the definition of nonuniformly hyperbolic trajectory are replaced by measurable functions  $\lambda(x)$  and  $\varepsilon(x)$ .

It follows from the previous statement that the following conditions are equivalent:

- (1)  $f$  is nonuniformly hyperbolic with respect to the measure  $\mu$ ;
- (2)  $\chi(x, v) \neq 0$  for each  $v \in T_x M$  and each  $x$  in a set with  $\mu$ -positive measure.

Therefore, the nonuniformly hyperbolic diffeomorphisms with respect to a given measure are precisely the diffeomorphisms with all Lyapunov exponents nonzero in a set of positive measure.

One of the standing problems of the theory of nonuniformly hyperbolic dynamical systems is to understand how 'common' this class is. Let  $M$  be a compact smooth Riemannian manifold. It was established by Katok in [Katok (1980)] when  $\dim M = 2$  and by Dolgopyat and Pesin in [Dolgopyat and Pesin (2002)] when  $\dim M \geq 3$  that there exists a  $C^k$  diffeomorphism  $f$  such that:

- (1)  $f$  preserves the Riemannian volume  $m$  on  $M$ ;
- (2)  $f$  has nonzero Lyapunov exponents at  $m$ -almost every point  $x \in M$ ;
- (3)  $f$  is a Bernoulli diffeomorphism.

For any compact smooth Riemannian manifold  $M$  of dimension at least 5, Brin constructed in [Brin (1981)] a  $C^k$  Bernoulli diffeomorphism which preserves the Riemannian volume and has all but one Lyapunov exponent nonzero. On the other hand, the construction of the above diffeomorphisms is not robust.

### 4.3 Quantum Formalism in Nano-Biodynamics

In this section we present quantum formalism, as is used in modern nano-biodynamics. Recall that biodynamics operates on four different biophysical levels of organization:

- (1) Level of a whole neuro-musculo-skeletal system;
- (2) Level of a single muscle, or a single neural network;
- (3) Level of a single muscle-fibre, or a single neuron, as a structural unit;
- (4) Nano-biodynamics: molecular muscular and neural level.

All the macroscopic levels (1–3) of biodynamic organization are governed by *classical biodynamics*. The molecular muscular and neural level (4) is governed by *quantum biodynamics*. In this section we present a minimum material necessary for later understanding the variety of quantum biodynamic phenomena, mainly associated with muscular proteins (this chapter) and neural microtubules (chapter 7). For the necessary mathematical background on Hilbert-space formalism, see Appendix.

#### 4.3.1 Quantum Mechanics in Biological Matter

Energy transfer across the cells, without dissipation, had been first conjectured to occur in biological matter by Fröhlich [Fröhlich and Kremer (1983)]. The phenomenon conjectured by Fröhlich was based on his 1D superconductivity model: in one dimensional electron systems with holes, the formation of solitonic structures due to electron-hole pairing results in the transfer of electric current without dissipation. In a similar manner, Fröhlich conjectured that energy in biological matter could be transferred without dissipation, if appropriate solitonic structures are formed inside the cells. This idea has lead theorists to construct various models for the energy transfer across the cell, based on the formation of kink classical solutions. In the early works no specific microscopic models had been considered. However, after the identification of microtubules (MT) as one of the most important structures of the cell, both functionally and structurally, a model for their dynamics has been presented in [Satarić *et al.* (1993); Satarić *et al.* (1998)], in which the formation of solitonic structures, and their role in energy transfer across the MT, is discussed in terms of classical physics. Later, in the work of Ellis *et al.* [Ellis *et al.* (1992); Ellis *et al.* (1999); Mavromatos and Nanopoulos (1995a); Mavromatos and Nanopoulos (1995b); Nanopoulos (1995)], the kink-soliton model for energy

transfer across the MT, obtained the proper, quantum-mechanical form.

On the other hand, quantum solitons have been used in Davydov's school of quantum biophysics [Davydov (1981); Davydov (1991)] to represent neural and muscular action potentials (see (musolit) above), where the simplest model of solitary particle-waves was given by the *nonlinear Schrödinger equation*.

### 4.3.2 Dirac's Canonical Quantization

The most important discoveries in natural sciences are in some or other way connected to quantum mechanics. There is also a bias that biological phenomena will be explained by quantum theory in the future, since quantum theory already contains all basic principles of particle interactions and these principles had success in molecular dynamics, the basis of life. Recall that a little book entitled *What is Life?*, written by E. Schrödinger, represents one of the great science classics of the twentieth century. A distinguished physicist's exploration of the question which lies at the heart of biology, it was written for the layman, but proved one of the spurs to the birth of molecular biology and the subsequent discovery of the structure of DNA, by Schrödinger's student, physicist (and another Noble Laureate), F. Crick.

To make a leap into the quantum realm, recall that classical state-space for the biodynamic system of  $n$  point-particles is its  $6ND$  phase-space  $\mathcal{P}$ , including all position and momentum vectors,  $\mathbf{r}_i = (x, y, z)_i$  and  $\mathbf{p}_i = (p_x, p_y, p_z)_i$ , respectively, for  $i = 1, \dots, n$ .

The *quantization* is performed as a *linear representation* of the real Lie algebra  $\mathcal{L}_P$  of the phase-space  $\mathcal{P}$ , defined by the Poisson bracket  $\{f, g\}$  of classical variables  $f, g$  – into the corresponding real Lie algebra  $\mathcal{L}_H$  of the Hilbert space  $\mathcal{H}$ , defined by the commutator  $[\hat{f}, \hat{g}]$  of skew-Hermitian operators  $\hat{f}, \hat{g}$ . This sounds like a functor, however it is not; as J. Baez says, 'First quantization is a mystery, but second quantization is a functor'. Mathematically, if quantization were *natural* it would be a functor from the category **Symplec**, whose objects are symplectic manifolds (i.e., phase-spaces) and whose morphisms are symplectic maps (i.e., canonical transformations) to the category **Hilbert**, whose objects are Hilbert spaces and whose morphisms are unitary operators.

Historically first, the so-called *canonical quantization* is based on the so-called *Dirac rules for quantization*. It is applied to 'simple' systems: finite number of degrees of freedom and 'flat' classical phase-spaces (an open set of  $\mathbb{R}^{2n}$ ). Canonical quantization includes the following data (see



e.g., [Dirac (1930)]):

- (1) *Classical description.* The system is described by the *Hamiltonian* or *canonical formalism*: its classical phase-space is locally coordinated by a set of *canonical coordinates*  $(q^j, p_j)$ , the *position* and *momentum* coordinates. Classical observables are real functions  $f(q^j, p_j)$ . Eventually, a Lie group  $G$  of symmetries acts on the system.
- (2) *Quantum description.* The quantum phase-space is a complex Hilbert space  $\mathcal{H}$ . Quantum observables are Hermitian (i.e., self-adjoint) operators acting on  $\mathcal{H}$ . (The Hilbert space is complex in order to take into account the interference phenomena of wave functions representing the quantum states. The operators are self-adjoint in order to assure their eigenvalues are real.) The symmetries of the system are realized by a group of unitary operators  $U_G(\mathcal{H})$ .
- (3) *Quantization method.* As a Hilbert space we take the space of square integrable complex functions of the configuration space; that is, functions depending only on the position coordinates,  $\psi(q^j)$ . The quantum operator associated with  $f(q^j, p_j)$  is obtained by replacing  $p_j$  by  $-i\hbar \frac{\partial}{\partial q^j}$ , and hence we have the correspondence  $f(q^j, p_j) \mapsto \hat{f}(q^j, -i\hbar \frac{\partial}{\partial q^j})$ . In this way, the classical commutation rules between the canonical coordinates are assured to have a quantum counterpart: the commutation rules between the quantum operators of position and momentum (which are related to the ‘uncertainty principle’ of quantum mechanics).

#### 4.3.2.1 Quantum States and Operators

Quantum systems have two modes of evolution in time. The first, governed by standard, *time-dependent Schrödinger equation*:

$$i\hbar \partial_t |\psi\rangle = \hat{H} |\psi\rangle, \quad (4.40)$$

(where  $\hat{H}$  is the *Hamiltonian energy operator* (in general,  $\hat{f}$  is a *Hermitian operator* obtained from the classical variable  $f$ ),  $i = \sqrt{-1}$  (imaginary unit), and  $\hbar$  is Planck’s constant divided by  $2\pi$  ( $\equiv 1$  in natural units)), describes the time evolution of quantum systems when they are undisturbed by measurements. ‘Measurements’ are defined as *interactions* of the quantum system with its classical environment. As long as the system is sufficiently isolated from the environment, it follows Schrödinger equation. If an interaction with the environment takes place, i.e., a measurement is performed, the system abruptly *decoheres* i.e., collapses or reduces to one of

its classically allowed states.

A *time-dependent state of a quantum system* is determined by a normalized, complex, *wave psi-function*  $\psi = \psi(t)$ . In Dirac's words, this is a unit *ket* vector  $|\psi\rangle$ , which is an element of the *Hilbert space*  $L^2(\psi)$  with a coordinate basis  $(q^i)$ . The state ket-vector  $|\psi(t)\rangle$  is subject to action of the Hermitian operators, obtained by the procedure of *quantization* of classical biodynamic quantities, and whose real eigenvalues are being measured.

*Quantum superposition* is a generalization of the algebraic principle of linear combination of vectors. The Hilbert space has a set of states  $|\varphi_i\rangle$  (where the index  $i$  runs over the degrees of freedom of the system) that form a basis and the most general state of such a system can be written as  $|\psi\rangle = \sum_i c_i |\varphi_i\rangle$ . The system is said to be in a state  $|\psi(t)\rangle$ , describing the motion of the *de Broglie waves* (named after *Nobel Laureate, Prince Louis V.P.R. de Broglie*), which is a linear superposition of the basis states  $|\varphi_i\rangle$  with weighting coefficients  $c_i$  that can in general be complex. At the microscopic or quantum level, the state of the system is described by the wave function  $|\psi\rangle$ , which in general appears as a linear superposition of all basis states. This can be interpreted as the system being in all these states at once. The coefficients  $c_i$  are called the *probability amplitudes* and  $|c_i|^2$  gives the probability that  $|\psi\rangle$  will collapse into state  $|\varphi\rangle$  when it decoheres (interacts with the environment). By simple normalization we have the constraint that  $\sum_i |c_i|^2 = 1$ . This emphasizes the fact that the wavefunction describes a *real, physical system*, which must be in one of its allowable classical states and therefore by summing over all the possibilities, weighted by their corresponding probabilities, one must obtain unity. In other words, we have the *normalization condition* for the psi-function, determining the unit length of the state ket-vector

$$\langle\psi(t)|\psi(t)\rangle = \int \psi^* \psi \, dV = \int |\psi|^2 \, dV = 1,$$

where  $\psi^* = \langle\psi(t)|$  denotes the *bra* vector, the complex-conjugate to the ket  $\psi = |\psi(t)\rangle$ , and  $\langle\psi(t)|\psi(t)\rangle$  is their scalar product, i.e., Dirac *bracket*. For this reason the scene of quantum mechanics is the functional space of square-integrable complex psi-functions, i.e., the Hilbert space  $L^2(\psi)$ .

When the system is in the state  $|\psi(t)\rangle$ , the average value  $\langle f \rangle$  of any physical observable  $f$  is equal to

$$\langle f \rangle = \langle\psi(t)| \hat{f} |\psi(t)\rangle,$$

where  $\hat{f}$  is the Hermitian operator corresponding to  $f$ .

A quantum system is *coherent* if it is in a linear superposition of its basis states. If a measurement is performed on the system and this means that the system must somehow interact with its environment, the superposition is destroyed and the system is observed to be in only one basis state, as required classically. This process is called *reduction* or *collapse* of the wavefunction or simply *decoherence* and is governed by the form of the wavefunction  $|\psi\rangle$ .

*Entanglement* on the other hand, is a purely quantum phenomenon and has no classical analogue. It accounts for the ability of quantum systems to exhibit correlations in counterintuitive ‘action-at-a-distance’ ways. Entanglement is what makes all the difference in the operation of quantum computers versus classical ones. Entanglement gives ‘special powers’ to quantum computers because it gives quantum states the potential to exhibit and maintain correlations that cannot be accounted for classically. Correlations between bits are what make information encoding possible in classical computers. For instance, we can require two bits to have the same value thus encoding a relationship. If we are to subsequently change the encoded information, we must change the correlated bits in tandem by explicitly accessing each bit. Since quantum bits exist as superpositions, *correlations* between them also exist in superposition. When the superposition is destroyed (e.g., one qubit is measured), the correct correlations are *instantaneously* ‘communicated’ between the qubits and this communication allows *many qubits* to be accessed *at once*, preserving their correlations, something that is absolutely impossible classically.

More precisely, the *first quantization* is a *linear representation* of all classical dynamical variables (like coordinate, momentum, energy, or angular momentum) by linear *Hermitian* operators acting on the associated Hilbert state-space  $L^2(\psi)$ , which has the following properties (see e.g., [Dirac (1930)]):

(1) Linearity:

$$\alpha f + \beta g \rightarrow \alpha \hat{f} + \beta \hat{g},$$

for all constants  $\alpha, \beta \in \mathbb{C}$ ;

- (2) A ‘dynamical’ variable, equal to unity everywhere in the phase-space, corresponds to unit operator:  $1 \rightarrow \hat{I}$ ; and  
 (3) *Classical Poisson brackets*

$$\{f, g\} = \frac{\partial f}{\partial q^i} \frac{\partial g}{\partial p_i} - \frac{\partial f}{\partial p_i} \frac{\partial g}{\partial q^i}$$

quantize to the corresponding commutators

$$\{f, g\} \rightarrow -i\hbar[\hat{f}, \hat{g}], \quad [\hat{f}, \hat{g}] = \hat{f}\hat{g} - \hat{g}\hat{f}.$$

Like Poisson bracket, commutator is bilinear and skew-symmetric operation, satisfying Jacobi identity. For Hermitian operators  $\hat{f}, \hat{g}$  their commutator  $[\hat{f}, \hat{g}]$  is anti-Hermitian; for this reason  $i$  is required in  $\{f, g\} \rightarrow -i\hbar[\hat{f}, \hat{g}]$ .

Property (2) is introduced for the following reason. In Hamiltonian mechanics each dynamical variable  $f$  generates some transformations in the phase-space via Poisson brackets. In quantum mechanics it generates transformations in the state-space by direct application to a state, i.e.,

$$\dot{u} = \{u, f\}, \quad \partial_t |\psi\rangle = \frac{i}{\hbar} \hat{f} |\psi\rangle. \quad (4.41)$$

Exponent of anti-Hermitian operator is unitary. Due to this fact, transformations, generated by Hermitian operators

$$\hat{U} = \exp \frac{i\hat{f}t}{\hbar},$$

are unitary. They are *motions* – scalar product preserving transformations in the Hilbert state-space  $L^2(\psi)$ . For this property  $i$  is needed in (4.41).

Due to property (2), the transformations, generated by classical variables and quantum operators, have the same algebra.

For example, the quantization of energy  $E$  gives:

$$E \rightarrow \hat{E} = i\hbar \partial_t.$$

The relations between operators must be similar to the relations between the relevant physical quantities observed in classical mechanics.

For example, the quantization of the classical equation  $E = H$ , where

$$H = H(p_i, q^i) = T + U$$

denotes the Hamilton's function of the total system energy (the sum of the kinetic energy  $T$  and potential energy  $U$ ), gives the Schrödinger equation of motion of the state ket-vector  $|\psi(t)\rangle$  in the Hilbert state-space  $L^2(\psi)$

$$i\hbar \partial_t |\psi(t)\rangle = \hat{H} |\psi(t)\rangle.$$

In the simplest case of a single particle in the potential field  $U$ , the operator of the total system energy – Hamiltonian is given by:

$$\hat{H} = -\frac{\hbar^2}{2m}\nabla^2 + U,$$

where  $m$  denotes the mass of the particle and  $\nabla$  is the classical gradient operator. So the first term on the r.h.s denotes the kinetic energy of the system, and therefore the momentum operator must be given by:

$$\hat{p} = -i\hbar\nabla.$$

Now, for each pair of states  $|\varphi\rangle, |\psi\rangle$  their scalar product  $\langle\varphi|\psi\rangle$  is introduced, which is [Nikitin (1995)]:

(1) Linear (for right multiplier):

$$\langle\varphi|\alpha_1\psi_1 + \alpha_2\psi_2\rangle = \alpha_1\langle\varphi|\psi_1\rangle + \alpha_2\langle\varphi|\psi_2\rangle;$$

(2) In transposition transforms to complex conjugated:

$$\langle\varphi|\psi\rangle = \overline{\langle\psi|\varphi\rangle};$$

this implies that it is ‘anti-linear’ for left multiplier:

$$\langle\alpha_1\varphi_1 + \alpha_2\varphi_2|\psi\rangle = \bar{\alpha}_1\langle\varphi_1|\psi\rangle + \bar{\alpha}_2\langle\varphi_2|\psi\rangle;$$

(3) Additionally it is often required, that the scalar product should be positively defined:

$$\text{for all } |\psi\rangle, \quad \langle\psi|\psi\rangle \geq 0 \quad \text{and} \quad \langle\psi|\psi\rangle = 0 \quad \text{iff} \quad |\psi\rangle = 0.$$

Complex conjugation of classical variables is represented as Hermitian conjugation of operators. We remind some definitions (see Appendix for details):

– two operators  $\hat{f}, \hat{f}^+$  are called Hermitian conjugated (or adjoint); if

$$\langle\varphi|\hat{f}\psi\rangle = \langle\hat{f}^+\varphi|\psi\rangle \quad \text{for all } \varphi, \psi.$$

This scalar product is also denoted by  $\langle\varphi|\hat{f}|\psi\rangle$  and called a matrix element of an operator.

– operator is Hermitian (self-adjoint) if  $\hat{f}^+ = \hat{f}$  and anti-Hermitian if  $\hat{f}^+ = -\hat{f}$ ;

– operator is unitary, if  $\hat{U}^+ = \hat{U}^{-1}$ ; such operators preserve the scalar product:

$$\langle \hat{U}\varphi | \hat{U}\psi \rangle = \langle \varphi | \hat{U}^+ \hat{U} | \psi \rangle = \langle \varphi | \psi \rangle.$$

Real classical variables should be represented by Hermitian operators; complex conjugated classical variables ( $a, \bar{a}$ ) correspond to Hermitian conjugated operators ( $\hat{a}, \hat{a}^+$ ).

Multiplication of a state by complex numbers does not change the state physically.

Any Hermitian operator in Hilbert space has only real eigenvalues:

$$\hat{f}|\psi_i\rangle = f_i|\psi_i\rangle, \quad f_i \in \mathbb{R}.$$

Eigenvectors  $|\psi_i\rangle$  form complete orthonormal basis (eigenvectors with different eigenvalues are automatically orthogonal; in the case of multiple eigenvalues one can form orthogonal combinations; then they can be normalized).

If the two operators  $\hat{f}$  and  $\hat{g}$  commute, i.e.,  $[\hat{f}, \hat{g}] = 0$  (see Heisenberg picture below), then the corresponding quantities can simultaneously have definite values. If the two operators do not commute, i.e.,  $[\hat{f}, \hat{g}] \neq 0$ , the quantities corresponding to these operators cannot have definite values simultaneously, i.e., the general *Heisenberg's uncertainty relation* is valid:

$$(\Delta\hat{f})^2 \cdot (\Delta\hat{g})^2 \geq \frac{\hbar}{4} [\hat{f}, \hat{g}]^2,$$

where  $\Delta$  denotes the deviation of an individual measurement from the mean value of the distribution. The well-known particular cases are ordinary uncertainty relations for coordinate–momentum ( $q - p$ ), and energy–time ( $E - t$ ):

$$\Delta q \cdot \Delta p_q \geq \frac{\hbar}{2}, \quad \text{and} \quad \Delta E \cdot \Delta t \geq \frac{\hbar}{2}.$$

For example, the rules of commutation, analogous to the classical ones written by the Poisson's brackets, are postulated for canonically–conjugate coordinate and momentum operators:

$$[\hat{q}^i, \hat{q}^j] = 0, \quad [\hat{p}_i, \hat{p}_j] = 0, \quad [\hat{q}^i, \hat{p}_j] = i\hbar\delta_j^i \hat{I},$$

where  $\delta_j^i$  is the Kronecker's symbol. By applying the commutation rules to the system Hamiltonian  $\hat{H} = \hat{H}(\hat{p}_i, \hat{q}^i)$ , the *quantum Hamilton's equations*

are obtained:

$$\frac{d(\hat{p}_i)}{dt} = -\frac{\partial \hat{H}}{\partial \hat{q}^i}, \quad \text{and} \quad \frac{d(\hat{q}^i)}{dt} = \frac{\partial \hat{H}}{\partial \hat{p}_i}.$$

A quantum state can be observed either in the *coordinate q-representation*, or in the *momentum p-representation*. In the *q-representation*, operators of coordinate and momentum have respective forms:  $\hat{q} = q$ , and  $\hat{p}_q = -i\hbar \frac{\partial}{\partial q}$ , while in the *p-representation*, they have respective forms:  $\hat{q} = i\hbar \frac{\partial}{\partial p_q}$ , and  $\hat{p}_q = p_q$ . The forms of the state vector  $|\psi(t)\rangle$  in these two representations are mathematically related by a *Fourier-transform pair* (within the Planck constant).

#### 4.3.2.2 Quantum Pictures

In the *q-representation* the quantum state is usually determined, i.e., the first quantization is performed, in one of the three *quantum pictures* (see e.g., [Dirac (1930)]):

- (1) *Schrödinger picture*,
- (2) *Heisenberg picture*, and
- (3) *Dirac interaction picture*.

These three pictures mutually differ in the time-dependence, i.e., time-evolution of the state vector  $|\psi(t)\rangle$  and the Hilbert coordinate basis  $(q^i)$  together with the system operators.

1. In the *Schrödinger (S) picture*, under the action of the *evolution operator*  $\hat{S}(t)$  the state-vector  $|\psi(t)\rangle$  rotates:

$$|\psi(t)\rangle = \hat{S}(t) |\psi(0)\rangle,$$

and the coordinate basis  $(q^i)$  is fixed, so the operators are constant in time:

$$\hat{F}(t) = \hat{F}(0) = \hat{F},$$

and the system evolution is determined by the Schrödinger wave equation:

$$i\hbar \partial_t |\psi^S(t)\rangle = \hat{H}^S |\psi^S(t)\rangle.$$

If the Hamiltonian does not explicitly depend on time,  $\hat{H}(t) = \hat{H}$ , which is the case with the absence of variables of macroscopic fields, the state vector

$|\psi(t)\rangle$  can be presented in the form:

$$|\psi(t)\rangle = \exp(-i\frac{E}{\hbar}t) |\psi\rangle,$$

satisfying the time-independent Schrödinger equation

$$\hat{H} |\psi\rangle = E |\psi\rangle,$$

which gives the eigenvalues  $E_m$  and eigenfunctions  $|\psi_m\rangle$  of the Hamiltonian  $\hat{H}$ .

2. In the *Heisenberg (H) picture*, under the action of the evolution operator  $\hat{S}(t)$ , the coordinate basis ( $q^i$ ) rotates, so the operators of physical variables evolve in time by the similarity transformation:

$$\hat{F}(t) = \hat{S}^{-1}(t) \hat{F}(0) \hat{S}(t),$$

while the state vector  $|\psi(t)\rangle$  is constant in time:

$$|\psi(t)\rangle = |\psi(0)\rangle = |\psi\rangle,$$

and the system evolution is determined by the *Heisenberg equation of motion*:

$$i\hbar \partial_t \hat{F}^H(t) = [\hat{F}^H(t), \hat{H}^H(t)],$$

where  $\hat{F}(t)$  denotes arbitrary Hermitian operator of the system, while the commutator, i.e., Poisson quantum bracket, is given by:

$$[\hat{F}(t), \hat{H}(t)] = \hat{F}(t) \hat{H}(t) - \hat{H}(t) \hat{F}(t) = iK.$$

In both Schrödinger and Heisenberg picture the evolution operator  $\hat{S}(t)$  itself is determined by the Schrödinger-like equation:

$$i\hbar \partial_t \hat{S}(t) = \hat{H} \hat{S}(t),$$

with the initial condition  $\hat{S}(0) = \hat{I}$ . It determines the Lie group of transformations of the Hilbert space  $L^2(\psi)$  in itself, the Hamiltonian of the system being the generator of the group.

3. In the *Dirac interaction (I) picture* both the state vector  $|\psi(t)\rangle$  and coordinate basis ( $q^i$ ) rotate; therefore the system evolution is determined by both the Schrödinger wave equation and the Heisenberg equation of motion:

$$i\hbar \partial_t |\psi^I(t)\rangle = \hat{H}^I |\psi^I(t)\rangle, \quad \text{and} \quad i\hbar \partial_t \hat{F}^I(t) = [\hat{F}^I(t), \hat{H}^O(t)].$$



Here:  $\hat{H} = \hat{H}^0 + \hat{H}^I$ , where  $\hat{H}^0$  corresponds to the Hamiltonian of the free fields and  $\hat{H}^I$  corresponds to the Hamiltonian of the interaction.

Finally, we can show that the stationary Schrödinger equation

$$\hat{H}\psi = \hat{E}\psi$$

can be obtained from the condition for the minimum of the *quantum action*:

$$\delta S = 0.$$

The quantum action is usually defined by the integral:

$$S = \langle \psi(t) | \hat{H} | \psi(t) \rangle = \int \psi^* \hat{H} \psi \, dV,$$

with the additional normalization condition for the unit-probability of the psi-function:

$$\langle \psi(t) | \psi(t) \rangle = \int \psi^* \psi \, dV = 1.$$

When the functions  $\psi$  and  $\psi^*$  are considered to be formally independent and only one of them, say  $\psi^*$  is varied, we can write the condition for an extreme of the action:

$$\delta S = \int \delta \psi^* \hat{H} \psi \, dV - E \int \delta \psi^* \psi \, dV = \int \delta \psi^* (\hat{H} \psi - E \psi) \, dV = 0,$$

where  $E$  is a Lagrangian multiplier. Owing to the arbitrariness of  $\delta \psi^*$ , the Schrödinger equation  $\hat{H}\psi - \hat{E}\psi = 0$  must hold.

#### 4.3.2.3 Spectrum of a Quantum Operator

To recapitulate, each *state* of a system is represented by a *state vector*  $|\psi\rangle$  with a unit-norm,  $\langle \psi | \psi \rangle = 1$ , in a complex Hilbert space  $\mathcal{H}$ , and vice versa. Each system *observable* is represented by a Hermitian operator  $\hat{A}$  in a Hilbert space  $\mathcal{H}$ , and vice versa. A Hermitian operator  $\hat{A}$  in a Hilbert space  $\mathcal{H}$  has its domain  $\mathcal{D}_{\hat{A}} \subset \mathcal{H}$  which must be dense in  $\mathcal{H}$ , and for any two state vectors  $|\psi\rangle, |\varphi\rangle \in \mathcal{D}_{\hat{A}}$  holds  $\langle \hat{A}\psi | \varphi \rangle = \langle \psi | \hat{A}\varphi \rangle$  (see e.g., [Messiah (2000)], as well as Appendix).

**Discrete Spectrum.** A Hermitian operator  $\hat{A}$  in a *finite-dimensional Hilbert space*  $\mathcal{H}_d$  has a *discrete spectrum*  $\{a_i, a \in \mathbb{R}, i \in \mathbb{N}\}$ , defined as a set of *discrete eigenvalues*  $a_i$ , for which the *characteristic equation*

$$\hat{A}|\psi\rangle = a|\psi\rangle \quad (4.42)$$

has the solution eigenvectors  $|\psi_a\rangle \neq 0 \in \mathcal{D}_{\hat{A}} \subset \mathcal{H}_d$ . For each particular eigenvalue  $a$  of a Hermitian operator  $\hat{A}$  there is a corresponding *discrete characteristic projector*  $\hat{\pi}_a = |\psi_a\rangle \langle \psi_a|$  (i.e., the projector to the eigensubspace of  $\hat{A}$  composed of all discrete eigenvectors  $|\psi_a\rangle$  corresponding to  $a$ ).

Now, the *discrete spectral form* of a Hermitian operator  $\hat{A}$  is defined as

$$\hat{A} = a_i \hat{\pi}_i = \sum_i a_i |i\rangle \langle i|, \quad \text{for all } i \in \mathbb{N} \quad (4.43)$$

where  $a_i$  are different eigenvalues and  $\hat{\pi}_i$  are the corresponding projectors subject to

$$\sum_i \hat{\pi}_i = \hat{I}, \quad \hat{\pi}_i \hat{\pi}_j = \delta_{ij} \hat{\pi}_j,$$

where  $\hat{I}$  is identity operator in  $\mathcal{H}_d$ .

A Hermitian operator  $\hat{A}$  defines, with its characteristic projectors  $\hat{\pi}_i$ , the *spectral measure* of any interval on the real axis  $\mathbb{R}$ ; for example, for a closed interval  $[a, b] \subset \mathbb{R}$  holds

$$\hat{\pi}_{[a,b]}(\hat{A}) = \sum_{a_i \in [a,b]} \hat{\pi}_i, \quad (4.44)$$

and analogously for other intervals,  $(a, b]$ ,  $[a, b)$ ,  $(a, b) \subset \mathbb{R}$ ; if  $a_i \in [a, b] = \emptyset$  then  $\hat{\pi}_{[a,b]}(\hat{A}) = 0$ , by definition.

Now, let us suppose that we measure an observable  $\hat{A}$  of a system in state  $|\psi\rangle$ . The *probability*  $P$  to obtain a result within the a priori given interval  $[a, b] \subset \mathbb{R}$  is given by its spectral measure

$$P([a, b], \hat{A}, \psi) = \langle \psi | \hat{\pi}_{[a,b]}(\hat{A}) | \psi \rangle. \quad (4.45)$$

As a consequence, the probability to obtain a discrete eigenvalue  $a_i$  as a result of measurement of an observable  $\hat{A}$  equals its *expected value*

$$P(a_i, \hat{A}, \psi) = \langle \psi | \hat{\pi}_i | \psi \rangle = \langle \hat{\pi}_i \rangle,$$

where  $\langle \hat{B} \rangle$  in general denotes the average value of an operator  $\hat{B}$ . Also, the probability to obtain a result  $a$  which is not a discrete eigenvalue of an observable  $\hat{A}$  in a state  $|\psi\rangle$  equals zero.

**Continuous Spectrum.** A Hermitian operator  $\hat{A}$  in an *infinite-dimensional Hilbert space*  $\mathcal{H}_c$  (the so-called *rigged Hilbert space*) has both a discrete spectrum  $\{a_i, a \in \mathbb{R}, i \in \mathbb{N}\}$  and a *continuous spectrum*  $[c, d] \subset \mathbb{R}$ .

In other words,  $\hat{A}$  has both a discrete sub-basis  $\{|i\rangle : i \in \mathbb{N}\}$  and a continuous sub-basis  $\{|s\rangle : s \in [c, d] \subset \mathbb{R}\}$ . In this case  $s$  is called the *continuous eigenvalue* of  $\hat{A}$ . The corresponding characteristic equation is

$$\hat{A}|\psi\rangle = s|\psi\rangle. \quad (4.46)$$

Equation (4.46) has the solution eigenvectors  $|\psi_s\rangle \neq 0 \in \mathcal{D}_{\hat{A}} \subset \mathcal{H}_c$ , given by the *Lebesgue integral*

$$|\psi_s\rangle = \int_a^b \psi(s) |s\rangle ds, \quad c \leq a < b \leq d,$$

where  $\psi(s) = \langle s|\psi\rangle$  are continuous, *square integrable Fourier coefficients*,

$$\int_a^b |\psi(s)|^2 ds < +\infty,$$

while the continuous eigenvectors  $|\psi_s\rangle$  are orthonormal,

$$\psi(t) = \langle t|\psi_s\rangle = \int_c^d \psi(s) \delta(s-t) ds, \quad (4.47)$$

i.e., normed on the Dirac  $\delta$ -function, with

$$\langle t|s\rangle = \delta(s-t), \quad s, t \in [c, d].$$

The corresponding *continuous projectors*  $\hat{\pi}_{[a,b]}^c(\hat{A})$  are defined as Lebesgue integrals

$$\hat{\pi}_{[a,b]}^c(\hat{A}) = \int_a^b |s\rangle ds \langle s| = |s\rangle \langle s|, \quad -c \leq a < b \leq d. \quad (4.48)$$

In this case, projecting any vector  $|\psi\rangle \in \mathcal{H}_c$  using  $\hat{\pi}_{[a,b]}^c(\hat{A})$  is given by

$$\hat{\pi}_{[a,b]}^c(\hat{A})|\psi\rangle = \left( \int_a^b |s\rangle ds \langle s| \right) |\psi\rangle = \int_a^b \psi(s) |s\rangle ds.$$

Now, the *continuous spectral form* of a Hermitian operator  $\hat{A}$  is defined as

$$\hat{A} = \int_c^d |s\rangle s ds \langle s|.$$

**Total Spectrum.** The *total Hilbert state-space* of the system is equal to the *orthogonal sum* of its *discrete* and *continuous subspaces*,

$$\mathcal{H} = \mathcal{H}_d \oplus \mathcal{H}_c. \quad (4.49)$$

The corresponding discrete and continuous projectors are mutually complementary,

$$\hat{\pi}_{a_i}(\hat{A}) + \hat{\pi}_{[c,d]}^c(\hat{A}) = \hat{I}.$$

Using the *closure property*

$$\sum_i |i\rangle\langle i| + \int_a^b |s\rangle ds \langle s| = \hat{I},$$

the *total spectral form* of a Hermitian operator  $\hat{A} \in \mathcal{H}$  is given by

$$\hat{A} = \sum_i a_i |i\rangle\langle i| + \int_c^d |s\rangle s ds \langle s|, \quad (4.50)$$

while an arbitrary vector  $|\psi\rangle \in \mathcal{H}$  is equal to

$$|\psi\rangle = \sum_i \psi_i |i\rangle + \int_c^d \psi(s) |s\rangle ds.$$

Here,  $\psi_i = \langle i|\psi\rangle$  are *discrete Fourier coefficients*, while  $\psi(s) = \langle s|\psi\rangle$  are continuous, square integrable, Fourier coefficients,

$$\int_a^b |\psi(s)|^2 ds < +\infty.$$

Using both discrete and continuous Fourier coefficients,  $\psi_i$  and  $\psi(s)$ , the *total inner product* of  $\mathcal{H}$  is defined as

$$\langle \varphi|\psi\rangle = \bar{\varphi}_i \psi_i + \int_c^d \bar{\varphi}(s) \psi(s) ds, \quad (4.51)$$

while the norm is

$$\langle \psi|\psi\rangle = \bar{\psi}_i \psi_i + \int_c^d \bar{\psi}(s) \psi(s) ds.$$

The *total spectral measure* is now given as

$$\hat{\pi}_{[a,b]}(\hat{A}) = \sum_i \hat{\pi}_i + \int_a^b |s\rangle ds \langle s|,$$

so the probability  $P$  to obtain a measurement result within the a priori given interval  $[a, b] \in \mathbb{R} \subset \mathcal{H}$  is given by

$$P([a, b], \hat{A}, \psi) = \sum_i \langle \psi | \hat{\pi}_i | \psi \rangle + \int_a^b |\psi(s)|^2 ds, \quad (4.52)$$

where  $|\psi(s)|^2 = \langle \psi | s \rangle \langle s | \psi \rangle$  is called the *probability density*. From this the expectation value of an observable  $\hat{A}$  is equal to

$$\langle \hat{A} \rangle = \sum_i a_i \langle \psi | \hat{\pi}_i | \psi \rangle + \int_a^b s |\psi(s)|^2 ds = \langle \psi | \hat{A} | \psi \rangle,$$

#### 4.3.2.4 General Representation Model

In quantum mechanics the total spectral form of the complete observable is given by relation (4.50). We can split this total spectral form into:

(1) *Pure discrete spectral form*,

$$\hat{A} = \sum_i a_i |i\rangle \langle i|,$$

with its discrete eigenbasis  $\{|i\rangle : i \in \mathbb{N}\}$ , which is orthonormal ( $\langle i | j \rangle = \delta_{ij}$ ) and closed ( $\sum_i |i\rangle \langle i| = \hat{I}$ ); and

(2) *Pure continuous spectral form*,

$$\hat{B} = \int_c^d |s\rangle s ds \langle s|,$$

with its continuous eigenbasis  $\{|s\rangle : s \in [c, d] \subset \mathbb{R}\}$ , which is orthonormal ( $\langle s | t \rangle = \delta(s - t)$ ) and closed ( $\int_c^d |s\rangle s ds \langle s| = \hat{I}$ ).

The completeness property of each basis means that any vector  $|\psi\rangle \in \mathcal{H}$  can be expanded/developed along the components of the corresponding basis. In case of the discrete basis we have

$$|\psi\rangle = \hat{I} |\psi\rangle = \sum_i |i\rangle \langle i | \psi \rangle = \sum_i \psi_i |i\rangle,$$

with discrete Fourier coefficients of the development  $\psi_i = \langle i | \psi \rangle$ .

In case of the continuous basis we have

$$|\psi\rangle = \hat{I} |\psi\rangle = \int_c^d |s\rangle ds \langle s | \psi \rangle = \int_c^d \psi(s) |s\rangle ds.$$

with continuous Fourier coefficients of the two development  $\psi(s) = \langle s|\psi\rangle$ , which are square integrable,  $\int_a^b |\psi(s)|^2 ds < +\infty$ .

#### 4.3.2.5 Direct Product Space

Let  $\mathcal{H}_1, \mathcal{H}_2, \dots, \mathcal{H}_n$  and  $\mathcal{H}$  be  $n+1$  given Hilbert spaces such that dimension of  $\mathcal{H}$  equals the product of dimensions of  $\mathcal{H}_i$ , ( $i = 1, \dots, n$  in this section). We say that the *composite Hilbert space*  $\mathcal{H}$  is defined as a direct product of the *factor Hilbert spaces*  $\mathcal{H}_i$  and write

$$\mathcal{H} = \mathcal{H}_1 \otimes \mathcal{H}_2 \otimes \dots \otimes \mathcal{H}_n$$

if there exists a one-to-one mapping of the set of all *uncorrelated vectors*  $\{|\psi_1\rangle, |\psi_2\rangle, \dots, |\psi_n\rangle\}$ ,  $|\psi_i\rangle \in \mathcal{H}_i$ , with zero inner product (i.e.,  $\langle \psi_i | \psi_j \rangle = 0$ , for  $i \neq j$ ) – onto their direct product  $|\psi_1\rangle \times |\psi_2\rangle \times \dots \times |\psi_n\rangle$ , so that the following conditions are satisfied:

1. Linearity per each factor:

$$\begin{aligned} & \left( \sum_{j_1=1}^{J_1} b_{j_1} |\psi_{j_1}\rangle \right) \times \left( \sum_{j_2=1}^{J_2} b_{j_2} |\psi_{j_2}\rangle \right) \times \dots \times \left( \sum_{j_n=1}^{J_n} b_{j_n} |\psi_{j_n}\rangle \right) \\ &= \sum_{j_1=1}^{J_1} \sum_{j_2=1}^{J_2} \dots \sum_{j_n=1}^{J_n} b_{j_1} b_{j_2} \dots b_{j_n} |\psi_{j_1}\rangle \times |\psi_{j_2}\rangle \times \dots \times |\psi_{j_n}\rangle. \end{aligned}$$

2. Multiplicativity of scalar products of uncorrelated vectors  $|\psi_i\rangle, |\varphi_i\rangle \in \mathcal{H}_i$ :

$$\begin{aligned} & (|\psi_1\rangle \times |\psi_2\rangle \times \dots \times |\psi_n\rangle, |\varphi_1\rangle \times |\varphi_2\rangle \times \dots \times |\varphi_n\rangle) \\ &= \langle \psi_1 | \varphi_1 \rangle \times \langle \psi_2 | \varphi_2 \rangle \times \dots \times \langle \psi_n | \varphi_n \rangle. \end{aligned}$$

3. Uncorrelated vectors generate the whole composite space  $\mathcal{H}$ , which means that in a general case a vector in  $\mathcal{H}$  equals the limit of linear combinations of uncorrelated vectors, i.e.,

$$|\psi\rangle = \lim_{K \rightarrow \infty} \sum_{k=1}^K b_k |\psi_1^k\rangle \times |\psi_2^k\rangle \times \dots \times |\psi_n^k\rangle.$$

Let  $\{|k_i\rangle\}$  represent arbitrary bases in the factor spaces  $\mathcal{H}_i$ . They induce the basis  $\{|k_1\rangle \times |k_2\rangle \times \dots \times |k_n\rangle\}$  in the composite space  $\mathcal{H}$ .

Let  $\hat{A}_i$  be arbitrary operators (either all linear or all antilinear) in the factor spaces  $\mathcal{H}_i$ . Their direct product,  $\hat{A}_1 \otimes \hat{A}_2 \otimes \dots \otimes \hat{A}_n$  acts on the

uncorrelated vectors

$$\begin{aligned} & (\hat{A}_1 \otimes \hat{A}_2 \otimes \dots \otimes \hat{A}_n) (|\psi_1\rangle \times |\psi_2\rangle \times \dots \times |\psi_n\rangle) \\ &= (\hat{A}_1 |\psi_1\rangle) \times (\hat{A}_2 |\psi_2\rangle) \times \dots \times (\hat{A}_n |\psi_n\rangle) \end{aligned}$$

#### 4.3.2.6 State-Space for $n$ Quantum Particles

Classical state-space for the system of  $n$  particles is its  $6ND$  phase-space  $\mathcal{P}$ , including all position and momentum vectors,  $\mathbf{r}_i = (x, y, z)_i$  and  $\mathbf{p}_i = (p_x, p_y, p_z)_i$  respectively, for  $i = 1, \dots, n$ .

The *quantization* is performed as a *linear representation* of the real Lie algebra  $\mathcal{L}_P$  of the phase-space  $\mathcal{P}$ , defined by the Poisson bracket  $\{A, B\}$  of classical variables  $A, B$  – into the corresponding real Lie algebra  $\mathcal{L}_H$  of the Hilbert space  $\mathcal{H}$ , defined by the commutator  $[\hat{A}, \hat{B}]$  of skew-Hermitian operators  $\hat{A}, \hat{B}$ .

We start with the *Hilbert space*  $\mathcal{H}_x$  for a single 1D quantum particle, which is composed of all vectors  $|\psi_x\rangle$  of the form

$$|\psi_x\rangle = \int_{-\infty}^{+\infty} \psi(x) |x\rangle dx,$$

where  $\psi(x) = \langle x|\psi\rangle$  are square integrable Fourier coefficients,

$$\int_{-\infty}^{+\infty} |\psi(x)|^2 dx < +\infty.$$

The position and momentum Hermitian operators,  $\hat{x}$  and  $\hat{p}$ , respectively, act on the vectors  $|\psi_x\rangle \in \mathcal{H}_x$  in the following way:

$$\begin{aligned} \hat{x}|\psi_x\rangle &= \int_{-\infty}^{+\infty} \hat{x} \psi(x) |x\rangle dx, & \int_{-\infty}^{+\infty} |x \psi(x)|^2 dx < +\infty, \\ \hat{p}|\psi_x\rangle &= \int_{-\infty}^{+\infty} -i\hbar \frac{\partial}{\partial x} \psi(x) |x\rangle dx, & \int_{-\infty}^{+\infty} \left| -i\hbar \frac{\partial}{\partial x} \psi(x) \right|^2 dx < +\infty. \end{aligned}$$

The *orbit Hilbert space*  $\mathcal{H}_1^o$  for a single 3D quantum particle with the full set of compatible observable  $\hat{\mathbf{r}} = (\hat{x}, \hat{y}, \hat{z})$ ,  $\hat{\mathbf{p}} = (\hat{p}_x, \hat{p}_y, \hat{p}_z)$ , is defined as

$$\mathcal{H}_1^o = \mathcal{H}_x \otimes \mathcal{H}_y \otimes \mathcal{H}_z,$$

where  $\hat{\mathbf{r}}$  has the common generalized eigenvectors of the form

$$|\hat{\mathbf{r}}\rangle = |x\rangle \times |y\rangle \times |z\rangle.$$

$\mathcal{H}_1^o$  is composed of all vectors  $|\psi_r\rangle$  of the form

$$|\psi_r\rangle = \int_{\mathcal{H}^o} \psi(\mathbf{r}) |\mathbf{r}\rangle d\mathbf{r} = \int_{-\infty}^{+\infty} \int_{-\infty}^{+\infty} \int_{-\infty}^{+\infty} \psi(x, y, z) |x\rangle \times |y\rangle \times |z\rangle dx dy dz,$$

where  $\psi(\mathbf{r}) = \langle \mathbf{r} | \psi_r \rangle$  are square integrable Fourier coefficients,

$$\int_{-\infty}^{+\infty} |\psi(\mathbf{r})|^2 d\mathbf{r} < +\infty.$$

The position and momentum operators,  $\hat{\mathbf{r}}$  and  $\hat{\mathbf{p}}$ , respectively, act on the vectors  $|\psi_r\rangle \in \mathcal{H}_1^o$  in the following way:

$$\begin{aligned} \hat{\mathbf{r}}|\psi_r\rangle &= \int_{\mathcal{H}_1^o} \hat{\mathbf{r}} \psi(\mathbf{r}) |\mathbf{r}\rangle d\mathbf{r}, & \int_{\mathcal{H}_1^o} |\mathbf{r} \psi(\mathbf{r})|^2 d\mathbf{r} < +\infty, \\ \hat{\mathbf{p}}|\psi_r\rangle &= \int_{\mathcal{H}_1^o} -i\hbar \frac{\partial}{\partial \mathbf{r}} \psi(\mathbf{r}) |\mathbf{r}\rangle d\mathbf{r}, & \int_{\mathcal{H}_1^o} \left| -i\hbar \frac{\partial}{\partial \mathbf{r}} \psi(\mathbf{r}) \right|^2 d\mathbf{r} < +\infty. \end{aligned}$$

Now, if we have a system of  $n$  3D particles, let  $\mathcal{H}_i^o$  denote the orbit Hilbert space of the  $i$ th particle. Then the composite orbit state-space  $\mathcal{H}_n^o$  of the whole system is defined as a direct product

$$\mathcal{H}_n^o = \mathcal{H}_1^o \otimes \mathcal{H}_2^o \otimes \dots \otimes \mathcal{H}_n^o.$$

$\mathcal{H}_n^o$  is composed of all vectors

$$|\psi_r^n\rangle = \int_{\mathcal{H}_n^o} \psi(\mathbf{r}_1, \mathbf{r}_2, \dots, \mathbf{r}_n) |\mathbf{r}_1\rangle \times |\mathbf{r}_2\rangle \times \dots \times |\mathbf{r}_n\rangle d\mathbf{r}_1 d\mathbf{r}_2 \dots d\mathbf{r}_n$$

where  $\psi(\mathbf{r}_1, \mathbf{r}_2, \dots, \mathbf{r}_n) = \langle \mathbf{r}_1, \mathbf{r}_2, \dots, \mathbf{r}_n | \psi_r^n \rangle$  are square integrable Fourier coefficients

$$\int_{\mathcal{H}_n^o} |\psi(\mathbf{r}_1, \mathbf{r}_2, \dots, \mathbf{r}_n)|^2 d\mathbf{r}_1 d\mathbf{r}_2 \dots d\mathbf{r}_n < +\infty,$$

The position and momentum operators  $\hat{\mathbf{r}}_i$  and  $\hat{\mathbf{p}}_i$  act on the vectors  $|\psi_r^n\rangle \in \mathcal{H}_n^o$  in the following way:

$$\begin{aligned} \hat{\mathbf{r}}_i |\psi_r^n\rangle &= \int_{\mathcal{H}_n^o} \{\hat{\mathbf{r}}_i\} \psi(\mathbf{r}_1, \mathbf{r}_2, \dots, \mathbf{r}_n) |\mathbf{r}_1\rangle \times |\mathbf{r}_2\rangle \times \dots \times |\mathbf{r}_n\rangle d\mathbf{r}_1 d\mathbf{r}_2 \dots d\mathbf{r}_n, \\ \hat{\mathbf{p}}_i |\psi_r^n\rangle &= \int_{\mathcal{H}_n^o} \left\{ -i\hbar \frac{\partial}{\partial \mathbf{r}_i} \right\} \psi(\mathbf{r}_1, \mathbf{r}_2, \dots, \mathbf{r}_n) |\mathbf{r}_1\rangle \times |\mathbf{r}_2\rangle \times \dots \times |\mathbf{r}_n\rangle d\mathbf{r}_1 d\mathbf{r}_2 \dots d\mathbf{r}_n, \end{aligned}$$



with the square integrable Fourier coefficients

$$\int_{\mathcal{H}_n^o} |\{\hat{\mathbf{f}}_i\} \psi(\mathbf{r}_1, \mathbf{r}_2, \dots, \mathbf{r}_n)|^2 d\mathbf{r}_1 d\mathbf{r}_2 \dots d\mathbf{r}_n < +\infty,$$

$$\int_{\mathcal{H}_n^o} \left| \left\{ -i\hbar \frac{\partial}{\partial \mathbf{r}_i} \right\} \psi(\mathbf{r}_1, \mathbf{r}_2, \dots, \mathbf{r}_n) \right|^2 d\mathbf{r}_1 d\mathbf{r}_2 \dots d\mathbf{r}_n < +\infty,$$

respectively. In general, any set of vector Hermitian operators  $\{\hat{\mathbf{A}}_i\}$  corresponding to all the particles, act on the vectors  $|\psi_r^n\rangle \in \mathcal{H}_n^o$  in the following way:

$$\hat{\mathbf{A}}_i |\psi_r^n\rangle = \int_{\mathcal{H}_n^o} \{\hat{\mathbf{A}}_i\} \psi(\mathbf{r}_1, \mathbf{r}_2, \dots, \mathbf{r}_n) |\mathbf{r}_1\rangle \times |\mathbf{r}_2\rangle \times \dots \times |\mathbf{r}_n\rangle d\mathbf{r}_1 d\mathbf{r}_2 \dots d\mathbf{r}_n,$$

with the square integrable Fourier coefficients

$$\int_{\mathcal{H}_n^o} \left| \{\hat{\mathbf{A}}_i\} \psi(\mathbf{r}_1, \mathbf{r}_2, \dots, \mathbf{r}_n) \right|^2 d\mathbf{r}_1 d\mathbf{r}_2 \dots d\mathbf{r}_n < +\infty.$$

#### 4.3.2.7 Quantum Measurement and Penrose Paradox

Now, to make a *measurement* or *observation* of the quantum system means to concentrate on those aspects of the system that can be *simultaneously magnified* to the classical level and from which the system must then choose. Therefore, by measuring we are *disturbing the quantum system* with the *magnifying device*, which results in *decoherence*. In other words, we get classical probabilities, highly reminiscent of a standard *particle-like behavior*. The ‘measurement/observation’ process has caused decoherence of the wavefunction and thus led to its *collapse* to a *specific state*.

Until now, our approach to the quantum world involves two components: the one component dubbed by Penrose [Penrose (1989); Penrose (1994); Penrose (1997)] the *U-part*, involves the *unitary evolution* of the system, in a *deterministic, continuous, time-symmetric* fashion, as described for example by the Schrödinger equation (4.40), i.e.,

$$\mathbf{U} : \quad i\hbar \partial_t \psi(t) = \hat{H} \psi(t). \quad (4.53)$$

Clearly such an evolution respects *quantum coherence*, as reflected by the quantum complex superposition principle implicit in (4.53). The second component, dubbed by Penrose the *R-part*, involves the *reduction of the*

state-vector or collapse of the wavefunction, that enforces coexisting alternatives to resolve themselves into *actual* alternatives, one or the other,

$$\mathbf{R}: \quad \psi = \sum_i c_i \psi_i \longrightarrow \sum_i |c_i|^2 |\psi_i|^2, \quad (4.54)$$

where  $|c_i|^2$  are classical probabilities describing *actual* alternatives. It is the  $\mathbf{R}$ -part of quantum physics that introduces ‘uncertainties’ and ‘probabilities’, thus involving *discontinuous, time-asymmetric quantum jumps* and leading to gross violations of quantum coherence. It is fair to say that almost universally, when physicists talk about quantum physics, they tacitly identify it with its  $\mathbf{U}$ -part only. It is the  $\mathbf{U}$ -part that has absorbed all our attention for about 70 years now, and in its more advanced form, relativistic quantum field theory, has become an icon of modern physics, with spectacular success, e.g., the *Standard Model*  $SU(3) \times SU(2) \times U(1)$ . On the other hand, the  $\mathbf{R}$ -part has been vastly and conveniently forgotten, tacitly assumed to be some mere technicality that gives us the right rules of ‘measurement’ or ‘observation’: different aspects of a quantum system are simultaneously magnified at the classical level, and between which the system must choose. This attitude has brought us finally to the *Penrose paradox*, and we need to reconsider our strategy. Actually, there is no way to deduce the  $\mathbf{R}$ -part from the  $\mathbf{U}$ -part, the  $\mathbf{R}$ -part being a completely different procedure from the  $\mathbf{U}$ -part, and effectively providing the *other ‘half’* of the interpretation of quantum mechanics. It is the  $(\mathbf{U} + \mathbf{R})$  parts *together* that are needed for the spectacular agreement of quantum mechanics with the observed facts. So, one is after some *new dynamics*,  $\mathbf{N}$ , that provides a unified and comprehensible picture of the whole  $(\mathbf{U} + \mathbf{R})$  process. In the work of [Ellis *et al.* (1992); Ellis *et al.* (1999); Mavromatos and Nanopoulos (1995a); Mavromatos and Nanopoulos (1995b); Nanopoulos (1995)] the above approach is presented by

$$\mathbf{U} \oplus \mathbf{R} \subseteq \mathbf{N}. \quad (4.55)$$

It should be stressed that the *New dynamics* involved in the  $\mathbf{N}$ -equation (4.55), because they have to approach at appropriate limits the  $\mathbf{U}$ -equation (4.53) and the  $\mathbf{R}$ -equation (4.54), i.e., almost anti-diametrical points of view, cannot be some smooth generalization of some wave dynamics. Apparently, the  $\mathbf{N}$ -equation (4.55) has to contain seeds of *non-relativistic invariance* and *time asymmetry*, but in such a way that when the  $\mathbf{R}$ -part or emergence of classicality is *neglected*, an approximately relativistic, time-symmetric (quantum field) theory emerges.

### 4.3.3 *The Problem of Quantum Measurement and Entropy*

Recall that what appears to be time reversal symmetry on the microscopic scale turns into time reversal asymmetry on the macroscopic scale. Our entire intuition concerning what constitutes the 'forward direction in time' is based upon our observed experience of the second law 'increase of entropy'. Yet the foundations of this thermodynamic break with reversible time are poorly understood [Srivastava *et al.* (1999)].

Notions of 'quantum measurements' are *also* not very well understood. The working physicist usually does not wish to think too hard about such a basic problem. For guidance one consults (and repeats) the following rules of *Nobel Laureate Niels Bohr*:

- (1) A measurement is an interaction between a classical apparatus and a quantum object.
- (2) All data are classical and thereby reside in the motion of a classical apparatus; and
- (3) One may never look directly at a quantum object.

If one asks experimentally what the quantum object is really doing, then the quantum object behaves in a classical fashion as an apparatus. If one asks theoretically what the quantum object is doing, then one risks being called a philosopher (or perhaps even worse). N. Bohr forbid A. Einstein to ask what the quantum object was really doing, and no agreed upon answer has yet been formulated (see [Fine (1986)]). Designing a great experiment using the Bohr rules is similar to creating a great sculpture employing a Lagrangian. The real art is in making those judgments that are not so well described by dry logical formal rules.

L. Landau and E. Lifshitz (see [Landau and Lifshitz (1977); Landau and Lifshitz (1978)]), in their classical treatises on theoretical physics, attempted to connect the above questions concerning the nature of the second law of thermodynamics and the quantum picture of measurements. They conjectured that second-law entropy increases are required for quantum measurements, and (conversely) that quantum measurements are responsible for the second law increase in entropy. A consequence of this conjecture is that the second law has no foundation in classical statistical thermodynamics. Quantum mechanics must be essential. However, Landau and Lifshitz (by their own evaluation) never really proved their conjecture. Alas, nor shall we. However, our purpose is to describe (in formal detail) the problems as they exist.

#### 4.3.3.1 The Classical Apparatus

Recall that from a classical viewpoint, we describe the classical apparatus motion as a path on a suitable  $n$ -manifold  $M$  with local coordinates

$$x = (x^1, \dots, x^n).$$

The path  $x(t)$  of the apparatus motion, were the apparatus not to interact with the quantum object, is determined by the Lagrangian

$$L_A(x, v) = \frac{1}{2} g_{ik}(x) v^i v^k - V(x), \quad (4.56)$$

where  $g_{ik}(x)$  is the Riemannian metric tensor, and the velocity tangent vector  $v^i = v^i(t)$  is defined as  $v^i = \dot{x}^i$ . If the apparatus does not interact with a quantum object, then the equations of motion read

$$\frac{d}{dt} \left( \frac{\partial L_A}{\partial v^i} \right) = \left( \frac{\partial L_A}{\partial x^i} \right).$$

Quantum measurements are performed when the quantum object causes the apparatus to deviate from the above unperturbed classical paths. Such deviations may be described by a renormalization of the apparatus Lagrangian induced by an interaction with a quantum object.

#### 4.3.3.2 Quantum Object

The Hamiltonian  $H(x)$  of the quantum object can be viewed as an operator whose matrix elements  $H_{ij}(x)$  depend on the apparatus coordinates. Recall that if the apparatus path  $x(t)$  is given, then the quantum object is thought to be described by the Schrödinger equation

$$i\hbar \partial_t |\psi(t)\rangle = H(x(t)) |\psi(t)\rangle. \quad (4.57)$$

There is no conceptual problem about how a classical apparatus will change the state of a quantum object. The manner in which a quantum object changes the path of  $x(t)$  is a bit more subtle.

The quantum object interacts with the classical apparatus in virtue of the variation of  $H(x)$  with  $x$ ; i.e., the force exerted on the apparatus by the quantum object is given by

$$F_i(x) = -\partial_{x^i} H(x).$$

The force is evidently a quantum operator on the quantum system which is supposed to have an effect on the classical path  $x(t)$ . How this occurs is not at once obvious [Srivastava *et al.* (1999)].

It is here convenient to invoke a unitary operator (see Appendix)

$$U^\dagger(x) = U^{-1}(x),$$

which obeys

$$W(x) = U^\dagger(x)H(x)U(x), \quad (4.58)$$

with  $W(x)$  a diagonal matrix. From (7.46), (4.58) and

$$|\psi(t)\rangle = U(x(t))|\Psi(t)\rangle,$$

it follows that

$$i\hbar \partial_t |\Psi(t)\rangle = H(x(t), v(t)) |\Psi(t)\rangle, \quad (4.59)$$

where

$$\mathcal{H}(x, v) = W(x) - v^i P_i(x), \quad (4.60)$$

and

$$P_i(x) = i\hbar U^\dagger(x) \partial_{x^i} U(x) = -i\hbar \partial_{x^i} U^\dagger(x) U(x). \quad (4.61)$$

From (7.5.7) and (7.48), it follows that  $\mathcal{H}(x, v)$  is the quantum object Hamiltonian when the interaction is with an apparatus whose motion exhibits coordinates  $x$  and velocities  $v$  [Srivastava *et al.* (1999)]. The force operator acting on the apparatus follows from (4.58) and (4.61) to be

$$U^\dagger(x) \mathcal{F}_i(x) U(x) = F_i(x) + f_i(x),$$

where

$$F_i(x) = -\partial_{x^i} W(x) \quad (4.62)$$

is the *adiabatic* part of the force, and

$$f_i(x) = -\frac{i}{\hbar} [W(x), P_i(x)] \quad (4.63)$$

is the *diabatic*, i.e., 'non-adiabatic', part of the force.

### 4.3.3.3 Adiabatic Measurement Lagrangians

The object Hamiltonian  $H(x) = H_{ij}(x)$  allows for the notion of a quantum measurement as a renormalization of the apparatus Lagrangian in (4.56). Explicitly, if one defines a measurement basis for the quantum object employing the adiabatic energy levels of (4.58),

$$H(x) |k\rangle = W_k(x) |k\rangle, \quad (4.64)$$

where

$$\langle k' | k \rangle = \delta_{k'}^k,$$

then a general wave function may be written in the adiabatic basis [Srivastava *et al.* (1999)]

$$|\psi\rangle = \sum_k C_k |k\rangle. \quad (4.65)$$

The renormalized measurement Lagrangian for the classical apparatus may be defined as a mapping from an adiabatic basis state to an effective apparatus Lagrangian corresponding to that state; i.e.,

$$|k\rangle \rightarrow \mathcal{L}_k(x, v) = L_A(x, v) - W_k(x), \quad (4.66)$$

where  $L_A(x, v)$  is defined in (4.56).

Quantum measurements are usually described as follows (see, e.g., [Townsend (1992)]):

- (1) All data are classical. For a classical apparatus with coordinates  $x$ , the ‘data’ are the ‘apparatus readings’, i.e., classical paths  $x(t)$ .
- (2) If the quantum object were in the state  $|k\rangle$ , then the renormalized apparatus Lagrangian  $\mathcal{L}_k(x, v)$  would control the classical path  $x(t)$  via

$$|k\rangle \rightarrow \left\{ \frac{d}{dt} \left( \frac{\partial \mathcal{L}_k}{\partial v^k} \right) = \left( \frac{\partial \mathcal{L}_k}{\partial x^k} \right) \right\}.$$

- (3) The probability that the state  $|k\rangle$  is ‘observed’ (i.e., that the apparatus yields a characteristic reading  $x(t)$  from the Lagrangian  $\mathcal{L}_k$ ) is given by

$$P_k = |C_k|^2,$$

where the amplitude  $C_k$  is defined in (4.65).

Thus, the quantum object Hamiltonian gives rise to a Lagrangian renormalization via (4.64) and (4.66). The measurement process assigns to each adiabatic state  $|k\rangle$  of the measurement basis an apparatus Lagrangian  $\mathcal{L}_k$  yielding a characteristic reading  $x(t)$  from state  $|k\rangle$  with quantum probability  $P_k = |C_k|^2$ . This prescription is in agreement with the N. Bohr's notion of how a quantum object yields a classical apparatus reading. This forms the basis of 'quantum measurements' in which all 'data' are classical in accordance with the so-called 'Copenhagen school'. A simple example of the above approach to measurements is the *Stern-Gerlach experiment* (see, e.g., [Townsend (1992)]).

#### 4.3.3.4 The Stern-Gerlach Experiment

As an example of the above formalism let us consider the Stern-Gerlach beam splitting experiment wherein a beam of spin one-half neutral atoms with a gyromagnetic ratio  $\gamma$  passes through a spatial region with an inhomogeneous field  $\mathbf{B}(\mathbf{r})$ . The two by two spin Hamiltonian matrix now reads as

$$H(\mathbf{r}) = -\hbar\gamma\mathbf{S} \cdot \mathbf{B}(\mathbf{r}),$$

while the eigenstates corresponding in (4.64) are determined by

$$H(\mathbf{r})|\pm\rangle = W_{\pm}(\mathbf{r})|\pm\rangle,$$

where

$$W_{\pm}(\mathbf{r}) = \mp \frac{1}{2} (\hbar\gamma|\mathbf{B}(\mathbf{r})|). \quad (4.67)$$

Thus, if the incoming beam is described as in (4.65) by the quantum state

$$|\psi\rangle = C_+|+\rangle + C_-|-\rangle, \quad (4.68)$$

then with probability  $P_+ = |C_+|^2$  an atom in the beam follows the classical path specified by the classical equation of motion

$$|+\rangle \rightarrow \{M\ddot{\mathbf{r}} = \mathbf{F}_+(\mathbf{r}) = -\nabla W_+(\mathbf{r})\}, \quad (4.69)$$

and with probability  $P_- = |C_-|^2$  an atom in the beam follows the classical path specified by the classical equation of motion

$$|-\rangle \rightarrow \{M\ddot{\mathbf{r}} = \mathbf{F}_-(\mathbf{r}) = -\nabla W_-(\mathbf{r})\}, \quad (4.70)$$

The Stern–Gerach experiment represents the success of the Bohr’s theoretical interpretation of quantum mechanics at its very best (see [Srivastava *et al.* (1999)]). The quantum object is simply the spin  $\mathbf{S}$  of the atom, which yields two possible states  $|\pm\rangle$ . The classical apparatus reading is the path  $\mathbf{r}(t)$  of the atom which obeys one of two possible classical equations of motion, (4.69) or (7.49). All of this may be described by the adiabatic Lagrangians, as in (4.66)

$$|\pm\rangle \rightarrow \mathcal{L}_{\pm}(\mathbf{r}, \mathbf{v}) = \frac{1}{2}M\mathbf{v}^2 - W_{\pm}(\mathbf{r}),$$

where  $W_{\pm}(\mathbf{r})$  is defined in (4.67). Thus, the triumphant Bohr could predict that for a beam described by the quantum state in (4.68), with probability  $|C_{\pm}|^2$  one would find an atom of the beam moving along a classical path with a reading controlled by the Lagrangian  $\mathcal{L}_{\pm}(\mathbf{r}, \mathbf{v})$ .

#### 4.3.3.5 Work and Heat

In the Lagrangian description above, the effective Lagrangians were computed from the adiabatic energy levels  $\{W_k(x)\}$ . When the external coordinates are changed, the resulting induced changes in the adiabatic energy levels describe the thermodynamic notion of *work* done by the classical environment on the quantum object(or the reverse).

Another method of changing the energy of the quantum object, is by causing a transition from one adiabatic energy level to another adiabatic energy level. In thermodynamic terms such diabatic transitions describe the *heat* flow from the classical environment to the quantum object (or the reverse).

Let us consider in more detail the decomposition of energy changes into ‘work’ and ‘heat’. The mean energy of quantum objects as members of a statistical ensemble may be written as

$$\bar{E} = \text{Tr}(\rho W), \quad (4.71)$$

where  $\rho$  is the density matrix of the ensemble which obeys

$$i\hbar\dot{\rho} = [\mathcal{H}, \rho],$$

where  $\mathcal{H}$  is defined in (7.48). From (4.71)

$$\dot{\bar{E}} = \text{Tr}(\dot{\rho}W) + \text{Tr}(\rho\dot{W}), \quad (\text{not the absolute derivative, } \dot{\bar{E}}) \quad (4.72)$$



which implies

$$\dot{\bar{E}} = -\frac{i}{\hbar} \text{Tr}([\mathcal{H}, \rho]W) + \text{Tr}\left(\rho \frac{\partial W}{\partial x^k}\right) v^k. \quad (4.73)$$

Note that the first term on the r.h.s of (4.72) may be simplified according to

$$\text{Tr}([\mathcal{H}, \rho]W) = \text{Tr}(\rho[W, v^k P_k]), \quad (4.74)$$

where (7.48) has been invoked. Furthermore, from (7.48), (4.62), (4.63), (4.73) and (4.74) it follows that

$$\dot{\bar{E}} = -(\bar{f}_k + \bar{F}_k) \dot{x}^k. \quad (4.75)$$

Equation (4.75) is the central result of this section. The mean energy changes in the quantum object (as a member of a statistical ensemble) can be decomposed into heat and work; i.e.

$$d\bar{E} = d'Q + d'W, \quad (4.76)$$

where the work done on the quantum object by the classical environment is determined by

$$d'W = -\bar{F}_k dx^k, \quad (4.77)$$

and where the heat is determined by

$$d'Q = -\bar{f}_k dx^k. \quad (4.78)$$

We employ the ‘inexact differential’  $d'$  notation for the heat  $d'Q$  (energy changes from quantum transitions between adiabatic energy levels) and the work  $d'W$  (energy changes from deformations in the given adiabatic energy levels). This decomposition of the mean energy change is exactly (i.e., rigorously) true, and constitutes a general derivation of the first law of thermodynamics.

#### 4.3.3.6 Statistical Thermodynamics

The decomposition of energy changes into work and heat in (4.76), (4.77) and (4.78) did not require that the quantum object be large or complex. An ensemble of two level atoms as used in the Stern–Gerlach atomic beam experiment is sufficient for the notion of introducing diabatic and adiabatic forces.

For the purpose of describing statistical thermodynamics, as employed for systems with a macroscopic number of particles, one normally introduces one (canonical or microcanonical) of the Gibbs probability distributions. For a macroscopic system, described by an infinite matrix  $W(x)$ , one may define  $\Omega(E, x)$  as the number of quantum states with energy equal or less than  $E$ ; i.e., with the step function

$$\vartheta(E) = \begin{cases} 1, & \text{if } E \geq 0, \\ 0, & \text{otherwise,} \end{cases}$$

we have

$$\Omega(E, x) = \text{Tr}[\vartheta(E - W(x))].$$

The microcanonical entropy of the quantum system is then

$$S(E, x) = k_B \ln \Omega(E, x). \quad (4.79)$$

The microcanonical temperature  $T$ ,

$$\frac{1}{T} = \left( \frac{\partial S(E, x)}{\partial E} \right), \quad (4.80)$$

is related to the microcanonical density of states,

$$G(E, x) = \text{Tr}[\delta(E - W(x))], \quad (4.81)$$

via

$$\Omega(E, x) = k_B T(E, x) G(E, x). \quad (4.82)$$

In the thermodynamic limit of large quantum objects, the mean adiabatic force on the apparatus is given in the microcanonical ensemble by

$$\bar{F}_k = - \left( \frac{\text{Tr}(\delta(E - W) \partial_{x^k} W)}{\text{Tr} \delta(E - W)} \right), \quad (4.83)$$

where (4.62) has been invoked. From equations (4.79)–(4.83), it follows that

$$\bar{F}_k = T \left( \frac{\partial S}{\partial x^k} \right)_E = \left( \frac{\partial E}{\partial S} \right)_x \left( \frac{\partial S}{\partial x^k} \right)_E,$$

or equivalently

$$\bar{F}_k(x, S) = -\partial_{x^k} E(x, S).$$

For quasi-static changes in a macroscopic thermodynamic system we have in the microcanonical ensemble both the first and second law of thermodynamics in the form

$$dE = TdS - \bar{F}_k dx^k. \quad (4.84)$$

Note, from (4.76), (4.77), (4.78), and (4.84), that the inexact heat differential from the diabatic forces has the temperature as an integrating factor

$$dS = \left( \frac{d'Q}{T} \right) = - \left( \frac{\bar{f}_k dx^k}{T} \right),$$

as required by the second law implied existence of an entropy function. If one makes the Gibbs microcanonical assumption for quasi-static (sufficiently slow) changes, then one achieves the thermodynamic laws in a consistent manner.

However we have not thus far justified the Gibbs microcanonical assumption by anything deeper than the mere observation that this assumption is reasonable. It is here that we fall short of a strict mathematical derivation of the thermodynamic second law.

Our instinct is that one must consider a quantum object with an infinite number of degrees of freedom, e.g. as conventionally done in quantum field theory. For the field theory case, the states corresponding to *different* values of  $x$  are not unitarily equivalent. Thus, there is no unitary transformation of the statistical state of the quantum object when one changes the  $x$  parameters from  $x_{\text{initial}}$  to  $x_{\text{final}} \neq x_{\text{initial}}$ . While the usual unitary time development involves *only* the Hamiltonian, the *necessarily* diabatic time development between *unitarily inequivalent* Hilbert spaces involves *also* the entropy, or equivalently the free energy [Srivastava *et al.* (1999)].

#### 4.3.3.7 Friction in a Macroscopic Apparatus

Let us now return to the apparatus viewed as having contact with a macroscopic thermodynamic system. In (4.56) we take the apparatus potential  $V(x)$  to be determined by the apparatus adiabatic energy function  $E_A(x, S)$ ; i.e.

$$L_A(x, v) = \frac{1}{2} g_{jk}(x) v^j v^k - E_A(x, S),$$

and we may further include the diabatic apparatus friction forces  $\{\bar{f}_{Ak}\}$  which heat the macroscopic degrees of freedom by

$$\frac{d}{dt} \left( \frac{\partial L_A}{\partial v^k} \right) - \left( \frac{\partial L_A}{\partial x^k} \right) = \bar{f}_{Ak}. \quad (4.85)$$

For small velocities it is often sufficient to take the apparatus friction forces to be linear functions of the velocities,

$$\bar{f}_{Ak} = \Gamma_{kj}(x)v^j. \quad (4.86)$$

Standard linear response theory gives expressions for the friction coefficients

$$\Gamma_{kj}(x) = \frac{i}{\hbar} \int_0^\infty \langle [f_{kA}(x, t), P_{Aj}(x)] \rangle dt,$$

where (7.48) and (4.63) has been invoked as well as the Heisenberg picture

$$f_{Ak}(x, t) = e^{iW_A(x)t/\hbar} f_{Ak}(x) e^{-iW_A(x)t/\hbar}.$$

If one employs the canonical density matrix,

$$\rho_A = \frac{1}{Z_A} e^{-\beta W_A(x)/\hbar}, \quad \beta = \left( \frac{\hbar}{k_B T} \right),$$

which is equivalent to the microcanonical ensemble (for sufficiently large thermal systems), then the expression for the friction coefficients reduce to the Nyquist-Kubo formula [Toda *et al.* (1991)],

$$\Gamma_{kj}(x) = \frac{1}{\hbar} \int_0^\beta d\lambda \int_0^\infty dt \langle f_{jA}(x, -i\lambda) f_{kA}(x, t) \rangle, \quad (4.87)$$

wherein the friction coefficient is related to the quantum fluctuations of the diabatic forces.

Thus in any apparatus one does expect some friction forces as in (4.85) [Srivastava *et al.* (1999)]. The total apparatus heating rate

$$\left( \frac{d'Q_A}{dt} \right) = f_{Ak} v^k,$$

in the linear regimes of (4.86), is described by the Rayleigh dissipation which is quadratic in the velocities

$$\left( \frac{d'Q_A}{dt} \right) = \Gamma_{kj}(x) v^k v^j.$$

For the case of the Stern-Gerlach experiment, the apparatus friction forces on the atoms with spin are quite small. The dissipation in this

experiment amounts to the small friction forces induced by Ohms law eddy currents inside the deflecting magnets in the beam splitter.

#### 4.3.3.8 Low Velocity Projective Measurements

Within the above discussion of quantum measurements in the adiabatic representation of  $W(x)$ , the statistical state of a quantum object is described by the matrix  $\rho = \rho_{ij}$ . The unitary time development of the statistical state obeys the equation of motion

$$i\hbar\dot{\rho} = [\mathcal{H}, \rho], \quad (4.88)$$

where  $\mathcal{H}$  is given in (7.48). However, in the fairly early days of quantum mechanics, von Neumann introduced, over and above the standard Bohr's Copenhagen interpretation, the notion of a projective measurement [von Neumann (1955)]. During a projective measurement, the density matrix is thought to obey a non-unitary time development governed by

$$\rho \rightarrow \rho_P = P_k \rho P_k, \quad (\text{summing}) \quad (4.89)$$

for a set of projection operators  $P_k = P_k^\dagger = P_k^2$  which is complete  $\sum_k P_k = 1$ . For the problem at hand  $P_k = |k\rangle\langle k|$ , so that the projected matrix  $\rho_P$  the diagonal form.

Note, from the above definitions of  $W(x)$  and  $\rho_P$ , as well as from (4.63), it follows that the mean diabatic (frictional heating) force on the quantum object obeys

$$\bar{f}_{Pk} = \text{Tr}(\rho_P f_k) = 0.$$

The frictional force is zero, when computed from the von Neumann projected density matrix. No diabatic heat is generated in a low velocity projective measurement. This strongly suggests that projective measurements (in general) violate energy conservation, which is indeed true. Suppose that the projection operator does not commute with the total energy operator of the apparatus plus the quantum object. Further suppose that before the measurement the system plus apparatus have a sharply defined energy. After the measurement the energy value will no longer be sharp since the projection operator does not commute with the total energy. Thus, with finite probability, the total energy is not conserved. We consider this violation to be a significant flaw in the projective measurement picture. Let us reconsider the situation without imposing the von Neumann projection postulate [Srivastava *et al.* (1999)].

In the Heisenberg (unitary time development) picture, the diabatic friction force operator obeys

$$\dot{f}_k = \left( \frac{\partial f_k}{\partial t} \right) + \frac{i}{\hbar} [\mathcal{H}, f_k].$$

With adiabatic Bohr transition frequencies

$$\hbar\omega_{ij}(x) = W_i(x) - W_j(x),$$

and for a slowly moving apparatus (small  $v^k$ ), the diabatic friction force operator has only quickly oscillating off diagonal matrix elements

$$\langle j|f_k(t)|i\rangle \sim e^{-i \int \omega_{ij}(x(t))dt} \langle j|f_k|i\rangle,$$

whose time average is virtually zero. Again, in a time averaged sense, the mean diabatic friction force is negligible,  $\bar{f}_k \approx 0$ .

Thus, in the general case, the mean energy changes of an ensemble of quantum objects decomposes into a ‘heat’ and ‘work’ term

$$d\bar{E} = d'Q + d'W,$$

with the inequality

$$|d'Q| < |d'W|, \quad \text{projective measurement.}$$

We stress that the diabatic friction forces can be small (on the average) if the apparatus velocities are also small. However, even if the diabatic forces during a projective measurement on the average are small, they are often still present as ‘noise’. Via the fluctuation–dissipation (4.87), such noise does give rise to friction at least for higher velocities if the apparatus is (at least in part) macroscopic. In the limit of an infinite number of degrees of freedom, one is not allowed to totally ignore heating, the diabatic forces are invoked as part of the dynamics of passing between two unitarily inequivalent spaces [Srivastava *et al.* (1999)].

#### 4.3.3.9 Information and Entropy

In some treatments of statistical thermodynamics, one associates the physical entropy to the statistical ‘information’ contained in  $\rho$  [von Neumann (1955); Townsend (1992)]; i.e.,

$$S = -k_B \text{Tr}(\rho \ln \rho). \quad (4.90)$$

The difficulty with this approach is that the information entropy  $S$  is not always simply related to thermodynamic heat  $d'Q = -\bar{f}_k dx^k$ . For example, von Neumann has proved [von Neumann (1955)] for the projective measurement in (4.89), that

$$S_P = -k_B \text{Tr}(\rho_P \ln \rho_P)$$

and that the change in statistical entropy obeys

$$\Delta S = S_P - S \geq 0.$$

Thus the statistical entropy of a projective measurement is thought to increase, yet the frictional heating (i.e., *thermodynamic entropy* increase  $d'Q/T$ ) in a low velocity projective measurement is virtually zero.

The paradox may be resolved when it is realized that during the *unitary time development* of (4.88), it is in fact rigorously true that the statistical entropy of (4.90) does not increase at all,

$$\dot{S} = -k_B \frac{d}{dt} \text{Tr}(\rho \ln \rho) = 0.$$

Thus it is only through the projection postulate itself, that the statistical entropy may be shown to increase.

Finally, non-unitary time development can enforce the approximate equality of the thermodynamic entropy in (4.79) and the statistical entropy (4.90). This is likely to happen in the limit of an infinite number of degrees of freedom. It is in such a limit that the information theory picture may be properly formulated, also with possible advantage in problems of quantum computation [Williams and Clearwater (1998)].

#### 4.3.4 Von Neumann's Density Matrix Quantization

There are various phenomena, like for example black hole evaporation, or *Hawking radiation*, that simply do not fit into the Copenhagen U-part quantum mechanics. Therefore, if we want to include the *mixed quantum states* in our description of a quantum-biodynamic system in order to get its more realistic picture, we may have to abandon the principle of quantum coherence, following Hawking (see [Penrose (1997)]), and turn to the von Neumann's *density matrix*  $\rho$ -formalism [von Neumann (1955)] ( $\rho$  is closely related to another von Neumann concept: *entropy*  $S = -\text{Tr}(\rho[\ln \rho])$ ). In the case of a pure state described by a wave vector  $|\psi\rangle$ , the von Neumann

density matrix operator  $\rho$  is given by:

$$\rho = |\psi\rangle\langle\psi|,$$

and in a representation  $\{a\}$  the matrix elements of  $\rho$  are:

$$\rho(a, a') \equiv \langle a' | \psi \rangle \langle \psi | a \rangle.$$

In general, for open systems one cannot always define a state vector, in which case the density matrix is defined over an ensemble of theories  $\mathcal{M}$ :

$$\rho \equiv \text{Tr}_{\mathcal{M}} |\psi\rangle\langle\psi|.$$

In the coordinate representation:  $\{a\} = \{\vec{x}\}$ , the diagonal element  $\rho(x, x; t)$  is the probability density  $\mathcal{P}(x, t)$ , which is given in the pure-state case by the wave function at the time  $t$ :

$$\rho(x, x; t) \equiv \mathcal{P}(x, t) \left( = |\psi(x, t)|^2 \right) \geq 0.$$

For well-defined representations  $\{a\}$  one must have the positivity property

$$\rho(a, a) \equiv \rho_a > 0.$$

Therefore, to define an appropriate density matrix, the operator  $\rho_a$  must have positive eigenvalues in the state-space  $\{a\}$  at any time  $t$ . Even if the matrix  $\rho(t = 0)$  has positive eigenvalues, it is not guaranteed that the time-evolved matrix  $\rho(t) = \omega(t)\rho(0)$  necessarily also has positive eigenvalues. This requirement of *simple positivity* (SP) has to be imposed, and restricts the general form of the environmental entanglement. Further restrictions apply when one considers  $\{a\}$  as coordinates of a subsystem within a larger system interacting with the environment, namely the requirements of *complete positivity* (CP).

Now, any *pure state* of a quantum system can be written as  $|\psi^a\rangle = \sum_i c_i^a |i\rangle$ , with  $c_i$  complex numbers obeying the conservation of probability condition  $\sum_i |c_i|^2 = 1$ . Then the scalar product  $\langle\psi^b|\psi^a\rangle = \sum_i c_i^{*b} c_i^a$  expresses the probability amplitude that starting with the state vector  $|\psi^a\rangle$  we end up in the state  $|\psi^b\rangle$ . Actually, one can consider all the tensor products  $|\psi^k\rangle\langle\psi^l|$  with the understanding that  $\langle\psi^l|\psi^k\rangle = \text{Tr}(|\psi^k\rangle\langle\psi^l|) = \sum_i c_i^{*l} c_i^k$ .

Here we introduce the density matrix  $\rho \equiv |\psi\rangle\langle\psi|$  with matrix elements  $\rho_{ij} = c_i c_j^*$ , such that  $\text{Tr} \rho = \text{Tr}(|\psi\rangle\langle\psi|) = \langle\psi|\psi\rangle = \sum_i c_i c_i^* = 1$ , i.e., the conservation of probability condition. Notice that, in the case of a pure state, the description of a quantum system by the state vector  $|\psi\rangle$  or by



the density matrix  $\rho$  is equivalent. For example, the measurable quantities  $\langle\psi|A|\psi\rangle$  correspond to  $\text{Tr}(\rho A)$ , with  $A$  denoting the quantum operator representing the 'measurable quantity', etc. The quantum equation (4.40), or (4.53), in the density matrix approach, becomes [Ellis *et al.* (1992); Ellis *et al.* (1999); Mavromatos and Nanopoulos (1995a); Mavromatos and Nanopoulos (1995b); Nanopoulos (1995)]

$$\dot{\rho}(t) = i[\rho, H],$$

which is the *quantum analogue* of the classical statistical mechanics *Liouville equation*, describing the time evolution of the phase-space density function (the *Liouville theorem*). The great advantage of the density matrix approach is its ability to describe not only *pure states*, but also *mixed states*.

#### 4.3.4.1 Dissipative Quantum Formalism

Now, in the realistic case of an *open quantum system*, which interacts with its environment, we must extend the equation (4.3.4) with a dissipative term. In this way, the quantum evolution is governed by a Markov-type stochastic process described by *generalized Liouville equation*, or *Master equation* of the form [Ellis *et al.* (1992); Ellis *et al.* (1999); Mavromatos and Nanopoulos (1995a); Mavromatos and Nanopoulos (1995b); Nanopoulos (1995)]:

$$\dot{\rho}(t) = i[\rho, H] + \hat{\delta}H\rho, \quad (4.91)$$

which accommodates the *pure state*  $\Rightarrow$  *mixed state* transition through the extra term  $\hat{\delta}H\rho$ . Here  $H$  denotes the appropriate Hamiltonian operator of the subsystem, and  $\hat{\delta}H\rho$  is the environmental, dissipative, non-Hamiltonian term. Clearly, the extra term  $\hat{\delta}H\rho$  leads to a *spontaneous dynamical decoherence* that enables the system to make a transition from a pure to a mixed state accommodating Hawking proposal.

To define  $\hat{\delta}H\rho$  term and explicitly obtain the time evolution of an open quantum system the non-critical string formalism is developed in [Ellis *et al.* (1992); Ellis *et al.* (1999); Mavromatos and Nanopoulos (1995a); Mavromatos and Nanopoulos (1995b); Nanopoulos (1995)], proposing the generalized Liouville equation (4.91) in the form

$$\dot{\rho}(t) = i[\rho, H] + iG_{ij}[\alpha_i, \rho]\beta^j,$$

where  $G_{ij}$  denotes some *positive definite metric* in the string-field space, while  $\beta^j$  is a characteristic function related to the field  $\alpha_j$  and representing *collectively* the agitation of the *physical world* on the  $\alpha_j$  dynamics.

**Wigner Functions.** Finally, recall that *Wigner functions* (named after Nobel Laureate Eugene P. Wigner) serve as a *phase-space distribution* alternative to the density matrix  $\rho$ , to whose matrix elements they are related by Fourier transformation. The diagonal, hence real, time-independent pure-state Wigner function  $f(q, p)$  corresponding to the eigenfunction  $\psi$  of  $\hat{H}\psi = E\psi$ , is given by

$$f(q, p) = \frac{1}{2\pi} \int dy \, e^{-iyp} \psi^*(q - \frac{\hbar}{2}y) \psi(q + \frac{\hbar}{2}y). \quad (4.92)$$

However, Wigner functions are not quite probability distribution functions, as they are not necessarily positive.

### 4.3.5 Geometric Quantization

#### 4.3.5.1 Motivation

Properties (1,3) in the subsection on Dirac quantization can be also realized using the following general construction [Nikitin (1995)].

*Natural Hilbert space:* arbitrary complex-valued functions on the phase-space with scalar product

$$\langle \varphi | \psi \rangle = \int \bar{\varphi} \psi \, dV$$

(integration over the phase volume  $dV = \prod_i dx^i dp_i$  in canonical coordinates).

Operators act as

$$\hat{f}|\psi\rangle = -i\hbar\{\psi, f\}.$$

Property (3) is satisfied due to Jacobi identity; real variables correspond to Hermitian operators due to conservation of phase volume in evolution with Hamiltonian  $f$ . Note that in such definition left and right equations in (3) coincide. This is a straightforward way to construct a quantum theory by means of classical theory itself.

Property (2) is violated:  $1 \rightarrow \hat{0}$ . To enable this axiom, let's represent symplectic form as the exterior derivative of the *symplectic potential*:

$$\omega = d\theta,$$

provided  $\omega$  is exact; only in this case the canonical variables can be defined globally. In canonical variables the symplectic potential can be written as

$$\theta = p_i dx^i.$$

Symplectic potential  $\omega$  is defined up to exterior derivative:  $\omega$  will not be changed in transformation  $\theta \rightarrow \theta + d\alpha$ . Therefore, more generally we can define  $\theta = (p_i + \partial a / \partial x^i) dx^i + \partial a / \partial p_i dp_i$ . The operators constructed below will also contain such arbitrariness.

Now let's define a function  $\theta(\omega \nabla f)$  instead of  $du = (dx, dp)$  in  $\theta$  we substitute velocities in Hamiltonian evolution,  $du = \omega \nabla f = \{u, f\}$ :

$$\theta(\omega \nabla f) = p_i \{x^i, f\} + \{a, f\}.$$

The following representation satisfy all axioms:

$$\hat{f}|\psi\rangle = -i\hbar\{\psi, f\} + (f - \theta(\omega \nabla f)) \cdot |\psi\rangle.$$

Usually we need to define action of operators for some complete set of variables in the phase-space, closed with respect to Poisson brackets; and then define their functions, fixing some prescription for ordering of products. For the first (independent) variables property (3) will be satisfied exactly, for others anomalies are possible.

The following remarkable fact should be noted. The constructed Hilbert space is reducible with respect to action of independent variables. This means that less subspace can be found in it, where all independent variables act, not moving the states out this subspace.

All products and functions of independent operators also act in such subspace. Actually, if a state is initially placed in this subspace, it will never leave this subspace in further evolution. Due to this fact one should speak namely about this subspace as an actual space of states. Thus, one more axiom is always implied:

Space of states should be irreducible for action of all operators in it.

A systematic way exists to construct such subspaces in the natural Hilbert space (called also prequantum Hilbert space). Functions in such subspaces depend only on a half of variables in  $2nD$  phase-space, for which Poisson brackets vanish. Particularly, these variables can be identified with  $n$  configuration variables in Lagrangian mechanics:  $\psi(x_i), \{x_i, x_j\} = 0$ . This pattern is most evident in considered example about coordinate and momentum representations of wave functions.

In this way modern quantum theory (called geometric quantization) deduces quantum uncertainty principle from more general axioms. We need to emphasize here, that such general methods are adequate only for quantization of phase-spaces with non-trivial topology, where old quantization fails. In the case of trivial topology these methods become identical.

#### 4.3.5.2 Geometric Prequantization

Recall that Dirac quantization states:

$$\{f, g\} = \frac{1}{i\hbar}[\hat{f}, \hat{g}],$$

which means that the quantum Poisson brackets (i.e., commutators) have the same values as the classical Poisson brackets. In other words, we can associate smooth functions defined on the symplectic phase-space manifold  $(M, \omega)$  of the classical biodynamic system with operators on a Hilbert space  $\mathcal{H}$  in such a way that the Poisson brackets correspond. Therefore, *there is a functor* from the category **Symplec** to the category **Hilbert**. This functor is called *prequantization*.

Let us start with the simplest symplectic manifold  $(M = T^*\mathbb{R}^n, \omega = dp_i \wedge dq^i)$  and state the *Dirac problem*: A prequantization of  $(T^*\mathbb{R}^n, \omega = dp_i \wedge dq^i)$  is a map  $\delta : f \mapsto \delta_f$ , taking smooth functions  $f \in C^\infty(T^*\mathbb{R}^n, \mathbb{R})$  to Hermitian operators  $\delta_f$  on a Hilbert space  $\mathcal{H}$ , satisfying the *Dirac conditions*:

- (1)  $\delta_{f+g} = \delta_f + \delta_g$ , for each  $f, g \in C^\infty(T^*\mathbb{R}^n, \mathbb{R})$ ;
- (2)  $\delta_{\lambda f} = \lambda \delta_f$ , for each  $f \in C^\infty(T^*\mathbb{R}^n, \mathbb{R})$  and  $\lambda \in \mathbb{R}$ ;
- (3)  $\delta_{1_{\mathbb{R}^n}} = Id_{\mathcal{H}}$ ; and
- (4)  $[\delta_f, \delta_g] = (\delta_f \circ \delta_g - \delta_g \circ \delta_f) = i\hbar \delta_{\{f, g\}_\omega}$ , for each  $f, g \in C^\infty(T^*\mathbb{R}^n, \mathbb{R})$ ;

The pair  $(\mathcal{H}, \delta)$ , where

$$\begin{aligned} \mathcal{H} &= L^2(\mathbb{R}^n, \mathbb{C}); \\ \delta : f &\in C^\infty(T^*\mathbb{R}^n, \mathbb{R}) \mapsto \delta_f : \mathcal{H} \rightarrow \mathcal{H}; \\ \delta_f &= -i\hbar X_f - \theta(X_f) + f; \quad \theta = p_i dq^i, \end{aligned}$$

gives a prequantization of  $(T^*\mathbb{R}^n, dp_i \wedge dq^i)$ , or equivalently, the answer to the Dirac problem is affirmative [Putz (1993)].

Now, let  $(M = T^*Q, \omega)$  be the cotangent bundle of an arbitrary manifold  $Q$  with its canonical symplectic structure  $\omega = d\theta$ . The prequantization of  $M$  is given by the pair  $(L^2(M, \mathbb{C}), \delta^\theta)$ , where for each  $f \in C^\infty(M, \mathbb{R})$ ,

the operator  $\delta_f^\theta : L^2(M, \mathbb{C}) \rightarrow L^2(M, \mathbb{C})$  is given by

$$\delta_f^\theta = -i\hbar X_f - \theta(X_f) + f.$$

Here, *symplectic potential*  $\theta$  is not uniquely determined by the condition  $\omega = d\theta$ ; for instance  $\theta' = \theta + du$  has the same property for any real function  $u$  on  $M$ . On the other hand, in the general case of an arbitrary symplectic manifold  $(M, \omega)$  (not necessarily the cotangent bundle) we can find only locally a 1-form  $\theta$  such that  $\omega = d\theta$ .

In general, a symplectic manifold  $(M, \omega = d\theta)$  is quantizable (i.e., we can define the Hilbert representation space  $\mathcal{H}$  and the prequantum operator  $\delta_f$  in a globally consistent way) if  $\omega$  defines an *integral cohomology class*. Now, by the *construction theorem of a fiber bundle*, we can see that this condition on  $\omega$  is also sufficient to guarantee the existence of a *complex line bundle*  $L^\omega = (L, \pi, M)$  over  $M$ , which has  $\exp(iu_{ji}/\hbar)$  as *gauge transformations* associated to an open cover  $\mathcal{U} = \{U_i | i \in I\}$  of  $M$  such that  $\theta_i$  is a symplectic potential defined on  $U_i$  (i.e.,  $d\theta_i = \omega$ ) and

$$\theta_i = \theta_j + du_{ji} \quad \text{on} \quad U_i \cap U_j.$$

In particular, for exact symplectic structures  $\omega$  (as in the case of cotangent bundles with their canonical symplectic structures) an integral cohomology condition is automatically satisfied, since then we have only one set  $U_i = M$  and do not need any gauge transformations.

Now, for each vector-field  $X \in M$  there exists an operator  $\nabla_X^\omega$  on the *space of sections*  $\Gamma(L^\omega)$  of  $L^\omega$ ,

$$\nabla_X^\omega : \Gamma(L^\omega) \rightarrow \Gamma(L^\omega)$$

given by

$$\nabla_X^\omega f = X(f) - \frac{i}{\hbar} \theta(X)f,$$

and it is easy to see that  $\nabla^\omega$  is a *connection* on  $L^\omega$  whose curvature is  $\omega/i\hbar$ . In terms of this connection the definition of  $\delta_f$  becomes

$$\delta_f = -i\hbar \nabla_{X_f}^\omega + f.$$

The complex line bundle  $L^\omega = (L, \pi, M)$  together with its compatible connection and Hermitian structure is usually called the *prequantum bundle* of the symplectic manifold  $(M, \omega)$ .

If  $(M, \omega)$  is a quantizable manifold then the pair  $(\mathcal{H}, \delta)$  defines its prequantization.

**Examples.** Each exact symplectic manifold  $(M, \omega = d\theta)$  is quantizable, for the cohomology class defined by  $\omega$  is zero. In particular, the cotangent bundle, with its canonical symplectic structure is always quantizable.

Let  $(M, \omega = d\theta)$  be an exact symplectic manifold. Then it is quantizable with the prequantum bundle given by [Puta (1993)]:

$$\begin{aligned} L^\omega &= (M \times \mathbb{C}, pr_1, M); \\ \Gamma(L^\omega) &\simeq C^\infty(M, \mathbb{C}); \\ \nabla_X^\omega f &= X(f) - \frac{i}{\hbar} \theta(X) f; \\ ((x, z_1), (x, z_2))_x &= \bar{z}_1 z_2; \\ \delta_f &= -i\hbar \left[ X_f - \frac{i}{\hbar} \theta(X_f) \right] + f. \end{aligned}$$

Let  $(M, \omega) = (T^*\mathbb{R}, dp \wedge dq)$ . It is quantizable with [Puta (1993)]:

$$\begin{aligned} L^\omega &= (\mathbb{R}^2 \times \mathbb{C}, pr_1, \mathbb{R}^2); \\ \Gamma(L^\omega) &= C^\infty(\mathbb{R}^2, \mathbb{C}); \\ \nabla_X^\omega f &= X(f) - \frac{i}{\hbar} pdq(X) f; \\ ((x, z_1), (x, z_2))_x &= \bar{z}_1 z_2; \\ \delta_f &= -i\hbar \left[ \frac{\partial f}{\partial p} \frac{\partial}{\partial q} - \frac{\partial f}{\partial q} \frac{\partial}{\partial p} \right] - p \frac{\partial f}{\partial p} + f. \end{aligned}$$

Therefore,

$$\begin{cases} \delta_q = i\hbar \frac{\partial}{\partial p} + q \\ \delta_p = -i\hbar \frac{\partial}{\partial q}, \end{cases}$$

which does not agree with the classical result of the Schrödinger quantization:

$$\begin{cases} \delta_q = q \\ \delta_p = -i\hbar \frac{\partial}{\partial q}, \end{cases}$$

Let  $\mathcal{H}$  be a complex Hilbert space and  $U_t : \mathcal{H} \rightarrow \mathcal{H}$  a continuous one-parameter unitary group, i.e., a homomorphism  $t \mapsto U_t$  from  $\mathbb{R}$  to the group of unitary operators on  $\mathcal{H}$  such that for each  $x \in \mathcal{H}$  the map  $t \mapsto U_t(x)$  is continuous. Then the generator  $A$  of  $U_t$ , defined by

$$Ax = \frac{1}{i} \frac{d}{dt} U_t(x) = \frac{1}{i} \lim_{h \rightarrow 0} \frac{U_h(x) - x}{h}$$

is self-adjoint.

Let  $(\mathbb{R}^2, \omega = dp \wedge dq, H = \frac{1}{2}(p^2 + q^2))$  be the Hamiltonian structure of the 1D harmonic oscillator.

If we take

$$\theta = \frac{1}{2}(pdq - qdp)$$

as the symplectic potential of  $\omega$ , then the spectrum of the prequantum operator

$$\delta_H = i\hbar \left( q \frac{\partial}{\partial p} - p \frac{\partial}{\partial q} \right)$$

is [Putz (1993)]

$$\text{Spec}(\delta_H) = \{\dots, -2\hbar, -\hbar, 0, \hbar, 2\hbar, \dots\},$$

where each eigenvalue occurs with infinite multiplicity.

Let  $\mathfrak{g}$  be the vector space spanned by the prequantum operators  $\delta_q, \delta_p, \delta_H$ , given by

$$\begin{aligned} \delta_q &= i\hbar \frac{\partial}{\partial p} + q, \\ \delta_p &= -i\hbar \frac{\partial}{\partial q}, \\ \delta_H &= i\hbar \left( q \frac{\partial}{\partial p} - p \frac{\partial}{\partial q} \right), \end{aligned}$$

and  $Id$ . Then [Putz (1993)]:

(1)  $\mathfrak{g}$  is a Lie algebra called the *oscillator Lie algebra*, given by:

$$\begin{aligned} [\delta_p, \delta_q] &= i\hbar \delta_{\{p,q\}_\omega} = i\hbar Id, \\ [\delta_H, \delta_q] &= i\hbar \delta_{\{H,q\}_\omega} = -i\hbar \delta_p, \\ [\delta_H, \delta_p] &= i\hbar \delta_{\{H,p\}_\omega} = i\hbar \delta_q, \end{aligned}$$

(2)  $[\mathfrak{g}, \mathfrak{g}]$  is spanned by  $\delta_q, \delta_p, \delta_H$  and  $Id$ , or equivalently, it is a *Heisenberg Lie algebra*.

(3) The oscillator Lie algebra  $\mathfrak{g}$  is *solvable*.

## 4.4 Variational Formalism in Biodynamics

In this section we present variational formalism, to be used in conservative biodynamics, following *Hilbert 19th and 23rd problems*.

### 4.4.1 Biodynamic Action Functional

*Biodynamic action* operates on four different biophysical levels of organization, with the following top-down structure:

- (1) Level of a whole musculo-skeletal system;
- (2) Level of a single muscle;
- (3) Level of a single muscle-fibre, as a structural muscle-unit;
- (4) Molecular muscular level of nano-biodynamics.

All the macroscopic levels (1–3) of biodynamic organization are governed by *classical biodynamic action*. The molecular level (4) is governed by *quantum biodynamic action*.

The integral form of the general biodynamic action is called *biodynamic action functional* (BAF, for short), with physical dimension of energy  $\times$  time. We have defined BAF as a *time integral over the Lagrangian energy function*  $L(x^i(t), \dot{x}^i(t); t)$ ,

$$S\{[x^i(t)]; t_1, t_2\} = \int_{t_1}^{t_2} dt L(x^i(t), \dot{x}^i(t); t). \quad (4.93)$$

Here,  $x^i$ ,  $i = 1, 2, \dots, N$  are generalized coordinates, i.e., points in  $ND$  biodynamic configuration space. Thus the set of trajectories ( $x^i(t)$ ) describes the behavior of the biodynamic system, and  $\dot{x}^i(t) = dx^i/dt$  determines its velocity along the path in the biodynamic configuration space. The end-points of the trajectory are given by  $x^i(t_1) = x_1^i$ , and  $x^i(t_2) = x_2^i$ .

The *principle of stationary action* says (see [Abraham and Marsden (1978); Arnold (1989); Marsden and Ratiu (1999)]): in response to infinitesimal variation of the integration path, the BAF is *stationary*, i.e.,  $\delta S = 0$ , for variations about correct path, provided the initial and final configurations are held fixed. On the other hand, if we permit infinitesimal changes of the trajectories  $x^i(t)$  at the initial and final times, including alterations of those times, the only contribution to  $\delta S$  comes from the end-point variations, or

$$\delta S = G(t_2) - G(t_1). \quad (4.94)$$



Equation (4.94) is the most general formulation of the biodynamic action principle. The fixed values  $G_1 = G(t_1)$  and  $G_2 = G(t_2)$  depend only on the endpoint path variables at the respective terminal times.

Given a muscle-system with the BAF, the actual time evolution in biodynamic configuration space follows that path about which general variations produce only endpoint contributions. The explicit form of  $G$  is dependent upon the special representation of the biodynamic action principle.

#### 4.4.2 Lagrangian Action

Each biodynamic point particle with mass  $m$  moves in a biophysical potential  $V(x^i, t)$ . Its Lagrangian function is defined as

$$L(x^i, \dot{x}^i; t) = \frac{m}{2} \dot{x}^i - V(x^i, t). \quad (4.95)$$

The dynamical variable  $x^i = x^i(t)$  denotes the actual classical trajectory of the particle which is parameterized by  $t$  with  $t_1 \leq t \leq t_2$ .

We consider the response of the biodynamic action functional (4.93) with respect to changes in the coordinates and in the time,  $\delta x^i(t)$  and  $\delta t$ , respectively.

If the time is not varied, we write  $\delta_0$  instead of  $\delta$ . The variation of  $x^i(t)$  is then given by

$$\delta x^i(t) = \delta_0 x^i(t) + \delta t \frac{d}{dt}(x^i(t)).$$

Similarly

$$\delta \dot{x}^i(t) = \delta_0 \dot{x}^i(t) + \delta t \frac{d}{dt}(\dot{x}^i(t)) = \frac{d}{dt}(\delta x^i) - \dot{x}^i \frac{d}{dt} \delta t.$$

The difference between  $\delta$  and  $\delta_0$  acting on  $t$ ,  $x^i(t)$  and  $\dot{x}^i(t)$  is expressed by the identity

$$\delta = \delta_0 + \delta t \frac{d}{dt},$$

Also, according to (4.93) we have

$$\delta L = \delta_0 L + \delta t \frac{d}{dt} L,$$

and the total variation of biodynamic Lagrangian is given by

$$\delta L = \frac{\partial L}{\partial x^i} \delta x^i + \frac{\partial L}{\partial \dot{x}^i} \delta \dot{x}^i + \frac{\partial L}{\partial t} \delta t.$$

Now, from (4.95) we substitute

$$\frac{\partial L}{\partial x^i} = -\frac{\partial V(x^i, t)}{\partial x^i}, \quad \frac{\partial L}{\partial \dot{x}^i} = \delta_k^i m \ddot{x}^k, \quad \frac{\partial L}{\partial t} = -\frac{\partial V(x^i, t)}{\partial t},$$

(where  $\delta^{ik} = \delta_k^i = \delta_{ik}$  is the Kronecker's symbol) so that we get,

$$\delta L = -\frac{\partial V}{\partial t} \delta t - \frac{\partial V}{\partial x^i} \delta x^i + m \dot{x}^i \frac{d}{dt} \delta x^i - m (\dot{x}^i)^2 \frac{d}{dt} \delta t.$$

Expression for the change of  $S$ ,  $\delta S$ , then becomes

$$\delta S = \int_{t_1}^{t_2} dt \left[ m \dot{x}^i \frac{d}{dt} \delta x^i - \frac{\partial V}{\partial t} \delta t - \frac{\partial V}{\partial x^i} \delta x^i + (L - m (\dot{x}^i)^2 \frac{d}{dt} \delta t) \right].$$

Using the definition of biodynamic mechanical energy

$$E = \frac{\partial L}{\partial \dot{x}^i} \dot{x}^i - L = \frac{m}{2} \left( \frac{dx^i}{dt} \right)^2 + V(x^i, t),$$

and reorganizing terms, we get

$$\begin{aligned} \delta S = & \int_{t_1}^{t_2} dt \frac{d}{dt} [m \dot{x}^i \delta x^i - E \delta t] \\ & + \int_{t_1}^{t_2} dt \left[ -\delta x^i \left( m \ddot{x}^i + \delta^{ik} \frac{\partial V}{\partial x^k} \right) + \delta t \left( \frac{dE}{dt} - \frac{\partial V}{\partial t} \right) \right]. \end{aligned}$$

Since  $\delta x^i$  and  $\delta t$  are independent variations, the biomechanical action principle  $\delta S = G_2 - G_1$  implies the following laws:

$$\begin{aligned} \delta x^i : \quad & m \ddot{x}^i = -\delta^{ik} \frac{\partial V(x^i, t)}{\partial x^k}, \quad (\text{Newton's law of motion}), \\ \delta t : \quad & \frac{dE}{dt} = \frac{\partial V(x^i, t)}{\partial t}, \end{aligned}$$

so that for a static potential,  $\partial V / \partial t = 0$ , the law of the conservation of biomechanical energy follows:  $dE / dt = 0$ . Here we have

$$\text{Surface term :} \quad G = m \dot{x}^i \delta x^i - E \delta t.$$

#### 4.4.3 Hamiltonian Action

As a function of the *total biodynamic energy*, given by *Hamiltonian*

$$H(x^i, p_i; t) = \frac{p_i^2}{2m} + V(x^i, t), \quad (4.96)$$

the biodynamic Lagrangian (4.95) can also be written as ( $p_i = \partial L / \partial \dot{x}^i$ ):

$$L = p_i \dot{x}^i - H(x^i, p_i; t).$$

Here the independent dynamical variables are  $x^i$  and  $p_i$ ;  $t$  is the independent time-parameter variable. Hence the change of BAF is

$$\delta S = \delta \int_{t_1}^{t_2} dt [p_i \dot{x}^i - H(x^i, p_i; t)] = \int_{t_1}^{t_2} dt \left[ p_i \frac{d}{dt} \delta x^i + \dot{x}^i \delta p_i - \delta H - H \frac{d}{dt} \delta t \right]$$

Upon using

$$\delta H = \left( \frac{\partial H}{\partial x^i} \delta x^i + \frac{\partial H}{\partial p_i} \delta p_i + \frac{\partial H}{\partial t} \delta t \right),$$

where, according to (4.96):  $\partial H / \partial x^i = \partial V / \partial x^i$  and  $\partial H / \partial p_i = p_i / m$ , we get

$$\begin{aligned} \delta S = & \delta \int_{t_1}^{t_2} dt [p_i \delta x^i - H \delta t] \\ & + \int_{t_1}^{t_2} dt \left[ -\delta x^i \left( \dot{p}_i + \frac{\partial V}{\partial x^i} \right) + \delta p_i \left( \dot{x}^i - \delta_j^i \frac{p_j}{m} \right) + \delta t \left( \dot{H} - \frac{\partial H}{\partial t} \right) \right]. \end{aligned}$$

The biomechanical action principle  $\delta S = G_2 - G_1$  then tells us that

$$\begin{aligned} \delta p_i : \quad \dot{x}^k &= \frac{\partial H}{\partial p_k} = \delta^{ik} \frac{p_k}{m}, \\ \delta x^i : \quad \dot{p}_k &= -\frac{\partial H}{\partial x^k} = -\frac{\partial V}{\partial x^k}. \end{aligned}$$

In this way we have obtained the *two* first-order Hamiltonian ODEs of motion. Also,

$$\begin{aligned} \delta t : \quad \dot{H} &= \frac{\partial H}{\partial t}, \quad \text{and} \\ \text{Surface term :} \quad G &= p_i \delta x^i - H \delta t. \end{aligned}$$

#### 4.4.4 Noether Theorem

The surface term  $G$  (see [Abraham and Marsden (1978); Arnold (1989); Marsden and Ratiu (1999)]) of the BAF (4.93) offers a connection between the conservation laws and the invariants of the biodynamic system, governed by the celebrated theorem of E. Noether.

Let us assume that our variation of the biodynamic action vanishes under certain circumstances:  $\delta S = 0$ . We then say that the biodynamic action, which remains unchanged, is invariant under that particular variation

of the path. The principle of stationary action then states:

$$\delta S = 0 = G_2 - G_1,$$

i.e.,  $G$  has the same value, independent of the initial and final configurations.

In particular, let us assume that the biodynamic action (in Hamiltonian formulation) is invariant for a variation around the actual path for which it holds that

$$\delta x^i(t_{1,2}) = 0, \quad \frac{d}{dt}(\delta t) = 0, \quad \text{therefore} \quad \delta t = \text{const} = \varepsilon.$$

Then it follows from the invariance of  $S$ -BAF under infinitesimal constant time translation:

$$\delta S = 0 = G_2 - G_1 = -H(t_2)\delta t_2 + H(t_1)\delta t_1 = -(H_2 - H_1)\varepsilon,$$

the conservation of biodynamic energy:

$$H(t_2) = H(t_1), \quad \text{meaning} \quad \dot{H} = 0.$$

Similarly, the conservation law for linear biodynamic momentum follows if we assume that the biodynamic action is invariant under constant space translation and the change of the terminal times vanishes:

$$\begin{aligned} \delta x^i &= \delta \varepsilon_i = \text{const}, & \delta t(t_{1,2}) &= 0, \\ \delta S = 0 &= G_2 - G_1 = (p_i \delta x^i)_2 - (p_i \delta x^i)_1 = (p_{i2} - p_{i1})\delta \varepsilon_i \end{aligned}$$

or

$$p_i(t_2) = p_i(t_1), \quad \text{meaning} \quad \dot{p}_i = 0.$$

Now let

$$H = \frac{p_i^2}{2m} + V(r),$$

i.e., biodynamic potential may only depend on the distance  $r = \sqrt{(x^i)^2}$ . Then no space direction is distinguished, and with respect to rigid rotations  $\delta \omega_i = \text{const.}$  and

$$\delta t(t_{1,2}) = 0, \quad \delta x^i = \varepsilon_k^{ij} \delta \omega_j x^k,$$

it can be proved that

$$\delta S = \delta \int_{t_1}^{t_2} dt \left[ p_i \dot{x}^i - \frac{p_i^2}{2m} - V(\sqrt{x^i}) \right] = 0.$$

Because

$$\begin{aligned}\delta S = 0 &= G_2 - G_1 = (p_i \delta x^i)_2 - (p_i \delta x^i)_1 \\ &= (p_i \varepsilon_k^{ij} \delta \omega_j x^k)_2 - (p_i \varepsilon_k^{ij} \delta \omega_j x^k)_1 \\ &= \delta \omega_i \{[(r \times p)_i]_2 - [(r \times p)_i]_1\}\end{aligned}$$

this implies the conservation for angular biodynamic momentum:

$$L(t_2) = L(t_1), \quad \text{meaning} \quad \dot{L} = 0.$$

Conversely, the conservation for angular biodynamic momentum corresponds to the invariance,  $\delta S = 0$ , under rigid rotation in space. The generalization of this statement is this: if a conservation law exists, then the  $S$ -BAF is stationary with respect to the infinitesimal transformation of a corresponding variable. The converse of this statement is also true: If the  $S$ -BAF is invariant with respect to an infinitesimal transformation,  $\delta S = 0$ , then the corresponding conservation is valid.

#### 4.4.5 Hamiltonian-Action Formulation of Biodynamics

Recall from chapter 3 that *Riemannian metric*  $g = \langle, \rangle$  on the configuration manifold  $M$  is a positive-definite quadratic form  $g : M \rightarrow \mathbb{R}$ , induced by the humanoid's kinetic energy (see [Arnold (1989); Ivancevic and Snoswell (2001); Ivancevic (2002); Ivancevic (2005)]). In local coordinates  $q^i \in U$ ,  $U$  open in  $M$ ,  $g$  is given as

$$g|_{q,m} \mapsto g_{ij}(q, m) dq^i dq^j, \quad (4.97)$$

where  $g_{ij}(q, m)$  is the *material covariant metric tensor* of the musculo-skeletal system, defining a relation between external and internal joint coordinates, and including  $n$  segmental masses  $m_\chi$  as

$$g_{ij}(q, m) = \sum_{\chi=1}^n m_\chi \delta_{rs} \frac{\partial x^r}{\partial q^i} \frac{\partial x^s}{\partial q^j}.$$

Here  $\delta_{rs}$  is the Kronecker-delta,  $x^r$  are external coordinates,  $r, s = 1, \dots, 6n$ ,  $i, j = 1, \dots, N \equiv 6n - h$  (where  $h$  denotes a number of holonomic constraints).

The *autonomous Hamiltonian function*  $H : T^*M \rightarrow \mathbb{R}$  of the musculo-skeletal biodynamics is, in local canonical coordinates  $q^i, p_i \in U_p$  on the momentum phase-space manifold, i.e., cotangent bundle  $T^*M$ , given by

equation

$$H(q, p) = \frac{1}{2} g^{ij}(q, m) p_i p_j + V(q), \quad (4.98)$$

where  $g^{ij}(q, m)$  denotes the *material contravariant metric tensor*, relating internal and external coordinates, and including  $n$  segmental masses  $m_\chi$  as

$$g^{ij}(q, m) = \sum_{\chi=1}^n m_\chi \delta_{rs} \frac{\partial q^i}{\partial x^r} \frac{\partial q^j}{\partial x^s}.$$

Now, consider the *space  $\Omega$  of paths*  $\gamma = \gamma(t)$  in the momentum phase-space manifold  $T^*M$ , starting at the zero section  $o_M$

$$\Omega = \{\gamma : [0, 1] \rightarrow T^*M \mid \gamma(0) \in o_M\}$$

as a fibration  $\pi_\Omega : \Omega \rightarrow M$  over the configuration manifold  $M$ , given by

$$\pi_\Omega(\gamma) = \pi_{T^*M}(\gamma(1)).$$

For the Hamiltonian function (4.98), the classical *action functional*  $\mathcal{I}_H : \Omega \rightarrow \mathbb{R}$  is defined by

$$\mathcal{I}_H = \int_\gamma p_i dq^i - \int_0^1 H(\gamma) dt. \quad (4.99)$$

If  $\xi$  is a vector-field along  $\gamma \in \Omega$ , the first variation of  $\mathcal{I}_H$  in  $\xi$ -direction equals

$$d\mathcal{I}_H(\gamma)\xi = \int_0^1 [\omega(\dot{\gamma}, \xi) - dH(\gamma)\xi] dt + \theta(\xi(1)),$$

where  $\omega = -d(p_i dq^i)$  is the *canonical symplectic 2-form* on  $T^*M$ . The *fibre derivative* of  $\mathcal{I}_H$  vanishes on the set of Hamiltonian orbits in  $T^*M$  given by

$$\mathcal{H}_{orb} \equiv \{\gamma \in \Omega \mid \dot{\gamma} \lrcorner \omega = dH(\gamma)\}.$$

For Hamiltonian vector-field,  $X_H = \left( \frac{\partial H}{\partial p_i}, -\frac{\partial H}{\partial q^i} \right)$  on  $M$ , there exists a base integral curve  $\gamma_0(t) = (q^i(t), p_i(t))$  iff  $\gamma_0(t)$  is a *geodesic*, given by *covariant force equation* (see [De Rham (1984); Ivancevic (2002); Ivancevic and Pearce (2001b); Ivancevic (2005)])

$$\dot{q}^k = g^{ki} p_i, \quad \dot{p}_i \equiv \dot{p}_i + \Gamma_{jk}^i g^{jl} g^{km} p_l p_m = 0), \quad (4.100)$$

where  $\Gamma_{jk}^i$  denote Christoffel symbols of the Levi-Civita connection  $\nabla$  in an open chart  $U$  on  $M$ , defined upon the Riemannian metric  $g = \langle, \rangle$  as

$$\Gamma_{jk}^i = g^{il} \Gamma_{jkl}, \quad \Gamma_{jkl} = \frac{1}{2} (\partial_{q^j} g_{kl} + \partial_{q^k} g_{jl} - \partial_{q^l} g_{jk}). \quad (4.101)$$

The l.h.s  $\dot{\hat{p}}_i$  of the covariant momentum equation (4.100) represents the *intrinsic* or *Bianchi covariant derivative* of the momentum with respect to time  $t$ . Basic relation  $\dot{\hat{p}}_i = 0$  defines the *parallel transport* on  $M$ , the simplest form of biodynamics. In that case Hamiltonian vector-field  $X_H$  is called the *geodesic spray* and its phase-flow is called the *geodesic flow* (for technical details see [Ivancevic (2002); Ivancevic and Snoswell (2001); Ivancevic and Pearce (2001b); Ivancevic (2005)]).

Now, the general deterministic biodynamic model is given by dissipative, driven Hamiltonian equations,

$$\dot{q}^i = \partial_{p_i} H + \partial_{p_i} R, \quad (4.102)$$

$$\dot{p}_i = F_i - \partial_{q^i} H + \partial_{q^i} R, \quad (4.103)$$

$$q^i(0) = q_0^i, \quad p_i(0) = p_i^0, \quad (4.104)$$

including *contravariant* equation (4.102) – the *velocity vector-field*, and *covariant* equation (4.103) – the *force 1-form*, together with initial joint angles and momenta (4.104). Here ( $i = 1, \dots, N$ ), and  $R = R(q, p)$  denotes the Raileigh nonlinear (biquadratic) dissipation function, and  $F_i = F_i(t, q, p)$  are covariant driving torques of *equivalent muscular actuators*, resembling muscular excitation and contraction dynamics in rotational joint form (see subsection (4.7.4.3) below). For technical details see [Hatze (1978); Ivancevic and Snoswell (2001); Ivancevic and Pearce (2001a); Ivancevic (1991)].

The velocity vector-field (4.102) and the force 1-form field (4.103) together define the generalized Hamiltonian vector-field  $X_H$ , which geometrically represents the *section* of the momentum phase-space manifold  $T^*M$ , which is itself the cotangent bundle of the biodynamics configuration manifold  $M$ , (Figure 1.2); the Hamiltonian (total energy) function  $H = H(q, p)$  is its generating function.

As the configuration manifold  $M$  is Hausdorff, for  $(q^i, p_i) \in U_p, U_p$  open in  $T^*M$ , there exists a unique one-parameter group of diffeomorphisms on  $T^*M$ , the *Hamiltonian phase-flow* [Ivancevic and Pearce (2001b); Ivancevic

(2002); Ivancevic (2005)]

$$\begin{aligned}\phi_t &: G_1 \times T^*M \rightarrow T^*M : \\ (p(0), q(0)) &\mapsto (p(t), q(t)), \\ (\phi_t \circ \phi_s &= \phi_{t+s}, \phi_0 = \text{identity}),\end{aligned}$$

given by (4.102–4.104) such that

$$\frac{d}{dt} \Big|_{t=0} \phi_t x = J \nabla H(x) = X_H, \quad \text{with} \quad J = \begin{pmatrix} 0 & I \\ -I & 0 \end{pmatrix},$$

where  $I$  denotes the  $n \times n$  identity matrix and  $\nabla$  is the gradient operator.

If  $\phi_t^H$  is a *Hamiltonian isotopy* generated by  $H$ , then we have the embedded *Lagrangian submanifold* (see [Milinkovic (1999)])

$$\phi_1^H(o_M) = \{d\mathcal{I}_H(\gamma) \mid \gamma \in \Sigma_{\mathcal{I}_H}\}.$$

For stochastic and fuzzy-set generalizations or the deterministic biodynamics defined above, see [Ivancevic and Snoswell (2001); Ivancevic (2002)].

#### 4.4.6 Feynman Quantum Action

So far we have analyzed the macroscopic biodynamic dynamics. To make description of the biodynamic action complete, in this section we give a glimpse of a deeper, microscopic, quantum biodynamic action.

Molecular model of biodynamic action describes oscillations of Amid I peptide groups with associated dipole electric momentum inside a spiral structure of myosin filament molecules. There is a simultaneous resonant interaction and strain interaction generating a collective interaction directed along the axis of the spiral. The resonance excitation jumping from one peptide group to another can be represented as an exciton, the local molecule strain caused by the static effect of excitation as a phonon and the resultant collective interaction as a *solitary particle-wave object*.

To find appropriate BAF for this particle-wave object, we start from the Lagrangian version of biodynamic action principle. To quantize the theory, we begin with the important concept of the *probability*, or *transition*, *amplitude*. The motion of a biodynamic particle between two space-time points is described here in a quantum-mechanical formulation of *Nobel Laureate Richard P. Feynman* [Feynman and Hibbs (1965)], by a phase



carrying *transition amplitude*.<sup>1</sup> Furthermore, all possible particle paths between these two points contribute to the transition amplitude.

At time  $t_1$ , we have a probability amplitude  $\psi(\mathbf{r}_1, t_1)$  of finding the biodynamic particle at the location given by the radius-vector  $\mathbf{r}_1$ . Similarly,  $\psi(\mathbf{r}_2, t_2)$  is the probability amplitude of finding the particle at the location  $\mathbf{r}_2$  at time  $t_2$ .

With  $K(\mathbf{r}_2, t_2 | \mathbf{r}_1, t_1)$  we want to denote the transition amplitude for a particle that is emitted at  $\mathbf{r}_1$  at time  $t_1$ , and is being detected at  $\mathbf{r}_2$  at time  $t_2$ .

If a particle is selected by a screen with openings  $\mathbf{r}_1$  to be at  $(\mathbf{r}_1, t_1)$  with the amplitude  $\psi(\mathbf{r}_1, t_1)$ , then propagates, (i.e., is emitted at  $(\mathbf{r}_1, t_1)$  and goes to  $(\mathbf{r}_2, t_2)$ , which is described by the quantum-mechanical transition amplitude  $K(\mathbf{r}_2, t_2 | \mathbf{r}_1, t_1)$ , and then is detected at  $(\mathbf{r}_2, t_2)$  – amplitude  $\psi(\mathbf{r}_2, t_2)$  – then the total amplitude  $\psi(\mathbf{r}_2, t_2)$  reads:

$$\psi(\mathbf{r}_2, t_2) = \int d^3\mathbf{r}_1 K(\mathbf{r}_2, t_2 | \mathbf{r}_1, t_1) \psi(\mathbf{r}_1, t_1). \quad (4.105)$$

This is the fundamental dynamical equation of the microscopic biodynamic theory. Our main concern now is to find  $K$ , the kernel of the integral micro-biodynamic equation. So we have to study  $K(\mathbf{r}_2, t_2 | \mathbf{r}_1, t_1)$ , the so-called *Feynman propagator* more closely.

In order to get from  $A(\mathbf{r}_1, t_1)$  to  $B(\mathbf{r}_2, t_2)$ , the biodynamic particle must have taken some path  $\gamma$ . Let  $\phi_{BA}[\gamma]$  be the amplitude for the path of the particle going from  $A$  to  $B$  along  $\gamma$ . Then it holds that

$$K(B|A) = \int [d\gamma] \phi_{BA}[\gamma], \quad (4.106)$$

where the integral (or the sum) has to be taken over all paths from  $A$  to  $B$ . Obviously, the integral is very complicated, as infinitely many paths exist

---

<sup>1</sup>Feynman summarizes his approach to quantum mechanics in [Feynman (1948)]: 'Non-relativistic quantum mechanics is formulated here in a different way. It is, however, mathematically equivalent to the familiar formulation. In quantum mechanics the probability of an event which can happen in several different ways is the absolute square of a sum of complex contributions, one from each alternative way. The probability that a particle will be found to have a path  $x(t)$  lying somewhere within a region of space time is the square of a sum of contributions, one from each path in the region. The contribution from a single path is postulated to be an exponential whose (imaginary) phase is the classical action (in units of  $\hbar$ ) for the path in question. The total contribution from all paths reaching  $x, t$  from the past is the wave function  $\psi(x, t)$ . This is shown to satisfy Schrödinger equation. The relation to matrix and operator algebra is discussed. Applications are indicated, in particular to eliminate the coordinates of the field oscillators from the equations of quantum electrodynamics.'

between  $A$  and  $B$ . The r.h.s of (4.106) is called the *Feynman path integral*.

For example, when we allow all possible paths in the  $(x, t)$ -plane between two points  $a$  and  $b$ , then the path integral is written as

$$K(b, a) = \int [dx(t)] \phi_{ba}[x(t)] \quad (4.107)$$

and the integral is taken over all possible paths from  $a$  to  $b$ .

We have until now reduced our problem to finding the amplitude  $\phi_{BA}[\gamma]$ . But one cannot determine this amplitude from a fundamental physical principle! We shall therefore postulate  $\phi_{BA}[\gamma]$  according to Dirac [Dirac (1930)]. Here we again come into contact with the Lagrangian version of the biodynamic action principle, where we assigned a classical  $S$ -BAF to each path:

$$S[\gamma] = \int_{t_1}^{t_2} dt L(\mathbf{r}, \dot{\mathbf{r}}; t). \quad (4.108)$$

Following an idea of Dirac, Feynman uses the following expression for  $\phi_{BA}[\gamma]$ :

$$\phi_{BA}[\gamma] = \exp\{i/\hbar S[\gamma]\}. \quad (4.109)$$

With this we get the following formula for the Feynman propagator:

$$K(\mathbf{r}_2, t_2; \mathbf{r}_1, t_1) = \int_{r(t_1)=r_1}^{r(t_2)=r_2} [d\mathbf{r}(t)] \exp \left[ \frac{i}{\hbar} \int_{t_1}^{t_2} dt L(\mathbf{r}(t), \dot{\mathbf{r}}(t); t) \right]. \quad (4.110)$$

We can see from this form of  $K = \int [d\mathbf{r}(t)] \exp[iS[\mathbf{r}(t)]/\hbar]$  that the plane is constructed in such a way that in the classical limit,  $S \gg \hbar$ , exactly the actual classical particle path results, for the classical path is constructed in such a manner that  $S$  does not change in first order in the vicinity of the classical trajectory; i.e., the phase  $S/\hbar$  stays constant in an infinitesimal neighborhood of the classical path  $\mathbf{r}_{cl}(t)$ . Outside of this vicinity of  $\mathbf{r}_{cl}(t)$ , the phase, in case  $S_{cl}/\hbar \gg 1$ , will change rapidly, so that the corresponding amplitudes will be washed out by destructive interference.

Since the main contribution to the propagator comes from the infinitesimal strip around the classical path, as first approximation it holds that in the classical limit  $\hbar \rightarrow 0$ :

$$K(\mathbf{r}_2, t_2; \mathbf{r}_1, t_1) \sim \exp \left[ \frac{i}{\hbar} \int_{t_1}^{t_2} dt L(\mathbf{r}_{cl}(t), \dot{\mathbf{r}}_{cl}(t); t) \right]. \quad (4.111)$$

For a typical classical problem, the strip is very 'narrow', but for a typical quantum mechanical problem, the strip is very 'wide'. Consequently, the classical path loses its meaning in a typical quantum mechanical solution.

As a first example, look at a free particle. For 1D case we have

$$K(x_2, t_2; x_1, t_1) = \int_{x(t_1)=x_1}^{x(t_2)=x_2} [dx(t)] e^{\frac{i}{\hbar} S} \quad (4.112)$$

with

$$S = \int_{t_1}^{t_2} dt L(x, \dot{x}; t). \quad (4.113)$$

For the deviation  $y = y(t)$  from the classical path (with fixed ends), the action is given as

$$S = S_{cl} + \frac{m}{2} \int_{t_1}^{t_2} dt \dot{y}^2, \quad (4.114)$$

where the classical action is equal

$$S_{cl} = \frac{m}{2} \frac{(x_2 - x_1)^2}{t_2 - t_1}. \quad (4.115)$$

So for the kernel-propagator we get

$$\begin{aligned} K(x_2, t_2; x_1, t_1) &= \exp \left[ \frac{i}{\hbar} \frac{m}{2} \frac{(x_2 - x_1)^2}{t_2 - t_1} \right] \\ &\times \int_{y(t_1)=0}^{y(t_2)=0} [dy(t)] \times \exp \left[ \frac{i}{\hbar} \int_{t_1}^{t_2} dt \frac{m}{2} \dot{y}^2(t) \right], \end{aligned} \quad (4.116)$$

which explicitly gives

$$K(x_2, t_2; x_1, t_1) = \sqrt{\frac{m}{2\pi i \hbar (t_2 - t_1)}} \exp \left[ \frac{i}{\hbar} \frac{m}{2} \frac{(x_2 - x_1)^2}{t_2 - t_1} \right].$$

In three dimensions we get instead

$$K(\mathbf{r}_2, t_2; \mathbf{r}_1, t_1) = \sqrt{\left( \frac{m}{2\pi i \hbar (t_2 - t_1)} \right)^3} \exp \left[ \frac{i}{\hbar} \frac{m}{2} \frac{(\mathbf{r}_2 - \mathbf{r}_1)^2}{t_2 - t_1} \right]. \quad (4.117)$$

Now,  $K(x, t; 0, 0)$  represents the Schrödinger wave function for a free particle which was emitted at  $x_1 = 0$  at time  $t_1 = 0$  and at  $(x, t)$  is described

by the probability amplitude  $\psi(x, t)$ :

$$\psi(x, t) = K(x, t; 0, 0) = \sqrt{\frac{m}{2\pi i \hbar t}} \exp \left[ \frac{i}{\hbar} \frac{m}{2} \frac{x^2}{t} \right]. \quad (4.118)$$

As a second example, we take the more general quadratic Lagrangian for a particle in a constant external field

$$L = a(t)x^2 + b(t)x\dot{x} + c(t)\dot{x}^2 + d(t)x + e(t)\dot{x} + f(t). \quad (4.119)$$

For the deviation  $y = y(t)$  from the classical path (with fixed ends), the action is given as

$$S = S_{cl} + \int_{t_1}^{t_2} dt (a(t)y^2 + b(t)y\dot{y} + c(t)\dot{y}^2), \quad (4.120)$$

where the classical action is equal

$$S_{cl} = \frac{m}{2} \frac{(x_2 - x_1)^2}{t_2 - t_1} + \frac{F(t_2 - t_1)}{2} (x_1 + x_2) - \frac{F^2(t_2 - t_1)^3}{24m}. \quad (4.121)$$

So the propagator of a particle in a constant external field is

$$K(x_2, t_2; x_1, t_1) = \sqrt{\frac{m}{2\pi i \hbar (t_2 - t_1)}} \times \quad (4.122)$$

$$\times \exp \left\{ \frac{i}{\hbar} \left[ \frac{m}{2} \frac{(x_2 - x_1)^2}{t_2 - t_1} + \frac{F}{2} (x_1 + x_2)(t_2 - t_1) - \frac{F^2(t_2 - t_1)^3}{24m} \right] \right\}.$$

Now, the simplest, linear model of the solitary particle-wave object, representing a single muscle-fibre, is *quantum harmonic oscillator* (see [9, 10]). Lagrangian of the oscillator is given by

$$L = \frac{m}{2} \dot{x}^2 - \frac{m}{2} \omega^2 x^2, \quad (4.123)$$

so for the propagator we have ( $T = t_2 - t_1$ ):

$$K(x_2, T; x_1, 0) = A(T) e^{\frac{i}{\hbar} S_{cl}}.$$

The classical BAF is equal

$$S_{cl} = \frac{m\omega}{2 \sin(\omega T)} [(x_1^2 + x_2^2) \cos(\omega T) - 2x_1 x_2], \quad \omega T \neq n\pi, \quad n \in Z, \quad (4.124)$$

so the propagator for the micro-biodynamic quantum harmonic oscillator is ( $T = t_2 - t_1$ ):

$$K(x_2, T; x_1, 0) = \sqrt{\frac{m\omega}{2\pi i\hbar \sin(\omega T)}} \times \exp \left\{ \frac{i}{\hbar} \frac{m}{2} \frac{\omega}{\sin(\omega T)} [(x_1^2 + x_2^2) \cos(\omega T) - 2x_1 x_2] \right\}. \quad (4.125)$$

Geometric and fields extensions of the Feynman path-integral formalism are used in chapter 7.

## 4.5 Nonholonomic Biodynamics

In this section we present nonholonomic formalism, as used in contemporary biodynamics. Note that for nonholonomic mechanical problems, an ordinary Hamilton principle is not valid.

### 4.5.1 Lagrangian Approach

We start with a configuration space  $M$  with local coordinates denoted  $q^i$ ,  $i = 1, \dots, n$  and a distribution  $\mathcal{D}$  on  $M$  that describes the kinematic nonholonomic constraints. The distribution is given by the specification of a linear subspace  $\mathcal{D}_q \subset T_q M$  of the tangent space to  $M$  at each point  $q \in M$ . In this section we consider only homogeneous velocity constraints.

The dynamics of a nonholonomically constrained mechanical system is governed by the *Lagrange-d'Alembert principle*. The principle states that the equations of motion of a curve  $q(t)$  in configuration space are obtained by setting to zero the variations in the integral of the Lagrangian subject to variations lying in the constraint distribution and that the velocity of the curve  $q(t)$  itself satisfies the constraints; that is,  $\dot{q}(t) \in \mathcal{D}_{q(t)}$ . Standard arguments in the calculus of variations show that this *constrained variational principle* is equivalent to the equations (see [Koon and Marsden (1997)])

$$-\delta L : \left( \frac{d}{dt} \frac{\partial L}{\partial \dot{q}^i} - \frac{\partial L}{\partial q^i} \right) \delta q^i = 0, \quad (4.126)$$

for all variations  $\delta q$  such that  $\delta q \in \mathcal{D}_q$  at each point of the underlying curve  $q(t)$ . These equations are often equivalently written as

$$\frac{d}{dt} \frac{\partial L}{\partial \dot{q}^i} - \frac{\partial L}{\partial q^i} = \lambda_i, \quad (4.127)$$

where  $\lambda_i$  is a set of *Lagrange multipliers* ( $i = 1, \dots, n$ ), representing the force of constraint. Intrinsically, this multiplier  $\lambda$  is a section of the cotangent bundle over  $q(t)$  that annihilates the constraint distribution. The Lagrange multipliers are often determined by using the condition that  $\dot{q}(t)$  lies in the distribution.

To explore the structure of the Lagrange–d'Alembert equations (4.127) in more detail, let  $\{\omega^a\}$ ,  $a = 1, \dots, k$  be a set of  $k$  independent one forms whose vanishing describes the constraints; i.e., the distribution  $\mathcal{D}$ . One can introduce local coordinates  $q^i = (r^\alpha, s^a)$  where  $\alpha = 1, \dots, n - k$ , in which  $\omega^a$  has the form

$$\omega^a(q) = ds^a + A_\alpha^a(r, s) dr^\alpha.$$

In other words, we are locally writing the distribution as

$$\mathcal{D} = \{(r; s, \dot{r}; \dot{s}) \in TM : \dot{s} + A_\alpha^a \dot{r}^\alpha = 0\}. \quad (4.128)$$

The equations of motion (4.126) may be rewritten by noting that the allowed variations  $\delta q^i = (\delta r^\alpha; \delta s^a)$  satisfy  $\delta s^a + A_\alpha^a \delta r^\alpha = 0$ . Substitution into (4.126) gives

$$\left( \frac{d}{dt} \frac{\partial L}{\partial \dot{r}^\alpha} - \frac{\partial L}{\partial r^\alpha} \right) = A_\alpha^a \left( \frac{d}{dt} \frac{\partial L}{\partial \dot{s}^a} - \frac{\partial L}{\partial s^a} \right).$$

Equation (4.128) combined with the constraint equations

$$\dot{s}^a = -A_\alpha^a \dot{r}^\alpha,$$

gives a complete description of the equations of motion of the system; this procedure may be viewed as one way of eliminating the Lagrange multipliers. Using this notation, one finds that  $\lambda = \lambda_a \omega^a$ , where  $\lambda_a = \frac{d}{dt} \frac{\partial L}{\partial \dot{s}^a} - \frac{\partial L}{\partial s^a}$ .

Now, we construct the geometric structures on the tangent bundle  $TM$  corresponding to those on the Hamiltonian side from the preceding subsection and formulate a similar procedure for obtaining the equations of motion.

First of all, we can define the energy function  $E$  simply as  $E = H \circ \mathbb{F}L$  (where  $\mathbb{F}L$  is the *fiber derivative*, or *Legendre transformation* defined above) and pull back to  $TM$  the canonical 2-form on  $T^*M$  and denote it by  $\Omega_L$ .

We define the distribution  $\mathcal{C} = (T\tau_M)^{-1}(\mathcal{D}) \subset TTM$ , where  $\tau_M : TM \rightarrow M$ . In coordinates, the distribution  $\mathcal{C}$  consists of vectors annihilated

by the form  $\tau_M^* \omega^a$ :

$$\mathcal{C} = \{u \in TTM \mid \langle \tau_M^* \omega^a, u \rangle = 0\}.$$

When  $\mathcal{C}$  is restricted to the constraint submanifold  $\mathcal{D} \subset TM$ , we get the constraint distribution  $\mathcal{K}$ :

$$\mathcal{K} = \mathcal{C} \cap T\mathcal{D}.$$

Clearly  $\mathcal{M} = \mathbb{F}L(\mathcal{D})$  and  $\mathcal{H} = T\mathbb{F}L(\mathcal{K})$ .

The dynamics is given by a vector-field  $X_{\mathcal{K}}$  on the manifold  $\mathcal{D}$  which takes values in  $\mathcal{K}$  and satisfies the equation

$$X_{\mathcal{K}} \lrcorner \Omega_{\mathcal{K}} = dE_{\mathcal{K}},$$

where  $dE_{\mathcal{K}}$  and  $\Omega_{\mathcal{K}}$  are the restrictions of  $dE_{\mathcal{D}}$  and  $\Omega_{\mathcal{D}}$  respectively to the distribution  $\mathcal{K}$  and where  $E_{\mathcal{D}}$  and  $\Omega_{\mathcal{D}}$  are the restrictions of  $E$  and  $\Omega_L$  to  $\mathcal{D}$ .

Consider a configuration space  $M$ , a hyperregular Lagrangian  $L$  and a distribution  $\mathcal{D}$  that describes the kinematic nonholonomic constraints. The  $\mathcal{K}$ -valued vector-field  $X_{\mathcal{K}}$  on  $\mathcal{D}$  given by the equation

$$X_{\mathcal{K}} \lrcorner \Omega_{\mathcal{K}} = dE_{\mathcal{K}}$$

defines dynamics that are equivalent to the Lagrange-d'Alembert equations together with the constraints.

#### 4.5.2 Hamiltonian Approach

The approach starts on the Lagrangian side with a configuration space  $M$  and a Lagrangian  $L$  of the form kinetic energy minus potential energy, i.e.,

$$L(q, \dot{q}) = \frac{1}{2} \langle \dot{q}, \dot{q} \rangle - V(q),$$

where  $\langle, \rangle$  is a metric on  $M$  defining the kinetic energy and  $V$  is a potential energy function. We do not restrict ourselves to Lagrangians of this form.

As above, our nonholonomic constraints are given by a distribution  $\mathcal{D} \subset TM$ . We also let  $\mathcal{D}^\circ \subset T^*M$  denote the annihilator of this distribution. As above, the basic equations are given by the Lagrange-d'Alembert principle.

The Legendre transformation  $\mathbb{F}L : TM \rightarrow T^*M$ , assuming that it is a diffeomorphism, is used to define the Hamiltonian  $H : T^*M \rightarrow \mathbb{R}$  in the

standard fashion (ignoring the constraints for the moment):

$$H = \langle p, \dot{q} \rangle - L = p_i \dot{q}^i - L.$$

Here, the momentum is  $p = \mathbb{F}L(v_q) = \partial L / \partial \dot{q}$ . Under this change of variables, the equations of motion are written in the Hamiltonian form as (see [Koon and Marsden (1997)])

$$\dot{q}^i = \frac{\partial H}{\partial p_i}, \quad \dot{p}_i = -\frac{\partial H}{\partial q^i} + \lambda_a \omega_i^a, \quad (4.129)$$

where  $i = 1, \dots, n$ , together with the constraint equations.

The *constrained Hamilton-d'Alembert equations* (4.129) can be rewritten as

$$X \lrcorner \Omega = dH + \lambda_a \pi_M^* \omega^a,$$

where  $X$  is the vector-field on  $T^*M$  governing the dynamics,  $\Omega$  is the canonical symplectic form on  $T^*M$ , and  $\pi_M : T^*M \rightarrow M$  is the cotangent bundle projection. We may write  $X$  in coordinates as  $X = \dot{q}^i \partial_{q^i} + \dot{p}_i \partial_{p_i}$ .

It is desirable to model the Hamiltonian equations without the Lagrange multipliers by a vector-field on a submanifold of  $T^*M$ . First, we define the set  $M = \mathbb{F}L(D) \subset T^*M$ ; so that the constraints on the Hamiltonian side are given by  $p \in M$ . Besides  $M$ , another basic object we deal with is defined as

$$\mathcal{F} = (T \pi_M)^{-1}(D) \subset TT^*M.$$

Using a basis  $\omega^a$  of the annihilator  $\mathcal{D}^0$ , we can write these spaces as

$$\mathcal{M} = \{p \in T^*M \mid \omega^a((\mathbb{F}L)^{-1}(p)) = 0\},$$

and

$$\mathcal{F} = \{u \in TT^*M \mid \langle \pi_M^* \omega^a, u \rangle = 0\}.$$

Finally, we define

$$\mathcal{H} = \mathcal{F} \cap T\mathcal{M}.$$

Using natural coordinates  $(q^i, p_i, \dot{q}^i, \dot{p}_i)$  on  $TT^*M$ , we see that the distribution  $\mathcal{F}$  naturally lifts the constraint on  $\dot{q}$  from  $TM$  to  $TT^*M$ . On the other hand, the space  $\mathcal{M}$  puts the associated constraints on the variable  $p$  and therefore the intersection  $\mathcal{H}$  puts the constraints on both variables.



To eliminate the Lagrange multipliers, we regard the Hamiltonian equations as a vector-field on the constraint submanifold  $\mathcal{M} \subset T^*M$  which takes values in the constraint distribution  $\mathcal{H}$ .

A result is that  $\Omega_{\mathcal{H}}$ , the restriction of the canonical 2-form  $\Omega$  of  $T^*M$  fiberwise to the distribution  $\mathcal{H}$  of the constraint submanifold  $\mathcal{M}$ , is non-degenerate. Note that  $\Omega_{\mathcal{H}}$  is not a true 2-form on a manifold, so it does not make sense to speak about it being closed. We speak of it as a fibre-restricted two form to avoid any confusion. Of course it still makes sense to talk about it being nondegenerate; it just means nondegenerate as a bilinear form on each fibre of  $\mathcal{H}$ . The dynamics is then given by the vector-field  $X_{\mathcal{H}}$  on  $\mathcal{M}$  which takes values in the constraint distribution  $\mathcal{H}$  and is determined by the condition

$$X_{\mathcal{H}} \lrcorner \Omega_{\mathcal{H}} = dH_{\mathcal{H}},$$

where  $dH_{\mathcal{H}}$  is the restriction of  $dH_{\mathcal{M}}$  to  $\mathcal{H}$ .

#### 4.5.3 Biodynamic Example: Bicycle Dynamics

In engineering terminology bicycle represents an *underactuated balance mechanical system with nonholonomic rolling constraints* (see [Koon and Marsden (1997)]). Such a system is beyond the rich of the Hamilton's action principle, and therefore cannot be described neither by Lagrangian, nor by Hamiltonian dynamics. It is governed by the Lagrange-d'Alembert principle.

The dynamics of an  $n$ -DOF nonholonomic mechanical system with  $k$  constraints, like a bicycle, are governed by the constrained Lagrange-d'Alembert equations (4.127), or Hamilton-d'Alembert equations (4.129). We will follow the later case here. The covariant term  $\lambda_a \omega_i^a$  in (4.129) denotes a set of Lagrange multipliers ( $i = 1, \dots, n$ ), representing the forces of constraint, where  $\{w_i^a\}$ ,  $a = 1, \dots, k$  is a set of  $k$  independent differential 1-forms whose vanishing describes the constraints, and coefficients  $\lambda_a$  are defined through coordinates of the constraints  $s^\alpha$  as

$$\lambda_a = \frac{d}{dt} \frac{\partial L}{\partial \dot{s}^\alpha} - \frac{\partial L}{\partial s^\alpha}.$$

For simplicity, a point mass bicycle is considered, with the wheels having negligible inertia moments, mass, and width, rolling without side or longitudinal slip, and having a fixed steering axis that is perpendicular to the ground. Under such simplifications, the configuration manifold of the

bicycle is  $M = SE(2) \times T^2$ , the direct product of the special 2D Euclidean group and the two-dimensional torus, parameterized by generalized coordinates  $q^i = \{x, y, \theta, \psi, \phi\}$  (see Figure 4.1).

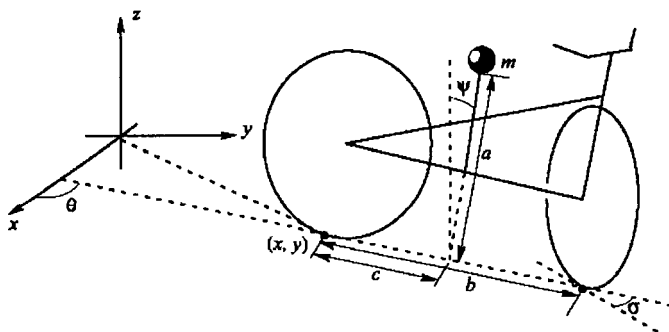


Fig. 4.1 Simple model of a bicycle (see text for explanation).

Consider a ground fixed inertial reference frame with  $x$  and  $y$  axis in the ground plane and  $z$ -axis perpendicular to the ground plane in the direction opposite to gravity. The intersection of the vehicle's plane of symmetry with the ground plane forms a contact line. The contact line is rotated about the  $z$ -direction by a yaw angle  $\theta$ . The contact line is considered directed, with its positive direction from the rear to the front of the vehicle. The yaw angle  $\theta$  is zero when the contact line is in the  $x$ -direction. The angle that the bicycle's plane of symmetry makes with the vertical direction is the roll angle  $\psi \in (-\frac{\pi}{2}, \frac{\pi}{2})$ . Front and rear wheel contacts are constrained to have velocities parallel to the lines of intersection of their respective wheel planes and the ground plane, but free to turn about an axis through the wheel/ground contact and parallel to the  $z$ -axis. Let  $\sigma \in (-\frac{\pi}{2}, \frac{\pi}{2})$  be the steering angle between the front wheel plane/ground plane intersection and the contact line. With  $\sigma$  we associate a moment of inertia  $J$  which depends both on  $\psi$  and  $\sigma$ . We will parameterize the steering angle by  $\phi = \tan \sigma/b$ .

Kinetic energy  $KE : TM \rightarrow \mathbb{R}$  is given by

$$KE = \frac{1}{2}J(\psi, \phi)\dot{\phi}^2 + \frac{m}{2} \left( (\cos \theta \dot{x} + \sin \theta \dot{y} + a \sin \psi \dot{\theta})^2 + ((-\sin \theta \dot{x} + \cos \theta \dot{y} - a \cos \psi \dot{\psi} + c \dot{\theta})^2 + (-a \sin \psi \dot{\psi})^2 \right),$$

where  $m$  is the mass of the bicycle, considered for simplicity to be a point mass, and  $J(\psi, \phi)$  is the moment of inertia associated with the steering

action. Potential energy  $PE : M \rightarrow \mathbb{R}$  is given by

$$PE = -mga \cos \psi.$$

The nonholonomic constraints associated with the front and rear wheels, assumed to roll without slipping, are expressed by

$$\dot{\theta} - \phi(\cos \theta \dot{x} + \sin \theta \dot{y}) = 0, \quad -\sin \theta \dot{x} + \cos \theta \dot{y} = 0,$$

which determine the *kinematic constraint distribution*

$$\mathcal{D}_q = \text{span}\{\partial_\psi, \partial_\phi, \cos \theta \partial_x + \sin \theta \partial_y + \phi \partial_\theta\}.$$

Using the nonholonomic momentum map on  $\mathcal{D}_q$ , the reduced Hamilton's equations of the bicycle motion are derived in the form (see [Koon and Marsden (1997)])

$$\begin{aligned} \dot{\psi} &= \frac{1}{ma} \left( \frac{K}{F} \frac{p_\psi}{a} + \frac{c\phi \cos \psi}{F} p \right), & \dot{\phi} &= \frac{p_\phi}{J}, \\ \dot{p}_\psi &= mga \sin \psi + \frac{1}{2J^2} p_\phi^2 \frac{\partial J}{\partial \psi} + m(1 + a\phi \sin \psi) a\phi \cos \psi \xi^2 + mca\phi \sin \psi \xi \dot{\psi}, \\ \dot{p}_\phi &= \frac{1}{2J^2} \frac{\partial J}{\partial \phi} p_\phi^2, \\ \dot{p} &= -\frac{\gamma \cos \psi (1 + a\phi \sin \psi)}{F} \frac{p_\psi}{a} \dot{\phi} + \frac{a \sin \psi (1 + a\phi \sin \psi) + \gamma^2 \phi \sin^2 \psi}{F} p \dot{\phi}, \end{aligned}$$

where

$$\begin{aligned} \xi &= \frac{c\phi \cos \psi}{K} \dot{\psi} + \frac{1}{mK} p = \frac{c\phi \cos \psi}{mF} \frac{p_\psi}{a} + \frac{1}{mF} p, \\ K &= (1 + a\phi \sin \psi)^2 + \gamma^2 \phi^2, \\ F &= (1 + a\phi \sin \psi)^2 + \gamma^2 \phi^2 \sin^2 \psi. \end{aligned}$$

## 4.6 Stochastic Formalism in Biodynamics

In this section we present stochastic formalism, as used in contemporary biodynamics.

*Stochastic Hamiltonian dynamics* is based on the concept of *Markov stochastic process*, which represents the probabilistic analogue to the deterministic dynamics. The Markov process is characterized by a *lack of memory*, i.e., the statistical properties of the immediate future are uniquely determined by the present, regardless of the past [Gardiner (1985)].

For example, a *random walk* is *Markov chain*, i.e., a discrete-time Markov process, such that the motion of the system in consideration is viewed as a sequence of states, in which the transition from one state to another depends only on the preceding one, or the probability of the system being in state  $k$  depends only on the previous state  $k - 1$ . The property of a Markov chain of prime importance in biodynamics is the existence of an *invariant distribution of states*: we start with an initial state  $x_0$  whose absolute probability is 1. Ultimately the states should be distributed according to a specified distribution.

Between pure deterministic (in which all DOF of the system in consideration are explicitly taken into account, leading to classical dynamical equations like Hamilton's) and pure stochastic dynamics (Markov process), there is so called *hybrid dynamics*, particularly *Brownian dynamics*, in which some of DOF are represented only through their *stochastic influence* on others. As an example, suppose a system of particles interacts with a viscous medium. Instead of specifying a detailed interaction of each particle with the particles of the viscous medium, we represent the medium as a *stochastic force* acting on the particle. The stochastic force *reduces the dimensionality* of the dynamics.

Recall from chapter 3, that the Brownian dynamics represents the phase-space trajectories of a collection of particles that individually obey *Langevin rate equations* in the field of force (i.e., the particles interact with each other via some deterministic force). For one free particle the Langevin equation of motion is given by [Gardiner (1985)]

$$m\dot{v} = R(t) - \beta v,$$

where  $m$  denotes the mass of the particle and  $v$  its velocity. The r.h.s represents the coupling to a *heat bath*; the effect of the random force  $R(t)$  is to heat the particle. This is exactly what happens in biodynamics in the heating of Hill's *muscular actuators* [Hill (1938)]. To balance overheating (on the average), the particle is subjected to *friction*  $\beta$ . In humanoid dynamics this is performed with the Rayleigh-Van der Pol's *joint dissipation*. Formally, the solution to the Langevin equation can be written as

$$v(t) = v(0) \exp\left(-\frac{\beta}{m}t\right) + \frac{1}{m} \int_0^t \exp[-(t-\tau)\beta/m] R(\tau) d\tau,$$

where the integral on the r.h.s is a *stochastic integral* and the solution  $v(t)$  is a random variable. The stochastic properties of the solution depend significantly on the stochastic properties of the random force  $R(t)$ . In the

Brownian dynamics the random force  $R(t)$  is Gaussian distributed. Then the problem boils down to finding the solution to the Langevin stochastic differential equation with the supplementary condition (mean zero and variance)

$$\langle R(t) \rangle = 0, \quad \langle R(t) R(0) \rangle = 2\beta k_B T \delta(t),$$

where  $\langle \rangle$  denotes the mean value,  $T$  is temperature,  $k_B$ —equipartition (i.e., uniform distribution of energy) coefficient, Dirac  $\delta(t)$ —function.

Algorithm for computer simulation of the Brownian dynamics (for a single particle) can be written as [Heermann (1990)]:

- (1) Assign an initial position and velocity.
- (2) Draw a random number from a Gaussian distribution with mean zero and variance.
- (3) Integrate the velocity to obtain  $v^{n+1}$ .
- (4) Add the random component to the velocity.

Another approach to taking account the coupling of the system to a heat bath is to subject the particles to collisions with *virtual particles* [Heermann (1990)]. Such collisions are imagined to affect only momenta of the particles, hence they affect the kinetic energy and introduce fluctuations in the total energy. Each stochastic collision is assumed to be an instantaneous event affecting only one particle.

The collision-coupling idea is incorporated into the Hamiltonian model of biodynamics by adding a stochastic force to the force canonical equation

$$\dot{q}^i = \frac{\partial H}{\partial p_i}, \quad \dot{p}_i = -\frac{\partial H}{\partial q^i} + R_i(t).$$

#### 4.6.1 Markov Stochastic Processes

The so-called *Ito stochastic integral* represents a kind of classical Riemann–Stieltjes integral from linear functional analysis, which is (in 1D case) for an arbitrary time-function  $G(t)$  defined as the *mean square limit*

$$\int_{t_0}^t G(t) dW(t) = ms \lim_{n \rightarrow \infty} \left\{ \sum_{i=1}^n G(t_{i-1}) [W(t_i) - W(t_{i-1})] \right\}.$$

Now, the general ND Markov process can be defined by *Ito stochastic*

differential equation (SDE),

$$\begin{aligned} dx_i(t) &= A_i[x^i(t), t]dt + B_{ij}[x^i(t), t] dW^j(t), \\ x^i(0) &= x_{i0}, \quad (i, j = 1, \dots, N) \end{aligned}$$

or corresponding *Ito stochastic integral equation*

$$x^i(t) = x^i(0) + \int_0^t ds A_i[x^i(s), s] + \int_0^t dW^j(s) B_{ij}[x^i(s), s],$$

in which  $x^i(t)$  is the variable of interest, the vector  $A_i[x(t), t]$  denotes deterministic *drift*, the matrix  $B_{ij}[x(t), t]$  represents continuous stochastic *diffusion fluctuations*, and  $W^j(t)$  is an  $N$ -variable *Wiener process* (i.e., generalized Brownian motion) [Wiener (1961)], and  $dW^j(t) = W^j(t+dt) - W^j(t)$ .

Now, there are three well-known special cases of the *Chapman-Kolmogorov equation* (see [Gardiner (1985)]):

- (1) When both  $B_{ij}[x(t), t]$  and  $W(t)$  are zero, i.e., in the case of pure deterministic motion, it reduces to the *Liouville equation*

$$\partial_t P(x', t' | x'', t'') = - \sum_i \frac{\partial}{\partial x^i} \{ A_i[x(t), t] P(x', t' | x'', t'') \}.$$

- (2) When only  $W(t)$  is zero, it reduces to the *Fokker-Planck equation*

$$\begin{aligned} \partial_t P(x', t' | x'', t'') &= - \sum_i \frac{\partial}{\partial x^i} \{ A_i[x(t), t] P(x', t' | x'', t'') \} \\ &+ \frac{1}{2} \sum_{ij} \frac{\partial^2}{\partial x^i \partial x^j} \{ B_{ij}[x(t), t] P(x', t' | x'', t'') \}. \end{aligned}$$

- (3) When both  $A_i[x(t), t]$  and  $B_{ij}[x(t), t]$  are zero, i.e., the state-space consists of integers only, it reduces to the *Master equation* of discontinuous jumps

$$\begin{aligned} \partial_t P(x', t' | x'', t'') &= \\ \int dx \{ W(x' | x'', t) P(x', t' | x'', t'') - W(x'' | x', t) P(x', t' | x'', t'') \}. \end{aligned}$$

The *Markov assumption* can now be formulated in terms of the conditional probabilities  $P(x^i, t_i)$ : if the times  $t_i$  increase from right to left, the conditional probability is determined entirely by the knowledge of the most recent condition. Markov process is generated by a set of conditional

probabilities whose probability-density  $P = P(x', t' | x'', t'')$  evolution obeys the general *Chapman-Kolmogorov integro-differential equation*

$$\begin{aligned} \partial_t P = & - \sum_i \frac{\partial}{\partial x^i} \{A_i[x(t), t] P\} \\ & + \frac{1}{2} \sum_{ij} \frac{\partial^2}{\partial x^i \partial x^j} \{B_{ij}[x(t), t] P\} \\ & + \int dx \{W(x' | x'', t) P - W(x'' | x', t) P\} \end{aligned}$$

including: *deterministic drift*, *diffusion fluctuations* and *discontinuous jumps* (given respectively in the first, second and third row).

#### 4.6.2 Statistical Mechanics of Oscillator Chains

Consider a model of a finite nonlinear chain of  $n$  oscillators, each of them  $d$ -dimensional ( $dD$ ), coupled to two Hamiltonian heat reservoirs initially at different temperatures  $T_L, T_R$ , each of which is described by a  $dD$  wave equation. A natural goal is to obtain a usable expression for the invariant (marginal) state of the chain analogous to the Boltzmann-Gibbs prescription  $\mu = Z^{-1} \exp(-H/T)$  which one has in equilibrium statistical mechanics [Bellet and Thomas (2000)]. We assume that the Hamiltonian  $H(p, q)$  of the isolated chain has the form

$$H(p, q) = \sum_{i=1}^n \frac{p_i^2}{2} + \sum_{i=1}^n U^{(1)}(q_i) + \sum_{i=1}^{n-1} U^{(2)}(q_i - q_{i+1}), \equiv \sum_{i=1}^n \frac{p_i^2}{2} + V(q), \quad (4.130)$$

where  $q_i$  and  $p_i$  are the coordinate and momentum of the  $i$ th particle, and where  $U^{(1)}$  and  $U^{(2)}$  are  $C^k$  confining potentials, i.e.,  $\lim_{|q| \rightarrow \infty} V(q) = +\infty$ .

The coupling between the reservoirs and the chain is assumed to be of dipole approximation type and it occurs at the boundary only: the first particle of the chain is coupled to one reservoir and the  $n$ th particle to the other heat reservoir. At time  $t = 0$  each reservoir is assumed to be in thermal equilibrium, i.e., the initial conditions of the reservoirs are distributed according to (Gaussian) Gibbs measure with temperature  $T_1 = T_L$  and  $T_n = T_R$  respectively. Projecting the dynamics onto the phase-space of the chain results in a set of integro-differential equations which differ from the Hamiltonian equations of motion by additional force terms in the equations for  $p_1$  and  $p_n$ . Each of these terms consists of a deterministic integral part independent of temperature and a Gaussian random part with

covariance proportional to the temperature. Due to the integral (memory) terms, the study of the long-time limit is a difficult mathematical problem. But by a further appropriate choice of couplings, the integral parts can be treated as auxiliary variables  $r_1$  and  $r_n$ , the random parts become Markovian. Thus we get (see [Eckmann *et al.* (1999)] for details) the following system of Markovian stochastic differential equations (SDEs) on the extended phase-space  $\mathbb{R}^{2dn+2d}$ : For  $x = (p, q, r)$  we have

$$\begin{aligned} \dot{q}_1 &= p_1, & \dot{p}_1 &= -\nabla_{q_1} V(q) + r_1, \\ \dot{q}_j &= p_j, & \dot{q}_j &= -\nabla_{q_j} V(q), & (j = 2, \dots, n-1) \\ \dot{q}_n &= p_n, & \dot{q}_n &= -\nabla_{q_n} V(q) + r_n, \\ dr_1 &= -\gamma(r_1 - \lambda^2 q_1)dt + (2\gamma\lambda^2 T_1)^{1/2}dw_1, \\ dr_n &= -\gamma(r_n - \lambda^2 q_n)dt + (2\gamma\lambda^2 T_n)^{1/2}dw_n. \end{aligned} \quad (4.131)$$

In equation (4.131),  $w_1(t)$  and  $w_n(t)$  are independent  $dD$  Wiener processes, and  $\lambda^2$  and  $\gamma$  are constants describing the couplings.

Now introduce a generalized Hamiltonian  $G(p, q, r)$  on the extended phase space, given by

$$G(p, q, r) = \sum_{i=1, n} \left( \frac{r_i^2}{2\lambda^2} - r_i q_i \right) + H(p, q), \quad (4.132)$$

where  $H(p, q)$  is the Hamiltonian of the isolated systems of oscillators given by (4.130). We also introduce the parameters  $\varepsilon$  (the mean temperature of the reservoirs) and  $\eta$  (the relative temperature difference):

$$\varepsilon = \frac{T_1 + T_n}{2}, \quad \eta = \frac{T_1 - T_n}{T_1 + T_n}. \quad (4.133)$$

Using (4.132), the equation (4.131) takes the form [Bellet and Thomas (2000)]

$$\begin{aligned} \dot{q} &= \nabla_p G, & \dot{p} &= -\nabla_q G, \\ dr &= -\gamma\lambda^2 \nabla_r G dt + \varepsilon^{1/2} (2\gamma\lambda^2 D)^{1/2} dw, \end{aligned} \quad (4.134)$$

where  $p = (p_1, \dots, p_n)$ ,  $q = (q_1, \dots, q_n)$ ,  $r = (r_1, r_n)$  and where  $D$  is the  $2d \times 2d$  matrix given by

$$D = \begin{pmatrix} 1 + \eta & 0 \\ 0 & 1 - \eta \end{pmatrix}.$$



The function  $G$  is a Lyapunov function, non-increasing in time, for the deterministic part of the flow (4.134). If the system is in equilibrium, i.e., if  $T_1 = T_n = \varepsilon$  and  $\eta = 0$ , it is not difficult to check that the generalized Gibbs measure

$$\mu_\varepsilon = Z^{-1} \exp(-G(p, q, r)/\varepsilon),$$

is an invariant measure for the Markov process solving (4.134).

## 4.7 Muscular Excitation–Contraction Dynamics

In this section, medically oriented and therefore rather descriptive in nature, we present muscular excitation–contraction dynamics on several biodynamic levels.

### 4.7.1 Human Musculo–Skeletal System

The human musculo–skeletal system consists of the skeleton, joints and muscles.

#### 4.7.1.1 Human Skeleton

The *skeleton* or *skeletal system* is the biological system providing support in living organisms. Skeletal systems are commonly divided into two types – external (an exoskeleton), and internal (an endoskeleton) [Marieb (1998); Wikipedia (2005); Gowitzke and Milner (1988); Ivancevic and Snoswell (2000)].

External skeletal systems are restricted in their maximum size so larger animals, such as the order chordata, have internal skeletal systems. Examples of this are found in arthropods and shellfish: the skeleton forms a hard shell-like covering protecting the internal organs.

An internal skeletal system consists of rigid structures within the body, moved by the muscular system. If the structures are mineralized or ossified, as they are in humans and other mammals, they are referred to as bones. Cartilage is another common component of skeletal systems, supporting and supplementing the skeleton. The human ear and nose are shaped by cartilage. Some organisms have a skeleton consisting entirely of cartilage and without any calcified bones at all, for example sharks. The bones or other rigid structures are connected by ligaments and connected to the muscular system via tendons.

The fully-developed human skeleton consists of 206 bones. The *human skeleton* is made up of bones, some of them joined together, supported and supplemented by a structure of ligaments, tendons, muscles, and cartilage.

The skeleton changes composition over a lifespan. A developing fetus has no hard skeleton at all – it forms gradually during the nine months in the womb. When a baby is born it actually has more bones than it will as an adult. On average, an adult human has 206 bones in their skeleton (the number can vary slightly from individual to individual), but a baby is born with approximately 270. The difference comes from a number of small bones that fuse together during growth. These include the bones in the skull and the spine. The sacrum (the bone at the base of the spine) consists of six bones which are separated at birth but fuse together into a solid structure in later years [Marieb (1998); Wikipedia (2005); Gowitzke and Milner (1988); Ivancevic and Snoswell (2000)].

There are 6 bones (three on each side) in the inner ear that articulate only with themselves, and one bone, the hyoid bone, which does not touch any other bones in the body.

Key parts of the human skeleton include: skull, jaw, rib cage, spine, pelvis and hip, femur, tibia and fibula, humerus, radius and ulna, patella, wrists and ankles, hands and feet.

In particular, the *spine* of a vertebrate is the vertebral column. It is divided, in most land mammals, into five sections: the cervical (neck) section, the thoracic section, the lumbar section, the sacrum, and the tail or coccyx.

The topmost vertebrae of the spine are the Axis and the atlas. These are specially adapted to allow a full range of movement for the skull.

The spine serves two major purposes – firstly, it gives the skeleton its strength by supporting the back, and second, it protects the vital spinal cord from damage.

The *skull* is the hard bony structure that protects the brain from damage and gives the head its shape. In humans, the skull is the uppermost portion of the human skeleton. It is made up of a number of bony parts – 7 in the skull proper (neurocranium) and 14 in the facial area (splanchnocranium). There are five main skull sections – one occipital, two frontal, two parietal. The sections are fused together in adults along sutures – metopic, coronal, sagittal and lambdoid. At birth these sutures are fibrous and moveable, necessary for birth and later growth. At the points where sutures meet are fontanelles, the main ones are the anterior and posterior. The anterior fontanelle is at the junction of the frontal and parietal bones, it is a 'soft

spot' on the heads of babies that can remain up to around two years of age. If the brain is bruised or injured it can be extremely serious. Normally the skull protects the brain from damage through its hard unyieldingness, but in cases of head injury (e.g., subdural haematoma) the intracranial pressure can cause brain damage unless an immediate operation is performed. This is why patients with concussion must be watched extremely carefully.

The skeleton can be affected by many diseases, affecting physical mobility and strength. These range from minor to extremely debilitating. Bone cancer and bone tumors are extremely serious and often require amputation of the affected limb. The various forms of arthritis attack the skeleton and cause extreme pain and debility. Osteoporosis is another danger, especially for post-menopausal women and the elderly. It greatly increases the likelihood of fractures and broken bones, although they can happen to anyone at any time if the bones suffer a trauma.

#### 4.7.1.2 Human Joints

A joint in the human body (and other animals) is the area where two bones interact, about which a movement can be formed.

There are many joints in the human body, but they can be divided into different groups [Marieb (1998); Wikipedia (2005); Gowitzke and Milner (1988); Ivancevic and Snoswell (2000)].

**Synovial Joints.** The ends of each bone are covered in smooth articular cartilage, they are also lubricated with *synovial fluid*, this reduces friction and enables smooth movements to be produced. The whole joint is contained in the *joint capsule*, which consists of a tough outer layer which helps to stabilise the joint, and a *synovial membrane* which produces synovial fluid.

Most of the joints that provide a lot of movement are synovial joints.

Synovial joints can be further grouped by their shape, which controls the movement they allow:

- *Hinge joints*, such as the elbow (between the humerus and the ulna). These joints act just like the hinge on a door, allowing *flexion* and *extension* in just one plane.
- *Ball-and-socket joints*, such as the hip joint. These allow a wide range of movement.
- *Condylloid* (or *ellipsoid*) *joints*, such as the knee. When the knee is *extended* there is no rotation, when it is flexed some rotation is possible.

A condyloid joint is where two bones fit together with an odd shape (e.g., an ellipse), and one bone is concave, the other convex.

- *Pivot joints*, such as the elbow (between the radius and the ulna). This is where one bone rotates about another.
- *Saddle joints*, such as the thumb (between the metacarpal and carpal). Named so because of their shape, saddle joints, allow movement in a variety of directions.
- *Gliding joints*, such as in the carpals of the wrist. These joints allow a wide variety of movement, but not much distance.

**Cartilaginous and Fibrous Joints.** Unlike synovial joints cartilaginous ones do not allow much movement. An example of this joint is the pubic symphysis. On the other hand, fibrous joints are not designed to allow any movement. The sutures in the skull are an example.

#### 4.7.1.3 Human Muscular System

The *muscular system* is the biological system of animals that allows them to move internally and externally. Animals use muscles to convert the chemical energy of adenosine three-phosphate (ATP) into mechanical work. The muscular system in vertebrates consists of three different types of muscles: cardiac, skeletal and smooth. Cardiac muscle is a striated muscle that makes up the heart. It is the only type of muscle consisting of branching fibers. Skeletal muscle consists of voluntary muscles attached to the frame of the skeletal system enabling bodily movement. Smooth muscle is the involuntary muscle that enables the movement of internal organs. Movement of all muscles is controlled through the nervous system.

Muscle is a tissue type found in the bodies of animals. The purpose of muscle is to move a part of the body, often by applying force to the bones. Muscles do this by contracting and relaxing. Contraction is caused by electrical impulses transmitted by the nerves. Muscles and muscular activity account for a lot of the body's energy consumption.

There are three general types of muscle [Marieb (1998); Wikipedia (2005); Gowitzke and Milner (1988); Ivancevic and Snoswell (2000)]:

- Skeletal muscle – often voluntary (over 640 in the human body). These enable movement and locomotion. The myofibrils of skeletal muscle are long, cylindrical cells that possess multiple, peripheral nuclei (see Figure 4.2).
- Smooth muscle – involuntary, such as in the intestines and blood vessels.

- Cardiac muscle – present in the heart.

These three types of cells have many differences, but all use the movement of actin against myosin to produce contraction. The strength of a skeletal muscle is directly proportional to its cross-sectional area. The strength of a body, however, is determined by biomechanical principles (the distance between muscle insertions and joints, muscle size, and so on).

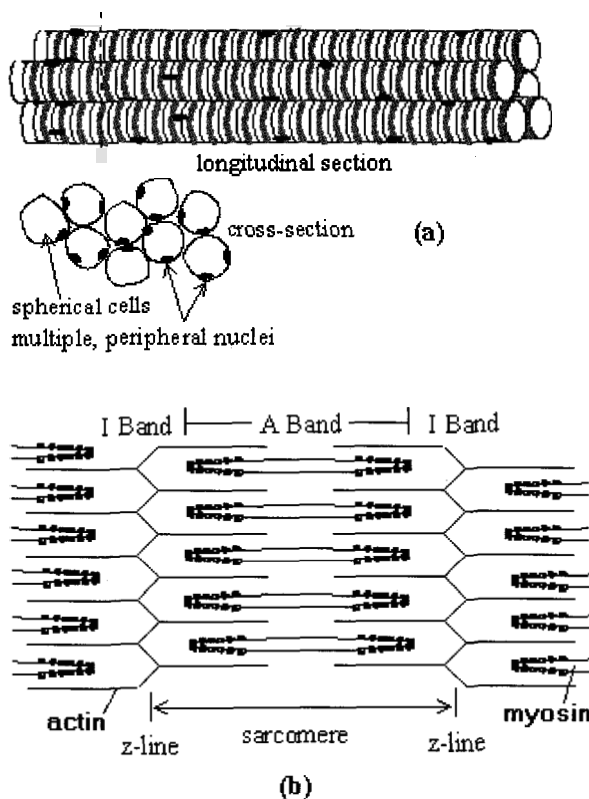


Fig. 4.2 Structure of the skeletal muscle: (a) muscular fibers with their cross-sections; (b) Sarcomere with overlapping myofilaments.

*Motor skills* are the abilities of proper use of the muscles. They depend also on the proper functioning of the brain, nerves and joints, and the bones being intact. One application of motor skills is locomotion.

The human muscular system consists of over 640 different muscles

[Marieb (1998); Wikipedia (2005); Gowitzke and Milner (1988); Ivancevic and Snoswell (2000)].

#### 4.7.1.4 Human Energy Flow

Human energy production spans the range of human movements from those requiring large bursts of energy over short periods of time (as in sprint running) – to those activities requiring small but sustained energy production (as in marathon running). Even within the same activity, the energy requirements change from one moment to the next (see [Marieb (1998); Gowitzke and Milner (1988); Bigland-Ritchie *et al.* (1995); Ivancevic (1991); Ivancevic and Snoswell (2000)]).

**Immediate Energy Source.** Adenosine triphosphate (*ATP*) is the immediately usable form of chemical energy for muscular activity. It is stored in most cells, particularly muscle cells. Other forms of chemical energy, such as that available from the foods we eat, must be transferred into the *ATP* form before they can be utilized by the muscle cells.

The chemical structure of *ATP* is complicated, but for our purposes it can be simplified, saying that *ATP* consists of a large complex of molecules called adenosine and three simpler components called phosphate groups. The last two phosphate groups represent ‘high energy bonds’. In other words, they store a high level of potential chemical energy. When the terminal phosphate bond is broken, energy is released, enabling the cell to perform work. The kind of work performed by the cell depends on the cell type. For example, mechanical work (contraction) is performed by muscle cells (skeletal, smooth and heart muscle), nerve conduction by nerve cells, secretion by secretory cells (e.g., endocrine cells), and so on. All ‘biological’ work performed by any cell requires the immediate energy derived from the breakdown of *ATP*.

**Principle of Coupled Reactions.** Since energy is released when *ATP* is broken down, it is not too surprising that energy is required to rebuild or resynthesize *ATP*. The building blocks for *ATP* synthesis are the byproducts of its breakdown, adenosine diphosphate (*ADP*) and inorganic phosphate ( $P_i$ ). Therefore, we have two essential formulas, the direct:  $ATP \rightarrow ADP + P_i + \text{energy}$ , and the inverse one:  $ADP + P_i \rightarrow ATP$ . The energy for *ATP* resynthesis comes from three different series of chemical reactions that take place within the body. Two of the three depend upon the food we eat, whereas the other depends upon a chemical compound called phosphocreatine. The energy released from any one of these series reactions

is coupled with the energy needs of the reaction that resynthesizes *ATP*. In other words, the separate reactions are functionally linked together in such a way that the energy released by the one is always used by the other. Biochemists refer to these functional links as coupled reactions, and it has been shown that such coupling is the fundamental principle involved in the metabolic production of *ATP*.

**Phosphagen System.** *PC* is an abbreviation for phosphocreatine, another one of those 'energy-rich' phosphate compounds closely related to *ATP*. For example, *PC*, like *ATP*, is stored in muscle cells, and when it is broken down (i.e., when its phosphate group is removed), a large amount of energy is released. The released energy, of course, is coupled to the energy requirement necessary for the resynthesis of *ATP*. In other words, as rapidly as *ATP* is broken down during muscular work, it is continuously reformed from *ADP* and  $P_i$  by the energy liberated during the breakdown of the stored *PC*:  $ADP + P_i \rightarrow ATP$ . For every mole of *PC* broken down, one mole of *ATP* is resynthesized.

The total muscular stores of both *ATP* and *PC* (collectively referred to as phosphagens) are very small – only about 0.3 mole in females and 0.6 mole in males. Thus, the amount of energy obtainable through this system is limited. In fact, if we were to run 100 m as fast as we could, the phosphagen stores in the working muscles would probably be empty by the end of the sprint. However, the usefulness of the *ATP* – *PC* system lies in the rapid availability of energy rather than in the quantity. For example, activities such as sprinting, jumping, swinging and other similar skills requiring only a few seconds to complete are all dependent upon the stored phosphagens for their primary energy source.

**Lactic Acid System.** This system is also known as 'anaerobic glycolysis'. 'Glycolysis' refers to the breakdown of sugar; 'anaerobic' means without oxygen. In this system, the breakdown of sugar (a carbohydrate, one of the foodstuffs) supplies the necessary energy from which *ATP* is manufactured. When the sugar is only partially broken down, one of the end products is lactic acid (hence the name lactic acid system).

When lactic acid accumulates in the muscles and blood reaches very high levels, temporary muscular fatigue results. This is a very definite limitation, and is the main cause of the 'early' fatigue. Another limitation of the lactic acid system that relates to its anaerobic quality is that only a few moles of *ATP* can be resynthesized from the breakdown of sugar as compared to the yield possible when oxygen is present. For example, only three moles of *ATP* can be manufactured from the anaerobic breakdown

of 180 *g* of glycogen (glycogen is the storage from glucose or sugar in the muscle). As we will soon see, the aerobic breakdown of 180 *g* of glycogen results in enough energy to resynthesize 39 *moles* of *ATP*!

The lactic acid system, like the *ATP* – *PC* system, is extremely important to us, primarily because it too provides for a rapid supply of *ATP* energy. For example, exercises that are performed at maximum rates for between 1 *min* and 3 *min*, such as sprinting 400 *m* and 800 *m*, depend heavily upon the lactic acid system for *ATP* energy. Also, in some performances, such as running 1500 *m* or a mile, the lactic acid system is used predominantly for the ‘kick’ at the end of the race.

**Aerobic System.** In the presence of oxygen, the complete breakdown of 180 *g* of glycogen to carbon dioxide ( $CO_2$ ) and water ( $H_2O$ ) yields enough energy to manufacture 39 *moles* of *ATP*. This series of reactions, like the anaerobic series, takes place within the muscle cell, but is confined to specialized subcellular compartments called mitochondria. Mitochondria are slipper-shaped cell bodies often referred to as the ‘powerhouse’ of the cell because they are the seat of the aerobic manufacture of *ATP* energy. Muscle cells are rich with mitochondria.

The aerobic breakdown of carbohydrates, fats, and even proteins provides energy for *ATP* resynthesis:  $ADP + P_i \rightarrow ATP$ . Since abundant *ATP* can be manufactured without yielding fatiguing by-product, the aerobic system is most suited for endurance activities. The carbon dioxide that is produced diffuses freely from the muscle cell into the blood and is carried to the lung, where it is exhaled. The water that is formed is useful within the cell itself, since the largest constituent of the cell is, in fact, water.

Another feature of the aerobic system that should be noticed is that concerned with the type of foodstuff required for breakdown. Not only glycogen but fats and proteins as well can be aerobically broken down to carbon dioxide and water, with energy released for *ATP* synthesis. For example, the breakdown of 256 *g* of fat will yield 130 *moles* of *ATP*. During exercise, both glycogen and fats, but not protein, are important sources of *ATP*-yielding energy.

The amount of oxygen we need to consume from the environment in order to synthesize one mole of *ATP* is approximately 3.5*l* if glycogen is the food fuel and about 4.0*l* with fat. At rest, most of us consume between 0.2*l* and 0.3*l* of oxygen per minute. In other words, a mole of *ATP* is aerobically manufactured every 12 *min* to 20 *min* under normal resting conditions. During maximal exercise, a mole of *ATP* can be aerobically



supplied to the working muscles every minute by most of us. For the highly trained endurance athlete, more than 1.5 *moles* of *ATP* can be aerobically synthesized and supplied to the muscles every minute during maximal effort.

In summary, then, the aerobic system is capable of utilizing both fats and glycogen for resynthesizing large amounts of *ATP* without simultaneously generating fatiguing by-products. Therefore, the aerobic system is particularly suited for manufacturing *ATP* during prolonged, endurance-type activities. For example, during marathon running, approximately 150 *moles* of *ATP* are required over 2.5 *h* the race takes. Such a large, sustained output of *ATP* energy is possible only because early fatigue can be avoided and large amounts of food (glycogen and fats) and oxygen are readily available.

**Energy Continuum Concept.** Therefore, *ATP* is immediate form of muscular energy, and is supplied in three ways:

- (1) by the stored phosphagens, *ATP* and *PC*;
- (2) by the lactic acid system (anaerobic glycolysis); and
- (3) by the oxygen, or aerobic, system. And ability of each system to supply the major portion of the *ATP* required in any given activity is related to the specific kind of activity performed.

For example, in short-term, high-intensity types of activities, such as the 100 *m* dash, most of the *ATP* is supplied by the readily available phosphagen system. In contrast, longer-term, lower intensity types of activities, such as the 42.2 *km*—marathon, are supported almost entirely by oxygen, or aerobic, system.

In the middle range of activities are those tasks that rely heavily on the lactic acid system for *ATP* production – e.g., the 400 *m* and 800 *m* dashes. Also in the middle are those activities that require a blend of both anaerobic and aerobic metabolism – e.g., the 1500 *m* and mile runs. In these latter activities, the anaerobic systems supply the major portion of *ATP* during the sprint at both the start and finish of the race, with the aerobic system predominating during the middle or steady-state period of the run.

Just from these examples it can be seen that what is at work in physical activities is an energy continuum, a continuum relating the way in which *ATP* is made available and the type of physical activity performed.

#### 4.7.1.5 Equivalent Muscular Actuator

A single skeletal muscle, (e.g., the triceps brachii muscle, see Figure 4.3), is attached at its *origin* to a large area of bone (the humerus in case of the triceps). At its other end, the *insertion*, it tapers into a glistening white *tendon* which, (in case of the triceps is attached to the ulna). As the triceps contracts, the insertion is pulled toward the origin and the arm is straightened or extended at the elbow. Thus the triceps is an *extensor*. Because skeletal muscle exerts force only when it contracts, a second muscle – a *flexor* – is needed to flex or bend the joint (e.g., the biceps brachii muscle is the flexor of the forearm). Together, they (the biceps and triceps) make up an antagonistic pair of muscles, which we will call forming the *equivalent muscular actuator*. Similar pairs, i.e., equivalent muscular actuators, working antagonistically across other joints, provide for almost all the movement of the skeleton. The equivalent muscular actuator has the role of ‘driver’ in biodynamics. It generates the equivalent muscular torque, which is the *primary cause* of human-like motion [Ivancevic (1991); Ivancevic and Snoswell (2001)].

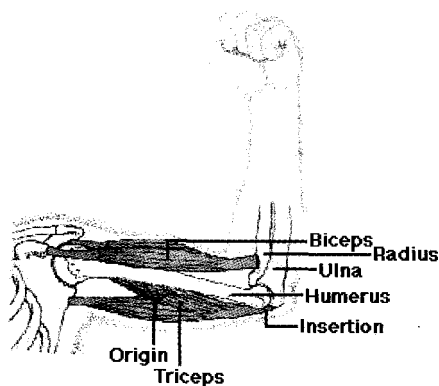


Fig. 4.3 An antagonistic pair of human skeletal muscles, one flexor and the other extensor (in the case of the forearm, biceps brachii and triceps brachii, respectively), forming the *equivalent muscular actuator* – the primary cause of the human-like motion.

#### 4.7.2 Molecular Muscular Dynamics

During muscular contraction the filamentous proteins actin and myosin, interacting via crossbridge cycles, move past one another within sarcom-

eres. A molecular description of this motion in real time involves the notion of *molecular motors* (compare with quantum biodynamics (4.3.1) above). Current models used to describe the properties of molecular motors and the energy transduction process fall under two distinct categories: continuous models [Magnasco (1993); Jülicher *et al.* (1997); Parmegiani *et al.* (1999)] and discrete models [Fisher and Kolomeisky (1999); Lipowsky (2000)]. Both represent a coarse grained description of a very complicated physico-chemical system and the use of one or the other depends on the quantities one is interested in. For example, continuous models are very useful to investigate the role of an external force on chemical kinetics [Lattanzi and Maritan (2001)], since the external force is inserted into the Fokker-Planck equations without any ambiguity. This is no longer true for discrete models, when one has to resort to some *ad hoc* principle or *a priori* reasoning to insert force in transition rates [Fisher and Kolomeisky (1999)]. Nonetheless discrete models present the important advantage of being analytically solvable, as it happens, for instance, in jump processes [Derrida (1983)]. On the other hand, an analytical solution is quite difficult to obtain in the general case of continuous models, and one has to resort to complex numerical integrations.

Also, all quantum models of muscular contraction belong here.

#### 4.7.3 *Mezoscopic Muscular Dynamics*

Skeletal muscle is made up of thousands of cylindrical *muscle fibers* often running all the way from origin to insertion. The fibers are bound together by connective tissue through which run blood vessels and nerves. Each muscle fibre contains numerous contractile elements – *myofibrils* ( $1 - 3 \mu$  in diameter) which are biological machines that utilize chemical energy from metabolism of food in the form of *adenosine triphosphate*, *ATP* hydrolysis to produce mechanical work. An understanding of contractility and muscle function requires, thus, both histo-mechanical and bio-energetic insight (see [Mountcastle (1980); Marieb (1998); Wikipedia (2005); Gowitzke and Milner (1988); Ivancevic and Snoswell (2000)]).

Contractile machinery unit of the myofibril, *sarcomere* ( $1.5 - 3.5 \mu$  long; on electron microscope it is seen as bounded by two *Z* lines, with *H* zone in the middle of the *A* band) is constituted of a great number of longitudinal protein filaments of two kinds: thick *myosin* filaments (about  $120 \text{ \AA}$  in diameter and about  $1.8 \mu$  long; they are located in the center of the sarcomere arranged in a hexagonal array about  $450 \text{ \AA}$  apart) and thin *actin*

filaments (about  $80 \text{ \AA}$  in diameter and about  $1.0 \mu$  long; they are anchored into the transverse filaments forming the Z line). Each myosin filament is surrounded by six actin filaments. Each myosin filament has two heads and two projections from opposite sides at about  $143 \text{ \AA}$  intervals along its length (see Figure 4.4).

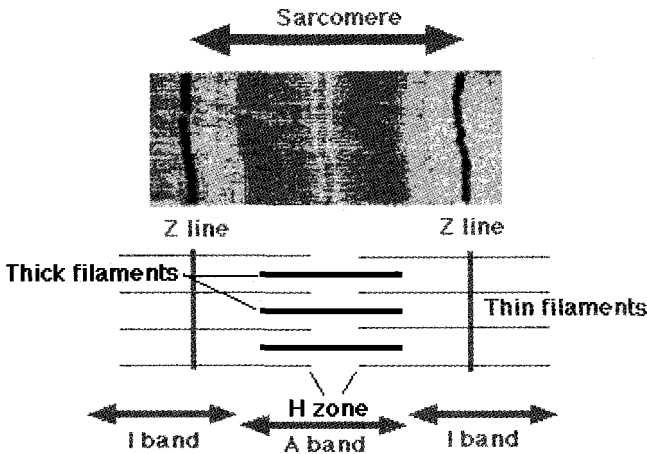


Fig. 4.4 Myofibrillar functional unit sarcomere.

Essential for the contraction process are *cross bridges*. They extend from myosin filaments to touch one of the adjacent actin filaments. Each thin filament receives cross bridges from the three adjacent thick filaments. During shortening the two sets of interdigitating filaments slide with respect to each other, cross and finally overlap each other. This process of muscle shortening involving progressive interdigitation of the two sets of protein filaments represents the *sliding filament mechanism*, discovered and mathematically formulated as a *microscopic theory of muscular contraction* in 1957, by Nobel Laureate Andrew F. Huxley [Huxley and Niedergerke (1954); Huxley (1957)].

According to Huxley, the myosin heads and cross bridges are elastic elements with a mechanism for attaching themselves transiently to specific sites on the thin filaments. The following cyclic events take place during muscular contraction:

- (1) The cross bridges extend from myosin filaments and attach themselves to specific sites on actin filaments. The probability that attachment

will occur is  $f(x)$ , where  $x$  is the instantaneous distance between the equilibrium position (0) and the maximum distance  $h$  for attachment along the myofibrillar axis.

(2) The cross bridges detach with probability  $g(x)$ .

If we let  $N$  equal the density of cross bridges and  $n$  the fraction of cross bridges that are attached, then  $nN$  equals the density of attached cross bridges. Huxley's rate equation for cross-bridge attachment-detachment, i.e., the *sliding filament model* of muscular contraction is now given by:

$$\dot{n} = f(x)[1 - n(x, t)] - g(x)n(x, t) = f(x) - [f(x) + g(x)]n(x, t). \quad (4.135)$$

Huxley's model (4.135) leads to expressions for the force developed by the cross bridges. For an *isometric steady-state contraction* the *contraction tension* or *contraction force* is given by:

$$F_0 = 0.5 N h^2 \frac{kf}{f + g}, \quad (4.136)$$

where  $k = k(x)$  is the stiffness of the cross-bridge spring. For *isotonic* steady states it recovers the classical *Hill's force-velocity* relation (4.137). The *static force* expression says that the force (or tension) generated in the muscle is the function of the interfilamentar overlap, and its maximum is about the middle of the shortening, where the acto-myosin overlap is maximal. This is the so-called *parabolic length-tension curve* of muscular contraction.

The classical *force-velocity relation* of muscular contraction was discovered in 1938 by Nobel Laureate Archibald V. Hill [Hill (1938)] in his thermodynamic studies of muscular work, and put into the basis of *macroscopic muscle-load dynamics*. Hill's celebrated *hyperbolic force-velocity curve* has the equation:

$$(F + a)v = (F_0 + F)b, \quad (4.137)$$

and says that the muscle force is greatest in isometric conditions (without motion), while the velocity of shortening is maximal without external load; in other words, muscle is either 'strong' or 'fast', but no both. Constants  $a$  and  $b$  correspond respectively to the energy dissipated during the contraction and the velocity of the chemo-mechanical processes.

Hill showed that energy change in muscle during contraction can be described by the following *thermodynamic relation*:

$$U = A + W + M, \quad (4.138)$$

where  $U$  is the total energy change associated with contraction,  $A$  is the *activation heat* (i.e., the heat production associated with the activation of the contractile elements),  $W$  is the mechanical work performed by the muscle by lifting a load,  $\alpha\Delta x$  is the *shortening heat*, and  $M$  is the *maintenance heat of contraction*.

The activation heat begins and is almost completely liberated before any tension is developed, i.e., it is predominantly connected with the excitation-contraction coupling process, and corresponds in time to the *latency relaxation* of muscle. It is associated with the internal work required to transform the contractile elements from the resting to the active state. Part of the activation heat probably is associated with a change in the elastic properties of muscle, but about two thirds of it is associated with the release of  $Ca^{++}$  ions from the triads, its binding by troponin and the subsequent rearrangement of the thin filament proteins. The activation heat is greatest for the first twitch after a period rest and becomes smaller with succeeding twitches.

The maintenance heat begins at about the time tension begins and can be divided into two parts: the labile maintenance heat and the stable maintenance heat. For isometric contractions at shorter than rest length, both the labile and the stable heats diminish. For stretched muscle, the labile heat is approximately constant, whereas the stable heat diminishes with stretching and is roughly proportional to the degree of interfilamentar overlap. The stable heat has quite different values in functionally different muscles; it is low when the muscle maintains tension efficiently and vice versa.

The shortening heat is proportional mainly to the distance of shortening and does not depend greatly on the load, the speed of shortening, or the amount of work performed. Since mechanical work is  $W = P\Delta x$ , substituting this in the above thermodynamic relation (4.138) gives the *muscular heat equation*:

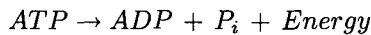
$$U = A + (P + \alpha)\Delta x + M.$$

From the analogy of the term  $(P + \alpha)$  in the heat equation (4.137) and the term  $(P + a)$  in the force-velocity equation (4.136), Hill was able to show a rough equivalence between the coefficient of the shortening heat  $\alpha$  and the force-velocity constant  $a$ . The shortening heat is greatest for the first twitch after a period of rest and is less for subsequent twitches.

Last, note should be made of *thermoelastic heat*. Generally speaking, resting muscle has rubberlike thermoelastic properties, whereas actively

contracting muscle has springlike thermoelastic properties. During the development of tension the change in elastic properties is accompanied by an absorption of heat by the muscle. As tension falls during relaxation, an equivalent amount of heat is released by the muscle owing to its elastic properties. The various kinds of muscle heat must be corrected for the thermoelastic heat. However, for a complete cycle of contraction and relaxation, the net heat produced by thermoelastic mechanisms is zero.

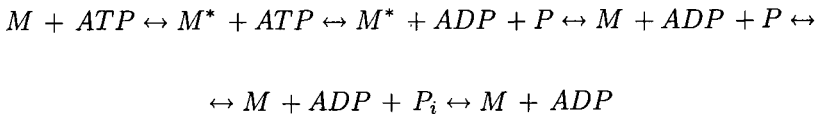
The immediate energy source for contraction in human muscles is adenosine triphosphate ATP (see e.g., [Mountcastle (1980); Marieb (1998)]). Muscle contains about  $2\text{ }\mu\text{mole}$  ATP/gram wet weight. The myosin head is the only site of the major ATP hydrolysis in active muscle. At the concentrations of ATP, ADP (*adenosine diphosphate*), and  $P_i$  (*inorganic phosphate*) present in the sarcoplasm, ATP hydrolysis yields about  $11.5\text{ kcal/mole}$ . About  $0.3\text{ }\mu\text{mole}$  of ATP/gram muscle is hydrolyzed by a single muscle twitch. The ATP hydrolysis overall scheme:



represents actually the complex 6-step chain-reaction  $\{k_i\}$ , ( $i = 1, \dots, 5$ ), which can be summarized as follows:

- (1) Myosin reacts rapidly with ATP to form a complex; the myosin is from its resting (low-energy) form converted to an energy-rich form.
- (2) While complexed to the myosin, ATP is hydrolyzed to ADP and  $P_i$ . Reaction 2 is much more rapid than reaction 1. (This step is extremely temperature sensitive).
- (3) In reaction 3, while the ADP and  $P_i$  are still attached to the myosin, the latter is converted to a low-energy form. This step is slow, rate limiting in the sequence of reactions, and insensitive to temperature changes.
- (4) Reactions 4 and 5 are rapid.

Therefore, the reaction sequence proceeds as follows:



where  $M$  is myosin in low-energy form,  $M^*$  is myosin in energy-rich form, and symbol  $\leftrightarrow$  actually represents a pair of reversible reactions  $\{k_i, k_{i-1}\}$ , ( $i = 1, \dots, 5$ ).

Muscles also contain about  $20\ \mu\text{mole CP/gram}$  (*creatine phosphate*). Creatine phosphate can phosphorylate ADP to form ATP in a reversible reaction catalyzed by the enzyme *creatine kinase*.

Muscle contains large amounts of creatine kinase; it amounts to more than 25 percent of the soluble cytoplasmic protein. As soon as ATP is hydrolyzed, the ADP formed is very rapidly rephosphorylated by CP and the ATP is regenerated. Thus CP forms a reservoir of energy-rich phosphate bonds to quickly replenish the sarcoplasmic ATP.

Ultimately, ATP is produced by *glycolysis* and respiration [Mountcastle (1980)]. In glycolysis (the so-called *Meyerhof pathway*, named after Nobel Laureate Otto F. Meyerhof), glucose is degraded to pyruvate, or to lactic acid in the absence of  $O_2$ , yielding 2 moles *ATP/mole* glucose metabolized. Intracellular glycogen granules provide a very readily available source of glucose. Muscles normally contain 9 to 16 gm/kg glycogen or, for a well-fed man of average height and weight, the total glycogen stores in muscle amount to 300 – 500 *gram*, with another 55 – 90 *gram* in the liver. Glycogen breakdown in muscle begins immediately on stimulation, and the amount of muscle glycogen depleted is proportional to the mechanical work done. Glycogen is hydrolyzed by the enzyme phosphorylase to *glucose-1-phosphate*, which then enters the glycolytic pathway.

*Red muscle fibers* respond to a stimulus with a relatively slow twitch (maximum shortening velocity about 17 mm/sec) and therefore are also called *slow fibers*, whereas *white muscle fibers* react to a stimulus with a rapid twitch (maximum shortening velocity about 42 mm/sec) and therefore are also called fast fibers. Red muscle has a more extensive blood supply than white muscle. Red muscle fibers are able to sustain activity for long periods of time whereas white muscle fibers characteristically produce short bursts of great tension followed by the rapid onset of fatigue.

Whole red and white muscles differ in *ATPase* activity, and, indeed, the purified contractile protein myosin extracted from red and white muscle differs in *ATPase* activity, a finding associated with different myosin light chains. White muscle and white muscle actomyosin show the greater *ATPase* activity. The innervation of red and white muscle differs, and, indeed, whether a given muscle is red or white results from trophic influences of the motor nerve.

Slow muscle fibers are generally thinner and possess many sarcosomes (mitochondria) containing large amounts of respiratory enzymes, as well as copious quantities of the  $O_2$ -carrying protein *myoglobin* in the sarcoplasm and many lipid droplets. The numerous sarcosomes and high level of myo-



globin give slow fibers their red color. Fast (or white) muscle fibers, on the other hand, are generally of larger diameter and contain large amounts of phosphorylase and glycolytic enzymes and large deposits of glycogen. Slow muscles derive energy predominantly from respiration, whereas in fast muscle fibers, glycolysis and lactate production are more prominent.

#### 4.7.3.1 *Myocybernetics*

In the series of papers, H. Hatze (see [Hatze (1977a); Hatze (1978); Hatze (1980)]) presented his *myocybernetic* model of the human skeletal muscle. In brief it can be divided into *excitation dynamics* and *contraction dynamics*. The excitation dynamics of a single muscle fibre stimulated by trains of normalized nerve impulses  $\alpha(t)$  is represented by the system

$$\ddot{\beta} + c_4\dot{\beta} + c_5\beta = c_6V_N\alpha(t), \quad \beta(0) = \dot{\beta}(0) = 0, \quad (4.139)$$

$$\ddot{\gamma} + (c_1\dot{\gamma} + c_2\gamma)/\rho^*(\xi) = c_3V_T\beta(t), \quad \gamma(0) = \dot{\gamma}(0) = 0,$$

$$\delta\dot{q} = d_1\{d_2[1 - k^2(\xi)][h(\dot{x}) - 1/(1 - q_0)] - \delta q\} \delta q(t_s) = 0,$$

where  $\rho^*(\xi)$  is *normalized Ca density function*,  $k(\xi)$  is *filamentary-overlap function*,  $h(\dot{x})$  is *velocity-dependence function*;  $c_1, \dots, c_6, d_1, d_2, V_N, V_T, q_0$  are defined constants;  $V_T\beta(t)$  is *action potential* as appearing in the interior of the  $T$ -system of the fibre, while  $\gamma(t)$  denotes the *free Ca-ion concentration* in the interfilamentary space; the variable  $\delta q$  expresses the *stretch potentiation* induced by an elongation of the tetanized fibre.

The variable  $\xi$  designates the *normalized length of the contractile element* of the fibre, and is defined by the contraction dynamics, i.e., by

$$\dot{\xi} = a_1[1/a_2 \arcsin h a_3 \ln(\frac{q^*k(\xi)}{b_2[f^{SE}/\bar{f} + b_1k_1(\xi)]} - a_4)] - \frac{1}{2}, \quad \xi(0) = \xi_0,$$

where  $a_1, \dots, a_4, b_1, b_2$  are defined constants,  $f^{SE}/\bar{f}$  is the *normalized force* across the *series elastic element*,  $b_1k_1(\xi)$  is the *passive sarcomere tension*, and  $q^*$  is the *active state*.

#### 4.7.4 *Macroscopic Muscular Dynamics*

##### 4.7.4.1 *Soft Tissue Dynamics of Relaxed Muscles*

**Statics of Relaxed Muscular Tissue.** Internal statics of relaxed muscular tissue can be represented as a *stress-strain* relation at each point of

the muscle tissue.

Let  $\Omega$  be the internal domain occupied by a skeletal muscle before its deformation. This domain is decomposed into a mesh of carefully selected spring elements. Using variational principles to minimize the potential energy of the whole muscle tissue, one gets a system of the form:

$$[\mathbf{K}]\{\mathbf{u}\} = \{\mathbf{f}\}, \quad (4.140)$$

where  $[\mathbf{K}]$  is *muscular stiffness matrix*,  $\{\mathbf{u}\}$  is the unknown *displacement vector-field* (i.e., the vector-field representing the displacement of every muscle point; otherwise it is called strain, or deformation), and  $\{\mathbf{f}\}$  is the *force vector-field* (i.e., the vector-field of internal and external forces applied to all muscle points; otherwise it is called stress, or load). Given the force vector-field  $\{\mathbf{f}\}$ , the finite element (FE) method computes the displacement vector-field  $\{\mathbf{u}\}$  over a mesh spanning the region  $\Omega$ .

**Dynamics of Relaxed Muscular Tissue.** Internal dynamics of relaxed muscular tissue can be represented as a dynamic extension of the static stress-strain relation at each point of the muscle tissue.

A *Lagrangian dynamics extension* of the stiffness equation (4.140) gives a *hyperbolic-parabolic* equation for internal structural dynamics of relaxed muscular tissue

$$[\mathbf{M}]\{\ddot{\mathbf{u}}\} + [\mathbf{C}]\{\dot{\mathbf{u}}\} + [\mathbf{K}]\{\mathbf{u}\} = \{\mathbf{f}\}, \quad (4.141)$$

where  $[\mathbf{M}]$  is the *consistent mass matrix*,  $[\mathbf{C}]$  is the *viscous damping matrix*,  $\{\dot{\mathbf{u}}\}$ , the first time derivative (i.e., rate of change with respect to time) of the displacement vector-field is the *velocity vector-field*, and  $\{\ddot{\mathbf{u}}\}$ , the second time derivative of the displacement, gives the *acceleration vector-field*.

To iteratively solve (4.141), we use a *time recurrence formula*, in which given  $\{\mathbf{u}_n\}$ ,  $\{\dot{\mathbf{u}}_n\}$  and  $\{\ddot{\mathbf{u}}_n\}$  at time point  $t_n$ , we seek the solutions of  $\{\mathbf{u}_{n+1}\}$ ,  $\{\dot{\mathbf{u}}_{n+1}\}$  and  $\{\ddot{\mathbf{u}}_{n+1}\}$  at time  $t_{n+1}$ .

#### Surface and Volume Preservation of Relaxed Muscular Tissue.

External smooth surface of relaxed muscular tissue can be modelled in a computer graphics environment as a *Bernstein-Bézier surface* (see section (3.10.2)), according to the following algorithm:

- (1) Define the generic  $n$ th degree Bernstein-polynomial function, by formula:

$$B_{i,n}(u) = \frac{n!}{i!(n-i)!} u^i (1-u)^{n-i}.$$

- (2) Define the Bezier surface  $\mathbf{S}(u, v)$  (summing from 0 to  $n$  and  $m$ ):

$$\mathbf{S}(u, v) = B_{i,n}(u) B_{j,m}(v) \mathbf{P}_{ij},$$

where  $\mathbf{P}_{ij}$  is the  $(n+1) \times (m+1)$ -closed control mesh to which the FE-springs are attached.

- (3) Calculate the muscular tissue volume as a double integral of the Bezier surface:

$$\mathbf{V}[\mathbf{S}(u, v)] = \int_0^n \int_0^m \mathbf{S}(u, v) dv du.$$

- (4) Keep the time derivative of the muscle's volume zero:  $\dot{\mathbf{V}} = 0$ , during its free-form deformation, to preserve its volume.

**Muscular Lagrangian Dynamics in the NURBS-Solid Framework.** A NURBS solid of degree  $p$  in the  $u$  direction, degree  $q$  in the  $v$  direction, and degree  $r$  in the  $w$  direction is a 3-variate vector-valued piecewise rational function of the form (summing from 0 to  $n, m, l$ )

$$\mathbf{X}(u, v, w) = R_{i,j,k}(u, v, w) \mathbf{P}_{i,j,k} \quad (4.142)$$

with piecewise rational basis functions

$$R_{i,j,k}(u, v, w) = \frac{N_{i,p}(u) N_{j,q}(v) N_{k,r}(w) w_{i,j,k}}{N_{i,p}(u) N_{j,q}(v) N_{k,r}(w) w_{i,j,k}}. \quad (4.143)$$

The  $\{\mathbf{P}_{i,j,k}\}$  form a 3-directional control net, the  $\{w_{i,j,k}\}$  are the weights, and the  $\{N_{i,p}(u)\}$ ,  $\{N_{j,q}(v)\}$  and  $\{N_{k,r}(w)\}$  are the nonrational B-spline basis functions defined on the knot vectors  $\{U, V, W\}$  (see [Piegl and Tiller (1997)]).

For the geometric modelling of virtual muscles we can use periodic NURBS  $N_{j,q}(v) = N_{j,q}(v + \text{phase})$  along the parameter  $v$  to produce closed isoparametric curves about the muscles central axis.

Although the shape of the NURBS solid is defined by its control lattice  $\mathbf{P}$ , the control points  $\mathbf{P}_{i,j,k}$  do not necessarily lie on the solid. Therefore, we can define an alternate but equal number of points,  $\mathbf{S} = \mathbf{S}_{i,j,k}$ , corresponding to spatial points evaluated at particular material coordinates. A linear system

$$\beta \mathbf{P} = \mathbf{S} \quad (4.144)$$

can be formed from Equations (4.142, 4.143), providing a way of finding the control points  $\mathbf{P}_{i,j,k}$  for a given set of  $\mathbf{S}_{i,j,k}$ . The sparse matrix  $\beta$

contains NURBS basis functions, similar to  $(N_{i,p}(u), N_{j,q}(v), N_{k,r}(w))$ , but evaluated at different material coordinates. In practice, the LU factors of  $\beta$  are pre-computed so as to solve (4.144) quickly and repeatedly for different  $\mathbf{S}_{i,j,k}$ . The spatial points  $\mathbf{S}_{i,j,k}$  allow us to associate mass properties with each of these points so that forces can be applied to them. In particular, the spatial points  $\mathbf{S}_{i,j,k}$  can be digitized directly from image data or muscle specimens.

Now, applying the Lagrangian equations to the spatial NURBS points  $\mathbf{S} = \mathbf{S}_{i,j,k}$ , in the same way as in the case of the B-spline solids, we get the equation of motion of the NURBS solid continuum,

$$\mathbf{M} \ddot{\mathbf{S}} = \mathbf{f}_s - \nabla_s V_{vol} + \mathbf{f}_d,$$

where  $\mathbf{M}$  is the diagonal mass matrix,  $\mathbf{f}_s$  is a vector of external forces applied to its corresponding components in  $\mathbf{S}$ , and  $\nabla_s V_{vol}$  is the gradient vector of the volume-preserving potential energy function  $V_{vol} = V_{vol}(\mathbf{S})$  which is itself defined by introducing a rest volume  $V_0$  (the desired volume to hold constant). A damping force  $\mathbf{f}_d$ , proportional to the velocity  $\dot{\mathbf{S}}$  of the spatial points  $\mathbf{S}$ , is applied to dampen oscillations and simulate energy loss caused by internal friction in the virtual musculo-tendons. As Lagrangian equations are simulated, at each time-step we also solve for  $\mathbf{P}_{i,j,k}$  to get the final NURBS-solid shape.

#### 4.7.4.2 Classical Hill's Model

In a seminal paper [Hill (1938)], A.V. Hill proposed a three-element model of the skeletal muscle-tendon complex (see Figure 4.5), which still remains the basis of *muscular mechanics*. In this model the length-tension property of muscle is represented by an active contractile element (CE) in parallel with a passive elastic element. Total isometric muscle force is assumed to be the sum of muscle force when it is inactive (passive) and when it is maximally excited (active). The muscle is in series with tendon, which is represented by a nonlinear spring. Pennation angle ( $\alpha$ ) is the angle between tendon and muscle fibers. Tendon slack length is the length of tendon at which force initially develops during tendon stretch. The model was scaled to represent each muscle by specifying the muscle's peak force, optimal fiber length, tendon slack length, and pennation angle based on data collected in anatomical experiments (see [Delp *et al.* (1998)]).

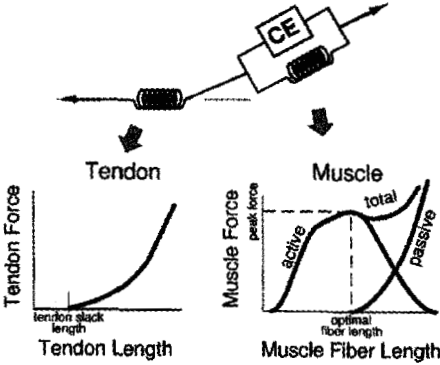


Fig. 4.5 Hill's model of the skeletal muscle-tendon complex (see text for explanation).

4.7.4.3 *Biodynamics of Load-Lifting*

As a simple practical example of the basic biodynamics equations (2.26–2.27), we have a 9 DOF, muscle-driven, lumped-spinal biodynamic model for 3D *symmetrical load-lifting* (see Figure 4.6; for biomechanical details, see [Ivancevic and Snoswell (2001)]).

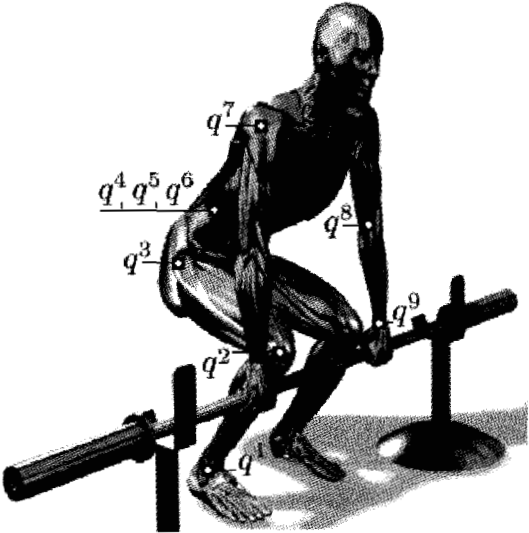


Fig. 4.6 A 9-DOF, muscle-driven, lumped-spinal biodynamic model for 3D symmetrical load-lifting.

The model is formulated under the following assumptions.

- Mechanical assumptions:

- (1) 3D load-lifting with symmetrical-hands is considered;
- (2) All described joint motions, except L5/S1 swivel-joint, are reduced to uniaxial,  $SO(2)$  rotational groups;
- (3) Distributed-parameter spine dynamics (according to the ergonomics literature) is represented by the lumped L5/S1 swivel-joint dynamics, and further decomposed into 3 uniaxial rotations: flexion-extension in the sagittal plane, lateral bending in the frontal plane and twisting in the horizontal plane; and
- (4) In each  $SO(2)$ -joint an *equivalent muscle torque* is generated by an antagonistic muscle-pair of flexor-extensor type. Input variables are equivalent muscle torques and output variables are time evolutions of joint angles and associated angular momenta.

- Anatomical assumptions:

Humanoid's joint-angles (see Figure 4.6) are defined as:  $q^1$  - ankle (flexion-extension),  $y$  - knee (flexion-extension),  $q^3$  - hip (flexion-extension),  $q^4$  - L5/S1-sagittal plane (flexion-extension),  $q^5$  - L5/S1-horizontal plane (twisting),  $q^6$  - L5/S1-frontal plane (lateral flexion),  $q^7$  - shoulder (flexion-extension),  $q^8$  - elbow (flexion-extension), and  $q^9$  - wrist (flexion-extension).

- Biomechanical assumptions:

The global load lifting-dynamical system can be separated into 3 parts:

- (1) Pure mechanical, rigid skeleton dynamics, defining conservative motion of body segments influenced by inertial, gravitational and Coriolis forces;
- (2) Active muscular (force-velocity-time) biodynamics, defining the excitation/contraction synergy of representative (i.e., equivalent) skeletal muscles;
- (3) Passive nonlinear joint damping, representing anatomical-synovial dissipation.

Under above assumptions, basic biodynamics equations (2.26–2.27), in vector form, read

$$\dot{\mathbf{q}} = \partial H / \partial \mathbf{p} + \partial R / \partial \mathbf{p}, \quad (4.145)$$

$$\dot{\mathbf{p}} = \mathbf{F} - \partial H / \partial \mathbf{q} + \partial R / \partial \mathbf{q}. \quad (4.146)$$

Without active muscular drives (i.e., for  $\mathbf{F} = 0$ ), the system (4.145–4.146) reduces:

- (1) with  $R = 0$ , to the conservative Hamiltonian system;
- (2) with  $H = 0$ , to the pure gradient system;

**Momentum Phase-Space.** The joint-angles  $q^i$  (Figure 4.6) now all represent the plane-rotational Lie-groups  $SO(2)^i$  ( $i = 1, \dots, 9$ ), and their 9-times tensor product gives a 9D torus  $T^9$ , which is an Abelian Lie group of all nondegenerate diagonal  $9 \times 9$ -matrices.

Consequently, the load lifting momentum phase-space is defined as an 18D cotangent bundle  $T^*T^9$ , including both the joint angles  $\mathbf{q} = q^i$  and the corresponding angular momenta  $\mathbf{p} = p_i$ , the canonically conjugate variables which are infinitesimal generators of joint rotations and consequently belong to the cotangent Lie-algebras  $so(2)_i^*$ ; otherwise they represent the impulses of the total joint-torques:

$$\mathbf{p} = \int_{t_0}^{t_1} \left( \mathbf{F}(\tau, \mathbf{q}, \mathbf{p}) - \frac{\partial H}{\partial \mathbf{q}} + \frac{\partial R}{\partial \mathbf{q}} \right) d\tau.$$

Thus, the biodynamics configuration manifold  $M$  is now reduced to the 9D torus  $T^9$  (with the active joint angles depicted on Figure 4.6) and the biodynamics momentum phase-space manifold  $T^*M$  is now reduced to the 18D cotangent bundle  $T^*T^9$ .

**Conservative Skeleton Dynamics.** On the load-lifting momentum phase-space manifold  $M = T^*T^9$  we have the natural action of the autonomous Hamiltonian (kinetic energy  $T$  plus potential energy  $V$ ) generating function  $H : M \rightarrow \mathbb{R}$ . The biodynamics Hamiltonian vector-field  $X_H$  on  $M$ , representing the conservative dynamical system of load-lifting, is now defined as  $X_H = (\partial H / \partial \mathbf{p}, -\partial H / \partial \mathbf{q})$ , representing the infinitesimal generator of the action  $\phi_t$  of the one-parameter group  $G_1$  of canonical diffeomorphisms on  $M$ , i.e., *autonomous conservative (symplectic) phase-flow*

$$\begin{aligned} \phi_t : G_1 \times M &\rightarrow M : (p(0), q(0)) \rightarrow (p(t), q(t)), \\ (\phi_t \circ \phi_s &= \phi_{t+s}, \quad \phi_0 = \text{identity}), \end{aligned} \quad (4.147)$$

determined by autonomous, conservative Hamilton's equations (in vector notation)

$$\dot{\mathbf{q}} = \partial H / \partial \mathbf{p}, \quad \dot{\mathbf{p}} = -\partial H / \partial \mathbf{q}.$$

To determine potential and kinetic energies, we define the two corresponding position vectors  $r_j^V$  and  $r_j^T$ , respectively

$$r_j^V = \sum_{j=1}^9 \sum_{i=1}^j \sigma_i L_i (1 - \cos q^i), \quad r_j^T = \sum_{j=1}^9 \sum_{i=1}^j L_i \cos q^i,$$

where  $\sigma = [-1, -1, -1, -1, 0, -1, 1, 1, 1]$  and  $L_i$  denote humanoid's segmental lengths. Using  $r_j^V$  and  $r_j^T$ , we get for the potential energy

$$V(q) = g m_j r_j^V,$$

(where  $g$  denotes gravitational acceleration, and  $m_i$  are segmental masses) and for the kinetic energy

$$T(q, p) = \frac{1}{2} g^{ij}(q) p_i p_j = \frac{1}{2} \left\{ [m_i (r_j^T)^2]^{-1} + [J_i]^{-1} \right\} p_i p_j,$$

where  $g^{ij} = g^{ij}(q, m)$ , corresponding to the term in the curly braces, is the contravariant metric tensor (i.e., inverse inertia matrix).

The autonomous conservative Hamilton's equations are derived (using the computer-algebra algorithm, see (A.7.1) in the Appendix) in the following expanded form

$$\dot{q}^i = p_i \left\{ [J_i]^{-1} + \left[ m_i \left( \sum_{k=1}^i L_k \cos q^k \right)^2 \right]^{-1} \right\}, \quad (4.148)$$

$$\begin{aligned} \dot{p}_i = & -g \sum_{k=i}^{10-i} L_k m_k \sin q^k \\ & - \sum_{k=i}^{10-i} L_k \sin q^k p_i p_k \left[ m_i \left( \sum_{k=1}^i L_k \cos q^k \right)^3 \right]^{-1}. \end{aligned} \quad (4.149)$$

The basic characteristic of the conservative Hamiltonian system (4.148–4.149) is that its symplectic phase-flow  $\phi_t$  (4.147) consists of canonical transformations *preserving the phase-space volume*, i.e., *Liouville measure*  $\text{vol}$ , defined as

$$\text{vol} = dq^1 \wedge \dots \wedge dq^9 \wedge dp_1 \wedge \dots \wedge dp_9,$$

as proposed by the Liouville theorem (see [Arnold (1989)]).

However, the preservation of volume *causes structural instability* of the conservative Hamiltonian system (4.148–4.149), i.e., the *phase-space*



*spreading effect* by which small phase regions  $R_t(\in M)$  will tend to get distorted from the initial one  $R_o(\in M)$  (during the conservative Hamiltonian system evolution). The problem is much more serious in higher dimensions than in lower dimensions, since there are so many 'directions' in which the region can locally spread (see [Penrose (1989)]). So, regardless of stability and accuracy of the supposed numerical integrator, the solutions of the conservative ODEs (4.148–4.149) necessarily diverges for any initial angles and momenta, and the flow  $\phi_t$  (4.147) could not be obtained.

**Dynamics of Joints and Muscles.** *Joint dynamics*, is described here by  $(q, p)$ -quadratic form of the *Rayleigh – Van der Pol's dissipation function* (see [Ivancevic and Snoswell (2001)])

$$R = \frac{1}{2} \sum_{i=1}^9 p_i^2 [a_i + b_i(q^i)^2], \quad (4.150)$$

where  $a_i$  and  $b_i$  denote dissipation parameters. Its partial derivatives  $\partial R/\partial p$  give rise to viscous forces in the joints which are linear in  $p_i$  and quadratic in  $q^i$ . It is based on the unforced Van der Pol's oscillator

$$\ddot{x} - (a + b x^2) \dot{x} + x = 0,$$

where the damping force  $F^{dmp}(\dot{x}) = -\partial R/\partial \dot{x}$  is given by the Rayleigh's dissipation function  $R = \frac{1}{2} (a + b x^2) \dot{x}^2$  – with the velocity term  $\dot{x}$  replaced by our momentum term  $p^2$ .

Thus, by including the biquadratic dissipation (4.150) into the symplectic phase-flow  $\phi_t$  (4.147), we try somehow to bound its naturally-unbounded diverging phase-trajectories, and hence to stabilize it in some kind of a *relaxation oscillatory regime*, which is quite natural for both biological and biomechanical systems (see [Ivancevic and Snoswell (2001)]).

*Muscular dynamics*, giving the driving torques  $F_i = F_i(t, q, p)$  for the biodynamics in general, as well as for our load-lifting task in particular, should describe the internal *excitation* and *contraction* dynamics [Ivancevic and Snoswell (2001)] of *equivalent muscular actuators*, anatomically represented by resulting action of *antagonistic muscle-pairs* for each uniaxial (i.e.,  $SO(2)$ ) humanoid joint. We attempt herein to describe the equivalent muscular dynamics in the simplest possible way (e.g., Hatze used 51 nonlinear first-order ODEs to derive his arguably most elaborate, myocybernetic model [Hatze (1978)]), and yet to include the main excitation and contraction relations.

- *Excitation dynamics* can be described by *impulse torque–time relation*

$$\begin{aligned} F_i^{imp} &= F_i^0(1 - e^{-t/\tau_i}) & \text{if stimulation} > 0 \\ F_i^{imp} &= F_i^0 e^{-t/\tau_i} & \text{if stimulation} = 0, \end{aligned}$$

where  $F_i^0$  denote the maximal isometric muscular torques applied at  $i$ -th joint ( $i = 1, \dots, 9$ ), while  $\tau_i$  denote the time characteristics of particular muscular actuators. This is a rotational-joint form of the solution of the Wilkie's *muscular active-state element equation* [Wilkie (1956)]

$$\dot{x} + \beta x = \beta S A, \quad x(0) = 0, \quad 0 < S < 1,$$

where  $x = x(t)$  represents the active state of the muscle,  $\beta$  denotes the element gain,  $A$  corresponds to the maximum tension the element can develop, and  $S = S(\tau)$  is the 'desired' active state as a function of motor unit stimulus rate  $\tau$ .

- *Contraction dynamics* has classically been described by the Hill's *hyperbolic force–velocity relation* [Hill (1938)], which we propose here in the rotational  $(q, p)$ -form

$$F_i^{Hill} = \frac{(F_i^0 b_i - a_i p_i)}{(p_i - b_i)}, \quad (i = 1, \dots, 9),$$

where  $a_i$  (having dimension of torque) and  $b_i$  (having dimension of momentum) denote the *rotational Hill's parameters* (see [Ivancevic and Snoswell (2001)]), corresponding to the energy dissipated during the contraction and the phosphagenic energy conversion rate, respectively.

Therefore, we can describe the excitation/contraction dynamics for the  $i$ -th equivalent muscle-joint actuator, i.e., antagonistic muscle pair (e.g., flexion/extension in the  $i$ -th joint) by the simple impulse-hyperbolic product-relation

$$F_i(t, q, p) = F_i^{imp} \times F_i^{Hill}, \quad (i = 1, \dots, 9).$$

**Total Load–Lifting Dynamics.** In this way, the total load lifting dynamics on  $M = T^*T^9$  is represented by the *dissipative, muscle-driven Hamiltonian phase-flow*

$$\begin{aligned} \phi_{md_t} : G_1 \times M &\rightarrow M : (p(0), q(0)) \rightarrow (p(t), q(t)), & (4.151) \\ (\phi_{md_t} \circ \phi_{md_s} &= \phi_{md_{t+s}}, \quad \phi_{md_0} = \text{identity}), \end{aligned}$$

generated by the Hamiltonian vector-field  $X_H$  on  $M$  given by *dissipative, driven Hamilton's equations* (4.145–4.146).

Here  $G_1$  is the one-parameter Lie group of muscle-driven and dissipative transformations of the momentum phase-space manifold  $M = T^*T^9$ . Therefore, the autonomous Hamiltonian function  $H(q, p) = T(q, p) + V(q)$  is conserved during the load lifting, but the flow  $\phi_{md_t}$  (4.151) is not conserved. This is a biodynamical 'escape' from the Liouville theorem. The dynamical equations (4.145–4.146) can be expanded (using the computer-algebra algorithm, see A.7.1 in the Appendix) as

$$\dot{q}^i = p_i \left\{ [J_i]^{-1} + \left[ m_i \left( \sum_{k=1}^i L_k \cos q^k \right)^2 \right]^{-1} + b_i q^i p_i \right\}, \quad (4.152)$$

$$\begin{aligned} \dot{p}_i = & F_i + p_i \left( a_i + b_i q^{i(2)} \right) - g \sum_{k=i}^{10-i} L_k m_k \sin q^k \\ & - \sum_{k=i}^{10-i} L_k \sin q^k p_i p_k \left[ m_i \left( \sum_{k=1}^i L_k \cos q^k \right)^3 \right]^{-1}. \end{aligned} \quad (4.153)$$

In the velocity-equation (4.152), the terms denote rotational velocities, translational velocities and velocity dampings for the  $i$ th joint ( $i = 1, \dots, 9$ ), respectively. The force-equation (4.153) contains terms of inertial torques (as differences between active-internal muscular torques and passive-external gravitational, Coriolis and centrifugal torques), plus passive-internal joint-damping torques. In the velocity-equation, the last segment-length  $L_i$  should, in every iteration, be replaced by the segmental centre-mass proximal distance  $a_i$ . Also, the  $L_i$ -terms with indices 4, 5, 6 are mutually exclusive; e.g., when vertical lifting is simulated, both  $L_5$  and  $L_6$  are zero. In the force-equation, the gravitational term is zero for the 5th (horizontal twisting) joint.

The system (4.152–4.153) is geometrically analogous to the *redundant manipulator* (a load-body with 6 external DOF, representing the *special Euclidean group of motions* is being lifted using 9 internal DOF – joint angles representing  $SO(2)$  rotational groups). Consequently, to each position of the load-body corresponds an infinite number of angle trajectories. So, the dissipative, driven phase-flow (4.151) has an infinite number of possible trajectories starting within the 'small' region of initial conditions (joint angles and momenta); for this reason, it is extremely sensitive to changes

of anthropomorphic parameters and initial conditions. However, this is the *general characteristics* of the biodynamics [Ivancevic and Snoswell (2001); Ivancevic (1991)]: *many DOF and highly nonlinear synergy even for very simple tasks*. Consequently, the utilization of energy is also mechanically inefficient. However, from the point of view of information and control, it is highly efficient.

## 4.8 Lie Functors in Biodynamics

In this section we present several Lie functors, as they are used in modern biodynamic research, all being different formulations of the *covariant force law*,  $F_i = mg_{ij}a^j$ , and giving different Lie representations of the fundamental *covariant force functor*  $\mathcal{F}_* : TT^*M \rightarrow TTM$  (see section 5.4 below in chapter 5).

### 4.8.1 Lie-Lagrangian Biodynamic Functor

Now we develop the *Lie-Lagrangian biodynamics functor* using a modern, nonlinear formulation of the classical robotics structure:

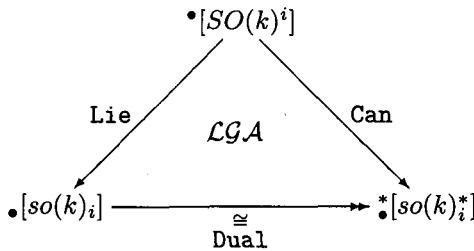
$$\begin{array}{llll} \textit{Kinematics} & \rightarrow & \textit{Dynamics} & \rightarrow & \textit{Control} \\ \textit{Lie groups} & \rightarrow & \textit{Exterior Lagrangian} & \rightarrow & \textit{Lie derivative} \end{array}$$

The conservative part of generalized Lagrangian formalism, as used in biodynamics, is derived from Lagrangian conservative energy function. It describes the motion of the conservative skeleton, which is free of control and dissipation. According to the Liouville theorem, this conservative dynamics is structurally unstable due to the phase-space spreading effect, caused by the growth of entropy (see [Ivancevic (1991); Ivancevic and Snoswell (2001)]). The dissipative part is derived from nonlinear dissipative function, and describes quadratic joint dampings, which prevent entropy growth. Its driving part represents equivalent muscular torques  $F_i$  acting in all DOF (or just in active joints, as used in the affine input control), in the form of in the form of force-time and force-velocity signals.

#### 4.8.1.1 Joint Kinematics

Recall from chapter 3 that human joints represented by internal coordinates  $x^i$  ( $i = 1, \dots, n$ ), constitute an  $n$ D smooth biodynamic configuration

manifold  $M$  (see Figure 3.1). Now we are going to perform some categorical transformations on the biodynamics configuration manifold  $M$ . If we apply the *functor*  $\text{Lie}$  to the *category*  $\bullet[SO(k)^i]$  of rotational Lie groups  $SO(k)^i$  and their homomorphisms we get the category  $\bullet[so(k)_i]$  of corresponding *tangent* Lie algebras  $so(k)_i$  and their homomorphisms. If we further apply the *isomorphic* functor  $\text{Dual}$  to the category  $\bullet[so(k)_i]$  we get the dual category  $\bullet[so(k)_i^*]$  of *cotangent*, or, *canonical* Lie algebras  $so(k)_i^*$  and their homomorphisms. To go directly from  $\bullet[SO(k)^i]$  to  $\bullet[so(k)_i^*]$  we use the canonical functor  $\text{Can}$  [Ivancevic and Snoswell (2001); Ivancevic (2002); Ivancevic (2005)]. Therefore we have a commutative triangle



Both the tangent algebras  $so(k)_i$  and the cotangent algebras  $so(k)_i^*$  contain infinitesimal group generators, angular velocities  $\dot{x}^i = \dot{x}^{\phi_i}$  in the first case and canonical angular momenta  $p_i = p_{\phi_i}$  in the second. As Lie group generators, angular velocities and angular momenta satisfy the respective commutation relations  $[\dot{x}^{\phi_i}, \dot{x}^{\psi_i}] = \epsilon_{\theta}^{\phi\psi} \dot{x}^{\theta_i}$  and  $[p_{\phi_i}, p_{\psi_i}] = \epsilon_{\phi\psi}^{\theta} p_{\theta_i}$ , where the structure constants  $\epsilon_{\theta}^{\phi\psi}$  and  $\epsilon_{\phi\psi}^{\theta}$  constitute totally antisymmetric third-order tensors.

In this way, the functor  $\text{Dual}_G : \text{Lie} \cong \text{Can}$  establishes a geometric duality between kinematics of angular velocities  $\dot{x}^i$  (involved in Lagrangian formalism on the tangent bundle of  $M$ ) and that of angular momenta  $p_i$  (involved in Hamiltonian formalism on the cotangent bundle of  $M$ ). This is analyzed below. In other words, we have two functors  $\text{Lie}$  and  $\text{Can}$  from a category of Lie groups (of which  $\bullet[SO(k)^i]$  is a subcategory) into a category of their Lie algebras (of which  $\bullet[so(k)_i]$  and  $\bullet[so(k)_i^*]$  are subcategories), and a natural equivalence (functor isomorphism) between them defined by the functor  $\text{Dual}_G$ . (As angular momenta  $p_i$  are in a bijective correspondence with angular velocities  $\dot{x}^i$ , every component of the functor  $\text{Dual}_G$  is invertible.)

Applying the functor  $\text{Lie}$  to the biodynamics configuration manifold  $M$  (Figure 1.2 above), we get the product-tree of the same anthropomorphic

structure, but having tangent Lie algebras  $so(k)_i$  as vertices, instead of the groups  $SO(k)^i$ . Again, applying the functor **Can** to  $M$ , we get the product-tree of the same anthropomorphic structure, but this time having cotangent Lie algebras  $so(k)_i^*$  as vertices.

The functor **Lie** defines the *second-order Lagrangian formalism on the tangent bundle*  $TM$  (i.e., the *velocity phase-space manifold*) while the functor **Can** defines the *first order canonical Hamiltonian formalism on the cotangent bundle*  $T^*M$  (i.e., the *momentum phase-space manifold*). As these two formalisms are related by the isomorphic functor **Dual**, they are equivalent. In this section we shall follow the Lagrangian functor **Lie**, using the powerful formalism of exterior differential systems and integral variational principles [Griffiths (1983); Choquet-Bruhat and DeWitt-Morete (1982)]. For the parallel, Hamiltonian treatment along the functor **Can**, more suitable for chaos theory and stochastic generalizations, see [Ivancevic and Snoswell (2001); Ivancevic (2002)].

#### 4.8.1.2 Exterior Lagrangian Dynamics

Let  $\Omega^p(M) = \sum \omega_I dx^I$  denote the space of differential  $p$ -forms on  $M$ . That is, if multi-index  $I \subset \{1, \dots, n\}$  is a subset of  $p$  elements then we have a  $p$ -form  $dx^I = dx_1^{i_1} \wedge dx_2^{i_2} \wedge \dots \wedge dx_p^{i_p}$  on  $M$ . We define the exterior derivative on  $M$  as  $d\omega = \sum \frac{\partial \omega^I}{\partial x_p} dx_p \wedge dx^I$ .

Now, from exterior differential systems point of view (see subsection 3.4.3 above as well as [Griffiths (1983)]), human-like motion represents an  $n$  DOF neuro-musculo-skeletal system  $\Xi$ , evolving in time on its  $nD$  configuration manifold  $M$ , (with local coordinates  $x^i$ ,  $i = 1, \dots, n$ ) as well as on its tangent bundle  $TM$  (with local coordinates  $(x^i; \dot{x}^i)$ ).

For the system  $\Xi$  we will consider a *well-posed variational problem*  $(I, \omega; \varphi)$ , on an associated  $(2n + 1)$ -D jet manifold  $X = J^1(\mathbb{R}, M) \cong \mathbb{R} \times TM$ , with local canonical variables  $(t; x^i; \dot{x}^i)$  (compare with section 4.4 above).

Here,  $(I, \omega)$  is called a *Pfaffian exterior differential system* on  $X$  (see [Griffiths (1983)]), given locally as

$$\begin{cases} \theta^i = dx^i - \dot{x}^i \omega = 0 \\ \omega \equiv dt \neq 0 \end{cases}, \quad (4.154)$$

with the structure equations

$$d\theta^i = -dx^i \wedge \omega.$$

Integral manifolds  $N \in J^1(\mathbb{R}, M)$  of the Pfaffian system  $(I, \omega)$  are locally one-jets  $t \rightarrow (t, x(t), \dot{x}(t))$  of curves  $x = x(t) : \mathbb{R} \rightarrow M$ .

$\varphi$  is a 1-form

$$\varphi = L\omega, \quad (4.155)$$

where  $L = L(t, x, \dot{x})$  is the system's *Lagrangian* function defined on  $X$ , having both coordinate and velocity partial derivatives, respectively denoted by  $L_{x^i} \equiv \partial_{x^i} L$ , and  $L_{\dot{x}^i} \equiv \partial_{\dot{x}^i} L$ .

A variational problem  $(I, \omega; \varphi)$  is said to be *strongly non-degenerate*, or *well-posed* [Griffiths (1983)], if the determinant of the matrix of mixed velocity partials of the Lagrangian is positive definite, i.e.,

$$\det \|L_{\dot{x}^i \dot{x}^j}\| > 0.$$

The *extended Pfaffian system*

$$\begin{cases} \theta^i = 0 \\ dL_{\dot{x}^i} - L_{x^i} \omega = 0 \\ \omega \neq 0 \end{cases}.$$

generates classical *Euler-Lagrange equations*

$$\frac{d}{dt} L_{\dot{x}^i} = L_{x^i}, \quad (4.156)$$

describing the *control-free and dissipation-free, conservative skeleton dynamics*.

If an *integral manifold*  $N$  satisfies the Euler-Lagrange equations (4.156) of a well-posed variational problem on  $X$  then

$$\frac{d}{dt} \left( \int_{N_t} \varphi \right)_{t=0} = 0$$

for any *admissible variation*  $N_t \in N$  that satisfies the *endpoint conditions*  $\omega = \theta^i = 0$ .

**Theorem:** *Under the above conditions, both the Lagrangian dynamics with initial conditions*

$$\begin{cases} \frac{d}{dt} L_{\dot{x}^i} = L_{x^i} \\ x(t_0) = x_0, \quad \dot{x}(t_0) = \dot{x}_0 \end{cases}$$

*and the Lagrangian dynamics with endpoint conditions*

$$\begin{cases} \frac{d}{dt} L_{\dot{x}^i} = L_{x^i} \\ x(t_0) = x_0, \quad x(t_1) = x_1 \end{cases}$$

have unique solutions. For the proof, see [Griffiths (1983)].

Now, if  $M$  is a smooth Riemannian manifold, its metric  $g = \langle \cdot, \cdot \rangle$  is locally given by a positive definite quadratic form (see Appendix as well as chapter 3)

$$ds^2 = g_{ij}(x) dx^i dx^j, \quad (4.157)$$

where the metric tensor is a  $C^k$  symmetric matrix  $g(x) = \|g_{ij}(x)\|$ .

*Kinetic energy* of the system  $\Xi$  is a function  $T = T(x, \dot{x})$  on the tangent bundle  $TM$ , which induces a positive definite quadratic form in each fibre  $T_x M \subset TM$ . In local coordinates, it is related to the Riemannian metric (4.157) by

$$T \omega^2 = \frac{1}{2} ds^2.$$

If potential energy of the system  $\Xi$  is a function  $U = U(x)$  on  $M$ , then the autonomous Lagrangian is defined as  $L(x, \dot{x}) = T(x, \dot{x}) - U(x)$ , i.e., kinetic minus potential energy.

The condition of well-posedness is satisfied, as

$$\det \|L_{\dot{x}^i \dot{x}^j}\| = \det \|g_{ij}(x)\| > 0.$$

Now, the *covariant Euler-Lagrange equations* (4.156) expand as

$$\frac{d}{dt} (g_{ij}(x(t)) \dot{x}^j(t)) = \frac{1}{2} \left( \frac{\partial g_{jk}(x(t))}{\partial x^i} \dot{x}^j(t) \dot{x}^k(t) \right) - F_i(x(t)), \quad (4.158)$$

where  $F_i(x(t)) = \frac{\partial U(x(t))}{\partial x^i}$  denote the *gradient force 1-forms*.

Letting  $\|g^{ij}(x)\|$  be the inverse matrix to  $\|g_{ij}(x)\|$  and introducing the *Christoffel symbols*

$$\Gamma_{jk}^i = g^{il} \Gamma_{jkl}, \quad \Gamma_{jkl} = \frac{1}{2} \left( \frac{\partial g_{kl}}{\partial x^j} + \frac{\partial g_{jl}}{\partial x^k} - \frac{\partial g_{jk}}{\partial x^l} \right)$$

the equations (4.158) lead to the classical *contravariant form* (see [Ivancevic (1991); Ivancevic and Pearce (2001b)])

$$\ddot{x}^i(t) + \Gamma_{jk}^i(x(t)) \dot{x}^j(t) \dot{x}^k(t) = -F^i(x(t)), \quad (4.159)$$

where  $F^i(x(t)) = g^{ij}(x) \frac{\partial U(x(t))}{\partial x^j}$  denote the *gradient force vector-fields*.



The above theorem implies that both the Lagrangian dynamics with initial conditions

$$\begin{cases} \ddot{x}^i(t) + \Gamma_{jk}^i(x(t)) \dot{x}^j(t) \dot{x}^k(t) = -F^i(x(t)) \\ x(t_0) = x_0, \quad \dot{x}(t_0) = \dot{x}_0 \end{cases} \quad (4.160)$$

and the Lagrangian dynamics with endpoint conditions

$$\begin{cases} \ddot{x}^i(t) + \Gamma_{jk}^i(x(t)) \dot{x}^j(t) \dot{x}^k(t) = -F^i(x(t)) \\ x(t_0) = x_0, \quad x(t_1) = x_1 \end{cases} \quad (4.161)$$

have unique solutions. We consider the system (4.160) to be the valid basis of human-like dynamics, and the system (4.161) to be the valid basis of the finite biodynamics control.

Now, recall from chapter 3, that any smooth  $n$ -manifold  $M$  gives rise to an  $n$ -category  $\Pi_n(M)$ , its fundamental  $n$ -groupoid. In  $\Pi_n(M)$ , 0-cells are *points* in  $M$ ; 1-cells are *paths* in  $M$  (i.e., parameterized smooth maps  $f : [0, 1] \rightarrow M$ ); 2-cells are *smooth homotopies* (denoted by  $\simeq$ ) of *paths* relative to endpoints (i.e., parameterized smooth maps  $h : [0, 1] \times [0, 1] \rightarrow M$ ); 3-cells are *smooth homotopies of homotopies* of paths in  $M$  (i.e., parameterized smooth maps  $j : [0, 1] \times [0, 1] \times [0, 1] \rightarrow M$ ). Categorical *composition* is defined by *pasting* paths and homotopies. In this way, the *recursive homotopy dynamics* emerges (see next page).

On the other hand, to describe the biomechanically realistic biodynamics, we have to generalize (4.159), so to include any other type of *external* contravariant forces (including excitation and contraction dynamics of muscular-like actuators, as well as nonlinear dissipative joint forces) to the r.h.s of (4.159); in this way we get the *general form of contravariant Lagrangian dynamics*

$$\ddot{x}^i(t) + \Gamma_{jk}^i(x(t)) \dot{x}^j(t) \dot{x}^k(t) = \mathcal{F}^i(t, x(t), \dot{x}(t)), \quad (4.162)$$

or, in exterior, *covariant* form

$$\frac{d}{dt} L_{\dot{x}^i} - L_{x^i} = \mathcal{F}_i(t, x(t), \dot{x}(t)). \quad (4.163)$$

# Recursive homotopy dynamics:

0 - cell :  $x_0 \bullet \quad x_0 \in M$ ; in the higher cells below:  $t, s \in [0, 1]$ ;

1 - cell :  $x_0 \bullet \xrightarrow{f} \bullet x_1 \quad f : x_0 \simeq x_1 \in M$ ,

$f : [0, 1] \rightarrow M, f : x_0 \mapsto x_1, x_1 = f(x_0), f(0) = x_0, f(1) = x_1$ ;

e.g., linear path:  $f(t) = (1 - t)x_0 + tx_1$ ; or

e.g., Euler-Lagrangian  $f$  - dynamics with endpoint conditions  $(x_0, x_1)$  :

$\frac{d}{dt}f_{\dot{x}^i} = f_{x^i}, \quad \text{with } x(0) = x_0, \quad x(1) = x_1, \quad (i = 1, \dots, n)$ ;

2 - cell :  $x_0 \bullet \begin{array}{c} \xrightarrow{f} \\ \Downarrow h \\ \xrightarrow{g} \end{array} \bullet x_1 \quad h : f \simeq g \in M$ ,

$h : [0, 1] \times [0, 1] \rightarrow M, h : f \mapsto g, g = h(f(x_0))$ ,

$h(x_0, 0) = f(x_0), h(x_0, 1) = g(x_0), h(0, t) = x_0, h(1, t) = x_1$

e.g., linear homotopy:  $h(x_0, t) = (1 - t)f(x_0) + tg(x_0)$ ; or

e.g., homotopy between two Euler-Lagrangian  $(f, g)$  - dynamics with the same endpoint conditions  $(x_0, x_1)$  :

$\frac{d}{dt}f_{\dot{x}^i} = f_{x^i}, \quad \text{and} \quad \frac{d}{dt}g_{\dot{x}^i} = g_{x^i} \quad \text{with } x(0) = x_0, \quad x(1) = x_1$ ;

3 - cell :  $x_0 \bullet \begin{array}{c} \xrightarrow{f} \\ \left( \begin{array}{c} \xrightarrow{h} \\ \Downarrow j \\ \xrightarrow{i} \end{array} \right) \\ \xrightarrow{g} \end{array} \bullet x_1 \quad j : h \simeq i \in M$ ,

$j : [0, 1] \times [0, 1] \times [0, 1] \rightarrow M, j : h \mapsto i, i = j(h(f(x_0)))$

$j(x_0, t, 0) = h(f(x_0)), j(x_0, t, 1) = i(f(x_0))$ ,

$j(x_0, 0, s) = f(x_0), j(x_0, 1, s) = g(x_0)$ ,

$j(0, t, s) = x_0, j(1, t, s) = x_1$

e.g., linear composite homotopy:  $j(x_0, t, s) = (1 - t)h(f(x_0)) + ti(f(x_0))$ ;

or, homotopy between two homotopies between above two Euler-

Lagrangian  $(f, g)$  - dynamics with the same endpoint conditions  $(x_0, x_1)$ .

#### 4.8.2 Lie–Hamiltonian Biodynamic Functor

The three fundamental and interrelated obstacles facing any researcher in the field of human-like musculo-skeletal dynamics, could be identified as [Ivancevic and Snoswell (2001)]:

- (1) *Deterministic chaos*,
- (2) *Stochastic forces*, and
- (3) *Imprecision of measurement* of the system numbers (SN): inputs, parameters and initial conditions.

Recall that the deterministic chaos is manifested as an irregular and unpredictable time evolution of purely deterministic nonlinear systems. If a nonlinear system is started twice, from slightly different initial conditions, its time evolution differs exponentially, while in case of a linear system, the difference in time evolution is linear.

Again, recall that the stochastic dynamics is based on the concept of *Markov stochastic process*<sup>2</sup>, which represents the probabilistic analogue to the deterministic dynamics. The property of a *Markov chain* of prime importance for humanoid dynamics is the existence of an *invariant distribution of states*: we start with an initial state  $x_0$  whose absolute probability is 1. Ultimately the states should be distributed according to a specified distribution.

Recall that *Brownian dynamics* represents the phase-space trajectories of a collection of particles that individually obey *Langevin rate equations* (see [Gardiner (1985)]) in the field of force (i.e., the particles interact with each other via some deterministic force). For one free particle the Langevin equation of motion is given by

$$m\dot{v} = R(t) - \beta v,$$

where  $m$  denotes the mass of the particle and  $v$  its velocity. The r.h.s represents the coupling to a *heat bath*; the effect of the random force  $R(t)$  is to heat the particle. To balance overheating (on the average), the particle is subjected to *friction*  $\beta$ .

---

<sup>2</sup>Recall that the Markov process is characterized by a *lack of memory*, i.e., the statistical properties of the immediate future are uniquely determined by the present, regardless of the past (see [Gardiner (1985)]).

Noe, between pure deterministic (in which all DOF of the system in consideration are explicitly taken into account, leading to classical dynamical equations like Hamilton's) and pure stochastic dynamics (Markov process), there is so-called *hybrid dynamics*, particularly the Brownian dynamics, in which some of DOF are represented only through their *stochastic influence* on others.

System theory and artificial intelligence have long investigated the topic of *uncertainty* in measurement, modelling and simulation. Research in artificial intelligence has enriched the spectrum of available techniques to deal with uncertainty by proposing a theory of possibility, based on the theory of fuzzy sets (see [Yager (1987); Dubois and Prade (1980); Cox (1992); Cox (1994)]). The field of qualitative reasoning and simulation [Berleant and Kuipers (1992)] is also interested in modelling incompletely known systems where qualitative values are expressed by intervals. Qualitative simulation techniques, however, reveal a low predictive power in presence of complex models. In this section we have combined qualitative and quantitative methods, in spirit of [Bontempi (1995); Ivancevic and Snoswell (2001)].

In this section we will deal with the general biodynamics from the point of view that mathematically and logically approaches a *general theory of systems*, i.e., that *makes the unique framework* for both linear and nonlinear, discrete and continuous, deterministic and stochastic, crisp and fuzzy, SISO and MIMO-systems, and *generalizes the robot dynamics* elaborated in the literature (see [Vukobratovic (1970); Vukobratovic *et al.* (1970); Vukobratovic and Stepanenko (1972); Vukobratovic and Stepanenko (1973); Vukobratovic (1975); Vukobratovic *et al.* (1990); Igarashi and Nogai (1992); Hurmuzlu (1993); Shih *et al.* (1993); Shih and Klein (1993); Lieh (1994); Channon *et al.* (1996); Seward *et al.* (1996); Has (1998); Sardain *et al.* (1999); Pratt and Pratt (1998); Yoshikawa (1984); Seraji (1989)]), including all necessary DOF to match the 'realistic' human-like motion. Yet, we wish to *avoid* all the mentioned fundamental system *obstacles*. To achieve this goal we have formulated the general *biodynamics functor machine*, covering a union of the three intersected frameworks:

- (1) Muscle-driven, dissipative, Hamiltonian (nonlinear, both discrete and continuous) MIMO-system;
- (2) Stochastic forces (including dissipative fluctuations and 'Master' jumps); and
- (3) Fuzzy system numbers.

#### 4.8.2.1 The Abstract Functor Machine

In this section we define the *abstract functor machine* [Ivancevic and Snoswell (2001)] (formalism used is modified from [Anderson *et al.* (1976)]) by a two-step generalization of the Kalman's modular theory of linear MIMO-systems (compare with chapter 6). The first generalization puts the Kalman's theory into the category **Vect** of vector spaces and linear operators (see [MacLane (1971)] for technical details about categorical language), thus formulating the unique, categorical formalism valid both for the discrete- and continual MIMO-systems.

We start with the unique, *continual-sequential state equation*

$$\dot{x}(t+1) = Ax(t) + Bu(t), \quad y(t) = Cx(t), \quad (4.164)$$

where the finite-dimensional vector spaces of *state*  $X \ni x$ , *input*  $U \ni u$ , and *output*  $Y \ni y$  have the corresponding linear operators, respectively  $A : X \rightarrow X$ ,  $B : U \rightarrow X$ , and  $C : X \rightarrow Y$ . The modular system theory comprises the *system dynamics*, given by a pair  $(X, A)$ , together with a *reachability map*  $e : U \rightarrow X$  of the pair  $(B, A)$ , and an *observability map*  $m : X \rightarrow Y$  of the pair  $(A, C)$ . If the reachability map  $e$  is surjection the system dynamics  $(X, A)$  is called *reachable*; if the observability map  $m$  is injection the system dynamics  $(X, A)$  is called *observable*. If the system dynamics  $(X, A)$  is both reachable and observable, a *composition*  $r = m \circ e : U \rightarrow Y$  defines the *total system's response*, which is given by solution of equation (4.164). If the unique solution to the continual-sequential state equation exists, it gives the answer to the (minimal) *realization problem*: find the system  $S$  that realizes the given response  $r = m \circ e : U \rightarrow Y$  (in the smallest number of discrete states and in the shortest time).

In categorical language, the system dynamics in the category **Vect** is a pair  $(X, A)$ , where  $X \in \text{Ob}(\text{Vect})$  is an object in **Vect** and  $A : X \rightarrow X \in \text{Mor}(\text{Vect})$  is a **Vect**-morphism. A *decomposable system* in **Vect** is such a sextuple  $S \equiv (X, A, U, B, Y, C)$  that  $(X, A)$  is the system dynamics in **Vect**, a **Vect**-morphism  $B : U \rightarrow X$  is an *input map*, and a **Vect**-morphism  $C : X \rightarrow Y$  is an *output map*. Any object in **Vect** is characterized by mutually *dual*<sup>3</sup> notions of its *degree* (a number of its input morphisms) and its *codegree* (a number of its output morphisms). Similarly, any decomposable system  $S$  in **Vect** has a *reachability map* given by an epimorphism

---

<sup>3</sup>Recall that in categorical language *duality* means reversing the (arrows of) morphisms; the knowledge of one of the two mutually dual terms automatically implies the knowledge of the other.

$e = A \circ B : U \rightarrow X$  and its dual *observability map* given by a monomorphism  $m = C \circ A : X \rightarrow Y$ ; their composition  $r = m \circ e : U \rightarrow Y$  in  $\text{Mor}(\text{Vect})$  defines the total system's response in  $\text{Vect}$  given by the unique solution of the continual-sequential state equation (4.164).

The second generalization gives an extension of the continual-sequential MIMO-system theory: from the linear category  $\text{Vect}$  – to an arbitrary nonlinear category  $\mathcal{K}$ . We do this extension (see [Ivancevic and Snoswell (2001)]) by formally applying the *action* of the *nonlinear process-functor*  $\mathcal{F} : \mathcal{K} \Rightarrow \mathcal{K}$  on the decomposable system  $S \equiv (X, A, U, B, Y, C)$  in  $\text{Vect}$ . Under the action of the process functor  $\mathcal{F}$  the linear system dynamics  $(X, A)$  in  $\text{Vect}$  transforms into a nonlinear  $\mathcal{F}$ -dynamics  $(\mathcal{F}[X], \mathcal{F}[A])$  in  $\mathcal{K}$ , creating the *functor machine* in  $\mathcal{K}$  represented by a *nonlinear decomposable system*  $\mathcal{F}[S] \equiv (\mathcal{F}[X], \mathcal{F}[A], \mathcal{F}[U], \mathcal{F}[B], \mathcal{F}[Y], \mathcal{F}[C])$ . The reachability map transforms into the *input process*  $\mathcal{F}[e] = \mathcal{F}[A] \circ \mathcal{F}[B] : \mathcal{F}[U] \rightarrow \mathcal{F}[X]$ , while its dual, observability map transforms into the *output process*  $\mathcal{F}[m] = \mathcal{F}[C] \circ \mathcal{F}[A] : \mathcal{F}[X] \rightarrow \mathcal{F}[Y]$ . In this way the total response of the linear system  $r = m \circ e : U \rightarrow Y$  in  $\text{Mor}(\text{Vect})$  transforms into the *nonlinear system behavior*  $\mathcal{F}[r] = \mathcal{F}[m] \circ \mathcal{F}[e] : \mathcal{F}[U] \rightarrow \mathcal{F}[Y]$  in  $\text{Mor}(\mathcal{K})$ . Obviously,  $\mathcal{F}[r]$ , if exists, is given by a nonlinear  $\mathcal{F}$ -transform of the linear state equation (4.164).

The purpose of this section is to formulate a nonlinear  $\mathcal{F}$ -transform for the linear state equation (4.164) for biodynamics, i.e., the biodynamics functor machine. In subsequent sections we give a three-step development of a fuzzy-stochastic-Hamiltonian formulation for the biodynamics functor machine  $\mathcal{F}[S]$ , with a corresponding nonlinear system behavior  $\mathcal{F}[r]$ .

#### 4.8.2.2 Muscle-Driven Hamiltonian Biodynamics

In this section we choose the functor  $\text{Can}$ , as the first order Hamiltonian formalism is more suitable for both stochastic and fuzzy generalizations to follow. Recall that the general deterministic Hamiltonian biodynamics, representing the canonical functor  $\text{Can} : \mathcal{S}^*[SO(n)^i] \Rightarrow \mathcal{S}_*^*[so(n)_i^*]$ , is given by dissipative, driven  $\delta$ -Hamiltonian equations (4.102–4.103), i.e.,

$$\dot{q}^i = \frac{\partial H}{\partial p_i} + \frac{\partial R}{\partial p_i}, \quad (4.165)$$

$$\dot{p}_i = F_i - \frac{\partial H}{\partial q^i} + \frac{\partial R}{\partial q^i}, \quad (4.166)$$

$$q^i(0) = q_0^i, \quad p_i(0) = p_i^0, \quad (4.167)$$

including *contravariant* equation (4.165) – the *velocity vector-field*, and *covariant* equation (4.166) – the *force 1-form*, together with initial joint angles and momenta (4.167). Here  $(i = 1, \dots, N)$ , and  $R = R(q, p)$  denotes the Raileigh nonlinear (biquadratic) dissipation function, and  $F_i = F_i(t, q, p)$  are covariant driving torques of *equivalent muscular actuators*, resembling muscular excitation and contraction dynamics in rotational form.

The velocity vector-field (4.165) and the force 1-form (4.166) together define the generalized Hamiltonian vector-field  $X_H$ , which geometrically represents the *section* of the momentum phase-space manifold  $T^*M$ , which is itself the cotangent bundle of the biodynamics configuration manifold  $M$ ; the Hamiltonian (total energy) function  $H = H(q, p)$  is its generating function.

As a Lie group, the configuration manifold  $M$  is Hausdorff [Abraham *et al.* (1988); Marsden and Ratiu (1999); Postnikov (1986)]. Therefore, for  $x = (q^i, p_i) \in U_p, U_p$  open in  $T^*M$ , there exists a unique one-parameter group of diffeomorphisms  $\phi_{\delta_t} : T^*M \rightarrow T^*M$ , the generalized deterministic  $\delta$ -Hamiltonian phase-flow

$$\begin{aligned} \phi_{\delta_t} : G_1 \times T^*M &\rightarrow T^*M : (p(0), q(0)) \mapsto (p(t), q(t)), \\ (\phi_{\delta_t} \circ \phi_{\delta_s} &= \phi_{\delta_{t+s}}, \phi_{\delta_0} = \text{identity}), \end{aligned} \quad (4.168)$$

given by (4.165–4.167) such that

$$\left. \frac{d}{dt} \right|_{t=0} \phi_{\delta_t} x = J \nabla H(x).$$

The  $\delta$ -Hamiltonian system (4.165–4.167), with its  $\delta$ -Hamiltonian phase-flow  $\phi_{\delta_t}$  (4.168), i.e., the canonical functor  $\text{Can}$ , represents our first, continual-deterministic model for the biodynamics functor machine  $\mathcal{F}[S]$  with the nonlinear system behavior  $\mathcal{F}[r]$ . In the two subsequent sections we generalize this model to include discrete stochastic forces and fuzzy SN.

### 4.8.3 Stochastic-Lie-Hamiltonian Biodynamic Functor

In terms of the Markov stochastic process, we can interpret the deterministic  $\delta$ -Hamiltonian biodynamic system (4.165–4.167) as deterministic drift corresponding to the *Liouville equation*. Thus, we can naturally (in the sense of Langevin) add the covariant vector  $\sigma_i(t)$  of stochastic forces (diffusion fluctuations and discontinuous-Master jumps)  $\sigma_i(t) = B_{ij}[q^i(t), t] dW^j(t)$  to the canonical force equation. In this way we get *stochastic*  $\sigma$ -Hamiltonian biodynamic system, a *stochastic transformation*

Stoch[Can] of the canonical functor Can,

$$dq^i = \left( \frac{\partial H}{\partial p_i} + \frac{\partial R}{\partial p_i} \right) dt, \quad (4.169)$$

$$dp_i = \left( F_i - \frac{\partial H}{\partial q^i} + \frac{\partial R}{\partial q^i} \right) dt + \sigma_i(t), \quad (4.170)$$

$$\sigma_i(t) = B_{ij}[q^i(t), t] dW^j(t), \quad q^i(0) = q_0^i, \quad p_i(0) = p_i^0.$$

In our low-dimensional example-case of symmetrical 3D load-lifting (see (4.7.4.3)), the velocity and force  $\sigma$ -Hamiltonian biodynamics equations (4.169–4.170) become

$$\begin{aligned} dq^i &= \left( p_i \left\{ [J_i]^{-1} + \left[ m_i \left( \sum_{j=1}^i L_j \cos q^j \right)^2 \right]^{-1} \right\} + \frac{\partial R}{\partial p_i} \right) dt, \\ dp_i &= B_{ij}[q^i(t), t] dW^j(t) + \left( F_i - g \sum_{j=i}^{10-i} L_j m_j \sin q^j \right. \\ &\quad \left. - \sum_{j=i}^{10-i} L_j \sin q^j p_i p_j \left[ m_i \left( \sum_{k=1}^i L_k \cos q^k \right)^3 \right]^{-1} + \frac{\partial R}{\partial q^i} \right) dt. \end{aligned}$$

Recall that Ito quadratic cotangent bundle  $I^*Q^N$  is defined as a Whitney sum

$$I^*Q^N = T^*Q^N \oplus SQ^N,$$

where  $SQ^N$  corresponds to *stochastic tensor bundle*, whose elements are 2nd-order tensor-fields composed of continual diffusion fluctuations and discontinuous jumps at every point of the manifold  $Q^N$ . On  $I^*Q^N$  is defined a non-degenerate, stochastic 2-form  $\alpha$  which is closed, i.e.,  $d\alpha = 0$ , and exact, i.e.,  $\alpha = d\beta$ , where 1-form  $\beta$  represents a section  $\beta : Q^N \rightarrow I^*Q^N$  of the Ito bundle  $I^*Q^N$ .

Now, the stochastic Hamiltonian vector-field  $\Xi_H$  represents a section  $\Xi_H : Q^N \rightarrow IQ^N$  of the *Ito quadratic tangent bundle*  $IQ^N$ , also defined as a Whitney sum

$$IQ^N = TM \oplus SQ^N.$$

The quadratic character of Ito stochastic fibre-bundles corresponds to the second term (trace of the 2nd-order tensor-field) of associate *stochastic*



*Taylor expansion* (see [Elworthy (1982); Mayer (1981)]).

Through stochastic  $\sigma$ -Hamiltonian biodynamic system (4.169–4.170), the deterministic  $\delta$ -Hamiltonian phase-flow  $\phi_{\delta_t}$  (4.168), extends into stochastic  $\sigma$ -Hamiltonian phase-flow  $\phi_{\sigma_t}$

$$\begin{aligned}\phi_{\sigma_t} : G_1 \times I^*M &\rightarrow I^*M : (p(0), q(0)) \mapsto (p(t), q(t)), \\ (\phi_{\sigma_t} \circ \phi_{\sigma_s} &= \phi_{\sigma_{t+s}}, \quad \phi_{\sigma_0} = \text{identity}),\end{aligned}\quad (4.171)$$

where  $I^*M$  denotes *Ito quadratic cotangent bundle* (see [Elworthy (1982); Mayer (1981)]) of biodynamic configuration manifold  $M$ .

Besides the  $\sigma$ -Hamiltonian phase-flow  $\phi_{\sigma_t}$  (4.171), including  $N$  individual random-phase trajectories, we can also define (see [Elworthy (1982)]) an *average* or *mean*  $\langle \sigma \rangle$ -Hamiltonian flow  $\langle \phi \rangle_{\sigma_t}$

$$\begin{aligned}\langle \phi \rangle_{\sigma_t} : G_1 \times I^*M &\rightarrow I^*M : (\langle p(0) \rangle, \langle q(0) \rangle) \mapsto (\langle p(t) \rangle, \langle q(t) \rangle), \\ (\langle \phi \rangle_{\sigma_t} \circ \langle \phi \rangle_{\sigma_s} &= \langle \phi \rangle_{\sigma_{t+s}}, \quad \langle \phi \rangle_{\sigma_0} = \text{identity}),\end{aligned}$$

which stochastically corresponds to the trajectory of the center of mass in the human-like dynamics, approximatively lumbo-sacral spinal  $SO(3)$ -joint.

The necessary conditions for existence of a unique *non-anticipating solution* of the  $\sigma$ -Hamiltonian biodynamic system in a fixed time interval are *Lipschitz condition* and *growth condition* (see [Elworthy (1982); Mayer (1981)]). For constructing an approximate solution a simple iterative Cauchy-Euler procedure could be used to calculate  $(q_{k+1}^i, p_i^{k+1})$  from the knowledge of  $(q_k^i, p_i^k)$  on the mesh of time points  $t^k$ ,  $k = 1, \dots, s$ , by adding discrete  $\delta$ -Hamiltonian drift-terms  $A^i(q_k^i)\Delta t^k$  and  $A_i(p_i^k)\Delta t^k$ , as well as a stochastic term  $B_{ij}(q_i^k, t^k)\Delta W_k^j$ .

$\sigma$ -Hamiltonian biodynamic system (4.169–4.170), with its  $\sigma$ -Hamiltonian phase-flow  $\phi_{\sigma_t}$  (4.171), i.e., the functor  $\text{Stoch}[\text{Can}]$ , represents our second, continual-discrete stochastic model for the biodynamics functor machine  $\mathcal{F}[S]$  with the nonlinear system behavior  $\mathcal{F}[r]$ . In the next section we generalize this model once more to include fuzzy SN.

#### 4.8.4 Fuzzy-Stochastic-Lie-Hamiltonian Functor

Generally, a fuzzy differential equation model (FDE-model, for short) is a symbolic description expressing a state of incomplete knowledge of the continuous world, and is thus an abstraction of an infinite set of ODEs models. Qualitative simulation (see [Berleant and Kuipers (1992)]) pre-

dicts the set of possible behaviors consistent with a FDE model and an initial state. Specifically, as a FDE we consider an ordinary deterministic (i.e., *crisp*) differential equation (CDE) in which some of the parameters (i.e., coefficients) or initial conditions are *fuzzy numbers*, i.e. uncertain and represented in a *possibilistic* form. As a *solution* of a FDE we consider a time evolution of a *fuzzy region of uncertainty* in the system's phase-space, which corresponds to its the *possibility distribution*.

Recall that a fuzzy number (see section (7.8) below) is formally defined as a convex, normalized fuzzy set [Dubois and Prade (1980); Cox (1992); Cox (1994)]. The concept of fuzzy numbers is an extension of the notion of real numbers: it encodes approximate quantitative knowledge. It is not probabilistic, but rather a possibilistic distribution. The mathematics of fuzzy numbers is founded on the *extension principle*, introduced by Zadeh [Yager (1987)]. This principle provides a general method for extending standard mathematical concepts in order to deal with fuzzy quantities [Dubois and Prade (1980)].

Let  $\Phi : Y^1 \times Y^2 \times \dots \times Y^n \rightarrow Z$  be a deterministic map such that  $z = \Phi(y^1, y^2, \dots, y^n)$  for all  $z \in Z$ ,  $y^i \in Y^i$ . The extension principle allows us to induce from  $n$  input fuzzy sets  $\bar{y}^i$  on  $Y^i$  an output fuzzy set  $\bar{z}$  on  $Z$  through  $\Phi$  given by

$$\mu_{\bar{z}}(t) = \sup_{t=\Phi(s^1, \dots, s^n)} \min(\mu_{\bar{y}^1}(s^1), \dots, \mu_{\bar{y}^n}(s^n)),$$

or,

$$\mu_{\bar{z}}(t) = 0 \quad \text{if} \quad \Phi^{-1}(t) = \emptyset,$$

where  $\Phi^{-1}(t)$  denotes the inverse image of  $t$  and  $\mu_{\bar{y}^i}$  is the membership function of  $\bar{y}^i$ , ( $i = 1, \dots, n$ ).

The extension principle provides a method to compute the fuzzy value of a fuzzy map but, in practice, its application is not feasible because of the infinite number of computations it would require. The simplest way of efficiently applying the extension principle is in the form of iterative repetition of several crisp Hamiltonian simulations (see [Bontempi (1995); Ivancevic and Snoswell (2001); Ivancevic and Pearce (2005a)]), within the range of included fuzzy SN.

Fuzzification of the crisp deterministic  $\delta$ -Hamiltonian biodynamic system (4.165–4.167) gives the fuzzified  $\mu$ -Hamiltonian biodynamic system, namely  $\delta$ -Hamiltonian biodynamic system with fuzzy SN, i.e., the *fuzzy transformation*  $\text{Fuzzy}[\text{Can}]$  of the canonical functor  $\text{Can}$

$$\dot{q}^i = \frac{\partial H(q, p, \sigma)}{\partial p_i} + \frac{\partial R}{\partial p_i}, \quad (4.172)$$

$$\dot{p}_i = \bar{F}_i(q, p, \sigma) - \frac{\partial H(q, p, \sigma)}{\partial q^i} + \frac{\partial R}{\partial q^i}, \quad (4.173)$$

$$q^i(0) = \bar{q}_0^i, \quad p_i(0) = \bar{p}_i^0, \quad (i = 1, \dots, N). \quad (4.174)$$

Here  $\sigma = \sigma_\mu$  (with  $\mu \geq 1$ ) denote fuzzy sets of conservative parameters (segment lengths, masses and moments of inertia), dissipative joint dampings and actuator parameters (amplitudes and frequencies), while the bar  $(\bar{\cdot})$  over a variable  $(\cdot)$  denotes the corresponding fuzzified variable.

In our example-case of symmetrical 3D load-lifting, the fuzzified  $\mu$ -Hamiltonian biodynamic system (4.172–4.174) becomes

$$\begin{aligned} \dot{q}^i &= p_i \left\{ [\bar{J}_i]^{-1} + \left[ \bar{m}_i \left( \sum_{j=1}^i \bar{L}_j \cos q^j \right)^2 \right]^{-1} \right\} + \frac{\partial R}{\partial p_i}, \\ \dot{p}_i &= \bar{F}_i(t, q^i, p_i, \{\sigma\}_\mu) - g \sum_{j=i}^{10-i} \bar{L}_j \bar{m}_j \sin q^j \\ &\quad - \sum_{j=i}^{10-i} \bar{L}_j \sin q^j p_i p_j \left[ \bar{m}_i \left( \sum_{k=1}^i \bar{L}_k \cos q^k \right)^3 \right]^{-1} + \frac{\partial R}{\partial q^i} \\ q^i(0) &= \bar{q}_0^i, \quad p_i(0) = \bar{p}_i^0, \quad (i = 1, \dots, 9). \end{aligned}$$

In this way, the crisp  $\delta$ -Hamiltonian phase-flow  $\phi_{\delta_t}$  (4.168) extends into fuzzy-deterministic  $\mu$ -Hamiltonian phase-flow  $\phi_{\mu_t}$

$$\begin{aligned} \phi_{\mu_t} : G_1 \times T^*M &\rightarrow T^*M : (\bar{p}_i^0, \bar{q}_0^i) \mapsto (p(t), q(t)), \\ (\phi_{\mu_t} \circ \phi_{\mu_s} &= \phi_{\mu_{t+s}}, \quad \phi_{\mu_0} = \text{identity}). \end{aligned}$$

Similarly, fuzzification of crisp stochastic  $\sigma$ -Hamiltonian biodynamic system (4.169–4.170) gives fuzzy-stochastic  $[\mu\sigma]$ -Hamiltonian biodynamic system, namely stochastic  $\sigma$ -Hamiltonian biodynamic system with fuzzy SN, i.e., the *fuzzy-stochastic transformation*  $\text{Fuzzy}[\text{Stoch}[\text{Can}]]$  of the canonical functor  $\text{Can}$

$$dq^i = \left( \frac{\partial H(q, p, \sigma)}{\partial p_i} + \frac{\partial R}{\partial p_i} \right) dt, \quad (4.175)$$

$$dp_i = B_{ij}[q^i(t), t] dW^j(t) + \left( \bar{F}_i(q, p, \sigma) - \frac{\partial H(q, p, \sigma)}{\partial q^i} + \frac{\partial R}{\partial q^i} \right) dt, \quad (4.176)$$

$$q^i(0) = \bar{q}_0^i, \quad p_i(0) = \bar{p}_i^0. \quad (4.177)$$

In our example-case of symmetrical 3D load-lifting, the velocity and force  $[\mu\sigma]$ -Hamiltonian biodynamic equations (4.175–4.176) become

$$\begin{aligned} dq^i &= \left( p_i \left\{ [\bar{J}_i]^{-1} + \left[ \bar{m}_i \left( \sum_{j=1}^i \bar{L}_j \cos q^j \right)^2 \right]^{-1} \right\} + \frac{\partial R}{\partial p_i} \right) dt, \\ dp_i &= B_{ij}[q^i(t), t] dW^j(t) + \left( \bar{F}_i(t, q^i, p_i, \{\sigma\}_\mu) - g \sum_{j=i}^{10-i} \bar{L}_j \bar{m}_j \sin q^j \right. \\ &\quad \left. - \sum_{j=i}^{10-i} \bar{L}_j \sin q^j p_i p_j \left[ \bar{m}_i \left( \sum_{k=1}^i \bar{L}_k \cos q^k \right)^3 \right]^{-1} + \frac{\partial R}{\partial q^i} \right) dt. \end{aligned}$$

In this way, the crisp stochastic  $\sigma$ -Hamiltonian phase-flow  $\phi_{\sigma_t}$  (4.171) extends into fuzzy-stochastic  $[\mu\sigma]$ -Hamiltonian phase-flow  $\phi_{[\mu\sigma]_t}$

$$\begin{aligned} \phi_{[\mu\sigma]_t} : G_1 \times I^*M &\rightarrow I^*M : (\bar{p}_i^0, \bar{q}_0^i) \mapsto (p(t), q(t)), \\ (\phi_{[\mu\sigma]_t} \circ \phi_{[\mu\sigma]_s} &= \phi_{[\mu\sigma]_{t+s}}, \quad \phi_{[\mu\sigma]_0} = \text{identity}). \end{aligned} \quad (4.178)$$

$[\mu\sigma]$ -Hamiltonian biodynamic system (4.175–4.177), with its phase-flow  $\phi_{[\mu\sigma]_t}$  (4.178), i.e., the functor  $\text{Fuzzy}[\text{Stoch}[\text{Can}]]$ , represents our final, continual-discrete and fuzzy-stochastic model for the biodynamic functor machine  $\mathcal{F}[S]$  with the nonlinear system behavior  $\mathcal{F}[r]$ .

## 4.9 Mechanics of Spinal Injuries

In this section we explore some new possibilities to understand, predict and prevent spinal injuries (see Appendix for a review of modern 3D neuro-imaging). We start from the proper construction of the spinal manifold  $M$  (see Figure 3.3 above).

#### 4.9.1 Spinal Dislocations, Disclinations and Fractures

According to the construction of the spinal manifold  $M$ , we have two general types of soft spinal injuries (excluding vertebral fractures), which agrees with the medical literature [Whiting and Zernicke (1998)]:

- The *intervertebral dislocations*, corresponding to translational movements in 25 gauge groups  $\mathbb{R}^3$ , and
- The *intervertebral disclinations*, corresponding to rotational movements in 25 gauge groups  $SO(3)$ .

Continuum mechanics of soft spinal defects comprises the following set of continuity equations [Kadic and Edelen (1983)]:

$$\dot{\alpha}^k = -dJ^k - S^k, \quad \dot{Q}^k = -dS^k, \quad d\alpha^k = Q^k, \quad dQ^k = 0,$$

where  $k = 1, \dots, 25 \times 3$ ;  $\alpha^k$ ,  $J^k$ ,  $S^k$ , and  $Q^k$  denote respectively 2-form of dislocation density, 1-form of dislocation flux, 2-form of disclination flux, and 3-form of disclination density, all spanned along the 25 movable spinal joints.

Now, the above picture is common for *all* movable (in particular, synovial) human joints included in the full biodynamic manifold  $M$  (see Figure 3.2): at all joints soft injuries can be classified as dislocations and disclinations defined above.

Regarding the hard injuries, *bone fractures*, we can say that they are generally *caused by*  $SE(3)$ -jolts, applied externally on the human bones (in particular, vertebrae, see the following subsections).

#### 4.9.2 Measuring the Risk of Local Intervertebral Injuries

In the literature on musculo-skeletal injuries, the description and classification of spinal injuries is usually based on the principal loading applied to the spine (see [Whiting and Zernicke (1998); McElhaney and Myers (1993)]). The *principal loading hypothesis* (PLH) predicts musculo-skeletal injury resulting from a combination of tension, compression, bending and shear that occurs as a direct consequence of the application of force beyond the joint thresholds in these dimensions. Now, while in the cases of severe injuries, like vertebral fractures, PLH might be valid, it is clearly not valid for the vastly greater number of cases where less severe disablement occurs, e.g., there is little evidence of structural damage accompanying cases of lower back pain [Waddell (1998)]. A more sensitive

model is needed, that is able to predict likely disablement over an extensive range of modelling musculo-skeletal injuries. In this comment we offer an alternative view regarding the mechanisms underlying functional and structural musculo-skeletal injury, and the conditions under which injury might occur [Ivancevic and Beagley (2003a); Ivancevic and Beagley (2003b); Ivancevic and Beagley (2003c)].

To be recurrent, musculo-skeletal injury must be associated with a histological change, i.e., the modification of associated tissues within the body. The incidence of injury is likely to be a continuum ranging from little or no evidence of structural damage through to the observable damage of muscles, joints or bones. The changes underlying functional injuries are likely to consist of torn muscle fibres, stretched ligaments, subtle erosion of joint tissues, and/or the application of pressure to nerves, all amounting to a disruption of function to varying degrees and a tendency toward spasm.

Given the assumption that an injury is the effect of tissue damage, it becomes important to understand the mechanism for such damage. The damage to the component tissues that make up the body's structural system is a consequence of a failure of any part of that system to dissipate externally imposed energy to either adjoining structural components, or to the surrounding environment. The components of the spine will break at the point that all of its vertebrae are at the extreme of their rotation and translation and when the tissues at their interface are at the limits of their elasticity. At this point, where no further motion is possible, the addition of further force will result in the failure of the system in the form of tissue damage at the weakest point.

At the same time, there is little evidence that static force, either internal (muscular), or external (loading), is the prime cause of injury, though it may aggravate an old injury. For example, maximal isometric muscle contractions, even in prolonged strength-endurance tests, are commonly used in the training of a variety of sports without injury. Similarly, the stretching techniques of gymnasts and ballet dancers are considered to be safe when performed very slowly i.e., under quasi-static conditions. These examples help to illustrate the body's ability to endure extreme static forces that, based on the theory of principal loading, would be expected to induce injury. Experience suggests that injuries occur, primarily, under situations where control over the situation is lost e.g., an abrupt change of direction when running or a shift in balance when lifting an awkward weight. We are not injured under high loading semi-static conditions because we are able to position our bodies (joints) in such a way that we dissipate forces

through compression rather than by potentially damaging motions of twisting or shearing. When control is lost, the joints may be forced in a rotation or direction for which they are not adapted to support.

Whilst it is evident that the body can endure extreme forces under static conditions, injuries appear to result from conditions where much lower peak forces are reached, if the transfer of energy is rapid and localized. In other words the primary cause of both functional and structural injury is the local dynamism of the force. We define the measure of local dynamism as the 'jolt' (see, for example [Wilder *et al.* (1996)]), or 'force-jerk', which is the time rate of change of the force. In other words, we suppose that the force is not constant (i.e., static), but rather that it is changing, and that we can measure the rate of its change. As the rate of change of the force increases it tends towards an Dirac impulse  $\delta$ -function. It is this instantaneous application of force that we consider to be the cause of injuries, at first only functional, i.e., reduction in function without obvious damage to tissue, and later even structural, i.e., loss of function directly attributable to specific localized tissue damage (e.g., a herniated intervertebral disc). It is the instantaneous nature of this applied force that defies the tissues' ability to dissipate energy with the consequence of raising the energy at that point to a level beyond the tolerance of the structural bonds that maintain the integrity of the tissue. The higher the rate of force change, the higher the risk of injury. Therefore, the same energy, or the same mechanical impulse, applied to the human body within the normal anatomical range of motion, can cause two totally different outcomes: the one with a constant or very slowly changing force would not cause any damage, while the other which is rapidly changing would cause injury.

Also, besides this time-locality of the force impact, we need to consider the space-locality measured as a pressure, i.e., the force per body area. In the spinal context it means the local point at which we expect an injury. When evaluating the risk of injury, it is not sufficient to simply consider a single translational force applied to the whole spine, neglecting the location of the load. The combination of additional mass and its eccentricity from the normal posture of the spine, measured by the distributed moments of inertia, i.e., the mass distribution, must be considered.

When determining a realistic mechanism of human spine injury, it must be emphasized that the natural dynamics of the spine is predominantly rotational, not translational as presumed by the principal loading hypothesis. Translation is evident in many cases of real world spinal injury, e.g., spinal compression. In the case of relatively low forces, e.g., carrying a weight

on the head, the symmetry of the body tends to allow these compressive forces to be absorbed without injury. In cases where much a larger compressive force is applied in a short time interval e.g., during an accident, the ability of the body to maintain symmetry is lost. Slight asymmetry in the body will have the effect of converting the external translational force into a rotational motion distributed along the structural components of the skeleton. At the extremes of a single joint's rotation, where no further movement is available to dissipate the force, disk deformation in the form of herniation will occur. At the global level, the importance of rotational dynamics can be illustrated by the accepted work practice for lifting and handling, summarized by the maxim: 'Bend in the knees to save the back.' By maintaining a 'straight' spine with the weight close to the body when lifting we reduce the rotational forces on the spine thus reducing the risk of injury. Mechanically, this means that we need to consider the action of various torques  $T$  on the human spine, rather than translational forces  $F$  (loadings). Torque  $T$  acting in the (spinal) joint is the (vector) product of the force  $F$  and its lever arm  $r$  for the particular joint. So, even with the constant loading  $F$ , the torque at the particular (spinal) joint can change rapidly due to the change of a particular lever arm  $r$ , and this change might cause an injury. That is why, in our opinion, the best measure for the risk of (spinal) injuries is the time rate of change of the total joint torque,  $\dot{T}$ , i.e., the *torque-jolt* (or, torque-jerk), as measured in  $[Nm/s]$ . The higher the torque-jolt  $\dot{T}$  at the certain point along the spine, the higher the risk of injuries, at first only functional, and later structural.

Using the torque-jolt concept, the *risk of local spinal injuries* is measured as a *distance in the spinal torque-jolt space*. Here, the *spinal torque-jolt space* is a set of triaxial torque-jolt trajectories calculated for each movable intervertebral joint; the *distance* is an instantaneous distance along the torque-jolt axis, still measured in  $[Nm/s]$ , between any two trajectories corresponding to the neighboring spinal joints.

We suggest that the energy imparted by a localized torque-jolt is a root cause of injury. At low levels, torque-jolt is dissipated within the associated tissues without lasting effect. Above various thresholds it will modify various tissues, i.e., cause damage, initially at a very low level and essentially invisible to diagnostic techniques. As the magnitude of the torque-jolt increases, the level of tissue damage would tend to increase up to a point where obvious structural damage may be observed.

If we take the example of muscle spasm, this may be due to chemical imbalances, usually following an injury. After about two weeks, if the ba-



sic injury has failed to repair, the spasm maintains an unnatural muscle contraction leading to the formation of knots. This happens most frequently for the small deep muscles of the spine, the rotatores, multifidus, interspinales, and intertransversarii. The stronger erector spine group, the iliocostalis, longissimus and spinalis, tends to be the last to be injured. Nevertheless, it is ready to go into painful spasm, whenever any of the smaller muscles is injured. The underlying point is that whilst this larger muscle group exhibits pain and a tendency to spasm without evidence of injury, the trigger for this pain and spasm is an underlying tissue change responsible for changes in the electrophysiology of surrounding tissues. In an attempt to reduce the risk of developing the symptoms of functional disturbance we are currently of the view that we must predict this localized tissue change. Our proposed mechanism and method of prediction is the *localized torque-jolt* [Ivancevic and Beagley (2003a); Ivancevic and Beagley (2003b); Ivancevic and Beagley (2003c)].

#### 4.9.2.1 Biodynamic Jerk Functions

The *covariant force law*,  $F_i = mg_{ij}a^j$ , together with its Hamiltonian formulation given in the previous section, has been applied for the prediction of spinal (and other neuro-musculo-skeletal) injuries. The *risk of spinal injuries* is measured using the *torque-jerk* quantity,  $\dot{\bar{T}}_i = \dot{T}_i - \Gamma_{ik}^j T_j \dot{x}^k$ , measured in  $[Nm/s]$ , defined as the *absolute time derivative of the total torque*  $T_i = F_i(t, q^i, p_i)$  acting along the joint Euler angles, in each movable intervertebral joint. This is the measure of the dynamism of the total torque: the sharper the shape of the torque, i.e., the more it approaches the shape of the Dirac's impulse  $\delta$ -function, both in time and along the spine, the higher is the risk of injury at that particular joint.

More precisely, by taking the absolute time derivative of the force equation (4.166),  $\dot{p}_i = T_i - \partial_{q^i} H + \partial_{q^i} R$ , we get the *deterministic biodynamic jerk function*,

$$\ddot{p}_i = \dot{\bar{T}}_i - \overline{\partial_{q^i} H} + \overline{\partial_{q^i} R}, \quad (4.179)$$

while differentiation of the fuzzy-stochastic equation (4.176),

$dp_i = B_{ij}[q^i(t), t] dW^j(t) + (\bar{T}_i(q, p, \sigma) - \partial_{q^i} H(q, p, \sigma) + \partial_{q^i} R) dt$ , - gives the *fuzzy-stochastic biodynamic jerk function*,

$$\overline{\dot{dp}_i} = B_{ij}[q^i(t), t] \overline{d\bar{W}^j}(t) + (\dot{\bar{T}}_i(q, p, \sigma) - \overline{\partial_{q^i} H}(q, p, \sigma) + \overline{\partial_{q^i} R}) dt. \quad (4.180)$$

Biodynamics jerk functions (4.179–4.180) are the quantities that need

to be controlled by the high-level, brain-like controller, both in humans and in humanoid robots.

In case of the spinal simulator, (4.179–4.180) read

$$\ddot{p}_i = \dot{T}_i(t, \dot{q}^i, \dot{p}_i) - (\dot{p}_i p_j + \dot{p}_j p_i) \sum_{j=i}^{76-i} L_j \sin q^j \left[ m_i \left( \sum_{k=1}^i L_k \cos q^k \right)^3 \right]^{-1} \quad (4.181)$$

$$+ \frac{\dot{p}_i}{\partial_{q^i} \bar{R}}, \quad \text{and}$$

$$\begin{aligned} \frac{d}{dt} \dot{p}_i = & B_{ij}[q^i(t), t] \frac{d}{dt} \dot{W}^j(t) + \left( \dot{T}_i(t, q^i, p_i, \{\sigma\}_\mu) \right. \\ & \left. - (\dot{p}_i p_j + \dot{p}_j p_i) \sum_{j=i}^{76-i} \bar{L}_j \sin q^j \left[ \bar{m}_i \left( \sum_{k=1}^i \bar{L}_k \cos q^k \right)^3 \right]^{-1} + \frac{\dot{p}_i}{\partial_{q^i} \bar{R}} \right) dt. \end{aligned} \quad (4.182)$$

Assuming well-behaved muscular actuators and weakly nonlinear (or even linear) joint dissipation functions, we see that both in the definition jerk functions (4.179–4.180) and in the expanded ones (4.181–4.182), the source of possible chaos can be the middle term with trigonometric couplings of joints, i.e.,

$$\frac{\dot{p}_i}{\partial_{q^i} \bar{H}} = (\dot{p}_i p_j + \dot{p}_j p_i) \sum_{j=i}^{76-i} L_j \sin q^j \left[ m_i \left( \sum_{k=1}^i L_k \cos q^k \right)^3 \right]^{-1}. \quad (4.183)$$

This term needs sophisticated, brain-like chaos control.

Finally, for the purpose of biomedical engineering, when muscular actuators  $T_i^{MUS}$  are insufficient to perform adequately, they can be complemented by D.C. motor-drives, to form the so-called ‘hybrid joint actuators’  $T_i = T_i^{MUS} + T_k^{DC}$  (see, e.g., [Vukobratovic *et al.* (1990)]). The D.C. motor-driven torques,  $T_k^{DC}$ , as implemented in standard hybrid joint actuators, are defined here in Hamiltonian form by

$$\begin{aligned} T_k^{DC} = & i_k(t) - \dot{p}_k(t) - B_k p_k(t), \quad (k = 1, \dots, N), \quad (4.184) \\ \text{with} \quad & l_k i_k(t) + R_k i_k(t) + C_k p_k(t) = u_k(t), \end{aligned}$$

where  $i_k(t)$  and  $u_k(t)$  denote currents and voltages in the rotors of the drives,  $R_k, l_k$  and  $C_k$  are resistances, inductances and capacitances in the rotors, respectively, while  $B_k$  correspond to the viscous dampings of the drives.

If we use a hybrid joint actuator  $T_i = T_i^{MUS} + T_k^{DC}$  – that resembles the brushless DC motor – then it can be chaotic itself [Chen and Dong (1998)].

#### 4.9.3 Measuring the Risk of Vertebral Fractures

In the previous subsection we left the possibility that principal loading hypothesis (PLH) might be valid for bone fractures. Now we want to show that even this is not the case, at least if the vague word 'loading' means *the force*. With the similar arguments as before, we claim that it is not the force itself that brakes the bones, but it is the sharp and local (along the spine) change of the force, i.e., the jolt, measured as [N/s]. Healthy bones (without signs of osteoporosis) can endure very high forces along all three axes, if these forces are predominantly static. However, moderately high forces with high jolts can break any bone. And the fracture is always localized, at the certain bone (vertebra, in the case of spine), and directed in a 3D space. Lots of evidence for this new jolt hypothesis can be obtained from any crash data, including road vehicle crashes, aircraft ejection seats, hard landing of parachutists, and land mine explosions. It is always the sharp peak of external force, i.e., translational jolt (as measured in [N/s]), or more generally  $SE(3)$ -jolt, that brakes human bones. General prevention of such injuries is threefold: (i) Strong deflection shield; (ii) High damping (shock-absorbing); and (iii) Distance from the point of impact.

##### 4.9.3.1 Research on Bone Injuries

J.C. Misra from Indian Institute of Technology, Karagpur, with his collaborators and PhD students, developed a body of mathematical and physical knowledge related to dynamics of bone fractures. In the following series of papers Misra explored: modelling biomechanics of vertebra bodies [Misra and Samanta (1988a)], stress concentration around cracks in long bones [Misra and Murthy (1981); Misra and Roy (1989b)], stress-field around simple fractures in human patella [Misra and Murthy (1983a)], effect of external loading on long bones [Misra and Bera (1991); Misra and Roy (1991)], physiology and mechanics of bone remodelling [Misra and Murthy (1983d); Misra and Roy (1989a); Misra *et al.* (1989); Misra and Murthy (1983c); Misra and Bera (1992); Misra and Murthy (2005); Misra and Samanta (1987)], propagation of torsional waves in tubular bones [Misra and Samanta (1983); Misra and Samanta (1984)], exterior star-shaped crack in a bone medium [Misra and Mishra (1984); Misra and Mishra (1985)], stresses in a tubular bone exposed to heat radiation from a distant heat source [Misra (1985)], distribution of stresses in a pre-cracked bone specimen [Misra (1986b)], and vibrations of a tubular bones [Misra *et al.* (1986); Misra and Samanta (1988b)].

## Chapter 5

# Natural Topology of Biodynamics

In this chapter we develop the basics of algebraic topology as is used in modern biodynamics research. It includes both tangent (Lagrangian) and cotangent (Hamiltonian) topological variations on the central theme of our *covariant force law*,  $F_i = mg_{ij}a^j$ . Here we basically follow the topological approach used in modern physics, regarding biodynamics as a physical science. Its biological part has a minor role here; it will dominate in the subsequent chapters. No background is assumed on the reader's side other than the natural language of biodynamics as already developed in the second chapter.

### 5.1 Category of (Co)Chain Complexes in Biodynamics

In this section we present the category of (co)chain complexes, as used in modern biodynamics. The central concept in cohomology theory is the *category*  $\mathbf{S}^\bullet(\mathbb{C})$  of *generalized cochain complexes* in an Abelian category  $\mathbb{C}$  [Dieudonne (1988)]. The *objects* of the category  $\mathbf{S}^\bullet(\mathbb{C})$  are infinite sequences

$$A^\bullet : \dots \longrightarrow A^{n-1} \xrightarrow{d^{n-1}} A^n \xrightarrow{d^n} A^{n+1} \longrightarrow \dots$$

where, for each  $n \in \mathbb{Z}$ ,  $A^n$  is an object of  $\mathbb{C}$  and  $d^n$  a morphism of  $\mathbb{C}$ , with the conditions

$$d^{n-1} \circ d^n = 0$$

for every  $n \in \mathbb{Z}$ . When  $A^n = 0$  for  $n < 0$ , one speaks of *cochain complexes*. The  $d^n$  are called *coboundary operators*.

The *morphisms* of the category  $\mathbf{S}^\bullet(\mathbb{C})$  are sequences  $f^\bullet = (f^n) : A^\bullet \rightarrow B^\bullet$  where, for each  $n \in \mathbb{Z}$ ,  $f^n : A^n \rightarrow B^n$  is a morphism of  $\mathbb{C}$ , and in the

diagram

$$\begin{array}{ccccccc}
 \dots & \longrightarrow & A^{n-1} & \xrightarrow{d^{n-1}} & A^n & \xrightarrow{d^n} & A^{n+1} \longrightarrow \dots \\
 & & \downarrow f^{n-1} & & \downarrow f^n & & \downarrow f^{n+1} \\
 \dots & \longrightarrow & B^{n-1} & \xrightarrow{d^{n-1}} & B^n & \xrightarrow{d^n} & B^{n+1} \longrightarrow \dots
 \end{array} \quad (5.1)$$

all squares are commutative; one says the  $f^n$  commute with the coboundary operators. One has  $\text{Im } d^{n+1} \subset \text{Ker } d^n \subset A^n$  for every  $n \in \mathbb{Z}$ ; the quotient  $H^n(A^\bullet) = \text{Ker } d^n / \text{Im } d^{n+1}$  is called the  $n$ th cohomology object of  $A^\bullet$ . From (5.1) it follows that there is a morphism

$$H^n(f^\bullet) : H^n(A^\bullet) \rightarrow H^n(B^\bullet)$$

deduced canonically from  $f^\bullet$ , and

$$(A^\bullet, f^\bullet) \Rightarrow (H^n(A^\bullet), H^n(f^\bullet))$$

is a *covariant functor* from  $\mathbf{S}^\bullet(\mathbb{C})$  to  $\mathbb{C}$ .

The *cohomology exact sequence*: if three cochain complexes  $A^\bullet, B^\bullet, C^\bullet$  are elements of a short exact sequence of morphisms

$$0 \longrightarrow A^\bullet \longrightarrow B^\bullet \longrightarrow C^\bullet \longrightarrow 0$$

then there exists an infinite sequence of canonically defined morphisms  $d^n : H^n(C^\bullet) \rightarrow H^{n-1}(A^\bullet)$  such that the sequence

$$\dots \longrightarrow H^n(A^\bullet) \longrightarrow H^n(B^\bullet) \longrightarrow H^n(C^\bullet) \longrightarrow H^{n-1}(A^\bullet) \longrightarrow \dots$$

is *exact*, that is the *image* of each homomorphism in the sequence is exactly the *kernel* of the next one.

The *dual* to the category  $\mathbf{S}^\bullet(\mathbb{C})$  is the *category* of  $\mathbf{S}_\bullet(\mathbb{C})$  of *generalized chain complexes*. Its objects and morphisms are obtained by formal inversion of all arrows and lowering all indices.

### 5.1.1 (Co)Homologies in Abelian Categories Related to $M$

Let  $\mathcal{M}^\bullet$  denote the Abelian category of cochains, (i.e.,  $p$ -forms) on the biodynamics configuration manifold  $M$  (see Figure 3.2). When  $\mathcal{C} = \mathcal{M}^\bullet$ , we have the category  $\mathcal{S}^\bullet(\mathcal{M}^\bullet)$  of generalized cochain complexes  $A^\bullet$  in  $\mathcal{M}^\bullet$ ,

and if  $A' = 0$  for  $n < 0$  we have a subcategory  $\mathcal{S}_{DR}^\bullet(\mathcal{M}^\bullet)$  of the *De Rham differential complexes* in  $\mathcal{M}^\bullet$

$$A_{DR}^\bullet : 0 \rightarrow \Omega^0(M) \xrightarrow{d} \Omega^1(M) \xrightarrow{d} \Omega^2(M) \cdots \xrightarrow{d} \Omega^n(M) \xrightarrow{d} \cdots$$

Here  $A' = \Omega^n(M)$  is the vector space over  $\mathbb{R}$  of all  $p$ -forms  $\omega$  on  $M$  (for  $p = 0$  the smooth functions on  $M$ ) and  $d_n = d : \Omega^{n-1}(M) \rightarrow \Omega^n(M)$  is the exterior differential. A form  $\omega \in \Omega^n(M)$  such that  $d\omega = 0$  is a closed form or  $n$ -cocycle. A form  $\omega \in \Omega^n(M)$  such that  $\omega = d\theta$ , where  $\theta \in \Omega^{n-1}(M)$ , is an exact form or  $n$ -coboundary. Let  $Z^n(M) = \text{Ker } d$  (resp.  $B^n(M) = \text{Im } d$ ) denote a real vector space of cocycles (resp. coboundaries) of degree  $n$ . Since  $d_{n+1} \circ d_n = d^2 = 0$ , we have  $B^n(M) \subset Z^n(M)$ . The quotient vector space

$$H_{DR}^n(M) = \text{Ker } d / \text{Im } d = Z^n(M) / B^n(M)$$

is the *De Rham cohomology group*. The elements of  $H_{DR}^n(M)$  represent equivalence sets of cocycles. Two cocycles  $\omega_1, \omega_2$  belong to the same equivalence set, or are cohomologous (written  $\omega_1 \sim \omega_2$ ) iff they differ by a coboundary  $\omega_1 - \omega_2 = d\theta$ . The de Rham's cohomology class of any form  $\omega \in \Omega^n(M)$  is  $[\omega] \in H_{DR}^n(M)$ . The De Rham differential complex (1) can be considered as a system of second-order DEs  $d^2\theta = 0$ ,  $\theta \in \Omega^{n-1}(M)$  having a solution represented by  $Z^n(M) = \text{Ker } d$ .

Analogously let  $\mathcal{M}_\bullet$  denote the Abelian category of chains on the configuration manifold  $M$ . When  $\mathcal{C} = \mathcal{M}_\bullet$ , we have the category  $\mathcal{S}_\bullet(\mathcal{M}_\bullet)$  of generalized chain complexes  $A_\bullet$  in  $\mathcal{M}_\bullet$ , and if  $A_n = 0$  for  $n < 0$  we have a subcategory  $\mathcal{S}_\bullet^{\mathcal{C}}(\mathcal{M}_\bullet)$  of chain complexes in  $\mathcal{M}_\bullet$ .

$$A_\bullet : 0 \leftarrow C^0(M) \xleftarrow{\partial} C^1(M) \xleftarrow{\partial} C^2(M) \cdots \xleftarrow{\partial} C^n(M) \xleftarrow{\partial} \cdots$$

Here  $A_n = C^n(M)$  is the vector space over  $\mathbb{R}$  of all finite chains  $C$  on the manifold  $M$  and  $\partial_n = \partial : C^{n+1}(M) \rightarrow C^n(M)$ . A finite chain  $C$  such that  $\partial C = 0$  is an  $n$ -cycle. A finite chain  $C$  such that  $C = \partial B$  is an  $n$ -boundary. Let  $Z_n(M) = \text{Ker } \partial$  (resp.  $B_n(M) = \text{Im } \partial$ ) denote a real vector space of cycles (resp. boundaries) of degree  $n$ . Since  $\partial_{n+1} \circ \partial_n = \partial^2 = 0$ , we have  $B_n(M) \subset Z_n(M)$ . The quotient vector space

$$H_n^{\mathcal{C}}(M) = \text{Ker } \partial / \text{Im } \partial = Z_n(M) / B_n(M)$$

is the  $n$ -homology group. The elements of  $H_n^{\mathcal{C}}(M)$  are equivalence sets of cycles. Two cycles  $C_1, C_2$  belong to the same equivalence set, or are

homologous (written  $C_1 \sim C_2$ ), iff they differ by a boundary  $C_1 - C_2 = \partial B$ . The homology class of a finite chain  $C \in C^n(M)$  is  $[C] \in H_n^C(M)$ .

The dimension of the  $n$ -cohomology (resp.  $n$ -homology) group equals the  $n$ th Betti number  $b^n$  (resp.  $b_n$ ) of the manifold  $M$ . *Poincaré lemma* says that on an open set  $U \in M$  diffeomorphic to  $\mathbb{R}^N$ , all closed forms (cycles) of degree  $p \geq 1$  are exact (boundaries). That is, the Betti numbers satisfy  $b^p = 0$  (resp.  $b = 0$ ) for  $p = 1, \dots, n$ .

The *De Rham theorem* states the following. The map  $\Phi: H_n \times H^n \rightarrow \mathbb{R}$  given by  $([C], [\omega]) \rightarrow \langle C, \omega \rangle$  for  $C \in Z_n, \omega \in Z^n$  is a bilinear nondegenerate map which establishes the duality of the groups (vector spaces)  $H_n$  and  $H^n$  and the equality  $b_n = b^n$ .

### 5.1.2 Reduction and Euler–Poincaré Characteristic

Recall (see subsection (3.5.3.2) above), that for the purpose of high-level control, the rotational biodynamic configuration manifold  $M$  (Figure 3.1), could be first, reduced to an  $n$ -torus, and second, transformed into an  $n$ -cube ‘hyper-joystick’, using the following topological techniques (see [Ivancevic (2002); Ivancevic and Pearce (2001b); Ivancevic (2005)]).

Let  $S^1$  denote the constrained unit circle in the complex plane, which is an Abelian Lie group. Firstly, we propose two reduction homeomorphisms, using the noncommutative semidirect product ‘ $\triangleright$ ’ of the constrained  $SO(2)$ -groups:

$$SO(3) \gtrsim SO(2) \triangleright SO(2) \triangleright SO(2), \quad \text{and} \quad SO(2) \approx S^1.$$

Next, let  $I^n$  be the unit cube  $[0, 1]^n$  in  $\mathbb{R}^n$  and ‘ $\sim$ ’ an equivalence relation on  $\mathbb{R}^n$  obtained by ‘gluing’ together the opposite sides of  $I^n$ , preserving their orientation. Therefore, the manifold  $M$  can be represented as the quotient space of  $\mathbb{R}^n$  by the space of the integral lattice points in  $\mathbb{R}^n$ , that is an oriented and constrained  $n$ D torus  $T^n$ :

$$\mathbb{R}^n / Z^n = I^n / \sim \approx \prod_{i=1}^n S_i^1 \equiv \{(q^i, i = 1, \dots, N) : \text{mod } 2\pi\} = T^n. \quad (5.2)$$

Now, using the *De Rham theorem* and the *homotopy axiom* for the De Rham cohomologies, we can calculate the *Euler–Poincaré characteristics* for  $T^n$  as well as for its two bundles,  $TT^n$  and  $T^*T^n$ , as (see [Ivancevic

(2002); Ivancevic (2005)])

$$\chi(T^n, TT^n) = \sum_{p=1}^n (-1)^p b_p,$$

where  $b_p$  are the *Betti numbers* defined as

$$\begin{aligned} b^0 &= 1, \\ b^1 &= n, \dots b^p = \binom{n}{p}, \dots b^{n-1} = n, \\ b^n &= 1, \quad (p = 0, \dots, n). \end{aligned} \tag{5.3}$$

## 5.2 Natural Duality in Biodynamics

The present section uncovers the underlying dual geometro-topological structure beneath the general biodynamics. It presents a parallel development of Hamiltonian and Lagrangian formulations of biodynamics (see[Ivancevic and Snoswell (2001); Ivancevic (2002); Ivancevic and Pearce (2001b); Ivancevic and Pearce (2001b); Ivancevic (2005)]), proves both differential-geometric and algebraic-topological dualities between these two formulations, and finally establishes a *unique functorial relation* between biodynamics geometry and biodynamics topology.

Lagrangian formulation of biodynamics is performed on the *tangent bundle*  $TM$ , while Hamiltonian formulation is performed on the *cotangent bundle*  $T^*M$ . Both *Riemannian* and *symplectic* geometry are used for these formulations. The geometric duality (see [Kolar *et al.* (1993); Choquet-Bruhat and DeWitt-Morete (1982)]) of Lie groups and algebras between these two biodynamics formulations is proved as an existence of natural equivalence between Lie and canonical functors. The topological duality (see [Dodson and Parker (1997)]) between these two biodynamics formulations is proved as an existence of natural equivalence between Lagrangian and Hamiltonian functors in both *homology* and *cohomology* categories. In the case of reduced configuration manifold, the Betti numbers and Euler-Poincaré characteristic are given.

### 5.2.1 Geometric Duality Theorem for $M$

**Theorem.** There is a geometric duality between rotational Lagrangian and Hamiltonian biodynamic formulations on  $M$  (as given by Figure 3.1).



In categorical terms, there is a unique natural geometric equivalence

$$\text{Dual}_G : \text{Lie} \cong \text{Can}$$

in biodynamics (symbols are described in the next subsection).

**Proof.** The proof has two parts: Lie-functorial and geometric.

#### 5.2.1.1 Lie-Functorial Proof

If we apply the functor  $\text{Lie}$  on the category  $\bullet[SO(n)^i]$  (for  $n = 2, 3$  and  $i = 1, \dots, N$ ) of rotational Lie groups  $SO(n)^i$  (and their homomorphisms) we get the category  $\bullet[so(n)_i]$  of corresponding *tangent* Lie algebras  $so(n)_i$  (and their homomorphisms). If we further apply the isomorphic functor  $\text{Dual}$  to the category  $\bullet[so(n)_i]$  we get the dual category  $\bullet[so(n)_i^*]$  of *cotangent*, or, *canonical* Lie algebras  $so(n)_i^*$  (and their homomorphisms). To go directly from  $\bullet[SO(n)^i]$  to  $\bullet[so(n)_i^*]$  we use the canonical functor  $\text{Can}$ . Therefore, we have a commutative triangle:

$$\begin{array}{ccc}
 & \bullet[SO(n)^i] & \\
 \text{Lie} \swarrow & & \searrow \text{Can} \\
 \bullet[so(n)_i] & \xrightarrow[\text{Dual}_A]{\cong} & \bullet[so(n)_i^*]
 \end{array}$$

$LGA$

Applying the functor  $\text{Lie}$  on the biodynamics configuration manifold  $M$ , we get the product-tree of the same anthropomorphic structure, but having tangent Lie algebras  $so(n)_i$  as vertices, instead of the groups  $SO(n)^i$ . Again, applying the functor  $\text{Can}$  on  $M$ , we get the product-tree of the same anthropomorphic structure, but this time having cotangent Lie algebras  $so(n)_i^*$  as vertices. Both the tangent algebras  $so(n)_i$  and the cotangent algebras  $so(n)_i^*$  contain infinitesimal group generators: angular velocities  $\dot{q}^i = \dot{q}^{\phi_i}$  – in the first case, and canonical angular momenta  $p_i = p_{\phi_i}$  – in the second case [Ivancevic and Snoswell (2001)]. As Lie group generators, both the angular velocities and the angular momenta satisfy the commutation relations:  $[\dot{q}^{\phi_i}, \dot{q}^{\psi_i}] = \epsilon_{\theta}^{\phi\psi} \dot{q}^{\theta_i}$  and  $[p_{\phi_i}, p_{\psi_i}] = \epsilon_{\phi\psi}^{\theta} p_{\theta_i}$ , respectively, where the structure constants  $\epsilon_{\theta}^{\phi\psi}$  and  $\epsilon_{\phi\psi}^{\theta}$  constitute the totally antisymmetric third-order tensors.

In this way, the functor  $\text{Dual}_G : \text{Lie} \cong \text{Can}$  establishes the unique geometric duality between kinematics of angular velocities  $\dot{q}^i$  (involved in

*Lagrangian* formalism on the tangent bundle of  $M$ ) and kinematics of angular momenta  $p_i$  (involved in *Hamiltonian* formalism on the cotangent bundle of  $M$ ), which is analyzed below. In other words, we have two functors, *Lie* and *Can*, from the *category of Lie groups* (of which  $\bullet[SO(n)^i]$  is a subcategory) into the *category of (their) Lie algebras* (of which  $\bullet[so(n)_i]$  and  $\bullet[so(n)^*_i]$  are subcategories), and a unique natural equivalence between them defined by the functor  $\text{Dual}_G$ . (As angular momenta  $p_i$  are in a bijective correspondence with angular velocities  $\dot{q}^i$ , every component of the functor  $\text{Dual}_G$  is invertible.) ■

### 5.2.1.2 Geometric Proof

Geometric proof is given along the lines of Riemannian and symplectic geometry of mechanical systems, as follows (see 4.1 and 4.2.2 above, as well as [Marsden and Ratiu (1999); Ivancevic and Snoswell (2001); Ivancevic (2002); Ivancevic and Pearce (2001b); Ivancevic (2005)]). Recall that the Riemannian metric  $g = \langle, \rangle$  on the configuration manifold  $M$  is a positive-definite quadratic form  $g : TM \rightarrow \mathbb{R}$ , given in local coordinates  $q^i \in U$  ( $U$  open in  $M$ ) as

$$g_{ij} \mapsto g_{ij}(q, m) dq^i dq^j, \quad \text{where}$$

$$g_{ij}(q, m) = m_\mu \delta_{rs} \frac{\partial x^r}{\partial q^i} \frac{\partial x^s}{\partial q^j}$$

is the covariant material metric tensor  $g$ , defining a relation between internal and external coordinates and including  $n$  segmental masses  $m_\mu$ . The quantities  $x^r$  are external coordinates ( $r, s = 1, \dots, 6n$ ) and  $i, j = 1, \dots, N \equiv 6n - h$ , where  $h$  denotes the number of holonomic constraints.

The *Lagrangian* of the system is a quadratic form  $L : TM \rightarrow \mathbb{R}$  dependent on velocity  $v$  and such that  $L(v) = \frac{1}{2} \langle v, v \rangle$ . It is given by

$$L(v) = \frac{1}{2} g_{ij}(q, m) v^i v^j$$

in local coordinates  $q^i$ ,  $v^i = \dot{q}^i \in U_v$  ( $U_v$  open in  $TM$ ). The *Hamiltonian* of the system is a quadratic form  $H : T^*M \rightarrow \mathbb{R}$  dependent on momentum  $p$  and such that  $H(p) = \frac{1}{2} \langle p, p \rangle$ . It is given by

$$H(p) = \frac{1}{2} g^{ij}(q, m) p_i p_j$$

in local canonical coordinates  $q^i, p_i \in U_p$  ( $U_p$  open in  $T^*M$ ). The inverse

(contravariant) metric tensor  $g^{-1}$ , is defined as

$$g^{ij}(q, m) = m_\mu \delta_{rs} \frac{\partial q^i}{\partial x^r} \frac{\partial q^j}{\partial x^s}.$$

For any smooth function  $L$  on  $TM$ , the *fibre derivative*, or *Legendre transformation*, is a diffeomorphism  $\mathbb{F}L : TM \rightarrow T^*M$ ,  $\mathbb{F}L(w) \cdot v = \langle w, v \rangle$ , from the momentum phase-space manifold to the velocity phase-space manifold associated with the metric  $g = \langle, \rangle$ . In local coordinates  $q^i, v^i = \dot{q}^i \in U_v$  ( $U_v$  open in  $TM$ ),  $\mathbb{F}L$  is given by  $(q^i, v^i) \mapsto (q^i, p_i)$ .

Recall that on the momentum phase-space manifold  $T^*M$  exists:

- (i) A unique canonical 1-form  $\theta_H$  with the property that, for any 1-form  $\beta$  on the configuration manifold  $M$ , we have  $\beta^* \theta_H = \beta$ . In local canonical coordinates  $q^i, p_i \in U_p$  ( $U_p$  open in  $T^*M$ ) it is given by  $\theta_H = p_i dq^i$ .
- (ii) A unique nondegenerate Hamiltonian symplectic 2-form  $\omega_H$ , which is closed ( $d\omega_H = 0$ ) and exact ( $\omega_H = d\theta_H = dp_i \wedge dq^i$ ). Each body segment has, in the general  $SO(3)$  case, a sub-phase-space manifold  $T^*SO(3)$  with

$$\omega_H^{(sub)} = dp_\phi \wedge d\phi + dp_\psi \wedge d\psi + dp_\theta \wedge d\theta.$$

Analogously, on the velocity phase-space manifold  $TM$  exists:

- (i) A unique 1-form  $\theta_L$ , defined by the *pull-back*  $\theta_L = (\mathbb{F}L)^* \theta_H$  of  $\theta_H$  by  $\mathbb{F}L$ . In local coordinates  $q^i, v^i = \dot{q}^i \in U_v$  ( $U_v$  open in  $TM$ ) it is given by  $\theta_L = L_{v^i} dq^i$ , where  $L_{v^i} \equiv \partial L / \partial v^i$ .
- (ii) A unique nondegenerate Lagrangian symplectic 2-form  $\omega_L$ , defined by the pull-back  $\omega_L = (\mathbb{F}L)^* \omega_H$  of  $\omega_H$  by  $\mathbb{F}L$ , which is closed ( $d\omega_L = 0$ ) and exact ( $\omega_L = d\theta_L = dL_{v^i} \wedge dq^i$ ).

Both  $T^*M$  and  $TM$  are orientable manifolds, admitting the standard volumes given respectively by

$$\Omega_{\omega_H} = \frac{(-1)^{\frac{N(N+1)}{2}}}{N!} \omega_H^N, \quad \text{and} \quad \Omega_{\omega_L} = \frac{(-1)^{\frac{N(N+1)}{2}}}{N!} \omega_L^N,$$

in local coordinates  $q^i, p_i \in U_p$  ( $U_p$  open in  $T^*M$ ), resp.  $q^i, v^i = \dot{q}^i \in U_v$  ( $U_v$  open in  $TM$ ). They are given by

$$\begin{aligned} \Omega_H &= dq^1 \wedge \cdots \wedge dq^N \wedge dp_1 \wedge \cdots \wedge dp_N, & \text{and} \\ \Omega_L &= dq^1 \wedge \cdots \wedge dq^N \wedge dv^1 \wedge \cdots \wedge dv^N. \end{aligned}$$

On the velocity phase-space manifold  $TM$  we can also define the *action*  $A : TM \rightarrow \mathbb{R}$  by  $A(v) = \mathbb{F}L(v) \cdot v$  and the energy  $E = A - L$ . In local coordinates  $q^i, v^i = \dot{q}^i \in U_v$  ( $U_v$  open in  $TM$ ) we have  $A = v^i L_{v^i}$ , so  $E = v^i L_{v^i} - L$ . The Lagrangian vector-field  $X_L$  on  $TM$  is determined

by the condition  $i_{X_L}\omega_L = dE$ . Classically, it is given by the second-order Lagrange equations

$$\frac{d}{dt}L_{v^i} = L_{q^i}. \quad (5.4)$$

The Hamiltonian vector-field  $X_H$  is defined on the momentum phase-space manifold  $T^*M$  by the condition  $i_{X_H}\omega = dH$ . The condition may be expressed equivalently as  $X_H = J\nabla H$ , where  $J = \begin{pmatrix} 0 & I \\ -I & 0 \end{pmatrix}$ .

In local canonical coordinates  $q^i, p_i \in U_p$  ( $U_p$  open in  $T^*M$ ) the vector-field  $X_H$  is classically given by the first-order Hamilton's canonical equations

$$\dot{q}^i = \partial_{p_i}H, \quad \dot{p}_i = -\partial_{q^i}H. \quad (5.5)$$

As a Lie group, the configuration manifold  $M$  is Hausdorff. Therefore for  $x = (q^i, p_i) \in U_p$  ( $U_p$  open in  $T^*M$ ) there exists a unique one-parameter group of diffeomorphisms  $\phi_t : T^*M \rightarrow T^*M$  such that  $\frac{d}{dt}|_{t=0} \phi_t x = J\nabla H(x)$ . This is termed *Hamiltonian phase-flow* and represents the maximal integral curve  $t \mapsto (q^i(t), p_i(t))$  of the Hamiltonian vector-field  $X_H$  passing through the point  $x$  for  $t = 0$ .

The flow  $\phi_t$  is *symplectic* if  $\omega_H$  is constant along it (that is,  $\phi_t^*\omega_H = \omega_H$ ) iff its Lie derivative vanishes (that is,  $\mathcal{L}_{X_H}\omega_H = 0$ ). A symplectic flow consists of canonical transformations on  $T^*M$ , that is, local diffeomorphisms that leave  $\omega_H$  invariant. By Liouville theorem, a symplectic flow  $\phi_t$  preserves the phase volume on  $T^*M$ . Also, the total energy  $H = E$  of the system is conserved along  $\phi_t$ , that is,  $H \circ \phi_t = H$ .

*Lagrangian flow* can be defined analogously (see [Abraham and Marsden (1978); Marsden and Ratiu (1999)]).

For a Lagrangian (resp. a Hamiltonian) vector-field  $X_L$  (resp.  $X_H$ ) on  $M$ , there is a base integral curve  $\gamma_0(t) = (q^i(t), v^i(t))$  (resp.  $\gamma_0(t) = (q^i(t), p_i(t))$ ) iff  $\gamma_0(t)$  is a geodesic. This is given by the contravariant velocity equation

$$\dot{q}^i = v^i, \quad \dot{v}^i + \Gamma_{jk}^i v^j v^k = 0, \quad (5.6)$$

in the former case, and by the covariant momentum equation

$$\dot{p}_i = g^{kj} p_j, \quad \dot{p}_i + \Gamma_{jk}^i g^{jl} g^{km} p_l p_m = 0, \quad (5.7)$$

in the latter. As before,  $\Gamma_{jk}^i$  denote the Christoffel symbols of an affine connection  $\nabla$  in an open chart  $U$  on  $M$ , defined by the Riemannian metric

$g = \langle, \rangle$  as:  $\Gamma_{jk}^i = g^{il}\Gamma_{jkl}$ ,  $\Gamma_{jkl} = \frac{1}{2}(\partial_{q^j}g_{kl} + \partial_{q^k}g_{jl} - \partial_{q^l}g_{jk})$ .

The l.h.s  $\dot{\tilde{v}}^i = \dot{v}^i + \Gamma_{jk}^i v^j v^k$  (resp.  $\dot{\tilde{p}}_i = \dot{p}_i + \Gamma_{jk}^i g^{jl}g^{km} p_l p_m$ ) in the second parts of (5.6) and (5.7) represent the *Bianchi covariant derivative* of the velocity (resp. momentum) with respect to  $t$ . Parallel transport on  $M$  is defined by  $\dot{\tilde{v}}^i = 0$ , (resp.  $\dot{\tilde{p}}_i = 0$ ). When this applies,  $X_L$  (resp.  $X_H$ ) is called the *geodesic spray* and its flow the *geodesic flow*.

For the dynamics in the gravitational potential field  $V : M \rightarrow \mathbb{R}$ , the Lagrangian  $L : TM \rightarrow \mathbb{R}$  (resp. the Hamiltonian  $H : T^*M \rightarrow \mathbb{R}$ ) has an extended form

$$\begin{aligned} L(v, q) &= \frac{1}{2} g_{ij} v^i v^j - V(q), \\ (\text{resp. } H(p, q) &= \frac{1}{2} g^{ij} p_i p_j + V(q)). \end{aligned}$$

A Lagrangian vector-field  $X_L$  (resp. Hamiltonian vector-field  $X_H$ ) is still defined by the second-order Lagrangian equations (5.4, 5.6) (resp. first-order Hamiltonian equations (5.5, 5.7)).

The fibre derivative  $\mathbb{F}L : TM \rightarrow T^*M$  thus maps Lagrange's equations (5.4, 5.6) into Hamilton's equations (5.5, 5.7). Clearly there exists a diffeomorphism  $\mathbb{F}H : T^*M \rightarrow TM$ , such that  $\mathbb{F}L = (\mathbb{F}H)^{-1}$ . In local canonical coordinates  $q^i, p_i \in U_p$  ( $U_p$ , open in  $T^*M$ ) this is given by  $(q^i, p_i) \mapsto (q^i, v^i)$  and thus maps Hamilton's equations (5.5, 5.7) into Lagrange's equations (5.4, 5.6).

A general form of the forced, non-conservative Hamilton's equations (resp. Lagrange's equations) is given as

$$\begin{aligned} \dot{q}^i &= \frac{\partial H}{\partial p_i}, \quad \dot{p}_i = -\frac{\partial H}{\partial q^i} + F_i(t, q^i, p_i), \\ (\text{resp. } \frac{d}{dt} \frac{\partial L}{\partial v^i} - \frac{\partial L}{\partial q^i} &= F_i(t, q^i, v^i)). \end{aligned}$$

Here the  $F_i(t, q^i, p_i)$  (resp.  $F_i(t, q^i, v^i)$ ) represent any kind of *covariant forces*, including dissipative and elastic joint forces, as well as actuator drives and control forces, as a function of time, coordinates and momenta. In covariant form we have

$$\begin{aligned} \dot{q}^k &= g^{ki} p_i, \quad \dot{p}_i + \Gamma_{jk}^i g^{jl} g^{km} p_l p_m = F_i(t, q^i, p_i), \\ (\text{resp. } \dot{q}^i &= v^i, \quad \dot{v}^i + \Gamma_{jk}^i v^j v^k = g^{ij} F_j(t, q^i, v^i)). \quad \blacksquare \end{aligned}$$

This proves the existence of the unique natural geometric equivalence

$$\text{Dual}_G : \text{Lie} \cong \text{Can}$$

in the rotational biodynamics.

### 5.2.2 Topological Duality Theorem for $M$

In this section we want to prove that the general biodynamics can be *equiv-  
alently* described in terms of two *topologically dual functors*  $\text{Lag}$  and  $\text{Ham}$ ,  
from  $\text{Diff}$ , the *category of smooth manifolds* (and their smooth maps) of  
class  $C^p$ , into  $\text{Bund}$ , the *category of vector bundles* (and vector-bundle  
maps) of class  $C^{p-1}$ , with  $p \geq 1$ .  $\text{Lag}$  is physically represented by the  
second-order Lagrangian formalism on  $TM \in \text{Bund}$ , while  $\text{Ham}$  is physically  
represented by the first-order Hamiltonian formalism on  $T^*M \in \text{Bund}$ .

**Theorem.** There is a topological duality between Lagrangian and  
Hamiltonian formalisms on  $M$  (as given by Figure 3.1). In categorical  
terms, there is a unique natural topological equivalence

$$\text{Dual}_T : \text{Lag} \cong \text{Ham}$$

in the general biodynamics.

**Proof.** The proof has two parts: cohomological and homological.

#### 5.2.2.1 Cohomological Proof

If  $\mathcal{C} = \mathcal{H}^\bullet \mathcal{M}$  (resp.  $\mathcal{C} = \mathcal{L}^\bullet \mathcal{M}$ ) represents the Abelian category of cochains  
on the momentum phase-space manifold  $T^*M$  (resp. the velocity phase-  
space manifold  $TM$ ), we have the category  $\mathcal{S}^\bullet(\mathcal{H}^\bullet \mathcal{M})$  (resp.  $\mathcal{S}^\bullet(\mathcal{L}^\bullet \mathcal{M})$ ) of  
generalized cochain complexes  $A^\bullet$  in  $\mathcal{H}^\bullet \mathcal{M}$  (resp.  $\mathcal{L}^\bullet \mathcal{M}$ ) and if  $A' = 0$  for  
 $n < 0$  we have a subcategory  $\mathcal{S}_{\mathcal{DR}}^\bullet(\mathcal{H}^\bullet \mathcal{M})$  (resp.  $\mathcal{S}_{\mathcal{DR}}^\bullet(\mathcal{L}^\bullet \mathcal{M})$ ) of De Rham  
differential complexes in  $\mathcal{S}^\bullet(\mathcal{H}^\bullet \mathcal{M})$  (resp.  $\mathcal{S}^\bullet(\mathcal{L}^\bullet \mathcal{M})$ )

$$\begin{aligned} A_{\mathcal{DR}}^\bullet : 0 \rightarrow \Omega^0(T^*M) \xrightarrow{d} \Omega^1(T^*M) \xrightarrow{d} \\ \xrightarrow{d} \Omega^2(T^*M) \xrightarrow{d} \dots \xrightarrow{d} \Omega^N(T^*M) \xrightarrow{d} \dots \\ \text{(resp. } A_{\mathcal{DR}}^\bullet : 0 \rightarrow \Omega^0(TM) \xrightarrow{d} \Omega^1(TM) \xrightarrow{d} \Omega^2(TM) \xrightarrow{d} \\ \dots \xrightarrow{d} \Omega^N(TM) \xrightarrow{d} \dots), \end{aligned}$$

where  $A' = \Omega^N(T^*M)$  (resp.  $A' = \Omega^N(TM)$ ) is the vector space of all  
 $N$ -forms on  $T^*M$  (resp.  $TM$ ) over  $\mathbb{R}$ .

Let  $Z^N(T^*M) = \text{Ker}(d)$  (resp.  $Z^N(T) = \text{Ker}(d)$ ) and  $B^N(T^*M) = \text{Im}(d)$  (resp.  $B^N(TM) = \text{Im}(d)$ ) denote respectively the real vector spaces of cocycles and coboundaries of degree  $N$ . Since  $d_{N+1}d_N = d^2 = 0$ , it follows that  $B^N(T^*M) \subset Z^N(T^*M)$  (resp.  $B^N(TM) \subset Z^N(TM)$ ). The quotient vector space

$$H_{DR}^N(T^*M) = \text{Ker}(d)/\text{Im}(d) = Z^N(T^*M)/B^N(T^*M)$$

(resp.  $H_{DR}^N(TM) = \text{Ker}(d)/\text{Im}(d) = Z^N(TM)/B^N(TM)$ ),

we refer to as the De Rham cohomology group (vector space) of  $T^*M$  (resp.  $TM$ ). The elements of  $H_{DR}^N(T^*M)$  (resp.  $H_{DR}^N(TM)$ ) are equivalence sets of cocycles. Two cocycles  $\omega_1$  and  $\omega_2$  are cohomologous, or belong to the same equivalence set (written  $\omega_1 \sim \omega_2$ ) iff they differ by a coboundary  $\omega_1 - \omega_2 = d\theta$ . Any form  $\omega_H \in \Omega^N(T^*M)$  (resp.  $\omega_L \in \Omega^N(TM)$ ) has a De Rham cohomology class  $[\omega_H] \in H_{DR}^N(T^*M)$  (resp.  $[\omega_L] \in H_{DR}^N(TM)$ ).

Hamiltonian symplectic form  $\omega_H = dp_i \wedge dq_i$  on  $T^*M$  (resp. Lagrangian symplectic form  $\omega_L = dL_{v^i} \wedge dq^i$  on  $TM$ ) is by definition both a closed 2-form or two-cocycle and an exact 2-form or two-coboundary. Therefore the 2D De Rham cohomology group of humanoid motion is defined as a quotient vector space

$$H_{DR}^2(T^*M) = Z^2(T^*M)/B^2(T^*M)$$

(resp.  $H_{DR}^2(TM) = Z^2(TM)/B^2(TM)$ ).

As  $T^*M$  (resp.  $TM$ ) is a compact Hamiltonian symplectic (resp. Lagrangian symplectic) manifold of dimension  $2N$ , it follows that  $\omega_H^N$  (resp.  $\omega_L^N$ ) is a volume element on  $T^*M$  (resp.  $TM$ ), and the  $2ND$  de Rham's cohomology class  $[\omega_H^N] \in H_{DR}^{2N}(T^*M)$  (resp.  $[\omega_L^N] \in H_{DR}^{2N}(TM)$ ) is nonzero. Since  $[\omega_H^N] = [\omega_H]^N$  (resp.  $[\omega_L^N] = [\omega_L]^N$ ), then  $[\omega_H] \in H_{DR}^2(T^*M)$  (resp.  $[\omega_L] \in H_{DR}^2(TM)$ ) and all of its powers up to the  $N$ -th must be zero as well. The existence of such an element is a necessary condition for  $T^*M$  (resp.  $TM$ ) to admit a Hamiltonian symplectic structure  $\omega_H$  (resp. Lagrangian symplectic structure  $\omega_L$ ).

The De Rham complex  $A_{DR}^\bullet$  on  $T^*M$  (resp.  $TM$ ) can be considered as a system of second-order ODEs  $d^2\theta_H = 0$ ,  $\theta_H \in \Omega^N(T^*M)$  (resp.  $d^2\theta_L = 0$ ,  $\theta_L \in \Omega^N(TM)$ ) having a solution represented by  $Z^N(T^*M)$  (resp.  $Z^N(TM)$ ). In local coordinates  $q^i$ ,  $p_i \in U_p$  ( $U_p$  open in  $T^*M$ ) (resp.  $q^i$ ,  $v^i \in U_v$  ( $U_v$  open in  $TM$ )) we have  $d^2\theta_H = d^2(p_i dq^i) = d(dp_i \wedge dq^i) = 0$ , (resp.  $d^2\theta_L = d^2(L_{v^i} dq^i) = d(dL_{v^i} \wedge dq^i) = 0$ ). ■

### 5.2.2.2 Homological Proof

If  $\mathcal{C} = \mathcal{H}_\bullet \mathcal{M}$ , (resp.  $\mathcal{C} = \mathcal{L}_\bullet \mathcal{M}$ ) represents an Abelian category of chains on  $T^*M$  (resp.  $TM$ ), we have a category  $\mathcal{S}_\bullet(\mathcal{H}_\bullet \mathcal{M})$  (resp.  $\mathcal{S}_\bullet(\mathcal{L}_\bullet \mathcal{M})$ ) of generalized chain complexes  $\mathcal{A}_\bullet$  in  $\mathcal{H}_\bullet \mathcal{M}$  (resp.  $\mathcal{L}_\bullet \mathcal{M}$ ), and if  $A = 0$  for  $n < 0$  we have a subcategory  $\mathcal{S}_\bullet^C(\mathcal{H}_\bullet \mathcal{M})$  (resp.  $\mathcal{S}_\bullet^C(\mathcal{L}_\bullet \mathcal{M})$ ) of chain complexes in  $\mathcal{H}_\bullet \mathcal{M}$  (resp.  $\mathcal{L}_\bullet \mathcal{M}$ )

$$\begin{aligned} \mathcal{A}_\bullet : 0 \leftarrow C^0(T^*M) \xleftarrow{\partial} C^1(T^*M) \xleftarrow{\partial} C^2(T^*M) \xleftarrow{\partial} \dots \\ \dots \xleftarrow{\partial} C^n(T^*M) \xleftarrow{\partial} \dots \\ (\text{resp. } \mathcal{A}_\bullet : 0 \leftarrow C^0(TM) \xleftarrow{\partial} C^1(TM) \xleftarrow{\partial} C^2(TM) \xleftarrow{\partial} \dots \\ \dots \xleftarrow{\partial} C^n(TM) \xleftarrow{\partial} \dots). \end{aligned}$$

Here  $A_N = C^N(T^*M)$  (resp.  $A_N = C^N(TM)$ ) is the vector space of all finite chains  $C$  on  $T^*M$  (resp.  $TM$ ) over  $\mathbb{R}$ , and  $\partial_N = \partial : C^{N+1}(T^*M) \rightarrow C^N(T^*M)$  (resp.  $\partial_N = \partial : C^{N+1}(TM) \rightarrow C^N(TM)$ ). A finite chain  $C$  such that  $\partial C = 0$  is an  $N$ -cycle. A finite chain  $C$  such that  $C = \partial B$  is an  $N$ -boundary. Let  $Z_N(T^*M) = \text{Ker}(\partial)$  (resp.  $Z_N(TM) = \text{Ker}(\partial)$ ) and  $B_N(T^*M) = \text{Im}(\partial)$  (resp.  $B_N(TM) = \text{Im}(\partial)$ ) denote respectively real vector spaces of cycles and boundaries of degree  $N$ . Since  $\partial_{N-1}\partial_N = \partial^2 = 0$ , then  $B_N(T^*M) \subset Z_N(T^*M)$  (resp.  $B_N(TM) \subset Z_N(TM)$ ). The quotient vector space

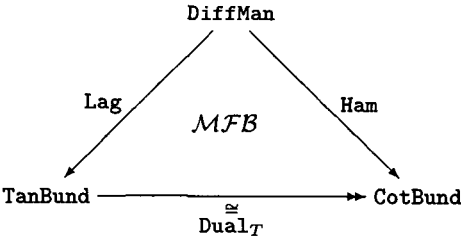
$$\begin{aligned} H_N^C(T^*M) &= Z_N(T^*M)/B_N(T^*M) \\ (\text{resp. } H_N^C(TM) &= Z_N(TM)/B_N(TM)) \end{aligned}$$

represents an  $ND$  biodynamics homology group (vector space). The elements of  $H_N^C(T^*M)$  (resp.  $H_N^C(TM)$ ) are equivalence sets of cycles. Two cycles  $C_1$  and  $C_2$  are homologous, or belong to the same equivalence set (written  $C_1 \sim C_2$ ) iff they differ by a boundary  $C_1 - C_2 = \partial B$ . The homology class of a finite chain  $C \in C^N(T^*M)$  (resp.  $C \in C^N(TM)$ ) is  $[C] \in H_N^C(T^*M)$  (resp.  $[C] \in H_N^C(TM)$ ). ■

### 5.2.3 Lagrangian Versus Hamiltonian Duality

In this way, we have proved a commutativity of a triangle:





which implies the existence of the unique natural topological equivalence

$$\text{Dual}_T : \text{Lag} \cong \text{Ham}$$

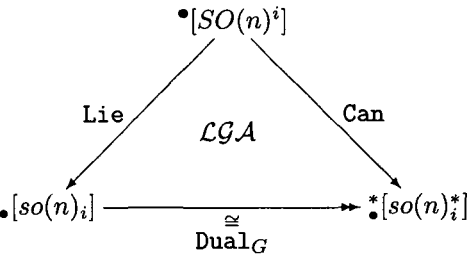
in the rotational biodynamics.

### 5.2.4 Globally Dual Structure of Rotational Biodynamics

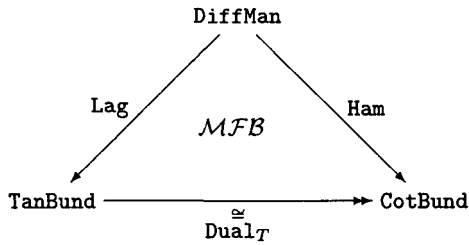
**Theorem.** Global dual structure of the rotational biodynamics is defined by the unique natural equivalence

$$\text{Dyn} : \text{Dual}_G \cong \text{Dual}_T.$$

**Proof.** This unique functorial relation, uncovering the natural equivalence between *geometric* and *topological* structures of biodynamics:



$$\begin{array}{c} \mathcal{F} \Big| \dashv \Big| \mathcal{G} \\ \downarrow \qquad \uparrow \end{array}$$



– has been established by parallel development of Lagrangian and Hamiltonian biodynamic formulations, i.e., functors  $\text{Lag}(\text{Lie})$  and  $\text{Ham}(\text{Can})$ .

### 5.3 Topological Phase Transitions and Hamiltonian Chaos

#### 5.3.1 Phase Transitions in Hamiltonian Systems

Recall from introduction to synergetics (chapter 2) that *phase transitions* (PTs) are phenomena which bring about *qualitative* physical changes at the macroscopic level in presence of the same microscopic forces acting among the constituents of a system (see also Appendix for details). Their mathematical description requires to translate into *quantitative* terms the mentioned qualitative changes. The standard way of doing this is to consider how the values of thermodynamic observables, obtained in laboratory experiments, vary with temperature, or volume, or an external field, and then to associate the experimentally observed discontinuities at a PT to the appearance of some kind of singularity entailing a loss of analyticity. Despite the smoothness of the statistical measures, after the *Yang–Lee theorem* [Yang and Lee (1952)] we know that in the  $N \rightarrow \infty$  limit non-analytic behaviors of thermodynamic functions are possible whenever the analyticity radius in the complex fugacity plane shrinks to zero, because this entails the loss of *uniform convergence* in  $N$  (number of degrees of freedom) of any sequence of real-valued thermodynamic functions, and all this depends on the distribution of the zeros of the grand canonical partition function. Also the other developments of the rigorous theory of PTs [Georgii (1988); Ruelle (1978)], identify PTs with the loss of analyticity.

In this subsection we will address a recently proposed geometric approach to thermodynamic phase transitions (see [Caiani *et al.* (1997); Franzosi *et al.* (1999); Franzosi *et al.* (2000); Franzosi and Pettini (2004)]). Given any Hamiltonian system, the configuration space can be endowed with a metric, in order to obtain a Riemannian geometrization of the dy-

namics (see chapter 3). At the beginning, several numerical and analytical studies of a variety of models showed that the fluctuation of the curvature becomes singular at the transition point. Then the following conjecture was proposed in [Caiani *et al.* (1997)]: The phase transition is determined by a change in the topology of the configuration space, and the loss of analyticity in the thermodynamic observables is nothing but a consequence of such topological change. The latter conjecture is also known as the *topological hypothesis*.

The topological hypothesis states that suitable topology changes of equipotential submanifolds of the Hamiltonian system's configuration manifold can entail thermodynamic phase transitions [Franzosi *et al.* (2000)]. The authors of the topological hypothesis gave both a theoretical argument and numerical demonstration in case of  $2d$  lattice  $\varphi^4$  model. They considered classical many-particle (or many-subsystem) systems described by standard *biodynamic-like Hamiltonians*

$$H(p, q) = \sum_{i=1}^N \frac{p_i^2}{2m} + V(q), \quad (5.8)$$

where the coordinates and momenta, ( $q^i = q^i(t)$ ,  $p_i = p_i(t)$ ,  $i = 1, \dots, N$ ), assume continuous values and the system's potential energy  $V(q)$  is bounded below.

Now, assuming a large number of subsystems  $N$ , the statistical behavior of physical systems described by Hamiltonians of the type (5.8) is usually encompassed, in the system's canonical ensemble, by the *partition function* in the system's phase space (see Appendix for details)

$$\begin{aligned} Z_N(\beta) &= \int \prod_{i=1}^N dp_i dq^i e^{-\beta H(p, q)} = \left(\frac{\pi}{\beta}\right)^{\frac{N}{2}} \int \prod_{i=1}^N dq^i e^{-\beta V(q)} \\ &= \left(\frac{\pi}{\beta}\right)^{\frac{N}{2}} \int_0^\infty dv e^{-\beta v} \int_{M_v} \frac{d\sigma}{\|\nabla V\|}, \end{aligned} \quad (5.9)$$

where the last term is written using a *co-area formula* [Federer (1969)], and  $v$  labels the *equipotential hypersurfaces*  $M_v$  of the system's configuration manifold  $M$ ,

$$M_v = \{(q^1, \dots, q^N) \in \mathbb{R}^N | V(q^1, \dots, q^N) = v\}. \quad (5.10)$$

Equation (5.9) shows that for Hamiltonians (3.5) the relevant statistical

information is contained in the *canonical configurational partition function*

$$Z_N^C = \int \prod_{i=1}^N dq^i \exp[-\beta V(q)].$$

Therefore, partition function  $Z_N^C$  is decomposed – in the last term of equation (5.9) – into an infinite summation of geometric integrals,  $\int_{M_v} d\sigma / \|\nabla V\|$ , defined on the  $\{M_v\}_{v \in \mathbb{R}}$ . Once the microscopic interaction potential  $V(q)$  is given, the configuration space of the system is automatically foliated into the family  $\{M_v\}_{v \in \mathbb{R}}$  of these equipotential hypersurfaces. Now, from standard statistical mechanical arguments we know that, at any given value of the inverse temperature  $\beta$ , the larger the number  $N$  of particles the closer to  $M_v \equiv M_{u_\beta}$  are the microstates that significantly contribute to the averages – computed through  $Z_N(\beta)$  – of thermodynamic observables. The hypersurface  $M_{u_\beta}$  is the one associated with the average potential energy computed at a given  $\beta$ ,

$$u_\beta = (Z_N^C)^{-1} \int \prod_{i=1}^N dq^i V(q) \exp[-\beta V(q)].$$

Thus, at any  $\beta$ , if  $N$  is very large the effective support of the canonical measure shrinks very close to a single  $M_v = M_{u_\beta}$ .

Explicitly, the topological hypothesis reads: the basic origin of a phase transition lies in a suitable topology change of the  $\{M_v\}$ , occurring at some  $v_c$ . This topology change induces the singular behavior of the thermodynamic observables at a phase transition. By change of topology we mean that  $\{M_v\}_{v < v_c}$  are not diffeomorphic to the  $\{M_v\}_{v > v_c}$ . In other words, canonical measure should ‘feel’ a big and sudden change of the topology of the equipotential hypersurfaces of its underlying support, the consequence being the appearance of the typical signals of a phase transition, i.e., almost singular (at finite  $N$ ) energy or temperature dependences of the averages of appropriate observables.

This point of view has the interesting consequence that – also at finite  $N$  – in principle *different* mathematical objects, i.e., manifolds of different cohomology type, could be associated to *different* thermodynamical phases, whereas from the point of view of measure theory [Yang and Lee (1952)] the only mathematical property available to signal the appearance of a phase transition is the loss of analyticity of the grand-canonical and canonical averages, a fact which is compatible with analytic statistical measures only in the mathematical  $N \rightarrow \infty$  limit.

As it is conjectured that the counterpart of a phase transition is a breaking of diffeomorphicity among the surfaces  $M_v$ , it is appropriate to choose a *diffeomorphism invariant* to probe if and how the topology of the  $M_v$  changes as a function of  $v$ . This is a very challenging task because we have to deal with high dimensional manifolds. Fortunately a topological invariant exists whose computation is feasible, yet demands a big effort. This is the *Euler characteristic*, a diffeomorphism invariant of the system's configuration manifold, expressing its fundamental topological information [Franzosi *et al.* (2000)].

### 5.3.2 Geometry of the Largest Lyapunov Exponent

Now, the topological hypothesis has recently been promoted into a *topological theorem* [Franzosi and Pettini (2004)]. The new theorem says that non-analyticity is the 'shadow' of a more fundamental phenomenon occurring in the system's configuration manifold: a *topology change* within the family of equipotential hypersurfaces (5.10). This topological approach to PTs stems from the numerical study of the Hamiltonian dynamical counterpart of phase transitions, and precisely from the observation of *discontinuous* or *cuspy patterns* (see Figure 7.45 below), displayed by the *largest Lyapunov exponent* at the transition energy (or temperature).

Recall from chapter 2 that the *Lyapunov exponents* measure the strength of *dynamical chaos* and cannot be measured in laboratory experiments, at variance with thermodynamic observables, thus, being genuine dynamical observables they are only measurable in numerical simulations of the microscopic dynamics. To get a hold of the reason why the largest Lyapunov exponent  $\lambda_1$  should probe configuration space topology, let us first remember that for standard Hamiltonian systems (see chapter 4),  $\lambda_1$  is computed by solving the *tangent dynamics equation* for Hamiltonian systems (see Jacobi equation of geodesic deviation (3.49), chapter 3)

$$\ddot{\xi}_i + \left( \frac{\partial^2 V}{\partial q^i \partial q^j} \right)_{q(t)} \xi^j = 0, \quad (5.11)$$

which, for the nonlinear Hamiltonian system

$$\begin{aligned} \dot{q}^1 &= p_1, & \dot{p}_1 &= -\partial_{q^1} V, \\ &\dots & &\dots \\ \dot{q}^N &= p_N, & \dot{p}_N &= -\partial_{q^N} V, \end{aligned}$$

expands into *linearized dynamics*

$$\begin{aligned}\dot{\xi}_1 &= \xi_{N+1}, & \dot{\xi}_{N+1} &= - \sum_{j=1}^N \left( \frac{\partial^2 V}{\partial q_1 \partial q_j} \right)_{q(t)} \xi_j, \\ &\dots & & \dots \\ \dot{\xi}_n &= \xi_{2N}, & \dot{\xi}_{2N} &= - \sum_{j=1}^N \left( \frac{\partial^2 V}{\partial q_N \partial q_j} \right)_{q(t)} \xi_j.\end{aligned}\quad (5.12)$$

Using (5.11) we can get the analytical expression for the largest Lyapunov exponent (compare with (2.15) in chapter 2)

$$\lambda_1 = \lim_{t \rightarrow \infty} \frac{1}{t} \log \frac{\left[ \xi_1^2(t) + \dots + \xi_N^2(t) + \dot{\xi}_1^2(t) + \dots + \dot{\xi}_N^2(t) \right]^{1/2}}{\left[ \xi_1^2(0) + \dots + \xi_N^2(0) + \dot{\xi}_1^2(0) + \dots + \dot{\xi}_N^2(0) \right]^{1/2}}. \quad (5.13)$$

If there are critical points of  $V$  in configuration space, that is points  $q_c = [\bar{q}^1, \dots, \bar{q}^N]$  such that  $\nabla V(q)|_{q=q_c} = 0$ , according to the *Morse lemma* (see e.g., [Hirsch (1976)]), in the neighborhood of any critical point  $q_c$  there always exists a coordinate system  $\tilde{q}(t) = [\bar{q}^1(t), \dots, \bar{q}^N(t)]$  for which

$$V(\tilde{q}) = V(q_c) - (\bar{q}^1)^2 - \dots - (\bar{q}^k)^2 + (\bar{q}^{k+1})^2 + \dots + (\bar{q}^N)^2, \quad (5.14)$$

where  $k$  is the index of the critical point, i.e., the number of negative eigenvalues of the Hessian of  $V$ . In the neighborhood of a critical point, equation (5.14) yields

$$\partial^2 V / \partial q^i \partial q^j = \pm \delta_{ij},$$

which, substituted into equation (5.11), gives  $k$  *unstable directions* which contribute to the exponential growth of the norm of the tangent vector  $\xi = \xi(t)$ . This means that the strength of dynamical chaos, measured by the largest Lyapunov exponent  $\lambda_1$ , is affected by the existence of critical points of  $V$ . In particular, let us consider the possibility of a sudden variation, with the potential energy  $v$ , of the number of critical points (or of their indexes) in configuration space at some value  $v_c$ , it is then reasonable to expect that the pattern of  $\lambda_1(v)$  – as well as that of  $\lambda_1(E)$  since  $v = v(E)$  – will be consequently affected, thus displaying *jumps* or *cusps* or other *singular patterns* at  $v_c$ .

On the other hand, recall that *Morse theory* teaches us that the existence of critical points of  $V$  is associated with topology changes of the hypersurfaces  $\{M_v\}_{v \in \mathbb{R}}$ , provided that  $V$  is a good *Morse function* (that is:

bounded below, with no vanishing eigenvalues of its Hessian matrix). Thus the existence of critical points of the potential  $V$  makes possible a conceptual link between dynamics and configuration space topology, which, on the basis of both direct and indirect evidence for a few particular models, has been formulated as a topological hypothesis about the relevance of topology for PTs phenomena (see [Franzosi *et al.* (2000); Franzosi and Pettini (2004); Grinza and Mossa (2004)]).

Here we give two simple examples of Hamiltonian systems of the biodynamic-like form (5.8), namely Peyrard–Bishop system and mean-field  $XY$  model.

**Peyrard–Bishop Hamiltonian System.** The *Peyrard–Bishop system* [Peyrard and Bishop (1989)]<sup>1</sup> exhibits a *second order phase transition*. It is defined by the following potential energy

$$V(q) = \sum_{i=1}^N \left[ \frac{K}{2} (q^{i+1} - q^i)^2 + D(e^{-aq^i} - 1)^2 + Dhaq^i \right], \quad (5.15)$$

which represents the energy of a string of  $N$  base pairs of reduced mass  $m$ . Each hydrogen bond is characterized by the stretching  $q^i$  and its conjugate momentum  $p_i = m\dot{q}^i$ . The elastic transverse force between neighboring pairs is tuned by the constant  $K$ , while the energy  $D$  and the inverse length  $a$  determine, respectively, the plateau and the narrowness of the on-site potential well that mimics the interaction between bases in each pair. It is understood that  $K$ ,  $D$ , and  $a$  are all positive parameters. The transverse, external stress  $h \geq 0$  is a computational tool useful in the evaluation of the susceptibility. Our interest in it lies in the fact that a phase transition can occur only when  $h = 0$ . We assume periodic boundary conditions.

The transfer operator technique [Dauxois *et al.* (2002)] maps the problem of computing the classical partition function into the easier task of evaluating the lowest energy eigenvalues of a ‘quantum’ mechanical Morse oscillator (no real quantum mechanics is involved, since the temperature plays the role of  $\hbar$ ). One can then observe that, as the temperature increases, the number of levels belonging to the discrete spectrum decreases, until for some critical temperature  $T_c = 2\sqrt{2KD}/(ak_B)$  only the continuous spectrum survives. This passage from a localized ground state to an unnormalizable one corresponds to the second order phase transition of the statistical model. Various critical exponents can be analytically computed

<sup>1</sup>The Peyrard–Bishop system has been proposed as a simple model for describing the DNA thermally induced denaturation [Grinza and Mossa (2004)].

and all applicable scaling laws can be checked. The simplicity of this model permits an analytical computation of the largest Lyapunov exponent by exploiting the geometric method proposed in [Caiani *et al.* (1997)].

**Mean-Field XY Hamiltonian System.** The mean-field XY model describes a system of  $N$  equally coupled planar classical rotators (see [Antoni and Ruffo (1995); Casetti *et al.* (1999)]). It is defined by a Hamiltonian of the class (2.28) where the potential energy is

$$V(\varphi) = \frac{J}{2N} \sum_{i,j=1}^N [1 - \cos(\varphi_i - \varphi_j)] - h \sum_{i=1}^N \cos \varphi_i. \quad (5.16)$$

Here  $\varphi_i \in [0, 2\pi]$  is the rotation angle of the  $i$ -th rotator and  $h$  is an external field. Defining at each site  $i$  a classical spin vector  $\mathbf{s}_i = (\cos \varphi_i, \sin \varphi_i)$  the model describes a planar (XY) Heisenberg system with interactions of equal strength among all the spins. We consider only the ferromagnetic case  $J > 0$ ; for the sake of simplicity, we set  $J = 1$ . The equilibrium statistical mechanics of this system is exactly described, in the thermodynamic limit, by the *mean-field theory* [Antoni and Ruffo (1995)]. In the limit  $h \rightarrow 0$ , the system has a continuous phase transition, with classical critical exponents, at  $T_c = 1/2$ , or  $\varepsilon_c = 3/4$ , where  $\varepsilon = E/N$  is the energy per particle (see Appendix).

The Lyapunov exponent  $\lambda_1$  of this system is extremely sensitive to the phase transition. According to reported numerical simulations (see [Casetti *et al.* (1999)]),  $\lambda_1(\varepsilon)$  is positive for  $0 < \varepsilon < \varepsilon_c$ , shows a sharp maximum immediately below the critical energy, and drops to zero at  $\varepsilon_c$  in the thermodynamic limit, where it remains zero in the whole region  $\varepsilon > \varepsilon_c$ , which corresponds to the thermodynamic disordered phase. In fact in this phase the system is integrable, reducing to an assembly of uncoupled rotators.

### 5.3.3 Euler Characteristics of Hamiltonian Systems

Recall that *Euler characteristic*  $\chi$  is a number that is a characterization of the various classes of geometric figures based only on the topological relationship between the numbers of vertices  $V$ , edges  $E$ , and faces  $F$ , of a geometric figure. This number,  $\chi = F - E + V$ , is the same for all figures the boundaries of which are composed of the same number of connected pieces. Therefore, the Euler characteristic is a *topological invariant*, i.e., any two geometric figures that are homeomorphic to each other have the same Euler characteristic.



More specifically, a standard way to analyze a geometric figure is to fragment it into other more familiar objects and then to examine how these pieces fit together. Take for example a surface  $M$  in the Euclidean 3D space. Slice  $M$  into pieces that are curved triangles (this is called a triangulation of the surface). Then count the number  $F$  of faces of the triangles, the number  $E$  of edges, and the number  $V$  of vertices on the tessellated surface. Now, no matter how we triangulate a compact surface  $\Sigma$ , its Euler characteristic,  $\chi(\Sigma) = F - E + V$ , will always equal a constant which is characteristic of the surface and which is invariant under diffeomorphisms  $\phi: \Sigma \rightarrow \Sigma'$ .

At higher dimensions this can be again defined by using higher dimensional generalizations of triangles (simplexes) and by defining the Euler characteristic  $\chi(M)$  of the  $n$ D manifold  $M$  to be the alternating sum:

$$\{\text{number of points}\} - \{\text{number of 2-simplices}\} + \\ \{\text{number of 3-simplices}\} - \{\text{number of 4-simplices}\} + \dots$$

i.e.,

$$\chi(M) = \sum_{k=0}^n (-1)^k (\text{number of faces of dimension } k). \quad (5.17)$$

and then define the Euler characteristic of a manifold as the Euler characteristic of any simplicial complex homeomorphic to it. With this definition, circles and squares have Euler characteristic 0 and solid balls have Euler characteristic 1.

The Euler characteristic  $\chi$  of a manifold is closely related to its *genus*  $g$  as  $\chi = 2 - 2g$ .<sup>2</sup>

Now, recall that in differential topology a more standard definition of  $\chi(M)$  is

$$\chi(M) = \sum_{k=0}^n (-1)^k b_k(M), \quad (5.18)$$

where  $b_k$  is the  $k$ th Betti number of  $M$ , as defined by (5.3) above.

---

<sup>2</sup>Recall that the *genus* of a topological space such as a surface is a topologically invariant property defined as the largest number of nonintersecting simple closed curves that can be drawn on the surface without separating it, i.e., an integer representing the maximum number of cuts that can be made through it without rendering it disconnected. This is roughly equivalent to the number of holes in it, or handles on it. For instance: a point, line, and a sphere all have genus 0; a torus has genus 1, as does a coffee cup as a solid object (solid torus), a Möbius strip, and the symbol 0; the symbols 8 and  $B$  have genus 2; etc.

In general, it would be hopeless to try to practically compute  $\chi(M)$  from (5.18) in the case of non-trivial physical models at large dimension. Fortunately, there is a possibility given by the *Gauss-Bonnet formula*, that relates  $\chi(M)$  with the total *Gauss-Kronecker curvature* of the manifold, (compare with (3.40) and (3.51) in chapter 3)

$$\chi(M) = \gamma \int_M K_G d\sigma, \quad (5.19)$$

which is valid for even dimensional hypersurfaces of Euclidean spaces  $\mathbb{R}^N$  [here  $\dim(M) = n \equiv N - 1$ ], and where:

$$\gamma = 2/\text{vol}(S_1^n)$$

is twice the inverse of the volume of an  $n$ -dimensional sphere of unit radius  $S_1^n$ ;  $K_G$  is the Gauss-Kronecker curvature of the manifold;

$$d\sigma = \sqrt{\det(g)} dx^1 dx^2 \cdots dx^n$$

is the invariant volume measure of  $M$  and  $g$  is its Riemannian metric (induced from  $\mathbb{R}^N$ ). Let us briefly sketch the meaning and definition of the Gauss-Kronecker curvature. The study of the way in which an  $n$ -surface  $M$  curves around in  $\mathbb{R}^N$  is measured by the way the normal direction changes as we move from point to point on the surface. The rate of change of the normal direction  $\xi$  at a point  $x \in M$  in direction  $v$  is described by the *shape operator*

$$L_x(v) = -\mathcal{L}_v \xi = [v, \xi],$$

where  $v$  is a tangent vector at  $x$  and  $\mathcal{L}_v$  is the Lie derivative, hence

$$L_x(v) = -(\nabla \xi_1 \cdot v, \dots, \nabla \xi_{n+1} \cdot v);$$

gradients and vectors are represented in  $\mathbb{R}^N$ . As  $L_x$  is an operator of the tangent space at  $x$  into itself, there are  $n$  independent eigenvalues  $\kappa_1(x), \dots, \kappa_n(x)$  which are called the principal curvatures of  $M$  at  $x$  [Thorpe (1979)]. Their product is the Gauss-Kronecker curvature:

$$K_G(x) = \prod_{i=1}^n \kappa_i(x) = \det(L_x).$$

Alternatively, recall that according to the Morse theory, it is possible to understand the topology of a given manifold by studying the regular critical points of a smooth Morse function defined on it. In our case, the

manifold  $M$  is the configuration space  $\mathbb{R}^N$  and the natural choice for the Morse function is the potential  $V(q)$ . Hence, one is lead to define the family  $M_v$  (5.10) of submanifolds of  $M$ .

A full characterization of the topological properties of  $M_v$  generally requires one to find the critical points of  $V(q)$ , which means solving the equations

$$\partial_{q^i} V = 0, \quad (i = 1, \dots, N). \quad (5.20)$$

Moreover, one has to compute the indexes of all the critical points, that is the number of negative eigenvalues of the Hessian  $\partial^2 V / (\partial q^i \partial q_j)$ . Then the Euler characteristic  $\chi(M_v)$  can be computed by means of the formula

$$\chi(M_v) = \sum_{k=0}^N (-1)^k \mu_k(M_v), \quad (5.21)$$

where  $\mu_k(M_v)$  is the total number of critical points of  $V(q)$  on  $M_v$  which have index  $k$ , i.e., the so-called *Morse numbers* of a manifold  $M$ , which happen to be upper bounds of the Betti numbers,

$$b_k(M) \leq \mu_k(M) \quad (k = 0, \dots, n). \quad (5.22)$$

Among all the Morse functions on a manifold  $M$ , there is a special class, called *perfect Morse functions*, for which the Morse inequalities (5.22) hold as equalities. Perfect Morse functions characterize completely the topology of a manifold.

Now, we continue with our two examples.

**Peyrard–Bishop System.** If applied to any generic model, calculation of (5.21) turns out to be quite formidable, but the exceptional simplicity of the Peyrard–Bishop model (5.15) makes it possible to carry on completely the topological analysis without invoking equation (5.21).

For the potential in exam, equation (5.20) results in the nonlinear system

$$\frac{a}{R}(q^{i+1} - 2q^i + q^{i-1}) = h - 2(e^{-2aq^i} - e^{-aq^i}),$$

where  $R = Da^2/K$  is a dimensionless ratio. It is easy to verify that a particular solution is given by

$$q^i = -\frac{1}{a} \ln \frac{1 + \sqrt{1 + 2h}}{2}, \quad (i = 1, \dots, N).$$

The corresponding minimum of potential energy is

$$V_{\min} = ND \left( \frac{1+h-\sqrt{1+2h}}{2} - h \ln \frac{1+\sqrt{1+2h}}{2} \right).$$

**Mean-Field XY Model.** In the case of the mean-field XY model (5.16) it is possible to show analytically that a topological change in the configuration space exists and that it can be related to the thermodynamic phase transition. Consider again the family  $M_v$  of submanifolds of the configuration space defined in (5.10); now the potential energy per degree of freedom is that of the mean-field XY model, i.e.,

$$\mathcal{V}(\varphi) = \frac{V(\varphi)}{N} = \frac{J}{2N^2} \sum_{i,j=1}^N [1 - \cos(\varphi_i - \varphi_j)] - h \sum_{i=1}^N \cos \varphi_i,$$

where  $\varphi_i \in [0, 2\pi]$ . Such a function can be considered a Morse function on  $M$ , so that, according to Morse theory, all these manifolds have the same topology until a critical level  $\mathcal{V}^{-1}(v_c)$  is crossed, where the topology of  $M_v$  changes.

A change in the topology of  $M_v$  can only occur when  $v$  passes through a critical value of  $\mathcal{V}$ . Thus in order to detect topological changes in  $M_v$  we have to find the critical values of  $\mathcal{V}$ , which means solving the equations

$$\partial \varphi_i \mathcal{V}(\varphi) = 0, \quad i = 1, \dots, N. \quad (5.23)$$

For a general potential energy function  $\mathcal{V}$ , the solution of (5.23) would be a formidable task, but in the case of the mean-field XY model, the mean-field character of the interaction greatly simplifies the analysis, allowing an analytical treatment of (5.23); moreover, a projection of the configuration space onto a 2D plane is possible [Casetti *et al.* (1999); Casetti *et al.* (2003)].

### 5.4 The Covariant Force Functor

We will summarize this chapter by stating that our central construct in lower, mechanical biodynamics, the *covariant force law*,  $F_i = mg_{ij}a^j$  (see subsection A.1.4 in Appendix), in topological language represents the *covariant force functor*  $\mathcal{F}_*$  defined by the following commutative diagram:

$$\begin{array}{ccc}
 TT^*M & \xrightarrow{\mathcal{F}_*} & TTM \\
 \uparrow F_i = \dot{p}_i & & \uparrow a^i = \dot{v}^i \\
 T^*M = \{x^i, p_i\} & & TM = \{x^i, v^i\} \\
 \swarrow p_i & & \nearrow v^i = \dot{x}^i \\
 M = \{x^i\} & & 
 \end{array}$$

saying that the force 1-form-field  $F_i = \dot{p}_i$ , defined on the mixed tangent-cotangent bundle  $TT^*M$ , causes the acceleration vector-field  $a^i = \dot{v}^i$ , defined on the second tangent bundle  $TTM$  of the configuration manifold  $M$ .

The Lie biodynamic functors defined in the section 4.8 above represent special versions of the fundamental force functor  $\mathcal{F}_* : TT^*M \rightarrow TTM$ .

The corresponding *contravariant acceleration functor* is defined as its inverse map  $\mathcal{F}^* : TTM \rightarrow TT^*M$ .

## Chapter 6

# Natural Control and Self-Organization in Biodynamics

In this third part, we present neural-like, control biodynamics, written predominantly using a self-organized synergetic language of *diversity in unity* of our *covariant force law*,  $F_i = mg_{ij}a^j$ , and its associated *covariant force functor*,  $\mathcal{F}_* : TT^*M \rightarrow TTM$  (see previous section). The exceptions of this deductive approach are medical sections, which are necessarily written in a ‘botanical way’, namely in ‘plain English with lots of figures’.

As a motivation for higher biodynamics, we cite here an extract from the *Nobel Lecture of Roger W. Sperry*: “...In closing it remains to mention briefly that one of the more important things to come out of the *split-brain work*, as an indirect spin-off, is a revised concept of the *nature of consciousness* and its fundamental relation to brain processing [Sperry (1965); Sperry (1969); Sperry (1980)]. The key development here is a switch from prior non-causal, parallelist views to a new causal, or ‘interactionist’ interpretation that ascribes to inner experience an integral causal control role in brain function and behavior. In effect, and without resorting to dualist views, the mental forces and properties of the conscious mind are restored to the brain of objective science from which they had long been excluded on materialist-behaviorist principles.

Acceptance of the revised ‘causal view’ and the reasoning involved, now becoming widespread, carries important implications for science and for scientific views of man and nature. Cognitive introspective psychology and related cognitive science can no longer be ignored experimentally, or written off as ‘a science of epiphenomena’, nor either as something that must, in principle, reduce eventually to neurophysiology. The events of inner experience, as emergent properties of brain processes, become themselves explanatory causal constructs in their own right, interacting at their own level with their own laws and dynamics. The whole world of inner experi-

ence (the world of the humanities) long rejected by 20th century scientific materialism, thus becomes recognized and included within the domain of science.

Basic revisions in concepts of causality are involved in which the whole, besides being 'different from and greater than the sum of the parts', also causally determines the fate of the parts, without interfering with the physical or chemical laws for the subentities at their own level. It follows that physical science no longer perceives the world to be reducible to quantum mechanics or to any other unifying ultra element or field force. The qualitative, holistic properties at all different levels become causally real in their own form and have to be included in the causal account. Quantum theory on these terms no longer replaces or subsumes classical mechanics but rather just supplements or complements.

The results add up to a fundamental change in what science has long stood for throughout the materialist-behaviorist era. The former scope of science, its limitations, world perspectives, views of human nature, and its societal role as an intellectual, cultural and moral force all undergo profound change. Where there used to be a chasm and irreconcilable conflict between the scientific and the traditional humanistic views of man and the world, we now perceive a continuum. A unifying new interpretative framework emerges with far reaching impact not only for science but for those ultimate value-belief guidelines by which mankind has tried to live and find meaning."

The purpose of the present chapter is to introduce just enough of modern control theory as a necessary background for the final chapter on brain-like control. It is not intended to be a complete description from either control theory or robotics perspective. We start with classical control and stability concepts. Then we present the basics of Lie algebra methods in nonlinear geometric control. After that we move on to Lagrangian and Hamiltonian control approaches for mechanical systems. After that we give a brief description of optimal nonlinear control. Then we present several examples of the current biodynamics control, introducing the fundamental *concept of learning* (i.e., adaptation, or training) as an introduction to brain dynamics exposed in chapter 7. The last section introduces humanoid robotics. No background is assumed on the reader's side apart from the previous chapters.

## 6.1 The Basics of Classical Control and Stability

In this section we present the basics of classical control and stability theory, to be used in the subsequent sections.

### 6.1.1 Introduction to Feedback Control

The feedback control form of our basic *sensory-motor adjunction* is reflected in the *basic formula of feedback control*,

$$\text{Sensing} + \text{Computation} + \text{Actuation} = \text{Feedback Control} \quad (6.1)$$

The formula (6.1) implies the *basic premise of control engineering*:

- Given a *system* to be controlled and the specifications of its *desired behavior*, construct a *feedback control law* to make the closed-loop system display its desired behavior.

The three basic goals of feedback control are (see [Murray (1997)]):

- (1) *Stability*, which states that bounded inputs produce bounded outputs;
- (2) *Performance*, which defines how to achieve desired response; and
- (3) *Robustness*, which balances stability versus performance in the presence of unknown dynamics.

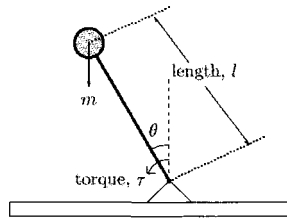


Fig. 6.1 An inverted pendulum (see text for explanation).

For example, consider the popular problem of stabilization of an *inverted pendulum* (see Figure 6.1), in which dynamics is governed by the Newtonian-like equation

$$J\ddot{\theta} - mgl \sin \theta = \tau,$$

and we want to start from a large angle, say  $\theta(0) = 60^\circ$  and move to the vertical upright position,  $\theta = 0$ .



One choice of a stabilizer is [Wilson (2000)]

$$\tau = -k_d \dot{\theta} - k_p \theta - mgl \sin \theta,$$

where  $\tau$  is the stabilizing torque, while  $k_d$  and  $k_p$  are positive constants. In this case, closed loop dynamics is given by

$$J\ddot{\theta} + k_d \dot{\theta} + k_p \theta = 0,$$

which is globally stable and linear.

An alternative controller is given by

$$\tau = -k_d \dot{\theta} - 2mgl \sin \theta,$$

leading to the globally stable nonlinear closed-loop dynamics

$$J\ddot{\theta} + k_d \dot{\theta} + mgl \sin \theta = 0.$$

This example shows how the feedback and feedforward control amounts to modifying the dynamics of the plant into a desired form. It is further expanded as a difficult nonholonomic problem of a unicycle (6.2.2.2) below.

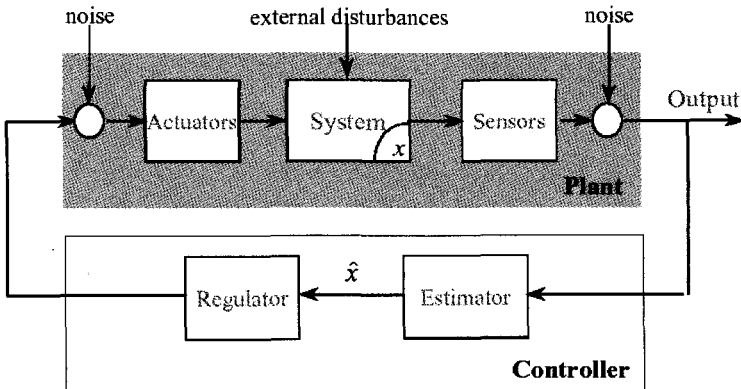


Fig. 6.2 The basic components of a feedback control system (see text for explanation).

To summarize, the basic components of a feedback control system (see Figure 6.2) are [Murray (1997)]:

- (1) Plant, including (bio)physical system, actuation and sensing;
- (2) Controller, including state estimator and regulator; and
- (3) Feedback, including interconnection between plant output and controller input.

Control systems are usually represented using:

- Linear or nonlinear ODEs; and
- Block diagrams with transfer functions (Laplace transform based).

Historically, four periods can be distinguished in control theory (see [Murray (1997)]):

(1) Classical control (1940–1960). This period is characterized by:

- Frequency domain based tools; stability via gain and phase margins;
- Mainly useful for single-input, single-output (SISO) systems;
- Control is one of the main tools for the practicing engineer.

(2) Modern control (1940–1960). In this period:

- The so-called *state-space approach* was developed for linear control theory;
- It works both for SISO and multi-input, multi-output (MIMO) systems;
- Performance and robustness measures are often not made explicit.

(3) Post-modern control (1940–1960). This period:

- Generalizes ideas in classical control to MIMO context; and
- Uses operator theory at its core, but can be easily interpreted in frequency domain.

(4) Nonlinear control (1990–). This period is characterized by specialized techniques for control of nonlinear plants.

Now, as already stated, the *goal of a control system* is to enhance automation within a system while providing improved performance and robustness. For instance, we may develop a *cruise control* system for an automobile to release drivers from the tedious task of speed regulation while they are on long trips. In this case, the *output* of the *plant* is the sensed vehicle speed,  $y$ , and the *input* to the plant is the throttle angle,  $u$ . Typically, control systems are designed so that the *plant output follows some reference input* (the driver-specified speed in the case of our cruise control example) while achieving some level of *disturbance rejection*. For the cruise control problem, a disturbance would be a road grade variation or wind. Clearly we would want our cruise controller to reduce the effects

of such disturbances on the quality of the speed regulation that is achieved [Spooner *et al.* (2002)].

In the area of *robust control* the focus is on the development of controllers that can maintain good performance even if we only have a poor model of the plant or if there are some plant parameter variations. In the area, of *adaptive control*, to reduce the effects of plant parameter variations, robustness is achieved by adjusting (i.e., adapting) the controller on-line. For instance, an adaptive controller for the cruise control problem would seek to achieve good speed tracking performance even if we do not have a good model of the vehicle and engine dynamics, or if the vehicle dynamics change over time (e.g., via a weight change that results from the addition of cargo, or due to engine degradation over time). At the same time it would try to achieve good disturbance rejection. Clearly, the performance of a good cruise controller should not degrade significantly as your automobile ages or if there are reasonable changes in the load the vehicle is carrying [Spooner *et al.* (2002)].

We use *adaptive mechanisms* within the control laws when certain *parameters* within the plant dynamics are *unknown*. An adaptive controller is used to improve the closed-loop system robustness while meeting a set of performance objectives. If the plant uncertainty cannot be expressed in terms of unknown parameters, one may be able to reformulate the problem by expressing the uncertainty in terms of a *fuzzy system*, *neural network*, or some other *parameterized nonlinear system*, like an *adaptive Lie-derivative controller*. The uncertainty then becomes recast in terms of a new set of unknown parameters that may be adjusted using adaptive techniques.

When developing a *robust control design*, the focus is on *maintaining stability* even in the presence of *unmodelled plant dynamics* or *external disturbances*. The approach in robust control is to accept *a priori* that there will be model uncertainty, and try to cope with it.

The issue of robustness has been studied extensively in the control literature [Spooner *et al.* (2002)]. When working with linear systems, one may define phase and gain margins which quantify the range of uncertainty a closed-loop system may withstand before becoming unstable. In the world of *nonlinear control design*, we often investigate the stability of a closed-loop system by studying the behavior of a *Lyapunov function candidate*. The Lyapunov function candidate is a mathematical function designed to provide a simplified measure of the control objectives allowing complex nonlinear systems to be analyzed using a scalar differential equation. When a controller is designed that drives the Lyapunov function to

zero, the control objectives are met. If some system uncertainty tends to drive the Lyapunov candidate away from zero, we often simply add an additional stabilizing term to the control algorithm that dominates the effect of the uncertainty, thereby making the closed-loop system more robust.

Now, by adding a static term in the control law that simply dominates the plant uncertainty, it is often easy to simply stabilize an uncertain plant, however, driving the system error to zero may be difficult if not impossible. Consider the case when the plant is defined by [Spooner *et al.* (2002)]

$$\dot{x} = \theta x + u, \quad (6.2)$$

where  $x \in \mathbb{R}$  is the plant state that we wish to drive to the point  $x = 1$ ,  $u \in \mathbb{R}$  is the plant input, and  $\theta$  is an unknown constant. Since  $\theta$  is unknown, one may not define a static controller that causes  $x = 1$  to be a stable equilibrium point. In order for  $x = 1$  to be a stable equilibrium point, it is necessary that  $\dot{x} = 0$  when  $x = 1$ , so  $u(x) = -\theta$  when  $x = 1$ . Since  $\theta$  is unknown, however, we may not define such a controller. In this case, the best that a static nonlinear controller may do is to keep  $x$  bounded in some region around  $x = 1$ . If dynamics are included in the nonlinear controller, then it turns out that one may define a control system that does drive  $x \rightarrow 1$  even if  $\theta$  is unknown.

On the other hand, an adaptive controller can be designed so that it estimates some uncertainty within the system, then automatically designs a controller for the estimated plant uncertainty. In this way the control system uses information gathered on-line to reduce the model uncertainty, that is, to figure out exactly what the plant is at the current time so that good control can be achieved. Considering the system defined by (A.19), an adaptive controller may be defined so that an *estimate* of  $\theta$  is generated, which we denote by  $\hat{\theta}$ . If  $\theta$  were known, then including a term  $-\theta x$  in the control law would cancel the effects of the uncertainty. If  $\hat{\theta} \rightarrow \theta$  over time, then including the term  $-\hat{\theta}x$  in the control law would also cancel the effects of the uncertainty over time. This approach is referred to as *indirect adaptive control* [Spooner *et al.* (2002)].

An indirect approach to adaptive control is made up of an *approximator* (often referred to as an *identifier* in the adaptive control literature) that is used to estimate unknown plant parameters and a certainty equivalence control scheme in which the plant controller is designed, assuming that the parameter estimates are their true values. Here the adjustable approximator is used to model some component of the system. Since the approximation is used in the control law, it is possible to determine if we

have a good estimate of the plant dynamics. If the approximation is good (i.e., we know how the plant should behave), then it is easy to meet our control objectives. If, on the other hand, the plant output moves in the wrong direction, then we may assume that our estimate is incorrect and should be adjusted accordingly.

As an example of an indirect adaptive controller, consider the cruise control problem where we have an approximator that is used to estimate the vehicle mass and aerodynamic drag. Assume that the vehicle dynamics may be approximated by

$$m\dot{x} = -\rho x^2 + u,$$

where  $m$  is the vehicle mass,  $\rho$  is the coefficient of aerodynamic drag,  $x$  is the vehicle velocity, and  $u$  is the plant input. Assume that an approximator has been defined so that estimates of the mass and drag are found such that  $\hat{m} \rightarrow m$  and  $\hat{\rho} \rightarrow \rho$ . Then the control law

$$u = \hat{\rho}x^2 + \hat{m}v(t)$$

may be used so that  $\dot{x} = v(t)$  when  $\hat{m} = m$  and  $\hat{\rho} = \rho$ . Here  $v(t)$  may be considered a new control input that is defined to drive  $x$  to any desired value [Spooner *et al.* (2002)].

## 6.1.2 Linear Stationary Systems and Operators

### 6.1.2.1 Basics of Kalman State-Space Theory

It is well-known that linear multiple input-multiple output (MIMO) control systems can always be put into Kalman canonical state-space form of order  $n$ , with  $m$  inputs and  $k$  outputs. In the case of *continual time systems* we have the state and output equations of the form<sup>1</sup>

$$\begin{aligned}\dot{\mathbf{x}} &= \mathbf{A}(t)\mathbf{x}(t) + \mathbf{B}(t)\mathbf{u}(t), \\ \mathbf{y}(t) &= \mathbf{C}(t)\mathbf{x}(t) + \mathbf{D}(t)\mathbf{u}(t),\end{aligned}\tag{6.3}$$

while in case of *discrete time systems* we have the state and output equations of the form

---

<sup>1</sup>In our covariant form, (6.4) reads

$$\dot{x}^i = a_j^i x^j + b_k^i u^k, \quad y^i = c_j^i x^j + d_k^i u^k, \quad (i, j = 1, \dots, n; k = 1, \dots, m).$$

$$\begin{aligned} \mathbf{x}(n+1) &= \mathbf{A}(n)\mathbf{x}(n) + \mathbf{B}(n)\mathbf{u}(n), \\ \mathbf{y}(n) &= \mathbf{C}(n)\mathbf{x}(n) + \mathbf{D}(n)\mathbf{u}(n). \end{aligned} \quad (6.4)$$

Both in (6.3) and in (6.4) the variables have the following meaning:

$\mathbf{x}(t) \in \mathbb{X}$  is an  $n$ -vector of *state variables* belonging to the *state space*  $\mathbb{X} \subset \mathbb{R}^n$ ;

$\mathbf{u}(t) \in \mathbb{U}$  is an  $m$ -vector of *inputs* belonging to the *input space*  $\mathbb{U} \subset \mathbb{R}^m$ ;

$\mathbf{y}(t) \in \mathbb{Y}$  is a  $k$ -vector of *outputs* belonging to the *output space*  $\mathbb{Y} \subset \mathbb{R}^k$ ;

$\mathbf{A}(t) : \mathbb{X} \rightarrow \mathbb{X}$  is an  $n \times n$  matrix of *state dynamics*;

$\mathbf{B}(t) : \mathbb{U} \rightarrow \mathbb{X}$  is an  $n \times m$  matrix of *input map*;

$\mathbf{C}(t) : \mathbb{X} \rightarrow \mathbb{Y}$  is an  $k \times n$  matrix of *output map*;

$\mathbf{D}(t) : \mathbb{U} \rightarrow \mathbb{Y}$  is an  $k \times m$  matrix of *input-output transform*.

Input  $\mathbf{u}(t) \in \mathbb{U}$  can be empirically determined by trial and error; it is properly defined by optimization process called *Kalman regulator*, or more generally (in the presence of noise), by *Kalman filter* (even better, *extended Kalman filter* to deal with stochastic nonlinearities) [Kalman (1960)].

Now, the most common special case of the general Kalman model (6.3), with constant state, input and output matrices (and relaxed bold-face vector-matrix notation), is the so-called *stationary linear model*. Such systems frequently serve as a baseline, against which other control systems are measured. We follow a common notational convention and let  $u$  denote the vector of *inputs*,  $y$  the vector of *outputs* and assume that they can be related through an intermediary *state* variable  $x$  according to the equations

$$\dot{x} = Ax + Bu, \quad y = Cx. \quad (6.5)$$

We refer to this as the deterministic *stationary linear model*. The stationary linear system (6.5) defines a variety of operators, in particular those related to: (i) regulators, (ii) end point controls, (iii) servomechanisms, and (iv) repetitive modes (see [Brockett (2001)]).

The discrete-time version of (6.5) is described in the section on Kalman filtering and biomechanical experiments (see (6.6) below).

### 6.1.2.2 Regulator Problem

Consider a variable, or set of variables, associated with a dynamical system. They are to be maintained at some desired values in the face of changing circumstances. There exist a second set of parameters that can be adjusted

so as to achieve the desired regulation. The effecting variables are usually called *inputs* and the affected variables called *outputs*. Specific examples include the regulation of the thrust of a jet engine by controlling the flow of fuel, as well as the regulation of the oxygen content of the blood using the respiratory rate.

Now, there is the steady state operator of particular relevance for the regulator problem. It is

$$y_{\infty} = -CA^{-1}Bu_{\infty},$$

which describes the map from constant values of  $u$  to the equilibrium value of  $y$ . It is defined whenever  $A$  is invertible but the steady state value will only be achieved by a real system if, in addition, the eigenvalues of  $A$  have negative real parts. Only when the rank of  $CA^{-1}B$  equals the dimension of  $y$  can we steer  $y$  to an arbitrary steady state value and hold it there with a constant  $u$ . A nonlinear version of this problem plays a central role in robotics where it is called the *inverse kinematics problem* (see, e.g., [Murray *et al.* (1994)]).

### 6.1.2.3 End Point Control Problem

Here we have inputs, outputs and trajectories. In this case the shape of the trajectory is not of great concern but rather it is the end point that is of primary importance. Standard examples include rendezvous problems such as one has in space exploration.

Now, the operator of relevance for the end point control problem, is the operator

$$x(T) = \int_0^T \exp[A(T - \sigma)] Bu(\sigma) d\sigma.$$

If we consider this to define a map from the  $mD$ -space  $L_2^m[0, T]$  (where  $u$  takes on its values) into  $\mathbb{R}^m$  then, if it is an onto map, it has a Moore–Penrose (least squares) inverse

$$u(\sigma) = B^T \exp[A^T(T - \sigma)] (W[0, T])^{-1} (x(T) - \exp(AT)x(0)),$$

with the symmetric positive definite matrix  $W$ , the *controllability Gramian*, being given by

$$W[0, T] = \int_0^T \exp[A(T - \sigma)] BB^T \exp[A^T(T - \sigma)] d\sigma.$$

#### 6.1.2.4 Servomechanism Problem

Here we have inputs, outputs and trajectories, as above, and an associated dynamical system. In this case, however, it is desired to cause the outputs to follow a trajectory specified by the input. For example, the control of an airplane so that it will travel along the flight path specified by the flight controller.

Now, because we have assumed that  $A$ ,  $B$  and  $C$  are constant

$$y(t) = C \exp(At) x(0) + \int_0^t C \exp[A(T - \tau)] B u(\tau) d\tau,$$

and, as usual, the Laplace transform  $\mathcal{L}$ , defined as a pair of inverse maps  $\mathcal{L} = \{F, f\} : \mathbb{R} \leftrightarrow \mathbb{C}$ ,

$$F(s) = \{\mathcal{L}f(t)\}(s) = \int_0^\infty e^{-st} f(t) dt, \quad (t \in \mathbb{R}, s \in \mathbb{C})$$

$$f(t) = \{\mathcal{L}^{-1}F(s)\}(t) = \frac{1}{2\pi i} \int_{\gamma-i\infty}^{\gamma+i\infty} e^{st} F(s) ds,$$

– can be used to convert convolution to multiplication. This brings out the significance of the Laplace transform pair

$$C \exp(At) B \xLeftrightarrow{\mathcal{L}} C(Is - A)^{-1} B \quad (6.6)$$

as a means of characterizing the input–output map of a linear model with constant coefficients.

#### 6.1.2.5 Repetitive Mode Problem

Here again one has some variable, or set of variables, associated with a dynamical system and some inputs which influence its evolution. The task has elements which are repetitive and are to be done efficiently. Examples from biology include the control of respiratory processes, control of the pumping action of the heart, control of successive trials in practicing a athletic event.

The relevant operator is similar to the servomechanism operator, however the constraint that  $u$  and  $x$  are periodic means that the relevant diagonalization is provided by Fourier series, rather than the Laplace transform. Thus, in the Fourier domain, we are interested in a set of complex-valued matrices

$$G(iw_i) = C(iw_i - A)^{-1} B, \quad (w_i = 0, w_0, 2w_0, \dots)$$



More general, but still deterministic, models of the input–state–output relation are afforded by the *nonlinear affine control system* (see, e.g., [Isidori (1989)])

$$\dot{x}(t) = f(x(t)) + g(x(t)) u(t), \quad y(t) = h(x(t));$$

and the still more general *fully nonlinear control system*

$$\dot{x}(t) = f(x(t), u(t)), \quad y(t) = h(x(t)).$$

### 6.1.2.6 Feedback Changes the Operator

No idea is more central to automatic control than the idea of feedback. When an input is altered on the basis of the difference between the actual output of the system and the desired output, the system is said to involve *feedback*. Man made systems are often constructed by starting with a basic element such as a motor, a burner, a grinder, etc. and then adding sensors and the hardware necessary to use the measurement generated by the sensors to regulate the performance of the basic element. This is the *essence of feedback control*. Feedback is often contrasted with open loop systems in which the inputs to the basic element is determined without reference to any measurement of the trajectories. When the word feedback is used to describe naturally occurring systems, it is usually implicit that the behavior of the system can best be explained by pretending that it was designed as one sees man made systems being designed [Brockett (2001)].

In the context of linear systems, the effect of feedback is easily described. If we start with the stationary linear system (6.5) with  $u$  being the controls and  $y$  being the measured quantities, then the effect of feedback is to replace  $u$  by  $u - Ky$  with  $K$  being a matrix of feedback gains. The closed-loop equations are then

$$\dot{x} = (A - BKC)x + Bu, \quad y = Cx.$$

Expressed in terms of the Laplace transform pairs (6.6), feedback effects the transformation

$$(C \exp(At)B; C(Is - A)^{-1}B) \mapsto C \exp(A - BKC)^t B; C(Is - A + BKC)^{-1}B.$$

Using such a transformation, it is possible to alter the dynamics of a system in a significant way. The modifications one can effect by feedback include influencing the location of the eigenvalues and consequently the stability of the system. In fact, if  $K$  is  $m$  by  $p$  and if we wish to select a gain matrix

$K$  so that  $A - BKC$  has eigenvalues  $\lambda_1, \lambda_2, \dots, \lambda_n$ , it is necessary to insure that

$$\det \begin{pmatrix} C(I\lambda_1 - A)^{-1}B - I \\ I \quad K \end{pmatrix} = 0, \quad (i = 1, 2, \dots, n).$$

Now, if  $CB$  is invertible then we can use the relationship  $C\dot{x} = CAx + CBu$  together with  $y = Cx$  to write  $\dot{y} = CAx + CBu$ . This lets us solve for  $u$  and recast the system as

$$\begin{aligned} \dot{x} &= (A - B(CB)^{-1}CA)x + B(CB)^{-1}\dot{y}, \\ u &= (CB)^{-1}\dot{y} - (CB)^{-1}CAx. \end{aligned}$$

Here we have a set of equations in which the roles of  $u$  and  $y$  are reversed. They show how a choice of  $y$  determines  $x$  and how  $x$  determines  $u$  [Brockett (2001)].

### 6.1.3 Stability and Boundedness

Let a time-varying dynamical system may be expressed as

$$\dot{x}(t) = f(t, x(t)), \quad (6.7)$$

where  $x \in \mathbb{R}^n$  is an  $n$ D vector and  $f : \mathbb{R}^+ \times D \rightarrow \mathbb{R}^n$  with  $D = \mathbb{R}^n$  or  $D = B_h$  for some  $h > 0$ , where  $B_h = \{x \in \mathbb{R}^n : |x| < h\}$  is a ball centered at the origin with a radius of  $h$ . If  $D = \mathbb{R}^n$  then we say that the dynamics of the system are defined *globally*, whereas if  $D = B_h$  they are only defined *locally*. We do not consider systems whose dynamics are defined over disjoint subspaces of  $\mathbb{R}^n$ . It is assumed that  $f(t, x)$  is piecemeal continuous in  $t$  and Lipschitz in  $x$  for existence and uniqueness of state solutions. As an example, the linear system  $\dot{x}(t) = Ax(t)$  fits the form of (6.7) with  $D = \mathbb{R}^n$  [Spooner *et al.* (2002)].

Assume that for every  $x_0$  the initial value problem

$$\dot{x}(t) = f(t, x(t)), \quad x(t_0) = x_0,$$

possesses a unique solution  $x(t, t_0, x_0)$ ; it is called a solution to (6.7) if  $x(t, t_0, x_0) = x_0$  and  $\frac{d}{dt}x(t, t_0, x_0) = f(t, x(t, t_0, x_0))$  [Spooner *et al.* (2002)].

A point  $x_e \in \mathbb{R}^n$  is called an *equilibrium point* of (6.7) if  $f(t, x_e) = 0$  for all  $t \geq 0$ . An equilibrium point  $x_e$  is called an *isolated equilibrium point* if there exists an  $\rho > 0$  such that the ball around  $x_e$ ,  $B_\rho(x_e) = \{x \in \mathbb{R}^n : |x - x_e| < \rho\}$ , contains no other equilibrium points besides  $x_e$  [Spooner *et al.* (2002)].

The equilibrium  $x_e = 0$  of (6.7) is said to be *stable in the sense of Lyapunov* if for every  $\epsilon > 0$  and any  $t_0 \geq 0$  there exists a  $\delta(\epsilon, t_0) > 0$  such that  $|x(t, t_0, x_0)| < \epsilon$  for all  $t \geq t_0$  whenever  $|x_0| < \delta(\epsilon, t_0)$  and  $x(t, t_0, x_0) \in B_h(x_e)$  for some  $h > 0$ . That is, the equilibrium is stable if when the system (6.7) starts close to  $x_e$ , then it will stay close to it. Note that stability is a property of an equilibrium, not a system. A system is stable if all its equilibrium points are stable. Stability in the sense of Lyapunov is a local property. Also, notice that the definition of stability is for a single equilibrium  $x_e \in \mathbb{R}^n$  but actually such an equilibrium is a trajectory of points that satisfy the differential equation in (6.7). That is, the equilibrium  $x_e$  is a solution to the differential equation (6.7),  $x(t, t_0, x_0) = x_e$  for  $t \geq 0$ . We call any set such that when the initial condition of (6.7) starts in the set and stays in the set for all  $t \geq 0$ , an *invariant set*. As an example, if  $x_e = 0$  is an equilibrium, then the set containing only the point  $x_e$  is an invariant set, for (6.7) [Spooner *et al.* (2002)].

If  $\delta$  is independent of  $t_0$ , that is, if  $\delta = \delta(\epsilon)$ , then the equilibrium  $x_e$  is said to be *uniformly stable*. If in (6.7)  $f$  does not depend on time (i.e.,  $f(x)$ ), then  $x_e$  being stable is equivalent to it being uniformly stable. Uniform stability is also a local property.

The equilibrium  $x_e = 0$  of (6.7) is said to be *asymptotically stable* if it is stable and for every  $t_0 \geq 0$  there exists  $\eta(t_0) > 0$  such that  $\lim_{t \rightarrow \infty} |x(t, t_0, x_0)| = 0$  whenever  $|x_0| < \eta(t_0)$ . That is, it is asymptotically stable if when it starts close to the equilibrium it will converge to it. Asymptotic stability is also a local property. It is a stronger stability property since it requires that the solutions to the ordinary differential equation converge to zero in addition to what is required for stability in the sense of Lyapunov.

The equilibrium  $x_e = 0$  of (6.7) is said to be *uniformly asymptotically stable* if it is uniformly stable and for every  $\epsilon > 0$  and  $t_0 \geq 0$ , there exist a  $\delta_0 > 0$  independent of  $t_0$  and  $\epsilon$ , and a  $T(\epsilon) > 0$  independent of  $t_0$ , such that  $|x(t, t_0, x_0) - x_e| \leq \epsilon$  for all  $t \geq t_0 + T(\epsilon)$  whenever  $|x_0 - x_e| < \delta_0$ . Again, if in (6.7)  $f$  does not depend on time (i.e.,  $f(x)$ ), then  $x_e$  being asymptotically stable is equivalent to it being uniformly asymptotically stable. Uniform asymptotic stability is also a local property.

The set  $X_d \subset \mathbb{R}^n$  of all  $x_0 \in \mathbb{R}^n$  such that  $|x(t, t_0, x_0)| \rightarrow 0$  as  $t \rightarrow \infty$  is called the *domain of attraction* of the equilibrium  $x_e = 0$  of (6.7). The equilibrium  $x_e = 0$  is said to be *asymptotically stable in the large* if  $X_d \subset \mathbb{R}^n$ . That is, an equilibrium is asymptotically stable in the large if no matter where the system starts, its state converges to the equilibrium asymptoti-

cally. This is a global property as opposed to the earlier stability definitions that characterized local properties. This means that for asymptotic stability in the large, the local property of asymptotic stability holds for  $B_h(x_e)$  with  $h = \infty$  (i.e., on the whole state-space).

The equilibrium  $x_e = 0$  is said to be *exponentially stable* if there exists an  $\alpha > 0$  and for every  $\epsilon > 0$  there exists a  $\delta(\epsilon) > 0$  such that  $|x(t, t_0, x_0)| \leq \epsilon e^{-\alpha(t-t_0)}$ , whenever  $|x_0| < \delta(\epsilon)$  and  $t \geq t_0 \geq 0$ . The constant  $\alpha$  is sometimes called the *rate of convergence*. Exponential stability is sometimes said to be a ‘stronger’ form of stability since in its presence we know that system trajectories decrease exponentially to zero. It is a local property; here is its global version. The equilibrium point  $x_e = 0$  is *exponentially stable in the large* if there exists  $\alpha > 0$  and for any  $\beta > 0$  there exists  $\epsilon(\beta) > 0$  such that  $|x(t, t_0, x_0)| \leq \epsilon(\beta)e^{-\alpha(t-t_0)}$ , whenever  $|x_0| < \beta$  and  $t \geq t_0 \geq 0$ .

An equilibrium that is not stable is called *unstable*.

Closely related to stability is the concept of *boundedness*, which is, however, a global property of a system in the sense that it applies to trajectories (solutions) of the system that can be defined over all of the state-space [Spooner *et al.* (2002)].

A solution  $x(t, t_0, x_0)$  of (6.7) is *bounded* if there exists a  $\beta > 0$ , that may depend on each solution, such that  $|x(t, t_0, x_0)| < \beta$  for all  $t \geq t_0 \geq 0$ . A system is said to possess *Lagrange stability* if for each  $t_0 \geq 0$  and  $x_0 \in \mathbb{R}^n$ , the solution  $x(t, t_0, x_0)$  is bounded. If an equilibrium is asymptotically stable in the large or exponentially stable in the large then the system for which the equilibrium is defined is also Lagrange stable (but not necessarily vice versa). Also, if an equilibrium is stable, it does not imply that the system for which the equilibrium is defined is Lagrange stable since there may be a way to pick  $x_0$  such that it is near an unstable equilibrium and  $x(t, t_0, x_0) \rightarrow \infty$  as  $t \rightarrow \infty$ .

The solutions  $x(t, t_0, x_0)$  are *uniformly bounded* if for any  $\alpha > 0$  and  $t_0 \geq 0$ , there exists a  $\beta(\alpha) > 0$  (independent of  $t_0$ ) such that if  $|x_0| < \alpha$ , then  $|x(t, t_0, x_0)| < \beta(\alpha)$  for all  $t \geq t_0 \geq 0$ . If the solutions are uniformly bounded then they are bounded and the system is Lagrange stable.

The solutions  $x(t, t_0, x_0)$  are said to be *uniformly ultimately bounded* if there exists some  $B > 0$ , and if corresponding to any  $\alpha > 0$  and  $t_0 > 0$  there exists a  $T(\alpha) > 0$  (independent of  $t_0$ ) such that  $|x_0| < \alpha$  implies that  $|x(t, t_0, x_0)| < B$  for all  $t \geq t_0 + T(\alpha)$ . Hence, a system is said to be uniformly ultimately bounded if eventually all trajectories end up in a  $B$ -neighborhood of the origin.

### 6.1.4 Lyapunov's Stability Method

A. M. Lyapunov invented two methods to analyze stability [Spooner *et al.* (2002)]. In his *indirect method* he showed that if we linearize a system about an equilibrium point, certain conclusions about local stability properties can be made (e.g., if the eigenvalues of the linearized system are in the left half plane then the equilibrium is stable but if one is in the right half plane it is unstable).

In his *direct method* the stability results for an equilibrium  $x_e = 0$  of (6.7) depend on the existence of an appropriate *Lyapunov function*  $V : D \rightarrow \mathbb{R}$  where  $D = \mathbb{R}^n$  for global results (e.g., asymptotic stability in the large) and  $D = B_h$  for some  $h > 0$ , for local results (e.g., stability in the sense of Lyapunov or asymptotic stability). If  $V$  is continuously differentiable with respect to its arguments then the derivative of  $V$  with respect to  $t$  along the solutions of (6.7) is

$$\dot{V}(t, x) = \partial_t V + \partial_x V f(t, x).$$

As an example, suppose that (6.7) is autonomous, and let  $V(x)$  is a quadratic form  $V(x) = x^T P x$  where  $x \in \mathbb{R}^n$  and  $P = P^T$ . Then,  $\dot{V}(x) = \frac{\partial V}{\partial x} f(t, x) = \dot{x}^T P x + x^T P \dot{x} = 2x^T P \dot{x}$  [Spooner *et al.* (2002)].

Lyapunov's direct method provides for the following ways to test for stability. The first two are strictly for local properties while the last two have local and global versions.

- *Stable*: If  $V(t, x)$  is continuously differentiable, positive definite, and  $\dot{V}(t, x) \leq 0$ , then  $x_e = 0$  is stable.
- *Uniformly stable*: If  $V(t, x)$  is continuously differentiable, positive definite, decreascent<sup>2</sup>, and  $V(t, x) \leq 0$ , then  $x_e = 0$  is uniformly stable.
- *Uniformly asymptotically stable*: If  $V(t, x)$  is continuously differentiable, positive definite, and decreascent, with negative definite  $\dot{V}(t, x)$ , then  $x_e = 0$  is uniformly asymptotically stable (uniformly asymptotically stable in the large if all these properties hold globally).
- *Exponentially stable*: If there exists a continuously differentiable  $V(t, x)$  and  $c, c_1, c_2, c_3 > 0$  such that

$$c_1 |x|^c \leq V(t, x) \leq c_2 |x|^c, \quad \dot{V}(t, x) \leq -c_3 |x|^c, \quad (6.8)$$

for all  $x \in B_h$  and  $t \geq 0$ , then  $x_e = 0$  is exponentially stable. If there

---

<sup>2</sup>A  $C^0$ -function  $V(t, x) : \mathbb{R}^+ \times B_h \rightarrow \mathbb{R}$  ( $V(t, x) : \mathbb{R}^+ \times \mathbb{R}^n \rightarrow \mathbb{R}$ ) is said to be *decreascent* if there exists a strictly increasing function  $\gamma$  defined on  $[0, r)$  for some  $r > 0$  (defined on  $[0, \infty)$ ) such that  $V(t, x) \leq \gamma(|x|)$  for all  $t \geq 0$  and  $x \in B_h$  for some  $h > 0$ .

exists a continuously differentiable function  $V(t, x)$  and equations (6.8) hold for some  $c, c_1, c_2, c_3 > 0$  for all  $x \in \mathbb{R}^n$  and  $t \geq 0$ , then  $x_e = 0$  is exponentially stable in the large [Spooner *et al.* (2002)].

### 6.1.5 Graphical Techniques for Nonlinear Systems

Graphical techniques preceded modern geometric techniques in nonlinear control theory. They started with simple plotting tools, like the so-called 'tracer plot'. It is a useful visualization tool for analysis of second order dynamical systems, which just adds time dimension to the standard 2D phase portrait. For example, consider a damped spring governed by

$$\ddot{x} = -k\dot{x} - x, \quad x(0) = 1.$$

Its tracer plot is given in Figure 6.3. Note the stable asymptote reached as  $t \rightarrow \infty$ .

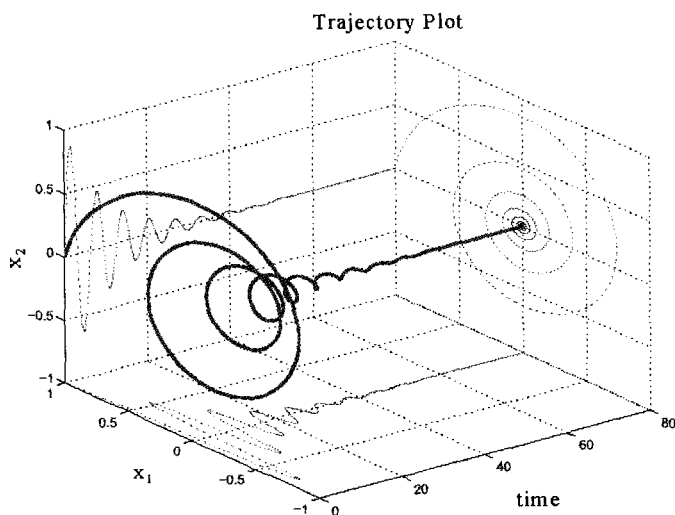


Fig. 6.3 Tracer plot of the damped spring.

The most important graphical technique is the so-called describing function analysis.

### 6.1.5.1 Describing Function Analysis

Describing function analysis extends classical linear control technique, frequency response analysis, for nonlinear systems. It is an *approximate* graphical method mainly used to predict *limit cycles* in nonlinear ODEs (see [Wilson (2000)] for technical details).

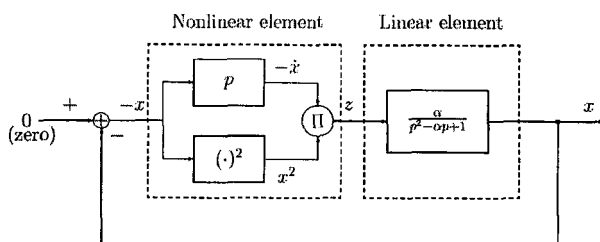


Fig. 6.4 Feedback interpretation of the Van Der Pol oscillator (see text for explanation).

For example, if we want to predict the existence of limit cycles in the classical *Van der Pol's oscillator* (2.9) given by

$$\ddot{x} + \alpha(x^2 - 1)\dot{x} + x = 0, \quad (6.9)$$

we need to rewrite (6.9) as a *linear* unstable low-pass block and a *nonlinear* block (see Figure 6.4). In this way, using the nonlinear block substitution,  $w = -\dot{x}x^2$ , we get

$$\begin{aligned} \ddot{x} - \alpha\dot{x} + x &= \alpha w, & \text{or} \\ x(p^2 - \alpha p + 1) &= \alpha w, \end{aligned}$$

or just considering the transfer function from  $w$  to  $x$ ,

$$\frac{x}{w} = \frac{\alpha}{p^2 - \alpha p + 1}.$$

Now, if we assume that the Van der Pol oscillator does have a limit cycle with a frequency of

$$x(t) = A \sin(\omega t),$$

so  $\dot{x} = Aw \cos(\omega t)$ , therefore the *output* of the nonlinear block is

$$\begin{aligned} z &= -x^2 \dot{x} = -A^2 \sin^2(wt) A w \cos(wt) - \frac{A^3 w}{2} (1 - \cos(2wt)) \cos(wt) \\ &= -\frac{A^3 w}{4} (\cos(wt) - \cos(3wt)). \end{aligned}$$

Note how  $z$  contains a third harmonic term, but this is attenuated by the low-pass nature of the linear block, and so does not effect the signal in the feedback. So we can approximate  $z$  by

$$z \approx \frac{A^3}{4} w \cos(wt) = \frac{A^2}{4} \frac{d}{dt} (-A \sin(wt)).$$

Therefore, the output of the nonlinear block can be approximated by the quasi-linear transfer function which depends on the signal amplitude,  $A$ , as well as frequency. The frequency response function of the quasi-linear element is obtained by substituting  $p \equiv s = iw$ ,

$$N(A, w) = \frac{A^2}{4}(iw).$$

Since the system is assumed to contain a sinusoidal oscillation,

$$x = A \sin(wt) = G(iw) z = G(iw) N(A, w) (-x),$$

where  $G(iw)$  is the transfer function of the linear block. This implies that,

$$\begin{aligned} \frac{x}{-x} &= -1 = G(iw) N(A, w), \quad \text{so} \\ 1 + \frac{A^2(iw)}{4} \frac{\alpha}{(iw)^2 - \alpha(iw) + 1} &= 0, \end{aligned}$$

which solving gives,

$$A = 2, \quad \omega = 1,$$

which is independent of  $\alpha$ . Note that in terms of the Laplace variable  $p \equiv s$ , the closed loop characteristic equation of the system is

$$1 + \frac{A^2(iw)}{4} \frac{\alpha}{p^2 - \alpha p + 1} = 0,$$

whose eigenvalues are

$$\lambda_{1,2} = -\frac{1}{8}\alpha(A^2 - 4) \pm \sqrt{\frac{\alpha^2(A^2 - 4)^2}{64} - 1}.$$



Corresponding to  $A = 2$  gives eigenvalues of  $\lambda_{1,2} = \pm i$  indicating an existence of a limit cycle of amplitude 2 and frequency 1 (see Figure 6.5). If  $A > 2$  eigenvalues are negative real, so stable, and the same holds for  $A < 2$ . The approximation of the nonlinear block with  $(A2/4)(iw)$  is called the *describing function*. This technique is useful because most limit cycles are approximately sinusoidal and most linear elements are low-pass in nature. So most of the higher harmonics, if they existed, are attenuated and lost.

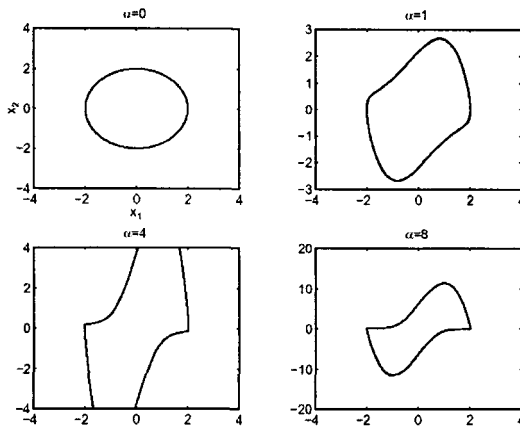


Fig. 6.5 Limit cycle of the Van der Pol oscillator (see text for explanation).

## 6.2 The Basis of Modern Geometric Control

In this section we present the basics of modern geometric control, as currently used in modern biodynamics.

### 6.2.1 Feedback Linearization

#### 6.2.1.1 Exact Feedback Linearization

The idea of feedback linearization is to algebraically transform the nonlinear system dynamics into a fully or partly linear one so that the linear control techniques can be applied. Note that this is not the same as a conventional linearization using Jacobians. In this subsection we will present the modern, geometric, Lie-derivative based techniques for exact feedback linearization

of nonlinear control systems.

**The Lie Derivative and Lie Bracket in Control Theory.** Recall (see (3.5.1) above) that given a scalar function  $h(x)$  and a vector-field  $f(x)$ , we define a new scalar function,  $\mathcal{L}_f h = \nabla h f$ , which is the Lie derivative of  $h$  w.r.t.  $f$ , i.e., the directional derivative of  $h$  along the direction of the vector  $f$ . Repeated Lie derivatives can be defined recursively:

$$\mathcal{L}_f^0 h = h, \quad \mathcal{L}_f^i h = \mathcal{L}_f (\mathcal{L}_f^{i-1} h) = \nabla (\mathcal{L}_f^{i-1} h) f, \quad (\text{for } i = 1, 2, \dots)$$

Or given another vector-field,  $g$ , then  $\mathcal{L}_g \mathcal{L}_f h(x)$  is defined as

$$\mathcal{L}_g \mathcal{L}_f h = \nabla (\mathcal{L}_f h) g.$$

For example, if we have a control system

$$\dot{x} = f(x), \quad y = h(x),$$

with the state  $x = x(t)$  and the the output  $y$ , then the derivatives of the output are:

$$\dot{y} = \frac{\partial h}{\partial x} \dot{x} = \mathcal{L}_f h, \quad \text{and} \quad \ddot{y} = \frac{\partial \mathcal{L}_f h}{\partial x} \dot{x} = \mathcal{L}_f^2 h.$$

Also, recall that the curvature of two vector-fields,  $g_1, g_2$ , gives a non-zero Lie bracket (3.5.1.2),  $[g_1, g_2]$  (see Figure 6.6). Lie bracket motions can generate new directions in which the system can move.

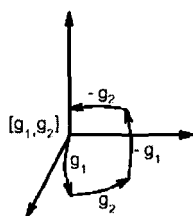


Fig. 6.6 'Lie bracket motion' is possible by appropriately modulating the control inputs (see text for explanation).

In general, the Lie bracket of two vector-fields,  $f(x)$  and  $g(x)$ , is defined by

$$[f, g] = \text{Ad}_f g = \nabla g f - \nabla f g = \frac{\partial g}{\partial x} f - \frac{\partial f}{\partial x} g,$$

where  $\nabla f = \partial f / \partial x$  is the Jacobian matrix. We can define Lie brackets recursively,

$$Ad_f^0 g = g, \quad Ad_f^i g = [f, Ad_f^{i-1} g], \quad (\text{for } i = 1, 2, \dots)$$

Lie brackets have the properties of bilinearity, skew-commutativity and Jacobi identity.

For example, if

$$f = \begin{pmatrix} \cos x_2 \\ x_1 \end{pmatrix}, \quad g = \begin{pmatrix} x_1 \\ 1 \end{pmatrix},$$

then we have

$$[f, g] = \begin{pmatrix} 1 & 0 \\ 0 & 0 \end{pmatrix} \begin{pmatrix} \cos x_2 \\ x_1 \end{pmatrix} - \begin{pmatrix} 0 & -\sin x_2 \\ 1 & 0 \end{pmatrix} \begin{pmatrix} x_1 \\ 1 \end{pmatrix} = \begin{pmatrix} \cos x_2 + \sin x_2 \\ -x_1 \end{pmatrix}.$$

**Input/Output Linearization.** Given a single-input single-output (SISO) system

$$\dot{x} = f(x) + g(x)u, \quad y = h(x), \quad (6.10)$$

we want to formulate a linear-ODE relation between output  $y$  and a new input  $v$ . We will investigate (see [Isidori (1989); Sastri and Isidori (1989); Wilson (2000)]):

- How to generate a linear input/output relation.
- What are the internal dynamics and zero-dynamics associated with the input/output linearization?
- How to design stable controllers based on the I/O linearization.

This linearization method will be exact in a finite domain, rather than tangent as in the local linearization methods, which use Taylor series approximation. Nonlinear controller design using the technique is called exact feedback linearization.

**Algorithm for Exact Feedback Linearization.** We want to find a nonlinear compensator such that the closed-loop system is linear (see Figure 6.7). We will consider only affine SISO systems of the type (6.10), i.e.  $\dot{x} = f(x) + g(x)u$ ,  $y = h(x)$ , and we will try to construct a *control law* of the form

$$u = p(x) + q(x)v, \quad (6.11)$$

where  $v$  is the setpoint, such that the *closed-loop nonlinear system*

$$\dot{x} = f(x) + g(x)p(x) + g(x)q(x)v, \quad y = h(x),$$

is linear from command  $v$  to  $y$ .

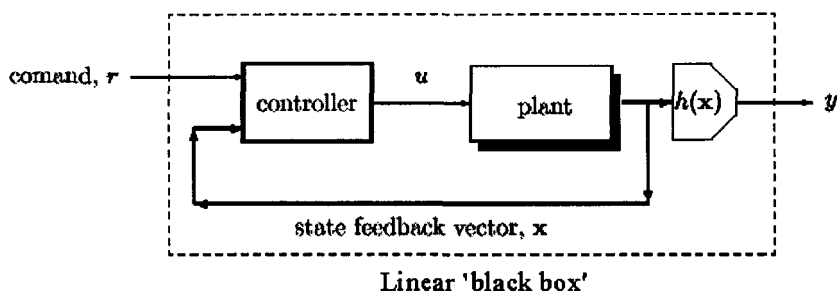


Fig. 6.7 Feedback linearization (see text for explanation).

The main idea behind the feedback linearization construction is to find a nonlinear change of coordinates which transforms the original system into one which is linear and controllable, in particular, a chain of integrators. The difficulty is finding the output function  $h(x)$  which makes this construction possible.

We want to design an exact nonlinear feedback controller. Given the nonlinear affine system,  $\dot{x} = f(x) + g(x)u$ ,  $y = h(x)$ , we want to find the controller functions  $p(x)$  and  $q(x)$ . The unknown functions inside our controller (6.11) are given by:

$$p(x) = \frac{-\left(\mathcal{L}_f^r h(x) + \beta_1 \mathcal{L}_f^{r-1} h(x) + \dots + \beta_{r-1} \mathcal{L}_f h(x) + \beta_r h(x)\right)}{\mathcal{L}_g \mathcal{L}_f^{r-1} h(x)},$$

$$q(x) = \frac{1}{\mathcal{L}_g \mathcal{L}_f^{r-1} h(x)}, \quad (6.12)$$

which are comprised of Lie derivatives,  $\mathcal{L}_f h(x)$ . Here, the *relative order*,  $r$ , is the smallest integer  $r$  such that  $\mathcal{L}_g \mathcal{L}_f^{r-1} h(x) \neq 0$ . For linear systems  $r$  is the difference between the number of poles and zeros.

To obtain the *desired response*, we choose the  $r$  parameters in the  $\beta$  polynomial to describe how the output will respond to the setpoint,  $v$  (pole-

placement).

$$\frac{d^r y}{dt^r} + \beta_1 \frac{d^{r-1} y}{dt^{r-1}} + \dots + \beta_{r-1} \frac{dy}{dt} + \beta_r y = v.$$

Here is the proposed algorithm [Isidori (1989); Sastri and Isidori (1989); Wilson (2000)]:

- (1) Given nonlinear SISO process,  $\dot{x} = f(x, u)$ , and output equation  $y = h(x)$ , then:
- (2) Calculate the relative order,  $r$ .
- (3) Choose an  $r$ th order desired linear response using pole-placement technique (i.e., select  $\beta$ ). For this could be used a simple  $r$ th order low-pass filter such as a Butterworth filter.
- (4) Construct the exact linearized nonlinear controller (6.12), using Lie derivatives and perhaps a symbolic manipulator (e.g., Mathematica, see Appendix).
- (5) Close the loop and obtain a linear input-output black-box (see Figure 6.7).
- (6) Verify that the result is actually linear by comparing with the desired response.

### 6.2.1.2 Relative Degree

A nonlinear SISO system

$$\dot{x} = f(x) + g(x)u, \quad y = h(x),$$

is said to have *relative degree*  $r$  at a point  $x_o$  if (see [Isidori (1989); Nijmeijer and van der Schaft (1990)])

- (1)  $L_g L_f^k h(x) = 0$  for all  $x$  in a neighborhood of  $x_o$  and all  $k < r - 1$ ; and
- (2)  $L_g L_f^{r-1} h(x_o) \neq 0$ .

For example, *controlled Van der Pol oscillator* has the state space form

$$\dot{x} = f(x) + g(x)u = \begin{bmatrix} x_2 \\ 2\omega\zeta(1 - \mu x_1^2)x_2 - \omega^2 x_1 \end{bmatrix} + \begin{bmatrix} 0 \\ 1 \end{bmatrix} u.$$

Suppose the output function is chosen as  $y = h(x) = x_1$ . In this case we have

$$L_g h(x) = \frac{\partial h}{\partial x} g(x) = [1 \ 0] \begin{bmatrix} 0 \\ 1 \end{bmatrix} = 0, \quad \text{and}$$

$$L_f h(x) = \frac{\partial h}{\partial x} f(x) = [1 \ 0] \begin{bmatrix} x_2 \\ 2\omega\zeta(1 - \mu x_1^2)x_2 - \omega^2 x_1 \end{bmatrix} = x_2.$$

Moreover

$$L_g L_f h(x) = \frac{\partial(L_f h)}{\partial x} g(x) = [0 \ 1] \begin{bmatrix} 0 \\ 1 \end{bmatrix} = 1,$$

and thus we see that the Vand der Pol oscillator system has relative degree 2 at any point  $x_o$ .

However, if the output function is, for instance  $y = h(x) = \sin x_2$ , then  $L_g h(x) = \cos x_2$ . The system has relative degree 1 at any point  $x_o$ , provided that  $(x_o)_2 \neq (2k + 1)\pi/2$ . If the point  $x_o$  is such that this condition is violated, no relative degree can be defined.

As another example, consider a *linear system* in the state space form

$$\dot{x} = Ax + Bu, \quad y = Cx.$$

In this case, since  $f(x) = Ax$ ,  $g(x) = B$ ,  $h(x) = Cx$ , it is easily seen that

$$L_f^k h(x) = C A^k x, \quad \text{and therefore,}$$

$$L_g L_f^k h(x) = C A^k B.$$

Thus, the integer  $r$  is characterized by the conditions

$$C A^k B = 0, \quad \text{for all } k < r - 1$$

$$C A^{r-1} B \neq 0, \quad \text{otherwise.}$$

It is well-known that the integer satisfying these conditions is exactly equal to the *difference* between the degree of the denominator polynomial and the degree of the numerator polynomial of the transfer function

$$H(s) = C(sI - A)^{-1}B$$

of the system.

### 6.2.1.3 Approximative Feedback Linearization

Consider a SISO system

$$\dot{x} = f(x) + g(x)u, \quad (6.13)$$

where  $f$  and  $g$  are smooth vector-fields defined on a compact contractible region  $M$  of  $\mathbb{R}^n$  containing the origin. (Typically,  $M$  is a closed ball in  $\mathbb{R}^n$ .) We assume that  $f(0) = 0$ , i.e., that the origin is an equilibrium for  $\dot{x} = f(x)$ . The classical problem of feedback linearization can be stated as follows: find in a neighborhood of the origin a smooth change of coordinates  $z = \Phi(x)$  (a local diffeomorphism) and a smooth feedback law  $u = k(x) + l(x)u_{new}$  such that the closed-loop system in the new coordinates with new control is linear,

$$\dot{z} = Az + Bu_{new},$$

and controllable (see [Banaszuk and Hauser (1996)]). We usually require that  $\Phi(0) = 0$ . We assume that the system (6.13) has the *linear controllability* property

$$\dim(\text{span}\{g, Ad_f g, \dots, Ad_f^{n-1} g\}) = n, \quad \text{for all } x \in M \quad (6.14)$$

(where  $Ad_f^i$  are iterated Lie brackets of  $f$  and  $g$ ). We define the *characteristic distribution* for (6.13)

$$\mathcal{D} = \text{span}\{g, Ad_f g, \dots, Ad_f^{n-2} g\},$$

which is an  $(n-1)$ D smooth distribution by assumption of linear controllability (6.14). We call any nowhere vanishing 1-form  $\omega$  annihilating  $\mathcal{D}$  a characteristic 1-form for (6.13). All the characteristic 1-forms for (6.13) can be represented as multiples of some fixed characteristic 1-form  $\omega_0$  by a smooth nowhere vanishing function (zero-form)  $\beta$ . Suppose that there is a nonvanishing  $\beta$  so that  $\beta\omega_0$  is exact, i.e.,  $\beta\omega_0 = d\alpha$  for some smooth function  $\alpha$ , where  $d$  denotes the exterior derivative. Then  $\omega_0$  is called *integrable* and is called an integrating factor for  $\omega_0$ . The following result is standard in nonlinear control: Suppose that the system (6.13) has the linear controllability property (6.14) on  $M$ . Let  $\mathcal{D}$  be the characteristic distribution and  $\omega_0$  be a characteristic 1-form for (6.13). The following statements are equivalent:

- (1) Equation (6.13) is feedback linearizable in a neighborhood of the origin in  $M$ ;

- (2)  $D$  is involutive in a neighborhood of the origin in  $M$ ; and
- (3)  $\omega_0$  is integrable in a neighborhood of the origin in  $M$ .

As is well known, a generic nonlinear system is not feedback linearizable for  $n > 2$ . However, in some cases, it may make sense to consider *approximate feedback linearization*.

Namely, if one can find a feedback linearizable system close to (6.13), there is hope that a control designed for the feedback linearizable system and applied to (6.13) will give satisfactory performance if the feedback linearizable system is close enough to (6.13). The first attempt in this direction goes back to [Krener (1984)], where it was proposed to apply to (6.13) a change of variables and feedback that yield a system of the form

$$\dot{z} = Az + B u_{new} + O(z, u_{new}),$$

where the term  $O(z, u_{new})$  contains higher-order terms. The aim was to make  $O(z, u_{new})$  of as high order as possible. Then we can say that the system (6.13) is approximately feedback linearized in a small neighborhood of the origin. Later [Hunt and Turi (1993)] introduced a new algorithm to achieve the same goal with fewer steps.

Another idea has been investigated in [Hauser *et al.* (1992)]. Roughly speaking, the idea was to neglect nonlinearities in (6.13) responsible for the failure of the involutivity condition in above theorem. This approach happened to be successful in the ball-and-beam system, when neglect of centrifugal force acting on ball yielded a feedback linearizable system. Application of a control scheme designed for the system with centrifugal force neglected to the original system gave much better results than applying a control scheme based on classical Jacobian linearization. This approach has been further investigated in [Xu and Hauser (1994); Xu and Hauser (1995)] for the purpose of approximate feedback linearization about the manifold of constant operating points. However, a general approach to deciding which nonlinearities should be neglected to get the best approximation has not been set forth.

All of the above-mentioned work dealt with applying a change of coordinates and a preliminary feedback so that the resulting system looks like linearizable part plus nonlinear terms of highest possible order around an equilibrium point or an equilibrium manifold. However, in many applications one requires a large region of operation for the nonlinearizable system. In such a case, demanding the nonlinear terms to be neglected to be of highest possible order may, in fact, be quite undesirable. One might prefer that



the nonlinear terms to be neglected be small in a uniform sense over the region of operation. In this section we propose an approach to approximate feedback linearization that uses a change of coordinates and a preliminary feedback to put a system (6.13) in a perturbed Brunovsky form,

$$\dot{z} = Az + B u_{new} + P(z) + Q(z) u_{new}, \quad (6.15)$$

where  $P(z)$  and  $Q(z)$  vanish at  $z = 0$  and are 'small' on  $M$ . We obtain upper bounds on uniform norms of  $P$  and  $Q$  (depending on some measures of noninvolutivity of  $\mathcal{D}$ ) on any compact, contractible  $M$ .

A different, indirect approach was presented in [Banaszuk and Hauser (1996)]. In this section, the authors present an approach for finding feedback linearizable systems that approximate a given SISO nonlinear system on a given compact region of the state-space. First, they it is shown that if the system is close to being involutive, then it is also close to being linearizable. Rather than working directly with the characteristic distribution of the system, the authors work with characteristic 1-forms, i.e., with the 1-forms annihilating the characteristic distribution. It is shown that homotopy operators can be used to decompose a given characteristic 1-form into an exact and an antiexact part. The exact part is used to define a change of coordinates to a normal form that looks like a linearizable part plus nonlinear perturbation terms. The nonlinear terms in this normal form depend continuously on the antiexact part, and they vanish whenever the antiexact part does. Thus, the antiexact part of a given characteristic 1-form is a measure of nonlinearizability of the system. If the nonlinear terms are small, by neglecting them we get a linearizable system approximating the original system. One can design control for the original system by designing it for the approximating linearizable system and applying it to the original one. We apply this approach for design of locally stabilizing feedback laws for nonlinear systems that are close to being linearizable.

Let us start with approximating characteristic 1-forms by exact forms using *homotopy operators* (compare with (3.11) above). Namely, on any contractible region  $M$  one can define a linear operator  $H$  that satisfies

$$\omega = d(H\omega) + Hd\omega \quad (6.16)$$

for any form  $\omega$ . The homotopy identity (6.16) allows to decompose any given 1-form into the *exact part*  $d(H\omega)$  and an 'error part'  $\epsilon = Hd\omega$ , which we call the *antiexact part of*  $\omega$ . For given  $\omega_0$  annihilating  $\mathcal{D}$  and a scaling factor  $\beta$  we define  $\alpha_\beta = H\beta\omega_0$  and  $\epsilon_\beta = Hd\beta\omega_0$ . The 1-form

$\epsilon_\beta$  measures how exact  $\omega_\beta = \beta\omega_0$  is. If it is zero, then  $\omega_\beta$  is exact and the system (6.13) is linearizable, and the zero-form  $\alpha_\beta$  and its first  $n - 1$  Lie derivatives along  $f$  are the new coordinates. In the case that  $\omega_0$  is not exactly integrable, i.e., when no exact integrating factor  $\beta$  exists, we choose  $\beta$  so that  $d\beta\omega_0$  is *smallest* in some sense (because this also makes  $\epsilon_\beta$  small). We call this  $\beta$  an *approximate integrating factor* for  $\omega_0$ . We use the zero-form  $\alpha_\beta$  and its first  $n - 1$  Lie derivatives along  $f$  as the new coordinates as in the linearizable case. In those new coordinates the system (6.13) is in the form

$$\dot{z} = Az + Bru + Bp + Eu,$$

where  $r$  and  $p$  are smooth functions,  $r \neq 0$  around the origin, and the term  $E$  (the obstruction to linearizability) depends linearly on  $\epsilon_\beta$  and some of its derivatives. We choose  $u = r^{-1}(u_{new} - p)$ , where  $u_{new}$  is a new control variable. After this change of coordinates and control variable the system is of the form (6.15) with  $Q = r^{-1}E$ ,  $P = -r^{-1}pE$ . We obtain estimates on the uniform norm of  $Q$  and  $P$  (via estimates on  $r$ ,  $p$ , and  $E$ ) in terms of the error 1-form  $\epsilon_\beta$ , for any fixed  $\beta$ , on any compact, contractible manifold  $M$ . Most important is that  $Q$  and  $P$  depend in a continuous way on  $\epsilon_\beta$  and some of its derivatives, and they vanish whenever  $\epsilon$  does (see [Banaszuk and Hauser (1996)]).

## 6.2.2 Controllability

### 6.2.2.1 Linear Controllability

A system is *controllable* if the set of all states it can reach from initial state  $x_0 = x(0)$  at the fixed time  $t = T$  contains a ball  $\mathcal{B}$  around  $x_0$ . Again, a system is *small time locally controllable* (STLC) iff the ball  $\mathcal{B}$  for  $t \leq T$  contains a neighborhood of  $x_0$ .<sup>3</sup>

In the case of a linear system in the standard state-space form (see subsection (4.8.2.1) above)

$$\dot{x} = Ax + Bu, \tag{6.17}$$

where  $A$  is the  $n \times n$  state matrix and  $B$  is the  $m \times n$  input matrix, all

<sup>3</sup>The above definition of controllability tells us only whether or not something can reach an open neighborhood of its starting point, but does not tell us how to do it. That is the point of the trajectory generation.

controllability definitions coincide, i.e.,

$$0 \rightarrow x(T), \quad x(0) \rightarrow 0, \quad x(0) \rightarrow x(T),$$

where  $T$  is either fixed or free.

*Rank condition* states: System (6.17) is controllable iff the matrix

$$W_n = (B \ AB \ \dots \ A^{n-1}B) \quad \text{has full rank.}$$

In the case of nonlinear systems the corresponding result is obtained using the formalism of Lie brackets, as Lie algebra is to nonlinear systems as matrix algebra is to linear systems.

### 6.2.2.2 Nonlinear Controllability

Nonlinear MIMO-systems are generally described by differential equations of the form (see [Isidori (1989); Nijmeijer and van der Schaft (1990); Goodwine (1998)]):

$$\dot{x} = f(x) + g_i(x) u^i, \quad (i = 1, \dots, n), \quad (6.18)$$

defined on a smooth  $n$ -manifold  $M$ , where  $x \in M$  represents the state of the control system,  $f(x)$  and  $g_i(x)$  are vector-fields on  $M$  and the  $u^i$  are control inputs, which belong to a set of *admissible controls*,  $u^i \in U$ . The system (6.18) is called *driftless*, or *kinematic*, or *control linear* if  $f(x)$  is identically zero; otherwise, it is called a *system with drift*, and the vector-field  $f(x)$  is called the *drift term*. The flow  $\phi_t^g(x_0)$  represents the solution of the differential equation  $\dot{x} = g(x)$  at time  $t$  starting from  $x_0$ . Geometric way to understand the *controllability* of the system (6.18) is to understand the geometry of the vector-fields  $f(x)$  and  $g_i(x)$ .

**Example: Car-Parking Using Lie Brackets.** In this popular example, the driver has two different transformations at his disposal. He can turn the steering wheel, or he can drive the car forward or back. Here, we specify the state of a car by four coordinates: the  $(x, y)$  coordinates of the center of the rear axle, the direction  $\theta$  of the car, and the angle  $\phi$  between the front wheels and the direction of the car.  $L$  is the constant length of the car. Therefore, the configuration manifold of the car is 4D,  $M = (x, y, \theta, \phi)$ .

Using (6.18), the driftless car kinematics can be defined as:

$$\dot{x} = g_1(x) u_1 + g_2(x) u_2, \quad (6.19)$$

with two vector-fields  $g_1, g_2 \in \mathcal{X}^k(M)$ .

The infinitesimal transformations will be the vector-fields

$$g_1(x) \equiv \text{DRIVE} = \cos \theta \frac{\partial}{\partial x} + \sin \theta \frac{\partial}{\partial y} + \frac{\tan \phi}{L} \frac{\partial}{\partial \theta} \equiv \begin{pmatrix} \cos \theta \\ \sin \theta \\ \frac{1}{L} \tan \phi \\ 0 \end{pmatrix},$$

$$\text{and } g_2(x) \equiv \text{STEER} = \frac{\partial}{\partial \phi} \equiv \begin{pmatrix} 0 \\ 0 \\ 0 \\ 1 \end{pmatrix}.$$

Now, STEER and DRIVE do not commute; otherwise we could do all your steering at home before driving on a trip. Therefore, we have a Lie bracket

$$[g_2, g_1] \equiv [\text{STEER}, \text{DRIVE}] = \frac{1}{L \cos^2 \phi} \frac{\partial}{\partial \theta} \equiv \text{ROTATE}.$$

The operation  $[g_2, g_1] \equiv \text{ROTATE} \equiv [\text{STEER}, \text{DRIVE}]$  is the infinitesimal version of the sequence of transformations: steer, drive, steer back, and drive back, i.e.,

$$\{\text{STEER}, \text{DRIVE}, \text{STEER}^{-1}, \text{DRIVE}^{-1}\}.$$

Now, ROTATE can get us out of some parking spaces, but not tight ones: we may not have enough room to ROTATE out. The usual tight parking space restricts the DRIVE transformation, but not STEER. A truly tight parking space restricts STEER as well by putting your front wheels against the curb.

Fortunately, there is still another commutator available:

$$\begin{aligned} [g_1, [g_2, g_1]] &\equiv [\text{DRIVE}, [\text{STEER}, \text{DRIVE}]] = [[g_1, g_2], g_1] \equiv \\ [\text{DRIVE}, \text{ROTATE}] &= \frac{1}{L \cos^2 \phi} \left( \sin \theta \frac{\partial}{\partial x} - \cos \theta \frac{\partial}{\partial y} \right) \equiv \text{SLIDE}. \end{aligned}$$

The operation  $[[g_1, g_2], g_1] \equiv \text{SLIDE} \equiv [\text{DRIVE}, \text{ROTATE}]$  is a displacement at right angles to the car, and can get us out of any parking place. We just need to remember to steer, drive, steer back, drive some more, steer, drive back, steer back, and drive back:

$$\{\text{STEER}, \text{DRIVE}, \text{STEER}^{-1}, \text{DRIVE}, \text{STEER}, \text{DRIVE}^{-1}, \text{STEER}^{-1}, \text{DRIVE}^{-1}\}.$$

We have to reverse steer in the middle of the parking place. This is not intuitive, and no doubt is part of the problem with parallel parking.

Thus from only two controls  $u_1$  and  $u_2$  we can form the vector-fields  $\text{DRIVE} \equiv g_1$ ,  $\text{STEER} \equiv g_2$ ,  $\text{ROTATE} \equiv [g_2, g_1]$ , and  $\text{SLIDE} \equiv [[g_1, g_2], g_1]$ , allowing us to move anywhere in the configuration manifold  $M$ . The car kinematics  $\dot{x} = g_1 u_1 + g_2 u_2$  is thus expanded as:

$$\begin{pmatrix} \dot{x} \\ \dot{y} \\ \dot{\theta} \\ \dot{\phi} \end{pmatrix} = \text{DRIVE} \cdot u_1 + \text{STEER} \cdot u_2 \equiv \begin{pmatrix} \cos \theta \\ \sin \theta \\ \frac{1}{L} \tan \phi \\ 0 \end{pmatrix} \cdot u_1 + \begin{pmatrix} 0 \\ 0 \\ 0 \\ 1 \end{pmatrix} \cdot u_2.$$

The *parking theorem* says: One can get out of any parking lot that is larger than the car.

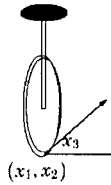


Fig. 6.8 The unicycle problem (see text for explanation).

**The Unicycle Example.** Now, consider the unicycle example (see Figure 6.8). Here we have

$$g_1 = \begin{pmatrix} \cos x_3 \\ \sin x_3 \\ 0 \end{pmatrix}, \quad g_2 = \begin{pmatrix} 0 \\ 0 \\ 1 \end{pmatrix}, \quad [g_1, g_2] = \begin{pmatrix} \sin x_3 \\ -\cos x_3 \\ 0 \end{pmatrix}.$$

The unicycle system is full rank and therefore controllable.

### 6.2.2.3 Controllability Condition

Nonlinear controllability is an extension of linear controllability. The nonlinear MIMO system

$$\dot{x} = f(x) + g(x)u \quad \text{is controllable}$$

if the set of vector-fields  $\{g, [f, g], \dots, [f^{n-1}, g]\}$  is independent.

For example, for the kinematic car system of the form (6.19), the *nonlinear controllability criterion* reads: If the Lie bracket tree:

$$g_1, \quad g_2, \quad [g_1, g_2], \quad [[g_1, g_2], g_1], \quad [[g_1, g_2], g_2], \quad [[[g_1, g_2], g_1], g_1], \\ [[[g_1, g_2], g_1], g_2], \quad [[[g_1, g_2], g_2], g_1], \quad [[[g_1, g_2], g_2], g_2], \dots$$

– has *full rank* then the system is *controllable* [Isidori (1989); Nijmeijer and van der Schaft (1990); Goodwine (1998)]. In this case the combined input

$$(u_1, u_2) = \begin{cases} (1, 0), & t \in [0, \varepsilon] \\ (0, 1), & t \in [\varepsilon, 2\varepsilon] \\ (-1, 0), & t \in [2\varepsilon, 3\varepsilon] \\ (0, -1), & t \in [3\varepsilon, 4\varepsilon] \end{cases}$$

gives the motion  $x(4\varepsilon) = x(0) + \varepsilon^2 [g_1, g_2] + O(\varepsilon^3)$ , with the flow given by (see (3.19) below)

$$F_t^{[g_1, g_2]} = \lim_{n \rightarrow \infty} \left( F_{\sqrt{t/n}}^{-g_2} F_{\sqrt{t/n}}^{-g_1} F_{\sqrt{t/n}}^{g_2} F_{\sqrt{t/n}}^{g_1} \right)^n.$$

#### 6.2.2.4 Distributions

In control theory, the set of all possible directions in which the system can move, or the set of all points the system can reach, is of obvious fundamental importance. Geometrically, this is related to *distributions*.

A *distribution*  $\Delta \subset \mathcal{X}^k(M)$  on the manifold  $M$  is a subbundle of its tangent bundle  $TM$ , which assigns a subspace of the tangent space  $T_x M$  to each point  $x \in M$  in a smooth way. The dimension of  $\Delta(x)$  over  $\mathbb{R}$  at a point  $x \in M$  is called the rank of  $\Delta$  at  $x$ .

A distribution  $\Delta$  is *involutive* if, for any two vector-fields  $X, Y \in \Delta$ , their Lie bracket  $[X, Y] \in \Delta$ .

A function  $f \in C^k(M)$  is called an *integral* of  $\Delta$  if  $df(x) \in \Delta^0(x)$  for each  $x \in M$ . An *integral manifold* of  $\Delta$  is a submanifold  $N$  of  $M$  such that  $T_x N \subset \Delta(x)$  for each  $x \in N$ . A distribution  $\Delta$  is *integrable* if, for any  $x \in M$ , there is a submanifold  $N \subset M$ , whose dimension is the same as the rank of  $\Delta$  at  $x$ , containing  $x$  such that the tangent bundle,  $TN$ , is exactly  $\Delta$  restricted to  $N$ , i.e.,  $TN = \Delta|_N$ . Such a submanifold is called the *maximal integral manifold* through  $x$ .

It is natural to consider distributions generated by the vector-fields appearing in the sequence of flows (3.18). In this case, consider the distribution defined by

$$\Delta = \text{span}\{f; g_1 \dots g_m\},$$

where the span is taken over the set of smooth real-valued functions. Denote by  $\bar{\Delta}$  the *involutive closure* of the distribution  $\Delta$ , which is the closure of  $\Delta$  under bracketing. Then,  $\bar{\Delta}$  is the smallest subalgebra of  $\mathcal{X}^k(M)$  which

contains  $\{f; g_1 \dots g_m\}$ . We will often need to 'add' distributions. Since distributions are, pointwise, vector spaces, define the sum of two distributions,

$$(\Delta_1 + \Delta_2)(x) = \Delta_1(x) + \Delta_2(x).$$

Similarly, define the intersection

$$(\Delta_1 \cap \Delta_2)(x) = \Delta_1(x) \cap \Delta_2(x).$$

More generally, we can arrive at a distribution via a *family of vector-fields*, which is simply a subset  $\mathcal{V} \subset \mathcal{X}^k(M)$ . Given a family of vector-fields  $\mathcal{V}$ , we may define a distribution on  $M$  by

$$\Delta_{\mathcal{V}}(x) = \langle X(x) | X \in \mathcal{V} \rangle_{\mathbb{R}}.$$

Since  $\mathcal{X}^k(M)$  is a Lie algebra, we may ask for the smallest Lie subalgebra of  $\mathcal{X}^k(M)$  which contains a family of vector-fields  $\mathcal{V}$ . It will be denoted as  $\overline{\text{Lie}}(\mathcal{V})$ , and will be represented by the set of vector-fields on  $M$  generated by repeated Lie brackets of elements in  $\mathcal{V}$ . Let  $\mathcal{V}^{(0)} = \mathcal{V}$  and then iteratively define a sequence of families of vector-fields by

$$\mathcal{V}^{(i+1)} = \mathcal{V}^{(i)} \cup \{[X, Y] | X \in \mathcal{V}^{(0)} = \mathcal{V} \text{ and } Y \in \mathcal{V}^{(i)}\}.$$

Now, every element of  $\overline{\text{Lie}}(\mathcal{V})$  is a linear combination of repeated Lie brackets of the form

$$[Z_k, [Z_{k-1}, [\dots, [Z_2, Z_1] \dots]]]$$

where  $Z_i \in \mathcal{V}$  for  $i = 1, \dots, k$ .

### 6.2.2.5 Foliations

Related to integrable distributions are foliations.

Frobenius' theorem asserts that integrability and involutivity are equivalent, at least locally. Thus, associated with an involutive distribution is a partition  $\Phi$  of  $M$  into disjoint connected immersed submanifolds called *leaves*. This partition  $\Phi$  is called a *foliation*. More precisely, a foliation  $\mathcal{F}$  of a smooth manifold  $M$  is a collection of disjoint immersed submanifolds of  $M$  whose disjoint union equals  $M$ . Each connected submanifold of  $\mathcal{F}$  is called a *leaf* of the foliation. Given an integrable distribution  $\Delta$ , the collection of maximal integral manifolds for  $\Delta$  defines a foliation on  $M$ , denoted by  $\mathcal{F}_D$ .

A foliation  $\mathcal{F}$  of  $M$  defines an equivalence relation on  $M$  whereby two points in  $M$  are equivalent if they lie in the same leaf of  $\mathcal{F}$ . The set of

equivalence classes is denoted  $M/\mathcal{F}$  and is called the *leaf space* of  $\mathcal{F}$ . A foliation  $\mathcal{F}$  is said to be simple if  $M/\mathcal{F}$  inherits a manifold structure so that the projection from  $M$  to  $M/\mathcal{F}$  is a surjective submersion.

In control theory, foliation leaves are related to the set of points that a control system can reach starting from a given initial condition. A foliation  $\Phi$  of  $M$  defines an equivalence relation on  $M$  whereby two points in  $M$  are equivalent if they lie in the same leaf of  $\Phi$ . The set of equivalence classes is denoted  $M/\Phi$  and is called the *leaf space* of  $\Phi$ .

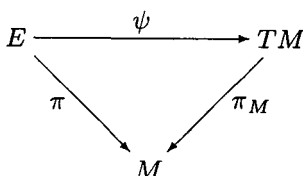
### 6.3 Modern Control Techniques for Mechanical Systems

In this section we present modern control techniques for mechanical systems, as used in modern biodynamics research. Much of the existing work on control of mechanical systems has relied on the presence of specific structure. The most common examples of the types of structure assumed are symmetry (conservation laws) and constraints. While it may seem counter-intuitive that constraints may help in control theory, this is sometimes in fact the case. The reason is that the constraints provide extra forces (forces of constraint) which can be used to advantage. probably, the most interesting work is done from the Lagrangian (respectively Hamiltonian) perspective where we study systems whose Lagrangians are 'kinetic energy minus potential energy' (resp. 'kinetic energy plus potential energy'). For these *simple mechanical control systems*, the controllability questions are different than those typically asked in nonlinear control theory. In particular, one is often more interested in what happens to configurations rather than states, which are configurations and velocities (resp. momenta) for these systems (see [Lewis (1995); Lewis and Murray (1997)]).

#### 6.3.1 Abstract Control System

In general, a nonlinear control system  $\Sigma$  can be represented as a triple  $(\Sigma, M, f)$ , where  $M$  is the system's *state-space* manifold with the tangent bundle  $TM$  and the general fibre bundle  $E$ , and  $f$  is a smooth map, such that the following bundle diagram commutes [Manikonda (1998)]





where  $\psi : (x, u) \mapsto (x, f(x, u))$ ,  $\pi_M$  is the natural projection of  $TM$  on  $M$ , the projection  $\pi : E \rightarrow M$  is a smooth fibre bundle, and the fibers of  $E$  represent the *input spaces*. If one chooses fibre-respecting coordinates  $(x, u)$  for  $E$ , then locally this definition reduces to  $\psi : (x, u) \mapsto (x, \psi(x, u))$ , i.e.,

$$\dot{x} = \psi(x, u).$$

The specific form of the map  $\psi$ , usually used in nonlinear control, is  $\psi : (x, u) \mapsto (x, f(x) + g(x, u))$ , with  $g(x, 0) = 0$ , producing standard nonlinear system equation

$$\dot{x} = f(x) + g(x, u).$$

### 6.3.2 Controllability of a Linear Control System

Consider a linear biodynamic control system (compare with (6.1.2) above):

$$\dot{x}(t) = Ax(t) + Bu(t), \quad (6.20)$$

where  $x \in \mathbb{R}^n$ ,  $u \in \mathbb{R}^m$ ,  $A \in L(\mathbb{R}^n, \mathbb{R}^n)$ , and  $B \in L(\mathbb{R}^m, \mathbb{R}^n)$ . One should think of  $t \mapsto u(t)$  as being a specified input signal, i.e., a function on the certain time interval,  $[0, T]$ . Now, control theory wants to design the signal to make the *state*  $t \mapsto x(t)$  do what we want. What this is may vary, depending on the situation at hand. For example, one may want to steer from an initial state  $x^i$  to a final state  $x_f$ , perhaps in an optimal way. Or, one may wish to design  $u : \mathbb{R}^n \rightarrow \mathbb{R}^m$  so that some state, perhaps  $x = 0$ , is stable for the dynamical system  $\dot{x}(t) = Ax + Bu(x)$ , which is called *state feedback* (often one asks that  $u$  be linear). One could also design  $u$  to be a function of both  $x$  and  $t$ , etc.

One of the basic control questions is *controllability*, which comes in many guises. Basically we are asking for 'reachable' points. In particular,

$$\mathcal{R}(0) = \text{span}_{\mathbb{R}}\{[B|AB|\dots|A^{n-1}B]\},$$

which is the smallest  $A$ -invariant subspace containing  $\text{Im}(B)$ , denotes the set of points reachable from  $0 \in \mathbb{R}^n$ . For the linear system (6.20), the basic controllability questions have definite answers. We want to do something similar for a class of simple mechanical systems [Lewis (1995); Lewis and Murray (1997)].

### 6.3.3 Affine Control System and Local Controllability

The nonlinear control system that we most often consider in biodynamics has state-space  $M$ , a smooth  $n$ -manifold, and is *affine* in the controls. Thus it has the form (see [Lewis (1995); Lewis and Murray (1997)])

$$\dot{x} = f(x) + u^a g_a(x), \quad x \in M, \quad (6.21)$$

where  $f, g_1, \dots, g_m$  are vector-fields on  $M$ . The *drift* vector-field  $f = f(x)$  describes how the system would evolve in the absence of any inputs. Each of the *control* vector-fields  $g_1, \dots, g_m$  specifies a direction in which one can supply actuation. To fully specify the control system properly, one should also specify the type of control action to be considered. Here we consider our controls to be taken from the set:  $U = \{u : \mathbb{R} \rightarrow \mathbb{R}^m \mid u \text{ is piecewise constant}\}$ . This class of controls is sufficient to deal with all analytic control systems. More generally, one may wish to consider measurable functions which take their values in a subset of  $\mathbb{R}^m$ .

Given an *affine control system* (6.21), it is possible to define a family of vector-fields on  $M$  by:  $V_\Sigma = \{f + u^a g_a \mid u \in \mathbb{R}^m\}$ .

A solution of the system (6.21) is a pair  $(\gamma, u)$ , where  $\gamma : [0, T] \rightarrow M$  is a piecewise smooth curve on  $M$  and  $u \in U$  such that

$$\dot{\gamma}(t) = f(\gamma(t)) + u^a(t) g_a(\gamma(t)), \quad \text{for each } t \in [0, T].$$

The *reachable set* from  $x_0$  in time  $T$  is

$$\begin{aligned} \mathcal{R}(x_0, T) &= \{x \mid \exists \gamma : [0, T] \rightarrow M \quad \text{and} \\ &\quad u : [0, T] \rightarrow \mathbb{R}^m \quad \text{satisfying (6.21)} \\ &\quad \text{with } \gamma(0) = x_0 \quad \text{and } \gamma(T) = x\}. \end{aligned}$$

Note that since the system has drift  $f$ , when we reach the point  $\gamma(T)$  we will not remain there if this is not an equilibrium point for  $f$ . Also, we have,  $\mathcal{R}(x_0, \leq T) = \bigcup_{0 < t \leq T} \mathcal{R}(x_0, t)$ .

Let  $x_0 \in M$ , let  $V$  be a neighborhood of  $x_0$ , and let  $T > 0$ . We say that equation (6.21) represents a *locally accessible system* at  $x_0$  if  $\mathcal{R}(x_0, \leq T)$

contains an open subset of  $M$  for each  $V$  and for each  $T$  sufficiently small. Furthermore, we say that the system (6.21) is *small-time local controllability* (STLC, see [Sussmann (1983); Sussmann (1987)]), if it is locally accessible and if  $x_0$  is in the interior of  $\mathcal{R}(x_0, \leq T)$  for each  $V$  and for each  $T$  sufficiently small.

### 6.3.4 Hamiltonian Control and Maximum Principle

#### 6.3.4.1 Hamiltonian Control Systems

Hamiltonian control system on a symplectic manifold  $(P, \omega)$  is defined as an affine control system whose drift and control vector-fields are Hamiltonian. It can be written as

$$\dot{p} = X_H(p) + u^a X_a(p),$$

where the vector-fields  $X_a$  are assumed to be Hamiltonian with Hamiltonian  $H_a$  for  $a = 1, \dots, m$ . Examples of systems which are (at least locally) Hamiltonian control systems are those which evolve on the symplectic manifold  $T^*M$  and where the control Hamiltonians are simply coordinate functions on  $M$ .

Alternatively, Hamiltonian control systems can be defined on Poisson manifolds, however for the purposes of this section, it will be more natural to work within the Poisson context. Recall (see (4.2.3) above) that given a smooth Hamiltonian function  $h : M \rightarrow \mathbb{R}$ , on the Poisson manifold  $M$ , the Poisson bracket  $\{, \} : C^\infty(M) \times C^\infty(M) \rightarrow C^\infty(M)$  (such that  $\{f, g\} = -\{g, f\}$ ,  $\{f, \{g, h\}\} + \{g, \{h, f\}\} + \{h, \{f, g\}\} = 0$ , and  $\{fg, h\} = \{f, h\}g + f\{g, h\}$ ) allows us to obtain a Hamiltonian vector-field  $X_h$  with Hamiltonian  $h$  through the equality

$$\mathcal{L}_{X_h} f = \{f, h\}, \quad \text{for all } f \in C^\infty(M),$$

where  $\mathcal{L}_{X_h} f$  is the Lie derivative of  $f$  along  $X_h$ . Note that the vector-field  $X_h$  is well defined since the Poisson bracket verifies the Leibniz rule and therefore defines a derivation on  $C^\infty(M)$  (see [Marsden and Ratiu (1999)]). Furthermore  $C^\infty(M)$  equipped with a Poisson bracket is a Lie algebra, called a Poisson algebra. Also, we say that the Poisson structure on  $M$  is nondegenerate if the  $\{, \}$ -associated map  $B^\# : T^*M \rightarrow TM$  defined by

$$dg(B^\#(x)(df)) = B(x)(df, dg),$$

(where  $df$  denotes the exterior derivative of  $f$ ) is an isomorphism for every  $x \in M$ .

An *affine Hamiltonian control system*  $\Sigma = (U, M, h)$  consists of a smooth manifold  $U$  (the *input space*), a Poisson manifold  $M$  with non-degenerate Poisson bracket (the *state-space*), and a smooth function  $H : M \times U \rightarrow \mathbb{R}$  (the *controlled Hamiltonian*). Furthermore,  $H$  is locally of the form  $H = h_0 + h_i u^i$  ( $i = 1, \dots, n$ ), with  $h_i$  locally defined smooth real valued maps and  $u^i$  local coordinates for  $U$  [Tabuada and Pappas (2001a); Tabuada and Pappas (2003)].

Using the controlled Hamiltonian and the Poisson structure on  $M$  we can recover the familiar system map  $F : M \times U \rightarrow TM$ , locally given by

$$F = X_{h_0} + X_{h_i} u^i,$$

and defines an affine distribution on  $M$  given by

$$\mathcal{D}_M(x) = X_{h_0}(x) + \text{span}\{X_{h_1}(x), X_{h_2}(x), \dots, X_{h_n}(x)\}.$$

This distribution captures all the possible directions of motion available at a certain point  $x$ , and therefore describes a control system, up to a parametrization by control inputs. This affine distribution will be our main object of interest here, and we will assume that the rank of  $\mathcal{D}_M$  does not change with  $x$ . Furthermore, we denote an affine distribution  $\mathcal{D}_M$  by  $X + \Delta$ , where  $X$  is a vector-field and  $\Delta$  a distribution. When this affine distribution is defined by a Hamiltonian control system we have  $X = X_{h_0}$  and  $\Delta = \text{span}\{X_{h_1}(x), X_{h_2}(x), \dots, X_{h_n}(x)\}$ . A similar reasoning is possible at the level of Hamiltonians. Locally, we can define the following affine space of smooth maps

$$\mathcal{H}_M = h_0 + \text{span}_{\mathbb{R}}\{h_1, h_1, \dots, h_n\},$$

which defines  $\mathcal{D}_M$  by the equality

$$\mathcal{D}_M = B^\#(d\mathcal{H}_M),$$

where we used the notation  $d\mathcal{H}_M$  to denote the set  $\cup_{h \in \mathcal{H}_M} dh$ . We also use the notation  $\mathcal{H}_M = h_0 + H_\Delta$  for an affine space of smooth maps where  $h_0$  is a smooth map and  $H_\Delta$  a linear space of smooth maps.

Having defined Hamiltonian control systems we turn to their trajectories or solutions: A smooth curve  $\gamma : I \rightarrow M$ ,  $I \subseteq \mathbb{R}_0^+$  is called a *trajectory of control system*  $\Sigma = (U, M, H)$ , iff there exists a curve  $\gamma^U : I \rightarrow U$  satisfying

[Tabuada and Pappas (2001a); Tabuada and Pappas (2003)]

$$\dot{\gamma}(t) = F(\gamma(t), \gamma^U(t)), \quad \text{for every } t \in I.$$

Now, given a Hamiltonian control system and a desired property, an abstracted Hamiltonian system is a reduced system that preserves the property of interest while ignoring modelling detail (see [Tabuada and Pappas (2001a); Tabuada and Pappas (2003)]). Property preserving abstractions of control systems are important for reducing the complexity of their analysis or design. From an analysis perspective, given a large scale control system and a property to be verified, one extracts a smaller abstracted system with equivalent properties. Checking the property on the abstraction is then equivalent to checking the property on the original system. From a design perspective, rather than designing a controller for the original large scale system, one designs a controller for the smaller abstracted system, and then refines the design to the original system while incorporating modelling detail.

This approach critically depends on whether we are able to construct hierarchies of abstractions as well as characterize conditions under which various properties of interest propagate from the original to the abstracted system and vice versa. In [Pappas *et al.* (2000)], hierarchical abstractions of linear control systems were extracted using computationally efficient constructions, and conditions under which controllability of the abstracted system implied controllability of the original system were obtained. This led to extremely efficient hierarchical controllability algorithms. In the same spirit, abstractions of nonlinear control affine systems were considered in [Pappas and Simic (2002)], and the canonical construction for linear systems was generalized to nonlinear control affine systems. In [Tabuada and Pappas (2001b)] existence of abstractions (regarded as quotients in a category) was shown for fully nonlinear control systems. Furthermore, a characterization of the relation between the state/input space of the original system with the state/input space of its abstraction was also presented.

In [Tabuada and Pappas (2001a); Tabuada and Pappas (2003)], abstractions of Hamiltonian control systems are considered, which are control systems completely specified by controlled Hamiltonians. This additional structure allows to simplify the abstraction process by working with functions instead of vector-fields or distributions as is the case for general nonlinear systems [Pappas and Simic (2002)]. This is possible since the controlled Hamiltonian contains all the relevant information

that must be captured by the abstracted system. On the other hand, to be able to relate the dynamics induced by the controlled Hamiltonians, we need to restrict the class of abstracting maps to those that preserve the Hamiltonian structure. More precisely, given a Hamiltonian control system on a Poisson manifold  $M$ , and a (quotient) Poisson map  $\phi : M \rightarrow N$ , one presents a canonical construction that extracts an abstracted Hamiltonian control system on  $N$ . One then characterizes abstracting maps for which the original and abstracted system are equivalent from a local accessibility point of view [Tabuada and Pappas (2001a); Tabuada and Pappas (2003)].

### 6.3.4.2 Pontryagin's Maximum Principle

*Pontryagin's Maximum Principle* (MP) applies to a general optimization problem called a *Bolza problem* (see [Pontryagin *et al.* (1986)]). To apply MP to optimal control, we need to define Hamiltonian function:

$$H(\psi, x, u) = (\psi, f(x, u)) = \psi_i f^i(x, u), \quad (i = 1, \dots, n). \quad (6.22)$$

Then in order for a control  $u(t)$  and a trajectory  $x(t)$  to be *optimal*, it is necessary that there exist a nonzero absolutely continuous vector function  $\psi(t) = (\psi_0(t), \psi_1(t), \dots, \psi_n(t))$  corresponding to the functions  $u(t)$  and  $x(t)$  such that:

- (1) The function  $H(\psi(t), x(t), u(t))$  attains its maximum at the point  $u = u(t)$  almost everywhere in the interval  $t_0 \leq t \leq T$ ,

$$H(\psi(t), x(t), u(t)) = \max_{u \in U} H(\psi(t), x(t), u(t)).$$

- (2) At the *terminal time*  $T$ , the relations  $\psi_0(T) \leq 0$  and  $H(\psi(T), x(T), u(T))$  are satisfied.

MP states the following algorithm: To maximize the set of *steering functions*  $\gamma_i x^i(t)$  (with  $n$  constants  $\gamma_i$ ) for controlling the changes in the *state variables*

$$\dot{x}^i(t) = f^i(x^i, u_k), \quad (i = 0, 1, \dots, n, \quad k = 1, \dots, m),$$

we maximize at each instant the Hamiltonian function (6.22), where

$$\dot{\psi}_i = -\psi_j \frac{\partial f^j}{\partial x^i} \quad \text{and} \quad \psi_i(T) = \gamma_i.$$

### 6.3.4.3 Affine Control Systems

Now, let us look at MP as applied to the *affine control system* (see [Lewis (2000)])

$$\dot{\gamma}(t) = f_0(\gamma(t)) + u^a(t) f_a(\gamma(t)),$$

with  $\gamma(t) \in M$ ,  $u$  taking values in  $U \subset \mathbb{R}^m$ , and objective function  $L(x, u)$ .

We need to have the control Hamiltonian on  $U \times T^*M$ :

$$H(\alpha_x, u) = \underbrace{\alpha_x(f_0(x))}_{H_1} + \underbrace{\alpha_x(u^a f_a(x))}_{H_2} - \underbrace{L(x, u)}_{H_3}.$$

One of several consequences of the MP is that if  $(u, \gamma)$  is a *minimizer* then there exists a 1-form field  $\lambda$  along  $\gamma$  with the property that  $t \mapsto \lambda(t)$  is an integral curve for the time-dependent Hamiltonian  $(\alpha_x, u) \mapsto H(\alpha_x, u)$ . The Hamiltonian  $H(\alpha_x, u)$  is a sum of three terms, and so too will be the Hamiltonian vector-field.

Let us look at the first term, that with (old) Hamiltonian  $H_1 = \alpha_x(f_0(x))$ . In local coordinates  $X_{H_1}$  is written as

$$\dot{x}^i = f_0^i(x), \quad \dot{p}_i = -\frac{\partial f_0^j(x)}{\partial x^i} p_j. \quad (6.23)$$

$X_{H_1}$  is the *cotangent lift* of  $f_0$  and, following [Lewis (2000)], we denote it  $f_0^{T*}$ . So we want to understand  $f_0^{T*}$  on  $TM$  with  $f_0 = Z$ .

Let  $f_0$  be a vector-field on a general manifold  $N$  with  $f_0^T$  its *tangent lift* defined by

$$f_0^T(v_x) = \left. \frac{d}{dt} \right|_{t=0} T_x F_t(v_x),$$

where  $F_t$  denotes the flow of  $f_0$ . Therefore,  $f_0^T$  is the ‘linearisation’ of  $f_0$  and in local coordinates it is given by (compare with (6.23))

$$\dot{x}^i = f_0^i(x), \quad \dot{v}^i = -\frac{\partial f_0^i(x)}{\partial x^j} v^j.$$

The flow of  $f_0^T$  measures how the integral curves of  $f_0$  change as we change the initial condition in the direction of  $v_x$ .

Now, perhaps we can understand  $Z^T$  on  $TM$  with  $f_0 = Z$  in the discussion of tangent lift. Let  $\gamma(t)$  be a geodesic. By varying the initial condition for the geodesic we generate an ‘infinitesimal variation’ which satisfies the

extended Jacobi equation (compare with (3.49) above),

$$\nabla_{\dot{y}(t)}^2 \xi(t) + R(\xi(t), \dot{y}(t)) \dot{y}(t) + \nabla_{\dot{y}(t)} (T(\xi(t), \dot{y}(t))) = 0. \quad (6.24)$$

To make the ‘connection’ between  $Z^T$  and the Jacobi equation, we perform constructions on the tangent bundle using the spray  $Z$ .  $\nabla$  comes from a linear connection on  $M$  which induces an *Ehresmann connection* on  $\tau_M : TM \rightarrow M$ . Thus we may write  $T_{v_q} TM \simeq T_q M \oplus T_q M$ . Now, if  $I_M : TTM \rightarrow TTM$  is the canonical involution then  $I_M^* Z^T$  is a spray. We use  $I_M^* Z^T$  to induce an Ehresmann connection on  $\tau_{TTM} : TTM \rightarrow TM$ . Thus,

$$T_{X_{v_q}} TTM \simeq T_{v_q} TM \oplus T_{v_q} TM \simeq \underbrace{T_q M \oplus T_q M}_{\text{geodesic equations}} \oplus \underbrace{T_q M \oplus T_q M}_{\text{variation equations}}.$$

One represents  $Z^T$  in this splitting and determines that the Jacobi equation sits ‘inside’ one of the four components. Now one applies similar constructions to  $T^*TM$  and  $Z^{T^*}$  to derive a 1-form version of the Jacobi equation (6.24), the so-called *adjoint Jacobi equation* [Lewis (2000)]:

$$\nabla_{\dot{y}(t)}^2 \lambda(t) + R^*(\lambda(t), \dot{y}(t)) \dot{y}(t) - T^*(\nabla_{\dot{y}(t)} \lambda(t), \dot{y}(t)) = 0, \quad (6.25)$$

where we have used  $\langle R^*(\alpha, u)v; \omega \rangle = \langle \alpha; R(\omega, u)v \rangle$ , and  $\langle T^*(\alpha, u); \omega \rangle = \langle \alpha; T(\omega, u) \rangle$ .

The adjoint Jacobi equation forms the backbone of a general statement of the MP for affine connection control systems. When objective function is the Lagrangian  $L(u, v_q) = \frac{1}{2}g(v_q, v_q)$ , when  $\nabla$  is the Levi-Civita connection for the Riemannian metric  $g$ , and when the system is fully actuated, then we recover the equation of [Noakes *et al.* (1989)]

$$\nabla_{\dot{y}(t)}^3 \dot{y}(t) + R(\nabla_{\dot{y}(t)} \dot{y}(t), \dot{y}(t)) = 0.$$

Therefore, the adjoint Jacobi equation (6.25) captures the interesting part of the Hamiltonian vector-field  $Z^{T^*}$ , which comes from the MP, in terms of affine geometry, i.e., from  $Z^{T^*}$  follows

$$\nabla_{\dot{y}(t)} \dot{y}(t) = 0, \quad \nabla_{\dot{y}(t)}^2 \lambda(t) + R^*(\lambda(t), \dot{y}(t)) \dot{y}(t) - T^*(\nabla_{\dot{y}(t)} \lambda(t), \dot{y}(t)) = 0.$$

The geometry of  $Z$  on  $TM$  provides a way of globally pulling out the adjoint Jacobi equation from the MP in an intrinsic manner, which is not generally possible in the MP [Lewis (2000)].



## 6.4 Locomotion Systems and Human Gait

In this section we present both human and man-made locomotion systems.

### 6.4.1 Control of Locomotion Systems

In this subsection we consider nonlinear kinematic controllability and motion planning of a class of systems called *stratified* (see [Goodwine (1998); Goodwine and Burdick (1997)]). Roughly speaking, such stratified systems have a configuration manifold  $M$  which can be decomposed into submanifolds upon which the system has a different set of equations of motion. For such systems, then, considering controllability and motion planning is difficult because of the discontinuous form of the equations of motion. We present two alternative forms of the controllability test. The first, analogous to Chow's theorem, is based upon a construction involving distributions. The second, uses tools from exterior differential systems and is based upon a construction which uses the derived flag.

Now, many mechanical systems can change dimension. The changing dimensionality for the kinematic systems comes, at least for legged robot examples, from intermittent contact with some physical boundary. Dynamical problems could also have this feature, but additionally they can have intermittent nonholonomic constraints. In this case we are primarily concerned with the problems of *controllability* and *motion planning* (see [Goodwine (1998); Goodwine and Burdick (1997)]).

Here we will consider the *driftless*, or *kinematic*, or *control linear* systems of the form:

$$\dot{x} = g_i(x) u^i, \quad (i = 1, \dots, m), \quad (6.26)$$

where  $g_i = g_i(x)$  are vector-fields and  $u^1$  are control inputs (for  $i = 1, \dots, m$ ). For example, the kinematic car (see (6.19) above) is a kinematic system with equation of motion:  $\dot{x} = g_1 u^1 + g_2 u^2$ .

Now, an involutive distribution for the system (6.26) is defined as

$$\bar{\Delta} = \text{span} \{g_1, \dots, g_n, [g_i, g_j], \dots, [g_i, [g_j, g_k]], \dots\}$$

and is associated with a submanifold  $S$ , which is the set of reachable system's points.

If the system's configuration manifold is  $nD$ , then the *Chow's theorem* says: If  $\dim(\bar{\Delta}) = m$  at a point  $x$ , then the system described by equation

(6.26) satisfies the Lie Algebra Rank Condition (LARC) at  $x$  and consequently it is STLC [Chow (1939)].

Recall that Frobenius' theorem equates involutivity of a distribution with its integrability, thus associated with any involutive distribution there exists a unique submanifold. The intuition here is that the collection of all the Lie brackets between the control vector-fields, and all the iterations thereof, gives us all the directions in which we can move. Therefore these directions are tangent to the hypersurface that represents the set of reachable points for the system.

#### 6.4.1.1 *Stratified Kinematic Controllability*

Consider a *biped robot*. The configuration manifold  $M$  for the biped describes the spatial position and orientation of a reference frame rigidly attached to the body of the robot mechanism as well as variables such as joint angles which describe the mechanism's internal geometry. The robot will be subjected to constraints if one or more of its feet is in contact with the ground. The set of configurations corresponding to one of the feet in contact with the ground is a codimension one submanifold of the configuration space. The same is true when the other foot contacts the ground. Similarly, when both feet are in contact with the ground, the system is on a codimension two submanifold of the configuration space formed by the intersection of the single contact submanifolds (see [Goodwine (1998); Goodwine and Burdick (1997)] for technical details).

We also note that when a foot contacts the ground, the biped is subjected to additional constraints. In particular, the velocity of the foot relative to the ground must be zero. Also, except for when the robot transitions from a state where a foot is off of the ground to one where a foot contacts the ground, the equations of motion for the system are smooth. In other words, restricted to each stratum, the equations of motion are smooth.

We will refer to the configuration manifold  $M$  for the biped robot as *stratified*. Classically, a regularly stratified set  $\mathcal{X}$  is a set  $\mathcal{X} \subset \mathbb{R}^m$  decomposed into a finite union of disjoint smooth manifolds, called strata, satisfying the Whitney condition. The dimension of the strata varies between zero, which are isolated point manifolds, and  $m$ , which are open subsets of  $\mathbb{R}^m$ . The Whitney condition requires that the tangent spaces of two neighboring strata 'meet nicely', and for our purposes it suffices to say that this condition is generically satisfied.

Therefore, the configuration space  $M$  of a kinematic biped contains

three strata  $\{S_1, S_2, S_3\}$  on which the system has different equations of motion. The biped would have a submanifold  $S_1$  corresponding to its left foot being in contact with the ground. Similarly, there will be a different submanifold,  $S_2$ , corresponding to its right foot being in contact with the ground. The intersection of these two submanifolds,  $S_3 = S_1 \cap S_2$  defines yet a third submanifold corresponding to both feet being in contact with the ground. We can observe that locomotion results from following a path in the configuration space which cyclically moves on and of each of these *leaves*, and without moving between at least some of the submanifolds, locomotion, and thus controllability would probably be impossible. The biped's locomotion is defined by cyclically changing strata.

On each submanifold we have different equations of motion. Controllability of the biped is dependent on equations of motion in each submanifold. In general, transitioning among strata are non-smooth. The standard controllability result for kinematic systems, the Chow's theorem, does not apply to this situation because it assumes that the equations of motion are smooth. Also, both the form and the number of  $g_i$ 's in the system's equation (6.26) may change in a non-smooth way between submanifolds – but are assumed smooth in each regime [Goodwine (1998); Goodwine and Burdick (1997)].

Now, by considering legged robot systems more general than the biped robot, we can develop a general definition of stratified configuration spaces. Let  $M$  denote the legged robot's entire configuration manifold (it will often be convenient to denote this space as  $S_0$ ). Let  $S_i \subset M$  denote the codimension one submanifold of  $M$  that corresponds to all configurations where only the  $i$ th foot contacts the terrain. Denote, the intersection of  $S_i$  and  $S_j$ , by  $S_{ij} = S_i \cap S_j$ . The set  $S_{ij}$  physically corresponds to states where both the  $i$ th and  $j$ th feet are on the ground. Further intersections can be similarly defined in a recursive fashion:  $S_{ijk} = S_i \cap S_j \cap S_k = S_i \cap S_{jk}$ , etc. Note that the ordering of the indices is irrelevant, i.e.,  $S_{ij} = S_{ji}$ . We will term the lowest dimension stratum containing the point  $x$  as the *bottom stratum*, and any other submanifolds containing  $x$  as *higher strata*. When making relative comparisons among different strata, we will refer to lower-dimensional (i.e., higher codimensional) strata as lower strata, and higher-dimensional (i.e., lower codimensional) strata as higher strata.

Furthermore, we will assume that on each stratum,  $S_i$ , our system may be subjected to constraints in addition to those present on  $M$ . Denote the set of constraints on  $M = S_0$  by  $\{\omega^{0,1}, \dots, \omega^{0,m}\}$ .

### 6.4.1.2 The Distributions Approach

Although the Chow's theorem does not apply, it will be useful to compute the involutive closure  $\bar{\Delta}$  of the control vector-fields separately on each of the biped's submanifolds  $\{S_1, S_2, S_3\}$ . This defines a *foliation* on each of the submanifolds. Intuitively, if the submanifolds which make up the various foliations on each strata collectively intersect transversely, then we have small time local controllability. More precisely, if there exists a nested sequence of submanifolds

$$S_{p_i} \subseteq S_{(p-1)_i} \subseteq \dots \subseteq S_{1_i} \subseteq M,$$

such that the associated involutive distributions satisfy

$$\bar{\Delta}_M|_x + \sum_{j=1}^p \bar{\Delta}_{S_{j_i}}|_x = T_x M,$$

then the system is STLC from  $x$  (see [Goodwine (1998); Goodwine and Burdick (1997)]).

For example, consider the six legged robot with 2DOF legs. The equations of motion are (see [Kelly and Murray (1995)])

$$\begin{aligned} \dot{x} &= \cos \theta (\alpha(h_1) u_1 + \beta(h_2) u_2), & \dot{y} &= \sin \theta (\alpha(h_1) u_1 + \beta(h_2) u_2), & (6.27) \\ \dot{\theta} &= l\alpha(h_1) u_1 - l\beta(h_2) u_2, & \dot{\phi}_1 &= u_1, & \dot{\phi}_2 &= u_2, & \dot{h}_1 &= v_1, & \dot{h}_2 &= v_2, \end{aligned}$$

where  $(x, y, \theta)$  represents the planar position of the center of mass,  $\phi_i$  is the angle of the legs and  $h_i$  is the height of the legs off the ground.

Now, if we call the strata corresponding to:

- (1) all feet in contact  $S_{12}$ ;
- (2) feet 1-4-5 in contact  $S_1$ ; and,
- (3) feet 2-3-6 in contact  $S_2$ ,

then it is simple to verify that

$$\bar{\Delta}_{S_{12}} + \bar{\Delta}_{S_1} + \bar{\Delta}_{S_2} = T_x M, \quad \text{for all } x \in M.$$

This implies STLC [Goodwine (1998); Goodwine and Burdick (1997)].

### 6.4.1.3 The Exterior Differential Systems Approach

The following analysis of controllability focuses on the constraint equations, rather than the equations of motion, and involves techniques from exterior

differential systems (EDS, see (3.4.3.3) above). Let  $\Omega^k$  denote the set of smooth exterior  $k$ -forms on  $M$ , let  $\Omega$  be the algebra of exterior differential forms on  $M$ , and let  $I$  be a codistribution on  $M$  spanned by a set of linearly independent 1-forms  $\{\omega^1, \dots, \omega^m\}$ . The ideal generated by  $I$  is

$$\mathcal{I} = \{\sigma \in \Omega : \sigma \wedge \omega^1 \wedge \dots \wedge \omega^m = 0\}.$$

The exterior derivative  $d : \Omega^k \rightarrow \Omega^{k+1}$  induces a map

$$\delta : \mathcal{I} \rightarrow \Omega^2(M)/\mathcal{I}, \quad \lambda \mapsto d\lambda \bmod(\mathcal{I}).$$

It follows from linearity that the kernel of  $\delta$  is a codistribution on  $M$ . Call the subspace  $I^{(1)}$  the *first derived system* of  $I$ . This construction can be continued to generate a nested sequence of codistributions

$$I = I^{(0)} \supset I^{(1)} \supset \dots \supset I^{(N)}. \quad (6.28)$$

If the dimension of each  $I^{(i)}$  is constant, then this construction terminates for some finite integer  $N$ . we call the relation (6.28) the *derived flag* of  $I$ . The following is the dual of Chow's theorem: Let  $I = \{\omega^1, \dots, \omega^m\}$  represent a set of constraints and assume that the derived flag of the system exists. Then, there exists a path  $x(t)$  between any two points satisfying  $\omega^i(x)\dot{x} = 0$  for all  $i$  if there exists an  $N$  such that  $I^{(N)} = 0$  (for details, see e.g., [Murray (1994)]).

In the case of the six legged robot with equations of motion (6.27), when all legs are in contact with the ground, the constraints are [Goodwine (1998); Goodwine and Burdick (1997)]

$$\begin{aligned} \omega^{12,1} &= dx - \cos \theta (d\phi_1 + d\phi_2) = 0, & \omega^{12,2} &= dy - \sin \theta (d\phi_1 + d\phi_2) = 0, \\ \omega^{12,3} &= d\theta - ld\phi_1 + ld\phi_2 = 0, & \omega^{12,4} &= dh_1 = 0, & \omega^{12,5} &= dh_2 = 0. \end{aligned}$$

Computing the derived system for this system,

$$\begin{aligned} I_{S_{12}}^{(1)} &= \{-\csc \theta d\phi_1 - \csc \theta d\phi_2 + \cot \theta dx - \cot^2 \theta dy + \csc^2 \theta dy, \\ &\quad ld\phi_2 - ld\phi_1 + d\theta, dh_1, dh_2\}, \\ I_{S_{12}}^{(2)} &= \{ld\phi_2 - ld\phi_1 + d\theta, dh_1, dh_2\}, \end{aligned}$$

which is clearly the bottom derived system.

When legs 1, 4 and 5 are in contact with the ground, but legs 2, 3 and 6 are not in contact, the constraints are

$$\begin{aligned} \omega^{1,1} &= dx - \cos \theta d\phi_1 = 0, & \omega^{1,2} &= dy - \sin \theta d\phi_1 = 0, \\ \omega^{1,3} &= d\theta - ld\phi_1 = 0, & \omega^{1,4} &= dh_1 = 0. \end{aligned}$$

Computing the derived flag for this system,

$$I_{S_1}^{(1)} = \{dy - \sin \theta d\phi_1, dx - \cos \theta d\phi_1, d\theta - ld\phi_1, dh_1\},$$

which is the bottom derived system on  $S_1$ .

When legs 2, 3 and 6 are in contact with the ground, but legs 1, 4 and 5 are not in contact, the constraints are

$$\begin{aligned} \omega^{2,1} = dx - \cos \theta d\phi_2 = 0, & \quad \omega^{2,2} = dy - \sin \theta d\phi_2 = 0, \\ \omega^{2,3} = d\theta - ld\phi_2 = 0, & \quad \omega^{2,4} = dh_2 = 0. \end{aligned}$$

Computing the derived flag for this system,

$$I_{S_2}^{(1)} = \{dy - \sin \theta d\phi_2, dx - \cos \theta d\phi_2, d\theta - ld\phi_2, dh_2\},$$

which is the bottom derived system on  $S_2$ .

When none of the legs are in contact with the ground,

$$\omega^{0,1} = dx = 0, \quad \omega^{0,2} = dy = 0, \quad \omega^{0,3} = d\theta = 0.$$

Clearly, the bottom derived system is

$$I_{S_0}^{(1)} = \{dx, dy, d\theta\}.$$

The intersection of the bottom derived systems associated with the nested sequence  $S_{12} \subset S_1$  contains only  $\{dh_1\}$ , so the system can reach an open set in  $S_1$ . Similarly, intersection of the bottom derived systems associated with the nested sequence  $S_{12} \subset S_2$  contains only  $\{dh_2\}$ , so the system can reach an open set in  $S_2$ . Thus, the robot is controllable in  $S_1 \cup S_2$ .

#### 6.4.1.4 On the Existence and Uniqueness of Solutions

Since, for the problems in which we are interested, the r.h.s of the kinematic differential equation

$$\dot{x} = g_i(x) u^i(x, t) = f(x, t), \quad i = 1, \dots, m. \quad (6.29)$$

is not continuous everywhere, we must generalize the notion of a solution of a differential equation [Goodwine (1998); Goodwine and Burdick (1997)]. If there is a  $C^0$ -function,  $\phi(t)$  which satisfies the initial conditions for equation (6.29) and

$$\dot{\phi}(t) = f(\phi(t), t) \quad \text{almost everywhere,} \quad (6.30)$$

then we say that  $\phi(t)$  is a solution of equation (6.29).

In order to assure existence and uniqueness of solutions, we make the following assumptions regarding the flow of the control system. Except for the points where the r.h.s of equation (6.29) is discontinuous, the differential equation has a unique solution. This corresponds to points in  $M$  which have a neighborhood that do not contain points  $x \in S_i$ . Also, restricted to any stratum, we assume that equations of motion have a unique solution for all points in that stratum which have neighborhoods that do not contain any substrata. Also, if the flow of the system encounters a stratum of the configuration space in which the r.h.s of the differential equation which describes the motion of the system is discontinuous, then the system evolves on the stratum for a finite time before leaving it. These assumptions eliminate the possibility, for instance, when, in a neighborhood of a stratum, all solution curves intersect the stratum, but on the stratum, the vector-fields are directed away from the stratum towards the region from which the solutions came. This is basically the 'chattering' problem in sliding mode control. In this case, a solution of the differential equation as defined by equation (6.30) will not exist (see [Filippov (1964)] for details).

The above assumptions now guarantee existence and uniqueness of solutions of equation (6.29) because of piecewise existence and uniqueness. Points of discontinuity of the r.h.s of (6.29) are encountered only when a trajectory encounters a substratum of the stratum on which it is evolving, or when the trajectory leaves the stratum on which it is evolving. In either case, since the point of discontinuity uniquely establishes initial conditions for the system, and we have assumed existence and uniqueness for the equations of motion restricted to any strata away from substrata, we have existence and uniqueness of solutions in the sense of equation (6.30) [Goodwine (1998); Goodwine and Burdick (1997)].

#### 6.4.1.5 Trajectory Generation Problem

**Smooth Systems.** Trajectory generation for general robot motion is not a trivial problem, as many robots are *underactuated*. For example, the kinematic car (see (6.2.2.2) above) has only two inputs, but four states that we want to control. By simply considering the rank of the system it is clear that, given a desired trajectory,  $\gamma(t)$ , in general it will be impossible to just invert the dynamics of the system to obtain the control inputs which will make the system track  $\gamma(t)$  [Goodwine (1998); Goodwine and Burdick (1997)]. In this case a Lie bracket motion is defined by  $[[g_1, g_2], g_1]$ .

Now, the question of controllability is useful, but, unlike in the linear context where controllability and controller design are essentially the same problem, in the nonlinear context controllability is of little use for the control synthesis problem. In contrast, the trajectory generation problem can be phrased as [Goodwine (1998); Goodwine and Burdick (1997)]: Determine the control inputs that will steer the kinematic system (6.26) from its initial condition to the desired final configuration. One approach to the trajectory generation problem for smooth, kinematic systems was proposed by [Lafferriere *et al.* (1993)]. The basic approach is to first consider an *extended system*, such that

$$\dot{x} = g_i u^i \quad \text{implies} \quad \dot{x} = f_j v^j,$$

where  $i = 1, \dots, m, j = 1, \dots, p$ , and the  $f_j$ 's include higher order Lie brackets between the  $g_i$ 's. These higher order brackets are chosen so that

$$\dim(\text{span}\{g_1, \dots, g_p\}) = \dim(M).$$

The higher order Lie brackets must belong to the Philip Hall basis for the Lie algebra. The trajectory generation problem for the extended system is easy to solve. Then the real controls,  $u^i$  are determined from the fictitious controls,  $v^j$  (which do not correspond in a simple manner to the real inputs  $u^i$ ). With the fictitious inputs, the trajectory generation problem reduces to calculating a matrix inverse or pseudo-inverse. The difficult problem is then to determine the real control inputs as a function of the fictitious inputs.

**Stratified Systems.** The extended system approach is valid for smooth systems. However, we can still apply it 'strata-wise' [Goodwine (1998); Goodwine and Burdick (1997)] for the locomotion systems. In this way we decompose the desired trajectory into components on the various strata in the configuration space, and apply the results from [Lafferriere *et al.* (1993)] in a piece-wise manner. Just like for the controllability problem, the main difficulty for us is to deal with the discontinuities introduced by the stratified nature of configuration space. As before, this creates problems because of the discontinuities, but also presents opportunities to exploit the specific structure of the configuration manifold  $M$ . This decomposition is not trivial because of the *Campbell-Baker-Hausdorff* (CBH) formula (compare with the CBH-flow formula 3.19 above):

$$\exp(g_1) \exp(g_2) = \exp(g_1 + g_2 + \frac{1}{2}[g_1, g_2] + \frac{1}{12}([g_1, [g_1, g_2]] - [g_2, [g_1, g_2]]) \dots).$$



Thus, we require ‘decoupling’ between the vector-fields on the various strata. In the simplest case, where the vector-fields on different strata are ‘decoupled’ in the sense that the Lie bracket between vector-fields on different strata is zero, then the inputs which would have to be executed simultaneously as a result of the approach [Lafferriere *et al.* (1993)] can be executed sequentially on different strata. This follows from the CBH formula.

In other words, the main difficulty is how to switch between the strata. The results in [Lafferriere *et al.* (1993)] assume that the equations of motion for the control system are smooth. In the stratified case, the equations of motion are non-smooth. However, since the equations of motion restricted to each strata are smooth, given the correct assumptions, we can effectively ‘project’ the trajectory generation method onto each strata.

To do this, we consider the stratified extended system, which simply is the sum of the extended systems defined by the equations of motion restricted to each strata [Goodwine (1998); Goodwine and Burdick (1997)],

$$\dot{x} = b_{I,i} u^{I,i}.$$

Now, the difficulty that arises is that the construction outlined for smooth systems yields control inputs that cannot easily be decomposed in a logical, sequential manner onto the various strata present in the configuration space  $M$ . If we assume complete decoupling: equations of motion independent of leg height. Another simplification is strata decoupling,

$$[b_{I,i}, b_{J,j}] = 0, \quad \text{for } I \neq J,$$

follows from the CBH formula. This allows us to sequentially order the flows corresponding to each strata, as well as to arbitrarily order the strata switching sequence, i.e., specify the gait.

#### 6.4.2 Gait Biodynamics

An outline of the basic steps involved in the production of voluntary movement is quite simple (see chapter 7 for details). Commands initiated in the brain are transmitted along nerves to muscles. When activated by nerves, muscles generate forces. Muscle forces are transferred to bones and produce angular motions of the joints. When the nervous system properly coordinates the activation of many muscles, the result is smooth, purposeful movement. Scientists fascinated by human and animal movement have

examined each of these steps and performed an extensive range of experiments to record neuromuscular excitation patterns, characterize muscular excitation—contraction dynamics, describe musculo-skeletal geometry, and quantify movement dynamics [Delp and Loan (2000)].

Computational models of human and animal movement provide a framework for integrating facts about the biology of movement. Once researchers develop and test a computer model of the neuro-musculo-skeletal system, they can use it to explore movement control, analyze athletic performance, and simulate treatments for musculo-skeletal and neurologic disorders. Researchers need simulations to complement experimental studies because important elements of movement, including neural signals and muscle forces, are extremely difficult to measure experimentally [Delp and Loan (2000)].

Developing accurate simulations of human and animal movement is challenging because of the intrinsic complexity of biologic systems, especially human. For example, the forces produced by muscles depend on their activation, length, and velocity. Muscles transmit forces through tendons, which have nonlinear properties. Tendons connect to bones that have complex geometry and span joints that have complicated kinematics. Understanding how the nervous system coordinates movement is especially difficult because many muscles work together to produce movement, and any individual muscle can accelerate all of the joints of the body. These complexities have important functional consequences and must be represented accurately if computational models are to provide insights into musculoskeletal performance. For this cause, Delp and coworkers [Delp and Loan (2000)] have developed the popular software package 'SIMM' (see Figure 6.9), that lets users develop, alter, and evaluate models of various musculoskeletal structures.

Using the 'SIMM'-software, the computer analysis of human gait [Delp *et al.* (1998); Piazza and Delp (1996)] is performed according to the diagram presented in Figure 6.10. For this simulation, Hill's musculo-tendon complex (see Figure 4.5) was implemented, and muscular activations were determined from EMG measurements.

During walking, forces generated by the body are transferred through the limb(s) to the ground. These forces arise in large part from the influence of gravity on body mass as well as from the net forces generated by muscles and ligaments. As weight is loaded onto the leading leg at initial contact, shear forces which would contribute to a forward foot slip are generated. In order to prevent a slip, sufficient friction at the foot-floor interface is required. When the shear forces exceed the available friction from the floor,

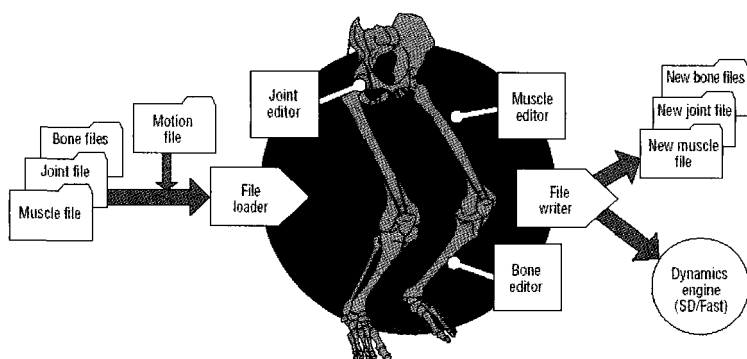


Fig. 6.9 Structure of musculoskeletal modelling software 'SIMM', based on popular dynamics engine, 'SD/Fast'.

a slip becomes imminent. If the head, arms and trunk, which represent two-thirds of body mass, are unable to re-align over the anteriorly slipping foot, a fall will result (see [Winter (1990); Winter (1995)]).

Slips are likely to occur when the utilized coefficient of friction (COF) between the foot and the floor exceeds the available surface slip resistance. As slips are a leading cause of falls, the following biomechanical experiment was conducted by Burnfield [Burnfield *et al.* (2003)], to analyze the slipping gait. Forty-nine healthy adults participated (28 males, 21 females; mean age =  $26 \pm 4$  years). All subjects wore the same style 'Rockport' walking shoes.

Ground reaction forces ('AMTI' force plates; 1200 Hz; 4<sup>th</sup> order, 45 Hz low-pass 'Butterworth' filter) and full-body kinematic data ('VICON' Motion Analysis, 6-cameras, 120 Hz) were recorded simultaneously as subjects walked at a self-selected speed along a 10-meter walkway.

The ratio of shear to vertical ground reaction forces (GRF's) was used to calculate the COF throughout stance for each subject's right leg. During weight acceptance, the peak COF resulting from a shear force that would contribute to a forward foot slip was identified. Center of pressure (CP) was calculated using force platform moment and force data. Whole body CM location was estimated using a 15-segment model ('VICON Plug-in-Gait Model').

Pearson correlation coefficients tested the collinearity between peak COF for each CM kinematic variable assessed. To determine whether the selected CM kinematic variables were predictive of the peak COF during

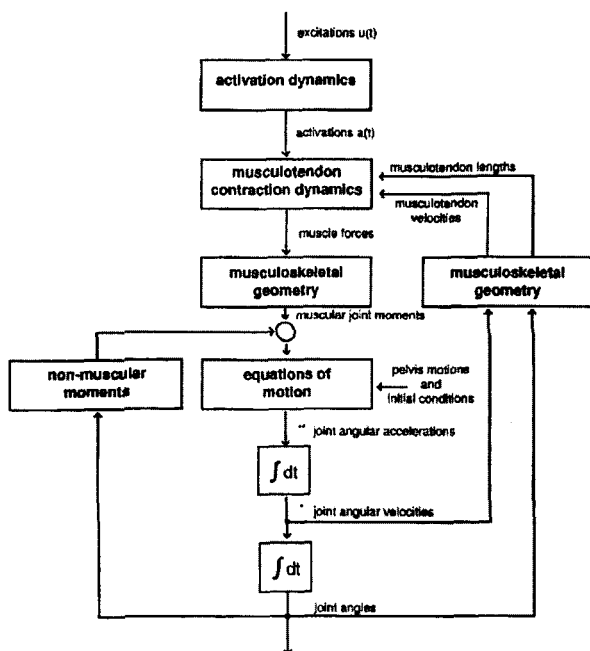


Fig. 6.10 Block diagram of the swing phase of human gait.

weight acceptance, stepwise regression analysis using a forward stepwise procedure was performed ( $F$  to enter = 0.05;  $F$  to remove = 0.10). Independent variables included the following at the instant of peak COF during weight acceptance:

- (1) Absolute distances between the CM and the CP in anterior-posterior, medial-lateral, and vertical directions;
- (2) CM acceleration in the anterior-posterior, medial-lateral, and vertical directions; and
- (3) The angle of CM to CP expressed relative to vertical (Figure 6.11).

Peak COF was the dependent variable. All statistics were calculated using the 'SPSS 10.0' statistical software (SPSS Inc., Chicago, IL).  $r = 0.75$ .

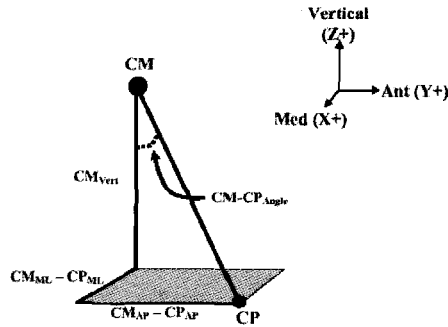


Fig. 6.11 Center of mass (COM) and center of pressure (COP) variables studied in the biomechanical experiment on slipping gait.

## 6.5 Biodynamic Control Policy, Learning and Self-Organization

In this section we present modern concepts of biodynamic control, learning, and self-organization.

### 6.5.1 Control Policy Learning by Robots

Robot learning, a subclass of the field of learning control, refers to the process of acquiring a sensory-motor control strategy for a particular movement task and movement system by trial and error. Learning control is usually distinguished from adaptive control in that the learning system is permitted to fail during the process of learning, while adaptive control emphasizes single trial convergence without failure. Thus, learning control resembles the way that humans and animals acquire new movement strategies, while adaptive control is a special case of learning control that fulfills stringent performance constraints, e.g., as needed in life-critical systems like airplanes and industrial robots [Schaal (1998)].

A key question in learning control is what it is that should be learned. In order to address this issue, it is helpful to view motor control as originally developed in the middle of the 20th century in the fields of optimization theory, optimal control, and in particular dynamic programming (see [Dyer and McReynolds (1970)]). Here, the goal of learning control was formalized as the need to acquire a *task dependent control policy*  $\pi$  that maps the continuous valued state vector  $x$  of a control system and its environment, possibly in a time-dependent way, to a continuous valued control vector  $u =$

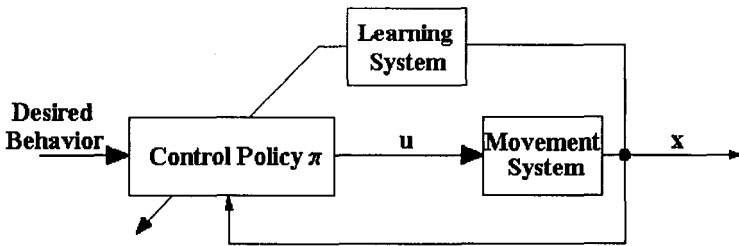


Fig. 6.12 Generic control diagram for learning control (see text for explanation).

$\pi(x, \alpha, t)$ . The parameter vector  $\alpha$  contains the problem specific parameters in the policy  $\pi$  that need to be adjusted by the learning system; Figure 6.12 illustrates the generic control diagram of learning a control policy. Since the controlled system can generally be expressed as a nonlinear function  $\dot{x} = f(x, u)$ , the *combined system-controller dynamics* reads

$$\dot{x} = f(x, \pi(x, \alpha, t)).$$

Thus, learning control means finding a (usually nonlinear) function  $\pi$  that is adequate for a given desired behavior and movement system. This formal viewpoint allows discussing robot learning in terms of the different methods that have been suggested for the learning of control policies [Schaal (1998)].

#### 6.5.1.1 Direct Learning of the Control Policy

To learn the control policy  $\pi$  directly, the desired behavior needs to be expressed as an optimization criterion  $r(t)$  to be optimized over a certain temporal horizon  $T$ , resulting in a cost function [Schaal (1998)]

$$J(x(t)) = \int_{t=0}^T r(x(s), u(s)) ds = \int_{t=0}^{\infty} \frac{1}{\tau} \exp\left(-\frac{t-s}{\tau}\right) r(x(s), u(s)) ds.$$

Here the rightmost term illustrates the use of an infinite horizon time window by introducing a discount factor that reduces the influence of values of  $r(t)$ , (which is usually a function of the state  $x$  and command  $u$  taken in  $x$ ) in the far future. Solving such kinds of optimization problems was developed in the framework of dynamic programming [Dyer and McReynolds (1970)] and its recent derivative, *reinforcement learning* (see [Sutton and Barto (1998)]). For reinforcement learning,  $r(t)$  corresponds to the *immediate reward*, and  $J(x(t))$  is called the *long-term reward*. For instance, in the classical task of balancing a pole on a finger, the immediate reward could

be +1 at every time step at which balancing was successful, and -1000 if the pole was dropped; the task goal would be to accumulate maximal long term reward, equivalent to balancing without dropping.

The policy  $\pi$  is acquired with reinforcement learning by, first, learning the optimal function  $J(x(t))$  for every state  $x$ , usually by a technique called *temporal-difference learning*, and then deducing the policy  $\pi$  as the command  $u$  in every state  $x$  that leads to the best future payoff, i.e.,

$$u = \max_{u'}(r(x(t), u'(t)) + J(x(t+1))),$$

with

$$x(t+1) = x(t) + f(x(t), u'(t)) \Delta t,$$

where  $\Delta t$  is an arbitrarily chosen constant time step for sampling the systems behavior. Many variations of reinforcement learning exist, including methods that avoid estimating the optimization function  $J(x(t))$ .

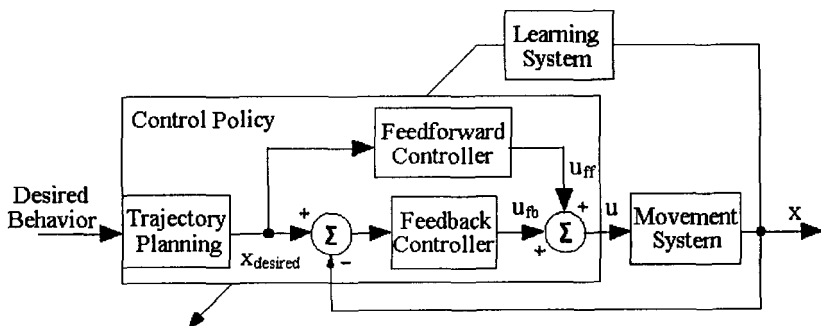


Fig. 6.13 Learning control with functional decomposition (see text for explanation).

#### 6.5.1.2 Indirect Learning of the Control Policy

For many movement systems, a direct control strategy is not advantageous since it fails to re-use modules in the policy that are common across multiple tasks. This view suggests modularization in terms of a functional structuring within each control policy. A typical example is to organize the control policy into several processing stages, as illustrated in Figure 6.13. Most commonly, the policy is decomposed into a planning and an execution stage, a strategy that is typical for most robot controllers but also likely to be used in motor control of primates. Planning generates a

*desired kinematic trajectory*, i.e., a prescribed way of how the state of the movement system is supposed to change in order to achieve the task goal. Execution transforms the plan into appropriate motor commands.

Separating planning and execution is highly advantageous. For instance, in reaching movements for a target, a direct approach to robot learning would require to learn a new policy for every target location the desired behavior is to minimize the distance between the hand and the target, and due to the complex dynamics of an arm, different target location require very different motor commands for reaching. In contrast, an indirect control approach only requires learning the movement execution module, which is valid for any target location. For simplicity, movement plans can be kept the same for every target location, e.g., a straight line between the target and the start position of the arm with a bell-shaped velocity profile the kinematics of the movement are independent of the target location. Thus, after the execution module has been acquired, reaching is a solved problem, no matter where the target is [Schaal (1998)].

Depending on the task, planning can take place in external kinematic variables, e.g., Cartesian or end-effector space, or in internal kinematic variables, e.g., joint space for a human-like arm. If the planning space does not coincide with the space where motor commands are issued, coordinate transformations are required to map the external motor plan into intrinsic coordinates. This problem is typically discussed as the inverse kinematics problem of robot control, a problem that equally needs to be addressed by biological movement systems.

To transform kinematic plans into motor commands, standard method from control theory can be employed. Figure 6.13 illustrates a typical example that uses a feedforward/feedback mechanism called computed torque controller that enjoys popularity in both robotic systems as well as models of biological motor control [Jordan (1996)]. The feedback controller is of classical PD type, while the feedforward controller contains an inverse dynamics model of the movement system.

From the point of robot learning, functional modularity also decomposes the learning problem into several independent learning problems. The modules of the execution stage can be learned with supervised learning techniques. For various types of movements, kinematic movement plans can be highly stereotyped, as described in the reaching example above. For complex movements, e.g., a tennis serve, planning requires more sophistication, and the same reinforcement learning methods of direct control can be applied; the only difference is that motor commands  $u$  are replaced



with a desired change in trajectory  $\dot{x}_d$ . Applying reinforcement learning to kinematic planning is of reduced complexity than solving the complete direct control problem, but still it remains an open research problem for high-dimensional movement systems.

### 6.5.1.3 *Learning of Motor Control Components*

Whether direct or indirect control is employed in a motor learning problem, the core of the learning system usually requires methods of supervised learning of regression problems, called *function approximation*. Function approximation is concerned with approximating a nonlinear function  $y = f(x)$  from noisy data, drawn according to the data generating model

$$y = f(x) + \varepsilon, \quad \text{for all } x \in \mathbb{R}^m, x \in \mathbb{R}^n, E\{\varepsilon\} = 0,$$

i.e.,  $\varepsilon$  is a zero-mean random noise variable [Schaal (1998)].

## 6.5.2 *Pathways to Self-Organization in Biodynamics*

By now it should be clear to the reader that the general biodynamics is an extremely complex control system, which represents the natural stage for *self-organization and cooperation* of its components, as already emphasized in the introductory section (2.3). Now we will explore the pathways to self-organization in biodynamics, following the general principles of Haken's synergetics (see chapter 2 as well as [Haken (1996); Haken (2000)]).

**Self-Organization Through Change of Control Parameters.** We may change the global impact of the surroundings on a certain biodynamic system, as expressed by its control parameters  $\{\sigma\}$  (e.g., changing a surrounding temperature  $\sigma = T$  causes faster muscular contractions [Hill (1938)]). When we slowly change the impact of the surroundings on the system, at certain points the system may acquire new states of higher order or structure (e.g., a 'warm up' of the human muscular system [Ivancevic (1991)]).

**Self-Organization Through Change of Components.** Self-organization can be caused by a mere increase of number of components of a certain biodynamic system (e.g., activating more muscular-like actuators enables more sophisticated motion patterns [Ivancevic (1991)]). Even if we put the same microscopic components together, entirely new behavior can arise on the macroscopic level (e.g., reducing the basic biodynamics model (2.26–2.27) to the macro-model (2.34)).

**Self-Organization Through Transients.** Self-organization can be also caused by a sudden change of control parameters when a certain biodynamic system (e.g., muscular-like actuator) tries to relax to a new state under the new conditions (constraints). Patterns in this system may be formed in a self-organized fashion when it passes from an initial disordered (or homogenous) state to another final state which we need not specify or which even does not exist. For example, if we have a musculo-skeletal-like state vector of the form

$$q(x, t) = u(t)v(x),$$

where  $v(x)$  describes some muscular-like spatial order, and the order parameter equation

$$\dot{o} = \lambda o.$$

When we change a control parameter  $\sigma$  quickly, so that  $\lambda < 0$  is quickly replaced by  $\lambda > 0$ , we get a transient state vector of the form

$$q(x, t) = \exp(\lambda t) v(x). \quad (6.31)$$

It clearly describes some structure, but it does not tend to a new stable state.

Now, to get the solution (6.31) started, some *fluctuations* must be present. Otherwise, the solution  $o \equiv 0$ , and thus  $q \equiv 0$  will persist forever.

**Self-Organization and Neural Networks.** The basic synergetic idea of self-organization by reduction of the system's dimension has been fully exploited in T. Kohonen's neural network model, the so-called *self-organizing map* (SOM) (for details see the next chapter, in particular (7.6.3.3) below). The SOM transforms the network's input of arbitrary dimension into a one or 2D discrete map subject to a topological (neighborhood preserving) constraint. The SOM is computed using Kohonen's special form of *unsupervised learning*. The output of the SOM can be used as input to a supervised classification feedforward network. This network's key advantage is the clustering produced by the SOM which reduces the input space into representative features using a self-organizing process. Hence the underlying structure of the input space is kept, while the dimensionality of the space is reduced.

### 6.5.3 Neuro-Muscular Excitation-Contraction Dynamics

Now we continue our exposition on muscular dynamics from chapter 4 (see (4.7.3) above), by including neural inputs and feedbacks. We follow the general scheme depicted in Figure 6.14, to be expanded in detail in chapter 7.

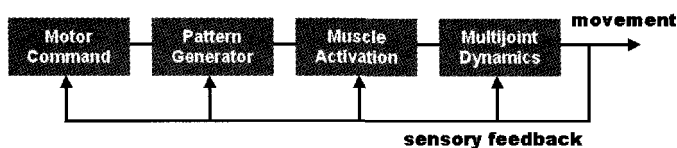


Fig. 6.14 General control scheme of human musculo-skeletal dynamics.

#### 6.5.3.1 Motor Units

All motor neurons (for technical details see section (7.2) in chapter 7 below) leading to skeletal muscles have branching axons, each of which terminates in a neuro-muscular junction with a single muscle fibre. Nerve impulses passing down a single motor neuron will thus trigger contraction in all the muscle fibers at which the branches of that neuron terminate. This minimum unit of contraction is called the *motor unit*.

The size of the motor unit is small in muscles over which we have precise control. For example, a single motor neuron triggers fewer than 10 fibers in the muscles controlling eye movements; the motor units of the muscles controlling the larynx are as small as 2 - 3 fibers per motor neuron. In contrast, a single motor unit for a muscle like the gastrocnemius (calf) muscle may include 1000–2000 fibers (scattered uniformly through the muscle). Although the *response* of a motor unit is *all-or-none*, the strength of the response of the entire muscle is determined by the *number* of motor units *activated*. Even at rest, most of our skeletal muscles are in a state of partial contraction called *tonus*. Tonus is maintained by the activation of a few motor units at all times even in resting muscle. As one set of motor units relaxes, another set takes over.

#### 6.5.3.2 Darwinian Oscillatory Neural Net

The classical *embedding field equation* (see e.g., [Grossberg (1969); Hopfield (1982)]) of the nonlinear oscillatory neural network  $\mathcal{N}$  can be presented in

the covariant form

$$\dot{x}^i = -D_j^i x^i + T_j^i g^i(x^i) + S^i, \quad (6.32)$$

where  $x^i(t)$  represents the mean soma potential of the  $i$ th neuron;  $g^i(x^i(t))$  is a smooth function that represents the short-term average of the firing rate of the  $i$ th neuron as a function of its potential;  $S^i$  is the constant external input to the network;  $D_j^i$  is diagonal tensor and its elements  $a_i^i > 0$  represent the time constant of the rate of change for the  $i$ th neuron's potential;  $T_j^i$  is the mixed second order tensor-field whose elements represent synaptic efficiency of the  $j$ th neuron's potential transmitted to the  $i$ th neuron.

For the proposed model  $\mathcal{N}$  sufficient conditions for existence and asymptotic stability of the network's equilibria were derived using perturbation theory (see [Barhen *et al.* (1989)]) and reduced to a set of piecewise linear inequality relations that can be solved by feedforward binary network. The storage capacity of the network was analyzed using geometric analysis based on the function  $g$  that models the firing rate of the system.

Each neuron in the network  $\mathcal{N}$  is regarded as a computing process and the interconnections between neurons as *virtual communication links* embedded in the hypercube topology. Associated with each neuron is a decision algorithm that determines its next state. This algorithm is akin to the cellular automata approach in that each neuron uses only local information to reach its decision.

According to the system (6.32) a computer model of a frequency-coded neural network  $\mathcal{N}^f$  for self-organization, learning, and coupling to simulated pulse-coded sensors was analyzed in [Barhen *et al.* (1989)]. A single  $i$ th neuron in this system  $\mathcal{N}$ , neglecting environmental influences, behaves according to the difference scheme  $\mathcal{N}^d$ , given by

$$\Delta x^i = bx^i(1 - y^i) - (x^i - P)y^i, \quad \Delta y^i = -vy^i + g(x^i + T_j^i y^j),$$

where  $v > 0$  is the rate of decay of the action potential,  $0 < b < v$  is the charging rate of the neuron,  $P$  is the value to which each neuron charges, and  $g(x^i)$  is the Heaviside unit step function translated to a firing threshold  $G > 0$ . The term  $(1 - y_i)$  acts to suppress the charging term when the node fires. Allowing the soma charging to compete with the axon firing, and choosing  $P$  to be zero, we may pass to a continuous system representing a forced oscillator  $\mathcal{N}^c$  [Ivancevic (1995); Ivancevic *et al.* (1995)]

$$\dot{x}^i = (b - y^i)x^i, \quad \dot{y}^i = -vy^i + g(x^i + T_j^i y^j). \quad (6.33)$$

This departure from the usual first-order membrane equations results in interesting dynamic behavior of the model. If the synaptic weights  $T_j^i$  are identically zero, these equations specify a nonlinear, free oscillator with a typical (noncircular) limit cycle [Grebogi *et al.* (1987)].

Each oscillator in this frequency-coded model  $\mathcal{N}^f$  is coupled to many identical oscillators [Barhen *et al.* (1989)]. The coupling is through the tensor-field  $T_j^i$  of synaptic weights. It has the following properties:

- (1) It is nonsymmetric and biased in a preferred direction within the network structure;
- (2) It has a dynamic evolution in time due to interaction with the environment; and
- (3) It represents a nonlinear feedback mechanism.

The field of oscillators, a threshold-feedback mechanism for focusing attention, the synaptic field for recording an internal representation of the external environment, and the external environment itself make up the essential components of the global system  $\mathcal{N}$  [Barhen *et al.* (1989)].

Since each neuron in  $\mathcal{N}$  is an oscillator with external feedback and an external forcing function (input from other neurons of the environment), phase changes in the system represent an important mode of information processing. The relative phase of an information loop (local attractor in the node firing dynamics) may be changed by incoming information having a higher frequency than the network average. The attention mechanism of the threshold control system ensures that the new information will be processed by the network until the stimulus drops back below the network average.

The possibility of chaotic behavior in a dynamical neural system  $\mathcal{N}$  makes *a priori* knowledge of system parameters (sensor firing rates, node refractory period, noise level of membrane potential) difficult if not impossible [Grebogi *et al.* (1987)]. If the system parameters are thought of as genes in a genetic space  $\mathcal{N}^p$  of possible synthetic creatures, then the methods of nature may be used [Dress and Knisley (1987)]. Darwinian variation and selection (with the natural competitive environment playing the selector role) can be abstracted and simplified [Kauffman and Smith (1986)] by merging the concepts of variation and mutation into a single random parameter change each generation, followed by a 'lifetime' during which the synthetic system is allowed to organize itself according to environmental constraints. The part of natural selection is played by an algorithm measuring the fitness of each genome instantiation.

Random mutations are made in the parameter set  $\mathcal{N}^p$  at the rate of one for each instantiation, and a change is accepted once each generation [Dress and Knisley (1987); Kauffman and Smith (1986)]. Which gene to vary, the amount of variation, and its sign are chosen randomly and limited by a control gene. If the variation is a success (i.e., if the daughter performs equal to or better than the mother), the daughter becomes a parent and another mutation of the same amount in the same direction is made in the parameter that failed. If both directions (increase and decrease) result in failure, a local maximum along a specific axis has probably been found, and another parameter is chosen at random for variation. Successful as well as neutral changes are thus accumulated, resulting in a process of behavioral selection and improvement over time.

A mechanism for evolving the genome necessitates appropriate mapping of the genes onto the parameter set  $\mathcal{N}^p$  as well as allowing for the appearance of new genes and the disappearance of old genes when they are no longer functional [Dress and Knisley (1987); Kauffman and Smith (1986)]. Not only will an individual synthetic creature evolve, but an optimal region in the genetic landscape will also be found. Successful evolution of the entire quasi species is seen as determining a bundle of trajectories in the embedding space. Any particular trajectory in the bundle represents an evolutionary history of the genome up to the end point.

The most natural application of such dynamical neural-net system  $\mathcal{N}$  can be found in a skeletal muscle system  $\mathcal{M}$  response to *efferent functional stimulation* (EFS)  $\mathcal{F}$  and its motor control system  $\mathcal{F}^{-1}$ .

### 6.5.3.3 Recurrent Neuro-Muscular Model

The EFS-response map  $\mathcal{F}$  of a skeletal muscle, i.e., the response of the muscle system  $\mathcal{M}$  to the efferent functional stimulation from the neural network system  $\mathcal{N}$ , can be modelled [Ivancevic (1991); Ivancevic *et al.* (1995)] as temporal behavior of the *force generator*

$$\mathcal{F} : \mathbb{R} \rightarrow \text{Hom}(\mathcal{N}, \mathcal{M}),$$

where:  $\mathbb{R} \ni t$  denotes stimulation time,  $\mathcal{N}$  and  $\mathcal{M}$  correspond to the left  $\mathbb{R}$ -moduli of neural and muscular systems. The mapping  $\mathcal{F}$  can be considered as an effect of a *fifth-order transmission cascade* ( $\mathcal{F}_1 \mapsto \mathcal{F}_2 \mapsto \mathcal{F}_3 \mapsto \mathcal{F}_4 \mapsto \mathcal{F}_5$ ), where  $\mathcal{F}_i$  ( $i = 1, \dots, 5$ ) represent *neural action potential*, *synaptic potential*, *muscular action potential*, *excitation-contraction coupling* and *muscle tension generating*, respectively (see [Hodgkin and Huxley (1952);

Hodgkin (1964); Noble (1962)]).

According to the Haken's synergetics (see section (2.3) above), all transmission components of the system ( $\mathcal{F}_1 \mapsto \mathcal{F}_2 \mapsto \mathcal{F}_3 \mapsto \mathcal{F}_4 \mapsto \mathcal{F}_5$ ), where  $\mathcal{F}_i$  ( $i = 1, \dots, 5$ ) can be considered as being some kind of *diffusion processes*, forming the fifth-order transmission *flux cascade*. Therefore, the map  $\mathcal{F}$  (for all included motor units in the particular muscle contraction) can be described as a fifth order *recurrent, distributed parameter diffusion system* [Ivancevic (1991); Ivancevic *et al.* (1995); Ivancevic (1995)]

$$C_k \frac{\partial V_k}{\partial t} = \frac{1}{R_k} \frac{\partial^2 V_{k-1}}{\partial z^2} - J_k(V_k), \quad (k = 1, \dots, 5) \quad (6.34)$$

with boundary condition (at  $z = 0$ )

$$V_k(0, t) = V_0 \sin(2\pi f t) = S(t).$$

The single element  $\mathcal{F}_k$ , ( $k = 1, \dots, 5$ ) behavior is now given by

$$V_k(z, t) = V_0 \exp(-z_k/m) \sin(2\pi f(t - z_k/n)),$$

$$m = 1/((R_k C_k f), \quad n = \frac{4\pi f}{R_k C_k}.$$

For muscle-mechanical purpose, the presented distributed mapping  $\mathcal{F}$  can be first - mathematically approximated with the corresponding lumped parameter  $R_k C_k$  electric circuit (where the second circuit represents the *model of synaptic activation* of the Nobel Laureate John C. Eccles [Eccles (1964); Eccles *et al.* (1967)], and the last one corresponds to the low-pass filter representing the contraction process itself), at  $x = tendon$

$$\dot{z}_k = \frac{1}{T_k} (b_k z_{k-1} - z_k), \quad (k = 1, \dots, 5) \quad (6.35)$$

$$z_k(0) = 0, z_0 = S(t), z_5 = F(t),$$

where  $T_k = R_k C_k$  are time characteristics of the circuits in cascade, and  $b_k$  are corresponding input gains (conversion factors).

The single muscle behavior in the lumped approximation form is given by the recurrent sum of its transient and weighting terms (with time legs  $\tau_k$ ) [Ivancevic (1995); Ivancevic *et al.* (1995)]

$$z_k(t) = b_k z_{k-1} (1 - \exp(-t/T_k)) + z_k \exp(-(t - \tau_k)/T_k).$$

The presented distributed mapping  $\mathcal{F}$  can be further physically approximated with a second order forced-dumped linear oscillator in a Cauchy

form [Ivancevic (1991)]

$$T\ddot{z} + 2aT\dot{z} + cz = bS, \quad z(0) = \dot{z}(0) = 0,$$

where  $a$  (having dimension of force) corresponds to energy dissipated during the contraction,  $b$  (having dimension of velocity) is the phosphagenic energy transducing rate, while  $c$  corresponds to the second derivative of the stress-strain curve of the series viscoelastic element [Wilkie (1956)] of the muscular actuator (assumed in exponential 3-parameter form).

The complete efferent neuro-muscular model  $(\mathcal{N}, \mathcal{M})$  is now given by the set (6.32,6.34), i.e.,

$$\begin{aligned} \dot{x}^i &= -D_j^i x^i + T_j^i g^i(x^i) + S^i, & (i = 1, \dots, n), \\ C_k \frac{\partial V_k}{\partial t} &= \frac{1}{R_k} \frac{\partial^2 V_{k-1}}{\partial z^2} - J_k(V_k), & (k = 1, \dots, 5), \end{aligned}$$

or, its simplified form (6.33,6.35)

$$\begin{aligned} \dot{x}^i &= (b - y^i)x^i, & \dot{y}^i &= -vy^i + g(x^i + T_j^i y^j), \\ \dot{z}_k &= \frac{1}{T_k}(b_k z_{k-1} - z_k), & (k = 1, \dots, 5), \\ z_k(0) &= 0, z_0 = S(t), z_5 = F(t). \end{aligned}$$

Equations (6.33,6.35) constitute a  $3nD$  phase-space (for  $n = 5$  or  $k = i$ ) being a *hyper-cube = neuro-muscular control space*. The feedback control  $\mathcal{F}^{-1}$  of the mapping  $\mathcal{F}$  is performed by the autogenetic muscular *motor servo*.

#### 6.5.3.4 Autogenetic Reflex Motor-Servo

It is now well-known [Houk (1979); Ivancevic (1995); Ivancevic *et al.* (1995)] that voluntary contraction force  $\mathcal{F}$  of a skeletal muscle system  $\mathcal{M}$  is reflexly excited (positive reflex feedback  $+\mathcal{F}^{-1}$  by responses of its *spindle receptors* to stretch and is reflexly inhibited (negative reflex feedback  $-\mathcal{F}^{-1}$  by responses of its *Golgi tendon organs* (named after *Nobel Laureate Camillo Golgi*) to contraction. Stretch and unloading reflexes are mediated by combined actions of several autogenetic neural pathways.

Term *autogenetic* (or *autogenic*) means that the stimulus excites receptors located in the same muscle that is the target of the reflex response (compare with (7.2.3.1) below). The most important of these muscle receptors are the primary and secondary endings in muscle spindles, sensitive



to length change – positive length feedback  $+\mathcal{F}^{-1}$ , and the Golgi tendon organs, sensitive to contractile force – negative force feedback  $-\mathcal{F}^{-1}$ .

The gain  $G$  of the length feedback  $+\mathcal{F}^{-1}$  can be expressed as the *positional muscle stiffness* (the ratio  $G \approx S = dF/dx$  of the force  $\mathcal{F}$ -change to the length  $x$ -change) of the muscle system  $\mathcal{M}$ . The greater the stiffness  $S$ , the less will the muscle be disturbed by a change in load and the more reliable will be the performance of the muscle system  $\mathcal{M}$  in executing controlled changes in length  $+\mathcal{F}^{-1}$ .

The autogenetic circuits  $(+\mathcal{F}^{-1})$  and  $(-\mathcal{F}^{-1})$  appear to function as *servoregulatory loops* that convey continuously graded amounts of excitation and inhibition to the large (*alpha*) skeletomotor neurons. Small (*gamma*) fusimotor neurons innervate the contractile poles of muscle spindles and function to modulate spindle-receptor discharge.

### 6.5.3.5 Biodynamics Control

**Dissipative and Driving Forces.** As stated previously, the l.h.s of both Lagrangian equations (4.162) and (4.163) – describes the unstable, conservative motion of the humanoid skeleton, which is control-free and dissipation-free; the forcing term on the right should include joint dampings and muscular-like excitation and contraction dynamics.

*Synovial joint dynamics*, giving the first stabilizing effect to the conservative skeleton dynamics, is described in biodynamics by  $(x, \dot{x})$ -form of the *Rayleigh – Van der Pol's dissipation function* (see (4.7.4.3) above)

$$R = \frac{1}{2} \sum_{i=1}^n (\dot{x}^i)^2 [\alpha_i + \beta_i (x^i)^2],$$

where  $\alpha_i$  and  $\beta_i$  denote dissipation parameters. Its partial derivatives give rise to the viscous-damping forces in the joints

$$\mathcal{F}_i^{joint} = \partial R / \partial \dot{x}^i,$$

which are linear in  $\dot{x}^i$  and quadratic in  $x^i$ .

*Muscular dynamics*, giving the driving torques  $\mathcal{F}_i^{muscle}(t, x, \dot{x})$  with  $(i = 1, \dots, n)$ , for biodynamics (see 4.7.4.3 above), describes the internal *excitation* and *contraction* dynamics of *equivalent muscular actuators* (anatomically resembling the resulting action of *antagonistic muscular pairs*) for each uniaxial humanoid joint axis (i.e., each rotational DOF labelled by  $i$ ).

- *Excitation dynamics* can be described by the impulse torque-time relation

$$\begin{aligned} F_i^{imp} &= F_i^0(1 - e^{-t/\tau_i}), & \text{if stimulation} > 0 \\ F_i^{imp} &= F_i^0 e^{-t/\tau_i}, & \text{if stimulation} = 0, \end{aligned}$$

where  $F_i^0$  denotes the maximal isometric muscular torque applied at the  $i$ th joint ( $i = 1, \dots, n$ ), while  $\tau_i$  denotes the time characteristic of the particular muscular actuator. This is a rotational-joint form of the solution of the Wilkie's muscular *active-state element* equation [Wilkie (1956)]

$$\dot{\mu} + \gamma\mu = \gamma SA, \quad \mu(0) = 0, \quad 0 < S < 1,$$

where  $\mu = \mu(t)$  represents the active state of the muscle,  $\gamma$  denotes the element gain,  $A$  corresponds to the maximum tension the element can develop, and  $S = S(r)$  is the 'desired' active state as a function of the motor unit stimulus rate  $r$ . This is the basis of the biodynamics force controller.

- *Contraction dynamics* has classically been described by the Hill's hyperbolic force-velocity relation (see 4.7.4.3), which we propose here in the rotational  $(x, \dot{x})$ -form

$$F_i^{Hill} = \frac{(F_i^0 b_i - \delta_{ij} a_i \dot{x}^j)}{(\delta_{ij} \dot{x}^j + b_i)},$$

where  $a_i$  (having dimension of torque) and  $b_i$  (having dimension of momentum) denote the *rotational Hill's parameters* (see [Ivancevic and Snoswell (2001); Ivancevic (1991)]), corresponding to the energy dissipated during the contraction and the phosphagenic energy conversion rate, respectively, while  $\delta_{ij}$  is the Kronecker's  $\delta$ -tensor.

In this way, biodynamics describes the excitation/contraction dynamics for the  $i$ th equivalent muscle-joint actuator, using the simple impulse-hyperbolic product relation

$$\mathcal{F}_i^{muscle}(t, x, \dot{x}) = F_i^{imp} \times F_i^{Hill}.$$

Now, for the purpose of the so-called *hybrid joint actuator*, the general biodynamics includes, along with muscular-like and damping forces, the D.C. motor drives, defined as (compare with Hamiltonian definition (4.184)

above)

$$\begin{aligned}\mathcal{F}_k^{DC} &= i_k(t) - J_k \ddot{x}_k(t) - B_k \dot{x}_k(t), \quad \text{with} \\ l_k \dot{i}_k(t) + R_k i_k(t) + C_k \dot{x}_k(t) &= u_k(t),\end{aligned}$$

where  $k = 1, \dots, n$ ,  $i_k(t)$  and  $u_k(t)$  denote currents and voltages in the rotors of the drives,  $R_k$ ,  $l_k$  and  $C_k$  are resistances, inductances and capacitances in the rotors, respectively, while  $J_k$  and  $B_k$  correspond to inertia moments and viscous dampings of the drives, respectively.

Finally, to make the model more realistic, we need to add some stochastic forces (see [Ivancevic and Snoswell (2001); Ivancevic (2002)])

$$\mathcal{F}_i^{stoch} = B_{ij}[x^i(t), t] dW^j(t),$$

where  $B_{ij}[x(t), t]$  represents continuous stochastic *diffusion fluctuations*, and  $W^j(t)$  is an  $N$ variable *Wiener process* (i.e., generalized Brownian motion), with  $dW^j(t) = W^j(t + dt) - W^j(t)$  for  $j = 1, \dots, N$ .

**Force and Velocity Servo-Controllers.** Hierarchical biodynamics control includes (as minimum) two control levels:

- (1) Lower force servo-controller; and
- (2) Higher velocity servo-controller.

The lower biodynamic *force servo-controller*  $\mathcal{F}_i^{reflex}$  resembles an *autogenetic motor servo* [Houk (1979)], acting on the spinal-reflex level of the human locomotion control. The voluntary contraction force  $F$  of human skeletal muscle is reflexively excited (positive feedback  $+F^{-1}$ ) by responses of its *spindle receptors* to stretch and is reflexively inhibited (negative feedback  $-F^{-1}$ ) by responses of its *Golgi tendon organs* to contraction. Stretch and unloading reflexes are mediated by combined actions of several autogenetic neural pathways, forming the so-called ‘motor-servo’. The term ‘autogenetic’ means that the stimulus excites receptors located in the same muscle that is the target of the reflex response. The most important of these muscle receptors are the primary and secondary endings in muscle-spindles, sensitive to length change – positive length feedback  $+F^{-1}$ , and the Golgi tendon organs, sensitive to contractile force – negative force feedback  $-F^{-1}$ .

The gain  $G$  of the length feedback  $+F^{-1}$  can be expressed as the *positional stiffness* (the ratio  $G \approx S = dF/dx$  of the force- $F$  change to the length- $x$  change) of the muscle system. The greater the stiffness  $S$ , the

less will the muscle be disturbed by a change in load and the more reliable will be the performance of the muscle system in executing controlled changes in length  $+F^{-1}$ . The autogenetic circuits  $+F^{-1}$  and  $-F^{-1}$  appear to function as *servoregulatory loops* that convey continuously graded amounts of excitation and inhibition to the large (*alpha*) skeletomotor neurons. Small (*gamma*) fusimotor neurons innervate the contractile poles of muscle spindles and function to modulate spindle-receptor discharge.

On the other hand, the higher biodynamic *velocity servo-controller* resembles the self-stabilizing and adaptive tracking action of the human motor controller – the cerebellum [Houk *et al.* (1996)]. Firstly, we introduce the *affine Lagrangian control* function  $L^a : TM \rightarrow \mathbb{R}$ , in local canonical coordinates on  $TM$  given as

$$L^a(x, \dot{x}, u) = L(x, \dot{x}) + L^j(x, \dot{x}) u_j,$$

with *coupling Lagrangians*  $L^j = L^j(x, \dot{x})$ ,  $j = 1, \dots, m \leq n$ , corresponding to the *active* biodynamics joints. (For equivalent, Hamiltonian formulation, see section (7.12) below.)

Secondly, by introducing the vector-fields  $f$  and  $g$ , given respectively by

$$f = (\dot{x}^i, L_{x^i}), \quad g = (-\dot{x}^j, L_{x^j}^a),$$

we get the affine controller in the standard nonlinear MIMO-system form (see [Isidori (1989); Nijmeijer and van der Schaft (1990)])

$$\dot{x}^i = f(x) + g(x) u_j. \quad (6.36)$$

Using the Lie derivative formalism, and applying the *constant relative degree*  $r$  to all biodynamics joints, the *control law* for asymptotic tracking of the reference outputs  $\sigma_R^j = \sigma_R^j(t)$  could be formulated as (generalized from [Isidori (1989)])

$$u_j = \frac{\dot{\sigma}_R^{(r)j} - \mathcal{L}_f^{(r)} x^i + \sum_{s=1}^r \gamma_{s-1} (\sigma_R^{(s-1)j} - \mathcal{L}_f^{(s-1)} x^j)}{\mathcal{L}_g \mathcal{L}_f^{(r-1)} x^j}, \quad (6.37)$$

where  $\gamma_{s-1}$  are the coefficients of the linear differential equation of order  $r$  for the *error function*  $e(t) = x^j(t) - \sigma_R^j(t)$

$$e^{(r)} + \gamma_{r-1} e^{(r-1)} + \dots + \gamma_1 e^{(1)} + \gamma_0 e = 0.$$

With this formulation the affine nonlinear MIMO control system (6.36) with the control law (6.37) resembles the self-stabilizing and synergistic

output tracking action of the human cerebellum (see [Houk *et al.* (1996); van der Smagt (1999); Schaal and Atkeson (1998); Schaal (1999)]).

If nominal reference outputs  $o_R^i = o_R^i(t)$  are known, the simple 'jerk controller', or 'PDDD servo' (extending the standard stiffness-servo [Whitney (1987)]) could be formulated, via error function  $e(t)$ , in covariant form

$$u_i = K_o \delta_{ij} (o^j - o_R^j) + K_{\dot{o}} \delta_{ij} (\dot{o}^j - \dot{o}_R^j) + K_{\ddot{o}} \delta_{ij} (\ddot{o}^j - \ddot{o}_R^j) + K_{\ddot{\ddot{o}}} \delta_{ij} (\ddot{\ddot{o}}^j - \ddot{\ddot{o}}_R^j),$$

where  $K$ s are the control-gains and  $\delta_{ij}$  is the Kronecker's tensor.

#### 6.5.4 Lie-Adaptive Biodynamic Control

In this subsection we develop the concept of *machine learning* in the framework of Lie derivative control formalism (see (6.2.1.1) above). Consider an  $nD$ , SISO system in the standard affine form (6.10), rewritten here for convenience:

$$\dot{x}(t) = f(x) + g(x)u(t), \quad y(t) = h(x), \quad (6.38)$$

As already stated, the feedback control law for the system (6.38) can be defined using Lie derivatives  $\mathcal{L}_f h$  and  $\mathcal{L}_g h$  of the system's output  $h$  along the vector-fields  $f$  and  $g$ .

If the SISO system (6.38) is a relatively simple (quasilinear) system with *relative degree*<sup>4</sup> = 1 it can be rewritten in a quasilinear form

$$\dot{x}(t) = \gamma_i(t) f_i(x) + d_j(t) g_j(x) u(t), \quad (6.39)$$

where  $\gamma_i$  ( $i = 1, \dots, n$ ) and  $d_j$  ( $j = 1, \dots, m$ ) are system's parameters, while  $f_i$  and  $g_j$  are smooth vector-fields.

In this case the feedback control law for *tracking* the *reference signal*  $y_R = y_R(t)$  is defined as (see [Isidori (1989); Nijmeijer and van der Schaft (1990)])

$$u = \frac{-\mathcal{L}_f h + \dot{y}_R + \alpha(y_R - y)}{\mathcal{L}_g h}, \quad (6.40)$$

<sup>4</sup>Relative degree equals the number of differentiations of the output function  $y$  required to have the input  $u$  appear explicitly. Technically, the system (6.38) is said to have relative degree  $r$  at the point  $x^0$  if (see [Isidori (1989); Nijmeijer and van der Schaft (1990)])

(i)  $\mathcal{L}_g \mathcal{L}_f^k h(x) = 0$  for all  $x$  in a neighborhood of  $x^0$  and all  $k < r - 1$ , and

(ii)  $\mathcal{L}_g \mathcal{L}_f^{r-1} h(x^0) \neq 0$ ,

where  $\mathcal{L}_f^k h$  denotes the  $k$ th Lie derivative of  $h$  along  $f$ .

where  $\alpha$  denotes the feedback gain.

Obviously, the problem of reference signal tracking is relatively simple and straightforward if we know all the system's parameters  $\gamma_i(t)$  and  $d_j(t)$  of (6.39). The question is can we apply a similar control law if the system parameters are unknown?

Now we have much harder problem of *adaptive signal tracking*. However, it appears that the feedback control law can be actually cast in a similar form (see [Sastri and Isidori (1989)], [Gómez (1994)]):

$$\hat{u} = \frac{-\widehat{\mathcal{L}_f h} + \dot{y}_R + \alpha(y_R - y)}{\widehat{\mathcal{L}_g h}}, \quad (6.41)$$

where Lie derivatives  $\mathcal{L}_f h$  and  $\mathcal{L}_g h$  of (6.40) have been replaced by their estimates  $\widehat{\mathcal{L}_f h}$  and  $\widehat{\mathcal{L}_g h}$ , defined respectively as

$$\widehat{\mathcal{L}_f h} = \hat{\gamma}_i(t) \mathcal{L}_{f_i} h, \quad \widehat{\mathcal{L}_g h} = \hat{d}_j(t) \mathcal{L}_{g_j} h,$$

in which  $\hat{\gamma}_i(t)$  and  $\hat{d}_j(t)$  are the estimates for  $\gamma_i(t)$  and  $d_j(t)$ .

Therefore, we have the straightforward control law even in the uncertain case, provided that we are able to estimate the unknown system parameters. Probably the best known *parameter update law* is based on the so-called *Lyapunov criterion* (see [Sastri and Isidori (1989)]) and given by

$$\dot{\psi} = -\gamma \epsilon W, \quad (6.42)$$

where  $\psi = \{\gamma_i - \hat{\gamma}_i, d_j - \hat{d}_j\}$  is the parameter estimation error,  $\epsilon = y - y_R$  is the output error, and  $\gamma$  is a positive constant, while the matrix  $W$  is defined as:

$$W = [W_1^T W_2^T]^T, \quad \text{with}$$

$$W_1 = \begin{bmatrix} \mathcal{L}_{f_1} h \\ \vdots \\ \mathcal{L}_{f_n} h \end{bmatrix}, \quad W_2 = \begin{bmatrix} \mathcal{L}_{g_1} h \\ \vdots \\ \mathcal{L}_{g_m} h \end{bmatrix} \cdot \frac{-\widehat{\mathcal{L}_f h} + \dot{y}_R + \alpha(y_R - y)}{\widehat{\mathcal{L}_g h}}.$$

The proposed adaptive control formalism (6.41–6.42) can be efficiently applied wherever we have a problem of tracking a given signal with an output of a SISO-system (6.38–6.39) with unknown parameters.

## 6.6 Essentials of Biodynamic Measurement: Kalman Filtering and Inertial Navigation

In this subsection we give a brief description of modern biomechanical measurement, based on the celebrated *Kalman filter*, a stochastic dynamical signal-processing system, rooted in the linear state-space control theory. An extended, adaptive version of the Kalman filter is used in contemporary biomechanics, and also provides a solid engineering basis for the theory of artificial neural networks (see chapter 7).

### 6.6.0.1 *Kalman Filter Basics*

The classical *Kalman filter* is an effective procedure for *combining noisy sensor outputs to estimate the state of a system with uncertain dynamics*. The Kalman filter provides a *recursive solution to the linear optimal filtering problem*. It applies to stationary as well as nonstationary environments. The solution is recursive in that each updated estimate of the state is computed from the previous estimate and the new input data, so only the previous estimate requires storage. In addition to eliminating the need for storing the entire past observed data, the Kalman filter is computationally more efficient than computing the estimate directly from the entire past observed data at each step of the filtering process.

Recall from section 6.3 above, that the *linear quadratic regulator* (LQR) represents a *linear state feedback control law*

$$u = -Kx$$

for the linear MIMO-system

$$\dot{x} = Ax + Bu$$

which minimizes a *quadratic cost function*

$$J = \int_0^\infty (x(t)^T Q x(t) + u(t)^T R u(t)) dt.$$

The control law is called *optimal with respect to the cost function J*.

Now, one might ask whether there is an optimal design technique for a *state estimator*. That is, is there an approach to *observer design* which is equivalent, in some sense, to the linear quadratic regulator?

Given the *observable system*

$$\dot{x} = Ax + Bu, \quad y = Cx,$$

one may define the *dual system*

$$\dot{\theta} = A^T \theta + C^T \gamma$$

and design an LQR controller to minimize the quadratic cost function

$$J = \int_0^\infty (\theta(t)^T Q \theta(t) + \gamma(t)^T R \gamma(t)) dt.$$

However, it is unclear how one should ‘penalize’  $\theta$  and  $\gamma$  in the cost function. Instead, consider the *extended observable system*

$$\dot{x} = Ax + Bu + w, \quad y = Cx + v,$$

in which the dynamics are subject to random disturbances  $w$  and the measurements are subject to random noise  $v$ . In parallel with the development of the linear quadratic regulator, Rudolph Kalman examined the following *optimal estimator problem*: Construct a full state observer which minimizes the combined effect of the disturbances and the noise, thus providing a ‘most likely’ estimate of the system state. Solving this problem requires some information about the random processes. If the processes are zero-mean, Gaussian white noise processes (see Appendix), then the optimal estimator design problem becomes perfectly analogous to the LQR control design problem. In 1960, Kalman published his famous paper describing a recursive solution to the discrete-data linear filtering problem [Kalman (1960)]. Since that time, due in large part to advances in digital computing, the Kalman filter has been the subject of extensive particularly in the area of autonomous or assisted navigation (see, e.g., [Haykin (2001); Grewal *et al.* (2001)]).

The Kalman filter is a *discrete-time, two-step process*, the steps of which are usually called *prediction* and *correction*, thus resembling a popular *Adams–Bashforth–Moulton integrator* for ODEs (see, e.g., [Welch and Bishop (1995)]). The *predictor*, or *time update*, projects the current system’s state estimate ahead in time. The *corrector*, or *measurement update*, adjusts the projected state estimate by an actual system’s measurement at that time. In this way, the correction step makes corrections to an estimate, based on new information obtained from sensor measurements. The continuous-time version is usually referred to as *Kalman–Bucy filter* or *smoother* [Stevens and Lewis (2003); Asif (2004)].

Consider a generic linear, discrete-time dynamical system. The concept of *discrete state* is fundamental to this description. The *state vector*, denoted by  $x_k$ , is defined as the minimal set of data that is sufficient to



uniquely describe the unforced dynamical behavior of the system; the subscript  $k$  denotes discrete time. In other words, the state is the least amount of data on the past behavior of the system that is needed to predict its future behavior. Typically, the state  $x_k$  is unknown. To estimate it, we use a set of observed data, denoted by the *observable* vector  $y_k$ .

The state-space model of a generic linear, discrete-time dynamical system includes the *process equation* (6.43) and the *measurement equation* (6.44)

$$x_{k+1} = F_{k+1,k} x_k + w_k, \quad (6.43)$$

$$y_k = H_k x_k + v_k, \quad (6.44)$$

where  $F_{k+1}$  is the *transition matrix* taking the state  $x_k$  from time  $k$  to time  $k+1$ ,  $H_k$  is the *measurement sensitivity matrix*, while  $w_k$  and  $v_k$  are independent, additive, zero-mean, white *Gaussian noise* processes, defined below.

The covariance matrix of the *process noise*  $w_k$  is defined by

$$E[w_n, w_k^T] = \begin{cases} Q_k, & \text{for } n = k, \\ 0, & \text{for } n \neq k. \end{cases}$$

Similarly, the covariance matrix of the *measurement noise*  $v_k$  is defined by

$$E[v_n, v_k^T] = \begin{cases} R_k, & \text{for } n = k, \\ 0, & \text{for } n \neq k. \end{cases}$$

The *Kalman filtering problem*, namely, the problem of jointly solving the process and measurement equations for the unknown state in an optimum manner may now be formally stated as follows: Use the entire observed data, consisting of the vectors  $y_1, y_2, \dots, y_k$ , to find for each  $k \geq 1$  the minimum mean-square error estimate of the state  $x_i$ . The problem is called *filtering* if  $i = k$ , *prediction* if  $i > k$ , and *smoothing* if  $1 \leq i < k$ .

The derivation of the Kalman filter is based on the following two theorems (see [Kalman (1960); Haykin (2001)]):

- *Conditional mean estimator.* If the stochastic processes  $\{x_k\}$  and  $\{y_k\}$  are jointly Gaussian, then the optimum estimate  $\hat{x}_k$  that minimizes the mean-square error  $J_k$  is the conditional mean estimator:

$$\hat{x}_k = E[x_k | y_1, y_2, \dots, y_k].$$

- *Principle of orthogonality.* Let the stochastic processes  $\{x_k\}$  and  $\{y_k\}$  be of zero means; that is,

$$E[x_k] = E[y_k] = 0, \quad \text{for all } k.$$

Then:

- (i) the stochastic process  $\{x_k\}$  and  $\{y_k\}$  are jointly Gaussian; or
- (ii) if the optimal estimate  $\hat{x}_k$  is restricted to be a linear function of the observables and the cost function is the mean-square error,
- (iii) then the optimum estimate  $\hat{x}_k$ , given the observables  $y_1, y_2, \dots, y_k$ , is the orthogonal projection of  $x_k$  on the space spanned by these observables.

The *Kalman filter design algorithm* consists of (see [Kalman (1960); Haykin (2001)]):

- (1) *Initialization:* For  $k = 0$ , set

$$\hat{x}_0 = E[x_0], \quad P_0 = E[(x_0 - E[x_0])(x_0 - E[x_0])^T].$$

and

- (2) *Computation:* For  $k = 1, 2, \dots$ , compute:

- (i) *State estimate propagation*

$$\hat{x}_{\bar{k}} = F_{k,k-1} \hat{x}_{\bar{k}-1};$$

- (ii) *Error covariance propagation*

$$P_{\bar{k}} = F_{k,k-1} P_{k-1} F_{k,k-1}^T + Q_{k-1};$$

- (iii) *Kalman gain matrix*

$$G_k = P_{\bar{k}} H_k^T [H_k P_{\bar{k}} H_k^T + R_k]^{-1};$$

- (iv) *State estimate update*

$$\hat{x}_k = \hat{x}_{\bar{k}} + G_k (y_k - H_k \hat{x}_{\bar{k}});$$

- (v) *Error covariance update*

$$P_k = (I - G_k H_k) P_{\bar{k}}.$$

Therefore, the basic Kalman filter is a linear, discrete-time, finite-dimensional system, which is endowed with a recursive structure that makes a digital computer well suited for its implementation. A key property of the Kalman filter is that it is the minimum mean-square (variance) estimator of the state of a linear dynamical system. The model is stochastic owing to the additive presence of process noise and measurement noise, which are assumed to be Gaussian with zero mean and known covariance matrices.

**Extended Kalman Filter.** The Kalman filtering problem considered so far has addressed the estimation of a state vector in a linear model of a dynamical system. If, however, the model is nonlinear, we may extend the use of Kalman filtering through a linearization procedure. The resulting filter is referred to as the *extended Kalman filter* (EKF) [Haykin (2001)]. Such an extension is feasible by virtue of the fact that the Kalman filter is described in terms of difference equations in the case of discrete-time systems. While the ordinary (i.e., linear) Kalman filter is defined in terms of the measurement sensitivity matrix  $H_k$ , the extended Kalman filter can be defined in terms of a suitably differentiable vector-valued measurement sensitivity function  $h(k, x_k)$ .

To set the stage for a development of the extended Kalman filter, consider a nonlinear dynamical system described by the state-space model

$$x_{k+1} = f(k, x_k) + w_k, \quad y_k = h(k, x_k) + v_k, \quad (6.45)$$

where, as before,  $w_k$  and  $v_k$  are independent zero-mean white Gaussian noise processes with covariance matrices  $R_k$  and  $Q_k$ , respectively. Here, however, the functional  $f(k, x_k)$  denotes a nonlinear transition matrix function that is possibly time-variant. Likewise, the functional  $h(k, x_k)$  denotes a vector-valued measurement sensitivity function, i.e., a nonlinear measurement matrix that may be time-variant, too [Haykin (2001)].

The basic idea of the extended Kalman filter is to linearize the state-space model (6.45) at each time instant around the most recent state estimate, which is taken to be either  $\hat{x}_k$  or  $\hat{x}_{\bar{k}}$ , depending on which particular functional is being considered. Once a linear model is obtained, the standard Kalman filter equations are applied.

The *EKF design algorithm* consists of [Haykin (2001)]:

- (1) The *discrete state-space model* (6.45).
- (2) *Definitions*

$$F_{k,k} = \left. \frac{\partial f(k, x)}{\partial x} \right|_{x=x_k}, \quad H_k = \left. \frac{\partial h(k, x)}{\partial x} \right|_{x=x_k}.$$

(3) *Initialization*: For  $k = 0$ , set

$$\hat{x}_0 = E[x_0], \quad P_0 = E[(x_0 - E[x_0])(x_0 - E[x_0])^T].$$

(4) *Computation*: For  $k = 1, 2, \dots$ , compute:

(i) *State estimate propagation*

$$\hat{x}_{\bar{k}} = F_{k,k-1} \hat{x}_{\bar{k}-1};$$

(ii) *Error covariance propagation*

$$P_{\bar{k}} = F_{k,k-1} P_{k-1} F_{k,k-1}^T + Q_{k-1};$$

(iii) *Kalman gain matrix*

$$G_k = P_{\bar{k}} H_k^T [H_k P_{\bar{k}} H_k^T + R_k]^{-1};$$

(iv) *State estimate update*

$$\hat{x}_k = \hat{x}_{\bar{k}} + G_k (y_k - H_k \hat{x}_{\bar{k}});$$

(v) *Error covariance update*

$$P_k = (I - G_k H_k) P_{\bar{k}}.$$

**Sensor Fusion in Hybrid Systems.** Kalman filter can be used to *combine* or *fuse* information from different sensors for hybrid systems (see Figure 6.15), like accelerometers and gyroscopes (see text below). The basic idea is to use the Kalman filter to weight the different mediums most heavily in the circumstances where they each perform best, thus providing more accurate and stable estimates than a system based on any one medium alone (see [Luinge (2002)]). In particular, the *indirect feedback Kalman filter* (also called a *complementary* or *error-state Kalman filter*) is often used to combine the two mediums [Maybeck (1979)]. In such a configuration, the Kalman filter is used to estimate the difference between the current inertial and optical (or acoustic) outputs, i.e. it continually estimates the error in the inertial estimates by using the optical system as a second (redundant) reference. This error estimate is then used to correct the inertial estimates. The *tuning* of the Kalman filter parameters then adjusts the weight of the correction as a function of frequency. By slightly modifying the Kalman

filter, adaptive velocity response can be incorporated also. This can be accomplished by adjusting (in real time) the expected optical measurement error as a function of the magnitude of velocity [Welch and Bishop (1995)]. Kalman filter has been used to investigate the human balancing system [van der Kooij *et al.* (2001); van der Kooij and Donker (2003)] (see below).

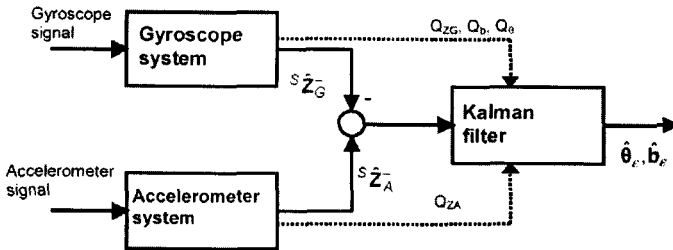


Fig. 6.15 Structure of *sensor fusion in Kalman filter estimation*. Both the accelerometer and the gyroscope system are used to make an estimate of the global vertical unit vector  $\mathbf{Z}$ . The difference between the two estimates is written as a function of orientation error  $\theta_e$  and offset error  $b_e$ . Kalman filter estimates both  $\theta_e$  and  $b_e$  using the error covariances of the orientation  $Q_\theta$ , offset  $Q_b$  and inclination estimation ( $Q_{ZG}$  and  $Q_{ZA}$ ). These estimated errors are used to correct the estimated.

### 6.6.0.2 Inertial Navigation

Now recall that, by the *Newton's first law of motion*, *inertia* is the property of bodies to maintain constant translational and rotational velocity, unless disturbed by forces of torques, respectively. Inertial reference frames are coordinate frames, neither rotating nor accelerating, in which Newton's laws of motion are valid.

Inertial sensors measure angular velocity (i.e., rotation rate) and translational (or, linear) acceleration, which are both vector-valued variables (see [Grewal *et al.* (2001)]):

(i) Gyroscopes are sensors for measuring rotation: rate gyroscopes measure rotation rate, and displacement gyroscopes (also called whole-angle gyroscopes) measure rotation angle.

(ii) Accelerometers are sensors for measuring acceleration (however, they cannot measure gravitational acceleration; that is, an accelerometer in free fall (or in orbit) has no detectable input).

Mechanics of inertial sensors [Soderkvist (1994)] actually resembles mechanics of the human vestibular system (see subsection 7.2.11.8 below), in an attempt to capture the three translations and three rotations from the

$SE(3)$  group of rigid body motions (see subsection 3.5.2.5 above). The input axis of an inertial sensor defines which vector component it measures. Multiaxial sensors measure more than one component.

Inertial navigation uses gyroscopes and accelerometers to maintain an estimate of the position, velocity, attitude, and attitude rates of the host vehicle on which the inertial sensors are carried.

In biomechanics, inertial sensors (mainly accelerometers) have been used for *inverse dynamic analysis of human movement*. In [van den Bogert *et al.* (1996)] a method was developed to calculate total resultant force and moment on a 3D body segment, from accelerometer data. The method was applied for an analysis of intersegmental loading at the hip joint during the single support phase of working and running, using four triaxial accelerometers mounted on the upper body. Results were compared to a conventional analysis using simultaneously recorded kinematics and ground reaction forces. The loading patterns obtained by both methods were similar, but the *accelerometry method* systematically underestimated the intersegmental force and moment at the hip by about 20%. This could be explained by the inertial and gravitational forces originating from the swing leg which were neglected in the analysis. In addition, the accelerometry analysis was not not reliable during the impact phase of running, when the upper body and accelerometers did not behave as a rigid body. For applications where these limitations are acceptable, the accelerometry method has the advantage that it does not require a gait laboratory environment and can be used for field studies with a completely body-mounted recording system. The method does not require differentiation or integration, and therefore provides the possibility of real-time inverse dynamics analysis.

An inertial navigation system (INS) consists of the following:

- (i) An *inertial measurement unit* (or inertial reference unit) containing a cluster of sensors: accelerometers (three or more) and gyroscopes (also three or more), which are rigidly mounted to a common base to maintain the same relative orientations.
- (ii) *Navigation computers* (one or more) calculate the gravitational acceleration (not measured by accelerometers) and doubly integrate the net acceleration to maintain an estimate of the position of the host vehicle.

There are many different designs of inertial navigation systems with different performance characteristics, but they fall generally into two categories: (i) *gimballed inertial systems*, and (ii) *strapdown inertial systems* (see [Grewal *et al.* (2001)] for technical details).

**Gimballed Inertial Systems.** A gimbal is a rigid frame with rotation

bearings for isolating the inside of the frame from external rotations about the bearing axes. If the bearings could be made perfectly frictionless and the frame perfectly balanced (which is unrealistic, however), then the rotational inertia of the frame would be sufficient to isolate it from rotations of the supporting body.

Alternatively, a gyroscope can be mounted inside the gimbal frame and used to detect any rotation to the frame due to torques from bearing friction or frame unbalance. The detected rotational disturbance can then be used in a feedback loop to provide restoring torques on the gimbal bearings to null out all rotations of the frame about the respective gimbal bearings.

At least three gimbals are required to isolate a subsystem from host vehicle rotations about the *three Euler angles*: *roll*  $\varphi$  (about the  $X$ -axis along the plane), *pitch*  $\psi$  (about the  $Y$ -axis which extends along the wings of the plane), and *yaw*, or *heading*  $\theta$  (about the  $Z$ -axis).

Recall from subsection 3.5.2 above, that the Euler-angle parametrization of the  $SO(3)$  group of motions defines the total three-axial rotation as the product of three one-parameter Euler rotations  $R_\varphi, R_\psi, R_\theta$ , giving the full transformation matrix.

The gimbals in an INS are mounted inside one another. Three gimbals (the minimum number required) will suffice for host vehicles with limited ranges of rotation in pitch and roll (such as land vehicles and surface ships), where the outermost axis is typically aligned with the host vehicle yaw axis (nominally vertical). In this way all three gimbal rotation axes will remain essentially orthogonal when the inner gimbal axes are kept level and the vehicle rotates freely about its yaw axis only.

A fourth gimbal is required for host vehicles with full freedom of rotation about all three axes (such as a high-performance aircraft). Otherwise, rotations of the host vehicle can align two of the three gimbal axes parallel to one another in a condition called *gimbal lock*.

**Strapdown Inertial Systems.** In strapdown systems, the inertial sensor cluster is 'strapped down' to the frame of the host vehicle, without using intervening gimbals for rotational isolation. The system computer must then integrate the full 6-DOF equations of motion. The additional processing functions, beyond those required for gimballed inertial navigation, include: (i) components for coordinate transformation update and acceleration coordinate transformation (the strapdown software effectively maintains virtual gimbals in the form of a coordinate transformation from the unconstrained, body-fixed sensor coordinates to the equivalent sensor coordinates of an inertial platform); and (ii) attitude rate compensation for

accelerometers, which was not required for gimballed systems.

**Common Error Models.** Theoretically, one should be able to recover the input from the sensor output so long as the input/output relationship is known and invertible. However, in practice, common types of *inertial sensor errors* are: (i) bias, which is any nonzero sensor output when the input is zero; (ii) scale factor error, often resulting from aging or manufacturing tolerances; (iii) nonlinearity, which is present in most sensors to some degree; (iv) scale factor sign asymmetry, often from mismatched push-pull amplifiers; (v) a dead zone, usually due to mechanical stiction of lock-in; and (vi) quantization error, inherent in all digitized systems.

For a cluster of three gyroscopes or accelerometers, of either gimballed or strapdown type, with nominally orthogonal input axes, the effects of individual scale factor deviations and input axis misalignments from their nominal values can be modelled by the equation

$$\mathbf{z}_{out} = S_{nom}(\mathbf{I} + \mathbf{M})\mathbf{z}_{in} + \mathbf{b}_z,$$

where the components of the vector  $\mathbf{b}_z$  are the three sensor output biases, the components of the  $\mathbf{z}_{in}$  and  $\mathbf{z}_{out}$  vectors are the sensed values (accelerations or angular velocities) and output values from the sensors, respectively,  $S_{nom}$  is the nominal sensor scale factor, and the elements  $m_{ij}$  of the scale factor and misalignment matrix  $\mathbf{M}$  represent the individual scale factor deviations and input axis misalignments, while  $\mathbf{I}$  is  $3 \times 3$  identity matrix.

**Kalman-Quaternion Filter for Attitude Estimation.** Now, although Euler angles are physically most plausible for representing rotations (as parameterizations of the  $SO(3)$ -group of rigid-body rotations), they 'flip' (i.e., have singularity) at the angle of  $\pm\pi/2$ . This is the reason for using Hamilton's quaternions instead (see Appendix). The *quaternion attitude estimation filter* was proposed at Monterey Naval Postgraduate School in a series of Master theses supervised by R.. McGhee (see [McGhee (1996)]) as an alternative representation and improvement to filters based on Euler angles. The quaternion attitude estimation filter is designed to track human limb segments through all orientations as part of an inertial tracking system. It uses a Kalman-fusion of three different types of sensors to obtain the information about the orientation of a tracked object. These sensors are a 3-axial accelerometer, a 3-axial gyroscope and a 3-axial *magnetometer* (digital compass).

An extended *Kalman-quaternion filter* for real-time estimation of rigid body motion altitude was proposed in [Joao (2000)]. A process model for rigid body angular motions and angular rate measurements is defined. The



process model converts angular rates into quaternion rates, which are in turn integrated to obtain quaternions. The outputs of the model are values of 3D angular rates, 3D linear accelerations, and 3D magnetic field vector. Gauss–Newton iteration is utilized to find the best quaternion that relates the measured linear accelerations and earth magnetic field in the body coordinate frame to calculated values in the earth coordinate frame. The quaternion obtained from the optimization algorithm is used as part of the observations for the Kalman filter. As a result, the measurement equations become linear.

#### 6.6.0.3 *Adaptive Estimation in Biomechanics*

The extended Kalman filter is widely used in biomechanical experiments. For example, an adaptive Kalman estimator model of human spatial orientation is presented in [van der Kooij *et al.* (2001); van der Kooij and Donker (2003)]. The adaptive Kalman model dynamically weights sensory error signals. More specific, the model weights the difference between expected and actual sensory signals as a function of environmental conditions. The model does not require any changes in model parameters. Differences with existing models of spatial orientation are in the following: (i) Environmental conditions are not specified but estimated; (ii) The sensor noise characteristics are the only parameters supplied by the model designer; (iii) History-dependent effects and mental resources can be modelled; and (iv) Vestibular thresholds are not included in the model; instead vestibular-related threshold effects are predicted by the model.

The model was applied to human stance control and evaluated with results of a visually induced sway experiment [van der Kooij *et al.* (2001); Peterka (2002)]. From these experiments it is known that the amplitude of visually induced sway reaches a saturation level as the stimulus level increases. This saturation level is higher when the support base is sway referenced. For subjects experiencing vestibular loss, these saturation effects do not occur. Unknown sensory noise characteristics were found by matching model predictions with these experimental results. Using only five model parameters, far more than five data points were successfully predicted. Model predictions showed that both the saturation levels are vestibular related since removal of the vestibular organs in the model removed the saturation effects, as was also shown in the experiments. It seems that the nature of these vestibular-related threshold effects is not physical, since in the model no threshold is included. The model results

suggest that vestibular-related thresholds are the result of the processing of noisy sensory and motor output signals. Model analysis suggests that, especially for slow and small movements, the environment postural orientation can not be estimated optimally, which causes sensory illusions. The model also confirms the experimental finding that postural orientation is history dependent and can be shaped by instruction or mental knowledge. In addition the model predicts the following: (i) Vestibular-loss patients cannot handle sensory conflicting situations and will fall down; (ii) During sinusoidal support-base translations vestibular function is needed to prevent falling; (iii) During sinusoidal support-base translations vestibular function is needed to prevent falling; (iv) During sinusoidal support-base translations vestibular function is needed to prevent falling; and (v) Loss of vestibular function results in falling for large support-base rotations with the eyes closed. These predictions agree with experiments [Peterka (2002)].

To relate neuromuscular disorders (impairments) with balance disorders (disabilities) a well-defined method that identifies the different factors determining balance control is essential. An adequate approach is to isolate different sensory sources and to calculate transfer functions between the input (e.g., perturbation) and output (e.g., body sway) signals. Using this system identification approach the dynamical behavior of postural control can be obtained and is well defined. The adaptive Kalman model of balance control [van der Kooij *et al.* (2001); Peterka (2002)] was successfully used to reproduce the experimental findings on *sensory-motor integration* in human postural control [Peterka (2002)] (see Figure 7.39 below).

## 6.7 Humanoid Robotics

### 6.7.1 *Honda Humanoid Series*

Corresponding to Honda's Slogan 'The Power of Dreams', Honda set itself the ambitious goal to create a two-legged walking robot by developing revolutionary new technology. Research began by envisioning the ideal robot form for use in human society. The robot would need to be able to maneuver between objects in a room, be able to go up and down stairs and need to be able to walk on uneven ground. For this reason it had to have two legs, just like a person.

The first Honda robot, E0, was made in 1986. A two legged robot was made to walk. Walking by putting one leg before the other was successfully

achieved. However, taking nearly five seconds between steps, it walked very slowly in a straight line. To increase walking speed, or to allow walking on uneven surfaces or slopes, fast walking must be realized.

In the period 1987–1991, Honda made the next three robots in E-series: E1, E2, and E3. Human walking was thoroughly researched and analyzed. Based on this data a fast walking program was created, input into the robot and experiments were begun. The E2 robot achieved fast walking at a speed of 1.2 km/h on a flat surface. The next step was realized fast, stable walking in the human living environment, especially on uneven surfaces, slopes and steps, without falling down.

In the period 1991–1993, Honda made the next three robots in E-series: E4, E5, and E6. Honda investigated techniques for stabilizing walking, and developed three control techniques: (i) floor reaction control, (ii) target ZMP control, and (iii) foot planting location control. In particular, E5 robot achieved stable, two legged walking, even on steps or slopping surfaces. The next step was to attach the legs to a body and create a *humanoid robot*.

In the period 1994–1997, Honda made three humanoid robots in the new P-series: P1, P2, and P3. The first humanoid, P1, can turn external electrical and computer switches on and off, grab doorknobs, and pick up and carry things. Its height is 1.91 m, and its weight is 175 kg.

P2, the worlds first self-regulating, two-legged humanoid walking robot debuted in December, 1996. Using wireless techniques, the torso contained a computer, motor drives, battery, wireless radio, all of which were build in. It is 1.82 m tall and weights 210 kg.

In September 1997 the two-legged humanoid walking robot P3 was completed. Size and weight were reduced by changing component materials and by decentralizing the control system. Its smaller size is better suited for use in the human environment. It is 1.60 m tall, and weights 130 kg.

Finally, in 2000 Honda released a humanoid robot Asimo. Using the know-how gained from the prototypes P2 and P3, research and development began on new technology for actual use. Asimo represents the fruition of this pursuit. Weight was reduced to 43 kg and height to 1.20 m.

### 6.7.2 Cerebellar Robotics

At the end of this chapter, as an introduction to the main theme of the last chapter: *brain-like biodynamics control*, we present in brief a new trend in robotics research, the so-called *cerebellar robotics*. In a series of papers published in prestigious journals, M. Kawato and his collab-

orators [Atkeson *et al.* (2000); Kawato (1999); Shidara *et al.* (1993); Gomi and Kawato (1996); Burdet *et al.* (2001); Imamizu *et al.* (2000); Imamizu *et al.* (2003); Wolpert and Kawato (1998)] investigated the information processing of the brain with the long-term goal that machines, either computer programs or robots, could solve the same computational problems as those that the human brain solves, while using essentially the same principles. With these general approaches, they made progresses in elucidating visual information processing, optimal control principles for arm trajectory planning, internal models in the cerebellum, teaching by demonstration for robots, human interfaces based on electromyogram, and applications in rehabilitation medicine.

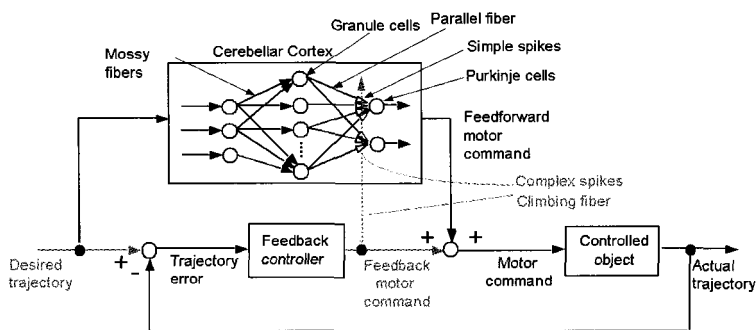


Fig. 6.16 Cerebellar feedback-error learning (see text for explanation).

They developed a 30 DOF humanoid robot 'DB' for computational neuroscience research. DB is quick in movements, very compliant, with the same dimension and weight with humans. It has four cameras, artificial vestibular sensor, joint angle sensors and force sensors for all the actuators. DB can demonstrate 24 different behaviors, classified into 3 main classes: (i) learning from demonstration, (ii) eye movements, and (iii) behavior depending on task dynamics, physical interaction, and learning.

Essential computational principles of some of these demonstrations are: (i) cerebellar internal models, (ii) reinforcement learning in the basal ganglia, and (iii) cerebral stochastic internal model.

Their feedback error learning for cerebellum (see Figure 6.16) includes the following data: (1) Simple spike represents feedforward motor command; (2) Parallel-fibre inputs represent desired trajectory; (3) Cerebellar cortex constitutes inverse model; and (4) Complex spike represents error in

motor-command coordinate.

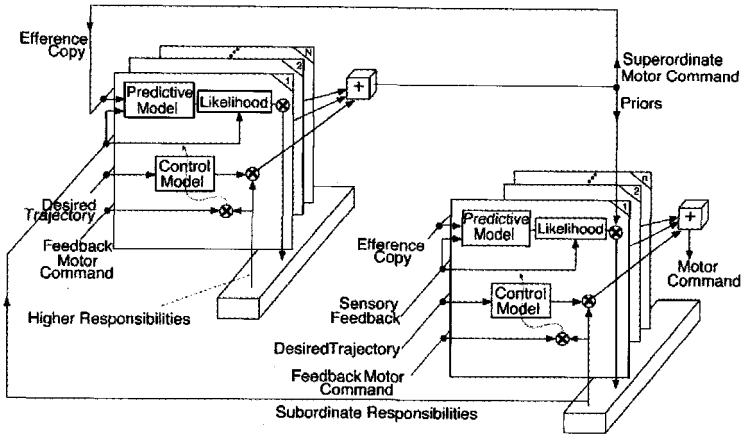


Fig. 6.17 Cerebellar modular selection and identification control (see text).

Theories of motor control postulate that the brain uses internal models of the body to control movements accurately. Internal models are neural representations of how, for instance, the arm would respond to a neural command, given its current position and velocity. The cerebellar cortex can acquire internal models through motor learning (see chapter 7). Because the human cerebellum is involved in higher cognitive function as well as in motor control, they proposed a coherent computational theory in which the phylogenetically newer part of the cerebellum similarly acquires internal models of objects in the external world (see Figure 6.17). While human subjects learned to use a new tool (a computer mouse with a novel rotational transformation), cerebellar activity was measured by functional magnetic resonance imaging. As predicted by their theory, two types of activity were observed. One was spread over wide areas of the cerebellum and was precisely proportional to the error signal that guides the acquisition of internal models during learning. The other was confined to the area near the posterior superior fissure and remained even after learning, when the error levels had been equalized, thus probably reflecting an acquired internal model of the new tool.

## Chapter 7

# Natural Brain Dynamics and Sensory–Motor Integration

This final chapter presents various aspects of the top level biodynamics, the brain-like control system, reflecting our *covariant force law*,  $F_i = mg_{ij}a^j$ , and its associated *covariant force functor*  $\mathcal{F}_* : TT^*M \rightarrow TTM$  (see section 5.4 above). Although this is supposed to be ‘biodynamic synthesis’, it is actually an inevitably incomplete and non-rigorous exposition, in many ways ‘botanical’ (see [Penrose (1997)]), which reflects the current development of the brain science (see Appendix for a review of modern 3D neuro-imaging). So, the real purpose of this chapter is to describe the *central biodynamic adjunction*, *coordination* = *sensory*  $\dashv$  *motor* : *brain*  $\rightleftarrows$  *body*, the *association–integration* between sensory and motor neural pathways, the mathematical unity in biodynamics diversity as well as the natural diversity in mathematical unity. The simplest form of this adjunction is the basis of all neural activity, namely, the reflex sensory–motor action. We start with the necessary minimum of neuro-anatomy and neuro-physiology and after that give a definition of our central sensory–motor adjunction. Then we move on to the brain dynamics and biological neural networks. Next we shift to artificial neural networks and related fuzzy logic systems. After that we present categorical generalization of the natural and neural-like systems, as well as concurrent machines. At the end we propose our own model for the brain-like control in biodynamics. Note that *Einstein’s summation convention over repeated indices* (not necessarily one subscript and the other superscript) *is assumed in the whole chapter*, unless otherwise stated. This is a bit unusual in neural community, but it simplifies notation and gives it a unified geometrodynamical expression.

## 7.1 Introduction to Brain

In this section, as a motivation, we give an informal introduction to human brain, mainly from the physical perspective. The *human brain* is the most complicated object, as far as we know, in the Universe. A closer look at the brain points to a rather recursively hierarchical structure and a very elaborate organization [Kandel *et al.* (1991); Braitenberg and Shulz (1991)]. An average brain weighs about 1.3 kg, and it is made of:  $\sim 77\%$  water,  $\sim 10\%$  protein,  $\sim 10\%$  fat,  $\sim 1\%$  carbohydrates,  $\sim 0.01\%$  DNA/RNA. The largest part of the human brain, the cerebrum, is found on the top and is divided down the middle into left and right cerebral hemispheres, and front and back into *frontal lobe*, *parietal lobe*, *temporal lobe*, and *occipital lobe*. Further down, and at the back lies a rather smaller, spherical portion of the brain, the *cerebellum*, and deep inside lie a number of complicated structures like the *thalamus*, *hypothalamus*, *hippocampus*, etc.

Both the cerebrum and the cerebellum have comparatively thin outer surface layers of grey matter and larger inner regions of white matter. The grey regions constitute what is known as the *cerebral cortex* and the *cerebellar cortex*. It is in the *grey matter* where various kinds of *computational tasks* seem to be performed, while the *white matter* consists of long nerve fibers (axons) carrying signals from one part of the brain to another. However, despite of its amazing computational abilities, brain is not a computer, at least not a 'Von Neumann computer' [von Neumann (1958)], but rather a huge, hierarchical, neural network. It is the cerebral cortex that is central to the higher brain functions, speech, thought, complex movement patterns, etc. On the other hand, the cerebellum seems to be more of an 'automaton'. It has to do more with precise coordination and control of the body, and with skills that have become our 'second nature'. Cerebellum actions seem almost to take place by themselves, without thinking about them. They are very similar to the unconscious reflex actions, e.g., reaction to pinching, which may not be mediated by the brain, but by the upper part of the spinal column.

Various regions of the cerebral cortex are associated with very specific functions. The *visual cortex*, a region in the occipital lobe at the back of the brain, is responsible for the reception and interpretation of vision. The *auditory cortex*, in the temporal lobe, deals mainly with analysis of sound, while the *olfactory cortex*, in the frontal lobe, deals with smell. The *somatosensory cortex*, just *behind* the division between frontal and parietal lobes, has to do with the sensations of touch. There is a very

specific mapping between the various parts of the surface of the body and the regions of the somatosensory cortex. In addition, just in *front* of the division between the frontal and parietal lobes, in the frontal lobe, there is the *motor cortex*. The *motor cortex* activates the movement of different parts of the body and, again here, there is a very specific mapping between the various muscles of the body and the regions of the motor cortex. All the above mentioned regions of the cerebral cortex are referred to as *primary*, since they are the one most directly concerned with the input and output of the brain. Near to these primary regions are the *secondary sensory* regions of the cerebral cortex, where information is processed, while in the *secondary motor* regions, conceived plans of motion get translated into specific directions for actual muscle movement by the primary motor cortex. The most abstract and sophisticated activity of the brain is carried out in the remaining regions of the cerebral cortex, the *association cortex*.

The basic building blocks of the brain are the nerve cells or neurons. Among about 200 types of different basic types of human cells, the neuron is one of the most specialized, exotic and remarkably versatile cell. The neuron is highly unusual in three respects: its *variation in shape*, its *electrochemical function*, and its *connectivity*, i.e., its ability to link up with other neurons in networks. Let us start with a few elements of neuron microanatomy [Kandel *et al.* (1991); Braitenberg and Shulz (1991)]. There is a central starlike bulb, called the *soma*, which contains the nucleus of the cell. A long nerve fibre, known as the *axon*, stretches out from one end of the soma. Its length, in humans, can reach up to few *cm*. The function of an axon is to transmit the neuron's output signal, in which it acts like a *coaxial cable*. The axon has the ability of multiple bifurcation, branching out into many smaller nerve fibers, and the very end of which there is always a *synaptic knob*. At the other end of the soma and often springing off in all directions from it, are the tree-like *dendrites*, along which input data are carried into the soma. The whole nerve cell, as basic unit, has a cell membrane surrounding soma, axon, synaptic knobs, and dendrites. Signals pass from one neuron to another at junctions known as *synapses*, where a synaptic knob of one neuron is attached to another neuron's soma or dendrites. There is very narrow gap, of a few *nm*, between the synaptic knob and the soma/dendrite to where the *synaptic cleft* is attached. The signal from one neuron to another has to propagate across this gap.

A nerve fibre is a cylindrical tube containing a mixed solution of NaCl and KCl, mainly the second, so there are  $\text{Na}^+$ ,  $\text{K}^+$ , and  $\text{Cl}^-$  ions within the



tube. Outside the tube the same type of ions are present but with more  $\text{Na}^+$  than  $\text{K}^+$ . In the *resting* state there is an excess of  $\text{Cl}^-$  over  $\text{Na}^+$  and  $\text{K}^+$  inside the tube, giving it a negative charge, while it has positive charge outside. A nerve signal is a region of *charge reversal* travelling along the fibre. At its head, *sodium gates* open to allow the sodium to flow inwards and at its tail *potassium gates* open to allow potassium to flow outwards. Then, metabolic pumps act to restore order and establish the *resting state*, preparing the nerve fibre for another signal. There is no major material (ion) transport that produces the signal, just in and out local movements of ions, across the cell membranes, i.e., a *small* and *local* depolarization of the cell. Eventually, the nerve signal reaches the attached synaptic knob, at the very end of the nerve fibre, and triggers it to emit chemical substances, known as *neurotransmitters*. It is these substances that travel across the synaptic cleft to another neuron's soma or dendrite. It should be stressed that the signal here is not electrical, but a chemical one. What really is happening is that when the nerve signal reaches the synaptic knob, the local depolarization cause little bags immersed in the *vesicular grid*, the *vesicles* containing molecules of the neurotransmitter chemical (e.g., acetylcholine) to release their contents from the neuron into the synaptic cleft, the phenomenon of *exocytosis*. These molecules then diffuse across the cleft to interact with *receptor proteins* on receiving neurons. On receiving a neurotransmitter molecule, the receptor protein opens a gate that causes a local depolarization of the receiver neuron.

It depends on the nature of the synaptic knob and of the specific synaptic junction, if the next neuron would be encouraged to *fire*, i.e., to start a new signal along its own axon, or it would be discouraged to do so. In the former case we are talking about *excitatory synapses*, while in the latter case about *inhibitory synapses*. At any given moment, one has to add up the effect of all excitatory synapses and subtract the effect of all the inhibitory ones. If the net effect corresponds to a positive electrical potential difference between the inside and the outside of the neuron under consideration, *and* if it is bigger than a critical value, then the neuron *fires*, otherwise it stays mute.

The basic dynamical process of neural communication can be summarized in the following three steps: [Nanopoulos (1995)]

- (1) The neural axon is an *all or none* state. In the *all state* a signal, called a *spike* or *action potential* (AP), propagates indicating that the summation performed in the soma produced an amplitude of the order

of tens of mV. In the *none state* there is no signal travelling in the axon, only the resting potential ( $\sim -70\text{mV}$ ). It is essential to notice that the presence of a travelling signal in the axon, *blocks* the possibility of transmission of a second signal.

- (2) The nerve signal, upon arriving at the ending of the axon, triggers the emission of neurotransmitters in the synaptic cleft, which in turn cause the receptors to open up and allow the penetration of ionic current into the *post synaptic* neuron. The *efficacy* of the synapse is a parameter specified by the amount of penetrating current per presynaptic spike.
- (3) The post synaptic potential (PSP) diffuses toward the soma, where all inputs in a short period, from all the presynaptic neurons connected to the postsynaptic are summed up. The amplitude of individual PSP's is about 1mV, thus quite a number of inputs is required to reach the 'firing' threshold, of tens of mV. Otherwise the postsynaptic neuron remains in the *resting* or *none* state.

The cycle-time of a neuron, i.e., the time from the emission of a spike in the presynaptic neuron to the emission of a spike in the postsynaptic neuron is of the order of 1 – 2 ms. There is also some recovery time for the neuron, after it fired, of about 1 – 2 ms, independently of how large the amplitude of the depolarizing potential would be. This period is called the absolute refractory period of the neuron. Clearly, it sets an upper bound on the spike frequency of 500 – 1000/sec. In the types of neurons that we will be interested in, the spike frequency is considerably lower than the above upper bound, typically in the range of 100/sec, or even smaller in some areas, at about 50/sec. It should be noticed that this rather exotic neural communication mechanism works very efficiently and it is employed universally, both by vertebrates and invertebrates. The vertebrates have gone even further in perfection, by protecting their nerve fibers by an insulating coating of myelin, a white fatty substance, which incidentally gives the white matter of the brain, discussed above, its color. Because of this insulation, the nerve signals may travel undisturbed at about 120 m/sec [Nanopoulos (1995)]

A very important anatomical fact is that each neuron receives some  $10^4$  synaptic inputs from the axons of other neurons, usually one input per presynaptic neuron, and that each branching neural axon forms about the same number ( $\sim 10^4$ ) of synaptic contacts on other, postsynaptic neurons. A closer look at our cortex then would expose a mosaic-type structure of assemblies of a few thousand densely connected neurons. These assemblies

are taken to be the basic cortical processing *modules*, and their size is about  $1(\text{mm})^2$ . The neural connectivity gets much sparser as we move to larger scales and with much less feedback, allowing thus for autonomous local collective, parallel processing and more serial and integrative processing of local collective outcomes. Taking into account that there are about  $10^{11}$  nerve cells in the brain (about  $7 \times 10^{10}$  in the cerebrum and  $3 \times 10^{10}$  in the cerebellum), we are talking about  $10^{15}$  synapses.

While the dynamical process of neural communication suggests that the brain action looks a lot like a computer action, there are some fundamental differences having to do with a basic brain property called *brain plasticity*. The interconnections between neurons are not fixed, as is the case in a computer-like model, but are changing all the time. These are *synaptic junctions* where the communication between different neurons actually takes place. The synaptic junctions occur at places where there are *dendritic spines* of suitable form such that contact with the synaptic knobs can be made. Under certain conditions these dendritic spines can shrink away and break contact, or they can grow and make new contact, thus determining the *efficacy* of the synaptic junction. Actually, it seems that it is through these dendritic spine changes, in synaptic connections, that long-term memories are laid down, by providing the means of storing the necessary information. A supporting indication of such a conjecture is the fact that such dendritic spine changes occur within *seconds*, which is also how long it takes for permanent memories to be laid down [Penrose (1989); Penrose (1994); Penrose (1997); Stapp (1993)].

Furthermore, a very useful set of phenomenological rules has been put forward by Hebb [Hebb (1949)], the *Hebb rules*, concerning the underlying mechanism of brain plasticity. According to Hebb, a synapse between neuron 1 and neuron 2 would be strengthened whenever the firing of neuron 1 is followed by the firing of neuron 2, and weakened whenever it is not. It seems that *brain plasticity* is a *fundamental property* of the activity of the brain.

Many mathematical models have been proposed to try to simulate *learning process*, based upon the close resemblance of the dynamics of neural communication to computers and implementing, one way or another, the essence of the Hebb rules. These models are known as *neural networks*. They are closely related to *adaptive Kalman filtering* (see (6.6) above) as well as *adaptive control* (see (6.5.4) above).

Let us try to construct a neural network model for a set of  $N$  interconnected neurons (see e.g., [Amari (1972)]). The activity of the neurons

is usually parameterized by  $N$  functions  $\sigma_i(t)$ ,  $i = 1, 2, \dots, N$ , and the synaptic strength, representing the synaptic efficacy, by  $N \times N$  functions  $j_{ik}(t)$ . The total stimulus of the network on a given neuron ( $i$ ) is assumed to be given simply by the sum of the stimuli coming from each neuron

$$S_i(t) = j_{ik}(t)\sigma_k(t), \quad (\text{summation over } k)$$

where we have identified the individual stimuli with the product of the synaptic strength  $j_{ik}$  with the activity  $\sigma_k$  of the neuron producing the individual stimulus. The dynamic equations for the neuron are supposed to be, in the simplest case

$$\dot{\sigma}_i = F(\sigma_i, S_i), \quad (7.1)$$

with  $F$  a nonlinear function of its arguments. The dynamic equations controlling the time evolution of the synaptic strengths  $j_{ik}(t)$  are much more involved and only partially understood, and usually it is assumed that the  $j$ -dynamics is such that it produces the synaptic couplings. The simplest version of a neural network model is the *Hopfield model* [Hopfield (1982)]. In this model the neuron activities are conveniently and conventionally taken to be *switch*-like, namely  $\pm 1$ , and the time  $t$  is also an integer-valued quantity. This *all*(+1) or *none*(-1) neural activity  $\sigma_i$  is based on the neurophysiology. The choice  $\pm 1$  is more natural the usual 'binary' one ( $b_i = 1$  or  $0$ ), from a physicist's point of view corresponding to a two-state system, like the fundamental elements of the ferromagnet, i.e., the electrons with their spins up (+) or (-).

The increase of time  $t$  by one unit corresponds to one step for the dynamics of the neuron activities obtainable by applying (for all  $i$ ) the rule

$$\sigma_i(t + \frac{i+1}{N}) = \text{sign}(S_i(t + i/N)), \quad (7.2)$$

which provides a rather explicit form for (7.1). If, as suggested by the Hebb rules, the  $j$  matrix is *symmetric* ( $j_{ik} = j_{ki}$ ), the Hopfield dynamics [Hopfield (1982)] corresponds to a sequential algorithm for looking for the minimum of the Hamiltonian

$$H = -S_i(t)\sigma_i(t) = -j_{ik}\sigma_i(t)\sigma_k(t).$$

The Hopfield model, at this stage, is very similar to the dynamics of a statistical mechanics *Ising-type* [Goldenfeld (1992)], or more generally a *spin-glass*, model [Stein (1992)]. This *mapping* of the Hopfield model to a spin-glass model is highly advantageous because we have now a justification

for using the statistical mechanics language of phase transitions, like critical points or attractors, etc, to describe neural dynamics and thus brain dynamics. This simplified Hopfield model has many *attractors*, corresponding to many different *equilibrium* or *ordered* states, endemic in spin-glass models, and an unavoidable prerequisite for successful storage, in the brain, of many different patterns of activities. In the neural network framework, it is believed that an internal representation (i.e., a pattern of neural activities) is associated with each object or category that we are capable of recognizing and remembering. According to neurophysiology, it is also believed that an object is memorized by suitably changing the synaptic strengths. *Associative memory* then is produced in this scheme as follows [Nanopoulos (1995)]: An external stimulus, suitably involved, produces synaptic strengths such that a specific learned pattern  $\sigma_i(0) = P_i$  is 'printed' in such a way that the neuron activities  $\sigma_i(t) \sim P_i$  (II *learning*), meaning that the  $\sigma_i$  will remain for all times close to  $P_i$ , corresponding to a stable attractor point (III *coded brain*). Furthermore, if a *replication signal* is applied, pushing the neurons to  $\sigma_i$  values *partially* different from  $P_i$ , the neurons should evolve toward the  $P_i$ . In other words, the memory is able to retrieve the information on the whole object, from the knowledge of a part of it, or even in the presence of wrong information (IV *recall process*). Clearly, if the external stimulus is very different from any preexisting  $\sigma_i = P_i$  pattern, it may either create a new pattern, i.e., create a new attractor point, or it may reach a chaotic, random behavior (I *uncoded brain*).

Despite the remarkable progress that has been made during the last few years in understanding brain function using the neural network paradigm, it is fair to say that neural networks are rather artificial and a very long way from providing a realistic model of brain function. It seems likely that the mechanisms controlling the changes in synaptic connections are much more complicated and involved than the ones considered in NN, as utilizing cytoskeletal restructuring of the sub-synaptic regions. *Brain plasticity* seems to play an essential, central role in the workings of the brain! Furthermore, the 'binding problem, i.e., how to *bind* together all the neurons firing to different features of the same object or category, especially when more than one object is perceived during a *single* conscious perceptual moment, seems to remain unanswered [Nanopoulos (1995)]. In this way, we have come a long way since the times of the 'grandmother neuron', where a *single* brain location was invoked for self observation and control, identified with the pineal glands by Descartes [Amit (1989)].

It has been long suggested that different groups of neurons, respond-

ing to a common object/category, fire *synchronously*, implying *temporal correlations* [Singer and Gray (1995)]. If true, such correlated firing of neurons may help us in resolving the binding problem [Crick (1994)]. Actually, brain waves recorded from the scalp, i.e., the EEGs, suggest the existence of some sort of *rhythms*, e.g., the ' $\alpha$ -rhythms' of a frequency of 10 Hz. More recently, oscillations were clearly observed in the visual cortex. Rapid oscillations, above EEG frequencies in the range of 35 to 75 Hz, called the ' $\gamma$ -oscillations' or the '40 Hz oscillations', have been detected in the cat's visual cortex [Singer and Gray (1995)]. Furthermore, it has been shown that these oscillatory responses can become *synchronized* in a stimulus-dependent manner. Studies of auditory-evoked responses in humans have shown inhibition of the 40 Hz coherence with *loss of consciousness* due to the induction of general anesthesia [Sayers and Beagley (1974)]. These striking results have prompted Crick and Koch to suggest that this *synchronized firing* on, or near, the beat of a ' $\gamma$ -oscillation' (in the 35–75 Hz range) might be the *neural correlate* of *visual awareness* [Crick (1994)]. Such a behavior would be, of course, a very special case of a much more general framework where coherent firing of *widely-distributed, non-local* groups of neurons, in the 'beats' of  $x$ -oscillation (of specific frequency ranges), *bind* them together in a mental representation, expressing the *oneness* of *consciousness* or *unitary sense of self*. While this is a bold suggestion [Crick (1994)], it should be stressed that in a physicist's language it corresponds to a phenomenological explanation, not providing the underlying physical mechanism, based on neuron dynamics, that triggers the synchronized neuron firing [Nanopoulos (1995)]. On the other hand, the *Crick-Koch proposal* [Crick and Koch (1990); Crick (1994)] is very suggestive (see Figure 7.33 below) and in compliance with our central biodynamic adjunction,

$$\text{coordination} = \text{sensory} \dashv \text{motor} : \text{brain} \rightleftarrows \text{body}.$$

## 7.2 Human Nervous System

In this section we proceed with a more formal, *neuroscience*, a medical field of study which deals with the structure, function, development, chemistry, pharmacology and pathology of the *human nervous system*. The biological study of the brain is an interdisciplinary field which involves many levels of study, from the molecular level through the cellular level (individual neurons), the level of relatively small assemblies of neurons like cortical

columns, that of larger subsystems like that which subserves visual perception, up to large systems like the cerebral cortex or the cerebellum, and at the highest level the nervous system as a whole. At this highest level the field largely merges with cognitive neuroscience, a discipline first populated mostly by cognitive psychologists, currently becoming a dynamic specialty of its own. Thus, the concern of neuroscience includes such diverse topics as the operation of neurotransmitters at the synapse; how genes contribute to neural development in the embryo and throughout life, including learning; the operation of relatively simpler neural structures of other organisms like marine snails; and the structure and functioning of complex neural circuits in perceiving, remembering, and speaking. Closely related and overlapping fields, besides cognitive neuroscience, include neurology, psychopharmacology, aphasiology, neurolinguistics, and several others.

The general function of the *nervous system* is to orchestrate the integration and communication of other body systems. These processes are accomplished by nerve impulses and are facilitated by neurons throughout the body. The nervous system of an animal coordinates muscle movement, monitors the organs, constructs and processes impressions from the senses, and initiates actions. In animals with brains, it also generates and conducts thoughts and emotions. Chemicals that target the activity of nerves generally are the most rapidly acting toxins, typically causing paralysis and/or death (see [Marieb (1998); Wikipedia (2005); Gowitzke and Milner (1988); Ivancevic and Snoswell (2000)]).

### 7.2.1 *Building Blocks of the Nervous System*

The nervous system consists basically of two types of cells: neurons and glia. *Neurons* (also called nerve cells, see Figure 7.1, as well as Figure 1.3 in the Introduction) are the primary cells, morphologic and functional units of the nervous system. They are found in the brain, the spinal cord and in the peripheral nerves and ganglia. Neurons consist of four major parts, including the *dendrites* (shorter projections), which are responsible for receiving stimuli; the *axon* (longer projection), which sends the nerve impulse away from the cell; the *cell body*, which is the site of metabolic activity in the cell; and the *axon terminals*, which connect neurons to other neurons, or neurons to other body structures. Each neuron can have several hundred axon terminals that attach to another neuron multiple times, attach to multiple neurons, or both. Some types of neurons, such as Purkinje cells, have over 1000 dendrites. The body of a neuron, from which the axon and dendrites

project, is called the soma and holds the nucleus of the cell. The nucleus typically occupies most of the volume of the soma and is much larger in diameter than the axon and dendrites, which typically are only about a micrometer thick or less. Neurons join to one another and to other cells through synapses.

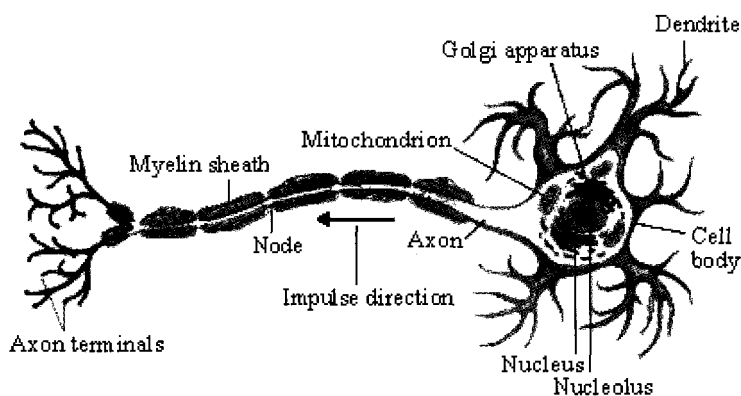


Fig. 7.1 A typical neuron, containing all of the usual cell organelles. However, it is highly specialized for the conductance of nerve impulse.

A defining feature of neurons is their ability to become 'electrically excited', that is, to undergo an action potential—and to convey this excitation rapidly along their axons as an impulse. The narrow cross section of axons and dendrites lessens the metabolic expense of conducting action potentials, although fatter axons convey the impulses more rapidly, generally speaking.

Many neurons have insulating sheaths of myelin around their axons, which enable their action potentials to travel faster than in unmyelinated axons of the same diameter. Formed by glial cells, the myelin sheathing normally runs along the axon in sections about 1 mm long, punctuated by unsheathed nodes of Ranvier. Neurons and glia make up the two chief cell types of the nervous system.

An action potential that arrives at its terminus in one neuron may provoke an action potential in another through release of neurotransmitter molecules across the synaptic gap.

There are three structural classes of neurons in the human body (see Figure 7.2):



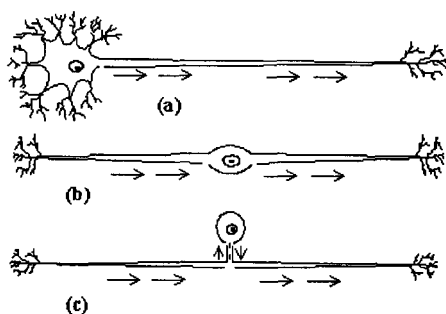


Fig. 7.2 Three structural classes of human neurons: (a) multipolar, (b) bipolar, and (c) unipolar .

- (1) The *multipolar neurons*, the majority of neurons in the body, in particular in the central nervous system.
- (2) The *bipolar neurons*, sensory neurons found in the special senses.
- (3) The *unipolar neurons*, sensory neurons located in dorsal root ganglia.

#### 7.2.1.1 Neuronal Circuits

Figure 7.3 depicts a general model of a convergent circuit, showing two neurons converging on one neuron. This allows one neuron or *neuronal pool* to receive input from multiple sources. For example, the neuronal pool in the brain that regulates rhythm of breathing receives input from other areas of the brain, baroreceptors, chemoreceptors, and stretch receptors in the lungs.

*Glia* are specialized cells of the nervous system whose main function is to 'glue' neurons together. Specialized glia called *Schwann cells* secrete myelin sheaths around particularly long axons. Glia of the various types greatly outnumber the actual neurons.

The human nervous system consists of the central and peripheral parts (see Figure 7.4). The *central nervous system* (CNS) refers to the core nervous system, which consists of the *brain* and *spinal cord* (as well as *spinal nerves*). The *peripheral nervous system* (PNS) consists of the nerves and neurons that reside or extend outside the central nervous system—to serve the limbs and organs, for example. The peripheral nervous system is further divided into the somato-motoric nervous system and the autonomic nervous system (see Figure 7.5).

The CNS is further divided into two parts: the *brain* and the *spinal*

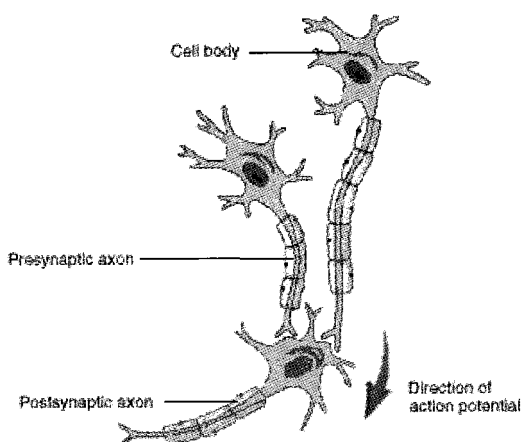


Fig. 7.3 A convergent neural circuit: nerve impulses arriving at the same neuron.

*cord*. The average adult human brain weighs 1.3 to 1.4 kg (approximately 3 pounds). The brain contains about 100 billion nerve cells (neurons) and trillions of 'support cells' called glia. Further divisions of the human brain are depicted in Figure 7.6. The spinal cord is about 43 cm long in adult women and 45 cm long in adult men and weighs about 35–40 grams. The vertebral column, the collection of bones (back bone) that houses the spinal cord, is about 70 cm long. Therefore, the spinal cord is much shorter than the vertebral column.

The PNS is further divided into two major parts: the *somatic nervous system* and the *autonomic nervous system*.

The somatic nervous system consists of *peripheral nerve fibers* that send sensory information to the central nervous system and *motor nerve fibers* that project to skeletal muscle.

The autonomic nervous system (ANS) controls smooth muscles of the viscera (internal organs) and glands. In most situations, we are unaware of the workings of the ANS because it functions in an involuntary, reflexive manner. For example, we do not notice when blood vessels change size or when our heart beats faster. The ANS is most important in two situations:

- (1) In *emergencies* that cause stress and require us to 'fight' or take 'flight', and
- (2) In *non-emergencies* that allow us to 'rest' and 'digest'.

The ANS is divided into three parts:

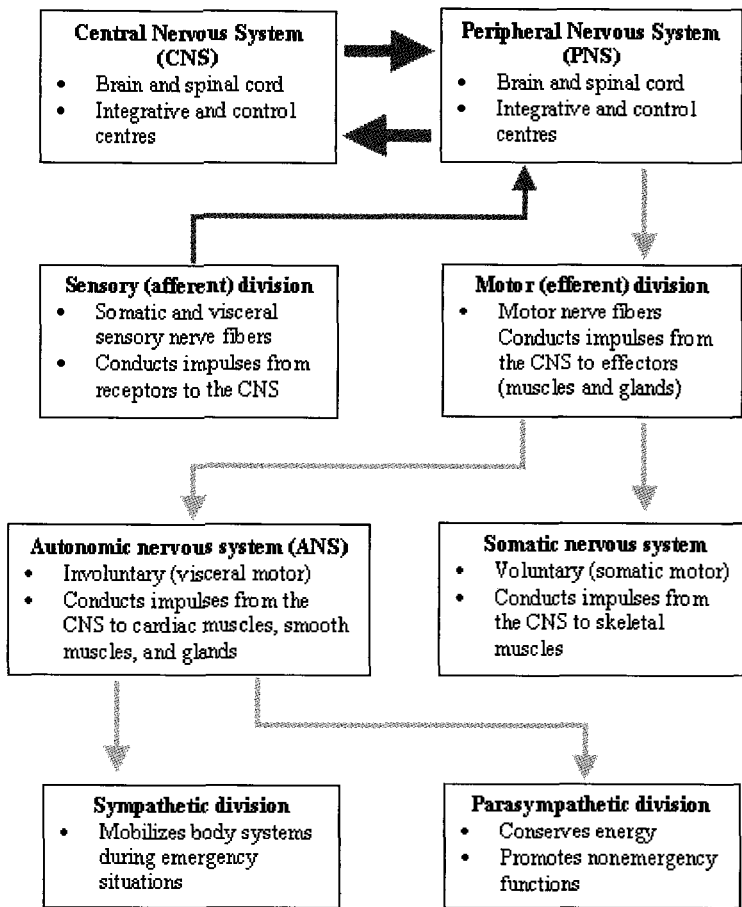


Fig. 7.4 Organization of the human nervous system.

- (1) The *sympathetic nervous system* (see Figure 7.7),
- (2) The *parasympathetic nervous system* (see Figure 7.8), and
- (3) The *enteric nervous system*, which is a meshwork of nerve fibers that innervate the viscera (gastrointestinal tract, pancreas, gall bladder).

In the PNS, neurons can be functionally divided in 3 ways:

- (1)
  - *sensory (afferent)* neurons – carry information into the CNS from sense organs, and
  - *motor (efferent)* neurons – carry information away from the CNS

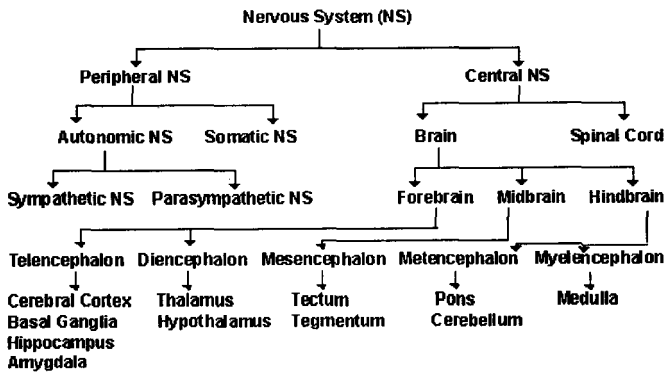


Fig. 7.5 Basic divisions of the human nervous system.

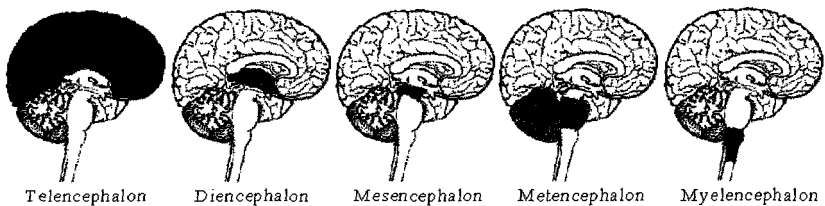


Fig. 7.6 Basic divisions of the human Brain.

(for muscle control).

- (2)
  - *cranial* neurons – connect the brain with the periphery, and
  - *spinal* neurons – connect the spinal cord with the periphery.
- (3)
  - *somatic* neurons – connect the skin or muscle with the central nervous system, and
  - *visceral* neurons – connect the internal organs with the central nervous system.

Some differences between the PNS and the CNS are:

- (1)
  - In the CNS, collections of neurons are called *nuclei*.
  - In the PNS, collections of neurons are called *ganglia*.
- (2)
  - In the CNS, collections of axons are called *tracts*.
  - In the PNS, collections of axons are called *nerves*.

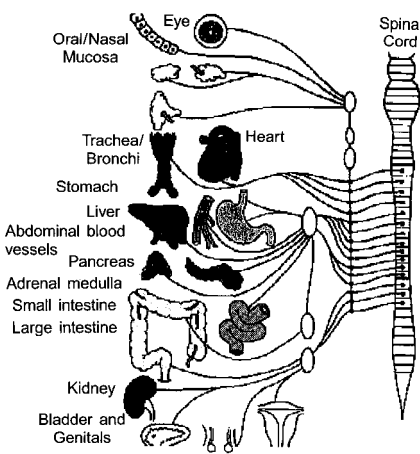


Fig. 7.7 Basic functions of the sympathetic nervous system.

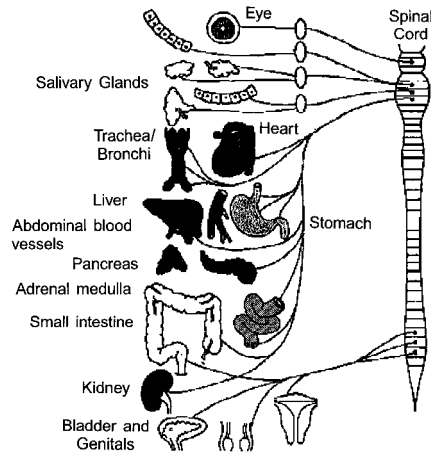


Fig. 7.8 Basic functions of the parasympathetic nervous system.

7.2.1.2 Basic Brain Partitions and Their Functions

**Cerebral Cortex.** The word ‘cortex’ comes from the Latin word for ‘bark’ (of a tree). This is because the cortex is a sheet of tissue that makes up the outer layer of the brain. The thickness of the cerebral cortex varies from 2 to 6 mm. The right and left sides of the cerebral cortex are connected by a

thick band of nerve fibers called the 'corpus callosum'. In higher mammals such as humans, the cerebral cortex looks like it has many bumps and grooves. A bump or bulge on the cortex is called a gyrus (the plural of the word gyrus is 'gyri') and a groove is called a sulcus (the plural of the word sulcus is 'sulci'). Lower mammals like rats and mice have very few gyri and sulci. The main cortical functions are: *thought, voluntary movement, language, reasoning, and perception.*

**Cerebellum.** The word 'cerebellum' comes from the Latin word for 'little brain'. The cerebellum is located behind the brain stem. In some ways, the cerebellum is similar to the cerebral cortex: the cerebellum is divided into hemispheres and has a cortex that surrounds these hemispheres. Its main functions are: *movement, balance, and posture.*

**Brain Stem.** The brain stem is a general term for the area of the brain between the *thalamus* and spinal cord. Structures within the brain stem include the medulla, pons, tectum, reticular formation and tegmentum. Some of these areas are responsible for the most basic functions of life such as breathing, heart rate and blood pressure. Its main functions are: *breathing, heart rate, and blood pressure.*

**Hypothalamus.** The *hypothalamus* is composed of several different areas and is located at the base of the brain. Although it is the size of only a pea (about 1/300 of the total brain weight), the hypothalamus is responsible for some very important functions. One important function of the hypothalamus is the control of body temperature. The hypothalamus acts like a 'thermostat' by sensing changes in body temperature and then sending signals to adjust the temperature. For example, if we are too hot, the hypothalamus detects this and then sends a signal to expand the capillaries in your skin. This causes blood to be cooled faster. The hypothalamus also controls the pituitary. Its main functions are: *body temperature, emotions, hunger, thirst, sexual instinct, and circadian rhythms.* The *hypothalamus* is 'the boss' of the ANS.

**Thalamus.** The thalamus receives sensory information and relays this information to the cerebral cortex. The cerebral cortex also sends information to the thalamus which then transmits this information to other areas of the brain and spinal cord. Its main functions are: *sensory processing and movement.*

**Limbic System.** The limbic system (or the limbic areas) is a group of structures that includes the amygdala, the hippocampus, mammillary bodies and cingulate gyrus. These areas are important for controlling the emotional response to a given situation. The hippocampus is also important

for memory. Its main function is *emotions*.

**Hippocampus.** The hippocampus is one part of the limbic system that is important for memory and learning. Its main functions are: *learning* and *memory*.

**Basal Ganglia.** The basal ganglia are a group of structures, including the globus pallidus, caudate nucleus, subthalamic nucleus, putamen and substantia nigra, that are important in coordinating movement. Its main function is *movement*.

**Midbrain.** The midbrain includes structures such as the superior and inferior colliculi and red nucleus. There are several other areas also in the midbrain. Its main functions are: *vision*, *audition*, *eye movement*, and *body movement*.

### 7.2.1.3 Nerves

A *nerve* is an enclosed, cable-like bundle of *nerve fibers* or *axons*, which includes the glia that ensheath the axons in myelin (see [Marieb (1998); Wikipedia (2005); Gowitzke and Milner (1988); Ivancevic and Snoswell (2000)]).

Nerves are part of the peripheral nervous system. *Afferent nerves* convey sensory signals to the brain and spinal cord, for example from skin or organs, while *efferent* nerves conduct stimulatory signals from the *motor neurons* of the brain and spinal cord to the muscles and glands.

These signals, sometimes called nerve impulses, are also known as action potentials: Rapidly travelling electrical waves, which begin typically in the cell body of a neuron and propagate rapidly down the axon to its tip or terminus'.

Nerves may contain fibers that all serve the same purpose; for example *motor nerves*, the axons of which all terminate on muscle fibers and stimulate contraction. Or they be *mixed nerves*.

An *axon*, or 'nerve fibre', is a long slender projection of a nerve cell or neuron, which conducts electrical impulses away from the neuron's cell body or soma. Axons are in effect the primary transmission lines of the nervous system, and as bundles they help make up nerves. The axons of many neurons are sheathed in myelin.

On the other hand, a *dendrite* is a slender, typically branched projection of a nerve cell or neuron, which conducts the electrical stimulation received from other cells through synapses to the body or soma of the cell from which it projects.

Many dendrites convey this stimulation passively, meaning without action potentials and without activation of voltage-gated ion channels. In such dendrites the voltage change that results from stimulation at a synapse may extend both towards and away from the soma. In other dendrites, though an action potential may not arise, nevertheless voltage-gated channels help to propagate excitatory synaptic stimulation. This propagation is efficient only toward the soma due to an uneven distribution of channels along such dendrites.

The structure and branching of a neuron's dendrites strongly influences how it integrates the input from many others, particularly those that input only weakly (more at synapse). This integration is in aspects 'temporal'—involving the summation of stimuli that arrive in rapid succession—as well as 'spatial'—entailing the aggregation of excitatory and inhibitory inputs from separate branches or 'arbors'.

*Spinal nerves* take their origins from the spinal cord. They control the functions of the rest of the body. In humans, there are 31 pairs of spinal nerves: 8 *cervical*, 12 *thoracic*, 5 *lumbar*, 5 *sacral* and 1 *coccygeal*.

#### 7.2.1.4 *Action potential*

As the travelling signals of nerves and as the localized changes that contract muscle cells, *action potentials* are an essential feature of animal life. They set the pace of thought and action, constrain the sizes of evolving anatomies and enable centralized control and coordination of organs and tissues (see [Marieb (1998); Wikipedia (2005); Gowitzke and Milner (1988); Ivancevic and Snoswell (2000)]).

**Basic Features.** When a biological cell or patch of membrane undergoes an action potential, the polarity of the transmembrane voltage swings rapidly from negative to positive and back. Within any one cell, consecutive action potentials typically are indistinguishable. Also between different cells the amplitudes of the voltage swings tend to be roughly the same. But the speed and simplicity of action potentials vary significantly between cells, in particular between different cell types.

Minimally, an action potential involves a *depolarization*, a *repolarization* and finally a *hyperpolarization* (or 'undershoot'). In specialized muscle cells of the heart, such as the pacemaker cells, a 'plateau phase' of intermediate voltage may precede repolarization.

**Underlying Mechanism.** The transmembrane voltage changes that take place during an action potential result from changes in the permeability



of the membrane to specific ions, the internal and external concentrations of which are in imbalance. In the axon fibers of nerves, depolarization results from the inward rush of sodium ions, while repolarization and hyperpolarization arise from an outward rush of potassium ions. Calcium ions make up most or all of the depolarizing currents at an axon's pre-synaptic terminus, in muscle cells and in some dendrites.

The imbalance of ions that makes possible not only action potentials but the resting cell potential arises through the work of pumps, in particular the sodium-potassium exchanger.

Changes in membrane permeability and the onset and cessation of ionic currents reflect the opening and closing of 'voltage-gated' ion channels, which provide portals through the membrane for ions. Residing in and spanning the membrane, these enzymes sense and respond to changes in transmembrane potential.

**Initiation.** Action potentials are triggered by an initial depolarization to the point of *threshold*. This threshold potential varies but generally is about 15 millivolts above the resting potential of the cell. Typically action potential initiation occurs at a synapse, but may occur anywhere along the axon. In his discovery of 'animal electricity', L. Galvani elicited an action potential through contact of his scalpel with the motor nerve of a frog he was dissecting, causing one of its legs to kick as in life.

**Wave Propagation.** In the fine fibers of simple (or 'unmyelinated') axons, action potentials propagate as waves, which travel at speeds up to 120 meters per second.

The propagation speed of these 'impulses' is faster in fatter fibers than in thin ones, other things being equal. In their *Nobel Prize* winning work uncovering the wave nature and ionic mechanism of action potentials, *Alan L. Hodgkin* and *Andrew F. Huxley* performed their celebrated experiments on the 'giant fibre' of Atlantic squid [Hodgkin and Huxley (1952)]. Responsible for initiating flight, this axon is fat enough to be seen without a microscope (100 to 1000 times larger than is typical). This is assumed to reflect an adaptation for speed. Indeed, the velocity of nerve impulses in these fibers is among the fastest in nature.

**Saltatory propagation.** Many neurons have insulating sheaths of myelin surrounding their axons, which enable action potentials to travel faster than in unmyelinated axons of the same diameter. The myelin sheathing normally runs along the axon in sections about 1 mm long, punctuated by unsheathed 'nodes of Ranvier'.

Because the salty cytoplasm of the axon is electrically conductive, and

because the myelin inhibits charge leakage through the membrane, depolarization at one node is sufficient to elevate the voltage at a neighboring node to the threshold for action potential initiation. Thus in myelinated axons, action potentials do not propagate as waves, but recur at successive nodes and in effect hop along the axon. This mode of propagation is known as *saltatory conduction*. Saltatory conduction is faster than smooth conduction. Some typical action potential velocities are as follows:

Fiber	Diameter	AP Velocity
Unmyelinated	0.2–1.0 micron	0.2–2 m/sec
Myelinated	2–20 microns	12–120 m/sec

The disease called *multiple sclerosis* (MS) is due to a breakdown of myelin sheathing, and degrades muscle control by destroying axons' ability to conduct action potentials.

**Detailed Features.** Depolarization and repolarization together are complete in about two milliseconds, while undershoots can last hundreds of milliseconds, depending on the cell. In neurons, the exact length of the roughly two-millisecond delay in repolarization can have a strong effect on the amount of neurotransmitter released at a synapse. The duration of the hyperpolarization determines a nerve's 'refractory period' (how long until it may conduct another action potential) and hence the frequency at which it will fire under continuous stimulation. Both of these properties are subject to biological regulation, primarily (among the mechanisms discovered so far) acting on ion channels selective for potassium.

A cell capable of undergoing an action potential is said to be *excitable*.

#### 7.2.1.5 *Synapses*

Synapses are specialized junctions through which cells of the nervous system signal to one another and to non-neuronal cells such as muscles or glands (see Figure 7.9). Synapses define the circuits in which the neurons of the central nervous system interconnect. They are thus crucial to the biological computations that underlie perception and thought. They also provide the means through which the nervous system connects to and controls the other systems of the body (see [Marieb (1998); Wikipedia (2005); Gowitzke and Milner (1988); Ivancevic and Snoswell (2000)]).

**Anatomy and Structure.** At a classical synapse, a mushroom-shaped bud projects from each of two cells and the caps of these buds press flat against one another (see Figure 7.10). At this interface, the membranes of the two cells flank each other across a slender gap, the narrowness of which

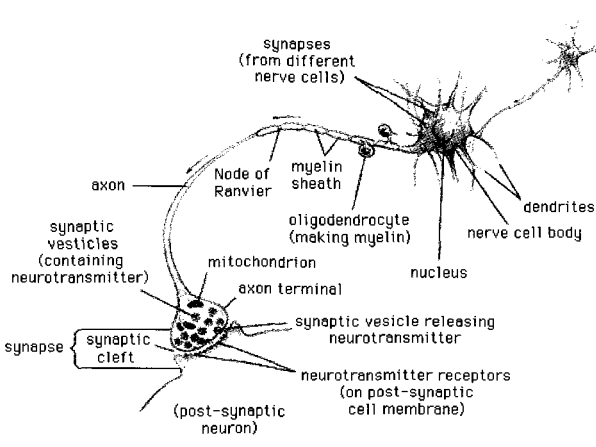


Fig. 7.9 Neuron forming a synapse.

enables signaling molecules known as neurotransmitters to pass rapidly from one cell to the other by diffusion. This gap is sometimes called the synaptic cleft.

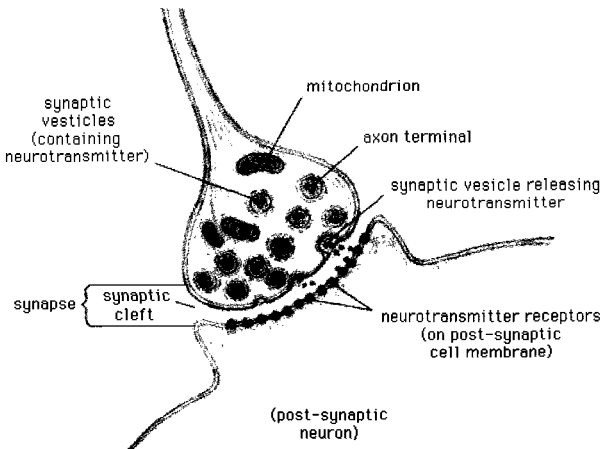


Fig. 7.10 Structure of a chemical synapse.

Synapses are asymmetric both in structure and in how they operate. Only the so-called pre-synaptic neuron secretes the neurotransmitter, which binds to receptors facing into the synapse from the post-synaptic cell. The pre-synaptic nerve terminal generally buds from the tip of an axon,

while the post-synaptic target surface typically appears on a dendrite, a cell body or another part of a cell.

**Signalling across the Synapse.** The release of neurotransmitter is triggered by the arrival of a nerve impulse (or action potential) and occurs through an unusually rapid process of cellular secretion: Within the pre-synaptic nerve terminal, vesicles containing neurotransmitter sit 'docked' and ready at the synaptic membrane. The arriving action potential produces an influx of calcium ions through voltage-dependent, calcium-selective ion channels, at which point the vesicles fuse with the membrane and release their contents to the outside. Receptors on the opposite side of the synaptic gap bind neurotransmitter molecules and respond by opening nearby ion channels in the post-synaptic cell membrane, causing ions to rush in or out and changing the local transmembrane potential of the cell. The result is *excitatory*, in the case of depolarizing currents, or *inhibitory* in the case of hyperpolarizing currents. Whether a synapse is excitatory or inhibitory depends on what type(s) of ion channel conduct the post-synaptic current, which in turn is a function of the type of receptors and neurotransmitter employed at the synapse.

Excitatory synapses in the brain show several forms of synaptic plasticity, including long-term potentiation (LTP) and long-term depression (LTD), which are initiated by increases in intracellular  $Ca^{2+}$  that are generated through NMDA (N-methyl-D-aspartate) receptors or voltage-sensitive  $Ca^{2+}$  channels. LTP depends on the coordinated regulation of an ensemble of enzymes, including  $Ca^{2+}$ /calmodulin-dependent protein kinase II, adenylyl cyclase 1 and 8, and calcineurin, all of which are stimulated by calmodulin, a  $Ca^{2+}$ -binding protein. [Xia and Storm (2005)] discussed the hypothesis that calmodulin is a central integrator of synaptic plasticity and that its unique regulatory properties allow the integration of several forms of signal transduction that are required for LTP and LTD.

**Synaptic strength.** The amount of current, or more strictly the change in transmembrane potential, depends on the 'strength' of the synapse, which is subject to biological regulation. One regulatory mechanism involves the simple coincidence of action potentials in the synaptically linked cells. Because the coincidence of sensory stimuli (the sound of a bell and the smell of meat, for example, in the experiments by *Nobel Laureate Ivan P. Pavlov*) can give rise to associative learning or conditioning, neuroscientists have hypothesized that synaptic strengthening through coincident activity in two neurons might underlie learning and memory. This is known as the *Hebbian theory* [Hebb (1949)]. It is related to *Pavlov's*

*conditional-reflex learning*: it is learning that takes place when we come to associate two stimuli in the environment. One of these stimuli triggers a reflexive response. The second stimulus is originally neutral with respect to that response, but after it has been paired with the first stimulus, it comes to trigger the response in its own right.

### Biophysics of Synaptic Transmission.

Technically, synaptic transmission happens in transmitter-activated ion channels. Activation of a presynaptic neuron results in a release of neurotransmitters into the synaptic cleft. The transmitter molecules diffuse to the other side of the cleft and activate receptors that are located in the postsynaptic membrane. So-called ionotropic receptors have a direct influence on the state of an associated ion channel whereas metabotropic receptors control the state of the ion channel by means of a biochemical cascade of  $g$ -proteins and second messengers. In any case the activation of the receptor results in the opening of certain ion channels and, thus, in an excitatory or inhibitory postsynaptic current (EPSC or IPSC, respectively). The transmitter-activated ion channels can be described as an explicitly time-dependent conductivity  $g_{syn}(t)$  that will open whenever a presynaptic spike arrives. The current that passes through these channels depends, as usual, on the difference of its reversal potential  $E_{syn}$  and the actual value of the membrane potential,

$$I_{syn}(t) = g_{syn}(t)(u - E_{syn}).$$

The parameter  $E_{syn}$  and the function  $g_{syn}(t)$  can be used to characterize different types of synapse. Typically, a superposition of exponentials is used for  $g_{syn}(t)$ . For inhibitory synapses  $E_{syn}$  equals the reversal potential of potassium ions (about -75 mV), whereas for excitatory synapses  $E_{syn} \approx 0$ .

The effect of fast *inhibitory* neurons in the central nervous system of higher vertebrates is almost exclusively conveyed by a neuro-transmitter called  $\gamma$ -aminobutyric acid, or GABA for short. In addition to many different types of inhibitory interneurons, cerebellar Purkinje cells form a prominent example of projecting neurons that use GABA as their neuro-transmitter. These neurons synapse onto neurons in the deep cerebellar nuclei (DCN) and are particularly important for an understanding of cerebellar function.

The parameters that describe the conductivity of transmitter-activated ion channels at a certain synapse are chosen so as to mimic the time course and the amplitude of experimentally observed spontaneous postsynaptic currents. For example, the conductance  $\tilde{g}_{syn}(t)$  of inhibitory synapses in

DCN neurons can be described by a simple exponential decay with a time constant of  $\tau = 5$  ms and an amplitude of  $\bar{g}_{syn} = 40$  pS,

$$g_{syn}(t) = \sum_f \bar{g}_{syn} \exp\left(-\frac{t - t^{(f)}}{\tau}\right) \Theta(t - t^{(f)}),$$

where  $t^{(f)}$  denotes the arrival time of a presynaptic action potential. The reversal potential is given by that of potassium ions, viz.  $E_{syn} = -75$  mV (see [Gabbiani *et al.* (1994)]).

Clearly, more attention can be paid to account for the details of synaptic transmission. In cerebellar granule cells, for example, inhibitory synapses are also GABAergic, but their postsynaptic current is made up of two different components. There is a fast component, that decays with a time constant of about 5 ms, and there is a component that is ten times slower. The underlying postsynaptic conductance is thus of the form

$$g_{syn}(t) = \sum_f \left( \bar{g}_{fast} \exp\left(-\frac{t - t^{(f)}}{\tau_{fast}}\right) + \bar{g}_{slow} \exp\left(-\frac{t - t^{(f)}}{\tau_{slow}}\right) \right) \Theta(t - t^{(f)}).$$

Now, most of *excitatory* synapses in the vertebrate central nervous system rely on glutamate as their neurotransmitter. The postsynaptic receptors, however, can have very different pharmacological properties and often different types of glutamate receptors are present in a single synapse. These receptors can be classified by certain amino acids that may be selective agonists. Usually, NMDA (N-methyl-D-aspartate) and non-NMDA receptors are distinguished. The most prominent among the non-NMDA receptors are AMPA-receptors. Ion channels controlled by AMPA-receptors are characterized by a fast response to presynaptic spikes and a quickly decaying postsynaptic current. NMDA-receptor controlled channels are significantly slower and have additional interesting properties that are due to a voltage-dependent blocking by magnesium ions (see [Gabbiani *et al.* (1994)]).

Excitatory synapses in cerebellar granule cells, for example, contain two different types of glutamate receptors, viz. AMPA- and NMDA-receptors. The time course of the postsynaptic conductivity caused by an activation of AMPA-receptors at time  $t = t^{(f)}$  can be described as follows,

$$g_{AMPA}(t) = \bar{g}_{AMPA} \cdot N \cdot \left( \exp\left(-\frac{t - t^{(f)}}{\tau_{decay}}\right) - \exp\left(-\frac{t - t^{(f)}}{\tau_{rise}}\right) \right) \Theta(t - t^{(f)}),$$

with rise time  $\tau_{rise} = 0.09$  ms, decay time  $\tau_{decay} = 1.5$  ms, and maximum conductance  $\bar{g}_{AMPA} = 720$  pS. The numerical constant  $N = 1.273$  normalizes the maximum of the braced term to unity (see [Gabbiani *et al.* (1994)]).

NMDA-receptor controlled channels exhibit a significantly richer repertoire of dynamic behavior because their state is not only controlled by the presence or absence of their agonist, but also by the membrane potential. The voltage dependence itself arises from the blocking of the channel by a common extracellular ion,  $Mg^{2+}$ . Unless  $Mg^{2+}$  is removed from the extracellular medium, the channels remain closed at the resting potential even in the presence of NMDA. If the membrane is depolarized beyond  $-50$  mV, then the  $Mg^{2+}$ -block is removed, the channel opens, and, in contrast to AMPA-controlled channels, stays open for 10–100 milliseconds. A simple ansatz that accounts for this additional voltage dependence of NMDA-controlled channels in cerebellar granule cells is

$$g_{NMDA}(t) = \bar{g}_{NMDA} \cdot N \cdot \left( \exp\left(-\frac{t - t^{(f)}}{\tau_{decay}}\right) - \exp\left(-\frac{t - t^{(f)}}{\tau_{rise}}\right) \right) g_{\infty} \Theta(t - t^{(f)}),$$

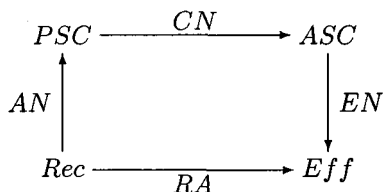
where  $g_{\infty} = (1 + e^{\alpha u} [Mg^{2+}]_o / \beta)$ ,  $\tau_{rise} = 3$  ms,  $\tau_{decay} = 40$  ms,  $N = 1.358$ ,  $\bar{g}_{NMDA} = 1.2$  nS,  $\alpha = 0.062$  mV $^{-1}$ ,  $\beta = 3.57$  mM, and the extracellular magnesium concentration  $[Mg^{2+}]_o = 1.2$  mM (see [Gabbiani *et al.* (1994)]).

Finally, Though NMDA-controlled ion channels are permeable to sodium and potassium ions, their permeability to  $Ca^{2+}$  is even five or ten times larger. Calcium ions are known to play an important role in intracellular signaling and are probably also involved in long-term modifications of synaptic efficacy. Calcium influx through NMDA-controlled ion channels, however, is bound to the coincidence of presynaptic (NMDA release from presynaptic sites) and postsynaptic (removal of the  $Mg^{2+}$ -block) activity. Hence, NMDA-receptors operate as a kind of a molecular coincidence detectors as they are required for a biochemical implementation of Hebb's learning rule [Hebb (1949)].

### 7.2.2 Reflex Action: the Basis of CNS Activity

The basis of all CNS activity, as well as the simplest example of our sensory-motor adjunction, is the *reflex (sensory-motor) action, R.A.* It occurs at all neural organizational levels. We are aware of some reflex acts, while others occur without our knowledge.

In particular, the spinal reflex action is defined as a composition of neural pathways,  $RA = EN \circ CN \circ AN$ , where  $EN$  is the efferent neuron,  $AN$  is the afferent neuron and  $CN = CN_1, \dots, CN_n$  is the chain of  $n$  connector neurons ( $n = 0$  for the simplest, stretch, reflex,  $n \geq 1$  for all other reflexes). In other words, the following diagram commutes:



in which  $Rec$  is the receptor (e.g., eye),  $Eff$  is the effector (e.g., muscle),  $PSC$  is the posterior (or, dorsal) horn of the spinal cord, and  $ASC$  is the anterior (or, ventral) horn of the spinal cord. In this way defined map  $RA : Rec \rightarrow Eff$  is the simplest, *one-to-one* relation between one receptor neuron and one effector neuron (e.g., patellar reflex, Figure 7.11; also, see subsection (7.2.3.1) below).

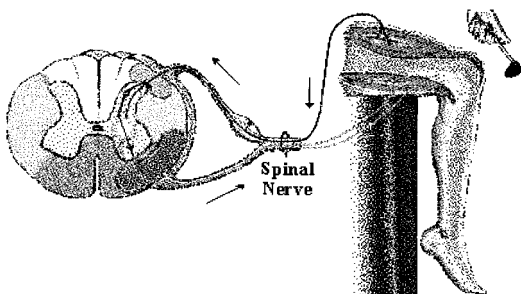


Fig. 7.11 Schematic of a simple knee-jerk reflex. Hammer strikes knee, generating sensory impulse to spinal cord. Primary neuron makes (monosynaptic, excitatory) synapse with anterior horn (motor) cell, whose axon travels via ventral root to quadriceps muscle, which contracts, raising foot. Hamstring (lower) muscle is simultaneously inhibited, via an internuncial neuron.

Now, in the majority of human reflex arcs a chain  $CN$  of many connector neurons is found. There may be link-ups with various levels of the brain and spinal cord. Every receptor neuron is potentially linked in the CNS with a large number of effector organs all over the body, i.e., the map  $RA : Rec \rightarrow Eff$  is *one-to-many*. Similarly, every effector neuron is potentially in communication with receptors all over the body, i.e., the map  $RA : Rec \rightarrow Eff$  is *many-to-one*.



However, the most frequent form of the map  $RA : Rec \rightarrow Eff$  is *many-to-many*. Other neurons synapsing with the effector neurons may give a complex link-up with centers at higher and lower levels of the CNS. In this way, higher centers in the brain can modify reflex acts which occur through the spinal cord. These centers can send suppressing or facilitating impulses along their pathways to the cells in the spinal cord [Ivancevic (1991)].

Through such 'functional' link-ups, neurons in different parts of the CNS, when active, can influence each other. This makes it possible for Pavlov's conditioned reflexes to be established. Such reflexes form the basis of all training, so that it becomes difficult to say where reflex (or involuntary) behavior ends and purely voluntary behavior begins [Anochin (1980)].

In particular, the control of voluntary movements is extremely complex. Many different systems across numerous brain areas need to work together to ensure proper motor control. Our understanding of the nervous system decreases as we move up to higher CNS structures.

### 7.2.3 The Spinal Cord Pathways

31 pairs of spinal nerves arise along the *spinal cord*. These are called 'mixed' nerves because each contain both *sensory* and *motor* axons. However, within the spinal column, all the *sensory axons* pass into the *dorsal root ganglion* where their cell bodies are located and then on into the spinal cord itself. Also, all the *motor axons* pass into the *ventral roots* before uniting with the sensory axons to form the mixed nerves (see Figure 7.12).

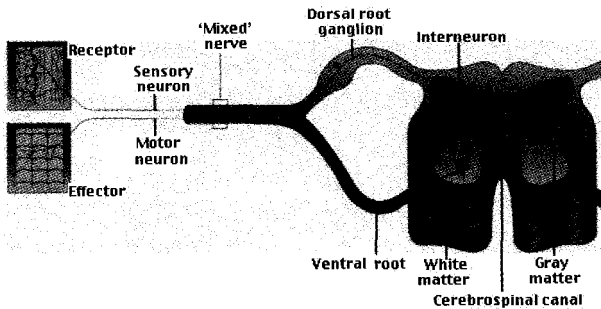


Fig. 7.12 The spinal cord with its sensory and motor axons.

The spinal cord carries out two main functions:

- It connects a large part of the peripheral nervous system to the brain. Information (nerve impulses) reaching the spinal cord through sensory neurons are transmitted up into the brain. Signals arising in the motor areas of the brain travel back down the cord and leave in the motor neurons.
- It also acts as a minor coordinating center responsible for some simple reflexes like the withdrawal reflex.

The interneurons carrying impulses to and from specific receptors and effectors are grouped together in *spinal tracts*. Impulses reaching the spinal cord from the left side of the body eventually pass over to tracts running up to the right side of the brain and vice versa. In some cases this crossing over occurs as soon as the impulses enter the cord. In other cases, it does not take place until the tracts enter the brain itself.

The *motor pathways* are pathways which originate in the brain or brainstem and descend down the spinal cord to control the  $\alpha$ -motor neurons (see Figure 7.13). These large neurons in the ventral horns of the spinal cord send their axons out via the spinal roots and directly control the muscles. The motor pathways can control posture, reflexes, and muscle tone, as well as the conscious voluntary movements that we think of when we hear 'motor system'. The most celebrated pathway is the so called 'pyramidal system', which begins with the large pyramidal neurons of the motor cortex, travels through the pyramids of the brainstem, (somewhere in here there is a coincidence), and finally ends on or near the  $\alpha$ -motor neurons.

#### 7.2.3.1 Spinal Lower Motor Neurons

Lower motor neurons (LMNs; also called alpha motor neurons), are directly responsible for generation of force by the muscles they innervate. A *motor unit* is a single LMN and all of the muscle fibers it innervates. The collection of LMNs that innervate a single muscle (say triceps) is called a *motor neuron pool*. LMNs respond to, and are therefore controlled by, inputs from three sources, dorsal root ganglia, interneurons (cells that do not project out of the area), and projections from higher centers such as the brain stem and cerebral cortex.

LMNs that control proximal and distal muscles are found mainly in the cervical and lumbosacral segments of the spinal cord. At these levels, the LMNs are distributed such that neurons controlling *axial* muscles lie *medial* to those LMNs controlling distal muscles and motor neurons controlling

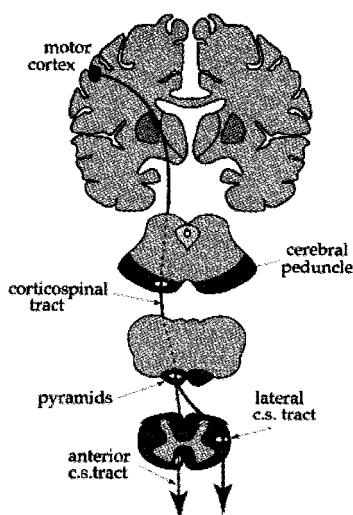


Fig. 7.13 The main pathways of the voluntary motor system.

*flexors* lie *dorsal* to those controlling extensors.

**Dorsal Root Inputs to LMNs: Stretch Reflex.** One of the most familiar reflexes is the *stretch reflex*, also known as the *knee-jerk reflex* and the *myotatic reflex* (compare with subsection (6.5.3.4) above). In its simplest form it is a 2-neuron loop, one afferent neuron and one efferent neuron. The afferent neuron is connected to a *muscle spindle*, which detects stretch in the muscle. The efferent neuron is the motor neuron, which causes the muscle to twitch. Stretch reflexes work to *resist lengthening* of a muscle. They are functionally efficient because they allow weight-bearing muscles to adjust to a changing load at the level of the spinal cord, without the information having to go all the way up to cortex for a decision.

There are actually several types of afferents reporting on the status of the muscle. Let's look more closely at the muscle spindle, which is a small group of muscle fibers walled off from the rest of the muscle by a collagen sheath (see Figure 7.14). The sheath has a spindle or 'fusiform' shape, so these fibers are called *intrafusal* fibers, and are contrasted with the *extrafusal* fibers, which are the power-generating muscle fibers. There are two types of nerve endings wrapped around this intrafusal fibre, both of which monitor its degree of stretch - as the muscle stretches, so does this capsule within it. These two *stretch receptors* are sensitive to different time

scales, however. The first is called a Ia fibre; the classification scheme is based on diameter and conduction velocity, so the Ia's are the largest and fastest. The Ia fibre fires like crazy when the muscle is stretching, but it is *rapidly adapting*. As soon as the muscle stops changing length, and holds a new position, the Ia adapts to the new length and stops firing. But we also need to know the position of our muscle when it is still. The second type of stretch receptor is called a II fibre, and it is slowly adapting. It also responds when the muscle is stretching, but it maintains a firing rate after the muscle has stopped moving (essentially, it is non-adapting). This information is part of what allows us to tell the position of our arm when our eyes are closed.

Rule of nomenclature – if there is a Ia, where is Ib? The Ib fibers are not connected to muscle spindles at all. Instead they are embedded in the tendon, and monitor overall muscle tension from there. They are also called *Golgi tendon organs*.

When the intrafusal fibre contracts, the entire spindle shortens, remaining taut, and the sensitivity is intact. There are small motor neurons in the ventral horn that innervate the intrafusal muscle fibers and cause them to contract – they are the  $\gamma$ -motor neurons. These neurons are excited every time the  $\alpha$ -motor neurons fire, so that as the muscle contracts, the intrafusals contract with it.

Now, Ia fibers are associated mainly with the nuclear bag intrafusal fibers and carry information regarding the *length* and *change in length* of the muscle. The II fibers are primarily concerned with the constant length of the muscle and thus bring information into the spinal cord from the nuclear chain fibers. These fibers are important in stretch reflexes. Stretch of the intrafusal muscle fibers results in contraction of the extrafusal muscle fibers in the same, i.e., homonymous muscle. This is a *monosynaptic reflex*, in that there is only one synapse between the incoming information and the outgoing signal to contract the muscle. It has been shown that this monosynaptic reflex takes about 1 ms; the synaptic delay between the sensory input and the LMN is between 0.5 and 0.9 ms. In the cat, a single Ia fibre makes excitatory connections with all homonymous motor neurons. This Ia *divergent* signal produces a very strong excitatory drive to the muscle within which it originates. This is called *autogenetic excitation*. The Ia fibre also makes monosynaptic connections with LMNs that innervate muscles that are *synergistic* to the homonymous muscle.

The incoming Ia fibre also synapses on a Ia *inhibitory interneuron* that in turn inhibits LMNs that innervate the antagonist muscles (stretch

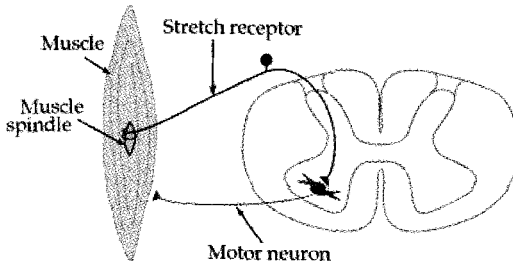


Fig. 7.14 The stretch reflex loop.

biceps—contract biceps—inhibit triceps; notice this is not a monosynaptic reflex). This is called *reciprocal innervation*. Ia inhibitory interneurons are also important for coordinating voluntary movements, as corticospinal axons make direct excitatory connections with LMNs and also send a collateral to the Ia inhibitory neuron. Thus, the cortex does not have to send separate messages to the opposing muscles.

The intrafusal muscle fibers can be controlled by the small gamma efferent neurons that lie in the ventral horn. These gamma efferent cells, which are controlled by descending inputs, bias the intrafusal muscle fibers in order to ensure that the intrafusal muscle fibers are always signaling information to the brain. For instance, contraction/shortening of the extrafusal muscle will put slack on the intrafusal fibers, and they will stop telling the brain about the length of the muscles. To get around this, the cortical input tells the gamma efferents to fire and tighten up the intrafusal muscle fibers (to keep them firing) when the extrafusal fibers contract. The gamma efferents that innervate the *bags* are called *gamma dynamics* while those targeting the *chains* are *gamma statics*.

**Inverse Stretch Reflex.** The Ib fibers are carrying information from Golgi tendon organs (GTOs, see subsection (6.5.3.4) above). Each GTO is comprised of collagen fibers intertwined with a Ib fibre. Thus, stretching of the tendon ‘squeezes’ the Ib fibre and it begins to fire. While muscle spindles are sensitive to changes in length of a muscle, GTOs are most sensitive to changes in muscle tension and thus signal the force in a muscle. GTOs provide the nervous system with precise information about the state of contraction of the muscle.

The *inverse stretch reflex* (see Figure 7.15) is also known as the *inverse myotatic reflex* or *Golgi tendon reflex*. This reflex involves Ib afferents, Ib inhibitory interneurons, and LMNs. Thus, increased firing of the Ib results

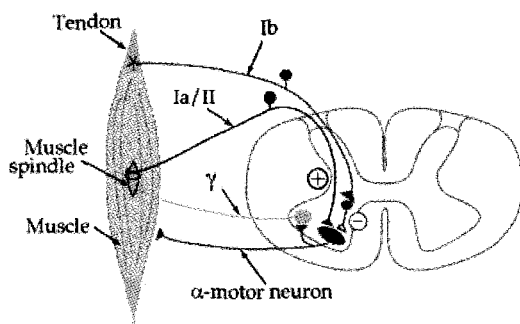


Fig. 7.15 The inverse stretch reflex loop.

in the inhibition of the homonymous muscle (*autogenetic inhibition*).

The inverse stretch reflex is *polysynaptic*, meaning that it involves more than one synapse. This reflex is therefore slower than the stretch reflex. However, the inverse stretch reflex can over-ride the stretch reflex, and serves two important functions. The first function is protective. If there is a very large stimulus, such as a strong blow to the patella tendon with a hammer, the quadriceps muscles will contract due to the stretch reflex. To prevent damage to the tendon due to the muscle pulling too hard on it, the inverse stretch reflex is initiated by increasing tension in the tendon, and the contraction of the muscle is inhibited. The inverse stretch reflex is therefore damping down the effect of the stretch reflex.

Now, the question is how are these two reflexes hooked together? There are two simple rules:

- (1) When the stretch receptors fire, the  $\alpha$ -motor neuron is excited, and the muscle contracts.
- (2) When the Golgi tendon organ fires, the  $\alpha$ -motor neuron is inhibited (via an inhibitory interneuron), and the muscle relaxes.

The purpose here is that the stretch receptors tell the muscle when it needs a little more force – that despite intending to contract the muscle is lengthening. This helps us to maintain the correct muscle tone. The Golgi tendon organs, on the other hand, begin to fire when the tension on the tendon is so great that we are in danger of injury. They have a protective function, and therefore they tell the muscle to ease off before it tears.

In general, response of the muscle-spindle sensory neuron to stretch of the muscle varies under various conditions. When passive stretch is applied

to a resting muscle in which the length of the intrafusal muscle fibers is matched to the length of the extrafusal fibers, the rate of action potential in the sensory neuron increases. During active contraction of the extrafusal muscle fibers, the muscle shortens and the load on the intrafusal muscle fibers is removed. This stops the firing of action potentials in the sensory neuron and prevents the sensory neuron from responding to a passive stretch of the muscle. The resting discharge and the sensitivity to stretch of the sensory neuron are restored if the intrafusal muscle fibers are stimulated to contract along with the extrafusal muscle fibers during contraction of the muscle.

**Flexion/Withdrawal Reflex.** Flexion/withdrawal reflex Pain and temperature fibers in the dorsal roots play a role in the *flexion reflex*, also known as the *withdrawal reflex*. At the spinal level, this reflex responds to noxious stimuli, such as a hot object on the skin. The result is a rapid flexion that confers a protective mechanism against damage by the stimulus. Another example of this reflex is stepping on a pin. The pin will be sensed by delta and C fibers, which synapse with a series of excitatory and inhibitory interneurons to produce a flexion response. The excitatory interneurons excite LMNs to the hamstring, while the inhibitory interneurons inhibit LMNs to the quadriceps (this is the celebrated *Sherrington reciprocal inhibition*, due to Nobel Laureate Charles S. Sherrington).

The flexion reflex is often accompanied by a crossed extension reflex acting on the contralateral limb. Using the example of stepping on a hot match, the crossed extension reflex would brace the other leg, helping to maintain balance. In this case, excitatory interneurons excite LMNs innervating the quadriceps, while inhibitory interneurons inhibit LMNs that project to the hamstrings.

We can see from the flexion/crossed extensor reflex that flexion withdrawal is a *complete motor act*. While this reflex is reasonably stereotyped, the spatial extent and force of muscle contraction is dependent upon stimulus intensity. For instance, a moderately painful stimulus will result in the production of a moderately fast withdrawal of your finger and wrist, while a real painful stimulus results in the forceful withdrawal of the entire limb. Thus reflexes are not simply repetitions of a stereotyped movement pattern, but instead are modulated by the properties of the stimulus. They are *adaptable* and control movements in a purposeful manner. For example, a perturbation (a disturbance of motion, course, arrangement, or state of equilibrium) of the left arm can cause contraction of the opposite elbow extensor in one situation (opposite arm used to prevent the body from being

pulled forward) but not the other, where the opposite arm holds a cup and the perturbation causes an inhibition of opposite elbow extensor.

Also, spinal reflexes are functionally efficient because they enable adjustments of movements to be made at the level of the spinal cord, without having to involve (and wait for) decisions from higher levels of the motor systems.

### 7.2.3.2 Central Pattern Generators in the Spinal Cord

Now, let us move 'up' slightly in the 'motor hierarchy', and in particular, to *neural networks* in the spinal cord that generate rhythmic alternating activity (see [Molavi (1997); Harting (1997); Marieb (1998)]). A *central pattern generator* (CPG) is a neuronal network capable of generating a rhythmic pattern of motor activity. Normally, these CPGs are controlled by higher centers in the brain stem and cortex. A simple spinal cord circuit is shown below and to the right. This circuitry underlies *alternating flexion/extension* because when some cells are *active* the others are *inhibited*. These cells lie in the ventral horn on the same side of the spinal cord and include flexor and extensor motor neurons, together with their associated interneurons. Descending inputs from higher levels provide continuous input to the excitatory interneurons. However, because of random fluctuations in excitability or other inputs, one half-center initially dominates and inhibits the other. Let us say, for example, that excitatory interneuron  $n_1^+$  turns on first. It will not only excite the flexor LMN and cause flexion, but it will also turn on inhibitory interneuron  $n_2^-$ , which inhibits excitatory interneuron  $n_2^+$  so that the extensor LMN is inhibited. Inhibitory interneuron  $n_2^-$  also inhibits itself, so the flexion will switch to extension when the inhibitory interneuron  $n_2^-$  stops firing. Also, the tonic inputs are exciting excitatory neuron  $n_2^+$ . This will mean that now the excitatory interneuron  $n_2^+$  will fire and excite inhibitory interneuron  $n_1^-$  (see Figure 7.16).

Sometimes these CPGs can be activated below the level of a spinal cord transection. For instance, if a quadriplegic's hips are extended, spontaneous uncontrollable rhythmic movements (flexion and extension) of the legs occur. Moreover, if babies are held erect and moved over a horizontal surface, rhythmic stepping movements take place. Granted, these stepping rhythmic activities in babies involve sensory input, but the circuitry for the rhythmicity of the movements is in the spinal cord. These two examples indicate that basic neuronal circuitry for locomotion is established genetically.



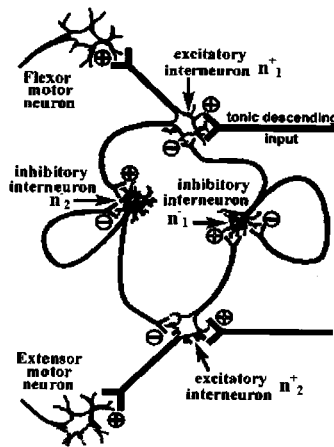


Fig. 7.16 Central pattern generators in the spinal cord.

#### 7.2.3.3 Influence of Higher Centers

The next level of organization in the motor systems hierarchy includes descending inputs to the spinal cord circuitry from a number of different nuclei in the brain stem and primary motor cortex. Descending pathways to the spinal cord can be divided into *ventromedial* and *dorsolateral* systems based upon which spinal cord funiculus the pathway travels in and the termination pattern of its axons in the spinal cord grey (see [Molavi (1997); Harting (1997); Marieb (1998)]).

**Ventromedial System: Control of Axial and Proximal Musculature.** Recall that the *tecto- and vestibulo-spinal tracts* (MVST and LVST, respectively) travel in the *ventral funiculus* and terminate on LMNs that control *axial* and *proximal* musculature. Thus, they keep the head balanced on the shoulders as the body navigates through space, and the head turns in response to new sensory stimuli.

The *pontine* and *medullary reticulospinal tracts* (PRST and MRST, respectively) also travel in the ventral funiculus. The PRST, which lies medial to the MRST in the ventral funiculus, arises from cells in the pons that lie around and near the PPRF. In contrast, the MRST has its origin from cells dorsal to the inferior olive. The reticular formation consists of those cells in the brain stem that do not comprise the sensory and motor nuclei.

The PRST enhances the anti-gravity reflexes of the spinal cord. Thus,

this pathway *excites* upper limb flexors and lower limb *extensors*. This is an important component of motor control, since most of the time the activity of ventral horn cells maintains, rather than changes, muscle length and tension. PRST cells are *spontaneously active* but they also receive excitatory input from the cerebellum and the cortex.

The MRST has the *opposite effect* of the PRST, in that it *inhibits* anti-gravity reflexes of spinal cord (inhibits upper limb flexors and lower limb extensors). MRST cells, like those in the PRST also receive excitatory input from the cerebellum and the cortex.

All of these *ventromedial pathways* (MVST, LVST, TST, MRST, PRST) innervate LMNs and interneurons that innervate axial and proximal limb muscles. Moreover, the axons in the ventromedial pathway distribute collaterals to many segments along their distribution in the spinal cord (for the coordination of intersegmental movements). Note that such a distribution is not well suited for the discrete control of a few muscles but rather for *control of groups of muscles* involved in *posture and balance*.

Lesions of the ventromedial pathways in animals result in difficulty in righting to a sitting or standing position and immobility of the body axis and proximal parts of the extremities. However, the hands and distal parts of the extremities are still active. Thus, descending pathways controlling LMNs that innervate these more distal muscles must not travel in the ventromedial part of the spinal cord.

**Dorsolateral System: Control of Distal Musculature.** Recall that the lateral corticospinal tract (LCST) is one of the two dorsolateral pathways. This pathway is especially important for the control of distal musculature and for steering extremities and manipulating the environment. The other pathway in the dorsolateral system is the rubrospinal tract (RST), which arises from the ruber-duber. Both of these pathways course within the lateral funiculus and are important for the control of distal limb musculature. Axons of the dorsolateral system terminate at only one or two segments (in contrast to the more extensive distribution of ventromedial axons) and reach the LMNs that lie more laterally in the ventral horn. Thus these pathways are involved in the finer motor control of the distal musculature (finger movements for example).

Lesions involving both dorsolateral pathways result in the inability to make fractionated (independent) movements of the wrist or fingers. Moreover, voluntary movements are slower and less accurate, however, the patient still has the ability to sit upright, and stand with relatively normal posture (via functioning pathways in the ventromedial system). A lesion of

only the LCST initially resembles the combined lesion involving the LCST and the RST, but after a while the main deficit is that there is weakness of the distal flexors and the inability to move the fingers independently (fractionated movements). Evidently, the functioning RST accounts for the recovered function of the wrist.

#### 7.2.4 First Look at the Brain

The *brain* is the supervisory center of the nervous system consisting of *grey matter* (superficial parts called *cortex* and deep brain nuclei) and *white matter* (deep parts except the brain nuclei). It controls and coordinates behavior, *homeostasis*<sup>1</sup> (i.e., negative feedback control of the body functions such as heartbeat, blood pressure, fluid balance, and body temperature) and mental functions (such as cognition, emotion, memory and learning) (see [Marieb (1998); Wikipedia (2005); Gowitzke and Milner (1988); Ivancevic and Snoswell (2000)]).

The *vertebrate brain* can be subdivided into: (i) *medulla oblongata* (or, *brain stem*); (ii) *myelencephalon*, divided into: *pons* and *cerebellum*; (iii) *mesencephalon* (or, *midbrain*); (iv) *diencephalon*; and (v) *telencephalon* (*cerebrum*).

Sometimes a gross division into three major parts is used: *hind-*

---

<sup>1</sup>*Homeostasis* is the property of an open system to regulation its internal environment so as to maintain a stable state of structure and functions, by means of multiple dynamic equilibrium controlled by interrelated regulation mechanisms. The term was coined in 1932 by W. Cannon from two Greek words [*homeo-man*] and [*stasis-stationary*]. Homeostasis is one of the fundamental characteristics of living things. It is the maintenance of the internal environment within tolerable limits. All sorts of factors affect the suitability of our body fluids to sustain life; these include properties like temperature, salinity, acidity (carbon dioxide), and the concentrations of nutrients and wastes (urea, glucose, various ion, oxygen). Since these properties affect the chemical reactions that keep bodies alive, there are built-in physiological mechanisms to maintain them at desirable levels. This control is achieved with various organs and glands in the body. For example [Marieb (1998); Wikipedia (2005); Gowitzke and Milner (1988); Ivancevic and Snoswell (2000)]: The *hypothalamus* monitors water content, carbon dioxide concentration, and blood temperature, sending nerve impulses to the pituitary gland and skin. The pituitary gland synthesizes ADH (anti-diuretic hormone) to control water content in the body. The muscles can shiver to produce heat if the body temperature is too low. Warm-blooded animals (homeotherms) have additional mechanisms of maintaining their internal temperature through homeostasis. The pancreas produces insulin to control blood-sugar concentration. The lungs take in oxygen and give out carbon dioxide. The kidneys remove urea and adjust ion and water concentrations. More realistic is dynamical homeostasis, or *homeokinesis*, which forms the basis of the *Anochin's theory of functional systems* [Anochin (1980)]

*brain* (including medulla oblongata and myelencephalon), *midbrain* (mesencephalon) and *forebrain* (including diencephalon and telencephalon). The cerebrum and the cerebellum consist each of two *hemispheres*. The *corpus callosum* connects the two hemispheres of the cerebrum.

The cerebrum and the cerebellum consist each of two hemispheres. The corpus callosum connects the two hemispheres of the cerebrum. The cerebellum is a cauliflower-shaped section of the brain (see Figure 7.17). It is located in the hindbrain, at the bottom rear of the head, directly behind the pons. The cerebellum is a complex computer mostly dedicated to the intricacies of managing walking and balance. Damage to the cerebellum leaves the sufferer with a gait that appears drunken and is difficult to control.

The spinal cord is the extension of the central nervous system that is enclosed in and protected by the vertebral column. It consists of nerve cells and their connections (axons and dendrites), with both gray matter and white matter, with the former surrounded by the latter.

*Cranial nerves* are nerves which start directly from the brainstem instead of the spinal cord, and mainly control the functions of the anatomic structures of the head. In human anatomy, there are exactly 12 pairs of them: (I) *olfactory nerve*, (II) *optic nerve*, (III) oculomotor nerve, (IV) Trochlear nerve, (V) Trigeminal nerve, (VI) Abducens nerve, (VII) Facial nerve, (VIII) Vestibulocochlear nerve (sometimes called the auditory nerve), (IX) Glossopharyngeal nerve, (X) Vagus nerve, (XI) Accessory nerve (sometimes called the spinal accessory nerve), and (XII) Hypoglossal nerve.

The optic nerve consists mainly of axons extending from the ganglionic cells of the eye's retina. The axons terminate in the lateral geniculate nucleus, pulvinar, and superior colliculus, all of which belong to the primary visual center. From the lateral geniculate body and the pulvinar fibers pass to the visual cortex.

In particular, the *optic nerve* contains roughly one million nerve fibers. This number is low compared to the roughly 130 million receptors in the retina, and implies that substantial pre-processing takes place in the retina before the signals are sent to the brain through the optic nerve.

In most vertebrates the mesencephalon is the highest integration center in the brain, whereas in mammals this role has been adopted by the telencephalon. Therefore the cerebrum is the largest section of the mammalian brain and its surface has many deep fissures (sulci) and grooves (gyri), giving an excessively wrinkled appearance to the brain.

The *human brain* can be subdivided into several distinct regions:

The *cerebral hemispheres* form the largest part of the brain, occupying

the anterior and middle cranial fossae in the skull and extending backwards over the tentorium cerebelli. They are made up of the cerebral cortex, the basal ganglia, tracts of synaptic connections, and the ventricles containing CSF.

The *diencephalon* includes the thalamus, hypothalamus, epithalamus and subthalamus, and forms the central core of the brain. It is surrounded by the cerebral hemispheres.

The *midbrain* is located at the junction of the middle and posterior cranial fossae.

The *pons* sits in the anterior part of the posterior cranial fossa; the fibres within the structure connect one cerebral hemisphere with its opposite cerebellar hemisphere.

The *medulla oblongata* is continuous with the spinal cord, and is responsible for automatic control of the respiratory and cardiovascular systems.

The *cerebellum* overlies the pons and medulla, extending beneath the tentorium cerebelli and occupying most of the posterior cranial fossa. It is mainly concerned with motor functions that regulate muscle tone, coordination, and posture.

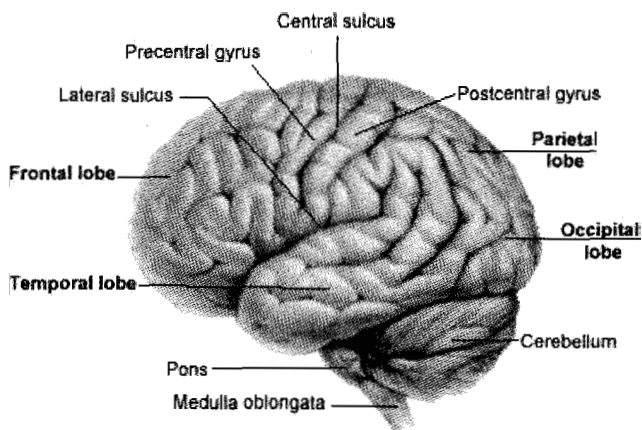


Fig. 7.17 The human cerebral hemispheres.

Now, the two *cerebral hemispheres* (see Figure 7.17) can be further divided into *four lobes*:

The *frontal lobe* is concerned with higher intellectual functions, such as abstract thought and reason, speech (Broca's area in the left hemisphere

only), olfaction, and emotion. Voluntary movement is controlled in the precentral gyrus (the primary motor area, see Figure 7.18).

The *parietal lobe* is dedicated to sensory awareness, particularly in the postcentral gyrus (the primary sensory area, see Figure 7.18). It is also associated with abstract reasoning, language interpretation and formation of a mental egocentric map of the surrounding area.

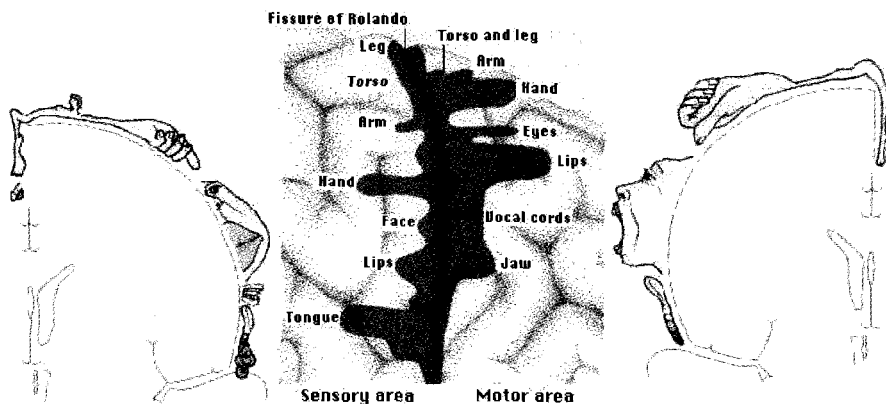


Fig. 7.18 Penfield's 'Homunculus', showing the primary somatosensory and motor areas of the human brain.

The *occipital lobe* is responsible for interpretation and processing of visual stimuli from the optic nerves, and association of these stimuli with other nervous inputs and memories.

The *temporal lobe* is concerned with emotional development and formation, and also contains the auditory area responsible for processing and discrimination of sound. It is also the area thought to be responsible for the formation and processing of memories.

A 3D model of the human brain in the *wireframe graphical mode* is presented in Figure 7.19.

## 7.2.5 Motor Pathways

### 7.2.5.1 Primary Motor Cortex

The *primary motor cortex* is also called area 4 of Brodmann and motor I (MI). Corticospinal cells in area 4 project directly to the lower motor neurons (LMNs) in the spinal cord and brain stem and tell these LMNs,

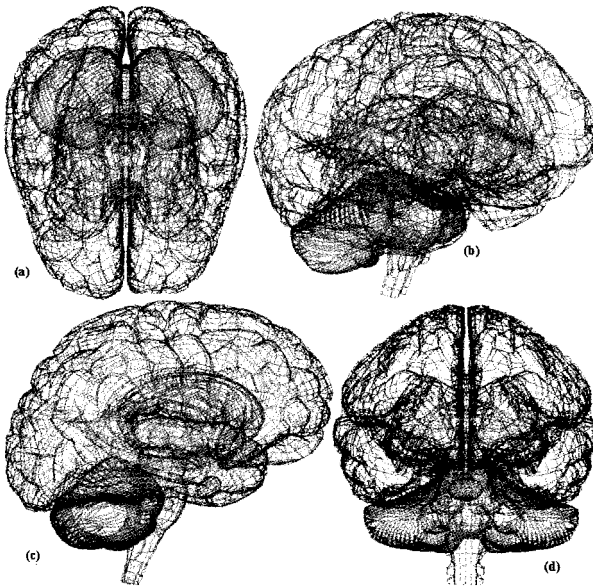


Fig. 7.19 A wireframe 3D-graphics model of the human brain: (a) top view, (b) perspective view, (c) left view, and (d) front view.

and in turn the muscles they innervate, what to do. They are the classic upper motor neurons (UMNs). MI is located in the precentral gyrus, which lies in front (rostral) of the central sulcus. MI occupies most of this gyrus along both its lateral and medial surfaces and is bound caudally by the central sulcus (see [Molavi (1997); Harting (1997); Marieb (1998)]).

**Somatotopic Organization of MI.** In the late 1950s W. Penfield studied the somatotopic organization of MI in patients by stimulating MI with relatively large electrodes (the patients gave their permission to do this as part of their surgery). He found a topographically organized representation of the entire head and body, which is schematically shown above and to the right as the classic *homunculus* (little man or person). The head and forelimbs are represented laterally, and the hind limb and feet medially. The cortical areas allotted to different bodily regions are of unequal size, with the degree of representation proportional to the amount of skilled movement that is required of the respective part of the body. Thus, in humans the face (particularly the tongue and lips used in speaking), thumb, and hand receive a disproportionate representation, giving these structures a correspondingly exaggerated appearance. Movements of limbs

evoked by stimulation of MI are strictly contralateral, but movements of the face (remember corticobulbars) may be bilateral.

The main outputs of MI are the now familiar corticospinal and corticobulbar pathways, which arise from cells that are pyramidal in shape and lie in layer 5 of MI (most of the cerebral cortex has 6 layers, 1 being most superficial and 6 the deepest). The largest corticospinal cells are called *Betz cells*.

**Physiology of Corticospinal Neurons.** Much of what we know about the physiology of cells that project into the corticospinal tract comes from single neuron recordings in awake monkeys trained to perform specific tasks. Since corticospinal neurons course within the pyramids when they are in the medulla, they are also called pyramidal tract neurons (PTNs). If a monkey is trained to move a handle by flexing and extending the wrist, then the PTNs can be studied. In the experiment shown above, a light comes on to signal to the monkey that he/she should either flex or extend their wrist. It takes a while for the brain to get the visual information (the light signal) to MI before the PTN will begin to fire. There are PTNs related to either flexion or extension of the wrist and the ones that fire depend on the light signal. If the light signal is a cue to flex, the PTNs involved in flexion will fire and send information down the corticospinal tract to the level of the medulla where the pathway decussates. The lateral corticospinal tract then continues to the LMNs in the ventral horn that innervate either the extensors or flexors of the wrist.

**Functions of MI.** Recent studies have shown that corticospinal cells are telling LMNs in the spinal cord what to do. In fact, corticospinal cells are involved in conveying a lot of details about amplitude, force and direction to the LMN. In other words, MI neurons are NOT leaving these decisions up to the LMNs, as they are too dumb. Thus, MI cells tell the LMNs (and in turn the muscles) what direction to move, how far to move (amplitude) and how much force to use. The corticospinals in MI are specifying some pretty basic stuff instead of just sitting back and saying grab that glass of water, arm and hand and leaving the rest of the work to the poor LMNs. Remember, MIs contributions to motor control include controlling the number of muscles and movement forces and trajectories. MI cells are mainly concerned with the actual execution of the movements.

In general, with lesions of MI there will be the usual constellation of signs associated with UMN lesions. There will be hemiplegia that is especially noticeable for voluntary movements of the distal extremities. Also a Babinski sign would be present if the lesion involves UMN of the lower



limb. Remember that skilled, independent movements of the distal extremities (fingers) are most affected. The rubrospinal tract (which along with the corticospinal tract is a component of the dorsolateral system) can help carry out some of its more distal (wrist) limb movement tasks but isn't much help when it comes to the more refined movements of the fingers). Also, recall that the ventromedial system is functioning and thus the axial and more proximal muscles are able to function.

#### 7.2.5.2 *Motor Association/Premotor Cortical Areas*

The primary motor cortex (MI; Brodmann area 4) was the first motor cortical area discovered. It takes relatively little stimulating current of this cortical area to evoke a movement. This is because the corticospinal neurons that lie in MI are directly connected to the LMNs in the brain stem and spinal cord. Movements also result from stimulation of other areas of cortex that lie immediately rostral to MI, and we call these motor association areas (supplementary motor area and lateral premotor area on the drawing below). Since these motor association areas influence LMNs primarily via their inputs to MI corticospinal cells, more current is needed to evoke movements. Premotor areas tell MI what movements to execute. That is, they are involved with the planning of a movement. The total size of these premotor areas is considerably larger than area 4, and thus these areas prove to be particularly important in the control of human voluntary movement and are often compromised in diseases. The two premotor areas we will talk about are the supplementary motor area and the lateral premotor area. They are both part of area 6 (see [Molavi (1997); Harting (1997); Marieb (1998)]).

**Lateral Premotor Area.** The *lateral premotor area* (PMI) lies on the lateral convexity of the hemisphere. Many motor actions are often responses to visual or auditory cues, and cells in PMI are active during such externally cued movements. For instance, we see an apple (external cue) and the apple cues a movement to reach out and grasp it. The pathways involved in this sensorimotor transformation (*seeing* it is *sensory* and *reaching* for and *grasping* it is *motor*) are seen in the adjacent drawing. The visual information (apple) falls first on the retina, and the retinal signal eventually reaches the primary visual cortex in the back of the brain (area 17). From area 17, the retinal information is conveyed rostrally and bilaterally to what is termed the posterior parietal cortex (areas 5 and 7 or just call it PPC). The PPC helps to transform visual information about the location of the

apple in extrapersonal space into the direction of a reaching movement (moving a body part relative to another body part is an example of a movement in intrapersonal space, while movements in extrapersonal space are movements executed in a 3D coordinate system fixed by points in the environment). Information from PPC is conveyed to PMl. PMl projects bilaterally to another premotor area called the supplementary motor area (SMA). The SMA contralateral to the apple then turns on MI to execute the reaching movement.

Lesions of the PMl result in apraxia, which is an inability to perform a purposeful movement (especially skilled) in the absence of any significant paralysis, sensory loss, or deficit in comprehension. For example, monkeys can be trained to turn or pull a handle (MI is OK) depending upon whether the handle is red or blue. If there is a lesion of PMl, the monkey can still turn and pull the handle, but they can not learn to associate the correct movement with the correct external visual cue (colors). That is, the monkeys deficit lies in finding that particular movement when they are presented with a particular cue.

**Supplementary Motor Cortex.** The SMA is located immediately rostral to area 4, and includes the caudal one-third of the medial, dorsal, and lateral surfaces of the *superior frontal gyrus*. The SMA is involved in the programming of all movement sequences. Thus, it will be active when reaching for the apple. The reaching movement needs to be sequenced by the SMAs (both sides are active) after the PPC gives the SMA the proper coordinates in extrapersonal space. The SMAs are involved in internally generated movements so, if we suddenly have the 'internal need' to reach out and grab something in front of us (this is not precipitated by an external cue), the memory/motor patterns necessary for this movement are encoded in cells within the SMA. Cells in the SMA will start to fire and, in turn, send the instructions for the movement to the workhorse, MI, so that the right muscles are moved with the correct amount of force and speed (execution of the movement). Interestingly, the two SMAs are interconnected by cortico-cortical fibers, and, unlike cells in MI, the activity in the SMA is usually *bilateral*. So, during the movement of the right arm/hand, cells in both SMAs start firing, but only cells in the left MI fire. Cells in SMA fire before those in MI but both areas will be firing during the movement. Interestingly, if we *just imagine* reaching out and grabbing something in front of us, cells in SMA will increase firing (bilaterally).

Monkeys with lesions of SMA have impaired ability to carry out a motor act that they had learned earlier, i.e., *apraxia*. There is no paralysis, only

problems in *planning*. For instance, monkeys who had learned how to open a latch box by opening three different latches in a particular *sequence* are greatly impaired following either uni- or bilateral lesions of SMA. Recall that the two SMAs are interconnected across the midline. A lesion of one affects the proper functioning of the other. For instance, a lesion of the *right* SMA means the right MI is not getting proper planning information. This affects the *left* arm/hand. In addition, the left SMA has lost its input from the right SMA so the left SMA input to the left MI is not normal. In the end, *bimanual coordination* is affected. So, we can put an equality  $SMA = bimanual\ coordination$ .

The role of the SMA in *sequencing* of movements is further exemplified by data from experiments in which monkeys were trained to do three movements; push, pull or turn a manipulandum (a joystick like we use with video games) in four different orders (e.g., push, turn, pull, would be one choice). Cells were found that increased their firing to a particular sequence (turn, push, pull but not turn, push, turn). So, SMA is big on sequencing and especially *internally* or *memory-guided movements*. Recall that in the above task with the manipulandum, the appearance (an *external cue*) of the apparatus gave no clue as to which movement to make first, or even the order of the movements.

We can see that *planning premotor areas* are more *specialized* than the execution cells in MI and are important for selecting and controlling movements made in particular behavioral contexts, such as when the direction of a movement that needs to be made must be remembered (internally generated) or selected on the basis of an available external cue (externally guided). The movement is the same but the areas that activate and tell MI which muscles to turn on (execution) differ.

**Studies of Regional Cerebral Blood Flow.** Additional information about the activation of cortical areas during different types of movements can be gathered by looking at the regional cerebral blood flow (rCBF) during particular tasks. In these studies an increase in rCBF means the cortical area is active. For example, it has been shown that fast flexions of the index finger against a spring loaded movable cylinder increases rCBF in the finger area of the *contralateral* MI and SI (primary somatosensory area). The increase in rCBF in the somatosensory cortex reflects the activation of peripheral receptors caused by the rapid finger flexions. Most important, no higher cortical motor area exhibited an increase in rCBF in this task. Thus, MI (and its associated LMNs), is the only motor cortical area involved in the control of *simple repetitive movements*.

When a person is asked to carry out from memory more sophisticated and complex movements, then other motor cortical area(s) besides MI exhibit an increase in rCBL. Such a complex movement is where the thumb, in quick succession, must touch the index finger twice, the middle finger once, the ring finger three times, and the little finger two times. Then, with the thumb opposed to the little finger, the whole sequence is reversed! This is a complex series of movements guided by memory and carried out in intrapersonal space (moving a body part relative to another body part). Again, there is increased rCBF in the contralateral MI and SI (a bigger area since more fingers are involved), but in addition there is increased rCBF within SMA bilaterally. Thus, a complex task involving a sequence of remembered movements requires the activity of both SMAs and the MI contralateral to the active fingers. Of course, MI is needed for the execution. Interestingly, if we just imagine the finger sequence movement, SMA lights up bilaterally, but not MI.

Now, what happens when we are asked to do a complex movement in space such as a memorized spiral movement of the arm and hand? Since this movement is made in extrapersonal space, the posterior parietal cortex (PPC) is needed. In addition to PPC, SMA is active bilaterally because the movement needs sequencing. Clearly, contralateral MI is active, as it is doing the labor (execution) and SI is active because it is receiving the sensory information generated by the movement.

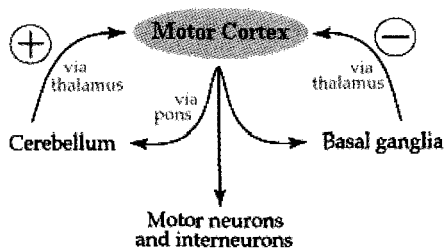


Fig. 7.20 Coordination feedback loops of cerebellum and basal ganglia.

### 7.2.6 Subcortical Motor 'Side Loops'

Two main subcortical 'side-loop' controllers of human movement are cerebellum and basal ganglia. The *cerebellum* and the *basal ganglia* are large collections of nuclei that modify movement on a minute-to-minute

basis: The *motor cortex* sends information to both, and both structures send information right back to cortex via the *thalamus*. The *output* of the *cerebellum* is *excitatory*, while the *basal ganglia* are *inhibitory* (see Figure 7.20). The balance between these two systems allows for smooth, coordinated movement, and a disturbance in either system will show up as movement disorders (see [Molavi (1997); Harting (1997); Marieb (1998)]).

#### 7.2.6.1 *The Cerebellum*

When someone compares learning a new skill to learning how to ride a bike they imply that once mastered, the task seems imbedded in our brain forever. Well, imbedded in the cerebellum to be exact. This brain structure is the commander of coordinated movement and possibly even some forms of cognitive learning. Damage to this area leads to motor or movement difficulties. Some scientists have discovered cognitive problems as well (see [Molavi (1997); Harting (1997); Marieb (1998); van der Smagt (1999)]).

Neuro-scientists believe the structure coordinates movement of muscles and joints by synthesizing data from the brain stem, the spinal cord, and another the cerebral cortex along with sensory input from muscles and other areas. The brain stem and spinal cord provide information on body positioning and the cerebral cortex is responsible for all conscious experience, including perception, emotion and planning.

Some scientists suspect that there are two main information pathways in the cerebellum that interact to synthesize incoming information. One carries a large amount of data from different brain and body areas and contains memory cells. The other originates in the brain stem and interacts with the first pathway to learn new patterns of movement based on incoming information. New skills are learned by trial and error and then coded into the cerebellar memory. Clinical observations suggest that mental activities also are coordinated in the cerebellum in a similar manner.

The cerebellum is a kind of a 'little brain', or a 'biocomputer', involved in the coordination of human movement. A simple way to look at its purpose is that it compares what we thought we were going to do (according to motor cortex) with what is actually happening down in the limbs (according to *proprioceptive feedback*), and corrects the movement if there is a problem. The cerebellum is also partly responsible for motor learning, such as riding a bicycle. Unlike the cerebrum, which works entirely on a *contralateral* basis, the cerebellum works *ipsilaterally*.

The cerebellum has convolutions similar to those of cerebral cortex, only the folds are much smaller. Like the cerebrum, the cerebellum has an outer cortex, an inner white matter, and deep nuclei below the white matter.

If we enlarge a single fold of cerebellum, or a *folium*, we can begin to see the organization of cell types. The outermost layer of the cortex is called the *molecular layer*, and is nearly cell-free. Instead it is occupied mostly by axons and dendrites. The layer below that is a monolayer of large cells called *Purkinje cells*, central players in the circuitry of the cerebellum. Below the Purkinje cells is a dense layer of tiny neurons called *granule cells*. Finally, in the center of each folium is the white matter, all of the axons travelling into and out of the folia. These cell types are hooked together in stereotypical ways throughout the cerebellum.

The human cerebellum has 7–14 million Purkinje cells. Each receives about 200,000 synapses, most onto dendritic splines. Granule cell axons form the *parallel fibers*. They make excitatory synapses onto Purkinje cell dendrites. Each parallel fibre synapses on about 200 Purkinje cells. They create a strip of excitation along the cerebellar folia.

*Mossy fibers* are one of two main sources of input to the cerebellar cortex (see Figure 7.21). A mossy fibre is an axon terminal that ends in a large, bulbous swelling. These mossy fibers enter the granule cell layer and synapse on the dendrites of granule cells; in fact the granule cells reach out with little ‘claws’ to grasp the terminals. The granule cells then send their axons up to the molecular layer, where they end in a T and run parallel to the surface. For this reason these axons are called *parallel fibers*. The parallel fibers synapse on the huge dendritic arrays of the Purkinje cells. However, the individual parallel fibers are not a strong drive to the Purkinje cells. The Purkinje cell dendrites fan out within a plane, like the splayed fingers of one hand. If we were to turn a Purkinje cell to the side, it would have almost no width at all. The parallel fibers run perpendicular to the Purkinje cells, so that they only make contact once as they pass through the dendrites.

Unless firing in bursts, parallel fibre EPSPs do not fire Purkinje cells. Parallel fibers provide excitation to all of the Purkinje cells they encounter. Thus, granule cell activity results in a strip of activated Purkinje cells.

Mossy fibers arise from the spinal cord and brainstem. They synapse onto granule cells and deep cerebellar nuclei. The Purkinje cell makes an inhibitory synapse (GABA) to the deep nuclei. Mossy fibre input goes to both cerebellar cortex and deep nuclei. When the Purkinje cell fires, it inhibits output from the deep nuclei.

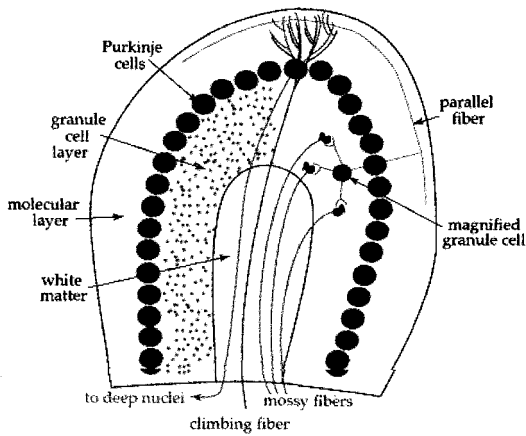


Fig. 7.21 Stereotypical ways throughout the cerebellum.

The *climbing fibre* arises from the inferior olive. It makes about 300 excitatory synapses onto one Purkinje cell. This powerful input can fire the Purkinje cell.

The parallel fibre synapses are plastic—that is, they can be modified by experience. When parallel fibre activity and climbing fibre activity converge on the same Purkinje cell, the parallel fibre synapses become weaker (EPSPs are smaller). This is called long-term depression. Weakened parallel fibre synapses result in less Purkinje cell activity and less inhibition to the deep nuclei, resulting in facilitated deep nuclei output. Consequently, the mossy fibre collaterals control the deep nuclei.

The *basket cell* is activated by parallel fibers afferents. It makes inhibitory synapses onto Purkinje cells. It provides lateral inhibition to Purkinje cells. Basket cells inhibit Purkinje cells lateral to the active beam.

*Golgi cells* receive input from parallel fibers, mossy fibers, and climbing fibers. They inhibit granule cells. Golgi cells provide feedback inhibition to granule cells as well as feedforward inhibition to granule cells. Golgi cells create a brief burst of granule cell activity.

Although each parallel fibre touches each Purkinje cell only once, the thousands of parallel fibers working together can drive the Purkinje cells to fire like mad.

The second main type of input to the folium is the *climbing fibre*. The climbing fibers go straight to the Purkinje cell layer and snake up the Purkinje dendrites, like ivy climbing a trellis. Each climbing fibre associates with

only one Purkinje cell, but when the climbing fibre fires, it provokes a large response in the Purkinje cell.

The Purkinje cell compares and processes the varying inputs it gets, and finally sends its own axons out through the white matter and down to the *deep nuclei*. Although the inhibitory Purkinje cells are the main output of the cerebellar cortex, the output from the cerebellum as a whole comes from the deep nuclei. The three deep nuclei are responsible for sending excitatory output back to the thalamus, as well as to postural and vestibular centers.

There are a few other cell types in cerebellar cortex, which can all be lumped into the category of inhibitory interneuron. The *Golgi cell* is found among the granule cells. The *stellate* and *basket cells* live in the molecular layer. The basket cell (right) drops axon branches down into the Purkinje cell layer where the branches wrap around the cell bodies like baskets.

The cerebellum operates in 3's: there are 3 highways leading in and out of the cerebellum, there are 3 main inputs, and there are 3 main outputs from 3 deep nuclei. They are:

The 3 highways are the *peduncles*. There are 3 pairs (see [Molavi (1997); Harting (1997); Marieb (1998)]):

- (1) The *inferior cerebellar peduncle* (restiform body) contains the dorsal spinocerebellar tract (DSCT) fibers. These fibers arise from cells in the ipsilateral Clarke's column in the spinal cord (C8-L3). This peduncle contains the cuneocerebellar tract (CCT) fibers. These fibers arise from the ipsilateral accessory cuneate nucleus. The largest component of the inferior cerebellar peduncle consists of the olivocerebellar tract (OCT) fibers. These fibers arise from the contralateral inferior olive. Finally, vestibulocerebellar tract (VCT) fibers arise from cells in both the vestibular ganglion and the vestibular nuclei and pass in the inferior cerebellar peduncle to reach the cerebellum.
- (2) The *middle cerebellar peduncle* (brachium pontis) contains the pontocerebellar tract (PCT) fibers. These fibers arise from the contralateral pontine grey.
- (3) The *superior cerebellar peduncle* (brachium conjunctivum) is the primary efferent (out of the cerebellum) peduncle of the cerebellum. It contains fibers that arise from several deep cerebellar nuclei. These fibers pass ipsilaterally for a while and then cross at the level of the inferior colliculus to form the decussation of the superior cerebellar peduncle. These fibers then continue ipsilaterally to terminate in the red nucleus ('ruber-duber') and the motor nuclei of the thalamus (VA,



VL).

The 3 inputs are: *mossy fibers* from the *spinocerebellar* pathways, climbing fibers from the *inferior olive*, and more mossy fibers from the *pons*, which are carrying information from *cerebral cortex* (see Figure 7.22). The mossy fibers from the spinal cord have come up ipsilaterally, so they do not need to cross. The fibers coming down from cerebral cortex, however, do need to cross (as the cerebrum is concerned with the opposite side of the body, unlike the cerebellum). These fibers synapse in the pons (hence the huge block of fibers in the cerebral peduncles labelled ‘corticopontine’), cross, and enter the cerebellum as mossy fibers.

The 3 deep nuclei are the *fastigial*, *interposed*, and *dentate nuclei*. The fastigial nucleus is primarily concerned with balance, and sends information mainly to vestibular and reticular nuclei. The dentate and interposed nuclei are concerned more with voluntary movement, and send axons mainly to thalamus and the red nucleus.

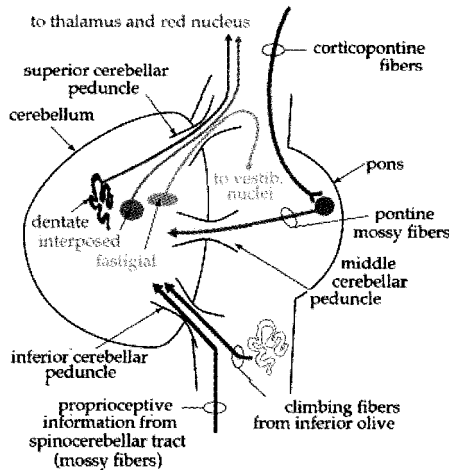


Fig. 7.22 Inputs and outputs of the cerebellum.

The main function of the cerebellum as a motor controller is depicted in Figure 7.23. A coordinated movement is easy to recognize, but we know little about how it is achieved. In search of the neural basis of coordination, a model of spinocerebellar interactions was recently presented in [Apps and Garwicz (2005)], in which the structure-functional organizing principle is a division of the cerebellum into discrete micro-complexes. Each micro-

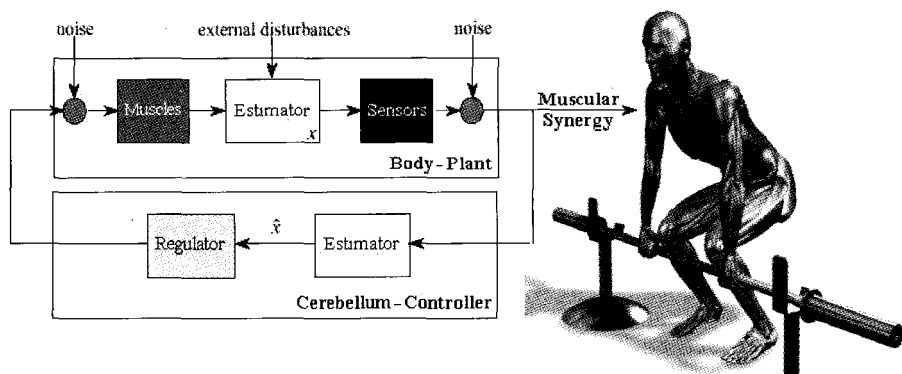


Fig. 7.23 The cerebellum as a motor controller.

complex is the recipient of a specific motor error signal - that is, a signal that conveys information about an inappropriate movement. These signals are encoded by spinal reflex circuits and conveyed to the cerebellar cortex through climbing fibre afferents. This organization reveals salient features of cerebellar information processing, but also highlights the importance of systems level analysis for a fuller understanding of the neural mechanisms that underlie behavior.

The authors of [Apps and Garwicz (2005)] reviewed anatomical and physiological foundations of cerebellar information processing. The cerebellum is crucial for the coordination of movement. The authors presented a model of the cerebellar paravermis, a region concerned with the control of voluntary limb movements through its interconnections with the spinal cord. They particularly focused on the olivo-cerebellar climbing fibre system.

Climbing fibres are proposed to convey motor error signals (signals that convey information about inappropriate movements) related to elementary limb movements that result from the contraction of single muscles. The actual encoding of motor error signals is suggested to depend on sensorimotor transformations carried out by spinal modules that mediate nociceptive withdrawal reflexes.

The termination of the climbing fibre system in the cerebellar cortex subdivides the paravermis into distinct microzones. Functionally similar but spatially separate microzones converge onto a common group of cerebellar nuclear neurons. The processing units formed as a consequence are termed 'multizonal microcomplexes' (MZMCs), and are each related to a

specific spinal reflex module.

The distributed nature of microzones that belong to a given MZMC is proposed to enable similar climbing fibre inputs to integrate with mossy fibre inputs that arise from different sources. Anatomical results consistent with this notion have been obtained.

Within an individual MZMC, the skin receptive fields of climbing fibres, mossy fibres and cerebellar cortical inhibitory interneurons appear to be similar. This indicates that the inhibitory receptive fields of Purkinje cells within a particular MZMC result from the activation of inhibitory interneurons by local granule cells.

On the other hand, the parallel fibre-mediated excitatory receptive fields of the Purkinje cells in the same MZMC differ from all of the other receptive fields, but are similar to those of mossy fibres in another MZMC. This indicates that the excitatory input to Purkinje cells in a given MZMC originates in non-local granule cells and is mediated over some distance by parallel fibres.

The output from individual MZMCs often involves two or three segments of the ipsilateral limb, indicative of control of multi-joint muscle synergies. The distal-most muscle in this synergy seems to have a roughly antagonistic action to the muscle associated with the climbing fibre input to the MZMC.

The model proposed in [Apps and Garwicz (2005)] indicates that the cerebellar paravermis system could provide the control of both single- and multi-joint movements. Agonist-antagonist activity associated with single-joint movements might be controlled within a particular MZMC, whereas coordination across multiple joints might be governed by interactions between MZMCs, mediated by parallel fibres.

#### 7.2.6.2 *The Basal Ganglia*

The *basal ganglia* are a collection of nuclei deep to the white matter of cerebral cortex. The name includes: *caudate*, *putamen*, *nucleus accumbens*, *globus pallidus*, *substantia nigra*, *subthalamic nucleus*, and historically the *claustrum* and the *amygdala* (see Figure 7.24).

The relationships between the nuclei of the basal ganglia are by no means completely understood. The caudate and putamen receive most of the input from cerebral cortex; in this sense they are the doorway into the basal ganglia. The caudate and putamen are reciprocally interconnected with the *substantia nigra*, but send most of their output to the *globus pal-*

*lidus*. The substantia nigra can be divided into two parts: the *substantia nigra pars compacta* (SNpc) and the *substantia nigra pars reticulata* (SNpr). The SNpc receives input from the caudate and putamen, and sends information right back. The SNpr also receives input from the caudate and putamen, but sends it outside the basal ganglia to control head and eye movements. The SNpc is the more celebrated of the two, as it produces dopamine, which is critical for normal movement. The globus pallidus can also be divided into two parts: the *globus pallidus externa* (GPe) and the *globus pallidus interna* (GPi). Both receive input from the caudate and putamen, and both are in communication with the subthalamic nucleus. It is the GPi, however, that sends the major inhibitory output from the basal ganglia back to thalamus. The GPi also sends a few projections to an area of midbrain, presumably to assist in postural control (see [Molavi (1997); Harting (1997); Marieb (1998)]).

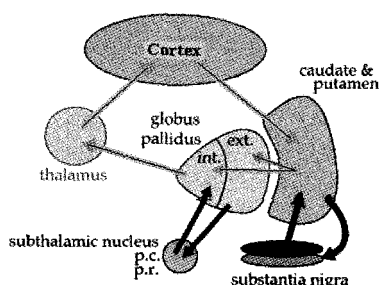


Fig. 7.24 The connections of the basal ganglia.

The function of the basal ganglia is often described in terms of a 'brake hypothesis'. To sit still, we must put the brakes on all movements except those reflexes that maintain an upright posture. To move, we must apply a brake to some postural reflexes, and release the brake on voluntary movement. In such a complicated system, it is apparent that small disturbances can throw the whole system out of whack, often in unpredictable ways. The deficits tend to fall into one of two categories: the presence of extraneous unwanted movements or an absence or difficulty with intended movements.

Lesions in specific nuclei tend to produce characteristic deficits. One well-known disorder is *Parkinson's disease*, which is the slow and steady loss of dopaminergic neurons in SNpc. An instant Parkinson-like syndrome will result if these neurons are damaged. This happened several years ago to an unfortunate group of people who took some home-brewed Demerol

in search of a high. It was contaminated by a very nasty byproduct, MPTP, which selectively zapped the SNpc neurons. The three symptoms usually associated with Parkinson's are *tremor*, *rigidity*, and *bradykinesia*. The tremor is most apparent at rest. Rigidity is a result of simultaneous contraction of flexors and extensors, which tends to lock up the limbs. Bradykinesia, or 'slow movement', is a difficulty initiating voluntary movement, as though the brake cannot be released.

*Huntington's disease*, or *chorea*, is a hereditary disease of unwanted movements. It results from degeneration of the caudate and putamen, and produces continuous dance-like movements of the face and limbs. A related disorder is *hemiballismus*, flailing movements of one arm and leg, which is caused by damage (i.e., stroke) of the subthalamic nucleus.

### 7.2.6.3 Cerebellar Movement Control

Recall that different regions of the cerebellum receive different inputs and project to different parts of the brain stem and thalamus. Here we will consider a biphasic movement that involves two sequences,  $mv1$  and  $mv2$  (see [Harting (1997); Marieb (1998)]). The first sequence,  $mv1$ , starts from  $SMA_{mv1}$  cell sending information directly to a  $MI_{mv1}$  cell (see Figure 7.25). At the same time, the  $SMA_{mv1}$  cell sends the same signal into the direct loop of the basal ganglia, so that the VA/VL can help  $MI_{mv1}$  reach an appropriate firing rate. The  $MI_{mv1}$  cell is a corticospinal neuron that sends its information to the contralateral LMNs in the spinal cord for execution of  $mv1$ .

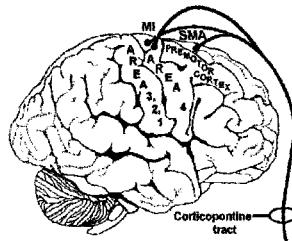


Fig. 7.25 Central motor pathways starting from the motor cortex.

At the same time, the  $MI_{mv1}$  cell sends the same signal about  $mv1$  to the ipsilateral pontine grey, via corticopontine fibers. Now, the cells in the pontine grey have axons called pontocerebellar fibers that cross and en-

ter the middle cerebellar peduncle and terminate in the cerebellar cortex. Each side of the cerebellum is divided into four different zones or regions called the flocculonodular, medial, intermediate, and lateral. The  $MI_{mv1}$  information is conveyed (via corticopontine and pontocerebellar fibers) to the intermediate zone. That is, the  $MI_{mv1}$  information does not reach the entire contralateral cerebellum (via the pontine grey), but instead reaches only one region and this is called the intermediate zone. As  $mv1$  is evolving, the dorsal spinocerebellar and cuneocerebellar pathways are signaling to the cerebellum exactly what the muscles are doing. This unconscious proprioceptive information also reaches the intermediate zone of the cerebellum. Thus, the incoming sensory information about what is happening in the muscles during  $mv1$  is compared to the information carried by the pontocerebellar fibers concerning what  $MI_{mv1}$  is commanding muscles 1,2,3 to do. Thus, the intermediate zone of the cerebellum is a region in which comparisons are made between the movement being commanded by  $MI_{mv1}$  and what the muscles involved in the movement are actually doing.

From this we can see that one function of the cerebellum, (and in particular the intermediate zone), is to update and correct the ongoing or current movement. It integrates/compares the pontocerebellar and spinocerebellar information about the current movement and then sends updated, corrective signals to other parts of the motor systems that actually carry out the correction/update. Now, the superior cerebellar peduncle is a major outflow tract of the cerebellum. The axons in the SCP arise from cells in deep cerebellar nuclei. Each cerebellar zone has a deep cerebellar nucleus. In the case of the intermediate zone (comparing/updating), axons arising in nucleus interpositus enter the superior cerebellar peduncle, cross, and synapse within the red nucleus and the motor related (VA/VL) nuclei of the thalamus. Signals sent down the rubrospinal tract update and correct the ongoing movement at the level of the spinal cord. In contrast, VA/VL inform  $MI_{mv1}$  about the correction that in turn is carried out via the corticospinal projection of  $MI_{mv1}$ .

Now, while  $mv1$  is taking place,  $mv2$  is being planned.  $SMA_{pl2}$  cells inform  $MI_{pl2}$  cells about the planned (next) movement. In addition,  $SMA_{pl2}$  sends the same planning information into the Indirect loop of the basal ganglia, as the basal ganglia are inhibiting VA/VL and  $mv2$ .

The  $SMA_{pl2}$  and  $MI_{pl2}$  cells send their planning information to the ipsilateral pontine grey (corticopontine) These planning pontine grey cells are in a different part of the pontine grey than those receiving corticopontine

input about the current movement  $mv1$ . These planning pontocerebellar cells send their axons into the opposite middle cerebellar peduncle (ponto-cerebellar) and terminate in the lateral zone of the cerebellum.

Now, one hypothesis is that the *lateral cerebellar zone* is involved in the storage and/or retrieval of long-term memory for motor skills. That is, when movement  $mv2$  was initially learned, circuitry in the lateral zone learned something about the movement that can now assist the *SMA* and *MI*. Thus, when  $SMA_{pl2}$  and  $MI_{pl2}$  information reaches the lateral zone (via corticopontine and then pontocerebellar fibers), specific cerebellar circuits that were laid down when the movement was initially learned are activated. So, information about  $mv2$  is contained not only in cortical areas ( $SMA_{pl2}$  and  $MI_{pl2}$ ), but also in the lateral zone of the cerebellum.

The integrated planning information is conveyed out of the lateral zone of the cerebellum via the deep cerebellar nucleus of the lateral zone, the dentate nucleus. Axons of dentate neurons enter the superior cerebellar peduncle, cross, and terminate in VA/VL. From the VA/VL, the planning information reaches  $SMA_{pl2}$  and  $MI_{pl2}$  cells.

We can see from the above analysis that the cerebellum is involved with updating/comparing and the planning of movements. There are other parts of the cerebellum that are involved in other aspects of motor functions. These are the medial zone and the flocculonodular lobe/zone.

The medial zone of the cerebellum receives sensory information (unconscious proprioception) from the dorsal spinocerebellar and cuneocerebellar tracts (just like the intermediate zone). This sensory information reaches the ipsilateral medial zone via the inferior cerebellar peduncle. To exit the cerebellum, the axons of cells in the deep cerebellar nucleus of the medial zone, the fastigial, pass ipsilaterally via the inferior cerebellar peduncle to reach the vestibular nuclei and the pontine and medullary reticular formation.

Now, the vestibular nuclei project to the PPRF (for horizontal eye movements) and the spinal cord (via the MVST and LVST) and that these two pathways are important components of the postural and balance-related ventromedial brain stem system. Pontine reticulospinal tract (PRST) and medullary reticulospinal tract (MRST) fibers travel in the ventral funiculus and are also part of the descending ventromedial system. The PRST enhances the antigravity reflexes of the spinal cord. Thus, this pathway facilitates extensors of the lower limb and flexors of the upper limb in order to help maintain posture against the force of gravity. This is an important component of motor control, since most of the time the activity of ventral

horn cells maintains, rather than changes, muscle length and tension. The MRST has the opposite effect of the PRST, in that it frees the antigravity muscles from reflex control (is inhibitory). Therefore, the descending cortical pathways that reach the pontine and medullary reticular formation preside over control of a delicate balance between the two pathways.

The remaining zone of the cerebellum is called the *flocculonodular* or *vestibular zone lobe*. This zone receives only vestibular information from the vestibular nerve and the vestibular nuclei. Interestingly, the deep cerebellar nuclei of the flocculonodular lobe are the vestibular nuclei, which give rise to the LVST and the MVST. Unlike the dentate, interpositus and fastigial, which are deep cerebellar nuclei that lie in the cerebellum, the vestibular nuclei are in the brain stem.

As a summary here is the 'global picture' of the cerebellar analysis of movement:

- (1) The cerebellum is involved in taking the  $MI_{mv1}$  signal and comparing it with the DSCT and CCT signals. It makes corrections via its outflow to the ruber (rubrospinal makes correction) and VA/VL; the latter project to  $MI_{mv1}$  for the correction. This updating/comparing/correcting takes place in the intermediate part or zone of the cerebellum and the outflow nucleus is the interpositus via the superior cerebellar peduncle to reach the ruber and VA/VL. The rubrospinal tract causes a fast correction while the VA/VL projection enables the thalamus to tell  $MI$  to make a certain correction.
- (2) The cerebellum is also involved in the planning of the next movement. Planning information from  $SMA$  and  $MI$  reaches the cerebellum and is integrated with circuits that contain other types of information regarding the planned movement. This planning takes place within the lateral region or zone of the cerebellum and the outflow nucleus is the dentate via the superior cerebellar peduncle to reach the VA/VL, which in turn tells planning areas of  $MI$  and  $SMA$  about the planning information that it picked up in the cerebellum.
- (3) The cerebellum is also involved in the control of posture, balance, and eye movements. It does this via the medial and flocculonodular zones. Thus, the medial zone receives DSCT and CCT unconscious proprioception and uses the outflow of the fastigial to control the reticular formation (PRST and MRST) and the LVST and MVST. We do not know what the circuitry of the cerebellum does to the DSCT and CCT signals, but there must be some integration before the fastigial sends



information out of the cerebellum.

- (4) The flocculonodular lobe receives only vestibular inputs and uses the vestibular nuclei as its deep cerebellar nucleus to control posture, balance and eye movements. Again, we do not know what happens to the vestibular information within the cerebellum.

### 7.2.7 Human Senses and their Pathways

The senses are the physiological methods of perception. A broadly acceptable definition of a sense would be 'a system that consists of a sensory cell type (or group of cell types) that respond to a specific kind of physical energy, and that correspond to a defined region (or group of regions) within the brain where the signals are received and interpreted'. Where disputes arise is with regard to the exact classification of the various cell types and their mapping to regions of the brain. Using this definition several senses can be identified.

*Seeing* or *vision* describes the ability to detect light and interpret it as 'sight'. There is disagreement as to whether or not this constitutes one, two or even three distinct senses. Neuroanatomists generally regard it as two senses, given that different receptors are responsible for the perception of color (the frequency of light) and brightness (the energy of light). Some argue that the perception of depth also constitutes a sense, but it is generally regarded that this is really a cognitive (that is, post-sensory) function derived from having stereoscopic vision (two eyes) and is not a sensory perception as such.

*Hearing* or *audition* is the sense of sound perception and results from tiny hair fibres in the inner ear detecting the motion of atmospheric particles within (at best) a range of 20 to 20000 Hz. Sound can also be detected as vibration by tactition. Lower and higher frequencies than can be heard are detected this way only.

*Taste* or *gustation* is one of the two 'chemical' senses. It is well-known that there are at least four types of *taste* 'bud' (receptor) and hence, as should now be expected, there are anatomists who argue that these in fact constitute four or more different senses, given that each receptor conveys information to a slightly different region of the brain.

The four well-known receptors detect sweet, salt, sour, and bitter, although the receptors for sweet and bitter have not been conclusively identified. A fifth receptor, called 'umami', detects the amino acid glutamate, a flavor commonly found in meat, and in artificial flavorings such

as monosodium glutamate.

*Smell* or *olfaction* is the other 'chemical' sense. Olfactory neurons differ from most other neurons in that they die and regenerate on a regular basis.

The remaining senses can be considered types of physical feeling.

*Tactition* is the sense of *pressure* perception. This definition is the one that differs the most from the Aristotelian model, as it specifically excludes the perception of pain and temperature (classified separately). Even within the limited field of 'pressure' there is still disagreement as to how many distinct senses there actually are. In the skin, for example, there are different receptors responsible for the detection of light against heavy pressure, as well as brief against sustained pressure. Adding to the complexity is the fact that there are also distinct receptors that detect pressure in the visceral organs, such as that caused by a full stomach, and endocrinal receptors that cause the feeling of 'tension', such as that associated with anxiety or excessive caffeine consumption.

*Thermoception* is the sense of *heat* and the absence of heat (*cold*). It is also the first of the group of senses not identified explicitly by Aristotle. Again there is some disagreement about how many senses this actually represents—the thermoreceptors in the skin are quite different from the homeostatic thermoreceptors which provide feedback on internal body temperature. How warm or cold something feels does not only depend on temperature, but also on specific heat capacity and heat conductance; e.g., warm metal feels warmer than warm wood, cold metal feels colder than cold wood because metal has a higher thermal conductivity than wood. Wind feels cold because of the heat withdrawn for evaporation of sweat or other moisture, and because an isolating layer of warm air around the body blows away; however, in the case of hot air, wind makes it feel hotter, for a similar reason as the latter.

*Nociception* is the perception of *pain*. It can be classified as from one to three senses, depending on the classification method. The three types of pain receptors are cutaneous (skin), somatic (joints and bones) and visceral (body organs).

*Equilibrioception* is the perception of *balance* and is related to cavities containing fluid in the inner ear. There is some disagreement as to whether or not this also includes the sense of 'direction' or orientation. However, as with depth perception earlier, it is generally regarded that 'direction' is a post-sensory cognitive awareness.

*Proprioception* is the perception of *body awareness* and is a sense that people rely on enormously, yet are frequently not aware of. More easily

demonstrated than explained, proprioception is the 'unconscious' awareness of where the various regions of the body are located at any one time. (This can be demonstrated by anyone closing their eyes and waving their hand around. Assuming proper proprioceptive function, at no time will the person lose awareness of where the hand actually is, even though it is not being detected by any of the other senses).

Based on this outline and depending on the chosen method of classification, somewhere between 9 and 21 human senses have been identified. Additionally there are some other candidate physiological experiences which may or may not fall within the above classification, for example the sensory awareness of hunger and thirst.

There are also some non-human senses.

*Electroception* (or *electroreception*), the most significant of the non-human senses, is the ability to detect electric fields. Several species of fish, sharks and rays have evolved the capacity to sense changes in electric fields in their immediate vicinity. Some fish passively sense changing nearby electric fields, some generate their own weak, electric fields and sense the pattern of field potentials over their body surface, and some use these generating and sensing capacities for social communication. The mechanisms by which electroceptive fishes construct a spatial representation from very small differences in field potentials involve comparisons of spike latencies from different parts of the fish's body.

The only known mammal which demonstrates electroception is the platypus.

*Magnetoception* (or *magnetoreception*) is the ability to detect fluctuations in magnetic fields and is most commonly observed in birds. Although there is no dispute that this sense exists in many avians (it is essential to the navigational abilities of migratory birds) it is not a well understood phenomenon.

*Echolocation* is the ability to determine orientation to other objects through interpretation of reflected sound (like sonar). Bats and dolphins are noted for this ability, though some other mammals and birds do as well. It is most often used to navigate through poor lighting conditions or to identify and track prey. There is presently an uncertainty as to whether this is simply an extremely developed post-sensory interpretation of auditory perceptions, or actually constitutes a separate sense. Resolution of the issue will require brain scans of animals while they actually perform echolocation, a task which has proved difficult in practice.

### 7.2.8 The Human-Like Vision

The *human eye* is a highly complex optical system, something like a highly sophisticated bio-camera. Its functioning supposes a perfect organization between various components (see Figure 7.26), among them:

- (1) The *iris* – equivalent to the diaphragm of the camera – regulates the quantity of light received;
- (2) The *lens* (biconvex) adjusts the focal distance; and
- (3) The *retina* (which is a kind of a film) contains about 125 millions of photosensitive cells (compare that value to the digital camera resolution). It receives a perfect image, pre-treats it and sends the information to the brain for final interpretation. We ‘see’ with our brains; our eyes merely collect the information to do so.

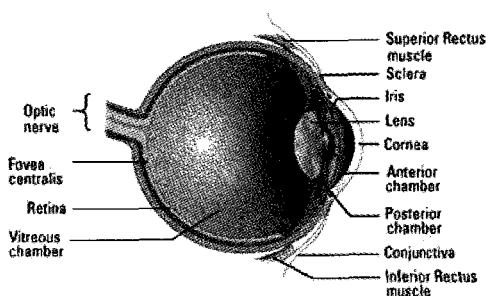


Fig. 7.26 The human eye.

The eye allows us to see and interpret the shapes, colors, and dimensions of objects in the world by processing the light they reflect or emit. The eye is able to see in bright light or in dim light, but it cannot see objects when light is absent.

Light from an object (such as a tree) enters the eye first through the clear cornea and then through the pupil, the circular aperture (opening) in the iris. Next, the light is converged by the crystalline lens to a nodal point immediately behind the lens; at that point, the image becomes inverted. The light progresses through the gelatinous vitreous humor and, ideally, back to a clear focus on the retina, the central area of which is the macula. In the retina, light impulses are changed into electrical signals and then sent along the optic nerve and back to the occipital (posterior) lobe of the brain, which interprets these electrical signals as visual images. Actually,

then, we do not ‘see’ with our eyes but, rather, with our brains; our eyes merely assist with the process.

#### 7.2.8.1 *Extraocular $SO(3)$ –Muscles*

There are six extraocular muscles which act to rotate an eye about its vertical, horizontal, and antero–posterior axes, pretty much in the  $SO(3)$ –group fashion (see chapter 3): the medial rectus (MR), the external rectus (ER), the superior rectus (SR), the inferior rectus (IR), the superior oblique (SO), and the inferior oblique (IO) (see [Montgomery (2003)]).

A given extraocular muscle moves an eye in a specific manner, as follows:

- (1) *medial rectus* (MR)—moves the eye toward the nose, innervated by cranial nerve III;
- (2) *external rectus* (ER)—moves the eye away from the nose, innervated by cranial nerve VI;
- (3) *superior rectus* (SR)—primarily moves the eye upward and secondarily rotates the top of the eye toward the nose, innervated by cranial nerve III;
- (4) *inferior rectus* (IR)—primarily moves the eye downward and secondarily rotates the top of the eye away from the nose, innervated by cranial nerve III;
- (5) *superior oblique* (SO)—primarily rotates the top of the eye toward the nose and secondarily moves the eye downward, innervated by cranial nerve IV; and
- (6) *inferior oblique* (IO)—primarily rotates the top of the eye away from the nose and secondarily moves the eye upward, innervated by cranial nerve III.

Recall that the primary muscle that moves a body segment, as well as an eye, in a given direction is known as the *prime mover* or *agonist muscle*. A muscle in the same eye that moves the eye in the same direction as the agonist is known as a *synergist*, while the muscle in the same eye that moves the eye in the opposite direction of the agonist is the *antagonist muscle*. According to Sherrington’s Law [Sherrington (1906)], increased innervation to any agonist muscle is accompanied by a corresponding decrease in innervation to its antagonist muscle(s).

All of the extraocular muscles, with the exception of the inferior oblique, form a ‘cone’ within the bony orbit. The apex of this cone is located in the posterior aspect of the orbit, while the base of the cone is the attachment of

the muscles around the midline of the eye. This conic structure is referred to as the 'annulus of Zinn', and within the cone runs the optic nerve (cranial nerve II), and within the optic nerve are contained the ophthalmic artery and the ophthalmic vein.

The superior oblique muscle, although part of the cone-shaped annulus of Zinn, differs from the recti muscles in that before it attaches to the eye it passes through a ring-like tendon, the *trochlea* (which acts as a pulley), in the nasal portion of the orbit. The inferior oblique, which is not a member of the annulus of Zinn, arises from the lacrimal fossa in the nasal portion of the bony orbit and attaches to the inferior portion of the eye.

When considering each eye separately, any movement is called a 'duction'. Describing movement around a vertical axis, 'abduction' is a horizontal movement away from the nose caused by a contraction of the ER muscle with an equal relaxation of the MR muscle. Conversely, 'adduction' is a horizontal movement toward the nose caused by a contraction of the MR muscle with an equal relaxation of the ER muscle.

Describing movement around a horizontal axis, 'supraduction' (elevation) is a vertical movement upward caused by the contraction of the SR and IO muscles with an equal relaxation of the IR and SO muscles. Conversely, 'infraduction' (depression) is a vertical movement downward caused by the contraction of the IR and SO muscles with an equal relaxation of the SR and IO muscles.

Describing movement around an antero-posterior axis, 'incycloduction' (intorsion) is a nasal or inward rotation (of the top of the eye) caused by the contraction of the SR and SO muscles with an equal relaxation of the IR and IO muscles. Conversely, 'excycloduction' (extorsion) is a temporal or outward rotation (of the top of the eye) caused by the contraction of the IR and IO muscles with an equal relaxation of the SR and SO muscles.

When considering the eyes' working together, a 'version' or 'conjugate' movement involves simultaneous movement of both eyes in the same direction. Agonist muscles in both eyes which work together to move the eyes in the same direction are said to be 'yoked' together. According to 'Herring's Law,' yoked muscles receive equal and simultaneous innervation. There are six principle versional movements: (1) *dextroversion* (looking right); (2) *levoversion* (looking left); (3) *supraversion* or *sursumversion* (looking up); (4) *infraversion* or *deorsumversion* (looking down); (5) *dextrocycloversion* (rotation to the right); and (6) *levocycloversion* (rotation to the left).

A 'vergence' or 'disconjugate' movement involves simultaneous movement of both eyes in opposite directions. There are two principle vergence

movements: (a) *convergence* (looking nasally or inward: 'crossed-eyes'), and (b) *divergence* (looking temporally or outward: 'wall-eyes').

The 'cardinal positions' are six positions of gaze which allow comparisons of the horizontal, vertical, and diagonal ocular movements produced by the six extraocular muscles. These are the six cardinal positions: *up/right*, *right*, *down/right*, *down/left*, *left*, and *up/left*.

In each position of gaze, one muscle of each eye is the primary mover of that eye and is yoked to the primary mover of the other eye.

Damage to cranial nerve III, IV, or VI often will cause a 'palsy' (paralysis or paresis) of the extraocular muscle(s) innervated by that nerve. The cause of the palsy usually is acquired (due to a lesion, a stroke, or other trauma), although occasionally it can be congenital.

### 7.2.8.2 *Retina*

The retina is the innermost layer of the eye (the tunica intima or internal tunic) and is comparable to the film inside of a camera. It is composed of nerve tissue which senses the light entering the eye. This complex system of nerves sends impulses through the optic nerve back to the brain, which translates these messages into images that we see (see [Montgomery (2003)]).

The retina is composed of 10 layers, from the outside (nearest the blood vessel enriched choroid) to the inside (nearest the gelatinous vitreous humor):

- (1) *pigmented epithelium*;
- (2) *photoreceptors* – bacillary layer (outer and inner segments of cone and rod photoreceptors);
- (3) *external* (outer) *limiting membrane*;
- (4) *outer nuclear* (cell bodies of cones and rods);
- (5) *outer plexiform* (cone and rod axons, horizontal cell dendrites, bipolar dendrites);
- (6) *inner nuclear* (nuclei of horizontal cells, bipolar cells, amacrine cells, and Müller cells);
- (7) *inner plexiform* (axons of bipolar cells and amacrine cells, dendrites of ganglion cells);
- (8) *ganglion cells* (nuclei of ganglion cells and displaced amacrine cells);
- (9) *axons* (nerve fibers from ganglion cells traversing the retina to leave the eye at the optic disk); and
- (10) *internal limiting membrane* (separates the retina from the vitreous).

Light entering the eye is converged first by the cornea, then by the crystalline lens. This focusing system is so powerful that the light rays intersect at a point just behind the lens (inside the vitreous humor) and diverge from that point back to the retina. The diverging light passes through 9 (clear) layers of the retina and, ideally, is brought into focus in an upside-down image on the first (outermost) retinal layer (pigmented epithelium). The image is reflected back onto the adjacent second layer, where the rods and cones are located.

Rods and cones actually face away from incoming light, which passes by these photoreceptors before being reflected back onto them. Light causes a chemical reaction with 'iodopsin' in cones and with 'rhodopsin' in rods, beginning the visual process. Activated photoreceptors stimulate bipolar cells, which in turn stimulate ganglion cells. The impulses continue into the axons of the ganglion cells, through the optic nerve, and to the visual center at the back of the brain, where the image is perceived as right-side up. The brain actually can detect one photon of light being absorbed by a photoreceptor.

There are about 6.5 to 7 million cones in each eye, and they are sensitive to bright light and to color. The highest concentration of cones is in the macula. The fovea centralis, at the center of the macula, contains only cones and no rods. There are 3 types of cone pigments, each most sensitive to a certain wavelength of light: short (430–440 nm), medium (535–540 nm) and long (560–565 nm). The wavelength of light perceived as brightest to the human eye is 555 nm, a greenish-yellow. Once a cone pigment is bleached by light, it takes about 6 minutes to regenerate.

There are about 120 to 130 million rods in each eye, and they are sensitive to dim light, to movement, and to shapes. The highest concentration of rods is in the peripheral retina, decreasing in density up to the macula. Rods do not detect color, which is the main reason it is difficult to tell the color of an object at night or in the dark. The rod pigment is most sensitive to the light wavelength of 500 nm. Once a rod pigment is bleached by light, it takes about 30 minutes to regenerate. Defective or damaged cones results in color deficiency; whereas, defective or damaged rods results in problems seeing in the dark and at night.

### 7.2.8.3 *Cornea*

One-sixth of the outer layer of the eye (called the tunica fibrosa or fibrous tunic) bulges forward as the cornea, the transparent dome which serves as



the outer window of the eye. The cornea is the primary (most powerful) structure focusing light entering the eye (along with the secondary focusing structure, the crystalline lens). It is composed, for the most part, of connective tissue with a thin layer of epithelium on the surface. Epithelium is the type of tissue that covers all free body surfaces (see [Montgomery (2003)]).

The cornea is composed of 5 layers, from the front to the back: *epithelium*; *Bowman's* (anterior limiting) *membrane*; *stroma* (substantia propria); *Descemet's* (posterior limiting) *membrane*; and *endothelium* (posterior epithelium);

The transparency of the cornea is due to the fact that it contains hardly any cells and no blood vessels (although blood vessels can creep in from around it if it is constantly irritated or infected). On the other hand, the cornea contains the highest concentration of nerve fibers of any body structure. The nerve fibers enter on the margins of the cornea and radiate toward the center. These fibers are associated with numerous pain receptors that have a very low threshold. Cold receptors also are abundant in the cornea, although heat and touch receptors seem to be lacking.

Along its circumference, the cornea is continuous with the *sclera*: the white, opaque portion of the eye. The sclera makes up the back five-sixths of the eye's outer layer. It provides protection and serves as an attachment for the extraocular muscles which move the eye.

Coating the outer surface of the cornea is a 'pre-corneal tear film'. People normally blink the eyelids of their eyes about every six seconds to replenish the tear film. Tears have four main functions on the eye: (i) Wetting the corneal epithelium, thereby preventing it from being damaged due to dryness; (ii) Creating a smooth optical surface on the front of the microscopically irregular corneal surface; (iii) Acting as the main supplier of oxygen and other nutrients to the cornea; and (iv) Containing an enzyme called 'lysozyme' which destroys bacteria and prevents the growth of microcysts on the cornea.

#### 7.2.8.4 Iris

The iris, visible through the clear cornea as the colored disc inside the eye, is a thin diaphragm composed mostly of connective tissue and smooth muscle fibers. It lies between the cornea and the crystalline lens. The iris divides the anterior compartment, the space separating the cornea and the lens, into the anterior chamber (between the cornea and the iris) and

the posterior chamber (between the iris and the lens) (see [Montgomery (2003)]).

The iris is composed of 3 *layers*, from the front to the back: *endothelium*; *stroma*; and *epithelium*.

The color of the iris, which is established genetically, is determined by the amount of pigment present in this eye structure. No pigment at all (in the case of an albino) results in a pink iris. Some pigment causes the iris to appear blue. Increasing amounts of iris pigment produce green, hazel, and brown irises (or *irides*). There actually are two pigments, melanin and lipochrome, which determine eye color. Melanin (brown) deposition is controlled by a gene on chromosome 15. Lipochrome (yellowish-brown) deposition is controlled by a gene on chromosome 19.

The iris acts like the shutter of a camera. The *pupil*, the (normally) circular hole in the middle of the iris, comparable to the aperture of a camera, regulates the amount of light passing through to the retina at the back of the eye.

As the amount of light entering the eye diminishes (such as in the dark or at night), the iris dilator muscle (which runs radially through the iris like spokes on a wheel) pulls away from the center, causing the pupil to 'dilate' and allowing more light to reach the retina. When too much light is entering the eye, the iris sphincter muscle (which encircles the pupil) pulls toward the center, causing the pupil to 'constrict' and allowing less light to reach the retina.

Constriction of the pupil also occurs when the crystalline lens accommodates (changes focus) to a near distance; this reaction is known as the 'near reflex'. A representation of parasympathetic pathways in the pupillary light reflex can be seen here, the so-called parasympathetic response.

Watching television in a dark room gives some people eye aches or headaches. This is because as the brightness of the television screen varies considerably every few seconds, the dilator and sphincter iris muscles controlling the pupil have to work overtime, constantly adjusting the ever-changing levels of light entering the eye. With a uniform background light present in the room, causing the pupils to slightly constricted, there is less variance in the size of the pupil as the television illumination changes, and the muscles controlling the pupil size become less tired.

The iris is the most anterior portion of the *uvea* or uveal tract (also known as the tunica vasculosa or vascular tunic). Anatomical structures posterior to the iris, which also are part of the uvea, are the ciliary body

(within which is the ciliary muscle which controls the shape of the crystalline lens) and the choroid (located underneath the retina and which contains the retina's blood supply).

#### 7.2.8.5 Pursuit Eye Control and Motion Perception

*Smooth pursuit eye movements* are eye rotations that are used to maintain fixation on a moving target. Such rotations complicate the interpretation of the retinal image, because they nullify the retinal motion of the target, while generating retinal motion of stationary objects in the background. This poses a problem for the oculomotor system, which must track the stabilized target image, while suppressing the optokinetic reflex, which would move the eye in the direction of the retinal background motion, which is opposite to the direction in which the target is moving. Similarly, the perceptual system must estimate the actual direction and speed of moving objects in spite of the confounding effects of the eye rotation. S. Grossberg and collaborators [Pack *et al.* (2001)], propose a neural model to account for the ability of primates to accomplish these tasks. The model, describing smooth pursuit control and motion perception by *cortical area MST*, simulates the neurophysiological properties of cell types found in the superior temporal sulcus of the macaque monkey, specifically the medial superior temporal (MST) region. These cells process signals related to target motion, background motion, and receive an efference copy of eye velocity during pursuit movements. The model focuses on the interactions between cells in the ventral and dorsal subdivisions of MST, which are hypothesized to process target velocity and background motion, respectively. The model explains how these signals can be combined to explain behavioral data about pursuit maintenance and perceptual data from human studies, including the *Aubert-Fleischl phenomenon* and the *Filehne Illusion*, thereby clarifying the functional significance of neurophysiological data about these MST cell properties. It is suggested that the connectivity used in the model may represent a general strategy used by the brain in analyzing the visual world.

The visual acuity of humans and other primates is marked by a central foveal region of high acuity and concentric regions of decreasing acuity. As such, it is advantageous to keep the fovea fixed on an object as it moves relative to the observer. This can be accomplished if the eye rotates at a speed equal to that of the target. Such rotations are called *smooth pursuit eye movements* (SPEMs). Humans can execute accurate SPEMs for target

motion in excess of  $30^\circ/\text{s}$ . A SPEM consists of at least two phases: one related to target selection and pursuit initiation, and another related to maintenance of ongoing pursuit movements. This model of [Pack *et al.* (2001)] focuses on the second phase.

The maintenance of SPEMs is often characterized in terms of a negative feedback system, meaning that the oculomotor system continuously attempts to match the velocity of the eye to that of the target. However, this description is likely to be incomplete for the simple reason that a successful SPEM stabilizes the target near the fovea. As a result, there is often little or no motion of the target on the retina. Therefore, the pursuit system cannot rely on retinal target velocity to drive a SPEM. A number of additional signals have been hypothesized to guide pursuit, including target position, target acceleration, and a 'memory' of target velocity, which is often described in terms of an oculomotor efference copy of eye velocity. An efference copy duplicates the neural signal sent to the muscles which move the eye, and as such carries information about the movement of the eye that is independent of the retinal image. The efference copy therefore maintains a prediction of pursuit velocity from moment to moment. Thus, the brain may combine retinal information about target motion or position with extraretinal information about the velocity of eye rotation.

An additional source of information relevant to pursuit maintenance is the existence of a visual background. A SPEM is typically made across a visual scene which contains stationary objects, and these objects sweep across the retinal image with a velocity opposite that of the target. This results in large-field coherent motion across the retina, which normally triggers an involuntary eye rotation known as *optokinetic nystagmus* (OKN). OKN causes the eye to move in the same direction as the large stimulus, so that an OKN movement to track retinal motion of a visual background during pursuit would be in the opposite direction of the ongoing pursuit movement. As such, it is crucial that optokinetic signals be suppressed during execution of a SPEM. On the other hand, such signals provide a reafferent stimulus to the visual system indicating that the eye is moving. Therefore the visual motion of the background can provide information about the velocity of ongoing SPEMs, even when the pursuit target is relatively stable on the retina. Such a signal could also be used to generate a prediction of target velocity. The visual motion of the background therefore has contradictory effects on the pursuit system, providing a potentially useful signal for pursuit maintenance, and a potentially destructive OKN signal.

An analogous problem exists for the perceptual system. During an ac-

curate SPEM, the retinal target motion is very small, while objects in the background move across the retina. Psychophysical experiments indicate that human subjects are able to estimate the velocity of objects during a SPEM, but that this ability is somewhat limited. Specifically, it is well-known that observers underestimate the velocity of a moving target during a SPEM when no visible background is present (the Aubert–Fleischl phenomenon), and perceive slight motion of a stationary visual background during a SPEM. More generally, distinguishing between the retinal motion caused by the movement of external objects and that caused by eye rotation is of primary importance for navigation and object tracking, as evidenced by the behavioral deficits that occur when localized cortical lesions disrupt this ability.

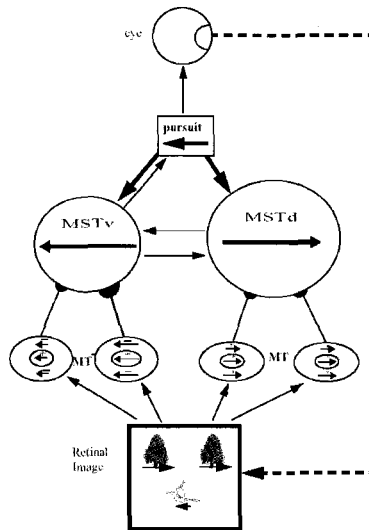


Fig. 7.27 A leftward eye movement channel, in which all connections are excitatory(see text for explanation).

The model of Pack [Pack *et al.* (2001)] consists of two levels of processing (see Figure 7.27). The first level contains 200 MT-like cells which have direction- and speed-selective responses to retinal image motion for stimuli within their receptive fields. Half of these cells have inhibitory surrounds, such that they are suppressed by large stimuli moving in a coherent direction. The other half have excitatory surrounds, exhibiting larger responses to larger stimulus sizes.

The two types of cells form distinct projections to the model MST, which is the second level of processing. Based on these projections, the model MST cells are divided into two functional classes, MSTd and MSTv. We simulate 2 cells in each class. The model MSTd cells integrate the responses of MT cells with excitatory surrounds, thereby enabling them to respond well to global motion of the background. The model MSTv cells integrate the responses of MT cells with inhibitory surrounds, thereby enabling them to respond well to discrete moving targets. The connections from MT to MST are weighted such that MT cells preferring higher speeds generate larger responses in the MSTv cells to which they connect. This generates a graded response to target speed in MSTv. This response is used to drive pursuit eye movements, and the resulting efference copy is fed back into the model at the level of MST. The excitatory connections from MSTd to MSTv enable increasing relative background motion to supplement decreasing relative target motion as the speed of the eye approaches that of the target. Thus model cells in MSTv code the predicted target speed, rather than the speed of the target on the retina.

#### 7.2.8.6 *Optical Flow*

In some evolutionary circles, it is believed that the estimation of the motion of predators advancing at a mobile animal was important to its ability to take flight away from the predator and hence survive. Here we deal with the problem of recovering the motion of objects in the 3D world from the motion of segments on the 2D image plane. The technical problem with estimating the motion of objects in 3D is that in the image formation process, due to the perspective projection of the 3D world onto the 2D image plane, some of the information is lost. We will now address several ways of recovering the 3D information from 2D images using *motion*, *binocular stereopsis*, *texture*, *shading* and *contour*. In particular, there is a lot of biological motivation for studying motion flow [Debevec *et al.* (1996)]:

- (1) Human beings do it all the time without even realizing it, for example, this is why we have saccadic eye movements (that is our eyes jump from focusing at one spot to another). Thus, if the scene has no motion, and we are still our eyes are moving. There are celebrated experiments made on the movements of the pupils of people looking for instance at the 'Mona Lisa' painting, showing the eyes darting from the eyes to the lips to the mouth and then the hair and so on.
- (2) Simple experiment can demonstrate how motion can reveal something

about the 3D structure. Fixating on something close and very far away and moving your head (either sideways or forward and backward), we can notice that the retinal image of the close by tree moves more than the one of a distant tree, i.e. the motion in the retinal plane is inversely proportional to the distance from the retinal plane.

- (3) There are a few examples from the animal world, where the motion helps the animals to obtain some information about the environment structure, e.g., pigeons move their necks to get the so-called ‘motion parallax’.

If the human eye or robot camera moves in the 3D scene, the resulting apparent motion in the image is called the *optical flow*. The optical flow describes the direction and the speed of motion of the features in the image. We now show how to compute the optical flow from sequence of images and then derive an equations relating the 3D structure of the world to our 2D measurements.

The optical flow vector  $v(x, y) \in \mathbb{R}^2$  has two components  $v_1(x, y)$  and  $v_2(x, y)$  describing the motion of a point feature in  $x$  and  $y$  Cartesian direction in the image plane respectively. In order to be able to measure optical flow we need to find corresponding points between two frames. One possibility would be to exploit the similarity between the image patches surrounding the individual points. There are two measures of similarity that are commonly used for optical flow vectors. One is *sum of squared differences* (SSD) between an image patch centered at a point  $P$ , which is a location  $(x_0, y_0)$  at time  $t_0$  and various other candidate locations  $(x_0 + \delta x, y_0 + \delta y)$  where that patch could have moved between two frames at time  $t$  and  $t + \delta t$ . The goal here is to find a displacement in the image plane  $(\delta x, \delta y)$ , which minimizes the SSD criterion [Debevec *et al.* (1996)]:

$$SSD(\delta x, \delta y) = \sum_{(x, y)} (I(x, y, t) - I(x + \delta x, y + \delta y, t + \delta t))^2,$$

where the summation ranges over the image patch centered at the feature of interest. The optical flow of the chosen point feature is

$$(v_1, v_2) = (\partial_t x, \partial_t y).$$

An alternative measure of similarity would be to maximize the cross-correlation between the neighboring patches in the images expressed as

$$Cor(\delta x, \delta y) = \sum_{(x,y)} I(x, y, t) \cdot I(x + \delta x, y + \delta y, t + \delta t).$$

It is important to note that the optical flow is not uniquely determined by the local information.

Next, we want to relate the motion of the camera frame to the optical flow pattern which it generates. For simplicity we will concentrate again only on a single point with 3D coordinates  $(X, Y, Z)$ . Assume that the camera moves with translational velocity  $T \in \mathbb{R}^3$  and the angular velocity  $\omega \in \mathbb{R}^3$  and the observed scene is stationary. This is referred to as *ego-motion*. By differentiating the equation for a projective transformation, we find that the optical flow of a point caused by the motion of the camera is [Debevec *et al.* (1996)]:

$$\begin{aligned} v_1(x, y) &= \left[ -\frac{T_1}{Z(x, y)} - \omega_2 + \omega_3 y \right] - x \left[ -\frac{T_1}{Z(x, y)} - \omega_1 y + \omega_2 x \right], \\ v_2(x, y) &= \left[ -\frac{T_2}{Z(x, y)} + \omega_1 - \omega_3 x \right] - y \left[ -\frac{T_3}{Z(x, y)} - \omega_1 y + \omega_2 x \right], \end{aligned}$$

where  $Z(x, y)$  gives the coordinates of the scene point corresponding to the image at  $(x, y)$ .

Another use of motion flow is in *rendering*. Here we take multiple 2D views of a fixed scene and use it to reconstruct the 3D shape of the object.

### 7.2.9 The Visual Pathway

Vision is generated by photoreceptors in the *retina*, a layer of cells at the back of the eye. The information leaves the eye by way of the *optic nerve*, and there is a partial crossing of axons at the *optic chiasm*. After the chiasm, the axons are called the *optic tract*. The optic tract wraps around the midbrain to get to the *lateral geniculate nucleus* (LGN), where all the axons must synapse. From there, the LGN axons fan out through the deep white matter of the brain as the *optic radiations*, which will ultimately travel to *primary visual cortex*, at the back of the brain.

Information about the world enters both eyes with a great deal of overlap. If we closing one eye, we will find that our range of vision in the remaining eye is mainly limited by our nose. The image projected onto our retina can be cut down the middle, with the *fovea* defining the center. Now we have essentially two halves of the retina, a left half and a right



half. Generally, the halves are referred to as a *temporal half* (next to the temple) and a *nasal half* (next to the nose).

Visual images are inverted as they pass through the lens. Therefore, in the right eye, the nasal retina sees the right half of the world, while the temporal retina sees the left half of the world. Notice also that the right nasal retina and the left temporal retina see pretty much the same thing. If we drew a line through the world at the nose, they would see everything to the right of that line. That field of view is called the *right hemifield*. Each eye gets information from both hemifields.

Now, why bother to divide the retinas at all? Recall that the brain works on a *crossed wires system*. The left half of the brain controls the right side of the body, and vice versa. Therefore the left half of the brain is only interested in visual input from the right side of the world. To insure that the brain does not get extraneous information, the fibers from the retina sort themselves out to separate right hemifield from left hemifield. Specifically, fibers from the nasal retinas cross over at the optic chiasm – whereas the temporal retinas, already positioned to see the opposite side of the world, do not cross (see Figure 7.28).

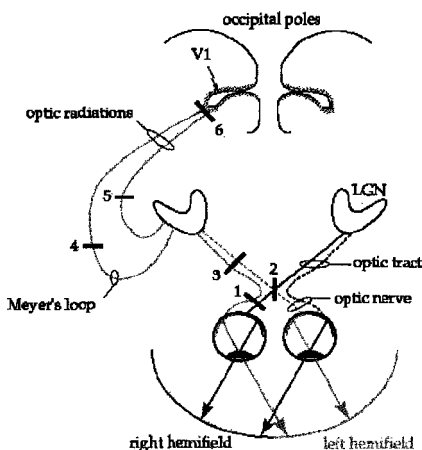


Fig. 7.28 Basic visual pathways.

The practical consequences of this crossing are that damaging the visual system before the chiasm will affect *one eye, both hemifields* – analogous to closing one eye. Damaging the pathway after the chiasm, though, will damage *parts of both eyes, and only one hemifield*.

Once the ganglion cell axons leave the retina, they travel through the optic nerve to the *optic chiasm*, a partial crossing of the axons. At the optic chiasm the left and right visual worlds are separated. After the chiasm, the fibers are called the optic tract. The optic tract wraps around the cerebral peduncles of the midbrain to get to the *lateral geniculate nucleus* (LGN; 'Geniculate' means knee-shaped, and it is a pretty accurate description of the LGN). The LGN is really a part of the thalamus, and remember that nothing gets up to cortex without synapsing in thalamus first (if the cortex is the boss, the thalamus is an excellent secretary). Almost all of the optic tract axons, therefore, synapse in the LGN. The remaining few branch off to synapse in nuclei of the midbrain: the *superior colliculi* and the *pretectal area*.

The neurons in the LGN send their axons directly to V1 (primary visual cortex, striate cortex, area 17) via the *optic radiations*. This highway of visual information courses through the white matter of the temporal and parietal lobes, and can be very vulnerable to strokes. Once the axons reach V1, they terminate primarily in a single sublayer of the cortex.

Recall that all cortical areas in the cerebrum are composed of six basic layers, but that each specific area of cortex may have modifications of layers to best serve its function. It was on the basis of layer appearance and cell types alone that Brodmann first subdivided the cortex into over 50 areas. These areas are known today to correspond to functionally distinct areas – area 17 is primary visual cortex, for example.

Now, to identify the general vicinity of visual cortex, we need first to find the *calcarine sulcus* on the medial surface of the occipital lobe. Primary visual cortex, or V1, is buried within this sulcus. In a fortuitous section, we may be able to see a fine white stripe running within the grey matter inside the sulcus. This stripe marks V1, and gives it a third name, *striate cortex*.

The layers of V1 are specialized in one primary way – layer 4 has been expanded into 4 sublayers: 4A, 4B, 4Ca, and 4Cb. Layer 4A is a dark layer, while the deeper 4B is a very pale layer full of myelin. 4B is actually visible without a microscope – it is the *line of Gennari*, the white stripe that gives V1 its other name, striate cortex. Layer 4C is important because it receives most of the input from the LGN. Due to these specializations, we too can see a transition between Brodmann areas. Follow along the 4B stripe, and we will see it suddenly disappear into a more compact layer 4. This is the transition between areas V1 and V2 (secondary visual cortex, area 18).

As the signal is transmitted to upper layers of cortex, the information

from the two eyes is mixed and binocular vision is created, but here in 4C the two eyes are still entirely separate. Therefore, if we could label the inputs from a single eye, in 4C we would see little pillars of label. If we were to cut tangentially (parallel to the surface) through layer 4C, we would see that all those pillars line up next to each other and form tiger stripes. These are the *ocular dominance stripes*.

Now, recall that the receptive fields of both ganglion cells and LGN neurons were center-surround, and that they responded optimally to points of light. Neurons in the cortex, however, respond very poorly to points of light. The optimal stimulus for most cortical neurons turns out to be a bar of light, in a very specific orientation. How did this come about? One hypothesis is that the key is in how the LGN axons converge on the cortical neurons.

What we see can be divided into several categories of vision: *color*, *linear pattern*, *motion*, etc. The perception of these different categories requires a wide variety of equipment, and some of the divisions are made as early as the retina. For example, rods see only black and white, and can function in dim light, whereas cones can see all colors but require full light. There are at least two types of ganglion cells as well. There are small ganglion cells that dominate in the fovea: they are color sensitive and are 'fine-grained', meaning their receptive fields are small enough that they can pick up a high level of detail. These small cells are called *P cells* (or small cells). The second type of ganglion cells have large dendritic arrays, and receive information from a wide radius of bipolar cells. They are mostly found in the peripheral retina, are not color-sensitive, and are 'coarse-grained' and relatively insensitive to detail. Their main asset is that they are sensitive to motion – we can imagine that due to their width they can track a signal flashing across several bipolar cells. These are the *M cells* (or large cells).

These two types of information, motion vs. color and form, are maintained in separate compartments all the way up the visual pathway. They are kept in separate layers in the LGN, enter V1 via separate sublayers (4Ca vs. 4Cb), and after passing through V2, go on to separate areas of associative cortex. In the end, the *parietal visual cortical areas* (such as MT and PP) end up dealing with motion of objects, navigation through the world, and spatial reasoning (which is essentially moving things around in your head). Temporal *visual areas* (such as V4 and IT) are involved with the complex perception of patterns and forms as recognizable objects.

**Primary Visual Cortex and Visual Awareness.** The primary visual cortex (V1) is probably the best characterized area of human cortex,

but whether this region contributes directly to conscious visual experience is controversial. Early neurophysiological and neuroimaging studies found that visual awareness was best correlated with neural activity in extrastriate visual areas, but recent studies have found similarly powerful effects in V1. Lesion and inactivation studies have provided further evidence that V1 might be necessary for conscious perception. Whereas hierarchical models propose that damage to V1 simply disrupts the flow of information to extrastriate areas that are crucial for awareness, interactive models propose that recurrent connections between V1 and higher areas form functional circuits that support awareness. Further investigation into V1 and its interactions with higher areas might uncover fundamental aspects of the neural basis of visual awareness [Tong (2003)].

#### 7.2.9.1 *Light Reflex and 3D Vision*

**Pupillary Light Reflex.** Recall that there are a few optic tract fibers which bypassed the LGN entirely, travelling instead to the less glamorous but equally essential midbrain. One of their targets in the midbrain is the *pretectal area*, which mediates the *pupillary light reflex*. This reflex can be demonstrated by shining a light in one eye; if all is working correctly, both pupils will constrict.

Light enters the retina and from there travels directly to the pretectal area. After synapsing, the information is sent to the *Edinger–Westphal nuclei* on both sides of the midbrain - this is the crucial step in ensuring that both eyes react to light. The Edinger–Westphal nuclei, via the *III nerve*, control the pupillary constrictors that narrow the pupils. Knowledge of all this enables us to test the status of your patient's visual system by shining a light into each eye.

**3D Shape Perception from Combined Depth Cues.** The brain combines multiple visual cues to yield a perception of depth, but little is known about the site for such combinatorial processing. A recent fMRI study [Welchman *et al.* (2005)] finds that activity in extrastriate areas LOC and MT reflects percepts derived from combining disparity and perspective cues.

Our perception of the world's 3D structure is critical for object recognition, navigation and planning actions. To accomplish this, the brain combines different types of visual information about depth structure, but at present, the neural architecture mediating this combination remains largely unknown. Neuroimaging correlates of human *3D shape perception* from the

combination of two depth cues were recently reported [Welchman *et al.* (2005)]. fMRI responses were measured while observers judged the 3D structure of two sequentially presented images of slanted planes defined by binocular disparity and perspective. The authors compared the behavioral and fMRI responses evoked by changes in one or both of the depth cues. fMRI responses in extrastriate areas (hMT+/V5 and lateral occipital complex), rather than responses in early retinotopic areas, reflected differences in perceived 3D shape, suggesting 'combined-cue' representations in higher visual areas. These findings provide insight into the neural circuits engaged when the human brain combines different information sources for unified 3D visual perception.

**3D Motion Perception.** The eyes receive slightly different views of the world, and the differences between their images (binocular disparity) are used to see depth. Several authors have suggested how the brain could exploit this information for three-dimensional (3D) motion perception, but here we consider a simpler strategy. Visual direction is the angle between the direction of an object and the direction that an observer faces. Recently, [Harris and Drga (2005)] described human behavioral experiments in which observers used visual direction, rather than binocular information, to estimate an object's 3D motion even though this causes them to make systematic errors. Many different trajectories correspond to a single visual direction, which suggests the use of Feynman path integral for modelling purposes (see section 4.4 above as well as section 7.13 below). This suggests that models of binocular 3D motion perception may not reflect the strategies that human observers actually use.

### 7.2.10 *Differential Geometry of the Striate Cortex*

In this subsection we describe how the *cortical fibre bundle map* can represent the neural attributes in the *cortical bundle category*. Recall from chapter 3, that in a trivial bundle, a total space  $E$  is composed of a base (or lattice) space  $B$  and a fibre  $F$ . Common physical examples of fibre are tangent vector space at each point in Euclidean space or internal phases of quantum particles. In case of the *human striate cortex*, a code (or feature, model) space becomes the fibre, while the cortex area becomes the base space. The *signal/feature vector-space* defined by the Cartesian components or the symbolic set in the symbolic computational architecture also becomes the fibre. The bundle transition (symmetry) group  $G$  is the group of homeomorphisms of the fibre  $F$ . Sometimes the transition group replaces

the fibre,  $G = F$  (i.e., *principal fibre bundle*), and the neural attributes would be represented by the group elements.<sup>2</sup>

Now, a series of experiments have suggested that important elements of the organization of *ocular dominance* (OD) and *orientation preference* (OP) maps in the striate cortex are not prespecified but emergent during an activity-driven, Hebbian-like self-organizing process [Hebb (1949)]. Modern brain-imaging techniques (see Appendix) revealed the detailed maps of OD and OP over small patches of the cortex, which prompted several models for the map generation in the brain and various attempts for the analysis of the properties in the observed cortical map patterns. In [Cho and Kim (2004)], a new *visual map formation method* was proposed with *neighborhood interactions*. The cortical map generation is described by *spin-like Hamiltonians* with *distance dependent interactions*. The statistical analysis of these Hamiltonians leads to the successful description of several pattern properties observed *in vivo*. In this analogy, the progress in the visual map formation corresponds to *relaxation dynamics in spin systems*, where, for example, the pinwheels in OP can be regarded as (in-plane) vortices.

According to [Cho and Kim (2004)], the *six layers of the neocortex* can be classified into three different functional types. The layer IV neurons first get the long range input currents, such as signals from the retina via the *lateral geniculate nucleus* (LGN) of the thalamus, and send them up vertically to layer II and III that are called the *true association cortex*. Output signals are sent down to the layer V and VI, and sent further to the thalamus or other deep and distant neural structures. Lateral connections also occur in the superficial (layer II and III) pyramidal neurons and have usual antagonistic propensity which sharpens responsiveness to an area. However, the superficial pyramidal neurons also send excitatory recurrent to adjacent neurons due to unmyelinated collaterals. Horizontal or lateral connections have such distance dependent ('Mexican hat' shaped) excitatory or inhibitory activity. Some bunches of neurons make columnar clusters called minicolumns and such aggregations are needed to consider higher dimensional properties of processing elements [Arbib (1998); Cho and Kim (2004)].

A Lie algebraic representation method for the feature vectors in cortical maps, called the *fibre bundle map* model was proposed in [Cho and Kim (2004)]. This starts from the assumption that the total cortical space  $E$  is composed of the lattice (or base) space  $B$  and the pattern (or fibre)

---

<sup>2</sup>Recall that principal fibre bundles admit connections (or vector potential) in Yang-Mills gauge theories.

space  $F$ . A transition function (or symmetry) group  $G = SO(3)$  of a homeomorphism of the fibre space  $F$  is necessary to describe what happens if there is 'excitatory' or 'inhibitory' activity.

If there are stimuli from lateral and LGN neurons in the OP columns, the changes in preferred angles  $\phi_i$  ( $0 \leq \phi_i < \pi$ ) for  $i$ th neuron group are described by

$$\dot{\phi}_i = -2\varepsilon I(\vec{r}_i, \vec{r}_j) \sin(2\phi_i - 2\phi_j) - 2\mu B_i \sin(2\phi_i - 2\phi'_i), \quad (7.3)$$

where  $\varepsilon$  and  $\mu$  are the change rates in the stimuli from lateral and LGN cells, respectively, and  $B$  and  $\phi'$  are the strength and the phase of LGN stimulus. The lateral neighborhood interaction function  $I$  was used as a modified output from a wavelet (with amplitude  $k$  and standard dev.  $\sigma$ ),

$$I_{WL}(\vec{r}_i, \vec{r}_j) = \left(1 - k \frac{|\vec{r}_i - \vec{r}_j|^2}{\sigma^2}\right) \exp\left(-\frac{|\vec{r}_i - \vec{r}_j|^2}{2\sigma^2}\right).$$

Note that there is also another well-known Mexican hat shaped function called the *difference of Gaussians filter* (or DOG-filter),

$$I_{DOG}(r) = \exp(-r^2/2\sigma_1^2) - k \exp(-r^2/2\sigma_2^2).$$

Equation (7.3) can be rewritten as a *gradient flow* with the Hamiltonian

$$H = -J(\vec{r}_i, \vec{r}_j) \mathbf{S}_i \cdot \mathbf{S}_j - \mathbf{h}_i \cdot \mathbf{S}_i,$$

where  $J(\vec{r}_i, \vec{r}_j) = \frac{\varepsilon}{2} I(\vec{r}_i, \vec{r}_j)$  is site distance dependent *interaction energy*. The site states  $\mathbf{S}_i = (\cos 2\phi_i, \sin 2\phi_i)$  and the external stimuli  $\mathbf{h}_i = (\mu B_i \cos 2\phi'_i, \mu B_i \sin 2\phi'_i)$  are 2-component vectors. In this form,  $H$  is similar to spin models in statistical physics. In the case of OD maps,  $\mathbf{S}_i$  has a one-component with  $\pm 1$  values similar to the Ising model (see subsection 7.7.2 below).

### 7.2.11 Auditory and Vestibular Pathways

#### 7.2.11.1 The Inner Ear

The auditory and vestibular systems are intimately connected. The receptors for both are located in the temporal bone, in a convoluted chamber called the *bony labyrinth*. A delicate continuous membrane is suspended within the bony labyrinth, creating a second chamber within the first. This chamber is called the *membranous labyrinth*. The entire fluid-filled structure is called the inner ear.

The inner ear has two membrane-covered outlets into the air-filled middle ear – the oval window and the round window. The oval window is filled by the plate of the stapes, the third middle ear bone. The stapes vibrates in response to vibrations of the eardrum, setting the fluid of the inner ear sloshing back and forth. The round window serves as a pressure valve, bulging outward as pressure rises in the *inner ear*.

The inner ear has two membrane-covered outlets into the air-filled middle ear – the oval window and the round window. The oval window is filled by the plate of the stapes, the third middle ear bone. The stapes vibrates in response to vibrations of the eardrum, setting the fluid of the inner ear sloshing back and forth. The round window serves as a pressure valve, bulging outward as pressure rises in the inner ear.

The oval window opens into a large central area within the inner ear called the *vestibule*. All of the inner ear organs branch off from this central chamber. On one side is the *cochlea*, on the other the *semicircular canals*. The *utricle* and *sacculle*, additional vestibular organs, are adjacent to the vestibule.

The membranous labyrinth is filled with a special fluid called *endolymph*. Endolymph is very similar to intracellular fluid: it is high in potassium and low in sodium. The ionic composition is necessary for vestibular and auditory hair cells to function optimally. The space between the membranous and bony labyrinths is filled with *perilymph*, which is very much like normal cerebral spinal fluid.

#### 7.2.11.2 Auditory Transduction

The transduction of sound into a neural signal occurs in the cochlea. As the stapes vibrates the oval window, the perilymph sloshes back and forth, vibrating the round window in a complementary rhythm. The membranous labyrinth is caught between the two, and bounces up and down with all this sloshing. Now let's take a closer look at the membranous labyrinth.

The membranous labyrinth of the cochlea encloses the endolymph-filled *scala media*. The two compartments of the bony labyrinth, which house the perilymph, are called the *scala vestibuli* and *tympani*. Within the *scala media* is the receptor organ, the *organ of Corti*. It rests on part of the membranous labyrinth, the *basilar membrane*.

The auditory hair cells sit within the organ of Corti. There are *inner hair cells*, which are the auditory receptors, and *outer hair cells*, which help to 'tune' the cochlea, as well as supporting cells. The sensitive stereocilia of



the inner hair cells are embedded in a membrane called the *tectorial membrane*. As the basilar membrane bounces up and down, the fine stereocilia are sheared back and forth under the tectorial membrane. When the stereocilia are pulled in the right direction, the hair cell depolarizes. This signal is transmitted to a nerve process lying under the organ of Corti. This neuron transmits the signal back along the auditory nerve to the brainstem. As with almost all sensory neurons (the exception is in the retina), its cell body lies outside the CNS in a ganglion. In this case, the ganglion is stretched out along the spiralling center axis of the cochlea, and is named the *spiral ganglion*.

The basilar membrane is actually thinner and narrower at the base of the cochlea than at the tip (apex), which seems backwards given that the cochlea is widest at the base. The properties of the basilar membrane change as its shape changes; just as with guitar strings, thin things vibrate to high pitches, and thick things vibrate to low pitches. This means that the basilar membrane vibrates to high frequencies at the base of the cochlea and to low frequencies at the apex. A hair cell at the base of the cochlea will respond best to high frequencies, since at those frequencies the basilar membrane underneath it will vibrate the most. Although the hair cells are arranged in order along the basilar membrane, from high-frequency to low-frequency, it is the properties of the basilar membrane that set up this gradient, not the properties of the hair cells.

Now, our ability to discriminate two close frequencies is actually much better than one would predict just from the mechanics of the basilar membrane. One theory to explain the mystery is that the outer hair cells help to 'sharpen the tuning'. Outer hair cells can actually move (change length) in response to nerve stimulation. If they could push the basilar membrane up and down, they could amplify or damp vibrations at will, making the inner hair cells more or less responsive.

### 7.2.11.3 Central Auditory Pathways

The auditory nerve carries the signal into the brainstem and synapses in the *cochlear nucleus*. From the cochlear nucleus, auditory information is split into at least two streams, much like the visual pathways are split into motion and form processing. Auditory nerve fibers going to the ventral cochlear nucleus synapse on their target cells with giant, hand-like terminals. Something about this tight connection allows the timing of the signal to be preserved to the microsecond (action potentials are on the order of

milliseconds, so it is no mean feat). The ventral cochlear nucleus cells then project to a collection of nuclei in the medulla called the *superior olive*. In the superior olive, the minute differences in the timing and loudness of the sound in each ear are compared, and from this we can determine the direction the sound came from. The superior olive then projects up to the *inferior colliculus* via a fibre tract called the *lateral lemniscus*.

The second stream of information starts in the *dorsal cochlear nucleus*. Unlike the exquisitely time-sensitive localization pathway, this stream analyzes the quality of sound. The dorsal cochlear nucleus, with fairly complex circuitry, picks apart the tiny frequency differences which make 'bet' sound different from 'bat' and 'debt'. This pathway projects directly to the inferior colliculus, also via the lateral lemniscus. Note that both pathways are bilateral. The consequence of this is that lesions anywhere along the pathway usually have no obvious effect on hearing. Deafness is essentially only caused by damage to the middle ear, cochlea, or auditory nerve.

From the inferior colliculus, both streams of information proceed to sensory thalamus. The auditory nucleus of thalamus is the *medial geniculate nucleus*. The medial geniculate projects to *primary auditory cortex*, located on the banks of the temporal lobes (see Figure 7.29).

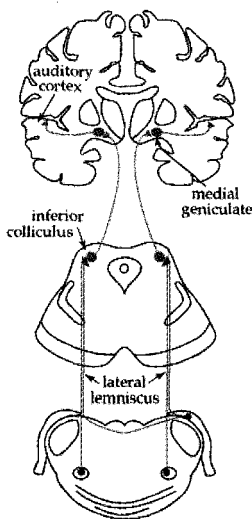


Fig. 7.29 Basic auditory pathways.

The auditory cortex, once thought to be a passive detector, is now

caught in the act of reshaping the frequency sensitivity of its neurons to intercept target sounds that are significant for a behavioral task, suggesting tuning properties can change ‘on-line’ [Middlebrooks (2004)].

#### 7.2.11.4 *The Vestibular System*

The purpose of the vestibular system is to keep tabs on the position and motion of your head in space. There are really two components to monitoring motion, however. You must be able to detect rotation, such as what happens when we shake or nod your head. In dynamics, this is called *angular acceleration*. You must also be able to detect motion along a line - such as what happens when the elevator drops beneath us, or on a more subtle note, what happens when your body begins to lean to one side. This is called *linear acceleration*. The vestibular system is divided into two receptor organs to accomplish these tasks.

#### 7.2.11.5 *The Semicircular Canals*

The *semicircular canals* detect *angular acceleration*. There are 3 canals, corresponding to the three dimensions in which we move, so that each canal detects motion in a single plane. Each canal is set up as shown below, as a continuous endolymph-filled hoop. The actual hair cells sit in a small swelling at the base called the *ampula* (see Figure 7.31 below).

The hair cells are arranged as a single tuft that projects up into a gelatinous mass, the cupula. When we turn our head in the plane of the canal, the inertia of the endolymph causes it to slosh against the cupula, deflecting the hair cells. Now, if we were to keep turning in circles, eventually the fluid would catch up with the canal, and there would be no more pressure on the cupula. If we stopped spinning, the moving fluid would slosh up against a suddenly still cupula, and we would feel as though we were turning in the other direction.

Naturally, we have the same arrangement (mirrored) on both sides of the head. Each tuft of hair cells is polarized – if we push it one way, it will be excited, but if we push it the other way, it will be inhibited. This means that the canals on either side of the head will generally be operating in a *push-pull* rhythm; when one is excited, the other is inhibited (see below). It is important that both sides agree as to what the head is doing. If there is disagreement, if both sides push at once, then we will feel debilitating vertigo and nausea. This is the reason that infections of the endolymph or damage to the inner ear can cause vertigo. However, if one vestibular nerve

is cut, the brain will gradually get used to only listening to one side – this can actually be a treatment for intractable vertigo.

A large role of the semicircular canal system is to keep your eyes still in space while your head moves around them. If you nod and shake and swivel your head, you will find that you have no trouble staying focused on this page. But hold a piece of paper in front of you and shake it around, and your eyes will not be able to keep up with the quick movements. The reason is that the semicircular canals exert direct control over the eyes, so they can directly compensate for head movements. Recall that the eye is controlled by three pairs of muscles; the medial and lateral rectus, the superior and inferior rectus, and the inferior and superior oblique. You may also remember that their directions of motion seemed to be at crazy diagonals. Those same crazy diagonals are matched closely by the three planes of the semicircular canals, so that a single canal (in general) interacts with a single muscle pair. The entire compensatory reflex is called the *vestibulo-ocular reflex* (VOR).

#### 7.2.11.6 The Vestibulo-Ocular Reflex

Although the VOR works on all three muscle pairs, the medial-lateral rectus pair, coupled to the horizontal canal, is geometrically the easiest to draw. The setup, looking down at a person's head is given in Figure 7.30.

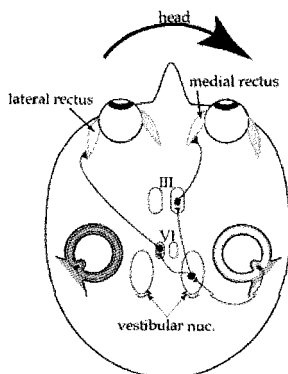


Fig. 7.30 Pathways of the vestibulo-ocular reflex.

The lateral rectus muscle will pull the eye laterally, and the medial rectus will pull the eye medially, both in the horizontal plane. The horizontal canal detects rotation in the horizontal plane.

If you move your head to the left, you will excite the left horizontal canal, inhibiting the right. To keep your eyes fixed on a stationary point, you need to fire the right lateral rectus and the left medial rectus, to move the eyes to the right.

The pathway is as follows: the vestibular nerve enters the brainstem and synapses in the vestibular nucleus. Cells that received information from the left horizontal canal project to the abducens nucleus on the right side, to stimulate the lateral rectus. They also project to the oculomotor nucleus on the left side, to stimulate the medial rectus. Although not shown on the diagram, the same vestibular cells also inhibit the opposing muscles (in this case, the right medial rectus, and the left lateral rectus).

What about the other side? The right horizontal canal is wired to the complementary set of muscles. Since it is inhibited, it will not excite its target muscles (the right medial rectus and the left lateral rectus), nor will it inhibit the muscles you want to use (the right lateral rectus and the left medial rectus).

A great deal of the VOR axon traffic travels via a fibre pathway called the MLF (medial longitudinal fasciculus). The integrity of this tract is crucial for the VOR to work properly. It is occasionally damaged by medial brainstem strokes.

#### 7.2.11.7 *The Utricle and Sacculle*

The *utricle* and *sacculle* detect *linear acceleration*. Each organ has a sheet of hair cells (the macula) whose cilia are embedded in a gelatinous mass, just like the semicircular canals. Unlike the canals, however, this gel has a clump of small crystals embedded in it, called an otolith (yes, all along you've had rocks in your head). The otoliths provide the inertia, so that when you move to one side, the otolith-gel mass drags on the hair cells. Once you are moving at a constant speed, such as in a car, the otoliths come to equilibrium and you no longer perceive the motion.

The hair cells in the utricle and sacculle are polarized, but they are arrayed in different directions so that a single sheet of hair cells can detect motion forward and back, side to side. Each macula can therefore cover two dimensions of movement. The utricle lays horizontally in the ear, and can detect any motion in the horizontal plane. The sacculle is oriented vertically, so it can detect motion in the sagittal plane (up and down, forward and back).

A major role of the sacculle and utricle is to keep you vertically oriented

with respect to gravity. If your head and body start to tilt, the vestibular nuclei will automatically compensate with the correct postural adjustments. This is not just something that happens if the floor tilts – if you watch someone trying to stand still, you will notice constant small wavers and rocking back and forth.

### 7.2.11.8 Mechanics of the Semicircular Canals

Recall that the *human vestibular system* consists of two sets of organs: the *otolithhic organs* (sacculle and utricle), which sense translational acceleration and gravity, and the *semicircular canals* (cupula), which sense *angular acceleration*. Natural purpose of the vestibular system is to capture the three translations and three rotations from the  $SE(3)$  group of rigid body motions (see subsection 3.5.2 above). Each ear has three semicircular canals that are oriented in a mutually orthogonal fashion in order to sense rotations about each of three axes (see Figure 7.31). The canals are filled with endolymph of density  $\rho$  and viscosity  $\mu$  similar to that of water. Each canal consists of a narrow *duct* connected to thicker *ampulla* and *vestibule* regions, which are in turn separated by the membranous cupula (see [Squires *et al.* (2005)]).

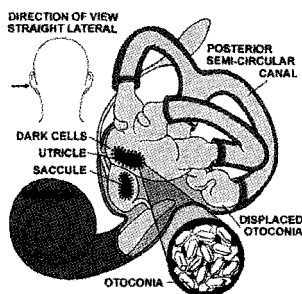


Fig. 7.31 The human vestibular system consists of the semicircular canals for sensing angular acceleration, the otolithhic organs (sacculle and utricle) for sensing linear/gravitational acceleration, and the cochlea for auditory sensing.

When the semicircular canal experiences an angular acceleration, inertia moment causes a lag in endolymph motion, distorting the *cupula* by a volume  $V_c$ . The cupular distortion triggers activation of embedded sensory hair cells, signalling the angular acceleration/velocity to the brain and causing a compensatory eye motion called *nystagmus*. Under sustained rotation, the elastic restoring force of the cupula pushes endolymph back through the canal, and the cupula slowly relaxes to its undisplaced position.

Neural signal processing in the brain stem modifies the transmitted signal in a process called *velocity storage* [Robinson (1977); Raphan *et al.* (1979)], which lengthens the typical time constant of the associated sensation and nystagmus. The typical time constant for cupular relaxation ( $\tau_c \approx 4$  s) is transformed into a nystagmus time constant of about  $\tau_v \approx 21$  s for rotation about the vertical axis of the head (yaw), where the lateral semicircular canal is stimulated.

To model geometry of the semicircular canal, a two-part, two-torus  $T^2$  of major radius  $R$ , with a thick *ampulla* region and a thin *duct* region is used in [Squires *et al.* (2005)]. The inner and outer radii of the canal as functions of angle ( $0 < \theta \leq 2\pi$ ) are represented as

$$R_{\text{out}} = R + b_d \quad \text{and} \quad R_{\text{in}}(\theta) = R - \left[ A + B \tanh\left(\frac{\theta - \theta_1}{\delta}\right) \right],$$

where  $A = 2b_c + b_d$  and  $B = 2b_c - b_d$ . The canal narrows from radius  $b_c$  in the ampulla to  $b_d$  in the duct roughly over an angle  $2\delta$ , centered around  $\theta_1$ .

#### 7.2.11.9 Endolymph Flow in the Semicircular Canals

Classical *Steinhausen model* of the normal functioning of the semicircular canals [Steinhausen (1933)], treats endolymph displacement with an overdamped pendulum equation. Two time scales appear in this work: a rapid time scale  $\tau_f$ , during which fluid moves ballistically through the canal, and a slow time scale  $\tau_c$  over which the cupula relaxes back to its undistorted position. Subsequent theoretical work has typically worked towards calculating these time scales from the physical parameters and length scales characteristic of the vestibular system. Examples include the transient and quasi-steady fluid motion in a torus with thin (duct) and thick (vestibule/utricle) sections [van Buskirk *et al.* (1976)], ducts with non-constant and non-circular cross section [Oman *et al.* (1987)], allowances for high-accelerations by calculating the fluid flow near the cupula partition rather than assuming a Poiseuille profile [Rabbitt and Damiano (1996)], fluid flow through a possibly porous cupula [Damiano (1999)], and the effects of multiple hydrodynamically-connected canals [Muller and Verhagen (1988)].

Furthermore, in [van Buskirk *et al.* (1976)] the time constants were

explicitly calculated in terms of the system dimensions and parameters as

$$\tau_c = \frac{8\mu\beta_d R}{\pi b_d^4 K} \quad \text{and} \quad \tau_f = \frac{\rho b_d^2}{\lambda_1^2 \mu},$$

where  $\lambda_1$  is the first zero of the Bessel function  $J_0(\lambda)$ , i.e.,  $\lambda_1 \approx 2.4$ . All physical parameters are known other than the elastic constant  $K$  of the cupula, here chosen to give the measured value ( $\tau_c = 4.2$  s) for the human cupular time constant [Dai *et al.* (1999)]. Following a step increase in angular velocity  $\alpha(t) = \Omega_0 \delta(t)$ , the endolymph in the duct (and therefore the cupula) experiences a maximum displacement of volume

$$V_c = \frac{4\rho\Omega_0(1 + \beta_u/\beta_d)\pi R b_d^4}{\lambda_1^4 \mu},$$

after a time  $\tau_f$ , after which the cupula relaxes back on a time scale  $\tau_c$ .

The influence of fluid inertia occurs over millisecond time scales, whereas the state of the fluid, cupula, and otoconium all change on significantly longer time scales. Therefore, we can neglect fluid inertia, so that the cupular membrane obeys a simple balance of pressures, in which three terms are important. A cupular membrane that is distorted to displace a volume  $V_c$  exerts an elastic restoring force that contributes an amount  $-KV_c$  to the transcupular pressure difference. Second, by conservation of mass, instantaneous cupular and endolymph volume displacements must be equal. The resulting *viscous force* contributes an amount  $-\gamma\dot{V}_c$  to the transcupular pressure. The last term to enter the pressure balance is an externally applied, time-dependent pressure difference  $\Delta P_c(t)$ , which in our case is given by the fluid pressure set up by a settling otoconium. These three pressures balance, giving an *equation for cupular volume displacement* [Squires *et al.* (2005)]

$$-KV_c - \gamma\dot{V}_c + \Delta P_c(t) = 0. \quad (7.4)$$

In normal vestibular functioning,  $\Delta P_c$  arises from angular acceleration of the canals, in which case (7.4) is consistent with the Steinhausen equation [Steinhausen (1933)] (if the effect of fluid inertia is neglected).

The viscous resistance coefficient  $\gamma$  for quasi-steady fluid flow through the duct can be derived in a straightforward manner. Fluid in a straight channel of length  $\beta_d R$  and circular cross-section of radius  $b_d$ , subject to an applied pressure difference  $\Delta P$ , moves with a parabolic velocity profile



directed along the cylinder axis  $\mathbf{e}_{||}$  [Leal (1992)],

$$\mathbf{u}(r) = \frac{\Delta P}{4\mu\beta_d R} (b_d^2 - r^2) \mathbf{e}_{||}.$$

Note that we have assumed the usual no-slip condition for a solid/fluid interface. From the flow rate  $\dot{V}_c = \pi b_d^4 \Delta P / 8\mu\beta_d R$ , the viscous coefficient  $\gamma$  is shown to be

$$\gamma = \frac{8\mu\beta_d R}{\pi b_d^4}.$$

This result can be expected to provide a very good approximation for the low-Reynolds-number flow in the slightly curved canal duct and slowly-varying geometries of interest here. The pressure drop along the duct (which varies approximately with  $\approx b_d^4/\beta_d$ ) is approximately a thousand times greater than that along the vestibule/utricle and ampulla (which varies with  $b_c^4/\beta_u$ ). Therefore, we can approximate the viscous resistance in the canal as occurring in the duct alone. Furthermore, we can approximate the channel as locally straight, because the radius of curvature of the channel  $R$  is large compared to the duct radius. This introduces errors of magnitude  $\mathcal{O}(b_d/R) \approx 0.05$  in the axial flow and  $\mathcal{O}(b_d^2/R^2) \approx 10^{-3}$  in the flow rate [Leal (1992)]. Finally, although the channel radius is not constant, it typically varies slowly within the duct [Squires *et al.* (2005)].

### 7.2.12 Somatosensory Pathways

The *somatosensory system* includes multiple types of sensation from the body - light touch, pain, pressure, temperature, and joint and muscle position sense (also called proprioception). However, these modalities are lumped into three different pathways in the spinal cord and have different targets in the brain. The first modality is called *discriminative touch*, which includes touch, pressure, and vibration perception, and enables us to ‘read’ raised letters with our fingertips, or describe the shape and texture of an object without seeing it. The second grouping is *pain and temperature*, which is just what it sounds like, and also includes the sensations of itch and tickle. The third modality is called *proprioception*, and includes receptors for what happens below the body surface: muscle stretch, joint position, tendon tension, etc. This modality primarily targets the *cerebellum*, which needs minute-by-minute feedback on what the muscles are doing.

These modalities differ in their receptors, pathways, and targets, and also in the level of crossing. Any sensory system going to the cerebral cortex

will have to cross over at some point, because the cerebral cortex operates on a contralateral (opposite side) basis. The discriminative touch system crosses high – in the medulla. The pain system crosses low – in the spinal cord. The proprioceptive system is going to the cerebellum, which works ipsilaterally (same side). Therefore this system does not cross.

#### 7.2.12.1 The Discriminative Touch System

The *discriminative touch system*, which is carried in the spinal cord, includes the entire body from the neck down; face information is carried by cranial nerves. The overall pathway is presented on Figure 7.32.

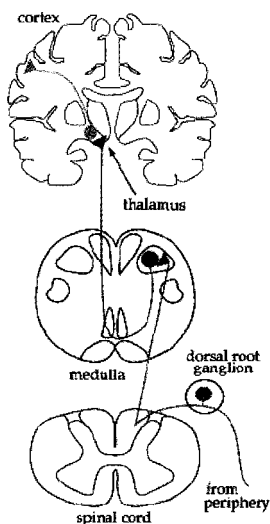


Fig. 7.32 The discriminative touch pathway.

Sensation enters the periphery via sensory axons. All sensory neurons have their cell bodies sitting outside the spinal cord in a clump called a *dorsal root ganglion*. There is one such ganglion for every spinal nerve. The sensory neurons are unique because unlike most neurons, the signal does not pass through the cell body. Instead the cell body sits off to one side, without dendrites, and the signal passes directly from the distal axon process to the proximal process.

The proximal end of the axon enters the dorsal half of the spinal cord, and immediately turns up the cord towards the brain. These axons are

called the *primary afferents*, because they are the same axons that brought the signal into the cord. (In general, afferent means towards the brain, and efferent means away from it.) The axons ascend in the dorsal white matter of the spinal cord.

At the medulla, the primary afferents finally synapse. The neurons receiving the synapse are now called the *secondary afferents*. The secondary afferents cross immediately, and form a new tract on the other side of the brainstem.

This tract of secondary afferents will ascend all the way to the *thalamus*, which is the clearinghouse for everything that wants to get into cortex. Once in thalamus, they will synapse, and a third and final neuron will go to *cerebral cortex*, the final target. Once in the thalamus, the secondary afferents synapse in a thalamic nucleus called the *ventrolateral posterior nucleus* (VPL). The thalamocortical afferents (from thalamus to cortex) travel up through the internal capsule to get to *primary somatosensory cortex*, the end of the pathway. Primary somatosensory cortex is located in the *post-central gyrus*, which is the fold of cortex just posterior to the central sulcus.

The discriminative touch is the perception of *pressure*, *vibration*, and *texture*. This system relies on four different receptors in the skin. They are: *Meissner's corpuscles*, *Pacinian corpuscles*, *Merkel's disks*, and *Ruffini endings*.

The first two are considered rapidly adapting (they quickly stop firing in response to a constant stimulus) and the second two are considered slowly adapting (they do not stop firing). To put this into an example, if one lays his pen down in his palm, the Meissner's and Pacinian corpuscles will fire rapidly as it first touches down, to let him know something has landed. If the pen lays still, they will stop firing almost right away. The Merkel's and Ruffini endings, however, will continue to fire to let him know that something is still there.

#### 7.2.12.2 The Pain and Temperature System

The *pain and temperature system* does not have specialized receptor organs. Instead, it uses *free nerve endings* throughout skin, muscle, bone, and connective tissue to perceive changes in temperature and pain peptides. Although pain will result from damage to a free nerve ending, in reality most pain is a result of substances released by damaged tissues: *prostaglandins*, *histamine*, and *substance P*. The free nerve ending has re-

ceptors for these substances and lets us know (stridently) when tissue has been damaged.

This system shares one major rule with the discriminative touch system: primary afferents synapse ipsilaterally, then secondary afferents cross. The crossings just occur at different levels.

Pain afferents (all of the following applies to temperature as well) enter the cord laterally, due to their small size, and synapse more or less immediately. 'More or less', because they actually can travel one or two segments up or down the cord before synapsing. *Lissauer's tract* is the tract carrying these migrating axons, but they are only in the tract for a short time. Within one or two levels, they enter the dorsal horn and synapse.

The dorsal horn is a multi-layered structure. The thin outermost layer is called the *posterior marginalis* layer. The wide pale second layer is called the *substantia gelatinosa*, and the layer deep to that is called the *nucleus proprius*.

### 7.2.12.3 The Proprioceptive System

The third modality, *proprioceptive sensation*, relies on receptors in muscles and joints. The muscle spindle is the major stretch receptor within muscles, and just like the cutaneous receptors, it has a rapidly-adapting and slowly-adapting component. There are also Golgi tendon organs and *joint afferents* to monitor stresses and forces at the tendons and joints.

The proprioceptive system arises from primarily the  $\alpha$ -afferents entering the spinal cord. These are the afferents from muscle spindles, Golgi tendon organs, and joint receptors. The axons travel for a little while with the discriminative touch system, in the posterior columns. Within a few segments, however, the proprioceptive information slips out of the dorsal white matter and synapses. After synapsing it ascends without crossing to the cerebellum.

Exactly where the axons synapse depends upon whether they originated in the legs or the arms. Leg fibers enter the cord at sacral or lumbar levels, ascend to the upper lumbar segments, and synapse in a medial nucleus called *Clarke's nucleus* (or nucleus dorsalis). The secondary afferents then enter the *dorsal spinocerebellar tract* on the lateral edge of the cord.

Fibers from the arm enter at cervical levels and ascend to the caudal medulla. Once there they synapse in a nucleus called the *external cuneate* (or lateral cuneate) nucleus, and the secondary axons join the leg information in the dorsal spinocerebellar tract.

The spinocerebellar tract stays on the lateral margin of the brainstem all the way up the medulla. Just before reaching the pons, it is joined by a large projection from the *inferior olive*. These axons together make up the bulk of the *inferior cerebellar peduncle*, which grows right out of the lateral medulla and enters the cerebellum.

**Normal and Pathological Oscillatory Communication in the Brain.** The huge number of neurons in the human brain are connected to form functionally specialized assemblies. The brain's amazing processing capabilities rest on local communication within and long-range communication between these assemblies. Even simple sensory, motor and cognitive tasks depend on the precise coordination of many brain areas. Recent improvements in the methods of studying long-range communication have allowed us to address several important questions [Schnitzler and Gross (2005)]. What are the common mechanisms that govern local and long-range communication and how do they relate to the structure of the brain? How does oscillatory synchronization subserve neural communication? And what are the consequences of abnormal synchronization?

According to [Schnitzler and Gross (2005)], the remarkable processing capabilities of the brain rely on efficient communication between the huge number of neurons and neuronal assemblies that constitute functionally specialized units. Abundant anatomical connections form the structural basis of communication. Functionally, the synchronization of oscillatory neuronal activity has increasingly been recognized as a mechanism for long-range communication.

Studies of the insect olfactory system provide the most direct evidence that oscillatory communication is behaviorally relevant. These and other studies point towards several mechanisms that function on different spatial scales to support interneuronal communication. Filtering and resonance phenomena indicate the dependence of neuronal activity on the frequency content of the input. Specific structural connectivity underlies the emergence of particular network properties that facilitate specific computations by spatiotemporal patterns of excitation and inhibition.

New analytical methods have allowed the non-invasive investigation of frequency-specific long-range communication in the human brain with magneto-encephalographic (MEG) recordings.

Recent studies in humans and monkeys have provided new evidence for the physiological relevance of oscillatory synchronization in motor and cognitive functions. Synchronization in the beta frequency band seems to have a particularly important role in long-range communication. The

functional relevance of desynchronization processes is also being increasingly recognized, and specific spatiotemporal patterns of synchronization desynchronization have been directly related to attentional processes and behavioral performance.

In the human motor system, oscillations in the primary motor cortex modulate the firing rate of spinal motor neurons. This modulation is evident as oscillatory coupling between motor cortex activity and muscle activity.

Electrophysiological recordings of basal ganglia-thalamocortical circuits in healthy monkeys, a monkey model of Parkinson's disease and patients with Parkinson's disease have provided new insights into the functional roles of oscillations and oscillatory synchronization in normal and disturbed motor behavior. Specifically, enhanced beta and reduced gamma oscillations are associated with the poverty and slowness of movement that is characteristic of Parkinson's disease. In addition, tremor seems to arise from abnormal synchronization of oscillations in several cortical and subcortical brain areas.

Chronic high-frequency deep brain stimulation, which can be delivered through electrodes that have been implanted in specific basal ganglia target structures, greatly improves motor symptoms in patients with Parkinson's disease, probably through desynchronizing effects.

Pathological changes in long-range synchronization are also evident in other movement disorders, as well as in neuropsychiatric diseases. Further work is needed to better understand the mechanisms that govern oscillatory communication and the consequences of disturbed communication. Hopefully, these studies will lead to the development of new therapeutic approaches.

**Associative Learning in the Brain.** According to a recent study by [Pasupathy and Miller (2005)], the neural correlates of *associative learning* appear in the caudate nucleus - part of the basal ganglia - earlier than in the prefrontal cortex (PFC). The findings shed new light on the interactions and relationships between the basal ganglia and cortex. The authors used a simple conditional association learning task to investigate the roles of the two brain areas. Monkeys had to learn to make a leftward eye movement in response to one visual cue, and a rightward eye movement in response to another. Correct responses were rewarded with fruit juice, and once a pair of cues had been learned the required responses were reversed so that the monkeys had to learn the new associations. New cues were used each day, and Pasupathy and Miller recorded the activity of neurons in both

the dorsolateral PFC and the caudate nucleus during the task. Both the dorsolateral PFC and the caudate nucleus are known to show task-related activity in this sort of task, and they are joined as part of a corticostriatal loop, but until now the temporal relationship between their activity has not been investigated. The authors found that neurons in both areas showed changes in activity during associative learning, but that the neurons in the caudate nucleus showed these changes much earlier, and more abruptly, than did neurons in the dorsolateral PFC. These results might support the idea that the basal ganglia can learn new associations rapidly, and then ‘train’ the PFC. Interestingly, the monkeys’ behavior showed slower learning of the new cue-response associations than did the activity of caudate neurons. Whereas caudate activity showed a sudden switch to the correct association, the monkeys’ performance improved more gradually, and was correlated more strongly with the changes in activity seen in the PFC. The authors suggest that although the caudate nucleus might ‘train’ the PFC, behavior depends more on PFC activity than on that of the basal ganglia.

### 7.3 The Sensory–Motor Adjunction

In this section we define our central biodynamic adjunction *coordination* =  $\text{sensory} \dashv \text{motor} : \text{brain} \rightleftarrows \text{body}$ . This central adjunction is clearly reflected by the *Crick–Koch binding hypothesis* [Crick and Koch (1990); Crick (1994)] (see section (7.1) as well as Figure 7.33).

#### 7.3.1 Summary on Sensory–Motor Pathways

In this subsection we will summarize the facts collected so far about our central biodynamic adjunction, *coordination* =  $\text{sensory} \dashv \text{motor} : \text{brain} \rightleftarrows \text{body}$ , the association between sensory and motor neural pathways. Anatomically, its top-level, association link can be visualized as a talk between the two Penfield’s homunculi (see Figure 7.18 above). Its lower levels can be depicted as in Figure 7.34.

**Sensory Pathways.** Recall that sensations from the skin, muscles, and internal organs of the body, are transmitted to the central nervous system via axons that enter via spinal nerves. Somatosensory information from the head and face is carried to the brain primarily via cranial nerve V, the trigeminal nerve. The cell bodies of these somatosensory receptors are located in clusters called dorsal root ganglia and cranial nerve ganglia.

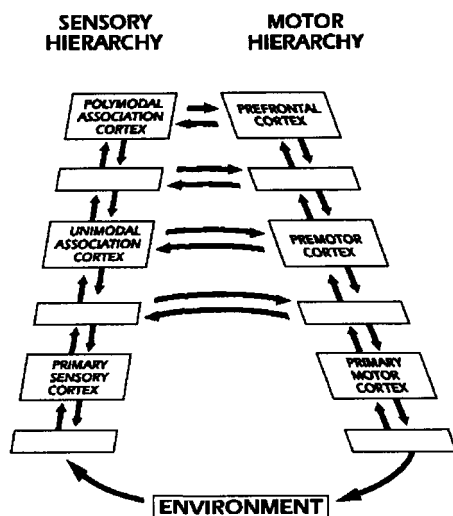


Fig. 7.33 Fiber connections between cortical regions participating in the *perception-action cycle*, reflecting again our sensory-motor adjunction. Empty rhomboids stand for intermediate areas or subareas of the labelled regions. Notice that there are connections between the two hierarchies at several levels, not just at the top level.

Two separate somatosensory pathways transmit information about sensations that are tightly localized (fine touch of the exteroceptive system and kinesthesia of the proprioceptive system) and poorly localized (temperature and pain of the exteroceptive system). Fine touch ascends via the segment of spinal cord white matter called the dorsal columns, whereas diffuse somatosensory information ascends via the spinothalamic tract of the spinal cord (the anterolateral system). Each pathway projects to distinct areas of the thalamus and somatosensory cortex located in parietal lobe.

The dorsal-column medial-lemniscal system begins with somatosensory axons entering the spinal cord via the dorsal root and ascending in the dorsal columns ipsilaterally. The first synapse point for this pathway is in the dorsal column nuclei located in the medulla. The axons of neurons originating in the dorsal column nuclei cross-over, ascending via the medial lemniscus to the contralateral ventral posterior thalamic nucleus (VPN). Somatosensory fibers of the trigeminal nerve (CN V), carrying information from the contralateral side of the face and head, also synapse in the VPN. The majority of VPN neurons project to the primary somatosensory cortex (SI), the remaining project to the secondary somatosensory cortex (SII) of the posterior parietal lobe.



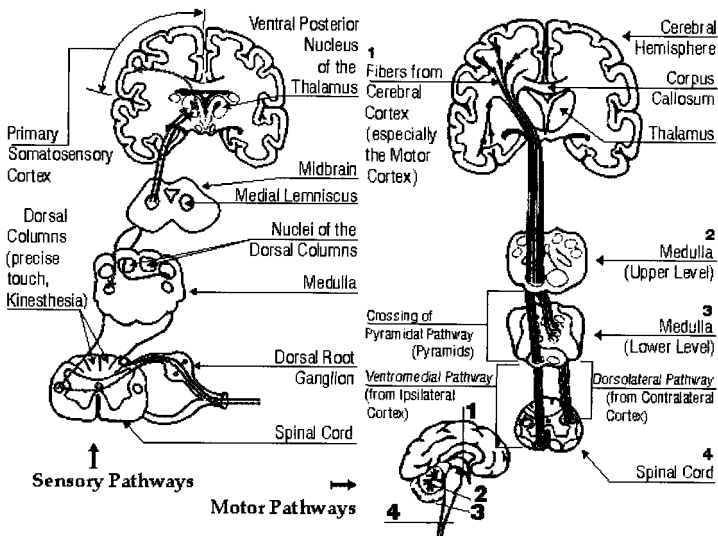


Fig. 7.34 Human sensory-motor pathways.

The anterolateral system begins with somatosensory axons entering the spinal cord via the dorsal root and synapsing upon entry. The majority of these second-order axons decussate, and ascend to the brain via the anterolateral portion of the spinal cord white matter. This ascending system is composed of three separate tracts, the spinothalamic tract, the spinoreticular tract, and the spinotectal tract. The spinothalamic tract projects to the ventral posterior nucleus of the thalamus. This tract is involved in the perception of touch, temperature, and sharp pain. The spinoreticular tract projects to the brain stem reticular formation on its way to the parafascicular nucleus and intralaminar nucleus of the thalamus. This pathway seems to be selectively involved in the perception of deep, chronic pain. The spinotectal tract projects to the tectum of midbrain. This tract is likely involved in some aspect of pain perception. The tracts of the anterolateral system project to both the primary and secondary somatosensory cortex, and to more posterior locations within the parietal lobe.

The selective area of skin innervated by the left and right dorsal roots of a particular spinal nerve is called a dermatome. The surface of the body has been mapped according to these dermatomes. It is important to note, however, that in reality the boundaries of these somatosensory regions overlap each other by approximately half of their width. Damage to a single

dorsal root, therefore, produces slight loss of sensation. Both the sensation type and region of body represented are kept somewhat separate along all levels of the somatosensory pathway.

**Motor Pathways.** Recall that the motor system executes control over the skeletal muscles of the body via several major tracts. The *pyramidal* and *extrapyramidal* motor systems utilize separate tracts. The pyramidal system conveys information via the corticospinal tract of the dorsolateral pathway. This tract conveys signals from the primary motor cortex to the alpha motor neurons found in the medulla and the spinal cord. The pyramidal, corticospinal tract crosses in the 'pyramids' of the medulla, to control discrete voluntary movement on the contralateral side of the body. The extrapyramidal system includes all pathways connecting the motor structures not included in the pyramidal system, including the basal ganglia, red nucleus, reticular formation, and the vestibular nuclei. The descending dorsolateral and ventromedial pathways include both pyramidal and extrapyramidal elements and are each composed of two major tracts, one which descends directly to the spinal cord and another that synapses for processing in the brain stem prior to acting on the spinal cord motor neurons or interneurons. The ventromedial pathway differs from the dorsolateral pathway, as it is much more diffuse in both its origin and distribution, affecting interneurons on both sides of the spinal cord along several segments. In addition, the ventromedial pathway affects the proximal muscles of the trunk and shoulder, while the dorsolateral pathway affects the distal muscles of the hand and fingers. The dorsolateral, corticospinal tract is synonymous with the pyramidal tract or system, and is the only pathway of control for fine finger movements. The dorsolateral, corticorubrospinal tract originates in motor cortex, but synapses in the red nucleus of the extrapyramidal system prior to controlling movement of the forearms, hands and feet. Both tracts of the dorsolateral pathway are involved in the control of reaching movements.

In addition, we have the *side-loop action* of the basal ganglia and the synergetic motor controller, the cerebellum (see Figure 7.20).

On the other hand, during goal-directed reaching in primates, a *sensory-motor transformation* generates a dynamical pattern of muscle activation (see ART-subsection 7.6.3.3 below). Within the context of this sensory-motor transformation, a fundamental question concerns the coordinate systems in which individual cells in the primary motor cortex (MI) encode movement direction. S. Grossberg and coworkers (in [Ajemian *et al.* (2000)]) develop a mathematical framework that computes, as a function of

the coordinate system in which an individual cell is hypothesized to operate, the spatial preferred direction (pd) of that cell as the arm configuration and hand location vary. Three coordinate systems were explicitly modelled: Cartesian spatial, shoulder-centered, and joint angle. The computed patterns of spatial probability densities were distinct for each of these three coordinate systems, and experimental approaches were described which can capitalize upon these differences to compare the empirical adequacy of each coordinate hypothesis. One particular experiment involving curved motion (see [Hocherman and Wise (1991)]) was analyzed from this perspective. Out of the three coordinate systems tested, the assumption of joint angle coordinates best explained the observed cellular response properties. The mathematical framework developed in [Ajemian *et al.* (2000)] can be also used to design new experiments that are capable of disambiguating between a given set of specified coordinate hypotheses.

### 7.3.2 Sensory-Motor Control

Human motor control studies all voluntary movements initiated and regulated by the central nervous system. Sensory-motor (or, sensorimotor) control concerns relationships between sensation and movement or, more broadly, between perception and action. The interplay of sensory and motor processes provides the basis of observable human behavior. In 1858, W. Wundt, the founder of *physiological psychology*, had realized that an understanding of complex behavioral patterns will be impossible without understanding the simple elements (see [Bernstein (1967); Bernstein (1982); Brooks (1986); Ghez (1990); Ghez (1991); Kandel *et al.* (1991); Latash (1993); Wiesendanger (1997); Prochazka (1996); Prochazka *et al.* (2002)]). Consequently, in trying to comprehend general human behavior, *motor control* is an integral part.

Now, a tensor-network model of the human sensory-motor control was proposed by Pellionisz [Pellionisz and Llinas (1979)] for describing how CNS converts patterns of sensory input (joint coordinates) into patterns of motor (muscular) activity. The model presents a 3-step tensorial scheme to transfer covariant sensory coordinates into contravariant components expressed in a different motor frame:

- (1) *Sensory metric tensor* ( $g^{pr}$ ), transforming a covariant reception vector ( $s_r$ ) to contravariant perception ( $s^p$ ). Here,  $s^p = g^{pr} s_r$ , where  $g^{pr} = |g_{pr}|^{-1} = |\cos(\Omega_{pr})|^{-1}$ , and  $|\cos(\Omega_{pr})|$  is the table of cosines of angles

among sensory unit-vectors.

- (2) *Sensory-motor covariant embedding tensor* ( $\gamma_{ip}$ ), transforming the sensory vector ( $s^p$ ) into covariant motor intention vector ( $m_i$ ). Covariant embedding is unique, including the case of overcompleteness, but results in a non-executable covariant expression:  $m_i = \gamma_{ip}s^p$ , where  $\gamma_{ip} = u_i w_p$ , and  $u_i$ ,  $w_p$  are the  $i$ th sensory unit vector and  $p$ th motor unit vector.
- (3) *Motor metric tensor* ( $g^{ei}$ ), that converts intention ( $m_i$ ) to executable contravariants ( $m^e$ ):  $m^e = g^{ei}m_i$ , (where ( $g^{ei}$ ) is computed as ( $g^{pr}$ ) in (1).

In case of *overcompleteness* of either or both the sensory and motor coordinate systems, tensor-network model suggests that the *CNS* uses the *Moore-Penrose generalized inverse* (*MPGI*) of the unique covariant metric tensor:  $g^{jk} = \sum_m \{ \frac{1}{\lambda^+} \cdot |E_m \rangle \langle E_m| \}$ , where  $E_m$  and  $\lambda^+$  are the  $m$ th eigenvector of  $g_{jk}$  and its eigenvalue.

From muscular synergy point of view, significant for human-motion control, *MPGI* technique is an efficient choice since it tends to minimize co-contraction of muscles with opposing actions thus preventing wasteful expenditure of energy [Humphrey and Freund (1991)].

From the geometric point of view, *MPGI* corresponds to a construction which we call the *Legendre's functor*, transforming the internal Riemannian metrics  $g_{(int)}$  on some internal-neural state-space, i.e., *CNS*-working manifold  $M$ , from  $g_{(int)} : TM \rightarrow \mathbb{R}$ , into  $g_{(int)}^{-1} : T^*M \rightarrow \mathbb{R}$ . This is completely analogous to the Hamiltonian transition of *external* metrics  $g_{(ext)}$  on the rotational biodynamic configuration manifold, the (*toral Lie group*)  $T^N$ , from  $g_{(ext)} : TT^N \rightarrow \mathbb{R}$ , into  $g_{(ext)}^{-1} : T^*T^N \rightarrow \mathbb{R}$ .

This supports our hypothesis that the brain-motor-controller performs the highest-level control of biodynamic coordination by performing some kind of its neurodynamics in the 'selector - command space', which we have identified with the internal unit-Tychonoff's cub  $I_{(int)}^N$ . Anatomically, these general stimuli-patterns of voluntary movements (the highest level of motor programming) are generated in the premotor cortex (i.e., Brodmann's cytoarchitectonic area 6) and flow down through the extrapyramidal neural pathway.

More specific (secondary or more skilled) movement patterns are generated in the motor cortex (i.e., *Brodmann's area 4*) and flow down through the pyramidal neural pathway. The command state-space for these specific movement patterns has obviously more complicated topology than  $I_{(int)}^N$ ,



- (3) Spatial coordination at the lower cortical, striato–pyramidal level;
- (4) Object–driven action control at the pre–motor/temporal cortex level;  
and
- (5) Semantic/symbolic coordination at the higher cortical levels.

Any of these levels, from the lowest (1) to the highest (5), can lead in regulating a motor task, depending on its complexity, with all the lower levels, providing background support to this leading–level regulation. For example, a musician's vibrato is controlled through proprioceptive automatisms at level (1); a gymnast's summersault is regulated by deliberate proprioceptive corrections at the level of muscular synergies (level 2); a child's drawing of a picture is regulated by visuo–spatial corrections, either direct (e.g., when drawing over a dotted sketch (level 3a)) or representational (e.g., when drawing from an external model (3b)); an athlete's discus slinging is driven by the meaning of the implement (level 4); and a teacher's sketching of a loose resemblance of a circle on the whiteboard to illustrate geometric explanations is driven by logic and semantics (level 5). Note that while up to and including level (3), motor control parameters rely on metric properties of the environment (e.g., copying contours at level 3a or scaling them up/down at 3b), motor coordination at levels (4) and (5) is driven by the object's topology rather than metrics: the space at these levels is organized in abstract categories, rather than in geometric forms.

#### 7.3.2.1 *Multisensory Integration for Motor Planning*

When planning target–directed reaching movements, human subjects combine visual and proprioceptive feedback to form two estimates of the arm's position: one to plan the reach direction, and another to convert that direction into a motor command. These position estimates are based on the same sensory signals but rely on different combinations of visual and proprioceptive input, suggesting that the brain weights sensory inputs differently depending on the computation being performed. [Sober and Sabes (2003); Sober and Sabes (2005)] showed that the relative weighting of vision and proprioception depended both on the sensory modality of the target and on the information content of the visual feedback, and that these factors affected the two stages of planning independently. The observed diversity of weightings demonstrated the flexibility of sensory integration and suggested a unifying principle by which the brain chose sensory inputs so as to minimize errors arising from the transformation of sensory signals between coordinate frames.

**Modeling the initial movement direction.** In building an explicit model of reach planning Sober [Sober and Sabes (2003); Sober and Sabes (2005)] had to specify which extrinsic and intrinsic variables were used. Behavioral studies have variously suggested that reach planning uses either kinematic or dynamic variables, and neurophysiological findings have supported both hypotheses. So, they fitted their data twice, using the two models (see Figure 7.36):

- (1) the *velocity command model*, in which the motor command is specified kinematically (as joint angle velocities), and
- (2) the *torque command model*, in which the motor command is specified dynamically (as joint torques).

The goal of these models was to understand how visual and proprioceptive signals from the sensory periphery combined to guide the initial, feedforward component of the reach. In these models, only the initial velocities or accelerations of movements were computed, and feedback control was not modelled. The authors assumed that the CNS weighted the visual ( $\hat{x}_{vis}$ ) and proprioceptive ( $\hat{x}_{prop}$ ) position estimates and added them to create two estimates of the position of the arm, ( $\hat{x}_{MV}$ ) ('movement vector') and ( $\hat{x}_{INV}$ ) ('inverse model'),

$$\begin{aligned}\hat{x}_{MV} &= \alpha_{MV}\hat{x}_{vis} + (1 - \alpha_{MV})\hat{x}_{prop}, \\ \hat{x}_{INV} &= \alpha_{INV}\hat{x}_{vis} + (1 - \alpha_{INV})\hat{x}_{prop}.\end{aligned}\tag{7.5}$$

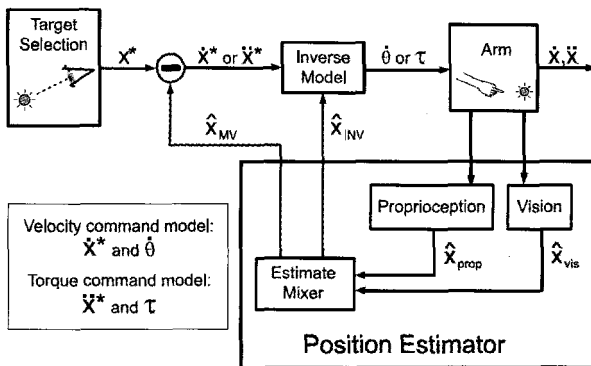


Fig. 7.36 Two models of feedforward motor planning.

The estimate  $\hat{x}_{MV}$  was used to determine the desired movement vector in both models. This vector specified desired initial fingertip velocity in the velocity command model and the desired initial fingertip acceleration in the torque command model. The second estimate,  $\hat{x}_{INV}$ , was used to convert the desired movement into an intrinsic motor command. This command was expressed as joint velocities in the velocity command model and as joint torques in the torque command model. In both models, therefore, the weighting parameters  $\alpha_{MV}$  and  $\alpha_{INV}$  characterized sensory integration at the two stages of reach planning.

**Velocity command model.** In the velocity command model, the planned movement vector was defined as the desired initial velocity of the fingertip ( $\dot{x}^*$ ). The direction of this velocity is specified by

$$\angle \dot{x}^* = \angle(x_d^* - \hat{x}_{MV}) + \omega_d,$$

where  $\angle x$  represents the angle of vector  $x$ ,  $x_d^*$  represents the location of target  $d \in [1, \dots, 8]$ ,  $\hat{x}_{MV}$  is the estimated hand position defined in (7.5), and  $\omega_d$  is an angular offset from the straight line connecting the estimated initial position and target  $x_d^*$ . The  $\omega_d$  terms were included to account for the fact that natural, unperturbed reaching movements were slightly curved, resulting in initial reach directions that differed from the target direction.

Given a desired Cartesian fingertip velocity  $\dot{x}^*$ , the ideal joint angle velocity command would be

$$\dot{\theta}_{ideal} = J^{-1}(\theta)\dot{x}^*,$$

where the Jacobian matrix  $J(\theta)$  represents the gradient of the fingertip location with respect to the joint angles,

$$J(\theta) = \nabla_{\theta} K(\theta) = \frac{dx}{d\theta}.$$

The kinematics equation  $x = K(\theta)$  describes the mapping from joint angles to fingertip locations.

As the arm was restricted to planar, two-joint movements, both the kinematics and the Jacobian were invertible. As the internal inverse model must rely on an estimate of the position of the arm ( $\hat{x}_{INV}$ ), the implemented motor command would be

$$\dot{\theta} = J^{-1}(\hat{\theta}_{INV})\dot{x}^*,$$



where

$$\hat{\theta}_{INV} = K^{-1}(\hat{x}_{INV}).$$

Finally, this joint velocity command was executed, and the arm moved with an initial fingertip velocity determined by the Jacobian (evaluated at the true arm position),

$$\dot{x} = J(\theta)\dot{\theta} = J(\theta)J^{-1}(\hat{\theta}_{INV})\dot{x}^*. \quad (7.6)$$

This model predicted that the initial velocity  $\dot{x}$  would be distorted from the desired velocity  $\dot{x}^*$  if the arm position was misestimated.

**Torque command model.** In addition to the velocity command model, which assumes that reaches are planned in kinematic coordinates, [Sober and Sabes (2003); Sober and Sabes (2005)] also considered a model in which the dynamics of the movement were controlled via the joint torques  $\tau$ . In the torque command model, the movement vector specified a desired initial acceleration,  $\ddot{x}^*$ , which was offset by some angle  $\omega_d$  from the target direction,

$$\angle \ddot{x}^* = \angle(x_d^* - \hat{x}_{MV}) + \omega_d,$$

where  $\omega_d$  was determined by measuring the average initial accelerations for reaches to each target in the baseline.

The ideal joint torque command could be computed from the desired acceleration as follows. The relationship between joint and endpoint acceleration is found by differentiating (7.6) with respect to time,

$$\ddot{x} = J(\theta)\ddot{\theta} + \frac{d}{dt}[J(\theta)]\dot{\theta} \approx J(\theta)\ddot{\theta}, \quad (7.7)$$

where the last approximation follows from the fact that only the initial component of the movement was considered, when the magnitude of the angular velocity was small. The relationship between the joint torques and the kinematic variables of the movement was given by the dynamics equations for the planar, two-joint arm,

$$\tau = I(\theta)\ddot{\theta} + H(\theta, \dot{\theta})\dot{\theta} \approx I(\theta)\ddot{\theta}, \quad (7.8)$$

where  $I(\theta)$  is the position-dependent, nonisotropic inertia of the arm, and the  $H$  term represents velocity-dependent centripetal forces, joint interaction torques, and damping forces at the joints. As this latter term varies linearly with respect to joint velocity, it is small at the onset of movement,

yielding the approximation of (7.8). By inverting (7.7) and combining it with (7.8), the ideal joint torque command is obtained,

$$\tau_{ideal} \approx I(\theta)J^{-1}(\theta)\ddot{x}^*.$$

However, the true value of the arm position is not available to the nervous system, which must make use of the estimated joint angles,  $\hat{\theta}_{INV}$  when computing the inverse model,

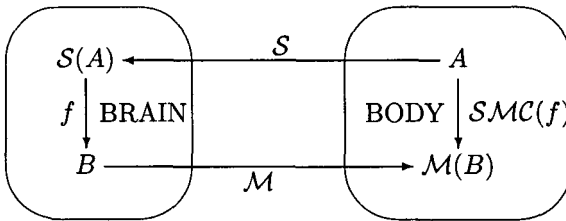
$$\tau \approx I(\hat{\theta}_{INV})J^{-1}(\hat{\theta}_{INV})\ddot{x}^*. \quad (7.9)$$

Finally, (7.9) could be inverted to determine the fingertip acceleration that results from a given joint torque command,

$$\ddot{x} \approx J(\theta)I^{-1}(\theta)I(\hat{\theta}_{INV})J^{-1}(\hat{\theta}_{INV})\ddot{x}^*.$$

### 7.3.2.2 The Sensory–Motor Adjunction

From categorical perspective, the human sensory–motor control system can be modelled as an adjunction between the afferent sensory functor  $\mathcal{S} : \mathcal{BODY} \rightarrow \mathcal{BRAIN}$  and the efferent motor functor  $\mathcal{M} : \mathcal{BRAIN} \rightarrow \mathcal{BODY}$ . Technically it is written,  $\mathcal{SMC} : \mathcal{S} \dashv \mathcal{M}$ ,  $(\mathcal{S}, \mathcal{M}) : \mathcal{BRAIN} \rightleftarrows \mathcal{BODY}$  and depicted as



This adjunction offers a mathematical answer to the fundamental question: How would *Nature* solve the general biodynamics control problem? *It is by using a weak functorial inverse of sensory neural pathways and motor neural pathways that Nature controls human behavior in general, and human motion in particular.*

### 7.3.3 The Central Biomechanical Adjunction

From biodynamic computer–simulation perspective, the motor control pathway incorporates the *central biodynamic adjunction* as the for-

ward/inverse dynamics (see Figure 7.37).

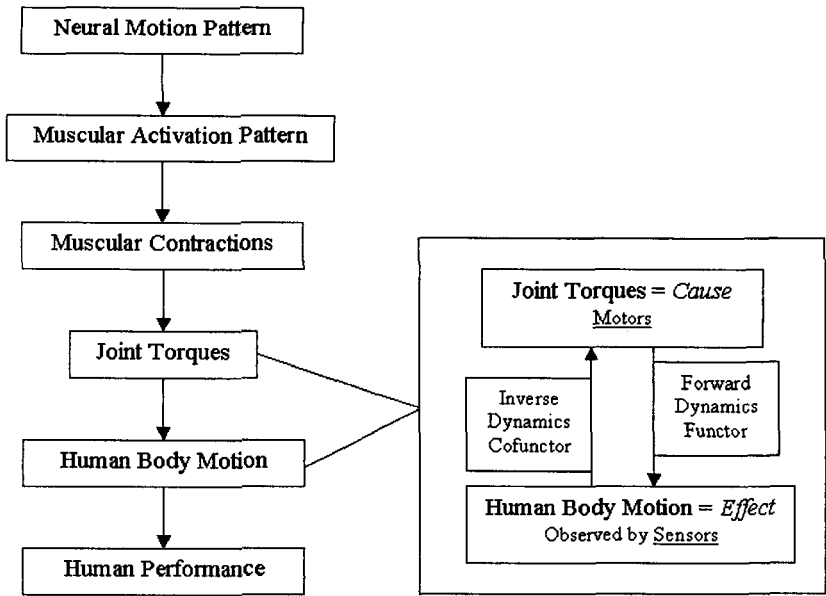


Fig. 7.37 The motor control pathway incorporates the *central biodynamic adjunction* as the forward/inverse dynamics.

Namely, in biomechanical studies, *inverse dynamics analysis* is the standard technique used to gain insight into the net summation of all muscle activity at each joint. In the inverse dynamics method, the joint forces and joint moments of force are calculated from a prescribed movement. Since the segmental movements, in contrast to the internal forces, can be measured, this method is commonly applied for the analysis of measured movements [Dariush (2003)]. A full kinematic description obtained from *motion capture* of marker positions is sufficient to obtain an inverse solution; however, motion capture is often combined with output from other sensors, including *force plates*, in order to improve the precision of the estimated joint loads. Since the optimal representation of the dynamic equations of motion will differ depending on the available sensors, inverse dynamics is in general considered a *multi-modal sensing problem* [Dariush (2002)]. Regardless of the sensing modes, there are two fundamental limitations associated with all inverse dynamics problems. Firstly, the inverse dynamics equations are functions of linear and angular accelerations of body segments, requiring the

calculations of higher order derivatives of experimental data contaminated by noise – a notoriously error prone operation [Cullum (1971)]. Second, the applicability of inverse dynamics not predictive, i.e., it is limited to the ‘analysis’ problem. In other words, the solution cannot be used directly to answer the ‘what if’ type questions (or the ‘synthesis’ problem) typically encountered in clinical applications and addressed by the *predictive forward dynamics* simulations.

Dariush [Dariush (2003)] proposed the forward dynamics solutions for multi-modal inverse dynamics biomechanical problems. He presented a new control-theoretic framework for the analysis and synthesis of human motion whereby the estimation of internal forces and moments had been formulated as a *trajectory tracking control problem*. The objective of the tracking controller was to obtain a set of forces and moments that when applied to a forward model would reproduce or track the measured kinematic data. In particular, tracking was achieved by employing a nonlinear control law that linearizes and decouples the states of the system. This technique represented a forward dynamics solution to the general multi-modal inverse dynamics problem. The proposed algorithm (see Figure 7.38) overcomes the limitations of the previous methods and represents a simple, yet powerful method for both the analysis and synthesis of human motion. In particular, the proposed method was stable, guaranteed to converge, computationally efficient (real time), did not require acceleration computations, and was predictive.

A typical application of inverse dynamics biomechanical analysis involves integration of motion capture and force plate measurements as inputs to an *iterative ‘ground up’ Newton-Euler inverse dynamics procedure* (see [van den Bogert *et al.* (1996)]).

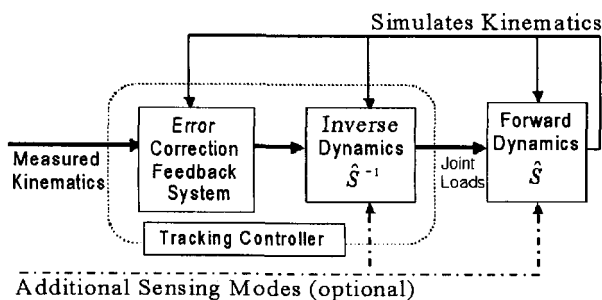


Fig. 7.38 Architecture for the proposed joint load estimation method.

Now, *rhythmic movements*, such as walking, chewing or scratching, are phylogenetically old motor behaviors found in many organisms, ranging from insects to primates. In contrast, *discrete movements*, such as reaching, grasping or kicking, are behaviors that have reached sophistication primarily in younger species, particularly primates. Neurophysiological and computational research on *arm motor control* has focused almost exclusively on discrete movements, essentially assuming similar neural circuitry for rhythmic tasks. In contrast, many behavioral studies have focused on rhythmic models, subsuming discrete movement as a special case. Using a human functional neuroimaging experiment, [Schaal *et al.* (2004)] showed that in addition to areas activated in rhythmic movement, discrete movement involved several higher cortical planning areas, even when both movement conditions were confined to the same single wrist joint. In their analysis, 'rhythmic-rest' and 'discrete-rest' plots demonstrated the main effects of brain activity during 'rhythmic' and 'Discrete' movement conditions. 'Rhythmic-discrete' showed brain areas where rhythmic movement had stronger activity than discrete movement. Only areas that were active in 'rhythmic-rest' were permitted to contribute to this contrast by using the active voxels of 'rhythmic-rest' as an inclusive mask. Analogously, 'discrete-Rhythmic' displays areas that showed significantly more activation than rhythmic movement, using 'discrete-rest' as an inclusive mask. These results provide neuroscientific evidence that rhythmic arm movement cannot be part of a more general discrete movement system and may require separate neurophysiological and theoretical treatment.

### 7.3.3.1 *Postural Control Experiments*

It is generally accepted that human bipedal upright stance is achieved by feedback mechanisms that generate an appropriate corrective torque based on body-sway motion detected primarily by visual, vestibular, and proprioceptive sensory systems. Because orientation information from the various senses is not always available (eyes closed) or accurate (compliant support surface), the postural control system must somehow adjust to maintain stance in a wide variety of environmental conditions. This is the *sensory-motor integration problem* that was investigated in [Peterka (2002)], by evoking anterior-posterior (AP) body sway using pseudorandom rotation of the visual surround and/or support surface (amplitudes  $0.5-8^\circ$ ) in both normal subjects and subjects with severe bilateral *vestibular loss* (VL). AP rotation of body *center-of-mass* (COM) was measured in response to six

conditions offering different combinations of available sensory information. Stimulus-response data were analyzed using spectral analysis to compute transfer functions and coherence functions over a frequency range from 0.017 to 2.23 Hz. Stimulus-response data were quite linear for any given condition and amplitude. However, overall behavior in normal subjects was nonlinear because gain decreased and phase functions sometimes changed with increasing stimulus amplitude. 'Sensory channel reweighting' could account for this nonlinear behavior with subjects showing increasing reliance on vestibular cues as stimulus amplitudes increased. VL subjects could not perform this reweighting, and their stimulus-response behavior remained quite linear. Transfer function curve fits based on a simple feedback control model provided estimates of postural stiffness, damping, and feedback time delay. There were only small changes in these parameters with increasing visual stimulus amplitude. However, stiffness increased as much as 60% with increasing support surface amplitude. To maintain postural stability and avoid resonant behavior, an increase in stiffness should be accompanied by a corresponding increase in damping. Increased damping was achieved primarily by decreasing the apparent time delay of feedback control rather than by changing the damping coefficient (i.e., corrective torque related to body-sway velocity). In normal subjects, stiffness and damping were highly correlated with body mass and moment of inertia, with stiffness always about 1/3 larger than necessary to resist the destabilizing torque due to gravity. The stiffness parameter in some VL subjects was larger compared with normal subjects, suggesting that they may use increased stiffness to help compensate for their loss. Overall results showed that the simple act of standing quietly depends on a remarkably complex sensory-motor control system.

To achieve further insight into the postural control behavior revealed in the experimental results, Peterka [Peterka (2002)] used a simple control system model to parameterize his transfer function results. This *independent channel model* (see Figure 7.39) uses negative feedback control from sensory systems to generate an active torque,  $T_a$ , and muscle/tendon stretch caused by body sway relative to the support surface to generate a passive torque,  $T_p$ .  $T_a$  and  $T_p$  sum to produce the total corrective torque,  $T_c$ , acting about the ankle joint. This model assumes that three types of sensory information contribute to the generation of  $T_a$ . The sensory information is provided by the visual system, detecting body orientation with respect to the visual environment, *proprioceptive system*, detecting body orientation with respect to the support surface, and *graviceptive system*, detecting

body orientation with respect to earth vertical. All sensory channels act separately, and the 'goal' of each channel is to minimize deviation from its individual internal reference.

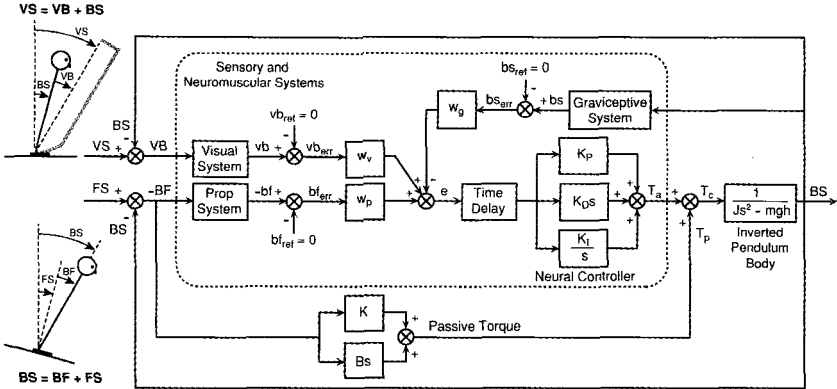


Fig. 7.39 'Independent channel model' of *sensory-motor integration* in postural control showing a weighted addition of contributions from visual, proprioceptive, and graviceptive systems to the generation of an active corrective torque,  $T_a$ , as well as a passive torque contribution,  $T_p$ , related to body movement relative to the feet.

The body rotation produced by  $T_c$  is described by the ODE of motion of a *single-link inverted pendulum*

$$J \frac{d^2(BS)}{dt^2} = mgh \sin(BS) + T_c,$$

where  $J$  is the body's moment of inertia about the ankle joint axis,  $m$  is body mass (not including the feet),  $g$  is acceleration due to gravity,  $h$  is the height of the COM above the ankle joint, and  $BS$  is the angular position of the body with respect to earth vertical. Both  $BS$  and  $T_c$  are time varying. Expressing this equation as a Laplace transform gives

$$\frac{BS(s)}{T_c(s)} = \frac{1}{Js^2 - mgh},$$

where  $s$  is the Laplace variable and the small angle approximation  $BS \approx \sin(BS)$  was used to simplify the equation.

An inverted pendulum is inherently unstable because a small deviation of body position from a perfect upright position produces a torque due to gravity,  $mgh \sin(BS)$ , that accelerates the body further from upright. To counteract this gravitational torque,  $T_c$  must be generated with a sign

opposite to the gravitational torque. The stability and dynamic behavior of the inverted pendulum control depends on the time course of  $T_c$  [Peterka (2002)].

#### 7.3.3.2 Learning Arm Movement Control

S. Grossberg and coworkers (in [Contreras-Vidal *et al.* (1997)]) proposed a neural network model of opponent cerebellar learning for arm movement control (see Figures 7.40–7.42). The model illustrates how a central pattern generator in cortex and basal ganglia, a neuromuscular force controller in spinal cord, and an adaptive cerebellum co-operate to reduce motor variability during multi-joint arm movements using mono- and bi-articular muscles.

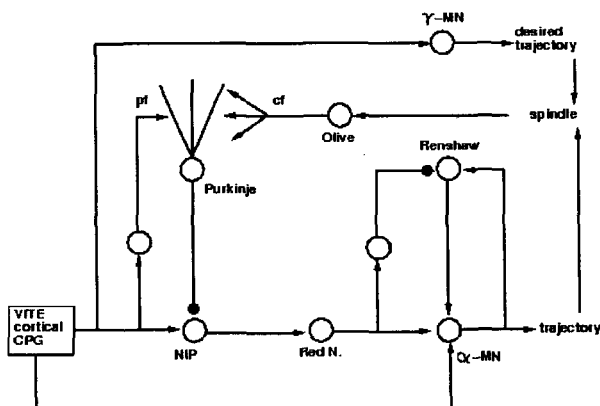


Fig. 7.40 Cortico-spino-cerebellar model structure (see text for explanation.

Cerebellar learning modifies velocity commands to produce phasic antagonist bursts at interpositus nucleus cells whose feedforward action overcomes inherent limitations of spinal feedback control of tracking. Excitation of  $\alpha$ -motoneuron pools combined with inhibition of their Renshaw cells by the cerebellum facilitate movement initiation and optimal execution. Transcerebellar pathways are opened by learning through long-term depression (LTD) of parallel fiber-Purkinje cell synapses in response to conjunctive stimulation of parallel fibers and climbing fiber discharges that signal muscle stretch errors. The cerebellar circuitry also learns to control opponent muscles pairs, allowing co-contraction and reciprocal inhibition of muscles. Learning is stable, exhibits load compensation properties, and generalizes



better across movement speeds if motoneuron pools obey the size principle. The intermittency of climbing fiber discharges maintains stable learning. Long-term potentiation (LTP) in response to uncorrelated parallel fiber signals enables previously weakened synapses to recover. Loss of climbing fibers, in the presence of LTP, can erode normal opponent signal processing. Simulated lesions of the cerebellar network reproduce symptoms of cerebellar disease, including sluggish movement onsets, poor execution of multi-joint plans, and abnormally prolonged endpoint oscillations.

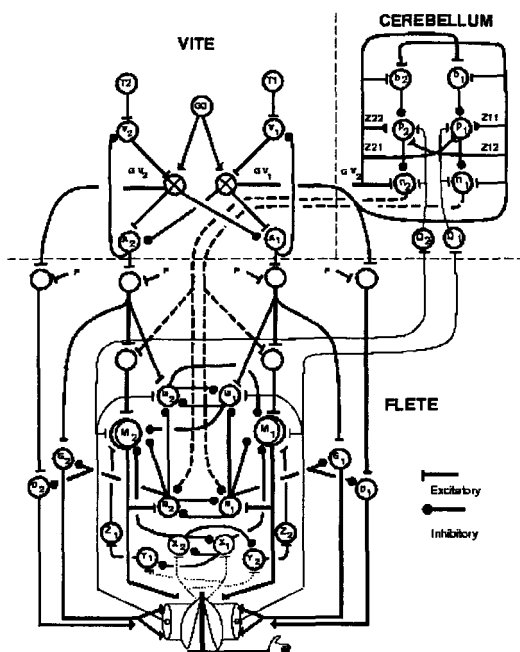


Fig. 7.41 Neural network representation of the neuromuscular control system including feedforward cerebellar control (see text). Key: B – basket cell, p – Purkinje cells, n – nucleus interpositus cells, O – inferior olive, CF – climbing fibers, z – long-term memory cells.

In Figure 7.40, the following symbols are used: CPG – central pattern generator, NIP – nucleus interpositus cells, pf – parallel fibers, cf – climbing fibers,  $\gamma$ -MN – gamma motoneurons,  $\alpha$ -MN – alpha motoneurons; arrow terminated pathways are excitatory, filled-circle terminated paths are inhibitory. Excitatory pathways from a central pattern generator (VITE) send velocity commands to motoneurons in the spinal cord as well

as mossy fiber collaterals which may bifurcate and send branches to both the cerebellar cortex and nuclei. The deep cerebellar nuclear cells ultimately project through the red nucleus to motoneurons and spinal interneurons such as Renshaw cells. Spindle error signals resulting from a comparison of the desired with the actual trajectory project to motoneurons and to the inferior olive, where they act as teaching signals via climbing fibers to the Purkinje cells. These teaching signals regulate long-term depression (LTD) at synapses where active parallel fibers contact Purkinje cells. It is hypothesized that for purpose of stability and economy of effort the path for velocity commands through the cerebellum is normally closed by Purkinje inhibition of nuclear cells, while the gain of excitatory signals through the motoneurons stage (both from descending commands and from proprioceptive reflexes) is low due to *Renshaw cells inhibition* of alpha motoneurons. However, LTD opens the gate in transcerebellar side-path and allows transient commands to simultaneously excite motoneurons and inhibit Renshaw cells.

In Figure 7.41, upper-left part represents the VITE model for variable-speed trajectory generation, while lower part represents the FLETE model of the opponently organized spino-muscular system. Dotted lines show feedback pathways from sensors embedded in muscles. The two lateral feedback pathways arise in spindle organs sensitive to muscle stretch and its first derivative. The two medial feedback pathways arise in Golgi tendon organs asensitive to muscle force. Signals  $A_1$  and  $A_2$  specify the desired position vector, and the signals  $V_1G$  and  $V_2G$  specify the desired velocity vector; signals  $T_1$  and  $T_2$  specify the target position vector; signal  $P$  scales the level of co-activation, and signal  $GO$  scales speed of movement. Upper-left part of the Figure represents feedforward cerebellar model, which computes transient inverse-dynamic signals that excite motoneurons and modulate the gain in spinal circuits.

In Figure 7.42, the following symbols are used:  $\Theta$  – shoulder joint angle;  $\Phi$  – elbow joint angle.  $a$ , insertion point for shoulder mono-articular muscle;  $a$  – insertion point for elbow bi-articular 2 muscle;  $lc$  – distance from clavicle/scapula to shoulder joint;  $ls$  – length of humerus;  $b$  – muscle origin distance from shoulder joint;  $D$  – normal to the line of pull of muscle.

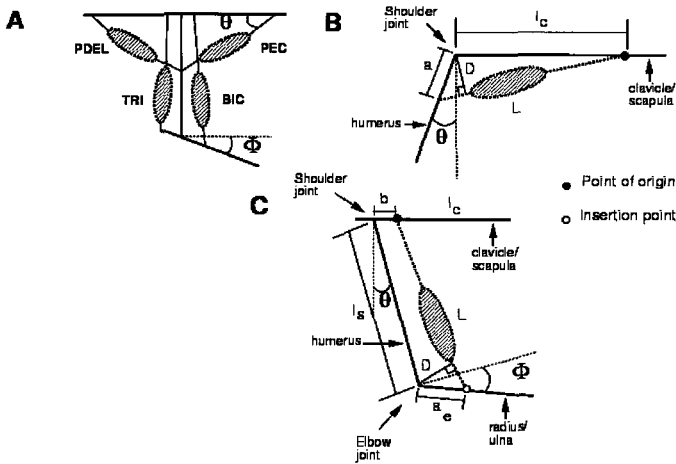


Fig. 7.42 (A) Geometry of origin and insertion points for mono- and bi-articular muscles; (B) Schematic of PEC muscle geometry. (C) Schematic of BIC muscle geometry (see text for explanation).

### 7.3.4 Mechanism of Brain Injuries

#### 7.3.4.1 Basic Dynamics of Brain Injuries

People usually take for granted that the *mechanism of brain injury* is very well known and there are plenty of measurement data to support this knowledge. Well, this is not the case. This mechanism is a 6 DOF *dynamical effect* (sudden brain rotation and translation) which is still pretty much a ‘black-box’. In brief, torque-jolt in the first neck joint (atlanto-occipital) can be used as a measure for sudden brain rotation; similarly, translational jolt in the same joint measures sudden brain translation. From the full head dynamics, both rotational and translational, we can infer what is happening, from dynamics point of view – inside the head.

Now, before we explain this in detail, let us recall some facts about biomechanical measurements (see section 6.6 above):

- (1) Measurement performed on dummies is not considered as valid in biomechanical community; measurement on cadavers is even worse; only ‘measurement in vivo’ is considered biomechanically valid.
- (2) While performing *measurements in vivo* we must be aware of the *problems of inverse dynamics* which [Dariush (2003)]:
  - (i) inputs kinematic noise;

- (ii) propagates this input noise through nonlinear dynamical system;
- (iii) amplifies this propagated noise using the error-prone calculations (like numerical differentiation); and
- (iv) at the end, it is supposed to give a precise information about forces and torques inside the human body.

It is obvious that after a series of noisy actions/amplifications, we cannot obtain a valid information. The only valid way is 'forward dynamics', which behaves as a low-pass filter.

- (3) The vast majority of human motion problems in biomechanics are solved using the formalism of 'linear' and angular momenta.<sup>3</sup> Now, while understanding the translational momenta is pretty straightforward, the understanding of angular momenta, in particular their compositions, requires understanding of the rigid body dynamics (see chapter 4).

Also, while it is clear that brain injuries have something to do with translational and rotational momenta, our previous experience with spinal injuries (see (4.9) above) suggests that it is rather the rate-of-change, i.e., the time derivative of these momenta, which are forces and torques that cause brain injuries. Finally, deeper look into the problem, analogous to the case of spinal injuries, reveals that it cannot be even the static force or torque that causes brain injury. It necessarily has to be a sharp force and/or torque, namely the jolt and/or the torque-jolt which actually causes brain injury.

Now we can explain what we mean by 'black-box' referred to above, emphasizing that *proper understanding is a necessary precondition for prediction and control/prevention*. We want to predict the brain injury. Prediction (as well as understanding, measurement and simulation) means dynamics itself, not the consequences of this dynamics (various traumas and lesions). In this game of dynamics, we have three players: brain injury, 'in vivo measurement', and simulation. All three are events happening in time as well as in  $SE(3)$  – the Special Euclidean group of rigid body motions (see (3.5.2.5) above), including (noncommutative) rotational dynamic data (torque-jolts, torques, angular accelerations, angular velocities, and angular displacements), as well as the corresponding (commutative) translational dynamic data.

---

<sup>3</sup>For everyone dealing with nonlinear mechanics it is clear that the common word 'linear momentum' (or 'linear acceleration') is not at all a good substitution for 'translational momentum' (or 'translational acceleration').

Predicting the brain injury means relating a dynamical event of the injury with dynamical events of measurement/simulation. Question: Can any one correlate an 'in vivo measurement' of dynamics happening in the brain's  $SE(3)$ -group, during the event of the brain injury? Obviously not. No one can measure even torques and forces acting on a freely moving hand, states contemporary biomechanics literature. And brain is an extremely complex tissue inside the three membranes damped with liquor inside the skull (which is the end-effector rigid body of the chain of 26 movable vertebral rigid bodies). Therefore, dynamical 'in vivo measurement' of the brain injury at the very instant of an injury is completely out of question, both for ethical and for the lack-of technology reasons. On the other hand, can we simulate the  $SE(3)$ -jolts (and all other  $SE(3)$ -dynamics, kinematics, statics), as well as the jolt distances between the neighboring spinal joints? Yes, that is exactly the purpose of biodynamic simulators, during various movements, impacts and loadings.

Now, medical statistics suggests that loss of consciousness in boxing knock-outs and road vehicle crashes is caused by *rotation of the brain-stem*, and related to the following syndromes: *Semi-Coma*, *Akinetic Mute*, and *Locked In*-syndrome, all three with the total loss of gesture, speech and movement. The cognitive abilities can still be intact, but the patient cannot express himself by either speech or gesture. Recall that the brain stem, including Midbrain, Pons and Medulla Oblongata, is located at the base of the brain. It is the connection between the cortex and the spinal cord, containing motor neural pathways for voluntary movement from the upper part of the brain. The brain stem also controls such automatic functions as breathing, heart rate, blood pressure, swallowing, sleep patterns and body temperature.

Weaker injuries include the following symptoms: *abnormal respiration* (hyperventilation and abnormal breathing patterns: ataxic, clustered, hiccups); *pupils*: dilated, fixed; and *movement* (if any): abnormal extensor.

From biodynamic perspective, this rotation of the brain stem is caused by noncommutative composition of angular momenta, or more appropriate, torques, or even more appropriate, torque jolts in the atlanto-occipital (first neck) joint. More precisely, torque-jolt (TJ) in the first neck joint (atlanto-occipital) measures the sudden rotation of the brain-stem. High TJ causes the 'knock-out' effect – loss of consciousness in boxing. Namely, 'upper-cut' is a high pitch-jolt in the neck, and 'cross-cut' is a high yaw-jolt in the neck. Upper-cut is similar to the localized whiplash effect in the rear-end car collisions. Moderate TJ at the same joint causes weaker symptoms.

Other brain injuries are caused by translational momenta, forces (more appropriate) and jolts (the most appropriate), respectively.

Therefore, combination of rotational and translational jolt-distances between the first and the second neck joint (atlanto-occipital and atlanto-axial joints, respectively) represents the best available measure of sudden rotational and translational forces acting on the skull, and consequently the best possible measure for the risk of brain injuries.

There are available biodynamics simulators that can simulate all  $SE(3)$ -jolts, forces and momenta in various impact situations (see e.g., *Human Biodynamics Engine*, developed in Defence Science & Technology Organisation, Australia).

#### 7.3.4.2 Research on Head and Brain Injuries

J.C. Misra from Indian Institute of Technology, Karagpur, with his collaborators and PhD students, developed a body of mathematical and physical knowledge related to dynamics of brain injuries. In the following series of papers Misra explored: general human head modelling [Misra and Chakravarty (1982c); Misra and Chakravarty (1984b)], effect of pulse loading on brain injury [Misra *et al.* (1977)], vibration of human skull-brain system [Misra *et al.* (1978); Misra (1978a); Misra and Chakravarty (1982a)], response of a human head to an impact [Misra (1978b)], general head impact modelling [Misra and Chakravarty (2005)], dynamics of brain injuries [Misra *et al.* (1977); Misra and Chakravarty (1984a)], stress-field analysis in the human cranial bone [Misra and Murthy (1979); Misra and Murthy (1983b)], stresses in the human head generated due to thermogenesis [Misra (1986a)], dynamic response of a head-neck system to an impulsive loads [Misra and Chakravarty (1985)], and effect of solar radiation on the human head [Misra and Chakravarty (1982b)].

### 7.4 Brain Dynamics

In this section we give the introduction to brain dynamics, to be developed in the subsequent sections. 'While the brain is totally unlike modern computers, much of what it does can be described as computation. Associative memory, logic and inference, recognizing an odor or a chess position, parsing the world into objects, and generating appropriate sequences of locomotor muscle commands are all describable as computation', says J. Hopfield, one of the pioneers of artificial neural networks. He adds, 'Any computer does

its computation by its changes in internal state. In neurobiology, the change of the potentials of neurons (and changes in the strengths of the synapses) with time is what performs the computations. Systems of (nonlinearly-coupled oscillatory) ODEs can represent these aspects of neurobiology. We seek to understand some aspects of neurobiological computation through studying the behavior of equations modelling the time-evolution of neural activity.'

According to our present understanding, information exchange between neurons is achieved by spikes along axons. There are several mechanisms considered so far [Haken (1996)]:

- (1) The signal intensity is encoded by spike rates.
- (2) Pulse sequences can become synchronized. This mechanism is invoked for an explanation of the binding problem, though still debates are going on here.
- (3) Mechanisms are studied by which neurons can decode inter-spike intervals. In these studies the spike intervals stem from chaotically produced signals.

#### 7.4.1 *Microscopic Neurodynamics of Microtubules*

##### 7.4.1.1 *Biochemistry of Microtubules*

Recent developments/efforts to understand aspects of the brain function at the *sub-neural* level are discussed in [Nanopoulos (1995)]. Microtubules (MTs), protein polymers constructing the cytoskeleton of a neuron, participate in a wide variety of dynamical processes in the cell. Of special interest for this section is the MTs participation in bioinformation processes such as *learning* and *memory*, by possessing a well-known binary error-correcting code [ $K_1(13, 2^6, 5)$ ] with 64 words. In fact, MTs and DNA/RNA are *unique* cell structures that possess a code system. It seems that the MTs' code system is strongly related to a kind of *mental code* in the following sense. The MTs' periodic paracrystalline structure make them able to support a *superposition* of coherent quantum states, as it has been recently conjectured by Hameroff and Penrose [Hameroff and Penrose (1996)], representing an *external* or *mental order*, for sufficient time needed for *efficient quantum computing*.

Living organisms are collective assemblies of cells which contain collective assemblies of organized material, including membranes, organelles, nuclei, and the *cytoplasm*, the bulk interior medium of living cells. Dy-

dynamic rearrangements of the cytoplasm within *eucaryotic cells*, the cells of all animals and almost all plants on Earth, account for their changing shape, movement, etc. This extremely important cytoplasmic structural and dynamical organization is due to the presence of networks of interconnected protein polymers, which are referred to as the *cytoskeleton* due to their bone-like structure [Hameroff and Penrose (1996); Dustin (1984)]. The cytoskeleton consists of MT's, actin microfilaments, intermediate filaments and an *organizing complex*, the *centrosome* with its chief component the *centriole*, built from two bundles of microtubules in a separated T shape. Parallel-arrayed MTs are interconnected by cross-bridging proteins (*MT-Associated Proteins*: MAPs) to other MTs, organelle filaments and membranes to form *dynamic networks* [Hameroff and Penrose (1996); Dustin (1984)]. MAPs may be contractile, structural, or enzymatic. A very important role is played by contractile MAPs, like dynein and kinesin, through their participation in cell movements as well as in intra-neural, or axoplasmic transport which moves material and thus is of fundamental importance for the *maintenance* and *regulation* of *synapses*. The structural bridges formed by MAPs stabilize MTs and prevent their disassembly. The MT-MAP 'complexes' or *cytoskeletal networks* determine the cell architecture and dynamic functions, such a *mitosis*, or *cell division*, *growth*, *differentiation*, *movement*, and for us here the very crucial, *synapse formation and function*, all essential to the living state. It is usually said that *microtubules* are ubiquitous through the entire biology [Hameroff and Penrose (1996); Dustin (1984)].

MTs are hollow cylinders comprised of an exterior surface of cross-section diameter 25 nm ( $1\text{ nm} = 10^{-9}$  meters) with 13 arrays (protofilaments) of protein dimers called tubulines [Dustin (1984)]. The interior of the cylinder, of cross-section diameter 14 nm, contains *ordered water* molecules, which implies the existence of an electric dipole moment and an electric field. The arrangement of the dimers is such that, if one ignores their size, they resemble triangular lattices on the MT surface. Each dimer consists of two hydrophobic protein pockets, and has an unpaired electron. There are two possible positions of the electron, called  $\alpha$  and  $\beta$  *conformations*. When the electron is in the  $\beta$ -conformation there is a  $29^\circ$  distortion of the electric dipole moment as compared to the  $\alpha$  conformation.

In standard models for the simulation of the MT dynamics [Satarić *et al.* (1993); Satarić *et al.* (1998)], the 'physical' DOF – relevant for the description of the energy transfer – is the projection of the electric dipole moment on the longitudinal symmetry axis ( $x$ -axis) of the MT cylinder.



The  $29^\circ$  distortion of the  $\beta$ -conformation leads to a displacement  $u_n$  along the  $x$ -axis, which is thus the relevant physical DOF.

There has been speculation for quite some time that MTs are involved in information processing: it has been shown that the particular geometric arrangement (packing) of the tubulin protofilaments obeys an error-correcting mathematical code known as the  $K_2(13, 2^6, 5)$ -code [Koruga *et al.* (1993)]. Error correcting codes are also used in classical computers to protect against errors while in quantum computers special error correcting algorithms are used to protect against errors by preserving quantum coherence among qubits.

Information processing occurs via interactions among the MT protofilament chains. The system may be considered as similar to a model of *interacting Ising chains* on a triangular lattice, the latter being defined on the plane stemming from filleting open and flattening the cylindrical surface of MT. Classically, the various dimers can occur in either  $\alpha$  or  $\beta$  conformations. Each dimer is influenced by the neighboring dimers resulting in the possibility of a transition. This is the basis for classical information processing, which constitutes the picture of a (classical) cellular automaton.

#### 7.4.1.2 Kink Soliton Model of MT-Dynamics

The *quantum nature* (see section (4.3) above) of an MT network results from the *assumption* that each dimer finds itself in a *superposition* of  $\alpha$  and  $\beta$  conformations. Viewed as a *two-state quantum mechanical system*, the MT tubulin dimers couple to conformational changes with  $10^{-9} - 10^{-11}$  sec transitions, corresponding to an angular frequency  $\omega \sim \mathcal{O}(10^{10}) - \mathcal{O}(10^{12})$  Hz [Nanopoulos (1995)].

The *quantum computer* character of the MT network [Penrose (1989)] results from the assumption that each dimer finds itself in a superposition of  $\alpha$  and  $\beta$  conformations [Hameroff (1987)]. There is a macroscopic coherent state among the various chains, which lasts for  $\mathcal{O}(1 \text{ sec})$  and constitutes the 'preconscious' state [Nanopoulos (1995)]. The interaction of the chains with (non-critical stringy) quantum gravity, then, induces self-collapse of the wave function of the coherent MT network, resulting in quantum computation.

In [Ellis *et al.* (1992); Ellis *et al.* (1999); Mavromatos and Nanopoulos (1995a); Mavromatos and Nanopoulos (1995b); Nanopoulos (1995)] the authors assumed that the collapse occurs mainly due to the interaction of each chain with quantum gravity, the interaction from neighboring chains

being taken into account by including mean-field interaction terms in the dynamics of the displacement field of each chain. This amounts to a modification of the effective potential by anharmonic oscillator terms. Thus, the effective system under study is 2D, possessing one space and one time coordinate.

Let  $u_n$  be the displacement field of the  $n$ th dimer in a MT chain. The continuous approximation proves sufficient for the study of phenomena associated with energy transfer in biological cells, and this implies that one can make the replacement

$$u_n \rightarrow u(x, t), \quad (7.10)$$

with  $x$  a spatial coordinate along the longitudinal symmetry axis of the MT. There is a time variable  $t$  due to fluctuations of the displacements  $u(x)$  as a result of the dipole oscillations in the dimers.

The effects of the neighboring dimers (including neighboring chains) can be phenomenologically accounted for by an effective potential  $V(u)$ . In the kink-soliton model<sup>4</sup> of ref. [Satarić *et al.* (1993); Satarić *et al.* (1998)] a double-well potential was used, leading to a classical kink solution for the  $u(x, t)$  field. More complicated interactions are allowed in the picture of Ellis *et al.*, where more generic polynomial potentials have been considered.

The effects of the surrounding water molecules can be summarized by a *viscous force* term that damps out the dimer oscillations,

$$F = -\gamma \partial_t u, \quad (7.11)$$

with  $\gamma$  determined phenomenologically at this stage. This friction should be viewed as an environmental effect, which however does not lead to energy dissipation, as a result of the non-trivial solitonic structure of the ground-state and the non-zero constant force due to the electric field. This is a well known result, directly relevant to energy transfer in biological systems.

In mathematical terms the effective equation of motion for the relevant field DOF  $u(x, t)$  reads:

$$u''(\xi) + \rho u'(\xi) = P(u), \quad (7.12)$$

where  $\xi = x - vt$ ,  $u'(\xi) = du/d\xi$ ,  $v$  is the velocity of the soliton,  $\rho \propto \gamma$  [Satarić *et al.* (1993); Satarić *et al.* (1998)], and  $P(u)$  is a polynomial in  $u$ , of a certain degree, stemming from the variations of the potential

---

<sup>4</sup>Kinks are solitary (non-dispersive) waves arising in various one-dimensional (bio)physical systems.

$V(u)$  describing interactions among the MT chains. In the mathematical literature there has been a classification of solutions of equations of this form. For certain forms of the potential the solutions include *kink solitons* that may be responsible for dissipation-free energy transfer in biological cells:

$$u(x, t) \sim c_1 (\tanh[c_2(x - vt)] + c_3), \quad (7.13)$$

where  $c_1, c_2, c_3$  are constants depending on the parameters of the dimer lattice model. For the form of the potential assumed in the model of [Satarić *et al.* (1993); Satarić *et al.* (1998)] there are solitons of the form  $u(x, t) = c'_1 + \frac{c'_2 - c'_1}{1 + e^{c'_3(c'_2 - c'_1)(x - vt)}}$ , where again  $c'_i$ ,  $i = 1, \dots, 3$  are appropriate constants.

A *semiclassical quantization* of such solitonic states has been considered by Ellis *et al.*. The result of such a quantization yields a *modified soliton equation* for the (quantum corrected) field  $u_q(x, t)$  [Tsue and Fujiwara (1991)]

$$\partial_t^2 u_q(x, t) - \partial_x^2 u_q(x, t) + \mathcal{M}^{(1)}[u_q(x, t)] = 0, \quad (7.14)$$

with the notation

$$M^{(n)} = e^{\frac{1}{2}(G(x, y, t) - G_0(x, y)) \frac{\partial^2}{\partial z^2} U^{(n)}(z)} \Big|_{z=u_q(x, t)}, \quad U^{(n)} \equiv d^n U / dz^n.$$

The quantity  $U$  denotes the potential of the original soliton Hamiltonian, and  $G(x, y, t)$  is a bilocal field that describes quantum corrections due to the modified boson field around the soliton. The quantities  $M^{(n)}$  carry information about the quantum corrections. For the kink soliton (7.13) the quantum corrections (7.14) have been calculated explicitly in [Tsue and Fujiwara (1991)], thereby providing us with a concrete example of a large-scale quantum coherent state.

A typical propagation velocity of the kink solitons (e.g., in the model of [Satarić *et al.* (1993); Satarić *et al.* (1998)]) is  $v \sim 2$  m/sec, although, models with  $v \sim 20$  m/sec have also been considered. This implies that, for moderately long microtubules of length  $L \sim 10^{-6}$  m, such kinks transport energy without dissipation in

$$t_F \sim 5 \times 10^{-7} \text{ s}. \quad (7.15)$$

Such time scales are comparable to, or smaller in magnitude than, the decoherence time scale of the above-described coherent (solitonic) states  $u_q(x, t)$ . This implies the possibility that fundamental quantum mechanical

phenomena may then be responsible for frictionless energy (and signal) transfer across microtubular arrangements in the cell [Nanopoulos (1995)].

### 7.4.2 *Mezoscopic Neurodynamics of Action Potentials*

Classically, it was known that the cell membrane carries a potential (whose rate-of-change is proportional to current) across the inner and outer surfaces, hence a basic model for a cell membrane is that of a capacitor and resistor in parallel. The *model equation* takes the form (see e.g., [Murray (1989)])

$$C_m \dot{V} = -(V - V_{eq})/R + I_a, \quad (7.16)$$

where  $C_m$  is the membrane capacitance,  $R$  the resistance,  $V_{eq}$  the rest potential,  $V$  the potential across the inner and outer surfaces, and  $I_a$  represents the applied current. In landmark patch clamp experiments in the early part of the 20th century, it was determined that many cell membranes are *excitable*, i.e., exhibit large excursions in potential if the applied current is sufficiently large. Examples include nerve cells and certain muscle cells, e.g., cardiac cells.

#### 7.4.2.1 *Hodgkin-Huxley Model*

Among spiking neuron models, the oldest one, celebrated *Hodgkin-Huxley model* (HH) [Hodgkin and Huxley (1952); Hodgkin (1964)], is expected to be the most realistic in the biological sense. Hodgkin and Huxley performed experiments on the giant axon of the squid and found three different types of ion current, viz., sodium, potassium, and a leak current that consists mainly of  $Cl^-$  ions. Specific voltage-dependent ion channels, one for sodium and another one for potassium, control the flow of those ions through the cell membrane. The leak current takes care of other channel types which are not described explicitly. From a biophysical point of view, action potentials are the result of currents that pass through ion channels in the cell membrane. In an extensive series of experiments on the giant axon of the squid, Hodgkin and Huxley succeeded to measure these currents and to describe their dynamics in the form of an analogous circuit (see Figure 7.43) which in turn can be characterized by a set of nonlinear ODEs. These equations contain an empirically adequate description of the feedback system which changes the conductances (or equivalently, the permeabilities) of the membrane as a function of time and potential difference.

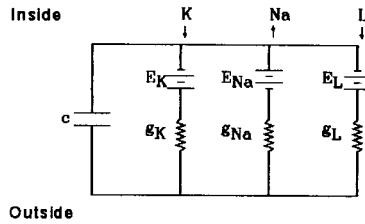


Fig. 7.43 Hodgkin-Huxley analogous circuit model, containing the three main ionic current circuits in parallel together with the observed membrane capacitance.

The HH-neuron model is described by the nonlinear coupled ODEs for the four variables,  $V$  for the membrane potential, and  $m, h$  and  $n$  for the gating variables of sodium and potassium channels (with HH-equation itself being a generalization of the model equation (7.16))

$$C\dot{V} = -g_{Na}m^3h(V - V_{Na}) - g_Kn^4(V - V_K) - g_L(V - V_L) + I_j^{\text{ext}},$$

$$\dot{m} = -(a_m + b_m)m + a_m, \quad \dot{h} = -(a_h + b_h)h + a_h, \quad \dot{n} = -(a_n + b_n)n + a_n,$$

where

$$a_m = 0.1(V + 40)/[1 - e^{-(V+40)/10}], \quad b_m = 4e^{-(V+65)/18},$$

$$a_h = 0.01(V + 55)/[1 - e^{-(V+55)/10}], \quad b_h = 0.125e^{-(V+65)/80},$$

$$a_n = 0.07e^{-(V+65)/20}, \quad b_n = 1/[1 + e^{-(V+35)/10}].$$

Here the reversal potentials of Na, an K channels and leakage are  $V_{Na} = 50$  mV,  $V_K = -77$  mV and  $V_L = -54.5$  mV; the maximum values of corresponding conductivities are  $g_{Na} = 120$  mS/cm<sup>2</sup>,  $g_K = 36$  mS/cm<sup>2</sup> and  $g_L = 0.3$  mS/cm<sup>2</sup>; the capacity of the membrane is  $C = 1$  μF/cm<sup>2</sup>. The external, input current is given by

$$I_j^{\text{ext}} = g_{syn}(V_a - V_c) \sum_n \alpha(t - t_{in}), \quad (7.17)$$

which is induced by the pre-synaptic spike-train input applied to the neuron  $i$ , given by

$$U_i(t) = V_a \sum_n \delta(t - t_{in}). \quad (7.18)$$

In (7.17) and (7.18),  $t_{in}$  is the  $n$ th firing time of the spike-train inputs,  $g_{syn}$  and  $V_c$  denote the conductance and the reversal potential, respectively, of

the synapse,  $\tau_s$  is the time constant relevant to the synapse conduction, and  $\alpha(t)$  is the alpha function given by

$$\alpha(t) = (t/\tau_s) e^{-t/\tau_s} \Theta(t),$$

where  $\Theta(t)$  is the Heaviside function. The HH model was originally proposed to account for the property of squid giant axons [Hodgkin and Huxley (1952); Hodgkin (1964)] and it has been generalized with modifications of ion conductances [Arbib (1998)]. The HH-type models have been widely adopted for a study on activities of *transducer neurons* such as motor and thalamus relay neurons, which transform the amplitude-modulated input to spike-train outputs. In this section, we pay our attention to *data-processing neurons* which receive and emit the spike-train pulses.

To make a network of HH-neurons, the interaction term was added to the HH-equation

$$C\dot{V} = -g_{Na}m^3h(V - V_{Na}) - g_Kn^4(V - V_K) - g_L(V - V_L) + I_j^{\text{ext}} + I_j^{\text{int}},$$

such that

$$I_j^{\text{int}} = G \left( \sum_{k(\neq j)} \sum_m (g_{jk}^{\text{exc}} - g_{jk}^{\text{inh}})(V_a - V_c) \alpha(t - \tau_{jk} - t_{okm}) \right),$$

where  $g_{jk}^{\text{exc}}$  and  $g_{jk}^{\text{inh}}$  denote respectively conductances of excitatory and inhibitory synapses of Hebbian or generalized Hebbian type.

Recently, the HH model has been revisited ([Arcas *et al.* (2003)]). The main point is that a spiking neuron ‘computes’ by transforming a complex dynamical input into a train of action potentials, or spikes. The computation performed by the neuron can be formulated as dimensional reduction, or feature detection, followed by a nonlinear decision function over the low-dimensional space. Generalizations of the reverse correlation technique with white noise input provide a numerical strategy for extracting the relevant low-dimensional features from experimental data, and information theory can be used to evaluate the quality of the low-dimensional approximation. The authors of ([Arcas *et al.* (2003)]) applied these methods to analyze the simplest biophysically realistic model neuron, the HH model, using this system to illustrate the general methodological issues. They focus on the features in the stimulus that trigger a spike, explicitly eliminating the effects of interactions between spikes. One can approximate this triggering ‘feature space’ as a 2D linear subspace in the high-dimensional space of input histories, capturing in this way a substantial fraction of the mutual

information between inputs and spike time. They found that an even better approximation, however, was to describe the relevant subspace as two dimensional but curved. In this way, one can capture 90% of the mutual information even at high time resolution. This analysis provides a new understanding of the computational properties of the HH model. While it is common to approximate neural behavior as ‘integrate and fire,’ the HH model is not an integrator, nor is it well described by a single threshold.

**Simple Model of Spiking Neurons.** According to [Izhikevich (2003)], to understand how the brain works, we need to combine experimental studies of animal and human nervous systems with numerical simulation of large-scale brain models. As we develop such large-scale brain models consisting of spiking neurons, we must find compromises between two seemingly mutually exclusive requirements: The model for a single neuron must be: (i) computationally simple, yet (ii) capable of producing rich firing patterns exhibited by real biological neurons. Using biophysically accurate HH-type models is computationally prohibitive, since we can simulate only a handful of neurons in real time. In contrast, using an integrate-and-fire model is computationally effective, but the model is unrealistically simple and incapable of producing rich spiking and bursting dynamics exhibited by cortical neurons. In this view, the author presented a simple model that reproduces *spiking* and *bursting* behavior of known types of cortical neurons. The model combines the biological plausibility of HH-type dynamics and the computational efficiency of *integrate-and-fire neurons*. Depending on four parameters, the model reproduces spiking and bursting behavior of known types of cortical neurons. It is presented as a 2D system of ODEs,

$$\dot{v} = 0.04v^2 + 5v + 140 - u + I, \quad \dot{u} = a(bv - u),$$

with the auxiliary after-spike resetting

$$\text{if } v \geq 30 \text{ mV then } \begin{cases} v \leftarrow c \\ u \leftarrow u + d \end{cases} \quad (7.19)$$

Here,  $v$  and  $u$  are dimensionless variables, and  $a, b, c$ , and  $d$  are dimensionless parameters. The variable  $v$  represents the membrane potential of the neuron and  $u$  represents a membrane recovery variable, which accounts for the activation of  $K^+$  ionic currents and inactivation of  $Na^+$  ionic currents, and it provides negative feedback to  $v$ . After the spike reaches its apex ( $+30\text{mV}$ ), the membrane voltage and the recovery variable are reset according to (7.19). Synaptic currents or injected dc-currents are delivered

via the variable  $I$ .

Using this model, one can simulate tens of thousands of spiking cortical neurons in real time (1 ms resolution) using a desktop PC.

#### 7.4.2.2 *FitzHugh-Nagumo Model*

Another plausible biological NN-model is *FitzHugh-Nagumo model* (FHN) [FitzHugh (1961); Nagumo *et al.* (1960)] (see (3.17) above), which is actually a lower-dimensional descendant of the HH-model. The FHN equations correspond to an excitable threshold model but, as will be seen briefly, due to their cubic nonlinearity, they exhibit the characteristic behavior of a bistable system. Our main objective is to show analytically the appearance of SR in this model under a periodic external forcing.

The reduced (without diffusion) 2D non-dimensional FHN equations read [Murray *et al.* (1994)]:

$$\dot{v} = v(a - v)(v - 1) - w + I_a, \quad (7.20)$$

$$\dot{w} = bv - \gamma w, \quad (7.21)$$

where  $0 < a < 1$  is essentially the threshold value,  $b$  and  $\gamma$  are positive constants and  $I_a$  is the applied current. The drift field for this model is given by

$$u_1(v, w) = v(a - v)(v - 1) - w, \quad u_2(v, w) = bv - \gamma w.$$

As can be seen from (7.21) the null cline of the deterministic dynamics of this equations is the line  $v = \frac{\gamma}{b}w$ . By substitution on the r.h.s of equation (7.20) we find the following equation for steady states

$$v(a - v)(v - 1) - \frac{b}{\gamma}v = 0.$$

When this system is in a noisy environment, in the limit of weak noise, we can approximate the dynamics of the fluctuations by the 1D *Langevin equation*

$$\dot{v} = v(a - v)(v - 1) - \frac{b}{\gamma}v + \xi(t),$$

that is, the fluctuations run along the line  $v = \frac{\gamma}{b}w$ .



## 7.5 Biological Neural Nets

Neuronal networks are built from neurons with different properties and from synapses of different strengths. [Hooper (2004)] suggests that networks can tune these parameters to many different combinations that nonetheless produce very similar network outputs. He provided example illustrating how different combinations of synaptic strength and intrinsic neuron properties could produce outputs that have the same cycle period, spike number and phase relationships (albeit with fine differences in action potential timing and slow-wave trajectories).

It is often assumed that cellular and synaptic properties need to be regulated to specific values to allow a neuronal network to function properly. To determine how tightly neuronal properties and synaptic strengths need to be tuned to produce a given network output, [Prinz *et al.* (2004)] simulated more than 20 million versions of a three-cell model of the pyloric network of the crustacean stomatogastric ganglion using different combinations of synapse strengths and neuron properties. They found that virtually indistinguishable network activity can arise from widely disparate sets of underlying mechanisms, suggesting that there could be considerable animal-to-animal variability in many of the parameters that control network activity, and that many different combinations of synaptic strengths and intrinsic membrane properties can be consistent with appropriate network performance.

In this section we continue the exposition on brain dynamics, giving a mathematical description of several important biological neural networks. The primary physical basis of oscillatory neural networks is given in Feynman's statistical-mechanics model of the vibrations of coupled oscillators in a crystal lattice (see Appendix, subsection A.6.3). This approach was later developed by J. Hopfield (see subsection 7.7.2 below).

### 7.5.1 Phase Dynamics of Oscillatory Neural Nets

In coupled oscillatory neuronal systems, under suitable conditions, the original dynamics can be reduced theoretically to a simpler phase dynamics. The state of the  $i$ th neuronal oscillatory system can be then characterized by a single phase variable  $\varphi_i$  representing the timing of the neuronal firings. The typical dynamics of *oscillator neural networks* are described by the *Kuramoto model* [Kuramoto (1984); Hoppensteadt and Izhikevich (1997); Strogatz (2000)], consisting of  $N$  equally weighted, all-to-all, phase-

coupled limit-cycle oscillators, where each oscillator has its own natural frequency  $\omega_i$  drawn from a prescribed distribution function:

$$\dot{\varphi}_i = \omega_i + \frac{K}{N} \sum_{j=1}^N J_{ij} \sin(\varphi_j - \varphi_i + \beta_{ij}). \quad (7.22)$$

Here,  $J_{ij}$  and  $\beta_{ij}$  are parameters representing the effect of the interaction, while  $K \geq 0$  is the coupling strength. For simplicity, we assume that all natural frequencies  $\omega_i$  are equal to some fixed value  $\omega_0$ . We can then eliminate  $\omega_0$  by applying the transformation  $\varphi_i \rightarrow \varphi_i + \omega_0 t$ . Using the complex representation  $W_i = \exp(i\varphi_i)$  and  $C_{ij} = J_{ij} \exp(i\beta_{ij})$  in (7.22), it is easily found that all neurons relax toward their stable equilibrium states, in which the relation  $W_i = h_i/|h_i|$  ( $h_i = \sum_{j=1}^N C_{ij} W_j$ ) is satisfied. Following this line of reasoning, as a synchronous update version of the oscillator neural network we can consider the alternative discrete form [Aoyagi and Nomura (1999)],

$$W_i(t+1) = \frac{h_i(t)}{|h_i(t)|}, \quad h_i(t) = C_{ij} W_j(t). \quad (7.23)$$

Now we will attempt to construct an extended model of the oscillator neural networks to retrieve sparsely coded phase patterns. In equation (7.23), the complex quantity  $h_i$  can be regarded as the local field produced by all other neurons. We should remark that the phase of this field,  $h_i$ , determines the timing of the  $i$ th neuron at the next time step, while the amplitude  $|h_i|$  has no effect on the retrieval dynamics (7.23). It seems that the amplitude can be thought of as the strength of the local field with regard to emitting spikes. Pursuing this idea, as a natural extension of the original model we stipulate that the system does not fire and stays in the resting state if the amplitude is smaller than a certain value. Therefore, we consider a network of  $N$  oscillators whose dynamics are governed by

$$W_i(t+1) = f(|h_i(t)|) \frac{h_i(t)}{|h_i(t)|}, \quad h_i(t) = C_{ij} W_j(t). \quad (7.24)$$

We assume that  $f(x) = \Theta(x - H)$ , where the real variable  $H$  is a threshold parameter and  $\Theta(x)$  is the unit step function;  $\Theta(x) = 1$  for  $x \geq 0$  and 0 otherwise. Accordingly, the amplitude  $|W_i^t|$  assumes a value of either 1 or 0, representing the state of the  $i$ th neuron as firing or non-firing. Consequently, the neuron can emit spikes when the amplitude of the local field  $h_i(t)$  is greater than the threshold parameter  $H$ .

Now, let us define a set of  $P$  patterns to be memorized as  $\xi_i^\mu = A_i^\mu \exp(i\theta_i^\mu)$  ( $\mu = 1, 2, \dots, P$ ), where  $\theta_i^\mu$  and  $A_i^\mu$  represent the phase and the amplitude of the  $i$ th neuron in the  $\mu$ th pattern, respectively. For simplicity, we assume that the  $\theta_i^\mu$  are chosen at random from a uniform distribution between 0 and  $2\pi$ . The amplitudes  $A_i^\mu$  are chosen independently with the probability distribution

$$P(A_i^\mu) = a\delta(A_i^\mu - 1) + (1 - a)\delta(A_i^\mu),$$

where  $a$  is the mean activity level in the patterns. Note that, if  $H = 0$  and  $a = 1$ , this model reduces to (7.23).

For the synaptic efficacies, to realize the function of the associative memory, we adopt the *generalized Hebbian rule* in the form

$$C_{ij} = \frac{1}{aN} \xi_i^\mu \tilde{\xi}_j^\mu, \quad (7.25)$$

where  $\tilde{\xi}_j^\mu$  denotes the complex conjugate of  $\xi_j^\mu$ . The overlap  $M_\mu(t)$  between the state of the system and the pattern  $\mu$  at time  $t$  is given by

$$M_\mu(t) = m_\mu(t) e^{i\varphi_\mu(t)} = \frac{1}{aN} \tilde{\xi}_j^\mu W_j(t), \quad (7.26)$$

In practice, the rotational symmetry forces us to measure the correlation of the system with the pattern  $\mu$  in terms of the amplitude component  $m_\mu(t) = |M_\mu(t)|$ .

Let us consider the situation in which the network is recalling the pattern  $\xi_i^1$ ; that is,  $m_1(t) = m(t) \sim O(1)$  and  $m_\mu(t) \sim O(1/\sqrt{N})$  ( $\mu \neq 1$ ). The local field  $h_i(t)$  in (7.24) can then be separated as

$$h_i(t) = C_{ij} W_j(t) = m_1 e^{i\varphi_1(t)} \xi_i^1 + z_i(t), \quad (7.27)$$

where  $z_i(t)$  is defined by

$$z_i(t) = \frac{1}{aN} \xi_i^\mu \tilde{\xi}_j^\mu W_j(t). \quad (7.28)$$

The first term in (7.27) acts to recall the pattern, while the second term can be regarded as the noise arising from the other learned patterns. The essential point in this analysis is the treatment of the second term as *complex Gaussian noise* characterized by

$$\langle z_i(t) \rangle = 0, \quad \langle |z_i(t)|^2 \rangle = 2\sigma(t)^2. \quad (7.29)$$

We also assume that  $\varphi_1(t)$  remains a constant, that is,  $\varphi_1(t) = \varphi_0$ . By applying the method of statistical neurodynamics to this model under the

above assumptions [Aoyagi and Nomura (1999)], we can study the retrieval properties analytically. As a result of such analysis we have found that the retrieval process can be characterized by some macroscopic order parameters, such as  $m(t)$  and  $\sigma(t)$ .

From (7.26), we find that the overlap at time  $t + 1$  is given by

$$m(t+1) = \left\langle \left\langle f(|m(t) + z(t)|) \frac{m(t) + z(t)}{|m(t) + z(t)|} \right\rangle \right\rangle, \quad (7.30)$$

where  $\langle \langle \dots \rangle \rangle$  represents an average over the complex Gaussian  $z(t)$  with mean 0 and variance  $2\sigma(t)^2$ . For the noise  $z(t+1)$ , in the limit  $N \rightarrow \infty$  we get [Aoyagi and Nomura (1999)]

$$z_i(t+1) \sim \frac{1}{aN} \sum_{j=1}^N \sum_{\mu=2}^P \xi_i^\mu \tilde{\xi}_j^\mu f(|h_{j,\mu}(t)|) \frac{h_{j,\mu}(t)}{|h_{j,\mu}(t)|} + z_i(t) \left( \frac{f'(|h_{j,\mu}(t)|)}{2} + \frac{f(|h_{j,\mu}(t)|)}{2|h_{j,\mu}(t)|} \right), \quad (7.31)$$

where  $h_{j,\mu}(t) = 1/aN \sum_{k=1}^N \sum_{\nu \neq \mu, 1}^P \xi_j^\nu \tilde{\xi}_k^\nu W_k(t)$ .

#### 7.5.1.1 Kuramoto Synchronization Model

The microscopic individual level dynamics of the Kuramoto model (7.22) is easily visualized by imagining oscillators as points running around on the unit circle. Due to rotational symmetry, the average frequency  $\Omega = \sum_{i=1}^N \omega_i / N$  can be set to 0 without loss of generality; this corresponds to observing dynamics in the co-rotating frame at frequency  $\Omega$ .

The governing equation (7.22) for the  $i$ th oscillator phase angle  $\varphi_i$  can be simplified to

$$\dot{\varphi}_i = \omega_i + \frac{K}{N} \sum_{j=1}^N \sin(\varphi_j - \varphi_i), \quad 1 \leq i \leq N. \quad (7.32)$$

It is known that as  $K$  is increased from 0 above some critical value  $K_c$ , more and more oscillators start to get synchronized (or phase-locked) until all the oscillators get fully synchronized at another critical value of  $K_{tp}$ . In the choice of  $\Omega = 0$ , the fully synchronized state corresponds to an exact steady state of the 'detailed', fine-scale problem in the co-rotating frame.

Such synchronization dynamics can be conveniently summarized by considering the fraction of the synchronized (phase-locked) oscillators, and conventionally described by a *complex-valued order parameter* [Kuramoto (1984); Strogatz (2000)],  $re^{i\psi} = \frac{1}{N} e^{i\varphi_j}$ , where the radius  $r$  measures the phase coherence, and  $\psi$  is the average phase angle.

**Transition from Full to Partial Synchronization.** Now, following [Moon and Kevrekidis (2005)], we restate certain facts about the nature of the second transition mentioned above, a transition between the full and the partial synchronization regime at  $K = K_{tp}$ , in the direction of decreasing  $K$ .

A fully synchronized state in the continuum limit corresponds to the solution to the mean-field type alternate form of equation (7.32),

$$\dot{\varphi}_i = \Omega = \omega_i + rK \sum_{i=1}^N \sin(\psi - \varphi_i), \quad (7.33)$$

where  $\Omega$  is the common angular velocity of the fully synchronized oscillators (which is set to 0 in our case). Equation (7.33) can be further rewritten as

$$\frac{\Omega - \omega_i}{rK} = \sum_{i=1}^N \sin(\psi - \varphi_i), \quad (7.34)$$

where the absolute value of the r.h.s is bounded by unity.

As  $K$  approaches  $K_{tp}$  from above, the l.h.s for the ‘extreme’ oscillator (the oscillator in a particular family that has the maximum value of  $|\Omega - \omega_i|$ ) first exceeds unity, and a real-valued solution to (7.34) ceases to exist. Different random draws of  $\omega_i$ ’s from  $g(\omega)$  for a finite number of oscillators result in slightly different values of  $K_{tp}$ .  $K_{tp}$  appears to follow the Gumbel type extreme distribution function [Kotz and Nadarajah (2000)], just as the maximum values of  $|\Omega - \omega_i|$  do:

$$p(K_{tp}) = \sigma^{-1} e^{-(K_{tp} - \mu)/\sigma} \exp[-e^{-(K_{tp} - \mu)/\sigma}],$$

where  $\sigma$  and  $\mu$  are parameters.

#### 7.5.1.2 Lyapunov Chaotic Synchronization

The notion of *conditional Lyapunov exponents* was introduced by Pecora and Carroll in their study of synchronization of chaotic systems. First, in [Pecora and Carroll (1991)], they generalized the idea of driving a stable system to the situation when the drive signal is chaotic. This led to the concept of conditional Lyapunov exponents and also generalized the usual criteria of the linear stability theorem. They showed that driving with chaotic signals can be done in a robust fashion, rather insensitive to changes in system parameters. The calculation of the stability criteria led naturally to an estimate for the convergence of the driven system to

its stable state. The authors focussed on a homogeneous driving situation that led to the construction of synchronized chaotic subsystems. They applied these ideas to the Lorenz and Rössler systems, as well as to an electronic circuit and its numerical model. Later, in [Pecora and Carroll (1998)], they showed that many coupled oscillator array configurations considered in the literature could be put into a simple form so that determining the stability of the synchronous state could be done by a master stability function, which could be tailored to one's choice of stability requirement. This solved, once and for all, the problem of synchronous stability for any linear coupling of that oscillator.

It turns out, that, like the full Lyapunov exponent, the conditional exponents are well defined ergodic invariants, which are reliable quantities to quantify the relation of a global dynamical system to its constituent parts and to characterize dynamical self-organization [Mendes (1998)].

Given a dynamical system defined by a map  $f : M \rightarrow M$ , with  $M \subset \mathbb{R}^m$  the conditional exponents associated to the splitting  $\mathbb{R}^k \times \mathbb{R}^{m-k}$  are the eigenvalues of the limit

$$\lim_{n \rightarrow \infty} (D_k f^{n*}(x) D_k f^n(x))^{\frac{1}{2n}},$$

where  $D_k f^n$  is the  $k \times k$  diagonal block of the full Jacobian.

Mendes [Mendes (1998)] proved that existence of the conditional Lyapunov exponents as well-defined ergodic invariants was guaranteed under the same conditions that established the existence of the Lyapunov exponents.

Recall that for measures  $\mu$  that are absolutely continuous with respect to the Lebesgue measure of  $M$  or, more generally, for measures that are smooth along unstable directions (SBR measures) Pesin's [Pesin (1977)] identity holds

$$h(\mu) = \sum_{\lambda_i > 0} \lambda_i,$$

relating *Kolmogorov-Sinai entropy*  $h(\mu)$  to the sum of the Lyapunov exponents. By analogy we may define the *conditional exponent entropies* [Mendes (1998)] associated to the splitting  $\mathbb{R}^k \times \mathbb{R}^{m-k}$  as the sum of the positive conditional exponents counted with their multiplicity

$$h_k(\mu) = \sum_{\xi_i^{(k)} > 0} \xi_i^{(k)}, \quad h_{m-k}(\mu) = \sum_{\xi_i^{(m-k)} > 0} \xi_i^{(m-k)}.$$

The Kolmogorov–Sinai entropy of a dynamical system measures the rate of information production per unit time. That is, it gives the amount of randomness in the system that is not explained by the defining equations (or the minimal model [Crutchfield and Young (1989)]). Hence, the conditional exponent entropies may be interpreted as a measure of the randomness that would be present if the two parts  $S^{(k)}$  and  $S^{(m-k)}$  were uncoupled. The difference  $h_k(\mu) + h_{m-k}(\mu) - h(\mu)$  represents the effect of the coupling.

Given a dynamical system  $S$  composed of  $N$  parts  $\{S_k\}$  with a total of  $m$  degrees of freedom and invariant measure  $\mu$ , one defines a *measure of dynamical self-organization*  $I(S, \Sigma, \mu)$  as

$$I(S, \Sigma, \mu) = \sum_{k=1}^N \{h_k(\mu) + h_{m-k}(\mu) - h(\mu)\}.$$

For each system  $S$ , this quantity will depend on the partition  $\Sigma$  into  $N$  parts that one considers.  $h_{m-k}(\mu)$  always denotes the conditional exponent entropy of the complementar of the subsystem  $S_k$ . Being constructed out of ergodic invariants,  $I(S, \Sigma, \mu)$  is also a well-defined ergodic invariant for the measure  $\mu$ .  $I(S, \Sigma, \mu)$  is formally similar to a mutual information. However, not being strictly a mutual information, in the information theory sense,  $I(S, \Sigma, \mu)$  may take negative values.

### 7.5.2 Complex Networks Dynamics

Recall that many systems in nature, such as neural nets, food webs, metabolic systems, co-authorship of papers, the worldwide web, etc. can be represented as *complex networks*, or *small-world networks* (see, e.g., [Watts and Strogatz (1998); Dorogovtsev and Mendes (2003)]). In particular, it has been recognized that many networks have scale-free topology; the distribution of the degree obeys the power law,  $P(k) \sim k^{-\gamma}$ . The study of the scale-free network now attracts the interests of many researchers in mathematics, physics, engineering and biology [Ichinomiya (2004)].

Another important aspect of complex networks is their dynamics, describing e.g., the spreading of viruses in the Internet, change of populations in a food web, and synchronization of neurons in a brain. In particular, [Ichinomiya (2004)] studied the synchronization of the random network of oscillators. His work follows the previous studies (see [Strogatz (2000)]) that showed that mean-field type synchronization, that Kuramoto observed in globally-coupled oscillators [Kuramoto (1984)], appeared also in the small-

world networks.

### 7.5.2.1 Continuum Limit of the Kuramoto Network

Ichinomiya started with the standard network with  $N$  nodes, described by a variant of the *Kuramoto model* (7.22). At each node, there exists an oscillator and the phase of each oscillator  $\theta_i$  is evolving according to

$$\dot{\theta}_i = \omega_i + K \sum_j a_{ij} \sin(\theta_j - \theta_i), \quad (7.35)$$

where  $K$  is the coupling constant,  $a_{ij}$  is 1 if the nodes  $i$  and  $j$  are connected, and 0 otherwise;  $\omega_i$  is a random number, whose distribution is given by the function  $N(\omega)$ .

For the analytic study, it is convenient to use the *continuum limit equation*. We define  $P(k)$  as the distribution of nodes with degree  $k$ , and  $\rho(k, \omega; t, \theta)$  the density of oscillators with phase  $\theta$  at time  $t$ , for given  $\omega$  and  $k$ . We assume that  $\rho(k, \omega; t, \theta)$  is normalized as

$$\int_0^{2\pi} \rho(k, \omega; t, \theta) d\theta = 1.$$

For simplicity, we also assume  $N(\omega) = N(-\omega)$ . Thus, we suppose that the collective oscillation corresponds to the stable solution,  $\dot{\rho} = 0$ .

Now we construct the continuum limit equation for the network of oscillators. The evolution of  $\rho$  is determined by the *continuity equation*  $\partial_t \rho = -\partial_\theta(\rho v)$  (see Appendix), where  $v$  is defined by the continuum limit of the r.h.s of (7.35). Because one randomly selected edge connects to the node of degree  $k$ , frequency  $\omega$ , phase  $\theta$  with the probability  $kP(k)N(\omega)\rho(k, \omega; t, \theta) / \int dk k P(k)$ ,  $\rho(k, \omega; t, \theta)$  obeys the equation

$$\begin{aligned} \partial_t \rho(k, \omega; t, \theta) = & -\partial_\theta [\rho(k, \omega; t, \theta) (\omega + \\ & + \frac{Kk \int d\omega' \int dk' \int d\theta' N(\omega') P(k') k' \rho(k', \omega'; t, \theta') \sin(\theta - \theta')}{\int dk' P(k') k'})]. \end{aligned}$$

The mean-field solution of this equation was studied by [Ichinomiya (2004)].

### 7.5.2.2 Path-Integral Approach to Complex Nets

Recently, [Ichinomiya (2005)] introduced the *path-integral* (see subsection 4.4.6 above) *approach* in studying the dynamics of complex networks. He considered the stochastic generalization of the Kuramoto network (7.35),



given by

$$\dot{x}_i = f_i(x_i) + \sum_{j=1}^N a_{ij} g(x_i, x_j) + \xi_i(t), \quad (7.36)$$

where  $f_i = f_i(x_i)$  and  $g_{ij} = g(x_i, x_j)$  are functions of network activations  $x_i$ ,  $\xi_i(t)$  is a *random force* that satisfies  $\langle \xi_i(t) \rangle = 0$ ,  $\langle \xi_i(t) \xi_j(t') \rangle = \delta_{ij} \delta(t-t') \sigma^2$ . He assumed  $x_i = x_{i,0}$  at  $t = 0$ . In order to discuss the dynamics of this system, he introduced the so-called *Matrin-Siggia-Rose* (MSR) *generating functional*  $Z$  (see [De Dominicis (1978)]) given by

$$Z[\{l_{ik}\}, \{\bar{l}_{ik}\}] = \left(\frac{1}{\pi}\right)^{NN_t} \left\langle \int \prod_{i=1}^N \prod_{k=0}^{N_t} dx_{ik} d\bar{x}_{ik} e^{-S} \exp(l_{ik} x_{ik} + \bar{l}_{ik} \bar{x}_{ik}) J \right\rangle,$$

where the *action*  $S$  is given by

$$S = \sum_{ik} \left[ \frac{\sigma^2 \Delta t}{2} \bar{x}_{ik}^2 + i \bar{x}_{ik} \{x_{ik} - x_{i,k-1} - \Delta t(f_i(x_{i,k-1}) + \sum_j a_{ij} g(x_{i,k-1}, x_{j,k-1}))\} \right],$$

and  $\langle \dots \rangle$  represents the average over the ensemble of networks.  $J$  is the functional Jacobian term,

$$J = \exp \left( -\frac{\Delta t}{2} \sum_{ijk} \frac{\partial(f_i(x_{ik}) + a_{ij} g(x_{ik}, x_{jk}))}{\partial x_{ik}} \right).$$

Ichinomiya considered such a form of the network model (7.36) in which

$$a_{ij} = \begin{cases} 1 & \text{with probability } p_{ij}, \\ 0 & \text{with probability } 1 - p_{ij}. \end{cases}$$

Note that  $p_{ij}$  can be a function of variables such as  $i$  or  $j$ . For example, in the 1D chain model,  $p_{ij}$  is 1 if  $|i - j| = 1$ , else it is 0. The average over all networks can be expressed as

$$\left\langle \exp \left[ \sum_{ik} i \Delta t \bar{x}_{ik} \sum_j a_{ij} g(x_{i,k-1}, x_{j,k-1}) \right] \right\rangle = \prod_{ij} \left[ p_{ij} \exp \left\{ \sum_k i \Delta t \bar{x}_{ik} g(x_{i,k-1}, x_{j,k-1}) \right\} + 1 - p_{ij} \right],$$

so we get

$$\langle e^{-S} \rangle = \exp(-S_0) \prod_{ij} \left[ p_{ij} \exp \left\{ \sum_k i \Delta t \bar{x}_{ik} g(x_{i,k-1}, x_{j,k-1}) \right\} + 1 - p_{ij} \right],$$

where 
$$S_0 = \sum_{ik} \frac{\sigma^2 \Delta t}{2} \bar{x}_{ik}^2 + i \bar{x}_{ik} \{x_{ik} - x_{i,k-1} - \Delta t f_i(x_{i,k-1})\}.$$

This expression can be applied to the dynamics of any complex network model. [Ichinomiya (2005)] applied this model to analysis of the *Kuramoto transition in random sparse networks*.

### 7.5.3 Complex Adaptive Systems

According to [Ahmed *et al.* (2005)], a *complex adaptive system* (CAS) consists of inhomogeneous, interacting adaptive agents, where the word *adaptive* means *capable of learning*. An *emergent property* of a CAS is a property of the system as a whole which does not exist at the individual elements (agents) level.

Typical CAS examples are the brain, the immune system, the economy, social systems, ecology, etc... Most of living systems are CAS.

Therefore to understand a complex system one has to study the system as a whole and not to decompose it into its constituents. This totalistic approach is against the standard reductionist one, which tries to decompose any system to its constituents and hopes that by understanding the elements one can understand the whole system.

The standard approaches to CAS modelling are: (i) ODEs, difference equations and PDEs; (ii) Cellular automata (CA) [Ilachinski (2001)]; (iii) Evolutionary game theory [Hofbauer and Sigmund (1998)]; (iv) Various agent based models; (v) Complex networks (see previous subsection); and (vi) Fractional calculus [Stanislavsky (2000)]. Most of these approaches are included in [Boccaro (2004)].

The ODE and PDE approaches have some difficulties as follows [Louzoun *et al.* (2003)]: (i) ODE and PDE assumes that local fluctuations have been smoothed out. (ii) Typically they neglect correlations between movements of different species. (iii) They assume instantaneous results of interactions.

Most biological systems show delay and do not satisfy the above assumptions. They concluded that a cellular automata (CA) [Ilachinski (2001)] type system called microscopic simulation is more suitable to model com-

plex biological systems. We agree that CA type systems are more suitable to model complex biological systems but such systems suffer from a main drawback namely the difficulty of obtaining analytical results. The known analytical results about CA type systems are very few compared to the known results about ODE and PDE.

A compromise was presented in [Ahmed *et al.* (2005)] in the form of a PDE, which avoids the delay and the correlations drawbacks. It is called *telegraph reaction diffusion equation* (TRD). To overcome the non-delay weakness in the *Fick law* (see (1.9), Introduction), it is replaced by

$$J(x, t) + \tau \partial_t J(x, t) = -D \partial_x c, \quad (7.37)$$

where the flux  $J(x, t)$  relaxes, with some given characteristic time constant  $\tau$  and  $c$  is the concentration of the diffusing substance. Combining (7.37) with the equation of continuity, one gets the *modified diffusion equation*, or the *telegraph equation*,  $\dot{c} = (D - \tau) \partial_{x^2} c$ . The corresponding TRD equation is given by

$$\tau \ddot{c} + \left(1 - \frac{df(c)}{dc}\right) \dot{c} = D \partial_{x^2} c + f(c), \quad (7.38)$$

where  $f(c)$  is a polynomial in  $c$ . Moreover it is known that TRD results from correlated random walk. This supports the conclusion that TRD equation (7.38) is more suitable for modeling complex systems than the usual diffusion one.

For example, a *human immune system* as a CAS was elaborated in [Segel and Cohen (2001)]. The emergent properties of the immune system (IS) included:

- \* The ability to distinguish any substance (typically called antigen Ag) and determine whether it is damaging or not. If Ag is non-damaging (damaging) then, typically, IS tolerates it (responds to it).
- \* If it decides to respond to it then IS determines whether to eradicate it or to contain it.
- \* The ability to memorize most previously encountered Ag, which enables it to mount a more effective reaction in any future encounters. This is the basis of vaccination processes.
- \* IS is complex thus it has a network structure.
- \* The immune network is not homogeneous since there are effectors with many connections and others with low number of connections.

- \* The Ag, which enters our bodies, has extremely wide diversity. Thus mechanisms have to exist to produce immune effectors with constantly changing random specificity to be able to recognize these Ag. Consequently IS is an adaptive complex system.
- \* Having said that, one should notice that the wide diversity of IS contains the danger of autoimmunity (attacking the body). Thus mechanisms that limit autoimmunity should exist.
- \* In addition to the primary clonal deletion mechanism, two further brilliant mechanisms exist: The first is that the IS network is a threshold or 'window' one i.e., no activation exists if the Ag quantity is too low or too high (This is called low and high zone tolerance).
- \* Thus an auto reactive immune effector (i.e., an immune effector that attacks the body to which it belongs) will face so many self-antigens that it has to be suppressed due to the high zone tolerance mechanism.
- \* Another mechanism against autoimmunity is the second signal given by antigen presenting cells (APC). If the immune effector is self reactive then, in most cases, it does not receive the second signal thus it becomes anergic.
- \* Also long term memory can be explained by the phenomena of high and low zone tolerance where IS tolerates Ag if its quantity is too high or too low. So persisting Ag is possible and continuous activation of immune effectors may occur.
- \* There is another possible explanation for long term memory using the immune system (extremal dynamics).
- \* Thus design principles of IS can explain important phenomena of IS.

The following Summary on CAS was given in [Ahmed *et al.* (2005)] (see also the literature cited there):

- (i) CAS should be studied as a whole hence reductionist point of view may not be reliable in some cases.
- (ii) CAS are open with nonlinear local interactions hence: (1) Long range prediction is highly unlikely. (2) When studying a CAS take into consideration the effects of its perturbation on related systems e.g. perturbation of lake Victoria has affected mosquitoes' numbers hence the locals quality of life. This is also relevant to the case of natural disasters where an earthquake at a city can cause a widespread power failure at other cities. (3) Expect side effects to any 'seemingly wise' decision. (4) Mathematical and computer models may be helpful in reducing such

side effects.

- (iii) Optimization in CAS should be multi-objective (not single objective).
- (iv) CAS are very difficult to control. Interference at highly connected sites may be a useful approach. The interlinked nature of CAS elements complicates both the unpredictability and controllability problems. It also plays an important role in innovations spread.
- (v) Memory effects should not be neglected in CAS. This lends more support for the proposed TRD equation (7.38). Also memory games have been studied. Also delay and fractional calculus are relevant to CAS.
- (vi) Mathematical topics motivated by CAS include ODE and PDE (non-autonomous, delayed, periodic coefficients, stability and persistence), multi-objective optimization (including biologically motivated methods e.g., ant colony optimization, extremal optimization, genetic algorithms, etc.), difference equations, cellular automata, networks, fractional calculus, control (e.g., bounded delayed control of distributed systems), game theory, nonlinear dynamics and fuzzy mathematics.

## 7.5.4 Noise Delayed Bifurcation in Coupled Neurons

### 7.5.4.1 The Theta-Neuron

The *theta-neuron model* developed by Ermentrout and Gutkin [Ermentrout (1996); Gutkin and Ermentrout (1998)] is derived from the observation that wide class of neuronal models of cortical neurons, based on the electro-physiological model of Hodgkin and Huxley, show a saddle-node type bifurcation at a critical parameter value. This parameter determines the dynamical behavior of the solutions of the corresponding system of ODEs. General dynamical systems theory tells us that the qualitative behavior in some neighborhood of the bifurcation point (which may be quite large as it extends up to the next bifurcation or other dynamic transition) is governed by the reduction of the system to the *center manifold* (see section 2.3 above). In the present case of the *saddle-node bifurcation* which is the simplest bifurcation type, this leads to the ODE:  $\dot{x} = \lambda + x^2$ . Here, the bifurcation parameter  $\lambda$  is considered as the input to the neuron while  $x$  records its activity. Obviously, a solution to this equation tends to infinity in finite time. This is considered as a spiking event, and the initial values are then reset to  $-\infty$ . In order to have a model that does not exhibit such formal singularities, one introduces a phase variable  $\theta$  that is  $2\pi$ -periodic via  $x = \tan(\frac{\theta}{2})$ .  $\theta$  is then a variable with domain the unit circle  $S^1$ , and a

spike now corresponds to a period of  $\theta$ . Spikes are no longer represented by transitions through infinity, but by changes of some discrete topological invariant. The original differential equation is then transformed into

$$\dot{\theta} = (1 - \cos \theta) + (1 + \cos \theta)\lambda. \quad (7.39)$$

Due to the nonlinearity of the transformation from  $x$  to  $\theta$ , the input  $\lambda$  is no longer additive. In fact, it is easy to show that  $(1 + \cos \theta)$  is the phase resetting function for the model [Ermentrout (1996)]. As before, the bifurcation occurs at  $\lambda = 0$ . There, we have precisely one rest point, namely  $\theta = 0$  which is degenerate. In any case, the sensitivity to the input  $\lambda$  is highest at  $\theta = 0$  and lowest at  $\theta = \pi$  which according to the derivation of our equation is considered as the spike point. When  $\lambda$  is positive, the equation does not have any rest point. In this case,  $\theta$  continues to increase all the time, and the neuron is perpetually firing. When  $\lambda$  is negative, however, there are two rest points, a stable one denoted by  $\theta_r$  and an unstable one  $\theta_t > \theta_r$ . If  $\theta$  is larger than  $\theta_t$  it increases until it completes a period and comes to rest at  $\theta_r + 2\pi$  which is identified with  $\theta_r$  as we are working on the unit circle  $S^1$ . Thus, if the phase is above the threshold value  $\theta_t$ , a spike occurs and the neuron returns to rest. So far, we have tacitly assumed that the input  $\lambda$  is constant. We now consider the situation where the input can be decomposed as  $\lambda = \beta + \sigma\eta$ , where  $\beta$  is a constant term, the so-called ‘bias’, while  $\eta$  is (white) noise and  $\sigma$  its intensity. In this case, sufficiently strong noise can occasionally push the phase  $\theta$  beyond the threshold value  $\theta_t$  causing intermittent firing. Equation (7.39) now becomes a canonical stochastic saddle-node oscillator which has been studied in [Gutkin and Ermentrout (1998)].

#### 7.5.4.2 Coupled Theta-Neurons

Here we consider the situation where we have two neurons (distinguished by subscripts  $i = 1, 2$ ). The dynamics then takes place on the product of two circles, i.e., on a 2D torus  $T$ , represented by the square  $[-\pi, \pi] \times [-\pi, \pi]$  in the plane, with periodic boundary identifications. We first consider the simple case of two uncoupled, noise-free neurons ( $\sigma_1 = \sigma_2 = 0$ ) with the same bias  $\beta$ . Their dynamics are independent. If  $\beta > 0$ , both neurons continue to fire, although their phase difference, if not 0 initially, is not constant, due to the nonlinearity of the differential equation governing it. If  $\beta = 0$ ,  $(0, 0)$  is a degenerate rest point. The two trajectories  $\theta_1 = \theta_2 = 0$  are homoclinic orbits and all flow lines eventually terminate at this fixed

point. One or both neurons will spike before returning to rest if their initial phase is between 0 and  $\pi$  [Gutkin and Ermentrout (1998)].

If  $\beta < 0$ , we have four fixed points – the attractor ( $\theta_1 = \theta_2 = \theta_r$ ), the repeller ( $\theta_1 = \theta_2 = \theta_t$ ), and the two saddles where one of the neurons has its phase at  $\theta_r$  (rest) and the other one at  $\theta_t$  (threshold). Some special heteroclinic orbits are given by the straight lines where one of the two neurons stays at  $\theta_t$  while the other one moves from the threshold to the rest value, spiking if its initial phase was above threshold. All other flow lines terminate at the attractor. We now add an interaction term  $s_i g_s$  to the input of neuron  $i$ .  $s_i$  is considered as the synaptic input from neuron  $j$  to neuron  $i$  ( $i \neq j$ ) and  $g_s$  is the synaptic intensity. (One could also study the case of a single neuron  $i$  for which  $s_i$  represents synaptic self-coupling, but here we are interested in the case of two coupled neurons). A precise equation for  $s_i$  can be derived from electrophysiological models, however for our qualitative study we only need the characteristic features that it stays bounded between 0 and 1. Typically, it is peaked near the spike of neuron  $j$ , i.e., where  $\theta_j = \pi$ . With this interaction term, the equation for neuron  $i$  then becomes

$$\dot{\theta}_i = (1 - \cos(\theta_i)) + (1 + \cos(\theta_i))(\beta + g_s s_i + \sigma \eta).$$

Since  $s_i$  represents the input that neuron  $i$  receives from neuron  $j$ ,  $s_i$  should essentially be considered as a function of the phase  $\theta_j$  of  $j$ . Once more, we first consider the situation without noise, i.e.  $\sigma = 0$  (although our final aim is to understand the effect of noise on the dynamic behavior of the coupled neurons). We also assume that we are in the excitable region, i.e.,  $\beta < 0$ .  $g_s$  is assumed to be positive (excitatory coupling), and so the coupling counteracts the effect of the bias to a certain extent, a crucial difference being, however, that the synaptic input to each neuron is time-dependent, in contrast to the constant bias. If  $g_s$  is sufficiently small, the qualitative situation does not change compared to the case without coupling, i.e.,  $g_s = 0$ . We still have a heteroclinic orbit from the saddle ( $\theta_1 = \theta_t, \theta_2 = \theta_r$ ) to the attractor ( $\theta_r, \theta_r$ ), although  $\theta_2$  does not stay constant anymore along that orbit, but increases first a little due to the input from neuron 1 before it descends again to the rest value [Gutkin and Ermentrout (1998)].

If  $g_s$  reaches some critical value  $g_s^*$ , however, the heteroclinic orbit starting at  $(\theta_t, \theta_r)$  does not terminate anymore at the attractor, and the value of the phase of neuron 2 is increased so much by the synaptic interaction that it reaches the other saddle  $(\theta_r, \theta_t)$ . Besides two heteroclinic orbits that go

from the repeller to the two saddles as before, all other orbits still terminate at the attractor  $(\theta_r, \theta_r)$ , for  $g_s = g_s^*$ . If  $g_s$  is increased beyond  $g_s^*$ , however, the heteroclinic orbit between the two saddles mutates into a stable attractor. It corresponds to sustained asynchronous firing of the two neurons. In fact, if the phase difference between the two neurons is too small, the dynamics converges towards the double rest point (except in some region in the vicinity of the node), and both neurons stop firing. This is caused by the fact that when the two neurons are close to synchrony, neither cell is sensitive enough to its synaptic input to maintain firing (an effective refractory period). Conversely, if they are out of synchrony, a single spike can induce the second neuron to fire at a time when the first one is close to rest, and sensitive to synaptic input itself. If  $g_s$  is only slightly above the critical value, the basin of attraction of that limit cycle will still be relatively small, but as  $g_s$  is increased further, the basin grows in size until eventually it is larger than the basin of attraction of the double rest point. On the basis of the preceding analysis, it is now straightforward to predict the effect of noise. If  $g_s$  is only slightly above the critical value  $g_s^*$ , a small amount of noise is more likely to kick the dynamics out of the narrow basin of attraction of the asynchronous limit cycle and into the large basin of the double rest point than vice versa. In effect, a small noise level increases the critical parameter value required for the qualitative transition to sustained asynchronous firing. A larger amount of noise, however, has the potential to move the dynamics from the rest point into the basin of attraction of the asynchronous limit cycle. Once in that basin, the neurons will fire. Thus, for large noise in that regime, one will observe that the neurons will fire, perhaps with some intermissions spent near the double rest point. So, a larger value of noise will cause intermittent periods of sustained firing of the two neurons even at somewhat smaller values of  $g_s$ . In effect, it decreases the value of the critical parameter. Thus, we observe a genuinely nonlinear effect of the noise level  $\sigma$ . For values of the coupling  $g_s$  that are substantially larger than the critical value  $g_s^*$ , even small amounts of noise have a good chance of perturbing the dynamics out of the attracting vicinity of the double rest point into the attracting region of the asynchronous limit cycle. This will further enhance the sustained asynchronous firing pattern of the two neurons [Gutkin and Ermentrout (1998)].



### 7.5.5 Classification of ‘Spiking’ Neuron Models

Recently, Izhikevich [Izhikevich (2004)] discussed biological plausibility and computational efficiency of some of the most useful models of *spiking and bursting neurons* (see Figure 7.44, permission from E. Izhikevich). He compared their applicability to large-scale simulations of cortical neural networks.

Following [Izhikevich (2004)], we present some widely used models of spiking and bursting neurons that can be expressed in the form of ODEs. Throughout this subsection,  $v$  denotes the membrane potential. All the parameters in the models are chosen so that  $v$  has  $mV$  scale and the time has  $ms$  scale. To compare computational cost, we assume that each model, written as a dynamical system  $\dot{x} = f(x)$ , is implemented using the simplest, fixed-step first-order Euler method, with the integration time step chosen to achieve a reasonable numerical accuracy.

**Integrate-and-Fire (I&F) Neuron.** One of the most widely used models in computational neuroscience is the *leaky integrate-and-fire neuron*, (I&F neuron, for short) given by

$$\dot{v} = I + a - bv, \quad \text{If } v \geq v_{trsh} \quad \text{Then } v \leftarrow c,$$

where  $v$  is the membrane potential,  $I$  is the input current, and  $a, b, c$ , and  $v_{trsh}$  are the parameters. When the membrane potential  $v$  reaches the threshold value  $v_{trsh}$ , the neuron is said to fire a *spike*, and  $v$  is reset to  $c$ . The I&F neuron can fire tonic spikes with constant frequency, and it is an integrator. The I&F neuron is *Class 1 excitable system* [Izhikevich (1999)]; it can fire tonic spikes with constant frequency, and it is an integrator. It is the simplest model to implement when the integration time step  $\tau$  is  $1\ ms$ . Because I&F has only one variable, it cannot have phasic spiking, bursting of any kind, rebound responses, threshold variability, bistability of attractors, or autonomous chaotic dynamics. Because of the fixed threshold, the spikes do not have latencies. In summary, despite its simplicity, I&F is one of the worst models to use in simulations, unless one wants to prove analytical results [Izhikevich (2004)].

**Integrate-and-Fire Neuron with Adaptation.** The I&F model is  $1D$ , hence it cannot burst or have other properties of cortical neurons. One may think that having a second linear equation

$$\dot{v} = I + a - bv + g(d - v), \quad \dot{g} = (e\delta(t) - g)/\tau,$$

describing activation dynamics of a high-threshold  $K$ -current, can make

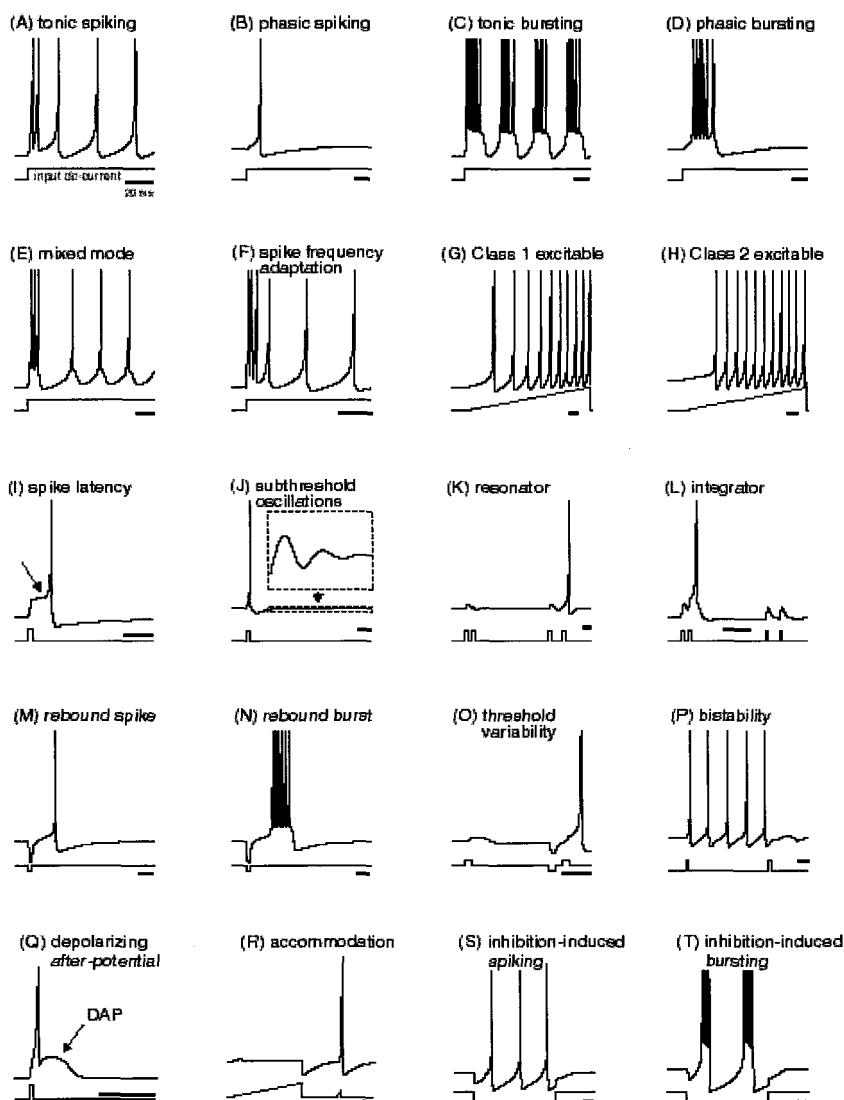


Fig. 7.44 Neuro-computational features of biological neurons.

an improvement, e.g., endow the model with spike-frequency adaptation. Indeed, each firing increases the  $K$ -activation gate via Dirac  $\delta$ -function and produces an outward current that slows down the frequency of tonic spiking. This model is fast, yet still lacks many important properties of

cortical spiking neurons.

**Integrate-and-Fire-or-Burst Neuron.** The *integrate-and-fire-or-burst neuron* model is given by

$$\begin{aligned} \dot{v} &= I + a - bv + gH(v - v_h)h(v_T - v), \\ \text{If } v \geq v_{trsh} \text{ Then } v &\leftarrow c, \quad \dot{h} = \begin{cases} \frac{-h}{\tau^-}, & \text{if } v > v_h, \\ \frac{1-h}{\tau^+}, & \text{if } v < v_h \end{cases} \end{aligned}$$

to model thalamo-cortical neurons. Here  $h$  describes the inactivation of the calcium  $T$ -current,  $g, v_h, v_T, \tau^+$  and  $\tau^-$  are parameters describing dynamics of the  $T$ -current, and  $H$  is the Heaviside step function. Having this kind of a second variable creates the possibility for bursting and other interesting regimes [Izhikevich (2004)], but is already a much slower (depending on the value of  $v$ ).

**Complex-Valued Resonate-and-Fire Neuron.** The *resonate-and-fire neuron* is a complex-valued (i.e.,  $2D$ ) analogue of the I&F neuron [Izhikevich (2001)], given by

$$\dot{z} = I + (b + iw)z, \quad \text{if } \text{Im } z = a_{trsh} \text{ then } z \leftarrow z_0(z), \quad (7.40)$$

where  $z = x + iy \in \mathbb{C}$  is a complex-valued variable that describes oscillatory activity of the neuron. Here  $b, w$ , and  $a_{trsh}$  are parameters,  $i = \sqrt{-1}$ , and  $z_0(z)$  is an arbitrary function describing activity-dependent after-spike reset. (7.40) is equivalent to the linear system

$$\dot{x} = bx - wy, \quad \dot{y} = wx + by,$$

where the real part  $x$  is the current-like variable, while the imaginary part  $y$  is the voltage-like variable. The resonate-and-fire model is simple and efficient. When the frequency of oscillation  $w = 0$ , it becomes an integrator.

**Quadratic Integrate-and-Fire Neuron.** An alternative to the leaky I&F neuron is the *quadratic I&F neuron*, also known as the *theta-neuron*, or the Ermentrout-Kopell canonical model [Ermentrout (1996); Gutkin and Ermentrout (1998)] (when it is written in a trigonometric form, see subsection 7.5.4.1 above). It can be presented as

$$\dot{v} = I + a(v - v_{rest})(v - v_{trsh}), \quad \text{If } v = v_{trsh} \text{ Then } v \leftarrow v_{rest},$$

where  $v_{rest}$  and  $v_{trsh}$  are the resting and threshold values of the membrane potential. This model is canonical in the sense that any *Class 1 excitable system* [Izhikevich (1999)] described by smooth ODEs can be transformed into this form by a continuous change of variables. It takes only seven

operations to simulate 1 ms of the model, and this should be the model of choice when one simulates large-scale networks of integrators. Unlike its linear analogue, the quadratic I&F neuron has spike latencies, activity dependent threshold (which is  $v_{trsh}$  only when  $I = 0$ ), and bistability of resting and tonic spiking modes.

**FitzHugh–Nagumo Neuron.** The parameters in the FitzHugh–Nagumo model (see subsection 7.4.2 above)

$$\dot{v} = a + bv + cv^2 + dv^3 - u, \quad \dot{u} = \varepsilon(ev - u),$$

can be tuned so that the model describes spiking dynamics of many resonator neurons. Since one needs to simulate the shape of each spike, the time step in the model must be relatively small, e.g.,  $\tau = 0.25$  ms. Since the model is a 2D system of ODEs, without a reset, it cannot exhibit autonomous chaotic dynamics or bursting. Adding noise to this, or some other 2D models, allows for stochastic bursting.

**Hindmarsh–Rose Neuron.** The *Hindmarsh–Rose thalamic neuron* model [Rose and Hindmarsh (1989)] can be written as a 3D ODE system

$$\dot{v} = I + u - F(v) - w, \quad \dot{u} = G(v) - u, \quad \dot{w} = (H(v) - w)/\tau,$$

where  $F, G$ , and  $H$  are some functions. This model is quite expensive to implement as a large-scale spike simulator [Izhikevich (2004)].

**Morris–Lecar Neuron.** Morris and Lecar [Morris and Lecar (1981)] suggested a simple 2D model to describe oscillations in barnacle giant muscle fiber. Because it has biophysically meaningful and measurable parameters, the *Morris–Lecar neuron* model became quite popular in computational neuroscience community. It consists of a membrane potential equation with instantaneous activation of  $Ca$  current and an additional equation describing slower activation of  $K$  current,

$$\begin{aligned} C\dot{V} &= I - g_L(V - V_L) - g_{Ca}m_\infty(V)(V - V_{Ca}) - g_Kn(V - V_K), \\ \dot{n} &= \lambda(V)(n_\infty(V) - n), \end{aligned}$$

where

$$\begin{aligned} m_\infty(V) &= \frac{1}{2} \left( 1 + \tanh \left[ \frac{V - V_1}{V_2} \right] \right), \\ n_\infty(V) &= \frac{1}{2} \left( 1 + \tanh \left[ \frac{V - V_3}{V_4} \right] \right), \\ \lambda(V) &= \bar{\lambda} \cosh \left[ \frac{V - V_3}{2V_4} \right], \end{aligned}$$

with parameters:  $C = 20 \mu\text{F}/\text{cm}^2$ ,  $g_L = 2 \text{ mmho}/\text{cm}^2$ ,  $V_L = -50 \text{ mV}$ ,  $g_{Ca} = 4 \text{ mmho}/\text{cm}^2$ ,  $V_{Ca} = 10 \text{ mV}$ ,  $g_K = 8 \text{ mmho}/\text{cm}^2$ ,  $V_K = -70 \text{ mV}$ ,  $V_1 = 0 \text{ mV}$ ,  $V_2 = 15 \text{ mV}$ ,  $V_3 = 10 \text{ mV}$ ,  $V_4 = 10 \text{ mV}$ ,  $\bar{\lambda} = 0.1 \text{ s}^{-1}$ , and applied current  $I(\mu\text{A}/\text{cm}^2)$ . The model can exhibit various types of spiking, but could exhibit tonic bursting only when an additional equation is added, e.g., slow inactivation of  $Ca$  current. In this case, the model becomes equivalent to the *Hodgkin-Huxley model* (see subsection 7.4.2 above), which is extremely expensive to implement.

### 7.5.6 Weakly Connected and Canonical Neural Nets

The assumption of weak neuronal connections is based on the observation that the typical size of a postsynaptic potential is less than  $1 \text{ mV}$ , which is small in comparison with the mean size necessary to discharge a cell (around  $20 \text{ mV}$ ) or the averaged size of the action potential (around  $100 \text{ mV}$ ); see detailed review of relevant electrophysiological data in [Hoppensteadt and Izhikevich (1997)]. From the mathematical point of view this results in *weakly-connected neural networks* of the form

$$\dot{x}^i = f(x^i, \lambda_i) + \varepsilon g_{ij}(x^i, x^j, \varepsilon), \quad (7.41)$$

where each vector  $x^i \in \mathbb{R}^m$  describes membrane potential, gating variables, and other electrophysiological variables of the  $i$ th neuron. Each vector  $\lambda_i \in \mathbb{R}^l$  denotes various biophysical parameters of the neuron. The function  $f$  describes the neuron's dynamics, and the functions  $g_{ij}$  describe connections between the neurons. The dimensionless parameter  $\varepsilon \ll 1$  is small, reflecting the strength of connections between neurons.

Now, bistable and hysteretic dynamics are ubiquitous in neural models, and they may play important roles in biological neurons [Arbib (1998)]. The *cusp bifurcation* (see Figure 7.45) is one of the simplest bifurcations leading to such dynamics. For example, the sigmoidal neuron

$$\dot{x} = -x + aS(x), \quad S(x) = 1/(1 + e^{-x}),$$

is at a cusp bifurcation point  $x = 0.5$  when  $a = 4$ . It is bistable when  $a > 4$ . If each neuron in the weakly connected network (7.41) is near a supercritical cusp bifurcation, then the entire network can be transformed into the *canonical form* [Hoppensteadt and Izhikevich (1997)],

$$\dot{y} = r_i - y_i^3 + s_{ij} y_j, \quad (7.42)$$

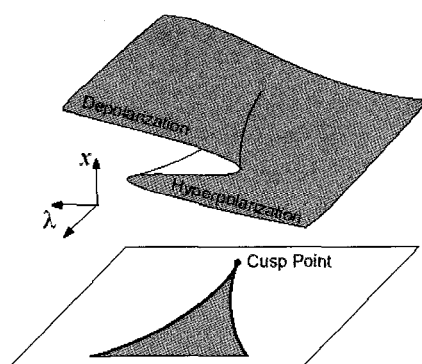


Fig. 7.45 Cusp surface.

where each scalar  $y_i \in \mathbb{R}$  describes re-scaled dynamics of the  $i$ th neuron. Particulars of the functions  $f$  and  $g_{ij}$  and the value of the parameters  $\lambda_i$  do not affect the form of the canonical model, but only particulars of the parameters  $r_i$  and  $s_{ij}$ . Thus, studying the canonical model (7.42) one can gain some insight into neuro-computational behavior of any neural model near a cusp bifurcation, whether it is a simple sigmoidal neuron or a biophysically detailed conductance-based (Hodgkin-Huxley-type) neuron [Hodgkin and Huxley (1952)].

The canonical model (7.42) is quite simple: Each equation has only one nonlinear term, namely,  $y_i^3$ , and two internal parameters,  $r_i$  and  $s_{ij}$ . Still, the *Cohen-Grossberg-Hopfield convergence theorem* [Cohen and Grossberg (1983)] applies, which means that the canonical model has the same neuro-computational properties as the standard Hopfield network: If the *connection matrix*  $S = (s_{ij})$  is *symmetric*, then the canonical neural network (7.42) is a *gradient* system.

One can easily check that

$$E(y) = -r_i y_i - \frac{1}{4} y_i^4 - \frac{1}{2} s_{ij} y_i y_j$$

is a *potential function* for the canonical model (7.42) in the sense that

$$\dot{y} = -\partial_{y_i} E.$$

### 7.5.7 Quantum Brain Model

The *conservative brain* model was originally formulated within the framework of the quantum field theory (QFT) by Umezawa and Ricciardi [Ricciardi and Umezawa (1967)] and subsequently developed in [Stuart *et al.* (1978); Stuart *et al.* (1979); Jibu and Yasue (1995); Jibu *et al.* (1996)]. The conservative brain model has been recently extended to the *dissipative quantum dynamics* in the work of G. Vitiello and collaborators [Vitiello (1995b); Alfinito and Vitiello (2000); Pessa and Vitiello (1999); Vitiello (2001); Pessa and Vitiello (2003); Pessa and Vitiello (2004)].

The canonical quantization procedure of a dissipative system requires to include in the formalism also the system representing the environment (usually the heat bath) in which the system is embedded. One possible way to do that is to depict the environment as the time-reversal image of the system [Celeghini *et al.* (1992)]: the environment is thus described as the *double* of the system in the time-reversed dynamics (the system image in the mirror of time).

Within the framework of dissipative QFT, the brain system is described in terms of an *infinite collection of damped harmonic oscillators*  $A_\kappa$  (the simplest prototype of a dissipative system) representing the DWQ [Vitiello (1995a)]. Now, the collection of damped harmonic oscillators is ruled by the Hamiltonian [Vitiello (1995a); Celeghini *et al.* (1992)]

$$H = H_0 + H_I, \quad \text{with} \\ H_0 = \hbar\Omega_\kappa(A_\kappa^\dagger A_\kappa - \tilde{A}_\kappa^\dagger \tilde{A}_\kappa), \quad H_I = i\hbar\Gamma_\kappa(A_\kappa^\dagger \tilde{A}_\kappa^\dagger - A_\kappa \tilde{A}_\kappa),$$

where  $\Omega_\kappa$  is the frequency and  $\Gamma_\kappa$  is the damping constant. The  $\tilde{A}_\kappa$  modes are the 'time-reversed mirror image' (i.e., the 'mirror modes') of the  $A_\kappa$  modes. They are the doubled modes, representing the environment modes, in such a way that  $\kappa$  generically labels their degrees of freedom. In particular, we consider the damped harmonic oscillator (DHO)

$$m\ddot{x} + \gamma\dot{x} + \kappa x = 0, \quad (7.43)$$

as a simple prototype for dissipative systems (with intention that thus obtained results also apply to more general systems). The damped oscillator (7.43) is a non-Hamiltonian system and therefore the customary canonical quantization procedure cannot be followed. However, one can face the problem by resorting to well known tools such as the *density matrix*  $\rho$  and the *Wigner function*  $W$ .

Let us start with the special case of a *conservative particle* in the absence of friction  $\gamma$ , with the standard Hamiltonian,  $H = -(\hbar\partial_x)^2/2m + V(x)$ .

Recall that the *density matrix equation of motion*, i.e., *quantum Liouville equation*, is given by

$$i\hbar\dot{\rho} = [H, \rho]. \quad (7.44)$$

The density matrix function  $\rho$  is defined by

$$\langle x + \frac{1}{2}y | \rho(t) | x - \frac{1}{2}y \rangle = \psi^*(x + \frac{1}{2}y, t) \psi(x - \frac{1}{2}y, t) \equiv W(x, y, t),$$

with the associated standard expression for the *Wigner function* (see [Feynman and Hibbs (1965)]),

$$W(p, x, t) = \frac{1}{2\pi\hbar} \int W(x, y, t) e^{(-i\frac{py}{\hbar})} dy.$$

Now, in the coordinate  $x$ -representation, by introducing the notation

$$x_{\pm} = x \pm \frac{1}{2}y, \quad (7.45)$$

the Liouville equation (7.44) can be expanded as

$$i\hbar\partial_t \langle x_+ | \rho(t) | x_- \rangle = \left\{ -\frac{\hbar^2}{2m} [\partial_{x_+}^2 - \partial_{x_-}^2] + [V(x_+) - V(x_-)] \right\} \langle x_+ | \rho(t) | x_- \rangle, \quad (7.46)$$

while the Wigner function  $W(p, x, t)$  is now given by

$$i\hbar\partial_t W(x, y, t) = H_o W(x, y, t)$$

with

$$H_o = \frac{1}{m} p_x p_y + V(x + \frac{1}{2}y) - V(x - \frac{1}{2}y),$$

and

$$p_x = -i\hbar\partial_x, \quad p_y = -i\hbar\partial_y.$$

The new Hamiltonian  $H_o$  (7.5.7) may be obtained from the corresponding Lagrangian

$$L_o = m\dot{x}\dot{y} - V(x + \frac{1}{2}y) + V(x - \frac{1}{2}y).$$



In this way, Vitiello concluded that the density matrix and the Wigner function formalism *required*, even in the conservative case (with zero mechanical resistance  $\gamma$ ), the introduction of a 'doubled' set of coordinates,  $x_{\pm}$ , or, alternatively,  $x$  and  $y$ . One may understand this as related to the introduction of the 'couple' of indices *necessary* to label the density matrix elements (7.46).

Let us now consider the case of the *particle interacting* with a *thermal bath* at temperature  $T$ . Let  $f$  denote the *random force* on the particle at the position  $x$  due to the bath. The interaction Hamiltonian between the bath and the particle is written as

$$H_{int} = -fx. \quad (7.47)$$

Now, in the *Feynman-Vernon formalism* (see [Feynman (1972)]), the *effective action*  $A[x, y]$  for the particle is given by

$$A[x, y] = \int_{t_i}^{t_f} L_o(\dot{x}, \dot{y}, x, y) dt + I[x, y],$$

with  $L_o$  defined by (7.5.7) and

$$e^{\frac{i}{\hbar} I[x, y]} = \langle (e^{-\frac{i}{\hbar} \int_{t_i}^{t_f} f(t)x_{-}(t)dt})_{-} (e^{\frac{i}{\hbar} \int_{t_i}^{t_f} f(t)x_{+}(t)dt})_{+} \rangle, \quad (7.48)$$

where the symbol  $\langle \cdot \rangle$  denotes the average with respect to the thermal bath; ' $(\cdot)_{+}$ ' and ' $(\cdot)_{-}$ ' denote time ordering and anti-time ordering, respectively; the coordinates  $x_{\pm}$  are defined as in (7.45). If the interaction between the bath and the coordinate  $x$  (7.47) were turned off, then the operator  $f$  of the bath would develop in time according to  $f(t) = e^{iH_{\gamma}t/\hbar} f e^{-iH_{\gamma}t/\hbar}$ , where  $H_{\gamma}$  is the Hamiltonian of the isolated bath (decoupled from the coordinate  $x$ ).  $f(t)$  is then the force operator of the bath to be used in (7.48).

The interaction  $I[x, y]$  between the bath and the particle has been evaluated in [Srivastava *et al.* (1995)] for a linear passive damping due to thermal bath by following Feynman-Vernon and Schwinger [Feynman and Hibbs (1965)]. The final result from [Srivastava *et al.* (1995)] is:

$$\begin{aligned} I[x, y] = & \frac{1}{2} \int_{t_i}^{t_f} dt [x(t)F_y^{ret}(t) + y(t)F_x^{adv}(t)] \\ & + \frac{i}{2\hbar} \int_{t_i}^{t_f} \int_{t_i}^{t_f} dt ds N(t-s)y(t)y(s), \end{aligned}$$

where the retarded force on  $y$ ,  $F_y^{ret}$ , and the advanced force on  $x$ ,  $F_x^{adv}$ , are given in terms of the retarded and advanced Green functions  $G_{ret}(t-s)$

and  $G_{adv}(t-s)$  by

$$F_y^{ret}(t) = \int_{t_i}^{t_f} ds G_{ret}(t-s)y(s), \quad F_x^{adv}(t) = \int_{t_i}^{t_f} ds G_{adv}(t-s)x(s),$$

respectively. In (7.49),  $N(t-s)$  is the *quantum noise* in the fluctuating random force given by  $N(t-s) = \frac{1}{2}\langle f(t)f(s) + f(s)f(t) \rangle$ .

The real and the imaginary part of the action are given by

$$\text{Re}(A[x, y]) = \int_{t_i}^{t_f} L dt, \quad (7.49)$$

$$L = m\dot{x}\dot{y} - \left[ V\left(x + \frac{1}{2}y\right) - V\left(x - \frac{1}{2}y\right) \right] + \frac{1}{2} [xF_y^{ret} + yF_x^{adv}], \quad (7.50)$$

$$\text{and} \quad \text{Im}(A[x, y]) = \frac{1}{2\hbar} \int_{t_i}^{t_f} \int_{t_i}^{t_f} N(t-s)y(t)y(s) dt ds, \quad (7.51)$$

respectively.

Equations (7.49–7.51), are *exact* results for linear passive damping due to the bath. They show that in the classical limit ' $\hbar \rightarrow 0$ ' nonzero  $y$  yields an 'unlikely process' in view of the large imaginary part of the action implicit in (7.51). Nonzero  $y$ , indeed, may lead to a negative real exponent in the evolution operator, which in the limit  $\hbar \rightarrow 0$  may produce a negligible contribution to the probability amplitude. On the contrary, at quantum level nonzero  $y$  accounts for quantum noise effects in the fluctuating random force in the system–environment coupling arising from the imaginary part of the action (see [Srivastava *et al.* (1995)]).

When in (7.50) we use

$$F_y^{ret} = \gamma\dot{y} \quad \text{and} \quad F_x^{adv} = -\gamma\dot{x} \quad \text{we get,}$$

$$L(\dot{x}, \dot{y}, x, y) = m\dot{x}\dot{y} - V\left(x + \frac{1}{2}y\right) + V\left(x - \frac{1}{2}y\right) + \frac{\gamma}{2}(x\dot{y} - y\dot{x}). \quad (7.52)$$

By using

$$V\left(x \pm \frac{1}{2}y\right) = \frac{1}{2}\kappa\left(x \pm \frac{1}{2}y\right)^2$$

in (7.52), the DHO equation (7.43) and its complementary equation for the  $y$  coordinate

$$m\ddot{y} - \gamma\dot{y} + \kappa y = 0. \quad (7.53)$$

are derived. The  $y$ -oscillator is the time-reversed image of the  $x$ -oscillator (7.43). From the manifolds of solutions to equations (7.43) and (7.53), we could choose those for which the  $y$  coordinate is constrained to be zero, they simplify to

$$m\ddot{x} + \gamma\dot{x} + \kappa x = 0, \quad y = 0.$$

Thus we get the classical damped oscillator equation from a Lagrangian theory at the expense of introducing an 'extra' coordinate  $y$ , later constrained to vanish. Note that the constraint  $y(t) = 0$  is *not* in violation of the equations of motion since it is a true solution to (7.43) and (7.53).

### 7.5.8 Open Liouville Neurodynamics and Self-Similarity

Recall (see section (4.3) above) that neurodynamics has its physical behavior both on the *macroscopic*, classical, *inter-neuronal level*, and on the *microscopic*, quantum, *intra-neuronal level*. On the *macroscopic* level, various models of neural networks (NNs, for short) have been proposed as goal-oriented models of the specific neural functions, like for instance, function-approximation, pattern-recognition, classification, or control (see, e.g., [Haykin (1994)]). In the physically-based, Hopfield-type models of NNs [Hopfield (1982); Hopfield (1984)] the information is stored as a content-addressable memory in which synaptic strengths are modified after the Hebbian rule (see [Hebb (1949)]). Its retrieval is made when the network with the symmetric couplings works as the point-attractor with the fixed points. Analysis of both *activation* and *learning dynamics* of Hopfield-Hebbian NNs using the techniques of statistical mechanics [Doman *et al.* (1991)], provides us with the most important information of storage capacity, role of noise and recall performance.

On the other hand, on the general *microscopic* intra-cellular level, energy transfer across the cells, without dissipation, had been first conjectured to occur in biological matter by [Frölich and Kremer (1983)]. The phenomenon conjectured by them was based on their 1D superconductivity model: in 1D electron systems with holes, the formation of *solitonic structures* due to electron-hole pairing results in the transfer of electric current without dissipation. In a similar manner, Frölich and Kremer conjectured

that energy in biological matter could be transferred without dissipation, if appropriate solitonic structures are formed inside the cells. This idea has lead theorists to construct various models for the energy transfer across the cell, based on the formation of *kink* classical solutions (see [Satarić *et al.* (1993); Satarić *et al.* (1998)]).

The interior of living cells is structurally and dynamically organized by *cytoskeletons*, i.e., networks of protein polymers. Of these structures, *microtubules* (MTs, for short) appear to be the most fundamental (see [Dustin (1984)]). Their dynamics has been studied by a number of authors in connection with the mechanism responsible for dissipation-free energy transfer. Hameroff and Penrose [Hameroff (1987)] have conjectured another fundamental role for the MTs, namely being responsible for *quantum computations* in the human neurons. [Penrose (1989); Penrose (1994); Penrose (1997)] further argued that the latter is associated with certain aspects of quantum theory that are believed to occur in the cytoskeleton MTs, in particular quantum superposition and subsequent collapse of the wave function of coherent MT networks. These ideas have been elaborated by [Mavromatos and Nanopoulos (1995a); Mavromatos and Nanopoulos (1995b)] and [Nanopoulos (1995)], based on the quantum-gravity EMN-language of [Ellis *et al.* (1992); Ellis *et al.* (1999)] where MTs have been physically modelled as non-critical (SUSY) bosonic strings. It has been suggested that the neural MTs are the microsites for the emergence of stable, macroscopic quantum coherent states, identifiable with the *preconscious states*; stringy-quantum space-time effects trigger an organized collapse of the coherent states down to a specific or *conscious state*. More recently, [Tabony *et al.* (1999)] have presented the evidence for biological self-organization and pattern formation during embryogenesis.

Now, we have two space-time biophysical scales of neurodynamics. Naturally the question arises: are these two scales somehow inter-related, is there a space-time self-similarity between them?

The purpose of this section is to prove the formal positive answer to the self-similarity question. We try to describe neurodynamics on both physical levels by the *unique form* of a single equation, namely *open Liouville equation*: NN-dynamics using its classical form, and MT-dynamics using its quantum form in the Heisenberg picture. If this formulation is consistent, that would prove the *existence* of the *formal neurobiological space-time self-similarity*.

### 7.5.8.1 Hamiltonian Framework

Suppose that on the macroscopic NN-level we have a conservative Hamiltonian system acting in a  $2ND$  symplectic phase-space  $T^*Q = \{q^i(t), p_i(t)\}$ ,  $i = 1 \dots N$  (which is the cotangent bundle of the NN-configuration manifold  $Q = \{q^i\}$ ), with a Hamiltonian function  $H = H(q^i, p_i, t) : T^*Q \times \mathbb{R} \rightarrow \mathbb{R}$ . The conservative dynamics is defined by classical Hamilton's canonical equations (3.5). Recall that within the conservative Hamiltonian framework, we can apply the formalism of classical Poisson brackets: for any two functions  $A = A(q^i, p_i, t)$  and  $B = B(q^i, p_i, t)$  their Poisson bracket is defined as

$$[A, B] = \left( \frac{\partial A}{\partial q^i} \frac{\partial B}{\partial p_i} - \frac{\partial A}{\partial p_i} \frac{\partial B}{\partial q^i} \right).$$

### 7.5.8.2 Conservative Classical System

Any function  $A(q^i, p_i, t)$  is called a *constant* (or *integral*) of motion of the conservative system (3.5) if

$$\dot{A} \equiv \partial_t A + [A, H] = 0, \quad \text{which implies} \quad \partial_t A = -[A, H]. \quad (7.54)$$

For example, if  $A = \rho(q^i, p_i, t)$  is a *density function* of ensemble phase-points (or, a probability density to see a state  $x(t) = (q^i(t), p_i(t))$  of *ensemble* at a moment  $t$ ), then equation

$$\partial_t \rho = -[\rho, H] = -iL\rho \quad (7.55)$$

represents the *Liouville theorem*, where  $L$  denotes the (Hermitian) *Liouville operator*

$$iL = [..., H] \equiv \left( \frac{\partial H}{\partial p_i} \frac{\partial}{\partial q^i} - \frac{\partial H}{\partial q^i} \frac{\partial}{\partial p_i} \right) = \text{div}(\rho \dot{\mathbf{x}}),$$

which shows that the conservative Liouville equation (7.55) is actually equivalent to the mechanical *continuity equation* (see Appendix)

$$\partial_t \rho + \text{div}(\rho \dot{\mathbf{x}}) = 0. \quad (7.56)$$

### 7.5.8.3 Conservative Quantum System

We perform the formal quantization of the conservative equation (7.55) in the Heisenberg picture: all variables become Hermitian operators (denoted by ' $\wedge$ '), the symplectic phase-space  $T^*Q = \{q^i, p_i\}$  becomes the Hilbert state-space  $\mathcal{H} = \mathcal{H}_{\hat{q}^i} \otimes \mathcal{H}_{\hat{p}_i}$  (where  $\mathcal{H}_{\hat{q}^i} = \mathcal{H}_{\hat{q}^1} \otimes \dots \otimes \mathcal{H}_{\hat{q}^N}$  and  $\mathcal{H}_{\hat{p}_i} =$

$\mathcal{H}_{\hat{p}_1} \otimes \dots \otimes \mathcal{H}_{\hat{p}_N}$ ), the classical Poisson bracket  $[ , ]$  becomes the quantum commutator  $\{ , \}$  multiplied by  $-i/\hbar$

$$[ , ] \longrightarrow -i\{ , \} \quad (\hbar = 1 \text{ in normal units}). \quad (7.57)$$

In this way the classical Liouville equation (7.55) becomes the *quantum Liouville equation*

$$\partial_t \hat{\rho} = i\{\hat{\rho}, \hat{H}\}, \quad (7.58)$$

where  $\hat{H} = \hat{H}(\hat{q}^i, \hat{p}_i, t)$  is the Hamiltonian evolution operator, while

$$\hat{\rho} = P(a)|\Psi_a\rangle\langle\Psi_a|, \quad \text{with} \quad \text{Tr}(\hat{\rho}) = 1,$$

denotes the von Neumann *density matrix operator*, where each quantum state  $|\Psi_a\rangle$  occurs with probability  $P(a)$ ;  $\hat{\rho} = \hat{\rho}(\hat{q}^i, \hat{p}_i, t)$  is closely related to another von Neumann concept: *entropy*  $S = -\text{Tr}(\hat{\rho}[\ln \hat{\rho}])$ .

#### 7.5.8.4 Open Classical System

We now move to the *open (nonconservative) system*: on the macroscopic NN-level the *opening operation* equals to the *adding* of a *covariant* vector of external (dissipative and/or motor) forces  $F_i = F_i(q^i, p_i, t)$  to (the r.h.s of) the covariant Hamilton's *force equation*, so that Hamilton's equations obtain the *open (dissipative and/or forced) form* (simplified from (2.26–2.27)):

$$\dot{q}^i = \frac{\partial H}{\partial p_i}, \quad \dot{p}_i = F_i - \frac{\partial H}{\partial q^i}. \quad (7.59)$$

In the framework of the open Hamiltonian system (7.59), dynamics of any function  $A(q^i, p_i, t)$  is defined by the *open evolution equation*:

$$\partial_t A = -[A, H] + \Phi,$$

where  $\Phi = \Phi(F_i)$  represents the general form of the scalar force term.

In particular, if  $A = \rho(q^i, p_i, t)$  represents the density function of ensemble phase-points, then its dynamics is given by the (dissipative/forced) *open Liouville equation*:

$$\partial_t \rho = -[\rho, H] + \Phi. \quad (7.60)$$

In particular, the scalar force term can be cast as a linear Poisson-bracket form

$$\Phi = F_i[A, q^i], \quad \text{with} \quad [A, q^i] = -\frac{\partial A}{\partial p_i}.$$

Now, in a similar way as the conservative Liouville equation (7.55) resembles the continuity equation (7.56) from continuum dynamics, also the open Liouville equation (7.60) resembles the probabilistic *Fokker-Planck equation* from statistical mechanics. If we have a  $ND$  stochastic process  $x(t) = (q^i(t), p_i(t))$  defined by the vector *Itô SDE*

$$dx(t) = f(x, t) dt + G(x, t) dW,$$

where  $f$  is a  $ND$  vector function,  $W$  is a  $KD$  Wiener process, and  $G$  is a  $N \times KD$  matrix valued function, then the corresponding probability density function  $\rho = \rho(x, t | \dot{x}, t')$  is defined by the  $ND$  Fokker-Planck equation (see, e.g., [Gardiner (1985)])

$$\partial_t \rho = -\text{div}[\rho f(x, t)] + \frac{1}{2} \frac{\partial^2}{\partial x^i \partial x_j} (Q_{ij} \rho), \quad (7.61)$$

where  $Q_{ij} = (G(x, t) G^T(x, t))_{ij}$ . It is obvious that the Fokker-Planck equation (7.61) represents the particular, stochastic form of our general open Liouville equation (7.60), in which the scalar force term is given by the (second-derivative) noise term

$$\Phi = \frac{1}{2} \frac{\partial^2}{\partial x^i \partial x_j} (Q_{ij} \rho).$$

Equation (7.60) will represent the open classical model of our macroscopic NN-dynamics.

#### 7.5.8.5 Continuous Neural Network Dynamics

The generalized NN-dynamics, including two special cases of *graded response neurons* (GRN) and *coupled neural oscillators* (CNO), can be presented in the form of a stochastic *Langevin rate equation*

$$\dot{\sigma}_i = f_i + \eta_i(t), \quad (7.62)$$

where  $\sigma_i = \sigma_i(t)$  are the continual neuronal variables of  $i$ th neurons (representing either membrane action potentials in case of GRN, or oscillator phases in case of CNO);  $J_{ij}$  are individual synaptic weights;  $f_i = f_i(\sigma_i, J_{ij})$  are the deterministic forces (given, in GRN-case, by

$f_i = \sum_j J_{ij} \tanh[\gamma \sigma_j] - \sigma_i + \theta_i$ , with  $\gamma > 0$  and with the  $\theta_i$  representing injected currents, and in CNO-case, by  $f_i = \sum_j J_{ij} \sin(\sigma_j - \sigma_i) + \omega_i$ , with  $\omega_i$  representing the natural frequencies of the individual oscillators); the noise variables are given as  $\eta_i(t) = \lim_{\Delta \rightarrow 0} \zeta_i(t) \sqrt{2T/\Delta}$  where  $\zeta_i(t)$  denote uncorrelated Gaussian distributed random forces and the parameter  $T$  controls the amount of noise in the system, ranging from  $T = 0$  (deterministic dynamics) to  $T = \infty$  (completely random dynamics).

More convenient description of the neural random process (7.62) is provided by the Fokker-Planck equation describing the time evolution of the probability density  $P(\sigma_i)$

$$\partial_t P(\sigma_i) = -\frac{\partial}{\partial \sigma_i} (f_i P(\sigma_i)) + T \frac{\partial^2}{\partial \sigma_i^2} P(\sigma_i). \quad (7.63)$$

Now, in the case of deterministic dynamics  $T = 0$ , equation (7.63) can be easily put into the form of the conservative Liouville equation (7.55), by making the substitutions:  $P(\sigma_i) \rightarrow \rho$ ,  $f_i = \dot{\sigma}_i$ , and  $[\rho, H] = \text{div}(\rho \dot{\sigma}_i) \equiv \sum_i \frac{\partial}{\partial \sigma_i} (\rho \dot{\sigma}_i)$ , where  $H = H(\sigma_i, J_{ij})$ . Further, we can formally identify the stochastic forces, i.e., the second-order noise-term  $T \sum_i \frac{\partial^2}{\partial \sigma_i^2} \rho$  with  $F^i[\rho, \sigma_i]$ , to get the open Liouville equation (7.60).

Therefore, on the NN-level deterministic dynamics corresponds to the conservative system (7.55). Inclusion of stochastic forces corresponds to the system opening (7.60), implying the *macroscopic arrow of time*.

#### 7.5.8.6 Open Quantum System

By formal quantization of equation (7.60) with the scalar force term defined by (2.27), in the same way as in the case of the conservative dynamics, we get the *quantum open Liouville equation*

$$\partial_t \hat{\rho} = i\{\hat{\rho}, \hat{H}\} + \hat{\Phi}, \quad \text{with } \hat{\Phi} = -i\hat{F}_i\{\hat{\rho}, \hat{q}^i\}, \quad (7.64)$$

where  $\hat{F}_i = \hat{F}_i(\hat{q}^i, \hat{p}_i, t)$  represents the covariant quantum operator of external friction forces in the Hilbert state space  $\mathcal{H} = \mathcal{H}_{\hat{q}^i} \otimes \mathcal{H}_{\hat{p}_i}$ .

Equation (7.64) will represent the open quantum-friction model of our microscopic MT-dynamics. Its system-independent properties are [Ellis *et al.* (1992); Ellis *et al.* (1999); Mavromatos and Nanopoulos (1995a); Mavromatos and Nanopoulos (1995b); Nanopoulos (1995)]:

(1) Conservation of probability  $P$

$$\partial_t P = \partial_t [\text{Tr}(\hat{\rho})] = 0.$$



(2) Conservation of energy  $E$ , on the average

$$\partial_t \langle \langle E \rangle \rangle \equiv \partial_t [\text{Tr}(\hat{\rho} E)] = 0.$$

(3) Monotonic increase in entropy

$$\partial_t S = \partial_t [-\text{Tr}(\hat{\rho} \ln \hat{\rho})] \geq 0,$$

and thus automatically and naturally implies a *microscopic arrow of time*, so essential in realistic biophysics of neural processes.

#### 7.5.8.7 Non-Critical Stringy MT-Dynamics

In EMN-language of non-critical (SUSY) bosonic strings, our MT-dynamics equation (7.64) reads

$$\partial_t \hat{\rho} = i\{\hat{\rho}, \hat{H}\} - i\hat{g}_{ij}\{\hat{\rho}, \hat{q}^i\}\hat{q}^j, \quad (7.65)$$

where the target-space density matrix  $\hat{\rho}(\hat{q}^i, \hat{p}_i)$  is viewed as a function of coordinates  $\hat{q}^i$  that parameterize the couplings of the generalized  $\sigma$ -models on the bosonic string world-sheet, and their conjugate momenta  $\hat{p}_i$ , while  $\hat{g}_{ij} = \hat{g}_{ij}(\hat{q}^i)$  is the quantum operator of the *positive definite metric* in the space of couplings. Therefore, the covariant quantum operator of external friction forces is in EMN-formulation given as  $\hat{F}_i(\hat{q}^i, \hat{q}^i) = \hat{g}_{ij} \hat{q}^j$ .

Equation (7.65) establishes the conditions under which a large-scale coherent state appearing in the MT-network, which can be considered responsible for loss-free energy transfer along the tubulins.

#### 7.5.8.8 Equivalence of Neurodynamic Forms

It is obvious that both the macroscopic NN-equation (7.60) and the microscopic MT-equation (7.64) have the same open Liouville form, which implies the arrow of time. These proves the existence of the formal neuro-biological space-time self-similarity.

In this way, we have described neurodynamics of both NN and MT ensembles, belonging to completely different biophysical space-time scales, by the unique form of open Liouville equation, which implies the arrow of time. The existence of the formal *neuro-biological self-similarity* has been proved.

## 7.6 Artificial Neural Nets in Biodynamics

In this section we introduce *artificial neural networks* (ANNs), as used in modern biodynamics. The ANNs are *nonlinear dynamical systems* that act as *functional approximators* [Kosko (1992)]. The ANN builds *discriminant functions* from its PEs. The ANN topology determines the *number* and *shape* of the discriminant functions. The shapes of the discriminant functions change with the topology, so ANNs are considered *semi-parametric classifiers*. One of the central advantages of ANNs is that they are sufficiently powerful to create arbitrary discriminant functions so ANNs can achieve optimal classification.

The placement of the discriminant functions is controlled by the network weights. Following the ideas of non-parametric training, the weights are adjusted directly from the training data without any assumptions about the data's statistical distribution. Hence one of the central issues in neural network design is to utilize systematic procedures, the so-called *training algorithm*, to modify the weights so that as accurate a classification as possible is achieved. The accuracy is quantified by an error criterion [Principe *et al.* (2000)].

The training is usually performed in the following way. First, data is presented, and an output is computed. An error is obtained by comparing the output  $\{y\}$  with a desired response  $\{d\}$  and it is used to modify the weights with a training algorithm. This procedure is repeated using all the data in the training set until a convergence criterion is met. Thus, in ANNs (and in adaptive systems in general) the designer does not have to specify the *parameters* of the system. They are automatically extracted from the input data and the desired response by means of the training algorithm. The two central issues in neural network design (semi-parametric classifiers) are the selection of the shape and number of the discriminant functions and their placement in pattern space such that the classification error is minimized [Principe *et al.* (2000)].

### 7.6.1 Biological Versus Artificial Neural Nets

In biological neural networks, signals are transmitted between neurons by electrical pulses (action potentials or spike trains) travelling along the axon. These pulses impinge on the afferent neuron at terminals called synapses. These are found principally on a set of branching processes emerging from the cell body (soma) known as dendrites. Each pulse occurring at a synapse

initiates the release of a small amount of chemical substance or neurotransmitter which travels across the synaptic cleft and which is then received at postsynaptic receptor sites on the dendritic side of the synapse. The neurotransmitter becomes bound to molecular sites here which, in turn, initiates a change in the dendritic membrane potential. This postsynaptic potential (PSP) change may serve to increase (hyperpolarize) or decrease (depolarize) the polarization of the postsynaptic membrane. In the former case, the PSP tends to inhibit generation of pulses in the afferent neuron, while in the latter, it tends to excite the generation of pulses. The size and type of PSP produced will depend on factors such as the geometry of the synapse and the type of neurotransmitter. Each PSP will travel along its dendrite and spread over the soma, eventually reaching the base of the axon (axonhillock). The afferent neuron sums or integrates the effects of thousands of such PSPs over its dendritic tree and over time. If the integrated potential at the axonhillock exceeds a threshold, the cell fires and generates an action potential or spike which starts to travel along its axon. This then initiates the whole sequence of events again in neurons contained in the efferent pathway.

ANNs are very loosely based on these ideas. In the most general terms, a ANN consists of large numbers of simple processors linked by weighted connections. By analogy, the processing nodes may be called artificial neurons. Each node output depends only on information that is locally available at the node, either stored internally or arriving via the weighted connections. Each unit receives inputs from many other nodes and transmits its output to yet other nodes. By itself, a single processing element is not very powerful; it generates a scalar output, a single numerical value, which is a simple non-linear function of its inputs. The power of the system emerges from the combination of many units in an appropriate way [Freeman and Skapura (1992); Ivancevic *et al.* (2003)].

ANN is specialized to implement different functions by varying the connection topology and the values of the connecting weights. Complex functions can be implemented by connecting units together with appropriate weights. In fact, it has been shown that a sufficiently large network with an appropriate structure and properly chosen weights can approximate with arbitrary accuracy any function satisfying certain broad constraints. In ANNs, the design motivation is what distinguishes them from other mathematical techniques: an ANN is a processing device, either an algorithm, or actual hardware, whose design was motivated by the design and functioning of animal brains and components thereof.

There are many different types of ANNs, each of which has different strengths particular to their applications. The abilities of different networks can be related to their structure, dynamics and learning methods.

## 7.6.2 Common Discrete ANNs

### 7.6.2.1 Multilayer Perceptrons

The most common ANN model is the *feedforward neural network* with one input layer, one output layer, and one or more hidden layers, called *multilayer perceptron* (MLP, see Figure 7.46). This type of neural network is known as a *supervised network* because it requires a desired output in order to learn. The goal of this type of network is to *create a model*  $f : x \rightarrow y$  that correctly maps the input  $x$  to the output  $y$  using historical data so that the model can then be used to produce the output when the desired output is unknown [Kosko (1992)].

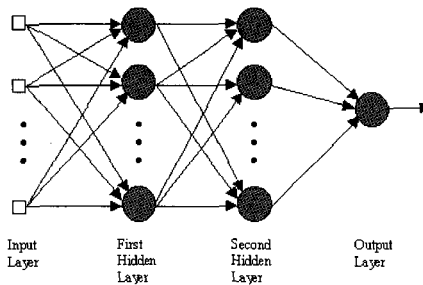


Fig. 7.46 Multilayer perceptron (MLP) with two hidden layers.

In MLP the inputs are fed into the input layer and get multiplied by interconnection weights as they are passed from the input layer to the first hidden layer. Within the first hidden layer, they get summed then processed by a nonlinear function (usually the hyperbolic tangent). As the processed data leaves the first hidden layer, again it gets multiplied by interconnection weights, then summed and processed by the second hidden layer. Finally the data is multiplied by interconnection weights then processed one last time within the output layer to produce the neural network output.

MLPs are typically trained with *static backpropagation*. These networks have found their way into countless applications requiring static pattern classification. Their main advantage is that they are easy to use, and that

they can approximate any input/output map. The key disadvantages are that they train slowly, and require lots of training data (typically three times more training samples than the number of network weights).

**McCulloch–Pitts Processing Element.** MLPs are typically composed of *McCulloch–Pitts neurons* (see [McCulloch and Pitts 1943]). This processing element (PE) is simply a sum-of-products followed by a threshold nonlinearity. Its input-output equation is

$$y = f(\text{net}) = f(w_i x^i + b), \quad (i = 1, \dots, D),$$

where  $D$  is the number of inputs,  $x^i$  are the inputs to the PE,  $w_i$  are the weights and  $b$  is a bias term (see e.g., [Minsky and Papert (1969)]). The activation function is a *hard threshold* defined by *signum* function,

$$f(\text{net}) = \begin{cases} 1, & \text{for } \text{net} \geq 0, \\ -1, & \text{for } \text{net} < 0. \end{cases}$$

Therefore, McCulloch–Pitts PE is composed of an adaptive linear element (*Adaline*, the weighted sum of inputs), followed by a signum nonlinearity [Principe *et al.* (2000)].

**Sigmoidal Nonlinearities.** Besides the hard threshold defined by signum function, other nonlinearities can be utilized in conjunction with the McCulloch–Pitts PE. Let us now smooth out the threshold, yielding a sigmoid shape for the nonlinearity. The most common nonlinearities are the *logistic* and the *hyperbolic tangent threshold activation functions*,

$$\begin{aligned} \text{hyperbolic} : \quad & f(\text{net}) = \tanh(\alpha \text{net}), \\ \text{logistic} : \quad & f(\text{net}) = \frac{1}{1 + \exp(-\alpha \text{net})}, \end{aligned}$$

where  $\alpha$  is a *slope parameter* and normally is set to 1. The major difference between the two sigmoidal nonlinearities is the range of their output values. The logistic function produces values in the interval  $[0, 1]$ , while the hyperbolic tangent produces values in the interval  $[-1, 1]$ . An alternate interpretation of this PE substitution is to think that the discriminant function has been generalized to

$$g(x) = f(w_i x^i + b), \quad (i = 1, \dots, D),$$

which is sometimes called a *ridge* function. The combination of the synapse and the tanh axon (or the sigmoid axon) is usually referred to as the modified McCulloch–Pitts PE, because they all respond to the full input space in basically the same functional form (a sum of products followed by a

global nonlinearity). The output of the logistic function varies from 0 to 1. Under some conditions, the logistic function allows a very powerful interpretation of the output of the PE as a posteriori probabilities for Gaussian-distributed input classes. The tanh is closely related to the logistic function by a linear transformation in the input and output spaces, so neural networks that use either of these can be made equivalent by changing weights and biases [Principe *et al.* (2000)].

**Gradient Descent on the Net's Performance Surface.** The search for the weights to meet a *desired response* or internal constraint is the essence of any *connectionist* computation. The central problem to be solved on the road to machine-based classifiers is how to automate the process of *minimizing the error* so that the machine can independently make these weight changes, without need for hidden agents or external observers. The optimality criterion to be minimized is usually the *mean square error* (MSE)

$$J = \frac{1}{2N} \sum_{i=1}^N \varepsilon_i^2,$$

where  $\varepsilon_i$  is the instantaneous error that is added to the output  $y_i$  (the linearly fitted value), and  $N$  is the number of observations. The function  $J(w)$  is called the *performance surface* (the total error surface plotted in the space of weights  $w$ ).

The search for the minimum of a function can be done efficiently using a broad class of methods based on *gradient information*. The gradient has two main advantages for the search:

- (1) it can be computed locally, and
- (2) it always points in the direction of maximum change.

The *gradient of the performance surface*,  $\nabla J = \nabla_w J$ , is a vector (with the dimension of  $w$ ) that always points toward the direction of maximum  $J$ -change and with a magnitude equal to the slope of the tangent of the performance surface. The minimum value of the error  $J_{min}$  depends on both the input signal  $x^i$  and the desired signal  $d_i$ ,

$$J_{min} = \frac{1}{2N} \left[ \sum_i d_i^2 - \frac{(d_i x^i)}{\sum_i x^i} \right], \quad (i = 1, \dots, D).$$

The location in coefficient space where the minimum  $w^*$  occurs also depends on both  $x^i$  and  $d_i$ . The performance surface shape depends only on the input signal  $x^i$  [Principe *et al.* (2000)].

Now, if the goal is to reach the minimum, the search must be in the direction opposite to the gradient. The overall method of gradient searching can be stated in the following way: Start the search with an arbitrary initial weight  $w(0)$ , where the iteration number is denoted by the index in parentheses. Then compute the gradient of the performance surface at  $w(0)$ , and modify the initial weight proportionally to the negative of the gradient at  $w(0)$ . This changes the operating point to  $w(1)$ . Then compute the gradient at the new position  $w(1)$ , and apply the same procedure again, that is,

$$w(n+1) = w(n) - \eta \nabla J(n),$$

where  $\eta$  is a small constant and  $\nabla J(n)$  denotes the gradient of the performance surface at the  $n$ th iteration. The constant  $\eta$  is used to maintain stability in the search by ensuring that the operating point does not move too far along the performance surface. This search procedure is called the *steepest descent method*.

In the late 1960s, [Widrow and Hoff (1960)] proposed an extremely elegant algorithm to estimate the gradient that revolutionized the application of gradient descent procedures. His idea is very simple: Use the instantaneous value as the estimator for the true quantity:

$$\nabla J(n) = \frac{\partial}{\partial w(n)} J \approx \frac{1}{2} \frac{\partial}{\partial w(n)} (\varepsilon^2(n)) = -\varepsilon(n) x(n),$$

i.e., instantaneous estimate of the gradient at iteration  $n$  is simply the product of the current input  $x(n)$  to the weight  $w(n)$  times the current error  $\varepsilon(n)$ . The amazing thing is that the gradient can be estimated with one multiplication per weight. This is the gradient estimate that led to the celebrated *least means square algorithm* (LMS):

$$w(n+1) = w(n) + \eta \varepsilon(n) x(n), \quad (7.66)$$

where the small constant  $\eta$  is called the *step size*, or the *learning rate*. The estimate will be noisy, however, since the algorithm uses the error from a single sample instead of summing the error for each point in the data set (e.g., the MSE is estimated by the error for the current sample).

Now, for fast convergence to the neighborhood of the minimum a large step size is desired. However, the solution with a large step size suffers from rattling. One attractive solution is to use a large learning rate in the beginning of training to move quickly toward the location of the optimal weights, but then the learning rate should be decreased to obtain good

accuracy on the final weight values. This is called *learning rate scheduling*. This simple idea can be implemented with a variable step size controlled by

$$\eta(n+1) = \eta(n) - \beta,$$

where  $\eta(0) = \eta_0$  is the initial step size, and  $\beta$  is a small constant [Principe *et al.* (2000)].

**Perceptron and Its Learning Algorithm.** *Rosenblatt perceptron* (see [Rosenblatt (1958); Minsky and Papert (1969)]) is a *pattern-recognition* machine that was invented in the 1950s for optical character recognition. The perceptron has an input layer fully connected to an output layer with multiple McCulloch–Pitts PEs,

$$y_i = f(\text{net}) = f(w_i x^i + b_i), \quad (i = 1, \dots, D),$$

where  $b_i$  is the bias for each PE. The number of outputs  $y_i$  is normally determined by the number of classes in the data. These PEs add the individual scaled contributions and respond to the entire input space.

F. Rosenblatt proposed the following procedure to directly minimize the error by changing the weights of the McCulloch–Pitts PE: Apply an input example to the network. If the output is correct do nothing. If the response is incorrect, tweak the weights and bias until the response becomes correct. Get the next example and repeat the procedure, until all the patterns are correctly classified. This procedure is called the *perceptron learning algorithm*, which can be put into the following form:

$$w(n+1) = w(n) + \eta(d(n) - y(n))x(n),$$

where  $\eta$  is the step size,  $y$  is the network output, and  $d$  is the desired response.

Clearly, the functional form is the same as in the LMS algorithm (7.66), that is, the old weights are incrementally modified proportionally to the product of the error and the input, but there is a significant difference. We cannot say that this corresponds to gradient descent since the system has a discontinuous nonlinearity. In the perceptron learning algorithm,  $y(n)$  is the output of the nonlinear system. The algorithm is directly minimizing the difference between the response of the McCulloch–Pitts PE and the desired response, instead of minimizing the difference between the Adaline output and the desired response [Principe *et al.* (2000)].



This subtle modification has tremendous impact on the performance of the system. For one thing, the McCulloch–Pitts PE learns only when its output is wrong. In fact, when  $y(n) = d(n)$ , the weights remain the same. The net effect is that the final values of the weights are no longer equal to the linear regression result, because the nonlinearity is brought into the weight update rule. Another way of phrasing this is to say that the weight update became much more selective, effectively gated by the system performance. Notice that the LMS update is also a function of the error to a certain degree. Larger errors have more effect on the weight update than small errors, but all patterns affect the final weights implementing a ‘smooth gate’. In the perceptron the net effect is that the placement of the discriminant function is no longer controlled smoothly by all the input samples as in the Adaline, only by the ones that are important for placing the discriminant function in a way that explicitly minimizes the output error.

**The Delta Learning Rule.** One can show that the LMS rule is equivalent to the chain rule in the computation of the *sensitivity* of the cost function  $J$  with respect to the unknowns. Interpreting the LMS equation (7.66) with respect to the sensitivity concept, we see that the gradient measures the sensitivity. LMS is therefore updating the weights proportionally to how much they affect the performance, i.e., proportionally to their sensitivity.

The LMS concept can be extended to the McCulloch–Pitts PE, which is a nonlinear system. The main question here is how can we compute the sensitivity through a nonlinearity? [Principe *et al.* (2000)] The so-called  $\delta$ -rule represents a direct extension of the LMS rule to nonlinear systems with smooth nonlinearities. In case of the McCulloch–Pitts PE, *delta-rule* reads:

$$w_i(n+1) = w_i(n) + \eta \varepsilon_p(n) x_p^i(n) f'(\text{net}(n)),$$

where  $f'(\text{net})$  is the partial derivative of the static nonlinearity, such that the *chain rule* is applied to the network topology, i.e.,

$$f'(\text{net}) x^i = \frac{\partial y}{\partial w_i} = \frac{\partial y}{\partial \text{net}} \frac{\partial}{\partial w_i}. \quad (7.67)$$

As long as the PE nonlinearity is smooth we can compute how much a change in the weight  $\delta w_i$  affects the output  $y$ , or from the point of view of the sensitivity, how sensitive the output  $y$  is to a change in a particular weight  $\delta w_i$ . Note that we compute this output sensitivity by a product

of partial derivatives through intermediate points in the topology. For the nonlinear PE there is only one intermediate point, net, but we really do not care how many of these intermediate points there are. The chain rule can be applied as many times as necessary. In practice, we have an error at the output (the difference between the desired response and the actual output), and we want to adjust all the PE weights so that the error is minimized in a statistical sense. The obvious idea is to distribute the adjustments according to the sensitivity of the output to each weight.

To modify the weight, we actually *propagate back the output error* to intermediate points in the network topology and scale it along the way as prescribed by (7.67) according to the element transfer functions:

$$\begin{aligned}
 \text{forward path : } & x^i \mapsto w_i \mapsto \text{net} \mapsto y \\
 \text{backward path 1 : } & w_i \xleftarrow{\partial \text{net} / \partial w} \text{net} \xleftarrow{\partial y / \partial \text{net}} y \\
 \text{backward path 2 : } & w_i \xleftarrow{\partial y / \partial w} y .
 \end{aligned}$$

This methodology is very powerful, because we do not need to know explicitly the error at intermediate places, such as net. The chain rule automatically derives the error contribution for us. This observation is going to be crucial for adapting more complicated topologies and will result in the *backpropagation* algorithm, discovered in 1988, by [Werbos (1989)].

Now, several key aspects have changed in the performance surface (which describes how the cost changes with the weights) with the introduction of the nonlinearity. The nice, parabolic performance surface of the linear least squares problem is lost. The performance depends on the topology of the network through the output error, so when nonlinear processing elements are used to solve a given problem the ‘performance – weights’ relationship becomes nonlinear, and there is no guarantee of a single minimum. The performance surface may have several minima. The minimum that produces the smallest error in the search space is called the *global minimum*. The others are called *local* minima. Alternatively, we say that the performance surface is *nonconvex*. This affects the search scheme because gradient descent uses local information to search the performance surface. In the immediate neighborhood, local minima are indistinguishable from the global minimum, so the gradient search algorithm may be caught in these suboptimal performance points, ‘thinking’ it has reached the global minimum [Principe *et al.* (2000)].

$\delta$ -rule extended to perceptron reads:

$$w_{ij}(n+1) = w_{ij}(n) - \eta \frac{\partial J}{\partial w_{ij}} = w_{ij}(n) + \eta \delta_{ip} x_p^j,$$

which are local quantities available at the weight, that is, the activation  $x_p^j$  that reaches the weight  $w_{ij}$  from the input and the local error  $\delta_{ip}$  propagated from the cost function  $J$ . This algorithm is local to the weight. Only the local error  $\delta_i$  and the local activation  $x^j$  are needed to update a particular weight. This means that it is immaterial how many PEs the net has and how complex their interconnection is. The training algorithm can concentrate on each PE individually and work only with the local error and local activation [Principe *et al.* (2000)].

**Backpropagation.** The multilayer perceptron constructs input-output mappings that are a nested composition of nonlinearities, that is, they are of the form

$$y = f \left( \sum f \left( \sum (\cdot) \right) \right),$$

where the number of function compositions is given by the number of network layers. The resulting map is very flexible and powerful, but it is also hard to analyze [Principe *et al.* (2000)].

MLPs are usually trained by generalized  $\delta$ -rule, the so-called *backpropagation* (BP). The weight update using backpropagation is

$$w_{ij}(n+1) = w_{ij}(n) + \eta f'(\text{net}_i(n)) \left( \varepsilon^k(n) f'(\text{net}_k(n)) w_{ki}(n) \right) y_j(n). \quad (7.68)$$

The summation in (7.68) is a sum of local errors  $\delta_k$  at each network output PE, scaled by the weights connecting the output PEs to the  $i$ th PE. Thus the term in parenthesis in (7.68) effectively computes the total error reaching the  $i$ th PE from the output layer (which can be thought of as the  $i$ th PE's contribution to the output error). When we pass it through the  $i$ th PE nonlinearity, we have its local error, which can be written as

$$\delta_i(n) = f'(\text{net}_i(n)) \delta^k w_{ki}(n).$$

Thus there is a unifying link in all the gradient-descent algorithms. All the weights in gradient descent learning are updated by multiplying the local error  $\delta_i(n)$  by the local activation  $x^j(n)$  according to Widrow's estimation of the instantaneous gradient first shown in the LMS rule:

$$\Delta w_{ij}(n) = \eta \delta_i(n) y_j(n).$$

What differs is the calculation of the local error, depending on whether the PE is linear or nonlinear and if the weight is attached to an output PE or a hidden-layer PE [Principe *et al.* (2000)].

**Momentum Learning.** Momentum learning is an improvement to the straight gradient-descent search in the sense that a memory term (the past increment to the weight) is used to speed up and stabilize convergence. In *momentum learning* the equation to update the weights becomes

$$w_{ij}(n+1) = w_{ij}(n) + \eta \delta_i(n) x_j(n) + \alpha (w_{ij}(n) - w_{ij}(n-1)),$$

where  $\alpha$  is the momentum constant, usually set between 0.5 and 0.9. This is called momentum learning due to the form of the last term, which resembles the momentum in mechanics. Note that the weights are changed proportionally to how much they were updated in the last iteration. Thus if the search is going down the hill and finds a flat region, the weights are still changed, not because of the gradient (which is practically zero in a flat spot), but because of the rate of change in the weights. Likewise, in a narrow valley, where the gradient tends to bounce back and forth between hillsides, the momentum stabilizes the search because it tends to make the weights follow a smoother path. Imagine a ball (weight vector position) rolling down a hill (performance surface). If the ball reaches a small flat part of the hill, it will continue past this local minimum because of its momentum. A ball without momentum, however, will get stuck in this valley. Momentum learning is a robust method to speed up learning, and is usually recommended as the default search rule for networks with nonlinearities.

**Advanced Search Methods.** The popularity of *gradient descent method* is based more on its simplicity (it can be computed locally with two multiplications and one addition per weight) than on its search power. There are many other search procedures more powerful than backpropagation. For example, *Newtonian method* is a second-order method because it uses the information on the curvature to adapt the weights. However Newtonian method is computationally much more costly to implement and requires information not available at the PE, so it has been used little in neurocomputing. Although more powerful, Newtonian method is still a local search method and so may be caught in local minima or diverge due to the difficult neural network performance landscapes. Other techniques such

as *simulated annealing*<sup>5</sup> and *genetic algorithms* (GA)<sup>6</sup> are global search procedures, that is, they can avoid local minima. The issue is that they are more costly to implement in a distributed system like a neural network, either because they are inherently slow or because they require nonlocal quantities [Principe *et al.* (2000)].

The problem of search with local information can be formulated as an approximation to the functional form of the *matrix cost function*  $J(\mathbf{w})$  at the operating point  $\mathbf{w}_0$ . This immediately points to the Taylor series expansion of  $J$  around  $\mathbf{w}_0$ ,

$$J(\mathbf{w} - \mathbf{w}_0) = J_0 + (\mathbf{w} - \mathbf{w}_0) \nabla J_0 + \frac{1}{2} (\mathbf{w} - \mathbf{w}_0) \mathbf{H}_0 (\mathbf{w} - \mathbf{w}_0)^T + \dots,$$

where  $\nabla J$  is our familiar gradient, and  $\mathbf{H}$  is the Hessian matrix, that is, the matrix of second derivatives with entries

$$H_{ij}(\mathbf{w}_0) = \left. \frac{\partial^2 J(w)}{\partial w_i \partial w_j} \right|_{w=\mathbf{w}_0},$$

evaluated at the operating point. We can immediately see that the Hessian cannot be computed with the information available at a given PE, since it uses information from two different weights. If we differentiate  $J$  with respect to the weights, we get

$$\nabla J(\mathbf{w}) = \nabla J_0 + \mathbf{H}_0 (\mathbf{w} - \mathbf{w}_0) + \dots \quad (7.69)$$

so we can see that to compute the full gradient at  $\mathbf{w}$  we need all the higher terms of the derivatives of  $J$ . This is impossible. Since the performance surface tends to be bowl shaped (quadratic) near the minimum, we are normally interested only in the first and second terms of the expansion [Principe *et al.* (2000)].

If the expansion of (7.69) is restricted to the first term, we get the gradient-search methods (hence they are called *first-order-search methods*), where the gradient is estimated with its value at  $\mathbf{w}_0$ . If we expand

---

<sup>5</sup>Simulated annealing is a global search criterion by which the space is searched with a random rule. In the beginning the variance of the random jumps is very large. Every so often the variance is decreased, and a more local search is undertaken. It has been shown that if the decrease of the variance is set appropriately, the global optimum can be found with probability one. The method is called simulated annealing because it is similar to the annealing process of creating crystals from a hot liquid.

<sup>6</sup>Genetic algorithms are global search procedures proposed by J. Holland that search the performance surface, concentrating on the areas that provide better solutions. They use 'generations' of search points computed from the previous search points using the operators of crossover and mutation (hence the name).

to use the second-order term, we get *Newton method* (hence the name second-order method). If we equate the truncated relation (7.69) to 0 we immediately get

$$w = w_0 - \mathbf{H}_0^{-1} \nabla J_0,$$

which is the equation for the Newton method, which has the nice property of quadratic termination (it is guaranteed to find the exact minimum in a finite number of steps for quadratic performance surfaces). For most quadratic performance surfaces it can converge in one iteration.

The real difficulty is the memory and the computational cost (and precision) to estimate the Hessian. Neural networks can have thousands of weights, which means that the Hessian will have millions of entries. This is why methods of approximating the Hessian have been extensively researched. There are two basic classes of approximations [Principe *et al.* (2000)]:

- (1) Line search methods, and
- (2) Pseudo-Newton methods.

The information in the first type is restricted to the gradient, together with line searches along certain directions, while the second seeks approximations to the Hessian matrix. Among the line search methods probably the most effective is the *conjugate gradient method*. For quadratic performance surfaces the conjugate gradient algorithm preserves quadratic termination and can reach the minimum in  $D$  steps, where  $D$  is the dimension of the weight space. Among the Pseudo-Newton methods probably the most effective is the *Levenberg-Marquardt algorithm* (LM), which uses the Gauss-Newton method to approximate the Hessian. LM is the most interesting for neural networks, since it is formulated as a sum of quadratic terms just like the cost functions in neural networks.

The *extended Kalman filter* (EKF, see (6.6) above) forms the basis of a second-order neural network training method that is a practical and effective alternative to the batch-oriented, second-order methods mentioned above. The essence of the recursive EKF procedure is that, during training, in addition to evolving the weights of a network architecture in a sequential (as opposed to batch) fashion, an approximate error covariance matrix that encodes second-order information about the training problem is also maintained and evolved.

**Homotopy Methods.** The most popular method for solving nonlin-

ear equations in general is the *Newton–Raphson method*. Unfortunately, this method sometimes fails, especially in cases when nonlinear equations possess multiple solutions (zeros). An emerging family of methods that can be used in such cases are homotopy (continuation) methods (see chapter 2). These methods are robust and have good convergence properties.

*Homotopy methods* or *continuation methods* have increasingly been used for solving variety of nonlinear problems in fluid dynamics, structural mechanics, systems identifications, and integrated circuits (see [Watson (1990)]). These methods, popular in mathematical programming, are globally convergent provided that certain coercivity and continuity conditions are satisfied by the equations that need to be solved [Watson (1990)]. Moreover, they often yield all the solutions to the nonlinear system of equations.

The idea behind a homotopy or continuation method is to embed a parameter  $\lambda$  in the nonlinear equations to be solved. This is why they are sometimes referred to as *embedding methods*. Initially, parameter  $\lambda$  is set to zero, in which case the problem is reduced to an easy problem with a known or easily-found solution. The set of equations is then gradually deformed into the originally posed difficult problem by varying the parameter  $\lambda$ . The original problem is obtained for  $\lambda = 1$ . Homotopies are a class of continuation methods, in which parameter  $\lambda$  is a function of a path arc length and may actually increase or decrease as the path is traversed. Provided that certain coercivity conditions imposed on the nonlinear function to be solved are satisfied, the homotopy path does not branch (bifurcate) and passes through all the solutions of the nonlinear equations to be solved.

The zero curve of the homotopy map can be tracked by various techniques: an *ODE-algorithm*, a *normal flow algorithm*, and an *augmented Jacobian matrix algorithm*, among others [Watson (1990)].

As a typical example, homotopy techniques can be applied to find the zeros of the gradient function  $F : \mathbb{R}^N \rightarrow \mathbb{R}^N$ , such that

$$F(\theta) = \frac{\partial E(\theta)}{\partial \theta_k}, \quad 1 \leq k \leq N,$$

where  $E = (\theta)$  is the certain error function dependent on  $N$  parameters  $\theta_k$ . In other words, we need to solve a system of nonlinear equations

$$F(\theta) = 0. \tag{7.70}$$

In order to solve equation (7.70), we can create a linear homotopy function

$$H(\theta, \lambda) = (1 - \lambda)(\theta - a) + \lambda F(\theta),$$

where  $a$  is an arbitrary starting point. Function  $H(\theta, \lambda)$  has properties that equation  $H(\theta, 0) = 0$  is easy to solve, and that  $H(\theta, 1) \equiv F(\theta)$ .

### 7.6.2.2 Summary of Supervised Learning Methods

**Gradient Descent Method.** Given the  $(D + 1)D$  weights vector  $\mathbf{w}(n) = [w_0(n), \dots, w_D(n)]^T$  (with  $w_0 = \text{bias}$ ), and the correspondent MSE-gradient (including partials of MSE w.r.t. weights)

$$\nabla \mathbf{e} = \left[ \frac{\partial e}{\partial w_0}, \dots, \frac{\partial e}{\partial w_D} \right]^T,$$

and the learning rate (step size)  $\eta$ , we have the vector learning equation

$$\mathbf{w}(n + 1) = \mathbf{w}(n) - \eta \nabla \mathbf{e}(n),$$

which in index form reads

$$w_i(n + 1) = w_i(n) - \eta \nabla e_i(n).$$

**LMS Algorithm:**

$$\mathbf{w}(n + 1) = \mathbf{w}(n) + \eta \varepsilon(n) \mathbf{x}(n),$$

where  $\mathbf{x}$  is an input (measurement) vector, and  $\varepsilon$  is a zero-mean Gaussian noise vector uncorrelated with input,

$$\text{or,} \quad w_i(n + 1) = w_i(n) + \eta \varepsilon(n) x^i(n).$$

**Newton's Method:**

$$\mathbf{w}(n + 1) = \mathbf{w}(n) - \eta \mathbf{R}^{-1} \mathbf{e}(n),$$

where  $\mathbf{R}$  is input (auto)correlation matrix,

$$\text{or,} \quad \mathbf{w}(n + 1) = \mathbf{w}(n) + \eta \mathbf{R}^{-1} \varepsilon(n) \mathbf{x}(n),$$

**Conjugate Gradient Method:**

$$\begin{aligned} \mathbf{w}(n + 1) &= \mathbf{w}(n) + \eta \mathbf{p}(n), \\ \mathbf{p}(n) &= -\nabla \mathbf{e}(n) + \beta(n) \mathbf{p}(n - 1), \\ \beta(n) &= \frac{\nabla \mathbf{e}(n)^T \nabla \mathbf{e}(n)}{\nabla \mathbf{e}(n - 1)^T \nabla \mathbf{e}(n - 1)}. \end{aligned}$$

**Levenberg-Marquardt Algorithm.**



Putting

$$\nabla \mathbf{e} = \mathbf{J}^T \mathbf{e},$$

where  $\mathbf{J}$  is the Jacobian matrix, which contains first derivatives of the network errors with respect to the weights and biases, and  $\mathbf{e}$  is a vector of network errors, LM algorithm reads

$$\mathbf{w}(n+1) = \mathbf{w}(n) - [\mathbf{J}^T \mathbf{J} + \mu \mathbf{I}]^{-1} \mathbf{J}^T \mathbf{e}. \quad (7.71)$$

### 7.6.2.3 Other Standard ANNs

**Generalized Feedforward Nets.** The *generalized feedforward network* (GFN, see Figure 7.47) is a generalization of MLP, such that connections can jump over one or more layers, which in practice, often solves the problem much more efficiently than standard MLPs. A classic example of this is the two-spiral problem, for which standard MLP requires hundreds of times more training epochs than the generalized feedforward network containing the same number of processing elements. Both MLPs and GFNs are usually trained using a variety of backpropagation techniques and their enhancements like the nonlinear LM algorithm (7.71). During training in the spatial processing, the weights of the GFN converge iteratively to the analytical solution of the 2D Laplace equation.

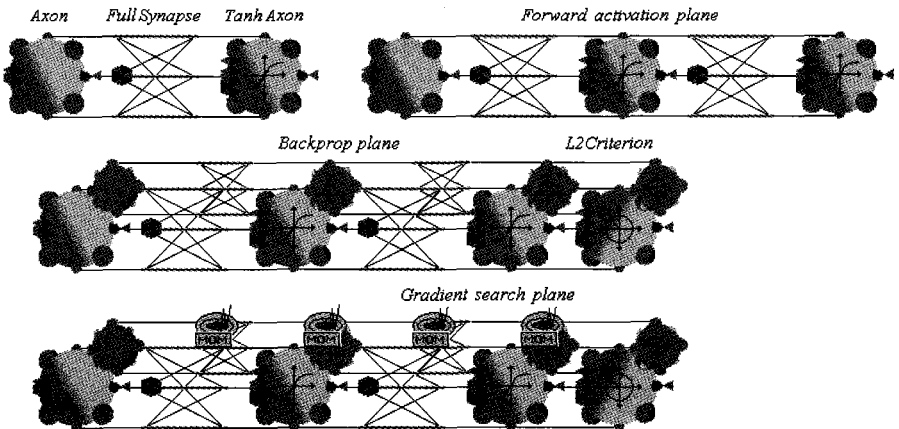


Fig. 7.47 Generalized feedforward network (GFN), arranged using *NeuroSolutions<sup>TM</sup>*.

**Modular Feedforward Nets.** The *modular feedforward networks* are a special class of MLP. These networks process their input using several parallel MLPs, and then recombine the results. This tends to create some structure within the topology, which will foster specialization of function in each submodule (see Figure 7.48). In contrast to the MLP, modular networks do not have full interconnectivity between their layers. Therefore, a smaller number of weights are required for the same size network (i.e., the same number of PEs). This tends to speed up training times and reduce the number of required training exemplars. There are many ways to segment a MLP into modules. It is unclear how to best design the modular topology based on the data. There are no guarantees that each module is specializing its training on a unique portion of the data.

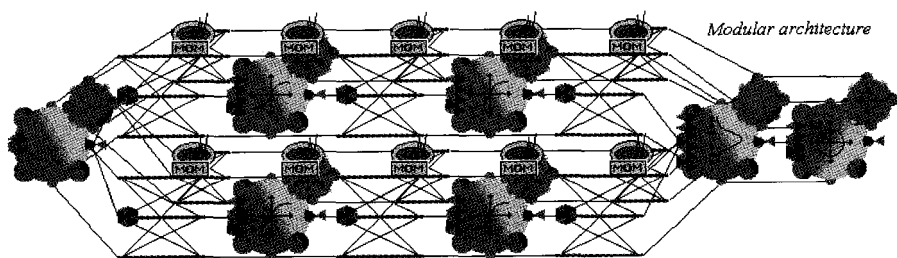


Fig. 7.48 Modular feedforward network, arranged using *NeuroSolutions<sup>TM</sup>*.

**Jordan and Elman Nets.** *Jordan and Elman networks* (see [Elman (1990)]) extend the multilayer perceptron with context units, which are processing elements (PEs) that remember past activity. Context units provide the network with the ability to extract temporal information from the data. In the Elman network, the activity of the first hidden PEs are copied to the context units, while the Jordan network copies the output of the network (see Figure 7.49). Networks which feed the input and the last hidden layer to the context units are also available.

**Kohonen Self-Organizing Map.** *Kohonen self-organizing map* (SOM, see Figure 7.50) is widely used for image pre-processing as well as a pre-processing unit for various hybrid architectures. SOM is a winner-take-all neural architecture that quantizes the input space, using a distance metric, into a discrete feature output space, where neighboring regions in the input space are neighbors in the discrete output space. SOM is usually applied to neighborhood clustering of random points along a circle using a variety

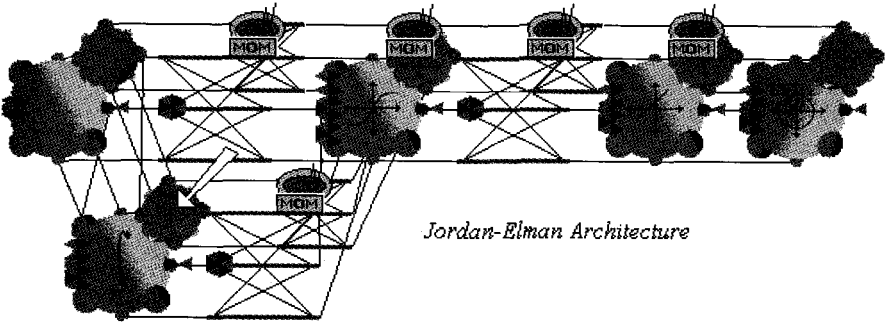


Fig. 7.49 Jordan and Elman network, arranged using *NeuroSolutions<sup>TM</sup>*.

of distance metrics: Euclidean,  $L_1$ ,  $L^2$ , and  $L^n$ , Machalanobis, etc. The basic SOM architecture consists of a layer of Kohonen synapses of three basic forms: line, diamond and box, followed by a layer of winner-take-all axons. It usually uses added Gaussian and uniform noise, with control of both the mean and variance. Also, SOM usually requires choosing the proper initial neighborhood width as well as annealing of the neighborhood width during training to ensure that the map globally represents the input space.

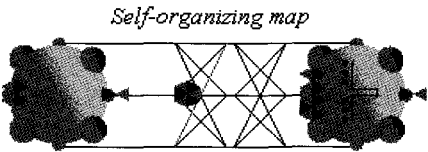


Fig. 7.50 Kohonen self-organizing map (SOM) network, arranged using *NeuroSolutions<sup>TM</sup>*.

The Kohonen SOM algorithm is defined as follows: Every stimulus  $\mathbf{v}$  of an Euclidian input space  $V$  is mapped to the neuron with the position  $\mathbf{s}$  in the neural layer  $R$  with the highest neural activity, the ‘center of excitation’ or ‘winner’, given by the condition

$$|\mathbf{w}_s - \mathbf{v}| = \min_{\mathbf{r} \in R} |\mathbf{w}_r - \mathbf{v}|,$$

where  $|\cdot|$  denotes the Euclidian distance in input space. In the Kohonen

model the learning rule for each synaptic weight vector  $\mathbf{w}_r$  is given by

$$\mathbf{w}_r^{\text{new}} = \mathbf{w}_r^{\text{old}} + \eta \cdot g_{rs} \cdot (\mathbf{v} - \mathbf{w}_r^{\text{old}}), \quad (7.72)$$

with  $g_{rs}$  as a gaussian function of Euclidian distance  $|\mathbf{r} - \mathbf{s}|$  in the neural layer. Topology preservation is enforced by the common update of all weight vectors whose neuron  $r$  is adjacent to the center of excitation  $s$ . The function  $g_{rs}$  describes the topology in the neural layer. The parameter  $\eta$  determines the speed of learning and can be adjusted during the learning process.

**Radial Basis Function Nets.** The *radial basis function network* (RBF, see Figure 7.51) provides a powerful alternative to MLP for function approximation or classification. It differs from MLP in that the overall input-output map is constructed from local contributions of a layer of Gaussian axons. It trains faster and requires fewer training samples than MLP, using the hybrid supervised/unsupervised method. The unsupervised part of an RBF network consists of a competitive synapse followed by a layer of Gaussian axons. The means of the Gaussian axons are found through competitive clustering and are, in fact, the weights of the Conscience synapse. Once the means converge the variances are calculated based on the separation of the means and are associated with the Gaussian layer. Having trained the unsupervised part, we now add the supervised part, which consists of a single-layer MLP with a soft-max output.

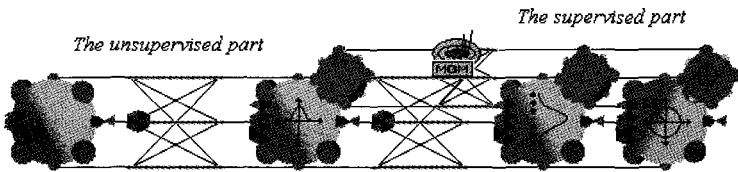


Fig. 7.51 Radial basis function network, arranged using *NeuroSolutions<sup>TM</sup>*.

**Principal Component Analysis Nets.** The *principal component analysis networks* (PCAs, see Figure 7.52) combine unsupervised and supervised learning in the same topology. Principal component analysis is an unsupervised linear procedure that finds a set of uncorrelated features, principal components, from the input. A MLP is supervised to perform the non-linear classification from these components. More sophisticated are the *independent component analysis networks* (ICAs) (see Appendix).

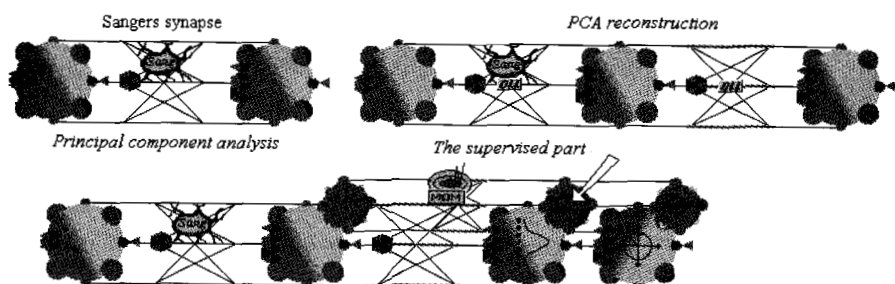


Fig. 7.52 Principal component analysis (PCA) network, arranged using *NeuroSolutions<sup>TM</sup>*.

**Co-active Neuro-Fuzzy Inference Systems.** The *co-active neuro-fuzzy inference system* (CANFIS, see Figure 7.53), which integrates adaptable fuzzy inputs with a modular neural network to rapidly and accurately approximate complex functions. Fuzzy-logic inference systems are also valuable as they combine the explanatory nature of rules (membership functions) with the power of 'black box' neural networks.

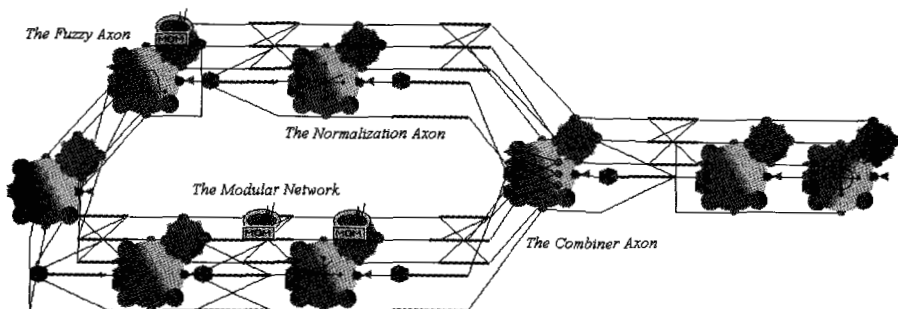


Fig. 7.53 Co-active neuro-fuzzy inference system (CANFIS) network, arranged using *NeuroSolutions<sup>TM</sup>*.

**Support Vector Machines.** The *support vector machine* (SVM, see Figure 7.54), implementing the statistical learning theory, is used as the most powerful classification and decision-making system. SVMs are a radically different type of classifier that has attracted a great deal of attention lately due to the novelty of the concepts that they bring to pattern recognition, their strong mathematical foundation, and their excellent results in practical problems. SVM represents the coupling of the following two concepts:

the idea that transforming the data into a high-dimensional space makes linear discriminant functions practical, and the idea of large margin classifiers to train the MLP or RBF. It is another type of a kernel classifier: it places Gaussian kernels over the data and linearly weights their outputs to create the system output. To implement the SVM-methodology, we can use the Adatron-kernel algorithm, a sophisticated nonlinear generalization of the RBF networks, which maps inputs to a high-dimensional feature space, and then optimally separates data into their respective classes by isolating those inputs, which fall close to the data boundaries. Therefore, the Adatron-kernel is especially effective in separating sets of data, which share complex boundaries, as well as for the training for nonlinearly separable patterns. The support vectors allow the network to rapidly converge on the data boundaries and consequently classify the inputs.

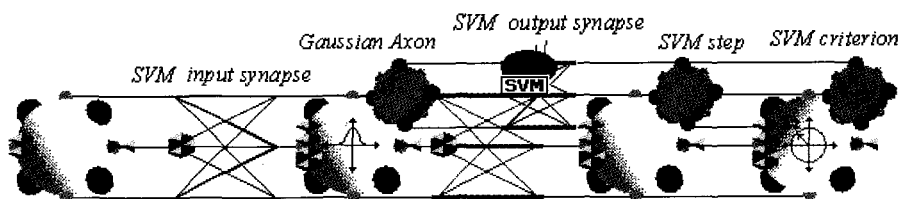


Fig. 7.54 Adatron-kernel based support vector machine (SVM) network, arranged using *NeuroSolutions<sup>TM</sup>*.

The main advantage of SVMs over MLPs is that the learning task is a *convex optimization problem* which can be reliably solved even when the example data require the fitting of a very complicated function [Vapnik (1995)]. A common argument in computational learning theory suggests that it is dangerous to utilize the full flexibility of the SVM to learn the training data perfectly when these contain an amount of noise. By fitting more and more noisy data, the machine may implement a rapidly oscillating function rather than the smooth mapping which characterizes most practical learning tasks. Its prediction ability could be no better than random guessing in that case. Hence, modifications of SVM training [Cristianini and Shawe-Taylor (2000)] that allow for training errors were suggested to be necessary for realistic noisy scenarios. This has the drawback of introducing extra model parameters and spoils much of the original elegance of SVMs.

Mathematics of SVMs is based on real *Hilbert space* methods (see Ap-

pendix).

**Genetic ANN–Optimization.** Genetic optimization, added to ensure and speed–up the convergence of all other ANN–components, is a powerful tool for enhancing the efficiency and effectiveness of a neural network. Genetic optimization can fine–tune network parameters so that network performance is greatly enhanced. Genetic control applies a *genetic algorithm* (GA [Goldberg (1988)], a part of broader *evolutionary computation*, see MIT journal with the same name) to any network parameters that are specified. Also through the *genetic control*, GA parameters such as mutation probability, crossover type and probability, and selection type can be modified.

**Time–Lagged Recurrent Nets.** The *time–lagged recurrent networks* (TLRNs, see Figure 7.55) are MLPs extended with short term memory structures [Werbos (1990)]. Most real–world data contains information in its time structure, i.e., how the data changes with time. Yet, most neural networks are purely static classifiers. TLRNs are the state of the art in nonlinear time series prediction, system identification and temporal pattern classification. Time–lagged recurrent nets usually use memory Axons, consisting of IIR filters with local adaptable feedback that act as a variable memory depth. The time–delay neural network (TDNN) can be considered a special case of these networks, examples of which include the Gamma and Laguerre structures. The Laguerre axon uses locally recurrent all–pass IIR filters to store the recent past. They have a single adaptable parameter that controls the memory depth. Notice that in addition to providing memory for the input, we have also used a Laguerre axon after the hidden Tanh axon. This further increases the overall memory depth by providing memory for that layer’s recent activations.

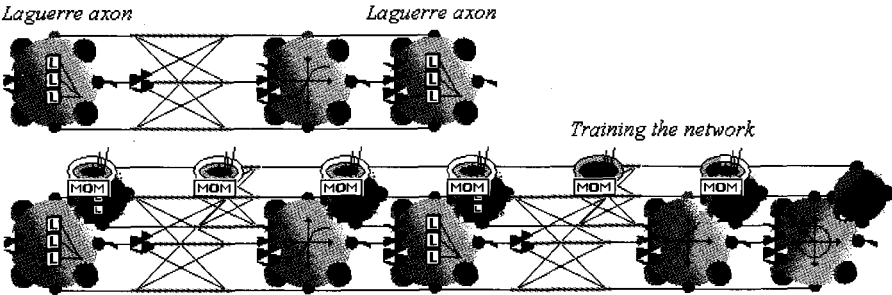


Fig. 7.55 Time–lagged recurrent network (TLRN), arranged using *NeuroSolutions<sup>TM</sup>*.

#### 7.6.2.4 Fully Recurrent ANNs

The *fully recurrent networks* feed back the hidden layer to itself. Partially recurrent networks start with a fully recurrent net and add a feedforward connection that bypasses the recurrency, effectively treating the recurrent part as a state memory. These recurrent networks can have an infinite memory depth and thus find relationships through time as well as through the instantaneous input space. Most real-world data contains information in its time structure. Recurrent networks are the state of the art in nonlinear time series prediction, system identification, and temporal pattern classification. In case of large number of neurons, here the firing states of the neurons or their membrane potentials are the microscopic stochastic dynamical variables, and one is mostly interested in quantities such as average state correlations and global information processing quality, which are indeed measured by macroscopic observables. In contrast to layered networks, one cannot simply write down the values of successive neuron states for models of recurrent ANNs; here they must be solved from (mostly stochastic) coupled dynamic equations. For nonsymmetric networks, where the asymptotic (stationary) statistics are not known, dynamical techniques from non-equilibrium statistical mechanics are the only tools available for analysis. The natural set of macroscopic quantities (or order parameters) to be calculated can be defined in practice as the smallest set which will obey closed deterministic equations in the limit of an infinitely large network.

Being high-dimensional nonlinear systems with extensive feedback, the dynamics of recurrent ANNs are generally dominated by a wealth of attractors (fixed-point attractors, limit-cycles, or even more exotic types), and the practical use of recurrent ANNs (in both biology and engineering) lies in the potential for creation and manipulation of these attractors through adaptation of the network parameters (synapses and thresholds) (see [Hopfield (1982); Hopfield (1984)]). Input fed into a recurrent ANN usually serves to induce a specific initial configuration (or firing pattern) of the neurons, which serves as a cue, and the output is given by the (static or dynamic) attractor which has been triggered by this cue. The most familiar types of recurrent ANN models, where the idea of creating and manipulating attractors has been worked out and applied explicitly, are the so-called attractor, associative memory ANNs, designed to store and retrieve information in the form of neuronal firing patterns and/or sequences of neuronal firing patterns. Each pattern to be stored is represented as a microscopic state vector. One then constructs synapses and thresholds such that the



dominant attractors of the network are precisely the pattern vectors (in the case of static recall), or where, alternatively, they are trajectories in which the patterns are successively generated microscopic system states. From an initial configuration (the cue, or input pattern to be recognized) the system is allowed to evolve in time autonomously, and the final state (or trajectory) reached can be interpreted as the pattern (or pattern sequence) recognized by network from the input. For such programmes to work one clearly needs recurrent ANNs with extensive ergodicity breaking: the state vector will during the course of the dynamics (at least on finite time-scales) have to be confined to a restricted region of state-space (an ergodic component), the location of which is to depend strongly on the initial conditions. Hence our interest will mainly be in systems with many attractors. This, in turn, has implications at a theoretical/mathematical level: solving models of recurrent ANNs with extensively many attractors requires advanced tools from disordered systems theory, such as replica theory (statics) and generating functional analysis (dynamics).

#### 7.6.2.5 *Dynamical Games and Recurrent ANNs*

**IPD Games.** Recall that *Prisoners' Dilemma* (PD) *game*<sup>7</sup> gets its name from the scenario where two people are arrested for some crime and are questioned separately. Each is given the opportunity to either cooperate with his/her accomplice and not give any information to the police, or defect against his/her partner by ratting to the police in exchange for some kind of immunity. The PD game is constructed to mimic this situation

---

<sup>7</sup>Recall that *game theory*, first formulated by John von Neumann and Oskar Morgenstern first formalised the subject in 1944 [von Neumann and Morgenstern (1944)] is a branch of applied mathematics that uses models to study interactions with formalized incentive structures ('games'). It has applications in a variety of fields, including economics, international relations, evolutionary biology, political science, and military strategy. Game theorists study the predicted and actual behavior of individuals in games, as well as optimal strategies. Seemingly different types of interactions can exhibit similar incentive structures, thus all exemplifying one particular game. The Prisoner's Dilemma game, as popularized by mathematician A. Tucker, furnishes an example of the application of game theory to real life; it has many implications for the nature of human co-operation. Another important concept in game theory is the *Nash equilibrium*, formulated by Nobel Laureate John Nash in his dissertation on Non-Cooperative Games in 1950. Nash showed that the various solutions for games that had been given earlier all yield Nash equilibria. For example, the Prisoner's dilemma has one Nash equilibrium: when both players defect. However, 'both defect' is inferior to 'both cooperate', in the sense that the total jail time served by the two prisoners is greater if both defect. The strategy 'both cooperate' is unstable, as a player could do better by defecting while their opponent still cooperates. Thus, 'both cooperate' is not an equilibrium.

by providing payoffs to the players based on how they both respond. A typical payoff is to give 3 points to each if they both cooperate (police have no case against criminals and can only get them for a very light crime). If one cooperates, and the other defects, the defector gets 5 points, while his partner receives none. If both players defect, they each only receive 1 point (police get them for a moderate crime, but not as severe as if only one person had taken the blame). The total payoff to both players is greatest for mutual cooperation (6 points), while a cooperate-defect play results in 5 points, and mutual defection only hands out 2 points. So, clearly, it is best for the collective system if all players cooperate, but here is the interesting paradox. Each player individually is better off by defecting in any given situation. If your partner cooperates, you can get 3 points by cooperating back, but you can get 5 by defecting. Similarly, if your partner defects, you get nothing if you cooperate, but you can still salvage 1 point by defecting back.

The extension of the PD game to permit repeated PD game play between players is known as the *Iterated Prisoner's Dilemma* (IPD) game. In 1979, R. Axelrod hosted a tournament at the University of Michigan to see what kinds of strategies would perform best over the long haul in the IPD game [Axelrod (1984)]. Various game theorists were solicited for IPD strategies in the form of computer algorithms, and the submitted strategies were then pitted against each other in repeated round-robin PD game play. The strategy that received the highest total payoff from this repeated PD game play was declared the winner of the tournament.

**Recurrent ANN Model for a Two-Player IPD Game.** A two-player IPD game was modelled using a *recurrent ANN* in [Taiji and Ikegami (1999)]. The authors created two *internal models* of game players. The first one was 'pure reductionist Bob', who made the opponent's model by a recurrent ANN. He thought that the opponent might behave with simple algorithms like finite automata, which could be expressed by the recurrent nets. The second one was 'clever Alice', who assumed that the opponent behaved like 'pure reductionist Bob'. She knew that the opponent made her model by recurrent nets and she decided the next action based on that model of herself. In other words, she builded the internal model of herself and treated that model as her image in the opponent.

Building the model of a player's behavior may involve many methods such as finite automata, Markov chain, etc. In [Taiji and Ikegami (1999)] the authors used *dynamical recognizers*, simple and powerful tools for studying dynamical behavior from the view points of cognitive studies. Dynamical

recognizers were first discussed by Pollack [Pollack (1991)], who showed that some automata could be learned very well by dynamical recognizers. When it could not learn automata, fractal-like patterns were generated in context spaces.

The so-called *cascaded recurrent ANN* consists of a function and a context net [Pollack (1991)]. It is quite similar to a two-layer linear perceptron, though the recurrent outputs are feedbacked not to the input nodes but to the weights of the function network. The recurrent outputs memorize the opponent's current status, and the context network converts the recurrent outputs to the weights of the function network which predicts the next action. The space constructed by the outputs from the function network (including both recurrent and network outputs) was called the *context space*. The output was taken from a node of the function network. In [Taiji and Ikegami (1999)], only one input and one output node were necessary since the IPD game had only two actions, cooperation and defection. The authors defined cooperation as 0 and defection as 1 in the network. The output was rounded off to 0 (cooperation) and 1 (defection). The network is described by the following equations,

$$z_i(n) = g(w_i y(n) + w_i^0), \quad w_i = u_{ij} z_j(n-1) + u_i^b, \quad w_i^0 = u_{ij}^0 z_j(n-1) + u_i^{0b},$$

where symbols have the following meanings:  $g(x) = (e^{-x} + 1)^{-1}$  is the sigmoid function,  $y(n)$  is the input,  $z_0(n)$  is the output,  $z_i(n)$ , ( $i = 1 \cdots N$ ) are the recurrent outputs,  $w_i$  is the weight of function network,  $w_i^0$  is the bias of function network,  $u_{ij}, u_{ij}^0$  is the weight of context network and  $u_i^b, u_i^{0b}$  is the bias of context network.

This recurrent ANN was trained by a form of the back-propagation method. In the game, the player knew only his or her own past actions and those of the opponent. In the case of 'pure reductionist Bob', the model of the opponent was built by the recurrent ANN. This means that the recurrent ANN takes the player's last action as an input and outputs the opponent's next action. Thus, the target for training is a series of the opponent's action when the inputs are the player's actions. However, since the number of training targets becomes too large as a game proceeds, the weights for learning are varied for each action so that far actions in the distant past are forgotten. Thus, the error  $E(n)$  after the  $n$ th game is  $E(n) = \sum_{k=1}^n \lambda^{n-k} (z_0(k) - d(k))^2$ , where  $d(k)$  is a target (i.e., the actual opponent's action in the  $k$ th game),  $z_0(k)$  is the predicted action by the recurrent ANN, and  $\lambda$  ( $= 0.9$  for most simulations) is a parameter which

controls the memory retention of the past actions.

To determine the player's next action, the authors of [Taiji and Ikegami (1999)] used the prediction of the opponent's future action based on the recurrent ANN. First, the algorithm for pure reductionist Bob was explained. Bob chose his forward actions up to  $M$  games. Then, he could predict the opponent's actions from his forward actions, and the expected score could be evaluated. The process was repeated for all possible strings of actions of length  $M$  and Bob chose the action with the highest score as the best action.

Clever Alice considered the opponent was a pure reductionist Bob, so she chose her forward  $M$  actions. She predicted the opponent's actions assuming that he behaved like pure reductionist Bob. Again the process was repeated for all strings of the length  $M$  and she chose the action string with the highest score as the best one. In other words, she predicted her image in the other person and tried to educate him to have a favorable image through her actions.

#### 7.6.2.6 Complex-Valued ANNs

It is expected that *complex-valued ANNs*, whose parameters (weights and threshold values) are all complex numbers, will have applications in all the fields dealing with complex numbers (e.g., telecommunications, quantum physics). A complex-valued, feedforward, multi-layered, back-propagation neural network model was proposed independently by [Nitta and Furuya (1991).; Nitta (1997); Nitta (2000); Nitta (2004)], [Georgiou *et al.* (1992)] and [Benvenuto and Piazza (1992)], and demonstrated its characteristics:

- (a) the properties greatly different from those of the real-valued back-propagation network, including 2D motion structure of weights and the orthogonality of the decision boundary of a complex-valued neuron;
- (b) the learning property superior to the real-valued back-propagation;
- (c) the inherent 2D motion learning ability (an ability to transform geometric figures); and
- (d) the ability to solve the XOR problem and detection of symmetry problem with a single complex-valued neuron.

Following [Nitta and Furuya (1991).; Nitta (1997); Nitta (2000); Nitta (2004)], we consider here the complex-valued neuron. Its input signals, weights, thresholds and output signals are all complex numbers. The net input  $U_n$  to a complex-valued neuron  $n$  is defined as

$$U_n = W_{mn}X_m + V_n,$$

where  $W_{mn}$  is the (complex-valued) weight connecting the complex-valued neurons  $m$  and  $n$ ,  $V_n$  is the (complex-valued) threshold value of the complex-valued neuron  $n$ , and  $X_m$  is the (complex-valued) input signal from the complex-valued neuron  $m$ . To obtain the (complex-valued) output signal, convert the net input  $U_n$  into its real and imaginary parts as follows:  $U_n = x + iy = z$ , where  $i = \sqrt{-1}$ . The (complex-valued) output signal is defined to be

$$\sigma(z) = \tanh(x) + i \tanh(y),$$

where  $\tanh(u) = (\exp(u) - \exp(-u)) / (\exp(u) + \exp(-u))$ ,  $u \in \mathbb{R}$ . Note that  $-1 < \operatorname{Re}[\sigma]$ ,  $\operatorname{Im}[\sigma] < 1$ . Note also that  $\sigma$  is not regular as a complex function, because the Cauchy-Riemann equations do not hold.

A complex-valued ANN consists of such complex-valued neurons described above. A typical network has 3 layers:  $m \rightarrow n \rightarrow 1$ , with  $w_{ij} \in \mathbb{C}$  – the weight between the input neuron  $i$  and the hidden neuron  $j$ ,  $w_{0j} \in \mathbb{C}$  – the threshold of the hidden neuron  $j$ ,  $c_j \in \mathbb{C}$  – the weight between the hidden neuron  $j$  and the output neuron ( $1 \leq i \leq m$ ;  $1 \leq j \leq n$ ), and  $c_0 \in \mathbb{C}$  – the threshold of the output neuron. Let  $y_j(z)$ ,  $h(z)$  denote the output values of the hidden neuron  $j$ , and the output neuron for the input pattern  $z = [z_1, \dots, z_m]^t \in \mathbb{C}^m$ , respectively. Let also  $\nu_j(z)$  and  $\mu(z)$  denote the net inputs to the hidden neuron  $j$  and the output neuron for the input pattern  $z \in \mathbb{C}^m$ , respectively. That is,

$$\begin{aligned} \nu_j(z) &= w_{ij}z_i + w_{0j}, & \mu(z) &= c_j y_j(z) + c_0, \\ y_j(z) &= \sigma(\nu_j(z)), & h(z) &= \sigma(\mu(z)). \end{aligned}$$

The set of all  $m \rightarrow n \rightarrow 1$  complex-valued ANNs described above is usually denoted by  $N_{m,n}$ . The Complex-BP learning rule [Nitta and Furuya (1991).; Nitta (1997); Nitta (2000); Nitta (2004)] has been obtained by using a steepest-descent method for such (multilayered) complex-valued ANNs.

### 7.6.3 Common Continuous ANNs

Virtually all computer-implemented ANNs (mainly listed above) are discrete dynamical systems, mainly using supervised training (except Kohonen SOM) in one of gradient-descent searching forms. They are good as problem-solving tools, but they fail as models of animal nervous system. The other category of ANNs are continuous neural systems that can be

considered as models of animal nervous system. However, *as models of the human brain, all current ANNs are simply trivial.*

### 7.6.3.1 Neurons as Functions

According to B. Kosko, neurons behave as functions [Kosko (1992)]; they transduce an unbounded input *activation*  $x(t)$  into output *signal*  $S(x(t))$ . Usually a sigmoidal (S-shaped, bounded, monotone-nondecreasing:  $S' \geq 0$ ) function describes the transduction, as well as the input-output behavior of many operational amplifiers. For example, the *logistic signal* (or, the *maximum-entropy*) function

$$S(x) = \frac{1}{1 + e^{-cx}}$$

is sigmoidal and strictly increases for positive scaling constant  $c > 0$ . Strict monotonicity implies that the *activation derivative* of  $S$  is positive:

$$S' = \frac{dS}{dx} = cS(1 - S) > 0.$$

An infinitely steep logistic signal function gives rise to a threshold signal function

$$S(x^{n+1}) = \begin{cases} 1, & \text{if } x^{n+1} > T, \\ S(x^n), & \text{if } x^{n+1} = T, \\ 0, & \text{if } x^{n+1} < T, \end{cases}$$

for an arbitrary real-valued threshold  $T$ . The index  $n$  indicates the discrete time step.

In practice signal values are usually binary or bipolar. *Binary signals*, like logistic, take values in the unit interval  $[0, 1]$ . *Bipolar signals* are signed; they take values in the bipolar interval  $[-1, 1]$ . Binary and bipolar signals transform into each other by simple scaling and translation. For example, the bipolar logistic signal function takes the form

$$S(x) = \frac{2}{1 + e^{-cx}} - 1.$$

Neurons with bipolar threshold signal functions are called *McCulloch-Pits neurons*.

A naturally occurring bipolar signal function is the *hyperbolic-tangent* signal function

$$S(x) = \tanh(cx) = \frac{e^{cx} - e^{-cx}}{e^{cx} + e^{-cx}},$$

with activation derivative

$$S' = c(1 - S^2) > 0.$$

The *threshold linear* function is a binary signal function often used to approximate neuronal firing behavior:

$$S(x) = \begin{cases} 1, & \text{if } cx \geq 1, \\ 0, & \text{if } cx < 0, \\ cx, & \text{else,} \end{cases}$$

which we can rewrite as

$$S(x) = \min(1, \max(0, cx)).$$

Between its upper and lower bounds the threshold linear signal function is trivially monotone increasing, since  $S' = c > 0$ .

*Gaussian*, or bell-shaped, signal function of the form  $S(x) = e^{-cx^2}$ , for  $c > 0$ , represents an important exception to signal monotonicity. Its activation derivative  $S' = -2cxe^{-cx^2}$  has the sign opposite the sign of the activation  $x$ .

*Generalized Gaussian* signal functions define potential or radial basis functions  $S_i(x^i)$  given by

$$S_i(x) = \exp\left[-\frac{1}{2\sigma_i^2} \sum_{j=1}^n (x_j - \mu_j^i)^2\right],$$

for input activation vector  $x = (x^i) \in \mathbb{R}^n$ , variance  $\sigma_i^2$ , and mean vector  $\mu_i = (\mu_j^i)$ . Each radial basis function  $S_i$  defines a spherical *receptive field* in  $\mathbb{R}^n$ . The  $i$ th neuron emits unity, or near-unity, signals for sample activation vectors  $x$  that fall in its receptive field. The mean vector  $\mu$  centers the receptive field in  $\mathbb{R}^n$ . The variance  $\sigma_i^2$  localizes it. The radius of the Gaussian spherical receptive field shrinks as the variance  $\sigma_i^2$  decreases. The receptive field approaches  $\mathbb{R}^n$  as  $\sigma_i^2$  approaches  $\infty$ .

The *signal velocity*  $\dot{S} \equiv dS/dt$  is the *signal time derivative*, related to the activation derivative by

$$\dot{S} = S'\dot{x},$$

so it depends explicitly on *activation velocity*. This is used in unsupervised learning laws that adapt with *locally available information*.

The signal  $S(x)$  induced by the activation  $x$  represents the neuron's firing frequency of action potentials, or pulses, in a sampling interval. The

firing frequency equals the average number of pulses emitted in a sampling interval.

*Short-term memory* is modelled by *activation dynamics*, and *long-term memory* is modelled by *learning dynamics*. The overall neural network behaves as an *adaptive filter* (see [Haykin (1991)]).

In the simplest and most common case, neurons are not topologically ordered. They are related only by the synaptic connections between them. Kohonen calls this *lack of topological structure in a field of neurons* the *zeroth-order topology*. This suggests that ANN-models are *abstractions*, not *descriptions* of the brain neural networks, in which order does matter.

### 7.6.3.2 Basic Activation and Learning Dynamics

One of the oldest continuous training methods, based on Hebb's biological synaptic learning [Hebb (1949)], is *Oja-Hebb learning rule* [Oja (1982)], which calculates the weight update according to the ODE

$$\dot{\omega}_i(t) = O(t) [I_i(t) - O(t) \omega_i(t)],$$

where  $O(t)$  is the output of a simple, linear processing element;  $I_i(t)$  are the inputs; and  $\omega_i(t)$  are the synaptic weights.

Related to the Oja-Hebb rule is a special matrix of synaptic weights called *Karhunen-Loeve covariance matrix*  $\mathbf{W}$  (KL), with entries

$$W_{ij} = \frac{1}{N} \omega_i^\mu \omega_j^\mu, \quad (\text{summing over } \mu)$$

where  $N$  is the number of vectors, and  $\omega_i^\mu$  is the  $i$ th component of the  $\mu$ th vector. The KL matrix extracts the principal components, or directions of maximum information (correlation) from a dataset.

In general, continuous ANNs are *temporal dynamical systems*. They have two coupled dynamics: activation and learning. First, a general system of coupled ODEs for the output of the  $i$ th *processing element* (PE)  $x^i$ , called the *activation dynamics*, can be written as

$$\dot{x}^i = g_i(x^i, \text{net}_i), \quad (7.73)$$

with the *net input* to the  $i$ th PE  $x^i$  given by  $\text{net}_i = \omega_{ij} x^j$ .

For example,

$$\dot{x}^i = -x^i + f_i(\text{net}_i),$$



where  $f_i$  is called *output*, or *activation*, *function*. We apply some input values to the PE so that  $\text{net}_i > 0$ . If the inputs remain for a sufficiently long time, the output value will reach an equilibrium value, when  $\dot{x}^i = 0$ , given by  $x^i = f_i(\text{net}_i)$ . Once the unit has a nonzero output value, removal of the inputs will cause the output to return to zero. If  $\text{net}_i = 0$ , then  $\dot{x}^i = -x^i$ , which means that  $x \rightarrow 0$ .

Second, a general system of coupled ODEs for the *update* of the synaptic weights  $\omega_{ij}$ , i.e., *learning dynamics*, can be written as a generalization of the Oja–Hebb rule, i.e..

$$\dot{\omega}_{ij} = G_i(\omega_{ij}, x^i, x^i),$$

where  $G_i$  represents the *learning law*; the learning process consists of finding weights that encode the knowledge that we want the system to learn. For most realistic systems, it is not easy to determine a closed-form solution for this system of equations, so the approximative solutions are usually enough.

### 7.6.3.3 Standard Models of Continuous Nets

**Hopfield Continuous Net.** One of the first physically-based ANNs was developed by J. Hopfield. He first made a discrete, Ising–spin based network in [Hopfield (1982)], and later generalized it to the continuous, graded-response network in [Hopfield (1984)], which we briefly describe here. Later we will give full description of Hopfield models. Let  $\text{net}_i = u_i$  – the net input to the the  $i$ th PE, biologically representing the summed action potentials at the axon hillock of a neuron. The PE *output function* is

$$v_i = g_i(\lambda u_i) = \frac{1}{2}(1 + \tanh(\lambda u_i)),$$

where  $\lambda$  is a constant called the *gain parameter*. The network is described as a transient RC circuit

$$C_i \dot{u}_i = T_{ij} v_j - \frac{u_i}{R_i} + I_i, \quad (7.74)$$

where  $I_i$ ,  $R_i$  and  $C_i$  are inputs (currents), resistances and capacitances, and  $T_{ij}$  are synaptic weights.

The Hamiltonian energy function corresponding to (7.74) is given as

$$H = -\frac{1}{2} T_{ij} v_i v_j + \frac{1}{\lambda} \frac{1}{R_i} \int_0^{v_i} g_i^{-1}(v) dv - I_i v_i, \quad (j \neq i) \quad (7.75)$$

which is a generalization of a discrete, *Ising-spin Hopfield network* with energy function

$$E = -\frac{1}{2}\omega_{ij}x^i x^j, \quad (j \neq i).$$

where  $g_i^{-1}(v) = u$  is the inverse of the function  $v = g(u)$ . To show that (7.75) is an appropriate *Lyapunov function* for the system, we shall take its time derivative assuming  $T_{ij}$  are symmetric:

$$\dot{H} = -\dot{v}_i(T_{ij}v_j - \frac{u_i}{R_i} + I_i) = -C_i\dot{v}_i\dot{u}_i = -C_i\dot{v}_i^2 \frac{\partial g_i^{-1}(v_i)}{\partial v_i}. \quad (7.76)$$

All the factors in the summation (7.76) are positive, so  $\dot{H}$  must decrease as the system evolves, until it eventually reaches the stable configuration, where  $\dot{H} = \dot{v}_i = 0$ . For further development on Hopfield nets, see section (7.7.2) below.

**Hecht-Nielsen Counterpropagation Net.** *Hecht-Nielsen counterpropagation network* (CPN) is a full-connectivity, graded-response generalization of the standard BP algorithm (see [Hecht-Nielsen (1987); Hecht-Nielsen (1990)]). The outputs of the PEs in CPN are governed by the set of ODEs

$$\dot{x}^i = -Ax_i + (B - x^i)I_i - x^i \sum_{j \neq i} I_j,$$

where  $0 < x^i(0) < B$ , and  $A, B > 0$ . Each PE receives a net excitation (on-center) of  $(B - x^i)I_i$  from its corresponding input value,  $I$ . The addition of inhibitory connections (off-surround),  $-x^i I_j$ , from other units is responsible for preventing the activity of the processing element from rising in proportion to the absolute pattern intensity,  $I_i$ . Once an input pattern is applied, the PEs quickly reach an equilibrium state ( $\dot{x}^i = 0$ ) with

$$x^i = \Theta_i \frac{BI_i}{A + I_i},$$

with the normalized *reflectance pattern*  $\Theta_i = I_i (\sum_i I_i)^{-1}$ , such that  $\sum_i \Theta_i = 1$ .

**Competitive Net.** Activation dynamics is governed by the ODEs

$$\dot{x}^i = -Ax_i + (B - x^i)[f(x^i) + \text{net}_i] - x^i \left[ \sum_{j \neq i} f(x_j) + \sum_{j \neq i} \text{net}_j \right],$$

where  $A, B > 0$  and  $f(x^i)$  is an output function.

### Kohonen's Continuous SOM and Adaptive Robotics Control.

*Kohonen continuous self organizing map* (SOM) is actually the original Kohonen model of the biological neural process (see [Kohonen (1988)]). SOM activation dynamics is governed by

$$\dot{x}^i = -r_i(x^i) + \sum_j z_{ij} x_j, \quad (7.77)$$

where the function  $r_i(x^i)$  is a general form of a loss term, while the final term models the lateral interactions between units (the sum extends over all units in the system). If  $z_{ij}$  takes the form of the Mexican-hat function, then the network will exhibit a bubble of activity around the unit with the largest value of net input.

SOM learning dynamics is governed by

$$\dot{\omega}_{ij} = \alpha(t)(I_i - \omega_{ij})U(x^i),$$

where  $\alpha(t)$  is the learning momentum, while the function  $U(x^i) = 0$  unless  $x^i > 0$  in which case  $U(x^i) = 1$ , ensuring that only those units with positive activity participate in the learning process.

Kohonen's continuous SOM (7.77–7.6.3.3) is widely used in adaptive robotics control (see subsection (6.5.2) above). Having an  $n$ -segment robot arm with  $n$  chained  $SO(2)$ -joints, for a particular initial position  $x$  and desired velocity  $\dot{x}_{desir}^j$  of the end-effector, the required torques  $T_i$  in the joints can be found as

$$T_i = a_{ij} \dot{x}_{desir}^j,$$

where the inertia matrix  $a_{ij} = a_{ij}(x)$  is learned using SOM.

**Adaptive Resonance Theory.** Principles derived from an analysis of experimental literatures in vision, speech, cortical development, and reinforcement learning, including attentional blocking and cognitive-emotional interactions, led to the introduction of S. Grossberg's *adaptive resonance theory* (ART) as a theory of human *cognitive information processing* (see [Carpenter and Grossberg (2003)]). The theory has evolved as a series of real-time neural network models that perform unsupervised and supervised learning, pattern recognition, and prediction. Models of unsupervised learning include ART1, for binary input patterns, and fuzzy-ART and ART2, for analog input patterns [Grossberg (1982); Carpenter and Grossberg (2003)]. ARTMAP models combine two unsupervised modules to carry out supervised learning. Many variations of the

basic supervised and unsupervised networks have since been adapted for technological applications and biological analyzes.

A central feature of all ART systems is a *pattern matching process* that compares an external input with the internal memory of an active code. ART matching leads either to a resonant state, which persists long enough to permit learning, or to a parallel memory search. If the search ends at an established code, the memory representation may either remain the same or incorporate new information from matched portions of the current input. If the search ends at a new code, the memory representation learns the current input. This match-based learning process is the foundation of ART *code stability*. Match-based learning allows memories to change only when input from the external world is close enough to internal expectations, or when something completely new occurs. This feature makes ART systems well suited to problems that require on-line learning of large and evolving databases (see [Carpenter and Grossberg (2003)]).

Many ART applications use fast learning, whereby adaptive weights converge to equilibrium in response to each input pattern. Fast learning enables a system to adapt quickly to inputs that occur rarely but that may require immediate accurate recall. Remembering details of an exciting movie is a typical example of learning on one trial. Fast learning creates memories that depend upon the order of input presentation. Many ART applications exploit this feature to improve accuracy by voting across several trained networks, with voters providing a measure of confidence in each prediction.

*Match-based learning* is complementary to *error-based learning*, which responds to a mismatch by changing memories so as to reduce the difference between a target output and an actual output, rather than by searching for a better match. Error-based learning is naturally suited to problems such as adaptive control and the learning of *sensory-motor maps*, which require ongoing adaptation to present statistics. Neural networks that employ error-based learning include backpropagation and other multilayer perceptrons (MLPs).

Activation dynamics of ART2 is governed by the ODEs [Grossberg (1982); Carpenter and Grossberg (2003)]

$$\epsilon \dot{x}_i = -Ax_i + (1 - Bx_i)I_i^+ - (C + Dx_i)I_i^-,$$

where  $\epsilon$  is the 'small parameter',  $I_i^+$  and  $I_i^-$  are excitatory and inhibitory inputs to the  $i$ th unit, respectively, and  $A, B, C, D > 0$  are parameters.

General *Cohen–Grossberg activation equations* have the form:

$$\dot{v}_j = -a_j(v_j)[b_j(v_j) - f_k(v_k)m_{jk}]_+, \quad (j = 1, \dots, N), \quad (7.78)$$

and the *Cohen–Grossberg theorem* ensures the global stability of the system (7.78). If

$$a_j = 1/C_j, b_j = v_j/R_j - I_j, f_j(v_j) = u_j,$$

and constant  $m_{ij} = m_{ji} = T_{ji}$ , the system (7.78) reduces to the Hopfield circuit model (7.74).

ART and distributed ART (dART) systems are part of a growing family of self-organizing network models that feature attentional feedback and stable code learning. Areas of technological application include industrial design and manufacturing, the control of mobile robots, face recognition, remote sensing land cover classification, target recognition, medical diagnosis, electrocardiogram analysis, signature verification, tool failure monitoring, chemical analysis, circuit design, protein/DNA analysis, 3D visual object recognition, musical analysis, and seismic, sonar, and radar recognition. ART principles have further helped explain parametric behavioral and brain data in the areas of visual perception, object recognition, auditory source identification, variable-rate speech and word recognition, and *adaptive sensory-motor control* (see [Carpenter and Grossberg (2003)]).

**Spatiotemporal Networks.** In *spatiotemporal networks*, activation dynamics is governed by the ODEs

$$\begin{aligned} \dot{x}^i &= A(-ax_i + b[I_i - \Gamma]^+), \\ \dot{\Gamma} &= \alpha(S - T) + \beta\dot{S}, \quad \text{with} \\ [u]^+ &= \begin{cases} u & \text{if } u > 0 \\ 0 & \text{if } u \leq 0 \end{cases}, \\ A(u) &= \begin{cases} u & \text{if } u > 0 \\ cu & \text{if } u \leq 0 \end{cases}. \end{aligned}$$

where  $a, b, \alpha, \beta > 0$  are parameters,  $T > 0$  is the *power-level target*,  $S = \sum_i x^i$ , and  $A(u)$  is called the *attack function*.

Learning dynamics is given by *differential Hebbian law*

$$\begin{aligned} \dot{\omega}_{ij} &= (-c\omega_{ij} + dx_i x_j)U(\dot{x}^i)U(-\dot{x}_j), \quad \text{with} \\ U(s) &= \begin{cases} 1 & \text{if } s > 0 \\ 0 & \text{if } s \leq 0 \end{cases} \quad \text{where } c, d > 0 \text{ are constants.} \end{aligned}$$

## 7.7 Distinguished ANN Models

In this section we continue the exposition on ANNs, giving several distinguished ANN models that are used in modern biodynamics.

### 7.7.1 Generalized Kohonen's SOM

As the brain is assumed to be optimized by evolution for information processing, one would postulate that maximal mutual information is a sound principle governing the setup of neural structures. For feedforward neural structures with lateral inhibition, an algorithm of maximal mutual information has been defined by Linsker [Linsker (1989)] using the gradient descent in mutual information. It requires computationally costly integrations, and has a highly nonlocal learning rule and therefore is less favorable as a model for biological maps and less feasible for technical applications [Claussen and Schuster (2002); Claussen (2002a)].

However, both biological network structures and technical applications are (due to realization constraints) not necessarily capable of reaching this optimum. This remains a question under discussion especially for the brain [Plumbley (1999)]. Even if one had quantitative experimental measurements of the magnification behavior, the question from what self-organizing dynamics the neural structure emerged remains. So overall it is desirable to formulate other learning rules that minimize mutual information in a simpler way.

The self-organizing feature map algorithm was proposed in 1982 by Kohonen [Kohonen (1982)] has become a successful model for topology preserving primary sensory processing in the cortex [Obermayer *et al.* (1992)], and an useful tool in technical applications [Ritter *et al.* (1992)].

The *self-organizing feature maps* map an input space, such as the retina or skin receptor fields, into a neural layer by feedforward structures with lateral inhibition. Biological maps show as defining properties topology preservation, error tolerance, plasticity (the ability of adaptation to changes in input space), and self-organized formation by a local process, since the global structure cannot be coded genetically [Claussen and Schuster (2002); Claussen (2002a)].

Compared to the *elastic net algorithm* of Durbin and Willshaw [Durbin and Willshaw (1987)] and the Linsker Algorithm [Linsker (1989)] which are performing gradient descent in a certain energy landscape, the Kohonen algorithm seems to have no energy function. Although the learning process

can be described in terms of a Fokker–Planck equation [Ritter and Schulten (1988)], the expectation value of the learning step is a nonconservative force [Obermayer *et al.* (1992)] driving the process so that it has no associated energy function. Furthermore, the relationships of the Kohonen model to both alternative models and general principles are still an open field [Kohonen (1991)].

#### 7.7.1.1 The Winner Relaxing Kohonen Algorithm

We now consider an energy function  $V$  that was at first proposed in [Ritter *et al.* (1992)] for the classical *Kohonen algorithm* (7.72). If we have a discrete input space, the potential function for the expectation value of the learning step is given by

$$V(\{\mathbf{w}\}) = \frac{1}{2} \sum_{\mathbf{r} \neq \mathbf{s}} g_{\mathbf{rs}}^{\gamma} \sum_{\mu | \mathbf{v}^{\mu} \in F_{\mathbf{s}}(\{\mathbf{w}\})} p(\mathbf{v}^{\mu}) \cdot |\mathbf{v}^{\mu} - \mathbf{w}_{\mathbf{r}}|^2,$$

where  $F_{\mathbf{s}}(\{\mathbf{w}\})$  is the cell of the *Voronoi tessellation* (or *Dirichlet tessellation*) of input space given by the weight vector configuration  $\{\mathbf{w}\}$ . The Voronoi tessellation is defined as the subset of vectors in input space that lead to firing of neuron  $\mathbf{s}$ . For discrete input space (where  $p(\mathbf{v})$  is a sum over delta peaks  $\delta(\mathbf{v} - \mathbf{v}^{\mu})$ ) the first derivative is not continuous at all weight vectors where the borders of the Voronoi tessellation are shifting over one of the input vectors.

Kohonen has, utilizing some approximations, shown in [Kohonen (1991)] for the 1D or 2D case that a gradient descent in  $V$  – note that the borders of the Voronoi tessellation  $F_{\mathbf{s}}(\{\mathbf{w}\})$  are shifting if one evaluates the gradient with respect to a weight vector  $\mathbf{w}_{\mathbf{r}}$  – results in a slightly different learning rule, which differs from the classical Kohonen rule only for the winning neuron  $\mathbf{s}$  itself:

$$\delta \mathbf{w}_{\mathbf{r}} = \eta \{ (\mathbf{v} - \mathbf{w}_{\mathbf{r}}) \cdot g_{\mathbf{rs}} - \frac{1}{2} \delta_{\mathbf{rs}} \sum_{\mathbf{r}' \neq \mathbf{s}} g_{\mathbf{r}'\mathbf{s}} (\mathbf{v} - \mathbf{w}_{\mathbf{r}'}) \}.$$

As the second term implies an additional elastic relaxation for the winning neuron, it is straightforward to call it ‘Winner Relaxing’ Kohonen algorithm. As the relaxing term acts only in one direction, the winner is relaxed to its neighbors, but the neighbors stay unattracted, it can not strictly be interpreted as an elastic force or physical interaction.

### 7.7.1.2 The Magnification Factor

Depending on the input probability density  $P(\mathbf{v})$  of the stimuli, any self-organizing map algorithm should show the property to spend more neurons to represent areas of higher probability density, according to a higher resolution, which is quantified by the magnification factor.

The magnification factor is defined as the density of neurons  $\mathbf{r}$  (i.e., the density of synaptic weight vectors  $\mathbf{w}_{\mathbf{r}}$ ) per unit volume of input space, and therefore is given by the inverse Jacobian of the mapping from input space to neuron layer:  $M = |J|^{-1} = |\det(d\mathbf{w}/d\mathbf{r})|^{-1}$ . (In the following we consider the case of non-inverting mappings, where  $J$  is positive. Further we assume the input space now to be continuous and of same dimension as the neural layer.) The magnification factor is a property of the networks' response to a given probability density of stimuli  $P(\mathbf{v})$ . To evaluate  $M$  in higher dimensions, one in general has to compute the equilibrium state of the whole network and needs therefore the complete global knowledge on  $P(\mathbf{v})$  [Claussen and Schuster (2002); Claussen (2002a)].

For 1D maps (and possibly for special separable but therefore less general cases in higher dimensions) the magnification factor can follow an universal magnification law, that is,  $M(\bar{\mathbf{w}}(\mathbf{r}))$  is a function of the local probability density  $P$  only and is independent of both the location  $\mathbf{r}$  in the neural layer and the location  $\bar{\mathbf{w}}(\mathbf{r})$  in input space.

For the classical Kohonen algorithm the magnification law (for 1D maps) is given by a power law  $M(\bar{\mathbf{w}}(\mathbf{r})) \propto P(\bar{\mathbf{w}}(\mathbf{r}))^\rho$  with exponent  $\rho = \frac{2}{3}$  [Ritter and Schulten (1986)].

Further it is nontrivial whether there exists a power law or not, as in the case of the Elastic Net, which has an universal magnification law which however is not a power law [Claussen and Schuster (2002)].

An optimal map from the view of information theory would reproduce the input probability exactly ( $M \sim P(\mathbf{v})^\rho$  with  $\rho = 1$ ), according to a power law with exponent 1. This is equivalent to the condition that all neurons in the layer are firing with same probability. An exponent  $\rho = 0$ , on the other hand, corresponds to a uniform distribution of weight vectors, which means there is no adaptation to the stimuli at all. So the magnification exponent is a direct indicator, how far a Self Organizing Map algorithm is away from the optimum predicted by information theory.

In the following subsection, the *Winner-relaxing Kohonen algorithm* (WRKA) is generalized introducing an additional parameter, and the magnification law in the 1D case is derived. This generalization can be used to



pre-select the magnification exponent between 1/2 and 1 by a fixed choice of the parameter.

### 7.7.1.3 Magnification Exponent

The necessary condition for the final state of the algorithm is that for all neurons  $\mathbf{r}$  the expectation value of the learning step vanishes:

$$\int d\mathbf{v} p(\mathbf{v}) \delta \mathbf{w}_{\mathbf{r}}(\mathbf{v}) = 0 \quad \text{for all } \mathbf{r} \in \mathbb{R}. \quad (7.79)$$

This is the *Chapman-Kolmogorov equation* for the *stochastic learning process* of serial presentation. Since this expectation value is equal to the learning step of the pattern parallel rule, (7.79) is the stationary state condition for *both* serial and parallel updating, and also for batch updating, so we can proceed for these variants simultaneously [Claussen and Schuster (2002); Claussen (2002a)].

Now we derive the magnification law for WRKA. We first introduce the following generalization, referred to as generalized WRKA, with free parameters  $\lambda$  and  $\mu$ :

$$\delta \mathbf{w}_{\mathbf{r}} = \eta \{ (\mathbf{v} - \mathbf{w}_{\mathbf{r}}) g_{\mathbf{r}\mathbf{s}}^{\gamma} + \mu (\mathbf{v} - \mathbf{w}_{\mathbf{r}}) \delta_{\mathbf{r}\mathbf{s}} - \lambda \delta_{\mathbf{r}\mathbf{s}} \sum_{\mathbf{r}' \neq \mathbf{s}} g_{\mathbf{r}'\mathbf{s}}^{\gamma} (\mathbf{v} - \mathbf{w}_{\mathbf{r}'} ) \},$$

where  $\mathbf{s}$  is the center of excitation for incoming stimulus  $\mathbf{v}$ , and  $g_{\mathbf{r}\mathbf{s}}^{\gamma}$  is a Gaussian function of distance in the neural layer with characteristic length  $\gamma$ . The original algorithm proposed by Kohonen in 1991 is obtained for  $\lambda = +1/2$  and  $\mu = 0$ , whereas the classical SOM algorithm is obtained for  $\lambda = 0$  and  $\mu = 0$ . Only for the special case  $\lambda = +1/2$  and  $\mu = 0$  the algorithm is associated with the potential function.

Insertion of the update rule (7.80) into the stationarity condition: for all  $\mathbf{r}$ ,  $\int d\mathbf{v} P(\mathbf{v}) \cdot \delta \mathbf{w}_{\mathbf{r}} = 0$ , and integration yields the differential equation (with  $\bar{P} = P(\bar{w}(r))$ ),

$$\gamma^2 \left( J \frac{d(\bar{P}J)}{dr} + \frac{\bar{P}J}{2} \frac{dJ}{dr} + \lambda \frac{\bar{P}J}{2} \frac{dJ}{dr} \right) = 0.$$

For  $\gamma \neq 0$ ,  $P \neq 0$ ,  $d\bar{P}/dr \neq 0$  and making the ansatz  $J(r) = J(\bar{P}(r))$  of an universal local magnification law (that may be expected for the 1D case) we get the differential equation

$$\frac{dJ}{d\bar{P}} = -\frac{2}{3 + \lambda} \frac{J}{\bar{P}},$$

with its solution (provided that  $\lambda \neq -3$ ):

$$M = \frac{1}{J} \sim P(v)^{\frac{2}{3+\lambda}}.$$

For WRKA ( $\lambda = 1/2$ ) the magnification factor follows an exact power law with magnification exponent  $\rho = 4/7$ , which is smaller than  $\rho = 2/3$  [Ritter and Schulten (1986)] for the classical SOM. Although WRKA was reported as ‘somewhat faster’ [Kohonen (1991)] in the initial ordering process, the resulting invariant mapping is slightly less optimal in terms of information theory [Claussen and Schuster (2002); Claussen (2002a)].

## 7.7.2 Dynamics of Hopfield’s Associative Recurrent Nets

### 7.7.2.1 Ising-Spin Neurons

The paradigm for the unsupervised, self-organizing, associative, and recurrent ANN is the discrete Hopfield network (see [Hopfield (1982)]). Hopfield gives a collection of simple threshold automata, called *formal neurons* by McCulloch & Pitts (see [Haykin (1994)]): two-state, ‘all-or-none’, firing or nonfiring units that can be modelled by *Ising spins* (uniaxial magnets)  $\{S_i\}$  such that  $S_i = \pm 1$  (where  $1 = |\uparrow\rangle$  = ‘spin up’ and  $-1 = |\downarrow\rangle$  = ‘spin down’; the label of the neuron is  $i$  and ranges between 1 and the size of the network  $N$ ). The neurons are connected by synapses  $J_{ij}$ .

Firing patterns  $\{\xi_i^\mu\}$  represent specific  $S_i$ -spin configurations, where the label of the pattern is  $\mu$  and ranges between 1 and  $q$ .

Using random patterns  $\xi_i^\mu = \pm 1$  with equal probability  $1/2$ , we have the *synaptic efficacy*  $J_{ij}$  of  $j$ th neuron operating on  $i$ th neuron given by

$$J_{ij} = N^{-1} \xi_i^\mu \xi_j^\mu \equiv N^{-1} \xi_i \cdot \xi_j. \quad (7.80)$$

*Postsynaptic potential* (PSP) represents an *internal local field*

$$h_i(t) = J_{ij} S_j(t). \quad (7.81)$$

Now, the *sequential (threshold) dynamics* is defined in the form of discrete equation

$$S_i(t + \Delta t) = \text{sgn}[h_i(t)]. \quad (7.82)$$

Dynamics (7.82) is equivalent to the rule that the state of a neuron is changed, or a spin is flipped iff the total network *energy*, given by *Ising*

### Hamiltonian

$$H_N = -\frac{1}{2} J_{ij} S_i S_j, \quad (7.83)$$

is lowered [Hopfield (1982); Hopfield and Tank (1985)]. Therefore, the Ising Hamiltonian  $H_N$  represents the monotonically decreasing *Lyapunov function* for the sequential dynamics (7.82), which converges to a local minimum or ground state of  $H_N$ . This holds for any *symmetric coupling*  $J_{ij} = J_{ji}$  with  $J_{ii} = 0$  and if spin-updating in (7.82) is asynchronous. In this case the patterns  $\{\xi_i^\mu\}$  after convergence become identical, or very near to, ground states of  $H_N$ , each of them at the bottom of the valley.

Data are *stored* in the neural net if, by a suitable choice of the  $J_{ij}$ , several specific patterns  $\{\xi_i^\mu\}$  are made local minima of  $H_N$ . If this can be achieved, the neural net will function as *content-addressable* or (auto)*associative memory*. A network state which 'somehow resembles' one of the stored prototypes corresponds to a location in the energy landscape which is close enough to the minimum representing that prototype to lie in its *basin of attraction*. By spontaneously moving downhill, or relaxing to the energy minimum, the network *recalls* the data or reconstructs the prototype.

Suppose that we have somehow stored several (stationary) patterns  $\{\xi_i^\mu\}$  in the  $J_{ij}$  and that the system is offered a noisy version of one of them. If the noise was not too strong, the system remains in the valley associated with that pattern and under its natural dynamics it will relax to the energy minimum where the stored patterns live. That is, the system has recalled the pattern.

In statistical mechanics, one is usually given the synapses  $J_{ij}$  and one of the first tasks consists in finding the minima of the Ising Hamiltonian  $H_N$  (7.83). In the theory of neural networks, however, one is given the patterns  $\{\xi_i^\mu\}$  and one is asked to solve the *inverse problem*: finding synapses  $J_{ij}$  such that the patterns  $\{\xi_i^\mu\}$  are minima of the Hamiltonian  $H_N$ .

To see why the Hopfield model with synapses given by (7.80) has patterns  $\{\xi_i^\mu\}$  as *attractors* of the dynamics (7.82), note that the sequential dynamical law embodies a two-step process, the evolution of the local field (PSP) (7.81), which is a *linear* operation, and a *nonlinear* decision process (7.82).

#### 7.7.2.2 Graded-Response Neurons

Graded-response neurons have continuous input-output relation (like nonlinear operational amplifiers) of the form  $V_i = g_i(\lambda u_i)$ , where  $u_i$  denotes

the input at  $i$ , a constant  $\lambda$  is called the gain parameter, and  $V_i$  is the output [Hopfield (1984)]. Usually,  $g_i$  are taken to be sigmoid functions, odd, and monotonically increasing (e.g.,  $g(\cdot) = \frac{1}{2}(1 + \tanh(\cdot))$ ), while discrete Ising spins have  $g_i(u_i) = \text{sgn}_i(u_i)$ . The behavior of the *continuous Hopfield network* is usually described by a set of coupled RC-transient equations

$$C_i \dot{u}_i = I_i + J_{ij} V_j - \frac{u_i}{R_i}, \quad (7.84)$$

where  $u_i = g^{-1}(V_i)$ ,  $R_i$  and  $C_i$  denote input capacitance and resistance, and  $I_i$  represents an external source.

The Hamiltonian of the continuous system (7.84) is given by

$$H = -\frac{1}{2} J_{ij} V_i V_j + \sum_{i=1}^N R_i^{-1} \int_0^{V_i} dV g^{-1}(V) - I_i V_i. \quad (7.85)$$

However, according to Hopfield [Hopfield (1984)] the synapses  $J_{ij}$  retain the form (7.80) with random patterns  $\xi_i^\mu = \pm 1$  with equal probability  $1/2$ , and the synaptic symmetry  $J_{ij} = J_{ji}$  implies that the continuous Hamiltonian (7.85) represents a *Lyapunov function* of the system (7.84), i.e.,  $H$  decreases under the continual neuro-dynamics governed by equation (7.84) as time proceeds.

More general form of synapses is

$$J_{ij} = N^{-1} Q(\xi_i; \xi_j),$$

for some synaptic kernel  $Q$  on  $\mathbb{R}^n \times \mathbb{R}^n$ . The vector  $\xi_i$  varies as  $i$  travels from 1 to  $N$ , but remains on a corner of the *Hamming hypercube*  $[-1, 1]^q$ .

### 7.7.2.3 Hopfield's Overlaps

Assuming that the number  $q$  of stored patterns is small compared to the number of neurons, i.e.,  $q/N \rightarrow 0$ , we find that the synapses (7.80) give rise to a local field of the form

$$h_i = \xi_i^\mu m_\mu, \quad (7.86)$$

where

$$m_\mu = N^{-1} \xi_i^\mu S_i \quad (7.87)$$

is the *auto-overlap* (or simply *overlap*)<sup>8</sup> of the network state  $\{S_i\}$  with the pattern  $\{\xi_i^\mu\}$ , measuring the proximity between them. We can see that  $m_\mu = 1$  (like peak-up in auto-correlation) if  $\{S_i\}$  and  $\{\xi_i^\mu\}$  are identical patterns,  $m_\mu = -1$  (like peak-down in autocorrelation) if they are each other's complement, and  $m_\mu = O(1/\sqrt{N})$  if they are uncorrelated (like no-peak in auto-correlation) with each other. Overlaps  $m_\mu$  are related to the Hamming distance  $d_\mu$  between the patterns (the fraction of spins which differ) by  $d_\mu = \frac{1}{2}(1 - m_\mu)$ .

As a pattern  $\xi_i^\mu$  represents (in the simplest case) a specific Ising-spin  $S_i$ -configuration, then  $(\xi_i^\mu)^2 = 1$ . If  $S_i = \xi_i^\mu$  for all  $i$ , then  $m_\mu = 1$ . Conversely, if  $m_\mu = 1$ , then  $S_i = \xi_i^\mu$ . In all other cases  $m_\mu < 1$ , by the Cauchy-Schwartz inequality. If  $\xi_i^\mu$  and  $S_i$  are uncorrelated, we may expect  $m_\mu$  to be of the order of  $N^{-1/2}$ , since the sum consists of  $N$  terms, each containing a  $\xi_i^\mu$ . On the other hand, if the  $S_i$  are positively correlated with  $\xi_i^\mu$ , then  $m_\mu$  is of the order of unity. So the overlaps give the global information about the network and hence are good order parameters. Also, according to Hopfield [Hopfield (1984)], the extension to the continual network is straightforward.

Using overlaps, the *Ising Hamiltonian* becomes

$$H_N = -\frac{1}{2}N \sum_{\mu=1}^q m_\mu^2. \quad (7.88)$$

The similarity between two different patterns  $\xi_i^\mu$  and  $\xi_i^\nu$  is measured by their *mutual overlap* or *cross-overlap*  $m_{\mu\nu}$  (in other parlance it is called *Karhunen-Loeve covariance matrix* (see [Freeman and Skapura (1992)]), which extracts the principal components from a data set)<sup>9</sup>, equal

$$m_{\mu\nu} = N^{-1} \xi_i^\mu \xi_i^\nu. \quad (7.89)$$

For similar patterns the cross-overlap is close to unity whereas for uncorrelated patterns it is random variable with zero mean and small  $(1/\sqrt{N})$  variance.

The symmetric *Hopfield synaptic matrix*  $J_{ij}$  can be expressed in terms of the cross-overlaps  $m_{\mu\nu}$  as

$$J_{ij} = N^{-1} \xi_i^\mu (m_{\mu\nu})^{-1} \xi_j^\nu = J_{ji}, \quad (7.90)$$

<sup>8</sup>resembling the auto-correlation function of a time-series, where distinct peaks indicate that the series at the certain time  $t$  is similar to the series at time  $t + \Delta t$

<sup>9</sup>resembling the cross-correlation function of two time-series, with several distinct peaks, indicating that the two series are very similar at each point in time where the peaks occur

where  $(m_{\mu\nu})^{-1}$  denotes the *Moore-Penrose pseudoinverse* of the cross-overlap matrix  $m_{\mu\nu}$ .

Besides the Hopfield model, the proposed pattern-overlap picture can be extended to cover some more sophisticated kinds of associative memory, among them (see, e.g., [Domany *et al.* (1991)]):

- (1) Forgetful memories, characterized by iterative synaptic prescription

$$J_{ij}^{(\mu)} = \phi(\epsilon \xi_i^\mu \xi_j^\mu + J_{ij}^{(\mu-1)}),$$

for some small parameter  $\epsilon$  and some odd function  $\phi$ . If  $\phi(\cdot)$  saturates as  $|\cdot| \rightarrow \infty$ , the memory creates storage capacity for new patterns by forgetting the old ones.

- (2) Temporal associative memories, which can store and retrieve a sequence of patterns, through synapses

$$NJ_{ij} = \xi_i^\mu \xi_j^\mu + \epsilon \sum_{\mu=1}^q \xi_i^{(\mu+1)} \xi_j^\mu, \quad (7.91)$$

where the second term on the right is associated with a temporal delay, so that one can imagine that the second term ‘pushes’ the neural system through an energy landscape created by the first term.

#### 7.7.2.4 Overlap Dynamics

According to Hopfield [Hopfield (1984)], the extension of the sequential dynamics  $S_i = \text{sgn}(\sum_\mu m_\mu \xi_i^\mu)$  of the network made of the simplest Ising-spin-neurons to the network made of continual graded-response amplifier-neurons, is straightforward using the probabilistic *Glauber dynamics*

$$\text{Prob}\{S_i \mapsto -S_i\} = \frac{1}{2}[1 - \tanh(\beta h_i S_i)], \quad i = 1, \dots, N, \quad (7.92)$$

where  $\beta$  represents the universal temperature ( $\beta = \frac{1}{k_B T}$ ,  $k_B$  is the normalized Boltzman’s constant and  $k_B T$  has dimension of energy).

Under the Glauber’s dynamics (7.92), and as  $N \rightarrow \infty$  (transition from the single neurons to the neural field), for time-dependent patterns  $\xi^\mu(t) = \xi_\mu(t)$ , vector auto-overlaps  $m_\mu(t)$ , and tensor cross-overlaps  $m_{\mu\nu}(t)$ , we propose the dynamics of overlaps governed by the following nonlinear differential equations (generalized from [Domany *et al.* (1991)], pp. 23), respectively in the vector form

$$\dot{m}_\mu(t) = -m_\mu(t) + \langle \xi_\mu(t) \tanh[\beta m_\mu(t) \xi^\mu(t)] \rangle, \quad (7.93)$$

and in the tensor form

$$\dot{m}_{\mu\nu}(t) = -m_{\mu\nu}(t) + \langle \xi_\mu(t) \xi_\nu(t) \tanh[\beta m_{\mu\nu}(t) \xi^\mu(t) \xi^\nu(t)] \rangle, \quad (7.94)$$

where the angular brackets denote an average over the  $q$  patterns  $\xi^\mu(t)$ .

The stationary solutions (for any fixed instant of time  $t = \tau$ ) of equations (7.93) and (7.94) are given by corresponding fixed-point vector and tensor equations

$$m_\mu = \langle \xi_\mu \tanh[\beta m_\mu \xi^\mu] \rangle, \quad (7.95)$$

and

$$m_{\mu\nu} = \langle \xi_\mu \xi_\nu \tanh[\beta m_{\mu\nu} \xi^\mu \xi^\nu] \rangle, \quad (7.96)$$

respectively.

#### 7.7.2.5 Hebbian Learning Dynamics

In terms of stochastic feed-forward multi-layer neural networks, the tensorial equation (7.94) corresponds to the average, general, self-organizing Hebbian neural learning scheme (see [Hebb (1949); Kosko (1992)])

$$\dot{m}_{\mu\nu}(t) = -m_{\mu\nu}(t) + \langle \mathcal{I}_{\mu\nu} \rangle, \quad (7.97)$$

with random signal *Hebbian innovation*

$$\mathcal{I}_{\mu\nu} = f_\mu[\xi^\mu(t)] f_\nu[\xi^\nu(t)] + \sigma_{\mu\nu}(t), \quad (7.98)$$

where  $\sigma_{\mu\nu}$ , denotes the tensorial, additive, zero-mean, Gaussian white-noise, independent of the main innovation function  $\mathcal{I}_{\mu\nu}$ , while  $f_{\mu,\nu}[\cdot]$  represent the hyperbolic tangent (sigmoid) neural activation functions. A single-layer Hebbian learning scheme, corresponding to the tensor equation (7.97), gives

$$\dot{m}_\mu(t) = -m_\mu(t) + \langle \mathcal{I}_\mu \rangle, \quad (7.99)$$

with the vector innovation

$$\mathcal{I}_\mu = f_\mu[\xi^\mu(t)] + \sigma_\mu(t),$$

where  $\sigma_\mu$ , denotes the vector additive zero-mean Gaussian white-noise, also independent of the main innovation function  $\mathcal{I}_\mu$ , while  $f_\mu[\cdot]$  represents the hyperbolic tangent (sigmoid) neural activation function.

If we assume the small absolute value of the average (stochastic) terms, the nonlinear overlap-dynamics equations (7.93) and (7.94) can be presented in the form of *weakly-connected neural networks* (see [Hoppensteadt and Izhikevich (1997)]), respectively, as a single-layer network

$$\dot{m}_\mu(t) = -m_\mu(t) + \varepsilon g_\mu(m_\mu, \varepsilon), \quad \varepsilon \ll 1, \quad (7.100)$$

and a multi-layer network

$$\dot{m}_{\mu\nu}(t) = -m_{\mu\nu}(t) + \varepsilon g_{\mu\nu}(m_{\mu\nu}, \varepsilon), \quad \varepsilon \ll 1, \quad (7.101)$$

where,  $g_\mu$  and  $g_{\mu\nu}$ , corresponding to the average (bracket) terms in (7.93) and (7.94), describe (vector and tensor, respectively) synaptic connections and the 'small' parameter  $\varepsilon$  describes their (dimensionless) strength. These weakly-connected neural systems represent  $\varepsilon$ -perturbations of the corresponding linear systems

$$\dot{m}_\mu(t) = -m_\mu(t) \quad \text{and} \quad \dot{m}_{\mu\nu}(t) = -m_{\mu\nu}(t),$$

with exponential maps as solutions

$$m_\mu(t) = m_\mu e^{-t} \quad \text{and} \quad m_{\mu\nu}(t) = m_{\mu\nu} e^{-t},$$

using the stationary (fixed-point) solutions (7.95, 7.96) as initial conditions  $m_\mu$  and  $m_{\mu\nu}$ . According to the *Hartman-Grobman theorem* from dynamical systems theory, the weakly-connected systems (7.100, 7.101) are topologically equivalent (homeomorphic) to the corresponding linear systems. Therefore the whole analysis for the linear vector and matrix flows can be applied here, with only difference that instead of increasing transients  $e^t$  here we have decreasing (i.e., asymptotically-stable) transients  $e^{-t}$ .

On the other hand, in terms of *synergetics* [Haken (1983)], both nonlinear overlap-dynamics equations (7.93–7.94) and Hebbian learning equations (7.97–7.98), represent (covariant) *order parameter equations*.

By introducing the scalar quadratic potential fields, dependent on vector and tensor order parameters (overlaps), respectively

$$V(m_\mu) = -\frac{1}{2} \sum_{\mu=1}^q m_\mu^2 \quad \text{and} \quad V(m_{\mu\nu}) = -\frac{1}{2} m_{\mu\nu}^2,$$

we can generalize the overlap-dynamics equations (7.93–7.94) to the *stochastic-gradient order parameter equations*, in vector and tensor form,



respectively

$$\dot{m}_\mu(t) = -\frac{\partial V(m_\mu)}{\partial m_\mu(t)} + F_\mu(t), \quad (7.102)$$

and

$$\dot{m}_{\mu\nu}(t) = -\frac{\partial V(m_{\mu\nu})}{\partial m_{\mu\nu}(t)} + F_{\mu\nu}(t). \quad (7.103)$$

$F_\mu(t)$  in (7.102) represents a vector fluctuating force, with average (over the stochastic process which produces the fluctuating force  $F_\mu(t)$ )

$$\langle F_\mu(t) \rangle = \langle \xi_\mu(t) \tanh[\beta m_\mu(t) \xi^\mu(t)] \rangle,$$

and variation

$$\langle F_\mu(t) F_\mu(t') \rangle = Q_\mu \delta(t - t'), \quad (7.104)$$

while  $F_{\mu\nu}(t)$  in (7.103) represents a tensor fluctuating force, with average (over the stochastic process which produces the fluctuating force  $F_{\mu\nu}(t)$ )

$$\langle F_{\mu\nu}(t) \rangle = \langle \xi_\mu(t) \xi_\nu(t) \tanh[\beta m_{\mu\nu}(t) \xi^\mu(t) \xi^\nu(t)] \rangle,$$

and variation

$$\langle F_{\mu\nu}(t) F_{\mu\nu}(t') \rangle = Q_{\mu\nu} \delta(t - t'). \quad (7.105)$$

Coefficients  $Q_\mu$  in (7.104) and  $Q_{\mu\nu}$  in (7.105) represent strengths of the corresponding stochastic processes, while Dirac  $\delta(t - t')$  express their short-term memories.

Recall that standard interpretation of synergetics (see [Haken (1983)]) describes the stochastic gradient systems (7.102–7.103) as the overdamped motion of (vector and tensor, respectively) representative particles in scalar potential fields  $V(m_\mu)$  and  $V(m_{\mu\nu})$ , subject to fluctuating forces  $F_\mu(t)$  and  $F_{\mu\nu}(t)$ . These particles undergo *nonequilibrium phase transitions* (in the similar way as the magnet undergoes transition from its unmagnetized state into a magnetized state, or a superconductor goes from its normal state into the superconducting state, only occurring now in systems far from thermal equilibrium), and associated phenomena, including a *symmetry breaking instability* and *critical slowing down* (see [Haken (1983)]).

The nonequilibrium phase transitions of vector and tensor order parameters (overlaps)  $m_\mu(t)$  and  $m_{\mu\nu}(t)$ , are in synergetics described in terms of

probability distributions  $p(m_\mu, t)$  and  $p(m_{\mu\nu}, t)$ , respectively, defined by corresponding *Fokker-Planck equations*

$$\dot{p}(m_\mu, t) = p(m_\mu, t) + \frac{1}{2} Q_\mu \frac{\partial^2 p(m_\mu, t)}{\partial m_\mu^2},$$

and

$$\dot{p}(m_{\mu\nu}, t) = p(m_{\mu\nu}, t) + \frac{1}{2} Q_{\mu\nu} \frac{\partial^2 p(m_{\mu\nu}, t)}{\partial m_{\mu\nu}^2}.$$

### 7.7.3 A Self-Organizing Bidirectional Competitive Net

Hopfield recurrent associative memory network can be generalized to get a *bidirectional associative memory* network, the so-called BAM model of Kosko [Kosko (1992)]. Here we derive an alternative self-organizing neural net model with competitive *Volterra-Lotka ensemble dynamics* [Ahmad (1993)].

We start from  $(n+m)$ D linear ODEs, describing two competitive neural ensembles participating in a two-party game,

$$\begin{aligned} \dot{R}^i &= -\alpha_B^j B_j, & R^i(0) &= R_0^i, \\ \dot{B}_j &= -\beta_i^R R^i, & B_j(0) &= B_j^0, \end{aligned} \quad (i = 1, \dots, n; j = 1, \dots, m), \quad (7.106)$$

where  $R^i = R^i(t)$  and  $B_j = B_j(t)$  respectively represent the numerical strengths of the two neural ensembles at time  $t$ ,  $R_0^i, B_j^0$  are their initial conditions, and  $\alpha_B$  and  $\beta^R$  represent the effective spiking rates (which are either constant, or Poisson random process). In this way, we generate a  $(n+m)$ D smooth manifold  $M$ , a *neural state-space*, and two dynamical objects acting on it: an  $n$ D smooth *vector-field*  $\dot{R}^i$ , and an  $m$ D differential *1-form*  $\dot{B}_j$ . Their dot product  $\dot{R}^i \cdot \dot{B}_j$ , represents a hypothetical *neural outcome*. This is a linear system, with the passive-decay couplings  $\alpha_B^j B_j$  and  $\beta_i^R R^i$ , fully predictable but giving only equilibrium solutions.

Secondly, to incorporate competitive dynamics of Volterra-Lotka style as commonly used in ecological modelling and known to produce a global chaotic attractor [Ahmad (1993)], we include to each of the neural ensembles a nonlinear competing term depending only on its own units,

$$\begin{aligned} \dot{R}^i &= a^i R^i(1 - b^i R^i) - \alpha_B^j B_j, \\ \dot{B}_j &= c_j B_j(1 - d_j B_j) - \beta_i^R R^i. \end{aligned} \quad (7.107)$$

Now we have a *competition between the two chaotic attractors*, one for the  $R^i$  and one for the  $B_j$  ensemble, i.e., the two self-organization patterns emerging far-from-equilibrium.

Thirdly, to make this even more realistic, we include the ever-present *noise* in the form of Langevin-type random forces  $F^i = F^i(t)$ , and  $G_j = G_j(t)$ , thus adding the ‘neural heating’, i.e., noise induced entropy growth, to the competitive dynamics

$$\begin{aligned}\dot{R}^i &= a^i R^i (1 - b^i R^i) - \alpha_B^j B_j + F^i, \\ \dot{B}_j &= c_j B_j (1 - d_j B_j) - \beta_i^R R^i + G_j.\end{aligned}\quad (7.108)$$

Finally, to overcome the deterministic chaos and stochastic noise with an adaptive *brain-like dynamics*, we introduce the *field competition potential*  $V$ , in the scalar form

$$V = -\frac{1}{2}(\omega_i^j R^i B_j + \varepsilon_i^j B_j R^i), \quad (7.109)$$

where  $\omega_i^j$  and  $\varepsilon_i^j$  represent *synaptic associative-memory* matrices for the  $R^i$  and  $B_j$  ensemble, respectively. From the negative potential  $V$ , we get a *Lyapunov-stable gradient system*  $\dot{R}^i = -\frac{\partial V}{\partial R^i}$ ,  $\dot{B}_j = -\frac{\partial V}{\partial B_j}$ . This robust system, together with the *sigmoidal activation functions*  $S(\cdot) = \tanh(\cdot)$ , and *control inputs*  $u_{OLN}^i = u_{OLN}^i(t)$  and  $v_j^{OLN} = v_j^{OLN}(t)$ , we incorporate into (7.108) to get the *full neural competitive-associative dynamics* (compare with [Ivancevic *et al.* (1999a)])

$$\begin{aligned}\dot{R}^i &= u_{OLN}^i - \alpha_B^j B_j + a^i R^i (1 - b^i R^i) + \omega_i^j S_j(B_j) + F^i, \\ \dot{B}_j &= v_j^{OLN} - \beta_i^R R^i + c_j B_j (1 - d_j B_j) + \varepsilon_i^j S^i(R^i) + G_j,\end{aligned}\quad (7.110)$$

with initial conditions

$$R^i(0) = R_0^i, \quad B_j(0) = B_j^0.$$

Now, each ensemble learns by trial-and-error from the opposite side. In a standard ANN-fashion, we model this learning on the spot by initially setting the random values to the synaptic matrices  $\omega_i^j$  and  $\varepsilon_i^j$ , and subsequently adjust these values using the standard *Hebbian learning scheme*:  
New Value = Old Value + Innovation. In our case it reads:

$$\begin{aligned}\dot{\omega}_i^j &= -\omega_i^j + \Phi_i^j(R^i, B_j), \\ \dot{\varepsilon}_i^j &= -\varepsilon_i^j + \Psi_i^j(B_j, R^i),\end{aligned}\quad (7.111)$$

with *innovation* given in tensor signal form (generalized from [Kosko

(1992)]

$$\begin{aligned}\Phi_i^j &= S_j(R^i) S_j(B_j) + \dot{S}_j(R^i) \dot{S}_j(B_j), \\ \Psi_i^j &= S^i(R^i) S^i(B_j) + \dot{S}^i(R^i) \dot{S}^i(B_j),\end{aligned}\tag{7.112}$$

where terms with overdots, equal  $\dot{S}(\cdot) = 1 - \tanh(\cdot)$ , denote the *signal velocities*.

## 7.8 Fuzzy Logic in Biodynamics

In this section we present the basics of *fuzzy logic*, as used in modern biodynamics. Fuzzy logic is a natural companion of ANNs.<sup>10</sup> It was initiated in 1965 by L. Zadeh [Yager (1987); Zadeh (1978)], professor of computer science at the University of California in Berkeley, as a way of processing data by allowing partial set membership rather than crisp set membership or non-membership. This approach to set theory was not really applied to control systems until the 90s due to insufficient computer capability prior to that time. Professor Zadeh reasoned that people did not require precise, numerical information input, and yet they were capable of highly adaptive control. If feedback controllers could be programmed to accept noisy, imprecise input, they would be much more effective and perhaps easier to implement.

### 7.8.1 The Concept of Fuzziness

#### 7.8.1.1 'Fuzzy Thinking'

'There is no logic in logic', pronounced the father of fuzzy logic, L. Zadeh [Yager (1987)]. His cryptic play-on-words, he explained, means that the kind of logic that people use to solve most real world problems rather than the artificial problems for which mathematical solutions are available is not the kind of logic that engineers are taught in school. 'An engineer can solve problems throughout his whole career without ever needing to resort to the brand of logic he was trained in', said Zadeh. 'Why? Because all people, even engineers, compute with words not the logical symbols taught in school', Zadeh maintained. 'In the future, computing will be done with words from natural languages, rather than with symbols that are far removed from daily life.'

<sup>10</sup>In the previous decade quite common were the joint conferences for neural networks and fuzzy expert systems.

In 1973, Zadeh proposed the concept of linguistic or fuzzy variables [Yager (1987); Zadeh (1978)]. Think of them as linguistic objects or words, rather than numbers. The sensor input is a noun, e.g. temperature, displacement, velocity, ow, pressure, etc. Since error is just the difference, it can be thought of the same way. The fuzzy variables themselves are adjectives that modify the variable (e.g., large positive error, small positive error, zero error, small negative error, and large negative error). As a minimum, one could simply have positive, zero, and negative variables for each of the parameters.

Additional ranges such as very large and very small could also be added to extend the responsiveness to exceptional or very nonlinear conditions, but are not necessary in a basic system. Normal logic is just not up to modelling the real world, claims B. Kosko [Kosko (1992); Kosko (1993); Kosko (1996); Kosko (1999)], perhaps the worlds most active proponent of fuzzy logic. According to Kosko, there is always *ambiguity* in our perceptions and measurements that is difficult to reflect in traditional logic. Probability attempts to reflect ambiguity by resorting to statistical averages over many events. But fuzzy theory describes the ambiguity of individual events. It measures the degree to which an event occurs, not whether it occurs.

### 7.8.1.2 Fuzzy Sets

Recall that a crisp (ordinary mathematical) set  $X$  is defined by a binary characteristic function  $\chi_X(x)$  of its elements  $x$

$$\chi_X(x) = \begin{cases} 1, & \text{if } x \in X, \\ 0, & \text{if } x \notin X, \end{cases}$$

while a fuzzy set is defined by a continuous characteristic function

$$\chi_X(x) = [0, 1],$$

including all (possible) real values between the two crisp extremes 1 and 0, and including them as special cases.

A fuzzy set set  $X$  is a collection of ordered pairs

$$X = \{(x, \mu(x))\}, \quad (7.113)$$

where  $\mu(x)$  is the *fuzzy membership function* representing the grade of membership of the element  $x$  in the set  $X$ . A single pair is called a fuzzy

*singleton.*

### 7.8.1.3 *Fuzziness of the Real World*

The real world consists of all subsets of the universe and the only subsets that are not fuzzy are the constructs of classical mathematics.

From small errors to satisfied customers to safe investments to noisy signals to charged particles, each element of the real world is in some measure fuzzy. For instance, satisfied customers can be somewhat unsatisfied, safe investments somewhat unsafe and so on. What is worse, most events more or less smoothly transition into their opposites, making classification difficult near the midpoint of the transition. Unfortunately, textbook events and their opposites are crisp, unlike the real world. Take the proposition that there is a 50% chance that an apple is in the refrigerator. That is an assertion of crisp logic. But suppose upon investigation it is found that there is half an apple in the refrigerator, that is fuzzy.

But regardless of the realities, the crisp logic in vogue today assumes that the world is really unambiguous and that the only uncertainty is the result of random samples from large sets. As the facts about these large sets become better known, the randomness supposedly dissipates, so that if science had access to all the facts, it would disappear. Unfortunately, if all the facts were in, a platypus would remain only roughly an mammal.

On the other hand, fuzzy logic holds that uncertainty is deterministic and does not dissipate as more elements of a set are examined. Take an ellipse, for instance. It is approximately a circle, to whatever degree that it resembles a perfect circle. There is nothing random about it. No matter how precisely it is measured it remains only approximately a circle. All the facts are in and yet uncertainty remains.

Traditional crisp logic has a difficult time applying itself to very large sets, since probability fades to unity, as well as to individual events where probabilities cannot be defined at all. Nevertheless, crisp logic continues to rein supreme based on long standing western traditions that maintain that rationality would vanish if there were not crisp logical ideals to which we should aspire. These laws of (rational) thought were first characterized by Aristotle as the principle of non-contradiction and the principle of the excluded middle. The principle of non-contradiction, stated in words, says that nothing can be both  $A$  and  $non - A$ . The law of the excluded middle says that anything must be either  $A$  or  $non - A$ .

'Fuzziness is the denial of both these so-called laws', says E. Cox [Cox

(1992); Cox (1994)]). The classical example is of a platypus which both is and is not a mammal. In such individual cases, even appending probability theory to crisp logic cannot resolve the paradox. For instance, take the now classical paradox formulated by B. Russell: If a barber shaves everyone in a village who does not shave himself, then who shaves the barber? This paradox was devised to assault G. Cantor's set theory as the foundation for G. Boole's digital logic. It has been restated in many forms, such as the liar from Crete who said that all Creatans are liars. Russell solved it by merely disqualifying such self-referential statements in his set theory. Probability theory solves it by assuming a population of barbers 50% of whom do, and 50% of whom do not, shave themselves. But fuzzy logic solves it by assigning to this individual barber a 50% membership value in the set self-shaving barbers. Further, it shows that there is a whole spectrum of other situations that are less fuzzy and which correspond to other degrees of set membership. Such as, barbers who shave themselves 70% of the time.

Kosko illustrates these various degrees of ambiguity by geometrically plotting various degrees of set membership inside a *unit fuzzy hypercube*  $[0, 1]^n$  [Kosko (1992); Kosko (1993); Kosko (1996); Kosko (1999)]. This sets-as-points approach holds that a fuzzy set is a point in a unit hypercube and a non-fuzzy set is a corner of the hypercube. Normal engineering practice often visualizes binary logical values as the corners of a hypercube, but only fuzzy theory uses the inside of the cube. Fuzzy logic is a natural filling-in of traditional set theory. Any engineer will recognize the 3D representation of all possible combinations three Boolean values:  $\{0, 0, 0\}, \{0, 0, 1\}, \{0, 1, 0\}, \{0, 1, 1\}, \{1, 0, 0\}, \{1, 0, 1\}, \{1, 1, 0\}, \{1, 1, 1\}$ , which correspond to the corners of the unit hypercube. But fuzzy logic also allows any other fractional values inside the hypercube, such as  $\{0.5, 0.7, 0.3\}$  corresponding to degrees of set membership.

Fuzzy logic holds that any point inside the unit hypercube is a fuzzy set with Russell's paradox located at the point of maximum ambiguity in the center of the hypercube.

#### 7.8.1.4 Fuzzy Entropy

Degrees of fuzziness are referred to as entropy by Kosko. *Fuzzy mutual entropy* measures the *ambiguity of a situation*, information and entropy are inversely related – if you have a maximum-entropy solution, then you have a minimum-information solution, and visa versa, according to Kosko. But

minimum-information does not mean that too little information is being used. On the contrary, the principle of maximum entropy ensures that only the relevant information is being used (compare with the concept of quantum entropy in (4.3.3) above).

This idea of maximizing entropy, according to Kosko, is present throughout the sciences, although it is called by different names. 'From the quantum level up to astrophysics or anywhere in-between for pattern recognition, you want to use all and only the available information,' Kosko claims. This emergent model proposes that scientists and engineers estimate the uncertainty structure of a given environment and maximize the entropy relative to the known information, similar to the Lagrange technique in mathematics. The principle of maximum entropy states that any other technique has to be biased, because it has less entropy and thus uses more information than is really available.

Fuzzy theory provides a measure of this entropy factor. It measures ambiguity with operations of union  $\cup$ , intersection  $\cap$  and complement  $-$ .

In traditional logic, these three operators are used to define a set of axioms that were proposed by Aristotle to be the immutable laws of (rational) thought, namely, the principle of *non-contradiction* and the principle of the *excluded middle*. The principle of non-contradiction, that nothing can be both  $A$  and  $-A$ , and the law of the excluded middle, that anything must be either  $A$  or  $-A$ , amounts to saying that the intersection of a set and its complement is always empty and that the union of a set and its complement always equals the whole *universe of discourse*, respectively. But if we do not know  $A$  with certainty, then we do not know  $-A$  with certainty either, else by double negation we would know  $A$  with certainty. This produces non-degenerate *overlap* ( $A \cap -A$ ), which breaks the law of non-contradiction. Equivalently, it also produced non-degenerate *underlap* ( $A \cup -A$ ) which breaks the law of the excluded middle. In fuzzy logic both these so-called laws are denied. A set and its complement can both be overlap and underlap.

What is worse, there is usually ambiguity in more than one parameter or dimension of a problem. To represent multi-dimensional ambiguity, Kosko shows fuzzy entropy geometrically with a hypercube.

All these relationships are needed in fuzzy logic to express its basic structures for *addition*, *multiplication*, and most important, *implication*  $IF \Rightarrow THEN$ . They all follow from the subsethood relationships between fuzzy sets. The subset relation by itself, corresponds to the implication relation in crisp logic. For instance,  $A \Rightarrow B$  is *false only* if the *antecedent*



$A$  is true and the consequent  $B$  is false. The same holds for subsets,  $A$  is a subset of  $B$  if there is no element that belongs to  $A$  but not to  $B$ .

But in fuzzy logic, degrees of subsethood permit some  $A$  to be somewhat of a subset of  $B$  even though some of its elements are not elements of  $B$ . The degree to which  $A$  is a subset of  $B$  can be measured as the distance from the origin to  $(A \cap B)$  divided by the distance from the origin to  $A$ .

This structure is derived as a theorem of fuzzy logic, whereas for probability theory equivalent conditional probability theorem has to be assumed, making fuzzy logic a more fundamental.

The *fuzzy mutual entropy* measures how close a fuzzy description of the world is to its own opposite [Kosko (1999)]. It has no random analogue in general. The *fuzzy fluid* leads to a type of wave equation. The wave shows how the *extended Shannon entropy potential*  $S : [0, 1]^n \rightarrow \mathbb{R}$ , defined on the *entire fuzzy cube*  $[0, 1]^n$ , fluctuates in time. It has the form of a *reaction-diffusion* equation

$$\dot{S} = -c \nabla^2 S, \quad (7.114)$$

where  $c$  is the *fuzzy diffusion parameter*. The *fuzzy wave equation* (7.114) implies  $\dot{S} > 0$ , and thus resembles the entropy increase of the  $S$ -theorem of the *Second Law of thermodynamics*.

Similar equations occur in all branches of science and engineering. The Schrödinger wave equation (see (4.3.1) above) has this form, as well as most models of diffusion. The fuzzy wave equation (7.114) assumes only that information is conserved. The total amount of information is fixed and we do not create or destroy information. Some form of the the wave equation would still apply if information were conserved locally or in small regions of system space. The space itself is a fuzzy cube of high dimension. It has as many dimensions as there are objects of interest. The Shannon entropy  $S$  changes at each point in this cube and defines a *fuzzy wave*. The obvious result is that the entropy  $S$  can only grow in time in the spirit of the second law.

The entropy always grows but its *rate of growth* depends on the system's position in the *fuzzy parameter space*. A deeper result is that entropy changes slowest at the fuzzy cube *midpoint of maximum fuzz*. That is the only point in the cube where the fuzzy description equals its own opposite. The Shannon entropy wave grows faster and faster away from the cube midpoint and near its skin. The skin or surface of the fuzzy cube is the only place where a 0 or 1 appears in the system description. The fuzzy wave equation (7.114) shows that the entropy  $S$  changes infinitely fast iff

it touches the cubes's skin. However, this is impossible in a universe with finite bounds on velocity like the speed of light. So, the result is never a *bit* – it is always a *fit* [Kosko (1999)].

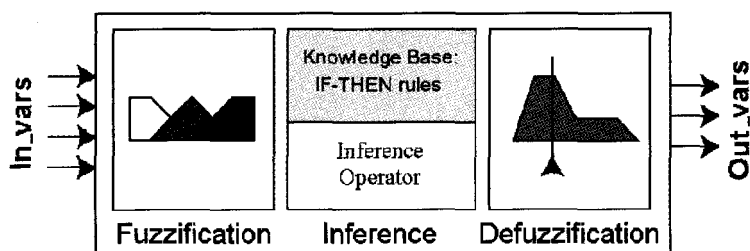


Fig. 7.56 Basic structure of the fuzzy inference engine.

### 7.8.2 Fuzzy Inference Engine

Like ANNs, the fuzzy logic systems are generic *nonlinear function approximators* [Kosko (1992)]. In the realm of fuzzy logic this generic nonlinear function approximation is performed by means of fuzzy inference engine. The *fuzzy inference engine* is an *input-output dynamical system* which *maps* a set of input linguistic variables (*IF*-part) into a set of output linguistic variables (*THEN*-part). It has three sequential modules (see Figure 7.56):

- (1) *Fuzzification*; in this module numerical crisp input variables are fuzzified; this is performed as an overlapping partition of their universes of discourse by means of fuzzy membership functions  $\mu(x)$  (7.113), which can have various shapes, like triangular-trapezoidal (see Figure 7.57), Gaussian-bell,  $\mu(x) = \exp \left[ \frac{-(x-m)^2}{2\sigma^2} \right]$  (with mean  $m$  and standard deviation  $\sigma$ ), sigmoid  $\mu(x) = \left[ 1 + \left( \frac{x-m}{\sigma} \right)^2 \right]^{-1}$ , or some other shapes. B. Kosko and his students have done extensive computer simulations looking for the best shape of fuzzy sets to model a known test system as closely as possible. They let fuzzy sets of all shapes and sizes compete against each other. They also let neural systems tune the fuzzy-set curves to improve how well they model the test system. The main conclusion from these experiments is that ‘triangles never do well’ in such contests. Suppose we want an adaptive fuzzy system  $F: \mathbb{R}^n \rightarrow \mathbb{R}$

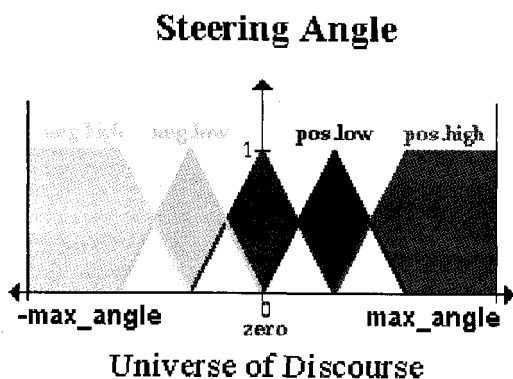


Fig. 7.57 Fuzzification example: set of triangular-trapezoidal membership functions partitioning the universe of discourse for the angle of the hypothetical steering wheel; notice the white overlapping triangles.

to approximate a test function (or, approximand)  $f : \mathbb{R}^n \rightarrow \mathbb{R}$  as closely as possible in the sense of minimizing the mean-squared error between them,  $(\|f - F\|^2)$ . Then the  $i$ th scalar 'sinc' function (as commonly used in signal processing),

$$\mu_i(x) = \frac{\sin\left(\frac{x-m_i}{d_i}\right)}{\frac{x-m_i}{d_i}}, \quad (i = 1, \dots, n), \quad (7.115)$$

with center  $m_i$  and dispersion (width)  $d_i = \sigma_i^2 > 0$ , often gives the best performance for  $IF$ -part mean-squared function approximation, even though this generalized function can take on negative values (see [Kosko (1999)]).

- (2) *Inference*; this module has two submodules:
  - (i) The expert-knowledge base consisting of a set of  $IF-THEN$  rules relating input and output variables, and
  - (ii) The inference method, or implication operator, that actually combines the rules to give the fuzzy output; the most common is *Mamdani Min-Max inference*, in which the membership functions for input variables are first combined inside the  $IF-THEN$  rules using  $AND$  ( $\cap$ , or *Min*) operator, and then the output fuzzy sets from different  $IF-THEN$  rules are combined using  $OR$  ( $\cup$ , or *Max*) operator to get the common fuzzy output (see Figure 7.58).
- (3) *Defuzzification*; in this module fuzzy outputs from the inference module

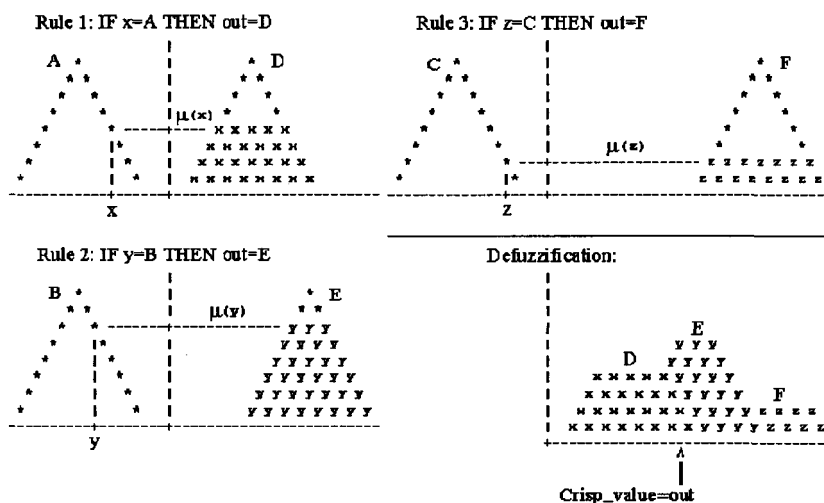


Fig. 7.58 Mamdani's Min-Max inference method and Center of Gravity defuzzification.

are converted to numerical crisp values; this is achieved by one of the several defuzzification algorithms; the most common is the Center of Gravity method, in which the crisp output value is calculated as the abscissa under the center of gravity of the output fuzzy set (see Figure 7.58).

In more complex technical applications of general function approximation (like in complex control systems, signal and image processing, etc.), two optional blocks are usually added to the fuzzy inference engine [Kosko (1992); Kosko (1996); Lee (1990)]:

(0) *Preprocessor*, preceding the fuzzification module, performing various kinds of normalization, scaling, filtering, averaging, differentiation or integration of input data; and

(4) *Postprocessor*, succeeding the defuzzification module, performing the analog operations on output data.

Common fuzzy systems have a simple feedforward mathematical structure, the so-called *Standard Additive Model* (SAM), which aids the spread of applications. Almost all applied fuzzy systems use some form of SAM, and some SAMs in turn resemble the ANN models (see [Kosko (1999)]).

In particular, an *additive fuzzy system*  $F : \mathbb{R}^n \rightarrow \mathbb{R}^p$  stores  $m$  rules of the patch form  $A_i \times B_i \subset \mathbb{R}^n \times \mathbb{R}^p$ , or of the word form 'If  $X = A_i$  Then  $Y = B_i$ ' and adds the 'fired' Then-parts  $B'_i(x)$  to give the output set  $B(x)$ ,

calculated as

$$B(x) = w_i B'_i(x) = w_i \mu_i(x) B_i(x), \quad (i = 1, \dots, n), \quad (7.116)$$

for a scalar rule weight  $w_i > 0$ . The factored form  $B'_i(x) = \mu_i(x) B_i(x)$  makes the additive system (7.116) a SAM system. The fuzzy system  $F$  computes its output  $F(x)$  by taking the centroid of the output set  $B(x)$ :  $F(x) = \text{Centroid}(B(x))$ . The *SAM theorem* then gives the centroid as a simple ratio,

$$F(x) = p_i(x) c_i, \quad (i = 1, \dots, n),$$

where the convex coefficients or discrete probability weights  $p_i(x)$  depend on the input  $x$  through the ratios

$$p_i(x) = \frac{w_i \mu_i(x) V_i}{w_k \mu_k(x) V_k}, \quad (i = 1, \dots, n). \quad (7.117)$$

$V_i$  is the finite positive volume (or area if  $p = 1$  in the codomain space  $\mathbb{R}^p$ ) [Kosko (1999)],

$$V_i = \int_{\mathbb{R}^p} b_i(y_1, \dots, y_p) dy_1 \dots dy_p > 0,$$

and  $c_i$  is the centroid of the Then-part set  $B_i(x)$ ,

$$c_i = \frac{\int_{\mathbb{R}^p} y b_i(y_1, \dots, y_p) dy_1 \dots dy_p}{\int_{\mathbb{R}^p} b_i(y_1, \dots, y_p) dy_1 \dots dy_p}.$$

### 7.8.3 Fuzzy Logic Control

The most common and straightforward applications of fuzzy logic are in the domain of nonlinear control [Kosko (1992); Kosko (1996); Lee (1990); Dote *et al.* (1996)]. Fuzzy control is a nonlinear control method based on fuzzy logic. Just as fuzzy logic can be described simply as computing with words rather than numbers, fuzzy control can be described simply as control with sentences rather than differential equations.

A fuzzy controller is based on the fuzzy inference engine, which acts either in the feedforward or in the feedback path, or as a supervisor for the conventional PID controller.

A fuzzy controller can work either directly with fuzzified dynamical variables, like direction, angle, speed, or with their fuzzified errors and rates of change of errors. In the second case we have rules of the form:

- (1) If error is *Neg* and change in error is *Neg* then output is *NB*.
- (2) If error is *Neg* and change in error is *Zero* then output is *NM*.

The collection of rules is called a rule base. The rules are in *IF – THEN* format, and formally the *IF*–side is called the condition and the *THEN*–side is called the conclusion (more often, perhaps, the pair is called antecedent – consequent). The input value *Neg* is a linguistic term short for the word Negative, the output value *NB* stands for *Negative\_Big* and *NM* for *Negative\_Medium*. The computer is able to execute the rules and compute a control signal depending on the measured inputs error and change in error.

The rulebase can be also presented in a convenient form of one or several rule matrices, the so-called *FAM*–matrices, where *FAM* is a shortcut for Kosko's *fuzzy associative memory* [Kosko (1992); Kosko (1996)]. For example, a  $9 \times 9$  graded FAM matrix can be defined in a symmetrical weighted form:

$$\text{FAM} = \begin{pmatrix} 0.6S4 & 0.6S4 & 0.7S3 & \dots & \text{CE} \\ 0.6S4 & 0.7S3 & 0.7S3 & \dots & 0.9B1 \\ 0.7S3 & 0.7S3 & 0.8S2 & \dots & 0.9B1 \\ \dots & \dots & \dots & \dots & 0.6B4 \\ \text{CE} & 0.9B1 & 0.9B1 & \dots & 0.6B4 \end{pmatrix},$$

in which the vector of nine linguistic variables  $L^9$  partitioning the *universes of discourse* of all three variables (with trapezoidal or Gaussian bell-shaped *membership functions*) has the form

$$L^9 = \{S4, S3, S2, S1, CE, B1, B2, B3, B4\}^T,$$

to be interpreted as: 'small 4', ... , 'small 1', 'center', 'big 1', ... , 'big 4'. For example, the left upper entry (1, 1) of the FAM matrix means: IF red is S4 and blue is S4, THEN result is 0.6S4; or, entry (3, 7) means: IF red is S2 and blue is B2, THEN result is center, etc.

Here we give design examples for two fuzzy controllers.

**Fan: the Temperature Control System.** In this simple example, the input linguistic variable is:

$$\text{temperature\_error} = \text{desired\_temperature} - \text{current\_temperature}.$$

The two output linguistic variables are:

*hot\_fan\_speed*, and *cool\_fan\_speed*. The universes of discourse, consisting

of membership functions, i.e., overlapping triangular–trapezoidal shaped intervals, for all three variables are:

*invar:*  $temperature\_error = \{Negative\_Big, Negative\_Medium, Negative\_Small, Zero, Positive\_Small, Positive\_Medium, Positive\_Big\}$ , with the range  $[-110, 110]$  degrees;

*outvars:*  $hot\_fan\_speed$  and  $cool\_fan\_speed = \{zero, low, medium, high, very\_high\}$ , with the range  $[0, 100]$  rounds-per-meter.

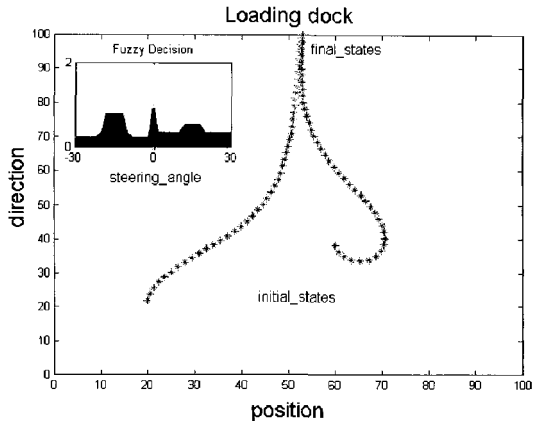


Fig. 7.59 Truck backer–upper steering control system.

**Truck Backer–Upper Steering Control System.** In this example there are two input linguistic variables: position and direction of the truck, and one output linguistic variable: steering angle (see Figure 7.59). The universes of discourse, partitioned by overlapping triangular–trapezoidal shaped intervals, are defined as:

*invars:*  $position = \{NL, NS, ZR, PS, PL\}$ , and

$direction = \{NL, NM, NS, ZR, PS, PM, PL\}$ , where *NL* denotes Negative\_Large, *NM* is Negative\_Medium, *NS* is Negative\_Small, etc.

*outvar:*  $steering\_angle = \{NL, NM, NS, ZR, PS, PM, PL\}$ .

The rule–base is given as:

If direction is *NL* and position is *NL*, Then steering angle is *NL*;

If direction is *NL* and position is *NS*, Then steering angle is *NL*;

If direction is *NL* and position is *ZR*, Then steering angle is *PL*;

If direction is *NL* and position is *PS*, Then steering angle is *PL*;

If direction is *NL* and position is *PL*, Then steering angle is *PL*;

If direction is *NM* and position is *NL*, Then steering angle is *ZR*;

.....  
 If direction is *PL* and position is *PL*, Then steering angle is *PL*.

The so-called *control surface* for the truck backer-upper steering control system is depicted in Figure 7.60.

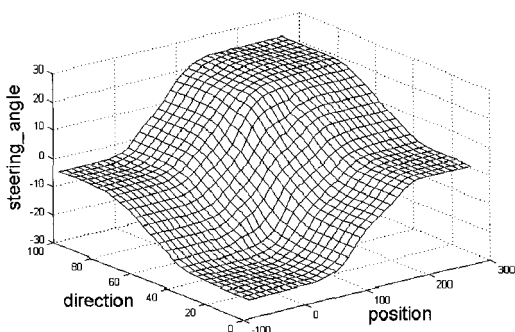


Fig. 7.60 Control surface for the truck backer-upper steering control system.

To distinguish between more and less important rules in the knowledge base, we can put weights on them. Such weighted knowledge base can be then trained by means of artificial neural networks. In this way we get *hybrid neuro-fuzzy trainable expert systems*.

Another way of the hybrid neuro-fuzzy design is the fuzzy inference engine such that each module is performed by a layer of hidden artificial neurons, and ANN-learning capability is provided to enhance the system knowledge (see Figure 7.61).

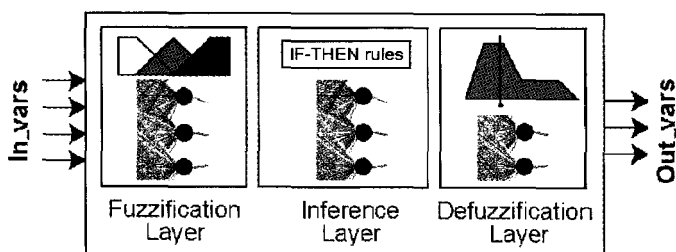


Fig. 7.61 Neuro-fuzzy inference engine.

Again, the fuzzy control of the BP learning (7.185–7.186) can be implemented as a set of heuristics in the form of fuzzy *IF – THEN* rules, for



the purpose of achieving a faster rate of convergence. The heuristics are driven by the behavior of the instantaneous sum of squared errors.

Finally, most *feedback fuzzy systems* are either discrete or continuous generalized SAMs [Kosko (1999)], given respectively by

$$x(k+1) = p_i(x(k))B_i(x(k)), \quad \text{or} \quad \dot{x}(t) = p_i(x(t))B_i(x(t)),$$

with coefficients  $p_i$  given by (7.117) above.

### 7.8.3.1 Fuzzy Control of Biodynamic Jerks

Recall from chapter 2, that according to OGY [Ott *et al.* (1990)], the simplest way to control the chaos is to adjust the parameters of a system to a regime of periodic rather than chaotic oscillation. This can be quite easily done by means of fuzzy-logic robust control. To control the nonlinear trigonometric coupling term (4.183) in the biodynamic jerk functions (4.179–4.180) and (4.181–4.182), we can use fuzzy-implication rules, like

If  $d_{KY}$  is very large or  $h_{KS}$  is very large, then  $\sigma_i$  is very large and/or  $\sigma_j$  is very small.

If  $d_{KY}$  is very small or  $h_{KS}$  is very small, then  $\sigma_i$  is very small and/or  $\sigma_j$  is very large.

Here  $\sigma_{i,j}$  denote two sample control parameters (e.g., inertia moments of body segments with respect to different Euler axes of rotation), while  $d_{KY}$  and  $h_{KS}$  are Kaplan–Yorke dimension and Kolmogorov–Sinai entropy, respectively. For these rules we can assign appropriate nonlinear membership functions  $\sigma_{i,j}(d_{KY})$  and  $\sigma_{i,j}(h_{KS})$ .

Otherwise, we can use the *occasional proportional feedback* [Hunt (1991); Lindner and Ditto (1995)], which is a variant of the original OGY chaos control method. Instead of using the unstable manifold of the attractor to compute corrections, it uses one of the dynamical variables, in a type of one-dimensional OGY method. This feedback could be applied continuously or discretely in time; in occasional proportional feedback it is applied discretely. Occasional proportional feedback exploits the strongly dissipative nature of the flows often encountered, enabling one to control them with a one-dimensional map. The method is easy to implement, and in many cases one can stabilize high period unstable orbits by using multiple corrections per period. It is a suitable method on which to base a fuzzy logic technique for the control of chaos, since it requires no knowledge of a system model, but merely an accessible system parameter [Calvo (1998)]. This technique can also be applied for control of the nonlinear trigonometric

coupling term (4.183) in the biodynamic jerk functions.

### 7.8.3.2 Characteristics of Fuzzy Control

Fuzzy logic offers several unique features that make it a particularly good choice for many control problems, among them [Lee (1990); Dote *et al.* (1996)]:

- (1) It is inherently robust since it does not require precise, noise-free inputs and can be programmed to fail safely if a feedback sensor quits or is destroyed. The output control is a smooth control function despite a wide range of input variations.
- (2) Since the fuzzy logic controller processes user-defined rules governing the target control system, it can be modified and tweaked easily to improve or drastically alter system performance. New sensors can easily be incorporated into the system simply by generating appropriate governing rules.
- (3) Fuzzy logic is not limited to a few feedback inputs and one or two control outputs, nor is it necessary to measure or compute rate-of-change parameters in order for it to be implemented. Any sensor data that provides some indication of a systems actions and reactions is sufficient. This allows the sensors to be inexpensive and imprecise thus keeping the overall system cost and complexity low.
- (4) Because of the rule-based operation, any reasonable number of inputs can be processed (1-8 or more) and numerous outputs (1-4 or more) generated, although defining the rulebase quickly becomes complex if too many inputs and outputs are chosen for a single implementation since rules defining their interrelations must also be defined. It would be better to break the control system into smaller chunks and use several smaller fuzzy logic controllers distributed on the system, each with more limited responsibilities.
- (5) Fuzzy logic can control nonlinear systems that would be difficult or impossible to model mathematically. This opens doors for control systems that would normally be deemed unfeasible for automation.

A *fuzzy logic controller* is usually designed using the following steps:

- (1) Define the control objectives and criteria: What am I trying to control? What do I have to do to control the system? What kind of response do I need? What are the possible (probable) system failure modes?

- (2) Determine the input and output relationships and choose a minimum number of variables for input to the fuzzy logic engine (typically error and rate-of-change of error).
- (3) Using the rule-based structure of fuzzy logic, break the control problem down into a series of *IF X AND Y THEN Z* rules that define the desired system output response for given system input conditions. The number and complexity of rules depends on the number of input parameters that are to be processed and the number fuzzy variables associated with each parameter. If possible, use at least one variable and its time derivative. Although it is possible to use a single, instantaneous error parameter without knowing its rate of change, this cripples the systems ability to minimize overshoot for a step inputs.
- (4) Create fuzzy logic membership functions that define the meaning (values) of Input/Output terms used in the rules.
- (5) Test the system, evaluate the results, tune the rules and membership functions, and re-test until satisfactory results are obtained.

Therefore, fuzzy logic does not require precise inputs, is inherently robust, and can process any reasonable number of inputs but system complexity increases rapidly with more inputs and outputs. Distributed processors would probably be easier to implement. Simple, plain-language rules of the form *IF X AND Y THEN Z* are used to describe the desired system response in terms of linguistic variables rather than mathematical formulas. The number of these is dependent on the number of inputs, outputs, and the designers control response goals. Obviously, for very complex systems, the rule-base can be enormous and this is actually the only drawback in applying fuzzy logic.

### 7.8.3.3 *Evolving Connectionist Systems*

Recently, [Kasabov (2002)] introduced a new type of fuzzy inference systems, denoted as dynamic evolving neuro-fuzzy inference system (DENFIS), for adaptive online and off-line learning, and their application for dynamic time series prediction. *DENFIS system* evolves through incremental, hybrid (supervised/ unsupervised), learning, and accommodates new input data, including new features, new classes, etc., through local element tuning. New fuzzy rules are created and updated during the operation of the system. At each time moment, the output of DENFIS is calculated through a fuzzy inference system based on *m*-most activated fuzzy rules which are dynamically chosen from a fuzzy rule set. Two approaches are

proposed: (i) dynamic creation of a first-order Takagi-Sugeno-type (see, e.g., [Tanaka and Wang (2001)]) fuzzy rule set for a DENFIS online model; and (ii) creation of a first-order Takagi-Sugeno-type fuzzy rule set, or an expanded high-order one, for a DENFIS offline model. A set of fuzzy rules can be inserted into DENFIS before or during its learning process. Fuzzy rules can also be extracted during or after the learning process. An evolving clustering method (ECM), which is employed in both online and off-line DENFIS models, is also introduced. It was demonstrated that DENFIS could effectively learn complex temporal sequences in an adaptive way and outperform some well-known, existing models.

#### 7.8.4 High-Resolution FAM Agents

In this subsection we extend the realm of biodynamics into the real-world *human performance modelling*.

Recall that the *agent theory* concerns the definition of BDI<sup>11</sup> agents and multi-agent systems, properties, architectures, communication, cooperation and coordination capabilities (see [Rao and Georgeff (1998)]). Its practical side concerns the agent languages and platforms for programming and experimenting with agents. According to [Ferber (1999)], a *BDI agent* is a physical or virtual entity which: (i) is capable of acting in an environment, (ii) can communicate directly with other agents, (iii) is driven by a set of tendencies (in the form of individual objectives or of a satisfaction/survival function which it tries to optimize), (iv) possesses resources of its own, which is capable of perceiving its environment (but to a limited extent), (v) has only a partial representation of its environment (and perhaps none at all), (vi) possesses skills and can offer services, (vii) may be able to reproduce itself, (viii) whose behavior tends towards satisfying its objectives, taking account of the resources and skills available to it and depending on its perception, its representation and the communications it receives. Agents' actions affect the environment which, in turn, affects future decisions of agents.

Multi-agent systems have already been successfully applied in numerous fields (see [Ferber (1999)] for the review). For example, the emerging field of *cellular robotics* relates to building robots on modular basis: a robot (say a manipulator arm), is considered as a multi-agent system, and each of its constituent parts (arm segments) is regarded as an agent (with the joints describing constraints on the set of acceptable movements). The coordi-

---

<sup>11</sup>BDI stands for 'belief', 'desire' and 'intention'.

nation of movement is thus a result of coordination involving an assembly of agents. It has been claimed that techniques similar to those used for modelling the multi-agent based eco-systems make it possible to accomplish complex movements with a minimum of computation. The head agent attempts to achieve the goal which has been set for it: if it can do it itself, it makes the movement and the system comes to a halt; if not, it brings in the neighboring agent, giving it goals which will help the head agent to get nearer to its objective. The process is repeated recursively, each agent trying to achieve the goals set for it by transmitting its desiderata to the neighboring agent.

This concept looks fine at the *low resolution level*. However, if we want a more sophisticated, high-resolution behavior of the arm manipulator, then we need to calculate a few derivatives of the nice and simple command 'Move'. This would give us proper robot kinematics: velocities and accelerations. In addition, if we want some more realism, we need to include inertial, gravity and friction forces, as well as to compensate them by driving forces. In this way we come to the proper dynamical system. Even further, to make it a proper control system, we need to add some feedbacks.

In the next subsection we propose a *high-resolution agent model*, suitable for human performance modelling.

#### 7.8.4.1 Generic Nonlinear MIMO Systems

In our opinion, a *good model* for human behavior/performance, i.e., a *model with both explanatory and predictive power*, is a nonlinear, multiple-input multiple-output (MIMO) *hybrid system*, predominantly continuous-time and smooth, but at the same time allowing discrete-time control and adaptation. It is based on (and resembling) a *real-life situation*, including noise, uncertainty, imprecision and misinformation. At the same time, to be a good predictor, it needs *full observability* and *controllability*, together with *stability* (as required by control theory [Isidori (1989); Nijmeijer and van der Schaft (1990)]), as well as *adaptability* (as required by complexity theory, see [Bar-Yam (1997)]). The main difference between our proposed approach and the standard control approach is that in addition to *immediate feedbacks*, we also have *long-term rewards*, which update the system parameters by means of human-like *trial-and-error*, thus *reinforcing* the change of long-term system behavior [Sutton and Barto (1998)]. Now, without denying both cybernetic and psychological values of feedback and reward, in our approach their role is to adjust, in discrete time steps

(as they are of lesser importance), only the system parameters, and not the system structure, which is predefined by the *instruction*; in other words, learning and training makes only local discrete-time adjustments to the global continuous-time dynamics predefined by the instruction.

The modelling tool that we use for this objective we call *adaptive fuzzy dynamics*. It consists of robust, observable, controllable and trainable, continuous-time, fuzzy-logic based MIMO systems, composed and fused in various ways. Our basic system has the form

$$\begin{array}{ccc} \text{INPUT} & \xrightarrow[\text{FAM}]{f} & \text{OUTPUT} \\ \text{SPACE} & & \text{SPACE} \end{array}$$

where  $\text{INPUT}_{\text{SPACE}}$  and  $\text{OUTPUT}_{\text{SPACE}}$  are nonlinear functional spaces consisting of a certain number of adaptive *fuzzy processes* (i.e., temporal fuzzy variables), partitioned by overlapping membership functions, which are either standard triangular/trapesoidal functions, or Gaussian functions of the form  $\mu(z) = \exp \left[ \frac{-(z-m)^2}{2\sigma^2} \right]$ , where  $z = z(t)$  denotes any fuzzy variable, while  $m$  and  $\sigma$  are its adjustable parameters, mean and standard deviation, respectively.

The corresponding adaptive  $n \times m$ -dimensional map  $\mathbb{R}^n \xrightarrow[\text{FAM}]{f} \mathbb{R}^m$  denotes the generalized *fuzzy associative memory* (FAM) (see [Kosko (1992); Kosko (1996)]), i.e., (possibly sparse) matrix  $R^{ij}$  of fuzzy IF-THEN rules of the form:

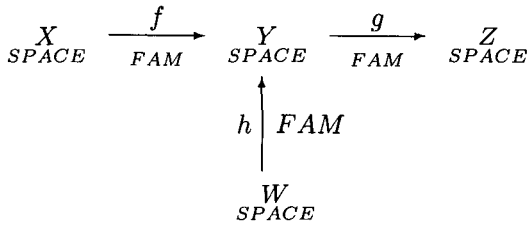
IF  $x_1$  is  $\mu(x)_1^i$  AND ...  $x_n$  is  $\mu(x)_n^i$  THEN  $y_1$  is  $\mu(y)_1^j$  AND ...  $y_m$  is  $\mu(y)_m^j$

each with its associated *rule-importance weight*  $w_{ij} \in [0, 1]$ .

To describe an adaptive FAM-map in plain English, consider the problem of teaching a violin to play some music: there is no known equation for mapping the music note inputs to the tonal frequencies coming out of the violin. However, by carefully observing an expert violin player, we can formulate an adaptive FAM-map to perform almost like him (as Japanese neuro-fuzzy-engineers already did in case of piano).

Given several FAM-maps, we will perform their *composition* as well as *fusion*<sup>12</sup> of the type

<sup>12</sup>This *input fusion* is similar to the *sensor fusion* usually performed by Kalman filters.



Using composition and fusion of FAM-maps, we can form hierarchical networks of nonlinear MIMO systems, for human behavior and performance modelling.

Both the rule-weights and Gaussian parameters (means and standard deviations) are adjusted using two forms of unsupervised trial-and-error learning: *Hebbian learning*, minimizing the error [Hebb (1949)] and *reinforcement learning*, maximizing the reward [Sutton and Barto (1998)]. We use both types of learning only as a minor parameter-adjusting tool, secondary to the primary fuzzy-logic *instruction*, setting-up the system's structure (i.e., FAM-map configuration). The learning is performed in discrete time steps, according to the general self-organized rule:

$$new\ value(n+1) = old\ value(n) + innovation(n)$$

The local learning/training dynamics is performed as a combination of two different ways:

- (1) Immediate, feedback-based, *Hebbian learning* rule [Hebb (1949)], occurring after each input-output system pass, comparing achieved output execution with the desired one and not considering the long-term rewards. Here the system learns its *optimal performance*:

$$innovation = |desired\ output - achieved\ output|$$

E.g., in case of the tennis game, this means the proper execution (i.e., precision, speed and spin) of the shot, without regard to the winning-points. It follows the simple tactic: 'Let me do my best shot, regardless of the opponent's actions'.

- (2) Long-term, reward-based, *reinforcement learning* rule [Sutton and Barto (1998)], occurring only after winning points and remembering the rewards. Here the system learns its *optimal policy*:

$$innovation = |reward - penalty|$$

In the tennis case, this means only the winning-point, no matter what was the actual execution of the shot. It follows the competitive tactics: 'The goal is to beat the opponent, no matter how (within the rules)'.

#### 7.8.4.2 *Alternative MIMO Systems*

Naturally a question arises: Why using adaptive FAM maps? Signals and MIMO systems are OK, but perhaps the same job could be done using some other, more appealing methodology instead of fuzzy. Let us consider other candidates for modelling *nonlinear adaptive complex systems*.

The first idea flashing in mind of a technically advanced reader, with a background combining control-engineering with Bayesian probability, is clear: *Kalman filter* (see subsection 6.6 above). It was developed by Rudolph Kalman in 1960 [Kalman (1960)], as a solution to the optimal estimator problem, based on Kalman's modular linear state-space theory of MIMO systems (in particular his optimal quadratic regulator). Kalman filter is the single most powerful and most popular algorithm and system of modern engineering. In 1960s, much before AI was born, it helped put men on the moon and bring them back; even today, it is the core of the Space Shuttle control system. If we insist on nonlinearity, there is an extended Kalman filter; if we insist on adaptivity, there is an adaptive Kalman filter. If we insist on continuous-time, there is the Kalman-Bucy smoother [Stevens and Lewis (2003)]. It is clear that, instead of any of our FAM-maps, we could use an adaptive, extended, continuous-time Kalman filter. However, to design the working chain of 20–30 interactive  $n$ D Kalman filters is most likely beyond comprehension.

The second idea flashing in mind of a mathematically advanced reader, with a background combining differential geometry and modern nonlinear control, would be *adaptive Lie-derivative* based controller [Sastri and Isidori (1989)]. Although, in practice such systems work much better as single-input single-output (SISO) controllers than MIMO ones, in theory it is possible to construct any nonlinear MIMO map using this methodology (see [Isidori (1989); Nijmeijer and van der Schaft (1990)]). So, we might say that, instead of any of our FAM-maps, we could use adaptive nonlinear MIMO map. However, to design the working chain of 20–30 of such maps is even further from comprehension than for Kalman filters.

Next come artificial neural networks (ANNs), where the most powerful candidate clearly is Kosko's own continuous-time *bidirectional associative memory* (BAM) system [Kosko (1992)]. It is designed as a coupled



system of two continuous-time *Hopfield nets* [Hopfield (1984)], nonlinear operational amplifiers, which are today embedded in VLSI-chips. Clearly, each FAM-map can be replaced by the corresponding BAM-map. The only disadvantage is that any ANN, including BAM, is a *black box*, without possibility for *knowledge representation*. The same disadvantage applies to *genetic algorithms* [Goldberg (1988)], *cellular automata* [Bar-Yam (1997)], and general *evolutionary computation* (see MIT journal with the same name), applied either alone or in conjunction with ANNs: no matter how we design or combine these popular soft-computing paradigms, the end-product is a black box, without any knowledge transparency.

Finally, the so-called 'strong AI expert systems' might do the same job. Recall that conventional expert systems have the following structure (MYCIN, developed in mid 1970s by E. Shortliffe): (i) Knowledge base (rules); (ii) Data Base (individual facts); and (iii) Inference Engine. Knowledge base and database resemble the first two premises of a syllogism; the inference engine descended from the first AI program, 'Logic Theorist', invented by A. Newell and H. Simon in 1956.

Most conventional expert systems are decision trees, or gardens of forking paths. They make one yes/no decision, then move on to another, and another. In general, according to Kosko [Kosko (1992)], a decision tree has four drawbacks: (i) It is prone to closed loops, in which the software reads both IF A THEN DO B and IF B THEN DO A and spins off to infinity. (ii) It is slow, and the more rules it has, the more 'koala-like' it becomes – it could hardly ever guide a robot across the room. (iii) It does not use all the data. The paths are independent. Instead, we want them to blend, but without causing closed loops. (iv) It is not combinable. As Kosko says, "A tree plus a tree does not equal a tree. This is the curse of AI. If you add three, four, or many expert systems, you will likely have a structure peppered with closed loops."

Fuzzy expert systems merge the rules. Instead of forking paths, the system takes many paths at once – it works in parallel. They work very much like the first fuzzy controller, Mamdani's steam plant: firing rules partially and fusing them for a result.

Fuzzy logic also addresses other problems with conventional expert systems. One, of course, is representing fuzziness itself while classical systems like MYCIN completely ignore the fundamental informational fuzziness.

Kosko contrasts AI and neural nets with fuzzy systems [Kosko (1992)]. He notes that traditional AI expert system is one-dimensional and its basic

unit is the symbol, a large, awkward item. Yet it also has structure, that is rules, and rules are priceless shortcuts. "The good news is you can represent structure in knowledge," he says. "The bad news is you can't do much with it because it's symbolically represented. In other words, you cannot take the derivative of a symbol. So the entire framework of mathematics and most of the hardware techniques for making chips are not available to you in AI."

Neural nets are just the opposite. They have the advantage of number. "You can prove theorems and you can build chips. The problem is that neural nets are unstructured." They cannot handle rules. For instance, a traffic-control system attempts to spur the flow of cars through city streets. What should it do if traffic grows heavier in one direction? The answer is pure common sense: Keep the green lights on longer. Unfortunately, one cannot just tell a neural network to do that. "You have to give it lots and lots and lots of examples," Kosko says, "and then maybe it'll learn."

Moreover, like brains, neural nets do not have indelible memory. They are volatile. Kosko continues, "You can't be sure it won't forget it when it learns new thing. And that's the problem with neural networks, and that's why you do not have neural network devices in the office, in the factory."

Adaptive fuzzy system is the best of both worlds. It has a rule-based structure like traditional AI expert systems. It also shows the mathematics of neural nets, and thus chips and learning.

In this way, adaptive FAM-maps represent today the only practically-realizable way to model predictable and controllable systems of the necessary complexity required for predictive human performance modelling, with the full knowledge transparency.

#### 7.8.4.3 *Biodynamics Example: Tennis Game*

In this subsection we will formulate a continuous-time *attack* (AT) and *counter-attack* (CA) model for the *tennis game* (with discrete-time learning). Tennis represents a competitive real-life situation within fully controlled conditions, depending on the individual's technical<sup>13</sup>, tactical<sup>14</sup> and strategic<sup>15</sup> skills as well as operational psycho-physical strengths. Here, we will formulate an adaptive, fuzzy-dynamics AT & CA, tennis perfor-

<sup>13</sup> *Technical skills* in sports are judged by the *biomechanical correctness of movements*.

<sup>14</sup> *Tactical skills* in sports include 'winners', 'changes of tempo', and 'applying pressure'.

<sup>15</sup> *Strategic skills* in sports include 'planning ahead' and 'weighting the relative importance of points' along the match.

mance model. Using compositions and fusions of FAM-maps (as described above), we will design a generic simulator for counter-attack and attack performance dynamics, based on the tennis game. We have chosen the tennis game as it allows: (i) complete analysis in every detail, (ii) full experimental validation, and (iii) training both in real-life situations and in a machine-learning environment.

### Attack Model: Tennis Serve

*A. Simple Attack: Serve Only.* The simple AT-dynamics is represented by a single FAM map

$$\begin{array}{ccc} \text{TARGET} & \xrightarrow[\text{FAM}]{f^{AT}} & \text{ATTACK} \\ \text{SPACE} & & \text{SPACE} \end{array}$$

In the case of simple tennis serve, this AT-scenario reads

$$\begin{array}{ccc} O \ni o_m & \xrightarrow{f^{AT}} & SR \ni sr_n \\ \text{OPPONENT-IN} & & \text{SERVE-OUT} \end{array}$$

where the two functional spaces,  $O_{\dim=2} \ni o_m$  and  $SR_{\dim=3} \ni sr_n$ , contain the fuzzy variables  $\{o_m = o_m(t)\}$  and  $\{sr_n = sr_n(t)\}$ , respectively opponent-related (target information) and serve-related, partitioned by overlapping Gaussians,  $\mu(z) = \exp \left[ \frac{-(z-m)^2}{2\sigma^2} \right]$ , and defined as:

$$\begin{array}{l} O_{\text{OPPONENT-IN}} : \\ o_1 = \text{Opp.Posit.Left.Right} : (\text{center, medium, wide}), \\ o_2 = \text{Opp.Anticip.Left.Right} : (\text{runCenter, stay, runWide}), \\ \\ sr_1 = 1.\text{Serve.Speed} : (\text{low, medium, high}) \\ SR_{\text{SERVE-OUT}} : sr_2 = 2.\text{Serve.Spin} : (\text{low, medium, high}) \\ sr_3 = 3.\text{Serve.Placement} : (\text{center, medium, wide}) \end{array}$$

In the fuzzy-matrix form this simple serve reads

$$\begin{bmatrix} O: \text{OPPONENT-IN} \\ o_1 = \text{Opp.Posit.Left.Right} \\ o_2 = \text{Opp.Anticip.Left.Right} \end{bmatrix} \xrightarrow{f^{AT}} \begin{bmatrix} SR: \text{SERVE-OUT} \\ sr_1 = 1.\text{Serve.Speed} \\ sr_2 = 2.\text{Serve.Spin} \\ sr_3 = 3.\text{Serve.Place} \end{bmatrix}$$

**B. Attack-Maneuver: Serve-Volley.** The generic advanced AT-dynamics is given by a composition of FAM maps

$$\begin{array}{ccccc} \text{TARGET} & \xrightarrow{f^{AT}} & \text{ATTACK} & \xrightarrow{g^{AT}} & \text{MANEUVER} \\ \text{SPACE} & \text{FAM} & \text{SPACE} & \text{FAM} & \text{SPACE} \end{array}$$

In the case of advanced tennis serve, this AT-scenario reads

$$\begin{array}{ccccc} O \ni o_m & \xrightarrow{f^{AT}} & SR \ni sr_n & \xrightarrow{g^{AT}} & RV \ni rv_p \\ \text{OPPONENT-IN} & & \text{SERVE-OUT} & & \text{RUN-VOLEY} \end{array}$$

where the new functional space,  $RV_{\dim=2} \ni rv_p$ , contains the opponent-anticipation driven volley-maneuver, expressed by fuzzy variables  $\{rv_p = rv_p(t)\}$ , partitioned by overlapping Gaussians and given by:

$$\begin{array}{l} RV \\ \text{RUN-VOLEY} \end{array} : \begin{array}{l} rv_1 = RV.For : (baseLine, center, netClose) \\ rv_2 = RV.L.R. : (left, center, right) \end{array}$$

In the fuzzy-matrix form this advanced serve reads

$$\begin{array}{ccc} \begin{array}{l} O: \text{OPPONENT-IN} \\ \left[ \begin{array}{l} o_1 = \text{Opp.Posit.L.R.} \\ o_2 = \text{Opp.Anticip.L.R.} \end{array} \right] \end{array} & \xrightarrow{f^{AT}} & \begin{array}{l} SR: \text{SERVE-OUT} \\ \left[ \begin{array}{l} sr_1 = 1.\text{Serve.Speed} \\ sr_2 = 2.\text{Serve.Spin} \\ sr_3 = 3.\text{Serve.Place} \end{array} \right] \end{array} \\ & \xrightarrow{g^{AT}} & \begin{array}{l} RV: \text{RUN-VOLEY} \\ \left[ \begin{array}{l} rv_1 = RV.For \\ rv_2 = RV.L.R. \end{array} \right] \end{array} \end{array}$$

### Counter-Attack Model: Tennis Return

**A. Simple Return.** The simple CA-dynamics reads:

$$\begin{array}{ccccc} \text{ATTACK} & \xrightarrow{f^{CA}} & \text{MANEUVER} & \xrightarrow{g^{CA}} & \text{RESPONSE} \\ \text{SPACE} & \text{FAM} & \text{SPACE} & \text{FAM} & \text{SPACE} \end{array}$$

In the case of simple tennis return, this CA-scenario consists purely of conditioned-reflex reaction, no decision process is involved, so it reads:

$$\begin{array}{ccccc} B \ni b_i & \xrightarrow{f^{CA}} & R \ni r_j & \xrightarrow{g^{CA}} & S \ni s_k \\ \text{BALL-IN} & & \text{RUNNING} & & \text{SHOT-OUT} \end{array}$$

where the functional spaces  $B_{\dim=5} \ni b_i$ ,  $R_{\dim=3} \ni r_j$ ,  $S_{\dim=4} \ni s_k$ , contain the fuzzy variables  $\{b_i = b_i(t)\}$ ,  $\{r_j = r_j(t)\}$  and  $\{s_k = s_k(t)\}$ , respectively defining the ball inputs, our player's running maneuver and his

shot-response, i.e.,

$$\begin{array}{c} B: BALL-IN \\ \left[ \begin{array}{l} b_1 = Dist.L.R. \\ b_2 = Dist.F.B. \\ b_3 = Dist.Vert \\ b_4 = Speed \\ b_5 = Spin \end{array} \right] \xrightarrow{f^{CA}} \begin{array}{c} R: RUNNING \\ \left[ \begin{array}{l} r_1 = Run.L.R. \\ r_2 = Run.F.B. \\ r_3 = Run.Vert \end{array} \right] \xrightarrow{g^{CA}} \begin{array}{c} S: SHOT-OUT \\ \left[ \begin{array}{l} s_1 = Backhand \\ s_2 = Forehand \\ s_3 = Voley \\ s_4 = Smash \end{array} \right] \end{array}
 \end{array}$$

Here, the existence of efficient weapons within the  $_{SHOT-OUT}^S$  arsenal-space, namely  $s_k(t) : s_1 = Backhand, s_2 = Forehand, s_3 = Voley$  and  $s_4 = Smash$ , is assumed.

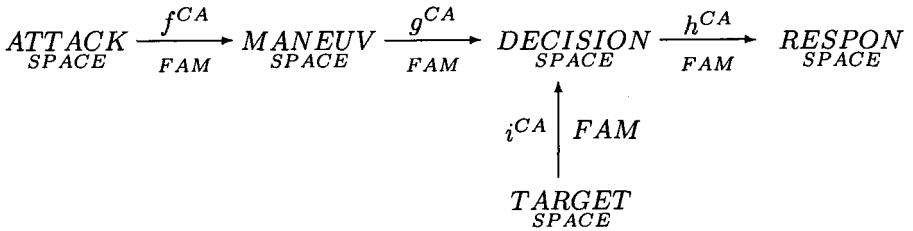
The universes of discourse for the fuzzy variables  $\{b_i(t)\}$ ,  $\{r_j(t)\}$  and  $\{s_k(t)\}$ , partitioned by overlapping Gaussians, are defined respectively as:

$$\begin{array}{c} B \\ BALL-IN : \end{array} \begin{array}{l} b_1 = Dist.L.R. : (veryLeft, left, center, right, veryRight), \\ b_2 = Dist.F.B. : (baseLine, center, netClose), \\ b_3 = Dist.Vert : (low, medium, high), \\ b_4 = Speed : (low, medium, high), \\ b_5 = Spin : (highTopSpin, lowTopSpin, flat, \\ lowBackSpin, highBackSpin). \end{array}$$

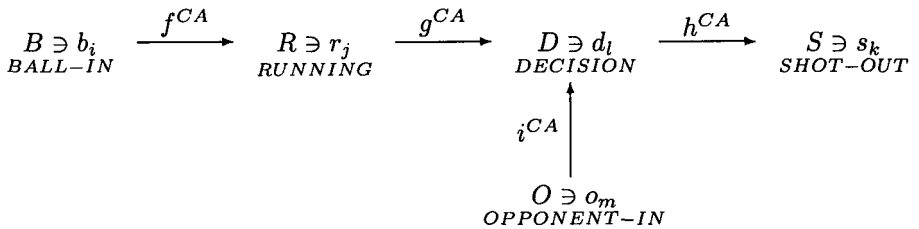
$$\begin{array}{c} R \\ RUNNING : \end{array} \begin{array}{l} r_1 = Run.L.R. : (veryLeft, left, center, right, veryRight), \\ r_2 = Run.F.B. : (closeFront, front, center, back, farBack), \\ r_3 = Run.Vert : (squat, normal, jump). \end{array}$$

$$\begin{array}{c} S \\ SHOT-OUT : \end{array} \begin{array}{l} s_1 = Backhand : (low, medium, high), \\ s_2 = Forehand : (low, medium, high), \\ s_3 = Voley : (backhand, block, forehand), \\ s_4 = Smash : (low, medium, high). \end{array}$$

*B. Advanced Return.* The advanced CA-dynamics includes both the information about the opponent and (either conscious or subconscious) decision making. This generic CA-scenario is formulated as composition + fusion of FAM maps:



where we have added two new functional spaces,  $\text{TARGET}_{\text{SPACE}}$  and  $\text{DECISION}_{\text{SPACE}}$ , respectively containing information about the opponent as a target, as well as our own aiming decision processes. In the case of advanced tennis return, this reads:



where the two additional functional spaces,  $O_{\text{dim}=4} \ni o_m$  and  $D_{\text{dim}=5} \ni d_l$ , contain the fuzzy variables  $\{o_m = o_m(t)\}$  and  $\{d_l = d_l(t)\}$ , respectively defining the opponent-related target information and the aim-related decision processes, both partitioned by overlapping Gaussians and defined as:

$$\begin{array}{l}
 O_{\text{OPPONENT-IN}} : \begin{array}{l}
 o_1 = \text{Opp.Posit.L.R.} : (\text{left}, \text{center}, \text{right}), \\
 o_2 = \text{Opp.Posit.F.B.} : (\text{netClose}, \text{center}, \text{baseLine}), \\
 o_3 = \text{Opp.Anticip.L.R.} : (\text{runLeft}, \text{stay}, \text{runRight}), \\
 o_4 = \text{Opp.Anticip.F.B.} : (\text{runNet}, \text{stay}, \text{runBase}).
 \end{array}
 \end{array}$$

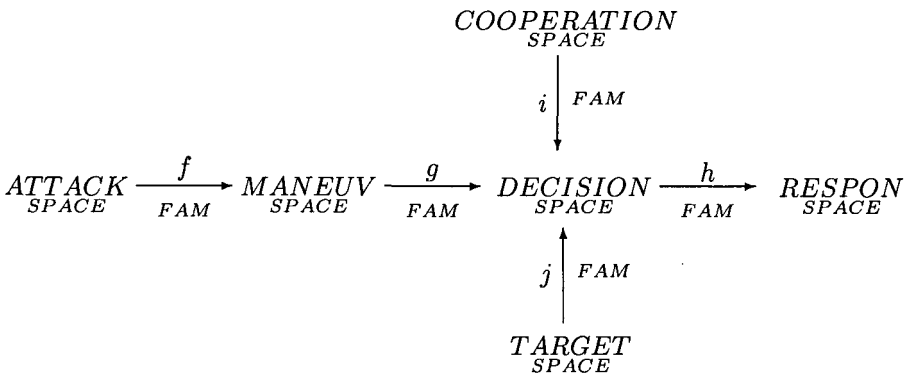
$$\begin{array}{l}
 D_{\text{DECISION}} : \begin{array}{l}
 d_1 = \text{Aim.L.R.} : (\text{left}, \text{center}, \text{right}), \\
 d_2 = \text{Aim.F.B.} : (\text{netClose}, \text{center}, \text{baseLine}), \\
 d_3 = \text{Aim.Vert} : (\text{low}, \text{medium}, \text{high}), \\
 d_4 = \text{Aim.Speed} : (\text{low}, \text{medium}, \text{high}), \\
 d_5 = \text{Aim.Spin} : (\text{highTopSpin}, \text{lowTopSpin}, \text{noSpin}, \\
 \text{lowBackSpin}, \text{highBackSpin}).
 \end{array}
 \end{array}$$

The corresponding fuzzy-matrices read:

$$\begin{array}{l}
 \begin{array}{l}
 B: \text{BALL-IN} \\
 \left[ \begin{array}{l}
 b_1 = \text{Dist.L.R.} \\
 b_2 = \text{Dist.F.B.} \\
 b_3 = \text{Dist.Vert} \\
 b_4 = \text{Speed} \\
 b_5 = \text{Spin}
 \end{array} \right],
 \end{array}
 \begin{array}{l}
 R: \text{RUNNING} \\
 \left[ \begin{array}{l}
 r_1 = \text{Run.L.R.} \\
 r_2 = \text{Run.F.B.} \\
 r_3 = \text{Run.Vert}
 \end{array} \right],
 \end{array}
 \begin{array}{l}
 D: \text{DECISION} \\
 \left[ \begin{array}{l}
 d_1 = \text{Aim.L.R.} \\
 d_2 = \text{Aim.F.B.} \\
 d_3 = \text{Aim.Vert} \\
 d_4 = \text{Aim.Speed} \\
 d_5 = \text{Aim.Spin}
 \end{array} \right],
 \end{array}
 \end{array}$$

$$\begin{array}{l}
 \begin{array}{l}
 O: \text{OPPONENT-IN} \\
 \left[ \begin{array}{l}
 o_1 = \text{Opp.Posit.L.R.} \\
 o_2 = \text{Opp.Posit.F.B.} \\
 o_3 = \text{Opp.Anticip.L.R.} \\
 o_4 = \text{Opp.Anticip.F.B.}
 \end{array} \right],
 \end{array}
 \begin{array}{l}
 S: \text{SHOT-OUT} \\
 \left[ \begin{array}{l}
 s_1 = \text{Backhand} \\
 s_2 = \text{Forehand} \\
 s_3 = \text{Voley} \\
 s_4 = \text{Smash}
 \end{array} \right].
 \end{array}
 \end{array}$$

**Generic FAM-Agents.** Finally, we briefly describe a generic *FAM-agent* as a following complex adaptive system, designed from five adaptive FAM-maps and six hybrid functional spaces:



Each generic FAM-agent is supposed to communicate with other FAM-agents and/or environment only by its inputs and outputs. It is both a feedback control system and an expert system, implementing: (i) feedbacks, (ii) instructions and (iii) common sense. It is a high-resolution human performance predictor-corrector system, which has to be designed in each specific case by consulting an expert from the field.

A *smart multi-agent organization* represents a brain-like sensory-motor system-of-systems, including hierarchical networks of generic FAM-agents, with the unique input and output. It is designed for the real-time implementation in the fastest Delphi-compiler for MS Windows.

## 7.9 Natural System in a Category

In this section we develop a categorical concept of *natural* and *neural systems*. Mathematical models for complex systems, such as neural, biological or social systems, have been given by several authors, in the general framework of 'relational biology'. This framework was defined in four major steps (followed by a number of authors, including M. Arbib [Arbib (1966); Arbib (1987)]):

- Rosen's [Rosen (1958)] theory of  $(M, R)$ -systems,
- Rashevsky's [Rashevsky (1967)] theory of *organismic* systems, and
- Louie's [Louie (1983)] theory of categorical systems *interacting with measuring devices*.
- A. Ehresmann's and Vanbremeersch's [Ehresmann and Vanbremeersch (1987); Ehresmann and Vanbremeersch (1996)] fully developed categorical theory of *natural* systems, which we present in this section in a form adapted for natural biodynamics.

### 7.9.1 Categorical Patterns and Hierarchical Links

In a category, a *pattern*  $P$  is modelled by the data of a family of objects  $N_i$  and of some distinguished links between them [Ehresmann and Vanbremeersch (1987); Ehresmann and Vanbremeersch (1996)]. A *collective link* from the pattern  $P$  to another object  $N'$  is a family of individual links  $f_i$  from each  $N_i$  to  $N'$ , correlated by the distinguished links of the pattern (see Figures 7.62 and 7.63 below).

The object binding the pattern (if it exists) in a category is modelled by the *colimit* (or *inductive limit*) [Kan (1958); MacLane (1971)] of the pattern. An object  $N$  is the colimit, or the binding, of the pattern  $P$  if it satisfies the two conditions:

1. There exists a collective link ( $c_i$ ) from the pattern to  $N$ ,
2. Each collective link ( $f_i$ ) from the pattern to any object  $N'$  binds into a unique arrow  $f$  from  $N$  to  $N'$ .

If a pattern has a colimit, it is unique (up to an isomorphism).

The situation can be seen 'upside-down': if an object  $N$  is the colimit of a pattern  $P$ , we say that  $N$  is a complex object admitting  $P$  as a *decomposition*. An object may have different decompositions. Indeed, while a pattern has at most one colimit (up to an isomorphism), several patterns may have the same colimit [Ehresmann and Vanbremeersch (1987);



Ehresmann and Vanbremeersch (1996)].

*Limit* (or *projective limit*) of a pattern  $P$  in a category actualizes the capacity of objects to collectively decode and classify information of which each receives only some part (see Figure 7.62).

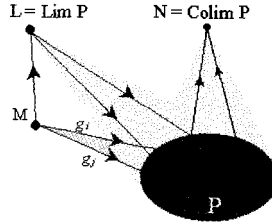


Fig. 7.62 A *limit* and a *colimit* of a *pattern* in a category.

A common message from an object  $M$  of the category to a pattern  $P$  is a family of individual links  $g_i$  from  $M$  to the  $N_i$ , which are correlated by the distinguished links of  $P$ . The limit of  $P$ , if it exists, is an object  $L$  which 'classifies' the common messages in the sense that the family  $(g_i)$  uniquely factors into an arrow  $g$  from  $M$  to  $L$ .

Formally, the *limit* is defined as the *colimit* of the pattern in the *dual* (opposite category).

In brain-like systems, the objects are partitioned into different complexity levels, each level satisfying its own rules. There are intra-level brain links, but also inter-level brain links. An object of brain level  $n + 1$  is an aggregate of objects of brain level  $n$ , bound by strong interactions between them which generate their cohesion in the brain aggregate.

Such a hierarchical brain-like organization is modelled in a category using the *colimit* operation [Kan (1958); MacLane (1971)]. A brain aggregate  $N$  can be modelled by the colimit of a brain pattern of linked objects representing its internal organization [Ehresmann and Vanbremeersch (1987); Ehresmann and Vanbremeersch (1996)].

A *pattern*  $P$  in a *brain category*  $\mathcal{B}$  is defined as a family of objects  $N_i$  of  $\mathcal{B}$  and some distinguished links between them [Ehresmann and Vanbremeersch (1987); Ehresmann and Vanbremeersch (1996)]. A *collective link* from  $P$  to an object  $N'$  is a family of arrows  $(f_i : N_i \rightarrow N')$  correlated by the distinguished arrows of the pattern. Collective links model coherent brain interactions (constraints, energy, or information transfer) effected by all the  $N_i$  acting in cooperation along their distinguished links, which could not be

realized by the objects of the pattern acting individually (see Figure 7.63).

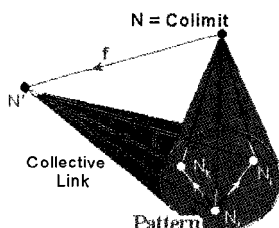


Fig. 7.63 A pattern in a category, a collective link, and a colimit.

A pattern  $P \in \mathcal{B}$  may have collective links toward several brain objects.  $P$  has an aggregate if, among those collective links, there is an 'optimal' one, i.e., a  $(c_i : N_i \rightarrow N)$  through which all the others factorize. In categorical terms, this means that  $N$  is the colimit of  $P$ ; we also say that  $N$  binds  $P$ , or, seen in the opposite direction, that  $P$  is a *decomposition* of the complex object  $N$ . The colimit has localized properties in being an objective representation of the brain pattern pattern it binds, that so acquires a dynamical stability; but it has also a 'global' implication for its surround through its 'universal' property of factorizing every collective link [Ehresmann and Vanbremeersch (1987); Ehresmann and Vanbremeersch (1996)].

The brain's colimit actualizes the potentiality of the objects to act together in a coherent manner by integrating the pattern in a higher unit. In a natural system where the links have a given 'strength', the formation of a colimit is characterized in two ways:

- (1) 'Locally and structurally', a strengthening of the distinguished brain links of the brain pattern restricts the DOF of the objects to ensure a more efficient cooperation among them;
- (2) 'Universally and functionally', the actions of the brain's colimit on the other objects of the brain system subsume the activity of the whole pattern (they correspond to its collective links).

The brain's colimit 'forgets' the precise organization of the brain pattern and records only its collective actions, and these can be the same for more or less differing brain patterns.

### 7.9.2 A General Natural System

The state of a *general natural system*, such as a neural, biological, or social system, at a given time  $t$  can be modelled by a category: its objects represent the components (of any level) of the system, and the morphisms their links in the system at this time. These links may represent more or less stable structural links such as causal or topological relations (e.g., desmosomes between adjacent cells), channels transmitting information, spatial or energetic constraints, or temporary interactions between two components (see [Ehresmann and Vanbremeersch (1987); Ehresmann and Vanbremeersch (1996)]).

The composite of two successive links  $N \rightarrow N'$  and  $N' \rightarrow N''$  represents the cumulative interaction from  $N$  to  $N''$  obtained by taking first the interaction from  $N$  to  $N'$ , then the interaction from  $N'$  to  $N''$ .

Thus an object  $N$  plays a double role:

- (1) It acts as an agent, or an emitter, through its links toward the other objects which represent its actions, or the messages it sends, and
- (2) It becomes a receptor, or an observer, through the links toward it, which correspond to the aspects it observes, or the information it receives, or the constraints which are imposed to it.

In a biological system, the identity of an object models its 'self'. The composition of links determines classes of paths which are 'functionally equivalent' (i.e., with the same practical effect), namely all the paths between two objects having the same composite; it allows to characterize the various temporally and energetically equivalent paths by which an information can be transmitted from a component to another one.

The system may have had some components before the time  $t$  which no more figure in it at  $t$ . These 'lost' components can be modelled by adding to the category a zero object (or initial object)  $0$ , i.e., an object such that there exists a unique link from  $0$  to any other object. We say that we have a category with a zero-object.

Categories modelling natural systems are often constructed in the following way [Ehresmann and Vanbremeersch (1987); Ehresmann and Vanbremeersch (1996)]. The graph  $G$  of generators is a *labelled graph* in the sense that a real number (or a vector), called its *arrow weight*, is associated to each arrow; this weight represents the force and/or the propagation delay with which information are transmitted by the arrow. A path of  $G$  is weighted by the sum of the weights of its factors; and the relations identify

two paths  $c$  and  $c'$  which have the same source, target and weight. The deduced category  $\mathcal{K}$  has for links from  $A$  to  $B$  classes of paths from  $A$  to  $B$  which have the same weight. It is a *weighted category* in the following sense: A category is weighted if it is a labelled graph and if the weight of a composite  $g \circ f$  is the sum of the weights of  $f$  and  $g$ .

### 7.9.3 The Category of Neurons

The *category of neurons*  $\mathcal{N}$  models a neuronal system at a given time  $t$ . It is constructed by the data of *generators* and *relations* [Ehresmann and Vanbreemersch (1987); Ehresmann and Vanbreemersch (1996)].

First we define the labelled graph  $G$  of its generators. Its vertices are the neurons; the activity of a neuron  $N$  at  $t$  is determined by its instantaneous frequency of spikes. An arrow from  $N$  to  $N'$  corresponds to a synapse such that  $N$  is the presynaptic neuron and  $N'$  the post-synaptic neuron. Let us remark that two neurons may be linked by one, several or no arrows. The weight of an arrow from  $N$  to  $N'$  represents the strength of the synapse, related to the probability that the activity of  $N$  be propagated to  $N'$  and to the delay of propagation. We adopt the usual convention that the activity of a neuron  $N$  is the summation of the activities of the neurons  $N_i$  to which it is linked, pondered by the weights of the synapses linking these  $N_i$  to  $N$ .

The category of paths  $\mathcal{C}$  on this graph admits the neurons for its objects, the links from  $N$  to  $N'$  are the paths formed by successive synapses, and the composition of paths is their concatenation. In this category, two paths from  $N$  to  $N'$  have the same weight if the activity of  $N$  is transmitted to  $N'$  in the same way along one of the other of the paths.

The category  $\mathcal{N}$  is deduced from the data of  $G$  and of the relations on  $\mathcal{C}(G)$  identifying two paths from  $N$  to  $N'$  which have the same weight. Thus its objects are still the neurons, but the links from  $N$  to  $N'$ , called *multisynaptic paths*, are classes of paths with the same weight. It is a weighted category.

### 7.9.4 Memory Evolutionary System

*Memory evolutionary system* (MES, for short [Ehresmann and Vanbreemersch (1987); Ehresmann and Vanbreemersch (1996)]) represents a categorical model to study biological, neural or social systems and to give plausible answers to several questions. The first question is how to model 'open' systems, whose components, with various complexity levels, change in time

through exchanges with the environment and through internal modifications such as the formation of new complex objects? This question has led to the introduction of the notion of an *evolutive system* (ES); in it the state of the system at a given time, with its components and their interactions, is modelled by a category; a 'complex' object is represented by the colimit (or inductive limit) of a pattern of linked objects standing for its internal organization; and the changes between successive states by 'transition' functors between the corresponding state categories. The ES is hierarchical if its objects are partitioned into complexity levels, so that an object of level  $n + 1$  is the colimit of a pattern of linked objects of level  $n$ . In an ES, the 'archetypal' changes (like birth/death) are modelled by a complexification process with respect to a 'strategy' of which the objectives are to add or suppress objects (external exchanges), and to form complex objects (adjunction of a colimit to a pattern) or to decompose complex objects.

This raises the problem of selection of strategies in an autonomous system. Whence the introduction of the notion of a partial internal *center of regulation* (CR), able to develop a stepwise 'trial-and-error' learning process, thanks to the formation, at each step, of its own internal (more or less deformed) representation of the system, its landscape, on which a strategy is selected.

The case of a neural system shows that its evolution depends on a whole net of competitive CRs. It has led to the definition of *memory evolutive systems* (MES): a MES is an ES with a net of cooperating/competitive CRs, which develop a hierarchical sub-ES, called *memory*, which allows to record past experiences in a flexible manner for a better later adaptation; each CR has its differential access to this memory. The links between objects have a 'strength' and a 'propagation delay' (represented by the set  $\mathbb{R}$  of real numbers).

In a MES, each  $CR_i$  acts on its landscape according to its own timescale, but the strategies of the different CRs compete for the common resources of the system, and at each time there is a 'play' among these possibly conflicting strategies, with a risk of fractures for some CRs; whence a dialectics between CRs which are heterogeneous by their complexity level and their timescale, generating the complexity of the system. Time has an essential role through the structural temporal constraints imposed on each CR, and repair processes develop for their being respected anew if they are transgressed. In particular, this leads to an aging theory for an organism based on a cascade of de/re-synchronizations for more and more complex CRs.

The problem of reductionism can be studied in the framework of MES:

an object of level  $n + 1$  is always the  $(n - k)$ -iterated colimit of a ramification [Ehresmann and Vanbremeersch (1987); Ehresmann and Vanbremeersch (1996)], based on the level  $k < n$ , but is it also 'reducible' to the level  $k$  in only one step, i.e., is it a simple colimit of a pattern of level  $k$ ? A more fine analysis of the form of the links between objects led to a characterization of such reducible objects, and proved that there exist non-reducible objects if the MES satisfies the multiplicity principle: there exist non-equivalent patterns which have the same colimit. In this case, a sequence of complexifications cannot be replaced by a unique complexification with respect to a strategy subsuming the intermediate strategies.

The preceding results applied to a neural system allow to describe an 'algebra of mental objects', and they explain the development of a procedural memory, and the formation of higher order cognitive processes. They suggest an approach to the mind/body problem: mental states are not simple physical states of the brain (activation of synchronous assemblies of neurons), but they dynamically supervene on such states through the progressive unfolding of a ramification based on the level of those physical states.

### 7.9.5 *Neural System in a Category*

**Assemblies of Neurons.** The response of a neuronal system to a simple signal is the activation of a specialized neuron; e.g., in the visual areas, there exist neurons activated by a segment of a certain direction ('simple' cells), or by an angle ('complex' cells),... [Ehresmann and Vanbremeersch (1987); Ehresmann and Vanbremeersch (1996)]. But more complex signals, apart from a few exceptions (e.g., a neuron representing a hand holding a banana in the monkey), do not have their own 'grandmother neuron'. The development of neuronal imagery shows that complex signals, or motor programs, are represented by the short synchronization of a specific assembly of neurons. And learning would consist in the formation of such synchronous assemblies, under the effect of the reinforcement of the synapses between their neurons, while following the Hebbian rule [Hebb (1949)]: a synapse between two neurons is strengthened if the two neurons are active at the same time, and its force decreases if one is active while the other is not.

These processes can be described in a MES modelling a neuronal system, and this model makes it possible to understand how they form the basis for the development of increasingly complex mental objects, enjoying a great flexibility.

**Memory Evolutive System of Neurons.** In such a MES, the state-categories will be obtained by successive complexifications of a category of neurons defined as follows [Ehresmann and Vanbremeersch (1987); Ehresmann and Vanbremeersch (1996)]:

Consider the graph whose vertices are the neurons at the time  $t$ , and the arrows  $f$  from  $N$  to  $N'$  are the synapses having  $N$  and  $N'$  respectively as their presynaptic and post-synaptic neurons. The category of paths of this graph is weighted, the weight of a synaptic path being connected to the probability that the activity of  $N$  (determined by its instantaneous frequency of impulses) is propagated to  $N'$ , and to the propagation delay of this activation. The category of neurons at  $t$  is obtained from this category by identifying two synaptic paths from  $N$  to  $N'$  with the same weight.

An assembly of neurons is represented by a pattern  $P$  in such a category of neurons. Its synchronization is then modelled by the emergence of a colimit of  $P$  in a complexification of the category; this colimit operates like a single 'neuron of a higher order' integrating the assembly, and which takes its own identity; it is called a neuron of category (or cat-neuron). The construction of the complexification determines which are 'the good' links between cat-neurons (namely the simple and complex links), therefore between synchronous assemblies of neurons. And, by iteration of the process of complexification, one can define cat-neurons of order 2 representative of assemblies of assemblies of neurons, then of order 3 etc..., modelling increasingly complex mental objects, or cognitive processes of a higher order. That makes it possible to describe explicitly how an *algebra of mental objects* develops [Ehresmann and Vanbremeersch (1987); Ehresmann and Vanbremeersch (1996)]. In particular, extension of the memory, under the effect of different CRs, leads to the emergence of cat-neurons of increasing orders. Among them, the cat-neurons which 'memorize' the strategies carried out and their results form the procedural memory.

**Semantics.** The neuronal system of a higher animal will be able to classify the items it recognizes by the formation of classes of invariance [Ehresmann and Vanbremeersch (1987); Ehresmann and Vanbremeersch (1996)].

For a lower CR, say  $E$ , this classification will be only 'pragmatic': two items 'are acted' as equivalent when their traces in the landscape activate the same pattern of agents: e.g., it is the same pattern of agents of a 'color' CR which is activated by all the blue objects.

But this classification will take a 'meaning' only at the level of a higher CR, with a longer period, which can determine what have in common the

different items that  $E$  has classified together, and memorize such a class in the form of an object called an  $E$ -concept. This object will be modelled by the limit of the pattern of agents of  $E$  activated by all the items of the class, and its various instances form the class of invariance of the concept (e.g., for the blue color-concept, all representations of blue objects).

The CR-concepts relating to the different CRs will form a Semantic Memory which is developed under the effect of successive complexifications, by addition of concepts classifying several attributes (such as a 'blue triangle'), then of more abstract concepts obtained as limits of patterns of such 'concrete' concepts, linked by complex links. A concept can be seen as a prototype for a class of items having a 'family air' (in the sense of Wittgenstein), and it does not suppose the existence of a language. The activation of a concept rests on a double indetermination: initially choice of a particular instance of the concept, then choice of a particular decomposition of this instance. It results from it that the introduction of a semantics makes the interplay among the strategies of the different CRs still more flexible; indeed the procedural memory will become semantic, so that, in higher CRs, the choice of a strategy can be made in the form of a concept, without specifying a particular object of the class of invariance of the concept. This gives a new DOF in the formation of the effective strategy on the system, since it makes it possible to activate the instance best adapted taking account of the strategies reflected by other CRs. For example the command for lifting an object will be modulated according to the shape and the size of the object to lift.

During the evolution of a MES, regrouping of emerging components and links can lead to the formation of new CRs of increasingly high levels, developing particular aptitudes. In particular, a MES equipped with a semantic memory can develop 'conscious' CRs, able to have an internal view of the semantics and of the concept of time. Such a CR can be characterized by the following capacities [Ehresmann and Vanbremeersch (1987); Ehresmann and Vanbremeersch (1996)]:

- (1) Retrospectively to extend its current landscape to lower levels of the recent past by an increase in attention, in particular after a fracture;
- (2) To operate a process of abduction in this extended landscape to find possible causes of the fracture; and
- (3) To plan a choice of strategies covering several future steps by the formation of 'virtual' landscapes in which the strategies (selected in the form of concepts) can be tested without energy cost.



From the neurological point of view, these properties rest on the existence of functional loops between various areas of the brain.

## 7.10 Brain–Mind Functorial Machines

In this section we propose two models of the *brain–mind functorial machines*: the first one is a psychologically–motivated top–down machine, while the second one is physically–motivated bottom–up solitary machine.

### 7.10.1 Neurodynamic 2–Functor

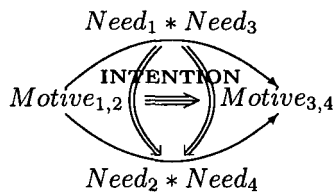
Here we define the goal–directed cognitive neurodynamics as an evolution 2–functor  $\mathcal{E}$  given by

$$\begin{array}{ccc}
 \begin{array}{ccc}
 A & \xrightarrow{f} & B \\
 \downarrow h & \text{CURRENT} & \downarrow g \\
 & \text{NEURAL} & \\
 & \text{STATE} & \\
 C & \xrightarrow{k} & D
 \end{array} & \xRightarrow{\mathcal{E}} & \begin{array}{ccc}
 \mathcal{E}(A) & \xrightarrow{\mathcal{E}(f)} & \mathcal{E}(B) \\
 \downarrow \mathcal{E}(h) & \text{DESIRED} & \downarrow \mathcal{E}(g) \\
 & \text{NEURAL} & \\
 & \text{STATE} & \\
 \mathcal{E}(C) & \xrightarrow{\mathcal{E}(k)} & \mathcal{E}(D)
 \end{array}
 \end{array} \quad (7.118)$$

In (7.118),  $\mathcal{E}$  represents a projection map from the *source 2–category* of the current neural state, defined as a commutative square of small categories  $A, B, C, D, \dots$  of *current neural ensembles* and their causal interrelations  $f, g, h, k, \dots$ , onto the *target 2–category* of the desired neural state, defined as a commutative square of small categories  $\mathcal{E}(A), \mathcal{E}(B), \mathcal{E}(C), \mathcal{E}(D), \dots$  of *evolved neural ensembles* and their causal interrelations  $\mathcal{E}(f), \mathcal{E}(g), \mathcal{E}(h), \mathcal{E}(k), \dots$

The evolution 2–functor  $\mathcal{E}$  can be horizontally decomposed in the following three neurodynamic components (see [Lewin (1997); Aidman and Leontiev (1991)]):

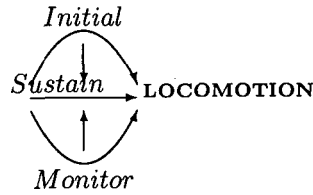
(1) *Intention*, defined as a 3–cell:



(2) *Action*, defined as a 1-cell:

ACTION  
→

(3) *Locomotion*, defined as a 2-cell:



Now, each causal arrow in (7.118), say  $f : A \rightarrow B$ , stands for a generic 'neuro-morphism', representing a self-organized, oscillatory neurodynamic system. We define a generic neuro-morphism  $f$  to be a nonlinear tensor-field  $(x, y, \omega)$ -system (7.119–7.124), acting as a bidirectional associative memory machine on a  $ND$  Riemannian manifold  $M^N$  of the human cortex. It is formed out of two distinct, yet nonlinearly-coupled neural subsystems:

- (1) Activation  $(x, y)$ -dynamics (7.119–7.120), defined as an interplay of an excitatory vector-field  $x^i = x^i(t) : M^N \rightarrow TM$ , representing a cross-section of the tangent bundle  $TM$ , and an inhibitory 1-form  $y_i = y_i(t) : M^N \rightarrow T^*M$ , representing a cross-section of the cotangent bundle  $T^*M$ .
- (2) Excitatory and inhibitory unsupervised learning  $(\omega)$ -dynamics (7.121–7.124) generated by random differential Hebbian learning process (7.123–7.124), defined respectively by contravariant synaptic tensor-field  $\omega^{ij} = \omega^{ij}(t) : M^N \rightarrow TTM_{im}^N$  and covariant synaptic tensor-field  $\omega_{ij} = \omega_{ij}(t) : M^N \rightarrow T^*T^*M$ , representing cross-sections of contravariant and covariant tensor bundles, respectively.

$(x, y, \omega)$ -system is analytically defined as a set of  $N$  coupled neurodynamic equations:

$$\dot{x}^i = A^i + \omega^{ij} f_j(y) - x^i, \quad (7.119)$$

$$\dot{y}_i = B_i + \omega_{ij} f^j(x) - y_i, \quad (7.120)$$

$$\dot{\omega}^{ij} = -\omega^{ij} + I^{ij}(x, y), \quad (7.121)$$

$$\dot{\omega}_{ij} = -\omega_{ij} + I_{ij}(x, y), \quad (7.122)$$

$$I^{ij} = f^i(x) f^j(y) + \dot{f}^i(x) \dot{f}^j(y) + \sigma^{ij}, \quad (7.123)$$

$$I_{ij} = f_i(x) f_j(y) + \dot{f}_i(x) \dot{f}_j(y) + \sigma_{ij}, \quad (7.124)$$

$$(i, j = 1, \dots, N).$$

Here  $\omega$  is a symmetric, second order synaptic tensor-field;  $I^{ij} = I^{ij}(x, y, \sigma)$  and  $I_{ij} = I_{ij}(x, y, \sigma)$  respectively denote contravariant-excitatory and

covariant-inhibitory random differential Hebbian innovation-functions with tensorial Gaussian noise  $\sigma$  (in both variances);  $f$ s and  $\dot{f}$ s denote sigmoid activation functions ( $f = \tanh(\cdot)$ ) and corresponding signal velocities ( $\dot{f} = 1 - f^2$ ), respectively in both variances;  $A^i = A^i(t)$  and  $B_i = B_i(t)$  are contravariant-excitatory and covariant-inhibitory neural inputs to the corresponding cortical cells, respectively;

Nonlinear activation  $(x, y)$ -dynamics, describes a two-phase biological neural oscillator field, in which the excitatory neural field excites the inhibitory neural field, which itself reciprocally inhibits the excitatory one.  $(x, y)$ -dynamics represents a nonlinear extension of a linear, Lyapunov-stable, conservative, gradient system, defined in local neural coordinates  $x^i, y_i \in V_y$  on  $T^*M$  as

$$\dot{x}^i = -\frac{\partial \Phi}{\partial y_i} = \omega^{ij} y_j - x^i, \quad \dot{y}_i = -\frac{\partial \Phi}{\partial x^i} = \omega_{ij} x^j - y_i. \quad (7.125)$$

The gradient system (7.125) is derived from scalar, neuro-synaptic action potential  $\Phi : T^*M \rightarrow \mathbb{R}$ , given by a negative, smooth bilinear form in  $x^i, y_i \in V_y$  on  $T^*M$  as

$$-2\Phi = \omega_{ij} x^i x^j + \omega^{ij} y_i y_j - 2x^i y_i, \quad (i, j = 1, \dots, N),$$

which itself represents a  $\Psi$ -image of the Riemannian metrics  $g : TM \rightarrow \mathbb{R}$  on the configuration manifold  $M^N$ .

The nonlinear oscillatory activation  $(x, y)$ -dynamics (7.119–7.122) is obtained from the linear conservative dynamics (7.125), by adding configuration dependent inputs  $A^i$  and  $B_i$ , as well as sigmoid activation functions  $f_j$  and  $f^j$ , respectively. It represents an interconnected pair of excitatory and inhibitory neural fields.

Both variant-forms of learning  $(\omega)$ -dynamics (7.121–7.122) are given by a generalized unsupervised (self-organizing) Hebbian learning scheme (see [Kosko (1992)]) in which  $\dot{\omega}_{ij}$  (resp.  $\dot{\omega}^{ij}$ ) denotes the new-update value,  $-\omega_{ij}$  (resp.  $\omega^{ij}$ ) corresponds to the old value and  $I_{ij}(x^i, y_j)$  (resp.  $I^{ij}(x^i, y_j)$ ) is the innovation function of the symmetric 2nd order synaptic tensor-field  $\omega$ . The nonlinear innovation functions  $I_{ij}$  and  $I^{ij}$  are defined by random differential Hebbian learning process (7.123–7.124). As  $\omega$  is a symmetric and zero-trace coupling synaptic tensor, the conservative linear activation dynamics (7.125) is equivalent to the rule that ‘the state of each neuron (in both neural fields) is changed in time if, and only if, the scalar action potential  $\Phi$  (52), is lowered’. Therefore, the scalar action potential  $\Phi$  represents the monotonically decreasing Lyapunov function (such that

$\dot{\Phi} \leq 0$ ) for the conservative linear dynamics (7.125), which converges to a local minimum or ground state of  $\Phi$ . That is to say, the system (7.125) moves in the direction of decreasing the scalar action potential  $\Phi$ , and when both  $\dot{x}^i = 0$  and  $\dot{y}_i = 0$  for all  $i = 1, \dots, N$ , the steady state is reached.

## 7.10.2 Solitary 'Thought Nets' and the Emerging Mind

### 7.10.2.1 Synergetic 'Thought Solitons'

Recall that synergetics teaches us that *order parameters* (and their spatio-temporal evolution) are *patterns, emerging from chaos*. In our opinion, the most important of these order parameters, both natural and man made, are *solitons*, because of their self-organizing quality to create order out of chaos. From this perspective, *nonlinearity* – the essential characteristic of nature – is the *cause* of both *chaos* and *order*. Recall that the solitary particle-waves, also called the 'light bullets', are localized space-time excitations  $\Psi(x, t)$ , propagating through a certain medium  $\Omega$  with constant velocities  $v_j$ . They describe a variety of nonlinear wave phenomena in one dimension and playing important roles in optical fibers, many branches of physics, chemistry and biology.

To derive our solitary network we start with modelling the conservative 'thought solitons', using the following three classical nonlinear equations, defining the time evolution of the spatio-temporal wave function  $\Psi(x, t)$  (which is smooth, and either complex-, or real-valued) (see [Novikov *et al.* (1984); Fordy (1990); Ablowitz and Clarkson (1991); Ivancevic and Pearce (2001a)]; also compare with (4.2.3.1) above):

#### (1) Nonlinear Schrödinger (NS) equation

$$i\Psi_t = 2\mu|\Psi|^2\Psi - \Psi_{xx}, \quad (7.126)$$

where  $\Psi = \Psi(x, t)$  is a complex-valued wave function with initial condition  $\Psi(x, t)|_{t=0} = \Psi(x)$  and  $\mu$  is a nonlinear parameter representing field strength. In the linear limit ( $\mu = 0$ ) NS becomes the ordinary Schrödinger equation for the wave function of the free 1D particle with mass  $m = 1/2$ . Its Hamiltonian function

$$H_{NS} = \int_{-\infty}^{+\infty} \left( \mu|\Psi|^4 + |\Psi_x|^2 \right) dx,$$

is equal to the total and conserved energy of the soliton. NS describes, for example, nonlinear Faraday resonance in a vertically oscillating wa-

ter, an easy-plane ferromagnet with a combination of a stationary and a high-frequency magnetic fields, and the effect of phase-sensitive amplifiers on solitons propagating in optical fibers.

(2) Korteweg-De Vries (KdV) equation

$$\Psi_t = 6\Psi\Psi_x - \Psi_{xxx},$$

with Hamiltonian (total conserved energy) given by

$$H_{KdV} = \int_{-\infty}^{+\infty} \left( \Psi^3 + \frac{1}{2} \Psi_x^2 \right) dx.$$

KdV is related to the ordinary Schrödinger equation by the inverse scattering method. KdV is a well-known model of 1D turbulence that was derived in various physical contexts, including chemical-reaction waves, propagation of combustion fronts in gases, surface waves in a film of a viscous liquid flowing along an inclined plane, patterns in thermal convection, rapid solidification, and others. Its discretization gives the Lotka-Volterra equation

$$\dot{x}^j(t) = x^j(t) (x^{j+1}(t) - x^{j-1}(t)),$$

which appears in a model of struggle for existence of biological species.

(3) Sine-Gordon (SG) equation

$$\Psi_{tt} = \Psi_{xx} - \sin \Psi,$$

with Hamiltonian (total conserved energy) given by

$$H_{SG} = \int_{-\infty}^{+\infty} (\Psi_t^2 + \Psi_x^2 + \cos \Psi) dx.$$

SG provides one of the simplest models of the unified field theory, can be found in the theory of dislocations in metals, in the theory of Josephson junctions and so on. It can be used also in interpreting certain biological processes like DNA dynamics. Its discretization gives a *system of coupled pendulums*.

Discrete solitons exist also in the form of the *soliton celular automata* (SCA) [Park *et al.* (1986)]. SCA is a 1(space)+1(time)-dimensional 'box and ball system' made of infinite number of zeros (or, boxes) and finite number of ones (or, balls). The value of the  $j$ th SCA cell  $a_t^j$  at a discrete

time  $t$ , is given as

$$a_{i+1}^j = \begin{cases} 1, & \text{if } a_t^j = 0 \text{ and } \sum_{i=-\infty}^{j-1} u_t^i > \sum_{i=-\infty}^{j-1} a_{t+1}^i, \\ 0, & \text{otherwise,} \end{cases}$$

where  $a_t^j = 0$  is assumed for  $|j| \gg 1$ . Any state of the SCA consists purely of solitons (particularly, KdV-solitons), possessing conserved quantities of the form of  $H_{KdV}$ . All of these properties have motivated a number of suggestive applications for a new kind of computational architecture that will utilize these evolution patterns of SCA in order to provide a 'gateless' implementation of logical operations.

In practice, both SCA and KdV are usually approximated by the *Toda lattice equation*,

$$\ddot{q}^i = e^{q^{i+1}-q^i} - e^{q^i-q^{i-1}}, \quad (i = 1, \dots, N) \quad (7.127)$$

with quasiperiodic

$$q^{N+i}(t) = q^i(t) + c,$$

or fast-dacaying boundary conditions

$$\lim_{i \rightarrow -\infty} q^i(t) = 0, \quad \lim_{i \rightarrow +\infty} q^i(t) = c.$$

The Toda equation (7.127) is a *gradient Newtonian equation* of motion

$$\ddot{q}^i = -\partial_q^i V, \quad V(q) = \sum_{i=1}^N e^{q^{i+1}-q^i}.$$

Otherwise, the Toda equation represents a Hamiltonian system

$$\dot{q}^i = p_i, \quad \dot{p}_i = e^{q^{i+1}-q^i} - e^{q^i-q^{i-1}},$$

with the phase-space  $P = \mathbb{R}^{2N}$  with coordinates  $(p_i, q^i)$ , standard Poisson structure

$$\{p_i, p_j\} = \{q^i, q^j\} = 0, \quad \{p_i, q^j\} = \delta_i^j,$$

and Hamiltonian function  $H = \sum_{i=1}^N \left( \frac{1}{2} p_i^2 + e^{q^{i+1}-q^i} \right), \quad (i, j = 1, \dots, N).$

Next, to make our conservative thought solitons *open to the environment*, we have to modify them by adding:

1. Input from the senses, in the form of the Weber–Fechner’s law,

$$S(t) = a_r \log s^r(t), \quad (r = 1, \dots, 5), \quad (7.128)$$

where  $S = S(t)$  is the *sensation*,  $s^r = s^r(t)$  the vector of stimuli from the five senses, and  $a_r$  a constant vector; and

2. Disturbances, in the form of additive, zero-mean Gaussian white noise  $\eta = \eta(t)$ , independent from the main soliton-signal.

In this way, we get the *modified solitary equations*:

$$\text{MNS : } i\Psi_t = 2\mu|\Psi|^2\Psi - \Psi_{xx} + a_r \log s^r\Psi + \eta,$$

$$\text{MKdV : } \Psi_t = 6\Psi\Psi_x - \Psi_{xxx} + a_r \log s^r\Psi + \eta,$$

$$\text{MSG : } \Psi_{tt} = \Psi_{xx} - \sin \Psi + a_r \log s^r\Psi + \eta,$$

representing the *three different models of the thought units*.

Now we will form a single emerging order-parameter, the general factor, that we call the *Mind*. It behaves like an orchestrated ensemble of thought solitons, defined as systems of trainable, coupled soliton equations. Their tensor couplings perform *self-organizing associative learning by trial and error*, similar to that of the neural ensemble.

The dynamics of the *soliton ensemble*, representing our model of the ‘mind’ can be described as one of the following three soliton systems; each of them performs *learning*, *growing* and *competing* between each other, and *communicates with environment* through the *inputs from the senses* and the *heating noise*:

1. Coupled modified nonlinear Schrödinger equations

$$\begin{aligned} i\Psi_t^k &= -\Psi_{xx}^k + 2\mu^k \sum_{j \neq k} |\Psi^j|^2 \mathbf{W}_k^j S^j(\Psi^j) \\ &+ \nu^k \Psi^k (1 - \epsilon^k \Psi^k) + a_r \log s^r \Psi^k + \eta^k, \end{aligned}$$

2. Coupled modified Korteweg–De Vries equations

$$\begin{aligned} \Psi_t^k &= 6\Psi_x^k \Psi^k - \Psi_{xxx}^k + \sum_{j \neq k} \mathbf{W}_k^j S^j(\Psi^j) \\ &+ \nu^k \Psi^k (1 - \epsilon^k \Psi^k) + a_r \log s^r \Psi^k + \eta^k, \end{aligned}$$

### 3. Coupled modified Sine-Gordon equations

$$\begin{aligned}\Psi_{tt}^k &= \Psi_{xx}^k - \sin \Psi^k + \sum_{j \neq k} \\ &+ \nu^k \Psi^k (1 - \epsilon^k \Psi^k) + a_r \log s^r \Psi^k + \eta^k,\end{aligned}$$

where  $\Psi^k = \Psi^k(x, t)$ , ( $k = 1, \dots, n$ ) is the set of wave functions of the solitary thoughts,  $S(\cdot)$  represents the sigmoidal threshold functions,  $\nu^k$  and  $\epsilon^k$  are *growing* and *competition* parameters.

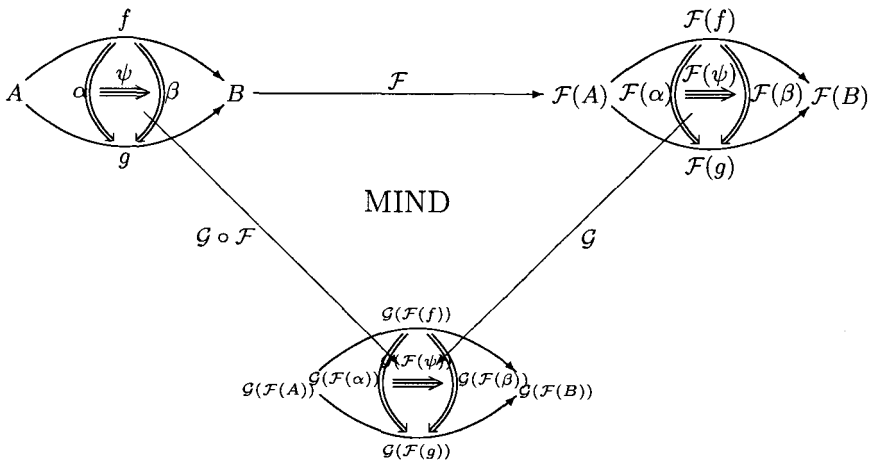
$\mathbf{W}_k^j = \mathbf{W}_k^j(\Psi)$  are *tensorial learning couplings*, evolving according to the Hebbian learning scheme (see [Kosko (1992)]):

$$\dot{\mathbf{W}}_k^j = -\mathbf{W}_k^j + \Phi_k^j(\Psi^k, \Psi^j),$$

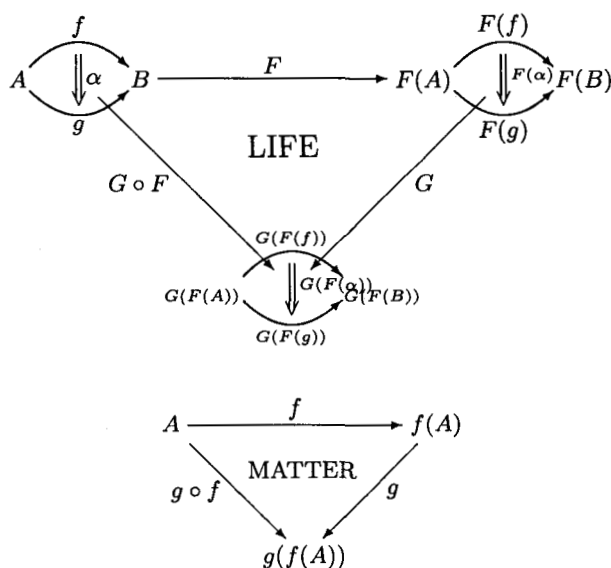
with *innovation* defined in tensor signal form (here  $\dot{S}(\cdot) = 1 - \tanh(\cdot)$ )

$$\Phi_k^j = S^j(\Psi^j) S^k(\Psi^k) + \dot{S}^j(\Psi^j) \dot{S}^k(\Psi^k).$$

**Categorical Structure of the MATTER $\Rightarrow$ LIFE $\Rightarrow$ MIND Emergence.** In this way, the solitary thought nets effectively simulate the following 3-categorical structure of MIND, emerging from the 2-categorical structure of LIFE, which is itself emerging from the 1-categorical structure of MATTER:







### 7.11 Body–Mind Adjunction and Natural Psychodynamics

In this section, which is written in the fashion of the *quantum brain* (see section 7.5 above), we present the top level of natural biodynamics, using geometric generalization of the *Feynman path integral* (see section 4.4 above). To formulate the basics of *natural psychodynamics*, we use the *action–amplitude picture* of the  $BODY \rightleftharpoons MIND$  adjunction:

↓ **Deterministic (causal) world of *Human BODY*** ↓

$$Action : S[q^n] = \int_{t_{in}}^{t_{out}} (E_k - E_p + Wrk + Src^{\pm}) dt$$

---


$$Amplitude : \langle out | in \rangle = \oint \mathcal{D}[w_n q^n] e^{iS[q^n]}$$

↑ **Probabilistic (fuzzy) world of *Human MIND*** ↑

In the action integral,  $E_k, E_p, Wrk$  and  $Src^{\pm}$  denote the kinetic end potential energies, work done by dissipative/driving forces and other energy

sources/sinks, respectively. In the amplitude integral, the peculiar sign  $\oint$  denotes integration along smooth paths and summation along discrete Markov chains;  $i$  is the imaginary unit,  $w_n$  are synaptic-like weights, while  $\mathcal{D}$  is the Feynman path differential (defined below) calculated along the configuration trajectories  $q^n$ . The action  $S[q^n]$ , through the *least action principle*  $\delta S = 0$ , leads to all biodynamic equations considered so far (in generalized Lagrangian and Hamiltonian form). At the same time, the action  $S[q^n]$  figures in the exponent of the path integral  $\oint$ , defining the probability transition amplitude  $\langle out|in \rangle$ . In this way, the whole body dynamics is incorporated in the mind dynamics. This *adaptive path integral* represents an *infinite-dimensional neural network*, suggesting an infinite capacity of human brain/mind.

For a long time the cortical systems for *language and actions* were believed to be independent modules. However, according to the recent research of [Pulvermüller (2005)], as these systems are reciprocally connected with each other, information about language and actions might interact in distributed neuronal assemblies. A critical case is that of action words that are semantically related to different parts of the body (e.g. 'pick', 'kick', 'lick',...). The author suggests that the comprehension of these words might specifically, rapidly and automatically activate the motor system in a somatotopic manner, and that their comprehension rely on activity in the action system.

### 7.11.1 *Natural Psychodynamics in the Life Space Foam*

Both the original *Lewinian force-field theory* in psychology (see [Lewin (1951); Gold (1999)]) and modern decision-field dynamics (see [Busemeyer and Townsend (1993); Roe *et al.* (2001); Busemeyer and Diederich (2002)]) are based on the classical Lewinian concept of an individual's *life space*.<sup>16</sup> As a topological construct, Lewinian life space represents a person's psychological environment that contains *regions* separated by dynamic permeable *boundaries*. As a field construct, on the other hand, the life space is not empty: each of its regions is characterized by *valence* (ranging from positive or negative and resulting from an interaction between the person's *needs* and the dynamics of their *environment*). Need is an energy construct, ac-

<sup>16</sup>The work presented in this subsection has been developed in collaboration with Dr. Eugene Aidman, Senior Research Scientist, Human Systems Integration, Land Operations Division, Defence Science & Technology Organisation, Australia.

according to Lewin. It creates *tension* in the person, which, in combination with other tensions, initiates and sustains behavior. Needs vary from the most primitive urges to the most idiosyncratic intentions and can be both internally generated (e.g., thirst or hunger) and stimulus-induced (e.g., an urge to buy something in response to a TV advertisement). Valences are, in essence, personal values dynamically derived from the person's needs and attached to various regions in their life space. As a field, the life space generates forces pulling the person towards positively-valenced regions and pushing them away from regions with negative valence. Lewin's term for these forces is *vectors*. Combinations of multiple vectors in the life space cause the person to move from one region towards another. This movement is termed *locomotion* and it may range from overt behavior to cognitive shifts (e.g., between alternatives in a decision-making process). Locomotion normally results in crossing the boundaries between regions. When their permeability is degraded, these boundaries become *barriers* that restrain locomotion. Life space model, thus, offers a meta-theoretical language to describe a wide range of behaviors, from goal-directed action to intrapersonal conflicts and multi-alternative decision-making.

In order to formalize the Lewinian life-space concept, a set of *action principles* need to be associated to Lewinian force-fields, (loco)motion paths (representing mental abstractions of biomechanical paths [Ivancevic (2004)]) and life space geometry. As an extension of the Lewinian concept, in this paper we introduce a new concept of *life-space foam* (LSF, see Figure 7.64). According to this new concept, Lewin's life space can be represented as a *geometric functor* with globally smooth macro-dynamics, which is at the same time underpinned by wildly fluctuating, non-smooth, local micro-dynamics, describable by *Feynman's*: (i) *sum-over-histories*  $\int_{paths}$ , (ii) *sum-over-fields*  $\int_{fields}$ , and (iii) *sum-over-geometries*  $\int_{geom}$ <sup>17</sup>.

LSF is thus a two-level *geometrodynamic functor*, representing these two distinct types of dynamics within the Lewinian life space. At its *macroscopic spatio-temporal level*, LSF appears as a 'nice & smooth' geometric functor with globally predictable dynamics – formally, a smooth  $n$ -dimensional manifold  $M$  with local Riemannian metrics  $g_{ij}(x)$ , smooth force-fields and smooth (loco)motion paths, as conceptualized in the

---

<sup>17</sup>In this section we use the peculiar Dirac's symbol  $\int$  to denote summation over 'discrete spectrum' and integration over 'continuous spectrum' of paths, fields and geometries in the microscopic level of the life space foam.

Lewinian theory. To model the global and smooth macro-level LSF-paths, fields and geometry, we use the general physics-like *principle of the least action*.

Now, the apparent smoothness of the macro-level LSF is achieved by the existence of another level underneath it. This *micro-level* LSF is actually a collection of wildly fluctuating force-fields, (loco)motion paths, curved regional geometries and topologies with holes. The micro-level LSF is proposed as an extension of the Lewinian concept: it is characterized by uncertainties and fluctuations, enabled by microscopic time-level, microscopic transition paths, microscopic force-fields, local geometries and varying topologies with holes. To model these fluctuating microscopic LSF-structures, we use three instances of *adaptive path integral*, defining a multi-phase and multi-path (also multi-field and multi-geometry) *transition* process from *intention* to the goal-driven *action*.

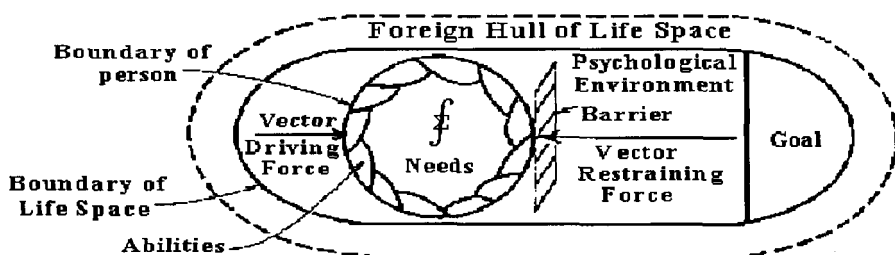


Fig. 7.64 Diagram of the *life space foam*: Lewinian life space with an adaptive path integral acting inside it and generating microscopic fluctuation dynamics.

We use the new LSF concept to develop modelling framework for motivational dynamics (MD) and induced cognitive dynamics (CD).

According to Heckhausen (see [Heckhausen (1977)]), *motivation* can be thought of as a process of *energizing* and *directing the action*. The process of energizing can be represented by Lewin's *force-field analysis* and Vygotsky's *motive formation* (see [Vygotsky (1982); Aidman and Leontiev (1991)]), while the process of directing can be represented by *hierarchical action control* (see [Bernstein (1947); Kuhl (1985)]).

Motivation processes both precede and coincide with every goal-directed action. Usually these motivation processes include the sequence of the following four feedforward *phases* [Vygotsky (1982); Aidman and Leontiev (1991)]: (\*)

- (1) *Intention Formation*  $\mathcal{F}$ , including: decision making, commitment building, etc.
- (2) *Action Initiation*  $\mathcal{I}$ , including: handling conflict of motives, resistance to alternatives, etc.
- (3) *Maintaining the Action*  $\mathcal{M}$ , including: resistance to fatigue, distractions, etc.
- (4) *Termination*  $\mathcal{T}$ , including parking and avoiding addiction, i.e., staying in control.

With each of the phases  $\{\mathcal{F}, \mathcal{I}, \mathcal{M}, \mathcal{T}\}$  in (\*), we can associate a *transition propagator* – an ensemble of (possibly crossing) feedforward paths propagating through the ‘wood of obstacles’ (including topological holes in the LSF, see Figure 7.65), so that the complete *transition functor*  $\mathcal{TA}$  is a product of propagators (as well as sum over paths). All the phases–propagators are controlled by a unique *Monitor* feedback process.

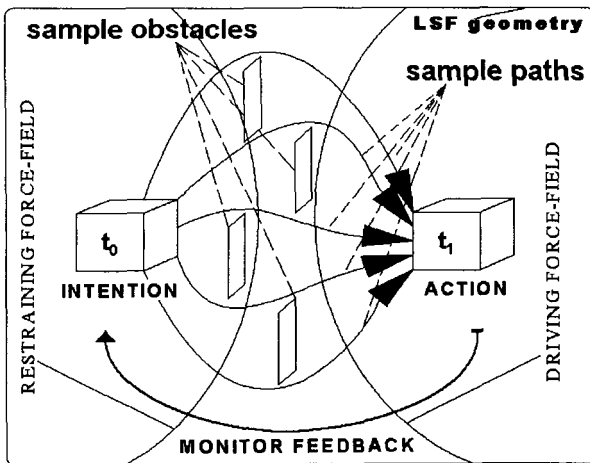


Fig. 7.65 *Transition-propagator* corresponding to each of the motivational phases  $\{\mathcal{F}, \mathcal{I}, \mathcal{M}, \mathcal{T}\}$ , consisting of an ensemble of feedforward paths propagating through the ‘wood of obstacles’. The paths affected by driving and restraining force-fields, as well as by the local LSF-geometry. Transition goes from *Intention*, occurring at a sample time instant  $t_0$ , to *Action*, occurring at some later time  $t_1$ . Each propagator is controlled by its own *Monitor* feedback. All together they form the transition functor  $\mathcal{TA}$ .

In this section we propose an *adaptive path integral* formulation for the motivational–transition functor  $\mathcal{TA}$ . In essence, we sum/integrate over different paths and make a product (composition) of different phases–

propagators. This is the most general description of the *general Markov stochastic process*:<sup>18</sup>

We will also attempt to demonstrate the utility of the same LSF-formalisms in representing cognitive functions, such as memory, learning and decision making. For example, in the classical *Stimulus encoding*  $\rightarrow$  *Search*  $\rightarrow$  *Decision*  $\rightarrow$  *Response* sequence [Sternberg (1969); Ashcraft (1994)], the environmental input-triggered *sensory memory* and *working memory* (WM) can be interpreted as operating at the micro-level force-field under the executive control of the *Monitor* feedback, whereas *search* can be formalized as a *control* mechanism guiding retrieval from the long-term memory (LTM, itself shaped by learning) and filtering material relevant to decision making into the WM. The essential measure of these mental processes, the *processing speed* (essentially determined by Sternberg's reaction-time) can be represented by our (loco)motion speed  $\dot{x}$ .

<sup>18</sup>Recall that *Markov stochastic process* is a stochastic (random) process characterized by a *lack of memory*, i.e., the statistical properties of the immediate future are uniquely determined by the present, regardless of the past [Gardiner (1985)]. This Markov assumption can be formulated in terms of the conditional probabilities  $P(x^i, t_i)$ : if the times  $t_i$  increase from right to left, the conditional probability is determined entirely by the knowledge of the most recent condition. The general, continuous + discrete Markov process is generated by a set of conditional probabilities whose probability-density evolution,  $P = P(x', t' | x'', t'')$ , obeys the general *Chapman-Kolmogorov integro-differential equation*

$$\begin{aligned} \partial_t P = & - \sum_i \frac{\partial}{\partial x^i} \{A_i[x(t), t] P\} + \frac{1}{2} \sum_{ij} \frac{\partial^2}{\partial x^i \partial x^j} \{B_{ij}[x(t), t] P\} \\ & + \int dx \{W(x' | x'', t) P - W(x'' | x', t) P\}, \end{aligned}$$

including: *deterministic drift* (the first term on the right, called the *Liouville equation*), *diffusion fluctuations* (the second term called the *Fokker-Planck equation*) and *discontinuous jumps* (the third term called the *Master equation*). It is this general Chapman-Kolmogorov integro-differential equation, with its conditional probability density evolution,  $P = P(x', t' | x'', t'')$ , that we are going to model by three forms of the Feynman

path integral: (i) *sum-over-histories*  $\oint_{paths}$ , (ii) *sum-over-fields*  $\oint_{fields}$ , and (iii)

*sum-over-geometries*  $\oint_{geom}$ , providing us with the psycho-physical insight behind the abstract probability densities. Besides, the *probability is defined and calculated in a different way*: the overall probability of the system's transition from some initial state *A* to some final state *B* is given *not* by adding up the probabilities for each history-route, but by adding up the *complex-valued amplitudes* for each route first (i.e., performing the sum-over-histories) and then squaring the total amplitude to get the real-valued probability (i.e., the sum of squares is different from the square of sums).

### 7.11.1.1 Six Faces of the Life Space Foam

The LSF has three forms of appearance: *paths + field + geometries*, acting on both macro-level and micro-level, which is six modes in total. In this section, we develop three least action principles for the macro-LSF-level and three adaptive path integrals for the micro-LSF-level. While developing our psycho-physical formalism, we will address the behavioral issues of motivational fatigue, learning, memory and decision making.

### 7.11.1.2 General Formalism

At both macro- and micro-levels, the total LSF represents a union of transition paths, force-fields and geometries, formally written as

$$\begin{aligned} LSF_{total} &:= LSF_{paths} \bigcup LSF_{fields} \bigcup LSF_{geom} \\ &\equiv \oint_{paths} + \oint_{fields} + \oint_{geom}. \end{aligned} \quad (7.129)$$

Corresponding to each of the three LSF-subspaces in (7.129) we formulate:

- (1) The *least action principle*, to model deterministic and predictive, macro-level MD & CD, giving a unique, global, causal and smooth path-field-geometry on the macroscopic spatio-temporal level; and
- (2) Associated *adaptive path integral* to model uncertain, fluctuating and probabilistic, micro-level MD & CD, as an ensemble of local paths-fields-geometries on the microscopic spatio-temporal level, to which the global macro-level MD & CD represents both time and ensemble *average* (which are equal according to the *ergodic hypothesis*).

In the proposed formalism, transition paths  $x^i(t)$  are affected by the force-fields  $\varphi^k(t)$ , which are themselves affected by geometry with metric  $g_{ij}$ .

**Global Macro-Level of  $LSF_{total}$ .** In general, at the *macroscopic* LSF-level we first formulate the *total action*  $S[\Phi]$ , the central quantity in our formalism that has psycho-physical dimensions of *Energy*  $\times$  *Time* = *Effort*, with immediate cognitive and motivational applications: *the greater the action – the higher the speed of cognitive processes and the lower the macroscopic fatigue* (which includes all sources of physical, cognitive and emotional fatigue that influence motivational dynamics). The action  $S[\Phi]$  depends on macroscopic paths, fields and geometries, commonly denoted by an abstract field symbol  $\Phi^i$ . The action  $S[\Phi]$  is formally defined as a temporal integral from the *initial* time instant  $t_{ini}$  to the *final* time

instant  $t_{fin}$ ,

$$S[\Phi] = \int_{t_{ini}}^{t_{fin}} \mathcal{L}[\Phi] dt, \quad (7.130)$$

with *Lagrangian density* given by

$$\mathcal{L}[\Phi] = \int d^n x \mathcal{L}(\Phi_i, \partial_{x^j} \Phi^i),$$

where the integral is taken over all  $n$  coordinates  $x^j = x^j(t)$  of the LSF, and  $\partial_{x^j} \Phi^i$  are time and space partial derivatives of the  $\Phi^i$ -variables over coordinates.

Second, we formulate the *least action principle* as a minimal variation  $\delta$  of the action  $S[\Phi]$

$$\delta S[\Phi] = 0, \quad (7.131)$$

which, using techniques from the calculus of variations gives, in the form of the so-called Euler-Lagrangian equations, a shortest (loco)motion path, an extreme force-field, and a life-space geometry of minimal curvature (and without holes). In this way, we effectively derive a *unique globally smooth transition functor*

$$TA : INTENTION_{t_{ini}} \Rightarrow ACTION_{t_{fin}}, \quad (7.132)$$

performed at a macroscopic (global) time-level from some initial time  $t_{ini}$  to the final time  $t_{fin}$ .

In this way, we get macro-objects in the global LSF: a single path described Newtonian-like equation of motion, a single force-field described by Maxwellian-like field equations, and a single obstacle-free Riemannian geometry (with global topology without holes).

For example, in 1945–1949 Wheeler and Feynman developed their *action-at-a-distance electrodynamics* [Wheeler and Feynman (1949)], in complete experimental agreement with the classical Maxwell's electromagnetic theory, but at the same time avoiding the complications of divergent self-interaction of the Maxwell's theory as well as eliminating its infinite number of field degrees of freedom. In Wheeler-Feynman view, "Matter consists of electrically charged particles," so they found a form for the action directly involving the motions of the charges only, which upon variation would give the Newtonian-like equations of motion of these charges. Here is the expression for this action in the flat space-time, which is in the core



of quantum electrodynamics:

$$S[x; t_i, t_j] = \frac{1}{2} m_i \int (\dot{x}_\mu^i)^2 dt_i + \frac{1}{2} e_i e_j \int \int \delta(I_{ij}^2) \dot{x}_\mu^i(t_i) \dot{x}_\mu^j(t_j) dt_i dt_j$$

with

$$I_{ij}^2 = [x_\mu^i(t_i) - x_\mu^j(t_j)] [x_\mu^i(t_i) - x_\mu^j(t_j)], \quad (7.133)$$

where  $x_\mu^i = x_\mu^i(t_i)$  is the four-vector position of the  $i$ th particle as a function of the proper time  $t_i$ , while  $\dot{x}_\mu^i(t_i) = dx_\mu^i/dt_i$  is the velocity four-vector. The first term in the action (7.133) is the ordinary mechanical action in Euclidean space, while the second term defines the electrical interaction of the charges, representing the Maxwell-like field (it is summed over each pair of charges; the factor  $\frac{1}{2}$  is to count each pair once, while the term  $i = j$  is omitted to avoid self-action; the interaction is a double integral over a delta function of the square of space-time interval  $I^2$  between two points on the paths; thus, interaction occurs only when this interval vanishes, that is, along light cones [Wheeler and Feynman (1949)]).

Now, from the point of view of Lewinian geometric force-fields and (loco)motion paths, we can give the following life-space interpretation to the Wheeler-Feynman action (7.133). The mechanical-like locomotion term occurring at the single time  $t$ , needs a covariant generalization from the flat 4D Euclidean space to the  $n$ D smooth Riemannian manifold, so it becomes (see e.g., [Ivancevic (2004)])

$$S[x] = \frac{1}{2} \int_{t_{ini}}^{t_{fin}} g_{ij} \dot{x}^i \dot{x}^j dt,$$

where  $g_{ij}$  is the Riemannian metric tensor that generates the total 'kinetic energy' of (loco)motions in the life space.

The second term in (7.133) gives the sophisticated definition of Lewinian force-fields that drive the psychological (loco)motions, if we interpret electrical charges  $e_i$  occurring at different times  $t_i$  as motivational charges – needs.

**Local Micro-Level of  $LSF_{total}$ .** After having properly defined macro-level MD & CD, with a unique transition map  $F$  (including a unique motion path, driving field and smooth geometry), we move down to the *microscopic* LSF-level of rapidly fluctuating MD & CD, where we cannot define a unique and smooth path-field-geometry. The most we can do at this level of *fluctuating uncertainty*, is to formulate an adaptive path integral and calculate overall probability amplitudes for ensembles of local transitions from one LSF-point to the neighboring one. This *probabilistic transi-*

*tion micro-dynamics* functor is defined by a multi-path (field and geometry, respectively) and multi-phase *transition amplitude*  $\langle \text{Action} | \text{Intention} \rangle$  of corresponding to the globally-smooth transition map (7.132). This absolute square of this probability amplitude gives the *transition probability* of occurring the final state of *Action* given the initial state of *Intention*,

$$P(\text{Action} | \text{Intention}) = |\langle \text{Action} | \text{Intention} \rangle|^2.$$

The total transition amplitude from the state of *Intention* to the state of *Action* is defined on  $LSF_{total}$

$$\mathcal{TA} \equiv \langle \text{Action} | \text{Intention} \rangle_{total} : INTENTION_{t_0} \Rightarrow ACTION_{t_1}, \quad (7.134)$$

given by adaptive generalization of the Feynman's path integral [Feynman and Hibbs (1965); Feynman (1972); Feynman (1998)]. The transition map (7.134) calculates the *overall probability amplitude* along a multitude of wildly fluctuating paths, fields and geometries, performing the *microscopic* transition from the micro-state  $INTENTION_{t_0}$  occurring at initial micro-time instant  $t_0$  to the micro-state  $ACTION_{t_1}$  at some later micro-time instant  $t_1$ , such that all micro-time instants fit inside the global transition interval  $t_0, t_1, \dots, t_s \in [t_{ini}, t_{fin}]$ . It is symbolically written as

$$\langle \text{Action} | \text{Intention} \rangle_{total} := \oint \mathcal{D}[w\Phi] e^{iS[\Phi]}, \quad (7.135)$$

where the Lebesgue integration is performed over all continuous  $\Phi_{con}^i = \text{paths} + \text{field} + \text{geometries}$ , while summation is performed over all discrete processes and regional topologies  $\Phi_{dis}^j$ ). The symbolic differential  $\mathcal{D}[w\Phi]$  in the general path integral (7.135), represents an *adaptive path measure*, defined as a weighted product

$$\mathcal{D}[w\Phi] = \lim_{N \rightarrow \infty} \prod_{s=1}^N w_s d\Phi_s^i, \quad (i = 1, \dots, n = con + dis), \quad (7.136)$$

which is in practice satisfied with a large  $N$  corresponding to infinitesimal temporal division of the four motivational phases (\*). Technically, the path integral (7.135) calculates the *amplitude* for the transition functor  $\mathcal{TA} : \text{Intention} \Rightarrow \text{Action}$ .

In the exponent of the path integral (7.135) we have the action  $S[\Phi]$  and the imaginary unit  $i = \sqrt{-1}$  ( $i$  can be converted into the real number  $-1$  using the so-called *Wick rotation*, see next subsection).

In this way, we get a range of micro-objects in the local LSF at the short time-level: ensembles of rapidly fluctuating, noisy and crossing paths,

force-fields, local geometries with obstacles and topologies with holes. However, by averaging process, both in time and along ensembles of paths, fields and geometries, we recover the corresponding global MD & CD variables.

**Infinite-dimensional neural network.** The adaptive path integral (7.135) incorporates the *local learning process* according to the basic formula: *New Value = Old Value + Innovation* (see section 7.6 above). The general weights  $w_s = w_s(t)$  in (7.136) are updated by the *MONITOR* feedback during the transition process, according to one of the two standard neural learning schemes, in which the micro-time level is traversed in discrete steps, i.e., if  $t = t_0, t_1, \dots, t_s$  then  $t + 1 = t_1, t_2, \dots, t_{s+1}$ :

- (1) A *self-organized, unsupervised* (e.g., Hebbian-like [Hebb (1949)]) learning rule:

$$w_s(t+1) = w_s(t) + \frac{\sigma}{\eta}(w_s^d(t) - w_s^a(t)), \quad (7.137)$$

where  $\sigma = \sigma(t)$ ,  $\eta = \eta(t)$  denote *signal* and *noise*, respectively, while superscripts *d* and *a* denote *desired* and *achieved* micro-states, respectively; or

- (2) A certain form of a *supervised gradient descent learning*:

$$w_s(t+1) = w_s(t) - \eta \nabla J(t), \quad (7.138)$$

where  $\eta$  is a small constant, called the *step size*, or the *learning rate* and  $\nabla J(n)$  denotes the gradient of the ‘performance hyper-surface’ at the  $t$ -th iteration.

Both Hebbian and supervised learning are used for the local decision making process (see below) occurring at the intention formation faze  $\mathcal{F}$ .

In this way, local micro-level of  $LSF_{total}$  represents an infinite-dimensional neural network. In the cognitive psychology framework, our adaptive path integral (7.135) can be interpreted as *semantic integration* (see [Bransford and Franks (1971); Ashcraft (1994)]).

### 7.11.1.3 Motion and Decision Making in $LSF_{paths}$

On the macro-level in the subspace  $LSF_{paths}$  we have the (loco)motion action principle

$$\delta S[x] = 0,$$

with the *Newtonian-like action*  $S[x]$  given by

$$S[x] = \int_{t_{ini}}^{t_{fin}} dt \left[ \frac{1}{2} g_{ij} \dot{x}^i \dot{x}^j + \varphi^i(x^i) \right], \quad (7.139)$$

where overdot denotes time derivative, so that  $\dot{x}^i$  represents *processing speed*, or (loco)motion velocity vector. The first bracket term in (7.139) represents the kinetic energy  $T$ ,

$$T = \frac{1}{2} g_{ij} \dot{x}^i \dot{x}^j,$$

generated by the *Riemannian metric tensor*  $g_{ij}$ , while the second bracket term,  $\varphi^i(x^i)$ , denotes the family of potential force-fields, driving the (loco)motions  $x^i = x^i(t)$  (the *strengths* of the fields  $\varphi^i(x^i)$  depend on their positions  $x^i$  in LSF, see  $LSF_{fields}$  below). The corresponding Euler-Lagrangian equation gives the Newtonian-like equation of motion

$$\frac{d}{dt} T_{\dot{x}^i} - T_{x^i} = -\varphi_{x^i}^i, \quad (7.140)$$

(subscripts denote the partial derivatives), which can be put into the standard Lagrangian form

$$\frac{d}{dt} L_{\dot{x}^i} = L_{x^i}, \quad \text{with} \quad L = T - \varphi^i(x^i).$$

In the next subsection we use the micro-level implications of the action  $S[x]$  as given by (7.139), for dynamical descriptions of the local decision-making process.

On the micro-level in the subspace  $LSF_{paths}$ , instead of a single path defined by the Newtonian-like equation of motion (7.140), we have an ensemble of fluctuating and crossing paths with weighted probabilities (of the unit total sum). This ensemble of micro-paths is defined by the simplest instance of our adaptive path integral (7.135), similar to the Feynman's original *sum over histories*,

$$\langle \text{Action} | \text{Intention} \rangle_{paths} = \int \mathcal{D}[wx] e^{iS[x]}, \quad (7.141)$$

where  $\mathcal{D}[wx]$  is a functional measure on the *space of all weighted paths*, and the exponential depends on the action  $S[x]$  given by (7.139). This procedure can be redefined in a mathematically cleaner way if we Wick-rotate the time variable  $t$  to imaginary values  $t \mapsto \tau = it$ , thereby making

all integrals real:

$$\oint \mathcal{D}[wx] e^{iS[x]} \xrightarrow{Wick} \oint \mathcal{D}[wx] e^{-S[x]}. \quad (7.142)$$

Discretization of (7.142) gives the *thermodynamic-like partition function*

$$Z = \sum_j e^{-w_j E^j / T}, \quad (7.143)$$

where  $E^j$  is the motion energy eigenvalue (reflecting each possible motivational energetic state),  $T$  is the temperature-like environmental control parameter, and the sum runs over all motion energy eigenstates (labelled by the index  $j$ ). From (7.143), we can further calculate all thermodynamic-like and statistical properties of MD & CD (see e.g., [Feynman (1972)]), as for example, *transition entropy*  $S = k_B \ln Z$ , etc.

From cognitive perspective, our adaptive path integral (7.141) calculates all (alternative) pathways of information flow during the transition *Intention*  $\rightarrow$  *Action*.

In the language of transition-propagators, the integral over histories (7.141) can be decomposed into the product of propagators (i.e., Fredholm kernels or Green functions) corresponding to the cascade of the four motivational phases (\*)

$$\langle \text{Action} | \text{Intention} \rangle_{\text{paths}} = \oint dx^{\mathcal{F}} dx^{\mathcal{I}} dx^{\mathcal{M}} dx^{\mathcal{T}} K(\mathcal{F}, \mathcal{I}) K(\mathcal{I}, \mathcal{M}) K(\mathcal{M}, \mathcal{T}), \quad (7.144)$$

satisfying the Schrödinger-like equation (see e.g., [Dirac (1930)])

$$i \partial_t \langle \text{Action} | \text{Intention} \rangle_{\text{paths}} = H_{\text{Action}} \langle \text{Action} | \text{Intention} \rangle_{\text{paths}}, \quad (7.145)$$

where  $H_{\text{Action}}$  represents the Hamiltonian (total energy) function available at the state of *Action*. Here our ‘golden rule’ is: the higher the  $H_{\text{Action}}$ , the lower the microscopic fatigue.

In the connectionist language, our propagator expressions (7.144–7.145) represent *activation dynamics*, to which our *Monitor* process gives a kind of *backpropagation* feedback, a version of the basic supervised learning (7.138).

**Mechanisms of decision making under uncertainty.** The basic question about our local decision making process, occurring under uncertainty at the intention formation faze  $\mathcal{F}$ , is: Which alternative to choose? (see [Roe *et al.* (2001); Grossberg (1982); Grossberg (1999); Grossberg (1988); Ashcraft (1994)]). In our path-integral language this reads: Which path (alternative) should be given the highest probability

weight  $w$ ? Naturally, this problem is iteratively solved by the learning process (7.137–7.138), controlled by the *MONITOR* feedback, which we term *algorithmic approach*.

In addition, here we analyze qualitative mechanics of the local decision making process under uncertainty, as a *heuristic approach*. This qualitative analysis is based on the micro-level interpretation of the Newtonian-like action  $S[x]$ , given by (7.139) and figuring both processing speed  $\dot{x}$  and LTM (i.e., the force-field  $\varphi(x)$ , see next subsection). Here we consider three different cases:

- (1) If the potential  $\varphi(x)$  is not very dependent upon position  $x(t)$ , then the more direct paths contribute the most, as longer paths, with higher mean square velocities  $[\dot{x}(t)]^2$  make the exponent more negative (after Wick rotation (7.142)).
- (2) On the other hand, suppose that  $\varphi(x)$  does indeed depend on position  $x$ . For simplicity, let the potential increase for the larger values of  $x$ . Then a direct path does not necessarily give the largest contribution to the overall transition probability, because the integrated value of the potential is higher than over another paths.
- (3) Finally, consider a path that deviates widely from the direct path. Then  $\varphi(x)$  decreases over that path, but at the same time the velocity  $\dot{x}$  increases. In this case, we expect that the increased velocity  $\dot{x}$  would more than compensate for the decreased potential over the path.

Therefore, the most important path (i.e., the path with the highest weight  $w$ ) would be one for which any smaller integrated value of the surrounding field potential  $\varphi(x)$  is more than compensated for by an increase in kinetic-like energy  $\frac{m}{2}\dot{x}^2$ . In principle, this is neither the most direct path, nor the longest path, but rather a middle way between the two. Formally, it is the path along which the average Lagrangian is minimal,

$$< \frac{m}{2}\dot{x}^2 + \varphi(x) > \longrightarrow \min, \quad (7.146)$$

i.e., the *path that requires minimal memory* (both LTM and WM, see  $LSF_{fields}$  below) and *processing speed*. This mechanical result is consistent with the ‘filter theory’ of *selective attention* [Broadbent (1958)], proposed in an attempt to explain a range of the existing experimental results. This theory postulates a low level filter that allows only a limited number of percepts to reach the brain at any time. In this theory, the importance of conscious, directed attention is minimized. The type of attention involving

low level filtering corresponds to the concept of *early selection* [Broadbent (1958)].

Although we termed this ‘heuristic approach’ in the sense that we can instantly feel both the processing speed  $\dot{x}$  and the LTM field  $\varphi(x)$  involved, there is clearly a psycho–physical rule in the background, namely the averaging minimum relation (7.146).

From the decision making point of view, all possible paths (alternatives) represent the *consequences* of decision making. They are, by default, *short-term consequences*, as they are modelled in the micro–time–level. However, the path integral formalism allows calculation of the *long-term consequences*, just by extending the integration time,  $t_{fin} \rightarrow \infty$ . Besides, this *averaging decision mechanics* – choosing the optimal path – actually performs the ‘averaging lift’ in the LSF: from micro– to the macro–level.

#### 7.11.1.4 Force–Fields and Memory in $LSF_{fields}$

At the macro–level in the subspace  $LSF_{fields}$  we formulate the *force–field action principle*

$$\delta S[\varphi] = 0, \quad (7.147)$$

with the action  $S[\varphi]$  dependent on Lewinian force–fields  $\varphi^i = \varphi^i(x)$  ( $i = 1, \dots, N$ ), defined as a temporal integral

$$S[\varphi] = \int_{t_{ini}}^{t_{fin}} \mathcal{L}[\varphi] dt, \quad (7.148)$$

with Lagrangian density given by

$$\mathcal{L}[\varphi] = \int d^n x \mathcal{L}(\varphi_i, \partial_{x^j} \varphi^i),$$

where the integral is taken over all  $n$  coordinates  $x^j = x^j(t)$  of the LSF, and  $\partial_{x^j} \varphi^i$  are partial derivatives of the field variables over coordinates.

On the micro–level in the subspace  $LSF_{fields}$  we have the Feynman–type *sum over fields*  $\varphi^i$  ( $i = 1, \dots, N$ ) given by the adaptive path integral

$$\langle \text{Action} | \text{Intention} \rangle_{fields} = \oint \mathcal{D}[w\varphi] e^{iS[\varphi]} \xrightarrow{\text{Wick}} \oint \mathcal{D}[w\varphi] e^{-S[\varphi]}, \quad (7.149)$$

with action  $S[\varphi]$  given by temporal integral (7.148). (Choosing special forms of the force–field action  $S[\varphi]$  in (7.149) defines micro–level MD & CD, in the  $LSF_{fields}$  space, that is similar to standard quantum–field equations,

see e.g., [Ramond (1990)].) The corresponding partition function has the form similar to (7.143), but with field energy levels.

Regarding topology of the force fields, we have in place *n-categorical Lagrangian-field structure* on the Riemannian LSF manifold  $M$ ,

$$\Phi^i : [0, 1] \rightarrow M, \quad \Phi^i : \Phi_0^i \mapsto \Phi_1^i,$$

generalized from the recursive homotopy dynamics (4.8.1.2) above, using

$$\frac{d}{dt} f_{\dot{x}^i} = f_{x^i} \longrightarrow \partial_\mu \left( \frac{\partial \mathcal{L}}{\partial_\mu \Phi^i} \right) = \frac{\partial \mathcal{L}}{\partial \Phi^i},$$

with  $[x_0, x_1] \longrightarrow [\Phi_0^i, \Phi_1^i].$

**Relationship between memory and force-fields.** As already mentioned, the subspace  $LSF_{fields}$  is related to our *memory storage* [Ashcraft (1994)]. Its global macro-level represents the *long-term memory* (LTM), defined by the least action principle (7.147), related to *cognitive economy* in the model of *semantic memory* [Ratcliff (1978); Collins and Quillian (1969)]. Its local micro-level represents *working memory* (WM), a limited-capacity ‘bottleneck’ defined by the adaptive path integral (7.149). According to our formalism, each of Miller’s  $7 \pm 2$  units [Miller (1956)] of the local WM are adaptively stored and averaged to give the global LTM capacity (similar to the physical notion of potential). This averaging memory lift, from WM to LTM represents *retroactive interference*, while the opposite direction, given by the path integral (7.149) itself, represents *proactive interference*. Both retroactive and proactive interferences are examples of the impact of cognitive contexts on memory. Motivational contexts can exert their influence, too. For instance, a reduction in task-related recall following the completion of the task is one of the clearest examples of force-field influences on memory: the amount of details remembered of a task declines as the force-field tension to complete the task is reduced by actually completing it.

Once defined, the global LTM potential  $\varphi = \varphi(x)$  is then affecting the locomotion transition paths through the path action principle (7.139), as well as general learning (7.137–7.138) and decision making process (7.146).

On the other hand, the two levels of  $LSF_{fields}$  fit nicely into the two levels of processing framework, as presented by [Craik and Lockhart (1972)], as an alternative to theories of separate stages for sensory, working and long-term memory. According to the *levels of processing framework*, stimulus information is processed at multiple levels simultaneously depending



upon its characteristics. In this framework, our macro-level memory field, defined by the fields action principle (7.147), corresponds to the *shallow memory*, while our micro-level memory field, defined by the adaptive path integral (7.149), corresponds to the *deep memory*.

#### 7.11.1.5 Geometries, Topologies and Noise in $LSF_{geom}$

On the macro-level in the subspace  $LSF_{geom}$  representing an  $n$ -dimensional smooth manifold  $M$  with the global Riemannian metric tensor  $g_{ij}$ , we formulate the *geometric action principle*

$$\delta S[g_{ij}] = 0,$$

where  $S = S[g_{ij}]$  is the  $n$ -dimensional *geodesic action* on  $M$ ,

$$S[g_{ij}] = \int d^n x \sqrt{g_{ij} dx^i dx^j}. \quad (7.150)$$

The corresponding Euler-Lagrangian equation gives the *geodesic equation* of the *shortest path* in the manifold  $M$ ,

$$\ddot{x}^i + \Gamma_{jk}^i \dot{x}^j \dot{x}^k = 0,$$

where the symbol  $\Gamma_{jk}^i$  denotes the so-called *affine connection* which is the source of *curvature*, which is geometric description for *noise* (see [Ingber (1997); Ingber (1998)]). The higher the local curvatures of the LSF-manifold  $M$ , the greater the noise in the life space. This noise is the source of our micro-level fluctuations. It can be internal or external; in both cases it curves our micro-LSF.

Otherwise, if instead we choose an  $n$ -dimensional Hilbert-like action (see [Misner *et al.* (1973)]),

$$S[g_{ij}] = \int d^n x \sqrt{\det |g_{ij}|} R, \quad (7.151)$$

where  $R$  is the scalar curvature (derived from  $\Gamma_{jk}^i$ ), we get the  $n$ -dimensional Einstein-like equation:  $G_{ij} = 8\pi T_{ij}$ , where  $G_{ij}$  is the Einstein-like tensor representing geometry of the LSF manifold  $M$  ( $G_{ij}$  is the trace-reversed Ricci tensor  $R_{ij}$ , which is itself the trace of the Riemann curvature tensor of the manifold  $M$ ), while  $T_{ij}$  is the  $n$ -dimensional *stress-energy-momentum* tensor. This equation explicitly states that *psychophysics of the LSF is proportional to its geometry*.  $T_{ij}$  is important quantity, representing motivational *energy*, geometry-imposed *stress* and *momentum* of (loco)motion. As before, we have our 'golden rule': *the greater*

the  $T_{ij}$ -components, the higher the speed of cognitive processes and the lower the macroscopic fatigue.

The choice between the geodesic action (7.150) and the Hilbert action (7.151) depends on our interpretation of time. If time is not included in the LSF manifold  $M$  (non-relativistic approach) then we choose the geodesic action. If time is included in the LSF manifold  $M$  (making it a relativistic-like  $n$ -dimensional space-time) then the Hilbert action is preferred. The first approach is more related to the information processing and the working memory. The later, space-time approach can be related to the long-term memory: we usually recall events closely associated with the times of their happening.

On the micro-level in the subspace  $LSF_{geom}$  we have the adaptive *sum over geometries*, represented by the path integral over all local (regional) Riemannian metrics  $g_{ij} = g_{ij}(x)$  varying from point to point on  $M$  (modulo diffeomorphisms),

$$\langle Action | Intention \rangle_{geom} = \int \mathcal{D}[wg_{ij}] e^{iS[g_{ij}]} \xrightarrow{Wick} \int \mathcal{D}[wg_{ij}] e^{-S[g_{ij}]}, \quad (7.152)$$

where  $\mathcal{D}[g_{ij}]$  is diffeomorphism equivalence class of  $g_{ij}(x) \in M$ .

To include the topological structure (e.g., a number of holes) in  $M$ , we can extend (7.152) as

$$\langle Action | Intention \rangle_{geom/top} = \sum_{topol.} \int \mathcal{D}[wg_{ij}] e^{iS[g_{ij}]}, \quad (7.153)$$

where the topological sum is taken over all connectedness-components of  $M$  determined by the *Euler characteristic*  $\chi$  of  $M$ . This type of integral defines the *theory of fluctuating geometries*, a propagator between  $(n-1)$ -dimensional boundaries of the  $n$ -dimensional manifold  $M$ . One has to contribute a meaning to the integration over geometries. A key ingredient in doing so is to approximate (using simplicial approximation and Regge calculus [Misner *et al.* (1973)]) in a natural way the smooth structures of the manifold  $M$  by piecewise linear structures (mostly using topological simplices  $\Delta$ ). In this way, after the Wick-rotation (7.142), the integral (7.152–7.153) becomes a *simple statistical system*, given by partition function  $Z = \sum_{\Delta} \frac{1}{C_{\Delta}} e^{-S_{\Delta}}$ , where the summation is over all triangulations  $\Delta$  of the manifold  $M$ , while  $C_T$  is the order of the automorphism group of the performed triangulation.

**Micro-level geometry: the source of noise and stress in LSF.**

The subspace  $LSF_{geom}$  is the source of noise, fluctuations and obstacles, as well as psycho-physical stress. Its micro-level is adaptive, reflecting the human ability to efficiently act within the noisy environment and under the stress conditions. By averaging it produces smooth geometry of certain curvature, which is at the same time the smooth psycho-physics. This macro-level geometry directly affects the memory fields and indirectly affects the (loco)motion transition paths.

**The Mental Force Law.** As an effective summary of this section, we state that the psychodynamic transition functor  $\mathcal{TA} : INTENTION_{t_{ini}} \Rightarrow ACTION_{t_{fin}}$ , defined by the generic path integral (7.135), can be interpreted as a *mental force law*, analogous to our musculo-skeletal *covariant force law*,  $F_i = mg_{ij}a^j$ , and its associated *covariant force functor*  $\mathcal{F}_* : TT^*M \rightarrow TTM$  (see section 5.4 above).

## 7.12 Brain-Like Control in a Nutshell

In this final section we propose our most recent model [Ivancevic and Beagley (2005)] for the mathematical unity in biodynamics diversity as well as the natural diversity in mathematical unity, in the specific form of complete biodynamic *brain-like control functor*. This is a neuro-dynamic reflection on our mechanical *covariant force law*,  $F_i = mg_{ij}a^j$ , and its associated *covariant force functor*  $\mathcal{F}_* : TT^*M \rightarrow TTM$  (see section 5.4 above).

Traditional hierarchical robot control (see, e.g., [Vukobratovic *et al.* (1990)], as well as chapter 6) consists of three levels: the *executive* control-level (at the bottom) performs tracking of nominal trajectories in internal-joint coordinates, the *strategic* control-level (at the top) performs ‘planning’ of trajectories of an end-effector in external-Cartesian coordinates, and the *tactical* control-level (in the middle) connects other two levels by means of inverse kinematics.

The modern version of the hierarchical robot control includes decision-making done by the neural (or, neuro-fuzzy) classifier to adapt the (manipulator) control to dynamically changing environment.

On the other hand, the so-called ‘intelligent’ approach to robot control typically represents a form of function approximation, which is itself based on some combination of neuro-fuzzy-genetic computations. Many special issues and workshops focusing on physiological models for robot control reflect the increased attention for the development of *cerebellar models* [van der Smagt (1999); Schaal and Atkeson (1998); Schaal (1999); Arbib (1998)]

for learning robot control with functional decomposition, where the main result could be formulated as: *the cerebellum is more than just the function approximator*.

In this section we try to fit between these three approaches for humanoid control, emphasizing the role of muscle-like robot actuators. We propose a new, physiologically based, tensor-invariant, hierarchical force control (FC, for short) for the 'biomechanically realistic' biodynamics. We consider the muscular torque one-forms  $F_i$  as the most important component of human-like motion; therefore we propose the sophisticated hierarchical system for the subtle  $F_i$ -control: corresponding to the spinal, the cerebellar and cortical levels of human motor control.  $F_i$  are first set-up as testing input-signals to biodynamics, and then covariantly updated as feedback 1-forms  $u_i$  on each FC-level. On the spinal FC-level the nominal joint-trajectory tracking is proposed in the form of affine Hamiltonian control; here the driving torques are given corrections by spinal-reflex controls. On the cerebellar FC-level, the relation is established between canonical joint coordinates  $q^i$ ,  $p_i$  and gradient *neural-image coordinates*  $x^i$ ,  $y_i$ , representing bidirectional, self-organized, associative memory machine; here the driving torques are given the cerebellar corrections. On the cortical FC-level the topological 'hyper-joystick' is proposed as the central FC command-space, selector, with the fuzzy-logic feedback-control map defined on it, giving the cortical corrections to the driving torques.

The model of the spinal FC-level formulated here resembles *autogenetic motor servo* (6.5.3.4), acting on the spinal-reflex level of the human locomotor control. The model of the cerebellar FC-level formulated here mimics the self-organizing, associative function of the excitatory granule cells and the inhibitory Purkinje cells of the cerebellum [Houk *et al.* (1996)]. The model of the cortical FC-level presented in this section mimics the synergistic *regulation of locomotor conditioned reflexes* by the cerebellum [Houk *et al.* (1996)].

We believe that (already mentioned) extremely high order of the driving force redundancy in biodynamics justifies the formulation of the three-level force control system. Also, both brain-like control systems can be easily extended to provide  $SE(3)$ -based force control for moving inverse kinematics (IK) chains of legs and arms.

### 7.12.1 Functor Control Machine

In this subsection we define the functor control-machine (compare with section (4.8) above), for the learning control with functional decomposition, by a two-step generalization of the Kalman's theory of linear MIMO-feedback systems. The first generalization puts the Kalman's theory into the pair of mutually dual linear categories  $\mathbf{Vect}$  and  $\mathbf{Vect}^*$  of vector spaces and linear operators, with a 'loop-functor' representing the closed-loop control, thus formulating the unique, categorical formalism valid both for the discrete and continual MIMO-systems.

We start with the *feedforward continual-sequential state equation*

$$\dot{x}(t+1) = Ax(t) + Bu(t), \quad y(t) = Cx(t), \quad (7.154)$$

where the finite-dimensional vector spaces of *state*  $X \ni x$ , *input*  $U \ni u$ , and *output*  $Y \ni y$  have the corresponding linear operators, respectively  $A : X \rightarrow X$ ,  $B : U \rightarrow X$ , and  $C : X \rightarrow Y$ . The modular system theory comprises the *system dynamics*, given by a pair  $(X, A)$ , together with a *reachability map*  $e : U \rightarrow X$  of the pair  $(B, A)$ , and an *observability map*  $m : X \rightarrow Y$  of the pair  $(A, C)$ . If the reachability map  $e$  is surjection the system dynamics  $(X, A)$  is called *reachable*; if the observability map  $m$  is injection the system dynamics  $(X, A)$  is called *observable*. If the system dynamics  $(X, A)$  is both reachable and observable, a *composition*  $r = m \circ e : U \rightarrow Y$  defines the *total system's response*, which is given by solution of equation (7.154). If the unique solution to the continual-sequential state equation exists, it gives the answer to the (minimal) *realization problem*: find the system  $S$  that realizes the given response  $r = m \circ e : U \rightarrow Y$  (in the smallest number of discrete states and in the shortest time).

The inverse map  $r^{-1} = e^{-1} \circ m^{-1} : Y \rightarrow U$  of the total system's response  $r : U \rightarrow Y$  defines the linear *feedback operator*  $K : Y \rightarrow U$ , given by standard feedback equation

$$u(t) = Ky(t). \quad (7.155)$$

In categorical language, the feedforward system dynamics in the category  $\mathbf{Vect}$  is a pair  $(X, A)$ , where  $X \in \mathbf{Ob}(\mathbf{Vect})$  is an object in  $\mathbf{Vect}$  and  $A : X \rightarrow X \in \mathbf{Mor}(\mathbf{Vect})$  is a  $\mathbf{Vect}$ -morphism. A *feedforward decomposable system* in  $\mathbf{Vect}$  is such a sextuple  $S \equiv (X, A, U, B, Y, C)$  that  $(X, A)$  is the system dynamics in  $\mathbf{Vect}$ , a  $\mathbf{Vect}$ -morphism  $B : U \rightarrow X$  is an *input map*, and a  $\mathbf{Vect}$ -morphism  $C : X \rightarrow Y$  is an *output map*. Any object in  $\mathbf{Vect}$  is characterized by mutually dual notions of its *degree* (a number of its input

morphisms) and its *codegree* (a number of its output morphisms). Similarly, any decomposable system  $S$  in  $\mathbf{Vect}$  has a *reachability map* given by an epimorphism  $e = A \circ B : U \rightarrow X$  and its dual *observability map* given by a monomorphism  $m = C \circ A : X \rightarrow Y$ ; their composition  $r = m \circ e : U \rightarrow Y$  in  $\mathbf{Mor}(\mathbf{Vect})$  defines the total system's response in  $\mathbf{Vect}$  given by the unique solution of the continual-sequential state equation (7.154) [Ivancevic and Snoswell (2001)].

The dual of the total system's response, defined by the feedback equation (7.155), is the *feedback morphism*  $K = e^{-1} \circ m^{-1} : Y \rightarrow U$  belonging to the dual category  $\mathbf{Vect}^*$ .

In this way, the linear, closed-loop, continual-sequential MIMO-system (7.154–7.155) represents the *linear iterative loop functor*  $\mathcal{L} : \mathbf{Vect} \Rightarrow \mathbf{Vect}^*$ .

Our second generalization represents a *natural system process*  $\Xi[\mathcal{L}]$ , that transforms the linear loop functor  $\mathcal{L} : \mathbf{Vect} \Rightarrow \mathbf{Vect}^*$  – into the *nonlinear loop functor*  $\mathcal{NL} : \mathcal{CAT} \Rightarrow \mathcal{CAT}^*$  between two mutually dual nonlinear categories  $\mathcal{CAT}$  and  $\mathcal{CAT}^*$ . We apply the natural process  $\Xi$ , separately

- (1) To the feedforward decomposable system  
 $S \equiv (X, A, U, B, Y, C)$  in  $\mathbf{Vect}$ , and
- (2) To the feedback morphism  $K = e^{-1} \circ m^{-1} : Y \rightarrow U$  in  $\mathbf{Vect}^*$ .

Under the action of the natural process  $\Xi$ , the linear feedforward system dynamics  $(X, A)$  in  $\mathbf{Vect}$  transforms into a nonlinear feedforward  $\Xi$ -dynamics  $(\Xi[X], \Xi[A])$  in  $\mathcal{CAT}$ , represented by a *nonlinear feedforward decomposable system*,  $\Xi[S] \equiv (\Xi[X], \Xi[A], \Xi[U], \Xi[B], \Xi[Y], \Xi[C])$ .

The reachability map transforms into the *input process*  $\Xi[e] = \Xi[A] \circ \Xi[B] : \Xi[U] \rightarrow \Xi[X]$ , while its dual, observability map transforms into the *output process*  $\Xi[m] = \Xi[C] \circ \Xi[A] : \Xi[X] \rightarrow \Xi[Y]$ . In this way the total response of the linear system  $r = m \circ e : U \rightarrow Y$  in  $\mathbf{Mor}(\mathbf{Vect})$  transforms into the *nonlinear system behavior*,  $\Xi[r] = \Xi[m] \circ \Xi[e] : \Xi[U] \rightarrow \Xi[Y]$  in  $\mathbf{Mor}(\mathcal{CAT})$ . Obviously,  $\Xi[r]$ , if exists, is given by a nonlinear  $\Xi$ -transform of the linear state equations (7.154–7.155).

Analogously, the linear feedback morphism  $K = e^{-1} \circ m^{-1} : Y \rightarrow U$  in  $\mathbf{Mor}(\mathbf{Vect}^*)$  transforms into the nonlinear feedback morphism  $\Xi[K] = \Xi[e^{-1}] \circ \Xi[m^{-1}] : \Xi[Y] \rightarrow \Xi[U]$  in  $\mathbf{Mor}(\mathcal{CAT}^*)$ .

In this way, the natural system process  $\Xi : \mathcal{L} \Rightarrow \mathcal{NL}$  is established. That means that the nonlinear loop functor  $L = \Xi[\mathcal{L}] : \mathcal{CAT} \Rightarrow \mathcal{CAT}^*$  is defined out of the linear, closed-loop, continual-sequential MIMO-system (7.154).

In this section we formulate the nonlinear loop functor  $L = \Xi[\mathcal{L}] :$

$\mathcal{CAT} \Rightarrow \mathcal{CAT}^*$  for various hierarchical levels of muscular-like FC.

### 7.12.2 Spinal Control Level

Our first task is to establish the nonlinear loop functor  $L = \Xi[\mathcal{L}] : \mathcal{EX} \Rightarrow \mathcal{EX}^*$  on the category  $\mathcal{EX}$  of spinal FC-level.

Recall that our dissipative, driven  $\delta$ -Hamiltonian biodynamic system on the configuration manifold  $M$  is, in local canonical-symplectic coordinates  $q^i, p_i \in U_p$  on the momentum phase-space manifold  $T^*M$ , given by autonomous equations

$$\dot{q}^i = \frac{\partial H_0}{\partial p_i} + \frac{\partial R}{\partial p_i}, \quad (i = 1, \dots, N) \quad (7.156)$$

$$\dot{p}_i = F_i - \frac{\partial H_0}{\partial q^i} + \frac{\partial R}{\partial q^i}, \quad (7.157)$$

$$q^i(0) = q_0^i, \quad p_i(0) = p_i^0, \quad (7.158)$$

including contravariant equation (7.156) – the velocity vector-field, and covariant equation (7.157) – the force 1-form, together with initial joint angles  $q_0^i$  and momenta  $p_i^0$ . Here the physical Hamiltonian function  $H_0 : T^*M \rightarrow \mathbb{R}$  represents the humanoid total energy function, in local canonical coordinates  $q^i, p_i \in U_p$  on  $T^*M$  given by

$$H_0(q, p) = \frac{1}{2} g^{ij} p_i p_j + V(q),$$

where  $g^{ij} = g^{ij}(q, m)$  denotes the contravariant material metric tensor.

Now, the *control Hamiltonian function*  $H_\gamma : T^*M \rightarrow \mathbb{R}$  of FC is in local canonical coordinates on  $T^*M$  defined by [Nijmeijer and van der Schaft (1990)]

$$H_\gamma(q, p, u) = H_0(q, p) - q^i u_i, \quad (i = 1, \dots, N) \quad (7.159)$$

where  $u_i = u_i(t, q, p)$  are feedback-control 1-forms, representing the spinal FC-level  $u$ -corrections to the covariant torques  $F_i = F_i(t, q, p)$ .

Using  $\delta$ -Hamiltonian biodynamic system (7.156–7.158) and the control Hamiltonian function (7.159), control  $\gamma_\delta$ -Hamiltonian FC-system can be

defined as

$$\begin{aligned}\dot{q}^i &= \frac{\partial H_\gamma(q, p, u)}{\partial p_i} + \frac{\partial R(q, p)}{\partial p_i}, \\ \dot{p}_i &= F_i - \frac{\partial H_\gamma(q, p, u)}{\partial q^i} + \frac{\partial R(q, p)}{\partial q^i}, \\ o^i &= -\frac{\partial H_\gamma(q, p, u)}{\partial u_i}, \quad (i = 1, \dots, N) \\ q^i(0) &= q_0^i, \quad p_i(0) = p_i^0,\end{aligned}$$

where  $o^i = o^i(t)$  represent FC natural outputs which can be different from commonly used joint angles.

If nominal reference outputs  $o_R^i = o_R^i(t)$  are known, the simple PD *stiffness-servo* [Whitney (1987)] could be formulated, via *error function*  $e(t) = o^j - o_R^j$ , in covariant form

$$u_i = K_o \delta_{ij} (o^j - o_R^j) + K_\dot{o} \delta_{ij} (\dot{o}^j - \dot{o}_R^j), \quad (7.160)$$

where  $K$ s are the control-gains and  $\delta_{ij}$  is the Kronecker tensor.

If natural outputs  $o^i$  *actually are* the joint angles and nominal canonical trajectories ( $q_R^i = q_R^i(t)$ ,  $p_i^R = p_i^R(t)$ ) are known, then the stiffness-servo (7.160) could be formulated in canonical form as

$$u_i = K_q \delta_{ij} (q^i - q_R^i) + K_p (p_i - p_i^R).$$

Now, using the fuzzified  $\mu$ -Hamiltonian biodynamic system with fuzzy system numbers (i.e, imprecise segment lengths, masses and moments of inertia, joint dampings and muscular actuator parameters)

$$\dot{q}^i = \frac{\partial H_0(q, p, \sigma_\mu)}{\partial p_i} + \frac{\partial R}{\partial p_i}, \quad (7.161)$$

$$\dot{p}_i = \bar{F}_i - \frac{\partial H_0(q, p, \sigma_\mu)}{\partial q^i} + \frac{\partial R}{\partial q^i}, \quad (7.162)$$

$$q^i(0) = \bar{q}_0^i, \quad p_i(0) = \bar{p}_i^0, \quad (i = 1, \dots, N), \quad (7.163)$$

(see 4.8.4 above) and the control Hamiltonian function (7.159),



$\gamma_\mu$ -Hamiltonian FC-system can be defined as

$$\begin{aligned}\dot{q}^i &= \frac{\partial H_\gamma(q, p, u, \sigma_\mu)}{\partial p_i} + \frac{\partial R(q, p)}{\partial p_i}, \\ \dot{p}_i &= \bar{F}_i - \frac{\partial H_\gamma(q, p, u, \sigma_\mu)}{\partial q^i} + \frac{\partial R(q, p)}{\partial q^i}, \\ \dot{\sigma}^i &= -\frac{\partial H_\gamma(q, p, u, \sigma_\mu)}{\partial u_i}, \quad (i = 1, \dots, N) \\ q^i(0) &= \bar{q}_0^i, \quad p_i(0) = \bar{p}_i^0,\end{aligned}$$

where  $\bar{\sigma}^i = \bar{\sigma}^i(t)$  represent the fuzzified natural outputs.

Finally, applying stochastic forces (diffusion fluctuations  $B_{ij}[q^i(t), t]$  and discontinuous jumps in the form of ND Wiener process  $W^j(t)$ ), i.e., using the fuzzy-stochastic  $[\mu\sigma]$ -Hamiltonian biodynamic system

$$dq^i = \left( \frac{\partial H_0(q, p, \sigma_\mu)}{\partial p_i} + \frac{\partial R}{\partial p_i} \right) dt, \quad (7.164)$$

$$\begin{aligned}dp_i &= B_{ij}[q^i(t), t] dW^j(t) + \\ &\quad \left( \bar{F}_i - \frac{\partial H_0(q, p, \sigma_\mu)}{\partial q^i} + \frac{\partial R}{\partial q^i} \right) dt, \quad (7.165)\end{aligned}$$

$$q^i(0) = \bar{q}_0^i, \quad p_i(0) = \bar{p}_i^0. \quad (7.166)$$

(see 4.8.4 above), and the control Hamiltonian function (7.159),  $\gamma_{\mu\sigma}$ -Hamiltonian FC-system can be defined as

$$\begin{aligned}dq^i &= \left( \frac{\partial H_\gamma(q, p, u, \sigma_\mu)}{\partial p_i} + \frac{\partial R(q, p)}{\partial p_i} \right) dt, \\ dp_i &= B_{ij}[q^i(t), t] dW^j(t) + \\ &\quad \left( \bar{F}_i - \frac{\partial H_\gamma(q, p, u, \sigma_\mu)}{\partial q^i} + \frac{\partial R(q, p)}{\partial q^i} \right) dt, \\ d\bar{\sigma}^i &= -\frac{\partial H_\gamma(q, p, u, \sigma_\mu)}{\partial u_i} dt, \quad (i = 1, \dots, N) \\ q^i(0) &= \bar{q}_0^i, \quad p_i(0) = \bar{p}_i^0.\end{aligned}$$

If we have the case that not all of the configuration joints on the configuration manifold  $M$  are active in the specified robot task, we can introduce the coupling Hamiltonians  $H^j = H^j(q, p)$ ,  $j = 1, \dots, M \leq N$ , corresponding to the system's active joints, and we come to *affine Hamiltonian function*  $H_a : T^*M \rightarrow \mathbb{R}$ , in local canonical coordinates on  $T^*M$

given as [Nijmeijer and van der Schaft (1990)]

$$H_a(q, p, u) = H_0(q, p) - H^j(q, p) u_j. \quad (7.167)$$

Using  $\delta$ -Hamiltonian biodynamic system (7.156–7.158) and the affine Hamiltonian function (7.167), affine  $a_\delta$ -Hamiltonian FC-system can be defined as

$$\dot{q}^i = \frac{\partial H_0(q, p)}{\partial p_i} - \frac{\partial H^j(q, p)}{\partial p_i} u_j + \frac{\partial R}{\partial p_i}, \quad (7.168)$$

$$\dot{p}_i = F_i - \frac{\partial H_0(q, p)}{\partial q^i} + \frac{\partial H^j(q, p)}{\partial q^i} u_j + \frac{\partial R}{\partial q^i}, \quad (7.169)$$

$$\dot{o}^i = -\frac{\partial H_a(q, p, u)}{\partial u_i} = H^j(q, p), \quad (7.170)$$

$$q^i(0) = q_0^i, \quad p_i(0) = p_i^0, \quad (7.171)$$

$$(i = 1, \dots, N; \quad j = 1, \dots, M \leq N).$$

Using the Lie-derivative exact feedback linearization (see (6.2.1.1) above), and applying the *constant relative degree*  $r$  (see [Isidori (1989); Sastri and Isidori (1989)]) to all  $N$  joints of the affine  $a_\delta$ -Hamiltonian FC-system (7.168–7.171), the control law for asymptotic tracking the reference outputs  $\sigma_R^j$  could be formulated as (compare with Lagrangian formulation (6.37) above)

$$u_j = \frac{\dot{o}_R^{(r)j} - \mathcal{L}_f^{(r)} H^j + \sum_{s=1}^r \gamma_{s-1} (o_R^{(s-1)j} - \mathcal{L}_f^{(s-1)} H^j)}{\mathcal{L}_g \mathcal{L}_f^{(r-1)} H^j},$$

where standard MIMO-vector-fields  $f$  and  $g$  are given by

$$f = \left( \frac{\partial H_0}{\partial p_i}, -\frac{\partial H_0}{\partial q^i} \right), \quad g = \left( -\frac{\partial H^j}{\partial p_i}, \frac{\partial H^j}{\partial q^i} \right)$$

and  $\gamma_{s-1}$  are the coefficients of linear differential equation of order  $r$  for the error function  $e(t) = o^j - \sigma_R^j$

$$e^{(r)} + \gamma_{r-1} e^{(r-1)} + \dots + \gamma_1 e^{(1)} + \gamma_0 e = 0.$$

Using the fuzzified  $\mu$ -Hamiltonian biodynamic system (7.161–7.163) and the affine Hamiltonian function (7.167), affine  $a_\mu$ -Hamiltonian FC-system can be defined as

$$\begin{aligned}
\dot{q}^i &= \frac{\partial H_0(q, p, \sigma_\mu)}{\partial p_i} - \frac{\partial H^j(q, p, \sigma_\mu)}{\partial p_i} u_j + \frac{\partial R(q, p)}{\partial p_i}, \\
\dot{p}_i &= \bar{F}_i - \frac{\partial H_0(q, p, \sigma_\mu)}{\partial q^i} + \\
&\quad \frac{\partial H^j(q, p, \sigma_\mu)}{\partial q^i} u_j + \frac{\partial R(q, p)}{\partial q^i}, \\
\dot{\sigma}^i &= - \frac{\partial H_a(q, p, u, \sigma_\mu)}{\partial u_i} = H^j(q, p, \sigma_\mu), \\
q^i(0) &= \bar{q}_0^i, \quad p_i(0) = \bar{p}_i^0, \quad (i = 1, \dots, N; \quad j = 1, \dots, M \leq N).
\end{aligned}$$

Using the fuzzy-stochastic  $[\mu\sigma]$ -Hamiltonian biodynamic system (7.164–7.166) and the affine Hamiltonian function (7.167), affine  $a_{\mu\sigma}$ -Hamiltonian FC-system can be defined as

$$\begin{aligned}
dq^i &= \left( \frac{\partial H_0(q, p, \sigma_\mu)}{\partial p_i} - \frac{\partial H^j(q, p, \sigma_\mu)}{\partial p_i} u_j + \frac{\partial R(q, p)}{\partial p_i} \right) dt, \\
dp_i &= B_{ij}[q^i(t), t] dW^j(t) \\
&\quad + \left( \bar{F}_i - \frac{\partial H_0(q, p, \sigma_\mu)}{\partial q^i} + \frac{\partial H^j(q, p, \sigma_\mu)}{\partial q^i} u_j + \frac{\partial R(q, p)}{\partial q^i} \right) dt, \\
d\sigma^i &= - \frac{\partial H_a(q, p, u, \sigma_\mu)}{\partial u_i} dt = H^j(q, p, \sigma_\mu) dt, \\
q^i(0) &= \bar{q}_0^i, \quad p_i(0) = \bar{p}_i^0, \quad (i = 1, \dots, N; \quad j = 1, \dots, M \leq N).
\end{aligned}$$

Being high-degree and highly nonlinear, all of these affine control systems are extremely sensitive upon the variation of parameters, inputs, and initial conditions. The sensitivity function  $S$  of the affine Hamiltonian  $H_a(q, p, u)$  upon the parameters  $\beta_i$  (representing segment lengths  $L_i$ , masses  $m_i$ , moments of inertia  $J_i$  and joint dampings  $b_i$ , see [Ivancevic and Snoswell (2001); Ivancevic (1991)]), is in the case of  $a_\delta$ -Hamiltonian FC-system defined as

$$S(H, \beta) = \frac{\beta_i}{H_a(q, p, u)} \frac{\partial H_a(q, p, u)}{\partial \beta_i},$$

and similarly in other two  $a_\mu$ - and  $a_{\mu\sigma}$ - cases.

The three affine FC-level systems  $a_\delta$ ,  $a_\mu$  and  $a_{\mu\sigma}$ , resemble (in a fuzzy-stochastic-Hamiltonian form), Houk's autogenetic motor servo of muscle spindle and Golgi tendon proprioceptors [Houk (1979)], correcting the co-

variant driving torques  $F_i = F_i(t, q, p)$  by local ‘reflex controls’  $u_i(t, q, p)$ . They form the nonlinear loop functor  $L = \Xi[\mathcal{L}] : \mathcal{E}\mathcal{X} \Rightarrow \mathcal{E}\mathcal{X}^*$ .

### 7.12.3 Cerebellar Control Level

Our second task is to establish the nonlinear loop functor  $L = \Xi[\mathcal{L}] : \mathcal{T}\mathcal{A} \Rightarrow \mathcal{T}\mathcal{A}^*$  on the category  $\mathcal{T}\mathcal{A}$  of the cerebellar FC-level. Here we propose an oscillatory neurodynamical  $(x, y, \omega)$ -system (adapted from [Ivancevic *et al.* (1999a)]), a bidirectional, self-organized, associative-memory machine, resembling the function of a set of excitatory granule cells and inhibitory Purkinje cells in the middle layer of the cerebellum [Houk *et al.* (1996)]. The neurodynamical  $(x, y, \omega)$ -system acts on *neural-image manifold*  $M_{im}^N$  of the configuration manifold  $M^N$  as a pair of smooth, ‘1 – 1’ and ‘onto’ maps  $(\Psi, \Psi^{-1})$ , where  $\Psi : M^N \rightarrow M_{im}^N$  represents the feedforward map, and  $\Psi^{-1} : M_{im}^N \rightarrow M^N$  represents the feedback map. Locally, it is defined in Riemannian neural coordinates  $x^i, y_i \in V_y$  on  $M_{im}^N$ , which are in bijective correspondence with symplectic joint coordinates  $q^i, p_i \in U_p$  on  $T^*M$ .

The  $(x, y, \omega)$ -system is formed out of two distinct, yet nonlinearly-coupled neural subsystems, with  $A^i(q)$  (7.174) and  $B_i(p)$  (7.175) as system inputs, and the feedback-control 1-forms  $u_i$  (7.180) as system outputs:

(1) Granule cells excitatory (contravariant) and Purkinje cells inhibitory (covariant) activation  $(x, y)$ -dynamics (7.172–7.175), defined respectively by a vector-field  $x^i = x^i(t) : M \rightarrow TM$ , representing a cross-section of the tangent bundle  $TM$ , and a 1-form  $y_i = y_i(t) : M \rightarrow T^*M$ , representing a cross-section of the cotangent bundle  $T^*M$ ; and

(2) Excitatory and inhibitory unsupervised learning  $(\omega)$ -dynamics (7.175–7.177) generated by random differential Hebbian learning process (7.178–7.180), defined respectively by contravariant synaptic tensor-field  $\omega^{ij} = \omega^{ij}(t) : M \rightarrow TTM_{im}^N$  and covariant synaptic tensor-field  $\omega_{ij} = \omega_{ij}(t) : M \rightarrow T^*T^*M$ , representing cross-sections of contravariant and covariant tensor bundles, respectively.

The system equations are:

$$\dot{x}^i = A^i(q) + \omega^{ij} f_j(y) - x^i, \quad (7.172)$$

$$\dot{y}_i = B_i(p) + \omega_{ij} f^j(x) - y_i, \quad (7.173)$$

$$A^i(q) = K_q(q^i - q_R^i), \quad (7.174)$$

$$B_i(p) = K_p(p_i^R - p_i), \quad (7.175)$$

$$\dot{\omega}^{ij} = -\omega^{ij} + I^{ij}(x, y), \quad (7.176)$$

$$\dot{\omega}_{ij} = -\omega_{ij} + I_{ij}(x, y), \quad (7.177)$$

$$I^{ij} = f^i(x) f^j(y) + \dot{f}^i(x) \dot{f}^j(y) + \sigma^{ij}, \quad (7.178)$$

$$I_{ij} = f_i(x) f_j(y) + \dot{f}_i(x) \dot{f}_j(y) + \sigma_{ij}, \quad (7.179)$$

$$u_i = \frac{1}{2}(\delta_{ij} x^i + y_i), \quad (i, j = 1, \dots, N). \quad (7.180)$$

Here  $\omega$  is a symmetric 2nd order synaptic tensor-field;  $I^{ij} = I^{ij}(x, y, \sigma)$  and  $I_{ij} = I_{ij}(x, y, \sigma)$  respectively denote contravariant-excitatory and covariant-inhibitory random differential Hebbian innovation-functions with tensorial Gaussian noise  $\sigma$  (in both variances);  $f$ s and  $\dot{f}$ s denote sigmoid activation functions ( $f = \tanh(\cdot)$ ) and corresponding signal velocities ( $\dot{f} = 1 - f^2$ ), respectively in both variances;

$A^i(q)$  and  $B_i(p)$  are contravariant-excitatory and covariant-inhibitory neural inputs to granule and Purkinje cells, respectively;  $u_i$  are the corrections to the feedback-control 1-forms on the cerebellar FC-level.

Nonlinear activation  $(x, y)$ -dynamics (7.172–7.175), describes a two-phase biological neural oscillator field, in which excitatory neural field excites inhibitory neural field, which itself reciprocally inhibits the excitatory one.  $(x, y)$ -dynamics represents a nonlinear extension of a linear, Lyapunov-stable, conservative, gradient system, defined in local neural coordinates  $x^i, y_i \in V_y$  on  $T^*M$  as

$$\dot{x}^i = -\frac{\partial \Phi}{\partial y_i} = \omega^{ij} y_j - x^i, \quad \dot{y}_i = -\frac{\partial \Phi}{\partial x^i} = \omega_{ij} x^j - y_i. \quad (7.181)$$

The gradient system (7.181) is derived from scalar, neuro-synaptic action potential  $\Phi : T^*M \rightarrow \mathbb{R}$ , given by a negative, smooth bilinear form in  $x^i, y_i \in V_y$  on  $T^*M$  as

$$-2\Phi = \omega_{ij} x^i x^j + \omega^{ij} y_i y_j - 2x^i y_i, \quad (i, j = 1, \dots, N), \quad (7.182)$$

which itself represents a  $\Psi$ -image of the Riemannian metrics  $g : TM \rightarrow \mathbb{R}$  on the configuration manifold  $M$ .

The nonlinear oscillatory activation  $(x, y)$ -dynamics (7.172–7.175) is obtained from the linear conservative dynamics (7.181) by adding configuration-dependent inputs  $A^i$  and  $B_i$ , as well as sigmoid activation functions  $f_j$  and  $\dot{f}^j$ , respectively. It represents an interconnected pair of excitatory and inhibitory neural fields.

Both variant-forms of learning ( $\omega$ )-dynamics (7.176–7.177) are given by generalized unsupervised (self-organizing) Hebbian learning scheme (see [Kosko (1992)]) in which  $\dot{\omega}_{ij}$  (resp.  $\dot{\omega}^{ij}$ ) denotes the new-update value,  $-\omega_{ij}$  (resp.  $-\omega^{ij}$ ) corresponds to the old value and  $I_{ij}(x^i, y_j)$  (resp.  $I^{ij}(x^i, y_j)$ ) is the innovation function of the symmetric 2nd order synaptic tensor-field  $\omega$ . The nonlinear innovation functions  $I_{ij}$  and  $I^{ij}$  are defined by random differential Hebbian learning process (7.178–7.179). As  $\omega$  is symmetric and zero-trace coupling synaptic tensor, the conservative linear activation dynamics (7.181) is equivalent to the rule that the state of each neuron (in both neural fields) is changed in time iff the scalar action potential  $\Phi$  given by (7.182), is lowered. Therefore, the scalar action potential  $\Phi$  represents the monotonically decreasing Lyapunov function (such that  $\dot{\Phi} \leq 0$ ) for the conservative linear dynamics (7.181), which converges to a local minimum or ground state of  $\Phi$ . That is to say, the system (7.181) moves in the direction of decreasing the scalar action potential  $\Phi$ , and when both  $\dot{x}^i = 0$  and  $\dot{y}_i = 0$  for all  $i = 1, \dots, N$ , the steady state is reached.

In this way, the neurodynamical  $(x, y, \omega)$ -system acts as tensor-invariant self-organizing (excitatory / inhibitory) associative memory machine, resembling the set of granule and Purkinje cells of cerebellum [Houk *et al.* (1996)].

The feedforward map  $\Psi : M \rightarrow M$  is realized by the inputs  $A^i(q)$  and  $B_i(p)$  to the  $(x, y, \omega)$ -system, while the feedback map  $\Psi^{-1} : M \rightarrow M$  is realized by the system output, i.e., the feedback-control 1-forms  $u_i(x, y)$ . These represent the cerebellar FC-level corrections to the covariant torques  $F_i = F_i(t, q, p)$ .

The tensor-invariant form of the oscillatory neurodynamical  $(x, y, \omega)$ -system (7.172–7.180) resembles the associative action of the granule and Purkinje cells in the tuning of the limb cortico-rubro-cerebellar recurrent network [Houk *et al.* (1996)], giving the cerebellar correction  $u_i(x, y)$  to the covariant driving torques  $F_i = F_i(t, q, p)$ . In this way  $(x, y, \omega)$ -system forms the nonlinear loop functor  $L = \Xi[\mathcal{L}] : \mathcal{TA} \Rightarrow \mathcal{TA}^*$  (see (A.7.2) in the Appendix).

A sample output from the leading human-motion simulator, *Human Biodynamics Engine* (developed by the authors in Defence Science & Technology Organisation, Australia), is given in Figure 7.66, giving the sophisticated 264 DOF analysis of adult male running with the speed of 5 m/s.

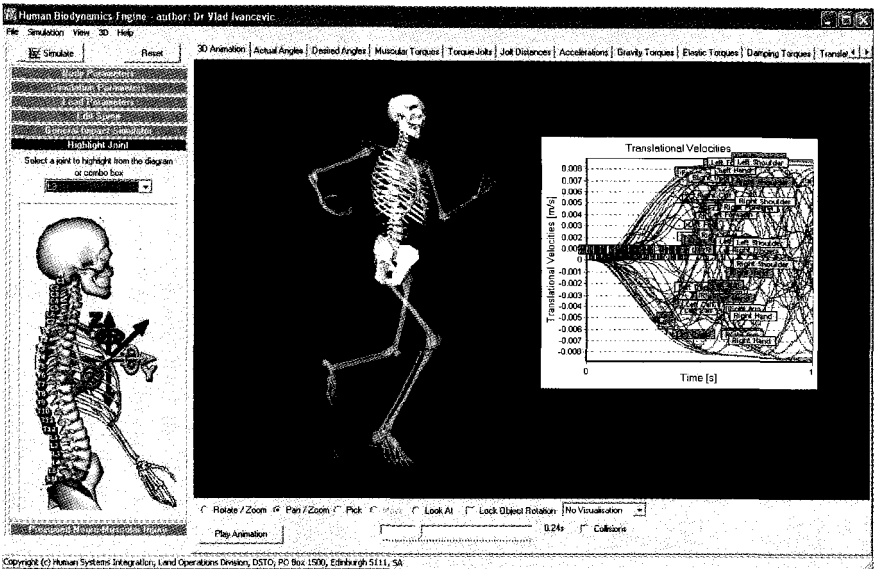


Fig. 7.66 Sample output from the Human Biodynamics Engine: running with the speed of 5 m/s.

7.12.4 Cortical Control Level

Our third task is to establish the nonlinear loop functor  $L = \Xi[\mathcal{L}] : ST \Rightarrow ST^*$  on the category  $ST$  of the cortical FC-level.

Recall that for the purpose of cortical control, the purely rotational biodynamic manifold  $M$  could be firstly reduced to  $N$ -torus and subsequently transformed to  $N$ -cube ('hyper-joystick'), using the following geometric techniques (see subsection (3.5.3.2) above).

Denote by  $S^1$  the constrained unit circle in the complex plane. This is an Abelian Lie group. We have two reduction homeomorphisms

$$SO(3) \gtrsim SO(2) \triangleright SO(2) \triangleright SO(2), \quad \text{and} \quad SO(2) \approx S^1,$$

where ' $\triangleright$ ' denotes the noncommutative semidirect product.

Next, let  $I^N$  be the unit cube  $[0,1]^N$  in  $\mathbb{R}^N$  and ' $\sim$ ' an equivalence relation on  $\mathbb{R}^N$  obtained by 'gluing' together the opposite sides of  $I^N$ , preserving their orientation. Therefore,  $M$  can be represented as the quotient space of  $\mathbb{R}^N$  by the space of the integral lattice points in  $\mathbb{R}^N$ , that is a

constrained ND torus  $T^N$ :

$$\mathbb{R}^N / Z^N = I^N / \sim \cong \prod_{i=1}^N S_i^1 \equiv \{(q^i, i = 1, \dots, N) : \text{mod } 2\pi\} = T^N.$$

In the same way, the momentum phase-space manifold  $T^*M$  can be represented by  $T^*T^N$ .

Conversely by ‘ungluing’ the configuration space we get the primary unit cube. Let ‘ $\sim^*$ ’ denote an equivalent decomposition or ‘ungluing’ relation. By the *Tychonoff product-topology theorem*, for every such quotient space there exists a ‘selector’ such that their quotient models are homeomorphic, that is,  $T^N / \sim^* \approx A^N / \sim^*$ . Therefore  $I_q^N$  represents a ‘selector’ for the configuration torus  $T^N$  and can be used as an  $N$ -directional ‘ $\hat{q}$ -command-space’ for FC. Any subset of DOF on the configuration torus  $T^N$  representing the joints included in the general biodynamics has its simple, rectangular image in the rectified  $\hat{q}$ -command space – selector  $I_q^N$ , and any joint angle  $q^i$  has its rectified image  $\hat{q}^i$ .

In the case of an end-effector,  $\hat{q}^i$  reduces to the position vector in external-Cartesian coordinates  $z^r$  ( $r = 1, \dots, 3$ ). If orientation of the end-effector can be neglected, this gives a topological solution to the standard inverse kinematics problem.

Analogously, all momenta  $\hat{p}_i$  have their images as rectified momenta  $\hat{p}_i$  in the  $\hat{p}$ -command space – selector  $I_p^N$ . Therefore, the total momentum phase-space manifold  $T^*T^N$  obtains its ‘cortical image’ as the  $(\widehat{q}, \widehat{p})$ -command space, a trivial 2ND bundle  $I_q^N \times I_p^N$ .

Now, the simplest way to perform the feedback FC on the cortical  $(\widehat{q}, \widehat{p})$ -command space  $I_q^N \times I_p^N$ , and also to mimic the cortical-like behavior [1,2], is to use the 2ND fuzzy-logic controller, in pretty much the same way as in popular ‘inverted pendulum’ examples [Kosko (1992); Kosko (1996)].

We propose the fuzzy feedback-control map  $\Xi$  that maps all the rectified joint angles and momenta into the feedback-control 1-forms

$$\Xi : (\hat{q}^i(t), \hat{p}_i(t)) \mapsto u_i(t, q, p), \quad (7.183)$$

so that their corresponding universes of discourse,  $\hat{M}^i = (\hat{q}_{max}^i - \hat{q}_{min}^i)$ ,  $\hat{P}_i = (\hat{p}_i^{max} - \hat{p}_i^{min})$  and  $U_i = (u_i^{max} - u_i^{min})$ , respectively, are mapped as

$$\Xi : \prod_{i=1}^N \hat{M}^i \times \prod_{i=1}^N \hat{P}_i \rightarrow \prod_{i=1}^N U_i. \quad (7.184)$$



The 2N-D map  $\Xi$  (7.183–7.184) represents a *fuzzy inference system*, defined by (adapted from [Ivancevic *et al.* (1999b)]):

- (1) *Fuzzification* of the crisp *rectified* and *discretized* angles, momenta and controls using Gaussian–bell membership functions

$$\mu_k(\chi) = \exp\left[-\frac{(\chi - m_k)^2}{2\sigma_k}\right], \quad (k = 1, 2, \dots, 9),$$

where  $\chi \in D$  is the common symbol for  $\hat{q}^i$ ,  $\hat{p}_i$  and  $u_i(q, p)$  and  $D$  is the common symbol for  $M^i$ ,  $\hat{P}_i$  and  $i$ ; the mean values  $m_k$  of the seven partitions of each universe of discourse  $D$  are defined as  $m_k = \lambda_k D + \chi_{min}$ , with partition coefficients  $\lambda_k$  uniformly spanning the range of  $D$ , corresponding to the set of nine linguistic variables  $L = \{NL, NB, NM, NS, ZE, PS, PM, PB, PL\}$ ; standard deviations are kept constant  $\sigma_k = D/9$ . Using the linguistic vector  $L$ , the  $9 \times 9$  FAM (fuzzy associative memory) matrix (a ‘linguistic phase–plane’), is heuristically defined for each humanoid joint, in a symmetrical weighted form

$$\mu_{kl} = \varpi_{kl} \exp\{-50[\lambda_k + u(q, p)]^2\}, \quad (k, l = 1, 2, \dots, 9)$$

with weights  $\varpi_{kl} \in \{0.6, 0.6, 0.7, 0.7, 0.8, 0.8, 0.9, 0.9, 1.0\}$ .

- (2) *Mamdani inference* is used on each FAM–matrix  $\mu_{kl}$  for all humanoid joints:

(i)  $\mu(\hat{q}^i)$  and  $\mu(\hat{p}_i)$  are combined inside the fuzzy IF–THEN rules using AND (Intersection, or Minimum) operator,

$$\mu_k[\bar{u}_i(q, p)] = \min\{\mu_{kl}(\hat{q}^i), \mu_{kl}(\hat{p}_i)\}.$$

(ii) the output sets from different IF–THEN rules are then combined using OR (Union, or Maximum) operator, to get the final output, fuzzy–covariant torques,

$$\mu[u_i(q, p)] = \max_k\{\mu_k[\bar{u}_i(q, p)]\}.$$

- (3) *Defuzzification* of the fuzzy controls  $\mu[u_i(q, p)]$  with the ‘center of gravity’ method

$$u_i(q, p) = \frac{\int \mu[u_i(q, p)] du_i}{\int du_i},$$

to update the crisp feedback-control 1-forms  $u_i = u_i(t, q, p)$ . These represent the cortical FC-level corrections to the covariant torques  $F_i = F_i(t, q, p)$ .

Operationally, the construction of the cortical  $\widehat{(q, p)}$ -command space  $I_q^N \times I_p^N$  and the 2ND feedback map  $\Xi$  (7.183–7.184), mimic the regulation of locomotor conditioned reflexes by the motor cortex [Houk *et al.* (1996)], giving the cortical correction to the covariant driving torques  $F_i$ . Together they form the nonlinear loop functor  $\mathcal{NL} = \Xi[\mathcal{L}] : \mathcal{ST} \Rightarrow \mathcal{ST}^*$  (derived using the computer-algebra system in (A.7.2), Appendix).

### 7.12.5 A Note on Muscular Training

In this subsection we extend the concept of affine Hamiltonian input-output control system to ‘intelligent’ biodynamics control system as a combination of mechanical feedforward part and neural-like feedback part.

Recall that AI neuro-fuzzy adaptive control theory attempts to design sophisticated control systems with high performance and flexibility, by combining ANNs and fuzzy logic control [Brown and Harris (1994)]. Integrating the most relevant elements of neuro-fuzzy algorithms, classical control and signal processing, these so-called ‘intelligent controllers’ have to cope with ill-defined, complex dynamics, characterized by spatial and temporal variations, yet be robust to minor faults and disturbances, and deal with nonlinear relationships over wide operating envelopes. Thus, they have to be self-organized, adaptive systems that automatically learn by interacting with their environment, with little ‘a priori’ knowledge.

Therefore, to emulate physiological motor control, we can use the neuro-fuzzy intelligent controller for optimization of our muscle-like input torques  $u_i = F_i(p, t)$ , defined by

$$F_i(p, t) = \frac{(F_i^0 b_i - a^i p_i)(1 - e^{-\frac{t}{\tau_i}})}{p_i - b_i}.$$

First, for the  $i$ th equivalent muscular actuator we can define the *torque state-space* as an exponential-hyperbolic surface in the  $\{F - p - t\}$  coordinate system (assuming the simplest possible, impulse case of the  $\{p - t\}$  relation).

Then, for the  $i$ th muscle-actuator we can define the torque optimization as the increase of all three  $F - p - t$  coordinates, which geometrically corresponds to the *homothetic transformation* of the surface. This actually

represents the *muscle training process*, equivalent to the transformation of the muscle-torque parameter set  $F_i = \{F, a, b, t|_i\}$  ( $i = 1, \dots, N$ ) for the  $i$ th muscular actuator. The control of the muscle training process can be performed by the use of the neuro-fuzzy controller, as follows.

The universal approximation theorem of Kolmogorov states [Haykin (1994)]: Let  $\phi(\cdot)$  be a nonconstant, bounded, and monotone-increasing  $C^0$ -function. Let  $I^N$  denote  $N$ D unit hypercube  $[0, 1]^N$ . The space of  $C^0$ -functions on  $I^N$  is denoted by  $C(I^N)$ . Then, given any function  $f \in C(I^N)$  and  $\epsilon > 0$ , there exist an integer  $M$  and sets of real constants  $\alpha_i, \theta_i, \omega_{ij}$ ,  $i = 1, \dots, M$ ;  $j = 1, \dots, N$  such that we may define

$$F(x_1, \dots, x_N) = \alpha_i \phi(\omega_{ij} x_j - \theta_i),$$

as an approximate realization of the function  $f(\cdot)$ ; that is

$$|F(x_1, \dots, x_N) - f(x_1, \dots, x_N)| < \epsilon \quad \text{for all } \{x_1, \dots, x_N\} \in I^N.$$

This theorem is directly applicable to multilayer perceptrons. First, the logistic function  $1/[1 + \exp(-v)]$  used as the sigmoidal nonlinearity in a neuron model for the construction of a multilayer perceptron is indeed a nonconstant, bounded, and monotone-increasing function; it therefore satisfies the conditions imposed on the function  $\phi(\cdot)$ . Second, the upper equation represents the output of a multilayer perceptron described as follows:

- (1) The network has  $n$  input nodes and a single hidden layer consisting of  $M$  neurons; the inputs are denoted by  $x_1, \dots, x_N$ .
- (2)  $i$ th hidden neuron has synaptic weights  $\omega_{i1}, \dots, \omega_{iN}$  and threshold  $\theta_i$ .
- (3) The network output  $y_j$  is a linear combination of the outputs of the hidden neurons, with  $\alpha_i, \dots, \alpha_M$  defining the coefficients of this combination.

The theorem actually states that a single hidden layer is sufficient for a multilayer perceptron to compute a uniform  $\epsilon$  approximation to a given training set represented by the set of inputs  $x_1, \dots, x_N$  and desired (target) output  $f(x_1, \dots, x_N)$ . However, the theorem does not say that a single layer is *optimum* in the sense of learning time or ease of implementation.

Recall that training of multilayer perceptrons is usually performed using a certain clone of the BP algorithm (7.6.2.1). In this forward-pass/backward-pass gradient-descending algorithm, the adjusting of

synaptic weights is defined by the extended  $\delta$ -rule, given by equation

$$\Delta\omega_{ji}(N) = \eta \cdot \delta_j(N) \cdot y_i(N), \quad (7.185)$$

where  $\Delta\omega_{ji}(N)$  corresponds to the *weight correction*,  $\eta$  is the *learning-rate parameter*,  $\delta_j(N)$  denotes the *local gradient* and  $y_i(N)$  – the *input signal of neuron  $j$* ; while the *cost function  $E$*  is defined as the instantaneous sum of squared errors  $e_j^2$

$$E(n) = \frac{1}{2} \sum_j e_j^2(N) = \frac{1}{2} \sum_j [d_j(N) - y_j(N)]^2, \quad (7.186)$$

where  $y_j(N)$  is the output of  $j$ th neuron, and  $d_j(N)$  is the desired (target) response for that neuron. The slow BP convergence rate (7.185–7.186) can be accelerated using the faster LM algorithm (see subsection 7.6.2.1 above), while its robustness can be achieved using an appropriate fuzzy controller (see (7.8.3) above).

In this way, the muscle training finite-control map  $TRN : F_0 \rightarrow F_1$  can be performed for the  $i$ th equivalent muscular actuator

$$TRN_i : \{F_\mu^0, a_0, b_0, \tau_0\}_i \mapsto \{F_\mu^1, a_1, b_1, \tau_1\}_i \quad i = 1, \dots, N,$$

(where indices  $^0$  and  $^1$  correspond to the *actual* and *desired* values, respectively), by the use of the neuro-fuzzy learning algorithm.

Muscle training is physiologically performed through the four basic types of muscular contraction:

- (1) *Isotonic (dynamic, concentric, myometric)* – muscle shortens as tensions developed;
- (2) *Isometric (static)* – muscle develops tension but does not change length;
- (3) *Eccentric (plyometric)* – muscle lengthens as tension develops; and
- (4) *Isokinetic* – muscle shortens as tension is developed through a full range of motion performed at constant speed.

In order to ensure the greatest benefits from any weight lifting-based training program, several guidelines should be followed [Ivancevic (1991); Ivancevic *et al.* (1995)]:

- (1) Muscles need to be overloaded, i.e., exercised against near maximal or maximal resistances;
- (2) The overload need to be progressive throughout the duration of the program; and

- (3) Larger muscle groups need to be exercised before smaller groups (like palmar and plantar flexors), and no two successive lifts or exercises should involve the same muscle groups.

### 7.12.6 Errors in Motion Control: Locomotor Injuries

Now, we can summarize what is meant herein under the statement ‘improper muscular synergy and configuration control’ of biodynamics (see [Ivancevic (1995); Ivancevic *et al.* (1995)]).

Mechanically, the improper control means incorrect, inadequate, muscular input torque one-forms,  $u_i = F_i^{tot}$ , in the covariant force model,  $F_i = mg_{ij}a^j$ , and this physiologically represents improper muscular synergy, anatomically realized by extrapyramidal neural pathway.

From the muscle training point of view, improper control means non-convergent neuro-fuzzy learning, representing the finite-control map on the muscle-torque state-space

$$TRN_i : \{F_\mu^0, a_0, b_0, \tau_0\}_i \mapsto \{F_\mu^1, a_1, b_1, \tau_1\}_i, \quad (i = 1, \dots, N).$$

Motor learning can now be defined as an internal quotient map,  $ML : I_{(int)}^N \rightarrow F_{(int)}^N$ , and improper motor learning is just the incorrect map  $ML$ , anatomically realized by transition from the *premotor cortex* to the *motor cortex*.

Finally, motor control can be defined as a map,  $MC : F_{(int)}^N \rightarrow F_{(ext)}^N$ , and improper motor control is just the incorrect map  $MC$ , representing the improper muscular synergy, anatomically realized by extrapyramidal neural pathway.

## Appendix A

### A.1 Basic Formulas from Tensor Analysis

Biodynamic laws must be independent of any particular coordinate systems used in describing them mathematically, if they are to be valid. In other words, all biodynamic equations need to be tensorial or *covariant*. Therefore, for the reference purpose, in this subsection, we give the basic formulas from the standard tensor calculus, which is used throughout the text. The basic notational convention used in tensor calculus is Einstein's summation convention over repeated indices. More on this subject can be found in any standard textbook on mathematical methods for scientists and engineers, or mathematical physics (we recommend [Misner *et al.* (1973)]).

#### A.1.1 General Functional Transformation

To introduce tensors, consider a standard linear  $nD$  matrix system,  $\mathbf{Ax} = \mathbf{b}$ . It can be rewritten in the so-called *covariant form* as

$$a_{ij}x^j = b_i, \quad (i, j = 1, \dots, n). \quad (\text{A.1})$$

Here,  $i$  is a *free index* and  $j$  is a *dummy index* to be summed upon, so the expansion of (A.1) gives

$$\begin{aligned} a_{11}x^1 + a_{12}x^2 + \dots + a_{1n}x^n &= b_1, \\ a_{21}x^1 + a_{22}x^2 + \dots + a_{2n}x^n &= b_2, \\ &\dots \\ a_{n1}x^1 + a_{n2}x^2 + \dots + a_{nn}x^n &= b_n, \end{aligned}$$

as expected from the original matrix form  $\mathbf{Ax} = \mathbf{b}$ . This indicial notation can be more useful than the matrix one, like e.g., in computer science,

where indices would represent loop variables. However, the full potential of tensor analysis is to deal with nonlinear multivariate systems, which are untractable by linear matrix algebra and analysis. The core of this *nonlinear multivariate analysis* is *general functional transformation*.

#### A.1.1.1 Transformation of Coordinates

Suppose that we have two sets of curvilinear coordinates that are single-valued, continuous and smooth functions of time,  $x^j = x^j(t)$ , ( $j = 1, \dots, m$ ) and  $\bar{x}^i = \bar{x}^i(t)$ , ( $i = 1, \dots, n$ ), respectively, representing trajectories of motion of some biodynamic system. Then a general  $(m \times n)$ D transformation (i.e., a nonlinear map)  $x^j \mapsto \bar{x}^i$  is defined by the set of transformation equations

$$\bar{x}^i = \bar{x}^i(x^j), \quad (i = 1, \dots, n; j = 1, \dots, m). \quad (\text{A.2})$$

In case of the square transformation,  $m = n$ , we can freely exchange the indices, like e.g., in general relativity theory. On the other hand, in the general case of rectangular transformation,  $m \neq n$ , like e.g., in robotics, and we need to take care of these 'free' indices.

Now, if the *Jacobian determinant* of this coordinate transformation is different from zero,

$$\left| \frac{\partial \bar{x}^i}{\partial x^j} \right| \neq 0,$$

then the transformation (A.2) is reversible and the inverse transformation,

$$x^j = x^j(\bar{x}^i),$$

exists as well. Finding the inverse transformation is the problem of matrix inverse: in case of the square matrix it is well defined, although the inverse might not exist if the matrix is singular. However, in case of the square matrix, its proper inverse does not exist, and the only tool that we are left with is the so-called *Moore–Penrose pseudoinverse*, which gives an optimal solution (in the least-squares sense) of an overdetermined system of equations. Every (overdetermined) rectangular coordinate transformation gives rise to a *redundant system*.

For example, in Euclidean 3D space  $\mathbb{R}^3$ , transformation from Cartesian coordinates  $y^k = \{x, y, z\}$  into spherical coordinates  $x^i = \{\rho, \theta, \varphi\}$  is given by

$$y^1 = x^1 \cos x^2 \cos x^3, \quad y^2 = x^1 \sin x^2 \cos x^3, \quad y^3 = x^1 \sin x^3, \quad (\text{A.3})$$

with the Jacobian matrix given by

$$\left( \frac{\partial y^k}{\partial x^i} \right) = \begin{pmatrix} \cos x^2 \cos x^3 & -x^1 \sin x^2 \cos x^3 & -x^1 \cos x^2 \sin x^3 \\ \sin x^2 \cos x^3 & x^1 \cos x^2 \cos x^3 & -x^1 \sin x^2 \sin x^3 \\ \sin x^3 & 0 & x^1 \cos x^3 \end{pmatrix} \quad (\text{A.4})$$

and the corresponding Jacobian determinant,  $\left| \frac{\partial y^k}{\partial x^i} \right| = (x^1)^2 \cos x^3$ .

An inverse transform is given by

$$\begin{aligned} x^1 &= \sqrt{(y^1)^2 + (y^2)^2 + (y^3)^2}, & x^2 &= \arctan \left( \frac{y^2}{y^1} \right), \\ x^3 &= \arctan \left( \frac{y^3}{\sqrt{(y^1)^2 + (y^2)^2}} \right), & \text{with } \left| \frac{\partial x^i}{\partial y^k} \right| &= \frac{1}{(x^1)^2 \cos x^3}. \end{aligned}$$

As a main biodynamic example, we have a rectangular transformation from 6 DOF external, end-effector (e.g., hand) coordinates, into  $n$  DOF internal, joint-angle coordinates. In most cases this is a redundant manipulator system, with infinite number of possible joint trajectories.

#### A.1.1.2 Scalar Invariants

A *scalar invariant* (or, a zeroth order tensor) with respect to the transformation (A.2) is the quantity  $\varphi = \varphi(t)$  defined as

$$\varphi(x^i) = \bar{\varphi}(\bar{x}^i),$$

which does not change at all under the coordinate transformation. In other words,  $\varphi$  is *invariant* under (A.2). Biodynamic examples of scalar invariants include various energies (kinetic, potential, biochemical, mental) with the corresponding kinds of work, as well as related thermodynamic quantities (free energy, temperature, entropy, etc.).

#### A.1.1.3 Vectors and Covectors

Any geometric object  $v^i = v^i(t)$  that under the coordinate transformation (A.2) transforms as

$$\bar{v}^i = v^j \frac{\partial \bar{x}^i}{\partial x^j}, \quad (\text{remember, summing upon } j\text{-index}),$$

represents a *vector*, traditionally called a *contravariant vector*, or, a first-order contravariant tensor. Standard biodynamic examples include both translational and rotational velocities and accelerations.



On the other hand, any geometric object  $v_i = v_i(t)$  that under the coordinate transformation (A.2) transforms as

$$\bar{v}_i = v_j \frac{\partial x^j}{\partial \bar{x}^i},$$

represents a *one-form* or *covector*, traditionally called a *covariant vector*, or, a first order covariant tensor. Standard biodynamic examples include both translational and rotational momenta, forces and torques.

#### A.1.1.4 Second-Order Tensors

Any geometric object  $t^{ik} = t^{ik}(t)$  that under the coordinate transformation (A.2) transforms as

$$\bar{t}^{ik} = t^{jl} \frac{\partial \bar{x}^i}{\partial x^j} \frac{\partial \bar{x}^k}{\partial x^l}, \quad (i, k = 1, \dots, n; j, l = 1, \dots, m),$$

represents a *second-order contravariant tensor*. It can be obtained as an *outer product* of two contravariant vectors,  $t^{ik} = u^i v^k$ .

Any geometric object  $t_{ik} = t_{ik}(t)$  that under the coordinate transformation (A.2) transforms as

$$\bar{t}_{ik} = t_{jl} \frac{\partial x^j}{\partial \bar{x}^i} \frac{\partial x^l}{\partial \bar{x}^k},$$

represents a *second-order covariant tensor*. It can be obtained as an outer product of two covariant vectors,  $t_{ik} = u_i v_k$ .

Any geometric object  $t_k^i = t_k^i(t)$  that under the coordinate transformation (A.2) transforms as

$$\bar{t}_k^i = t_l^j \frac{\partial \bar{x}^i}{\partial x^j} \frac{\partial x^l}{\partial \bar{x}^k},$$

represents a *second-order mixed tensor*. It can be obtained as an outer product of a covariant vector and a contravariant vector,  $t_k^i = u^i v_k$ .

Standard biodynamic examples include:

- (1) The fundamental (material) covariant metric tensor  $\mathbf{g} \equiv g_{ik}$ , i.e., inertia matrix, given usually by the transformation from Cartesian coordinates  $y^j$  to curvilinear coordinates  $x^i$ ,

$$g_{ik} = \frac{\partial y^j}{\partial x^i} \frac{\partial y^j}{\partial x^k}, \quad (\text{summing over } j).$$

It is used in the quadratic metric form  $ds^2$  of the space in consideration (e.g., a certain biodynamic configuration space)

$$ds^2 \equiv dy^j dy^j = g_{ik} dx^i dx^k,$$

where the first term on the r.h.s denotes the *Euclidean metrics*, while the second term is the *Riemannian metric* of the space, respectively.

(2) Its inverse  $\mathbf{g}^{-1} \equiv g^{ik}$ , given by

$$g^{ik} = (g_{ik})^{-1} = \frac{G_{ik}}{|g_{ik}|}, \quad G_{ik} \text{ is the cofactor of the matrix } (g_{ik});$$

(3) The *Kronecker-delta* symbol  $\delta_k^i$ , given by

$$\delta_k^i = \begin{cases} 1 & \text{if } i = k \\ 0 & \text{if } i \neq k \end{cases},$$

used to denote the metric tensor in Cartesian orthogonal coordinates.  $\delta_k^i$  is a discrete version of the *Dirac  $\delta$ -function*. The *generalized Kronecker-delta symbol*  $\delta_{lmn}^{ijk}$  (in 3D) is the product of *Ricci antisymmetric tensors*  $\varepsilon^{ijk}$  and  $\varepsilon_{lmn}$ ,

$$\delta_{lmn}^{ijk} = \varepsilon^{ijk} \varepsilon_{lmn} = \begin{cases} 0 & \text{if at least two indices are equal} \\ +1 & \text{if both } ijk \text{ and } lmn \text{ are either even or odd} \\ -1 & \text{if one of } ijk, lmn \text{ is even and the other is odd} \end{cases}.$$

For example, to derive components of the metric tensor  $\mathbf{g} \equiv g_{ij}$  in standard spherical coordinates, we use the relations (A.3–A.4) between the spherical coordinates  $x^i = \{\rho, \theta, \varphi\}$  and the Cartesian coordinates  $y^k = \{x, y, z\}$ , and the definition,  $g_{ij} = \frac{\partial y^k}{\partial x^i} \frac{\partial y^k}{\partial x^j}$ , to get the metric tensor (in matrix form)

$$(g_{ij}) = \begin{pmatrix} 1 & 0 & 0 \\ 0 & (x^1)^2 \cos^2 x^3 & 0 \\ 0 & 0 & (x^1)^2 \end{pmatrix} = \begin{pmatrix} 1 & 0 & 0 \\ 0 & \rho^2 \cos^2 \varphi & 0 \\ 0 & 0 & \rho^2 \end{pmatrix}, \quad (\text{A.5})$$

and the inverse metric tensor

$$(g^{ij}) = \begin{pmatrix} 1 & 0 & 0 \\ 0 & \frac{1}{(x^1)^2 \cos^2 x^3} & 0 \\ 0 & 0 & \frac{1}{(x^1)^2} \end{pmatrix} = \begin{pmatrix} 1 & 0 & 0 \\ 0 & \frac{1}{\rho^2 \cos^2 \varphi} & 0 \\ 0 & 0 & \frac{1}{\rho^2} \end{pmatrix}. \quad (\text{A.6})$$

Given a tensor, we can derive other tensors by raising and lowering its indices, by their multiplication with covariant and contravariant metric

tensors. In this way, the so-called *associated tensors* to the given tensor are formed. For example,  $v^i$  and  $v_i$  are associated tensors, related by

$$v_i = g_{ik}v^k \quad \text{and} \quad v^i = g^{ik}v_k.$$

Given two vectors,  $\mathbf{u} \equiv u^i$  and  $\mathbf{v} \equiv v^i$ , their inner (dot, or scalar) product is given by

$$\mathbf{u} \cdot \mathbf{v} \equiv g_{ij}u^i v^j,$$

while their vector (cross) product (in 3D) is given by

$$\mathbf{u} \times \mathbf{v} \equiv \varepsilon_{ijk}u^j v^k.$$

#### A.1.1.5 Higher-Order Tensors

As a generalization of above tensors, consider a geometric object  $R^i_{kps} = R^i_{kps}(t)$  that under the coordinate transformation (A.2) transforms as

$$\bar{R}^i_{kps} = R^j_{lqt} \frac{\partial \bar{x}^i}{\partial x^j} \frac{\partial x^l}{\partial \bar{x}^k} \frac{\partial x^q}{\partial \bar{x}^p} \frac{\partial x^t}{\partial \bar{x}^s}, \quad (\text{all indices} = 1, \dots, n). \quad (\text{A.7})$$

Clearly,  $R^i_{kjl} = R^i_{kjl}(x, t)$  is a fourth order tensor, once contravariant and three times covariant, representing the central tensor in Riemannian geometry, called the *Riemann curvature tensor*. As all biodynamic configuration spaces are Riemannian manifolds, they are all characterized by curvature tensors. In case  $R^i_{kjl} = 0$ , the corresponding Riemannian manifold reduces to the Euclidean space of the same dimension, in which  $g_{ik} = \delta^i_k$ .

If one contravariant and one covariant index of a tensor a set equal, the resulting sum is a tensor of rank two less than that of the original tensor. This process is called *tensor contraction*.

If to each point of a region in an  $n$ D space there corresponds a definite tensor, we say that a *tensor-field* has been defined. In particular, this is a *vector-field* or a *scalar-field* according as the tensor is of rank one or zero. It should be noted that a tensor or tensor field is not just the set of its components in one special coordinate system, but all the possible sets of components under any transformation of coordinates.

#### A.1.1.6 Tensor Symmetry

A tensor is called *symmetric* with respect to two indices of the same variance if its components remain unaltered upon interchange of the indices;

e.g.,  $a_{ij} = a_{ji}$ , or  $a^{ij} = a^{ji}$ . A tensor is called *skew-symmetric* (or, *antisymmetric*) with respect to two indices of the same variance if its components change sign upon interchange of the indices; e.g.,  $a_{ij} = -a_{ji}$ , or  $a^{ij} = -a^{ji}$ . Regarding tensor symmetry, in the following we will prove several useful propositions.

(i) *Every second-order tensor can be expressed as the sum of two tensors, one of which is symmetric and the other is skew-symmetric.* For example, a second order tensor  $a_{ij}$ , which is for  $i, j = 1, \dots, n$  given by the  $n \times n$ -matrix

$$a_{ij} = \begin{pmatrix} a_{11} & a_{12} & \dots & a_{1n} \\ a_{21} & a_{22} & \dots & a_{n2} \\ \dots & \dots & \dots & \dots \\ a_{n1} & a_{n2} & \dots & a_{nn} \end{pmatrix},$$

can be rewritten as

$$\begin{aligned} a_{ij} &= \frac{1}{2}a_{ij} + \frac{1}{2}a_{ij} + \frac{1}{2}a_{ji} - \frac{1}{2}a_{ji}, \quad \text{that can be rearranged as} \\ &= \frac{1}{2}a_{ij} + \frac{1}{2}a_{ji} + \frac{1}{2}a_{ij} - \frac{1}{2}a_{ji}, \quad \text{which can be regrouped as} \\ &= \frac{1}{2}(a_{ij} + a_{ji}) + \frac{1}{2}(a_{ij} - a_{ji}), \quad \text{which can be written as} \\ &= a_{(ij)} + a_{[ij]}, \end{aligned}$$

where  $a_{(ij)}$  denotes its symmetric part, while  $a_{[ij]}$  denotes its skew-symmetric part, as required.

(ii) *Every quadratic form can be made symmetric.* For example, a quadratic form  $a_{ij}x^i x^j$ , that (for  $i, j = 1, \dots, n$ ) expands as

$$\begin{aligned} a_{ij}x^i x^j &= a_{11}x^1 x^1 + a_{12}x^1 x^2 + \dots + a_{1n}x^1 x^n + \\ &\quad + a_{21}x^2 x^1 + a_{22}x^2 x^2 + \dots + a_{2n}x^2 x^n + \\ &\quad \dots \\ &\quad + a_{n1}x^n x^1 + a_{n2}x^n x^2 + \dots + a_{nn}x^n x^n, \end{aligned}$$

with a non-symmetric second order tensor  $a_{ij}$ , can be made symmetric in

the following way.

$$a_{ij}x^ix^j = \frac{1}{2}a_{ij}x^ix^j + \frac{1}{2}a_{ij}x^ix^j.$$

If we swap indices in the second term, we get

$$\begin{aligned} &= \frac{1}{2}a_{ij}x^ix^j + \frac{1}{2}a_{ji}x^jx^i, \quad \text{which is equal to} \\ &= \frac{1}{2}(a_{ij} + a_{ji})x^ix^j. \end{aligned}$$

If we now use a substitution,

$$\begin{aligned} \frac{1}{2}(a_{ij} + a_{ji}) &\equiv b_{ij} = b_{ji}, \quad \text{we get} \\ a_{ij}x^ix^j &= b_{ij}x^ix^j, \end{aligned}$$

where  $a_{ij}$  is non-symmetric and  $b_{ij}$  is symmetric, as required.

(iii) *Every second order tensor that is the sum  $a^{ij} = u^iv^j + u^jv^i$ , or,  $a_{ij} = u_iv_j + u_jv_i$  is symmetric.* In both cases, if we swap the indices  $i$  and  $j$ , we get  $a^{ji} = u^jv^i + u^iv^j$ , (resp.  $a_{ji} = u_jv_i + u_iv_j$ ), which implies that the tensor  $a^{ij}$  (resp.  $a_{ij}$ ) is symmetric.

(iv) *Every second order tensor that is the difference  $b^{ij} = u^iv^j - u^jv^i$ , or,  $b_{ij} = u_iv_j - u_jv_i$  is skew-symmetric.* In both cases, if we swap the indices  $i$  and  $j$ , we get  $b^{ji} = -(u^jv^i - u^iv^j)$ , (resp.  $b_{ji} = -(u_jv_i - u_iv_j)$ ), which implies that the tensor  $b^{ij}$  (resp.  $b_{ij}$ ) is skew-symmetric.

### A.1.2 Euclidean Tensors

#### A.1.2.1 Basis Vectors and the Metric Tensor in $\mathbb{R}^n$

The natural *Cartesian coordinate basis* in an  $n$ D Euclidean space  $\mathbb{R}^n$  is defined as a set of  $n$ D unit vectors  $e^i$  given by

$$e^1 = [\{1, 0, 0, \dots\}^t, e^2 = \{0, 1, 0, \dots\}^t, e^3 = \{0, 0, 1, \dots\}^t, \dots, e^n = \{0, 0, \dots, 1\}^t],$$

(where index  $t$  denotes transpose) while its dual basis  $e_i$  is given by:

$$e_1 = [\{1, 0, 0, \dots\}, e_2 = \{0, 1, 0, \dots\}, e_3 = \{0, 0, 1, \dots\}, \dots, e_n = \{0, 0, \dots, 1\}],$$

(no transpose) where the definition of the dual basis is given by the Kronecker's  $\delta$ -symbol, i.e., the  $n \times n$  identity matrix:

$$e^i \cdot e_j = \delta_j^i = \begin{bmatrix} 1 & 0 & 0 & \dots & 0 \\ 0 & 1 & 0 & \dots & 0 \\ 0 & 0 & 1 & \dots & 0 \\ \dots & \dots & \dots & \dots & \dots \\ 0 & 0 & 0 & \dots & 1 \end{bmatrix},$$

that is the metric tensor in Cartesian coordinates equals  $\mathbf{g} = \delta_j^i$ . In general, (i.e., curvilinear) coordinate system, the metric tensor  $\mathbf{g} = g_{ij}$  is defined as the scalar product of the dual basis vectors, i.e., the  $n \times n$  matrix:

$$g_{ij} = e_i \cdot e_j = \begin{bmatrix} g_{11} & g_{12} & g_{13} & \dots & g_{1n} \\ g_{21} & g_{22} & g_{23} & \dots & g_{2n} \\ g_{31} & g_{32} & g_{33} & \dots & g_{3n} \\ \dots & \dots & \dots & \dots & \dots \\ g_{n1} & g_{n2} & g_{n3} & \dots & g_{nn} \end{bmatrix}.$$

#### A.1.2.2 Tensor Products in $\mathbb{R}^n$

Let  $\mathbf{u}$  and  $\mathbf{v}$  denote two vectors in  $\mathbb{R}^n$ , with their components given by

$$u^i = \mathbf{u} \cdot \mathbf{e}^i, \quad \text{and} \quad v^j = \mathbf{v} \cdot \mathbf{e}^j,$$

where  $u = |\mathbf{u}|$  and  $v = |\mathbf{v}|$  are their respective norms (or, lengths). Then their inner product (i.e., scalar, or dot product)  $\mathbf{u} \cdot \mathbf{v}$  is a scalar invariant  $S$ , defined as

$$S = u^i \cdot v^j = g_{ij} u^i v^j.$$

Besides the dot product of two vectors  $\mathbf{u}, \mathbf{v} \in \mathbb{R}^n$ , there is also their tensor product (i.e., generalized vector, or cross product), which is a second order tensor

$$\mathbf{T} = \mathbf{u} \otimes \mathbf{v}, \text{ in components, } T^{ij} = u^i \otimes v^j.$$

In the natural basis  $\mathbf{e}_i$  this tensor is expanded as

$$\mathbf{T} = T^{ij} \mathbf{e}_i \otimes \mathbf{e}_j,$$

while its components in the dual basis read:

$$T^{ij} = T(\mathbf{e}^i, \mathbf{e}^j),$$

where  $T = |\mathbf{T}|$  is its norm. To get its components in curvilinear coordinates, we need first to substitute it in Cartesian basis:

$$T^{ij} = T^{mn}(e_m \otimes e_n)(e^i, e^j),$$

then to evaluate it on the slots:

$$T^{ij} = T^{mn} e_m \cdot e^i e_n \cdot e^j,$$

and finally to calculate the other index configurations by lowering indices, by means of the metric tensor:

$$T_j^i = g_{jm} T^{im}, \quad T_{ij} = g_{im} g_{jn} T^{mn}.$$

### A.1.3 Tensor Derivatives on Riemannian Manifolds

Consider now some  $n$ D Riemannian manifold  $M$  with the metric form (i.e., line element)  $ds^2 = g_{ik} dx^i dx^k$ , as a configuration space for a certain biodynamic system (e.g., human spine, or arm-shoulder complex).

#### A.1.3.1 Christoffel's Symbols

Partial derivatives of the metric tensor  $g_{ik}$  form themselves special symbols that do not transform as tensors (with respect to the coordinate transformation (A.2)), but nevertheless represent important quantities in tensor analysis. They are called *Christoffel symbols of the first kind*, defined by

$$\Gamma_{ijk} = \frac{1}{2}(\partial_{x^i} g_{jk} - \partial_{x^j} g_{ki} + \partial_{x^k} g_{ij}), \quad \left( \text{remember, } \partial_{x^i} \equiv \frac{\partial}{\partial x^i} \right)$$

and *Christoffel symbols of the second kind*, defined by

$$\Gamma_{ij}^k = g^{kl} \Gamma_{ijl}.$$

The Riemann curvature tensor  $R_{ijk}^l$  (A.7) of the manifold  $M$ , can be expressed in terms of the later as

$$R_{ijk}^l = \partial_{x^j} \Gamma_{ik}^l - \partial_{x^k} \Gamma_{ij}^l + \Gamma_{rj}^l \Gamma_{ik}^r - \Gamma_{rk}^l \Gamma_{ij}^r.$$

For example, in 3D spherical coordinates,  $x^i = \{\rho, \theta, \varphi\}$ , with the metric tensor and its inverse given by (A.5, A.6), it can be shown that the only

nonzero Christoffel's symbols are:

$$\begin{aligned}\Gamma_{12}^2 = \Gamma_{21}^2 = \Gamma_{13}^3 = \Gamma_{31}^3 &= \frac{1}{\rho}, & \Gamma_{23}^3 = \Gamma_{32}^2 &= -\tan \theta, \\ \Gamma_{22}^1 &= -\rho, & \Gamma_{33}^1 &= -\rho \cos^2 \theta, & \Gamma_{33}^2 &= \sin \theta \cos \theta.\end{aligned}\quad (\text{A.8})$$

### A.1.3.2 Geodesics

From the Riemannian metric form  $ds^2 = g_{ik}dx^i dx^k$  it follows that the distance between two points  $t_1$  and  $t_2$  on a curve  $x^i = x^i(t)$  in  $M$  is given by

$$s = \int_{t_1}^{t_2} \sqrt{g_{ik} \dot{x}^i \dot{x}^k} dt.$$

That curve  $x^i = x^i(t)$  in  $M$  which makes the distance  $s$  a minimum is called a *geodesic* of the space  $M$  (e.g., in a sphere, the geodesics are arcs of great circles). Using the calculus of variations, the geodesics are found from the differential *geodesic equation*,

$$\ddot{x}^i + \Gamma_{jk}^i \dot{x}^j \dot{x}^k = 0, \quad (\text{A.9})$$

where overdot means derivative upon the line parameter  $s$ .

For example, in 3D spherical coordinates  $x^i = \{\rho, \theta, \varphi\}$ , using (A.8), geodesic equation (A.9) becomes a system of three scalar ODEs,

$$\begin{aligned}\ddot{\rho} - \rho \dot{\theta}^2 - \rho \cos^2 \theta \dot{\varphi}^2 &= 0, & \ddot{\theta} + \frac{2}{\rho} \dot{\rho} \dot{\theta} + \sin \theta \cos \theta \dot{\varphi}^2 &= 0, \\ \ddot{\varphi} + \frac{2}{\rho} \dot{\rho} \dot{\varphi} - 2 \tan \theta \dot{\theta} \dot{\varphi} &= 0.\end{aligned}\quad (\text{A.10})$$

### A.1.3.3 The Covariant Derivative

Ordinary total and partial derivatives of vectors (covectors) *do not transform as vectors* (covectors) with respect to the coordinate transformation (A.2). For example, let  $y^k$  be Cartesian coordinates and  $x^i$  be general curvilinear coordinates of a dynamical system (with  $i, k = 1, \dots, n$ ). We have:  $x^i(t) = x^i[y^k(t)]$ , which implies that

$$\frac{dx^i}{dt} = \frac{\partial x^i}{\partial y^k} \frac{dy^k}{dt}, \quad \text{or equivalently,} \quad \dot{x}^i = \frac{\partial x^i}{\partial y^k} \dot{y}^k,$$

that is a transformation law for the contravariant vector, which means that the velocity  $v^i \equiv \dot{x}^i \equiv \frac{dx^i}{dt}$  is a proper contravariant vector. However, if we



perform another time differentiation, we get

$$\frac{d^2 x^i}{dt^2} = \frac{\partial x^i}{\partial y^k} \frac{d^2 y^k}{dt^2} + \frac{\partial^2 x^i}{\partial y^k \partial y^m} \frac{dy^k}{dt} \frac{dy^m}{dt},$$

which means that  $\frac{d^2 x^i}{dt^2}$  is not a proper vector.

$\frac{d^2 x^i}{dt^2}$  is an acceleration vector only in a special case when  $x^i$  are another Cartesian coordinates; then  $\frac{\partial^2 x^i}{\partial y^k \partial y^m} = 0$ , and therefore the original coordinate transformation is linear,  $x^i = a_k^i y^k + b^i$  (where  $a_k^i$  and  $b^i$  are constant).

Therefore,  $\frac{d^2 x^i}{dt^2}$  represents an acceleration vector only in terms of Newtonian mechanics in a Euclidean space  $\mathbb{R}^n$ , while it is not a proper acceleration vector in terms of Lagrangian or Hamiltonian mechanics in general curvilinear coordinates on a smooth manifold  $M^n$ . And we know that Newtonian mechanics in  $\mathbb{R}^n$  is sufficient only for fairly simple mechanical systems.

The above is true for any tensors. So we need to find another derivative operator to be able to preserve their tensor character. The solution to this problem is called the *covariant derivative*.

The covariant derivative  $v_{;k}^i$  of a contravariant vector  $v^i$  is defined as

$$v_{;k}^i = \partial_{x^k} v^i + \Gamma_{jk}^i v^j.$$

Similarly, the covariant derivative  $v_{i;k}$  of a covariant vector  $v_i$  is defined as

$$v_{i;k} = \partial_{x^k} v_i - \Gamma_{ik}^j v_j.$$

Generalization for the higher order tensors is straightforward; e.g., the covariant derivative  $t_{kl;q}^j$  of the third order tensor  $t_{kl}^j$  is given by

$$t_{kl;q}^j = \partial_{x^q} t_{kl}^j + \Gamma_{qs}^j t_{kl}^s - \Gamma_{kq}^s t_{sl}^j - \Gamma_{lq}^s t_{ks}^j.$$

The covariant derivative is the most important tensor operator in general relativity (its zero defines *parallel transport*) as well as the basis for defining other differential operators in mechanics and physics.

#### A.1.3.4 Vector Differential Operators

**Gradient.** If  $\varphi = \varphi(x^i, t)$  is a scalar field, the gradient one-form  $\text{grad}(\varphi)$  is defined by

$$\text{grad}(\varphi) = \nabla \varphi = \varphi_{;i} = \partial_{x^i} \varphi.$$

**Divergence.** The divergence  $\text{div}(v^i)$  of a vector-field  $v^i = v^i(x^i, t)$  is defined by contraction of its covariant derivative with respect to the coordinates  $x^i = x^i(t)$ , i.e., the contraction of  $v^i_{;k}$ , namely

$$\text{div}(v^i) = v^i_{;i} = \frac{1}{\sqrt{g}} \partial_{x^i} (\sqrt{g} v^i).$$

**Curl.** The curl  $\text{curl}(\theta_i)$  of a one-form  $\theta_i = \theta_i(x^i, t)$  is a second order covariant tensor defined as

$$\text{curl}(\theta_i) = \theta_{i;k} - \theta_{k;i} = \partial_{x^k} \theta_i - \partial_{x^i} \theta_k.$$

**Laplacian.** The Laplacian  $\Delta\varphi$  of a scalar invariant  $\varphi = \varphi(x^i, t)$  is the divergence of  $\text{grad}(\varphi)$ , or

$$\Delta\varphi = \nabla^2\varphi = \text{div}(\text{grad}(\varphi)) = \text{div}(\varphi_{;i}) = \frac{1}{\sqrt{g}} \partial_{x^i} (\sqrt{g} g^{ik} \partial_{x^k} \varphi).$$

#### A.1.3.5 The Absolute Derivative

The *absolute covariant derivative* (or *intrinsic*, or *Bianchi's derivative*) of a contravariant vector  $v^i$  along a curve  $x^k = x^k(t)$  is denoted by  $\dot{v}^i \equiv Dv^i/dt$  and defined as the inner product of the covariant derivative of  $v^i$  and  $\dot{x}^k \equiv dx^k/dt$ , i.e.,  $v^i_{;k} \dot{x}^k$ , and is given by

$$\dot{v}^i = v^i + \Gamma^i_{jk} v^j \dot{x}^k.$$

Similarly, the absolute derivative  $\dot{v}_i$  of a covariant vector  $v_i$  is defined as

$$\dot{v}_i = v_i - \Gamma^j_{ik} v_j \dot{x}^k.$$

Generalization for the higher order tensors is straightforward; e.g., the absolute derivative  $\dot{t}^j_{kl}$  of the third order tensor  $t^j_{kl}$  is given by

$$\dot{t}^j_{kl} = t^j_{kl} + \Gamma^j_{qs} t^s_{kl} \dot{x}^q - \Gamma^s_{kq} t^j_{sl} \dot{x}^q - \Gamma^s_{lq} t^j_{ks} \dot{x}^q.$$

The absolute derivative is the most important operator in biodynamics, as it is the basis for the covariant form of both Lagrangian and Hamiltonian equations of motion of many biodynamic systems.

**Application to Curve Geometry.** Given three unit vectors: *tangent*  $\tau^i$ , *principal normal*  $\beta^i$ , and *binormal*  $\nu^i$ , as well as two scalar invariants:

curvature  $K$  and torsion  $T$ , of a curve  $\gamma(s) = \gamma[x^i(s)]$ , the so-called *Frenet-Serret formulae* are valid<sup>19</sup>

$$\begin{aligned}\dot{\tau}^i &\equiv \dot{\tau}^i + \Gamma_{jk}^i \tau^j \dot{x}^k = K \beta^i, \\ \dot{\beta}^i &\equiv \dot{\beta}^i + \Gamma_{jk}^i \beta^j \dot{x}^k = -(K \tau^i + T \nu^i), \\ \dot{\nu}^i &\equiv \dot{\nu}^i + \Gamma_{jk}^i \nu^j \dot{x}^k = T \beta^i.\end{aligned}$$

**Application to Mechanical Definitions of Acceleration and Force.** In modern analytical mechanics, the two fundamental notions of *acceleration* and *force* in general curvilinear coordinates are substantially different from the corresponding terms in Cartesian coordinates as commonly used in engineering mechanics. Namely, the acceleration vector *is not* an ordinary time derivative of the velocity vector; 'even worse', the force, which is a paradigm of a vector in statics and engineering vector mechanics, *is not* a vector at all. Proper mathematical definition of the acceleration vector is the absolute time derivative of the velocity vector, while the force is a differential one-form.

To give a brief look at these 'weird mathematical beasts', consider a material dynamical system described by  $n$  curvilinear coordinates  $x^i = x^i(t)$ . First, recall from subsection A.1.3.3 above, that an ordinary time derivative of the velocity vector  $v^i(t) = \dot{x}^i(t)$  *does not transform as a vector* with respect to the general coordinate transformation (A.2). Therefore,  $a^i \neq \dot{v}^i$ . So, we need to use its absolute time derivative to define the acceleration vector (with  $i, j, k = 1, \dots, n$ ),

$$a^i = \dot{v}^i \equiv \frac{Dv^i}{dt} = v_{;k}^i \dot{x}^k \equiv \dot{v}^i + \Gamma_{jk}^i v^j \dot{x}^k \equiv \ddot{x}^i + \Gamma_{jk}^i \dot{x}^j \dot{x}^k, \quad (\text{A.11})$$

which is equivalent to the l.h.s of the geodesic equation (A.9). Only in the particular case of Cartesian coordinates, the general acceleration vector (A.11) reduces to the familiar engineering form of the Euclidean acceleration vector<sup>20</sup>,  $\mathbf{a} = \dot{\mathbf{v}}$ .

For example, in standard spherical coordinates  $x^i = \{\rho, \theta, \varphi\}$ , we have the components of the acceleration vector given by (A.10), if we now rein-

<sup>19</sup>In this paragraph, the overdot denotes the total derivative with respect to the line parameter  $s$  (instead of time  $t$ ).

<sup>20</sup>Any Euclidean space can be defined as a set of Cartesian coordinates, while any Riemannian manifold can be defined as a set of curvilinear coordinates. Christoffel's symbols  $\Gamma_{jk}^i$  vanish in Euclidean spaces defined by Cartesian coordinates; however, they are nonzero in Riemannian manifolds defined by curvilinear coordinates (see chapter 3 for geometric details).

terpret overdot as the time derivative,

$$a^\rho = \ddot{\rho} - \rho \dot{\theta}^2 - \rho \cos^2 \theta \dot{\varphi}^2, \quad a^\theta = \ddot{\theta} + \frac{2}{\rho} \dot{\rho} \dot{\varphi} + \sin \theta \cos \theta \dot{\varphi}^2,$$

$$a^\varphi = \ddot{\varphi} + \frac{2}{\rho} \dot{\rho} \dot{\varphi} - 2 \tan \theta \dot{\theta} \dot{\varphi}.$$

Now, using (A.11), the *Newton's fundamental equation of motion, that is the basis of all science*,  $\mathbf{F} = m \mathbf{a}$ , gets the following tensorial form

$$F^i = m a^i = m \dot{v}^i = m(v_{;k}^i \dot{x}^k) \equiv m(\dot{v}^i + \Gamma_{jk}^i v^j \dot{x}^k) = m(\ddot{x}^i + \Gamma_{jk}^i \dot{x}^j \dot{x}^k), \quad (\text{A.12})$$

which defines Newtonian force as a contravariant vector.

However, modern Hamiltonian dynamics reminds us that: (i) Newton's own force definition was not really  $\mathbf{F} = m \mathbf{a}$ , but rather  $\mathbf{F} = \dot{\mathbf{p}}$ , where  $\mathbf{p}$  is the system's momentum, and (ii) the momentum  $\mathbf{p}$  is not really a vector, but rather a dual quantity, a differential one-form<sup>21</sup> (see chapter 3 for details). Consequently, the force, as its time derivative, is also a one-form (see Figure A.1). This new force definition includes the precise definition of the mass distribution within the system, by means of its Riemannian metric tensor  $g_{ij}$ . Thus, (A.12) has to be modified as

$$F_i = m g_{ij} \dot{x}^j \equiv m g_{ij} (v_{;k}^j \dot{x}^k) \equiv m g_{ij} (\dot{v}^j + \Gamma_{ik}^j v^i \dot{x}^k) = m g_{ij} (\ddot{x}^j + \Gamma_{ik}^j \dot{x}^i \dot{x}^k), \quad (\text{A.13})$$

where the quantity  $m g_{ij}$  is called the *material metric tensor*, or *inertia matrix*. Equation (A.13) generalizes the notion of the Newtonian force  $\mathbf{F}$ , from Euclidean space  $\mathbb{R}^n$  to the Riemannian manifold  $M$  (see chapter 3).

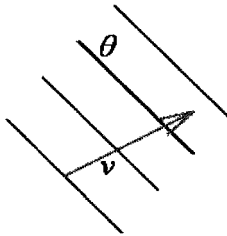


Fig. A.1 A one-form  $\theta$  (which is a family of parallel (hyper)surfaces, the so-called *Grassmann planes*) pierced by the vector  $v$  to give a scalar product  $\theta(v) \equiv \langle \theta, v \rangle = 2.6$ .

<sup>21</sup>For example, in Dirac's  $\langle \text{bra} | \text{ket} \rangle$  formalism, *kets* are vectors, while *bras* are one-forms; in matrix notation, columns are vectors, while rows are one-forms.

**Application to Fluid Mechanics: Continuity Equation.** The most important equation in continuum mechanics, in particular in fluid mechanics, is the celebrated *equation of continuity*,

$$\partial_t \rho + \operatorname{div}(\rho \dot{\mathbf{x}}) = 0. \quad (\text{A.14})$$

Here we derive the continuity equation (A.14), using the absolute time derivative and starting from the *mass conservation principle*,

$$\frac{\dot{dm}}{dm} = 0, \quad (\text{A.15})$$

where  $dm$  denotes an infinitesimal mass of a fluid (continuum) particle. If we introduce the fluid density  $\rho = dm/dv$ , where  $v$  is the infinitesimal volume of a fluid particle, then the mass conservation principle (A.15) can be rewritten as

$$\frac{\dot{\rho}}{\rho dv} = 0,$$

which is the absolute derivative of a product, and therefore expands into

$$\dot{\rho} dv + \rho \dot{dv} = 0. \quad (\text{A.16})$$

Now, as the fluid density is a function of both time  $t$  and spatial coordinates  $x^k$ , i.e., a scalar-field,  $\rho = \rho(x^k, t)$ , its total time derivative  $\dot{\rho}$ , figuring in (A.16), is defined by

$$\dot{\rho} = \partial_t \rho + \partial_{x^k} \rho \partial_t x^k \equiv \partial_t \rho + \rho_{,k} \dot{x}^k \equiv \partial_t \rho + \operatorname{grad}(\rho) \cdot \dot{\mathbf{x}}. \quad (\text{A.17})$$

Regarding  $\dot{dv}$ , the other term figuring in (A.16), we start by expanding an elementary volume  $dv$  along the sides  $\{dx_{(p)}^i, dx_{(q)}^j, dx_{(r)}^k\}$  of an elementary parallelepiped,

$$dv = \frac{1}{3!} \delta_{ijk}^{pqr} dx_{(p)}^i dx_{(q)}^j dx_{(r)}^k, \quad (i, j, k, p, q, r = 1, 2, 3)$$

so that its absolute derivative becomes

$$\begin{aligned} \frac{\dot{dv}}{dv} &= \frac{1}{2!} \delta_{ijk}^{pqr} \frac{\dot{dx}^i}{dx_{(p)}^i} dx_{(q)}^j dx_{(r)}^k \\ &= \frac{1}{2!} \dot{x}_{,l}^i \delta_{ijk}^{pqr} dx_{(p)}^l dx_{(q)}^j dx_{(r)}^k \quad (\text{using } \frac{\dot{dx}^i}{dx_{(p)}^i} = \dot{x}_{,l}^i dx_{(p)}^l), \end{aligned}$$

which finally simplifies into

$$\frac{\dot{dv}}{dv} = \dot{x}_{,k}^k dv \equiv \operatorname{div}(\dot{\mathbf{x}}) dv. \quad (\text{A.18})$$

Substituting (A.17) and (A.18) into (A.16) gives

$$\overline{\rho dv} \equiv (\partial_t \rho + \rho_{;k} \dot{x}^k) dv + \rho \dot{x}^k_{;k} dv = 0. \quad (\text{A.19})$$

Now, as we are dealing with arbitrary fluid particles,  $dv \neq 0$ , so from (A.19) it follows

$$\partial_t \rho + \rho_{;k} \dot{x}^k + \rho \dot{x}^k_{;k} \equiv \partial_t \rho + (\rho \dot{x}^k)_{;k} = 0. \quad (\text{A.20})$$

Equation (A.20) is the covariant form of the continuity equation, which in standard vector notation becomes (A.14).

In classical biomechanics, the continuity equation (A.14) forms the basis of *hemodynamics*, or blood flow dynamics.

#### A.1.4 The Covariant Force Law in Biodynamics

Objective of this final tensor subsection is to generalize the fundamental Newtonian 3D equation,  $\mathbf{F} = m\mathbf{a}$ , for the generic biodynamic system, consisting of a number of flexibly-coupled rigid segments (see Figures 3.2–3.3 above), and thus to formulate the fundamental law of lower biodynamics: *the covariant force law*.

To be able to apply the covariant formalism, we need to start with the suitable coordinate transformation (A.2), in this case as a relation between the 6 *external*  $SE(3)$  rigid-body coordinates,  $y^e = y^e(t)$  ( $e = 1, \dots, 6$ ), and  $2n$  *internal joint coordinates*,  $x^i = x^i(t)$  ( $i = 1, \dots, 2n$ ) ( $n$  angles, forming the constrained  $n$ -torus  $T^n$ , plus  $n$  very restricted translational coordinates, forming the hypercube  $I^n \subset \mathbb{R}^n$ ). Similarly, we can have any two sets of coordinates, one external (e.g., body coordinates) and one internal (e.g., brain coordinates), and perform the functional transformation (A.2),

$$x^i = x^i(y^e). \quad (\text{A.21})$$

Now, although the coordinate transformation (A.21) is nonlinear and even unknown at this stage, there is something known and simple about it: the corresponding transformation of differentials is *linear and homogenous*,

$$dx^i = \frac{\partial x^i}{\partial y^e} dy^e,$$

which implies the *linear and homogenous transformation of velocities*,

$$\dot{x}^i = \frac{\partial x^i}{\partial y^e} \dot{y}^e. \quad (\text{A.22})$$

Our *internal velocity vector-field* is defined by the set of ODEs (A.22), at each *representative point*  $x^i = x^i(t)$  of the biodynamic configuration manifold  $M = T^n \times I^n$ , as  $v^i \equiv v^i(x^i, t) := \dot{x}^i(x^i, t)$ .

Note that in general, a *vector-field* represents a field of vectors defined at every point  $x^i$  within some region  $U$  (e.g., movable segments/joints only) of the total configuration manifold  $M$  (consisting of all the segments/joints). Analytically, vector-field is defined as a set of autonomous ODEs (in our case, the set (A.22)). Its solution gives the *flow*, consisting of *integral curves* of the vector-field, such that all the vectors from the vector-field are tangent to integral curves at different representative points  $x^i \in U$ . In this way, through every representative point  $x^i \in U$  passes both a curve from the flow and its tangent vector from the vector-field. Geometrically, vector-field is defined as a cross-section of the tangent bundle  $TM$ , the so-called *velocity phase-space*. Its *geometrical dual* is the *1-form-field*, which represents a field of one-forms (see Figure A.1), defined at the same representative points  $x^i \in U$ . Analytically, 1-form-field is defined as an *exterior differential system*, an algebraic dual to the autonomous set of ODEs. Geometrically, it is defined as a cross-section of the cotangent bundle  $T^*M$ , the so-called *momentum phase-space*. Together, the vector-field and its corresponding 1-form-field define the *scalar potential field* (e.g., kinetic and/or potential energy) at the same movable region  $U \subset M$ . See chapter 3 for technical details.

Now, we are on the half-way to covariant biodynamics. We need to formulate the internal acceleration vector-field,  $a^i \equiv a^i(x^i, \dot{x}^i, t)$ , acting in all movable joints, and at the same time generalizing the 3D Newtonian acceleration vector  $\mathbf{a}$ .

According to Newton, acceleration is a rate-of-change of velocity. But, from the previous subsections, we know that  $a^i \neq \dot{v}^i$ . However,

$$a^i := \dot{v}^i = \dot{v}^i + \Gamma_{jk}^i v^j v^k = \ddot{x}^i + \Gamma_{jk}^i \dot{x}^j \dot{x}^k. \quad (\text{A.23})$$

Once we have the *internal acceleration vector-field*  $a^i = a^i(x^i, \dot{x}^i, t)$ , defined by the set of ODEs (A.23) (including affine connections  $\Gamma_{jk}^i$  of the configuration manifold  $M$ ), we can finally define the *internal force 1-form field*,  $F_i = F_i(x^i, \dot{x}^i, t)$ , as a family of force one-forms, half of them rotational and half translational, acting in all movable joints,

$$F_i := mg_{ij} a^j = mg_{ij} (\dot{v}^j + \Gamma_{ik}^j v^i v^k) = mg_{ij} (\ddot{x}^j + \Gamma_{ik}^j \dot{x}^i \dot{x}^k), \quad (\text{A.24})$$

where we have used the simplified *material metric tensor*,  $mg_{ij}$ , for the

biodynamic system (considering, for simplicity, all segments to have equal mass  $m$ ), defined by its *Riemannian kinetic energy form*

$$T = \frac{1}{2} mg_{ij} v^i v^j.$$

Equation  $F_i = mg_{ij} a^j$ , defined properly by (A.24) at every representative point  $x^i$  of the biodynamic configuration manifold  $M$ , formulates the sought for *covariant force law*, that generalizes the fundamental Newtonian equation,  $\mathbf{F} = m\mathbf{a}$ , for the generic biodynamic system. Its meaning is:

**Force 1-form-field = Mass distribution  $\times$  Acceleration vector-field**

In other words, the field (or, family) of force one-forms  $F_i$ , acting in all movable joints (with constrained rotations on  $T^n$  and very restricted translations on  $I^n$ ), causes both rotational and translational accelerations of all body segments, within the mass distribution  $mg_{ij}$ <sup>22</sup>, along the flow-lines of the vector-field  $a^j$ .

From the control theory perspective, a vector-field is a dynamical system, a set of differential equations (A.23) that has a set of force one-forms  $F_i$  as its inputs (see chapter 6).

The purpose of chapter 3 is to put this *core biodynamic law* into rigorous settings of smooth manifolds and their (co)tangent bundles.

### A.1.5 The Essence of Natural Hamiltonian Biodynamics

The *covariant force law*,  $F_i = mg_{ij} a^j$ , defined by (A.24) above, has the following Hamiltonian reformulation. We start with the *conservative Hamiltonian biodynamics* on the cotangent bundle  $T^*M$  of the system's *configuration manifold*  $M$  (see Figures 3.2–3.3 above), given by (chapter 4)

$$\dot{q}^\alpha = \partial_{p_\alpha} H(q^\alpha, p_\alpha), \quad \dot{p}_\alpha = -\partial_{q^\alpha} H(q^\alpha, p_\alpha), \quad (\alpha = 1, \dots, n).$$

The *forced Hamiltonian biodynamics* on  $T^*M$  is given by

$$\dot{q}^\alpha = \partial_{p_\alpha} H(q^\alpha, p_\alpha), \quad \dot{p}_\alpha = F_\alpha(t, q^\alpha, p_\alpha) - \partial_{q^\alpha} H(q^\alpha, p_\alpha),$$

---

<sup>22</sup>More realistically, instead of the simplified metric  $mg_{ij}$  we have the *material metric tensor*  $G_{ij}$ , including all  $k$  segmental masses  $m_\chi$ , as well as the corresponding moments and products of inertia,

$$G_{ij}(x, m) = \sum_{\chi=1}^k m_\chi \delta_{rs} \frac{\partial y^r}{\partial x^i} \frac{\partial y^s}{\partial x^j}, \quad (r, s = 1, \dots, 6; i, j = 1, \dots, 2n),$$

as defined in Figures 3.2–3.3 above.



where  $F_\alpha$  are muscular torques.

The *generalized Hamiltonian biodynamics* (forced & dissipative) on  $T^*M$  is

$$\begin{aligned}\dot{q}^\alpha &= \partial_{p_\alpha} H(q^\alpha, p_\alpha) - \partial_{p_\alpha} R(q^\alpha, p_\alpha), \\ \dot{p}_\alpha &= F_\alpha(t, q^\alpha, p_\alpha) - \partial_{q^\alpha} H(q^\alpha, p_\alpha) - \partial_{q^\alpha} R(q^\alpha, p_\alpha).\end{aligned}\tag{A.25}$$

The generalized Hamiltonian system (A.25) covers several types of classical dynamical systems: (see chapter 4)

- (i) in case  $F_\alpha = 0$ ,  $R = 0$  and  $H \neq 0$  – conservative Hamiltonian system;
- (ii) in case  $F_\alpha = 0$ ,  $R \neq 0$  and  $H \neq 0$  – dissipative Hamiltonian system;
- (iii) in case  $F_\alpha = 0$ ,  $R \neq 0$  and  $H = 0$  – bidirectional gradient system;
- (iv) in case  $F_\alpha \neq 0$ ,  $R = 0$  and  $H = 0$  – simple Newtonian system;
- (v) in case  $F_\alpha \neq 0$ ,  $R = 0$  and  $H \neq 0$  – generalized Newtonian system.

The *generalized Hamiltonian control system* on  $T^*M$  is obtained from the generalized Hamiltonian system on  $T^*M$  in the following way. First we introduce the *control Hamiltonian function*,  $H_C : T^*M \times \mathbb{R} \rightarrow \mathbb{R}$ . In the local coordinates  $q^\alpha, p_\alpha \in U_p \subset T^*M$ , the control Hamiltonian is given by

$$H_C(q, p, u) = H_0(q, p) - q^\alpha u_\alpha, \quad (\alpha = 1, \dots, n)$$

where  $u_\alpha = u_\alpha(t, q, p)$  are *neural control inputs*, and the physical Hamiltonian  $H_0(q, p)$  represents the system's *total energy function*  $H_0 : T^*M \times \mathbb{R} \rightarrow \mathbb{R}$ . The *natural input-output control system* is now defined as

$$\begin{aligned}\dot{q}^\alpha &= \partial_{p_\alpha} H_C(q, p, u) + \partial_{p_\alpha} R(q, p), & \dot{p}_\alpha &= F_\alpha - \partial_{q^\alpha} H_C(q, p, u) + \partial_{q^\alpha} R(q, p), \\ y^\alpha &= -\partial_{u_\alpha} H_C(q, p, u),\end{aligned}$$

where  $y^\alpha$  are *control outputs* (see chapter 6).

### A.1.6 Neuro-Hamiltonian Control in Biodynamics

In this last tensorial subsection we present the union of neurodynamics (chapter 7) and natural Hamiltonian control (chapter 6). It takes place between the internal (neural, knowledge) coordinates  $(\xi^i, \psi^i) \in U_{int}^i \subset M$  and the external (canonical, motion) coordinates  $(q^\alpha, p_\alpha) \in U_{ex}^\alpha \subset T_{ex}^*M$ . This relation between internal and external coordinates is threefold:

- (i) geometrical, provided by means of the Riemannian metric  $g_{\alpha\beta}(q, \xi)$

(ii) general Hamiltonian inputs,  $A^i = A^i[(q^\alpha, p_\alpha), (\xi^i, \psi^i), t]$  and  $B_i = B_i[(q^\alpha, p_\alpha), (\xi^i, \psi^i), t]$ , and

(iii) general control forces  $F_\alpha = F_\alpha[(q^\alpha, p_\alpha), (\xi^i, \psi^i), t]$ .

In thus correlated internal and external coordinates, the *neuro-Hamiltonian control system* is described as a double-feedback (or, double-coupled) system

$$\begin{aligned}\dot{q}^\alpha &= \partial_{p_\alpha} H_0(q, p) - \partial_{p_\alpha} H^\gamma(q, p) u_\gamma + \partial_{p_\alpha} R, \\ \dot{p}_\alpha &= F_\alpha - \partial_{q^\alpha} H_0(q, p) + \partial_{q^\alpha} H^\gamma(q, p) u_\gamma + \partial_{q^\alpha} R, \\ \dot{y}^\gamma &= -\partial_{u_\gamma} H_A(q, p, u) = H^\gamma(q, p), \\ F_\alpha &= F_\alpha[(q^\alpha, p_\alpha), (\xi^i, \psi^i), t], \\ \dot{x}^i &= A^i[(q^\alpha, p_\alpha), (\xi^i, \psi^i), t] + \omega^{ij} f_j(y_j) - x^i, \\ \dot{y}_i &= B_i[(q^\alpha, p_\alpha), (\xi^i, \psi^i), t] + \omega_{ij} f^j(x^j) - y_i, \\ \dot{\omega}^{ij} &= -\omega^{ij} + \mathcal{I}^{ij}(x^i, y_j), \quad \dot{\omega}_{ij} = -\omega_{ij} + \mathcal{I}_{ij}(x^i, y_j), \\ (\alpha &= 1, \dots, n), \quad (i, j = 1, \dots, N),\end{aligned}$$

together with:

- (i) known initial state (given by external coordinates at zero-time:  $q^\alpha(0) = q_0^\alpha$ ,  $p_\alpha(0) = p_\alpha^0$ ),
- (ii) known Hamiltonian inputs,
- (iii) zero initial activation ( $\mathbf{x}, \mathbf{y}$ )-field,
- (iii) random initial synaptic  $\mathbf{W}$ -field,
- (iv) neural activation output given as a mean- $(\mathbf{x}, \mathbf{y})$ -field, and
- (v) innovation functions  $\mathcal{I}^{ij}(x^i, y_j)$  (resp.  $\mathcal{I}_{ij}(x^i, y_j)$ ) given by one of the Hebbian models (see chapter 7).

## A.2 Frequently Used Neurophysiological Terms

In this section we give a brief glossary of frequently used neurophysiological terms. For more details, see e.g., [Matthews (2001); Marieb (1998)].

### A band

A darker band at the middle of a sarcomere of a striated muscle fibre, corresponding to the length of the thick filaments.

### absolute refractory period

The period of time after an action potential during which a second action potential cannot be triggered. This period corresponds to the time

when sodium channel inactivation gates remain closed after repolarization.

**acetylcholine (ACh)**

A neurotransmitter in both the central and peripheral nervous system, formed by the combination of acetate and choline, a reaction catalyzed by the synthetic enzyme choline acetyltransferase.

**acetylcholinesterase**

The degradative enzyme for acetylcholine, which cleaves the ester bond and releases acetate and choline.

**ACh receptor**

The receptor molecule that detects the presence of acetylcholine in the extracellular space and initiates the postsynaptic response to the neurotransmitter.

**actin**

A motor protein. Actin forms the backbone of the thin filaments of striated muscle cells and is also involved in other cellular motions, such as the movement of growth cones.

**action potential (AP)**

The long-distance signal of the nervous system. Action potentials are triggered in excitable cells in response to depolarization that exceeds the threshold potential.

**active zone**

The subregion of a presynaptic terminal where synaptic vesicles fuse with the plasma membrane, releasing their neurotransmitter content into the synaptic cleft.

**ADP – Adenosine diphosphate**

ADP results from hydrolysis of ATP by ATPase or kinase enzymes, with the concomitant release of the terminal phosphate group of ATP.

**afferent pathway**

A pathway carrying incoming sensory information into the nervous system.

**afterhyperpolarization**

A period after an action potential during which the membrane potential is more negative than usual.

**agnosia**

A collective term for the inability to identify objects based on sensory information, even though the primary sensory cortex is intact.

**alpha motor neurons**

Large motor neurons that innervate the extrafusal muscle fibers of skeletal muscles.

**Alzheimer's disease**

The most common type of age-related, progressive dementia, produced by death of neurons in a variety of brain regions. The disease is characterized by two pathological features in the brain: neuritic plaques and neurofibrillary tangles.

**angular gyrus**

A gyrus located at the border between the temporal, parietal, and occipital lobes of the cerebral cortex. Lesions in the angular gyrus of the language-dominant hemisphere interfere with reading and writing.

**anterolateral system**

The sensory projection system carrying pain and temperature information through the lateral sensory tract of the spinal cord to the brainstem, thalamus, and somatosensory cortex.

**aphasia**

A disorder of understanding or production of spoken language.

**apraxia**

A deficit in programming complex series of movements, without paralysis, sensory defects, or difficulty performing simple movements.

**archicortex**

A simple form of cortex having only a single layer of cells, as opposed to the multiple cell layers found in the neocortex. The hippocampus is an example of archicortex.

**arcuate fasciculus**

A fibre tract in the cortical white matter containing axons that interconnect Wernicke's and Broca's areas. Damage in this fibre tract produces a form of aphasia called conduction aphasia.

**area MT**

A portion of the middle temporal cortex (MT) involved in the detection of visual motion. Also called area V5.

**area V1**

Another name for the primary visual cortex, or striate cortex, located in the occipital lobe.

**ATP – Adenosine triphosphate**

The high-energy phosphate compound that is the primary source of energy for a variety of energy-requiring cellular processes. ATP also provides the donor phosphate group for phosphorylation of protein molecules by kinase enzymes. The second messenger, cyclic AMP, is synthesized from ATP by the enzyme adenylyl-cyclase.

**autonomic nervous system**

One of the major subdivisions of the nervous system, containing neurons that provide involuntary control of heart muscle, smooth muscle, and glands. The autonomic nervous system consists of the sympathetic and parasympathetic divisions.

**axon**

The neurite that carries action potentials leaving the cell body of a neuron and distributes the signal to postsynaptic target cells.

**basal ganglia**

An interconnected group of three forebrain nuclei involved in motor control. The three nuclei are the caudate nucleus, the putamen, and the globus pallidus.

**basilar membrane**

A membrane within the cochlea that vibrates in response to sound stimuli. The sensory structure of the ear (the organ of Corti) rides on top of the basilar membrane.

**bipolar cell**

A neuron type found in the retina. Bipolar cells are second-order neurons that receive synaptic input from photoreceptors and make synapses on amacrine cells and ganglion cells.

**blobs**

Groups of neurons within the primary visual cortex, containing color-sensitive cells. The cells within the blobs have high numbers of mitochondria, which are revealed by staining for the mitochondrial enzyme, cytochrome oxidase.

**brainstem**

A collective term for the midbrain (mesencephalon) and hindbrain (rhombencephalon).

**Broca's area**

Region of the frontal lobe of the dominant cortical hemisphere for language, where damage produces deficits in production of speech (expressive aphasia). Broca's area is located just anterior to the portion of the primary motor cortex that controls the muscles of the mouth and tongue.

**calcium-induced calcium release channel**

The ion channel of the sarcoplasmic reticulum that allows calcium ions to flow out of the sarcoplasmic reticulum to trigger contraction of skeletal muscle cells.

**caudate nucleus**

One of the basal ganglia of the forebrain. Together with the putamen, the caudate nucleus is part of the striatum.

**central sulcus**

The large infolding, or groove, in the dorsal surface of the cerebral cortex, approximately midway between the anterior and posterior poles of the brain.

**cerebellum**

A major part of the brainstem in mammalian brains, involved in integration of sensory information and motor commands.

**cerebral cortex**

The outer surface of the cerebrum, containing most of the neurons in the cerebrum.

**cerebral ventricles**

The fluid-filled canal at the center of the brain.

**cerebrospinal fluid (CSF)**

The fluid filling the cerebral ventricles and the spinal canal.

**cerebrum**

A major subdivision of the forebrain. Together, the cerebrum and basal ganglia make up the telencephalon.

**C-fibers**

Small-diameter, unmyelinated axons of peripheral nerves. C-fibers carry pain and temperature information.

**chemoreceptors**

Sensory neurons that detect chemical sensory stimuli.

**cholinergic neuron**

A neuron that uses the neurotransmitter acetylcholine.

**cingulate gyrus**

Part of the limbic system, this outfolding of the cerebral cortex runs front to back, hidden from view within the interhemispheric fissure that separates the two cerebral hemispheres.

**cingulum**

An axon bundle that contains axons projecting from the cingulate gyrus to the entorhinal cortex in the limbic system.

**cochlea**

Part of the inner ear that contains the sensory hair cells of the sense of hearing.

**cochlear nucleus**

A nucleus in the brainstem that receives synaptic input from the spiral ganglion neurons of the cochlea.

**collagen**

A structural protein that forms the backbone of the extracellular matrix

in many tissues.

**cones**

One of the two major classes of photoreceptors, the other being rods. Cones are less sensitive to light than rods and mediate color vision.

**corpus callosum**

The large fibre bundle containing axons interconnecting neurons of the two cerebral hemispheres.

**corticobulbar system**

The motor pathway carrying descending motor commands from the motor cortex to the brainstem.

**corticospinal system**

The motor pathway carrying axons from the motor cortex to the spinal cord, bypassing the brainstem motor centers.

**cranial nerves**

Nerves that directly connect the brain to peripheral targets. The human nervous system includes twelve distinct cranial nerves.

**cross bridge**

A structure visible through the electron microscope, connecting adjacent thick and thin filaments of a myofibril. The cross bridges are formed by myosin molecules that make up the thick filament.

**cuneate nucleus**

One of the dorsal column nuclei in the brainstem. The cuneate nucleus receives somatosensory inputs from the lateral portions of the dorsal columns of the spinal cord.

**decussation**

A cross over of axons from one side of the brain to the other.

**dendrite**

A neurite that receives synaptic inputs from other neurons.

**dendritic spine**

A short, hair-like projection from dendrite. Excitatory synapses commonly contact dendrites of CNS neurons at dendritic spines.

**dentate nucleus**

One of the deep nuclei of the cerebellum, in the brainstem.

**depolarization**

Movement of the membrane potential in the positive direction, from its normal negative level.

**diencephalon**

A subdivision of the forebrain, comprising the thalamus and hypothalamus.

**dorsal column nuclei**

Nuclei in the brainstem that receive synaptic inputs from somatosensory neurons whose axons are located in the dorsal columns. The dorsal column nuclei are the gracile nucleus and the cuneate nucleus.

**dorsal column**

A fibre bundle along the dorsal surface of the spinal cord, primarily consisting of branches of primary somatosensory neurons ascending from the spinal cord to the brainstem.

**dorsal root ganglion**

A ganglion located just outside the spinal cord at each vertebral segment, containing the cell bodies of sensory neurons whose axons enter the spinal cord at that segment.

**dorsal root**

The fibre bundle containing incoming (afferent) sensory axons entering the spinal cord at each vertebral segment.

**efferent pathway**

A pathway carrying outgoing motor information from neurons.

**emboliform nucleus**

One of the deep nuclei of the cerebellum, in the brainstem.

**end-plate**

The synaptic zone of a skeletal muscle cell, where postsynaptic ACh receptors are clustered at high density across from the synaptic terminal of the motor neuron.

**end-plate potential**

The postsynaptic electrical response elicited in a skeletal muscle cell by activation of its motor neuron.

**entorhinal cortex**

A part of the olfactory system and the limbic system. The entorhinal cortex provides input to the hippocampus, and receives synaptic connections from the cingulate gyrus. The entorhinal cortex is an example of paleocortex, having only two cellular layers.

**epinephrine, or adrenaline**

A hormone secreted by adrenal chromaffin cells into the bloodstream. Also used as a neurotransmitter.

**equilibrium potential**

The value of membrane potential at which a permeant ion is at equilibrium. The equilibrium potential is calculated from the *Nernst equation* (named after Nobel Laureate Walther H. Nernst).

**excitation-contraction coupling**



The process through which an action potential triggers contraction of a muscle cell.

**excitatory postsynaptic potential (EPSP)**

A postsynaptic change in membrane potential that promotes firing of an action potential in the postsynaptic cell, by bringing the membrane potential toward the threshold potential.

**exteroceptors**

Sensory receptors that detect stimuli originating outside the organism. For example, photoreceptors are exteroceptors.

**extrafusal muscle fibers**

The muscle cells of a skeletal muscle that generate the contractile force of the muscle and are located outside of muscle spindles.

**extraocular muscles**

The skeletal muscles that control the movements of the eyes.

**fastigial nucleus**

One of the deep nuclei of the cerebellum, in the brainstem.

**forebrain**

The most anterior of the three brain vesicles that arise from the neural tube early in brain development. Also, the adult brain region that arises from the forebrain vesicle. The forebrain consists of the telencephalon and diencephalon.

**fornix**

A large fibre bundle that contains output axons leaving the hippocampus.

**fourth ventricle**

The part of the cerebral ventricles located in the hindbrain.

**fovea**

The part of the retina that receives light from the center of the visual field, at the normal fixation point of the eye.

**frontal eye field**

Part of the frontal lobe where neurons generate commands that trigger saccades of the eyes.

**GABA – gamma aminobutyric acid**

A major inhibitory neurotransmitter in the brain. GABA is synthesized from glutamate by the enzyme glutamic acid decarboxylase.

**gamma motor neuron**

A special class of motor neurons that innervate the intrafusal muscle fibers within muscle spindles in skeletal muscles.

**ganglion (plural: ganglia)**

A cluster of neuronal cell bodies, usually located outside the central nervous system in vertebrates. Invertebrate central nervous systems consist of a series of ganglia connected by nerve bundles.

**gap junction**

A site of electrical connection between two cells, where gap junction channels bridge the gap between the insides of the two cells and allow small molecules such as ions to cross directly from one cell to the other.

**geniculostriate pathway**

The visual pathway leading from the lateral geniculate nucleus of the thalamus to the primary visual cortex (i.e., striate cortex).

**glial cell**

A non-neuronal cell in the nervous system that helps regulate the extracellular environment, including uptake of neurotransmitters released from synapses.

**globus pallidus**

One of the basal ganglia of the forebrain.

**Golgi tendon organ**

A specialized sensory structure that provides an indication of the force applied to a tendon by active contraction of a skeletal muscle.

**gracile nucleus**

One of the dorsal column nuclei in the brainstem. The gracile nucleus receives somatosensory inputs from the medial portion of the dorsal columns in the spinal cord.

**gray matter**

A portion of the central nervous system containing predominantly neuronal cell bodies. The relative lack of myelinated axons makes gray matter less opaque than surround areas containing fewer cell bodies and more myelinated fibers (white matter).

**gyrus (plural: gyri)**

An outfolding of the cerebral cortex in brains in which the cortex is highly folded (convoluted), such as the human brain.

**habituation**

Reduction in the strength of a reflexive response produced by repeated presentation of the eliciting stimulus.

**hair cell**

A ciliated sensory cell that produces changes in membrane potential in response to movements of the cilia induced by sensory stimuli.

**hair follicle receptor**

A type of sensory neuron that innervates hair follicles in the skin and

is activated when the hair is deflected.

**hindbrain**

The most posterior of the three brain vesicles that arise at the anterior end of the neural tube during embryonic development of the brain. Also, the most posterior part of the adult brain, which develops from the hindbrain vesicle, including the pons, medulla, and cerebellum.

**hippocampus**

A simplified form of cerebral cortex (archicortex) located under the lower lip of the neocortex at the medial border of the temporal lobe. The hippocampus is part of the limbic system and is thought to be involved in certain types of memory.

**homeostasis**

The maintenance of a relatively constant internal environment despite large changes in external conditions.

**horizontal cell**

A neuron type found in the retina. Horizontal cells are lateral interneurons that receive synaptic inputs from photoreceptors.

**hyperpolarization**

A change in membrane potential in the negative direction, making the cell interior more negative.

**hypothalamus**

A part of the diencephalon involved in a variety of homeostatic functions, in the control of the pituitary, and in motivation and drive. The hypothalamus is a major part of the limbic system.

**I band**

In a striated muscle cell, the part of the sarcomere corresponding the region occupied only by thin filaments, where thin and thick filaments do not overlap.

**inferior colliculus**

The more posterior of the two colliculi, located on the dorsal surface of the midbrain. The inferior colliculus is a processing center for auditory information ascending from the cochlear nucleus and superior olivary nucleus in the brainstem.

**inhibitory postsynaptic potential (IPSP)**

A postsynaptic change in membrane potential that tends to prevent firing of an action potential in the postsynaptic cell, by bringing the membrane potential away from the threshold potential.

**initial segment**

The initial part of the axon as it leaves the cell body of a neuron. The

initial segment is often the point at which action potentials are initiated in response to depolarization.

**intermediolateral gray matter**

The part of the spinal cord gray matter containing the cell bodies of sympathetic preganglionic neurons.

**interneuron**

A neuron in the nervous system that receives inputs from other neurons and makes synaptic contact with other neurons.

**interoceptors**

Sensory receptor cells that detect stimuli arising within the organism. Muscle spindle receptors are an example of interoceptors.

**intrafusal muscle fibers**

The specialized subset of skeletal muscle cells found within the muscle spindle.

**inverse myotatic reflex**

The reflex stimulated by activation of sensory neurons of Golgi tendon organs (also called the tendon organ reflex). Activation of this reflex leads to inhibition of the motor neurons for the same muscle, causing a reduction in muscle tension.

**ion channel**

A membrane protein that forms an aqueous pore through which charged ions can cross the membrane.

**isometric contraction**

A muscle contraction in which muscle length does not change although muscle tension increases.

**isotonic contraction**

A muscle contraction in which muscle tension remains constant during the contraction.

**labyrinth**

A collective term for the cochlea, semicircular canals, and otolith organs in the inner ear.

**lateral column**

The lateral white matter of the spinal cord.

**lateral geniculate nucleus**

The part of the thalamus that receives synaptic inputs from retinal ganglion cells and projects to the primary visual cortex.

**lateral inhibition**

Inhibition mediated by lateral interneurons, in which sensory stimuli at a particular location on the sensory surface inhibits activity in sensory

pathways originating from adjacent regions of the sensory surface.

**lateral intraparietal area**

A part of the parietal lobe of the cerebral cortex involved in integrating visual stimuli with the control of eye movements.

**lateral lemniscus**

An axon tract carrying auditory information from the cochlear nucleus and superior olivary nucleus in the brainstem to the inferior colliculus in the midbrain.

**lateral line organ**

A sensory system found in aquatic vertebrates, containing hair cells that respond to water movement.

**lateral sensory tract**

Part of the lateral white matter in the spinal cord, containing axons of interneurons that receive inputs from nociceptors and temperature-sensitive sensory neurons.

**lateral ventricles**

The portion of the cerebral ventricles found in the telencephalon.

**ligand-gated ion channel**

An ion channel in which channel gating is controlled by binding of a chemical signal (the ligand) to a specific binding site on the channel protein. The ACh-gated ion channel of the neuromuscular junction is an example.

**limbic system**

A brain system involved in the regulation of emotion, motivation, and homeostasis.

**Long-term depression (LTD)**

A reduction in the strength of a synaptic connection lasting for hours or days.

**Long-term potentiation (LTP)**

An enhancement of postsynaptic response amplitude lasting hours or days, produced by a burst of presynaptic activity. LTP is commonly studied as a cellular model of learning and memory.

**M line**

In the sarcomere of a striated muscle cell, the transverse line at the midpoint of the sarcomere. The M line consists of filaments connecting the thick filaments at their midpoint.

**mammillothalamic tract**

A fibre tract containing axons projecting from the mammillary bodies of the hypothalamus to the thalamus in the limbic system.

**marginal zone**

The relatively cell free region at the outer edge of the neural tube.

**mechanoreceptors**

Sensory receptor neurons that respond to mechanical displacement of the sensory surface. Examples are muscle spindle receptors and hair cells.

**medial geniculate nucleus**

The portion of the thalamus that processes auditory information. The medial geniculate nucleus receives synaptic input from the inferior colliculus and sends axons to the primary auditory cortex.

**medial lemniscus**

A fibre tract carrying ascending somatosensory information from the dorsal column nuclei of the brainstem to the thalamus in the diencephalon.

**medulla oblongata**

The most posterior part of the brainstem, at the border between the brain and the spinal cord.

**Meissner corpuscle**

A rapidly adapting skin mechanoreceptor that is sensitive to touch and pressure.

**membrane potential**

The electrical voltage difference between the inside and the outside of a cell.

**Merkel receptor**

A slowly adapting skin mechanoreceptor that signals sustained pressure.

**mesencephalon**

The midbrain.

**midbrain**

The middle of the three brain vesicles that arise from the neural tube during embryonic development. In the adult brain, the midbrain consists of brain structures such as the superior colliculus, the inferior colliculus, and parts of the reticular formation.

**miniature end-plate potential**

A small postsynaptic depolarization at the neuromuscular junction, arising from spontaneous fusion of a single synaptic vesicle in the synaptic terminal.

**motor neuron**

A neuron that makes synaptic contact with the final target cell, such as a skeletal muscle cell.

**motor unit**

A single motor neuron and all of the muscle cells that receive synaptic connections from that motor neuron.

**muscle fibre**

A muscle cell.

**muscle spindle**

An encapsulated sensory structure activated by stretch of skeletal muscles.

**myelin**

The insulating sheath around axons, formed by certain types of glial cells.

**myofibril**

A bundle of thick and thin filaments that forms an organizational unit within a single muscle cell, which contains several myofibrils.

**myosin**

The protein that makes up the thick filaments of a myofibril. ATP hydrolysis by myosin provides the energy to drive filament sliding during muscle contraction.

**myotatic, or stretch reflex**

The spinal reflex triggered by activation of muscle spindles.

**neocortex**

A type of cerebral cortex characterized by multiple layers of cells. Most of the cerebral cortex in the human brain consists of neocortex. Examples of neocortex are the primary somatosensory cortex and the primary motor cortex.

**neurite**

A collective term for the dendrites and axons of a neuron.

**neurogenesis**

The stage of neural development when neuronal precursor cells proliferate to produce neurons.

**neurohypophysis**

The posterior part of the pituitary gland, where nerve terminals of hypothalamic magnocellular neurosecretory cells release the hormones oxytocin and vasopressin.

**neuromuscular junction**

The synaptic junction between the motor neuron and its postsynaptic skeletal muscle cell.

**neuron**

A nerve cell.

**neurotransmitter**

The chemical messenger released from a synaptic terminal to influence a postsynaptic target cell.

**nodes of Ranvier**

Periodic breaks in the myelin sheath, where voltage-dependent sodium channels are clustered and sodium influx occurs to support action potential propagation.

**norepinephrine, or noradrenaline**

A neurotransmitter released by sympathetic motor neurons and by some neurons in the central nervous system.

**nucleus (plural: nuclei)**

A cluster of neuronal cell bodies within the central nervous system.

**olfactory bulb**

The part of the central nervous system that receives synaptic projections from olfactory sensory neurons, via the olfactory nerve.

**oligodendrocyte**

A type of glial cell that myelinates axons in the central nervous system.

**optic chiasm**

The cross over point of the optic nerve, where ganglion cell axons from the temporal and nasal portions of the retina are sorted to ipsilateral or contralateral projections to the lateral geniculate nucleus.

**organ of Corti**

The sensory structure within the cochlea, where sensory hair cells are located.

**osmosis**

The movement of water down its concentration gradient.

**otolith organ**

A sensory structure containing hair cells that detect the organism's orientation with respect to gravity.

**Pacinian corpuscle**

A rapidly adapting skin mechanoreceptor that is sensitive to touch and pressure.

**paleocortex**

A form of cerebral cortex characterized by two layers of cells, as opposed to the multiple layers of cells found in the neocortex. Entorhinal cortex of the olfactory system is an example of paleocortex.

**Papez circuit**

The central core of the limbic system, consisting of a loop from the cingulate gyrus, entorhinal cortex, hippocampus, hypothalamus, thalamus, and back to the cingulate gyrus.

**parasympathetic division**

The acetylcholine-releasing division of the autonomic nervous system.



**paravertebral ganglia**

The chain of sympathetic ganglia that parallel the spinal column.

**Parkinson's disease**

A human disease characterized by muscle tremor and difficulty in initiating and sustaining locomotion. The disease results from degeneration of dopamine-releasing neurons of the substantia nigra.

**pituitary gland**

A master control endocrine gland at the base of the brain. The pituitary gland is controlled in turn by the hypothalamus.

**pons**

A major subdivision of the hindbrain.

**postcentral gyrus**

The gyrus located just posterior to the central sulcus, consisting of the primary somatosensory cortex.

**postsynaptic cell**

The target cell at a synapse.

**post-tetanic potentiation**

Synaptic potentiation that follows a sustained, high-frequency burst of presynaptic action potentials.

**precentral gyrus**

The gyrus located just anterior to the central sulcus, consisting of the primary motor cortex.

**premotor cortex**

Part of the frontal lobe anterior to the primary motor cortex, containing neurons that encode complex movements.

**preoptic area**

Part of the telencephalon just anterior and superior to the anterior end of the hypothalamus. The preoptic area is closely associated with the hypothalamus and is usually considered to be part of the hypothalamus.

**presynaptic cell**

The input cell at a synapse.

**prevertebral ganglia**

Sympathetic ganglia located in the abdominal cavity.

**primary visual cortex**

The visual cortical area that receives direct input from the lateral geniculate nucleus. The primary visual cortex (area V1; striate cortex) is located at the posterior pole of the occipital lobe.

**process**

Another name for a neurite.

**proprioceptor**

A sensory receptor neuron that detects limb or joint position, muscle length, or muscle tension.

**prosencephalon**

The forebrain.

**Purkinje cell**

The output cells of the cerebellum.

**putamen**

One of the basal ganglia of the forebrain. Together, the putamen and the caudate nucleus form the striatum.

**pyramidal cell**

A type of cortical neuron shaped like a pyramid, with a long apical dendrite originating from the narrow end of the cell.

**pyramids**

The fibre bundles consisting of descending axons from the primary motor cortex. radial glial cell. A glial cell that extends from the ventricular zone to the marginal zone during early neural development. Migrating neurons leaving the ventricular zone follow the long thin radial glial cells.

**raphe nucleus**

A nucleus located near the midline of the brainstem, containing (among other neurons) the omnidirectional pause neurons that allow saccades to proceed.

**receptive field**

The portion of the sensory surface where stimuli affect the activity of a sensory neuron.

**receptor potential**

The change in membrane potential in a primary sensory receptor neuron in response to a sensory stimulus.

**red nucleus**

A brainstem motor control nucleus that gives rise to the rubrospinal tract. Activation of the rubrospinal tract promotes limb flexion.

**Renshaw cell**

An inhibitory interneuron in the spinal cord that receives excitatory input from a motor neuron and makes inhibitory synapses back onto the same motor neuron.

**resting potential**

The steady state membrane potential of a neuron in the absence of incoming synaptic or sensory influences.

**reticular formation**

A diffuse network of neurons in the midbrain and hindbrain, involved in a variety of sensory and motor functions.

**reticulospinal tract**

A fibre tract consisting of descending axons from neurons in the reticular formation to spinal interneurons and motor neurons.

**retina**

The multilayered structure at the back of the eye responsible for light reception and processing of visual information. The retina consists of the neural retina, containing the neurons and glial cells, and the retinal pigmented epithelium, which absorbs stray light and supports the outer segments of photoreceptor cells.

**retinal (retinaldehyde)**

The light-absorbing chromophore group that is chemically attached to the opsin protein to form a visual pigment molecule.

**retinal ganglion cell**

The output cells of the retina, whose axons form the optic nerve and project to the lateral geniculate nucleus of the thalamus, the accessory optic system, and the suprachiasmatic nucleus of the hypothalamus.

**retinohypothalamic tract**

The fibre tract consisting of axons of retinal ganglion cells projecting to the suprachiasmatic nucleus of the hypothalamus.

**rhodopsin**

The visual pigment molecule of rod photoreceptors.

**rhombencephalon**

The hindbrain.

**rods**

A subtype of photoreceptor found in the vertebrate retina. Rods are more sensitive to light than cones are responsible for vision under dim illumination.

**rubrospinal tract**

The fibre tract containing axons descending to the spinal cord from the red nucleus of the brainstem.

**Ruffini corpuscle**

A slowly adapting skin mechanoreceptor that signals sustained pressure.

**saccade**

A rapid eye movement used to alter eye position within the orbit, causing a rapid adjustment of the fixation point to different positions in the visual world.

**saccule**

The horizontally oriented otolith organ of the labyrinth.

**saltatory conduction**

A form of action potential propagation found in myelinated axons, in which action potentials jump from one node of Ranvier to the next.

**sarcomere**

The basic repeating unit of striation along the length of myofibrils of striated muscle cells. The sarcomere is defined as extending from one Z line to the next Z line.

**sarcoplasmic reticulum**

An intracellular store of calcium ions wrapped around the contractile apparatus of myofibrils in striated muscle cells. Calcium released from the sarcoplasmic reticulum triggers contraction.

**Schwann cell**

A type of glial cell that forms the myelin sheath around axons in the peripheral nervous system.

**semicircular canals**

Bio-accelerometers (i.e., acceleration-sensing organs), which are fluid-filled loops that form part of the labyrinth.

**sensitization**

Enhancement of the strength of a reflexive response produced by the presentation of a noxious stimulus.

**sensory adaptation**

The reduction in activity of a sensory neuron during sustained application of a sensory stimulus.

**sensory neuron**

A neuron whose activity is affected by the presence of a particular type of sensory stimulus.

**sensory transduction**

The conversion of stimulus energy into an electrical signal in a primary sensory receptor neuron.

**skeletal muscle**

A type of striated muscle responsible for movement of body parts.

**soma**

The cell body of a cell, where the nucleus is located.

**somatic nervous system**

The division of the nervous system that controls the skeletal muscles, as distinguished from the autonomic nervous system.

**somatopic map**

A form of neural organization in which neighboring regions of a body

structure project to or are controlled by neighboring neurons in the brain region that receive sensory inputs from or send motor output to the body structure.

**somatosensory system**

The sensory system that receives and processes sensory information from the body, including the skin, muscles, and joints.

**spatial summation**

Summation of postsynaptic responses in a postsynaptic cell from two or more synaptic inputs that are active at about the same time.

**spinal canal**

The fluid filled space at the center of the spinal cord. The spinal canal is continuous with the ventricles of the brain.

**spinal nerve**

The mixed motor and sensory nerve connected to the spinal cord at a particular vertebral segment.

**spinocerebellar tract**

The sensory pathway in the spinal cord carrying ascending axons to the cerebellum.

**spiral ganglion**

The ganglion in the cochlea containing the cell bodies of sensory neurons that receive inputs from the cochlear hair cells and send axons via the auditory nerve (cranial nerve VIII) to the cochlear nucleus of the brainstem.

**stellate cell**

A neuron whose dendrites radiate approximately equally in all directions from the soma, producing a starlike pattern.

**stem cell**

An undifferentiated precursor cell that retains the ability to give rise to a variety of cell types. In the nervous system, stem cells can give rise to various neuron subtypes and to glial cells.

**striated muscle cell**

A type of muscle cell in which the contractile machinery forms a regular, repeating array, which gives the cell a striped (striated) appearance when viewed through the light microscope.

**striatum**

A collective term for the caudate nucleus and putamen, which are two of the basal ganglia of the forebrain.

**substantia nigra**

A midbrain region involved in the control of motor behavior. Loss of dopamine-releasing neurons of the substantia nigra underlies the movement

disorder called Parkinson's disease.

**sulcus (plural: sulci)**

An infolding, or groove, in the cortical surface. A sulcus separates neighboring gyri.

**superior colliculus**

A brain region on the dorsal surface of the midbrain that is involved in the control of eye movements.

**superior olivary nucleus (superior olive)**

A nucleus in the brainstem that is involved in the processing of auditory information. The superior olivary nucleus receives inputs from the cochlear nuclei and sends outputs to the inferior colliculus.

**supplemental motor area**

A higher order cortical motor area located in the medial part of the frontal lobe, just anterior to the primary motor cortex.

**suprachiasmatic nucleus**

A nucleus of the hypothalamus responsible for synchronizing circadian rhythms in other organs and tissues.

**Sylvian fissure**

The large sulcus that separates the temporal lobe from the rest of the cerebral cortex. It is also called the lateral sulcus.

**sympathetic chains**

A series of interconnected sympathetic nuclei (the paravertebral ganglia) that parallel both sides of the vertebral column.

**sympathetic division**

A division of the autonomic nervous system, containing autonomic motor neurons that release the neurotransmitter norepinephrine. Actions of the sympathetic nervous system typically oppose the actions of the other division of the autonomic nervous system, the parasympathetic division.

**synapse**

The contact point where a neuron transfers information to a target cell.

**synaptic cleft**

The extracellular space separating the presynaptic cell and the postsynaptic cell at a synapse.

**synaptic vesicle**

A small, membrane-bound structure in which neurotransmitter molecules are stored within synaptic terminals.

**taste bud**

A cluster of cells on the surface of the tongue, containing taste receptor cells.

**tectorial membrane**

A sheet of tissue overlying the organ of Corti in the cochlea. Cilia of outer hair cells are embedded into the surface of the tectorial membrane.

**telencephalon**

A subdivision of the forebrain, comprising the cerebrum and the basal ganglia.

**temporal summation**

Summation of successive postsynaptic responses in a postsynaptic cell from two or more action potentials arriving within a brief period in the same synaptic terminal.

**tetrodotoxin**

A biological toxin that blocks voltage-dependent sodium channels.

**thalamus**

One of the two subdivisions of the diencephalon. The thalamus receives and processes sensory information and sends the sensory information to the appropriate regions of the cerebral cortex. The thalamus also plays important roles in motor control.

**thermoreceptors**

Primary sensory neurons that respond to changes in skin or body temperature. thick filament. A longitudinal filament found in striated muscle cells, made up of the protein myosin.

**thin filament**

A longitudinal filament found in striated muscle cells, made up of the protein actin and the associated proteins tropomyosin and troponin.

**third ventricle**

The part of the brain ventricles that extends from the midbrain through the diencephalon.

**threshold (threshold potential)**

The value of membrane potential that must be reached in an excitable cell to trigger an action potential.

**tonotopic map**

The orderly projection of inputs originating from the cochlea to sensory areas in the brain, such that neighboring neurons in the target regions respond to progressively higher frequencies.

**transverse tubules**

Invaginations of the plasma membrane in skeletal muscle cells that provide a path for depolarization during the muscle action potential to spread to the cell interior.

**tropomyosin**

A protein associated with the thin filaments of striated muscle cells. Tropomyosin controls the access of myosin to the myosin binding site of actin.

**troponin**

A calcium binding molecule associated with the thin filaments of striated muscle cells. Binding of calcium to troponin initiates contraction.

**tubulin**

A protein molecule that polymerizes to form the backbone of microtubules. tympanic membrane. The eardrum, which transfers sound pressure waves to the bones of the middle ear.

**undershoot**

The transient period of increased negativity at the termination of an action potential.

**utricle**

The vertically oriented otolith organ of the labyrinth.

**ventral column**

The white matter on the ventral surface of the spinal cord, containing descending motor axons of the corticospinal tract, the vestibulospinal tract, and the reticulospinal tract.

**ventral corticospinal tract**

The portion of the ventral column containing descending axons of neurons whose cell bodies are located in the primary motor cortex.

**ventral root**

The fibre bundle containing outgoing (efferent) motor axons exiting the spinal cord at each vertebral segment.

**ventricles**

The fluid-filled core of the brain, filled with cerebrospinal fluid.

**ventricular zone**

The inner layer of the neural tube, next to the fluid-filled ventricle. Dividing precursor cells that give rise to the nervous system are found in the ventricular zone.

**vestibular ganglion**

A ganglion located just outside the labyrinth of the inner ear, containing the cell bodies of sensory neurons that receive inputs from the hair cells of the semicircular canals.

**vestibular nuclei**

Nuclei in the brainstem that receive synaptic inputs from sensory neurons of the vestibular ganglion.

**vestibulo-ocular reflex**



The reflex that induces eye movements in response to head rotation to keep the eyes fixated at a constant point in space.

**vestibulospinal tract**

A fibre pathway originating in the vestibular nucleus of the brainstem and projecting to the spinal cord. Activation of the vestibulospinal tract promotes limb extension.

**voltage-sensitive sodium channel**

A sodium channel whose conducting state depends on voltage. Opening of voltage-sensitive sodium channels underlies the depolarizing phase of the action potential.

**Wernicke's area**

Part of the temporal lobe surrounding the primary auditory cortex. Damage in Wernicke's area produces deficits in understanding spoken language (receptive aphasia).

**white matter**

Regions of the central nervous system containing few neuronal cell bodies and many myelinated axons. The myelin sheaths are opaque compared to surrounding regions containing mostly neuronal cell bodies (gray matter).

**Z line**

A crosswise line connecting thin filaments within a myofibril. The sarcomere is defined as extending from one Z line to the next Z line.

### **A.3 Modern 3D Neuroimaging**

#### **A.3.1 Nuclear Magnetic Resonance in 2D Medical Imaging**

The *Nobel Prize in Physiology or Medicine in 2003* was jointly awarded to *Paul C. Lauterbur* and *Peter Mansfield* for their discoveries concerning *magnetic resonance imaging* (MRI), a technique for using strong magnetic fields to produce images of the inside of the human body.

Atomic nuclei in a strong magnetic field rotate with a frequency that is dependent on the strength of the magnetic field. Their energy can be increased if they absorb radio waves with the same resonant frequency. When the atomic nuclei return to their previous energy level, radio waves are emitted. These discoveries were awarded the *Nobel Prize in Physics in 1952*, jointly to *Felix Bloch* and *Edward M. Purcell*. During the following decades, magnetic resonance was used mainly for studies of the chemical structure of substances. In the beginning of the 1970s, Lauterbur and

Mansfield made pioneering contributions, which later led to the applications of nuclear magnetic resonance (NMR) in medical imaging.

Paul Lauterbur discovered the possibility to create a 2D picture by introducing gradients in the magnetic field. By analysis of the characteristics of the emitted radio waves, he could determine their origin. This made it possible to build up 2D pictures of structures that could not be visualized with other methods.

Peter Mansfield further developed the utilization of gradients in the magnetic field. He showed how the signals could be mathematically analyzed, which made it possible to develop a useful imaging technique. Mansfield also showed how extremely fast imaging could be achievable. This became technically possible within medicine a decade later.

*Magnetic resonance imaging* (MRI), is now a routine method within medical diagnostics. Worldwide, more than 60 million investigations with MRI are performed each year, and the method is still in rapid development. MRI is often superior to other imaging techniques and has significantly improved diagnostics in many diseases. MRI has replaced several invasive modes of examination and reduced the risk and discomfort for patients.

### A.3.2 3D Magnetic Resonance Imaging of Human Brain

Modern technology of human brain imaging emphasizes 3D investigation of brain structure and function, using three variations of MRI. Brain *structure* is commonly imaged using *anatomical MRI*, or aMRI, while brain *physiology* is usually imaged using *functional MRI*, or fMRI (see Figure A.2). For bridging the gap between brain anatomy and function, as well as exploring natural brain connectivity, a *diffusion MRI*, or dMRI is used, based on the state-of-the-art *diffusion tensor* (DT) technique (see [Le Bihan *et al.* (1995); Le Bihan (1996); Le Bihan (2000); Le Bihan *et al.* (2001); Le Bihan and van Zijl (2002); Le Bihan (2003)]).

The ability to visualize anatomical connections between different parts of the brain, non-invasively and on an individual basis, has opened a new era in the field of functional neuro-imaging. This major breakthrough for neuroscience and related clinical fields has developed over the past ten years through the advance of *diffusion magnetic resonance imaging* (dMRI). The concept of dMRI is to produce MRI quantitative maps of microscopic, natural displacements of water molecules that occur in brain tissues as part of the physical diffusion process. Water molecules are thus used as a probe that can reveal microscopic details about tissue architecture, either normal

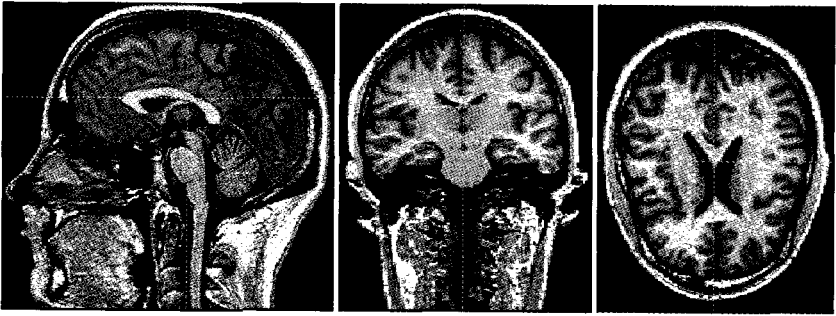


Fig. A.2 3D display from brain fMRI: left-sagittal, middle-coronal, and right-transversal view.

or in a diseased state.

### A.3.3 Diffusion MRI in 3D Volume

*Molecular diffusion* refers to the *Brownian motion* of molecules, which results from the thermal energy carried by these molecules. Molecules travel randomly in space over a distance that is statistically well described by a *diffusion coefficient*,  $D$ . This coefficient depends only on the size (mass) of the molecules, the temperature and the nature (viscosity) of the medium. In the spatially varying magnetic field, induced through a magnetic field gradient, the amplitude and timing of which are characterized by a so-called *b-factor*, moving molecules emit radiofrequency signals with slightly different phases. In a small 3D-volume (voxel) containing a large number of diffusing molecules, these phases become randomly distributed, directly reflecting the diffusion process, i.e., the trajectory of individual molecules. This diffusive phase distribution of the signal results in an *attenuation*  $A$  of the MRI signal, which quantitatively depends on the gradient characteristics of the *b-factor* and the diffusion coefficient  $D$ .

dmRI is, thus, deeply rooted in the concept that, during their diffusion-driven displacements, molecules probe tissue structure at a *microscopic scale* well beyond the usual *millimetric image resolution*. During typical diffusion times of about 50–100 ms, water molecules move in brain tissues on average over distances around 1–15  $\mu\text{m}$ , bouncing, crossing or interacting with many tissue components, such as cell membranes, fibres or macromolecules. Because of the tortuous movement of water molecules around those obstacles, the actual diffusion distance is reduced compared to free water. Hence, the non-invasive observation of the water diffusion-driven

displacement distributions *in vivo* provides unique clues to the fine structural features and geometric organization of neural tissues, and to changes in those features with physiological or pathological states.

### A.3.4 *Imaging Diffusion with MRI*

While early water diffusion measurements were made in biological tissues using Nuclear Magnetic Resonance in the 1960s and 70s, it is not until the mid 1980s that the basic principles of dMRI were laid out. MRI signals can be made sensitive to diffusion through the use of a pair of sharp magnetic field gradient pulses, the duration and the separation of which can be adjusted. The result is a signal (echo) attenuation which is precisely and quantitatively linked to the amplitude of the molecular displacement distribution: Fast (slow) diffusion results in a large (small) distribution and a large (small) signal attenuation. Naturally, the effect also depends on the intensity of the magnetic field gradient pulses.

In practice, any MRI imaging technique can be sensitized to diffusion by inserting the adequate magnetic field gradient pulses. By acquiring data with various gradient pulse amplitudes one gets images with different degrees of diffusion sensitivity. Contrast in these images depends on diffusion, but also on other MRI parameters, such as the water relaxation times. Hence, these images are often numerically combined to determine, using a global diffusion model, an estimate of the diffusion coefficient in each image location. The resulting images are maps of the diffusion process and can be visualized using a quantitative scale.

Because the overall signal observed in a MRI image voxel, at a millimetric resolution, results from the integration, on a statistical basis, of all the microscopic displacement distributions of the water molecules present in this voxel it was suggested to portray the complex diffusion processes that occur in a biological tissue on a voxel scale using a global, statistical parameter, the *apparent diffusion coefficient* (ADC). The ADC concept has been largely used since then in the literature. The ADC now depends not only on the actual diffusion coefficients of the water molecular populations present in the voxel, but also on experimental, technical parameters, such as the voxel size and the diffusion time.

### A.3.5 3D Diffusion Tensor

Now, as diffusion is really a 3D process, water molecular mobility in tissues is not necessarily the same in all directions. This *diffusion anisotropy* may result from the presence of obstacles that limit molecular movement in some directions. It is not until the advent of diffusion MRI that anisotropy was detected for the first time *in vivo*, at the end of the 1980s, in spinal cord and brain white matter (see [Le Bihan *et al.* (1995); Le Bihan (1996); Le Bihan (2000); Le Bihan *et al.* (2001); Le Bihan and van Zijl (2002); Le Bihan (2003)]). Diffusion anisotropy in white matter grossly originates from its specific organization in bundles of more or less myelinated axonal fibres running in parallel: Diffusion in the direction of the fibres (whatever the species or the fiber type) is about 3–6 times faster than in the perpendicular direction. However the relative contributions of the intra-axonal and extracellular spaces, as well as the presence of the myelin sheath, to the ADC, and the exact mechanism for the anisotropy is still not completely understood, and remains the object of active research. It quickly became apparent, however, that this anisotropy effect could be exploited to map out the orientation in space of the white matter tracks in the brain, assuming that the direction of the fastest diffusion would indicate the overall orientation of the fibres. The work on diffusion anisotropy really took off with the introduction in the field of diffusion MRI of the more rigorous formalism of the diffusion tensor.

More precisely, with plain diffusion MRI, diffusion is fully described using a single (scalar) parameter, the diffusion coefficient,  $D$ . The effect of diffusion on the MRI signal (most often a spin-echo signal) is an attenuation,  $A$ , which depends on  $D$  and on the  $b$  factor, which characterizes the the gradient pulses (timing, amplitude, shape) used in the MRI sequence:

$$A = \exp(-bD).$$

However, in the presence of anisotropy, diffusion can no longer be characterized by a single scalar coefficient, but requires a 3D tensor-field  $\mathbf{D} = \mathbf{D}(t)$  (see chapter 3 above), give by the matrix of ‘moments’ (on the main diagonal) and ‘product’ (off-diagonal elements) [Le Bihan *et al.* (2001)]:

$$\mathbf{D}(t) = \begin{pmatrix} D_{xx}(t) & D_{xy}(t) & D_{xz}(t) \\ D_{yx}(t) & D_{yy}(t) & D_{yz}(t) \\ D_{zx}(t) & D_{zy}(t) & D_{zz}(t) \end{pmatrix},$$

which fully describes molecular mobility along each direction and correla-

tion between these directions. This tensor is symmetric ( $D_{ij} = D_{ji}$ , with  $i, j = x, y, z$ ).

Now, in a *reference frame*  $[x', y', z']$  that coincides with the principal or self directions of diffusivity, the off-diagonal terms do not exist, and the tensor is reduced only to its diagonal terms,  $\{D_{x'x'}, D_{y'y'}, D_{z'z'}\}$ , which represent molecular mobility along axes  $x'$ ,  $y'$ , and  $z'$ , respectively. The *echo attenuation* then becomes:

$$A = \exp(-b_{x'x'}D_{x'x'} - b_{y'y'}D_{y'y'} - b_{z'z'}D_{z'z'}),$$

where  $b_{ii}$  are the elements of the **b**-tensor, which now replaces the scalar *b*-factor, expressed in the coordinates of this reference frame.

In practice, unfortunately, measurements are made in the reference frame  $[x, y, z]$  of the MRI scanner gradients, which usually does not coincide with the diffusion frame of the tissue [Le Bihan *et al.* (2001)]. Therefore, one must also consider the coupling of the nondiagonal elements,  $b_{ij}$ , of the **b**-tensor with the nondiagonal terms,  $D_{ji}$ , ( $i \neq j$ ), of the diffusion tensor (now expressed in the scanner frame), which reflect correlation between molecular displacements in perpendicular directions:

$$A = \exp(-b_{xx}D_{xx} - b_{yy}D_{yy} - b_{zz}D_{zz} - 2b_{xy}D_{xy} - 2b_{xz}D_{xz} - 2b_{yz}D_{yz}).$$

Hence, it is important to note that by using diffusion-encoding gradient pulses along one direction only, signal attenuation not only depends on the diffusion effects along this direction but may also include contribution from other directions.

Now, calculation of the the **b**-tensor may quickly become complicated when many gradient pulses are used, but the full determination of the diffusion tensor **D** is necessary if one wants to assess properly and fully all anisotropic diffusion effects.

To determine the diffusion tensor **D** fully, one must first collect diffusion-weighted images along several gradient directions, using diffusion-sensitized MRI pulse sequences such as *echoplanar imaging* (EPI) [Le Bihan (1995)]. As the diffusion tensor is symmetric, measurements along only 6 directions are mandatory (instead of 9), along with an image acquired without diffusion weighting ( $b = 0$ ).

In the case of axial symmetry, only four directions are necessary (tetrahedral encoding), as suggested in the *spinal cord* [Clark *et al.* (2000)]. The acquisition time and the number of images to process are then reduced.

In this way, with *diffusion tensor imaging* (DTI), diffusion is no longer

described by a single diffusion coefficient, but by an array of 9 coefficients (dependent on the sampling discrete time) that fully characterize how diffusion in space varies according to direction. Hence, diffusion anisotropy effects can be fully extracted and exploited, providing even more exquisite details on tissue microstructure.

With DTI, diffusion data can be analyzed in three ways to provide information on tissue microstructure and architecture for each voxel: (i) the *mean diffusivity*, which characterizes the overall mean-squared displacement of molecules and the overall presence of obstacles to diffusion; (ii) the *degree of anisotropy*, which describes how much molecular displacements vary in space and is related to the presence and coherence of oriented structures; (iii) the *main direction of diffusivities* (main ellipsoid axes), which is linked to the orientation in space of the structures.

**Mean Diffusivity.** To obtain an overall evaluation of the diffusion in a voxel or 3D-region, one must avoid anisotropic diffusion effects and limit the result to an invariant, i.e., a quantity that is independent of the orientation of the reference frame [Basser *et al.* (1994)]. Among several combinations of the tensor elements, the trace of the diffusion tensor,  $\text{Tr}(\mathbf{D}) = D_{xx} + D_{yy} + D_{zz}$ , is such an invariant. The mean diffusivity is then given by  $\text{Tr}(\mathbf{D})/3$ .

**Diffusion Anisotropy Indices.** Several scalar indices have been proposed to characterize diffusion anisotropy. Initially, simple indices calculated from diffusion-weighted images, or ADCs, obtained in perpendicular directions were used, such as  $ADC_x/ADC_y$  and displayed using a color scale [Douek *et al.* (1991)]. Other groups have devised indices mixing measurements along  $x$ ,  $y$ , and  $z$  directions, such as  $\frac{\max[ADC_x, ADC_y, ADC_z]}{\min[ADC_x, ADC_y, ADC_z]}$ , or the standard deviation of  $ADC_x$ ,  $ADC_y$ , and  $ADC_z$  divided by their mean value [van Gelderen *et al.* (1994)]. Unfortunately, none of these indices are really quantitative, as they do not correspond to a single meaningful physical parameter and, more importantly, are clearly dependent on the choice of directions made for the measurements. The degree of anisotropy would then vary according to the respective orientation of the gradient hardware and the tissue frames of reference and would generally be underestimated. Here again, invariant indices must be found to avoid such biases and provide an objective, intrinsic structural information [Basser and Pierpaoli (1996)].

Invariant indices are thus made of combinations of the eigen-values  $\lambda_1$ ,  $\lambda_2$ , and  $\lambda_3$  of the diffusion tensor  $\mathbf{D}$ . The most commonly used invariant indices are the *relative anisotropy* (RA), the *fractional anisotropy* (FA), and the *volume ratio* (VR).

**Fiber Orientation Mapping.** The last family of parameters that can

be extracted from the DTI concept relates to the mapping of the orientation in space of tissue structure. The assumption is that the direction of the fibers is collinear with the direction of the eigen-vector associated with the *largest eigen-diffusivity*. This approach opens a completely new way to gain direct and in vivo information on the organization in space of oriented tissues, such as muscle, myocardium, and brain or spine white matter, which is of considerable interest, both clinically and functionally. Direction orientation can be derived from DTI directly from diffusion/orientation-weighted images or through the calculation of the diffusion tensor  $\mathbf{D}$ . Here, a first issue is to display fiber orientation on a voxel-by-voxel basis. The use of color maps has first been suggested, followed by representation of ellipsoids, octahedra, or vectors pointing in the fiber direction [Le Bihan *et al.* (2001)].

#### A.3.6 Brain Connectivity Studies

Studies of neuronal connectivity are important to interpret functional MRI data and establish the networks underlying cognitive processes. Basic DTI provides a means to determine the overall orientation of white matter bundles in each voxel, assuming that only one direction is present or predominant in each voxel, and that diffusivity is the highest along this direction. 3D vector-field maps representing fiber orientation in each voxel can then be obtained back from the image data through the diagonalization (a mathematical operation which provides orthogonal directions coinciding with the main diffusion directions) of the diffusion tensor determined in each voxel. A second step after this *inverse problem* is solved consists in *connecting* subsequent voxels on the basis of their respective fibre orientation to infer some continuity in the fibers (see Figure A.3). Several algorithms have been proposed. *Line propagation algorithms* reconstruct tracts from voxel to voxel from a seed point. Another approach is based on *regional energy minimization* (minimal bending) to select the most likely trajectory among several possible [Le Bihan *et al.* (2001); Le Bihan and van Zijl (2002); Le Bihan (2003)].





Fig. A.3 Several approaches have been developed to 'connect' voxels after white matter fibers have been identified and their orientation determined; left: 3D display from fMRI of a brain hemisphere showing sulci and connections; right: 3D display of the motor cortex, central structures and connections.

### A.3.7 Brain Waves and Independent Component Analysis

Among all the techniques used today for monitoring functions, only *electroencephalography* (EEG) has requisite temporal resolution and portability for detection of rapid changes in the brain. Magnetoencephalography (MEG) is often too expensive and lacks portability. Haemodynamic techniques such as functional MRI (described above) and positron emission tomography (PET) are too slow to detect transient responses to external events; they lack portability; and are also too expensive.

Activity at each EEG electrode reflects 1500 ms of neural activity on the scalp in the microvolt range, volume conducted from underlying brain structures. It demonstrates event-related activity indexing different and multiple mental events. Brain electrical fields reliably capture both tonic and phasic brain states with spatiotemporal sensitivity.

However, there are still challenges to the efficient EEG applications, like extracting signal from background endogenous noise in the brain. This problem can be solved using *independent component analysis* (ICA), a statistical and computational technique for revealing hidden factors that underlie sets of random variables, measurements, or signals (see [Hyvärinen *et al.* (2001)]).

ICA defines a generative model for the observed multivariate data, which is typically given as a large database of samples. In the model, the data

variables are assumed to be linear mixtures of some unknown latent variables, and the mixing system is also unknown. The latent variables are assumed non-gaussian and mutually independent, and they are called the independent components of the observed data. These independent components, also called sources or factors, can be found by ICA.

ICA is superficially related to principal component analysis and factor analysis. ICA is a much more powerful technique, capable of finding the underlying factors or sources when these classic methods fail completely.

The data analyzed by ICA could originate from many different kinds of application fields, including digital images, document databases, economic indicators and psychometric measurements. In many cases, the measurements are given as a set of parallel signals or time series; the term *blind source separation* is used to characterize this problem. Typical examples are mixtures of simultaneous speech signals that have been picked up by several microphones, brain waves recorded by multiple sensors, interfering radio signals arriving at a mobile phone, or parallel time series obtained from some industrial process.

## A.4 Complex Functions, Manifolds and Hilbert Spaces

### A.4.1 Complex Numbers and Vectors

For a *complex number*  $z = a + bi \in \mathbb{C}$ , (with imaginary unit,  $i = \sqrt{-1}$ ), its *complex-conjugate* is  $\bar{z} = \overline{a + bi} = a - bi \in \mathbb{C}$ ; then  $z\bar{z} = a^2 + b^2 \in \mathbb{C}$ ; its *absolute value* or *modules* is  $|z| = |a + bi| = \sqrt{z\bar{z}} = \sqrt{a^2 + b^2}$ .  $z$  is *real*,  $z \in \mathbb{R}$ , iff  $\bar{z} = z$ .

Using *Euler's formula*

$$e^{i\theta} = \cos \theta + i \sin \theta,$$

the *polar* and *exponential* forms of a complex number  $z \in \mathbb{C}$  are given by

$$z = r(\cos \theta + i \sin \theta) = r \operatorname{cis} \theta = r e^{i\theta},$$

where  $r = |z| = \sqrt{a^2 + b^2}$  and  $\theta$  (*argument*, or *amplitude*) are polar coordinates, giving also

$$\begin{aligned} \cos \theta &= \frac{1}{2}(e^{i\theta} + e^{-i\theta}) = \frac{1}{2} \left( z + \frac{1}{z} \right), \\ \sin \theta &= \frac{1}{2i}(e^{i\theta} - e^{-i\theta}) = \frac{1}{2i} \left( z - \frac{1}{z} \right). \end{aligned}$$

*Product of two complex numbers* is now given as

$$z_1 z_2 = r_1 r_2 [\cos(\theta_1 + \theta_2) + i \sin(\theta_1 + \theta_2)] = r_1 r_2 \operatorname{cis}(\theta_1 + \theta_2) = r_1 r_2 e^{i(\theta_1 + \theta_2)},$$

there *quotient* is

$$\frac{z_1}{z_2} = \frac{r_1}{r_2} [\cos(\theta_1 - \theta_2) + i \sin(\theta_1 - \theta_2)] = \frac{r_1}{r_2} \operatorname{cis}(\theta_1 - \theta_2) = \frac{r_1}{r_2} e^{i(\theta_1 - \theta_2)},$$

the  $n$ th power *De Moivre's theorem* holds (with  $n \in \mathbb{N}$ )

$$z^n = [r(\cos \theta + i \sin \theta)]^n = [r(\cos n\theta + i \sin n\theta)] = r^n \operatorname{cis}(n\theta) = r^n e^{in\theta},$$

while the  $n$ th root is (with  $n, k \in \mathbb{N}$ )

$$z^{1/n} = \left[ r \left( \cos \frac{\theta + 2k\pi}{n} + i \sin \frac{\theta + 2k\pi}{n} \right) \right]^{1/n} = r^{1/n} \operatorname{cis} \frac{\theta + 2k\pi}{n} = r^{1/n} e^{i \frac{\theta + 2k\pi}{n}},$$

The elements of  $\mathbb{C}^n$  are  $n$ -vectors. For any two  $n$ -vectors  $x, y \in \mathbb{C}^n$  their *inner product* is defined as

$$x \cdot y = \langle x | y \rangle = \sum_{i=1}^n x_i y_i.$$

The *norm* of an  $n$ -vector  $x \in \mathbb{C}^n$  is

$$\|x\| = \sqrt{x \cdot x} = \sqrt{\langle x | x \rangle}.$$

The space  $\mathbb{C}^n$  with operations of vector addition, scalar multiplication, and inner product, is called *complex Euclidean  $n$ -space*.

M. Eastwood and R. Penrose (see [Eastwood, M., Penrose, R. (2000)]) developed a method for *drawing with complex numbers* in an ordinary Euclidean 3D space  $\mathbb{R}^3$ . They showed how the algebra of complex numbers can be used in an elegant way to represent the images of ordinary 3D figures, orthographically projected to the plane  $\mathbb{R}^2 = \mathbb{C}$ . For inspiration, see [Hilbert and Cohn-Vossen (1999)].

#### A.4.1.1 Quaternions and Rotations

Recall (from topology) that the set of Hamilton's *quaternions*  $\mathbb{H}$  represents an extension of the set of complex numbers  $\mathbb{C}$ . Quaternions are widely used to represent rotations<sup>23</sup>. Instead of one imaginary unit  $i = \sqrt{-1}$ , we have

<sup>23</sup>Quaternions are superior to Euler angles in representing rotations, as they do not 'flip' at the angle of  $\pm\pi/2$  (the well-known singularity of Euler angles).

three different numbers that are all square roots of  $-1$  – labelled  $i$ ,  $j$ , and  $k$ , respectively,

$$i \cdot i = -1, \quad j \cdot j = -1, \quad k \cdot k = -1.$$

When we multiply two quaternions, they behave similarly to cross products of the unit basis vectors,

$$i \cdot j = -j \cdot i = k, \quad j \cdot k = -k \cdot j = i, \quad k \cdot i = -i \cdot k = j.$$

The conjugate and magnitude of a quaternion are found in much the same way as complex conjugate and magnitude. If a quaternion  $q$  has length 1, we say that  $q$  is a *unit quaternion*

$$q = w + xi + yj + zk,$$

$$q' = w - xi - yj - zk,$$

$$|q| = \sqrt{q \cdot q'} = \sqrt{w^2 + x^2 + y^2 + z^2},$$

$$\text{unit quaternions: } |q| = 1 \Rightarrow q^{-1} = q',$$

$$\text{quaternions are associative: } (q_1 \cdot q_2) \cdot q_3 = q_1 \cdot (q_2 \cdot q_3),$$

$$\text{quaternions are not commutative: } q_1 \cdot q_2 \neq q_2 \cdot q_1.$$

We can represent a quaternion in several ways: (i) as a linear combination of 1,  $i$ ,  $j$ , and  $k$ , (ii) as a vector of the four coefficients in this linear combination, or (iii) as a scalar for the coefficient of 1 and a vector for the coefficients of the imaginary terms.

$$q = w + xi + yj + zk = [x \ y \ z \ w] = (s, v),$$

$$s = w, \quad v = [x \ y \ z].$$

We can write the product of two quaternions in terms of the  $(s, v)$  representation using standard vector products in the following way:

$$q_1 = (s_1, v_1), \quad q_2 = (s_2, v_2),$$

$$q_1 \cdot q_2 = (s_1 s_2 - v_1 \cdot v_2, \ s_1 v_2 + s_2 v_1 + v_1 \times v_2).$$

**Representing Rotations with Quaternions.** We will compute a rotation about the unit vector,  $\mathbf{u}$  by an angle  $\theta$ . The quaternion that computes this rotation is

$$q = (s, v) = \left( \cos \frac{\theta}{2}, \ u \sin \frac{\theta}{2} \right).$$

We will represent a point  $p$  in 3D space by the quaternion  $P = (0, p)$ . We compute the desired rotation about that point by

$$P = (0, p), \quad P_{\text{rotated}} = q \cdot P \cdot q^{-1}.$$

Now, the quaternion  $P_{\text{rotated}}$  should be  $(0, p_{\text{rotated}})$ . Actually, we could put any value into the scalar part of  $P$ , i.e.,  $P = (c, p)$  and after performing the quaternion multiplication, we should get back  $P_{\text{rotated}} = (c, p_{\text{rotated}})$ .

You may want to confirm that  $q$  is a *unit quaternion*, since that will allow us to use the fact that the inverse of  $q$  is  $q'$  if  $q$  is a unit quaternion.

**Concatenating Rotations.** Suppose we want to perform two rotations on an object. This may come up in a manipulation interface where each movement of the mouse adds another rotation to the current object pose. This is very easy and numerically stable with a quaternion representation.

Suppose  $q_1$  and  $q_2$  are unit quaternions representing two rotations. We want to perform  $q_1$  first and then  $q_2$ . To do this, we apply  $q_2$  to the result of  $q_1$ , regroup the product using associativity, and find that the composite rotation is represented by the quaternion  $q_2 \cdot q_1$ .

$$q_2 \cdot (q_1 \cdot P \cdot q_1^{-1}) \cdot q_2^{-1} = (q_2 \cdot q_1) \cdot P \cdot (q_1^{-1} \cdot q_2^{-1}) = (q_2 \cdot q_1) \cdot P \cdot (q_2 \cdot q_1)^{-1}.$$

Therefore, the only time we need to compute the matrix is when we want to transform the object. For other operations we need only look at the quaternions. A matrix product requires many more operations than a quaternion product so we can save a lot of time and preserve more numerical accuracy with quaternions than with matrices.

**Matrix Representation for Quaternion Multiplication.** We can use the rules above to compute the product of two quaternions.

$$\begin{aligned} q_1 &= w_1 + x_1i + y_1j + z_1k, \\ q_2 &= w_2 + x_2i + y_2j + z_2k, \\ q_1 \cdot q_2 &= (w_1w_2 - x_1x_2 - y_1y_2 - z_1z_2) \\ &\quad + (w_1x_2 + x_1w_2 + y_1z_2 - z_1y_2)i \\ &\quad + (w_1y_2 - x_1z_2 + y_1w_2 + z_1x_2)j \\ &\quad + (w_1z_2 + x_1y_2 - y_1x_2 + z_1w_2)k. \end{aligned}$$

If we examine each term in this product, we can see that each term depends linearly on the coefficients for  $q_1$ . Also each term depends linearly on the coefficients for  $q_2$ .

So, we can write the product of two quaternions in terms of a matrix multiplication.

When the matrix  $L_{\text{row}}(q_1)$  multiplies a row vector  $q_2$ , the result is a row vector representation for  $q_1 \cdot q_2$ . When the matrix  $R_{\text{row}}(q_2)$  multiplies a row vector  $q_1$ , the result is also a row vector representation for  $q_1 \cdot q_2$ .

$$q_1 \cdot q_2 = q_2 L_{\text{row}}(q_1) = [x_2 \ y_2 \ z_2 \ w_2] \begin{bmatrix} w_1 & z_1 & -y_1 & -x_1 \\ -z_1 & w_1 & x_1 & -y_1 \\ y_1 & -x_1 & w_1 & -z_1 \\ x_1 & y_1 & z_1 & w_1 \end{bmatrix},$$

$$q_1 R_{\text{row}}(q_2) = [x_1 \ y_1 \ z_1 \ w_1] \begin{bmatrix} w_2 & -z_2 & y_2 & -x_2 \\ z_2 & w_2 & -x_2 & -y_2 \\ -y_2 & x_2 & w_2 & -z_2 \\ x_2 & y_2 & z_2 & w_2 \end{bmatrix}.$$

**Computing Rotation Matrices from Quaternions.** Now we have all the tools we need to use quaternions to generate a rotation matrix for the given rotation. We have a matrix form for left-multiplication by  $q$

$$P \cdot L_{\text{row}}(q) = [x_p \ y_p \ z_p \ 0] \begin{bmatrix} w_q & z_q & -y_q & -x_q \\ -z_q & w_q & x_q & -y_q \\ y_q & -x_q & w_q & -z_q \\ x_q & y_q & z_q & w_q \end{bmatrix},$$

and a matrix form for right-multiplication by  $q^{-1}$ .

$$q^{-1} = q' = [-x_q \ -y_q \ -z_q \ w_q],$$

$$P \cdot R_{\text{row}}(q^{-1}) = [x_p \ y_p \ z_p \ 0] \begin{bmatrix} w_q & z_q & -y_q & x_q \\ -z_q & w_q & x_q & y_q \\ y_q & -x_q & w_q & z_q \\ -x_q & -y_q & -z_q & w_q \end{bmatrix}.$$

The resulting rotation matrix is the product of these two matrices,

$$Q_{\text{row}} = R_{\text{row}}(q^{-1}) \cdot L_{\text{row}}(q)$$

$$= \begin{bmatrix} w_q & z_q & -y_q & x_q \\ -z_q & w_q & x_q & y_q \\ y_q & -x_q & w_q & z_q \\ -x_q & -y_q & -z_q & w_q \end{bmatrix} \cdot \begin{bmatrix} w_q & z_q & -y_q & -x_q \\ -z_q & w_q & x_q & -y_q \\ y_q & -x_q & w_q & -z_q \\ x_q & y_q & z_q & w_q \end{bmatrix}$$

$$= \begin{bmatrix} w^2 + x^2 - y^2 - z^2 & 2xy + 2wz & 2xz - 2wy & 0 \\ 2xy - 2wz & w^2 - x^2 + y^2 - z^2 & 2yz + 2wx & 0 \\ 2xz + 2wy & 2yz - 2wx & w^2 - x^2 - y^2 + z^2 & 0 \\ 0 & 0 & 0 & w^2 + x^2 + y^2 + z^2 \end{bmatrix}$$

Although matrices do not generally commute (in general  $AB \neq BA$ ), because these matrices represent left and right multiplication and quaternion multiplication is associative, these particular matrices do commute. So, we could write  $Q_{\text{row}} = L_{\text{row}}(q) \cdot R_{\text{row}}(q^{-1})$  instead of  $Q_{\text{row}} = R_{\text{row}}(q^{-1}) \cdot L_{\text{row}}(q)$  and we would get the same result. So using this matrix, we could compute  $P_{\text{rotated}}$  another way:

$$P_{\text{rotated}} = P Q_{\text{row}}.$$

#### A.4.2 Complex Functions

Now we return to complex variable theory. If to each of a set of complex numbers which a variable  $z$  may assume there corresponds one or more values of a variable  $w$ , then  $w$  is called a *function of the complex variable*  $z$ , written  $w = f(z)$ . A function is *single-valued* if for each value of  $z$  there corresponds only one value of  $w$ ; otherwise it is *multiple-valued* or *many-valued*. In general we can write  $w = f(z) = u(x, y) + iv(x, y)$ , where  $u$  and  $v$  are real functions of  $x$  and  $y$  (called the *real and imaginary parts* of  $w$ , respectively).

Definitions of limits and continuity for functions of a complex variable are analogous to those for a real variable. Thus,  $f(z)$  is said to have the *limit*  $l$  as  $z$  approaches  $z_0$  if, given any  $\epsilon > 0$ , there exists a  $\delta > 0$ , such that  $|f(z) - l| < \epsilon$  whenever  $0 < |z - z_0| < \delta$ . Similarly,  $f(z)$  is said to be *continuous* at  $z_0$  if, given any  $\epsilon > 0$ , there exists a  $\delta > 0$ , such that  $|f(z) - f(z_0)| < \epsilon$  whenever  $0 < |z - z_0| < \delta$ ; alternatively,  $f(z)$  is continuous at  $z_0$  if  $\lim_{z \rightarrow z_0} f(z) = f(z_0)$ .

If  $f(z)$  is single-valued in some region of the  $z$  plane, the *derivative* of  $f(z)$  is defined as

$$f'(z) = \lim_{\Delta z \rightarrow 0} \frac{f(z + \Delta z) - f(z)}{\Delta z}, \quad (\text{A.26})$$

provided the limit exists independent of the manner in which  $\Delta z \rightarrow 0$ . If the limit (A.26) exists for  $z = z_0$ , then  $f(z)$  is called *differentiable* at  $z_0$ . If the limit exists for all  $z$  such that  $|z - z_0| < \delta$  for some  $\delta > 0$ , then  $f(z)$

is called *holomorphic function*, or *analytic in a region*  $\mathcal{R}$  in the complex plane  $\mathbb{C} \approx \mathbb{R}^2$ . In order to be analytic,  $f(z)$  must be single-valued and continuous. The converse is not necessarily true.

A *necessary condition* that  $w = f(z) = u(x, y) + iv(x, y)$  be holomorphic (or, analytic) in a region  $\mathcal{R} \in \mathbb{C}$  is that  $u$  and  $v$  satisfy the *Cauchy-Riemann equations*

$$\frac{\partial u}{\partial x} = \frac{\partial v}{\partial y}, \quad \frac{\partial u}{\partial y} = -\frac{\partial v}{\partial x}. \quad (\text{A.27})$$

If the partial derivatives in (A.27) are continuous in  $\mathcal{R} \in \mathbb{C}$ , the equations are also *sufficient conditions* that  $f(z)$  be analytic in  $\mathcal{R} \in \mathbb{C}$ .

If the second derivatives of  $u$  and  $v$  with respect to  $x$  and  $y$  exist and are continuous, we find by differentiating (A.27) that the real and imaginary parts satisfy 2D Laplace equation

$$\frac{\partial^2 u}{\partial x^2} + \frac{\partial^2 u}{\partial y^2} = 0, \quad \frac{\partial^2 v}{\partial x^2} + \frac{\partial^2 v}{\partial y^2} = 0.$$

Functions satisfying Laplace equation\* are called *harmonic functions*.

A holomorphic function  $w = f(z)$  gives a *surjective mapping* (or, transform) of its *domain of definition* in the complex  $z$ -plane *onto* its *range of values* in the complex  $w$ -plane (both planes are in  $\mathbb{C}$ ). This mapping is *conformal*, i.e., the angle between two curves in the  $z$  plane intersecting at  $z = z_0$ , has the same magnitude and orientation as the angle between the images of the two curves, so long as  $f'(z_0) \neq 0$ . In other words, the mapping defined by analytic function  $f(z)$  is conformal, except at *critical points* at which the derivative  $f'(z) = 0$  (the *conformal property of analytic functions*).

If  $f(z)$  is defined, single-valued and continuous in a region  $\mathcal{R} \subset \mathbb{C}$ , we define the *integral* of  $f(z)$  along some path  $c \in \mathcal{R}$  from point  $z_1$  to point  $z_2$ , where  $z_1 = x_1 + iy_1$ ,  $z_2 = x_2 + iy_2$ , as

$$\begin{aligned} \int_c f(z) dz &= \int_{(x_1, y_1)}^{(x_2, y_2)} (u + iv)(dx + idy) \\ &= \int_{(x_1, y_1)}^{(x_2, y_2)} u dx - v dy + i \int_{(x_1, y_1)}^{(x_2, y_2)} v dx + u dy. \end{aligned} \quad (\text{A.28})$$

With this definition the integral of a function of a complex variable can be made to depend on line integrals of functions of real variables. It is equivalent to the definition based on the limit of a sum.



Let  $c$  be a simple closed curve in a region  $\mathcal{R} \subset \mathbb{C}$ . If  $f(z)$  is analytic in  $\mathcal{R}$  as well as on  $c$ , then we have the *Cauchy's theorem*

$$\oint_c f(z) dz = 0. \quad (\text{A.29})$$

Expressed in another way, (A.29) is equivalent to the statement that  $\int_{z_1}^{z_2} f(z) dz$  has a value *independent of the path* joining  $z_1$  and  $z_2$ . Such integrals can be evaluated as  $F(z_2) - F(z_1)$  where  $F'(z) = f(z)$ .

If  $f(z)$  is analytic within and on a simple closed curve  $c$  and  $a$  is any point interior to  $c$ , then

$$f(a) = \frac{1}{2\pi i} \oint_c \frac{f(z)}{z-a} dz, \quad (\text{A.30})$$

where  $c$  is traversed in the positive (counterclockwise) sense. Similarly, the  $n$ th derivative of  $f(z)$  at  $z = a$  is given by

$$f^{(n)}(a) = \frac{n!}{2\pi i} \oint_c \frac{f(z)}{(z-a)^{n+1}} dz. \quad (\text{A.31})$$

These are the *Cauchy's integral formulas*. They are quite remarkable because they show that if the function  $f(z)$  is known *on* the closed curve  $c$  then it is also known *within*  $c$ , and the various derivatives at points within  $c$  can be calculated. Thus if a function of a complex variable has a first derivative, it has all higher derivatives as well, which is not necessarily true for functions of real variables.

Let  $f(z)$  be analytic inside and on a circle having its center at  $z = a$ . Then for all points  $z$  in the circle we have the *Taylor series* representation of  $f(z)$  given by

$$f(z) = f(a) + f'(a)(z-a) + \frac{f''(a)}{2!}(z-a)^2 + \frac{f'''(a)}{3!}(z-a)^3 + \dots \quad (\text{A.32})$$

A singular point of a function  $f(z)$  is a value of  $z$  at which  $f(z)$  fails to be analytic. If  $f(z)$  is analytic everywhere in some region  $\mathcal{R} \subset \mathbb{C}$  except at an interior point  $z = a$ , we call  $z = a$  an *isolated singularity* of  $f(z)$ .

If  $f(z) = \frac{\phi(z)}{(z-a)^n}$ ,  $\phi(a) \neq 0$ , where  $\phi(z)$  is analytic everywhere in  $\mathcal{R}$ , with  $n \in \mathbb{N}$ , then  $f(z)$  has an isolated singularity at  $z = a$  which is called a *pole of order  $n$* . If  $n = 1$ , the pole is called a *simple pole*; if  $n = 2$  it is called a *double pole*, etc.

If  $f(z)$  has a pole of order  $n$  at  $z = a$  but is analytic at every other point inside and on a circle  $c \subset \mathbb{C}$  with a center at  $a$ , then  $(z-a)^n f(z)$  is

analytic at all points inside and on  $c$  and has a Taylor series about  $z = a$  so that

$$f(z) = \frac{a_{-n}}{(z-a)^n} + \frac{a_{-n+1}}{(z-a)^{n-1}} + \dots + \frac{a_{-1}}{z-a} + a_0 + a_1(z-a) + a_2(z-a)^2 + \dots \quad (\text{A.33})$$

This is called a *Laurent series* for  $f(z)$ . The part  $a_0 + a_1(z-a) + a_2(z-a)^2 + \dots$  is called the *analytic part*, while the remainder consisting of inverse powers of  $z-a$  is called the *principal part*. More generally, we refer to the series  $\sum_{k=-\infty}^{\infty} a_k(z-a)^k$  as a Laurent series where the terms with  $k < 0$  constitute the principal part. A function which is analytic in a region bounded by two concentric circles having center at  $z = a$  can always be expanded into such Laurent series.

The coefficients in (A.33) can be obtained in the customary manner by writing the coefficients for the Taylor series corresponding to  $(z-a)^n f(z)$ . Specially, the coefficient  $a_{-1}$ , called the *residue* of  $f(z)$  at the pole  $z = a$ , written  $\text{Res}_{z=a} f(z)$ , is very important. It can be found from the formula

$$\text{Res}_{z=a} f(z) = \frac{1}{(n-1)!} \lim_{z \rightarrow a} \frac{d^{n-1}}{dz^{n-1}} [(z-a)^n f(z)],$$

where  $n$  is the order of the pole. For simple poles the calculation of the residue is simple

$$\text{Res}_{z=a} f(z) = \lim_{z \rightarrow a} (z-a) f(z).$$

*Cauchy's residue theorem:* If  $f(z)$  is analytic within and on the boundary  $c$  of a region  $\mathcal{R} \subset \mathbb{C}$  except at a finite number of poles  $a, b, c, \dots \in \mathcal{R}$ , having residues  $a_{-1}, b_{-1}, c_{-1}, \dots$  respectively, then

$$\begin{aligned} \oint_c f(z) dz &= 2\pi i (a_{-1} + b_{-1} + c_{-1} + \dots) \\ &= 2\pi i \sum_{i=1}^k \text{Res}_{z=z_i} f(z), \end{aligned} \quad (\text{A.34})$$

i.e., the integral of  $f(z)$  equals  $2\pi i$  times the sum of residues of  $f(z)$  at the poles enclosed by  $c$ . Cauchy's theorem and integral formulas are special cases of this result. It is used for evaluation of various definite integrals of both real and complex functions.

For example, (A.34) is used in *inverse Laplace transform*.

If  $F(s) = L\{f(t)\} = \int_0^\infty e^{-st} f(t) dt$ , then  $L^{-1}\{F(s)\}$  is given by

$$\begin{aligned} f(t) &= L^{-1}\{F(s)\} = \frac{1}{2\pi i} \oint_c e^{st} F(s) ds \\ &= \sum \text{Res} [e^{st} F(s)] \text{ at poles of } F(s) \end{aligned}$$

where  $c \subset \mathbb{C}$  is the so-called *Bromwich contour*.

### A.4.3 Complex Manifolds

Recall from chapter 3 that a *topological manifold* consists of the minimal mathematical structure on a set of points  $M$  so that we can define a notion of *continuity*. Additionally, with respect to this notion of continuity,  $M$  is required to locally look like a piece of  $\mathbb{R}^n$  for some fixed value of  $n$ . The next refinement is to pass from topological manifolds to *differentiable* or *smooth* manifolds. Whereas a topological manifold is the structure necessary to define a notion of continuity, a smooth manifold has just enough additional structure to define a notion of *differentiation*.

The second refinement is the notion of a *complex manifold*. Just as a differentiable manifold has enough structure to define the notion of differentiable functions, a complex manifold is one with enough structure to define the notion of holomorphic (or, analytic) functions  $f : X \rightarrow \mathbb{C}$ . Namely, if we demand that the transition functions  $\phi_j \circ \phi_i^{-1}$  in the charts  $U_i$  on  $M$  (see Figure A.4) satisfy the Cauchy–Riemann equations (A.27), then the analytic properties of  $f$  can be studied using its coordinate representative  $f \circ \phi_i^{-1}$  with assurance that the conclusions drawn are patch independent. Introducing local complex coordinates in the charts  $U_i$  on  $M$ , the  $\phi_i$  can be expressed as maps from  $U_i$  to an open set in  $\mathbb{C}^{\frac{n}{2}}$ , with  $\phi_j \circ \phi_i^{-1}$  being a holomorphic map from  $\mathbb{C}^{\frac{n}{2}}$  to  $\mathbb{C}^{\frac{n}{2}}$ . Clearly,  $n$  must be even for this to make sense. In local complex coordinates, we recall that a function  $h : \mathbb{C}^{\frac{n}{2}} \rightarrow \mathbb{C}^{\frac{n}{2}}$  is holomorphic if  $h(z_1, \bar{z}_1, \dots, z_{\frac{n}{2}}, \bar{z}_{\frac{n}{2}})$  is actually independent of all the  $\bar{z}_j$  [Greene (1996)].

In Figure A.4, we schematically illustrate the form of a complex manifold  $M$ . In a given patch on any even dimensional manifold, we can always introduce local complex coordinates by, for instance, forming the combinations  $z_j = x_j + ix_{\frac{n}{2}+j}$ , where the  $x_j$  are local real coordinates on  $M$ . The real test is whether the transition functions from one patch to another — when expressed in terms of the local complex coordinates — are holomorphic maps. If they are, we say that  $M$  is a complex manifold of complex

dimension  $d = n/2$ . The local complex coordinates with holomorphic transition functions provide  $M$  with a *complex structure*.

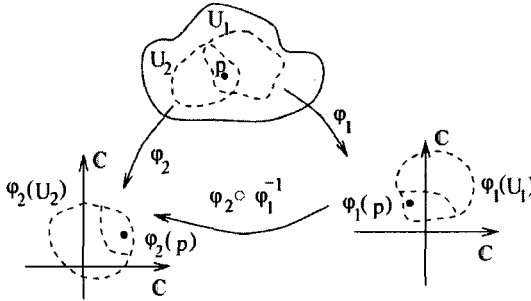


Fig. A.4 The charts for a complex manifold  $M$  have the complex coordinates.

As an example, consider a real two-torus  $T^2$  defined by  $\mathbb{R}^2/\Lambda$ , where  $\Lambda$  is a lattice  $\Lambda = \{\omega_1 m + \omega_2 n | m, n \in \mathbb{Z}\}$ . Since  $\mathbb{R}^2$  is  $\mathbb{C}$ , we can equally well think of  $T^2$  as  $\mathbb{C}/\Lambda$ . In this way we directly see that the two-torus is a complex manifold. It inherits complex coordinates from the ambient space  $\mathbb{C}$  in which it is embedded. The only distinction is that points labelled by  $z$  are identified with those labelled by  $z + \lambda$ , where  $\lambda$  is any element of  $\Lambda$ .

Given a differentiable manifold with real dimension  $n$  being even, it can be a difficult question to determine whether or not a complex structure exists. On the other hand, if some differentiable manifold  $M$  does admit a complex structure, we are not able to decide whether it is unique, i.e., there may be numerous inequivalent ways of defining complex coordinates on  $M$  [Greene (1996)].

Now, in the same way as a *homeomorphism* defines an equivalence between topological manifolds, and a *diffeomorphism* defines an equivalence between smooth manifolds, a *biholomorphism* defines an equivalence between complex manifolds. If  $M$  and  $N$  are complex manifolds, we consider them to be equivalent if there is a map  $\phi : M \rightarrow N$  which in addition to being a diffeomorphism, is also a holomorphic map. That is, when expressed in terms of the complex structures on  $M$  and  $N$  respectively,  $\phi$  is holomorphic. It is not hard to show that this necessarily implies that  $\phi^{-1}$  is holomorphic as well and hence  $\phi$  is known as a biholomorphism. Such a map allows us to identify the complex structures on  $M$  and  $N$  and hence they are isomorphic as complex manifolds.

These definitions are important because there are pairs of smooth man-

ifolds  $M$  and  $N$  which are homeomorphic but not diffeomorphic, as well as, there are complex manifolds  $M$  and  $N$  which are diffeomorphic but not biholomorphic. This means that if one simply ignored the fact that  $M$  and  $N$  admit local complex coordinates (with holomorphic transition functions), and one only worked in real coordinates, there would be no distinction between  $M$  and  $N$ . The difference between them only arises from the way in which complex coordinates have been laid down upon them.

As an example, consider the torus  $T^2$  which is a 2D real manifold and at the same time a 1D complex manifold. Consider two choices for the defining lattice  $\Lambda$ :  $(\omega_1, \omega_2) = ((1, 0), (0, 1))$  and  $(\omega'_1, \omega'_2) = ((1, 0), (0, 2))$ . As smooth manifolds, these two tori are equivalent since the map  $\phi$  provides an explicit diffeomorphism:

$$\phi : X \rightarrow Y, \quad (y_1, y_2) = \phi(x_1, x_2) = (x_1, 2x_2),$$

where  $(x_1, x_2)$  and  $(y_1, y_2)$  are local coordinates on  $M$  and  $N$ . The map  $\phi$  clearly meets all of the conditions of a diffeomorphism. However, using local complex coordinates  $w = x_1 + ix_2$  and  $z = y_1 + iy_2$ , we see that

$$(z, \bar{z}) = \phi(w, \bar{w}) = \frac{3}{2}w - \frac{1}{2}\bar{w}$$

and the latter is *not* a holomorphic function of  $w$ . Thus,  $M$  and  $N$  are diffeomorphic but not biholomorphic. They are equivalent as differentiable manifolds but not as complex manifolds. In fact, a simple extension of this reasoning shows that for more general choices of  $\Lambda$  and  $\Lambda'$ , the tori have the same complex structure if (but not only if) the ratio  $\frac{\omega_2}{\omega_1}$  equals  $\frac{\omega'_2}{\omega'_1}$ . This ratio is usually called  $\tau$  [Greene (1996)].

Again, recall from chapter 3 that a *tangent space* to a manifold  $M$  at a point  $p$  is the closest flat approximation to  $M$  at that point. A convenient basis for the tangent space of  $M$  at  $p$  consists of the  $n$  linearly independent partial derivative operators:

$$T_p M : \{\partial_{x^1}|_p, \dots, \partial_{x^n}|_p\}. \quad (\text{A.35})$$

A vector  $v \in T_p M$  can then be expressed as  $v = v^\alpha \partial_{x^\alpha}|_p$ .

Also, every vector space  $V$  has a dual space  $V^*$  consisting of real valued linear maps on  $V$ . Such is the case as well for  $V = T_p M$  with the dual space being denoted  $T_p^* M$ . A convenient basis for the latter is the basis of one-forms, which is dual to (A.35) and usually denoted by

$$T_p^* M : \{dx^1|_p, \dots, dx^n|_p\}, \quad (\text{A.36})$$

where, by definition,  $dx^i : T_p M \rightarrow \mathbb{R}$  is a linear map with  $dx_p^i(\partial_{x^j}|_p) = \delta_j^i$ .

Now, if  $M$  is a complex manifold of complex dimension  $d = n/2$ , there is a notion of the *complexified tangent space* of  $M$ , denoted by  $T_p M^{\mathbb{C}}$ , which is the same as the real tangent space  $T_p M$  except that we allow complex coefficients to be used in the vector space manipulations. This is often denoted by writing  $T_p M^{\mathbb{C}} = T_p M \otimes \mathbb{C}$ . We can still take our basis to be as in (A.35) with an arbitrary vector  $v \in T_p M^{\mathbb{C}}$  being expressed as  $v = v^\alpha \frac{\partial}{\partial x^\alpha}|_p$ , where the  $v^\alpha$  can now be complex numbers. In fact, it is convenient to rearrange the basis vectors in (A.35) to more directly reflect the underlying complex structure. Specifically, we take the following linear combinations of basis vectors in (A.35) to be our new basis vectors:

$$\begin{aligned} T_p M^{\mathbb{C}} : \quad & \{(\partial_{x^1} + i\partial_{x^{d+1}})|_p, \dots, \\ & (\partial_{x^d} + i\partial_{x^{2d}})|_p, (\partial_{x^1} - i\partial_{x^{d+1}})|_p, \dots, (\partial_{x^d} - i\partial_{x^{2d}})|_p\}. \end{aligned} \quad (\text{A.37})$$

In terms of complex coordinates we can write the basis (A.37) as

$$T_p M^{\mathbb{C}} : \{\partial_{z^1}|_p, \dots, \partial_{z^d}|_p, \partial_{\bar{z}^1}|_p, \dots, \partial_{\bar{z}^d}|_p\}.$$

From the point of view of real vector spaces,  $\partial_{x^j}|_p$  and  $i\partial_{x^j}|_p$  would be considered linearly independent and hence  $T_p M^{\mathbb{C}}$  has real dimension  $4d$ .

In exact analogy with the real case, we can define the dual to  $T_p M^{\mathbb{C}}$ , which we denote by  $T_p^* M^{\mathbb{C}} = T_p^* M \otimes \mathbb{C}$ , with the one-forms basis

$$T_p^* M^{\mathbb{C}} : \{dz^1|_p, \dots, dz^d|_p, d\bar{z}^1|_p, \dots, d\bar{z}^d|_p\}.$$

For certain types of complex manifolds  $M$ , it is worthwhile to refine the definition of the complexified tangent and cotangent spaces, which pulls apart the holomorphic and anti-holomorphic directions in each of these two vector spaces. That is, we can write

$$T_p M^{\mathbb{C}} = T_p M^{(1,0)} \oplus T_p M^{(0,1)},$$

where  $T_p M^{(1,0)}$  is the vector space spanned by  $\{\partial_{z^1}|_p, \dots, \partial_{z^d}|_p\}$  and  $T_p M^{(0,1)}$  is the vector space spanned by  $\{\partial_{\bar{z}^1}|_p, \dots, \partial_{\bar{z}^d}|_p\}$ . Similarly, we can write

$$T_p^* M^{\mathbb{C}} = T_p^* M^{(1,0)} \oplus T_p^* M^{(0,1)},$$

where  $T_p^* M^{(1,0)}$  is the vector space spanned by  $\{dz^1|_p, \dots, dz^d|_p\}$  and  $T_p^* M^{(0,1)}$  is the vector space spanned by  $\{d\bar{z}^1|_p, \dots, d\bar{z}^d|_p\}$ . We call  $T_p M^{(1,0)}$  the *holomorphic tangent space*; it has complex dimension  $d$  and we call  $T_p^* M^{(1,0)}$  the *holomorphic cotangent space*. It also has complex dimension

d. Their complements are known as the *anti-holomorphic* tangent and cotangent spaces respectively [Greene (1996)].

Now, recall from subsection 3.7.2 above, a definition of the *Kähler manifold*. Let  $M$  be a smooth manifold and  $g$  a Riemannian metric on  $M$ . Let  $J$  be a complex structure on  $M$ , that is,  $J : TM \rightarrow TM$ ,  $J^2 = -\text{Id}$  and  $J$  is  $g$ -orthogonal.  $M$  is called a *Kähler manifold* if  $\nabla J = 0$ , where  $\nabla$  is the Levi-Civita connection of  $g$  and  $J$  is regarded as a  $(1,1)$  tensor.

Finally, a special class of Kähler manifolds is the core of modern *string theory*. Namely, a *Calabi-Yau manifold* is a Kähler manifold of complex dimension  $n$  with a covariant constant holomorphic  $n$ -form. Equivalently it is a Riemannian manifold with *holonomy* contained in  $SU(n)$ .

#### A.4.4 Hilbert Space

A *norm* on a complex vector space  $\mathcal{H}$  is a mapping from  $\mathcal{H}$  into the complex numbers,  $\|\cdot\| : \mathcal{H} \rightarrow \mathbb{C}$ ;  $h \mapsto \|h\|$ , such that the following set of norm-axioms hold:

(N1)  $\|h\| \geq 0$  for all  $h \in \mathcal{H}$  and  $\|h\| = 0$  implies  $h = 0$  (positive definiteness);

(N2)  $\|\lambda h\| = |\lambda| \|h\|$  for all  $h \in \mathcal{H}$  and  $\lambda \in \mathbb{C}$  (homogeneity); and

(N3)  $\|h_1 + h_2\| \leq \|h_1\| + \|h_2\|$  for all  $h_1, h_2 \in \mathcal{H}$  (triangle inequality).

The pair  $(\mathcal{H}, \|\cdot\|)$  is called a *normed space*.

A *Hermitian inner product* on a complex vector space  $\mathcal{H}$  is a mapping  $\langle \cdot, \cdot \rangle : \mathcal{H} \times \mathcal{H} \rightarrow \mathbb{C}$  such that the following set of inner-product-axioms hold:

(IP1)  $\langle h h_1 + h_2 \rangle = \langle h h_1 + h h_2 \rangle$ ;

(IP2)  $\langle \alpha h, h_1 \rangle = \alpha \langle h, h_1 \rangle$ ;

(IP3)  $\langle h_1, h_2 \rangle = \overline{\langle h_1, h_2 \rangle}$  (so  $\langle h, h \rangle$  is real);

(IP4)  $\langle h, h \rangle \geq 0$  and  $\langle h, h \rangle = 0$  provided  $h = 0$ .

These properties are to hold for all  $h, h_1, h_2 \in \mathcal{H}$  and  $\alpha \in \mathbb{C}$ ;  $\bar{z}$  denotes the complex conjugate of the complex number  $z$ . (IP2) and (IP3) imply that  $\langle \alpha h, h_1 \rangle = \bar{\alpha} \langle h_1, h_2 \rangle$ . As is customary, for a complex number  $z$  we shall denote by  $\text{Re} z = \frac{z+\bar{z}}{2}$ ,  $\text{Im} z = \frac{z-\bar{z}}{2}$ ,  $|z| = (z\bar{z})^{1/2}$  its real and imaginary parts and its absolute value.

The *standard inner product* on the product space  $\mathbb{C}^n = \mathbb{C} \times \cdots \times \mathbb{C}$  is defined by  $\langle z, w \rangle = \sum_{i=1}^n z_i \bar{w}_i$ , and axioms (IP1)–(IP4) are readily checked. Also  $\mathbb{C}^n$  is a normed space with  $\|z\|^2 = \sum_{i=1}^n |z_i|^2$ .

The pair  $(\mathcal{H}, \langle \cdot, \cdot \rangle)$  is called an *inner product space*.

In an inner product space  $\mathcal{H}$ , two vectors  $h_1, h_2 \in \mathcal{H}$  are called *orthogonal*, and we write  $h_1 \perp h_2$ , provided  $\langle h_1, h_2 \rangle = 0$ . For a subset

In an inner product space  $\mathcal{H}$ , two vectors  $h_1, h_2 \in \mathcal{H}$  are called orthogonal, and we write  $h_1 \perp h_2$ , provided  $\langle h_1, h_2 \rangle = 0$ . For a subset  $A \subset \mathcal{H}$ , the set  $A^\perp$  defined by  $A^\perp = \{h \in \mathcal{H} \mid \langle h, x \rangle = 0 \text{ for all } x \in A\}$  is called the orthogonal complement of  $A$ .

In an inner product space  $\mathcal{H}$  the *Cauchy-Schwartz inequality* holds:  $|\langle h_1, h_2 \rangle| \leq \langle h_1, h_1 \rangle^{1/2} \langle h_2, h_2 \rangle^{1/2}$ . Here, equality holds provided  $h_1, h_2$  are linearly dependent.

Let  $(\mathcal{H}, \|\cdot\|)$  be an inner product space and set  $\|h\| = \langle h, h \rangle^{1/2}$ . Then  $(\mathcal{H}, \|\cdot\|)$  is a normed space.

Let  $(\mathcal{H}, \langle \cdot, \cdot \rangle)$  be an inner product space and  $\|\cdot\|$  the corresponding norm. Then we have

(1) *Polarization law*:

$$4 \langle h_1, h_2 \rangle = \|h_1 + h_2\|^2 - \|h_1 - h_2\|^2 + i \|h_1 + i h_2\|^2 - i \|h_1 - i h_2\|^2,$$

and

(2) *Parallelogram law*:

$$2 \|h_1\|^2 + 2 \|h_2\|^2 = \|h_1 + h_2\|^2 + \|h_1 - h_2\|^2.$$

Let  $(\mathcal{H}, \|\cdot\|)$  be a normed space and define  $d(h_1, h_2) = \|h_1 - h_2\|$ . Then  $(\mathcal{H}, d)$  is a metric space.

Let  $(\mathcal{H}, \|\cdot\|)$  be a normed space. If the corresponding metric  $d$  is complete, we say  $(\mathcal{H}, \|\cdot\|)$  is a Banach space. If  $(\mathcal{H}, \|\cdot\|)$  is an inner product space whose corresponding metric is complete, we say  $(\mathcal{H}, \|\cdot\|)$  is a *Hilbert space* (see, e.g., [Abraham *et al.* (1988)]).

If  $\mathcal{H}$  is a Hilbert space and  $F$  its closed subspace, then  $\mathcal{H}$  splits into two mutually orthogonal subspaces,  $\mathcal{H} = F \oplus F^\perp$ , where  $\oplus$  denotes the *orthogonal sum*. Thus every closed subspace of a Hilbert space splits.

Let  $\mathcal{H}$  be a Hilbert space. A set  $\{h_i\}_{i \in I}$  is called orthonormal if  $\langle h_i, h_j \rangle = \delta_{ij}$ , the Kronecker delta. An orthonormal set  $\{h_i\}_{i \in I}$  is a *Hilbert basis* if  $\text{closure}(\text{span}\{h_i\}_{i \in I}) = \mathcal{H}$ . Any Hilbert space has a Hilbert basis.

In the finite dimensional case equivalence and completeness are automatic. Let  $\mathcal{H}$  be a finite-dimensional vector space. Then (i) there is a norm on  $\mathcal{H}$ ; (ii) all norms on  $\mathcal{H}$  are equivalent; (iii) all norms on  $\mathcal{H}$  are complete.

Consider the space  $L^2([a, b], \mathbb{C})$  of *square-Lebesgue-integrable* complex-valued functions defined on an interval  $[a, b] \subset \mathbb{C}$ , that is, functions  $f$  that satisfy  $\int_a^b |f(x)|^2 dx < \infty$ . It is a Banach space with the norm defined by  $\|f\| = \left( \int_a^b |f(x)|^2 dx \right)^{1/2}$ , and a Hilbert space with the inner product defined by  $\langle f, g \rangle = \int_a^b f(x) \overline{g(x)} dx$ .



Recall from elementary linear algebra that the dual space of a finite dimensional vector space of dimension  $n$  also has dimension  $n$  and so the space and its dual are isomorphic. It is also true for Hilbert space.

**Riesz Representation Theorem.** Let  $\mathcal{H}$  be a real (resp., complex) Hilbert space. The map  $h \mapsto \langle \cdot, h \rangle$  is a linear (resp., antilinear) norm-preserving isomorphism of  $\mathcal{H}$  with  $\mathcal{H}^*$ ; for short,  $\mathcal{H} \cong \mathcal{H}^*$ . (A map  $A : \mathcal{H} \rightarrow F$  between complex vector spaces is called *antilinear* if we have the identities  $A(h + h') = Ae + Ae'$ , and  $A(\alpha h) = \bar{\alpha} Ae$ .)

Let  $\mathcal{H}$  and  $F$  be Banach spaces. We say  $\mathcal{H}$  and  $F$  are in *strong duality* if there is a non-degenerate continuous bilinear functional  $\langle \cdot, \cdot \rangle : \mathcal{H} \times F \rightarrow \mathbb{R}$ , also called a *pairing* of  $\mathcal{H}$  with  $F$ . Now, let  $\mathcal{H} = F$  and  $\langle \cdot, \cdot \rangle : \mathcal{H} \times \mathcal{H} \rightarrow \mathbb{R}$  be an inner product on  $\mathcal{H}$ . If  $\mathcal{H}$  is a Hilbert space, then  $\langle \cdot, \cdot \rangle$  is a *strongly non-degenerate pairing* by the Riesz representation theorem.

## A.5 Classical Lie Theory

In this section we present the basics of *classical theory of Lie groups* and their Lie algebras, as developed mainly by Sophus Lie, Elie Cartan, Felix Klein, Wilhelm Killing and Hermann Weyl. For more comprehensive treatment see e.g., [Chevalley (1955); Helgason (2001)].

### A.5.1 Basic Tables of Lie Groups and Their Lie Algebras

One classifies Lie groups regarding their algebraic properties (simple, semisimple, solvable, nilpotent, Abelian), their connectedness (connected or simply connected) and their compactness (see Tables A.1–A.3). This is the content of the *Hilbert 5th problem* (see, e.g., [Weisstein (2004); Wikipedia (2005)]).

## Some real Lie groups and their Lie algebras:

Lie group	Description	Remarks	Lie algb.	Description	dim / $\mathbb{R}$
$\mathbb{R}^n$	Euclidean space with addition	Abelian, simply connected, not compact	$\mathbb{R}^n$	the Lie bracket is zero	$n$
$\mathbb{R}^\times$	nonzero real numbers with multiplication	Abelian, not connected, not compact	$\mathbb{R}$	the Lie bracket is zero	1
$\mathbb{R}^{>0}$	positive real numbers with multiplication	Abelian, simply connected, not compact	$\mathbb{R}$	the Lie bracket is zero	1
$S^1 = \mathbb{R}/\mathbb{Z}$	complex numbers of absolute value 1, with multiplication	Abelian, connected, not simply connected, compact	$\mathbb{R}$	the Lie bracket is zero	1
$\mathbb{H}^\times$	non-zero quaternions with multiplication	simply connected, not compact	$\mathbb{H}$	quaternions, with Lie bracket the commutator	4
$S^3$	quaternions of absolute value 1, with multiplication; a 3-sphere	simply connected, compact, simple and semi-simple, isomorphic to $SU(2)$ , $SO(3)$ and to $Spin(3)$	$\mathbb{R}^3$	real 3-vectors, with Lie bracket the cross product; isomorphic to $\mathfrak{su}(2)$ and to $\mathfrak{so}(3)$	3
$GL(n, \mathbb{R})$	general linear group: invertible $n$ -by- $n$ real matrices	not connected, not compact	$M(n, \mathbb{R})$	$n$ -by- $n$ matrices, with Lie bracket the commutator	$n^2$
$GL^+(n, \mathbb{R})$	$n$ -by- $n$ real matrices with positive determinant	simply connected, not compact	$M(n, \mathbb{R})$	$n$ -by- $n$ matrices, with Lie bracket the commutator	$n^2$

## Classical real Lie groups and their Lie algebras:

Lie group	Description	Remarks	Lie algb.	Description	dim / $\mathbb{R}$
$SL(n, \mathbb{R})$	special linear group: real matrices with determinant 1	simply connected, not compact if $n > 1$	$\mathfrak{sl}(n, \mathbb{R})$	square matrices with trace 0, with Lie bracket the commutator	$n^2 - 1$
$O(n, \mathbb{R})$	orthogonal group: real orthogonal matrices	not connected, compact	$\mathfrak{so}(n, \mathbb{R})$	skew-symmetric square real matrices, with Lie bracket the commutator; $\mathfrak{so}(3, \mathbb{R})$ is isomorphic to $\mathfrak{su}(2)$ and to $\mathbb{R}^3$ with the cross product	$n(n-1)/2$
$SO(n, \mathbb{R})$	special orthogonal group: real orthogonal matrices with determinant 1	connected, compact, for $n \geq 2$ : not simply connected, for $n = 3$ and $n \geq 5$ : simple and semisimple	$\mathfrak{so}(n, \mathbb{R})$	skew-symmetric square real matrices, with Lie bracket the commutator	$n(n-1)/2$
$Spin(n)$	spinor group	simply connected, compact, for $n = 3$ and $n \geq 5$ : simple and semisimple	$\mathfrak{so}(n, \mathbb{R})$	skew-symmetric square real matrices, with Lie bracket the commutator	$n(n-1)/2$
$U(n)$	unitary group: complex unitary $n$ -by- $n$ matrices	isomorphic to $S^1$ for $n = 1$ , not simply connected, compact	$\mathfrak{u}(n)$	square complex matrices $A$ satisfying $A = -A^*$ , with Lie bracket the commutator	$n^2$
$SU(n)$	special unitary group: complex unitary $n$ -by- $n$ matrices with determinant 1	simply connected, compact, for $n \geq 2$ : simple and semisimple	$\mathfrak{su}(n)$	square complex matrices $A$ with trace 0 satisfying $A = -A^*$ , with Lie bracket the commutator	$n^2 - 1$

Basic complex Lie groups and their Lie algebras:<sup>24</sup>

Lie group	Description	Remarks	Lie algb.	Description	dim / $\mathbb{C}$
$\mathbb{C}^n$	group operation is addition	Abelian, simply connected, not compact	$\mathbb{C}^n$	the Lie bracket is zero	$n$
$\mathbb{C}^\times$	nonzero complex numbers with multiplication	Abelian, not simply connected, not compact	$\mathbb{C}$	the Lie bracket is zero	1
$GL(n, \mathbb{C})$	general linear group: invertible $n$ -by- $n$ complex matrices	simply connected, not compact, for $n = 1$ : isomorphic to $\mathbb{C}^\times$	$M(n, \mathbb{C})$	$n$ -by- $n$ matrices, with Lie bracket the commutator	$n^2$
$SL(n, \mathbb{C})$	special linear group: complex matrices with determinant 1	simple, semisimple, simply connected, for $n \geq 2$ : not compact	$\mathfrak{sl}(n, \mathbb{C})$	square matrices with trace 0, with Lie bracket the commutator	$n^2 - 1$
$O(n, \mathbb{C})$	orthogonal group: complex orthogonal matrices	not connected, for $n \geq 2$ : not compact	$\mathfrak{so}(n, \mathbb{C})$	skew-symmetric square complex matrices, with Lie bracket the commutator	$n(n-1)/2$
$SO(n, \mathbb{C})$	special orthogonal group: complex orthogonal matrices with determinant 1	for $n \geq 2$ : not compact, not simply connected, for $n = 3$ and $n \geq 5$ : simple and semisimple	$\mathfrak{so}(n, \mathbb{C})$	skew-symmetric square complex matrices, with Lie bracket the commutator	$n(n-1)/2$

## A.5.2 Representations of Lie groups

The idea of a *representation of a Lie group* plays an important role in the study of continuous symmetry (see, e.g., [Helgason (2001)]). A great deal is known about such representations, a basic tool in their study being the use of the corresponding 'infinitesimal' representations of Lie algebras.

Formally, a representation of a Lie group  $G$  on a vector space  $V$  (over a field  $K$ ) is a group homomorphism  $G \rightarrow \text{Aut}(V)$  from  $G$  to the automorphism group of  $V$ . If a basis for the vector space  $V$  is chosen, the representation can be expressed as a homomorphism into  $GL(n, K)$ . This is known as a *matrix representation*.

<sup>24</sup>The dimensions given are dimensions over  $\mathbb{C}$ . Note that every complex Lie group/algebra can also be viewed as a real Lie group/algebra of twice the dimension.

On the Lie algebra level, there is a corresponding linear map from the Lie algebra of  $G$  to  $\text{End}(V)$  preserving the Lie bracket  $[\cdot, \cdot]$ .

If the homomorphism is in fact an monomorphism, the representation is said to be *faithful*.

A unitary representation is defined in the same way, except that  $G$  maps to unitary matrices; the Lie algebra will then map to skew-Hermitian matrices.

Now, if  $G$  is a semisimple group, its finite-dimensional representations can be decomposed as direct sums of irreducible representations. The irreducibles are indexed by highest weight; the allowable (*dominant*) highest weights satisfy a suitable positivity condition. In particular, there exists a set of *fundamental weights*, indexed by the vertices of the *Dynkin diagram* of  $G$  (see below), such that dominant weights are simply non-negative integer linear combinations of the fundamental weights.

If  $G$  is a commutative compact Lie group, then its irreducible representations are simply the continuous characters of  $G$ . A *quotient representation* is a quotient module of the group ring.

### A.5.3 Root Systems and Dynkin Diagrams

A *root system* is a special configuration in Euclidean space that has turned out to be fundamental in Lie theory as well as in its applications. Also, the classification scheme for root systems, by *Dynkin diagrams*, occurs in parts of mathematics with no overt connection to Lie groups (such as singularity theory, see e.g., [Helgason (2001); Weisstein (2004); Wikipedia (2005)]).

#### A.5.3.1 Definitions

Formally, a *root system* is a finite set  $\Phi$  of non-zero vectors (*roots*) spanning a finite-dimensional Euclidean space  $V$  and satisfying the following properties:

- (1) The only scalar multiples of a root  $\alpha$  in  $V$  which belong to  $\Phi$  are  $\alpha$  itself and  $-\alpha$ .
- (2) For every root  $\alpha$  in  $V$ , the set  $\Phi$  is symmetric under reflection through the hyperplane of vectors perpendicular to  $\alpha$ .
- (3) If  $\alpha$  and  $\beta$  are vectors in  $\Phi$ , the projection of  $2\beta$  onto the line through  $\alpha$  is an integer multiple of  $\alpha$ .

The *rank* of a root system  $\Phi$  is the dimension of  $V$ . Two root systems may be combined by regarding the Euclidean spaces they span as mutually orthogonal subspaces of a common Euclidean space. A root system which does not arise from such a combination, such as the systems  $A_2$ ,  $B_2$ , and  $G_2$  in Figure A.5, is said to be *irreducible*.

Two irreducible root systems  $(V_1, \Phi_1)$  and  $(V_2, \Phi_2)$  are considered to be the same if there is an invertible linear transformation  $V_1 \rightarrow V_2$  which preserves distance up to a scale factor and which sends  $\Phi_1$  to  $\Phi_2$ .

The group of isometries of  $V$  generated by reflections through hyperplanes associated to the roots of  $\Phi$  is called the Weyl group of  $\Phi$  as it acts faithfully on the finite set  $\Phi$ , the Weyl group is always finite.

### A.5.3.2 Classification

It is not too difficult to classify the root systems of rank 2 (see Figure A.5).

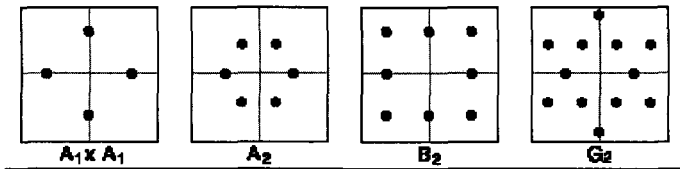


Fig. A.5 Classification of root systems of rank 2.

Whenever  $\Phi$  is a root system in  $V$  and  $W$  is a subspace of  $V$  spanned by  $\Psi = \Phi \cap W$ , then  $\Psi$  is a root system in  $W$ . Thus, our exhaustive list of root systems of rank 2 shows the geometric possibilities for any two roots in a root system. In particular, two such roots meet at an angle of 0, 30, 45, 60, 90, 120, 135, 150, or 180 degrees.

In general, irreducible root systems are specified by a family (indicated by a letter  $A$  to  $G$ ) and the rank (indicated by a subscript  $n$ ). There are four *infinite families*:

- $A_n$  ( $n \geq 1$ ), which corresponds to the special unitary group,  $SU(n+1)$ ;
- $B_n$  ( $n \geq 2$ ), which corresponds to the special orthogonal group,  $SO(2n+1)$ ;
- $C_n$  ( $n \geq 3$ ), which corresponds to the symplectic group,  $Sp(2n)$ ;
- $D_n$  ( $n \geq 4$ ), which corresponds to the special orthogonal group,  $SO(2n)$ ,

as well as five *exceptional cases*:  $E_6, E_7, E_8, F_4, G_2$ .

### A.5.3.3 Dynkin Diagrams

A Dynkin diagram is a graph with a few different kinds of possible edges (see Figure A.6). The connected components of the graph correspond to the irreducible subalgebras of  $\mathfrak{g}$ . So a simple Lie algebra's Dynkin diagram has only one component. The rules are restrictive. In fact, there are only certain possibilities for each component, corresponding to the classification of semi-simple Lie algebras (see, e.g., [Conway *et al.* (1985)]).

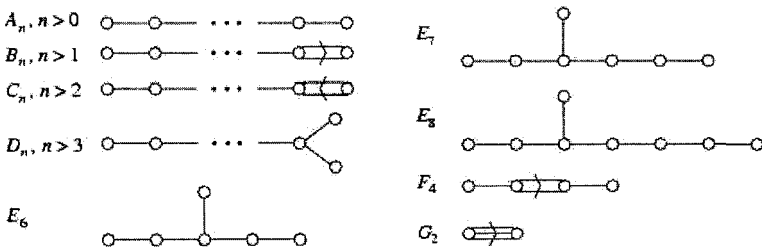


Fig. A.6 The problem of classifying irreducible root systems reduces to the problem of classifying connected Dynkin diagrams.

The *roots* of a complex Lie algebra form a lattice of rank  $k$  in a *Cartan subalgebra*  $\mathfrak{h} \subset \mathfrak{g}$ , where  $k$  is the Lie algebra rank of  $\mathfrak{g}$ . Hence, the *root lattice* can be considered a lattice in  $\mathbb{R}^k$ . A vertex, or node, in the Dynkin diagram is drawn for each *Lie algebra simple root*, which corresponds to a generator of the root lattice. Between two nodes  $\alpha$  and  $\beta$ , an edge is drawn if the simple roots are not perpendicular. One line is drawn if the angle between them is  $2\pi/3$ , two lines if the angle is  $3\pi/4$ , and three lines are drawn if the angle is  $5\pi/6$ . There are no other possible angles between Lie algebra simple roots. Alternatively, the number of lines  $N$  between the simple roots  $\alpha$  and  $\beta$  is given by

$$N = A_{\alpha\beta}A_{\beta\alpha} = \frac{2\langle\alpha,\beta\rangle}{|\alpha|^2} \frac{2\langle\beta,\alpha\rangle}{|\beta|^2} = 4\cos^2\theta,$$

where  $A_{\alpha\beta} = \frac{2\langle\alpha,\beta\rangle}{|\alpha|^2}$  is an entry in the *Cartan matrix* ( $A_{\alpha\beta}$ ) (for details on Cartan matrix see, e.g., [Helgason (2001); Weisstein (2004)]). In a Dynkin diagram, an arrow is drawn from the longer root to the shorter root (when the angle is  $3\pi/4$  or  $5\pi/6$ ).

Here are some properties of *admissible Dynkin diagrams*:

- (1) A diagram obtained by removing a node from an admissible diagram is admissible.
- (2) An admissible diagram has no loops.
- (3) No node has more than three lines attached to it.
- (4) A sequence of nodes with only two single lines can be collapsed to give an admissible diagram.
- (5) The only connected diagram with a triple line has two nodes.

A *Coxeter-Dynkin diagram*, also called a *Coxeter graph*, is the same as a Dynkin diagram, but without the arrows. The Coxeter diagram is sufficient to characterize the algebra, as can be seen by enumerating connected diagrams.

The simplest way to recover a simple Lie algebra from its Dynkin diagram is to first reconstruct its Cartan matrix  $(A_{ij})$ . The  $i$ th node and  $j$ th node are connected by  $A_{ij}A_{ji}$  lines. Since  $A_{ij} = 0$  iff  $A_{ji} = 0$ , and otherwise  $A_{ij} \in \{-3, -2, -1\}$ , it is easy to find  $A_{ij}$  and  $A_{ji}$ , up to order, from their product. The arrow in the diagram indicates which is larger. For example, if node 1 and node 2 have two lines between them, from node 1 to node 2, then  $A_{12} = -1$  and  $A_{21} = -2$ .

However, it is worth pointing out that each simple Lie algebra can be constructed concretely. For instance, the infinite families  $A_n$ ,  $B_n$ ,  $C_n$ , and  $D_n$  correspond to the special linear Lie algebra  $\mathfrak{gl}(n+1, \mathbb{C})$ , the odd orthogonal Lie algebra  $\mathfrak{so}(2n+1, \mathbb{C})$ , the symplectic Lie algebra  $\mathfrak{sp}(2n, \mathbb{C})$ , and the even orthogonal Lie algebra  $\mathfrak{so}(2n, \mathbb{C})$ . The other simple Lie algebras are called *exceptional Lie algebras*, and have constructions related to the *octonions*.

To prove this classification theorem, one uses the angles between pairs of roots to encode the root system in a much simpler combinatorial object, the Dynkin diagram. The Dynkin diagrams can then be classified according to the scheme given above.

To every root system is associated a corresponding Dynkin diagram. Otherwise, the Dynkin diagram can be extracted from the root system by choosing a *base*, that is a subset  $\Delta$  of  $\Phi$  which is a basis of  $V$  with the special property that every vector in  $\Phi$  when written in the basis  $\Delta$  has either all coefficients  $\geq 0$  or else all  $\leq 0$ .

The vertices of the Dynkin diagram correspond to vectors in  $\Delta$ . An edge is drawn between each non-orthogonal pair of vectors; it is a double edge if they make an angle of 135 degrees, and a triple edge if they make an angle of 150 degrees. In addition, double and triple edges are marked



with an angle sign pointing toward the shorter vector.

Although a given root system has more than one base, the Weyl group acts transitively on the set of bases. Therefore, the root system determines the Dynkin diagram. Given two root systems with the same Dynkin diagram, we can match up roots, starting with the roots in the base, and show that the systems are in fact the same.

Thus the problem of classifying root systems reduces to the problem of classifying possible Dynkin diagrams, and the problem of classifying irreducible root systems reduces to the problem of classifying connected Dynkin diagrams. Dynkin diagrams encode the inner product on  $E$  in terms of the basis  $\Delta$ , and the condition that this inner product must be positive definite turns out to be all that is needed to get the desired classification (see Figure A.6).

In detail, the individual root systems can be realized case-by-case, as in the following paragraphs:

**A<sub>n</sub>.** Let  $V$  be the subspace of  $\mathbb{R}^{n+1}$  for which the coordinates sum to 0, and let  $\Phi$  be the set of vectors in  $V$  of length  $\sqrt{2}$  and with integer coordinates in  $\mathbb{R}^{n+1}$ . Such a vector must have all but two coordinates equal to 0, one coordinate equal to 1, and one equal to  $-1$ , so there are  $n^2 + n$  roots in all.

**B<sub>n</sub>.** Let  $V = \mathbb{R}^n$ , and let  $\Phi$  consist of all integer vectors in  $V$  of length 1 or  $\sqrt{2}$ . The total number of roots is  $2n^2$ .

**C<sub>n</sub>:** Let  $V = \mathbb{R}^n$ , and let  $\Phi$  consist of all integer vectors in  $V$  of  $\sqrt{2}$  together with all vectors of the form  $2\lambda$ , where  $\lambda$  is an integer vector of length 1. The total number of roots is  $2n^2$ . The total number of roots is  $2n^2$ .

**D<sub>n</sub>.** Let  $V = \mathbb{R}^n$ , and let  $\Phi$  consist of all integer vectors in  $V$  of length  $\sqrt{2}$ . The total number of roots is  $2n(n-1)$ .

**E<sub>n</sub>.** For  $V_8$ , let  $V = \mathbb{R}^8$ , and let  $E_8$  denote the set of vectors  $\alpha$  of length  $\sqrt{2}$  such that the coordinates of  $2\alpha$  are all integers and are either all even or all odd. Then  $E_7$  can be constructed as the intersection of  $E_8$  with the hyperplane of vectors perpendicular to a fixed root  $\alpha$  in  $E_8$ , and  $E_6$  can be constructed as the intersection of  $E_8$  with two such hyperplanes corresponding to roots  $\alpha$  and  $\beta$  which are neither orthogonal to one another nor scalar multiples of one another. The root systems  $E_6$ ,  $E_7$ , and  $E_8$  have 72, 126, and 240 roots respectively.

**F<sub>4</sub>.** For  $F_4$ , let  $V = \mathbb{R}^4$ , and let  $\Phi$  denote the set of vectors  $\alpha$  of length 1 or  $\sqrt{2}$  such that the coordinates of  $2\alpha$  are all integers and are either all even or all odd. There are 48 roots in this system.

$G_2$ . There are 12 roots in  $G_2$ , which form the vertices of a *hexagram*.

#### A.5.3.4 *Root Systems and Lie Theory*

Irreducible root systems classify a number of related objects in Lie theory, notably:

- (1) Simple complex Lie algebras;
- (2) Simple complex Lie groups;
- (3) Simply connected complex Lie groups which are simple modulo centers;  
and
- (4) Simple compact Lie groups.

In each case, the roots are non-zero weights of the adjoint representation.

A root system can also be said to describe a *plant's root* and associated systems.

#### A.5.4 *Simple and Semisimple Lie Groups and Algebras*

A *simple Lie group* is a Lie group which is also a simple group. These groups, and groups closely related to them, include many of the so-called *classical groups* of geometry, which lie behind projective geometry and other geometries derived from it by the *Erlangen programme* of Felix Klein. They also include some *exceptional groups*, that were first discovered by those pursuing the classification of simple Lie groups. The exceptional groups account for many special examples and configurations in other branches of mathematics. In particular the classification of finite simple groups depended on a thorough prior knowledge of the 'exceptional' possibilities.

The complete listing of the simple Lie groups is the basis for the theory of the semisimple Lie groups and reductive groups, and their representation theory. This has turned out not only to be a major extension of the theory of compact Lie groups (and their representation theory), but to be of basic significance in mathematical physics.

Such groups are classified using the prior classification of the complex simple Lie algebras. It has been shown that a simple Lie group has a simple Lie algebra that will occur on the list given there, once it is complexified (that is, made into a complex vector space rather than a real one). This reduces the classification to two further matters.

The groups  $SO(p, q, \mathbb{R})$  and  $SO(p + q, \mathbb{R})$ , for example, give rise to different real Lie algebras, but having the same Dynkin diagram. In general

there may be different *real forms* of the same complex Lie algebra.

Secondly, the Lie algebra only determines uniquely the simply connected (universal) cover  $G^*$  of the component containing the identity of a Lie group  $G$ . It may well happen that  $G^*$  is not actually a simple group, for example having a non-trivial center. We have therefore to worry about the global topology, by computing the fundamental group of  $G$  (an Abelian group: a Lie group is an  $H$ -space). This was done by Elie Cartan.

For an example, take the special orthogonal groups in even dimension. With  $-I$  a scalar matrix in the center, these are not actually simple groups; and having a two-fold spin cover, they aren't simply-connected either. They lie 'between'  $G^*$  and  $G$ , in the notation above.

Recall that a *semisimple module* is a module in which each submodule is a direct summand. In particular, a *semisimple representation* is completely reducible, i.e., is a direct sum of irreducible representations (under a descending chain condition). Similarly, one speaks of an Abelian category as being semisimple when every object has the corresponding property. Also, a semisimple ring is one that is semisimple as a module over itself.

A *semisimple matrix* is diagonalizable over any algebraically closed field containing its entries. In practice this means that it has a diagonal matrix as its Jordan normal form.

A Lie algebra  $\mathfrak{g}$  is called *semisimple* when it is a direct sum of *simple Lie algebras*, i.e., non-trivial Lie algebras  $\mathfrak{L}$  whose only ideals are  $\{0\}$  and  $\mathfrak{L}$  itself. An equivalent condition is that the *Killing form*

$$B(X, Y) = \text{Tr}(Ad(X) Ad(Y))$$

is non-degenerate [Schafer (1996)]. The following properties can be proved equivalent for a finite-dimensional algebra  $\mathfrak{L}$  over a field of characteristic 0:

1.  $\mathfrak{L}$  is semisimple.
2.  $\mathfrak{L}$  has no nonzero Abelian ideal.
3.  $\mathfrak{L}$  has zero radical (the radical is the biggest solvable ideal).
4. Every representation of  $\mathfrak{L}$  is fully reducible, i.e., is a sum of irreducible representations.
5.  $\mathfrak{L}$  is a (finite) direct product of simple Lie algebras (a Lie algebra is called simple if it is not Abelian and has no nonzero ideal).

A *connected Lie group* is called *semisimple* when its Lie algebra is semisimple; and the same holds for algebraic groups. Every finite dimensional representation of a semisimple Lie algebra, Lie group, or algebraic group in characteristic 0 is semisimple, i.e., completely reducible, but the

converse is not true. Moreover, in characteristic  $p > 0$ , semisimple Lie groups and Lie algebras have finite dimensional representations which are not semisimple. An element of a semisimple Lie group or Lie algebra is itself semisimple if its image in every finite-dimensional representation is semisimple in the sense of matrices.

Every semisimple Lie algebra  $\mathfrak{g}$  can be classified by its Dynkin diagram [Helgason (2001)].

## A.6 Phase Transitions, Partition Function and Noise

In this section we present the basic principles of equilibrium phase transitions, which are used in *synergetics* (see chapter 2), *quantum biodynamics* (see chapter 4) and *topological biodynamics* (see chapter 5). We also give a brief on *partition function*, the most important quantity in statistical mechanics.

### A.6.1 Equilibrium Phase Transitions

In *thermodynamics*, a *phase transition* represents the transformation of a system from one phase to another. Here the term *phase* denotes a set of states of a macroscopic physical system that have relatively uniform chemical composition and physical properties (i.e., density, crystal structure, index of refraction, and so forth.) The most familiar examples of phases are solids, liquids, and gases. Less familiar phases include plasmas, Bose-Einstein condensates and fermionic condensates and the paramagnetic and ferromagnetic phases of magnetic materials.

In essence, all thermodynamic properties of a system (entropy, heat capacity, magnetization, compressibility, and so forth) may be expressed in terms of the *free energy potential*  $\mathcal{F}$  and its partial derivatives. For example, the *entropy*  $S$  is the first derivative of the free energy  $\mathcal{F}$  with respect to the temperature  $T$ , i.e.,  $S = -\partial\mathcal{F}/\partial T$ , while the *specific heat capacity*  $C$  is the second derivative,  $C = T \partial S/\partial T$ . As long as the free energy  $\mathcal{F}$  remains analytic, all the thermodynamic properties will be well-behaved.

Now, the distinguishing characteristic of a phase transition is an *abrupt sudden change in one or more physical properties*, in particular the specific heat  $c$ , with a small change in a thermodynamic variable such as the temperature  $T$ . Standard examples of phase transitions are (see e.g., [Landau and Lifshitz (1978); Wikipedia (2005)]):

- (1) The transitions between the solid, liquid, and gaseous phases (boiling, melting, sublimation, etc.)
- (2) The transition between the ferromagnetic and paramagnetic phases of magnetic materials at the Curie point.
- (3) The emergence of superconductivity in certain metals when cooled below a critical temperature.
- (4) Quantum condensation of bosonic fluids, such as Bose–Einstein condensation and the superfluid transition in liquid helium.
- (5) The breaking of symmetries in the laws of physics during the early history of the universe as its temperature cooled.

When a system goes from one phase to another, there will generally be a stage where the free energy is non-analytic. This is known as a phase transition. Familiar examples of phase transitions are melting (solid to liquid), freezing (liquid to solid), boiling (liquid to gas), and condensation (gas to liquid). Due to this *non-analyticity*, the free energies on either side of the transition are two different functions, so one or more thermodynamic properties will behave very differently after the transition. The property most commonly examined in this context is the heat capacity. During a transition, the heat capacity may become infinite, jump abruptly to a different value, or exhibit a ‘kink’ or *discontinuity* in its derivative<sup>25</sup>.

Therefore, phase transitions come about when the free energy of a system is non-analytic for some choice of thermodynamic variables. This non-analyticity generally stems from the interactions of an extremely large number of particles in a system, and does not appear in systems that are too small.

#### A.6.1.1 *Classification of Phase Transitions*

**Ehrenfest Classification.** The first attempt at classifying phase transitions was the *Ehrenfest classification scheme*, which grouped phase transitions based on the degree of non-analyticity involved. Though useful,

---

<sup>25</sup>In practice, each type of phase is distinguished by a handful of relevant thermodynamic properties. For example, the distinguishing feature of a solid is its rigidity; unlike a liquid or a gas, a solid does not easily change its shape. Liquids are distinct from gases because they have much lower compressibility: a gas in a large container fills the container, whereas a liquid forms a puddle in the bottom. Not all the properties of solids, liquids, and gases are distinct; for example, it is not useful to compare their magnetic properties. On the other hand, the ferromagnetic phase of a magnetic material is distinguished from the paramagnetic phase by the presence of bulk magnetization without an applied magnetic field.

Ehrenfest's classification is flawed, as we will discuss in the next section.

Under this scheme, phase transitions were labelled by the lowest partial derivative of the free energy that is discontinuous at the transition. *First-order phase transitions* exhibit a discontinuity in the first derivative of the free energy with respect to a thermodynamic variable. The various solid $\Rightarrow$ liquid $\Rightarrow$ gas transitions are classified as first-order transitions, as the density, which is the first partial derivative of the free energy with respect to chemical potential, changes discontinuously across the transitions<sup>26</sup>. *Second-order phase transitions* have a discontinuity in a second derivative of the free energy. These include the ferromagnetic phase transition in materials such as iron, where the magnetization, which is the first derivative of the free energy with the applied magnetic field strength, increases continuously from zero as the temperature is lowered below the Curie temperature. The magnetic susceptibility, the second derivative of the free energy with the field, changes discontinuously. Under the *Ehrenfest classification scheme*, there could in principle be third, fourth, and higher-order phase transitions.

**Modern Classification.** The Ehrenfest scheme is an inaccurate method of classifying phase transitions, for it is based on the *mean-field theory* of phases, which is inaccurate in the vicinity of phase transitions, as it neglects the role of thermodynamic fluctuations. For instance, it predicts a finite discontinuity in the heat capacity at the ferromagnetic transition, which is implied by Ehrenfest's definition of second-order transitions. In real ferromagnets, the heat capacity diverges to infinity at the transition.

In the modern classification scheme, phase transitions are divided into two broad categories, named similarly to the Ehrenfest classes:

- The *first-order phase transitions*, or, *discontinuous phase transitions*, are those that involve a latent heat. During such a transition, a system either absorbs or releases a fixed (and typically large) amount of energy. Because energy cannot be instantaneously transferred between the system and its environment, first-order transitions are associated with *mixed-phase regimes* in which some parts of the system have completed the transition and others have not. This phenomenon is familiar to anyone who has boiled a pot of water: the water does not instantly turn into gas, but forms a turbulent mixture of water and water vapor bubbles. Mixed-phase systems are difficult to study, because their dynamics are violent and hard to control. However, many important

---

<sup>26</sup>The pressure must be continuous across the phase boundary in equilibrium.

phase transitions fall in this category, including the solid $\Rightarrow$ liquid $\Rightarrow$ gas transitions.

- The *second-order phase transitions* are the *continuous phase transitions*. These have no associated latent heat. Examples of second-order phase transitions are the ferromagnetic transition, the superfluid transition, and Bose-Einstein condensation.

#### A.6.1.2 Basic Properties of Phase Transitions

**Critical Points.** In systems containing liquid and gaseous phases, there exist a special combination of pressure and temperature, known as the *critical point*, at which the transition between liquid and gas becomes a second-order transition. Near the critical point, the fluid is sufficiently hot and compressed that the distinction between the liquid and gaseous phases is almost non-existent.

This is associated with the phenomenon of critical opalescence, a milky appearance of the liquid, due to density fluctuations at all possible wavelengths (including those of visible light).

**Symmetry.** Phase transitions often (but not always) take place between phases with different symmetry. Consider, for example, the transition between a fluid (i.e., liquid or gas) and a crystalline solid. A fluid, which is composed of atoms arranged in a disordered but homogenous manner, possesses continuous translational symmetry: each point inside the fluid has the same properties as any other point. A crystalline solid, on the other hand, is made up of atoms arranged in a regular lattice. Each point in the solid is *not* similar to other points, unless those points are displaced by an amount equal to some lattice spacing.

Generally, we may speak of one phase in a phase transition as being more symmetrical than the other. The transition from the more symmetrical phase to the less symmetrical one is a *symmetry-breaking* process. In the fluid-solid transition, for example, we say that continuous translation symmetry is broken.

The ferromagnetic transition is another example of a symmetry-breaking transition, in this case the symmetry under reversal of the direction of electric currents and magnetic field lines. This symmetry is referred to as 'up-down symmetry' or 'time-reversal symmetry'. It is broken in the ferromagnetic phase due to the formation of magnetic domains containing aligned magnetic moments. Inside each domain, there is a magnetic field pointing in a fixed direction chosen spontaneously during the phase transi-

tion. The name *time-reversal symmetry* comes from the fact that electric currents reverse direction when the time coordinate is reversed.

The presence of symmetry-breaking (or nonbreaking) is important to the behavior of phase transitions. It was pointed out by Landau that, given any state of a system, one may unequivocally say whether or not it possesses a given symmetry [Landau and Lifshitz (1978)]. Therefore, it cannot be possible to analytically deform a state in one phase into a phase possessing a different symmetry. This means, for example, that it is impossible for the solid-liquid phase boundary to end in a critical point like the liquid-gas boundary. However, symmetry-breaking transitions can still be either first or second order.

Typically, the more symmetrical phase is on the high-temperature side of a phase transition, and the less symmetrical phase on the low-temperature side. This is certainly the case for the solid-fluid and ferromagnetic transitions. This happens because the Hamiltonian of a system usually exhibits all the possible symmetries of the system, whereas the low-energy states lack some of these symmetries (this phenomenon is known as spontaneous symmetry breaking.) At low temperatures, the system tends to be confined to the low-energy states. At higher temperatures, thermal fluctuations allow the system to access states in a broader range of energy, and thus more of the symmetries of the Hamiltonian.

When symmetry is broken, one needs to introduce one or more extra variables to describe the state of the system. For example, in the ferromagnetic phase one must provide the net magnetization, whose direction was spontaneously chosen when the system cooled below the Curie point. Such variables are instances of *order parameters*. However, note that order parameters can also be defined for symmetry-nonbreaking transitions.

Symmetry-breaking phase transitions play an important role in cosmology. It has been speculated that, in the hot early universe, the vacuum (i.e., the various quantum fields that fill space) possessed a large number of symmetries. As the universe expanded and cooled, the vacuum underwent a series of symmetry-breaking phase transitions. For example, the electroweak transition broke the  $SU(2) \times U(1)$  symmetry of the electroweak field into the  $U(1)$  symmetry of the present-day electromagnetic field. This transition is important to understanding the asymmetry between the amount of matter and antimatter in the present-day universe.

**Critical Exponents and Universality Classes.** Continuous phase transitions are easier to study than first-order transitions due to the absence of latent heat, and they have been discovered to have many interesting



properties. The phenomena associated with continuous phase transitions are called *critical phenomena*, due to their association with critical points.

It turns out that continuous phase transitions can be characterized by parameters known as critical exponents. For instance, let us examine the behavior of the heat capacity near such a transition. We vary the temperature  $T$  of the system while keeping all the other thermodynamic variables fixed, and find that the transition occurs at some critical temperature  $T_c$ . When  $T$  is near  $T_c$ , the heat capacity  $C$  typically has a *power law* behavior:  $C \sim |T_c - T|^{-\alpha}$ . Here, the constant  $\alpha$  is the critical exponent associated with the heat capacity. It is not difficult to see that it must be less than 1 in order for the transition to have no latent heat. Its actual value depends on the type of phase transition we are considering. For  $-1 < \alpha < 0$ , the heat capacity has a 'kink' at the transition temperature. This is the behavior of liquid helium at the 'lambda transition' from a normal state to the superfluid state, for which experiments have found  $\alpha = -0.013 \pm 0.003$ . For  $0 < \alpha < 1$ , the heat capacity diverges at the transition temperature (though, since  $\alpha < 1$ , the divergence is not strong enough to produce a latent heat.) An example of such behavior is the 3D ferromagnetic phase transition. In the 3D Ising model for uniaxial magnets, detailed theoretical studies have yielded the exponent  $\alpha \sim 0.110$ .

Some model systems do not obey this power law behavior. For example, mean-field theory predicts a finite discontinuity of the heat capacity at the transition temperature, and the 2D Ising model has a logarithmic divergence. However, these systems are an exception to the rule. Real phase transitions exhibit power law behavior.

Several other critical exponents –  $\beta$ ,  $\gamma$ ,  $\delta$ ,  $\nu$ , and  $\eta$  – are defined, examining the power law behavior of a measurable physical quantity near the phase transition.

It is a remarkable fact that phase transitions arising in different systems often possess the same set of critical exponents. This phenomenon is known as *universality*. For example, the critical exponents at the liquid–gas critical point have been found to be independent of the chemical composition of the fluid. More amazingly, they are an exact match for the critical exponents of the ferromagnetic phase transition in uniaxial magnets. Such systems are said to be in the same *universality class*. Universality is a prediction of the renormalization group theory of phase transitions, which states that the thermodynamic properties of a system near a phase transition depend only on a small number of features, such as dimensionality and symmetry, and is insensitive to the underlying microscopic properties of the system.

### A.6.2 Landau's Theory of Phase Transitions

*Landau's theory of phase transitions* is a simple but powerful empirical thermodynamic theory by which the behavior of crystals at phase transitions can be described. It is based simply on a power series expansion of the free energy of the crystal with respect to one or a few prominent parameters distorting the symmetry of the crystal. The symmetry of the distortion decides which terms may be present, and which not. For example, odd terms on the power series expansion often are not allowed because the energy of the system is symmetric with respect to positive or negative distortion. With Landau's theory, the thermodynamics of the crystal (free energy, entropy, heat capacity) can be directly linked to its structural state (volume, deviation from high symmetry, etc.), and both can be described as they change as a function of temperature or pressure.

More precisely, in Landau's theory, the probability (density) distribution function  $f$  is exponentially related to the potential  $\mathcal{F}$ ,

$$f \approx e^{-\mathcal{F}(T)}, \quad (\text{A.38})$$

if  $\mathcal{F}$  is considered as a function of the order parameter  $o$ . Therefore, the most probable order parameter is determined by the requirement  $\mathcal{F} = \min$ .

When  $M_{\uparrow}$  elementary magnets point upwards and  $M_{\downarrow}$  elementary magnets point downwards, the magnetization order parameter  $o$  is given by

$$o = (M_{\uparrow} - M_{\downarrow}) m, \quad (\text{A.39})$$

where  $m$  is the magnetic moment of a single elementary magnet.

We expand the potential  $\mathcal{F} = \mathcal{F}(o, T)$  into a power series of  $o$ ,

$$\mathcal{F}(o, T) = \mathcal{F}(0, T) + \mathcal{F}'(0, T)o + \dots + \frac{1}{4!}\mathcal{F}''''(0, T)o^4 + \dots, \quad (\text{A.40})$$

and discuss  $\mathcal{F}$  as a function of  $o$ . In a number of cases  $\mathcal{F}' = \mathcal{F}''' = 0$ , due to inversion symmetry. In this case,  $\mathcal{F}$  has the form

$$\mathcal{F}(o, T) = \mathcal{F}(0, T) + \frac{\sigma}{2}o^2 + \frac{\beta}{4}o^4, \quad (\text{A.41})$$

where  $\beta > 0$ , and  $\sigma = a(T - T_c)$ , ( $a > 0$ ), i.e., it changes its sign at the critical temperature  $T = T_c$ .

Recall that the (negative) first partial derivative of the free energy potential  $\mathcal{F}$  with respect to the *control parameter* – temperature  $T$  is the

entropy

$$S = -\frac{\partial \mathcal{F}(q, T)}{\partial T}. \quad (\text{A.42})$$

For  $T > T_c$ ,  $\sigma > 0$ , and the minimum of  $\mathcal{F}$  lies at  $o = o_0 = 0$ , and

$$S = S_0 = -\frac{\partial \mathcal{F}(0, T)}{\partial T}.$$

Also recall that the second partial derivative of  $\mathcal{F}$  with respect to  $T$  is the specific heat capacity (besides the factor  $T$ )

$$C = T \frac{\partial S}{\partial T}. \quad (\text{A.43})$$

One may readily check that  $S$  is continuous at  $T = T_c$  for  $\sigma = 0$ . However, when we calculate the specific heat we get two different expressions above and below the critical temperature and thus a discontinuity at  $T = T_c$ .

Closely related to the Landau's theory of phase transitions is *Ginzburg–Landau model of superconductivity* (named after Nobel Laureates Vitaly L. Ginzburg and Lev D. Landau). It does not purport to explain the microscopic mechanisms giving rise to superconductivity. Instead, it examines the macroscopic properties of a superconductor with the aid of general thermodynamic arguments. Based on Landau's previously-established theory of second-order phase transitions, Landau and Ginzburg argued that the free energy  $F$  of a superconductor near the superconducting transition can be expressed in terms of a complex *order parameter*  $\psi$ , which describes how deep into the superconducting phase the system is. By minimizing the free energy with respect to fluctuations in the order parameter and the vector potential, one arrives at the *Ginzburg–Landau equation*, which is a generalization of the *nonlinear Schrödinger equation* (7.126).

### A.6.3 Partition Function

Recall that in *statistical mechanics*, the *partition function*  $Z$  is used for statistical description of a system in thermodynamic equilibrium.  $Z$  depends on the physical system under consideration and is a function of temperature  $T$  as well as other parameters (such as volume  $V$  enclosing a gas etc.). The partition function forms the basis for most calculations in statistical mechanics. It is most easily formulated in *quantum statistical mechanics* (see e.g., [Feynman (1972); Weisstein (2004)]).

### A.6.3.1 Classical Partition Function

A system subdivided into  $N$  subsystems, where each subsystem (e.g., a particle) can attain any of the energies  $\epsilon_j$  ( $j = 1, \dots, N$ ), has the partition function given by the sum of its Boltzmann factors,

$$\zeta = \sum_{j=0}^{\infty} e^{-\beta \epsilon_j},$$

where  $\beta = \frac{1}{k_B T}$  and  $k_B$  is Boltzmann constant. The interpretation of  $\zeta$  is that the probability that the subsystem will have energy  $\epsilon_j$  is  $e^{-\beta \epsilon_j} / \zeta$ . When the number of energies  $\epsilon_j$  is definite (e.g., particles with spin in a crystal lattice under an external magnetic field), then the indefinite sum is replaced with a definite sum. However, the total partition function for the system containing  $N$  subsystems is of the form

$$Z = \prod_{j=1}^N \zeta_j = \zeta_1 \zeta_2 \zeta_3 \dots,$$

where  $\zeta_j$  is the partition function for the  $j$ th subsystem. Another approach is to sum over all system's total energy states,

$$Z = \sum_{r=1}^N e^{-\beta E_r}, \quad \text{where} \quad E_j = n_1^{(j)} \epsilon_1 + n_2^{(j)} \epsilon_2 + \dots$$

In case of a system containing  $N$  non-interacting subsystems (e.g., a real gas), the system's partition function is given by

$$Z = \frac{1}{N!} \zeta^N.$$

This equation also has the more general form

$$Z = \frac{1}{N! h^{3N}} \int \prod_{i=1}^N d^3 q^i d^3 p_i \sum_{i=1}^N e^{-\beta H_i},$$

where  $H_i = H_i(q^i, p_i)$  is the  $i$ th subsystem's Hamiltonian, while  $h^{3N}$  is a normalization factor.

Given the partition function  $Z$ , the system's free energy  $F$  is defined as

$$F = -k_B T \ln Z,$$

while the *average energy*  $U$  is given by

$$U = \frac{1}{Z} E_i e^{-\frac{E_i}{k_B T}} = -\frac{d}{d\beta} (\ln Z).$$

**Liner Harmonic Oscillators in Thermal Equilibrium.** The partition function  $Z$ , free energy  $F$ , and average energy  $U$  of the system of  $M$  oscillators can be found as follows: The oscillators do not interact with each other, but only with the *heat bath*. Since each oscillator is independent, one can find  $F_i$  of the  $i$ th oscillator and then  $F = \sum_{i=1}^M F_i$ . For each  $i$ th oscillator (that can be in one of  $N$  states) we have [Feynman (1972)]

$$Z_i = \sum_{n=1}^N e^{-\frac{E_n^i}{k_B T}}, \quad F_i = -k_B T \ln Z_i, \quad U_i = \frac{1}{Z} \sum_{n=1}^N E_n^i e^{-\frac{E_n^i}{k_B T}}.$$

#### A.6.3.2 Quantum Partition Function

Partition function  $Z$  of a quantum-mechanical system may be written as a trace over all states (which may be carried out in any basis, as the trace is basis-independent),

$$Z = \text{Tr}(e^{-\beta \hat{H}}),$$

where  $\hat{H}$  is the system's Hamiltonian operator. If  $\hat{H}$  contains a dependence on a parameter  $\lambda$ , as in  $\hat{H} = \hat{H}_0 + \lambda \hat{A}$ , then the statistical average over  $\hat{A}$  may be found from the dependence of the partition function on the parameter, by differentiation,

$$\langle \hat{A} \rangle = -\beta^{-1} \frac{d}{d\lambda} \ln Z(\beta, \lambda).$$

However, if one is interested in the average of an operator that does not appear in the Hamiltonian, one often adds it artificially to the Hamiltonian, calculates  $Z$  as a function of the extra new parameter and sets the parameter equal to zero after differentiation.

More general, in *quantum field theory*, we have a *generating functional*  $J$  of the *field*  $\phi(q)$  and the partition function is usually expressed by the *Feynman path integral* [Feynman (1972)]

$$Z[J] = \int \mathcal{D}\phi e^{i(S[\phi] + \int d^N q J(q)\phi(q))},$$

where  $S = S[\phi]$  is the *field action functional*.

### A.6.3.3 Vibrations of Coupled Oscillators

In this subsection, following [Feynman (1972)], we give both classical and quantum analysis of vibrations of coupled oscillators. R. Feynman used this method as a generic model for the crystal lattice.

Consider a *crystal lattice* with  $A$  atoms per unit cell, such that  $3A$  coordinates  $\alpha$  must be given to locate each atom. Also let  $Q_{\alpha,N}$  denote the *displacement* from equilibrium of the coordinate  $\alpha$  in the  $N$ th cell.  $Q_{\alpha,N+M}$  is the displacement of an atom in a cell close to  $N$ .

The *kinetic energy* of the lattice is given by

$$T = \frac{1}{2} \dot{Q}_{\alpha,N} \dot{Q}_{\alpha,N},$$

while its *potential energy* (in linear approximation) is given by

$$V = \frac{1}{2} C_{\alpha\beta}^M Q_{\alpha,N} Q_{\beta,N+M}.$$

**Classical Problem.** The so-called *original Hamiltonian* is given by

$$H = \sum_i \frac{p_i'^2}{2m_i} + \frac{1}{2} C_{ij}' q^i q^j,$$

where the  $q^i$  are the coordinates of the amount of the lattice displacement from its equilibrium,  $p_i' = m_i \dot{q}^i$  are the canonical momenta, and  $C_{ij}' = C_{ji}'$  are constants. To eliminate the mass constants  $m_i$ , let

$$q^i = q^i' \sqrt{m_i} \quad \text{and} \quad C_{ij} = \frac{C_{ij}'}{\sqrt{m_i m_j}}.$$

Then

$$p_i = \frac{\partial L}{\partial \dot{q}^i} = \frac{p_i'}{\sqrt{m_i}}, \quad (L \text{ is the Lagrangian of the system})$$

and we get the *simplified Hamiltonian*

$$H = \frac{1}{2} \sum_i p_i^2 + \frac{1}{2} C_{ij} q^i q^j.$$

The Hamilton's equations of motion now read

$$\dot{q}^i = \partial_{p_i} H = p_i, \quad \dot{p}_i = -\partial_{q^i} H = -C_{ij} q^j = \ddot{q}^i.$$

We now break the motion of the system into *modes*, each of which has its own frequency  $\omega$ . The total motion of the system is a sum of the motions

of the modes. Let the  $\alpha$ th mode have frequency  $\omega_\alpha$  so that

$$q_{(\alpha)}^i = e^{-i\omega_\alpha t} a_i^{(\alpha)}$$

for the motion of the  $\alpha$ th mode, with  $a_i^{(\alpha)}$  independent of time. Then

$$\omega_\alpha^2 a_i^{(\alpha)} = C_{ij} a_j^{(\alpha)}.$$

In this way, the classical problem of vibrations of coupled oscillators has been reduced to the problem of finding eigenvalues and eigenvectors of the real, symmetric matrix  $\|C_{ij}\|$ . In order to get the  $\omega_\alpha$  we must solve the characteristic equation

$$\det \|C_{ij} - \omega^2 \delta_{ij}\| = 0.$$

Then the eigenvectors  $a_i^{(\alpha)}$  can be found. It is possible to choose the  $a_i^{(\alpha)}$  so that

$$a_i^{(\alpha)} a_i^{(\beta)} = \delta_{\alpha\beta}.$$

The general solution for  $q^i$  is

$$q^i = C_\alpha q_{(\alpha)}^i,$$

where the  $C_\alpha$  are arbitrary constants. If we take

$$Q_\alpha = C_\alpha e^{-i\omega_\alpha t},$$

we get

$$q^i = a_i^{(\alpha)} Q_\alpha.$$

From this it follows that

$$a_i^{(j)} q^i = a_i^{(j)} a_i^{(\alpha)} Q_\alpha = \delta_{\alpha j} Q_\alpha = Q_j.$$

Making the change of variables,  $Q_j = a_i^{(j)} q^i$ , we get  $H = \sum_\alpha H_\alpha$ , where

$$H_\alpha = \frac{1}{2} p_\alpha^2 + \frac{1}{2} \omega_\alpha^2 Q_\alpha.$$

This has the expected solutions:  $Q_\alpha = C_\alpha e^{-i\omega_\alpha t}$ .

**Quantum-Mechanical Problem.** Again we have the original Hamiltonian

$$H = \sum_i \frac{p_i'^2}{2m_i} + \frac{1}{2} C'_{ij} q^i q^j,$$

where this time

$$p_i' = \frac{1}{i} \frac{\partial}{\partial q_i'} \quad (\text{in normal units } \hbar = 1).$$

Making the same change of variables as before, we get

$$Q_\alpha = a_i^{(\alpha)} q^i = a_i^{(\alpha)} \sqrt{m_i} q^i l, \\ H = \sum_\alpha H_\alpha, \quad \text{where} \quad H_\alpha = -\frac{1}{2} \frac{\partial^2}{\partial Q_\alpha^2} + \frac{1}{2} \omega_\alpha^2 Q_\alpha.$$

It follows immediately that the eigenvalues of our original Hamiltonian are

$$E = \sum_\alpha (N_\alpha + \frac{1}{2}) \omega_\alpha.$$

The solution of a quantum-mechanical system of coupled oscillators is trivial once we have solved the characteristic equation

$$0 = \det \| C_{ij} - \omega^2 \delta_{ij} \| = \det \left\| \frac{C_{ij}'}{\sqrt{m_i m_j}} - \omega^2 \delta_{ij} \right\|.$$

If we have a solid with  $\frac{1}{3}(10^{23})$  atoms we must apparently find the eigenvalues of a  $10^{23}$  by  $10^{23}$  matrix. But if the solid is *crystal*, the problem is enormously simplified. The *classical Hamiltonian for a crystal* is

$$H = \frac{1}{2} \sum_{\alpha, N} \dot{Q}_{\alpha, N}^2 + \frac{1}{2} \sum_{\alpha, \beta, N, M} C_{\alpha\beta}^M Q_{\alpha, N} Q_{\beta, N+M},$$

and the *classical equation of motion for a crystal lattice* is (using  $C_{\alpha\beta}^M = C_{\beta\alpha}^{-M}$ )

$$\ddot{Q}_{\alpha, N} = - \sum_{M, \beta} C_{\alpha\beta}^M Q_{\beta, N+M}.$$

In a given mode, if one cell of the crystal is vibrating in a certain manner, it is reasonable to expect all cells to vibrate the same way, but with different phases. So we try

$$Q_{\alpha, N} = a_\alpha(K) e^{-i\omega t} e^{iK \cdot N},$$

where  $K$  expresses the relative phase between cells. The  $e^{iK \cdot N}$  factor allows for wave motion. We now want to find the dispersion relations, or  $\omega =$



$\omega(K)$ .

$$\omega^2 a_\alpha e^{iK \cdot N} = \sum_{M, \beta} (C_{\alpha\beta}^M a_\beta e^{iK \cdot M}) e^{iK \cdot N}.$$

Let

$$\gamma_{\alpha\beta}(K) = \sum_M C_{\alpha\beta}^M e^{iK \cdot M}$$

(note that  $\gamma_{\alpha\beta}(K)$  is Hermitian).

Then  $\omega^2 a_\alpha = \sum_\beta \gamma_{\alpha\beta} a_\beta$ , and we must solve the characteristic equation of a  $3A$ -by- $3A$  matrix:

$$\det |\gamma_{\alpha\beta} - \omega^2 \delta_{\alpha\beta}| = 0.$$

The solutions of the characteristic equation are

$$\omega^{(r)}(K) = \omega_K^{(r)},$$

where  $r$  runs from 1 to  $3A$ . The motion of a particular mode can be written

$$Q_{\alpha,N}^{(r)}(K) = a_\alpha^r(K) e^{-i\omega^{(r)}(K)r} e^{iK \cdot N},$$

where

$$a_\alpha^r a_\alpha^{*r'} = \delta_{rr'}.$$

Then the general motion can be described by

$$Q_{\alpha,N} = \sum_{K,r} C_r(K) a_\alpha^r(K) e^{-i\omega^{(r)}(K)r} e^{iK \cdot N},$$

where  $C_r(K)$  are arbitrary constants.

Let  $Q_r(K) = C_r(K) e^{-i\omega^{(r)}(K)r}$ .  $Q_r(K)$  describe the motion of a particular mode. Then we have

$$Q_{\alpha,N} = \sum_{K,r} Q_r(K) a_\alpha^r(K) e^{iK \cdot N}.$$

It follows that

$$Q_r(K) \propto \sum_{\alpha,N} Q_{\alpha,N} a_\alpha^{*r}(K) e^{-iK \cdot N}, \quad (\propto \text{ means 'proportional to'}),$$

and the Hamiltonian for the system is

$$\begin{aligned} H &= \frac{1}{2} \sum_{\alpha, N} \left[ \dot{Q}_{\alpha, N}^2 + \sum_{\beta, M} C_{\alpha\beta}^M Q_{\alpha, N} Q_{\beta, N+M} \right] \\ &= \frac{1}{2} \sum_{K, r} \left[ |\dot{Q}_r(K)|^2 + \omega^{2(r)}(K) |Q_r(K)|^2 \right]. \end{aligned}$$

**A Cubic Lattice of Harmonic Oscillators.** Assume the unit cell to be a cubic lattice with one atom per cell. Each atom behaves as an harmonic oscillator, with spring constants  $k_A$  (nearest neighbors), and  $k_B$  (diagonal-, or next-nearest neighbors). This case is fairly simple, and we can simplify the notation:  $\alpha = 1, 2, 3$ .

$$Q_{1, N} = X_N, \quad Q_{2, N} = Y_N, \quad Q_{3, N} = Q_N.$$

We wish to find the 3 natural frequencies associated with each  $k$  of the crystal. To do this, we must find  $C_{\alpha\beta}^M$  and then  $\gamma_{\alpha\beta}$ . In complex coordinates,

$$V = \sum_{\alpha, \beta} V_{\alpha\beta}, \quad \text{where} \quad V_{\alpha\beta} = \sum_{N, M} C_{\alpha\beta}^M Q_{\alpha, N}^* Q_{\beta, N+M},$$

where  $*$  denotes complex conjugation. For example,

$$V_{11} = \sum_{N, M} C_{11}^M X_N^* X_{N+M}.$$

If we express the displacement of atom  $N$  from its normal position as  $X_N$ , then the *potential energy* from the distortion of the spring between atoms  $N$  and  $M$  is

$$\frac{1}{2} k_M \left[ (X_N - X_{N+M}) \cdot \frac{M}{|M|} \right]^2,$$

where  $k_M = k_A$  for  $N + M$  a nearest neighbor to  $N$ ,  $k_M = k_B$  for  $N + M$  a next-nearest neighbor.

In summing over  $N$  and  $M$  to get the total potential energy we must *divide  $V$  by two*, for we count each spring twice. If we use complex coordinates, however, we *multiply  $V$  by two* to get the correct equations of motion:

$$V = \frac{1}{2} \sum_{N, M} k_M \left[ (X_N - X_{N+M}) \cdot \frac{M}{|M|} \right]^2,$$

$$\begin{aligned}
 V_{11} &= \frac{1}{2} \sum_{N,M} k_M \left( \frac{M_X}{|M|} \right)^2 (X_N^* - X_{N+M}^*) (X_N - X_{N+M}) = \\
 &\frac{1}{2} \sum_{N,M} k_M \left( \frac{M_X}{|M|} \right)^2 [(X_N^* X_N + X_{N+M}^* X_{N+M}) - (X_N^* X_{N+M} + X_N X_{N+M}^*)] \\
 &= \sum_{N,M} k_M \left( \frac{M_X}{|M|} \right)^2 [X_N^* X_N - X_N X_{N+M}^*].
 \end{aligned}$$

Comparing the above expressions we see that

$$C_{11}^0 = 2k_A + 4k_B, \quad C_{11}^{\pm(1,0,0)} = -k_A, \quad \text{and so on.}$$

In this way, all the  $C_{\alpha\beta}^M$  can be found. We can then calculate

$$\gamma_{\alpha\beta}(K) = \sum_M C_{\alpha\beta}^M e^{iK \cdot M}.$$

We wish to solve

$$\det |\gamma_{\alpha\beta} - \omega^2 \delta_{\alpha\beta}| = 0.$$

For each relative phase  $K$ , there are 3 solutions for  $\omega$ . Thus we get  $3N$  values of  $\omega$  and  $\omega^{(r)}(K)$ .

#### A.6.4 Noise-Induced Nonequilibrium Phase Transitions

*Noise* is usually thought of as a phenomenon which perturbs the observation and creates disorder (see section 4.6.1). This idea is based mainly on our day to day experience and, in the context of physical theories, on the study of equilibrium systems. The effect of noise can, however, be quite different in *nonlinear nonequilibrium systems*. Several situations have been documented in the literature, in which the noise actually participates in the creation of ordered states or is responsible for surprising phenomena through its interaction with the nonlinearities of the system [Horsthemke and Lefever (1984)]. Recently, a quite spectacular phenomenon was discovered in a specific model of a spatially distributed system with multiplicative noise, white in space and time. It was found that the noise generates an *ordered symmetry-breaking state* through a genuine *second-order phase transition*, whereas no such transition is observed in the absence of noise [van den Broeck *et al.* (1994); van den Broeck *et al.* (1997)].

Recently it has been shown that a white and *Gaussian multiplicative noise* can lead an *extended* dynamical system (fulfilling appropriate conditions) to undergo a *phase transition* towards an *ordered* state, characterized by a nonzero order parameter and by the breakdown of ergodicity

[van den Broeck *et al.* (1994)]. This result—first obtained within a Curie–Weiss-like *mean-field approximation*, and further extended to consider the simplest correlation function approach—has been confirmed through extensive numerical simulations [van den Broeck *et al.* (1997)]. In addition to its *critical* nature as a function of the noise intensity  $\sigma$ , the newly found noise-induced phase transition has the noteworthy feature of being *reentrant*: for each value of  $D$  above a threshold one, the ordered state exists only inside a window  $[\sigma_1, \sigma_2]$ . At variance with the known case of *equilibrium* order  $\Rightarrow$  disorder transitions that are induced (in the simplest lattice models) by the nearest-neighbor coupling constant  $D$  and rely on the bistability of the local potential, the transition in the case at hand is led by the *combined effects* of  $D$  and  $\sigma$  through the nonlinearities of the system. Neither the zero-dimensional system (corresponding to the  $D = 0$  limit) nor the deterministic one ( $\sigma = 0$ ) show any transition.

#### A.6.4.1 General Zero-Dimensional System

To smoothly introduce the subject, we will start from the well-known *logistic equation*, and add to it a multiplicative white noise.

**Noisy Logistic Equation.** Recall that the logistic equation (also called the *Verhulst model* or *logistic growth curve*) is a model of population growth first published by P. Verhulst in 1845 (see [Weisstein (2004)]). The model is continuous in time, but a modification of the continuous equation to a discrete quadratic recurrence equation known as the *logistic map* is widely used in *chaos theory* (see chapter 2). The standard logistic equation

$$\dot{x} = \lambda x - x^2, \quad (\text{A.44})$$

where the parameter  $\lambda$  is usually constrained to be positive, has a solution

$$x(t) = \frac{1}{1 + \left(\frac{1}{x_0} - 1\right) e^{-\lambda t}}.$$

Now, if we add a *multiplicative zero-mean Gaussian white noise*  $\xi = \xi(t)$  with *noise intensity*  $\sigma$  to (A.44), we get the *Langevin SDE* (stochastic differential equation)

$$\dot{x} = \lambda x - x^2 + x \xi. \quad (\text{A.45})$$

If we apply the *Stratonovitch interpretation* to the Langevin equation (A.45), we get the corresponding *Fokker–Planck equation*

$$\partial_t P(x, t) = -\partial_t (\lambda x - x^2) P(x, t) + \frac{\sigma^2}{2} \partial_x x \partial_x P(x, t) \quad (\text{A.46})$$

determining the *probability density*  $P(x, t)$  for the variable  $x(t)$ . The equation (A.46) has the *stationary probability density*

$$P_{st}(x) = \frac{1}{Z} x^{\frac{2\lambda}{\sigma^2}-1} \exp\left(-\frac{2x}{\sigma^2}\right)$$

(where  $Z$  is a normalization constant), with *two extrema*:

$$x_1 = 0, \quad x_2 = \lambda - \frac{\sigma^2}{2}.$$

**General Zero-Dimensional Model.** Now, following [van den Broeck *et al.* (1994); van den Broeck *et al.* (1997)], we consider the following SDE that generalizes noisy logistic equation (A.45),

$$\dot{x} = f(x) + g(x) \xi, \quad (\text{A.47})$$

where, as above,  $\xi = \xi(t)$  denotes the Gaussian white noise with first two moments

$$\langle \xi(t) \rangle = 0, \quad \langle \xi(t) \xi(t') \rangle = \sigma^2 \delta(t - t').$$

If we interpret equation (A.47) according to the Stratonovitch interpretation, we get the corresponding Fokker-Planck equation

$$\partial_t P(x, t) = -\partial_x [f(x) + P(x, t)] + \frac{\sigma^2}{2} \partial_x (g(x) \partial_x [g(x) P(x, t)]),$$

with the *steady-state solution*

$$P_{st}(x) = \frac{1}{Z} \exp\left(\int_0^x \frac{f(y) - \frac{\sigma^2}{2} g(y) g'(y)}{\frac{\sigma^2}{2} g^2(y)} dy\right), \quad (\text{A.48})$$

where  $g'(x)$  stands for the derivative of  $g(x)$  with respect to its argument. The extrema of the steady-state probability density obey the following equation

$$f(x) - \frac{\sigma^2}{2} g(x) g'(x) = 0. \quad (\text{A.49})$$

Note that this equation is not identical to the equation  $f(x) = 0$  for the steady states in the absence of multiplicative noise. As a result, the most probable states need not coincide with the deterministic stationary states.

More importantly, solutions can appear or existing solutions can be destabilized by the noise. These changes in the asymptotic behavior of the system have been generally named noise-induced phase transitions [Horsthemke and Lefever (1984)].

To illustrate this phenomenon, consider the case of a deterministically stable steady state at  $x = 0$ , e.g.,

$$f(x) = -x + o(x),$$

perturbed by a multiplicative noise. As is clear from equations (A.48–A.49), a noise term of the form

$$g(x) = 1 + x^2 + o(x^2)$$

will have a stabilizing effect, since

$$-(\sigma^2/2)g(x)g'(x) = -\sigma^2 x + o(x^2),$$

and it makes the coefficient of  $x$  more negative. On the other hand, noise of the form

$$g(x) = 1 - x^2 + o(x^2)$$

i.e., with maximal amplitude at the reference state  $x = 0$ , has the tendency to ‘destabilize’ the reference state. In fact, above a critical intensity  $\sigma^2 > \sigma_c^2 = 1$ , the stationary probability density will no longer have a maximum at  $x = 0$ , and ‘noise-induced’ maxima can appear. This phenomenon remains possible even if the deterministic steady-state equation, obtained by fixing the random value of the noise to a constant value  $\lambda$ , namely,  $f(x) + \lambda g(x) = 0$ , has a unique solution for all  $\lambda$  [van den Broeck *et al.* (1994); van den Broeck *et al.* (1997)].

Following the formalism for equilibrium states, it is tempting to introduce the notion of a ‘stochastic potential’  $U_{st}(x)$  by writing:

$$P_{st}(x) \sim \exp[-U_{st}(x)].$$

One concludes that for a system undergoing a noise-induced transition, e.g., for  $g(x) = 1 - x^2 + o(x^2)$ , and for  $\sigma^2 > \sigma_c^2$ , the stochastic potential has two minima. Consider now a spatially extended system obtained by coupling such units. The coupling is such that it favors the nearest-neighbor units, to stay at the same maximum of the probability density (minimum of the stochastic potential). In analogy to what happens for equilibrium models (such as the Landau–Ginzburg model), one expects that this system will

undergo a phase transition for some critical value of the ‘temperature’ (noise intensity)  $\sigma^2$ . However, it turns out that this is not the case. It was shown in [van den Broeck *et al.* (1994); van den Broeck *et al.* (1997)] that one needs a noise of precisely the other type, namely  $g(x) = 1 + x^2 + o(x^2)$ , to generate a genuine phase transition.

#### A.6.4.2 General $d$ -Dimensional System

The general model has been introduced in [van den Broeck *et al.* (1994); van den Broeck *et al.* (1997)]: a  $dD$  extended system of typical linear size  $L$  is restricted to a hypercubic lattice of  $N = L^d$  points, whereas time is still regarded as a continuous variable. The state of the system at time  $t$  is given by the set of stochastic variables  $\{x_i(t)\}$  ( $i = 1, \dots, N$ ) defined at the sites  $\mathbf{r}_i$  of this lattice, which obey a system of coupled ordinary SDEs (with implemented Stratonovich interpretation)

$$\dot{x}_i = f(x_i) + g(x_i)\eta_i + \frac{D}{2d} \sum_{j \in n(i)} (x_j - x_i), \quad (\text{A.50})$$

Equations (A.50) are the discrete version of the *partial* SDE which in the continuum would determine the state of the extended system: we recognize in the first two terms the generalization of Langevin’s equation for site  $i$  to the case of multiplicative noise ( $\eta_i$  is the *colored multiplicative noise* acting on site  $\mathbf{r}_i$ ). For the specific example, perhaps the simplest one exhibiting the transition under analysis,

$$f(x) = -x(1 + x^2)^2, \quad g(x) = 1 + x^2. \quad (\text{A.51})$$

The last term in (A.50) is the lattice version of the Laplacian  $\nabla^2 x$  of the extended stochastic variable  $x(\mathbf{r}, t)$  in a reaction–diffusion scheme.  $n(i)$  stands for the set of  $2d$  sites which form the immediate neighborhood of the site  $\mathbf{r}_i$ , and the coupling constant  $D$  between neighboring lattice sites is the diffusion coefficient.

Here we want to investigate the effects of the self-correlation time  $\tau$  of the multiplicative noise on the model system just described [Mangioni *et al.* (2000)]. To that end we must assume a specific form for the noises  $\{\eta_i = \eta_i(t)\}$ : we choose *Ornstein–Uhlenbeck noise*, i.e., Gaussian distributed stochastic variables with zero mean and exponentially decaying correlations,

$$\langle \eta_i(t) \eta_j(t') \rangle = \delta_{ij}(\sigma^2/2\tau) \exp(-|t - t'|/\tau). \quad (\text{A.52})$$

They arise as solutions of an *uncoupled* set of Langevin SDEs,

$$\tau \dot{\eta}_i = -\eta_i + \sigma \xi_i \quad (\text{A.53})$$

where the  $\{\xi_i = \xi_i(t)\}$  are white noises—namely, Gaussian stochastic variables with zero mean and  $\delta$ -correlated:

$$\langle \xi_i(t) \xi_j(t') \rangle = \delta_{ij} \delta(t - t').$$

For  $\tau \rightarrow 0$ , the Ornstein–Uhlenbeck noise  $\eta_i(t)$  approaches the white-noise limit  $\xi_i^W(t)$  with correlations

$$\langle \xi_i^W(t) \xi_j^W(t') \rangle = \sigma^2 \delta_{ij} \delta(t - t').$$

**Mean-Field Approximation.** The mean-field approximation here follows closely Curie–Weiss’ mean-field approach to magnetism (see [Mangioni *et al.* (2000)]), and consists in replacing the last term in (A.50)

$$\Delta_i \equiv \frac{D}{2d} \sum_{j \in n(i)} (x_j - x_i) \quad (\text{A.54})$$

by

$$\bar{\Delta}_i \equiv D(\bar{x} - x_i), \quad (\text{A.55})$$

where  $\bar{x}$  is the *order parameter* that will be determined self-consistently. In other words, the (short-ranged) interactions are substituted by a time- and space-independent ‘external’ field whose value *depends on the state* of the system. Since in this approximation equations (A.50) get immediately decoupled, there is no use in keeping the subindex  $i$  and we may refer to the systems in (A.50) and (A.53) as if they were single equations (Hereafter, the primes will indicate derivatives with respect to  $x$  (clearly  $\bar{\Delta}' = -D$ )).

If we take the time derivative of (A.50), replace first  $\dot{\eta}$  in terms of  $\eta$  and  $\xi$  from (A.53) and then  $\eta$  in terms of  $\dot{x}$  and  $x$  from (A.50), we get the following *non-Markovian* SDE:

$$\tau(\ddot{x} - \frac{g'}{g} \dot{x}^2) = - \left( 1 - \tau \left[ (f + \bar{\Delta})' - \frac{g'}{g} (f + \bar{\Delta}) \right] \right) \dot{x} + (f + \bar{\Delta}) + \sigma g \xi. \quad (\text{A.56})$$

Now, following [Mangioni *et al.* (2000)], we perform an *adiabatic elimination* of variables, namely, neglecting  $\ddot{x}$  and  $\dot{x}^2$ , so that the system’s dynamics becomes governed by a Fokker–Planck equation. The resulting



equation, being *linear* in  $\dot{x}$  (but not in  $x$ ), can be immediately solved for  $\dot{x}$ , giving

$$\dot{x} = Q(x; \bar{x}) + S(x; \bar{x})\xi, \quad (\text{A.57})$$

with

$$Q(x; \bar{x}) \equiv (f + \bar{\Delta})\theta, \quad (\text{A.58})$$

$$S(x; \bar{x}) \equiv \sigma g\theta, \quad (\text{A.59})$$

$$\theta(x; \bar{x}) \equiv \{1 - \tau g[(f + \bar{\Delta})/g]'\}^{-1}. \quad (\text{A.60})$$

The Fokker–Planck equation associated to the SDE (A.57) is

$$\partial_t P(x, t; \bar{x}) = -\partial_x [R_1(x; \bar{x})P(x, t; \bar{x})] + \frac{1}{2}\partial_x^2 [R_2(x; \bar{x})P(x, t; \bar{x})], \quad (\text{A.61})$$

with *drift* and *diffusion* coefficients given by

$$R_1(x; \bar{x}) = Q + \frac{1}{4}(S^2)' \quad (\text{A.62})$$

$$R_2(x; \bar{x}) = S^2. \quad (\text{A.63})$$

The solution of the time-independent Fokker–Planck equation leads to the stationary probability density

$$P_{st}(x; \bar{x}) = \frac{1}{Z} \exp \left[ \int_0^x dx' \frac{2R_1(x'; \bar{x}) - \partial_{x'} R_2(x'; \bar{x})}{R_2(x'; \bar{x})} \right]. \quad (\text{A.64})$$

The value of  $\bar{x}$  arises from a *self-consistency relation*, once we equate it to the average value of the random variable  $x_i$  in the stationary state

$$\bar{x} = \langle x \rangle \equiv \int_{-\infty}^{\infty} dx x P_{st}(x; \bar{x}) \equiv F(\bar{x}). \quad (\text{A.65})$$

Now, the condition

$$\left. \frac{dF}{d\bar{x}} \right|_{\bar{x}=0} = 1 \quad (\text{A.66})$$

allows us to find the *transition line* between the *ordered* and the *disordered phases*.

**Results.** The mean-field approximation of the general  $dD$  extended system are the following (see [Mangioni *et al.* (2000)]):

- (A) As in the white-noise case  $\tau = 0$ , the ordering phase transition is *reentrant with respect to  $\sigma$* : for a range of values of  $D$  that depends on  $\tau$ , ordered states can only exist within a window  $[\sigma_1, \sigma_2]$ . The fact

that this window shifts to the right for *small*  $\tau$  means that, for fixed  $D$ , color *destroys* order just above  $\sigma_1$  but *creates* it just above  $\sigma_2$ .

- (B) For fixed  $\sigma > 1$  and  $\tau \neq 0$ , ordered states exist *only within a window* of values for  $D$ . Thus the ordering phase transition is *also reentrant with respect to D*. For  $\tau$  small enough the maximum value of  $D$  compatible with the ordered phase increases rather steeply with  $\sigma$ , reaching a maximum around  $\sigma \sim 5$  and then decreases gently. For  $\tau \geq 0.1$  it becomes evident (in the ranges of  $D$  and  $\sigma$  analyzed) that the region sustaining the ordered phase is *closed*, and shrinks to a point for a value slightly larger than  $\tau = 0.123$ .
- (C) For fixed values of  $\sigma > 1$  and  $D$  larger than its minimum for  $\tau = 0$ , the system *always* becomes disordered for  $\tau$  large enough. The maximum value of  $\tau$  consistent with order altogether corresponds to  $\sigma \sim 5$  and  $D \sim 32$ . In other words, ordering is possible *only* if the multiplicative noise inducing it has short memory.
- (D) The fact that the region sustaining the ordered phase finally shrinks to a point means that even for that small region in the  $\sigma$ - $D$  plane for which order is induced by color, a further increase in  $\tau$  destroys it. In other words, the phase transition is *also reentrant with respect to  $\tau$* . For  $D$  large enough there may exist even *two* such windows.

**Order Parameter.** As already mentioned above, the *order parameter* in this system is  $m \equiv |\bar{x}|$ , namely, the positive solution of the consistency equation (A.65). Consistently with what has been discussed in (A) and (C), we see that as  $\tau$  increases the window of  $\sigma$  values where ordering occurs shrinks until it disappears. One also notices that at least for this  $D$ , the value of  $\sigma$  corresponding to the maximum order parameter varies very little with  $\tau$ .

The *short-time evolution* of  $\langle x \rangle$  can be obtained multiplying (A.61) by  $x$  and integrating:

$$\frac{d\langle x \rangle}{dt} = \int_{-\infty}^{\infty} dx R_1(x; \bar{x}) P(x, t; \bar{x}). \quad (\text{A.67})$$

Let us assume an initial condition such that at early times  $P(x, t \sim 0; \bar{x}) = \delta(x - \bar{x})$ . Equating  $\bar{x} = \langle x \rangle$  as before, we get the *order parameter equation*

$$\frac{d\langle x \rangle}{dt} = R_1(\bar{x}, \bar{x}). \quad (\text{A.68})$$

The solution of (A.68) has an initial *rising* period (it is initially *unstable*)

reaching very soon a maximum and tending to zero afterwards.

For  $D/\sigma^2 \rightarrow \infty$ , equation (A.68) is valid also in the *asymptotic regime* since  $P_{st}(x) = \delta(x - \bar{x})$  [van den Broeck *et al.* (1997)]. According to this criterion, in the  $D/\sigma^2 \rightarrow \infty$  limit the system undergoes a second-order phase transition *if* the corresponding zero-dimensional model presents a *linear instability in its short-time dynamics*, i.e., if after linearizing (A.68):

$$\langle \dot{x} \rangle = -\alpha \langle x \rangle, \quad (\text{A.69})$$

one finds that  $\alpha < 0$ . We then see that the trivial (disordered) solution  $\langle x \rangle = 0$  is stable only for  $\alpha > 0$ . For  $\alpha < 0$  other stable solutions with  $\langle x \rangle \neq 0$  appear, and the system develops order through a genuine *phase* transition. In this case,  $\langle x \rangle$  can be regarded as the *order parameter*. In the white noise limit  $\tau = 0$  this is known to be the case for sufficiently large values of the coupling  $D$  and for a window of values for the noise amplitude  $\sigma \in [\sigma_1, \sigma_2]$ .

In summary, we have:

- (A) Multiplicative noise can shift or induce phase transitions in 0D systems.
- (B) Multiplicative noise can induce phase transitions in spatially extended systems.
- (C) Mean-field approximation predicts a minimal coupling strength for the appearance of noise induced phase transitions.
- (D) Mean-field approximation predicts, that the phase transition is reentrant, i.e., the ordered phase is destroyed by even higher noise intensity.
- (E) Appearance of an ordered phase results from a nontrivial cooperative effect between multiplicative noise, nonlinearity and diffusion.

## A.7 *Mathematica*<sup>TM</sup> Derivation of Main Biodynamic Functions

### A.7.1 *Load-Lifting Biodynamics*

The expanded dissipative, driven Hamiltonian biodynamic system (4.152–4.153) was derived using the simple computer-algebra algorithm.

Algorithm is straightforward:

- (A) Topology of the mechanism on the momentum phase-space manifold  $M = T^*T^9$  is presented in the form of position vectors  $rkin_i$  and  $rpot_i$ , for kinetic and potential energies, respectively.

- (B) Hamiltonian function  $H(q, p) = KE(q, p) + PE(q)$  is formed as a sum of kinetic and potential energy, and dissipation function  $DF(q, p)$  is separately given.
- (C) Synergy of active muscular contractions is represented by the muscular-actuator torques  $F_i(t, q, p)$ .
- (D) Dissipative, driven Hamilton's equations  $\{\dot{q}^i = \dots\}$  and  $\{\dot{p}_i = \dots\}$  are derived according to (4.152–4.153).

Implementation of the algorithm in 'Mathematica' reads:

Number of DOF:

$n = 9;$

Position vectors for the potential and kinetic energies:

$\text{Do}[\text{rpot}[j] = \text{Sum}[\text{sg}[i] * L[i] * (1 - \text{Cos}[q[i]]), \{i, j\}], \{j, n\}];$

$\text{Do}[\text{rkin}[j] = \text{Sum}[L[i] * \text{Cos}[q[i]], \{i, j\}], \{j, n\}];$

Energies: potential, kinetic, dissipative, Hamiltonian:

$\text{PE} = \text{Sum}[m[i] * g * \text{rpot}[i], \{i, n\}];$

$\text{KE} = \text{Sum}[p[i]^2 / (m[i] * \text{rkin}[i]^2) + p[i]^2 / J[i], \{i, n\}] / 2;$

$\text{DF} = \text{Sum}[p[i]^2 * (a[i] + b[i] * q[i]^2), \{i, n\}] / 2;$

$\text{HAM} = \text{PE} + \text{KE};$

Muscular actuator torques:

$\text{Do}[\text{F}[i] = (\text{FF}[i] * \text{B}[i] - \text{A}[i] * p[i]) / (p[i] - \text{B}[i]) * (1 - \text{Exp}[-t/T[i]]) * \text{Exp}[-t/T[i]], \{i, n\}];$

Dissipative, driven Hamilton's equations of motion:

$\text{Do}[q'[i] = D[\text{HAM}, p[i]] + D[\text{DF}, q[i]], \{i, n\}];$

$\text{Do}[p'[i] = F[i] - D[\text{HAM}, q[i]] + D[\text{DF}, p[i]], \{i, n\}];$

$\text{Do}[\text{Print}["q'[", i, "] = ", q'[i]], \{i, n\}];$

$\text{Do}[\text{Print}["p'[", i, "] = ", p'[i]], \{i, n\}];$

## A.7.2 Brain-Like Control Functions

### A.7.2.1 Spinal FC-level

Total rotational DOF  $n$  and active DOF  $m$ :

$n = 75; \quad m = 22;$

Position vectors (including segmental lengths  $L_i$ ):

$\text{Table}[\text{rk}_j = \sum_{i=1}^j L_i \text{Cos}[q_i[t]], \{j, n\}];$

$\text{Table}[\text{rp}_j = \sum_{i=1}^j L_i ((1 - \text{Cos}[q_i[t]])), \{j, n\}];$

Potential and kinetic energies and dissipation (including segmental masses  $M_i$  and inertia moments  $J_i$ , as well as linear and quadratic dis-

sipation parameters  $a_i$  and  $b_i$ ):

$$\text{PE} = 9.81 \sum_{i=1}^n M_i r p_i;$$

$$\text{KE} = \frac{1}{2} \sum_{i=1}^n \left( \frac{p_i[t]^2}{M_i r k_j^2} + \frac{p_i[t]^2}{J_i} \right);$$

$$\text{DE} = \frac{1}{2} \sum_{i=1}^n p_i[t]^2 (a_i + b_i q_i[t]^2);$$

Inner Hamiltonian Ho:

$$\text{Ho} = \text{PE} + \text{KE};$$

Muscular covariant torques (for simplicity, modelled here as Gaussian bell-functions with amplitudes  $\text{ampl}_i$ , means  $\text{mean}_i$ , and standard deviations  $\text{stdv}_i$ ):

$$\text{Table}[F_i = \text{ampl}_i \text{Exp}\left[-\frac{(t - \text{mean}_i)^2}{2 \text{stdv}_i^2}\right], \{i, n\}];$$

Test affine inputs (for simplicity, modelled here in the periodical sinus form with amplitudes  $\alpha$ , phases  $\beta_k$ , and frequencies  $\gamma_k$ ):

$$\text{Table}[u_k[t] = \alpha_k \text{Sin}[\beta_k + \gamma_k t], \{k, m\}];$$

Coupling (interaction) Hamiltonians  $\text{HI}_k$ :

$$\text{Table}[\text{HI}_k = q_k[t] q_{k-1}[t], \{k, m\}];$$

Affine Hamiltonian HA:

$$\text{HA} = \text{Ho} - \sum_{i=1}^m \text{HI}_k u_k[t];$$

Affine In-Out Hamiltonian equations:

$$\begin{aligned} \text{Eqns}_A = \text{Table}[\{ \\ q'_i[t] &= \partial_{p_i[t]} \text{Ho} - \sum_{k=1}^m \partial_{p_k[t]} \text{HI}_k u_k[t] + \partial_{q_i[t]} \text{DE}, \\ p'_i[t] &= F_i - \partial_{q_i[t]} \text{HA} + \sum_{k=1}^m \partial_{q_k[t]} \text{HI}_k u_k[t] + \partial_{p_i[t]} \text{DE}, \\ \}, \{i, n\}]; \end{aligned}$$

Affine outputs  $o_k$ :

$$\text{Table}[o_k[t] = \text{HI}_k, \{k, m\}];$$

Lie derivative function defined through gradient operator:

$$\text{Grad}[s, x\_List] := \partial_{\#} s \&/\& @ x;$$

$$\text{LieDer}[v\_List, s, x\_List] := \text{Grad}[s, x] . v;$$

Hamiltonian version of the standard MIMO  $f$  and  $g$  vector-fields defined:

$$f = \text{Table}[\{\partial_{p_i[t]} \text{Ho}, -\partial_{q_i[t]} \text{Ho}\}, \{i, n\}];$$

$$g = \text{Table}[\{-\partial_{p_i[t]} \text{HI}_k, \partial_{q_i[t]} \text{HI}_k\}, \{i, n\}, \{k, m\}];$$

Control law for tracking reference output trajectories  $oR_k[t]$  with coefficients  $c_k$  (for simplicity, we take relative degree  $r = 1$ , using only first Lie derivatives):

$$X = \{q_i[t], p_i[t]\};$$

$$\begin{aligned} \text{Table}[ \\ u_k[t] &= oR'_k[t] - \\ \text{LieDer}[f, \text{HI}_k, X] + c_k(oR_k[t] - o_k[t]) / \text{LieDer}[g, \text{HI}_k, X], \end{aligned}$$

$\{k, m\}$ };

(In the general case of  $r \neq 1$ , we would need  $r$ th-order recursive Lie derivatives:

$\text{Lie2Der}[f, \text{HI}_k, X] = \text{LieDer}[f, \text{LieDer}[f, \text{HI}_k, X], X], \dots)$

Provided all the parameters, as well as initial angles and momenta are given, the numerical solution could be obtained using NDSolve, the powerful built-in ODE solver:

$\text{Sol}_A$   
 $= \text{NDSolve}[\text{Eqns}_A, \text{Flatten}[\text{Table}[\{q_i, p_i\}, \{i, n\}], \{t, Tfin\}], \text{MaxSteps} \rightarrow 10000];$

#### A.7.2.2 Cerebellar FC-level

Set up ( $n$  = number of neurons in each neural activation field, equal to the total humanoid DOF,  $Tfin$  is the duration of each simulation,  $Iter$  is number of iterations):

$n = 75; \quad Tfin = .01; \quad Iter = 100;$

Defined excitatory and inhibitory inputs for each joint:

$\text{Table}[A_i[q_-] := K_q (q_i[t] - qR_i[t]), \{i, n\}];$

$\text{Table}[B_i[p_-] := K_p (pR_i[t] - p_i[t]), \{i, n\}];$

Hyperbolic tangent activation functions defined:

$\text{Do}[Sx_i = \text{Tanh}[x^i[t]], \{i, n\}];$

$\text{Do}[Sy_i = \text{Tanh}[y_i[t]], \{i, n\}];$

Derivatives of activation functions defined:

$\text{Do}[Sdx_i = 1 - Sx_i^2, \{i, n\}];$

$\text{Do}[Sdy_i = 1 - Sy_i^2, \{i, n\}];$

Synaptic weights initialized as random  $[-1, 1]$  numbers:

$\text{Do}[\{W_{i,j} = \text{Random}[\text{Real}, \{-1, 1\}]\}, \{i, n\}, \{j, n\}];$

Noise tensor  $\sigma_{i,j}$  defined simply as a random matrix:

$\text{Do}[\{\sigma_{i,j} = \text{Random}[\text{Real}, \{0, 1\}]\}, \{i, n\}, \{j, n\}];$

Main loop - all  $x, y$  and  $\omega$  equations are, for the zero initial activations and random initial weights, numerically solved using the sophisticated ODE-solver NDSolve, to give control torques  $F$ :

$\text{For}[\text{LoopVar} = 1, \text{LoopVar} \leq Iter, \quad (* \text{ loop start } *)$

$\text{Eqns} = \text{Flatten}[\text{Join}[$

$\text{Table}[\{ \quad \quad \quad (* X \text{ equation } *)$

$x^i[t] == A_i[q] - x^i[t] + \sum_{j=1}^m Sy_i \omega_{i,j}[t],$

$x^i[0] == 0$

$\}, \{i, n\} \quad ],$

```

Table[{
    (* Y equation *)
     $y'_i[t] == B_i[p] - y'_i[t] + \sum_{j=1}^m Sx_i \omega_{i,j}[t],$ 
     $y_i[0] == 0$ 
}, {i, n} ],
Table[{
    (* W equation *)
     $\omega'_{i,j}[t] == -\omega_{i,j}[t] + Sq_i Sp_j$ 
     $+ Sdq_i Sdp_j + \sigma_{i,j},$ 
     $\omega_{i,j}[0] == W_{i,j}, \{i, n\}, \{j, n\}$ 
}];
Sol = NDSolve[
    Eqns, Flatten[
        Join[
            Table[xi, {i, n}],
            Table[yi, {i, n}],
            Table[ $\omega_{i,j}$ , {i, n}, {j, n}]
        ], {t, 0, Tfin},
    StartingStepSize → 10-7
];
(* using the final values of x, y and  $\omega$ 
as initial conditions for the next person *)
Do[Xi = Evaluate[xi[Tfin] /. Sol][[1]], {i, n}];
Do[Yi = Evaluate[yi[Tfin] /. Sol][[1]], {i, n}];
Do[Wi,j = Evaluate[ $\omega_{i,j}$ [Tfin] /. Sol][[1]], {i, n}, {j, n}];

(* print output control 1-forms in each iteration *)
Print[Table[ui =  $\frac{1}{2}(X_i + Y_i)$ , {i, n}]];

LoopVar++] (* loop end *)

```

### A.7.2.3 Cortical FC-level

Defining a Gaussian-bell curve  $\mu$  with mean  $m$  and standard deviation  $\sigma$ :

$$\mu[x_-, m_-, \sigma_-] := \text{Exp}\left[-\frac{(x-m)^2}{2\sigma^2}\right];$$

The universe of discourse  $Dq$  and the fuzzy sets  $qSets[q]$  for the rectified and discretized input angle  $q$  are defined as:

$$Qmin = \text{Min}[q[t]]; \quad Qmax = \text{Max}[q[t]]; \quad$$

$$Dq = Qmax - Qmin;$$

$$mQ1 = .05Dq + Qmin; \quad qNL[q_-] := \mu[q, mQ1, \sigma Q];$$

$$mQ2 = .16Dq + Qmin; \quad qNB[q_-] := \mu[q, mQ2, \sigma Q];$$

$$\begin{aligned}
mQ3 &= .27Dq + Qmin; & qNM[q_-] &:= \mu[q, mQ3, \sigma Q]; \\
mQ4 &= .38Dq + Qmin; & qNS[q_-] &:= \mu[q, mQ4, \sigma Q]; \\
mQ5 &= .50Dq + Qmin; & qZE[q_-] &:= \mu[q, mQ5, \sigma Q]; \\
mQ6 &= .62Dq + Qmin; & qPS[q_-] &:= \mu[q, mQ6, \sigma Q]; \\
mQ7 &= .73Dq + Qmin; & qPM[q_-] &:= \mu[q, mQ7, \sigma P]; \\
mQ8 &= .84Dq + Qmin; & qPB[q_-] &:= \mu[q, mQ8, \sigma Q]; \\
mQ9 &= .95Dq + Qmin; & qPL[q_-] &:= \mu[q, mQ9, \sigma Q]; \\
\sigma Q &= .1Uq; \\
qSets[q_-] &:= \{qNL[q], qNB[q], qNM[q], qNS[q], qZE[q], \\
&\quad qPS[q], qPM[q], qPB[q], qPL[q]\};
\end{aligned}$$

The universe of discourse  $Dp$  and the fuzzy sets  $pSets[p]$  for the rectified and discretized input momentum  $p$  are defined as:

$$\begin{aligned}
Pmin &= \text{Min}[p[t]]; & Pmax &= \text{Max}[p[t]]; \\
Dp &= Pmax - Pmin; \\
mP1 &= .05Dp + Pmin; & pNL[p_-] &:= \mu[p, mP1, \sigma P]; \\
mP2 &= .16Dp + Pmin; & pNB[p_-] &:= \mu[p, mP2, \sigma P]; \\
mP3 &= .27Dp + Pmin; & pNM[p_-] &:= \mu[p, mP3, \sigma P]; \\
mP4 &= .38Dp + Pmin; & pNS[p_-] &:= \mu[p, mP4, \sigma P]; \\
mP5 &= .50Dp + Pmin; & pZE[p_-] &:= \mu[p, mP5, \sigma P]; \\
mP6 &= .62Dp + Pmin; & pPS[p_-] &:= \mu[p, mP6, \sigma P]; \\
mP7 &= .73Dp + Pmin; & pPM[p_-] &:= \mu[p, mP7, \sigma P]; \\
mP8 &= .84Dp + Pmin; & pPB[p_-] &:= \mu[p, mP8, \sigma P]; \\
mP9 &= .95Dp + Pmin; & pPL[p_-] &:= \mu[p, mP9, \sigma P]; \\
\sigma P &= .1Dp; \\
pSets[p_-] &:= \{pNL[p], pNB[p], pNM[p], pNS[p], pZE[p], \\
&\quad pPS[p], pPM[p], pPB[p], pPL[p]\};
\end{aligned}$$

The universe of discourse  $Du$  and the fuzzy sets  $uSets[u]$  for the rectified and discretized output control  $u$  are defined as:

$$\begin{aligned}
Umin &= \text{Min}[u[t]]; & Umax &= \text{Max}[u[t]]; \\
Du &= Umax - Umin; \\
mU1 &= .05Du + Umin; & uNL[u_-] &:= \mu[u, mU1, \sigma U]; \\
mU2 &= .16Du + Umin; & uNB[u_-] &:= \mu[u, mU2, \sigma U]; \\
mU3 &= .27Du + Umin; & uNM[u_-] &:= \mu[u, mU3, \sigma U]; \\
mU4 &= .38Du + Umin; & uNS[u_-] &:= \mu[u, mU4, \sigma U]; \\
mU5 &= .50Du + Umin; & uZE[u_-] &:= \mu[u, mU5, \sigma U]; \\
mU6 &= .62Du + Umin; & uPS[u_-] &:= \mu[u, mU6, \sigma U]; \\
mU7 &= .73Du + Umin; & uPM[u_-] &:= \mu[u, mU7, \sigma U]; \\
mU8 &= .84Du + Umin; & uPB[u_-] &:= \mu[u, mU8, \sigma U]; \\
mU9 &= .95Du + Umin; & uPL[u_-] &:= \mu[u, mU9, \sigma U];
\end{aligned}$$



$$\sigma P = .1Du;$$

$$uSets[u] := \{uNL[u], uNB[u], uNM[u], uNS[u], uZE[u], \\ uPS[u], uPM[u], uPB[u], uPL[u]\};$$

The  $9 \times 9$  FAM (fuzzy associative memory) matrix is defined as:

$$FAM[u] :=$$

$$\begin{pmatrix} .6 uNL[u] & .6 uNL[u] & \dots & .9 uNS[u] & uZE[u] \\ .6 uNL[u] & .7 uNB[u] & \dots & uZE[u] & .9 uPS[u] \\ .7 uNB[u] & .7 uNB[u] & \dots & .9 uPS[u] & .9 uPS[u] \\ .7 uNB[u] & .8 uNM[u] & \dots & .9 uPS[u] & .8 uPM[u] \\ .8 uNM[u] & .8 uNM[u] & \dots & .8 uPM[u] & .8 uPM[u] \\ .8 uNM[u] & .9 uNS[u] & \dots & .8 uPM[u] & .7 uPB[u] \\ .9 uNS[u] & .9 uNS[u] & \dots & .7 uPB[u] & .7 uPB[u] \\ .9 uNS[u] & uZE[u] & \dots & .7 uPB[u] & .6 uPL[u] \\ uZE[u] & .9 uPS[u] & \dots & .6 uPL[u] & .6 uPL[u] \end{pmatrix}$$

Implementing the discrete form of the centroid defuzzification  $u_C = \int \mu(u) du / \int du :$

$$defuzzify[fuzzySet, \{u, min, max, du\}] := \\ Sum[t * fuzzySet, \{u, min, max, du\}] / \\ Sum[fuzzySet, \{u, min, max, du\}];$$

Defuzzification of output controls:

$$Uout[q, p] := defuzzify[Max[Flatten[ \\ MapThread[Min, \{Outer[Min, qSets[q], \\ pSets[p]], FAM[u]\}, 2]]] \\ /.Min[0, _] \rightarrow 0, \{u, Umin, Umax, .1Du\}];$$

### A.7.3 Anatomical Description of Human Movements

#### A.7.3.1 Movements in Synovial Joints

- ankleMov = {dorsi\_flexion[right\_ankle], plantar\_flexion[right\_ankle], supination[right\_ankle], pronation[right\_ankle], dorsi\_flexion[left\_ankle], plantar\_flexion[left\_ankle], supination[left\_ankle], pronation[left\_ankle]};
- kneeMov = {flexion[right\_knee], extension[right\_knee], lateral\_rotation[right\_knee], medial\_rotation[right\_knee], flexion[left\_knee], extension[left\_knee], lateral\_rotation[left\_knee], medial\_rotation[left\_knee]};
- hipMov = {flexion[right\_hip], extension[right\_hip], abduction[right\_hip], adduction[right\_hip], lateral\_rotation[right\_hip], medial\_rotation[right\_hip], flexion[left\_hip], extension[left\_hip], abduction[left\_hip], adduction[left\_hip], lateral\_rotation[left\_hip], medial\_rotation[left\_hip]};
- spineMov = {flexion[spine], extension[spine], left\_lateral\_flexion[spine],

right\_lateral\_flexion[spine], left\_rotation[spine], right\_rotation[spine]);

- neckMov = {flexion[neck], extension[neck], left\_lateral\_flexion[neck], right\_lateral\_flexion[neck], left\_rotation[neck], right\_rotation[neck]};
- shoulderMov = {flexion[right\_shoulder], extension[right\_shoulder], abduction[right\_shoulder], adduction[right\_shoulder], lateral\_rotation[right\_shoulder], medial\_rotation[right\_shoulder], elevation[right\_shoulder], depression[right\_shoulder], flexion[left\_shoulder], extension[left\_shoulder], abduction[left\_shoulder], adduction[left\_shoulder], lateral\_rotation[left\_shoulder], medial\_rotation[left\_shoulder], elevation[left\_shoulder], depression[left\_shoulder]};
- elbowMov = {flexion[right\_elbow], extension[right\_elbow], supination[right\_elbow], pronation[right\_elbow], flexion[left\_elbow], extension[left\_elbow], supination[left\_elbow], pronation[left\_elbow]};
- wristMov = {dorsi\_flexion[right\_wrist], palmar\_flexion[right\_wrist], medial\_flexion[right\_wrist], lateral\_flexion[right\_wrist], dorsi\_flexion[left\_wrist], palmar\_flexion[left\_wrist], medial\_flexion[left\_wrist], lateral\_flexion[left\_wrist]};
- baseMovements = {ankleMov, kneeMov, hipMov, spineMov, neckMov, shoulderMov, elbowMov, wristMov} // Flatten
- rangeAmplitude = {full\_amplitude, big\_amplitude, half\_amplitude, smallAmplitude};
- rangeMovements = Table[Map[rangeAmplitude[[i]], baseMovements], {i, Length[rangeAmplitude]}] // Flatten;
- speed = {extremely\_fast, very\_fast, moderately\_fast, slow, very\_slow, extremely\_slow};
- RSJM = Table[Map[speed[[i]], rangeMovements], {i, Length[speed]}] // Flatten;

### A.7.3.2 Examples of Sport Movements

- Sprint running:  
rightLegJump = RSJM[[2]] & & RSJM[[10]] & & RSJM[[18]]; leftLegSwing = RSJM[[23]] & & RSJM[[13]] & & RSJM[[5]]; rightArmForw = RSJM[[185]] & & RSJM[[777]] & & fixed[right\_wrist]; leftArmBack = RSJM[[194]] & & RSJM[[782]] & & fixed[left\_wrist]; fixed[spine] & & fixed[neck];
- High Jump – take off:  
rightLegJump = RSJM[[2]] & & RSJM[[10]] & & RSJM[[18]]; leftLegSwing = RSJM[[23]] & & RSJM[[13]] & & RSJM[[5]]; rightArm = RSJM[[41]] & & RSJM[[777]] & & fixed[right\_wrist]; spineMov = RSJM[[318]] & & RSJM[[321]]; neckMov = RSJM[[324]] & & RSJM[[471]];
- Freestyle swimming:  
rightArmIn = RSJM[[617]] & & RSJM[[618]] & & RSJM[[777]] & &

```
RSJM[[778]] && RSJM[[780]] && fixed[right_wrist]; leftArmOut =
RSJM[[627]] & & RSJM[[625]] & & RSJM[[781]] && RSJM[[784]] &&
fixed[left_wrist]; spinNeck = RSJM[[753]] & & RSJM[[759]] & & RSJM[[754]]
& & RSJM[[760]]; rightLeg = RSJM[[815]] & & RSJM[[733]] && RSJM[[816]]
& & RSJM[[734]] && relaxed[left_ankle];
```

- Freestyle swimming start – take off:

```
rightLegJump = RSJM[[2]] & & RSJM[[10]] && RSJM[[18]]; rightArm =
RSJM[[41]] && RSJM[[777]] && fixed[right_wrist]; spineMov = RSJM[[318]];
neckMov = RSJM[[755]];
```

- Backstroke swimming:

```
rightArmIn = RSJM[[618]] & & RSJM[[617]] && RSJM[[777]] &&
RSJM[[778]] && RSJM[[780]] && fixed[right_wrist]; leftArmOut =
RSJM[[625]] & & RSJM[[638]] & & RSJM[[784]] && fixed[left_wrist];
spineNeck = RSJM[[606]] & & fixed[neck]; rightLeg = RSJM[[815]] & &
RSJM[[733]] && RSJM[[816]] & & RSJM[[734]] && relaxed[left_ankle];
```

- Butterfly swimming:

```
rightArmIn = RSJM[[617]] && RSJM[[618]] & & RSJM[[777]] &&
RSJM[[778]] && RSJM[[780]] && RSJM[[619]] && RSJM[[617]] &&
RSJM[[780]] && fixed[right_wrist]; spinNeck = RSJM[[606]] & &
RSJM[[755]]; rightLeg = RSJM[[743]] & & RSJM[[733]] && RSJM[[816]]
& & RSJM[[302]] && relaxed[left_ankle];
```

- Tennis serve:

```
rightArmSrv = RSJM[[617]] && RSJM[[633]] && RSJM[[42]] &&
RSJM[[58]] && fixed[right_wrist]; leftArm = RSJM[[625]] && RSJM[[638]]
&& RSJM[[50]] && RSJM[[781]] && relaxed[right_wrist]; spineNeck =
RSJM[[749]] & & RSJM[[753]] & & fixed[neck]; rightLeg = RSJM[[306]] &
& relaxed[right_knee] & & relaxed[right_ankle]; leftLeg = RSJM[[294]] & &
RSJM[[302]] && RSJM[[312]].
```

# Bibliography

- Ablowitz, M.J., Clarkson, P.A. (1991). Solitons, nonlinear evolution equations and inverse scattering. London Math. Soc., **149**, CUP, Cambridge.
- Abraham, R., Marsden, J. (1978). Foundations of Mechanics. Benjamin, Reading.
- Abraham, R., Marsden, J., Ratiu, T. (1988). Manifolds, Tensor Analysis and Applications. Springer, New York.
- Abraham, R., Shaw, C. (1992). Dynamics: the Geometry of Behavior. Addison-Wesley, Reading.
- Acheson, D. (1997). From Calculus to Chaos. Oxford Univ. Press, Oxford.
- Ahmed, E., Elgazzar, A.S., Hegazi, A.S. (2005). An Overview of Complex Adaptive Systems. Mansoura J. Math. (to appear).
- Aidman, E.V., Leontiev, D.A. (1991). From being motivated to motivating oneself: a Vygotskian perspective. Stud. Sov. Thought, **42**, 137–151.
- Ajemian, R., Bullock, D., Grossberg, S. (2000). Kinematic coordinates in which motor cortical cells encode movement direction. J. Neurophysiol., **84**, 2191–2203.
- Ahmad, S. (1993). On the nonautonomous Volterra–Lotka competition equations. Proc. Amer. Math. Soc., **117**, 199–205.
- Aleshinsky, S.Y., Zatsiorsky, V.M. (1978). Human locomotion in space analysed biomechanically through a multi-link chain model. J. Biomech., **11**, 101–108.
- Alfinito, E., Vitiello, G., (2000). Formation and life-time of memory domains in the dissipative quantum model of brain, Int. J. Mod. Phys. B, **14**, 853–868.
- Amari, S. (1972). Characteristics of random nets of analog neuron-like elements. IEEE Trans. Syst. Man Cybern. SMC-2, **5**, 643–657.
- Amaral, L.A.N., Goldberger, A.L., Ivanov, P.Ch., Stanley, H.E. (1998). Scale-independent measures and pathologic cardiac dynamics. Phys. Rev. Lett., **81**, 2388–2391.
- Amit, D.J. (1989). Modelling Brain Function. Cambridge Univ. Press, Cambridge.
- Anderson, B.D., Arbib, M.A., Manes, E.G. (1976). Foundations of System Theory: Finitary and Infinitary Conditions. Lecture Notes in Economics and Mathematical Systems Theory, Springer, New York.
- Andrecut, M. (2001). Biomorphs, program for *Mathcad*<sup>TM</sup>, Mathcad Application

Files, Mathsoft.

- Anochin, P.K. (1980). *Theory of Functional Systems*, (in Russian). Science, Moscow.
- Anosov, D.V., Sinai, Ya.G. (1982). Certain smooth ergodic systems. *Russ. Math. Surv.*, **22**, 103–167.
- Anosov, D. (1969). Geodesic flows on closed Riemann manifolds with negative curvature. *Proc. Steklov Inst. Math.*, **90**, Amer. Math. Soc.
- Antoni, M., Ruffo, S. (1995). Clustering and relaxation in long-range Hamiltonian dynamics. *Phys. Rev. E*, **52**, 2361–2374.
- Aoyagi, T., Nomura, M. (1999). Oscillator Neural Network Retrieving Sparsely Coded Phase Patterns. *Phys. Rev. Lett.* **83**, 1062–1065.
- Apps, R., Garwicz, M. (2005). Anatomical and physiological foundations of cerebellar information processing. *Nature Rev. Neurosci.*, **6**, 297–311.
- Arbib, M.A. (1966). Categories of  $(M, R)$ –systems. *Bull. Math. Biol.*, **28**, 511–517.
- Arbib, M. (1987). *Brains, Machines and Mathematics*. Springer.
- Arbib, M. (ed.) (1998). *Handbook of Brain Theory and Neural Networks* (2nd ed.). MIT Press, Cambridge.
- Arcas, B.A., Fairhall, A.L., Bialek, W. (2003). Computation in a Single Neuron: Hodgkin and Huxley Revisited. *Neural Computation*, **15**(8), 1715–1750.
- Arnold, V.I. (1978). *Ordinary Differential Equations*. MIT Press, Cambridge.
- Arnold, V.I. (1988). *Geometrical Methods in the Theory of Ordinary differential equations*. Springer, New York.
- Arnold, V.I. (1989). *Mathematical Methods of Classical Mechanics* (2nd ed). Springer, New York.
- Arnold, V.I. (1992). *Catastrophe Theory*. Springer, Berlin.
- Arnold, V.I. (1993). *Dynamical systems*. *Encyclopaedia of Mathematical Sciences*, Springer, Berlin.
- Ashcraft, M.H. (1994). *Human Memory and Cognition* (2nd ed). HarperCollins, New York.
- Asif, A. (2004). Fast implementations of the Kalman–Bucy filter for satellite data assimilation. *IEEE Sig. Proc. Lett.*, **11**(2), 235–238.
- Atkeson, C.G., Hale J., Pollick F., Riley M., Kotosaka S., Schaal S., Shibata T., Tevatia G., Vijayakumar S., Ude A., Kawato M. (2000) Using humanoid robots to study human behavior. *IEEE Intelligent Systems: Special Issue on Humanoid Robotics*, **15**, 46–56.
- Axelrod, R. (1984). *The Evolution of Cooperation*. Basic Books, New York.
- Baez, J. (1997). An introduction to  $n$ –categories. *7th Conference on Category Theory and Computer Science*, E. Moggi and G. Rosolini (eds), *Lecture Notes in Computer Science*, Springer, Berlin.
- Baez, J., Dolan, J. (1995). Higher dimensional algebra and topological quantum field theory. *J. Math. Phys.* **36**, 6073–6105.
- Baez, J., Dolan, J. (1998). Higher–Dimensional Algebra III:  $n$ –categories and the Algebra of Opetopes. *Adv. Math.* **135**(2), 145–206.
- Baez, J. (2002). Categorified gauge theory. *Lecture in the Joint Spring Meeting of the Pacific Northwest Geometry Seminar and Cascade Topology Seminar*.

- von Baeyer, H.C. (1998). All Shook Up. *The Sciences*, **38**(1), 12–14.
- Baker, G.L., Gollub, J.P. (1996). *Chaotic Dynamics: An Introduction* (2nd ed.), Cambridge Univ. Press, Cambridge.
- Banaszuk, A., Hauser, J. (1996). Approximate feedback linearization: a homotopy operator approach. *SIAM J. Cont. & Optim.*, **34**(5), 1533–1554.
- Barhen, J., Dress, W.B., and Jorgensen, C.C. (1989). Applications of Concurrent Neuromorphic Algorithms for Autonomos Robots. in *Neural computers* (ed. Eckmiller, R., Malsburg, C.) Springer, Berlin.
- Barreira, L. (1996). A non-additive thermodynamic formalism and applications to dimension theory of hyperbolic dynamical systems. *Ergodic Theory Dynam. Systems* **16**, 871–927.
- Barreira, L., Pesin, Y. (2002). *Lyapunov Exponents and Smooth Ergodic Theory*, Univ. Lecture Series 23, Am. Math. Soc.
- Barrow-Green, J. (1997). *Poincaré and the Three Body Problem*. American Mathematical Society, Providence, RI.
- Barry, J.C. (1993). *Matrices, Monads and the Fast Fourier Transform*. Univ. Tech., Sidney.
- Bar-Yam, Y. (1997). *Dynamics of Complex Systems*. Perseus Books, Reading.
- Basser, P.J., Mattiello, J., Le Bihan, D. (1994). MR diffusion tensor spectroscopy and imaging. *Biophys. J.* **66**, 259–267.
- Basser, P.J., Pierpaoli, C. (1996). Microstructural and physiological features of tissues elucidated by quantitative–diffusion–tensor MRI. *J. Magn. Reson. B*, **111**, 209–219.
- Bellet, L.R., Thomas, L.E. (2000). Asymptotic Behavior of Thermal Non-Equilibrium Steady States for a Driven Chain of Anharmonic Oscillators. *Commun. Math. Phys.* **215**, 1–24.
- Benvenuto, N., Piazza, F. (1992). On the complex backpropagation algorithm. *IEEE Trans. Sig. Proc.*, **40**(4), 967–969.
- Berleant, D., Kuipers, B. (1992). Qualitative–Numeric Simulation with Q3, in *Recent Advances in Qualitative Physics*. eds. Boi Faltings and Peter Struss, MIT Press, Cambridge.
- Bénabou, J., (1967). *Introduction to bicategories*. In: *Lecture Notes in Mathematics*. Springer, New York.
- Bernstein, N.A. (1935). *Investigations in Biodynamics of Locomotion* (in Russian). WIEM, Moscow.
- Bernstein, N.A. (1947). *On the structure of motion* (in Russian). Medgiz, Moscow.
- Bernstein, N.A. (1967). *The Coordination and Regulation of Movement*. Pergamon Press, Oxford.
- Bernstein, N. (1982). Some emergent problems of the regulation of motor acts. In: H.T.A. Whiting (Ed) *Human Motor Actions: Bernstein Reassessed*, North Holland, Amsterdam.
- Bigland-Ritchie, B., Rice, C.L., Garland, S.J. and Walsh, M.L. (1995). Task-dependent factors in fatigue of human voluntary contractions. In: *Fatigue* (Ed. S.C. Gandevia), Plenum, 361–380.
- Bielawski, S., Derozier, D., Glorieux, P. (1993). Experimental characterization of unstable periodic orbits by controlling chaos. *Phys. Rev. A*, **47**, 2492.

- Billingsley, P. (1965). *Ergodic theory and information*, Wiley, New York.
- Boccaletti, S., Grebogi, C., Lai, Y.-C., Mancini, H., Maza, D. (2000). The Control of Chaos: Theory and Applications. *Physics Reports* **329**, 103–197.
- Boccaro, N. (2004). *Modeling complex systems*. Springer, Berlin.
- Boffetta, G., Cencini, M., Falcioni, M., Vulpiani, A. (2002). Predictability: a way to characterize Complexity, *Phys. Rep.*, **356**, 367–474.
- Borelli, R.L., Coleman, C., Boyce, W.E. (1992). *Differential Equations Laboratory Workbook*. Wiley, New York.
- Brin, M. (1981). Bernoulli diffeomorphisms with nonzero exponents. *Ergod. Th. Dyn. Syst.*, **1**, 1–7.
- Brooks, V.B. (1986). *The Neural Basis of Motor Control*. Oxford Univ. Press, New York.
- Bontempi, G. (1995). Modelling with uncertainty in continuous dynamical systems: the probability and possibility approach. IRIDIA - ULB Technical Report, 95–16.
- Braitenberg, V., Shulz, A. (1991). *Anatomy of the Cortex*. Springer, Berlin.
- Bransford, J.D., Franks, J.J. (1971). The Abstraction of Linguistic Ideas. *Cogn. Psych.*, **2**, 331–350.
- Brockett, R. (2001). New Issues in the Mathematics of Control. In *Mathematics Unlimited – 2001 and Beyond*, Springer, New York.
- Broadbent, D.E. (1958). *Perception and communications*. Pergamon Press, London.
- Brown, M., Harris, C. (1994). *Neurofuzzy Adaptive Modelling and Control*, Prentice Hall, New York.
- Bryant, R., Griffiths, P., Grossman, D. (2003). *Exterior Differential Systems and Euler–Lagrange Partial differential Equations*. Univ. Chicago Press, Chicago.
- Burdet, E., Osu, R., Franklin, D., Milner, T., Kawato, M. (2001). The central nervous system stabilizes unstable dynamics by learning optimal impedance. *Nature*, **414**, 446–449.
- Burnfield, J.M., Few, C.D., Tsai, J., Powers, C.M. (2003). Prediction of Peak Utilized Coefficient of Friction Requirements During Walking Based on Center of Mass Kinematics, *Proceedings of ISB'03*, Univ. Otago, Dunedin.
- Busmeyer, J.R., Townsend, J.T. (1993). Decision field theory: A dynamic-cognitive approach to decision making in an uncertain environment. *Psych. Rev.*, **100**, 432–459.
- Busmeyer, J.R., Diederich, A., (2002). Survey of decision field theory. *Math. Soc. Sci.*, **43**, 345–370.
- Calvo, O. (1998). Fuzzy Control of Chaos. *Int. J. Bif. Chaos*, **8**, 1743–1747.
- Cao, H.D., Chow, B. (1999). Recent Developments on the Ricci Flow. *Bull. Amer. Math. Soc.* **36**, 59–74.
- Carpenter, G.A., Grossberg, S. (2003). Adaptive Resonance Theory. In M.A. Arbib (Ed.), *The Handbook of Brain Theory and Neural Networks*, Second Edition, Cambridge, MA: MIT Press, 87–90.
- Casetti, L., Cohen, E.G.D., Pettini, M. (1999). Origin of the Phase Transition in a Mean-Field Model. *Phys. Rev. Lett.*, **82**, 4160.

- Casetti, L., Pettini, M., Cohen, E.G.D. (2003). Phase transitions and topology changes in configuration space. *J. Stat. Phys.*, **111**, 1091.
- Celeghini, E., Rasetti, M., Vitiello, G. (1992). Quantum Dissipation. *Annals Phys.*, **215**, 156.
- Channon, P., Hopkins, S. and Pham, D. (1996). A variational approach to the optimization of gait for a bipedal robot. *J. Mech. Eng. Sci.*, **210**, 177–186.
- Chen, G., Dong, X. (1998). *From Chaos to Order. Methodologies, Perspectives and Application*. World Scientific, Singapore.
- Chevalley, C. (1955). *Theorie differential equations groupes de Lie*. vol. 1–3. Hermann D.C., Paris.
- Chiel, H.J., Beer, R.D., Quinn, R.D., Espenschied, K.S. (1992). Robustness of a distributed neural network controller for locomotion in a hexapod robot. *IEEE Trans. Rob. Aut.*, **8**, 293–303.
- Cho, M.W., Kim, S. (2004). Understanding visual map formation through vortex dynamics of spin Hamiltonian models. *Phys. Rev. Lett.* 92(1), 18101.
- Choquet-Bruhat, Y., DeWitt-Morete, C. (1982). *Analysis, Manifolds and Physics* (2nd ed). North-Holland, Amsterdam.
- Choquet-Bruhat, Y., DeWitt-Morete, C. (2000). *Analysis, Manifolds and Physics, Part II: 92 Applications* (rev. ed). North-Holland, Amsterdam.
- Chow, C.K., Jacobson, D.H. (1970). *Studies of human locomotion via optimal programming*. Tech. Rep. no 617, Div. Eng. Appl. Phys., Harvard Univ., Cambridge.
- Chow, W.L. (1939). Über systeme von linearen partiellen differentialgleichungen erster ordnung. *Math. Ann.*, **117**, 98–105.
- Caiani, L., Casetti, L., Clementi, C., Pettini, M. (1997). Geometry of dynamics, Lyapunov exponents and phase transitions. *Phys. Rev. Lett.* **79**, 4361.
- Celeghini, E., Rasetti, M., Vitiello, G. (1992). Quantum Dissipation, *Annals Phys.*, **215**, 156.
- Clark, C.A., Werring, D.J., Miller, D.H. (2000). Diffusion imaging of the spinal cord in vivo: estimation of the principal diffusivities and application to multiple sclerosis. *Magn. Reson. Med.* **43**, 133–138.
- Claussen, J.C., Schuster, H.G. (1998). Stability borders of delayed measurement from time-discrete systems. *arXiv nlin. CD/0204031*.
- Claussen, J.C., Mausbach, T., Piel, A. Schuster, H.G. (1998). Improved difference control of unknown unstable fixed points: Drifting parameter conditions and delayed measurement. *Phys. Rev. E*, **58**(6), 7256–7260.
- Claussen, J.C., Mausbach, T., Piel, A. Schuster, H.G. (1998). Memory difference control of unknown unstable fixed points: Drifting parameter conditions and delayed measurement. *Phys. Rev. E* **58**(6), 7260–7273.
- Claussen, J.C. (2002). Generalized Winner Relaxing Kohonen Feature Maps. *arXiv cond-mat/0208414*.
- Claussen, J.C. (2002) Floquet Stability Analysis of Ott-Grebogi-Yorke and Difference Control. *arXiv nlin.CD/0204060*.
- Claussen, J.C., Schuster, H.G. (2002). Asymptotic Level Density of the Elastic Net Self-Organizing Feature Map. 939-944 in: J. R. Dorronsoro (Ed.): *Artificial Neural Networks – ICANN’2002*, Springer LNCS, Berlin.



- Cohen, M.A., Grossberg, S. (1983). Absolute stability of global pattern formation and parallel memory storage by competitive neural networks. *IEEE Trans. Syst., Man, Cybern.*, **13**(5), 815–826.
- Cole, G.K., Nigg, B.M., Ronsky, J.L., Yeadon, M.R. (1993). Application of the joint coordinate system to three-dimensional joint attitude and movement representation: a standardization proposal. *J. Biomech. Eng.*, **115**, 344–349.
- Coleman, S. (1988). *Aspects of Symmetry : Selected Erice Lectures*. Cambridge Univ. Press, Cambridge.
- Collins, A.M., Quillian, M.R. (1969). Retrieval Time From Semantic Memory, *J. Verb. Learn. & Verb. Behav.*, **8**, 240–248.
- Contreras-Vidal, J.L., Grossberg, S., Bullock, D. (1997). A neural model of cerebellar learning for arm movement control: Cortico-spino-cerebellar dynamics. *Learning and Memory*, **3**, 475–502.
- Conway, J.H., Curtis, R.T., Norton, S.P., Parker, R.A., Wilson, R.A. (1985). *Atlas of Finite Groups: Maximal Subgroups and Ordinary Characters for Simple Groups*. Clarendon Press, Oxford.
- Cox, E. (1992). Fuzzy Fundamentals, *IEEE Spectrum*, 58–61.
- Cox, E. (1994). *The Fuzzy Systems Handbook*. AP Professional.
- Craik, F., Lockhart, R. (1972). Levels of processing: A framework for memory research. *J. Verb. Learn. & Verb. Behav.*, **11**, 671–684.
- Crane, L., Frenkel, I. (1994). Four dimensional topological quantum field theory, Hopf categories, and the canonical bases. *Jour. Math. Phys.* **35**, 5136–5154.
- Crick, F. (1994). *The Astonishing Hypothesis*. Charles Scribner's Sons, New York.
- Crick, F., Koch, C. (1990). Towards a neurobiological theory of consciousness. *Sem Neurosci* **2**, 263–275.
- Cristianini, N., Shawe-Taylor, J. (2000). *Support Vector Machines*. Cambridge Univ. Press, Cambridge.
- Crutchfield, J.P., Young, K. (1989). Computation at the onset of chaos. In *Complexity, Entropy and the Physics of Information*, pag. 223, SFI Studies in the Sciences Complexity, vol. VIII, W.H. Zurek (Ed.), Addison-Wesley, Reading.
- Cullum, J. (1971). Numerical differentiation and regularization, *SIAM J. Numer. Anal.* **8**(2), 254–265.
- Dai, M., Klein, A., Cohen, B., Raphan, T. (1999). Model-based study of the human cupular time constant. *J. Vest. Res.*, **9**, 293–301.
- Damiano, E.R. (1999). A poroelastic model of the cupula partition and the response dynamics of the vestibular semicircular canal. *J. Biomech. Eng.*, **121**, 449–461.
- Dariush, B. (2002). Multi-modal analysis of human movement from external measurements. *J. Dyn. Sys. Meas. & Control.* **123**(2), 272–278.
- Dariush, B. (2003). Forward dynamics solutions to multi-modal inverse dynamics problems. *Proceedings of ISB'03*, Univ. Otago, Dunedin, NZ.
- Dauvois, T., Theodorakopoulos, N., Peyrard, M. (2002). Thermodynamic instabilities in one dimension: correlations, scaling and solitons. *J. Stat. Phys.* **107**, 869.

- Davydov, A.S. (1981). *Biology and Quantum Mechanics*, Pergamon Press, New York.
- Davydov, A.S. (1991). *Solitons in Molecular Systems*. (2nd ed), Kluwer, Dordrecht.
- Debevec, P.E., Taylor, C.J., Malik, J. (1996). Modeling and rendering architecture from photographs. *Proc. SIGGRAPH '96*.
- Delp, S.L., Arnold, A.S., Piazza, S.J. (1998). Graphics-based modeling and analysis of gait abnormalities. *Bio-Med. Mat. Eng.*, **8**, 227–240.
- Delp, S.L., Loan, J.P., (2000). A computational framework for simulation and analysis of human and animal movement, *IEEE Com Sci. Eng.*, **2**(5), 46–55.
- De Rham, G. (1984). *Differentiable Manifolds*. Springer, Berlin.
- Derrida, B. (1983). Velocity and diffusion constant of a periodic one-dimensional hopping model. *J. Stat. Phys.*, **31**, 433–450.
- Dieudonne, J.A. (1969). *Foundations of Modern Analysis* (in four volumes). Academic Press, New York.
- Dieudonne, J.A. (1988). *A History of Algebraic and Differential Topology 1900–1960*. Birkhäuser, Basel.
- Ding, M., Grebogi, C., Yorke, J.A. (1997). Chaotic dynamics, in *The Impact of Chaos on Science and Society*, Eds. C. Grebogi and J.A. Yorke, 1–17, United Nations Univ. Press, Tokyo.
- Dirac, P.A.M. (1930). *The Principles of Quantum Mechanics*, Oxford Univ. Press, Oxford.
- Dodson, C.T.J., Parker, P.E. (1997). *A User's Guide to Algebraic Topology*. Kluwer, Dordrecht.
- Dolgopyat, D., Pesin, Ya. (2002). Every compact manifold carries a completely hyperbolic diffeomorphism. *Ergodic Theory Dynam. Systems* **22**, 409–435.
- Domany, E., Van Hemmen, J.L., Schulten, K. (eds.) (1991). *Models of Neural Networks*. Springer, Berlin.
- De Dominicis, C. (1978). Dynamics as a substitute for replicas in systems with quenched random impurities. *Phys. Rev. B* **18**, 4913–4919.
- Dorigo, M., Schnepf, U. (1993). Genetics-based machine learning and behavior-based robotics: a new synthesis. *IEEE Trans. Syst. Man, Cyber.*, **A 23**, 141–154.
- Dorogovtsev, S.N., Mendes, J.F.F. (2003). *Evolution of Networks*. Oxford Univ. Press, Oxford.
- Dote, Y., Strefezza, M., and Suitno, A. (1996). Neuro fuzzy robust controllers for drive systems. in *Neural Networks Applications*, ed. P.K. Simpson, IEEE Tec. Upd. Ser., New York.
- Douek, P., Turner, R., Pekar, J., Patronas, N.J., Le Bihan, D. (1991). MR color mapping of myelin fiber orientation. *J. Comput. Assist. Tomogr.*, **15**, 923–929.
- Dress, W.B., Knisley, J.R. (1987). A Darwinian approach to artificial neural systems. *Proc IEEE Conf. Sys., Man Cybern.*
- Dubois, D., Prade, H. (1980). *Fuzzy Sets and Systems*. Academic Press, New York.

- Durbin, R., Willshaw, D. (1987). An analogue approach to the Travelling Salesman Problem using an Elastic Net Method. *Nature* **326**, 689–691.
- Dustin, P. (1984). *Microtubules*. Springer, Berlin.
- Dyer, P., McReynolds, S.R. (1970). *The computation and theory of optimal control*. Academic Press, New York.
- Eastwood, M., Penrose, R. (2000). *Drawing with Complex Numbers*. arXiv math.MG/0001097.
- Eccles, J.C. (1964). *The Physiology of Synapses*. Springer, Berlin.
- Eccles, J.C., Ito M., Szentagothai J. (1967). *The Cerebellum as a Neuronal Machine*. Springer, Berlin.
- Eckmann, J.P., Ruelle, D. (1985). Ergodic theory of chaos and strange attractors, *Rev. Mod. Phys.*, **57**, 617–630.
- Eckmann, J.P., Pillet, C.A., Rey-Bellet, L. (1999). Non-equilibrium statistical mechanics of anharmonic chains coupled to two heat baths at different temperatures. *Commun. Math. Phys.*, **201**, 657–697.
- Ehresmann, A.C., Vanbremeersch, J.-P. (1987). Hierarchical Evolutive Systems: A Mathematical Model for Complex Systems. *Bul. Math. Bio.* **49**(1), 13–50.
- Ehresmann, A.C., Vanbremeersch, J.-P. (1996). Multiplicity Principle and emergence in MES. *Journ. Syst. Analysis, Modelling, Simulation* **26**, 81–117.
- Ellis, J., Mavromatos, N., Nanopoulos, D.V. (1992). String theory modifies quantum mechanics. CERN-TH/6595.
- Ellis, J., Mavromatos, N. and Nanopoulos, D.V. (1999). A microscopic Liouville arrow of time. *Chaos, Solit. Fract.*, **10**(2–3), 345–363.
- Elman, J. (1990). Finding structure in time. *Cog. Sci.* **14**, 179–211.
- Elworthy, K.D. (1982). *Stochastic Differential Equations on Manifolds*. Cambridge Univ. Press, Cambridge.
- Ermentrout, G.B. (1996). Type I membranes, phase resetting curves, and synchrony. *Neural Computation*, **8**(5), 979–1001.
- Federer, H. (1969). *Geometric Measure Theory*. Springer, New York.
- Ferber, J. (1999). *Multi-Agent Systems. An Introduction to Distributed Artificial Intelligence*. Addison-Wesley, Reading.
- Feynman, R.P. (1948). Space-time approach to non-relativistic quantum mechanics. *Rev. Mod. Phys.* **20**, 367–387.
- Feynman, R.P., Hibbs, A.R. (1965). *Quantum Mechanics and Path Integrals*, McGraw-Hill, New York.
- Feynman, R.P. (1972). *Statistical Mechanics, A Set of Lectures*. WA Benjamin, Inc., Reading, Massachusetts.
- Feynman, R.P. (1998). *Quantum Electrodynamics. Advanced Book Classics*, Perseus Publishing.
- Filippov, A.F. (1964). Differential equations with discontinuous right-hand sides. *AMS Translations, Ser. 2*, **42**, 199–231.
- Fine, A. (1986). *The Shaky Game: Einstein, Realism and Quantum Theory*, Univ. Chicago Press, Chicago.
- Fisher, M.E., Kolomeisky, A.B. (1999). The force exerted by a molecular motor. *Proc. Natl. Acad. Sci. USA*, **96**, 6597–6602.
- FitzHugh, R.A. (1961). Impulses and physiological states in theoretical models of

- nerve membrane. *Biophys J.*, **1**, 445–466.
- Fordy, A.P. (ed.) (1990). *Soliton Theory: A Survey of Results*. MUP, Manchester.
- Forsyth, A.R. (1960). *Calculus of Variations*. Dover, New York.
- Franzosi, R., Casetti, L., Spinelli, L., Pettini, M. (1999). Topological aspects of geometrical signatures of phase transitions. *Phys. Rev. E*, **60**, 5009–5012.
- Franzosi, R., Pettini, M., Spinelli, L. (2000). Topology and phase transitions: a paradigmatic evidence. *Phys. Rev. Lett.* **84**(13), 2774–2777.
- Franzosi, R., Pettini, M. (2004). Theorem on the origin of phase transitions. *Phys. Rev. Lett.*, **92**(6), 60601.
- Freeman, J.A., Skapura, D.M. (1992). *Neural Networks: Algorithms, Applications, and Programming Techniques*. Addison-Wesley, Reading.
- Frölich, H., Kremer, F. (1983). *Coherent Excitations in Biological Systems*. Springer, New York.
- Gabbiani, F., Midtgaard, J., and Knoepfl, T. (1994). Synaptic integration in a model of cerebellar granule cells. *J. Neurophysiol.*, **72**, 999–1009.
- Gardiner, C.W. (1985). *Handbook of Stochastic Methods for Physics, Chemistry and Natural Sciences* (2nd ed). Springer, Berlin.
- van Gelderen, P., de Vleeschouwer, M.H.M., des Pres, D., et al. (1994). Water diffusion and acute stroke. *Magn. Reson. Med.* **31**, 154–163.
- Georgii, H.O. (1988). *Gibbs Measures and Phase Transitions*. Walter de Gruyter, Berlin.
- Georgiou, G.M., Koutsougeras, C. (1992). Complex domain backpropagation. *Anal. Dig. Sig. Proc.*, **39**(5), 330–334.
- Ghez, C. (1990). Introduction to motor system. In: Kandel, E.K. and Schwarz, J.H. (eds.) *Principles of neural science*. 2nd ed. Elsevier, Amsterdam, 429–442.
- Ghez, C. (1991). Muscles: Effectors of the Motor Systems. In: *Principles of Neural Science*. 3rd Ed. (Eds. E.R. Kandel, J.H. Schwartz, T.M. Jessell), Appleton and Lange, Elsevier, 548–563.
- Gleick, J. (1997). *Chaos*. Minerva, UK.
- Gold, M. (1999). *A Kurt Lewin Reader, the Complete Social Scientist*. Am. Psych. Assoc., Washington.
- Goldberg, D. (1988). *Genetic Algorithms*, Addison-Wesley, Reading.
- Goldberger, A.L. (1999). Nonlinear Dynamics, Fractals, and Chaos Theory: Implications for Neuroautonomic Heart Rate Control in Health and Disease, in: Bolis CL, Licinio J, eds. *The Autonomic Nervous System*. World Health Organization, Geneva.
- Goldenfeld, N. (1992). *Lectures on Phase Transitions and the Renormalization Group*. Addison-Wesley, Reading.
- Goldstein, H., (1980). *Classical mechanics*. Addison-Wesley, Reading.
- Gómez, J.C. (1994). Using symbolic computation for the computer aided design of nonlinear (adaptive) control systems. Tech. Rep. EE9454, Dept. Electr. and Comput. Eng., Univ. Newcastle, Callaghan, NSW, AUS.
- Gomi, H., Kawato, M. (1996). Equilibrium-point control hypothesis examined by measured arm-stiffness during multi-joint movement. *Science*, **272**, 117–120.

- Goodwine, J.W. (1998). Control of Stratified Systems with Robotic Applications. PhD thesis, California Institute of Technology, Pasadena.
- Goodwine, B., Burdick, J. (1997). Trajectory generation for kinematic legged robots. In IEEE Int. Conf. Rob. Aut., 2689–2696. IEEE Press.
- Gottlieb, H.P.W. (1996). Question #38. What is the simplest jerk function that gives chaos? *Am. J. Phys.*, **64**(5), 525.
- Gowitzke, B.A., Milner, M. (1988). Scientific Bases of Human Movement. Williams and Wilkins, Baltimore.
- Grebogi, C., Ott, E., Yorke, J.A. (1987). Chaos, strange attractors, and fractal basin boundaries in nonlinear dynamics. *Science*, **238**, 632–637.
- Greene, B.R. (1996). String Theory on Calabi-Yau Manifolds. Lectures given at the TASI-96 summer school on Strings, Fields and Duality.
- Greene, B.R. (2000). The Elegant Universe: Superstrings, Hidden Dimensions, and the Quest for the Ultimate Theory. Random House.
- Grewal, M.S., Weill, L.R., Andrews, A.P. (2001). Global Positioning Systems, Inertial Navigation, and Integration. Wiley, New York.
- Griffiths, P.A. (1983). Exterior Differential Systems and the Calculus of Variations, Birkhauser, Boston.
- Grinza, P., Mossa, A. (2004). Topological origin of the phase transition in a model of DNA denaturation. *Phys. Rev. Lett.* **92**(15), 158102.
- Grossberg, S. (1969). Embedding fields: A theory of learning with physiological implications. *J. Math. Psych.* **6**, 209–239.
- Grossberg, S. (1982). Studies of Mind and Brain. Dordrecht, Holland.
- Grossberg, S. (1988). Neural Networks and Natural Intelligence. MIT Press, Cambridge.
- Grossberg, S. (1999). How does the cerebral cortex work? Learning, attention and grouping by the laminar circuits of visual cortex. *Spatial Vision* **12**, 163–186.
- Gutkin, B.S., Ermentrout, B. (1998). Dynamics of membrane excitability determine interspike interval variability: A link between spike generation mechanisms and cortical spike train statistics. *Neural Comput.*, **10**(5), 1047–1065.
- Haken, H. (1983). Synergetics: An Introduction (3rd ed). Springer, Berlin.
- Haken, H. (1993). Advanced Synergetics: Instability Hierarchies of Self-Organizing Systems and Devices (3rd ed.). Springer, Berlin.
- Haken, H. (1996). Principles of Brain Functioning: A Synergetic Approach to Brain Activity, Behavior and Cognition, Springer, Berlin.
- Haken, H. (2000). Information and Self-Organization: A Macroscopic Approach to Complex Systems. Springer, Berlin.
- Haken, H. (2002). Brain Dynamics, Synchronization and Activity Patterns in Pulse-Codupled Neural Nets with Delays and Noise, Springer, New York.
- Hale, J.K., Lunel, S.M.V. (1993). Introduction to Functional Differential Equations. Springer, New York.
- Hameroff, S.R. (1987). Ultimate Computing: Biomolecular Consciousness and Nanotechnology. North-Holland, Amsterdam.
- Hameroff, S.R., Penrose, R. (1996). Orchestrated reduction of quantum coherence in brain microtubules: A model for consciousness. In: Hameroff, S. R.,

- Kaszniak, A.W. and Scott, A.C. Eds: *Toward a Science of Consciousness: the First Tucson Discussion and Debates*, 507–539. MIT Press, Cambridge.
- Hamilton, R.S. (1982). Three-manifolds with positive Ricci curvature, *J. Differential Geom.* **17**, 255–306.
- Harris, J.M., Drga, V.F. (2005). Using visual direction in three-dimensional motion perception. *Nature Neurosci.*, **8**, 229–233.
- Harting, J.K. (1997). *The Global Anatomy* (electronic text), Univ. Wisconsin Medical School.
- Has, S. (1998). Humanoid robots in Waseda University: Hadaly-2 and Wabian. In *IARP First International Workshop on Humanoid and Human Friendly Robotics*, 1–2, Waseda Univ., Waseda.
- Hat, N.G. (1996). Coupling the neural and physical dynamics in rhythmic movements. *Neural Computation*, **8**, 567–581.
- Hatze, H. (1977). A myocybernetic control model of skeletal muscle. *Biol. Cyber.* **25**, 103–119.
- Hatze, H. (1977). A complete set of control equations for the human musculoskeletal system. *J. Biomech.* **10**, 799–805.
- Hatze, H. (1978). A general myocybernetic control model of skeletal muscle. *Biol. Cyber.*, **28**, 143–157.
- Hatze, H. (1980). Neuromusculoskeletal Control Systems Modelling — a Critical Survey of Recent Developments. *IEEE Trans. Aut. Con.* **25**(3), 375–385.
- Hatze, H. (1981). A comprehensive model for human motion simulation and its application to the take-off phase of the long jump. *J. Biomech.* **14**, 135–142.
- Hauser, J., Sastry, S., Kokotovic, P. (1992). Nonlinear control via approximate input-output linearization: The ball and beam example, *IEEE Trans. Aut. Con.*, **AC-37**, 392–398.
- Haykin, S. (1991). *Adaptive Filter Theory*. Prentice-Hall, Englewood Cliffs.
- Haykin, S. (1994). *Neural Networks: A Comprehensive Foundation*. Macmillan.
- Haykin, S. (ed.) (2001). *Kalman Filtering and Neural Networks*. Wiley, New York.
- Hebb, D.O. (1949). *The Organization of Behaviour*. Wiley, New York.
- Heermann, D.W. (1990). *Computer Simulation Methods in Theoretical Physics*. (2nd ed), Springer, Berlin.
- Helgason, S. (2001). *Differential Geometry, Lie Groups and Symmetric Spaces*. (2nd ed.) American Mathematical Society, Providence, RI.
- Hemami, H., Wyman, B.F. (1979). Modelling and control of constrained dynamic systems with application to biped locomotion in the frontal plane, *IEEE Trans. Aut. Con.*, **AC-24**, **4**, 526–535.
- Hilbert, D., Cohn-Vossen, S. (1999). *Geometry and the Imagination*. (Reprint ed.), Amer. Math. Soc.
- Hill, A.V. (1938). The heat of shortening and the dynamic constants of muscle, *Proc. R. Soc. B*, **76**, 136–195.
- Hirsch, M.W., Smale, S. (1974). *Differential Equations, Dynamical Systems and Linear Algebra*. Academic Press, New York.
- Hirsch, M.W. (1976). *Differential Topology*. Springer, New York.
- Heckhausen, H. (1977). Achievement motivation and its constructs: a cognitive model. *Motiv. Emot*, **1**, 283–329.

- Hecht-Nielsen, R. (1987). Counterpropagation networks. *Applied Optics*, **26**(23), 4979–4984.
- Hecht-Nielsen, R. (1990). *NeuroComputing*. Addison-Wesley, Reading.
- Hocherman, S., Wise, S.P. (1991). Effects of hand movement path on motor cortical activity in awake, behaving rhesus monkeys. *Exp. Brain Res.* **83**, 285–302.
- Hodgkin, A.L., Huxley, A.F. (1952). A quantitative description of membrane current and application to conduction and excitation in nerve. *J. Physiol.*, **117**, 500–544.
- Hodgkin, A.L. (1964). *The Conduction of the Nervous Impulse*. Liverpool Univ. Press, Liverpool.
- Hofbauer, J., Sigmund, K. (1998). *Evolutionary games and population dynamics*, Cambridge Univ. Press, U.K.
- Hooper, S.L. (2004). Multiple routes to similar network output. *Nature Neurosci.* **7**, 1287–1288.
- Hoover, W.G. (1995). Remark on “Some Simple Chaotic Flows,” *Phys. Rev. E*, **51**(1), 759–760.
- Hopf, E. (1939). Statistik der Geodatischen Linien in Mannigfaltigkeiten Negativer Krümmung. *Ber. Verh. S<sup>ach</sup>s. Akad. Wiss.*, Leipzig, **91**, 261–304.
- Hopfield, J.J. (1982). Neural networks and physical systems with emergent collective computational activity. *Proc. Natl. Acad. Sci. USA.*, **79**, 2554–2558.
- Hopfield, J.J. (1984). Neurons with graded response have collective computational properties like those of two-state neurons. *Proc. Natl. Acad. Sci. USA*, **81**, 3088–3092.
- Hopfield, J.J., Tank, D.W. (1985). Neural computation of decisions in optimisation problems. *Biol. Cybern.*, **52**, 114–152.
- Hoppensteadt, F.C., Izhikevich, E.M. (1997). *Weakly Connected Neural Networks*. Springer, New York.
- Horsthemke, W., Lefever, R. (1984). *Noise-Induced Transitions*. Springer, Berlin.
- Houk, J.C. (1979). Regulation of stiffness by skeletomotor reflexes. *Ann. Rev. Physiol.*, **41**, 99–114.
- Houk, J.C., Buckingham, J.T., Barto, A.G. (1996). Models of the cerebellum and motor learning. *Behavioral and Brain Sciences*, **19**(3), 368–383.
- Humphrey, D.R., Freund, H.J. (1991). *Motor Control: Concepts and Issues*. Wiley, Chichester, UK.
- Hunt, E.R. (1991). Stabilizing high period orbits in a chaotic system, *Phys. Rev. Lett.*, **67**, 1953–1955.
- Hunt, L., Turi, J. (1993). A new algorithm for constructing approximate transformations for nonlinear systems. *IEEE Trans. Aut. Con.*, **AC-38**, 1553–1556.
- Hurmuzlu, Y. (1993). Dynamics of bipedal gait. *J. Appl. Mech.*, **60**, 331–343.
- Huston, R.L., Passerello, C.E. (1971). On the dynamics of a human body model. *J. Biomech.*, **4**, 369–378.
- Huxley, A.F. (1957). Muscle structure and theories of contraction. *Progr. Biophys. Chem.*, **7**, 255–328.
- Huxley, A.F., Niedergerke, R. (1954). Changes in the cross-striations of muscle during contraction and stretch and their structural interpretation. *Nature*,

173, 973–976.

- Hyvärinen, A., Karhunen, J., Oja, E. (2001). *Independent Component Analysis*. Wiley.
- Ichinomiya, T. (2004). Frequency synchronization in random oscillator network. *Phys. Rev. E* **70**, 026116.
- Ichinomiya, T. (2005). Path-integral approach to the dynamics in sparse random network. *Phys. Rev. E* **72**, 016109.
- Igarashi, E., Nogai, T. (1992). Study of lower level adaptive walking in the sagittal plane by a biped locomotion robot. *Advanced Robotics*, **6**, 441–459.
- Ilachinski, A. (2001). *Cellular automata*. World Scientific, Singapore.
- Imamizu, H., Miyauchi, S., Tamada, T., Sasaki, Y., Takino, R., Puetz, B., Yoshioka, T., Kawato, M. (2000). Human cerebellar activity reflecting an acquired internal model of a novel tool. *Nature*, **403**, 192–195.
- Imamizu, H., Kuroda, T., Miyauchi, S., Yoshioka, T., Kawato, M. (2003). Modular organization of internal models of tools in the human cerebellum. *Proc Natl Acad Sci USA*, **100**, 5461–5466.
- Ingber, L. (1997). Statistical mechanics of neocortical interactions: Applications of canonical momenta indicators to electroencephalography, *Phys. Rev. E*, **55**(4), 4578–4593.
- Ingber, L. (1998). Statistical mechanics of neocortical interactions: Training and testing canonical momenta indicators of EEG, *Mathl. Computer Modelling* **27**(3), 33–64.
- Isidori, A. (1989). *Nonlinear Control Systems. An Introduction*, (2nd ed) Springer, Berlin.
- Ivancevic, T. (1995). Some Possibilities of Multilayered Neural Networks' Application in Biomechanics of Muscle Contractions, Man Locomotion and Sport Training, Master Thesis (in Serbo-Croatian), Univ. Novi Sad.
- Ivancevic, T., Jain, L.C., Bottema, M. (1999). New Two-feature GBAM–Neurodynamical Classifier for Breast Cancer Diagnosis, *Proc. from KES'99*, IEEE Press.
- Ivancevic, T., Jain, L.C., Bottema, M. (1999). A New Two-Feature FAM–Matrix Classifier for Breast Cancer Diagnosis, *Proc. from KES'99*, IEEE Press.
- Ivancevic, T., Pearce, C.E.M., Graves, I. (2003). *Review of Facial Recognition Algorithms*. DSTO, Adelaide.
- Ivancevic, V. (1991). *Introduction to Biomechanical Systems: Modelling, Control and Learning* (in Serbian). Scientific Book, Belgrade.
- Ivancevic, V., Lukman, L., Ivancevic, T. (1995) *Selected Chapters in Human Biomechanics*. Textbook (in Serbian). Univ. Novi Sad Press, Novi Sad.
- Ivancevic, V., Snoswell, M. (2000). *Torson Sports Cybernetics*. Torson Group. Inc., Adelaide.
- Ivancevic, V., Snoswell, M. (2001). Fuzzy–stochastic functor machine for general humanoid–robot dynamics. *IEEE Trans. on Sys, Man, Cyber. B*, **31**(3), 319–330.
- Ivancevic, V., Pearce, C.E.M. (2001). Poisson manifolds in generalised Hamiltonian biomechanics. *Bull. Austral. Math. Soc.* **64**, 515–526.
- Ivancevic, V., Pearce, C.E.M. (2001). Topological duality in humanoid robot



- dynamics. ANZIAM J. **43**, 183–194.
- Ivancevic, V. (2002). Generalized Hamiltonian biodynamics and topology invariants of humanoid robots. *Int. J. Mat. Mat. Sci.*, **31**(9), 555–565.
- Ivancevic, V., Beagley, N. (2003). Human Biodynamics Engine: The Full Spine Simulator. *Proc. Int. Soc. Biomech. XIX Congress*, Dunedin, NZ.
- Ivancevic, V., Beagley, N. (2003). Predicting spinal injury. Cover story for Connections, Defence Science & Technology Organisation, Australia, **73**, August.
- Ivancevic, V., Beagley, N. (2003). Mathematical twist reveals the agony of back pain – 3D Model Reveals Cause of Back Pain, *New Scientist – Frontiers*, p.15, 9th August.
- Ivancevic, V. (2004). Symplectic Rotational Geometry in Human Biomechanics. *SIAM Rev.*, **46**(3), 455–474.
- Ivancevic, V. (2005). Dynamics of Humanoid Robots: Geometrical and Topological Duality. To appear in *Biomathematics: Modelling and simulation* (ed. J.C. Misra), World Scientific, Singapore.
- Ivancevic, V., Beagley, N. (2005). Brain-like functor control machine for general humanoid biodynamics. *Int. J. Math. Math. Sci.* (to appear).
- Ivancevic, V., Pearce, C.E.M. (2005). A qualitative Hamiltonian model for the dynamics of human motion. In *Differential Equations and Applications*, Vol. 3 Eds. Y.J. Cho, J.K. Kim and K.S. Ha, Nova Science, New York.
- Ivanov, P. Ch., Amaral, L. A. N., Goldberger, A. L., Havlin, S., Rosenblum, M. B., Struzik, Z. & Stanley, H. E. (1999). Multifractality in healthy heartbeat dynamics. *Nature*, **399**, 461–465.
- Iyanaga, S., Kawada, Y. (eds.) (1980). Pontrjagin's Maximum Principle. In *Encyclopedic Dictionary of Mathematics*. MIT Press, Cambridge, MA, 295–296.
- Izhikevich, E.M. (1999). Class 1 neural excitability, conventional synapses, weakly connected networks, and mathematical foundations of pulse-coupled models. *IEEE Trans. Neu. Net.*, **10**, 499–507.
- Izhikevich, E.M. (2001). Resonate-and-fire neurons. *Neu. Net.*, **14**, 883–894.
- Izhikevich, E.M. (2003). Simple model of spiking neurons. *IEEE Trans. Neu. Net.*, **14**, 1569–1572.
- Izhikevich, E.M. (2004). Which model to use for cortical spiking neurons? *IEEE Trans. Neu. Net.*, **15**, 1063–1070.
- Jibu, M., Yasue, K. (1995). Quantum brain dynamics and consciousness. John Benjamins, Amsterdam.
- Jibu, M., Pribram, K.H., Yasue, K. (1996). From conscious experience to memory storage and retrieval: the role of quantum brain dynamics and boson condensation of evanescent photons, *Int. J. Mod. Phys. B*, **10**, 1735.
- Joao, M.L. (2000). An Extended Kalman Filter for Quaternion-Based Attitude Estimation. Master thesis, Computer Science Department, Naval Postgraduate School, Monterey, CA.
- Jordan, M.I. (1996). Computational aspects of motor control and motor learning. In H. Heuer, & S. W. Keele (Eds.), *Handbook of Perception and Action*. Academic Press, New York.
- Jülicher, F., Ajdari, A., Prost, J. (1997). Modelling molecular motors. *Rev. Mod.*

- Phys., **69**, 1269–1281.
- Just, W., Bernard, T., Ostheimer, M., Reibold, E., Benner, H. (1997). Mechanism of time-delayed feedback control. *Phys. Rev. Lett.*, **78**, 203–206.
- Kadic, A., Edelen, D.G.B. (1983). *A Gauge theory of Dislocations and Disclinations*, New York, Springer.
- Kalman, R.E. (1960). A new approach to linear filtering and prediction problems. *Transactions of the ASME, Ser. D, J. Bas. Eng.*, **82**, 34–45.
- Kan, D.M. (1958). Adjoint Functors. *Trans. Am. Math. Soc.* **89**, 294–329.
- Kandel, E.R., Schwartz, J.H., Jessel, T.M. (1991). *Principles of neural sciences*. Elsevier, Amsterdam.
- Kaplan, J.L., Yorke, J.A. (1979). Numerical Solution of a Generalized Eigenvalue Problem for Even Mapping. Peitgen, H.O., Walther, H.O. (Eds.): *Functional Differential Equations and Approximations of Fixed Points*, Lecture Notes in Mathematics, **730**, 228–256, Springer, Berlin.
- Kaplan, D.T., Furman, M.I., Pincus, S.M., Ryan, S.M., Lipsitz, L.A., Goldberger, A.L. (1991). Aging and the complexity of cardiovascular dynamics, *Biophys. J.*, **59**, 945–949.
- Kasabov, N. (2002). *Evolving connectionist systems: Methods and applications in bioinformatics, brain study and intelligent machines*. Springer, London.
- Katok, A. (1980). Lyapunov exponents, entropy and periodic orbits for diffeomorphisms. *Inst. Hautes Études Sci. Publ. Math.* **51**, 137–173.
- Kauffman, S.A., Smith, R.G. (1986). Adaptive automata based on Darwinian selection. *Physica D*, **22**, 68–82.
- Kawato, M. (1999). Internal models for motor control and trajectory planning. *Current Opinion in Neurobiology*, **9**, 718–727.
- Kelly, S.D., Murray, R.M. (1995). Geometric phases and robotic locomotion. *J. Robotic Systems*, **12**(6), 417–431.
- Ko, H., Badler, N. (1996). Animating human locomotion with inverse dynamics. *IEEE Comp. Graph. Appl.* **16**, 50–59.
- Kock, A., (1981). *Synthetic Differential Geometry*, London Math.Soc. Lecture Notes Series No. 51, Cambridge Univ. Press, Cambridge.
- Kock, A. (2001). Infinitesimal aspects of the Laplace operator. *Theory and Applications of Categories*, **9**(1), 1–16.
- Kock, A., Reyes, G.E. (2003). Some calculus with extensive quantities: wave equation. *Theory and Applications of Categories*, **11**(14), 321–336.
- Kohonen, T. (1982). Self-Organized Formation of Topologically Correct Feature Maps. *Biological Cybernetics* **43**, 59–69.
- Kohonen, T. (1988). *Self Organization and Associative Memory*. Springer.
- Kohonen, T. (1991). Self-Organizing Maps: Optimization Approaches. In: *Artificial Neural Networks*, ed. T. Kohonen et al. North-Holland, Amsterdam.
- Kolar, I., Michor, P.W., Slovak, J. (1993). *Natural Operations in Differential Geometry*. Springer, Berlin.
- Koon, W.S., Marsden, J.E. (1997). The Hamiltonian and Lagrangian approaches to the dynamics of nonholonomic systems. *Reports on Math Phys.* **40**, 21–62.
- Koruga, D.L., Hameroff, S.I., Sundareshan, M.K., Withers, J., Loutfy, R. (1993).

- Fullerence C60: History, Physics, Nanobiology and Nanotechnology. Elsevier Science Pub.
- Kosko, B. (1992). *Neural Networks and Fuzzy Systems, A Dynamical Systems Approach to Machine Intelligence*. Prentice-Hall, New York.
- Kosko, B. (1993). *Fuzzy Thinking*. Disney Books, Hyperion.
- Kosko, B. (1996). *Fuzzy Engineering*. Prentice Hall, New York.
- Kosko, B. (1999). *The Fuzzy Future: From Society and Science to Heaven in a Chip*. Random House, Harmony.
- Kotz, S., Nadarajah, S. (2000). *Extreme Value Distributions*. Imperial College Press, London.
- Krener, A. (1984). Approximate linearization by state feedback and coordinate change, *Systems Control Lett.*, 5, 181–185.
- Kuhl, J. (1985). Volitional Mediator of cognition-Behaviour consistency: Self-regulatory Processes and action versus state orientation (pp. 101-122). In: J. Kuhl & S. Beckman (Eds.) *Action control: From Cognition to Behaviour*. Springer, Berlin.
- Kuramoto, Y. (1984). *Chemical Oscillations. Waves and Turbulence*, Springer, New York.
- Lafferriere, G., Sussmann, J.J. (1993). A differential geometric approach to motion planning. In Z. Li and J. F. Canny (ed.) *Nonholonomic Motion Planning*, 235–270. Kluwer, Dordrecht.
- Lai, Y.-C. (1994). Controlling chaos. *Comput. Phys.*, 8, 62–67.
- Landau, L.D., Lifshitz, E.M. (1977). *Quantum Mechanics: Non-Relativistic Theory*, Pergamon Press, Oxford.
- Landau, L.D., Lifshitz, E.M. (1978). *Statistical Physics*, Pergamon Press, Oxford.
- Latash, M. (1993). *Control of Human Movement*. Human Kinetics Publ. Urbana-Champaign.
- Lattanzi, G., Maritan, A. (2001). Force dependence of the michaelis constant in a two-state ratchet model for molecular motors. *Phys. Rev. Lett*, 86, 1134–1137.
- Lavendhomme, R. (1996). *Basic Concepts of Synthetic Differential Geometry*. Kluwer, Dordrecht.
- Lawvere, F.W. (1979). *Categorical Dynamics. Topos Theoretic Methods in Geometry* (ed. A. Kock). Aarhus Various Publ, Series 30.
- Leal, L.G. (1992). *Laminar Flow and Convective Transport Processes*. Butterworth-Heinemann, Boston.
- Le Bihan, D., Jezzard, P., Haxby, J., Sadato, N., Rueckert, L., Mattay, V. (1995). Functional magnetic resonance imaging of the brain. *Ann. Intern. Med.*, 122(4), 296–303.
- Le Bihan, D. (1995). *Diffusion and perfusion magnetic resonance imaging. Applications to functional MRI*. Raven Press, New York.
- Le Bihan, D. (1996). Functional MRI of the brain: principles, applications and limitations. *J. Neuroradiol.*, 23(1), 1–5.
- Le Bihan, D. (2000). What to expect from MRI in the investigation of the central nervous system? *CR Acad. Sci. III*, 323(4), 341–50.
- Le Bihan, D., Mangin, J.F., Poupon, C., Clark, C.A., Pappata, S., Molko, N,

- Chabriat, H. (2001). Diffusion tensor imaging: concepts and applications. *J. Magn. Reson. Imaging*, **13**(4), 534–46.
- Le Bihan, D., van Zijl, P. (2002). From the diffusion coefficient to the diffusion tensor. *NMR Biomed.*, **15**(7-8), 431–4.
- Le Bihan, D. (2003). Looking into the functional architecture of the brain with diffusion MRI. *Nature Rev. Neurosci.*, **4**(6), 469–80.
- Lee, C.C. (1990). Fuzzy Logic in Control Systems. *IEEE Trans. Sys., Man, Cybern.*, **20**(2), 404–435.
- Lee, J.M. (2000). *Introduction to Topological Manifolds*. Springer, New York.
- Lee, J.M. (2002). *Introduction to Smooth Manifolds*. New York, Springer.
- Leinster, T. (2002). A survey of definitions of  $n$ -category. *Theor. Appl. Categ.*, **10**, 1–70.
- Leinster, T. (2003). *Higher Operads, Higher Categories*, London Mathematical Society Lecture Notes Series, Cambridge Univ. Press, Cambridge.
- Leinster, T. (2004). Operads in higher-dimensional category theory. *Theor. Appl. Categ.*, **12**, 73–194.
- Lewin, K. (1951). *Field Theory in Social Science*. Univ. Chicago Press, Chicago.
- Lewin, K. (1997). *Resolving Social Conflicts: Field Theory in Social Science*, American Psych. Assoc., New York.
- Lewis, A.D. (1995). *Aspects of Geometric Mechanics and Control of Mechanical Systems*. Technical Report CIT-CDS 95-017 for the Control and Dynamical Systems Option, California Institute of Technology, Pasadena, CA.
- Lewis, A.D., Murray, R.M. (1997). Controllability of simple mechanical control systems, *SIAM J. Con. Opt.*, **35**(3), 766–790.
- Lewis, A.D. (2000). Affine connection control systems. *Proceedings of the IFAC Workshop on Lagrangian and Hamiltonian Methods for Nonlinear Control* 128–133, Princeton.
- Lieh, J. (1994). Computer oriented closed-form algorithm for constrained multi-body dynamics for robotics applications. *Mechanism and Machine Theory*, **29**, 357–371.
- Lindner, J.F., Ditto, W.L. (1995). Removal, suppression, and control of chaos by nonlinear design, *Appl. Mech. Rev.*, **48**, 795–808.
- Linsker, R. (1989). How To generate Ordered maps by Maximizing the Mutual Information between Input and Output Signals. *Neural Computation* **1**, 402–411.
- Linz, S.J. (1997). Nonlinear Dynamical Models and Jerky Motion. *Am. J. Phys.*, **65**(6), 523–526.
- Lipowsky, R. (2000). Universal aspects of the chemomechanical coupling for molecular motors. *Phys. Rev. Lett.*, **85**(20), 4401–4404.
- Liverani, C., Wojtkowski, M.P. (1995). Ergodicity in Hamiltonian systems. *Dynamics Reported*, **4**, 130–202.
- Lorenz, E.N., (1963). Deterministic Nonperiodic Flow. *J. Atmos. Sci.*, **20**, 130–141.
- Louie, A.H. (1983). Categorical system theory and the phenomenological calculus. *Bull. Math. Biol.*, **45**, 1029–1045; Categorical system theory. *Bull. Math. Biol.*, **45**, 1047–1072.

- Luinge, H.J. (2002). Inertial Sensing of Human Movement. Ph.D. thesis Univ. Twente, Twente Univ. Press
- Louzoun, Y., Solomon, S., Atlan, H., Cohen, I.R. (2003). Proliferation and competition in discrete biological systems. *Bull. Math. Biol.* **65**, 375.
- MacKay, R.S. (1986). Stability of equilibria of Hamiltonian systems. In *Nonlinear Phenomena and Chaos* (S. Sarkar, ed.), 254–270, Hilger, Bristol.
- MacLane, S. (1971). *Categories for the Working Mathematician*. Springer, New York.
- Magnasco, M.O. (1993). Forced thermal ratchets. *Phys. Rev. Lett.*, **71**, 1477–1481.
- Malasoma, J.M. (2000). What is the Simplest Dissipative Chaotic Jerk Equation which is Parity Invariant? *Phys. Lett. A*, **264**(5), 383–389.
- Mangioni, S.E., Deza, R.R., Toral, R., Wio, H.S. (2000). Nonequilibrium phase ransitions induced by multiplicative noise: effects of self-correlation. *Phys. Rev. E*, **61**, 223–231.
- Manikonda, V. (1998). Control and Stabilization of a Class of Nonlinear Systems with Symmetry. PhD Thesis, Center for Dynamics and Control of Smart Structures, Harvard Univ., Cambridge.
- Marieb, E.N. (1998). *Human Anatomy and Physiology*. (4th ed.), Benjamin/Cummings, Menlo Park, CA.
- Marsden, J.E., Ratiu, T.S. (1999). *Introduction to Mechanics and Symmetry: A Basic Exposition of Classical Mechanical Systems*. (2nd ed), Springer, New York.
- Matthews, G.G. (2001). *Neurobiology: Molecules, Cells and Systems* (2nd ed), Blackwell Sci. Inc.
- Mavromatos, N.E., Nanopoulos, D.V. (1995). A Non-critical String (Liouville) Approach to Brain Microtubules: State Vector reduction, Memory coding and Capacity. ACT-19/95, CTP-TAMU-55/95, OUTP-95-52P.
- Mavromatos, N.E., Nanopoulos, D.V. (1995). Non-Critical String Theory Formulation of Microtubule Dynamics and Quantum Aspects of Brain Function. ENSLAPP-A-524/95.
- May, R. (1976). Simple Mathematical Models with Very Complicated Dynamics. *Nature*, **261**(5560), 459–467.
- Maybeck, P.S. (1979). *Stochastic Models, Estimation, and Control*, Volume 1, Academic Press, New York.
- Mayer, P.A. (1981). *A Differential Geometric Formalism for the Ito Calculus*. *Lecture Notes in Mathematics*, **851**, Springer, New York.
- McCulloch W., Pitts W. 1943. A logical calculus of the ideas imminent in the nervous activity. *Bull. Math. Biophys.* **5**, 115–133.
- McGhee, R.B., Frank, A.A. (1968). On the stability properties of quadruped creeping gaits, *Math. Biosci.*, **3**.
- McGhee, R.B. (1996). Research Notes: A Quaternion Attitude Filter Using Angular Rate Sensors, Accelerometers, and a 3-Axis Magnetometer, Computer Science Department, Naval Postgraduate School, Monterey, CA.
- McGeer, T. (1990). Passive dynamic walking. *Int. J. Robot. Res.*, **9**, 62–82.
- McElhaney, J.H., Myers, B.S. (1993). *Biomechanical Aspects of Cervical Trauma*.

- in: A.M. Nahum and J.W. Melvin (Eds.), *Accidental injury: Biomechanics and Prevention*, Springer, New York.
- Mendes, R.V. (1998). Conditional exponents, entropies and a measure of dynamical self-organization. *Phys. Let. A* **248**, 167–1973.
- Messiah, A. (2000). *Quantum Mechanics: Two Volumes Bound As One*. Dover Pubs.
- Meyer, K.R., Schmidt, D.S. (2000). From the restricted to the full three-body problem. *Trans. Amer. Math. Soc.*, **352**, 2283–2299.
- Meyer, K.R., Hall, G.R. (1992). *Introduction to Hamiltonian Dynamical Systems and the N-body Problem*. Springer, New York.
- Middlebrooks, J.C. (2004). The acquisitive auditory cortex. *Nature Neurosci.* **6**, 1122–1123.
- Michor, P.W. (2001). *Topics in Differential Geometry*. Lecture notes of a course in Vienna.
- Miller, G.A. (1956). The magical number seven, plus or minus two: Some limits on our capacity for processing information, *Psych. Rev.*, **63**, 81–97.
- Milinkovic, D. (1999). Morse homology for generating functions of Lagrangian submanifolds. *Trans. Amer. Math. Soc.* **351**(10), 3953–3974.
- Minsky, M., Papert, S. (1969). *Perceptrons*. MIT Press, Cambridge, MA.
- Misner, C.W., Thorne, K.S., Wheeler, J.A. (1973). *Gravitation*. Freeman, San Francisco.
- Misra, J.C., Hartung, C., Mahrenholtz, O. (1977). Effect of pulse loading on brain injury. *Mech. Res. Com.*, **4**, 297–302.
- Misra, J.C. (1978). Axisymmetric vibration of human skull-brain system. *Ing. Arch.* **47**, 11–19.
- Misra, J.C., Hartung, C., Mahrenholtz, O. (1978). Stresses in a human skull due to pulse loading. *Ing. Arch.* **47**, 329–337.
- Misra, J.C. (1978). Response of a human head to an impact. *Med. Life Sci. Eng.* **4**, 142–152.
- Misra, J.C., Murthy, V.V.T.N. (1979). An analytical estimate of the stress-field in the vicinity of a crack in the human cranial bone. *Med. Life Sci. Eng.* **5**, 95–107.
- Misra, J.C., Murthy, V.V.T.N. (1981). Stress concentration around cracks in long bones. *For. Im. Ing.* **47**, 37–40.
- Misra, J.C., Chakravarty, S. (1982). A free vibration analysis for the human cranial system. *J. Biomech.* **15**, 635–645.
- Misra, J.C., Chakravarty, S. (1982). Effect of solar radiation on the human head. *Int. J. Eng. Sci.* **20**, 445–454.
- Misra, J.C., Chakravarty, S. (1982). Stability of fluid-filled shells –mathematical models for human head. *Acta Mech.* **44**, 159–168.
- Misra, J.C., Murthy, V.V.T.N. (1983). A model for studying the stress-field around simple fractures in human patella. *Aer. Quat.* **34**, 303–313.
- Misra, J.C., Murthy, V.V.T.N. (1983). An estimate of the stress-field in an osseous medium having a no-slip interface crack. *Eng. Frac. Mech.* **18**, 075–1086.
- Misra, J.C., Murthy, V.V.T.N. (1983). Surface remodelling of bones induced by intramedullary nailing. *Rhe. Acta*, **22**, 512–518.

- Misra, J.C., Murthy, V.V.T.N. (1983). A mathematical model for studying the physiological process of internal bone remodelling. *Bull. Tech. Univ. Istanbul*, **36**, 67-80.
- Misra, J.C., Samanta, S. (1983). Propagation of torsional waves in tubular bones. *J. Math. Anal. Appl.* **96**, 313-319.
- Misra, J.C., Chakravarty, S. (1984). A study on rotational brain injury. *J. Biomech.* **17**, 459-466.
- Misra, J.C., Chakravarty, S. (1984). A poroelastic shell model for studying the problem of head injury. *J. Math. Anal. Appl.* **103**, 323-343.
- Misra, J.C., Samanta, S. (1984). Wave propagation in tubular bones. *Int. J. Sol. Str.* **20**, 55-62.
- Misra, J.C., Mishra, M. (1984). Exterior star-shaped crack in a bone medium. *Eng. Frac. Mech.* **19**, 101-112.
- Misra, J.C., Mishra, M. (1985). Stress-field in a bone medium having a star-shaped crack. *Eng. Frac. Mech.* **22**, 65-76.
- Misra, J.C., Chakravarty, S. (1985). Dynamic response of a head-neck system to an impulsive load. *Math. Model.* **6**, 83-96.
- Misra, J.C. (1985). Stresses in a tubular bone exposed to heat radiation from a distant heat source. *Rhe. Acta*, **24**, 520-533.
- Misra, J.C. (1986). Stresses in the human head generated due to thermogenesis. *Rhe. Acta*, **25**, 201-205.
- Misra, J.C. (1986). Distribution of stresses in a pre-cracked bone specimen. *Rhe. Acta*, **25**, 485-490.
- Misra, J.C., Bera, G.C., Samanta, S. (1986). Vibration of a tubular bone in axial planes. *Math. Model.* **7**, 483-492.
- Misra, J.C., Samanta, S. (1987). Effect of material damping on bone remodelling. *J. Biomech.* **20**, 241-249.
- Misra, J.C., Samanta, S. (1988). A Mathematical Model for the Biomechanics of the Body of a Vertebra. *Comp. Math. Appl.* **15**, 85-96.
- Misra, J.C., Samanta, S. (1988). A mathematical analysis of the vibration characteristics of the human tibia. *Comp. Math. Appl.* **16**, 1017-1026.
- Misra, J.C., Roy, S. (1989). Mechanics of bone remodelling vis-à-vis nonhomogeneity of osseous tissues. *Model., Sim. Con., C*, **15**(4), 41-63.
- Misra, J.C., Roy, S. (1989). Stresses in the neighbourhood of an exterior crack in a bone specimen. *Comp. Math. Appl.* **17**, 1493-1502.
- Misra, J.C., Bera, G.C., Samanta, S. (1989). Influence of non-isotropy of osseous tissues and cross-sectional non-uniformity of a long bone on the internal remodelling dynamics of osseous tissues. *Math. Model.* **12**, 611-624.
- Misra, J.C., Bera, G.C., (1991). A mathematical study of the stress field in a long bone subjected to an external load. *J. Math. Anal. Appl.* **161**, No. 1, 474-507.
- Misra, J.C., Roy, S. (1991). Mathematical analysis of a specimen of tubular bone subjected to torsional loading. *Comp. Math. Appl.* **21**(2-3) 141-147.
- Misra, J.C., Bera, G.C. (1992). Remodelling of diaphysial surfaces of a long bone induced due to force-fitting of a modullary pin. *Comp. Math. Appl.* **24**(7) 3-15.

- Misra, J.C., Chakravarty, S. (2005). Modelling of Head Impact Problems. In Misra, J.C.(Ed.): *Mathematical Models for Bioengineering and Probilistic Systems*, Narosa Publ. House, New Delhi, Chapter 1, pp. 1-26
- Misra, J.C., Murthy, V.V.T.N. (2005). Mathematical Models in Fracture and Remodelling of Bones. In Misra, J.C.(Ed.): *Mathematical Models for Bioengineering and Probilistic Systems*, Narosa Publ. House, New Delhi, Chapter 2, pp. 27-53.
- Moerdijk, I., Reyes, G.E. (1991). *Models for Smooth Infinitesimal Analysis*. Springer, New York.
- Molavi, D.W. (1997). Neuroscience Tutorial (electronic text). Washington Univ. School of Medicine.
- Montgomery, T.M. (2003). *Anatomy, Physiology & Pathology of the Human Eye*. [http://www.tedmontgomery.com/the\\_eye](http://www.tedmontgomery.com/the_eye).
- Moon, S.J., Kevrekidis, I.G. (2005). An equation-free approach to coupled oscillator dynamics: the Kuramoto model example. Submitted to *Int. J. Bifur. Chaos*.
- Moreinis, I.S., Grycenko, G.P. (1974). Physical and mathematical model of human locomotor apparatus, (in Russian). *Prost. Prost. Design*, Moscow, **33**.
- Morris, C., Lecar, H. (1981). Voltage oscillations in the barnacle giant muscle fiber. *Biophys. J.*, **35**, 193-213.
- Mosekilde, E. (1996). *Topics in Nonlinear Dynamics: Application to Physics, Biology and Economics*. World Scientific, Singapore.
- Mountcastle, V.N. (1980). *Medical Physiology (XIV ed)*. C.V. Mosby Comp., St Louis.
- Muller, M., Verhagen, J.H.G. (1988). A mathematical approach enabling the calculation of the total endolymph flow in the semicircular ducts. *J. Theo. Biol.*, **134**(4), 503-529.
- Murray, J.D. (1989). *Mathematical Biology*. Springer, Berlin.
- Murray, R.M. (1994). Nilpotent bases for a class of nonintegrable distributions with applications to trajectory generation for nonholonomic systems. *Math. Control Signals Systems*, **7**, 58-75.
- Murray, R.M. (1997). *A Brief Introduction to Feedback Control*, CDS 110, California Institute of Technology, San Diego.
- Murray, R.M., Li, X., Sastry, S. (1994). *Robotic Manipulation*, CRC Press, Boca Raton, FL.
- Mustafa, M.T. (1999). Restrictions on harmonic morphisms. *Confomal Geometry and Dynamics (AMS)*, **3**, 102-115.
- Muybridge, F. (1957). *Animals in Motion*, Dover, New York.
- Nagumo, J., Arimoto, S., Yoshizawa, S. (1960). An active pulse transmission line simulating 1214-nerve axons, *Proc. IRL*, **50**, 2061-2070.
- Nanopoulos, D.V. (1995). *Theory of Brain Function, Quantum Mechanics and Superstrings*. CERN-TH/95128.
- Nash, C., Sen, S. (1983). *Topology and Geometry for Physicists*. Academic Press, London.
- Nayfeh, A.H. (1973). *Perturbation Methods*, Wiley, New York.
- von Neumann, J., Morgenstern, O. (1944). *Theory of Games and Economic Be-*



- havior. Princeton Univ. Press, Princeton.
- von Neumann, J. (1955). *Mathematical Foundations of Quantum Mechanics*. Princeton Univ. Press, Princeton.
- von Neumann, J. (1958). *The Computer and the Brain*. Yale Univ. Press.
- Nicolis, G., Prigogine, I. (1977). *Self-Organization in Nonequilibrium Systems: From Dissipative Structures to Order through Fluctuations*. Wiley Europe.
- Nijmeijer, H., van der Schaft, A.J. (1990). *Nonlinear Dynamical Control Systems*. Springer, New York.
- Nikitin, I.N. (1995). Quantum string theory in the space of states in an indefinite metric. *Theor. Math. Phys.* **107**(2), 589601.
- Nitta, T., Furuya, T. (1991). A complex back-propagation learning. *Transactions of Information Proc. Soc. Japan*, **32**(10), 1319–1329, (in Japanese).
- Nitta, T. (1997). An extension of the back-propagation algorithm to complex numbers. *Neu. Net.*, **10**(8), 1392–1415.
- Nitta, T. (2000). An analysis on fundamental structure of complex-valued neuron. *Neu. Proc. Let.*, **12**(3), 239–246.
- Nitta, T. (2004). Reducibility of the Complex-valued Neural Network. *Neu. Inf. Proc.*, **2**(3), 53–56.
- Noakes, L., Heinzinger, G., Paden, B. (1989). Cubic splines on curved spaces, *IMA J. Math. Con. Inf.*, **6**(4), 465–473.
- Noble, D. (1962). A modification of the Hodgkin–Huxley equations applicable to Purkinie fibre action and peace-maker potentials. *J. Physiol.*, **160**, 317–330.
- Novikov, S.P., Manakov, S.V., Pitaevskii, L.P., Zakharov, V.E. (1984). *Theory of Solitons*, Plenum/Kluwer, Dordrecht.
- Obermayer, K., Blasdel, G.G., Schulten, K. (1992). *Phys. Rev. A* **45**, 7568–7589.
- Oja, E. (1982). A simplified neuron modeled as a principal component analyzer. *J. Math. Biol.* **15**, 267–273.
- Olver, P.J. (1986). *Applications of Lie Groups to Differential Equations* (2nd ed.) Graduate Texts in Mathematics, vol. 107, Springer, New York.
- Oman, C.M., Marcus, E.N., Curthoys, I.S. (1987). The influence of semicircular canal morphology on endolymph flow dynamics. *Acta Otolaryngol.*, **103**, 1–13.
- Oseledets, V.I. (1968). A Multiplicative Ergodic Theorem: Characteristic Lyapunov Exponents of Dynamical Systems. *Trans. Moscow Math. Soc.*, **19**, 197–231.
- Ott, E., Grebogi, C., Yorke, J.A. (1990). Controlling chaos. *Phys. Rev. Lett.*, **64**, 1196–1199.
- Pappas, G.J., Lafferriere, G., Sastry, S. (2000). Hierarchically consistent control systems. *IEEE Trans. Aut. Con.*, **45**(6), 1144–1160.
- Pappas, G.J., Simic, S. (2002). Consistent hierarchies of affine nonlinear systems. *IEEE Trans. Aut. Con.*, **47**(5), 745–756.
- Pasupathy, A., Miller, E.K. (2005). Different time courses of learning-related activity in the prefrontal cortex and striatum. *Nature*, **433**, 873–876.
- Parmeggiani, A., Jülicher, F., Ajdari, A., Prost, J. (1999). Energy transduction of isothermal ratchets: Generic aspects and specific examples close to and far from equilibrium. *Phys. Rev. E*, **60**, 2127–2140.

- Pack, C., Grossberg, S., Mingolla, E. (2001). A Neural Model of Smooth Pursuit Control and Motion Perception by Cortical Area MST, *J. Cog. Neurosci.*, **13**, 102–120.
- Park, J.K., Steiglitz, K. and Thurston, W.P., (1986). Soliton-like Behavior in Automata. *Physica D*, **19**, 423–432.
- Pecora, L.M., Carroll T.L. (1991). Driving systems with chaotic signals. *Phys. Rev. A*, **44**, 2374–2383.
- Pecora, L.M., Carroll T.L. (1998). Master stability functions for synchronized coupled systems. *Phys. Rev. Lett.* **80**, 2109–2112.
- Pellionisz, A., Llinas, R. (1979). Brain modeling by tensor network theory and computer simulation. *NeuroScience*, **4**, 323–348.
- Penrose, R. (1967). Twistor algebra. *J. Math. Phys.*, **8**, 345–366.
- Penrose, R. (1989). *The Emperor's New Mind*, Oxford Univ. Press, Oxford.
- Penrose, R. (1994). *Shadows of the Mind*. Oxford Univ. Press, Oxford.
- Penrose, R. (1997). *The Large, the Small and the Human Mind*. Cambridge Univ. Press, Cambridge.
- Pessa, E., Vitiello, G. (1999). Quantum dissipation and neural net dynamics, *Bioelectrochem. Bioener.*, **48**, 339–342.
- Pessa, E., Vitiello, G. (2003). Quantum noise, entanglement and chaos in the quantum field theory of mind/brain states, *Mind and Matter*, **1**, 59–79.
- Pessa, E., Vitiello, G. (2004). Quantum noise induced entanglement and chaos in the dissipative quantum model of brain, *Int. J. Mod. Phys. B*, **18** 841–858.
- Pesin, Ya.B. (1977). Lyapunov Characteristic Exponents and Smooth Ergodic Theory. *Russ. Math. Surveys*, **32**(4), 55–114.
- Peterka, R.J. (2002). Sensorimotor Integration in Human Postural Control. *J. Neurophysiol.* **88**, 1097–1118.
- Petersen, P. (1998). *Riemannian Geometry*. Springer, New York.
- Petersen, P. (1999). Aspects of Global Riemannian Geometry. *Bull. Amer. Math. Soc.*, **36**(3), 297–344.
- Peterson, I. (1993). *Newton's Clock: Chaos in the Solar System*. W. H. Freeman, San Francisco.
- Peyrard, M., Bishop, A.R. (1989). Statistical mechanics of a nonlinear model for DNA denaturation, *Phys. Rev. Lett.* **62**, 2755.
- Piazza, S.J., Delp, S.L. (1996). Influence of muscles on knee flexion during the swing phase of normal gait. *J. Biomech.*, **29**, 723–733.
- Pickover, C.A. (1986). Computer Displays of Biological Forms Generated From Mathematical Feedback Loops. *Computer Graphics Forum*, **5**, 313.
- Pickover, C.A. (1987). Mathematics and Beauty: Time-Discrete Phase Planes Associated with the Cyclic System. *Computer Graphics Forum*, **11**, 217.
- Piegl, L., Tiller, W. (1997). *The NURBS book*, (2nd ed.), Springer Monographs in Visual Communication, Berlin.
- Plumbley, M.D. (1999). Do cortical maps adapt to optimize information density?, *Network*, **10**, 41–58.
- Poincaré, H. (1890). Sur le problème differential equations trois corps et les équations de la dynamique. *Acta Math.*, **13**, 1–270.
- Pollack, J.B. (1991). The induction of dynamical recognizers. *Mach. Learn.*, **7**,

227–252.

- Pontryagin, L.S., Boltyanskii, V.G., Gamkrelidze, R.V., Mishchenko, E.F. (1986). *The Mathematical Theory of Optimal Processes*, Gordon & Breach Science Publishers, New York.
- Posch, H.A., Hoover, W.G., Vesely, F.J. (1986). Canonical Dynamics of the Nosé Oscillator: Stability, Order, and Chaos. *Phys. Rev. A*, **33**(6), 4253–4265.
- Postnikov, M.M. (1986). *Lectures in Geometry V, Lie Groups and Lie Algebras*. Mir Publ., Moscow.
- Pratt, J., Pratt, G. (1998). Exploiting natural dynamics in the control of a planar bipedal walking robot. In *Proceedings of the 36 Annual Allerton Conference on Communication, Control, and Computing*, 739–748, Allerton.
- Pribe, C., Grossberg, S., Cohen, M.A. (1997). Neural control of interlimb oscillations. II, Biped and quadruped gaits and bifurcations. *Biol. Cyber.* **77**, 141–152.
- Principe, J., Euliano, N., Lefebvre, C. (2000). *Neural and Adaptive Systems: Fundamentals Through Simulations*. Wiley, New York.
- Prinz, A.A., Bucher, D., Marder, E. (2004). Similar network activity from disparate circuit parameters. *Nature Neurosci.* **7**, 1345–1352.
- Prochazka, A., Gritsenko, V., Yakovenko, S. (2002). Sensory Control of Locomotion: Reflexes Versus Higher-Level Control, In: *Sensorimotor Control*, eds., S.G. Gandevia, U. Proske and D.G. Stuart, Kluwer, Dordrecht.
- Prochazka, A. (1996). Proprioceptive feedback and movement regulation. In: Rowell L, Sheperd JT (ed) *Handbook of Physiology. Section 12. Exercise: Regulation and Integration of Multiple Systems* American Physiological Society, New York, 89–127.
- Pulvermüller, F. (2005). Brain mechanisms kinking language and action. *Nature Rev. Neurosci.* **6**, 576–582.
- Putz, M. (1993). *Hamiltonian Mechanical Systems and Geometric Quantization*, Kluwer, Dordrecht.
- Pyragas, K. (1992). Continuous control of chaos, by self-controlling feedback. *Phys. Lett. A*, **170**, 421–428.
- Pyragas, K. (1995). Control of chaos via extended delay feedback. *Phys. Lett. A*, **206**, 323–330.
- Rabbitt, R.D., Damiano, E.R. (1996). A singular perturbation model of fluid dynamics in the vestibular semicircular canal and ampulla. *J. Fluid. Mech.*, **307**, 333–372.
- Ramond, P. (1990). *Field Theory: a Modern Primer*. Addison–Wesley, Reading.
- Rao, A.S., Georgeff, M.P. (1998). Decision Procedures for BDI Logics. *J. Logic Comp.*, **8**(3), 292–343.
- Raphan, T., Matsuo, V., Cohen, B. (1979). Velocity storage in the vestibulo-ocular reflex arc (vor). *Exp. Brain Res.*, **35**, 229–248.
- Rashevsky, N. (1967). Organismic sets. Outline of a general theory of biological and sociological organisms. *Bull. Math. Biophys.*, **29**, 139–152.
- Ratcliff, R. (1978). A theory of memory retrieval. *Psych. Rev.*, **85**, 59–108.
- Ricciardi, L.M., Umezawa, H. (1967). Brain physics and many-body problems, *Kibernetik*, **4**, 44.

- Ritter, H., Schulten, K. (1986). On the Stationary State of Kohonen's Self-Organizing Sensory Mapping. *Biological Cybernetics*, **54**, 99–106.
- Ritter, H., Schulten, K. (1988). Convergence Properties of Kohonen's Topology Conserving Maps: Fluctuations, Stability and Dimension Selection. *Biological Cybernetics*, **60**, 59–71.
- Ritter, H., Martinetz, T., Schulten, K. (1992). *Neural Computation and Self-Organizing Maps: An Introduction*, Addison-Wesley, Reading.
- Robinson, D.A. (1977). Linear addition of optokinetic and vestibular signals in the vestibular nucleus. *Exp. Brain Res.*, **30**, 447–450.
- Roe, R.M., Busemeyer, J.R., Townsend, J.T. (2001). Multi-alternative decision field theory: A dynamic connectionist model of decision making. *Psych. Rev.*, **108**, 370–392.
- Rose, R.M., Hindmarsh, J.L. (1989). The assembly of ionic currents in a thalamic neuron. I The three-dimensional model. *Proc. R. Soc. Lond. B*, **237**, 267–288.
- Rosen, R. (1958). The representation of biological systems from the standpoint of the theory of categories. *Bull. Math. Biophys.*, **20**, 245–260; A relational theory of biological systems. *Bull. Math. Biophys.*, **20**, 317–341.
- Rosenblatt, F. (1958). The perceptron: a probabilistic model for information storage and organization in the brain. *Physiol. Rev.*, **65**, 386–408.
- Rössler, O.E. (1976). An Equation for Continuous Chaos. *Phys. Lett. A*, **57**(5), 397–398.
- Ruelle, D. (1978). *Thermodynamic formalism. Encyclopaedia of Mathematics and its Applications*. Addison-Wesley, Reading.
- Rumelhart, D., McClelland, J. (eds.) (1987). *Parallel Distributed Processing. Vols I & II*, MIT Press, Cambridge.
- Sardain, P., Rostami, M., Bessonet, G. (1999). An anthropomorphic biped robot: dynamic concepts and technological design. *IEEE Trans. Syst. Man, Cyber. A*, **28**, 823–838.
- Sastri, S.S., Isidori, A. (1989). Adaptive control of linearizable systems. *IEEE Trans. Aut. Con.*, **34**(11), 1123–1131.
- Satarić, M.V., Tuszyński, J.A. and Zakula, R.B. (1993). Kinklike excitations as an energy-transfer mechanism in microtubules. *Phys. Rev. E*, **48**, 589–597.
- Satarić, M.V., Zeković, S., Tuszyński, J.A., Pokorný, J. (1998). Mössbauer effect as a possible tool in detecting nonlinear excitations in microtubules. *Phys. Rev. E*, **58**, 6333–6339.
- Sayers, B.McA., Beagley, H.A. (1974). Objective evaluation of auditory evoked EEG responses. *Nature*, **251**, 608–609.
- Schaal, S. (1998). Robot learning. In M. Arbib (ed). *Handbook of Brain Theory and Neural Networks* (2nd ed.), MIT Press, Cambridge.
- Schaal, S., Atkeson, C.G. (1998). Constructive incremental learning from only local information. *Neural Comput.*, **10**, 2047–2084.
- Schaal, S. (1999). Is imitation learning the route to humanoid robots?. *Trends Cogn. Sci.*, **3**, 233–242.
- Schaal, S., Sternad, J.C., Osu, R., Kawato, M. (2004). Rhythmic arm movement is not discrete. *Nature Neurosci.* **7**, 1136–1143.

- Schafer, R.D. (1996). *An Introduction to Nonassociative Algebras*. Dover, New York.
- Schiff, S.J., Jerger, K., Duong, D.H., Chang, T., Spano, M.L., Ditto, W.L. (1994). Controlling chaos in the brain, *Nature*, **370**, 615–620.
- Schnitzler, A., Gross, J. (2005). Normal and pathological oscillatory communication in the brain. *Nature Rev. Neurosci.*, **6**, 285–296.
- Schot, S.H. (1978). Jerk: The Time Rate of Change of Acceleration. *Am. J. Phys.*, **46**(11), 1090–1094.
- Segel, L.A., Cohen, I.R.(eds.), (2001). *Design principles for the immune system and other distributed autonomous systems*, Oxford Univ. Press, U.K.
- Seiler, W.M. (1995). Involution and constrained dynamics II: The Faddeev-Jackiw approach, *J. Phys. A*, **28**, 7315–7331.
- Sejnowski, T., Koch, C., Churchland, P. (1988). *Computational Neuroscience*. Science, **241**, 1299–1306.
- Seraji, H. (1989). Configuration control of redundant manipulators: theory and implementation. *IEEE Trans. Rob. Aut.*, **5**, 437–443.
- Seward, D., Bradshaw, A. and Margrave, F. (1996). The anatomy of a humanoid robot. *Robotica*, **14**, 437–443.
- Sherrington, C. (1906). *The Integrative Action of the Nervous System*. Yale Univ. Press.
- Shidara, M., Kawano, K., Gomi, H., Kawato, M. (1993). Inverse-dynamics model eye movement control by Purkinje cells in the cerebellum. *Nature*, **365**, 50–52.
- Shih, C.L., Gruver, W., Lee, T. (1993). Inverse kinematics and inverse dynamics for control of a biped walking machine. *J. Robot. Syst.*, **10**, 531–555.
- Shih, C.L., Klein, C.A. (1993). An adaptive gait for legged walking machines over rough terrain. *IEEE Trans. Syst. Man, Cyber. A*, **23**, 1150–1154.
- Sinai, Ya.G. (1970). Dynamical systems with elastic reflections. *Russ. Math. Surveys*, **25**, 137–189.
- Singer, W., Gray, C.M. (1995). Visual feature integration and temporal correlation hypothesis. *Ann. Rev. Neurosci.*, **18**, 555–586.
- Smale, S. (1967). Differentiable dynamical systems, *Bull. Amer. Math. Soc.*, **73**, 747–817.
- Sober, S.J., Sabes, P.N. (2003). Multisensory integration during motor planning. *J. Neurosci.* **23**(18), 6982–92.
- Sober, S.J., Sabes, P.N. (2005). Flexible strategies for sensory integration during motor planning. *Nature Neurosci.* **8**, 490–497.
- Soderkvist, J. (1994). Micromachined gyroscopes. *Sensors and Actuators A*, **43**, 65–71.
- Sperry, R.W. (1965). Mind, brain and humanist values. In: J. R. Platt (Ed.), *New Views of the Nature of Man*. 71–92, Univ. Chicago Press, Chicago.
- Sperry, R.W. (1969). A modified concept of consciousness. *Psych. Rev.*, **76**, 532–536.
- Sperry, R.W. (1980). Mind–brain interaction: Mentalism, yes; dualism, no. *Neurosci.*, **5**, 195–206.
- Sparrow, C. (1982). *The Lorenz Equations: Bifurcations, Chaos, and Strange*

- Attractors, Springer, New York.
- Spooner, J.T., Maggiore, M., Ordonez, R., Passino, K.M. (2002). *Stable Adaptive Control and Estimation for Nonlinear Systems: Neural and Fuzzy Approximator Techniques*. Wiley, New York.
- Sprott, J.C., Linz, S.J. (2000). Algebraically Simple Chaotic Flows, *Int. J. Chaos Theory and Appl.*, **5**(2), 3–22.
- Sprott, J.C. (1993). Automatic Generation of Strange Attractors. *Comput. & Graphics*, **17**(3), 325–332.
- Sprott, J.C. (1993). *Strange Attractors: Creating Patterns in Chaos*. M&T Books, New York.
- Sprott, J.C. (1994). Some Simple Chaotic Flows. *Phys. Rev. E*, **50**(2), R647–R650.
- Sprott, J.C. (1997). Some Simple Chaotic Jerk Functions. *Am. J. Phys.*, **65**(6), 537–543.
- Squires, T.M., Weidman, M.S., Hain, T.C., Stone, H.A. (2005) A mathematical model for top-shelf vertigo: the role of sedimenting otoconia in BPPV. *J. Biomech.* (to appear)
- Srivastava, Y.N., Vitiello, G., Widom, A. (1995). Quantum dissipation and quantum noise, *Annals Phys.*, **238**, 200.
- Srivastava, Y.N., Widom, A., Vitiello, G. (1999). Quantum measurements, information and entropy production. *Int. J. Mod. Phys. B* **13**, 3369–3382.
- Stanislavsky, A.A. (2000). Memory effects and macroscopic manifestation of randomness. *Phys. Rev. E* **61**, 4752.
- Stapp, H.P., (1993). *Mind, Matter and Quantum Mechanics*. Springer, New York.
- Stasheff, J.D. (1963). Homotopy associativity of H-spaces I & II. *Trans. Amer. Math. Soc.*, **108**, 275–292, 293–312.
- Steenrod, N. (1951). *The Topology of Fibre Bundles*. Princeton Univ. Press, Princeton.
- Stein, D.L. (1992). *Spin Glasses in Biology*. World Scientific, Singapore.
- Steinhausen, W. (1933). Über die beobachtung der cupula in den bogengangsampullen des labyrinth des lebenden hechts. *Pflügers Arch. Ges. Physiol.*, **232**, 500–523.
- Sternberg, S. (1969). Memory-scanning: Mental processes revealed by reaction-time experiments. *Am. Sci.*, **57**(4), 421–457.
- Stevens, B.L., Lewis, F.L. (2003). *Aircraft Control and Simulation* (2nd ed.). Wiley, Hoboken, NJ.
- Stong, R.E. (1968). *Notes on Cobordism Theory*. Princeton Univ. Press, Princeton.
- Strogatz, S. (2000). From Kuramoto to Crawford: exploring the onset of synchronization in populations of coupled oscillators. *Physica D*, **143**, 1–20.
- Stuart, J. (1999). *Calculus* (4th ed.). Brooks/Cole Publ., Pacific Grove, CA.
- Stuart, C.I.J., Takahashi, Y., Umezawa, H. (1978). On the stability and non-local properties of memory, *J. Theor. Biol.* **71**, 605–618.
- Stuart, C.I.J., Takahashi, Y., Umezawa, H. (1979). Mixed system brain dynamics: neural memory as a macroscopic ordered state, *Found. Phys.* **9**, 301.
- Sussmann, H.J. (1983). Lie brackets and local controllability: a sufficient condi-

- tion for scalar-input systems, *SIAM J. Con. Opt.*, **21**(5), 686–713.
- Sussmann, H.J. (1987). A general theorem on local controllability, *SIAM J. Con. Opt.*, **25**(1), 158–194.
- Sutton, R.S., Barto, A.G. (1998). *Reinforcement Learning: An Introduction*. MIT Press, Cambridge.
- Switzer, R.K. (1975). *Algebraic Topology – Homology and Homotopy*. (in *Classics in Mathematics*), Springer, New York.
- Tabony, J., Vuillard, L., Papaseit, C. (1999). Biological self-organisation and pattern formation by way of microtubule reaction-diffusion processes. *Adv. Complex Syst.* **2**(3), 221–276.
- Tabuada, P., Pappas, G.J. (2001). Abstractions of Hamiltonian Control Systems. *Proceedings of the 40th IEEE Conf. Decis. Con.*, Orlando, FL.
- Tabuada, P., Pappas, G.J. (2001). Quotients of fully nonlinear control systems. *SIAM J. Con. Opt.*
- Tabuada, P., Pappas, G.J. (2003). Abstractions of Hamiltonian Control Systems. Submitted to *Automatica*.
- Taiji, M., Ikegami, T. (1999). Dynamics of internal models in game players. *Physica D*, **134**, 253–266.
- Tanaka, K., Wang, H.O. (2001). *Fuzzy control systems design and analysis*. Wiley, New York.
- Thirring, W. (1979). *A Course in Mathematical Physics* (in four volumes). Springer, New York.
- Thom, R. (1975). *Structural Stability and Morphogenesis*. Addison–Wesley, Reading.
- Thorpe, J.A. (1979). *Elementary Topics in Differential Geometry*. Springer, New York.
- Toda, M., Kubo, R., Saito, N. (1991). *Statistical Physics 2*, Springer, New York.
- Townsend, J.S. (1992). *A modern Approach to Quantum Mechanics*, McGraw Hill Inc., New York.
- Tomovic, R., McGhee, R.B. (1966). A finite state approach to the synthesis of bioengineering control systems. *IEEE Trans. Hum. Fact. Elec.*, **7**(2), 65–69.
- Tong, F. (2003). Primary Visual Cortex and Visual Awareness. *Nature Rev. Neurosci.*, **4**, 219–229.
- Tsue, Y., Fujiwara, Y. (1991). Time-Dependent Variational Approach to (1+1)-Dimensional Scalar-Field Solitons, *Progr. Theor. Phys.* **86**(2), 469–489.
- van Buskirk, W.C., Watts, R.G., Liu, Y.K. (1976). The fluid mechanics of the semicircular canals. *J. Fluid Mech.*, **78**, 87–98.
- van den Bogert, A.J., Read, L., Nigg, B.M. (1996). A method for inverse dynamic analysis using accelerometry. *J. Biomech.*, **29**(7), 949–954.
- van den Broeck, C., Parrondo, J.M.R., Toral, R. (1994). Noise-Induced Nonequilibrium Phase Transition. *Phys. Rev. Lett.* **73**, 3395–3398.
- van den Broeck, C., Parrondo, J.M.R., Toral, R., Kawai, R. (1997) Nonequilibrium phase transitions induced by multiplicative noise. *Phys. Rev. E* **55**, 4084–4094.
- van der Helm, F.C.T., Pronk, G.M. (1995). Three-dimensional recording and

- description of motions of the shoulder mechanism. *J. Biomech. Eng.*, **117**, 27–40.
- van der Kooij, H., Jacobs R., van der Helm F. (2001). An adaptive model of sensory integration in a dynamic environment applied to human stance control. *Biol. Cybern* **84**, 103–115.
- van der Kooij, H., Donker, S. (2003). Use of Adaptive Model of Balance Control in the Identification of Postural Dynamics. Proceedings of ISB'03, Univ. Otago, Dunedin, NZ.
- van der Smagt, P. (ed.) (1999). Self-Learning Robots. Workshop: Brainstyle Robotics, IEE, London.
- Vapnik, V. (1995). *The Nature of Statistical Learning Theory*. Springer, New York.
- Verhás, J. (1997). *Thermodynamics and Rheology*, Akadémiai Kiadó, Budapest.
- Vitiello, G. (1995). Dissipation and memory capacity in the quantum brain model, *Int. J. Mod. Phys., B* **9**, 973.
- Vitiello, G. (1995). Dissipation and memory capacity in the quantum brain model, *Int. J. Mod. Phys. B*, **9**, 973–989.
- Vitiello, G. (2001). *My Double Unveiled*, John Benjamins, Amsterdam.
- Vygotsky, L.S. (1982). Historical meaning of the Psychological crisis. *Collected works*. vol. 1. Pedag. Publ., Moscow.
- Vladimirov, V.S., (1971). *Equations of Mathematical Physics*. Marcel Dekker, Inc., New York.
- Vladimirov, V.S. (1986). *A Collection of Problems on the Equations of Mathematical Physics*. Springer, Berlin.
- Vukobratovic, M., Borovac, B., Surla, D., Stokic, D., (1990). *Biped Locomotion: Dynamics, Stability, Control, and Applications*. Springer, Berlin.
- Vukobratovic, M. (1970). On the stability of biped locomotion. *IEEE Trans. Biom. Eng.*, **17**, 25–36.
- Vukobratovic, M., Juricic, D., Frank, A. (1970). On the control and stability of one class of biped locomotion systems. *ASME J. Basic Eng.*, **92**, 328–332.
- Vukobratovic, M., Stepanenko, Y. (1972). On the stability of anthropomorphic systems. *Math. Biosci.* **15**, 1–37.
- Vukobratovic, M., Stepanenko, Y. (1973). Mathematical models of general anthropomorphic systems. *Math. Biosci.* **17**, 191–242.
- Vukobratovic, M. (1975). *Legged Locomotion Robots and Anthropomorphic Mechanisms*. Mihailo Pupin Institute, Belgrade.
- Vukobratovic, M. *et al.* (1982–1988). *Scientific Fundamentals of Robotics* (Vols. 1–7), Springer, Berlin.
- Waddell, G. (1998). *The Back Pain Revolution*. Churchill Livingstone, Edinburgh.
- Watson, L.T. (1990). Globally convergent homotopy algorithms for nonlinear systems of equations. *Nonlinear Dynamics*, **1**, 143–191.
- Watts, D.J., Strogatz, S.H. (1998). Collective dynamics of ‘small-world’ networks. *Nature*, **393**, 440–442.
- Weinstein, A. (1990). Affine Poisson structures. *Internat. J. Math.*, **1**, 343–360.
- Weisstein, E.W. (2004). *MathWorld—A Wolfram Research Web Resource*. <http://mathworld.wolfram.com>.



- Welch, G., Bishop, G. (1995). An Introduction to the Kalman Filter. Univ. North Carolina, Dep. Comp. Sci., TR 95-041.
- Welchman, A.E., Deubelius, A., Conrad, V., Bulthoff, H.H., Kourtzi, Z. (2005). 3D shape perception from combined depth cues in human visual cortex. *Nature Neurosci. AOP*, **8**(5), doi:10.1038/nrn1458.
- Werbos, P.J. (1989). Backpropagation and neurocontrol: A review and prospectus. In *IEEE/INNS Int. Joint Conf. Neu. Net.*, Washington, D.C., **1**, 209-216.
- Werbos, P. (1990). Backpropagation through time: what it does and how to do it. *Proc. IEEE*, **78**(10).
- Wheeler, J.A., Feynman, R.P. (1949). Classical Electrodynamics in Terms of Direct Interparticle Action, *Rev. Mod. Phys.*, **21**, 425-433.
- Widrow, B., Hoff, M. (1960). Adaptive Switching Circuits. IRE Wescon Rept. 4.
- Wiener, N. (1961). *Cybernetics*. Wiley, New York.
- Wiesendanger, M. (1997). Path of Discovery in Human Motor Control. In: Hepp-Reymond, M.C., Marini, G. *Perspectives of Motor Behavior and its Neural Basis*. Karger Publ., Basel.
- Whiting, W.C., Zernicke, R.F. (1998). *Biomechanics of Musculoskeletal Injury, Human Kinetics*, Champaign, IL.
- Whitney, D.E. (1987). Historical perspective and state of the art in robot force control. *Int. J. Robot. Res.*, **6**(1), 3-14.
- Wiggins, S. (1990). *Introduction to Applied Dynamical Systems and Chaos*. Springer, New York.
- Wikipedia, the free encyclopedia. (2005) <http://wikipedia.org>.
- Wilder, D.G., Pope, M.H., Magnusson M.S. (1996). Mechanical stress reduction during seated jolt/vibration exposure, *Perinatol.*, **20**(1), 54-60.
- Wilkie, D.R. (1956). The mechanical properties of muscle. *Brit. Med. Bull.*, **12**, 177-182.
- Williams, C.P., Clearwater, S.H. (1998). *Explorations in Quantum Computing*, Springer, New York.
- Wilson, D. (2000). *Nonlinear Control, Advanced Control Course (Student Version)*, Karlstad Univ.
- Winter, D.A. (1990). *Biomechanics and Motor Control of Human Movement*, (2nd ed.) Wiley, New York.
- Winter, D.A. (1995). *Gait & Posture*, **3**(4), 193-214.
- Witten, E. (1998). Magic, mystery, and matrix. *Notices AMS*, **45**(9), 1124-1129.
- Wolf, A., Swift, J.B., Swinney, H.L., Vastano, J.A. (1985). Determining Lyapunov Exponents from a Time Series. *Physica D*, **16**(3), 285-317.
- Wolpert, D., Kawato, M. (1998). Multiple paired forward and inverse models for motor control. *Neural Networks*, **11**, 1317-1329.
- Xia, Z., Storm, D.R. (2005). The role of calmodulin as a signal integrator for synaptic plasticity. *Nature Rev. Neurosci.* **6**, 267-276.
- Xu, Z., Hauser, J. (1994). Higher order approximate feedback linearization about a manifold, *J. Math. Sys. Est. Con.*, **4**, 451-465.
- Xu, Z., Hauser, J. (1995). Higher order approximate feedback linearization about a manifold for multi-input systems, *IEEE Trans. Aut. Con*, AC-40, 833-840.

- Yager, R.R. (1987). *Fuzzy Sets and Applications: Selected Papers by L.A. Zadeh*, Wiley, New York.
- Yang, C.N., Lee, T.D. (1952). Statistical theory of equation of state and phase transitions I: Theory of condensation. *Phys. Rev.* **87**, 404–409.
- Yorke, J.A., Alligood, K., Sauer, T., Chaos (1996). *An Introduction to Dynamical Systems*. Springer, New York.
- Yoshikawa, T. (1984). Analysis and Control of Robot Manipulators with Redundancy. In *Robotics Research*, Eds. M. Brady and R. Paul, 735–747, MIT Press, Cambridge.
- Zatsiorsky, V.M. (1998). *Kinematics of Human Motion*. Human Kinetics Publ., Champaign, IL.
- Zadeh, L.A. (1978). Fuzzy sets as a basis for a theory of possibility. *Fuzzy Sets and Systems*, **1**(1), 3–28.

This page intentionally left blank

# Index

- 1-form-field, 854
- 3D scale vector, 260
- 3D shape perception, 619
- 3D-graphics, 242
- 3D-layering, 242
- 3D-printing, 242
- 3DS Max, 260
  
- Abelian category, 57
- Abelian group, 35
- absolute covariant derivative, 198, 204, 849
- abstract functor machine, 412
- abstract theory of Lyapunov exponents, 308
- acceleration, 128, 197, 850
- acceleration vector, 114
- accelerometer, 532
- actin, 386
- action, 238, 680, 793, 803
- action of the flow, 64
- action potential, 544
- action-amplitude picture, 800
- action-angle system of canonical coordinates, 300
- action-angle variables, 272
- action-at-a-distance electrodynamics, 807
- activation derivative, 733
- activation dynamics, 735, 812
- Adaline, 708
- Adams-Bashforth-Moulton integrator, 527
- adaptability, 772
- adaptive, 681
- adaptive control, 458, 546
- adaptive filter, 735
- adaptive fuzzy dynamics, 773
- adaptive Kalman filtering, 546
- adaptive Lie-derivative, 775
- adaptive path integral, 801, 803, 804, 806
- adaptive path measure, 809
- adaptive resonance theory, 738
- adaptive sensory-motor control, 740
- adaptive signal tracking, 525
- additive functor, 58
- additive fuzzy system, 763
- adenosine diphosphate, 390
- adenosine triphosphate, 386
- adiabatic, 332
- adiabatic elimination, 935
- adjoint group action, 176
- adjoint Jacobi equation, 495
- adjoint map, 166
- adjunction, 47, 48
- admissible controls, 482
- admissible Dynkin diagrams, 910
- admissible variation, 406
- afferent nerves, 558
- affine connection, 200, 816
- affine control system, 489, 494
- affine Hamiltonian control, 491
- affine Lagrangian control, 523

- agent action cycle, 243
- agonist muscle, 604
- Akinetic Mute, 660
- algebra, 161
- algebra homomorphism, 161
- algebra of classical observables, 266
- algebra of mental objects, 790
- algorithmic approach, 813
- alternating flexion/extension, 575
- amplitude, 809
- ampula, 626
- analytic in a region, 895
- anatomical MRI, 881
- angular acceleration, 626, 629
- Anosov diffeomorphism, 304
- antagonist muscle, 604
- anthropomorphic product-tree, 181
- anti-holomorphic, 902
- anticontrol of chaos, 71
- antiderivation, 138
- approximate feedback linearization, 479
- arc-element, 200
- area-preserving map, 80
- arm motor control, 652
- arrows, 39
- artificial neural networks, 24, 705
- associated tensors, 842
- associative composition, 39
- associative learning, 637
- associative memory, 548
- associativity of morphisms, 40
- asymptotically stable, 268, 466
- atlas, 118
- ATPase, 391
- attack function, 740
- attracting focus, 66
- attracting Jordan node, 66
- attracting line, 66
- attracting node, 66
- attracting set, 269
- attracting spiral, 67
- Aubert-Fleischl phenomenon, 610
- auditory cortex, 542
- auto-overlap, 748
- autocatalator, 79
- autogenetic excitation, 571
- autogenetic inhibition, 573
- autogenetic motor servo, 522
- autonomic nervous system, 553
- autonomous ODE, 60, 148
- average energy, 924
- averaging decision mechanics, 814
- axon, 550
- back adjunction, 48
- backpropagation, 714, 812
- backward Lyapunov exponent, 308
- ball-and-socket joints, 171, 378
- Banach manifold, 119
- Banach space, 119
- basal ganglia, 588, 594
- basic formula of feedback control, 455
- basilar membrane, 623
- basin of attraction, 99, 269
- basket cell, 590
- BDI agent, 771
- Belousov-Zhabotinski reaction, 83
- Bendixon's criterion, 271
- Betti, 42
- Betti numbers, 43, 143, 431
- Betz cells, 583
- Bianchi covariant derivative, 264, 291
- Bianchi relation, 239
- Bianchi symmetry condition, 203
- bidirectional associative memory, 753, 775
- bifurcation, 69, 150
- bifurcation point, 150
- biholomorphism, 899
- bijection, 41
- bijective, 28
- bilinear map, 217
- bimanual coordination, 586
- binary signals, 733
- binormal, 849
- biodynamic action, 351
- biodynamic bundles, 121
- biodynamic manifold, 117
- biodynamic-like Hamiltonians, 442
- biodynamics functor machine, 411
- biodynamics homology group, 439

- biomechanical force-velocity relation, 101
- biomechanical transformation matrix, 258
- biomorph, 81
- biomorphic systems, 81
- biped robot, 497
- bipolar neurons, 552
- bipolar signals, 733
- black box, 776
- blind source separation, 889
- Bloch, 880
- body scheme, 260
- Bohr, 330
- Boltzmann constant, 923
- Bolza problem, 493
- bone fractures, 420
- bony labyrinth, 622
- boundary, 59
- brain dynamics, 71
- brain injury, 658
- brain plasticity, 546, 548
- brain-control, 1
- brain-like control functor, 818
- brain-mind functorial machines, 792
- brain-motor-controller, 183
- Brodmann's area, 643
- Bromwich contour, 898
- Brouwer degree of the Gauss map, 209
- Brownian dynamics, 410
- Brownian motion, 224
- brute-force, 97
- bursting, 670
- butterfly effect, 73
- Calabi-Yau manifolds, 242, 902
- calculus of variations, 11
- Campbell-Baker-Hausdorff, 156, 503
- canonical configurational partition function, 443
- canonical coordinates, 265
- canonical quantization, 311
- canonical transformation, 218
- capacity dimension, 80, 87
- captured motion, 244
- Cartan subalgebra, 910
- Cartan's magic formula, 158
- Cartesian coordinate basis, 844
- Cartesian product, 28, 34
- cascaded recurrent ANN, 730
- catastrophes, 70
- categorification, 51, 240
- category, 39, 408
- category of Lie groups, 121, 433
- category of neurons, 787
- category of smooth manifolds, 437
- category of vector bundles, 437
- Cauchy's integral formulas, 896
- Cauchy's theorem, 279, 896
- Cauchy-Riemann equations, 895
- Cauchy-Schwartz inequality, 903
- causality-determination principle, 10
- causes of motion, 114
- Cauchy's residue theorem, 897
- cellular automata, 776
- cellular robotics, 771
- center, 67
- center manifold, 684
- central biodynamic adjunction, 541
- central nervous system, 552
- central pattern generator, 575
- cerebellar cortex, 542
- cerebellar models, 818
- cerebellar robotics, 538
- cerebellum, 183, 580, 587, 632
- cerebral cortex, 542
- cerebral hemispheres, 579
- chain complex, 59
- chain coupling, 102
- chain rule, 27, 123, 140
- chaos, 2
- chaos control, 2, 84
- chaos theory, 68, 931
- chaotic (strange) attractor, 152
- chaotic attractor, 99
- chaotic sets, 151
- Chapman-Kolmogorov equation, 373, 744
- Chapman-Kolmogorov integro-differential equation, 374, 805

- Chapman–Kolmogorov law, 125, 132
- characteristic distribution, 478
- characteristic equation, 320, 926
- characteristic Lyapunov exponents, 85
- chemical kinetics, 79
- Chow's theorem, 496
- Christoffel symbols, 200, 291, 846
- Chua–Matsumoto circuit, 83
- class of objects, 39
- classical biodynamic action, 351
- classical theory of Lie groups, 904
- climbing fibre, 590
- closed form, 59, 140
- closed path, 32
- closed-loop nonlinear system, 475
- closure property, 323
- co-active neuro-fuzzy inference system, 724
- coadjoint group action, 177
- cobasis, 137
- coboundary, 59
- coboundary operators, 427
- cochain complex, 59
- cochlea, 623
- cochlear nucleus, 624
- cocomplete category, 48
- cocycle, 59
- codifferential, 147
- codomain, 28, 39
- coframing, 137
- cofunctor, 43
- cognitive economy, 815
- cognitive information processing, 738
- Cohen–Grossberg activation equations, 740
- Cohen–Grossberg theorem, 740
- cohomology exact sequence, 428
- cohomology object, 59
- coimage, 57
- cokernel, 57
- colimit, 47
- colimits, 48
- collective link, 783
- colored multiplicative noise, 934
- combining noisy sensor outputs, 526
- commensurate, 272
- commutative diagram, 39
- commutative diagrams of arrows, 32
- commutative flow, 33
- commutator, 292
- compact, 30
- compactness, 30
- complete motor act, 574
- complete subcategory, 41
- complex, 140
- complex adaptive system, 681
- complex Gaussian noise, 674
- complex manifold, 898
- complex networks, 678
- complex phase-space manifold, 276
- complex structure, 899
- complex-valued amplitudes, 805
- complex-valued ANNs, 731
- complex-valued order parameter, 675
- complexified tangent space, 901
- components, 32
- composite Hilbert space, 325
- composition, 26, 773
- conatural projection, 124
- concept of learning, 454
- conditional exponent entropies, 677
- conditional Lyapunov exponents, 676
- conditional reflexes, 3
- condyloid, 378
- configuration manifold, 13, 114, 855
- configuration space, 12, 261
- conformal  $z$ -map, 80
- conjugate gradient method, 717
- connected, 32
- connected Lie group, 914
- connectedness, 30
- connection, 197, 198
- connection homotopy, 202
- connectionist, 709
- conscious state, 699
- consequences, 814
- conservative brain, 694
- conservative Hamiltonian biodynamics, 855
- conservative particle, 695
- conservative-reversible systems, 15

- constant of motion, 267
- constrained Hamilton–d’Alembert equations, 367
- constrained variational principle, 364
- context space, 730
- continual time systems, 460
- continual–sequential state equation, 412
- continuity, 28
- continuity equation, 679, 700
- continuous deformation, 29
- continuous eigenvalue, 322
- continuous Hopfield network, 747
- continuous phase transition, 105
- continuous phase transitions, 918
- continuous projectors, 322
- continuous spectral form, 322
- continuous spectrum, 321
- continuum limit equation, 679
- contraction, 136
- contraction dynamics, 392, 521
- contravariant acceleration functor, 452
- contravariant functor, 43
- contravariant Hom–functor, 45
- contravariant Lagrangian dynamics, 408
- contravariant vector, 839
- control, 805
- control Hamiltonian function, 856
- control law, 523
- control of motion, 114
- control outputs, 856
- control parameter, 105, 921
- control parameters, 17, 72, 103
- controllability, 772
- controlled Van der Pol oscillator, 476
- convex optimization problem, 725
- coordinate chart, 118
- coordinate transformation, 838
- corrector, 527
- correlation function, 224
- cotangent bundle, 114, 123, 181
- cotangent Lie algebra, 175
- cotangent lift, 494
- cotangent map, 124
- cotangent space, 123
- counit natural transformation, 48
- coupling Lagrangians, 523
- covariant, 837
- covariant derivative, 848
- covariant differentiation, 196
- covariant Euler–Lagrange equations, 407
- covariant force equation, 357
- covariant force functor, 403, 452, 453, 541, 818
- covariant force law, 2, 60, 101, 113, 114, 261, 403, 424, 427, 452, 453, 541, 818, 855
- covariant form, 837, 849
- covariant functor, 43
- covariant Hom–functor, 45
- covariant vector, 840
- covector, 840
- covector–field, 134
- cover, 30
- covering, 30, 120
- Coxeter graph, 911
- Coxeter–Dynkin diagram, 911
- Crick–Koch binding hypothesis, 638
- Crick–Koch proposal, 549
- critical phenomena, 920
- critical points, 213
- critical slowing down, 104, 105, 752
- cross bridges, 387
- cross–overlap, 748
- cupula, 629
- curvature, 239, 816
- curvature operator, 196, 203
- curve, 114
- curve on a manifold, 121
- cusp bifurcation, 692
- cycle, 59
- damping rate, 99
- data–processing neurons, 669
- De Rham cohomology group, 143, 429
- De Rham complex, 140
- De Rham differential complexes, 429
- De Rham theorem, 141, 143, 146, 430
- decoherence, 314



- decomposable system, 412
- deep memory, 816
- deep nuclei, 591
- defuzzification, 762, 832
- degree of anisotropy, 886
- degree of order, 103
- delta distribution, 220
- delta-rule, 712
- dendrites, 550
- DENFIS system, 770
- density matrix, 694
- density matrix equation of motion, 695
- density matrix operator, 701
- depolarization, 559
- derivative map, 131
- derivative matrix, 62
- describing function, 472
- desired kinematic trajectory, 511
- desired response, 475
- deterministic biodynamic jerk function, 424
- deterministic chaos, 68, 410
- deterministic drift, 374, 805
- diabatic, 332
- diagonal functor, 45
- diencephalon, 580
- diffeomorphism, 41, 121
- difference, 477
- difference of Gaussians filter, 622
- differential, 153
- differential Hebbian law, 740
- diffusion, 16
- diffusion anisotropy, 884
- diffusion coefficient, 882
- diffusion fluctuations, 373, 374, 805
- diffusion magnetic resonance imaging, 881
- diffusion MRI, 881
- diffusion tensor, 881
- Dirac delta function, 220
- Dirac interaction picture, 318
- Dirac matrices, 161
- Dirac rules for quantization, 311
- direct system, 38
- directing the action, 803
- direction cosines, 257
- directional derivative, 152
- Dirichlet tessellation, 742
- discontinuous jumps, 374, 805
- discontinuous phase transition, 105
- discontinuous phase transitions, 917
- discrete characteristic projector, 321
- discrete eigenvalues, 320
- discrete movements, 652
- discrete spectral form, 321
- discrete spectrum, 320
- discrete time systems, 460
- discriminant functions, 705
- discriminative touch, 632
- discriminative touch system, 633
- disorder  $\Rightarrow$  order, 106
- displacement vector-field, 393
- dissipation function, 400
- dissipation-fluctuation theorem, 226
- dissipative quantum dynamics, 694
- dissipative structures, 16
- distribution, 485
- distributions, 226
- domain, 26, 28, 39
- dorsal root ganglion, 633
- double, 694
- drawing with complex numbers, 890
- dual, 123, 134
- dual Bianchi relation, 238
- dual Hodge star operator, 238
- dual picture, 43
- dual system, 527
- Duffing oscillator, 75
- dummy index, 837
- dynamical recognizers, 729
- dynamical system, 148
- Dynkin diagram, 908
- early selection, 814
- eccentric, 835
- Eccles, 518
- echo attenuation, 885
- echolocation, 602
- echoplanar imaging, 885
- Edinger-Westphal nuclei, 619
- effective action, 167, 696

- effects of motion, 114
- efferent functional stimulation, 517
- Ehrenfest classification scheme, 916
- Ehresmann connection, 495
- eigenvalues, 926
- eigenvectors, 926
- Einstein, 111
- Einstein equations, 237
- Einstein's summation convention, xv, 541
- elastic net algorithm, 741
- elastic pendulum, 78
- electroception, 602
- electroencephalography, 888
- embedding field equation, 514
- embedding methods, 718
- emergent property, 681
- endolymph, 623
- endpoint conditions, 406
- energizing, 803
- entanglement, 314
- enteric nervous system, 554
- entropy, 19, 102, 701, 915
- epic, 58
- epimorphism, 40
- epimorphisms, 28
- equation of continuity, 852
- equations of mathematical physics, 226
- equilibrioception, 601
- equilibrium point, 62, 465
- equilibrium solution, 268
- equilibrium state, 62
- equipartition, 372
- equipotential hypersurfaces, 442
- equivalence relation, 28
- equivalent muscular actuator, 385
- ergodic hypothesis, 806
- ergodicity, 301
- Erlangen programme, 913
- error term, 62
- essence of feedback control, 464
- Euclidean metrics, 841
- Euler, 42
- Euler characteristic, 447, 817
- Euler's formula, 889
- Euler's vector equation, 294
- Euler–Lagrange differential equation, 12
- Euler–Lagrange equation, 202, 262
- Euler–Poincaré characteristics, 143, 430
- evolution laws, 17
- evolution operator, 125
- evolutionary computation, 726, 776
- evolutive system, 788
- exact, 57, 697
- exact form, 59, 140
- excitation dynamics, 392, 521
- excitatory, 563
- existence of identity morphism, 40
- existence–uniqueness theorem, 22
- exponential map, 165, 173, 187
- exponentially stable, 467
- exponentially stable in the large, 467
- exponentiation, 186
- extended Hamilton oscillator, 110
- extended Jacobi equation, 495
- extended Kalman filter, 530, 717
- extended Pfaffian system, 406
- extended phase-space, 148
- extension principle, 417
- extensive quantities, 226
- exterior algebra, 134
- exterior derivative, 114, 138
- exterior differential system, 854
- exterior differential systems, 137
- external coordinates, 180
- extract order from chaos, 72
- extrapyramidal, 641
- factor Hilbert spaces, 325
- faithful functor, 45
- Faraday tensor, 238
- fast variable, 151
- feedback fuzzy systems, 768
- feedforward neural network, 707
- Feigenbaum number, 79
- ferromagnet, 104
- Feynman, 7
- Feynman path integral, 361, 800, 924
- Feynman propagator, 360

- Feynman–Vernon formalism, 696
- fiber derivative, 365
- fibre, 124
- fibre bundle map, 621
- fibre derivative, 434
- Fick equation, 16
- Fick law, 682
- field, 37
- field action functional, 924
- Filehne Illusion, 610
- final, 806
- final object, 39
- finite-dimensional Hilbert space, 320
- first derived system, 500
- first integral, 267
- first quantization, 314
- first return time, 149
- first variation formula, 202
- first-order phase transitions, 917
- first-order-search methods, 716
- fisherman's derivative, 152
- FitzHugh–Nagumo model, 151, 671
- fixed point, 268
- fixed points, 21
- flexion reflex, 574
- Floquet multiplier, 93
- Floquet stability analysis, 93
- flow, 131, 148, 854
- flow line, 128, 133
- flow property, 132
- fluctuating force, 225
- fluctuating uncertainty, 808
- flux, 20
- Fokker–Planck equation, 373, 702, 753, 805, 931
- foliation, 486
- force, 20, 850
- force equation, 101, 291
- force servo-controller, 522
- force vector-field, 393
- force-field action principle, 814
- force-field analysis, 803
- force-velocity relation, 388
- forced Hamiltonian biodynamics, 855
- forced Van der Pol oscillator, 75
- forgetful memories, 749
- formal exponential, 132
- forward kinematics, 180
- forward Lyapunov exponent, 307
- Fourier equation, 16
- Fréchet derivative, 292
- fractal, 73, 80
- free action, 167
- free energy, 923
- free energy potential, 104, 915
- free index, 837
- free nerve endings, 634
- Frenet–Serret formulae, 850
- front adjunction, 48
- frontal lobe, 542
- full coupling, 101
- full embedding, 45
- full functor, 45
- full observability, 772
- fully nonlinear control system, 464
- fully recurrent networks, 727
- function, 26
- function approximation, 512
- function space, 31
- functional approximators, 705
- functional derivative, 293
- functional MRI, 881
- functional systems, 3
- functor, 43
- functor category, 46
- functor machine, 413
- functor morphism, 45
- fundamental group, 44
- fundamental groupoid, 42
- Fundamental theorem of calculus, 235
- fusion, 773
- fuzzification, 761
- fuzzy associative memory, 765, 773
- fuzzy diffusion parameter, 760
- fuzzy inference engine, 761
- fuzzy inference system, 832
- fuzzy logic, 755
- fuzzy logic controller, 769
- fuzzy membership function, 756
- fuzzy mutual entropy, 758, 760
- fuzzy numbers, 417
- fuzzy parameter space, 760

- fuzzy processes, 773
- fuzzy region of uncertainty, 417
- fuzzy wave equation, 760
- fuzzy-stochastic biodynamic jerk function, 424
- fuzzy-stochastic transformation, 418
- Galilei group, 9
- game, 728
- game theory, 728
- gamma dynamics, 572
- gamma statics, 572
- Gauss curvature, 196
- Gauss-Bonnet formula, 196, 449
- Gauss-Bonnet theorem, 144
- Gauss-Kronecker curvature, 449
- Gaussian bell-shaped curve, 220
- Gaussian multiplicative noise, 930
- general functional transformation, 838
- general linear Lie algebra, 156
- general Markov stochastic process, 805
- general natural system, 786
- general theory of systems, 411
- generalized chain complexes, 428
- generalized cochain complexes, 427
- generalized feedforward network, 720
- generalized functions, 226
- generalized Gaussian, 734
- generalized Hamiltonian
  - biodynamics, 856
- generalized Hamiltonian control system, 856
- generalized Hebbian rule, 674
- generalized Kronecker-delta symbol, 841
- generating functional, 680, 924
- genetic algorithm, 726
- genetic algorithms, 716, 776
- genetic control, 726
- genus, 448
- geodesic, 129, 199, 202, 847
- geodesic action, 816
- geodesic deviation, 205
- geodesic equation, 202, 816, 847
- geodesic equations, 162
- geodesic flow, 265, 291, 436
- geodesic spray, 130, 265, 291, 436
- geometric action principle, 816
- geometric modelling, 242
- geometric spirit, 7
- geometrical dual, 854
- geometrodynamic functor, 802
- geometrostatics, 114
- Gibbs ensemble, 23
- gimballed inertial systems, 533
- Ginzburg-Landau equation, 922
- Ginzburg-Landau model, 922
- Glauber dynamics, 749
- glia, 552
- gliding joints, 379
- global complex analysis, 276
- global solution, 133
- globus pallidus, 595
- glycolysis, 391
- goal of a control system, 457
- Golgi cells, 590
- Golgi tendon organs, 519
- Golgi tendon reflex, 572
- gradient, 131, 201
- gradient descent method, 715
- gradient flow, 622
- gradient force 1-forms, 407
- gradient force vector-fields, 407
- gradient information, 709
- gradient Newtonian equation, 797
- gradient of the performance surface, 709
- granule cells, 589
- Grassmann algebra, 134
- Grassmann planes, 851
- Green's function, 222
- Green-Gauss-Ostrogradsky Divergence theorem, 233
- grey matter, 542
- group, 35, 42, 64
- group action, 35, 171
- group conjugation, 176
- group homomorphism, 36
- group monomorphism, 36
- groupoid, 42

- grows exponentially, 68
- grows linearly, 68
- growth condition, 416
- gyroscope, 532
- Hénon map, 80
- Haar measure, 167
- Hamilton oscillator, 109
- Hamilton's equations, 266
- Hamilton's principle, 262
- Hamilton–Poisson biodynamic system, 294
- Hamiltonian biodynamics, 124
- Hamiltonian chaos, 98
- Hamiltonian energy function, 15, 265
- Hamiltonian energy operator, 312
- Hamiltonian flow, 269
- Hamiltonian formalism, 115
- Hamiltonian function, 161, 289
- Hamiltonian mechanical system, 265
- Hamiltonian phase-flow, 435
- Hamiltonian vector-field, 265, 289
- Hamming hypercube, 747
- harmonic, 147
- harmonic functions, 895
- Hartman–Grobman theorem, 751
- heading, 534
- hearing, 600
- heat bath, 410, 924
- heat conduction, 16
- heat equation, 188, 194, 210
- Heaviside's step function, 221
- Hebb rules, 546
- Hebbian innovation, 750
- Hebbian learning, 774
- Hebbian theory, 563
- Hecht–Nielsen counterpropagation network, 737
- Heisenberg picture, 297, 318
- Heisenberg's uncertainty relation, 317
- hemodynamics, 853
- Hermitian inner product, 902
- Hermitian operator, 312
- Hessian, 201
- heuristic approach, 813
- hierarchical action control, 803
- Hilbert, 37
- Hilbert 19th problem, 351
- Hilbert 23rd problem, 351
- Hilbert 4th problem, 200
- Hilbert 5th problem, 904
- Hilbert 6th problem, 7
- Hilbert action principle, 237
- Hilbert basis, 903
- Hilbert manifold, 119
- Hilbert space, 119, 313, 725, 903
- Hill, 388
- Hindmarsh–Rose thalamic neuron, 691
- hinge joints, 171, 378
- Hodge Laplacian, 147
- Hodge star operator, 137, 146
- Hodgkin–Huxley, 560
- Hodgkin–Huxley model, 667, 692
- holomorphic cotangent space, 901
- holomorphic function, 895
- holomorphic tangent space, 901
- holonomic constraints, 14
- holonomy, 239, 902
- Hom-bifunctor, 45
- homeomorphism, 41, 67
- homeostasis, 578
- homoclinic orbit, 150, 271
- homogenous transformation, 258
- homological algebra, 42
- homology group, 43, 44
- homology object, 59
- homotopic, 30
- homotopies of homotopies, 54
- homotopy, 30, 31
- homotopy axiom, 430
- homotopy classes, 31
- homotopy methods, 718
- homotopy of loops, 32
- homotopy operators, 142, 480
- homunculus, 582
- Hopf bifurcation, 99
- Hopfield model, 547
- Hopfield nets, 776
- Hopfield synaptic matrix, 748
- human animation, 242
- Human Biodynamics Engine, 661, 829

- human brain, 542
- human eye, 603
- human nervous system, 549
- human performance modelling, 771
- human skeleton, 377
- human striate cortex, 620
- human vestibular system, 629
- human-like locomotor system, 101
- humanoid robot, 538
- humanoid robots, 6
- Huntington's disease, 596
- Huxley, 387
- hybrid dynamics, 411
- hybrid joint actuator, 521
- hybrid system, 772
- hyperbolic force-velocity curve, 388
- hyperbolic force-velocity relation, 401
- hyperbolic point, 269
- hyperbolic structure, 151
- hyperbolic tangent threshold
  - activation functions, 708
- hyperpolarization, 559
- hysteresis effect, 104, 105
  
- ideal, 37
- identity, 39
- identity functor, 45
- image, 57
- immediate feedbacks, 772
- immune system, 682
- imprecision of measurement, or
  - estimation, 410
- impulse function, 220
- impulse torque-time relation, 401
- inclusion functor, 45
- incommensurate, 272
- independent component analysis, 888
- independent component analysis
  - networks, 723
- index, 137, 213
- indirect adaptive control, 459
- inductive limit, 783
- inertia, 532
- inertia matrix, 851
- inertial reference frames, 532
- inertial sensor errors, 535
- inertial sensors, 532
- inference, 762
- inferior cerebellar peduncle, 591
- infinite-dimensional Hilbert space, 321
- infinite-dimensional neural network, 801
- infinitesimal generator, 173
- infinitesimal generator of the action, 168
- information, 85
- inhibitory, 563
- initial, 806
- initial object, 39, 41
- injection, 28, 40
- inner ear, 623
- inner hair cells, 623
- inner product space, 902
- input fusion, 773
- input map, 412
- input process, 413
- insertion operator, 136
- instability sequence, 104
- instruction, 773, 774
- integral curve, 127, 132
- integral curves, 854
- integral element, 138
- integral manifold, 406, 485
- integrate-and-fire neuron, 688
- integrate-and-fire neurons, 670
- integrate-and-fire-or-burst neuron, 690
- intensive quantities, 226
- intention, 792, 803
- inter-neuronal level, 698
- interaction energy, 622
- interior product, 136
- internal acceleration vector-field, 854
- internal force 1-form field, 854
- internal joint coordinates, 180, 853
- internal models, 729
- internal velocity vector-field, 854
- intervertebral disclinations, 420
- intervertebral dislocations, 420
- intra-neuronal level, 698
- invariant, 839

- invariant manifold, 150
- invariant tori, 271
- inverse dynamic analysis of human movement, 533
- inverse dynamics analysis, 650
- inverse kinematics, 180
- inverse kinematics problem, 462
- inverse loop, 32
- inverse myotatic reflex, 572
- inverse stretch reflex, 572
- inverse system, 38
- inverted driven pendulum, 77
- inverted pendulum, 455
- involution, 186
- involutive closure, 485
- iris, 603
- irregular and unpredictable, 68
- irreversible processes, 16
- Ising Hamiltonian, 746, 748
- Ising–spin Hopfield network, 737
- isokinetic, 835
- isolated equilibrium point, 465
- isometric, 835
- isometric steady–state contraction, 388
- isomorphism, 41
- isotonic, 835
- isotropy group, 168
- Itô SDE, 702
- Iterated Prisoner's Dilemma, 729
- Ito, 372
- Ito quadratic cotangent bundle, 416
- Ito quadratic tangent bundle, 415
- Ito stochastic integral, 372
- Ito stochastic integral equation, 373
- Jacobi equation of geodesic deviation, 205
- Jacobi fields, 205
- Jacobi identity, 161, 292
- Jacobian determinant, 27, 838
- Jacobian matrix, 62
- jerk function, 98
- jet space, 189
- joint afferents, 635
- jolt, 422
- Jordan and Elman networks, 721
- Jordan canonical form, 66
- Kähler manifold, 220, 902
- Kalman filter, 461, 526, 775
- Kalman filtering problem, 528
- Kalman regulator, 461
- Kalman–Bucy filter, 527
- Kalman–quaternion filter, 535
- Kaplan–Yorke dimension, 87
- Karhunen–Loeve covariance matrix, 735, 748
- kernel, 57
- key–frame animation, 242
- kick equation, 222
- Killing form, 914
- kinematic constraint distribution, 370
- kinematic singularities, 180
- kinematic structure equation, 258
- kinetic energy, 115, 925
- kink solitons, 666
- knowledge representation, 776
- Kohonen algorithm, 742
- Kohonen continuous self organizing map, 738
- Kohonen self–organizing map, 721
- Kolmogorov–Arnold–Moser (KAM) theory, 301
- Kolmogorov–Sinai, 87
- Kolmogorov–Sinai entropy, 85, 677
- Korteveg–De Vries equation, 195, 296, 796
- Kronecker–delta, 841
- Kuramoto model, 672, 679
- lack of memory, 410
- Lagrange multipliers, 365
- Lagrange stability, 467
- Lagrange–d'Alembert principle, 364
- Lagrangian, 264
- Lagrangian biodynamics, 123
- Lagrangian density, 807
- Lagrangian flow, 435
- Lagrangian formalism, 115
- Lagrangian–field structure, 815
- Landau, 73

- Landau's theory of phase transitions, 921
- Langevin rate equation, 224, 371, 410, 702
- language and actions, 801
- Laplace equation, 190
- Laplace transform, 463, 897
- Laplace–Beltrami operator, 201
- Laplacian, 201
- Laplacian operator, 235
- largest eigen–diffusivity, 887
- largest Lyapunov exponent, 85, 444
- lateral geniculate nucleus, 621
- lateral premotor area, 584
- Laurent series, 897
- Lauterbur, 880
- laws of motion, 125
- leaf space, 487
- learning, 2
- learning dynamics, 735, 736
- learning rate, 710, 810
- learning rate scheduling, 711
- least action principle, 801, 806, 807
- least means square algorithm, 710
- Lebesgue integral, 322
- left adjoint, 48
- left cancellable, 40
- left exact, 58
- left extension, 164
- left ideal, 161
- left invariant vector–field, 163
- left inverse, 40
- Legendre transformation, 13, 365, 366, 434
- Legendre's functor, 643
- lens, 603
- level curves, 270
- level set, 126
- levels of processing framework, 815
- Levenberg–Marquardt algorithm, 717
- Levi–Civita connection, 198, 291
- Lie algebra, 156, 161, 292
- Lie algebra homomorphism, 161
- Lie algebra simple root, 910
- Lie bracket, 155, 161
- Lie bracket property, 194
- Lie derivative, 152, 266
- Lie derivative formalism, 116
- Lie functor, 164
- Lie group, 162
- Lie subalgebra, 161
- Lie–Lagrangian biodynamics functor, 403
- Lie–Poisson bracket, 177, 292
- life space foam, 803
- limit, 47
- limit cycle, 75
- limit set, 148, 269
- limits, 48
- linear, 61
- linear acceleration, 628
- linear approximation, 62
- linear controllability, 478
- linear flow, 63
- linear quadratic regulator, 526
- linear representation, 311
- linear system, 477
- linearization, 268
- linearized dynamics, 445
- linearly equivalent, 65
- Liouville equation, 344, 373, 414, 805
- Liouville measure, 103, 399
- Liouville operator, 700
- Liouville theorem, 103, 149, 298, 700
- Lipschitz condition, 130, 416
- Lissajous curves, 78
- local bifurcations, 150
- local learning process, 810
- locally accessible system, 489
- locally exact, 140
- Locked In, 660
- locomotion, 793
- logistic equation, 931
- logistic map, 79, 90
- long-term behavior, 61
- long-term consequences, 814
- long-term memory, 735, 815
- long-term rewards, 772
- loop, 32
- Lorenz attractor, 73
- Lorenz equations, 97
- Lorenz mask, 73



- Lorenz system, 73
- Lyapunov criterion, 525
- Lyapunov dimension, 87
- Lyapunov exponent, 288
- Lyapunov function, 458, 468, 737
- machine learning, 524
- macroscopic, 806
- macroscopic arrow of time, 703
- macroscopic spatio-temporal level, 802
- magnetic resonance imaging, 880
- magnetoception, 602
- magnetometer, 535
- main direction of diffusivities , 886
- Mamdani inference, 832
- Mandelbrot and Julia sets, 80
- manifold with boundary, 142
- manipulability measure, 180
- Mansfield, 880
- Markov assumption, 373
- Markov chain, 371, 410
- Markov stochastic process, 370, 410, 805
- mass conservation principle, 852
- Master equation, 373, 805
- match-based learning, 739
- material covariant metric tensor, 356
- material metric tensor, 851, 854, 855
- matrix commutator, 156
- matrix cost function, 716
- matrix representation, 907
- maximal geodesic, 129
- maximal integral curve, 128
- maximal integral manifold, 485
- maximum-entropy, 733
- Maxwell's equations, 238
- Maxwell-Haken laser equations, 74
- Maya, 260
- McCulloch-Pitts neurons, 708
- mean diffusivity, 886
- mean kinetic energy, 225
- mean square error, 709
- mean square limit, 372
- mean-field, 109
- mean-field approximation, 931
- mean-field theory, 447, 917
- measurement equation, 528
- medulla oblongata, 580
- Melnikov function, 276
- membranous labyrinth, 622
- memory, 24
- memory evolutive system, 787
- memory storage, 815
- memory term, 100
- memory-guided movements, 586
- mental force law, 818
- metric tensor, 197, 291
- Meyerhof pathway, 391
- micro-level, 803
- microscopic, 808, 809
- microscopic arrow of time, 704
- microscopic theory of muscular contraction, 387
- microtubules, 662, 699
- midbrain, 580
- middle cerebellar peduncle, 591
- millimetric image resolution, 882
- mind, 798
- minimizing the error, 709
- model of synaptic activation, 518
- model space, 119
- modified solitary equations, 798
- modular feedforward networks, 721
- module, 37
- molecular motors, 386
- momentum, 161
- momentum learning, 715
- momentum map, 173
- momentum phase-space, 182, 289, 854
- monic, 58
- monomorphism, 40
- monomorphisms, 28
- Moore-Penrose pseudoinverse, 181, 259, 749, 838
- morphism of vector-fields, 133
- morphisms, 39
- Morris-Lecar neuron, 691
- Morse function, 213, 445
- Morse theory, 213, 445
- mossy fibers, 592

- motion action principle, 810
- motion capture, 242, 243
- motivation, 803
- motive formation, 803
- motor axons, 568
- motor cortex, 543, 588
- motor metric tensor, 643
- motor nerve fibers, 553
- motor pathways, 569
- motor skills, 380
- motor unit, 514
- multi-kick equation, 223
- multi-modal sensing problem, 650
- multilayer perceptron, 707
- multiplicative zero-mean Gaussian
  - white noise noise, 931
- multipolar neurons, 552
- muscle, 1
- muscle fibers, 386
- muscle spindle, 570
- muscle training process, 834
- muscular dynamics, 520
- muscular heat equation, 389
- muscular mechanics, 395
- muscular stiffness matrix, 393
- muscular system, 379
- mutual overlap, 748
- myofibrils, 386
- myoglobin, 391
- myosin, 386
- myotatic reflex, 570
  
- n-categories, 49
- Nash equilibrium, 728
- natural equivalence, 46
- natural Hilbert space, 345
- natural inclusion, 46
- natural input-output control system,
  - 856
- natural isomorphism, 46
- natural projection, 122
- natural psychodynamics, 800
- natural transformation, 45
- nature of consciousness, 453
- nearest neighbor coupling, 102
- necessary, 696
  
- nerve impulses, 23
- nervous system, 23
- neural control inputs, 856
- neural state-space, 753
- neural-image coordinates, 819
- neural-image manifold, 827
- neuro-biological self-similarity, 704
- neuro-Hamiltonian control system,
  - 857
- neurons, 23, 550
- neutral line, 66
- Newton-Raphson method, 718
- Newtonian method, 715
- Newtonian-like action, 811
- nociception, 601
- Noether, 42
- Noether theorem, 354
- Noetherian module, 38
- Noetherian ring, 37
- noise, 810, 816
- non-anticipating solution, 416
- non-periodic orbit, 65
- nondegenerate, 217
- nonequilibrium phase transitions, 752
- nonholonomic rolling constraints, 368
- nonlinear, 61
- nonlinear adaptive complex systems,
  - 775
- nonlinear affine control system, 464
- nonlinear control, 116
- nonlinear control design, 458
- nonlinear controllability criterion, 484
- nonlinear decomposable system, 413
- nonlinear dynamics, 2, 115
- nonlinear function approximators, 761
- nonlinear multivariate analysis, 838
- nonlinear nonequilibrium systems,
  - 930
- nonlinear process-functor, 413
- nonlinear Schrödinger equation, 295,
  - 311, 922
- nonlinear Schrödinger equation, 795
- nonlinear system behavior, 413
- nonlinearity, 18, 795
- nontrivial recurrence, 305
- nonuniform hyperbolicity, 306

- nonuniformly hyperbolic dynamical systems, 305
- nonwandering set, 269
- norm, 161, 902
- normal form of a vector-field, 151
- normal subgroup, 36
- normal vector-field, 126
- normalization, 151
- normalization condition, 313
- normed space, 902
- null object, 41
- numerical invariants of spaces, 42
- nystagmus, 629
- objects, 39
- observability map, 412
- occasional proportional feedback, 768
- occipital lobe, 542
- ocular dominance, 621
- Oja-Hebb learning rule, 735
- olfactory cortex, 542
- one parameter subgroup, 164
- one-form, 840
- one-parameter family of maps, 148
- one-to-one, 28, 40
- Onsager relations, 21
- onto, 28, 40
- open cover, 30
- open evolution equation, 701
- open Liouville equation, 701
- optical flow, 614
- optimal estimator problem, 527
- optimal performance, 774
- optimal policy, 774
- optokinetic nystagmus, 611
- orbifolding, 242
- orbit, 148, 168
- orbit Hilbert space, 326
- orbit space, 168
- orbits, 36, 64
- order parameter, 72, 105, 795, 919, 935, 937
- order parameter equation, 105, 751, 937
- ordered symmetry-breaking state, 930
- ordering chaos, 70
- organ of Corti, 623
- orientation, 142
- orientation preference, 621
- Ornstein-Uhlenbeck noise, 934
- orthogonal sum, 322
- oscillator neural networks, 672
- otolithic organs, 629
- outer hair cells, 623
- outer product, 840
- output map, 412
- output process, 413
- overall probability amplitude, 809
- overlap, 748
- pain and temperature system, 634
- parabolic Einstein equation, 209
- parabolic length-tension curve, 388
- parallel transport, 265, 436
- parallelogram law, 903
- parameter update law, 525
- parasympathetic nervous system, 554
- parietal lobe, 542
- parking theorem, 484
- Parkinson's disease, 595
- partial order, 28
- partially ordered set, 28
- particle interacting, 696
- partition function, 442, 922
- path, 32
- path components, 32
- path connected, 32
- path that requires minimal memory, 813
- path-integral, 679
- pattern, 783
- pattern matching process, 739
- pattern-recognition, 711
- Pavlov, 563
- Pavlov's conditional-reflex learning, 564
- peduncles, 591
- Penrose paradox, 329
- perceptron, 711
- perfect Morse functions, 450
- performance, 455

- performance surface, 709
- perilymph, 623
- period, 144
- period doubling bifurcations, 79
- period-doubling bifurcation, 90
- periodic orbit, 65
- peripheral nerve fibers, 553
- peripheral nervous system, 552
- perturbation theory, 273
- Peyrard-Bishop system, 446
- Pfaffian exterior differential system, 405
- phase function, 221
- phase space, 15
- phase trajectory, 15, 268
- phase transition, 69, 104, 915
- phase transition of first order, 105
- phase transition of second order, 105
- phase transitions, 20, 441
- phase-space distribution, 345
- phase-space for, 148
- phase-space spreading effect, 400
- phase-transition effects, 104
- phase-transition theory, 73
- phases, 803
- physically based geometric modelling, 242
- Pickover's biomorphs, 83
- pitch, 534
- pivot joints, 379
- Poincaré, 7, 42
- Poincaré lemma, 140, 142, 430
- Poincaré map, 149
- Poincaré section, 75, 92, 149
- Poincaré-Bendixson theorem, 69
- Poincaré-Hopf theorem, 144
- point orbit, 65
- pointed set, 32
- pointed topological space, 32
- Poisson bracket, 266
- Poisson evolution equation, 292
- Poisson manifold, 292
- Poisson process, 224
- polarization law, 903
- pons, 580
- Pontryagin's Maximum Principle, 493
- position of equilibrium, 16
- positional muscle stiffness, 520
- positive leading Lyapunov exponent, 86
- possibility distribution, 417
- post-central gyrus, 634
- postsynaptic potential, 745
- potential energy, 925, 929
- potential system, 11
- practically rigid body, 112
- preconscious states, 699
- predictability time, 86
- predictive forward dynamics, 651
- predictor, 527
- prequantization, 347
- Prigogine, 16
- primary afferents, 634
- primary auditory cortex, 625
- primary motor cortex, 581
- primary somatosensory cortex, 634
- prime mover, 604
- principal component analysis
  - networks, 723
- principal fibre bundle, 621
- principal loading hypothesis, 420
- principal normal, 849
- Principia, 8
- Prisoners' Dilemma, 728
- proactive interference, 815
- probabilistic transition
  - micro-dynamics, 809
- probability amplitudes, 313
- probability density, 932
- process equation, 528
- processing elements, 24
- processing speed, 805, 811, 813
- product of two complex numbers, 890
- products, 16
- projective limit, 784
- prolongation, 188
- prolonged group action, 192
- proprioception, 601, 632
- proprioceptive feedback, 588
- proprioceptive sensation, 635
- protozoan morphology, 82
- pull-back diagram, 34

- Purcell, 880
- pure continuous spectral form, 324
- pure discrete spectral form, 324
- Purkinje cells, 589
- Pyragas control, 93
- pyramidal, 641
- quadratic cost function, 526
- quadratic I&F neuron, 690
- qualitative analysis, 61
- quantization, 311
- quantum biodynamic action, 351
- quantum biodynamics, 310
- quantum brain, 800
- quantum commutator, 297
- quantum computations, 699
- quantum computer, 664
- quantum computing, 662
- quantum evolution equation, 297
- quantum field theory, 924
- quantum Hamilton's equations, 317
- quantum Liouville equation, 695, 701
- quantum noise, 697
- quantum open Liouville equation, 703
- quantum pictures, 318
- quantum statistical mechanics, 922
- quantum stringy geometry, 241
- quantum superposition, 313
- quasiperiodic motions, 301
- quaternion attitude estimation filter, 535
- quaternions, 890
- quotient representation, 908
- quotient space, 183
- Rössler, 97
- radial basis function network, 723
- random force, 680, 696
- random walk, 371
- range, 26, 39
- rank condition, 482
- rate of error growth, 85
- Rayleigh-Bernard convection, 83
- reachability map, 412
- reachable set, 489
- reactants, 16
- reactive agents, 242
- real-life situation, 772
- realization problem, 412
- reciprocal innervation, 572
- recurrent ANN, 729
- recursive homotopy dynamics, 408
- red muscle fibers, 391
- reduction equivalence relation, 183
- redundancy, 180
- redundant manipulator, 402
- redundant system, 838
- reflectance pattern, 737
- reflex, 566
- regional energy minimization, 887
- regular points, 22
- reinforcement learning, 509, 774
- reinforcing, 772
- relation, 28
- relative acceleration, 205
- relative degree, 476
- relative order, 475
- relaxation dynamics in spin systems, 621
- relaxation oscillator, 75
- Renshaw cells inhibition, 657
- repelling focus, 66
- repelling Jordan node, 66
- repelling line, 66
- repelling node, 66
- repelling spiral, 67
- repolarization, 559
- representation of a category, 45
- representation of a group, 45
- representation of a Lie group, 907
- representative point, 15, 854
- required, 696
- residue, 897
- resonate-and-fire neuron, 690
- restricted 3-body problem, 2
- retina, 603
- retraction, 40
- retroactive interference, 815
- rhythmic movements, 652
- Ricci antisymmetric tensors, 841
- Ricci curvature, 197
- Ricci flow, 209

- Ricci tensor, 197, 203
- Riemann, 7
- Riemann curvature tensor, 196, 202, 842
- Riemannian kinetic energy form, 855
- Riemannian manifold, 137, 261
- Riemannian metric, 115, 196, 291, 356, 811, 841
- Riesz Representation Theorem, 904
- rigged Hilbert space, 321
- right adjoint, 48
- right cancellable, 40
- right exact, 59
- right ideal, 161
- right inverse, 40
- rigid body motions, 14
- rigid body with a fixed point, 282
- ring, 37
- risk of local spinal injuries, 423
- robust control, 458
- robustness, 455
- Rodrigues relation, 175
- roll, 534
- root system, 908
- Rosenblatt, 711
- Rosler system, 77
- rotation of the brain-stem, 660
- route to chaos, 70, 99
- rule-importance weight, 773
  
- sacculae, 623, 628
- saddle, 66
- saddle joints, 379
- saltatory conduction, 561
- sarcomere, 386
- scala media, 623
- scala vestibuli, 623
- scalar curvature, 197, 205
- scalar invariant, 839
- scalar potential field, 854
- scalar-field, 842
- Schrödinger picture, 318
- Schwann cells, 552
- search, 709, 805
- second order phase transition, 446
- second variation formula, 206
- second-order contravariant tensor, 840
- second-order covariant tensor, 840
- second-order mixed tensor, 840
- second-order phase transition, 930
- second-order phase transitions, 918
- section, 40
- sectional curvature, 204
- sections of biodynamic bundles, 124
- seeing, 600
- selective attention, 813
- self-consistency relation, 936
- self-organization and cooperation, 512
- self-organizing feature maps, 741
- self-organizing learning dynamics, 68
- self-organizing map, 513
- semantic integration, 810
- semantic memory, 815
- Semi-Coma, 660
- semi-parametric classifiers, 705
- semicircular canals, 623, 626, 629
- semiclassical quantization, 666
- semidirect product, 178, 183
- semisimple representation, 914
- sensitivity to initial conditions, 68
- sensitivity to parameters, 68
- sensor fusion, 773
- sensor fusion in hybrid systems, 531
- sensory axons, 568
- sensory memory, 805
- sensory metric tensor, 642
- sensory-motor adjunction, 455
- sensory-motor coordination, 23
- sensory-motor covariant embedding tensor, 643
- sensory-motor transformation, 641
- separatrix, 271
- sequence of period doublings, 99
- sequential (threshold) dynamics, 745
- servomechanism, 244
- set of morphisms, 39
- shallow memory, 816
- shape operator, 449
- Sherrington reciprocal inhibition, 574
- short exact sequence, 58

- short-term consequences, 814
- short-term memory, 735
- short-term predictability, 69
- short-time evolution, 937
- shortest path, 816
- signal, 810
- signal velocity, 734
- signal/feature vector-space, 620
- simple Lie group, 913
- simple mechanical control systems, 487
- simple mechanical systems, 263
- simple statistical system, 817
- simulated annealing, 716
- Sine-Gordon equation, 796
- single-link inverted pendulum, 654
- singular perturbation theory, 151
- singularity, 268
- six layers of the neocortex, 621
- skeletal system, 376
- skeleton, 376
- sliding filament mechanism, 387
- slope parameter, 708
- slow manifold, 151
- slow variable, 151
- small time locally controllable, 481
- small-time local controllability, 490
- small-world networks, 678
- smell, 601
- smooth, 119
- smooth homomorphism, 163
- smooth map, 120
- smooth pursuit eye movements, 610
- Sobolev-Schwartz, 226
- soliton, 295, 795
- soliton celular automata, 796
- soliton equation, 666
- solitonic structures, 698
- solution, 61
- solution curve, 65
- somatic nervous system, 553
- somatosensory cortex, 542
- somatosensory system, 632
- source, 43
- space of all weighted paths, 811
- spatiotemporal networks, 740
- special Euclidean group in 3D space, 177
- special Euclidean group in the plane, 175
- special Euclidean group of motions, 402
- special Euclidean groups, 14
- specific heat capacity, 915
- speed, 128
- Sperry, 453
- spike, 688
- spike function , 221
- spiking, 670
- spiking and bursting neurons, 688
- spin-like Hamiltonians, 621
- spinal cord, 568
- spinal frogs, 260
- spinal nerves, 559
- spinal torque-jolt space, 423
- spindle receptors, 519
- spinor, 160
- spiral ganglion, 624
- split-brain work, 453
- spray, 133
- stability, 61, 455, 772
- stable, 268
- stable in the sense of Lyapunov, 466
- stable set, 150
- stable submanifold, 303
- Standard Additive Model, 763
- standard saddle, 67
- standard sink, 67
- standard source, 67
- star-shaped, 142
- state feedback, 488
- state vector, 61
- state-space, 61
- state-space approach, 457
- static backpropagation, 707
- stationary probability density, 932
- steepest descent method, 710
- steering functions, 493
- Steinhausen model, 630
- step size, 710, 810
- stereolithography, 242
- Stern-Gerlach experiment, 334

- stochastic force, 371
- stochastic forces, 410
- stochastic Hamiltonian dynamics, 370
- stochastic influence, 411
- stochastic integral, 371
- stochastic learning process, 744
- stochastic Taylor expansion, 416
- stochastic tensor bundle, 415
- stochastic transformation, 414
- stochastic-gradient order parameter equations, 751
- Stokes formula, 143
- Stokes theorem, 233
- strange, 73
- strange attractor, 75
- strapdown inertial systems, 533
- Stratonovitch interpretation, 931
- strengths, 811
- stress-energy-momentum, 816
- stretch reflex, 570
- stretch-and-fold, 76
- string theory, 902
- structural instability, 103
- structurally stable, 150
- structure equations, 212
- subgroup, 36
- substantia nigra, 594
- sum over fields, 814
- sum over geometries, 817
- sum over histories, 811
- sum-over-fields, 805
- sum-over-geometries, 805
- sum-over-histories, 805
- superior cerebellar peduncle, 591
- superior frontal gyrus, 585
- supervised network, 707
- support vector machine, 724
- surjection, 28, 40
- symmetric, 201
- symmetric affine connection, 198
- symmetrical load-lifting, 396
- symmetry breaking instability, 104, 752
- symmetry group, 188
- symmetry-breaking, 918
- sympathetic nervous system, 554
- symplectic form, 217, 218
- symplectic group, 218
- symplectic Lie algebra, 179
- symplectic Lie group, 179
- symplectic manifold, 218, 265
- symplectic map, 218
- symplectic matrix, 179
- symplectomorphism, 217
- synaptic junctions, 546
- synaptic weights, 24
- synergetics, 68, 72, 751
- synergist, 604
- synovial joint dynamics, 520
- synthetic differential geometry, 227
- system dynamics, 412
- system of coordinates, 112
- system parameters, 101
- system with uncertain dynamics, 526
- tactition, 601
- tangent, 849
- tangent bundle, 114, 122, 181
- tangent dynamics equation, 444
- tangent Lie algebra, 174
- tangent map, 121, 123
- tangent space, 121
- tangent vector-field, 126
- target, 43
- taste, 600
- tectorial membrane, 624
- telegraph equation, 682
- telegraph reaction diffusion equation, 682
- temporal associative memories, 749
- temporal dynamical systems, 735
- temporal lobe, 542
- tensor contraction, 842
- tensor-field, 842
- terminal object, 41
- thalamus, 588
- the saddle-node bifurcation, 684
- the sectional curvature, 196
- theory of fluctuating geometries, 817
- thermal bath, 696
- thermal equilibrium, 73
- thermoception, 601



- thermodynamic equilibrium, 18
- thermodynamic relation, 388
- thermodynamic-like partition function, 812
- theta-neuron, 684, 690
- thought solitons, 795
- three Euler angles, 534
- time-dependent flow, 125
- time-dependent Schrödinger equation, 312
- time-dependent vector-field, 132
- time-lagged recurrent networks, 726
- time-reversal symmetry, 919
- Toda lattice equation, 797
- topological group, 163
- topological hypothesis, 442
- topological invariant, 447
- topological manifold, 117
- topological space, 29
- topologically dual functors, 437
- topologically equivalent, 67, 149
- torque command model, 646
- torque-jerk, 424
- torque-jolt, 423
- torsion, 200
- torsion free, 201
- total action, 806
- total derivative, 193
- total energy function, 856
- total Hilbert state-space, 322
- total spectral form, 323
- total spectral measure, 323
- total system's response, 412
- trajectory, 114, 130
- transducer neurons, 669
- transformation matrix, 258
- transient chaos, 152
- transition, 803
- transition amplitude, 360, 809
- transition entropy, 812
- transition functor, 804
- transition maps, 118
- transition probability, 809
- transition propagator, 804
- transitive action, 167
- trapping region, 269
- trial-and-error, 772
- triangular identities, 57
- true association cortex, 621
- two-sided ideal, 161
- two-sided inverse, 40
- Tychonoff product-topology theorem, 831
- tympani, 623
- uniaxial rotational joint, 267
- uniformly asymptotically stable, 466
- uniformly bounded, 467
- uniformly stable, 466
- uniformly ultimately bounded, 467
- unipolar neurons, 552
- unique functorial relation, 431
- unique globally smooth transition functor, 807
- unit natural transformation, 48
- universal properties, 34, 47
- universality class, 920
- unstable directions, 445
- unstable set, 150
- unstable submanifold, 303
- unsupervised learning, 513
- utricle, 623, 628
- Van der Pol's oscillator, 75, 470
- variation vector-field, 202
- vector, 839
- vector-field, 61, 126, 842, 854
- vector-fields, 114
- velocity, 128, 197
- velocity command model, 646
- velocity equation, 101
- velocity phase-space, 182, 263, 854
- velocity servo-controller, 523
- velocity storage, 630
- velocity vector, 114
- Verhulst model, 931
- vertebrate brain, 578
- vestibule, 623
- vestibulo-ocular reflex, 627
- virtual communication links, 515
- viscous force, 665
- visual cortex, 542

- visual map formation method, 621
- Volterra–Lotka ensemble dynamics, 753
- volume form, 147, 291
- Voronoi tessellation, 742
  
- water vapor, 103
- wave psi-function, 313
- weak functorial inverse, 47
- weakly-connected neural networks, 692, 751
- wedge product, 134, 136
- weighted category, 787
- weights, 810
- well-posed variational problem, 405
- white matter, 542
- Wick rotation, 809
- Wiener process, 373
- Wigner function, 345, 694, 695
- winding number, 278
- Winner-relaxing Kohonen algorithm, 743
- wireframe graphical mode, 581
- withdrawal reflex, 574
- working memory, 805, 815
  
- Yang–Lee theorem, 441
- Yang–Mills relation, 239
- yaw, 534
  
- zero morphism, 41